MOLECULAR DYNAMICS

and Theory of Broad Band Spectroscopy

MYRON EVANS

GARETH J. EVANS
The University College of Wales, Aberystwyth
Aberystwyth, Wales

WILLIAM T. COFFEY
School of Engineering
Trinity College
Dublin, Ireland

PAOLO GRIGOLINI
University of Pisa
Pisa, Italy

A Wiley-Interscience Publication
JOHN WILEY & SONS
New York · Chichester · Brisbane · Toronto · Singapore

I would like to express my warmest thanks to Dr. B. K. P. Scaife, Professor of Engineering Science in the University of Dublin, for very many discussions concerning the material of Chapters 2 and 3. A large proportion of these chapters has been taken from my doctoral dissertation written under his supervision. I would like to thank most warmly Professor J. H. Calderwood of the University of Salford and of University College Galway for helpful conversations and encouragement. It is also my pleasure to thank Professor H. Fröhlich, FRS, and Professor R. A. Sack of the University of Salford, Professor J. R. McConnell of the School of Theoretical Physics, Dublin Institute for Advanced Studies, Professor W. Schröer of the University of Bremen, Dr. J. K. Vij of Trinity College, and Dr. A. Morita of Akita University, Japan, for stimulating criticism.

I would like to thank Professor W. Wright and the Engineering School of Trinity College for providing much assistance toward the task of producing his book. I wish to express my warm thanks to the University of Salford for he award of a Visiting Fellowship during the tenure of which a great part of he manuscript was written. My thanks are also due to Professor J. S. Rowlinson for the hospitality of his department at Oxford University during he period in which the book was being printed.

Special thanks must go to Mr. G. C. R. Lyons of Trinity College for his neticulous care in the preparation of diagrams.

The authors would like to thank Dr. J. Yarwood for his help in producing Chapter 12, and we thank all other Research Workers from whom we have aken material.

With reference to the interrelation between theory and experiment stressed hroughout the volume, we can do no better than recall the words of Laplace:

'est ainsi que les théories les plus abstraites, en se répandant par de ombreuses applications, sur la nature et sur les arts, sont devenues 'inépuisables sources de biens et de jouissances pour celui même qui les nore.

raité de Mécanique Céleste, Vol. 3, J. B. M. Duprat, Paris, 1802.

W. T. C.

Contents

Notes on Symbolic Consistency

There being too many physical quantities for half a dozen alphabets (excluding that of the Chinese) we decided to aim for a degree of consistency within each chapter and accordingly each is prefaced with a list of symbols which is not intended to be comprehensive but rather to concentrate on those unfortunate coincidences in notation which could cause even more confusion than necessary. In particular we have tried to differentiate carefully between scalars, vectors, tensors, and supertensors. Some letters of the Roman and Greek alphabets change their meaning between chapters and the chapter lists are intended to define these as necessary. The standard practice is in itself often very confusing, for example the symbol α is used for power absorption coefficient, complex polarizability, and to denote the α loss process at low frequencies. It is therefore next to impossible to follow the standard notation and keep to this throughout the book. In the particular case of power absorption coefficient this is denoted by the Gothic $\mathfrak{A}$ to avoid confusion with the polarizability.

In Chapters 9 and 10 we have made extensive use of ket notation in order to facilitate comparison of quantum and classical equations of motion and in order to describe succinctly ground and excited vibrational states.

Book and Review References

These are intended to supplement the text of each chapter in so far as they may not be specifically referred to but are relevant background reading. In some cases the books are supplemented by periodicals and circulars (Chapter 3). Specific text references are of direct relevance and are listed separately for each chapter. In addition, Chapter 12 contains a bibliography (with titles) in the main body of the text for the molecules methyl fluoride, methyl iodide, and dichloro methane.

Chapter 1

1. Balescu, R., *Equilibrium and Non-Equilibrium Statistical Mechanics*, Wiley, New York (1975).
2. Berne, B. J. and Pecora, R., *Dynamic Light Scattering with Applications to Chemistry, Biology and Physics*, Wiley-Interscience, New York (1976).
3. Debye, P., *Polar Molecules*, Chemical Catalog Co., New York (1929).
4. de Gennes, P. G., *The Physics of Liquid Crystals*, Oxford University Press, Oxford (1974).
5. Doob, J. L., *Stochastic Processes*, Wiley, New York (1963).
6. Einstein, A., *Investigations on the Theory of the Brownian Movement*, edited by R. Fürth, Dover, New York (1956).
7. Fox, R. F., "Gaussian Stochastic Processes in Physics," Phys. Rep., **48**, 179–283 (1978).
8. Kac, M., *Probability and Related Topics in Physical Sciences*, Interscience, New York (1959).

8a. Khinchin, A. I., *Statistical Mechanics*, translated by Gamow, Dover, New York (1949).

9. Kubo, R., *Statistical Mechanics of Equilibrium and Non-Equilibrium*, North-Holland, Amsterdam (1965).
10. McDonald, I. R. and Hansen, J. P., *Theory of Simple Liquids*, Academic, New York (1976).
11. McQuarrie, D. A., *Statistical Mechanics*, Harper and Row, New York (1975).
12. Nelson, E., *Dynamical Theories of Brownian Motion*, Princeton University Press, Princeton, N.J. (1967).
13. Prigogine, I., *Non-Equilibrium Statistical Mechanics*, Interscience, New York (1962).

14. Resibois, P., *Physics of Many Particle Systems*, edited by E. Meeron, Gordon and Breach, New York (1966).

15. Rice, S. A. and Gray, P., *The Statistical Mechanics of Simple Liquids*, Interscience, New York (1965).

15a. Sveshnikov, A. A., *Applied Methods of the Theory of Random Functions*, translated by J. Berry, Pergamon, New York (1966).

16. Tolman, R. C., *The Principles of Statistical Mechanics*, Oxford University Press, Oxford (1938).

17. Uhlenbeck, G. E. and Ford, G. W., *Lectures in Statistical Mechanics*, American Mathematical Society, New York (1963).

18. Wax, N. (Ed.), *Selected Papers on Noise and Stochastic Processes*, Dover, New York (1954).

Chapter 2 (see also book and review references to Chapter 1)

1. Brink, D. M., and Satchler, G. R., *Angular Momentum*, Oxford University Press, New York (1968).

2. Edmunds, A. R., *Angular Momentum in Quantum Mechanics*, Princeton University Press, Princeton, N.J. (1957).

3. Favro, L. D., in *Fluctuation Phenomena in Solids*, Academic, New York (1965).

4. Fano, V. and Racah, G., *Irreducible Tensorial Sets*, Academic, New York (1959).

5. Goulon, J., "Theories Stochastiques des Phenomènes de Transport (cas des Mouvements de Reorientations Moleculaire)," Deuxieme Thèse d'État, University of Nancy I (1972).

6. Jeffreys, H., *Cartesian Tensors*, Cambridge University Press, Cambridge (1961).

7. Margenau, H. and Murphy, G. M., *The Mathematics of Physics and Chemistry*, van Nostrand, New York, 1962.

8. Rose, M. E., *Elementary Theory of Angular Momentum*, Wiley, New York (1957).

9. Spiegel, M. R., *Theory and Problems of Vector Analysis*, Schaum, New York, 1958.

Chapter 3

Volumes on Dielectrics

1. Bordewijk, P. and Bottcher, C. J. F., *Theory of Electric Polarisation*, Vols. I and II, Elsevier, Amsterdam (1973, 1979).

2. Brot, C., *Dielectric and Related Molecular Processes*, Chem. Soc., Specialist Per. Rep., Chem. Soc., London, Vol. 2, p.1 (1975).

2a. Cole, R. H. (Ed.), *J. G. Kirkwood—Collected Works*, Gordon/Breach Series: "Documents on Modern Physics."

3. Fröhlich, H., *Theory of Dielectrics*, Oxford University Press, Oxford (1958).

3a. Hasted, J. B., *Aqueous Dielectrics*, Chapman and Hall, London (1973). Müller, K. D., and Rothschild, W. G., *Far Infra-red Spectroscopy*, Wiley-Interscience, New York, (1971). This contains references to a further 1512 papers up to 1970.

4. Hill, N. E., Vaughan, W. E., Price, A. H., and Davies, M., *Dielectric Properties and Molecular Behaviour*, van Nostrand/Reinhold, London (1969).

5. Scaife, B. K. P. (Ed.) *Complex Permittivity*, The English Universities Press, London (1971).

6. Smyth, C. P., *Dielectric Behaviour and Structure*, McGraw-Hill, New York (1965).

Volumes on Liquid Properties

1. Buckingham, A. D. (Ed.), *Organic Liquids—Structure, Dynamics and Chemical Properties*, Wiley, New York (1979).

2. Chantry, G., *Submillimetre Spectroscopy*, Academic, New York (1971).

3. Croxton, C., *Introduction to Liquid State Physics*, Wiley, New York (1975) (paperback).

4. Croxton, C. (Ed.), *Progress in Liquid Physics*, Wiley-Interscience, New York (1978).

5. Egelstaff, P. A., *An Introduction to the Liquid State*, Academic, New York (1967).

6. Kohler, F., *The Liquid State*, Verlag Chemie, Berlin (1972).

7. Kruus, P., *Liquids and Solutions, Structure and Dynamics*, Marcel Dekker, New York (1977).

8. Rowlinson, J. S., *Liquids and Liquid Mixtures*, 2nd ed., Butterworth, London (1969).

9. Stuart, H. A., *Molekulstruktur*, Springer-Verlag, Berlin (1967).

10. Ubbelohde, A. R., *The Molten State of Matter*, Wiley, New York (1979).

Review Periodicals

Molecular Relaxation Processes, Chemical Society Special Publication No. 20, The Chemical Society/Academic, New York (1966).

Birks, J. B. and Schulman, J. H. (Ed.), *Progress in Dielectrics*, Heywood & Co. Ltd., London.

Davies, M. (Ed.), *Dielectric and Related Molecular Processes*, Chemical Society (London), Specialist Periodical Report, Vols. 1–3.

National Research Council (U.S.A.), *Digest of Literature on Dielectrics*, National Academy of Sciences, U.S.A.

Orville-Thomas, W. J. (Ed.), *Advances in Molecular Relaxation and Interaction Processes*, Elsevier, Amsterdam.

Prigogine, I. and Rice, S. A. (Eds.), *Advances in Chemical Physics*, Wiley-Interscience, New York.

Chapter 5

1. Balescu, R., Lebovitz, J. L., Prigogine, I., Resibois, P., and Salsburg, Z. W., *Lectures in Statistical Physics*, Springer/Verlag, Berlin (1971).

2. Happel, J. and Brenner, H., *Low Reynolds Number Hydrodynamics*, Prentice-Hall, Englewood Cliffs, N.J. (1965).
3. Resibois, P. and de Leener, M., *Classical Kinetic Theory of Fluids*, Wiley-Interscience, New York (1977).
4. Zubarev, D. N., *Non-Equilibrium Statistical Thermodynamics*, Consultants Bureau, Plenum, New York (1975).

Chapter 7

1. Abramowitz, M. and Stegun, I. A., *Handbook of Mathematical Functions*, Dover, New York (1965).
2. Flory, P. J., *Statistical Mechanics of Chain Molecules*, Interscience, New York (1969).
3. McCrum, N. G., Read, B. E., and Williams, G., *Anelastic and Dielectric Effects in Polymeric Solids*, Wiley, New York (1967).
4. Prins, J. A. (Ed.), *Physics of Non-Crystalline Solids*, North-Holland, Amsterdam (1965).
5. Williams, G., Chem. Rev. **72**, 55 (1972); *Dielectric and Related Molecular Processes*, Chemical Society, London (1975), Vol. 2, p. 151.
6. Wong, J. and Angell, C. A., *Glass Structure by Spectroscopy*, Marcel Dekker, New York (1976).
7. Wyllie, G., Ref. 5, (1972), Vol. 1, p. 32.

Chapter 8

1. Brown, G. H. (Ed.), *Advances in Liquid Crystallography*, Academic, New York.
2. de Gennes, P. G., *The Physics of Liquid Crystals*, Oxford University Press, Oxford (1974).
3. de Vries, (Ed.,), *Molecular Crystals and Liquid Crystals*, Harper and Row, New York (periodical).
4. Emsley J. W. and Lindon, J. C., *N.M.R. Spectroscopy using Liquid Crystal Solvents*, Pergamon, New York (1975).
5. Faber, T. E. and Luckhurst, G. R., *Ann. Rep. Chem. Soc.* **72A**, 31 (1975).
6. Gray, G. W. and Windsor, P. A. (Eds.), *Liquid Crystals and Plastic Crystals*, Ellis Horwood Ltd., London (1974).
7. Johnson, J. F. and Porter, R. S. (Eds.), *Liquid Crystals and Ordered Fluids*, Plenum, New York (1970).
8. Meier, G., in *Dielectric and Related Molecular Processes*, Chemical Society, London (1975), Vol. 2, p. 183, Liquid Crystals, 5th Faraday Society Symposium (1971).

Chapter 11

1. McQuarrie, D. A., *Statistical Mechanics*, Harper and Row, New York (1975).
2. Muller, K. D. and Rothschild, W. G., *Far Infra-red Spectroscopy*, Wiley-Interscience, New York (1971).

MOLECULAR DYNAMICS

1
Statistics and Spectra

LIST OF SYMBOLS

$\hat{}$	Operator
$\cdot$	Vector dot product
$\times$	Vector cross product
$[\,]$	Poisson bracket operator
$(,)$	Inner product operator
$*$	Complex conjugate
a_n	The nth coefficient of the time series expansion of the correlation function
A	The general variate or random variable
$\hat{A}$	The quantum mechanical operator equivalent to A
$A^{(n)}$	The nth time derivative of A, assumed to exist
$\mathbf{A}$	A column matrix made up of dynamical variables, assumed linearly independent
α	The power absorption coefficient
$B(t)$	The Wiener process
β	The friction coefficient of the Langevin equation
ξ	A difference of Wiener terms
$C(t)$	The time-correlation function
$\hat{C}(t)$	The quantum-mechanical operator equivalent to $C(t)$
D	Diffusion coefficient of Einstein
δ	Dirac delta function in t
$E(X)$	Expectation value of X
$\mathbf{E}$	Electric field strength vector
ϵ''	The frequency dependent dielectric loss
ϵ'	The frequency dependent dielectric permittivity
ϵ	The complex dielectric permittivity ($\equiv \epsilon' - i\epsilon''$)
f	Measure of discrete probability, or continuous probability density
$F(x)$	Distribution function of x
$\mathbf{F}_A$	The random noise term of the projected Liouville equation for $\mathbf{A}$
Γ	A point in the phase space of positions and momenta
$\hbar$	Planck's constant
H	Hamiltonian
i	Root of minus one
I	Moment of inertia (scalar or tensor)
J	Rotational quantum number
$\mathbf{J}$	The resultant molecular angular momentum vector

k	Boltzmann's constant
κ	The torque term—$\boldsymbol{\mu} \times \mathbf{F}$
$\mathscr{L}$	The Liouville operator
m	Molecular mass
$\boldsymbol{\mu}$	The resultant molecular dipole moment vector
μ	(Scalar) mean value
N	The resultant molecular torque vector (= $\dot{\mathbf{J}}$)
$\bar{\nu}$	Wave number (in cm^{-1})
$\mathbf{p}_r$	Momentum of the rth particle
$\hat{P}$	Projection operator
P	General measure of probability
$\hat{\phi}_A$	The memory kernel of the projected Liouville equation for **A**
ϕ_n	The nth memory function
$\mathbf{q}_r$	Position of the rth particle
$\hat{Q}$	Projection operator orthogonal to $\hat{P}$ ($\equiv \hat{1} - \hat{P}$)
R	Real part of
S	Order parameter
$\sigma(X)$	[or Var(X)] The variance of X
t	Time
T	(Superscript) transpose of the vector
θ	The angle between the dipole vector $\boldsymbol{\mu}$ at time $t = 0$ and t; in general, a measure of angular displacement
u	(Scalar) a velocity component of the Wiener/Langevin equation
$\mathbf{u}$	(Vector) the dipole unit vector ($= \boldsymbol{\mu}/\lvert\boldsymbol{\mu}\rvert$)
$\mathbf{v}$	Center of mass linear velocity
V	An external potential term of the Langevin equation
ω	Angular frequency in radians per second
Ω	(Scalar) the probability sample space
$\hat{\Omega}_A$	(Operator) the resonance operator of the projected Liouville equation for the column vector **A**
$\langle x \rangle$	Mean value, ensemble or running time average of x, according to context
X	The variate, or random variable; also A and B
z	($= x - x'$) The linear displacement coordinate of the Smoluchowski equation, whose volume element is d^3z

1.1 THE PROBLEM

The dynamics and interactions of molecules in the condensed phases of matter are those of a crowd in which the individual governs and is governed by the behavior of the whole. In many ways what follows deals with this interrelation. Analytically, the problem is that of approximating the Liouville equation for the interaction and motion of bodies which have electric (and magnetic) properties. The development of fast and powerful computers provides an opportunity for simulating the motions of molecules given an analytical form for the potential energy of interaction. Methods of analysis are used in order to describe the molecular trajectories in terms of

a finite number of quantities—*averages* built up from information on the molecular scale and accessible to spectroscopic measurement. The fluid and plastic states of matter absorb and disperse radiation in the range up to 10^{12} Hz (200 or 300 cm^{-1} in the far infrared). The resulting spectral features reflect molecular motions on a temporal scale of picoseconds to that of years. A time scale of picoseconds may be associated reasonably with the dynamics of an isolated molecule (such as rotation in the gas phase); one of years can only be cooperative in molecular terms.

It may be possible soon to compute the cooperative motions of many molecules using the quantum probability laws governing the orbiting electrons. In this volume, however, the computer is used to check the indications of molecular spectroscopy obtained by means of statistical mechanics. It is inevitable that in development we often lose sight of the electrons; that is, molecules and particles become one and the same. When this is the case we cannot then be satisfied that the crudest of theories seems to work when viewed in a particular experimental light. For example, the theory of Brownian motion can be adapted for rotational motions of molecules (Section 1.6) and, following Debye (1929), can be made to describe absorptions and dispersions at the low frequency end of the 0–THz range (Fig. 1.1.1). Far infrared technological innovations have recently made it possible to extend the range of measurement to frequen-

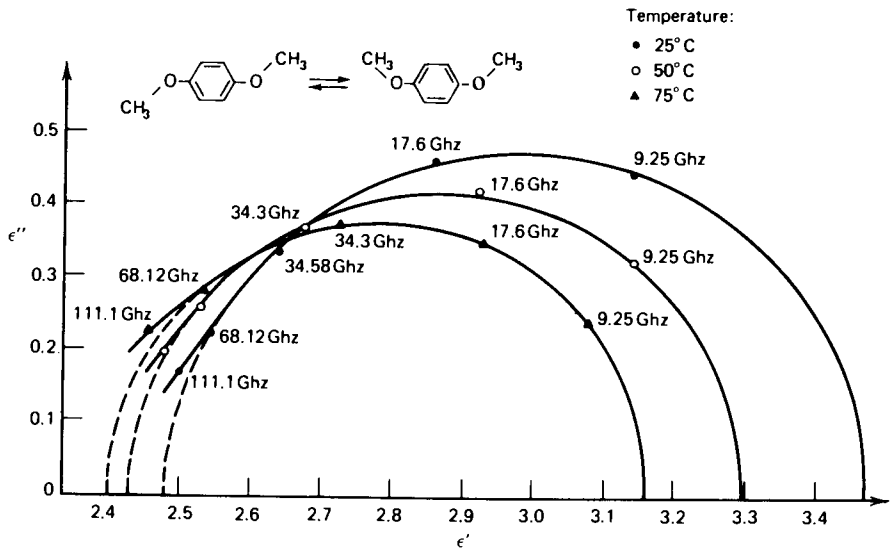

Figure 1.1.1 Plots of dielectric loss [$\epsilon''(\omega)$] against dielectric permittivity [$\epsilon'(\omega)$] for a solution of dimethoxybenzene in CCl_4 at 298, 323, and 348°K. The data fall on a semicircle, but at high frequencies (approaching those of the far infrared), there is a suspicion that the theory (solid line) is no longer adequate. [Reproduced by permission from J. Goulon et al., *Mol. Phys.*, **30**(4), 973 (1975).

cies higher than the gigahertz (microwave). It can now be seen by direct comparison with data (Fig. 1.1.2) that the Debye equations for the dielectric loss [$\epsilon''(\omega)$] and permittivity [$\epsilon'(\omega)$] can no longer be used. They imply that all dipolar liquids would be more or less opaque in the range $>10^{12}$ Hz, including, of course, the visible. There are different ways of explaining why this should be so, which is part of the purpose of what follows.

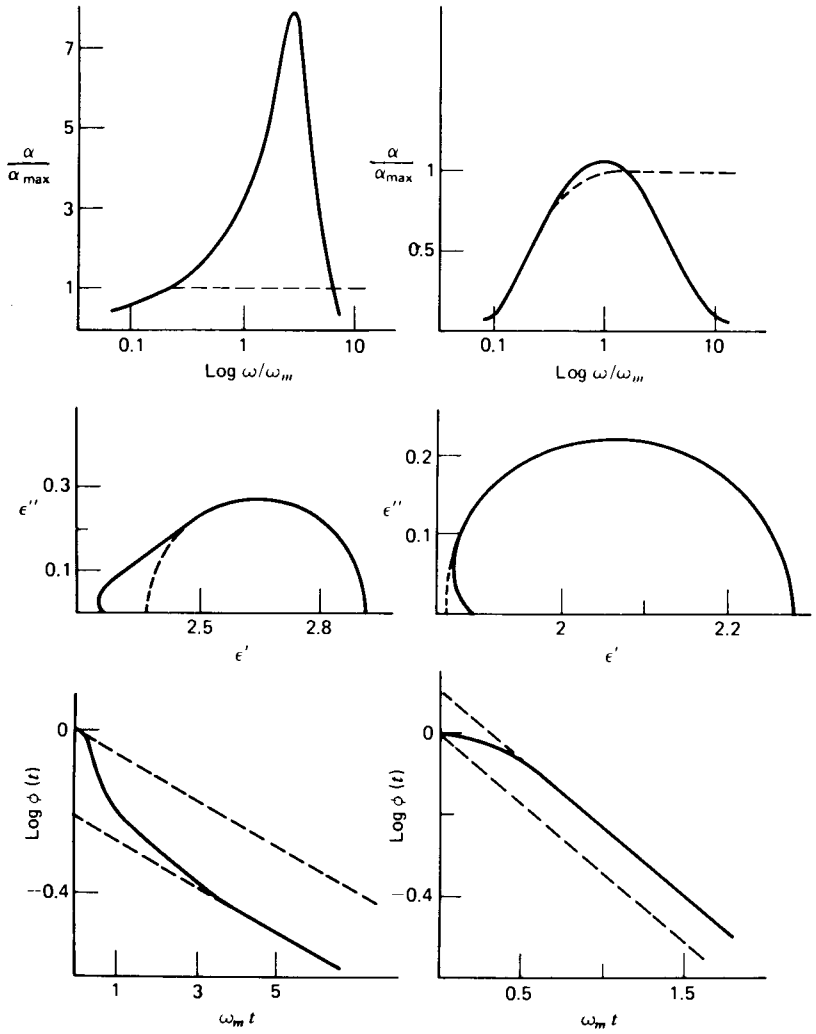

Figure 1.1.2 The suspicion arising from Figure 1.1.1 is confirmed by adequate frequency coverage, as in this composite diagram by Desplanques. Left, a solution of CH_3CN in CCl_4, 5% mole fraction; and right, 20% mole fraction $(CH_3)_3CCl$ in hexane at 298°K. The dashed curves are from the Debye theory of rotational diffusion. α = power absorption coefficient (Np/cm); $\phi(t)$ = orientational correlation function; ω = frequency (rad/sec); t = time. (Reproduced by permission from P. Desplanques, thèse d'État, Univ. of Lille, 1973, p. 45.)

At the outset, we emphasize that a wide range of data (from different techniques) is needed to disprove a hypothesis. A theory cannot be proved. It is not meaningful therefore to overuse adjustable parameters to marry fancy and fact. It is better to examine the source of disagreement. Unfortunately this is an adage with which for purely practical reasons we sometimes fail to comply. In summary, we seek to do the following:

1. To describe statistically the interaction and motion of molecules on the microscopic scale.
2. To interpret spectral data in terms of these dynamics, and to use the information to disprove and "improve" the theoretical hypotheses.
3. To make use of computing power to provide exact trajectories (and thereby averages) of molecules (and molecular properties) using known potential forms in the Newton equations of motion.

In each chapter we hope to explain, whenever possible, how these three aspects interact in the progress toward solution.

1.2 SOLUTIONS

It is not self-evident that there exists a solution that does not invite more questioning. It is not yet possible or desirable to describe 1 ml of liquid in terms of the trajectory of each molecule from $t = 0$ to the present time. We use instead the ideas of thermodynamics and statistical mechanics. Chapters 2 and 3 are devoted to the difference between the statistics of particles and the statistics of molecules, respectively. In other words, the potential energy in a molecular ensemble is modified considerably by electrodynamic interactions (Chapter 3), which may be expressed as the motion of multipoles. This influence has recently been investigated directly by computer simulation (Fig. 1.2.1). In some cases the electrodynamic effect is obvious without recourse to any kind of calculating machine. A mole of liquid benzene mixed with a mole of liquid hexafluorobenzene at room temperature immediately produces solidification owing to an exceptionally strong quadrupolar interaction.

An adequate solution to the problem of condensed phase molecular dynamics must therefore be concerned with electrodynamics as well as with mechanics. This is true on the microscopic scale and particularly so when dealing with the relation between what is measured in 0–THz spectroscopy and what the theories and computer simulators are able to supply. Whenever a solution describing the ensemble dynamic situation is found at the microscopic level, the relation of the measuring field to the displaced field in the dielectric medium must also be predictable before the macroscopic spectral band shapes can be calculated. The most we can

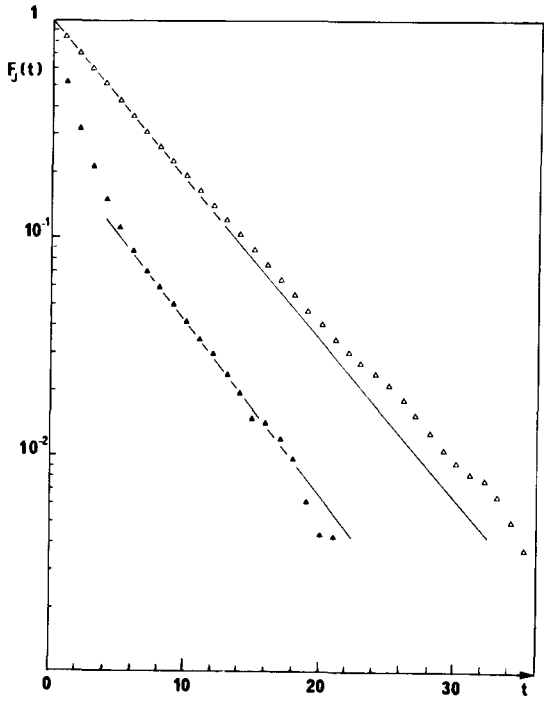

Figure 1.2.1 A computer simulation by Brot and co-workers of the angular velocity autocorrelation function of ▲, a diatomic molecule represented by a type of Lennard–Jones intermolecular potential (with both an attractive and repulsive part); △ a purely repulsive potential. The straight lines represent an exponential decay (Debye's theory). At short times (far infrared frequencies) this is adequate for △ but not for ▲, whose collisions are not elastic. At very long times Debye's theory fails because it does not take account of the vortex effects set up by the rotating molecule. [Reproduced by permission from C. Brot et al., *Mol. Phys.*, **34**, 1295 (1977).]

hope from this problem of the internal field is an approximate solution for $\epsilon(\omega)$ based on some self-consistent technique such as molecular dynamics simulation, or by incisive analysis of set problems, such as that of the translationally invariant lattice of interacting dipoles. There are some cases (such as that of water) where dipole-dipole coupling is very strong, but only one macroscopic relaxation time *seems* to appear. This suggests that in such cases the concept of "microscopic relaxation time" is meaningless, and that we are dealing with a cooperative process involving many molecules. Figure 1.2.2 illustrates the great difference between the loss curve of pure liquid water and that of its individual molecules freed from hydrogen bonding, studied recently in the far infrared. The hydrogen bonding in this example is of course an extreme example of dipole electrodynamic influences on the system Hamiltonian.

Solutions of problems 1–3 listed above must be general enough to

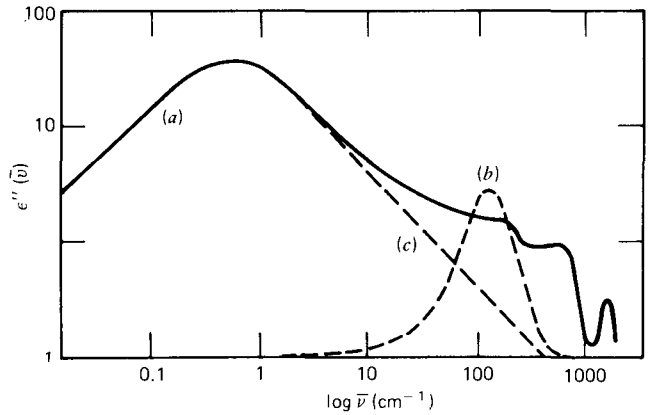

Figure 1.2.2 Plots of dielectric loss for (*a*) pure liquid water and (*b*) 0.01% (w/w) water in carbon tetrachloride, at room temperature and pressure. (*c*) Extrapolation of Debye's Theory to higher frequencies.

encompass the known spectral features (such as those in Fig. 1.2.3) at the extremes of the existence of the liquid phase. In particular, the most characteristic feature of the power absorption coefficient [$\alpha(\omega)$ in Np/cm] in the far infrared region is the movement of the peak absorption frequency. Figure 1.2.3 illustrates this feature for chloroform along the gas–liquid coexistence curve. As we shall see in Chapter 3 this is an incisive and convenient method for probing the deficiencies of some molecular dynamical models. (A dynamic model is an approximate solution of the classical or quantum equations of motion.) Figure 1.2.3 is a spectral representation of gradual inhibition of molecular rotation and interruption of free translation as the liquid state is approached, leading to an interaction and coupling between these freedoms.

At this point it is convenient to sketch out a justification for the use throughout this volume of classical equations in the analysis and simulation of small molecules such as water and nitrogen. In some cases their use seems clearly inadequate, because the remnants of the free rotor quantum lines are observable in the liquid phase (Fig. 1.2.4). The use of classical theory implies that the incoherent motion of individual molecules can be described by constructing a wave packet (Atkins, 1978) with mean energy and width sufficiently large compared with the quantum mechanical spacings of the rotational energy levels. For HCl and H_2O, it may be shown that

$$\left|\frac{\mu E}{\epsilon_J}\right| \doteqdot \frac{100}{J(J+1)} \qquad \left|\frac{\mu E}{\Delta_J}\right| \doteqdot \left(\frac{50}{J+1}\right) \tag{1.2.1}$$

Here ϵ_J and Δ_J are the energy and spacing of a free rotator, and J is the rotational quantum number. μE is the interaction energy between the

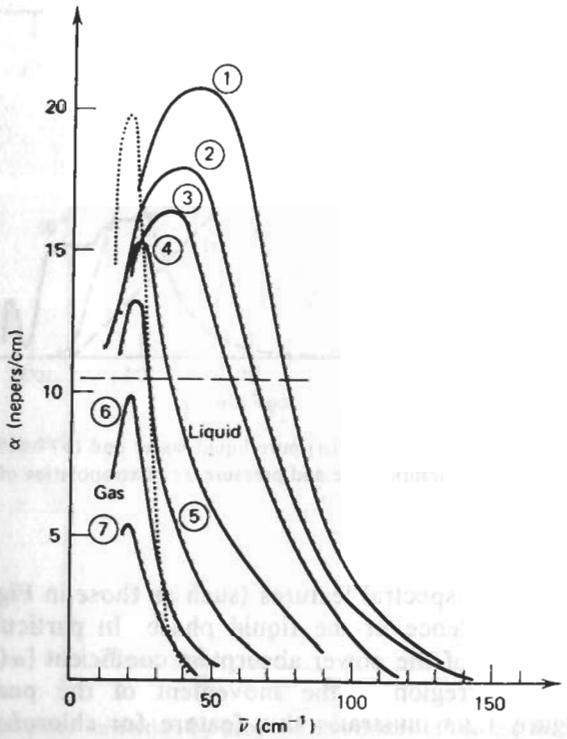

Figure 1.2.3 Far infrared spectra of $CHCl_3$. (1–5) liquid; (6, 7) gas. The dotted line represents the free rotator absorption at 534°K. The dashed line represents the "Debye plateau" at 300°K. [Reproduced by permission from A. Gerschel et al., *Mol. Phys.*, **23**, 317 (1972).]

molecule and the collective polarization field in a sample of dielectric. Equation 1.2.1 shows that a wave packet made up from rotator states would exhibit a large occupation over many levels (since $|\mu E/\epsilon_J|$ and $|\mu E/\Delta_J|$ are significant for large J). This partly justifies a classical description of liquid HCl and liquid H_2O, but the fact remains that the far infrared $\Delta_J = 1$ transitions are observable in liquid solutions of HCl. Either the classical Liouville equation must be replaced by a stochastic equation (Chapters 9 and 10) or some quantum character must be incorporated into the classical equations of statistical mechanics. This is discussed further in Chapters 9–11.

At the other extreme the transition of liquid to crystalline solid means that the specimen becomes more capable of supporting collective behavior which shows up in spectral terms as collective modes in the far infrared. These are related to the liquid phase "plasmons" (Chapter 3) in the same kind of way that a shear wave in the liquid would give way to a transverse phonon mode in the solid. Each is synthesized from the coherent motion of a very large number of molecules, and its frequency of maximum ab-

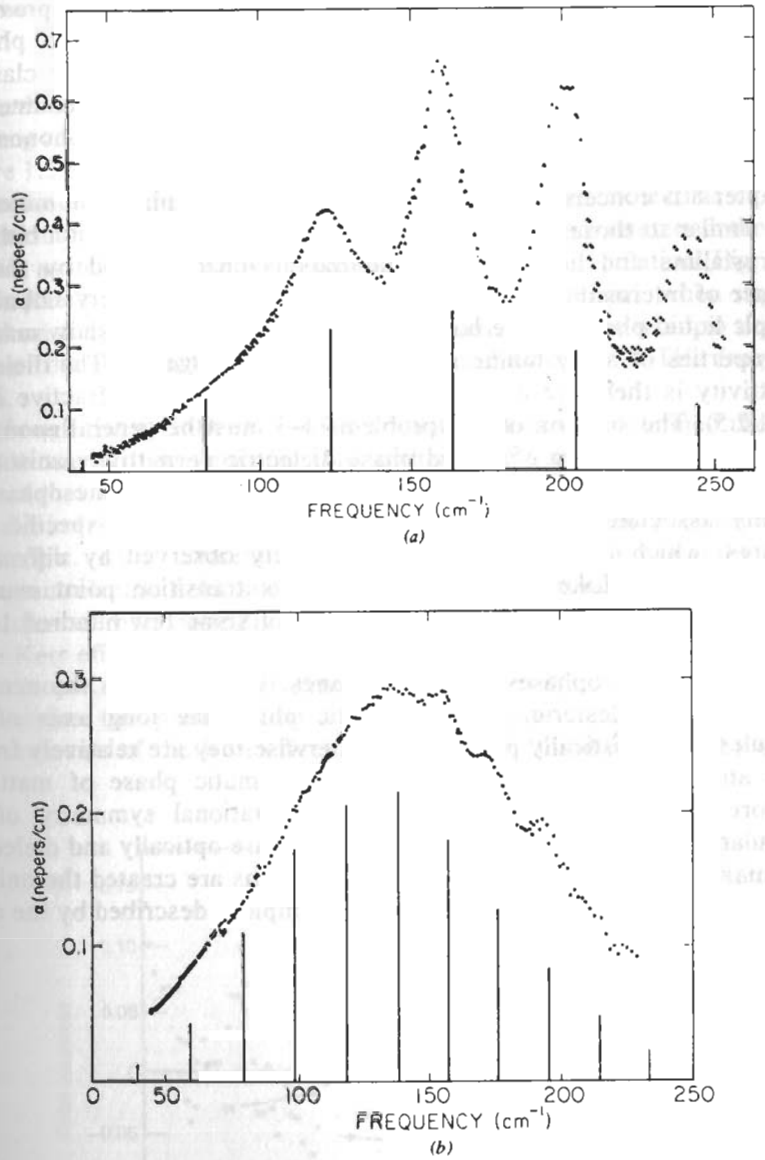

Figure 1.2.4 (*a*) Absorption of HF dissolved in *liquid* SF_6 at 273°K. The bars represent the frequency and relative intensity (Maxwell–Boltzmann) of the "pure rotational" quantum lines in the gas. [Reproduced by permission from G. Birnbaum, *Mol. Phys.*, **25**, 241 (1973).] Note that the broadening on the *low frequency* side is more significant. (*b*) Absorption of NH_3 in liquid SF_6 at 273°K.

sorption can be calculated classically. Sound waves in a crystal provide a simple example. Once a dynamic matrix is constructed, the phonon frequencies and polarization vectors are obtained by a strictly classical calculation. Quantum effects are entirely statistical, and are accounted for by use of the Planck function for the thermal equilibrium phonon distribution.

Chapter 8 is concerned with the description of mesophases in molecular terms similar to those used in the isotropic liquid. The transition between the crystalline and liquid crystal materials is characterized by the appearance of intermediate states or mesophases between the crystalline and isotropic liquid phase. These have an ordered structure and show many of the properties of a crystalline solid, such as birefringence. The dielectric permittivity is therefore a tensor quantity and so is the refractive index (Fig. 1.2.5). The solution of our problems 1–3 must be general enough to allow for the formation of a fluid phase dielectric permittivity anisotropy using only intermolecular potential forms. The existence of mesophases is normally associated with well-defined energy changes at specific temperatures, which in most cases can be readily observed by differential thermal analysis. Like the melting point, this transition point marks a first-order phase transition with a latent heat of some few hundred Joules per mole.

Well-defined mesophases exist (de Gennes, 1974), such as the nematic, smectic, and cholesteric. In the nematic phase the long axes of the molecules are statistically parallel, but otherwise they are relatively free to rotate and translate. The viscosity of the nematic phase of matter is therefore fairly low. It follows from the rotational symmetry of the molecular ordering that nematic liquid crystals are optically and dielectrically uniaxial. In practice, unless special conditions are created the uniform orientation along the symmetry axis of the sample is described by the order

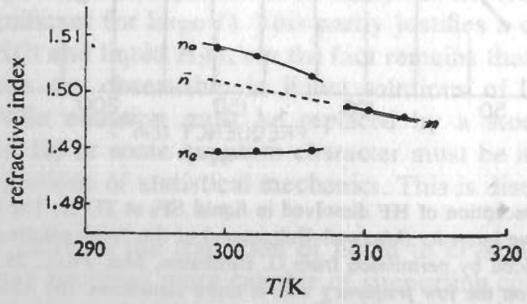

Figure 1.2.5 Variation of the refractive index (D line) of cholesteryl oleyl carbonate with temperature in the cholesteric and isotropic liquid phases. n_o and n_e are the refractive indexes of the ordinary and extraordinary rays, n the mean refractive index, and $\bar{n}$ that of the isotropic phase. [Reproduced by permission from M. Evans et al., *J. Chem. Soc. Faraday Trans. II*, 71, 1854 (1975).]

parameter S, defined by

$$S = \tfrac{1}{2}\langle 3\cos^2\theta - 1\rangle$$

where the brackets denote a time or space average and θ is the angle between the long molecular axis and the preferred, or symmetry (or director) axis. Figure 1.2.6 shows that on average S is very small in a computer simulation, for instance, of a C_{3v} triatomic. $S = 1$ means that all molecular axes are parallel to the symmetry axis. Nematic liquids have S parameters in the range 0.4–0.7, as indeed do lathlike potentials in a computer simulation (Fig. 1.2.7). In Chapter 8 we see that a strong intermolecular potential, when superimposed on the usual isotropic phase Hamiltonian, may be used to describe some of the spectral features of the nematic phase in the 0–THz frequency range.

Although the nematic → isotropic transition seems well-defined there are delicate ways of investigating this further. One such is by making use of the fact that under a voltage gradient a dielectric (or insulator) develops an optical birefringence. Molecules are polarizable, and their polarizability is anisotropic. As a consequence they have a preferred orientation in a permanent electric field, and it is this that makes the medium of which the molecules are part optically anisotropic. The induced optical birefringence is the Kerr effect, which in the nematic phase is enormously greater than in the isotropic. Our molecular dynamics theories and solutions must be able to describe the pretransition effects which are clearly discernible by measurements of the Kerr effect in the isotropic liquid removed by quite a

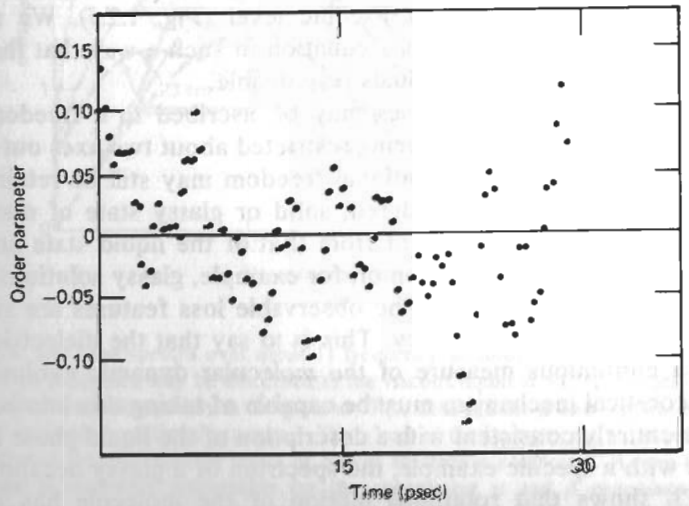

Figure 1.2.6 The rotational order parameter in a molecular dynamics simulation by the authors of a triatomic molecule with an included angle of 60° (C_{2v} symmetry). Note that the mean over many time steps is close to zero.

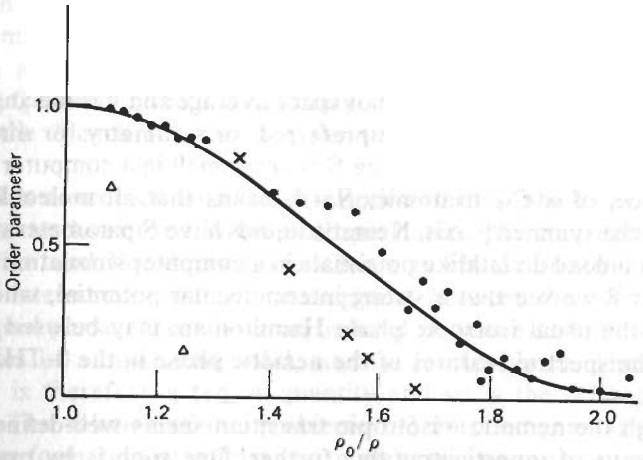

Figure 1.2.7 The variation of the rotational order parameter with density for highly elongated molecules; a molecular dynamics simulation produces the results × and △. The dots are from a Monte Carlo study in two dimensions of the equation of state of ellipses of axial ratio 6. [Reproduced by permission from J. Kushick and B. J. Berne, *J. Chem. Phys.*, **64**, 1362 (1976).]

few degrees from the visible transition temperature. These pretransition effects provide one of the elegant experimental challenges embodied in our problems 1–3. In the isotropic phase there is no long-range order in the alignment of the molecules, but at short range there is, persisting over the *characteristic coherence length*. What the Kerr effect indicates is that this starts to become dramatically longer *well before* the sample develops a tensor permittivity on the macroscopic level (Fig. 1.2.5). We must approximate the stochastic Liouville equation in such a way that the rush to conform is traced to the individuals responsible.

The fluidity of the mesophases may be ascribed to a freedom of the molecular translation, rotation being restricted about two axes out of three. However, when this is lost rotational freedom may still be retained. This corresponds to a plastic, disordered, solid or glassy state of matter. The viscosity is dramatically different from that of the liquid state and this is mirrored in the 0–THz absorption of, for example, glassy solutions of small dipolar molecules (Fig. 1.2.8). The observable loss features are significant over many *decades* of frequency. This is to say that the dielectric permittivity is a continuous measure of the molecular dynamic evolution. Any viable theoretical mechanism must be capable of taking this into account in a manner entirely consistent with a description of the liquid phase itself. To illustrate with a specific example, the spectrum of a glassy decalin solution of CH_2Cl_2 shows that rotational motion of the molecule has not been stopped by the highly viscous environment (Chapter 7). At frequencies in the kilohertz range there is a broad maximum in the loss which moves rapidly to higher frequencies as the temperature of the glass is raised. As

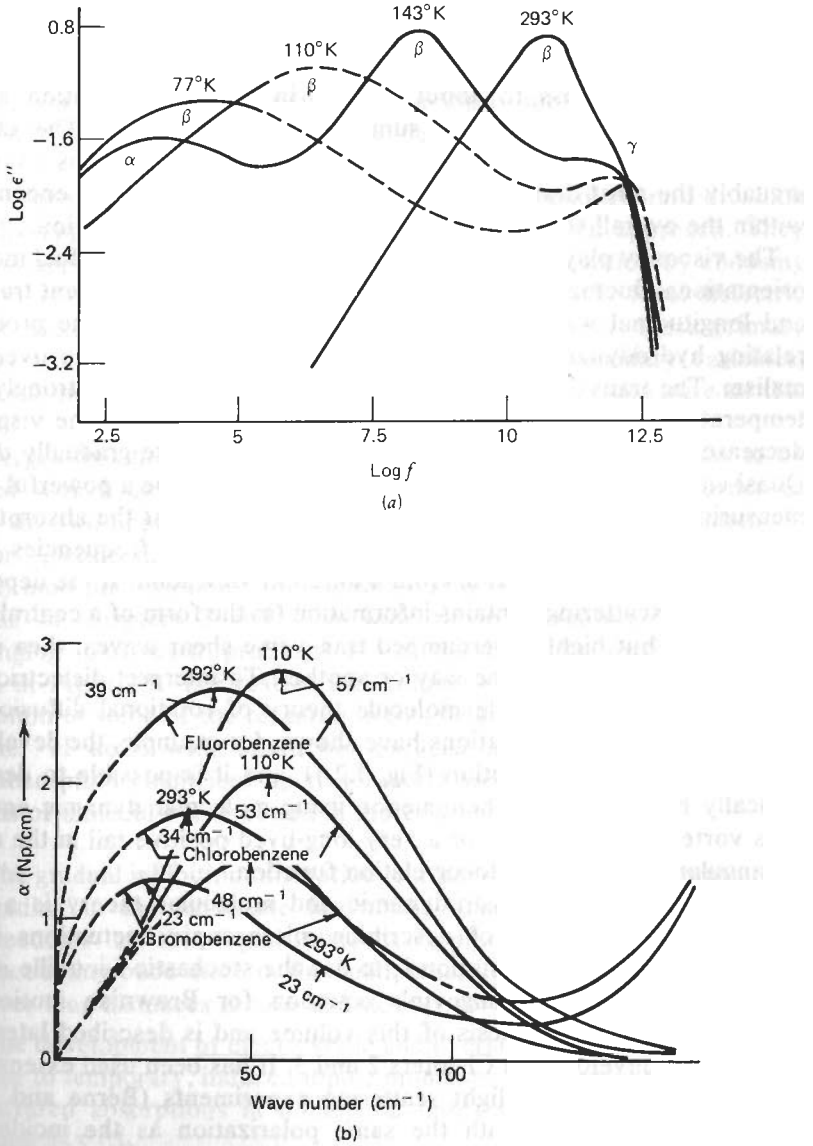

Figure 1.2.8 (*a*) Loss spectra over about 11 frequency decades of 10% v/v fluorobenzene in decalin. Three processes may be discerned in the viscous liquid at 143°K, labeled α, β, and γ. The first shifts to zero frequency in the glass at 77°K, although the β and γ peaks evidence the survival of molecular rotational processes. The γ part of the loss process is that observable in the far infrared (*b*), this time in terms of power absorption coefficient. A long-lived vortex phenomenon is obviously responsible for the cooperative α and β processes, which are rototranslational in origin. (Reproduced by permission from C. J. Reid, Thesis, University of Wales, 1979.)

the glass gives way to the liquid there is a sudden shift to gigahertz frequencies (microwave). In the far infrared a secondary loss feature appears which shifts downwards in frequency at the same time from about $116\,cm^{-1}$ in the glass to about $50\,cm^{-1}$ in the liquid solution at room temperature. The spectra are summarized in Fig. 1.2.8. The effect of viscosity on the molecular dynamics (or vice versa) in this example is arguably the most dramatic of all the variables, and must be encompassed within the overall solution of the molecular equations of motion.

The viscosity plays a significant role in the ability of individual molecular orientational fluctuations to give rise to long range and coherent transverse and longitudinal waves in the fluid state. This embodies the problem of relating hydrodynamic and molecular description within one overall formalism. The transverse (or shearing) waves are propagated strongly at low temperatures in supercooled (very viscous) liquids, but as the viscosity is decreased they become progressively "softer" and are gradually diffused. Quasi-elastic depolarized light scattering is known to be a powerful tool for measuring these phenomena. It is less well-known that the absorption and dispersion of electromagnetic waves up to terahertz frequencies provide the same type of information from a different viewpoint. If the depolarized line of light scattering contains information (in the form of a central dip) on propagative but highly overdamped transverse shear waves, then so must 0–THz spectroscopy in one way or another. To interpret dielectric results in terms of Debye's single molecule theory of rotational diffusion is no longer satisfactory. Simulations have shown, for example, the development of a long-lived vortex motion (Fig. 1.2.1), and it is possible to describe a typically hydrodynamic phenomenon using molecular dynamic equations. This vortex is responsible for a very long-lived positive tail in the molecular angular momentum autocorrelation function.

The interrelation of hydrodynamic and molecular theory is a central problem similar to that of describing microscopic fluctuations in thermodynamic terms. One solution is to use the stochastic Liouville equation in a form similar to Langevin's equation for Brownian motion. This derivation is a central thesis of this volume and is described later in this chapter and developed in Chapters 2 and 3. It has been used extensively to describe the results of light scattering experiments (Berne and Pecora, 1976). Light scattered with the same polarization as the incident light contains information about isotropic or coherent fluctuations which are hydrodynamic in nature, whereas depolarized scattering contains information about anisotropic fluctuations arising from molecular reorientations. It is essential to investigate the interrelation between the two kinds of information. As we see in Chapters 5–7, this is closely connected with the problem of describing the mutual and subtle effects of rotation and translation on the molecular scale.

To take one specific example of the nature of the problem it is possible to describe the central dip observed in a spectrum of scattered and depolarized light in hydrodynamic and molecular terms.

Hydrodynamically, the viscoelastic theory, for example, assumes a priori the existence of a frequency-dependent shear modulus which couples the stress and strain tensors. Fluctuations in the strain tensor produce light scattering via a photoelastic coefficient. The dip is implied by a modulation of the strain tensor produced by the damped shear (and longitudinal) waves.

Molecularly, a great number of theories have been proposed which outwardly appear quite different, but are very similar in approach. They consist in approximating the "generalized" Langevin equation by choosing one (or more) "primary" variables which are coupled to the local dielectric constant. Generally an orientation or polarizability tensor, these primary variables are allowed to interact with one or more secondary variables, generally a momentum density tensor, within the overall structure of this equation.

It emerges that the relaxation time of the shear strain tensor has to be identified with a correlation time for molecular orientation in order to identify the two approaches. This is discussed in Chapter 7. The methods used for relating macroscopic and microscopic (the collective and individual) molecular motions, the "macro-micro correlation" theorems, are discussed in Chapters 3 and 8. A wide range of features, demanding wide-ranging solutions to problems 1–3 of the preceding section are summarized in Fig. 1.2.9. The rest of this volume is designed as a guide and introduction to some of the research in this field.

Chapter 11 deals with *interaction-induced* absorption. The loss and power absorption coefficient up to terahertz frequencies may be used as measures of molecular interaction in more than one sense:

1. The gradual inhibition of rotation and interruption of free translation, leading to the inevitable interaction and coupling between these freedoms as the liquid state is approached. Their subsequent decoupling once more in the solid, where center of mass translation over long distances is rare and slow.
2. The development of electrostatic and overlap interactions which give rise to temporary, induced dipole moments, and thus to rotational far infrared absorptions in nondipolar gases such as N_2 and solvents such as CCl_4.

In Chapter 11 we introduce this second aspect, both the experimental and theoretical techniques, and show how they may be used to gain information on the analytical form of the intermolecular potential and on the molecular dynamics. Figure 1.2.10 is an example of how the the induced far infrared spectrum of a few hundred N_2 molecules, nondipolar but quadrupolar, may be simulated by computer given a particular form for the intermolecular potential, which must be capable of accounting for the *molecular polarizability*. This again emphasizes the difference between real molecules and particles such as hard spheres, where the potential is purely repulsive,

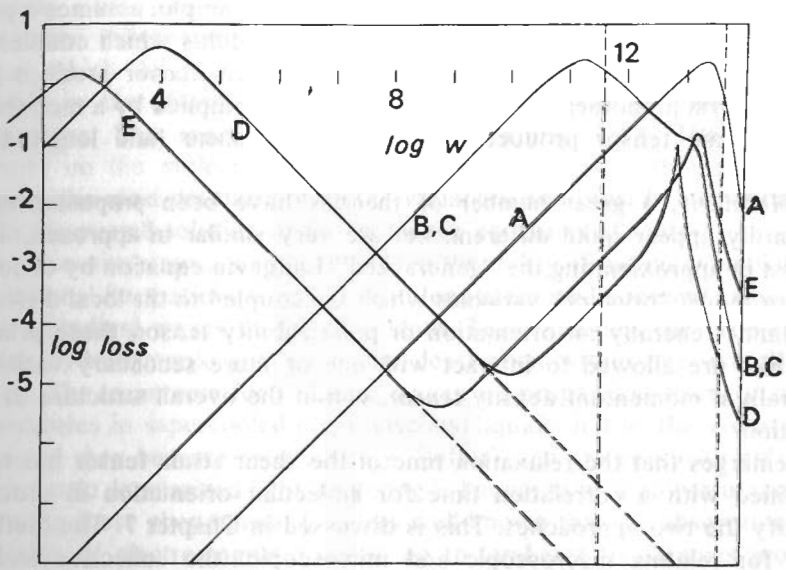

Figure 1.2.9 Composite schematic of the major loss features observable in some condensed phases of matter. (*A*) Water free from hydrogen bonding (in dilute solution); gas-like rototranslation in the liquid state. (*B, C*) Liquids such as benzonitrile and plastic crystals such as $(CH_3)_3CCl$ where the far infrared part of the loss is resolved on the *high frequency* side of the Debye curve. (*D*) Mesophase, such as the nematic, in this unoriented. The far infrared part of the loss is considerably sharper than in cases *B* and *C* and well separated on the frequency scale. (*E*) Glasses, such as those of Fig. 1.2.8.

with no electrostatic embellishment. The nondipolar N_2 molecule absorbs in the far infrared because intermolecular electrostatic fields distort the overall symmetry of a given molecule's electron cloud, producing upon "collision" a small dipole moment that changes in magnitude and direction rapidly with time. Thus compressed gaseous mixtures of rare gas atoms absorb in the far infrared, whereas the components when separated and moderately pressurized do not. A pair of colliding helium atoms, for example, do not possess a resultant electronic cloud of dipolar symmetry, whereas a helium-neon pair modulate the electromagnetic field over a broad band of far infrared frequencies commensurate with the most probable frequencies at which interatomic collisions occur. Atomic-induced absorption is purely translational in origin, a mechanism which therefore also persists in molecular fluids such as hydrogen and nitrogen as an absorption corresponding to no rotational energy change: that is, $\Delta J = 0$. A dipole moment set up between a pair of colliding molecules additionally absorbs by rotational means since, even without relative translation of molecular centers, the effects on each other of their rotatory electrostatic fields (expanded as multipole moments) do not cancel. A practical means of dealing with these intermolecular absorption mechanisms is to treat them separately. The rotational absorption is dealt with by expanding the field in

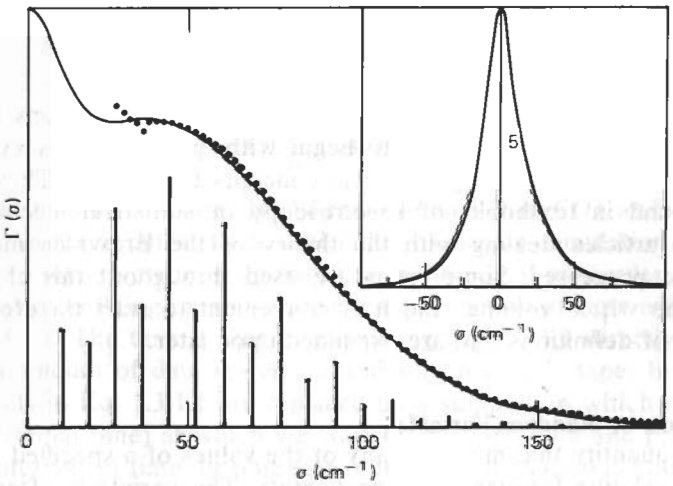

Figure 1.2.10 Computer simulation of the *induced* far infrared absorption of compressed nitrogen gas (124°K). Experiment (points) and reconstruction (solid line) with the help of a molecular dynamics simulation of the mean square torque. The vertical bars indicate the position and intensity of *quadrupolar-induced* rotational transitional. The zero-frequency contribution is *translational* in origin. [Reproduced by permission from U. Buontempo, S. Cunsolo, and G. Jacucci, *J. Chem. Phys.*, **59**, 3750 (1973).]

terms of multipole tensors, which all vanish in the case of spherical symmetry such as that of atoms. The consequences of this are explored for the compressed gas phase in Chapter 11, where we also extend our range to the liquid and plastic crystalline states of nondipolar molecules. What, for example, happens to interaction-induced absorption as the nondipolar gas is compressed into the liquid, which may subsequently be frozen or compressed into a solid state? Spectra in the 0–THz frequency range are sensitive to the molecular details of how a gas becomes liquefied and subsequently solidifies. The collision-induced absorption per molecule decreases as the sample is condensed, a sensitive indication of the change from two-body to multibody interaction and dynamics. Neutron scattering experiments on molecules of T_d symmetry in the liquid state have shown in a complementary fashion that the dynamics in the liquid proceed in a cogwheel fashion, so that translation and rotation are mutually effective to a greater extent than in either the gas or rotator phase solid. In a molecular crystal the collision-induced absorption should disappear because of the symmetry of packing, but any disturbance of this symmetry results in a broad 0–THz absorption band if the molecules are possessed of any degree of vestigial rotational freedom. Induced absorption in such solids is therefore useful as a probe into the rotational disorder of nondipolar molecules and semistochastic simulations by computer form a useful complement. Chapter 12 closes with a discussion of the possibilities in these fields of endeavor, at present very much open and unexplored.

1.3 GLOSSARY OF STATISTICAL CONCEPTS AND EQUATIONS OF MOTION

Before proceeding to the statistical description of the motions and interactions of many molecules, or to begin with, particles, it is *essential* to know about the underlying statistical concepts themselves. These are not easily found in textbooks of spectroscopy or statistical mechanics, but rather in articles dealing with the theory of the Brownian motion and stochastic processes. Some terms are used throughout this chapter and indeed the whole volume, and it is convenient to start therefore with a short list of definitions that are expanded upon later.

The Variate or Random Variable

This is a quantity that may take any of the values of a specified set with a specified relative frequency, or *probability*. The variate is often called a random variable. This could be a vector molecular property such as center of mass velocity, angular momentum, or dipole orientation, or a tensor such as the polarizability. It is regarded as defined not only by a set of permissible values such as an ordinary mathematical variable, but by an associated *probability function* expressing how often these values appear in the situation under discussion.

Stochastic Process

A stochastic variable is one in which at least one of the elements is a variate, and a stochastic process is one wherein the system incorporates an element of randomness as opposed to a determinate system.

Correlation

In general, correlation is the interdependence between quantitative or qualitative data. In a narrower sense, it is a relationship between measurable variates.

Autocorrelation Function

This function is the internal correlation between a number or series of observations (μ) in time or space. The normalized autocorrelation of a stochastic process is defined by

$$\rho(\tau) = \lim_{T\to\infty} \left\{ \frac{1}{T} \int_{-T/2}^{T/2} \mu(t)\mu(t+\tau)\, dt \Big/ \int_{-T/2}^{T/2} \mu^2(t)\, dt \right. \qquad (1.3.1.1)$$

for a series with zero mean and range $-T/2 < t < T/2$, defined at each point in time. The numerator in the equation is called the *autocovariance* and the denominator the *variance*. The limits $-T/2$ and $T/2$ may be infinite, subject to the existence of the integrals or sums involved.

The Spectral Function

If $C(t)$ is a time autocorrelation function of a stochastic process, then it is expressible in the form (the Wiener–Khinchin theorem)

$$C(t) = \int_0^\infty \cos \omega t\, dF(\omega) \qquad (1.3.1.2)$$

$F(\omega)$ is a spectral function. N. Wiener showed that $C(t)$ and $F(\omega)$ are Fourier transform pairs. In a molecular dynamics simulation (using a computer to solve Newton's equations for hundreds of molecules at a time) the process of building up an autocorrelation function of time is illustrated in Fig. 1.3.1.1. The task is that of evaluating Eq. 1.3.1.1 directly from an enormous amount of data stored on a disk or magnetic tape. In practice, the integrals in Eq. 1.3.1.1 are replaced by a summation which runs from the point (initial time) at which we start to store the data and proceeds at discrete intervals of time (or time steps) until the simulation is finished. The total time may be in the region 10^{-10} sec, some thousands of steps. At each time step, information must be averaged for a sample of a few hundred molecules, which explains the double summation of Fig. 1.3.1.1. The relation illustrated schematically in Eq. 1.3.1.1 provides a direct link between the motions of individual molecules and spectral functions such as the 0–THz power absorption coefficient or dielectric loss. The task of analytical theory, in contrast to a simulation, is to attempt to describe the spectral function in terms of a very few thermodynamic equilibrium

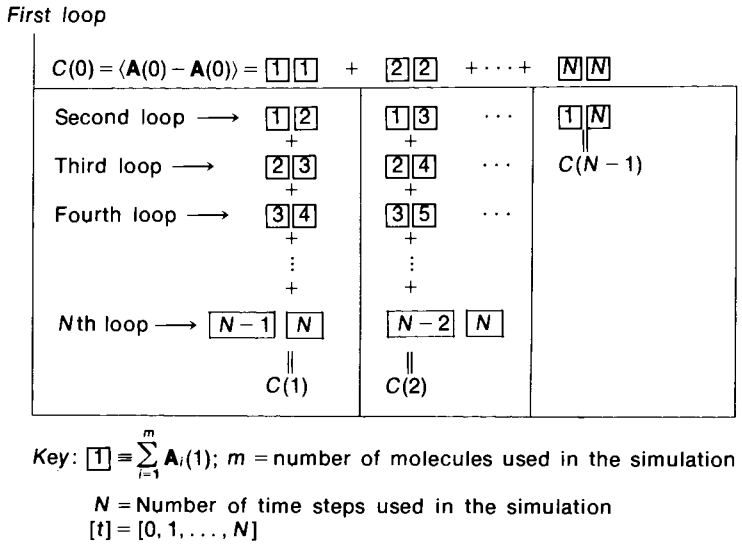

Figure 1.3.1.1 Construction by computer of a correlation function of the dynamical variable **A**(*t*).

averages or phenomenological variables. To do this we use hypotheses other than Newton's equations.

Markov's Hypothesis

Only the last state occupied by a process is relevant in determining its future behavior. If the probability (q) that each state will be occupied after the $(n+1)$th transition, given the entire trajectory or history of state occupancies through time n, is

$$q[s(n+1)=j \mid s(n)=i, s(n-1)=k, \ldots, s(0)=m] \qquad (1.3.1.3)$$

where $s(n)$ is the state at time n, then Markov's assumption reduces this to

$$q[s(n+1)=j \mid s(n)=i] \qquad (1.3.1.4)$$

That is, the probability of making a transition to each state of the process depends only on its present state. *If a process is non-Markovian, the history of the system before the last state occupied influences future behavior.*

Doob's Theorem

This is a rigorous mathematical relation defining the autocorrelation function (a.c.f.) of a Markovian statistical process. With some loss of rigor we can say that the a.c.f. of a Markov process decays exponentially to zero as time evolves from $t=0$. If we are to concern ourselves with the dynamic evolution of atoms and molecules, then Fig. 1.3.1.2, from a simulation of liquid nitrogen, and Fig. 1.3.1.3, derived from 0–THz spectroscopy, illustrate that we must ultimately aim at describing *non-Markovian* processes. However, we could hardly describe non-Markovian processes without first knowing something about the use of Markov's hypothesis in, for example, the classical theory of the Brownian motion.

Stationary Process or Stationarity

The point at which one starts the exercise of correlating a property X at $t=t$ and X at $t=t'$ is of no consequence. Doob's theorem applies to this type of process. In building up an a.c.f. in a simulation it is assumed that if the data on magnetic tape are statistically stationary, then, if we can construct the autocovariance of a property X (e.g., the velocity of each molecule) at time steps t and t',

$$C_{XX}(t)=\langle [X(t)-\langle X(t')\rangle][X(t+t')-\langle X(t+t')\rangle]\rangle \qquad (1.3.1.5)$$

this should be the same whenever we choose to start the process illustrated in Fig. 1.3.1.1. In Eq. 1.3.1.5 we have introduced the angular brackets $\langle\,\rangle$ to denote the averaging process. Often the symbol $\langle\,\rangle_0$ is used to denote averaging at thermodynamic equilibrium.

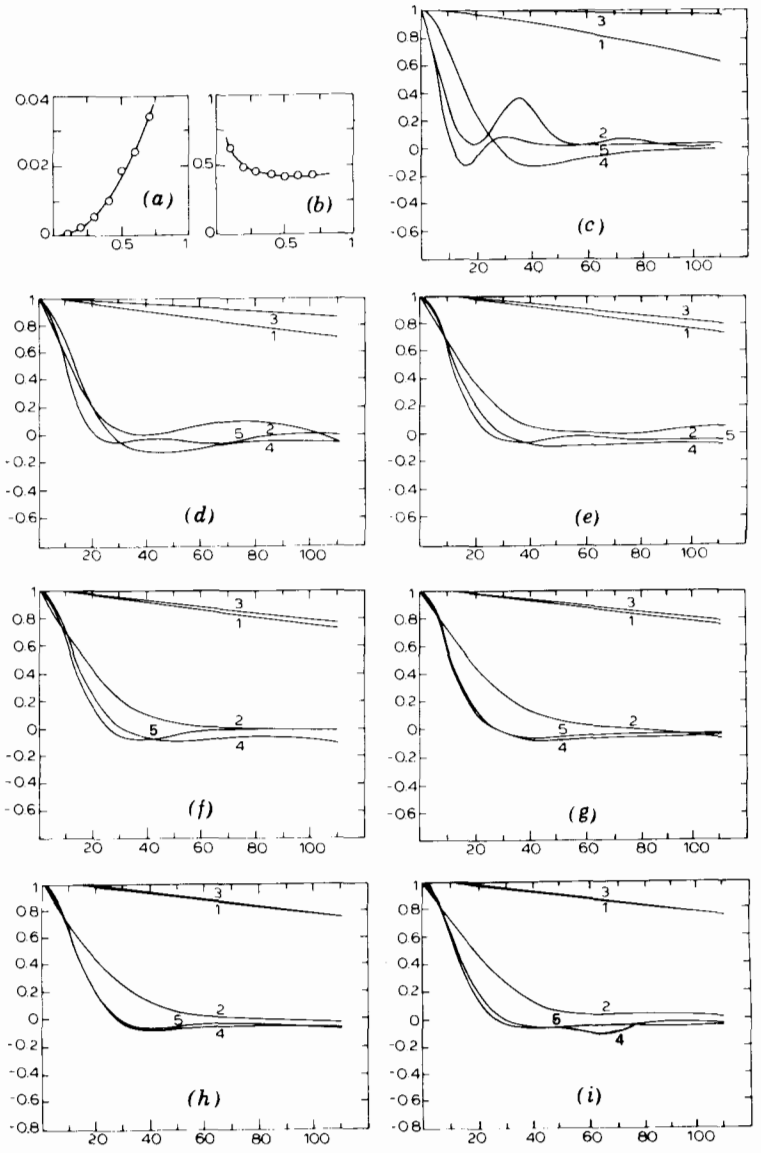

Figure 1.3.1.2 Molecular dynamics simulation of some a.c.f.'s for a diatomic of varying bond length. Variation with bond length of (*a*) mean square torque and (*b*) mean square force. (*c–i*) Time a.c.f.'s with *decreasing* bond length: (1) velocity; (2) orientation; (3) angular velocity; (4) force; (5) torque. Abscissae: (*a*), (*b*) bond length; (*c*) to (*i*) time steps. [Reproduced by permission from M. Evans et al., *Adv. Mol. Rel. Int. Proc.*, **11**, 295 (1977).]

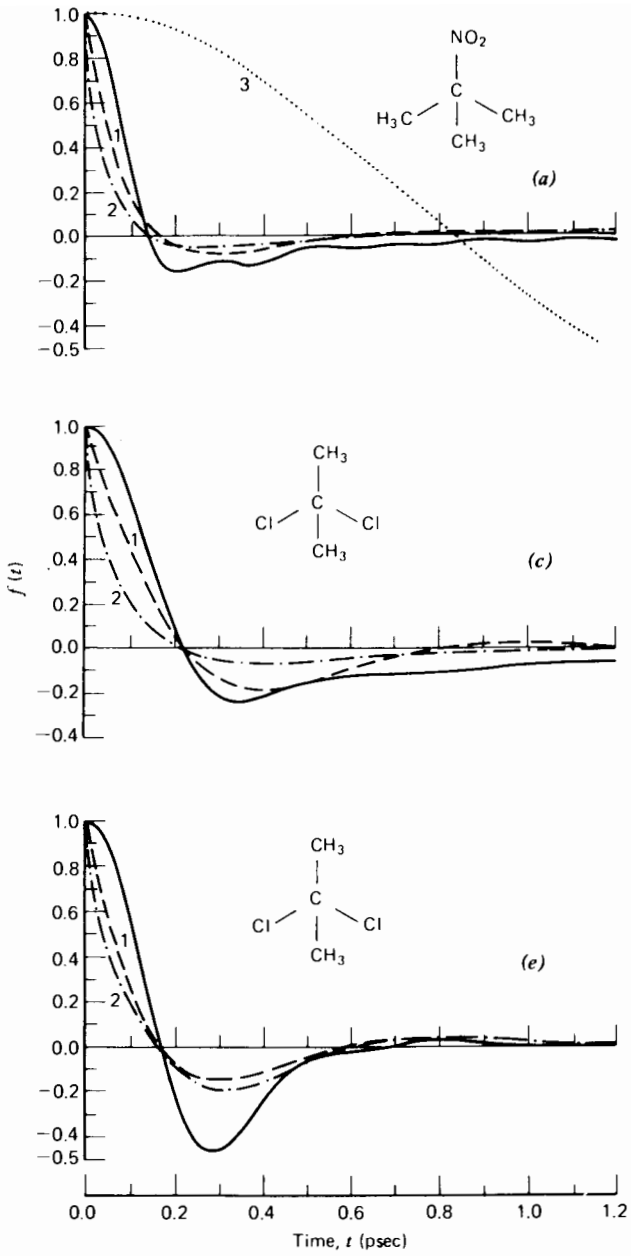

Figure 1.3.1.3 Orientational velocity correlation functions (i.e., those of $\langle \dot{\mathbf{u}}(0) \cdot \dot{\mathbf{u}}(t) \rangle$ where $\mathbf{u}$ is the dipole unit vector from far infrared/dielectric spectra, accompanied by theories 1 and 2, which involve Markov statistics in some way and are unrealistic at short times. Curve 3 is a "free rotor" function. (*a*) plastic crystal at 294°K; (*b*) at 273°K and (·----·----·) 219°K; (*c*) liquid at 295°K; (*d*) at 241°K; (*e*) plastic crystal at 235°K; (*f*) at 192°K. [Reproduced by permission from M. Evans, *J. Chem. Soc. Faraday Trans. II*, **71**, 2051 (1975).]

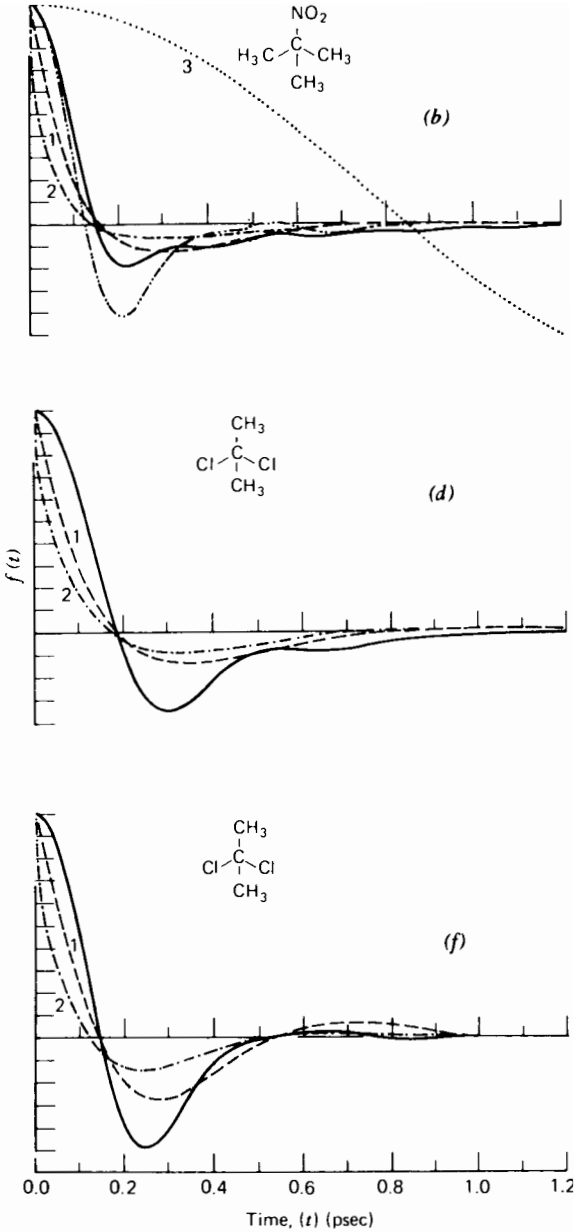

Figure 1.3.1.3 (*Continued*)

Gaussian Process

If an event has probability p of appearing at any one trial, the probability of r appearances in n independent trials is

$$\frac{n!}{(n-r)!r!}q^{n-r}p^r \qquad (1.3.1.6)$$

where $q = 1 - p$. This is the term involving p^r in the binomial expansion of $(q+p)^n$. A limiting form of the binomial distribution is the continuous frequency distribution of infinite range represented by

$$dF(x) = \frac{1}{\sigma\sqrt{2\pi}}\exp\left[-\frac{1}{2}\left(\frac{x-m}{\sigma}\right)^2\right]dx \qquad (-\infty < x < \infty) \qquad (1.3.1.7)$$

where m is the mean of the statistical data. For example, if we are concerned with molecular center of mass velocity in a sample of liquid that is not flowing, then *at thermodynamic equilibrium* m is zero. However, if a small measuring field is applied to the specimen, the mean of such variates as the angular momentum is finite, and regresses to zero only after the field is removed. The period of regression is known as a *transient*, or *transient regime*. σ is the standard deviation. The form 1.3.1.7 is known as the Gaussian distribution, and is a theoretical cornerstone of equilibrium statistical mechanics. More details are available in a number of excellent treatises (Balescu, 1975; McQuarrie, 1976).

However, the magnetic tape data from a molecular dynamics simulation *do not obey Gaussian statistics* (Fig. 1.3.1.4). This is despite the fact that initially such quantities as the molecular or atomic velocity are distributed in this manner using a random number generator. We must aim therefore at a theoretical treatment which is general enough to take this discovery in its stride.

Ergodicity

A stochastic, stationary process $X(t)$ is ergodic if

$$X(t) = \frac{1}{t}\int_0^t X(t')\,dt' \to \langle\alpha\rangle \qquad \text{as } t \to \infty$$

This allows us to build up an a.c.f. using a *running time average*, such as that of Fig. 1.3.1.1.

Khinchin's Theorem

A sufficient condition for a system of n stationary, stochastic processes to be ergodic is that all correlation functions $C(t) \to 0$ as $t \to \infty$.

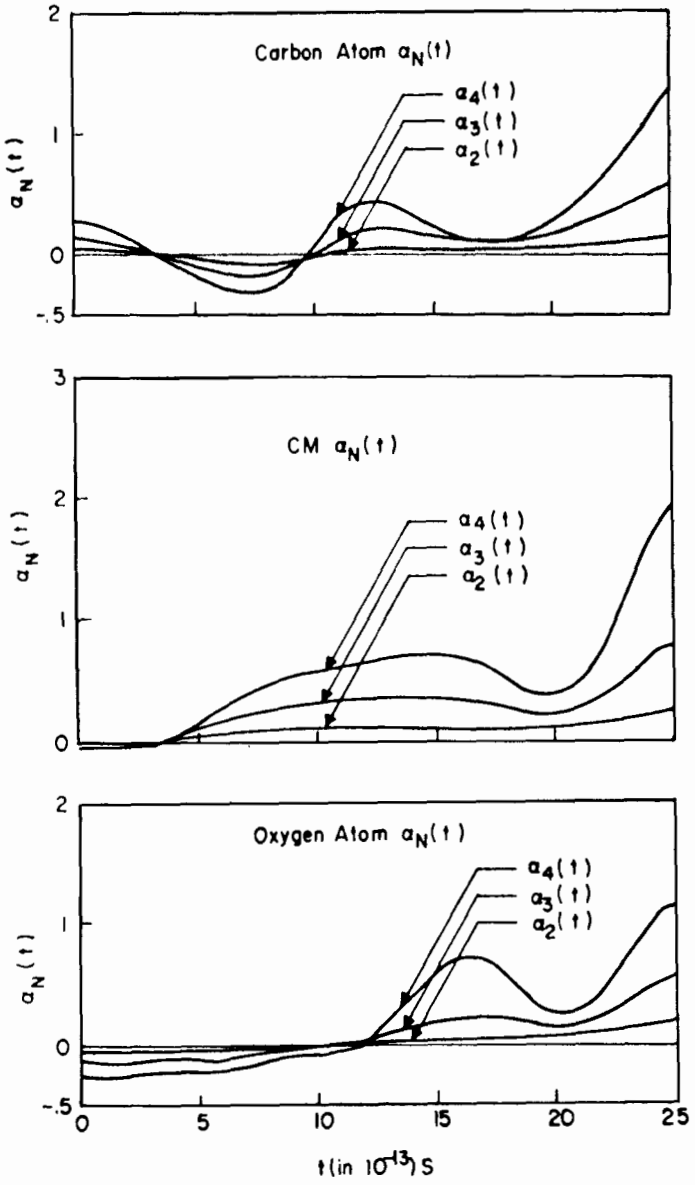

Figure 1.3.1.4 Some ratios $[\alpha_N(t)]$ of the left- to the right-hand sides of Eq. 1.4.10.1b from a simulation by Berne and Harp of liquid carbon monoxide. CM denotes center of mass. [Reproduced by permission from B. J. Berne and G. D. Harp, *Adv. Chem. Phys.*, **17**, 205 (1970).]

1.4 THE THEORY OF PROBABILITY

1.4.1 Classical Definition

If an event can occur in n mutually exclusive and equally likely ways and if n_A of these ways have an attribute A then the probability of the event A is the factor n_A/n. For example, the probability of picking an ace is 4/52.

1.4.2 Relative Frequency Definition

If an event has occurred in n mutually exclusive ways and if n_A of the outcomes have an attribute A, then the probability of A is the number to which n_A/n tends as n tends to infinity.

In the following it is assumed that a probability has already been assigned to an event under consideration. This probability is such that it satisfies the following axioms. Let Ω be the set of all outcomes of a particular experiment (Ω is termed the *sample space*). To each event $A \subset$ (belonging to) Ω is assigned a real number $P(A)$ called the probability of the event A, satisfying the following conditions:

1. $P(\Omega) = 1$.
2. $0 \leq P(A) \leq 1$.
3. If A and B are mutually exclusive events $\subset \Omega$ (i.e., events which cannot occur together) then
$$P[A \cup B] = P(A) + P(B) \quad \text{or} \quad P(A \cap B) = \phi.$$
4. If $(A_1, A_2, \ldots, A_n)$ are n mutually exclusive events $\subset \Omega$ then
$$P[A_1 \cup A_2 \cup \cdots A_{i-1} \cup A_i \cup \cdots \cup A_n] = P(A_1) + P(A_2) + \cdots + P(A_n)$$

In these four axioms, $A \cup B$ (read A union B), means that *either* event A *or* event B happens. $A \cap B$ (read A intersection B) means both events A and B occur. (For $\subset$ read "in a subset of".) In general we call a space, consisting of a sample space Ω, a collection of events $\subset \Omega$ (the measurable subsets $\mathcal{F}$ of Ω) and a probability P assigned to these events a *probability space*. We denote this space by $(\Omega, \mathcal{F}, P)$. P is termed a *probability measure* on the space Ω.

1.4.3 Conditional Probability

Define the probability of the event A *given that the event* B *occurs* as

$$P(A \mid B) = \frac{P(A \cap B)}{P(B)} \tag{1.4.3.1}$$

This probability satisfies the above four axioms.

The events A and B are *independent* if and only if

$$P(A \mid B) = \frac{P(A \cap B)}{P(B)} = P(A) \tag{1.4.3.2}$$

That is, $P(A \cap B) = P(A)P(B)$. This is true, for example, if we regard the rotational and translational motions of molecules as statistically independent. In Chapter 5 we show that this is sometimes *not* the case.

1.4.4 Random Variables—A Physical Analogy

Suppose X is a variable that can take on the values $(x_1, x_2, \ldots, x_n)$ with probabilities $[p(x_1), p(x_2), \ldots, p(x_n)]$, where

$$\sum_{i=1}^{n} p(x_i) = 1$$

Then X is called a random variable (r.v.), stochastic variable, or variate. There is a physical problem whose analogy to probability theory will help with the concepts that follow.

Suppose we have a unit mass that can be broken up into n smaller masses (not necessarily equal) $m_1 + m_2 + m_3 + \cdots$. Clearly

$$\sum_{i=1}^{n} m_i = 1$$

Let these masses be distributed arbitrarily on the x axis. The distance to any mass from the origin is denoted by x. We may construct the mechanical definitions:

$$\text{Center of mass (first moment)} = m_1x_1 + m_2x_2 + \cdots + m_nx_n$$
$$\text{Moment of inertia} = m_1x_1^2 + m_2x_2^2 + \cdots + m_nx_n^2$$

If we imagine now that X is a r.v. assuming the values $(x_1, \ldots, x_n)$ with probabilities $[p(x_1), \ldots, p(x_n)]$, the *expected value* may be defined as

$$E(X) = \langle X \rangle \tag{1.4.4.1}$$

which is the *mean value* or *average value* of $(x_1, \ldots, x_n)$,

$$\langle X \rangle = \sum_{i=1}^{n} x_i p(x_i)$$

Note that $\langle\ \rangle$ is a linear operator since Σ is a linear operator. We have

$$\langle X \rangle = \bar{X}; \qquad \langle X - \bar{X} \rangle = \langle X' \rangle = 0$$

X' is a r.v. with zero mean, a *centered* r.v. The reduction of X to X' is always possible. In general we may define the expected value of a function $g(X)$ of X by the equation

$$\langle g(X) \rangle = \sum_{i=1}^{n} g(x_i) p(x_i)$$

Consider $\langle (X-a)^2 \rangle$ where a is a constant; then

$$\begin{aligned}\langle (X-a)^2 \rangle &= \sum_i (x_i - a)^2 p(x_i) \\ &= \sum_i x_i^2 p(x_i) - 2a \sum_i x_i p(x_i) + a^2 \sum_i p(x_i) \\ &= \langle X^2 \rangle - 2a\langle X \rangle + a^2\end{aligned}$$

Now let $\langle X \rangle = a$; then $\langle (X-a)^2 \rangle$ is called the *variance* of the random variable X; that is,

$$\sigma_X^2 \equiv \mathrm{Var}[X] = \langle (X-a)^2 \rangle = \langle (X - \langle X \rangle)^2 \rangle$$

σ_X is called the standard deviation or root mean square (r.m.s.) value of the r.v. X. In terms of our mass distribution σ_X is the radius of gyration about the center of mass origin. Since $\langle X \rangle = a$ we have

$$\langle (X-a)^2 \rangle = \langle X^2 \rangle - \langle X \rangle^2$$

which in our mechanical model is the parallel axis theorem of mechanics.

1.4.5 Probability and Distribution Functions

The function $p(X)$ which takes on the discrete values $[p(x_1), \ldots, p(x_n)]$ at the points $(x_1, \ldots, x_n)$ is called the *probability function* (p.f.) or *frequency function of the distribution.*

We may write

$$p(x_i) = P(X = x_i)$$

so that

$$\sum_{i=1}^{n} p(x_i) = 1$$

Another important function associated with a random variable X is the *distribution function* $F(x)$ (d.f.).

It is defined as

$$F(x) = P(X \leq x_i) = \sum_{x_i \leq x} p(x_i)$$

From the definition of the p.f. $P(X)$ we see that $F(x)$ is a *step function* whose jumps are equal to $p(x_i)$ (Fig. 1.4.5.1).

1.4.5.1 Multidimensional Random Variables

Consider two random variables (r.v.'s) X and Y. Let X be defined as above and let Y assume the values $(y_1, \ldots, y_m)$ with respective probabilities $[q(y_1), \ldots, q(y_m)]$. Write $p(x_i, y_i)$ as the probability that $X = x_i$ and $Y = y_j$; then

$$p(x_i, y_j) = P(X = x_i, Y = y_j)$$

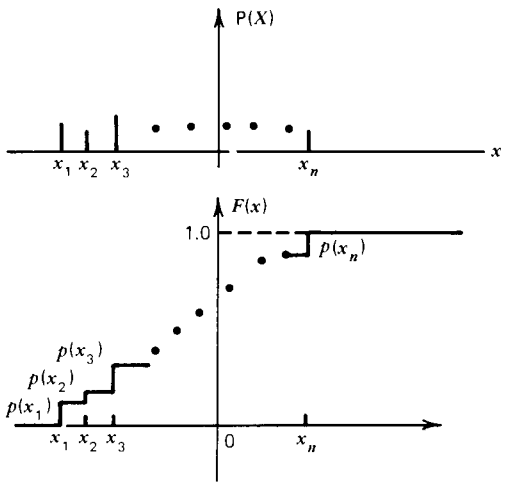

Figure 1.4.5.1 Illustration of the step function $F(x)$.

and

$$\sum p(x_i, y_j) = 1$$

The d.f. is

$$\begin{aligned}F(x, y) &= P(X \leq x, Y \leq y) \\ &= \sum_{x_i \leq X} \sum_{y_i \leq Y} p(x_i, y_j)\end{aligned}$$

Now

$$\begin{aligned}F(x) = P(X \leq x) &= P(X \leq x, Y < \infty) \\ &= \sum_{x_i \leq X} \sum_{j=1}^{m} p(x_i, y_j) = \sum_{x_i \leq X} p(x_i)\end{aligned}$$

which shows the relation between the d.f. of X and the joint d.f., $F(x, y)$ of X and Y. $F(x)$ is here termed a *marginal* distribution function. The corresponding marginal probability function is

$$p(x_i) = P(X = x_i, Y < \infty) = \sum_{j=1}^{m} p(x_i, y_j)$$

From axiom 2 we can define the *conditional probability* $p_{y_j}(x_i)$ as the probability that $X = x_i$, knowing that $Y = y_j$, or explicitly:

$$\begin{aligned}p_{y_j}(x_i) &= \frac{P(X = x_i, Y = y_j)}{P(Y = y_j)} \\ &= \frac{p(x_i, y_j)}{q(y_j)}\end{aligned}$$

A similar formula holds for the conditional probability $q_{x_i}(y_j)$. The cor-

responding conditional d.f. $F_{y_j}(x)$ is given by

$$F_{y_j}(x) = \frac{P(X \leq x,\ Y = y_j)}{P(Y = y_j)}$$
$$= \sum_{x_i \leq x} p(x_i, y_j)$$

The mean value of $g(X, Y)$ is defined by

$$\langle g(X, Y)\rangle = \sum_i^n \sum_j^m g(x_i, y_j)p(x_i, y_j)$$

It may be shown that

$$\langle (X + Y)\rangle = \langle X\rangle + \langle Y\rangle \qquad (1.4.5.1.1)$$

and if X and Y are independent:

$$\langle XY\rangle = \langle X\rangle\langle Y\rangle \qquad (1.4.5.1.2)$$

Equations 1.4.5.1.1 and 1.4.5.1.2 are important results which the reader might like to derive independently.

1.4.5.2 Worked Example—The Binomial Distribution

Let X be a r.v. which assumes the integral values: $(0, 1, 2, \ldots, n)$ with the respective probabilities $(B_0, B_1, \ldots, B_n)$ of assuming these values where B_r is given by

$$B_r = {}^nC_r p^r (1-p)^{n-r} \qquad 0 \leq p \leq 1$$

Then X has the binomial distribution. Also

$$\sum_{r=0}^n B_r = 1$$

for if $q = 1 - p$ and x is a number, we have

$$(px + q)^n = \sum_{r=0}^n {}^nC_r p^r q^{n-r} x^r \qquad x = 1,\ (p + q)^n = 1$$
$$= \sum_{r=0}^n p^r q^{n-r}\, {}^nC_r = \sum_{r=0}^n B_r$$

To determine $\langle X\rangle$ we have by differentiation with respect to x

$$n(px + q)^{n-1} p = \sum_{r=0}^n r\, {}^nC_r p^r q^{n-r} x^{r-1} \qquad (1.4.5.2.1)$$

and setting $x = 1$

$$n(p + q)^{n-1} p = \sum_{r=0}^n r\, {}^nC_r p^r q^{n-r} = \langle X\rangle$$

so that $\langle X\rangle = np$. The variance is now

$$\mathrm{Var}[X] = \sigma^2 = \langle (X - np)^2\rangle = \langle X^2\rangle - (np)^2$$

Multiplying Eq. 1.4.5.2.1 by x and differentiating with respect to x, we have, on letting $x = 1$,

$$n(n-1)p^2 + np = \sum_{r=0}^n r^2\, {}^nC_r p^r q^{n-r} = \langle X^2\rangle$$

so that

$$\langle X^2\rangle - (np)^2 = npq$$
$$= \langle X^2 - \langle X\rangle^2\rangle$$

1.4.6 Continuous Distributions

Hitherto we have assumed that the r.v. X can take only a finite number of discrete values. Consider again our mechanical analogy. Suppose that instead of being discretely distributed the mass is continuously distributed. Then we cannot speak of the mass at any one point since it is zero, but we can speak of the mass Δm lying in some small interval Δx of the x axis. If the limit $\Delta m/\Delta x$ exists as $\Delta x \to 0$, we call it the density of mass $\rho(x)$. The mass contained in any interval $[a, b]$ is therefore given by the integral $\int_a^b \rho(x)\, dx$. In an analogous fashion we define $f(X)$, the mass density or *probability density* of the r.v. X, by the relation

$$f(X) = \lim_{\Delta x \to 0} \frac{P(x \leq X \leq x + \Delta x)}{\Delta x} \qquad (1.4.6.1)$$

Hence

$$P(a \leq X \leq b) = \int_a^b f(X)\, dX \qquad (1.4.6.2)$$

and

$$\int_{-\infty}^{\infty} f(X)\, dX = 1$$

The corresponding d.f. is $F(x) = P(X \leq x) = \int_{-\infty}^{x} f(X)\, dX$. Let us suppose that $f(X)$ is continuous, then

$$\frac{dF(x)}{dx} = f(x)$$

In many cases $f(x)$ is not continuous and we must use the Stieljes integral:

$$F(x) = \int_{-\infty}^{x} dF(u)$$

(which is used in our glossary definition of the spectral function).

Illustration

We recall the definition of sample space in the discrete case. Here in the continuous case we must in general consider a continuum of values. In the

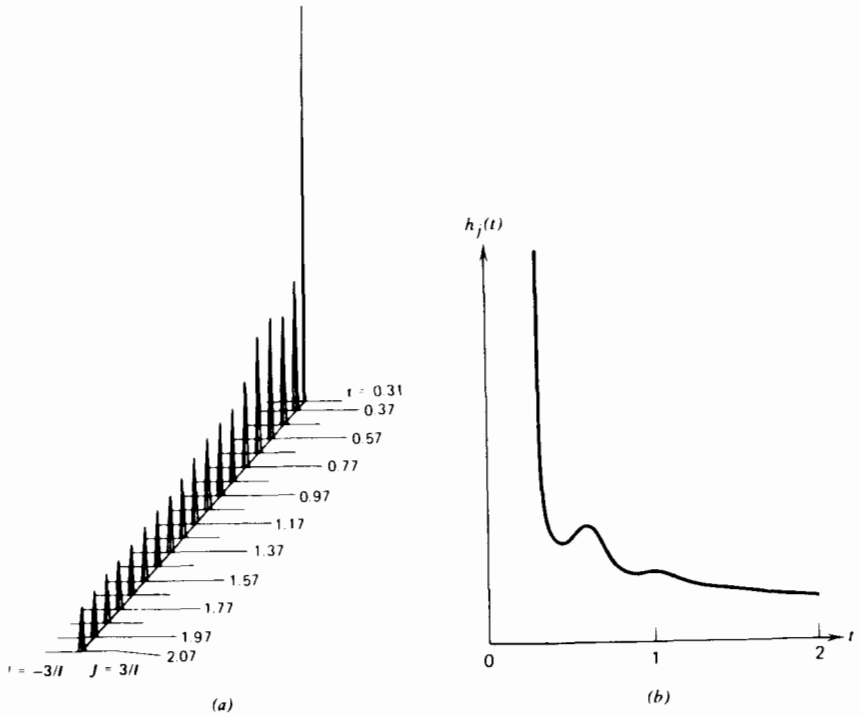

Figure 1.4.6.1 (*a*) Probability density function of angular momentum (J), plotted on the vertical axis. $|J|$ is plotted on the horizontal axes (from $-3/I$ to $3/I$), where I is the moment of inertia, and time t on the diagonal axis. (*b*) Plot of peak height versus time (psec). [Reproduced from A. R. Davies et al., *Mol. Phys.*, **35**, 864 (1978).]

above example our space consists of the real line R. Then instead of considering events as sets of sample points, we must consider subsets of R. The natural concept to use is to consider the space R upon which a probability measure has been defined, and to use the class of all Borel measurable sets (Pitt, 1963).

The probability density function (p.d.f.) is basic to the development in Chapters 2-5. It may be a multidimensional function but Fig. 1.4.6.1 illustrates the form it takes when considering a type of angular motion labeled by us as itinerant oscillation (see Chapter 4).

1.4.7 Two-Dimensional Continuous Distributions

Let (X, Y) be two continuous r.v.'s; then their joint p.d.f. $f(X, Y)$ may be described as

$$f(X, Y)\,dX\,dY = P(x \leq X \leq x + dx;\ y \leq Y \leq y + dy)$$

The corresponding joint d.f. is

$$F(x, y) = P(X \leq x,\ Y \leq y) = \int_{-\infty}^{y}\int_{-\infty}^{x} f(X, Y)\,dX\,dY$$

Thus if F is differentiable

$$f(x, y) = \frac{\partial^2 F(x, y)}{\partial x\,\partial y}$$

and

$$\int_{-\infty}^{\infty}\int_{-\infty}^{\infty} f(X, Y)\,dX\,dY = 1$$

The marginal d.f. $F(x)$ of X is

$$F(x) = P(X \leq x, Y < y) = \int_{-\infty}^{\infty}\int_{-\infty}^{\infty} f(X, Y)\,dX\,dY$$

$$= \int_{-\infty}^{x} f(X)\,dX$$

where $f(X)$ is the marginal p.d.f. of X.

Illustration

The marginal p.d.f. of X is $f(x)$ so that

$$f(x) = \frac{\partial}{\partial x} F(x, \infty) = \int_{-\infty}^{\infty} f(x, Y)\,dY$$

The conditional density function (c.d.f.) of X given that $Y = y$ is

$$F_y(x) = \lim_{\Delta y \to 0} \frac{P(X \leq x,\ y \leq Y \leq y + \Delta y)}{P(y \leq Y \leq y + \Delta y)}$$

$$= \lim_{\Delta y \to 0} \frac{\int_{-\infty}^{x}\int_{y}^{y+\Delta y} f(X, Y)\,dX\,dY}{\int_{y}^{y+\Delta y} q(Y)\,dY}$$

$$= \frac{\int_{-\infty}^{x} f(X, Y)\,dX}{q(y)}$$

while the corresponding conditional p.d.f. (c.p.d.f.) $f_y(x)$ is

$$f_y(x) = \frac{\partial}{\partial x} F_y(x) = \frac{f(x, y)}{q(y)}$$

In terms of probabilities we may write

$$f_y(x)\,dx = \frac{P(x \leq X \leq x + dx,\ y \leq Y \leq y + dy)}{P(y \leq Y \leq y + dy)}$$

A similar analysis can be made in order to obtain the c.d.f. and c.p.d.f. of Y.

1.4.7.1 *Mean Values for Two-Dimensional Distributions*

$$\langle g(X, Y)\rangle = \int_{-\infty}^{\infty}\int_{-\infty}^{\infty} g(X, Y)f(X, Y)\,dX\,dY$$

$$\langle X + Y\rangle = \langle X\rangle + \langle Y\rangle$$

are two of the fundamental equations. Note also that

$$\langle XY\rangle = \int_{-\infty}^{\infty}\int_{-\infty}^{\infty} XY\,f(X, Y)\,dX\,dY$$

If (X, Y) are independent,

$$f(X, Y) = f_Y(X)q_X(Y)$$

or

$$f(X, Y) = f(X)q(Y)$$

so that

$$\langle XY\rangle = \int_{-\infty}^{\infty} Xf(X)\,dX \int_{-\infty}^{\infty} Yq(Y)\,dY$$
$$= \langle X\rangle\langle Y\rangle$$

Generally, if $(X_1, \ldots, X_n)$ are independent r.v.'s,

$$\langle X_1X_2\cdots X_n\rangle = \langle X_1\rangle\langle X_2\rangle\cdots\langle X_n\rangle$$

1.4.8 The Normal (Gaussian) Distribution

Let us consider the following p.d.f.:

$$f(X) = \frac{1}{\sqrt{2\pi}\,\sigma}\exp\left[-\frac{(X-\mu)^2}{2\sigma^2}\right] \qquad -\infty < X < \infty$$

If X has this p.d.f. it is said to have the normal distribution with parameters μ and σ^2; usually this is written $X \sim N(\mu, \sigma^2)$. This distribution has the following fundamental properties:

1. If $X \sim N(\mu, \sigma^2)$, $f(X)$ has a stationary point at $X = \mu$.
2. As $X \to \infty$, $f(X) \to 0$.
3. $\langle X\rangle = \mu$, $\langle X^2 - \langle X\rangle^2\rangle = \sigma^2$.

The mean value is given by

$$\langle X\rangle = \int_{-\infty}^{\infty} \frac{X}{\sqrt{2\pi}\,\sigma}\exp\left(-\frac{(X-\mu)^2}{2\sigma^2}\right)dX$$
$$= \mu$$

since

$(1/\sqrt{2\pi})\exp(-y^2/2)$ is the p.d.f. of $N(0, 1)$. Similarly, $\langle X^2 - \langle X\rangle^2\rangle = \sigma^2$.

1.4.9 Moment Generating and Spectral Functions

The moment generating function (m.g.f.) is an integral transform of a d.f., and is therefore very useful for the description of spectra in stochastic terms. In particular, we consider the Fourier transform of the d.f. and we suppose that X is a continuous r.v. possessing a p.d.f. $f(X)$. Then the Fourier transform of the p.d.f. $f(X)$ is

$$\phi_X(t) = \int_{-\infty}^{\infty} e^{itX}f(X)\,dX = \langle e^{itX}\rangle$$

termed the *characteristic function* of X.

Illustrations

1. If two r.v.'s have the same c.f., they have the same probability distribution.
2. If two r.v.'s have the same probability distribution, they have the same characteristic function.
3. For a normal distribution, the characteristic function is

$$\phi_X(t) = \exp\left(i\mu t - \frac{\sigma^2t^2}{2}\right) \equiv \exp\left(i\langle X\rangle t - \frac{\langle X^2\rangle t^2}{2}\right)$$

4. In particular, if $t = 1$,

$$\langle e^{iX}\rangle = \exp\left(i\langle X\rangle - \frac{\langle X^2\rangle}{2}\right)$$

which is an exceptionally useful result.

Sometimes it is useful to make the following integral transform:

$$M_X(t) = \int_{-\infty}^{\infty} e^{tX}f(X)\,dX$$

If $X \sim N(\mu, \sigma^2)$, then

$$M_X(t) = \exp\left(t\mu + \frac{\sigma^2t^2}{2}\right)$$

The nth derivative of $M_X(t)$ with respect to t gives the nth moment of the r.v. X about zero, so that

$$\langle X^n\rangle = \left(\frac{d^n}{dt^n}M_X(t)\right)_{t=0}$$

Theorem

If X_1 and X_2 are *independent* r.v.'s and

$$Z = \alpha_1X_1 + \alpha_2X_2$$

then

$$M_Z(t) = \langle e^{\alpha_1 X_1 t}\rangle\langle e^{\alpha_2 X_2 t}\rangle$$

A linear combination of independent normally distributed r.v.'s is also a normally distributed r.v. with mean

$$\mu = \sum_{i=1}^{n} \alpha_i \mu_i$$

and variance

$$\sum_{i=1}^{n} \alpha_i^2 \sigma_i^2 = \sigma^2$$

This is a result of particular importance in the theory of neutron scattering, where it is fundamentally supposed that rotational and translational variables are statistically independent. That this is *not necessarily so* is illustrated by the moment averages of Fig. 1.4.9.1, estimated from a molecular dynamics simulation of diatomic molecules.

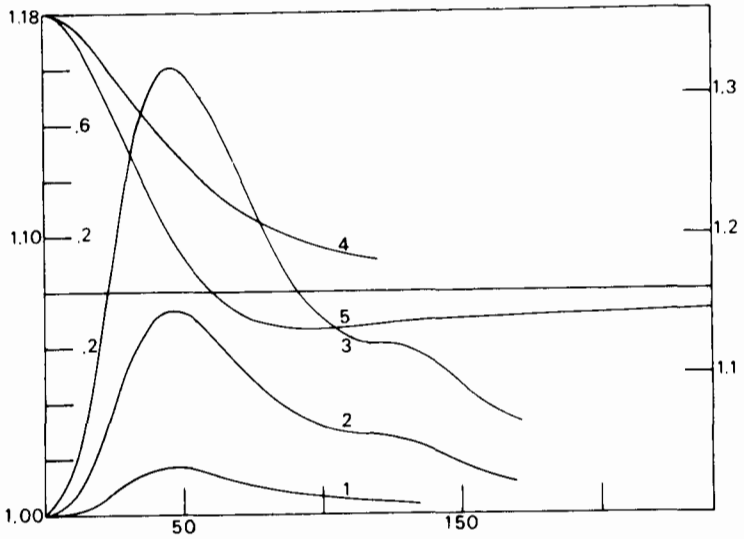

Figure 1.4.9.1 Moments of mixed a.c.f.'s of linear (v) and angular velocity (ω) from a computer simulation of liquid nitrogen. Abscissa: time steps.
(1) $\langle |\mathbf{v}(0)|\,|\boldsymbol{\omega}(t)|\rangle / \langle |\mathbf{v}(0)|\,|\boldsymbol{\omega}(0)|\rangle$.
(2) $\langle v^2(0)\omega^2(t)\rangle / \langle v^2(0)\omega^2(0)\rangle$.
(3) $\langle v^4(0)\omega^4(t)\rangle / \langle v^4(0)\omega^4(0)\rangle$.
(4) $\langle \mathbf{v}(0)\cdot\mathbf{v}(t)\rangle / \langle \mathbf{v}(0)\cdot\mathbf{v}(0)\rangle$.
(5) $\langle \boldsymbol{\omega}(0)\cdot\boldsymbol{\omega}(t)\rangle / \langle \boldsymbol{\omega}(0)\cdot\boldsymbol{\omega}(0)\rangle$.
[Reproduced by permission from M. Evans et al., *Adv. Chem. Phys.* **44**, 255–481 (1980).]

1.4.10 Higher Moments of the Gaussian Distribution

If $X \sim N(0, 1)$, then by successive integrations

$$\langle X^{2n+1}\rangle = 0 \qquad (1.4.10.1a)$$

$$\langle X^{2n}\rangle = 1\cdot 3\cdot 5\cdot \cdots \cdot (2n-1)\langle X^2\rangle^n \qquad (1.4.10.1b)$$

It is precisely these relations that are *not* obeyed (Chapter 10) in a molecular dynamics simulation such as that of Fig. 1.3.1.4. However, the Gaussian distribution has been historically of such fundamental importance in the field of molecular dynamics that very little effort has yet been made to expand in other directions. Our task (in Chapter 10) is to lay the foundations for this expansion.

1.4.11 The Central Limit Theorem

Let $[X_1, X_2, X_3, \ldots, X_n]$ be n *independent* random variables with *arbitrary* distributions. Then the sum

$$X = \frac{X_1 + X_2 + \cdots + X_n}{\sqrt{n}}$$

approaches a normally distributed r.v. as n approaches infinity. Further if X_i has mean zero and variance $\sigma_i^2 < \infty$, that is,

$$\langle X_i\rangle = 0, \qquad \langle X_i^2\rangle = \sigma_i^2, \qquad i = 1, 2, \ldots, n$$

then X also has mean zero and variance σ^2, where

$$\sigma^2 = \frac{(\sigma_1^2 + \sigma_2^2 + \sigma_3^2 + \cdots + \sigma_n^2)}{n}$$

Illustration

One way of explaining the non-Gaussian results may be that because the number of molecules used, $n = 10^2 - 10^3$, is relatively small compared with Avogadro's number, $N_{AV} = 6.023 \times 10^{23}$ the process becomes Gaussian for a sample of real liquid by the central limit theorem. This is an interesting question which remains to be resolved. However, as we shall see later, there is no a priori reason for assuming that molecular dynamics in a liquid is governed by Gaussian statistics.

1.4.12 Covariance and Autocorrelation Functions

These are the most useful of definitions when judged by the literature in this field of the last decade or so. The covariance of any two r.v.'s X_1 and X_2 is written $\mathrm{Cov}[X_1, X_2]$ and is defined by

$$\mathrm{Cov}[X_1, X_2] = \langle (X_1 - \langle X_1\rangle)(X_2 - \langle X_2\rangle)\rangle$$
$$= \langle X_1 X_2\rangle - \langle X_1\rangle\langle X_2\rangle \qquad (1.4.12.1)$$

If X_1 and X_2 are independent,

$$\mathrm{Cov}[X_1, X_2] = 0$$

and X_1 and X_2 are said to be uncorrelated. Further, since X_1 and X_2 are uncorrelated,

$$\langle X_1 X_2 \rangle = \langle X_1 \rangle \langle X_2 \rangle$$
$$\mathrm{Var}[X_1 + X_2] = \mathrm{Var}[X_1] + \mathrm{Var}[X_2] \qquad (1.4.12.2)$$

The proof of Eq. 1.4.12.2 is short and illuminating. Since

$$\begin{aligned}&\mathrm{Var}[X_1 + X_2] - \mathrm{Var}[X_1] - \mathrm{Var}[X_2] \\ &= \langle (X_1 + X_2)^2 \rangle - \langle X_1 + X_2 \rangle^2 - \langle X_1^2 \rangle + \langle X_1 \rangle^2 - \langle X_2^2 \rangle + \langle X_2 \rangle^2 \\ &= 2\langle X_1 \rangle \langle X_2 \rangle - (\langle X_1 \rangle + \langle X_2 \rangle)^2 + \langle X_1 \rangle^2 + \langle X_2 \rangle^2 = 0\end{aligned}$$

1.4.13 The Multidimensional Normal Distribution

The n dimensional Gaussian distribution is defined as follows; let $(X_1 \cdots X_n)$ be n (not necessarily independent) r.v.'s with means equal to zero. Let $f(X_1 \cdots X_n)$ be their joint p.d.f. then we say $(X_1 \cdots X_n)$ are normally distributed in n dimensions if their p.d.f. is of the form

$$f(\mathbf{X}) = \frac{\exp[-\frac{1}{2}\det(\mathbf{X}'\mathbf{M}^{-1}\mathbf{X})]}{(2\pi)^{n/2}\sqrt{\det \mathbf{M}}} \qquad (1.4.13.1)$$

where $\mathbf{M} = \mu_{ij}$ is the matrix of the second moments

$$\mu_{ij} = \langle X_i X_j \rangle, \qquad i, j = 1, 2, \ldots, n;$$

$\mathbf{M}^{-1}$ is the inverse matrix; $\det \mathbf{M}$ is the determinant of the matrix $\mathbf{M}$; $\mathbf{X}$ is the column vector with the components $(X_1 \cdots X_n)$ and $\mathbf{X}'$ is its transpose

$$\det(\mathbf{X}'\mathbf{M}^{-1}\mathbf{X}) = \sum_{i=1}^{n}\sum_{j=1}^{n} \frac{M_{ij}X_iX_j}{\det \mathbf{M}}.$$

The marginal distributions $f(X_{i_1}, X_{i_2}, \ldots, X_{i_r})$ for the multidimensional normal distribution may be determined in the usual fashion as

$$f(X_{i_1} \cdots X_{i_r}) = \int_{-\infty}^{\infty}\int_{-\infty}^{\infty} \cdots \int_{-\infty}^{\infty} f(X_{i_1} \cdots X_{i_n}) dX_{i_{r-1}} \cdots dX_{i_n}$$

These are r dimensional normal distributions. If the X_i are independent then

$$\langle X_i X_j \rangle = 0 \qquad i \neq j$$

and $\mathbf{M}$ becomes a pure diagonal matrix. In this case

$$f(X_1 \cdots X_n) = f(X_1) f(X_2) \cdots f(X_n)$$

where each $f(X_i)$ is a one-dimensional normal distribution with mean zero and variance μ_{ii}.

For the two-dimensional case, with p.d.f. $f(X_1, X_2)$,

$$\mathbf{M} = \begin{bmatrix} \mu_{11} & \mu_{12} \\ \mu_{21} & \mu_{22} \end{bmatrix}; \qquad \mathbf{M}^{-1} = \begin{bmatrix} \mu_{22} & -\mu_{21} \\ -\mu_{12} & \mu_{11} \end{bmatrix} \frac{1}{\det \mathbf{M}}$$

and $\det \mathbf{M} = \mu_{11}\mu_{22} - \mu_{12}^2$.

The vectors $\mathbf{X}$ and $\mathbf{X}'$ are

$$\mathbf{X} = \begin{bmatrix} X_1 \\ X_2 \end{bmatrix}; \qquad \mathbf{X}' = [X_1 X_2]$$

and $\det(\mathbf{X}'\mathbf{M}^{-1}\mathbf{X}) = (\det \mathbf{M})^{-1}(\mu_{22}X_1^2 - 2\mu_{12}X_1X_2 + \mu_{11}X_2^2)$. If we now introduce the standard notation

$$\mu_{11} = \sigma_X^2, \qquad \mu_{22} = \sigma_Y^2, \qquad \mu_{12} = \sigma_X\sigma_Y$$

where σ_X and σ_Y are the standard deviations of X_1 and X_2 and τ is the *correlation function of* X_1 *and* X_2, then the p.d.f. assumes the standard form (Coffey and Evans, 1978):

$$f(X, Y) = \{2\pi[(1-\tau^2)\sigma_X\sigma_Y]^{1/2}\} \exp\left[-\frac{1}{2(1-\tau^2)}\left(\frac{X^2}{\sigma_X^2} - \frac{2\tau XY}{\sigma_X\sigma_Y} + \frac{Y^2}{\sigma_Y^2}\right)\right] \qquad (1.4.13.2)$$

If X and Y are independent then X and Y are uncorrelated and

$$f(X, Y) = \frac{e^{-X^2/(2\sigma_X^2)}}{\sigma_X\sqrt{2\pi}} \frac{e^{-Y^2/(2\sigma_Y^2)}}{\sigma_Y\sqrt{2\pi}} \qquad (1.4.13.3)$$

If X is molecular linear velocity for example, and Y an angular velocity about an axis fixed in the laboratory frame of reference, then as we see below, the *conditional* counterparts of Eqs. 1.4.13.2 and 1.4.13.3 provide us with a means of identifying the presence or absence of translation/rotation interaction depending as to whether or not τ, the mixed correlation coefficient exists.

1.5 STOCHASTIC PROCESSES

A stochastic process is a family of r.v.'s $[X(t), t \in T]$ where t is some parameter, generally the time, defined on a set T. It is convenient to decompose this set T into instants $t_1 < t_2 < t_3 \cdots < t_n < T$ and then to approximate the family of r.v.'s $[X(t)]$ by $X(t_1)$, $X(t_2)$, etc. We may describe the process by the following family of joint probability distributions: $f_1(x_1, t_1)\,dx_1$, is the probability of finding $X(t_1)$ in $(x_1, x_1 + dx_1)$; $f_2(x_1, t_1, x_2, t_2)\,dx_1\,dx_2$ of finding $X(t_1)$ in $(x_1, x_1 + dx_1)$ and $X(t_2)$ in $(x_2, x_2 + dx_2)$; and $f_3(x_1, t_1, x_2, t_2, x_3, t_3)\,dx_1\,dx_2\,dx_3$ of finding $X(t_1)$ in $(x_1, x_1 + dx_1)$, $X(t_2)$ in $(x_2, x_2 + dx_2)$, $X(t_3)$ in $(x_3, x_3 + dx_3)$, etc.; to $f_n(x_1, t_1, x_2, t_2, \ldots, x_n, t_n)$.

The process is *stationary* when the probability distribution underlying the process during a given interval of time depends only on the length of that interval and not on when that interval began. The underlying mechanism which causes r.v.'s $[X(t)]$ to fluctuate does not change with the course of time is another way of saying this.

A *purely random process* is identifiable when all its joint distributions may be written as follows:

$$f_1(x_1, t_1)$$
$$f_2(x_1, t_1, x_2, t_2) = f_1(x_1, t_1) f_1(x_2, t_2)$$
$$f_3(x_1, t_1, x_2, t_2, x_3, t_3) = f_1(x_1, t_1) f_1(x_2, t_2) f_1(x_3, t_3) \quad \text{etc.}$$

All the information is contained in the first p.d.f. f_1.

However, no molecular dynamic ensemble can be described by purely random statistics since this contravenes the laws of motion and the laws of thermodynamics. *The Markov process* (see glossary), as we shall see later, also strictly limits the dynamic possibilities, but is a more useful statistical concept, where all information about the process is contained in f_2. It is convenient at this point to introduce the *conditional probability density function*, c.d.f..

If the probability that $X(t_n)$ is in $(x_n, x_n + dx_n)$ at time t_n *depends* on $X(t_{n-1})$, x_n, and t_n, then

$$f_n(x_n, t_n \mid x_{n-1}, t_{n-1}, \ldots, x_1, t_1) = f_2(x_n, t_n \mid x_{n-1}, t_{n-1}).$$

This defines the Markov concept. A c.p.d.f. *depends* on other events, and is thus more in accord with the dynamical ideas governing, for example, atomic or molecular collisions.

Illustration

If a dynamic system could be found where the angular momentum or linear momentum of a very large number of molecules were subject to events which infinitely quickly changed them infinitesimally, then the system is describable by a Markov process. The artificial nature of this system may be shown by taking the Newtonian definition of force (F):

$$F = m \frac{d\mathbf{v}}{dt}$$

where m is the mass and $\mathbf{v}$ the linear velocity. An infinitely fast change in $\mathbf{v}$, written symbolically, means $d\mathbf{v}/dt \to \infty$. The force in such a system becomes infinite at each "collision." The dynamic "history" of the molecular velocity extends no further than the collision event itself, upon which it is solely dependent. The velocity is governed statistically by a "random" force which is Markovian (and Gaussian). The reader might already have discarded such a system because of its artificial nature, but if we balance

the propagative effect of the collisions by an even stranger concept—hydrodynamic friction on the molecular scale—we obtain a *seemingly* perfect description of the *low frequency* dielectric loss and dispersion of many dipolar liquids. Nobody should be content with this state of affairs and especially not far infrared spectroscopists, being naturally non-Markovian historians.

1.5.1 The Chapman–Kolmogorov and Smoluchowski Equations

Consider a set of instants $t_1 < t_2 < t_3$, where we suppose for the moment that t_1 and x_1 are fixed. Define $f_2(x_2, t_2 \mid x_1, t_1)\, dx_2 =$ probability that $X(t_2)$ is in $(x_2, x_2 + dx_2)$ given that $X(t_1)$ had the value x_1 at time t_1. $f_3(x_3, t_3 \mid x_2, t_2; x_1, t_1)\, dx_3 =$ probability that $X(t_3)$ is in $(x_3, x_3 + dx_3)$ given that $X(t_2)$ has the value x_2 at time t_2 and that $X(t_1)$ has the value x_1 at time t_1.

If we multiply f_2 and f_3 and integrate with respect to x_2, all dependence on x_2 vanishes. The new p.d.f. depends only on x_1 at t_1:

$$f_3(x_3, t_3 \mid x_1, t_1)\, dx_3 = \int_{-\infty}^{\infty} f_2(x_2, t_2 \mid x_1, t_1) f_3(x_3, t_3 \mid x_2, t_2; x_1, t_1)\, dx_2\, dx_3$$

or

$$f_3(x_3, t_3 \mid x_1, t_1) = \int_{-\infty}^{\infty} f_2(x_2, t_2 \mid x_1, t_1) f_3(x_3, t_3 \mid x_2, t_2; x_1, t_1)\, dx_2 \quad (1.5.1.1)$$

If we confine ourselves to Markov processes,

$$f_3(x_3, t_3 \mid x_2, t_2; x_1, t_1) = f_2(x_3, t_3 \mid x_2, t_2)$$

and

$$f_2(x_3, t_3 \mid x_1, t_1) = \int_{-\infty}^{\infty} f_2(x_2, t_2 \mid x_1, t_1) f_2(x_3, t_3 \mid x_2, t_2)\, dx_2 \quad (1.5.1.2)$$

Equation 1.5.1.1 is termed the *Chapman–Kolmogorov equation* and Eq. 1.5.1.2 the *Smoluchowski equation*. These relations may be used to construct some fundamentally useful stochastic differential equations for the diffusion of probability densities. These are the Fokker–Planck class of equations, which approximate Eqs. 1.5.1.1 and 1.5.1.2. During the past 15 years it has been shown that the whole structure of quantum mechanics may be derived and even *generalized* by means of stochastic equations. However, this field of *stochastic electrodynamics* is outside the scope of this book.

1.5.2 Probability Density Diffusion Equations

We are in danger of losing sight of the molecules in a probabilistic universe and it is refreshing when such a theory can be used as proof for their existence. This is illustrated in this section where we derive fundamental

forms for the evolution of p.d.f.'s in time for Markov processes only. The generalization to non-Markov processes is described later.

Take the Smoluchowski equation as starting point. For notational convenience we drop x_1, t_1 and write $t_2 = t$ and $t_3 = t + \delta t$, so that

$$f_2(x_3, t_3) = f(x_3, t + \delta t) = \int_{-\infty}^{\infty} f(x_2, t) f(x_3, t + \delta t \mid x_2, t)\, dx_2 \quad (1.5.2.1)$$

Now we introduce the variable $z = x_3 - x_2$, and fix x_2. Then x_3 will determine z, so that

$$f(x_3, t + \delta t \mid x_2, t) = q(z, \delta t \mid x_2, t)$$

say.

In the simplest case q is independent of the value x_2 from which the transition is made and independent of the time t_2, so that

$$f(x_3, t + \delta t \mid x_2, t) = q(z, \delta t)$$

Equation 1.5.2.1 becomes now, dropping the subscript 3,

$$f(x, t + \delta t) = \int_{-\infty}^{\infty} q(z, \delta t) f(x - z, t)\, dz \quad (1.5.2.2)$$

To approximate the true solution of Eq. 1.5.2.2 $f(x, t + \delta t)$ and $f(x - z, t)$ are expanded in Taylor series:

$$f(x - z, t) = f(x, t) - z \frac{\partial f}{\partial x}(x, t) + \frac{z^2}{2!} \frac{\partial^2 f}{\partial x^2}(x, t) \cdots$$

$$f(x, t + \delta t) = f(x, t) + \delta t \frac{\partial f}{\partial t}(x, t) + \frac{(\delta t)^2}{2!} \frac{\partial^2 f}{\partial t^2}(x, t) \cdots$$

This is always possible, and stringent mathematical proofs are available in many textbooks (for example, Balescu, 1975). We have already assumed, in forming the Smoluchowski equation, that a p.d.f. is integrable, and in forming the Taylor series we assume that it is differentiable.

Assume that δt is very small, so that we can ignore terms $O(\delta t)^2$, then

$$f(x, t) + \delta t \frac{\partial f}{\partial t}(x, t) = f(x, t) \int_{-\infty}^{\infty} q(z, \delta t)\, dz - \frac{\partial f(x, t)}{\partial x} \int_{-\infty}^{\infty} z q(z, \delta t)\, dz$$
$$+ \frac{1}{2!} \frac{\partial^2 f(x, t)}{\partial x^2} \int_{-\infty}^{\infty} z^2 q(z, \delta t)\, dz - \frac{1}{3!} \frac{\partial^3 f(x, t)}{\partial x^3} \int_{-\infty}^{\infty} z^3 q(z, \delta t)\, dz \cdots$$

If $\langle z \rangle = \int_{-\infty}^{\infty} z q(z, \delta t)\, dz = 0$ (which is the case, for example, when dealing with angular velocities of molecules in an *isotropic* liquid, but not otherwise), then

$$\langle z^2(\delta t) \rangle = \int_{-\infty}^{\infty} z^2 q(z, \delta t)\, dz$$

and

$$\frac{\partial f(x, t)}{\partial} = \frac{1}{2!} \frac{\langle z^2(\delta t) \rangle}{\partial t} \frac{\partial^2 f(x, t)}{\partial}$$

If $\lim_{\delta t \to 0} \frac{1}{2} \langle z^2(\delta t) \rangle / \delta t$ exists, then denote it by the factor D, so that

$$\frac{\partial f(x, t)}{\partial t} = D \frac{\partial^2 f(x, t)}{\partial x^2} \quad (1.5.2.3)$$

This is a diffusion equation for the *transition probability density function*:

$$f(x, t \mid x_1, t_1) = f(x, t)$$

derived from the Smoluchowski equation with simplifying assumptions. Equation 1.5.2.3 forms the basis of Einstein's (1905) theory of the Brownian movement of translating, (but not rotating) particles.

Illustration

Equation 1.5.2.3 is Markovian, so that its use with molecules, as opposed to particles, is subject to limitations which are severe. The same type of equation is the basis of Debye's theory (1929) of the so-called "rotational Brownian motion," and which leads to the spectroscopic catastrophe of the Debye plateau at terahertz frequencies. The rotational motions of molecules at short times are not Markovian, because Newton's laws are operable between and during "collisions," giving the system a dynamic memory. Neither are they Markovian at long times, because of the vortex effect (Chapter 5).

In deriving Eq. 1.5.2.3 Einstein made use of calculations based on the fact that an external force applied to a suspension of particles in equilibrium is balanced by the osmotic pressure of the suspension. In effect this implies that the Brownian motion is described as that of a massive body immersed in a bath of very many and much smaller particles which may be thought of as changing its linear velocity infinitesimally and infinitely quickly. D may be described in hydrodynamic terms:

$$D = \frac{kT}{6\pi\eta a} = \frac{kT}{m\beta} \quad (1.5.2.4)$$

where η is the macroscopic viscosity of the fluid, a is the radius of a Brownian particle, and m is its mass. The formula assumes that the Brownian particle is a rigid sphere so that the Stokes law applies.

The fundamental solution of Eq. 1.5.2.3 is that corresponding to a "narrow spike of probability density centered on the origin $x = 0$." Physically this means that the Brownian particles are initially found in a narrow region symmetric about the origin and diffuse outwards with time. Figure 1.4.6.1 illustrates this schematically in the rotational case considered later. The solution is

$$f(x, t) = (4\pi D t)^{-1/2} \exp\left(-\frac{x^2}{4Dt}\right) \quad (1.5.2.5)$$

which is infinite at $t = 0$. Equation 1.5.2.5 is a Gaussian distribution with zero mean, and variance $\sigma^2 = 2Dt$, $t > 0$. J. Perrin tested this equation by measuring the displacement of a large number of granules in an emulsion. He obtained the value $N_{AV} = 6.82 \times 10^{23}$ for Avogadro's number, the accepted value being now 6.023×10^{23}. Despite the simplifications, Eq. 1.5.2.3 therefore seems to provide evidence for the existence of molecules and to account roughly for some observable dynamical features, such as the mean square displacement, or σ^2, at observable times *t very long indeed* compared with the picosecond scales associated with molecular dynamics simulations. An account of Perrin's work is given by Chandrasekhar (Wax, 1954).

1.5.3 The Wiener Process

We shall demonstrate eventually that the Liouville theorem and Liouville equation of classical mechanics may be derived from stochastic concepts and probability. To facilitate this aim the fundamental properties of the Wiener process are set out in this section.

Let $X(t)$ denote the displacement after a time t of a particle undergoing Brownian motion so that $X(0) = 0$ by definition. Consider a time interval (s, t) which is long compared with the time between impacts of the particles of the surrounding medium on the Brownian particle. This is to say that the Brownian particle has been "drummed" during (s, t). We make the following assumptions (Calderwood and Coffey, 1977):

1. The displacement $[X(t) - X(s)]$ of the Brownian particle over the time interval (s, t) is the sum $\Sigma_{k=1}^{n}[X(t_k) - X(t_{k-1})]$ of the small displacements $[X(t_k) - X(t_{k-1})]$ of the Brownian particle caused by the impacts of the particles of the surrounding medium.
2. The probability distribution of $X(t_k)$ depends only on $X(t_{k-1})$ and not on $X(t_{k-2})$, $X(t_{k-3})$, etc., so that we have a Markovian process, from which it follows that

$$[X(t_1) - X(s)], [X(t_2) - X(t_1)], \ldots, [X(t) - X(t_{n-1})]$$

   are independent random variables. The process has independent increments.
3. Since $[X(t) - X(s)]$ is the sum of a large number of independent random variables $[X(t_k) - X(t_{k-1})]$, each having *arbitrary distributions*, it follows from the central limit theorem that $[X(t) - X(s)]/\mathrm{Var}[X(t) - X(s)]$ approaches a Gaussian distribution as $n \to \infty$. This is the same as saying that the characteristic function of $[X(t) - X(s)]$ is

$$\phi(u)_{X(t)-X(s)} = \exp\{-\tfrac{1}{2}u^2 \,\mathrm{Var}[X(t) - X(s)]\}$$

A stochastic process is a Wiener process $[X(t), t \geq 0]$ if:

a. $[X(t), t \geq 0]$ has stationary independent increments. This is so if the surrounding medium is in equilibrium.
b. $X(t)$ is normally distributed for $t \geq 0$.
c. $\langle X(t)\rangle = 0$ for $t \geq 0$.
d. $X(0) = 0$.

1.5.3.1 The Variance of the Wiener Process

Assuming that $\mathrm{Var}[X(t)] = f(t)$, we have

$$\begin{aligned} f(t_1 + t_2) &= \langle X^2(t_1 + t_2)\rangle \\ &= \langle [X(t_1 + t_2) - X(t_1) + X(t_1) - X(0)]^2\rangle \end{aligned}$$

since $X(0) = 0$. On multiplying out,

$$f(t_1 + t_2) = \langle [X(t_1 + t_2) - X(t_1)]^2\rangle + \langle [X(t) - X(0)]^2\rangle \qquad (1.5.3.1.1)$$

since

$$\langle [X(t_1 + t_2) - X(t_1)][X(t_1) - X(0)]\rangle = \langle [X(t_1 + t_2) - X(t_1)\rangle\langle X(t_1) - X(0)]\rangle = 0$$

because $[X(t_1 + t_2) - X(t_1)]$ and $[X(t_1) - X(0)]$ are independent random variables and $\langle X(t)\rangle = 0$.

By stationarity we may express Eq. 1.5.3.1.1 as

$$\begin{aligned} f(t_1 + t_2) &= \langle [X(t_2) - X(0)]^2\rangle + \langle [X(t_1) - X(0)]^2\rangle \\ &= \langle X^2(t_2)\rangle + \langle X^2(t_1)\rangle \\ &= f(t_2) + f(t_1) \end{aligned}$$

Let $t_2 = t$, $t_1 = -s$; then

$$f(t - s) = f(t) + f(-s)$$

and the only function which satisfies this functional equation is

$$f(t - s) = c^2(t - s) \qquad (1.5.3.1.2)$$

where c is constant and to be determined.

By stationarity:

$$\begin{aligned} \mathrm{Var}[X(t) - X(s)] &= \mathrm{Var}[X(t - s) - X(0)] \\ &= \mathrm{Var}[X(t - s)] \end{aligned}$$

[since $X(0) = 0$]; so that from Eq. 1.5.3.1.2

$$\begin{aligned} \mathrm{Var}[X(t) - X(s)] &= c^2(t - s) \\ &= c^2|t - s| \qquad (1.5.3.1.3) \end{aligned}$$

in order to ensure a positive variance. Therefore $[X(t) - X(s)]$ is a Gaussian random variable with p.d.f.

$$[c(2\pi|t - s|)^{1/2}]^{-1} \exp\left(\frac{-[X(t) - X(s)]^2}{2c^2|t - s|}\right)$$

1.5.3.2 *The Covariance of the Wiener Process*

We wish to evaluate $K(s, t)$ where

$$K(s,t) = \mathrm{Cov}[X(s), X(t)]$$
$$= \langle [X(s) - \langle X(s)\rangle][X(t) - \langle X(t)\rangle]\rangle$$

Now $\langle X(s)\rangle = \langle X(t)\rangle = 0$, so that

$$K(s,t) = \langle X(s)X(t)\rangle \text{ (the a.c.f.)}$$
$$= \langle X(s)[X(t) - X(s) + X(s)]\rangle$$
$$= \langle X(s)[X(t) - X(s)]\rangle + \langle X^2(s)\rangle$$
$$= \langle X^2(s)\rangle$$

since $X(s)$ and $[X(t) - X(s)]$ are *independent*. Therefore

$$K(s,t) = \langle X^2(s)\rangle = \mathrm{Var}[X(s)] = c^2 s$$
$$= c^2 \min(s,t) = c^2 s \wedge t$$

We now demonstrate the usefulness of these relations in the classical context—the Ornstein–Uhlenbeck theory of the Brownian motion.

1.6 CLASSICAL BROWNIAN THEORY

This is based on *the Langevin equation* (Ornstein and Uhlenbeck), which in its simplest form is (Wax, 1954)

$$\dot{\mathbf{v}}(t) = -\beta \mathbf{v}(t) + \mathbf{A}(t) \tag{1.6.1}$$

This is Newton's law of motion applied to a particle after dividing through by the mass. $\mathbf{v}$ is the center of mass velocity. The first term on the right is due to the frictional resistance imposed by the surrounding medium on the particle. This is represented by the friction coefficient β, related to the viscosity and Einstein diffusion coefficient by Eq. 1.5.2.4. The second term $\mathbf{A}(t)$ represents the random forces or particle impacts. It is the Markov–Gauss stochastic force to which we alluded in an earlier illustration (Section 1.5.2).

This strange equation has inherent in it mathematical inconsistencies that have been largely ignored in physical texts because of its profound intuitive associations. Attempts at rectifying these inconsistencies have been very fruitful, especially, as we shall see later, when dealing with the coefficient β. These attempts have resulted in discoveries such as the Ito–Stratonovich calculi, and were used by Onsager in the context of nonequilibrium thermodynamics and the reciprocal relations. Equation 1.6.1 is also intimately related to the Fokker–Planck class of equations and is a limiting (albeit unphysical) form of the stochastic Liouville equation.

The inconsistencies are not hard to find, and here we summarize the criticisms by Doob (1942).

Let $X(t)$ be the x-coordinate of a particle at time t. Einstein and Smoluchowski treated $X(t)$ as a random variable and found the distribution of $[X(t) - X(0)]$ to be Gaussian with mean zero and a variance $\alpha|t|$ (see preceding sections). However, such a set of random variables $[X(t)]$ is more accurately a *temporally homogeneous* differential stochastic process, that is, a *Wiener process* whose properties we have just described. The sample functions $X(t)$ of this stochastic process are continuous with probability 1. More to the point, $[X(s+t) - X(s)]$ has a standard deviation $\alpha|t|$ so that $[X(s+t) - X(s)]$ is of the order of magnitude of $|t|^{1/2}$. *This implies that $dX(s)/ds$ cannot be finite; that is, the velocity function of the Langevin equation has no time derivative.* However, this directly contravenes the fact that probability hypotheses are imposed on $A(t)$, *including relations between* $A(t)$ and $\mathbf{v}(t)$, (i.e., between *force and velocity*) in order to determine the $\mathbf{v}(t)$ distribution. (If we impose a deterministic relation between force and velocity, then this implies that the velocity must be differentiable.) This velocity distribution cannot, then, satisfy the Langevin equation, *$d\mathbf{v}/dt$ cannot exist* by Wiener statistical algebra, and physically, *the particles in question do not have a finite acceleration*, or in other words the force is indeterminate, as discussed in Section 1.5.2. As we shall see in the rotational context, this has its greatest effect in the far infrared region, that is, at short times.

A different stochastic process describing the $X(t)$ was derived by Uhlenbeck and Ornstein (see Wax, 1954). This new distribution of $X(s-t) - X(s)$ is Gaussian with mean zero and variance

$$\frac{\alpha}{\beta}[\exp(-\beta|t|) - 1 + \beta|t|]$$

approximately $\alpha|t|$ for large t, but $\alpha\beta t^2/2$ for small t. Here β is a second physically determined constant. The displacement function as discussed by Ornstein and Uhlenbeck *has a derivative* $\dot{\mathbf{v}}(t)$, and all the probability distributions needed can be derived from those of $\mathbf{v}(t)$. However, the variance of $[\mathbf{v}(s+t) - \mathbf{v}(s)]$ is

$$\langle [\mathbf{v}(s+t) - \mathbf{v}(s)]^2\rangle = \mathrm{const}(1 - e^{-\beta|t|})$$
$$\sim \mathrm{const}\ \beta|t|$$

Thus $\mathbf{v}(s+t) - \mathbf{v}(s)$ is of the order of magnitude of $|t|^{1/2}$ and $\dot{\mathbf{v}}$ *cannot exist.*

How then, are we to interpret Eq. 1.6.1? The answer is provided by the use of the Wiener process as follows.

1.6.1 Interpretation of the Langevin Equation

Let us write it, following Doob (1942), in the form

$$du(t) = -\beta u(t)\, dt + dB(t) \tag{1.6.1.1}$$

Here $B(t)$ is a differential process, that is, if $t_1 < t_2 < \cdots < t_n$ we suppose that $[B(t_2) - B(t_1)], \ldots, [B(t_n) - B(t_{n-1})]$ are mutually independent random variables. Assume that $B(s+t) - B(s)$ is independent of the initial value s, and that

$$\langle B(s+t) - B(s) \rangle = 0$$
$$\langle [B(s+t) - B(s)]^2 \rangle = c^2 t$$

so that $B(t)$ satisfies the requirements for a Wiener process.

Multiply Eq. 1.6.1.1 by $f(t)$, any continuous function of time, and integrate both sides. Then for all a and b,

$$\int_{t=a}^{b} f(t)\, du(t) = -\beta \int_a^b f(t)u(t)\, dt + \int_a^b f(t)\, dB(t)$$

all the integrals being *well-defined.*

If $f(t) = 1$, then

$$u(b) - u(a) = -\beta \int_a^b u(t)\, dt + B(b) - B(a) \qquad (1.6.1.2)$$

In the Ornstein–Uhlenbeck process $u(t)$ exists and so does the displacement so Eq. 1.6.1.2 may be written for $a = 0$, $b = t$, as

$$B(t) - B(0) = u(t) - u(0) + \beta[X(t) - X(0)] \qquad (1.6.1.3)$$

The time interval $(b - a)$ is long compared with the (infinitesimally small) time between impacts, so that $B(b) - B(a)$ may be written as the series

$$B(b) - B(a) = \sum_{k=1}^{n} [B(t_k) - B(t_{k-1})]$$

with

$$t_0 = a < t_1 < t_2 \cdots < t_{n-1} < t_n = b$$

Therefore we see that the second term on the right of Eq. 1.6.1.2 *may be represented as a Wiener process.* In the rest of this volume we always interpret the Langevin equation in this way. Setting $f(t) = \exp(\beta t)$ we obtain the "classical" solution

$$u(t) = u(0)e^{-\beta t} + \int_0^t e^{-\beta(t-s)}\, dB(s) \qquad (1.6.1.4)$$

which may be obtained in a less rigorous manner from Eq. 1.6.1 by the method of Laplace transforms.

1.6.2 The Properties of $B(t)$

Using the properties of the Wiener stochastic process:

$$\langle B(t_1)B(t_2) \rangle = c^2 \min(t_1, t_2)$$
$$\langle B(t_1) \rangle = \langle B(t_2) \rangle = 0 \qquad (1.6.2.1)$$
$$\langle [B(t_2) - B(t_1)]^2 \rangle = c^2 |t_2 - t_1|$$

We now write

$$t_2 - t_1 = \Delta; \qquad B(t_2) - B(t_1) = \xi(\Delta)$$
$$t_2' - t_1' = \Delta'; \qquad B(t_2') - B(t_1') = \xi(\Delta')$$

in order to discuss the very useful properties of Wiener integrals.

1.6.3 Wiener Integrals

We first note that

$$\begin{aligned}\langle \xi(\Delta)\xi(\Delta') \rangle &= B(t_2)B(t_2') - B(t_1)B(t_2') - B(t_2)B(t_1') + B(t_1)B(t_1') \\ &= c^2|t_2 - t_1'| \\ &= c^2|\Delta \cap \Delta'|\end{aligned}$$

and write $dB(s)$ in terms of ξ:

$$dB(s) = B(s + ds) - B(s) = \xi(ds)$$

Therefore,

$$\int_{-\infty}^{\infty} f(s)\, dB(s) = \int_{-\infty}^{\infty} \xi(ds) f(s)$$

which is termed a *Wiener integral*, and denoted

$$\xi[f] = \int_{-\infty}^{\infty} f(t)\xi(dt) \qquad (1.6.3.1)$$

In Fig. 1.6.3.1 we illustrate how we may approximate any continuous function on $(-\infty, \infty)$ by a series of step functions, and as the number of step functions is increased we obtain the exact representation of the function. So we may approximate the continuous function $f(t)$ and also define $\xi[f]$ by (Nelson, 1967)

$$\xi[f] = \lim_{n \to \infty} \xi[f_n]$$

where f_n is a series of steps (Fig. 1.6.3.1). Therefore

$$\begin{aligned}\langle \xi[f_n] \rangle &= c_1\langle B(t_1) - B(t_1') \rangle + c_2\langle B(t_2) - B(t_2') \rangle + \cdots + c_n\langle B(t_n) - B(t_n') \rangle \\ &= c_1\langle \xi(\Delta_1) \rangle + c_2\langle \xi(\Delta_2) \rangle + \cdots + c_n\langle \xi(\Delta_n) \rangle = 0\end{aligned}$$

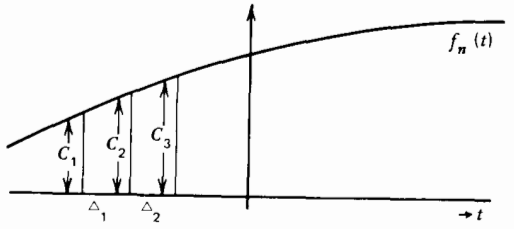

Figure 1.6.3.1 Approximation of a continuous function by step functions.

Here c_1, Δ_1, etc. are defined by reference to Fig. 1.6.3.1. Consider now

$$\xi[f_n] = \int_{-\infty}^{\infty} f_n(t)\xi(dt) = \sum_{r=1}^{n} c_i \xi(\Delta_i)$$

$$\left[\int_{-\infty}^{\infty} f_n(t)\xi(dt)\right]^2 = \sum_{j=1}^{n}\sum_{i=1}^{n} c_i c_j \xi(\Delta_i)\xi(\Delta_j)$$

so that

$$\left\langle\left[\int_{-\infty}^{\infty} f_n(t)\xi(dt)\right]^2\right\rangle = c^2 \sum_{j=1}^{n}\sum_{i=1}^{n} c_i c_j |\Delta_i \cap \Delta_j| = \sum_{i=1}^{n} c_i^2 |\Delta_i| = \int_{-\infty}^{\infty} f^2(t)\, dt$$

Thus we obtain the following very useful result (see Chapter 5):

$$\langle \xi^2[f]\rangle = c^2 \int_{-\infty}^{\infty} f^2(t)\, dt \tag{1.6.3.2}$$

Illustration

1. In exactly the same way we may show that if f and g are continuous functions on $(-\infty, \infty)$, then (Nelson, 1967)

$$\left\langle \int_{-\infty}^{\infty} f(t)\xi(dt) \int_{-\infty}^{\infty} g(t)\xi(dt)\right\rangle = c^2 \int_{-\infty}^{\infty} f(t)g(t)\, dt$$

that is

$$\langle \xi[f]\xi[g]\rangle = c^2 \int_{-\infty}^{\infty} f(t)g(t)\, dt$$

as the reader might like to verify.

1.6.4 The Kramers, Fokker–Planck, and Liouville Equations

The Langevin equation for the motion of a particle of mass m under the influence of an external field of force of potential V is

$$\begin{aligned} m\dot{\mathbf{v}}(t) &= -\nabla V(u_1, u_2, u_3) \\ &\quad - m\beta \mathbf{v}(t) + mb\dot{\mathbf{W}}(t) \end{aligned} \tag{1.6.4.1}$$

This potential may be due to an applied measuring field or, for example, a strong director such as that in the nematic phase of rodlike molecules (Chapter 8). Here $b\dot{\mathbf{W}}(t)$ is a Wiener process, β is time-independent, and $\mathbf{v}$ is the center of mass velocity, with m the mass.

The *Kramers equation*, Klein (1921), is a probability diffusion equation, corresponding to Eq. 1.6.4.1, defined in six-dimensional phase space (i.e., the space of positions and momenta). The derivation is instructive and we follow it through in detail.

If $[u_1(t), u_2(t), u_3(t)]$ are the *Cartesian* coordinates of the particle at time t, then Eq. 1.6.4.1 may be written as

$$d\begin{bmatrix} u_1 \\ u_2 \\ u_3 \\ v_1 \\ v_2 \\ v_3 \end{bmatrix} = \begin{bmatrix} v_1 \\ v_2 \\ v_3 \\ -(\beta v_1 + m^{-1}\partial V/\partial u_1) \\ -(\beta v_2 + m^{-1}\partial V/\partial u_2) \\ -(\beta v_3 + m^{-1}\partial V/\partial u_3) \end{bmatrix} dt + \begin{bmatrix} 0 \\ 0 \\ 0 \\ dW_1 \\ dW_2 \\ dW_3 \end{bmatrix} b$$

which in turn becomes

$$d\begin{bmatrix} x_1 \\ . \\ . \\ . \\ x_6 \end{bmatrix} = \begin{bmatrix} g_1 \\ . \\ . \\ . \\ g_6 \end{bmatrix} dt + b \begin{bmatrix} 0 & 0 & 0 & 0 & 0 & 0 \\ 0 & 0 & 0 & 0 & 0 & 0 \\ 0 & 0 & 0 & 0 & 0 & 0 \\ 0 & 0 & 0 & 1 & 0 & 0 \\ 0 & 0 & 0 & 0 & 1 & 0 \\ 0 & 0 & 0 & 0 & 0 & 1 \end{bmatrix} \begin{bmatrix} dW_1 \\ . \\ . \\ . \\ dW_6 \end{bmatrix}$$

with $X_1 = u_1$; $X_2 = u_2$; ...; $X_6 = v_3$; $g_1 = v_1$; ...; $g_6 = -(\beta v_3 + m^{-1}\partial V/\partial u_3)$. The Langevin equation has the matrix form

$$d\mathbf{x}(t) = \mathbf{g}(t, \mathbf{x})\, dt + b\mathbf{A}\, d\mathbf{W}(t)$$

and as in the one-dimensional case, the Smoluchowski equation is

$$f(\mathbf{x}, t+\delta t) = \int_{-\infty}^{\infty} f(\mathbf{x}, t+\delta t \mid \mathbf{x}', t) f(\mathbf{x}', t)\, d\mathbf{x}' \tag{1.6.4.2}$$

where $\mathbf{x}$ is a vector in $\mathbf{R}^6$ and

$$\int_{-\infty}^{\infty} \equiv \int_{-\infty}^{\infty} \cdots\cdots \int_{-\infty}^{\infty} = \int_{\mathbf{R}^6}$$

We note that Eq. 1.6.4.2 restricts us to the consideration of a *Markovian* f. This is lifted when we consider the Liouville equation for stochastic processes. As in the preceding, we find

$$f(\mathbf{x}, t+\delta t) = \int_{-\infty}^{\infty} q(\mathbf{z}, \delta t \mid \mathbf{x}-\mathbf{z}, t) f(\mathbf{x}-\mathbf{z}, t)\, d\mathbf{z}$$

$$\mathbf{z} = \mathbf{x} - \mathbf{x}'$$

$d^6\mathbf{z}$ is the volume element $(d\mathbf{z}_1 \cdots d\mathbf{z}_6)$. In this case we do *not* make the assumption that q is independent of the value $\mathbf{x}'$ from which the transition is made, and our calculation is more general. Again, assume that the integrand may be expanded in a Taylor series. To this end define

$$r(\mathbf{x}-\mathbf{z}, t, \mathbf{z}, \delta t) = q(\mathbf{z}, \delta t \mid \mathbf{x}-\mathbf{z}, t) f(\mathbf{x}-\mathbf{z}, t)$$

r may be written explicitly as follows:

$$r(x_1 - z_1, x_2 - z_2, \ldots, x_6 - z_6) = qf = \exp\left(-z_1 \frac{\partial}{\partial x_1}\right) r(x_1, x_2 - z_2, \ldots, x_6 - z_6)$$

where

$$\exp\left(-z_1 \frac{\partial}{\partial x_1}\right) = 1 - z_1 \frac{\partial}{\partial x_1} + \frac{1}{2!}\left(z_1 \frac{\partial^2}{\partial x_1^2}\right)^2$$

This implies

$$\begin{aligned} &r(x_1 - z_1, x_2 - z_2, \ldots, x_6 - z_6) \\ &= \exp\left[-\left(z_1 \frac{\partial}{\partial x_1} + z_2 \frac{\partial}{\partial x_2} + \cdots + z_6 \frac{\partial}{\partial x_6}\right)\right] r(x_1 \cdots x_6) \\ &= r(x_1, \ldots, x_6) - \left(z_1 \frac{\partial}{\partial x_1} + \cdots + z_6 \frac{\partial}{\partial x_6}\right) r(x_1 \cdots x_6) \\ &\quad + \frac{1}{2!}\left[\left(z_1 \frac{\partial}{\partial x_1} + \cdots + z_6 \frac{\partial}{\partial x_6}\right)^2\right] r(x_1 \cdots x_6) + \cdots \end{aligned}$$

Therefore, with Eq. 1.6.4.2,

$$\begin{aligned} f(\mathbf{x}, t + \delta t) = &\int_{R^6} r(x_1 \cdots x_6)\, dz_1 \cdots dz_6 \\ &- \sum_{l=1}^{6} \int_{R^6} z_l \frac{\partial}{\partial x_l} r(x_1 \cdots x_6)\, dz_1 \cdots dz_6 \\ &+ \frac{1}{2!} \sum_{l=1}^{6} \sum_{m=1}^{6} \int_{R^6} z_l z_m \frac{\partial^2 r(x_1 \cdots x_6)\, dz_1 \cdots dz_6}{\partial x_l \partial x_m} \end{aligned}$$

We can replace $r(x_1 \cdots x_6)$ by $q(z_1 \cdots z_6,\ \delta t \mid x_1 \cdots x_6,\ t) f(x_1 \cdots x_6, t)$. Now

$$f(x_1 \cdots x_6, t + \delta t) = f(x_1 \cdots x_6, t) + \delta t \frac{\partial f}{\partial t} + O(\delta t)^2$$

and therefore

$$\begin{aligned} \delta t \frac{\partial f}{\partial t} = &- \sum_{l=1}^{6} \frac{\partial}{\partial x_6} [\langle z_l(\delta t, x_1 \cdots x_6, t)\rangle f(x_1 \cdots x_6, t)] \\ &+ \frac{1}{2!} \sum_{l=1}^{6} \sum_{m=1}^{6} \frac{\partial^2}{\partial x_l \partial x_m} [\langle z_l z_m(\delta t, x_1 \cdots x_6, t)\rangle f(x_1 \cdots x_6, t)] \end{aligned}$$

where

$$\langle z_l \rangle = \int_{R^6} z_l q(z_1 \cdots z_6, \delta t \mid x_1 \cdots x_6, t)\, dz_1 \cdots dz_6$$

$$\langle z_l z_m \rangle = \int_{R^6} z_l z_m q(z_1 \cdots z_6, \delta t \mid x_1 \cdots x_6, t)\, dz_1 \cdots dz_6$$

Our next task is to evaluate the limits

$$\lim_{\delta t \to 0} \frac{\langle z_l(\delta t, x_1 \cdots x_6, t)\rangle}{\delta t}$$

and

$$\lim_{\delta t \to 0} \frac{\langle z_l z_m(\delta t, x_1 \cdots x_6, t)\rangle}{\delta t}$$

To do this the Langevin equation (Eq. 1.6.4.1) is integrated between t and $t + \delta t$:

$$\begin{aligned} \mathbf{x}(t + \delta t) - \mathbf{x}(t) &= \int_t^{t+\delta t} \mathbf{g}[\theta, \mathbf{x}(\theta)]\, d\theta + b \int_t^{t+\delta t} \mathbf{A}\, d\mathbf{W}(\theta) \\ &= \mathbf{g}[t, \mathbf{x}(t)]\delta t + b\mathbf{A}[\mathbf{W}(t + \delta t) - \mathbf{W}(t)] \end{aligned}$$

By definition, $\mathbf{x}(t + \delta t) - \mathbf{x}(t) = \mathbf{z}$, and therefore

$$\mathbf{z} = \mathbf{g}[t, \mathbf{x}(t)]\delta t + b\mathbf{A}\xi(\delta t)$$

and

$$\langle \mathbf{z} \rangle = \mathbf{g}[t, \mathbf{x}(t)]\delta t$$

It follows that

$$\lim_{\delta t \to 0} \frac{\langle z_l(\delta t, x_1 \cdots x_6, t)\rangle}{\delta t} = g_l(t, \mathbf{X})$$

and

$$\lim_{\delta t \to 0} \frac{\langle z_m z_l(\delta t, x_1 \cdots x_6, t)\rangle}{\delta t} = b^2 c^2 \delta_{l,m}, \qquad l = 4, 5, 6;\ m = 4, 5, 6$$

where b and c are constants. The second equality follows by taking two distinct components z_l and z_m, multiplying these, ignoring terms in $O(\delta t^2)$, and using the fact that

$$\langle \xi_l(t) \rangle = \langle \xi_m(\delta t) \rangle = 0$$

Therefore one arrives finally at the relation (Kramers, 1940)

$$\frac{\partial f}{\partial t} + \sum_{l=1}^{3} \frac{\partial}{\partial u_l}(v_l f) - \sum_{l=1}^{3} \frac{\partial}{\partial v_l}\left[\left(\beta v_l + \frac{1}{m}\frac{\partial V}{\partial u_l}\right) f\right] - \frac{c^2 b^2}{2} \sum_{l=1}^{3} \frac{\partial^2 f}{\partial v_l^2} = 0 \qquad (1.6.4.3)$$

or in vector notation

$$\frac{\partial f}{\partial t} + \mathbf{v} \cdot \nabla_{\mathbf{u}} f - \frac{1}{m}(\nabla_{\mathbf{v}} f) \cdot \nabla_{\mathbf{u}} V = \beta \nabla_{\mathbf{v}} \cdot (\mathbf{v} f) + \frac{c^2 b^2}{2} \nabla_{\mathbf{v}}^2 f = \frac{Df}{Dt} \qquad (1.6.4.4)$$

with

$$f \equiv f(u_1, u_2, u_3, v_1, v_2, v_3, t + \delta t \mid u_1', u_2', u_3', v_1', v_2', v_3', t)$$

This is the Kramers equation in six-space, the coordinates of a point in this space being $(u_1, u_2, u_3, v_1, v_2, v_3)$. Equations 1.6.4.3 and 1.6.4.4 do not change their form when the space being considered becomes $6N$-dimensioned, which is the usual one of classical statistical mechanics where N is the number of particles, each having three velocity and three displacement coordinates.

In $6N$ space Eq. 1.6.4.4 represents the *generalization* of *Liouville's theorem*, which in classical mechanics is

$$\frac{Df}{Dt} = 0 \tag{1.6.4.5}$$

to include Brownian movement. In particular, on the left hand side of Eq. 1.6.4.4 we have the Stokes operator:

$$\frac{D}{Dt} = \frac{\partial}{\partial t} + \mathbf{v} \cdot \text{grad}$$

while on the right-hand side we have terms arising from the Brownian motion. Equation 1.6.4.4 may be considerably simplified if we assume that the condition $t \gg$ time between collisions is satisfied (i.e., $t \gg \beta^{-1}$). If this is fulfilled then Eq. 1.6.4.4 becomes one in configuration space (u_1, u_2, u_3), only, (Kramers, 1940)

$$\frac{\partial f}{\partial t} = \text{div grad}\left(\frac{kT}{m\beta} + \frac{V}{m\beta}\right) f = \text{div}\left(\frac{kT}{m\beta}\,\text{grad}\, f - \frac{\kappa f}{m\beta}\right) \tag{1.6.4.6}$$

which is also known as Smoluchowski's equation. This is not the same, of course, as his integral equation (Eq. 1.6.4.2).

Illustration

The Smoluchowski equation (Eq. 1.6.4.6) is the starting point of *Debye's theory of rotational Brownian motion* of a sphere. In this case m is replaced by the moment of inertia I and $-\kappa$ by $\mu F \sin\theta (\equiv |\boldsymbol{\mu} \times \mathbf{F}|)$, where $\boldsymbol{\mu}$ is a dipole moment embedded in the sphere and $\mathbf{F}$ the external field vector. Even when corrected for inertial effects, Debye's theory cannot account for the far infrared absorption and is derived within a framework of *Markov statistics*. The breakdown of the Debye equations in the far infrared is illustrated for benzonitrile in Fig. 1.6.4.1. Transparency is regained when inertial effects are fully considered, but otherwise the Debye (1929) theory bears very little resemblance to the measured spectral data. Part of the reason for this is that far infrared frequencies correspond to $t \doteqdot \beta^{-1}$. Also, more realistically, the statistics are non-Markovian, so that β, the friction coefficient, develops a dynamic memory, that is, becomes dependent on time. As we shall see later, β is in general an effective Liouvillian often called the *memory function*.

The *simplest type of Fokker–Planck* equation is an equation in the velocity space spanned by (v_1, v_2, v_3) (in general a $3N$ space). One may show in a manner similar to that by which we derived the Kramers equation that this is

$$\frac{\partial f}{\partial t} = \beta \nabla_{\mathbf{v}} \cdot (\mathbf{v} f) + \frac{c^2 b^2}{2} \nabla_{\mathbf{v}}^2 f \tag{1.6.4.7}$$

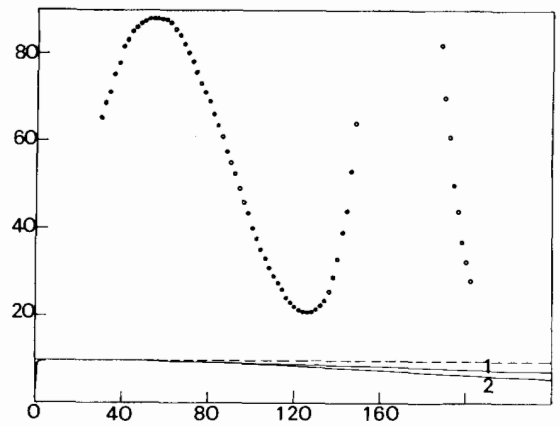

Figure 1.6.4.1 Breakdown of the rotational Smoluchowski equation (cf. Eq. 1.6.4.5) (Debye's theory) in the far infrared, illustrated for liquid benzonitrile. Ordinate: $\alpha(\bar{\nu})$ (Np/cm). Abscissa: $\bar{\nu}(\text{cm}^{-1})$. The low frequency peak is part of the loss process in which we are interested; the other is proper mode of intramolecular origin. The solid line is for (1) a spherical top and (2) the true asymmetric top. The dashed line is the so-called Debye plateau, obtained when inertial effects are neglected. [Reproduced by permission from M. Evans et al., *J. Chem. Soc. Faraday Trans. II*, 75, 1428 (1979).] Note from Fig. 1.1.1 that *the same inertialess* theory gives a seemingly perfect fit over a restricted range of low frequencies. This illustrates the importance of taking an overall view of data from different sources.

For a particle moving along the x axis Eq. 1.6.4.7 reduces to

$$\frac{\partial f}{\partial t} = \beta \frac{\partial}{\partial v_x}(v_x f) + \frac{D}{2}\frac{\partial^2 f}{\partial v_x^2} \tag{1.6.4.8}$$

where $D = c^2 b^2$ is the Einstein diffusion coefficient. This equation is the diffusion equation corresponding to the Langevin equation for a free Brownian particle (i.e., no external potential V):

$$\dot{v}_x(t) = -\beta v_x(t) + A_x(t)$$

where

$$A_x(t) = b\frac{dW_x}{dt}$$

1.7 THE LIOUVILLE EQUATION—NON-MARKOVIAN PROCESSES

The Liouville theorem has already been alluded to above. This is usually written in the standard texts (e.g., Tolman, 1938) as

$$\frac{Df}{Dt} = \frac{\partial f}{\partial t} + \sum_r \left[\dot{\mathbf{q}}_r \frac{\partial f}{\partial \mathbf{q}_r} + \dot{\mathbf{p}}_r \frac{\partial f}{\partial \mathbf{p}_r}\right] = \frac{\partial f}{\partial t} + \sum_r \left[\frac{\partial H}{\partial \mathbf{p}_r}\frac{\partial f}{\partial \mathbf{q}_r} + \frac{\partial H}{\partial \mathbf{q}_r}\frac{\partial f}{\partial \mathbf{p}_r}\right]$$
$$\equiv \frac{\partial f}{\partial t} + \widehat{[H, f]} \equiv \frac{\partial f}{\partial t} + \hat{\mathscr{L}} f = 0 \tag{1.7.1}$$

Here $\mathbf{q}_r$ is the coordinate and $\mathbf{p}_r$ the momentum of the rth particle, H the Hamiltonian, [^] the Poisson bracket operator, and $\hat{\mathscr{L}}$ the Liouville operator, as usual. Equation 1.7.1 describes the statistical behavior of a classical macroscopic assembly under the action of external and internal forces. If N is the number of degrees of freedom of the system then f is a probability distribution in $2N$ dimensions. This is an equation which contains about 10^{20} variables (in the region of Avogadro's number) when we are dealing with molecular motion and interactions. The molecular dynamics simulators reduce this to about 10^2–10^3, so that their dynamic system is just tractable with the maximum computing power available at present.

For analytical purposes it is necessary to modify Eq. 1.7.1 by both reducing and generalizing it, for example, to Kramers' equation. Reduction is the subject of this section. In the past few years this technique has proved to be very fruitful and consists of limiting the degrees of freedom to a small but representative set of thermodynamic averages which define the potential part of the Hamiltonian successively more accurately. Generalization is accomplished by the addition of terms on the right-hand side to account for the mean interaction between this set and the remaining degrees of freedom: the background or heat bath (Sack, 1957).

Df/Dt vanishes because in statistical equilibrium f is independent of the nature of the interaction between the set considered and the background. Of the various possible types of interactions, the ones most often investigated belong to the class of *adiabatic collisions*, which are of such short duration compared with other explicitly considered time intervals such as periods of oscillation or rotation, that they can be treated as instantaneous. Brownian motion is an example where the collisions do not alter the positions of the particles, and their velocities are altered by such small amounts as to be infinitesimal. Correlation between successive impulses is negligible; the effect of such collisions appears as a viscous retardation, $d\mathbf{v}/dt = -\beta\mathbf{v}$, superimposed on which are random fluctuations. There is a succession of small collisions, the explicitly considered particle being surrounded by a heat bath of much smaller ones. However, if the opposite applies, that is, the molecules of the heat bath are much heavier, then adiabatic collisions are such that the positions of the particles remain unaltered on impact, but all coherence between their initial and final velocities is destroyed. After these "large" collisions a particle may have any velocity with a probability according to Boltzmann's law for the given temperature. The processes here are Gaussian and Markovian. The Kramers equation is *restricted to this class*, that is, to the description of adiabatic interactions. In what follows we show how the stochastic Liouville equation may be reduced to a form where this restriction is lifted and where the system can be described in terms of successive thermodynamics averages. First we introduce the concept of *projection* in a Hilbert space.

1.7.1 Projection Operators

A monograph by Berne and Pecora (1976) deals with this subject lucidly. Balescu (1975) describes the rigorous theory in great detail. To proceed we write the Liouville equation making use of the definition:

$$i\hat{\mathscr{L}} = \sum_r \left[\frac{\partial H}{\partial \mathbf{p}_r}\frac{\partial}{\partial \mathbf{q}_r} - \frac{\partial H}{\partial \mathbf{q}_r}\frac{\partial}{\partial \mathbf{p}_r}\right]$$

Define a point $\mathbf{\Gamma}$ in the phase space of positions and momenta used in deriving the Kramers equation:

$$\mathbf{\Gamma} = (\mathbf{q}_1, \ldots, \mathbf{q}_r, \mathbf{p}_1, \ldots, \mathbf{p}_r)$$

The Liouville equation now takes the standard form:

$$\dot{\mathbf{\Gamma}} = \widehat{[\mathbf{\Gamma}, H]} = i\hat{\mathscr{L}}\mathbf{\Gamma}$$

Consider now a linearly independent set $[A_j(t)]$, $j = 1, \ldots, n$ of real valued (implicitly) time-dependent dynamical variables of the given r-particle system. We say that the set of all possible dynamic variables is a real Hilbert space. Now we construct an *ensemble average* in this space, denoted by the brackets $\langle\ \rangle$. We note that this is an *inner product*, so that

$$(A, B) \equiv \langle A(0)B(t)\rangle$$

where A and B are separate variables. If A is for some reason complex, then

$$(A^*, B) \equiv \langle A^*(0)B(t)\rangle$$

(where A^* is the complex conjugate of A) is defined as the inner, or *scalar* product of A and B.

We have at our disposal some fundamental concepts of statistical mechanics to write the inner product (or correlation function) in terms of, for example, the equilibrium canonical distribution function, defined by

$$f(\mathbf{\Gamma}_0) = \frac{\exp(-H(\mathbf{\Gamma}_0)/kT)}{\int e^{-H/kT}\, d\mathbf{\Gamma}_0}$$

where $\mathbf{\Gamma}_0$ is $\mathbf{\Gamma}$ at $t = 0$, and H is the Hamiltonian. We have

$$(A^*, B) = \int d\mathbf{\Gamma} f(\mathbf{\Gamma}) B(\mathbf{\Gamma}) A^*(\mathbf{\Gamma})$$

The properties A and B (or A^* and B) depend on the time only through the dependence of the state $\mathbf{\Gamma}$ on the time—they are implicitly time-dependent. Therefore

$$\dot{A} = \widehat{[A, H]} = i\hat{\mathscr{L}}A$$

which has the formal solution

$$A(\Gamma, t) = \exp(i\hat{\mathscr{L}}t)A(\Gamma, 0) \qquad (1.7.1.1)$$

The time a.c.f. of A may now be defined as

$$C(t) = (A(t),\ A^*) = (e^{i\hat{\mathscr{L}}t}\ A,\ A^*) \tag{1.7.1.2}$$

The a.c.f. is very important to the development of this volume, since it is related by Fourier transform to observable spectral characteristics. Its properties are considered in detail in Section 1.9. Note that

$$C(t) = \int d\Gamma f(\Gamma) A^*(\Gamma) e^{i\hat{\mathscr{L}}t} A(\Gamma) \tag{1.7.1.3}$$

Because of the formal identity of $C(t)$ and the quantum mechanical scalar product (Chapters 9 and 10), the mathematical techniques of quantum mechanics may be used to study classical time-correlation functions.

Definitions (Quantum Mechanical Analogy)

1. Two properties A and B are orthogonal if $(A^*,\ B) = 0$.
2. The propagator $\exp(i\hat{\mathscr{L}}t)$ is an orthogonal operator.
3. If the *norm* $(A^*,\ A)^{1/2}$ is unity then A is *normalized.*
4. By analogy, $f^{1/2}A \equiv \psi_A(\Gamma)$ is a quantum mechanical wave function.
5. The linear, Hermitian operator $\hat{\mathscr{L}}$ is known as the Liouvillian.
6. $C(t)$ is the expectation value of $\exp(i\hat{\mathscr{L}}t)$ in the state ψ_A.
7. The operator $\exp(i\hat{\mathscr{L}}t)$ is unitary; it preserves the norm of A.

The time evolution of $A_j(t)$, the jth dynamical variable, is therefore *a rotation in Liouville space,* with

$$\langle A_j(t)A_k(t)\rangle = \langle A_j(0)A_k(0)\rangle \qquad (j,\ k = 1, \ldots, n)$$

A may be a single molecule or multimolecule property (such as hydrodynamic spin density, number density, etc.). In general it denotes an $n \times 1$ column vector with elements $A_j(t)$, and in this case $\mathbf{A}^T(0)$ denotes its corresponding row vector. Then $\langle \mathbf{A}(t)\mathbf{A}^T(t)\rangle$ denotes the $n \times n$ matrix with elements $\langle A_j(t)A_k(t)\rangle$. By stationarity

$$\langle \mathbf{A}(t)\mathbf{A}^T(t)\rangle = \langle \mathbf{A}(0)\mathbf{A}^T(0)\rangle$$

In this section we wish to show that the column vector $\mathbf{A}(t)$ evolves in time according to the equation

$$\dot{\mathbf{A}}(t) = i\hat{\Omega}_A\mathbf{A}(t) - \int_0^t d\tau \hat{\phi}_A(t-\tau)\mathbf{A}(\tau) + \mathbf{F}_A(t) \tag{1.7.1.4}$$

by using the geometric analogy of Liouville space rotation mentioned already. In this equation $\hat{\Omega}_A$ and $\hat{\phi}_A$ are *operators,* and $\mathbf{F}_A(t)$ a *vector* of random quantities. For the moment, let us confine our discussion to a scalar A.

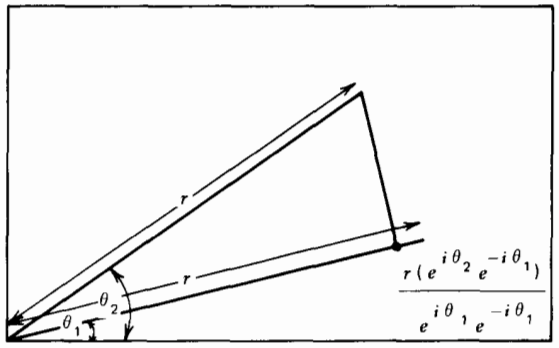

Figure 1.7.1.1 Rotation of a vector in the complex plane.

Rotate the complex number $(r\cos\theta_1, ir\sin\theta_1) \equiv re^{i\theta_1}$ to a new position defined by $(r\cos\theta_2, ir\sin\theta_2) \equiv re^{i\theta_2}$ on the complex plane (Fig. 1.7.1.1). The projection of the second vector onto the first is $[r\cos(\theta_2-\theta_1), ir\sin(\theta_2-\theta_1)]$ which may be written as $r(e^{i\theta_2}e^{-i\theta_1})/(e^{i\theta_1}e^{-i\theta_1})$. Since $A(t) = e^{i\hat{\mathscr{L}}t}A(0)$, then by analogy the scalar product of the two forms *a projection in Liouville space.* The time a.c.f. of A is a projection of $A(t)$ onto $A(0)$. We may project any B onto $A(0)$ using the operator

$$\hat{P} \equiv (\ \ , A^*)(A,\ A^*)^{-1}A$$

That is,

$$\hat{P}B = (B,\ A^*)(A,\ A^*)^{-1}A \tag{1.7.1.5}$$

analogously with the projection in the complex plane.

Definitions

1. Clearly the projection of A onto itself *at the same* t has no effect, $\hat{P}A = A$.
2. Having already projected, say, B onto A with $\hat{P}B$, a further projection $\hat{P}(\hat{P}B) \equiv \hat{P}^2B$ has no further effect by note 1. Therefore $\hat{P}_2^2 = \hat{P}$ and $\hat{P}(\hat{1} - \hat{P}) = \hat{0}$.
3. $(\hat{1} - \hat{P})B$ projects B onto a subspace orthogonal to A, because

$$\begin{aligned}((\hat{1} - \hat{P})B,\ A^*) &= (B,\ A^*) - (B,\ A^*)(A,\ A^*)^{-1}(A,\ A^*)\\ &= 0\end{aligned}$$

The analogy on the Argand diagram is that $\hat{1} - \hat{P}(\equiv \hat{Q})$ performs the projection of Fig. 1.7.1.1, so that the new complex number is $[r\cos(\pi/2-\theta_1), i\sin(\pi/2-\theta_1)]$. That is,

$$re^{i(\pi/2-\theta_1)} = re^{i\pi/2}\,e^{-i\theta_1} = r(\sin\theta_1 - i\cos\theta_1)$$

which is related to the original vector by a rotation through $\pi/2$, and is therefore orthogonal.

4. $\hat{P}$ is a Hermitian operator.
5. $\hat{P} + \hat{Q} = \hat{1}$.
6. Choose any two operators $\hat{\alpha}$ and $\hat{\beta}$; then

$$\hat{\alpha}^{-1} - \hat{\beta}^{-1} \equiv \hat{\alpha}^{-1}(\hat{\beta} - \hat{\alpha})\hat{\beta}^{-1}$$

Further define $\hat{O}_1 + \hat{O}_2 = \hat{1}$ where $\hat{O}_1$ and $\hat{O}_2$ are any two operators. If we choose $\hat{\alpha} = (s\hat{1} - i\hat{\mathscr{L}})$, $\hat{\beta} = (s\hat{1} - i\hat{O}_1\hat{\mathscr{L}})$, where s is the Laplace variable, then (Berne and Pecora, 1976)

$$\frac{\hat{1}}{\hat{1}s - i\hat{\mathscr{L}}} \equiv \frac{\hat{1}}{\hat{1}s - i\hat{O}_1\hat{\mathscr{L}}} + \frac{\hat{1}}{\hat{1}s - i\hat{\mathscr{L}}}\, i(\hat{1} - \hat{O}_1)\hat{\mathscr{L}}\, \frac{\hat{1}}{\hat{1}s - i\hat{O}_1\hat{\mathscr{L}}}$$

Because $\hat{O}_1 + \hat{O}_2 = \hat{1}$, $(\hat{1} - \hat{O}_1) = \hat{O}_2$ and Laplace inversion (Jaeger, 1949) gives

$$e^{i\hat{\mathscr{L}}t} \equiv e^{i\hat{O}_1\hat{\mathscr{L}}t} + \int_0^t d\tau\, e^{i\hat{\mathscr{L}}(t-\tau)}\, i\hat{O}_2\hat{\mathscr{L}} e^{i\hat{O}_1\hat{\mathscr{L}}\tau}$$

That is,

$$e^{i\hat{\mathscr{L}}t} \equiv e^{i\hat{Q}\hat{\mathscr{L}}t} + \int_0^t d\tau\, e^{i\hat{\mathscr{L}}(t-\tau)}\, i\hat{P}\hat{\mathscr{L}} e^{i\hat{Q}\hat{\mathscr{L}}\tau} \qquad (1.7.1.6)$$

is an *operator identity.*

Using these definitions we can proceed to derive Eq. 1.7.1.4. The first step is to *change nothing in a fruitful way*; that is, differentiating the Liouville equation,

$$\dot{A}(t) = e^{i\hat{\mathscr{L}}t} i\hat{\mathscr{L}}A(0) \equiv e^{i\hat{\mathscr{L}}t}(\hat{P} + \hat{Q})i\hat{\mathscr{L}}A(0) \qquad (1.7.1.7)$$

We *stress the obvious* that the final equation we derive from Eq. 1.7.1.7, whatever form it takes, is identical to the Liouville equation from which we started. Any approximate solution of that equation is therefore an approximation to the Liouville equation itself. There is, furthermore, *no hidden assumption* such as that of adiabatic collisions as used in generalizing the Liouville equation to the Kramers equation.

Define now

$$i\hat{\Omega}A(t) \equiv e^{i\hat{\mathscr{L}}(t)}\, \hat{P}_i\hat{\mathscr{L}}A(0) = e^{i\hat{\mathscr{L}}t}\, A(0)(i\hat{\mathscr{L}}A,\, A^*)(A,\, A^*)^{-1}$$

or

$$\hat{\Omega} \equiv (\hat{\mathscr{L}}A,\, A^*)(A,\, A^*)^{-1} \qquad (1.7.1.8)$$

The operator $i\hat{\Omega} = (\dot{A},\, A^*)(A,\, A^*)^{-1}$ may be rewritten as

$$i\hat{\Omega} = \frac{d}{dt}\,[\langle A(t)A^*(0)\rangle\langle A(0)A^*(0)\rangle]_{t\to 0}$$

which, as we shall see later, is identically zero for a.c.f.'s of single

The Liouville equation takes now the form

$$\dot{A}(t) = i\hat{\Omega}A(t) + \exp(i\hat{Q}\hat{\mathscr{L}}t)\hat{Q}i\hat{\mathscr{L}}A(0) + \int_0^t d\tau e^{i\hat{\mathscr{L}}(t-\tau)} i\hat{P}\hat{\mathscr{L}} e^{i\hat{Q}\hat{\mathscr{L}}\tau}\hat{Q}i\hat{\mathscr{L}}A(0) \qquad (1.7.1.9)$$

The second two terms involve the projection operator $\hat{Q}$, which projects an arbitrary variable onto a subspace orthogonal to $A(0)$, so that there is no correlation between the quantity

$$F(t) \equiv e^{i\hat{Q}\hat{\mathscr{L}}t}G = e^{i\hat{Q}\hat{\mathscr{L}}t}\hat{Q}i\hat{\mathscr{L}}A(0) = \hat{Q}e^{i\hat{Q}\hat{\mathscr{L}}\tau}G \equiv \hat{Q}F(t)$$

and $A^*(0)$; that is,

$$(F(t),\, A^*(0)) \equiv \langle F(t)A^*(0)\rangle = 0 \qquad (1.7.1.10)$$

By analogy with the Langevin theory of Brownian motion, $F(t)$ is called the random force, since it has the units of the latter if $A^*(0)$ denotes velocity, and is *uncorrelated* with $A(0)$ for all t.

Definitions

1. If $\mathbf{A}(t)$ is a column vector then $\mathbf{F}$ is of course more than a force, and is in general sometimes said to be Mori-propagated from $\mathbf{A}(0)$, after Mori's work of 1965, described in fuller detail in Chapter 10.
2. In a phenomenon involving the movement of molecules cooperatively, $i\hat{\Omega}$, involving only $\hat{P}$, measures the extent to which the cooperative motion is a *resonance* of its components. In consequence $i\hat{\Omega}$ is known as the *resonance operator.*

1.7.2 The Memory Function and the Kubo Theorem of Fluctuation-Dissipation. Non-Markovian Processes

The integral in Eq. 1.7.1.9 is

$$\int_0^t d\tau \exp[i\hat{\mathscr{L}}(t-\tau)]i\hat{P}\hat{\mathscr{L}}F(\tau)$$

A large part of this volume is devoted to approximating this integral in such a way as to conform with the spectral facts. Using the properties of $\hat{P}$ and $\hat{Q}$,

$$i\hat{P}\hat{\mathscr{L}}F(\tau) = i\hat{P}\hat{\mathscr{L}}\hat{Q}F(\tau) = (i\hat{\mathscr{L}}\hat{Q}F(\tau),\, A^*(0))(A(0),\, A^*(0))^{-1}A(0)$$

Using the *Hermitian* properties of $\hat{P}$ and $\hat{Q}$ we have

$$(i\hat{\mathscr{L}}\hat{Q}F(\tau),\, A^*(0)) = -(F(\tau),\, (\hat{Q}i\hat{\mathscr{L}}A(0))^*) = -(F(\tau),\, F^*(0))$$

so that

$$i\hat{P}\hat{\mathcal{L}}F(\tau) = -(F(\tau),\ F^*(0))(A(0),\ A^*(0))^{-1}A(0)$$

Defining

$$\phi(\tau) \equiv (F(\tau),\ F(0)^*)(A(0),\ A^*(0))^{-1} \tag{1.7.2.1}$$

gives us Eq. 1.7.1.4 for scalar A and F.

Note

It should be clear that Eq. 1.7.1.4 is not the *only way* of rewriting the Liouville equation. The a.c.f. $\phi(t)$ is that of the "random force" $F(t)$. If this is a delta function and if $i\hat{\Omega} = \hat{0}$, Eq. 1.7.1.4, that is, the Liouville equation, reduces to the Langevin equation, taking for A the center of mass linear velocity of a single Brownian particle. The random force of Eq. 1.7.1.4, known also as the Mori equation, *cannot then be Markovian in nature, by Doob's theorem.* The a.c.f. $\langle A(t)A(0)\rangle$ is not exponential. In fact,

$$\dot{C}(t) = i\hat{\Omega}C(t) - \int_0^t d\tau\phi(\tau)C(t-\tau) \tag{1.7.2.2}$$

as the reader might try to verify independently or by reference, for example, to Berne and Pecora (1976) or to McDonald and Hansen (1976). Here $C(t) = (A(t),\ A^*(0)) = \langle A(t)A(0)\rangle$ for real A. Equation 1.7.2.2 illustrates that ϕ is a function that provides the a.c.f. $C(t)$ with a non-Markovian character, that is, gives it a *memory* of dynamic events. Equation 1.7.2.1 shows that it involves the *effective Liouvillian* $\hat{\mathcal{L}}\hat{Q}$ operating on $F(\tau)$. ϕ is therefore often known as the memory function, and Eq. 1.7.2.1 as the *fluctuation-dissipation theorem* of Kubo (1965), who derived it in a different way. In the chapter on liquid crystals, we treat the effect of an arbitrarily large imposed potential on Eq. 1.7.1.4; that is, we generalize the Kramers equation, *removing the constraint of adiabatic collisions.* This in turn allows us to treat the motions of molecules, rather than the dubious elastic particles of "classical" theory.

1.7.3 Mode–Mode Coupling, Single and Multimolecule Motions

The "hidden" power of the Mori equation lies partly in the fact that A is in general a column vector (or matrix) of linearly independent dynamical variables, in this context denoted by **A**. The memory function ϕ is now a matrix operator, and **F** is also a column vector. Equation 1.7.1.4 may be used in various ways to describe the interaction between modes of motion, such as translation and rotation, and also between the motion of a single molecule and many. It is sometimes termed as an equation for mode–mode coupling dynamics. The use of the Mori equation in this way is illustrated in Chapter 5.

The column vector **A** could be assigned the form $\mathbf{A} = \begin{bmatrix}\mathbf{p}\\ \mathbf{J}\end{bmatrix}$ where **p** is the linear momentum and **J** the angular momentum of one single molecule which is translating and rotating, the trajectory being interrupted continually by contact with other molecular potentials. In this case (Chapter 5), the Mori equation allows us to consider a rational approximation scheme for the Liouville equation describing the system. Note that a rototranslational equation of motion is needed if we forego the assumption (as in Brownian motion) that collisions do not alter the positions of the particles involved. More information can be extracted from the system if we include in **A** the angular and linear coordinates, the Euler angles, and Cartesian frame, for example. This is illustrated in Chapter 5.

The most convenient way of describing the cooperative motions of many molecules is to use in **A** *hydrodynamic density variables.* These are introduced in Chapter 5. They are especially useful in the modern theories of light scattering (appendix to Chapter 7), where a component of the polarizability tensor is included with them in **A**, and the spectral consequences evaluated using symmetry rules to simplify the calculation.

Finally, the individual and collective motions may be interrelated by using both molecular and hydrodynamic types of variables in Eq. 1.7.1.4. The results are often known as *macro–micro correlation theorems* (Chapter 3).

1.7.4 The Continued Fraction Theorem—Thermodynamic-Equilibrium Averages

The memory function $\hat{\phi}(t)$ (designated as an operator) is a matrix of correlation functions—in the scalar case $[\phi(t)]$ an a.c.f. of the random force. However, Eq. 1.7.2.2 shows how *any* a.c.f. may be associated via an integro-differential equation with a convolution kernel. We suspect, therefore, that the memory function may be describable in terms of its own memory function $[\phi_1(t)]$. This function $\phi_1(t)$ would be related to $\phi(t)$ in the same way as $\phi(t)$ is related to $C(t)$ by Eq. 1.7.2.2. Therefore $\phi_1(t)$ would also have the properties of an a.c.f. There is nothing, it seems, to prevent us extending the reasoning to $\phi_n(t)$, $n \to \infty$. Let us investigate this in the scalar case.

If we regard F rather than A as the dynamic variable in Eq. 1.7.1.7, then by exactly the same route we arrive at an equation analogous to Eq. 1.7.2.2:

$$\dot{\phi}(t) = i\hat{\Omega}_1\phi(t) - \int_0^t d\tau\phi_1(\tau)\phi(t-\tau) \tag{1.7.4.1}$$

where ϕ_1 is the correlation function of a dynamical variable F_1 which must be orthogonal both to F and to A; that is,

$$\phi_1(t) = \langle F_1(t)F_1(0)\rangle\langle F(0)F(0)\rangle^{-1} \tag{1.7.4.2}$$

for real F_1 and F. Now note that

$$F(t) = e^{i\hat{Q}\hat{\mathscr{L}}t}\hat{Q}i\hat{\mathscr{L}}A(0)$$

so that

$$F(0) = \hat{Q}i\hat{\mathscr{L}}A(0) = \hat{Q}\dot{A}(0) \tag{1.7.4.3}$$

$$= \dot{A}(0) - [\langle \dot{A}(0)A(0)\rangle\langle A(0)A(0)\rangle^{-1}]A(0)$$

$$= \dot{A}(0) \tag{1.7.4.4}$$

if $A(0)$ is real and a single molecule property only, so that $\dot{A}(0)$ and $A(0)$ are uncorrelated. For example, there is no relation between position $\mathbf{q}(0)$ and momentum $\mathbf{p}(0)$, its time derivative. Therefore if we define A as *angular momentum*, the memory function at $t = 0$ is related to the *equilibrium* ($t = 0$) *mean square torque*. This is *undefined* in Langevin's equation for rotational Brownian motion because the collisions are adiabatic. As we see later the correct definition of the mean square torque has all-important spectral consequences, especially in the far infrared (Chapter 4).

Next, note that

$$F_1(t) = e^{i\hat{Q}_1\hat{\mathscr{L}}_1 t}\hat{Q}_1 i\hat{\mathscr{L}}_1 F(0) \tag{1.7.4.5}$$

where we have used a new Liouvillian $\hat{\mathscr{L}}_1$ and projection operator $\hat{Q}_1$. At $t = 0$:

$$\begin{aligned}
F_1(0) &= \hat{Q}_1\dot{F}(0) \\
&= \hat{Q}_1\frac{d}{dt}(\hat{Q}\dot{A}(0)) \\
&= \frac{d}{dt}(\hat{Q}\dot{A}(0)) - \left\{\left\langle\frac{d}{dt}(\hat{Q}\dot{A}(0))F(0)\right\rangle\langle F(0)F(0)\rangle^{-1}\right\}F(0) \\
&= \ddot{A}(0) - [\langle\dot{A}(0)A(0)\rangle\langle A(0)A(0)\rangle + \langle\ddot{A}(0)F(0)\rangle\langle F(0)F(0)\rangle^{-1} \\
&\quad - \langle\dot{A}(0)A(0)\rangle\langle\dot{A}(0)F(0)\rangle\langle A(0)A(0)\rangle^{-1}\langle F(0)F(0)\rangle^{-1}]\dot{A}(0) \\
&\quad - [\langle\ddot{A}(0)A(0)\rangle\langle A(0)A(0)\rangle^{-1} - \langle\dot{A}(0)A(0)\rangle^2\langle A(0)A(0)\rangle^{-2} \\
&\quad - \langle\dot{A}(0)A(0)\rangle\langle\ddot{A}(0)F(0)\rangle\langle A(0)A(0)\rangle^{-1}\langle F(0)F(0)\rangle^{-1} \\
&\quad + \langle\dot{A}(0)A(0)\rangle^2\langle\dot{A}(0)F(0)\rangle\langle A(0)A(0)\rangle^{-2}\langle F(0)F(0)\rangle^{-1}]A(0)
\end{aligned}$$

For single-particle dynamics this equilibrium average reduces to

$$F_1(0) = \ddot{A}(0) - \langle\ddot{A}(0)A(0)\rangle\langle A(0)A(0)\rangle^{-1}A(0) \tag{1.7.4.6}$$

where we have used the fact that $F(0) = \dot{A}(0)$. We may now use a theorem on a.c.f.'s proved later:

$$\frac{d^2}{dt^2}\langle A(t)A(0)\rangle = \langle\ddot{A}(t)A(0)\rangle = -\langle\dot{A}(t)\dot{A}(0)\rangle$$

so that, finally,

$$F_1(0) = \ddot{A}(0) + \frac{\langle\dot{A}(0)^2\rangle}{\langle A(0)^2\rangle}A(0) \tag{1.7.4.7}$$

The zero-time, equilibrium value of the second memory function is

$$\langle F_1(0)F_1(0)\rangle = \langle\ddot{A}(0)^2\rangle - \frac{\langle\dot{A}(0)^2\rangle^2}{\langle A(0)^2\rangle} \tag{1.7.4.8}$$

This is expressible therefore in terms of the mean square torque and the mean square torque derivative, if we take A as the molecular angular momentum.

We see that by taking a series of integro-differential equations to approximate the Liouville equation, the potential energy of the Hamiltonian is described by *successive equilibrium averages*, the values of the memory functions at $t = 0$. We have therefore achieved our aim of relating the $\sim 10^{20}$ variables of the Liouville equation to a few thermodynamic variables. The question is how many. The answer is provided by spectral and simulation data. In the most general case where $\mathbf{A}$ is a column vector the Liouville equation may be expressed as a set of integro-differential equations.

$$\begin{aligned}
\dot{\mathbf{C}}(t) &= i\hat{\Omega}_0\mathbf{C}(t) - \int_0^t d\tau\hat{\phi}_0(\tau)\mathbf{C}(t-\tau) \\
\dot{\hat{\phi}}_0(t) &= i\hat{\Omega}_i\dot{\hat{\phi}}_0(t) - \int_0^t d\tau\hat{\phi}_1(\tau)\hat{\phi}_0(t-\tau) \\
&\vdots \qquad\qquad\qquad \vdots \\
\dot{\hat{\phi}}_{n-1}(t) &= i\hat{\Omega}_n\hat{\phi}_{n-1}(t) - \int_0^t d\tau\hat{\phi}_n(\tau)\hat{\phi}_{n-1}(t-\tau)
\end{aligned} \tag{1.7.4.9}$$

The continued fraction theorem is named after the form obtained when Eqs. 1.7.4.9 are *Laplace transformed.*

Notes

1. The Laplace transform of a function $f(t)$ is denoted by $\tilde{f}(s)$, and for our purposes may be defined as (Jaeger, 1949)

$$\tilde{f}(s) = \int_0^\infty f(t)e^{-st}\,dt \equiv \hat{\mathscr{L}}_a[f(t)]$$

2. A rigorous proof by mathematical induction of the series theorem (Eqs. 1.7.4.9) has been given by Berne and Harp (1970), using bra-ket quantum mechanical notation (see Chapters 9 and 10).
3. It is not straightforward to evaluate the consequences of taking n to infinity in Eqs. 1.7.4.9. This in any case defeats our immediate purpose of trying to approximate the system by a *small* number of averages, $C(0)$, $\phi_0(0)$, etc. In the cases of interest, the series is always *truncated* with $n = 2$ or 3.

Laplace transformation of the matrix equations results in the *continued fraction of matrices*:

$$\tilde{\mathbf{C}}_{\mathbf{A}}(s) = \hat{\mathscr{L}}_a[\langle \mathbf{A}(t)\mathbf{A}^T(0)\rangle\langle \mathbf{A}(0)\mathbf{A}^T(0)\rangle^{-1}] \tag{1.7.4.10}$$

$$= \cfrac{\mathbf{1}}{\mathbf{1}s - i\hat{\Omega}_0 + \cfrac{\mathbf{1}}{\mathbf{1}s - i\hat{\Omega}_1 + \cfrac{\mathbf{1}}{\ddots + \cfrac{\mathbf{1}}{\mathbf{1}s - i\hat{\Omega}_{n-1} + \hat{\phi}_n(s)}\hat{\phi}_{n-1}(0)}\hat{\phi}_1(0)}\hat{\phi}_0(0)}$$

first derived by Mori. Tractable expressions for $\mathbf{C}_{\mathbf{A}}(t)$ are thus generated by finite approximants of the continued fraction. The components of this system may be expressed formally as

$$i\hat{\Omega}_j = \langle \dot{\mathbf{F}}\mathbf{F}_j^T\rangle\langle \mathbf{F}_j\mathbf{F}_j^T\rangle^{-1} \tag{1.7.4.11}$$

$$\hat{\phi}_j(0) = \langle \mathbf{F}_j\mathbf{F}_j^T\rangle\langle \mathbf{F}_{j-1}\mathbf{F}_{j-1}^T\rangle^{-1} \tag{1.7.4.12}$$

$$\mathbf{F}_j = \left[\hat{1} - \sum_{k=0}^{j-1}\hat{P}_k\right] i\hat{\mathscr{L}}\mathbf{F}_{j-1}, \quad j \geq 0; \qquad \hat{P}_0 \equiv \hat{P}$$

$$\dot{\mathbf{F}}_j = \left[\hat{1} - \sum_{k=0}^{j-1}\hat{P}_k\right] i\hat{\mathscr{L}}\mathbf{F}_j, \qquad j \geq 0 \tag{1.7.4.13}$$

where $\hat{P}_k$ projects into the subspace spanned by $\mathbf{F}_k(0)$.

Comments

1. It is *nowhere assumed* in the derivation of the continued fraction that the statistics governing the system are Gaussian or Markovian. However, truncating at a given n implies that one of the memory functions is to be given an analytical dependence on time. If this is, for example, an exponential, then the random force associated with this memory function will be Markovian, and, by implication, Gaussian. In Chapter 3 we show that in this case the Liouville equation takes on a *multidimensional* Markov form.
2. Many models of molecular dynamics in the literature are approximants of this expansion. Indeed, for reasons of consistency it is difficult to see why a model should *not* fit into the expansion represented by Eq. 1.7.1.4, unless of course there is an applied potential of the Kramers kind. The generalization of the Kramers equation is dealt with in Chapters 8–10. The real power of the continued fraction is its general validity for classifying not only molecular but also hydrodynamic and ferromagnetic phenomena (i.e., *transport phenomena*) within the same theoretical frame-

3. The *convergence* of the continued fraction is an open question. Intuitively, it cannot be expected to represent the closed solution when only one or two terms of the series are involved. It is also necessary to choose the dynamic variables making up the vector **A** so as to account for the results from a wide range of experiments. Far infrared and dielectric spectra provide a demanding test of the convergence, or alternatively of the need to choose **A** carefully, so as to take in all the various possibilities of mode–mode coupling. Figure 1.7.4.1 illustrates the behavior of some early approximants in the far infrared region.
4. The meaning of the generalized force $\mathbf{F}_{\mathbf{A}}(t)$ should not be confused with that of the generalized force in classical Lagrangian dynamics. In the Mori formalism $\mathbf{F}_{\mathbf{A}}(0)$ is the component of $\mathbf{A}(0)$ orthogonal to $\mathbf{A}(0)$, whereas $\mathbf{F}_{\mathbf{A}}(t)$ is propagated from $\mathbf{F}_{\mathbf{A}}(0)$ by the special propagator $\exp(i\hat{Q}\hat{\mathscr{L}}t)$.

1.7.4.1 Molecular Rotation

The simplest physical realizations of Eq. 1.7.1.4 occur, for example, in the rotational motion of a sphere, or an asymmetric top about a *fixed* axis. Equation 1.7.1.4 then becomes

$$\dot{\mathbf{J}} + \int_0^t d\tau\hat{\phi}_{\mathbf{J}}(t-\tau)\mathbf{J}(\tau) = \mathbf{F}_{\mathbf{J}}(t) \tag{1.7.4.1.1}$$

where $\mathbf{J}$ is the angular momentum of the rotator, the operator $\hat{\Omega}_{\mathbf{J}}$ is null, $\hat{\phi}_{\mathbf{J}}(t)$ is a tensor, and $\mathbf{F}_{\mathbf{J}}(t)$ is a random driving torque of finite correlation time with mean $\langle \mathbf{F}_{\mathbf{J}}(t)\rangle = \mathbf{0}$. Equation 1.7.4.1.1 is such that the components of each vector are referred to principal body axes (i.e., a frame of reference fixed along the directions of the principal molecular moments of

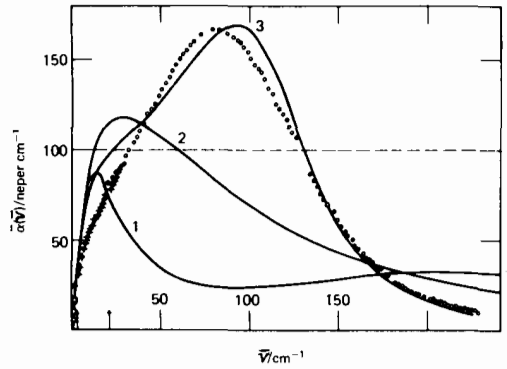

Figure 1.7.4.1 Absorption of CH_2Cl_2 (liquid) in the far infrared compared with some dynamic models (labeled 1–3). The comparison is carried out in such a way that the low frequency loss data are reproduced perfectly in all cases (as in Fig. 1.1.1). We discuss this result further in Chapter 6. [Reproduced by permission from M. W. Evans et al., *J. Chem. Soc. Faraday Trans. II*, 74, 2143 (1978).]

inertia), and $\dot{\mathbf{J}}_k$ denotes rate of change along these axes. Rotational motion of the asymmetric top, treated in Chapter 2, is very complicated. The more general angular equation,

$$\dot{\mathbf{J}}(t) - i\hat{\Omega}_J \mathbf{J}(t) + \int_0^t d\tau \hat{\phi}_J(t-\tau)\mathbf{J}(\tau) = \mathbf{F}_J(t)$$

is *formally valid* for the asymmetric top, but then the quantities $\hat{\Omega}_J$, $\hat{\phi}_J$, and $\mathbf{F}_J$ may not have obvious *physical* meaning. This problem may be circumvented by rewriting the Mori continued fraction as a *multidimensional* Markov equation (Chapters 9 and 10).

Again, when dealing with a *freely rotating body*, it is required that the continued fraction be structured so that it preserves the initial value of the angular momentum a.c.f.: $\langle \mathbf{J}(t)\cdot\mathbf{J}(0)\rangle / \langle \mathbf{J}(0)\cdot\mathbf{J}(0)\rangle = 1$ for all t. This is so only if the "dynamic memory" is totally preserved and, is not possible mathematically if the continued fraction is truncated. Free rotation must be described with an "infinite" continued fraction (Chapter 2). It follows that it is not possible to describe the angular momentum a.c.f. of an *interacting* system with an infinite continued fraction. The same is true of the linear momentum, whose a.c.f. is also conserved when the trajectory is not interrupted. The infinite continued fraction is therefore the Liouville equation for a system consisting of molecules that have neither linear nor angular acceleration. This is possible only when the molecules are infinitely far apart, so that they are not mutually affected by their force fields, that is, when they carry memory intact from the infinite past into the infinite future. The distribution of angular momenta in this case is Maxwellian. It seems obvious that the concept of free rotation (or translation), although convenient, is in conflict with those of entropy maximization, relativity, and the oscillating universe. We may therefore conclude that a system of interacting molecules may be described by successive approximants of the Mori continued fraction, but not by an infinite continued fraction. Strictly speaking, a Mori approximant is an approximation of the Liouville equation in the sense that something is assumed about the statistical distribution of a particular dynamical variable which causes loss of memory at some point in the dynamical history of the system. We are assuming then that the universe is not deterministic.

The generalized force $\mathbf{F}_A(t)$ may or may not be Gaussian depending on the nature of $\mathbf{A}(t)$ and on the geometry of the molecule. For example, if we consider the angular velocity $\boldsymbol{\omega}$ of the sphere, the corresponding random driving torque $\mathbf{F}_\omega(t)$ may be *assumed* Gaussian (although non-Markovian), and so $\boldsymbol{\omega}$ is *conditionally* Gaussian. If, however, we consider the total Euler angle:

$$\theta(t) = \int_0^t \omega_1(\tau)\, d\tau$$

then it is not obvious whether $\mathbf{F}_\theta(t)$ is Gaussian. Here θ is the total angle [illegible] which is

restricted to the range $-\pi \leqslant \theta \leqslant \pi$. In fact, the angular distribution has a *wrapped normal distribution* which we consider later. One possible way of investigating the Gaussian or non-Gaussian nature of $\mathbf{F}_A(t)$ for a given $\mathbf{A}(t)$ is to expand the operator $\exp(i\hat{Q}\hat{\mathscr{L}}t)$. Since $\hat{Q}$ and $\hat{\mathscr{L}}$ commute, and $\hat{Q}^m = \hat{Q}$ (idempotency) for $m \geqslant 1$, we have

$$\mathbf{F}_A(t) = \hat{Q}\dot{\mathbf{A}}(0) + t\hat{Q}i\hat{\mathscr{L}}\dot{\mathbf{A}}(0) - \tfrac{1}{2}t^2\hat{Q}\hat{\mathscr{L}}^2\dot{\mathbf{A}}(0) + \cdots$$

As a simple illustration consider $\mathbf{F}_\theta(t)$ for a disk rotating in its own plane under a Gaussian restoring torque:

$$\Gamma(t) = -k_r[\theta(t) - \theta(0)]$$

where k_r is a constant. The Liouville operator is

$$i\hat{\mathscr{L}} = I\dot{\theta}\frac{\partial}{\partial\theta} - k_r\theta\frac{\partial}{\partial\dot{\theta}}$$

where I is the moment of inertia of the disk, so that

$$(i\hat{\mathscr{L}})^{2m}\dot{\theta} = (-Ik_r)^m\dot{\theta}$$
$$(i\hat{\mathscr{L}})^{2m+1}\dot{\theta} = I^m(-k_r)^{m+1}\theta$$

Since $\hat{Q}\theta(0) = 0$ and $\hat{Q}\dot{\theta}(0) = \dot{\theta}(0)$, it follows that

$$F_\theta(t) = \dot{\theta}(0)\left[1 - \frac{Ik_rt^2}{2!} + \frac{(Ik_r)^2t^4}{4!} - \cdots\right]$$
$$= \dot{\theta}(0)\cos[(Ik_r)^{1/2}t]$$

Similarly, we can show that

$$F_{\dot{\theta}}(t) = \left(\frac{\Gamma(0)}{T}\right)\cos[(Ik_r)^{1/2}t]$$

so that $F_{\dot{\theta}}(t)$ is Gaussian, while the nature of $F_\theta(t)$ is determined by that of $\dot{\theta}(0)$.

The conditional p.d.f.'s discussed above are the most informative functions that can be extracted from a statistical treatment of the microscopic ensemble dynamics, more so than the correlation and memory functions, which are integrals over the density functions. In Chapters 2 and 3 we show that these satisfy a generalized diffusion equation *provided* that $\mathbf{F}_A(t)$ is assumed Gaussian. This equation is similar in form to the Fokker–Planck equation presented already for adiabatic collisions.

1.8 SPECTRAL MOMENTS, AUTOCORRELATION, AND MEMORY FUNCTIONS

The relation of autocorrelation and memory functions to spectral functions is a convenient method of bringing to light the essential properties of the former. These functions of course allow us to relate the statistical space-

time microscopic distribution to spectral information. It is possible to take either time correlations or space correlations, or both, as in the correlation function for the fluctuation of the density:

$$\langle n(0, \mathbf{0}) n(t, \mathbf{r}) \rangle$$

where $\mathbf{r}$ is the molecular center of mass and t the time. This is the normalized probability that a molecule is at $\mathbf{r}$ at the instant t when the probability is unity at the origin at the instant $t = 0$.

The *dipolar* a.c.f. $\langle \mathbf{u}(t) \cdot \mathbf{u}(0) \rangle$ is the mean value of the angular fluctuation, after a time t, of an unit vector lying in the molecule, $\mathbf{u} = \boldsymbol{\mu}/|\boldsymbol{\mu}|$, where $\boldsymbol{\mu}$ is the dipole moment (Scaife, 1959).

In these two examples, and indeed generally, the origin of the coordinate and time can be chosen arbitrarily because of the translational invariance in liquids, and because the correlation functions are stationary in the time for which the liquid is supposed to be in equilibrium. In cases such as dielectric spectroscopy it is necessary to apply an external force field to observe the molecular motions so that the system is perturbed. However, this can be accounted for quite generally by involving in the Mori equation an arbitrarily large extra potential term (as in Chapters 9 and 10). The response of the system can be calculated in the first degree using the spontaneous fluctuations at equilibrium: the fluctuation-dissipation theorem. The Gibbs ensemble average, denoted by $\langle \cdots \rangle$, as we have already seen, can be interpreted using the ergodic theorem, as time averages taken over arbitrary initial times, by which means one can then take spatial averages over the coordinates (see Fig. 1.3.1.1).

Time-correlation functions are well-adapted for a classical mechanical description of molecular behavior, because the equations of motion can be written naturally as functions of time for both translation and rotation. The quantum mechanical analogy is the Heisenberg system rather than the Schrödinger. The interaction between translation and rotation in molecular systems, or alternatively between translation and orientation, is discussed at length in Chapter 5, where *mixed* a.c.f.'s of the form $\langle A(t)B(0) \rangle$ are useful.

The correlation function (denoted by $C(t)$) of two arbitrary and stationary functions of time can be written (Scaife, 1959, 1963)

$$C(t) = \langle A(t)B(0) \rangle$$

where

$$\langle \cdots \rangle \equiv \int_\Gamma dp\, dq\, f_0 \tag{1.8.1}$$

as we have already seen. In classical mechanics, the correlation function is a *real* function of time. Because of the stationary property of the arbitrary function A we may write

$$C(t) = \langle A(t)A(0) \rangle = \langle A(-t)A(0) \rangle = \langle A(0)A(-t) \rangle \tag{1.8.2}$$

so that $C(t)$ is also an *even* function of time.

Derivatives of Correlation Functions with Respect to Time

We have the fundamental relationships (Scaife, 1959, 1963)

$$C(t) = \langle A(t)B(0) \rangle = \langle A(t+\tau)B(\tau) \rangle = \langle A(\tau - t)B(\tau) \rangle$$

so that

$$\frac{\partial C(t)}{\partial t} = \langle \dot{A}(t+\tau)B(\tau) \rangle = -\langle \dot{A}(\tau - t)B(\tau) \rangle \tag{1.8.3}$$

If $t = 0$, then the following results are obtained:

(1) $$\langle \dot{A}(t)B(0) \rangle = -\langle A(t)\dot{B}(0) \rangle \tag{1.8.4}$$

(2) $$\langle \dot{A}(0)A(0) \rangle = 0 \tag{1.8.5}$$

Theorem 1 follows from the fact that, using stationarity,

$$-\langle \dot{A}(\tau - t)B(\tau) \rangle = \langle \dot{A}(\tau)B(\tau + t) \rangle$$

Theorem 2 is the only solution to theorem 1 when $t = 0$ and $A = B$. We have already used these theorems in discussing the equilibrium averages of the Mori continued fraction. Theorem 2 is of course a well-known result since $\dot{A}(0)$ and $A(0)$ are linearly independent, that is, uncorrelated (but *not* for all t).

Taking the second derivative of the *auto*correlation function, then

$$\begin{aligned} \frac{\partial^2}{\partial t^2} \langle A(t+\tau)A(\tau) \rangle &= \frac{\partial}{\partial t} \langle \dot{A}(t+\tau)A(\tau) \rangle \\ &= -\frac{\partial}{\partial t} \langle \dot{A}(\tau)A(t+\tau) \rangle \\ &= -\langle \dot{A}(\tau)\dot{A}(t+\tau) \rangle \end{aligned}$$

and continuing the process we arrive at the following important result:

$$\frac{\partial^{2n}}{\partial t^{2n}} \langle A(t)A(0) \rangle = (-1)^n \left\langle \frac{\partial^n}{\partial t^n} A(t) \left(\frac{\partial^n}{\partial t^n} [A(t)] \right)_{t=0} \right\rangle \tag{1.8.6}$$

This property is valuable when working in the *frequency domain*, because it allows us to relate a correlation function to even spectral moments, that is, to derive sum rules for the areas beneath measurable spectral bands. Before proceeding it is necessary to discuss the relation between the frequency and time domains embodied in the Fourier transforms.

1.8.1 Time Fourier Transforms—Spectral Moments

The Fourier transform of $C(t)$ is defined as (Titchmarsh, 1937)

$$C(\omega) = \frac{1}{2\pi} \int_{-\infty}^{\infty} C(t) e^{-i\omega t}\, dt \tag{1.8.1.1}$$

This implies mathematically that

$$C(t) = \int_{-\infty}^{\infty} C(\omega) e^{i\omega t}\, d\omega \tag{1.8.1.2}$$

Note that to calculate a spectral distribution $[C(\omega)]$ from a *Laplace* transform $\tilde{C}(s)$ of $C(t)$, one need only replace $\tilde{C}(s)$ by $\tilde{C}(-i\omega)$. This is a very useful bit of mathematical manipulation which allows us, for example, to calculate spectra *directly* from the Mori continued fraction without going through the usually intractable process of calculating the time-correlation function itself.

A particularly useful case of Eq. 1.8.1.2 is

$$C(\omega) = \delta(\omega) \tag{1.8.1.3}$$

$$C(t) = \frac{1}{2\pi}$$

where δ denotes a point distribution of frequency, which is the monochromatic line.

Denote by $C^{(n)}(t)$ the nth time derivative of $C(t)$; then

$$C^{(n)}(\omega) = \frac{1}{2\pi} \int_{-\infty}^{\infty} C^{(n)}(t) e^{-i\omega t}\, dt \equiv (i)^n \omega^n C(\omega)$$

$$C^{(n)}(t) = (i)^n \int_{-\infty}^{\infty} \omega^n C^{(n)}(\omega) e^{i\omega t}\, d\omega \tag{1.8.1.4}$$

and developing the integral in Eq. 1.8.1.5,

$$C(t) = \int_{-\infty}^{\infty} C(\omega)\, d\omega + it \int_{-\infty}^{\infty} \omega C(\omega)\, d\omega + \cdots + \frac{i^n t^n}{n!} \int_{-\infty}^{\infty} \omega^n C(\omega)\, d\omega \tag{1.8.1.5}$$

The successive integrals are called *moments* of order 1, 2, 3, etc., of the spectrum $C(\omega)$. Developing now the exponential in Eq. 1.8.1.4,

$$C^{(n)}(t) = i^n \int_{-\infty}^{\infty} \omega^n C^{(n)}(\omega) \left(1 + i\omega t + \frac{(i\omega t)^2}{2!} + \cdots\right) d\omega$$

so that

$$C^{(n)}(0) = i^n \int_{-\infty}^{\infty} \omega^n C(\omega)\, d\omega \tag{1.8.1.6}$$

Equation 1.8.1.6 is a fundamental theorem relating the even spectral moments of a classical a.c.f. to its time derivatives at equilibrium ($t = 0$). The even spectral moments of order $2n$ are equal to the time derivatives of order n at the origin of the correlation functions. Note that this implies that a classical correlation function must be expanded as

$$C(t) = \langle A^2(0)\rangle - \frac{t^2}{2!}\langle \dot{A}^2(0)\rangle + \frac{t^4}{4!}\langle \ddot{A}^2(0)\rangle - \cdots \tag{1.8.1.7}$$

where

$$\langle A^2(0)\rangle = \int_{-\infty}^{\infty} C(\omega)\, d\omega \tag{1.8.1.8a}$$

$$\langle \dot{A}^2(0)\rangle = \int_{-\infty}^{\infty} \omega^2 C(\omega)\, d\omega \tag{1.8.1.8b}$$

$$\vdots$$

$$\langle \dot{A}^{2n}(0)\rangle = \int_{-\infty}^{\infty} \omega^{2n} C(\omega)\, d\omega \tag{1.8.1.8c}$$

Illustrations

1. At short times, that is, as $t \to 0$, a classical correlation function behaves asymptotically as

$$C(t) \doteqdot \langle A^2(0)\rangle - \frac{t^2}{2!}\langle \dot{A}^2(0)\rangle$$

A classical a.c.f. therefore starts to evolve with a zero slope. The exponential a.c.f. of velocity from the Langevin equation contravenes this general law because the mean square force is not defined, and all the odd t powers in the expression of $C(t)$ are still finite if $C(t)$ is exponential. This implies that the Markovian assumption is a rough approximation to the fundamental properties of correlation functions of stationary and ergodic ensembles.

2. The Mori continued fraction should be truncated ideally with a phenomenological function which expands in even t powers. A Markovian assumption anywhere along the chain of memory functions contravenes Eq. 1.8.1.7.

Equation 1.8.1.8a defines the zeroth moment, a spectral integral of the correlation function, which is to say that it defines a sum rule for the area beneath the band of experimental interest. This is independent of all modeling techniques. Equation 1.8.1.8b is useful for far infrared spectroscopy, as we shall see, but the evaluation of mean squares of derivatives of higher order rapidly becomes difficult, and is not a practical way of evaluating the correlation functions at long times.

1.8.2 The Correlation Function in Quantum Mechanics: Detailed Balancing

In quantum mechanics the situation is more complicated. The random variable A is now considered as an operator with which we can no longer form the commutative relation of the classical Eq. 1.8.2. This means that the correlation function, or scalar product, is ***no longer even in time***, and has an imaginary part. Assume for the moment that the spectral density $C(\omega)$ is related to an observable real spectrum. The Fourier integral

theorem implies that the *real part* of $C(t)$ is even, and the imaginary part is odd.

To relate these two parts of $C(t)$ we relate their respective Fourier transforms using a term by term comparison method known as *detailed balancing*. *Denote by* $\hat{\rho}C(\omega)$ and $\hat{\sigma}C(\omega)$, respectively, the even and odd parts of the Fourier transform or spectral density. Then it follows that

$$\frac{\hat{\sigma}C(\omega)}{\hat{\rho}C(\omega)} = \frac{C(\omega) - C(-\omega)}{C(\omega) + C(-\omega)} \tag{1.8.2.1}$$

We assume that $C(\omega)$ is equal to the number of absorption transitions (from the zero level to the level $\hbar\omega$) and that $C(-\omega)$ is equal to the number of transitions (stimulated emission) in the system supposed at equilibrium with the radiation field at the temperature T. These numbers of transitions are respectively proportional to the population of the levels initially. The proportionality coefficient is that of Einstein in the case of a photon radiation. One has

$$\left.\begin{aligned} C(\omega) &\propto e^0 = 1 \\ C(-\omega) &\propto \exp\left(\frac{-\hbar\omega}{kT}\right) \\ C(-\omega) &= \exp\left(\frac{-\hbar\omega}{kT}\right) C(\omega) \end{aligned}\right\} \tag{1.8.2.2}$$

Furthermore,

$$\hat{\sigma}C(\omega) = \tanh\left(\frac{\hbar\omega}{2kT}\right)\hat{\rho}C(\omega) \tag{1.8.2.3}$$

and

$$C(\omega) = \left(1 + \tanh\frac{\hbar\omega}{2kT}\right)\hat{\rho}C(\omega) \tag{1.8.2.4}$$

Denoting by $\hat{R}$ and $\hat{I}$ the real and imaginary parts of the correlation function, it follows that

$$\hat{\rho}C(\omega) = \frac{1}{2\pi}\int_{-\infty}^{\infty} \hat{R}C(t)e^{i\omega t}\,dt \tag{1.8.2.5}$$

with

$$\begin{aligned} \hat{R}C(t) &= \frac{1}{2}[C(t) + C(-t)] \\ &= \frac{1}{2}[\langle\hat{A}(0)\hat{A}(t)\rangle + \langle\hat{A}(0)\hat{A}(-t)\rangle] \\ &= \frac{1}{2}\langle\hat{A}(0)\hat{A}(t) + \hat{A}(t)\hat{A}(0)\rangle \end{aligned} \tag{1.8.2.6}$$

where $\hat{A}$ emphasizes that A is to be regarded as a quantum mechanical operator (Chapters 9 and 10). The last form is the symmetrical quantum correlation function which is real and even, and easily related to the classical correlation function. The spectrum corresponding to this is (from Eqs. 1.8.1.1 and 1.8.1.2) *asymmetric*. This is the case dealing with infrared and Raman line broadening.

The relation between the imaginary and real parts of $C(t)$ can be derived similarly as follows. Comparing imaginary parts in Eq. 1.8.2.4, one has

$$i\hat{I}C(t) = \int_{-\infty}^{\infty} \hat{\sigma}C(\omega)e^{i\omega t}\,d\omega \tag{1.8.2.7}$$

Take the Fourier transform of Eq. 1.8.2.4 and develop the tanh function in ω:

$$i\hat{I}C(t) = \frac{\hbar}{2kT}\int_{-\infty}^{\infty} d\omega e^{i\omega t}\omega\hat{\rho}C(\omega) - \frac{1}{3}\left(\frac{\hbar}{2kT}\right)^3\int_{-\infty}^{\infty} d\omega e^{i\omega t}\omega^3\hat{\rho}C(\omega) + \cdots$$

or

$$\begin{aligned} \hat{I}C(t) &= -\frac{\hbar}{2kT}\frac{d}{dt}\hat{R}C(t) - \frac{1}{3}\left(\frac{\hbar}{2kT}\right)^3\frac{d^3}{dt^3}\hat{R}C(t) \\ &\doteq -\frac{\hbar}{2kT}\frac{d}{dt}\hat{R}C(t) \end{aligned} \tag{1.8.2.8}$$

to a first approximation. In this case the classical and quantum correlation functions are related by

$$C(t) = C_{\text{class}}\left(t - \frac{i\hbar}{2kT}\right) \tag{1.8.2.9}$$

1.8.3 Memory Functions—Series Expansions

The correlation function takes the form (classically)

$$C(t) = \sum_{n=0}^{\infty} a_n \frac{t^{2n}}{(2n)!} \tag{1.8.3.1}$$

where successive a_n are alternatively positive and negative. For single-particle dynamics the memory functions ϕ_0, ϕ_1, etc. must also take the form of Eq. 1.8.3.1. This follows from a consideration of the form of the integro-differential relations of Eqs. 1.7.4.9 when the resonance operator is null. Therefore

$$\begin{aligned} \phi_0(t) &= \sum_{n=0}^{\infty} {}^0k_n \frac{t^{2n}}{(2n)!} \\ &\vdots \\ \phi_m(t) &= \sum_{n=0}^{\infty} {}^mk_n \frac{t^{2n}}{(2n)!} \end{aligned} \tag{1.8.3.2}$$

The coefficients ${}^0k_n, \ldots, {}^mk_n$ are known in terms of the a_n. For example,

$$
\begin{aligned}
{}^0k_0 &\equiv \phi_0(0) = -\frac{a_1}{a_0} = \frac{\langle \dot{A}(0)^2 \rangle}{\langle A(0)^2 \rangle} \\
{}^0k_1 &= -a_2 - {}^0k_0 a_1 = a_1^2 - a_2 \\
{}^1k_0 &\equiv \phi_1(0) = a_1 - \frac{a_2}{a_1} \\
&= \frac{\langle \ddot{A}(0)^2 \rangle}{\langle \dot{A}(0)^2 \rangle} - \frac{\langle \dot{A}(0)^2 \rangle}{\langle A(0)^2 \rangle}
\end{aligned}
\tag{1.8.3.3}
$$

We note that these results for ${}^0k_0$ and ${}^1k_0$ agree with those derived from operating directly on the Liouville equation with $\hat{P}$ and $\hat{Q}$ in Section 1.7. This emphasizes the general nature of the Mori continued fraction.

1.9 CALCULATION OF EQUILIBRIUM AVERAGES IN CLASSICAL MECHANICS—SUM RULES FOR SPECTRAL ANALYSIS

Finally in this chapter on statistics and spectra we illustrate how an equilibrium average such as $\langle A(0)^2 \rangle$, $\langle \dot{A}(0)^2 \rangle$, or $\langle \ddot{A}^2(0) \rangle$ may be calculated for single-molecule motions.

1.9.1 Angular Momentum Autocorrelation Function

We take as an informative example

$$
\langle \mathbf{J}(t) \cdot \mathbf{J}(0) \rangle = \langle \mathbf{J}(0) \cdot \mathbf{J}(0) \rangle - \langle \dot{\mathbf{J}}(0) \cdot \dot{\mathbf{J}}(0) \rangle \frac{t^2}{2!} + \cdots
$$

where $\mathbf{J}$ is the molecular angular momentum. Using the equipartition theorem (described in textbooks on statistical mechanics), the mean square angular momentum $\langle \mathbf{J}(0) \cdot \mathbf{J}(0) \rangle$ may be calculated knowing only the geometric structure of the molecule. It is independent of the precise nature of the intermolecular interaction. The latter is embodied in the product $k_B T$, where T is the absolute temperature and k_B is Boltzmann's constant. Without loss of generality we may limit the following calculation to the angular motion of a *symmetrical top* molecule.

The orientation of the molecule is defined by reference to a unit vector $\mathbf{u}(t)$ along the symmetry axis of the symmetrical top. The angular momentum is now $\mathbf{J} = I'\boldsymbol{\omega}_\parallel + I\boldsymbol{\omega}_\perp$, where I' and I are moments of inertia parallel and perpendicular to $\mathbf{u}$, and $\boldsymbol{\omega}_\parallel$ and $\boldsymbol{\omega}_\perp$ are angular velocities. The rotational kinetic energy is $E = \frac{1}{2} I' \omega_\parallel^2 + \frac{1}{2} I \omega_\perp^2 = 2k_B T$ on average.

As the limit of "free rotation" is approached, $\mathbf{J}$ and E are constant so that $|\boldsymbol{\omega}_\parallel|$ and $|\boldsymbol{\omega}_\perp|$ are also constant. It follows that the angle between $\mathbf{J}$ and $\mathbf{u}$ is likewise constant. The molecular motion is compounded of a rotational motion about its symmetry axis (angular speed $|\boldsymbol{\omega}_\parallel|$) and a *precessional* movement about $\mathbf{J}$ (angular speed $\Omega = |\mathbf{J}|/I$). Introduce now an external force field, that is, an angular *acceleration* caused by an external torque $\mathbf{N}$, so that

$$
\mathbf{N} = \dot{\mathbf{J}} = I'\dot{\boldsymbol{\omega}}_\parallel + I\dot{\boldsymbol{\omega}}_\perp \tag{1.9.1.1}
$$

In this equation the derivatives operate by reference to an external fixed frame. In contrast, the axes of the principal moments of inertia (labeled as in spectroscopic treatises as A, B, C) constitute a mobile frame of reference (m) fixed in the rotating molecule. In Chapter 2 we consider the relation between these frames of reference in greater detail. Using a fundamental theorem of mechanics, one can write

$$
\dot{\mathbf{J}} = \dot{\mathbf{J}}_m + \boldsymbol{\omega} \times \mathbf{J}
$$

where $\boldsymbol{\omega} = \boldsymbol{\omega}_\parallel + \boldsymbol{\omega}_\perp$. Using this we have

$$
\begin{aligned}
\mathbf{N}_\parallel &= I'\dot{\boldsymbol{\omega}}_{\parallel_m} \\
\mathbf{N}_\perp &= I\dot{\boldsymbol{\omega}}_{\perp_m} + (I - I')\boldsymbol{\omega}_\parallel \times \boldsymbol{\omega}_\perp
\end{aligned}
\tag{1.9.1.2}
$$

where $\mathbf{N}_\parallel$ and $\mathbf{N}_\perp$ are the components of the torque $\mathbf{N}$ respectively parallel and perpendicular to the unit vector $\mathbf{u}$. Equations 1.9.1.2 are equivalent to those of *Euler*, with $I_A = I_B = I$, $I_C = I'$; that is,

$$
\begin{aligned}
N_A &= I\dot{\omega}_A - (I - I')\omega_C\omega_B \\
N_B &= I\dot{\omega}_B + (I - I')\omega_C\omega_A \\
N_C &= I'\dot{\omega}_C
\end{aligned}
\tag{1.9.1.3}
$$

Furthermore, we have

$$
\dot{\boldsymbol{\omega}}_\perp = \dot{\boldsymbol{\omega}}_{\perp_m} + \boldsymbol{\omega}_\parallel \times \boldsymbol{\omega}_\perp \tag{1.9.1.4}
$$

Comparing Eqs. 1.9.1.2 and 1.9.1.4,

$$
I\dot{\boldsymbol{\omega}}_\perp = \mathbf{N}_\perp + I'\boldsymbol{\omega}_\parallel \times \boldsymbol{\omega}_\perp
$$

Taking the square

$$
I^2 \boldsymbol{\omega}_\perp \cdot \boldsymbol{\omega}_\perp = N_\perp^2 + I'\omega_\parallel^2\omega_\perp^2 + 2I'\mathbf{N}_\perp \cdot (\boldsymbol{\omega}_\parallel \times \boldsymbol{\omega}_\perp)
$$

The last term vanishes on averaging because

$$
\mathbf{N}_\perp \cdot (\boldsymbol{\omega}_\parallel \times \boldsymbol{\omega}_\perp) = \boldsymbol{\omega}_\parallel \cdot (\boldsymbol{\omega}_\perp \times \mathbf{N}_\perp) = \omega_C(N_B\omega_A - N_A\omega_B)
$$

and $N_B\omega_A$ and $N_A\omega_B$ are equiprobable. Finally we obtain an expression

$$
\langle \boldsymbol{\omega}_\perp \cdot \boldsymbol{\omega}_\perp \rangle = \frac{\langle N_\perp^2 \rangle}{I^2} + \frac{I'}{2I}\left(\frac{2kT}{I}\right)^2 \tag{1.9.1.5}
$$

1.9.1.1 *The Maxwell Distribution of Angular Velocity Components* ($E_\parallel$ *and* $E_\perp$)

The probability distribution of rotational kinetic energies (E) is governed by

$$f(E) = [(kT)^{n/2}\Gamma(n/2)]^{-1} \exp\left(\frac{-E}{kT}\right) E^{n/2-1} \qquad (1.9.1.1.1)$$

where n is the number of degrees of freedom of the relevant kinematic variable. Γ is the gamma function. By the equipartition principle,

$$\langle E \rangle = \int_0^\infty E f(E)\, dE = \frac{nkT}{2}$$

We obtain in this way the probability density of $E_\parallel (n = 1)$ and $E_\perp (n = 2)$

$$f(E_\parallel) = \frac{1}{\sqrt{\pi kT}} \exp\left(\frac{-E_\parallel}{kT}\right) (E_\parallel)^{-1/2}$$

$$f(E_\perp) = \frac{1}{kT} \exp\left(\frac{-E_\perp}{kT}\right)$$

so that

$$\langle \omega_\parallel^{2n} \rangle = \left\langle \left(\frac{2E_\parallel}{I'}\right)^{2n} \right\rangle = \left(\frac{2}{I'}\right)^n \int_0^\infty E_\parallel^n f(E_\parallel)\, dE_\parallel$$

$$= \frac{(2n)!}{2^n n!} \left(\frac{kT}{I'}\right)^n \qquad (1.9.1.1.2)$$

$$\langle \omega_\perp^{2n} \rangle = \left\langle \left(\frac{2E_\perp}{I}\right)^{2n} \right\rangle = n! \left(\frac{2kT}{I}\right)^n \qquad (1.9.1.1.3)$$

Equations 1.9.1.5, 1.9.1.1.2, and 1.9.1.1.3 together provide us with a convenient framework for evaluation not only of successive moments of the angular-momentum a.c.f. but also the *orientational* a.c.f. $\langle \mathbf{u}(t) \cdot \mathbf{u}(0) \rangle$. This is very important from the spectral point of view because the latter is what is observed effectively in 0–THz spectroscopy, and (in a modified form) depolarized light scattering spectroscopy.

1.9.2 Moments of the Orientational Autocorrelation Function

We are interested in the expansion

$$\langle \mathbf{u}(t) \cdot \mathbf{u}(0) \rangle = \langle \mathbf{u}(0) \cdot \mathbf{u}(0) \rangle - \frac{\langle \dot{\mathbf{u}}(0) \cdot \dot{\mathbf{u}}(0) \rangle t^2}{2!} + \cdots \qquad (1.9.2.1)$$

where $\mathbf{u}$ may be defined as, for example, the unit dipole vector $\boldsymbol{\mu}/|\boldsymbol{\mu}|$ of a symmetrical top such as methyl fluoride. It is possible in principle to calculate all the moments using the *purely kinematic* (i.e., completely general) relations:

$$\dot{\mathbf{u}} = \boldsymbol{\omega}_\perp \times \mathbf{u} \qquad (1.9.2.2)$$

$$\boldsymbol{\omega}_\perp = \mathbf{u} \times \dot{\mathbf{u}} \qquad (1.9.2.3)$$

First Moment

By definition,

$$\langle \mathbf{u} \cdot \mathbf{u} \rangle = 1 \qquad [\mathbf{u} \equiv \mathbf{u}(0)]$$

Second Moment

We have

$$\langle \dot{\mathbf{u}} \cdot \dot{\mathbf{u}} \rangle = \langle (\mathbf{u} \times \dot{\mathbf{u}}) \cdot (\mathbf{u} \times \dot{\mathbf{u}}) \rangle = \langle \omega_\perp^2 \rangle$$

$$= \frac{2kT}{I} \qquad (1.9.2.4)$$

since $\mathbf{u} \cdot \mathbf{u} = 1$, $\mathbf{u} \cdot \dot{\mathbf{u}} = 0$.

Third Moment

In this case we use

$$\dot{\boldsymbol{\omega}}_\perp = \mathbf{u} \times \ddot{\mathbf{u}}; \qquad \dot{\boldsymbol{\omega}}_\perp \times \dot{\boldsymbol{\omega}}_\perp = \dot{\mathbf{u}} \cdot \dot{\mathbf{u}} - (\dot{\mathbf{u}} \cdot \ddot{\mathbf{u}})^2$$

so that

$$\langle \ddot{\mathbf{u}} \cdot \ddot{\mathbf{u}} \rangle = \langle \omega_\perp^4 \rangle + \langle \dot{\boldsymbol{\omega}}_\perp \cdot \dot{\boldsymbol{\omega}}_\perp \rangle$$

$$= 2\left(\frac{2kT}{I}\right)^2 \left(1 + \frac{I'}{4I}\right) + \frac{\langle N_\perp^2 \rangle}{I^2} \qquad (1.9.2.5)$$

using Eqs. 1.9.1.5 and 1.9.1.1.3.

Quite generally, therefore, the third moment of $\langle \mathbf{u}(t) \cdot \mathbf{u}(0) \rangle$ may be related to the mean square torque component $\langle N_\perp^2 \rangle$. This method may be extended to the following:

1. Higher moments, although the complexity rapidly increases.
2. A rotating body of any shape, termed the asymmetric top.

Illustrations

1. Figure 1.3.1.2 illustrates the behavior of the mean square torque as simulated for various diatomics in a molecular dynamics run.
2. Figure 1.9.2.1 is a simulation of the torque correlation function and torque derivative correlation function. The latter oscillates very rapidly. In general, the force field governing the dynamic evolution of $\mathbf{u}$ is such that its higher derivatives become effective at long times only. At times very shortly after the arbitrary $t = 0$ the $\mathbf{u}$ vector is reorienting "freely." However, in the absence of a force field, $\langle \mathbf{u}(t) \cdot \mathbf{u}(0) \rangle$ *decays* (unlike $\langle \mathbf{J}(t) \cdot \mathbf{J}(0) \rangle$) owing to the presence of terms such as $2(2kT/I)^2(1 + I'/4I)$, the *centripetal acceleration* arising from the fact that $\mathbf{u}$ is fixed in length.
3. Gordon has calculated the first two odd moments of quantum mechanical origin, as well as quantum contributions to the even moments in this case.

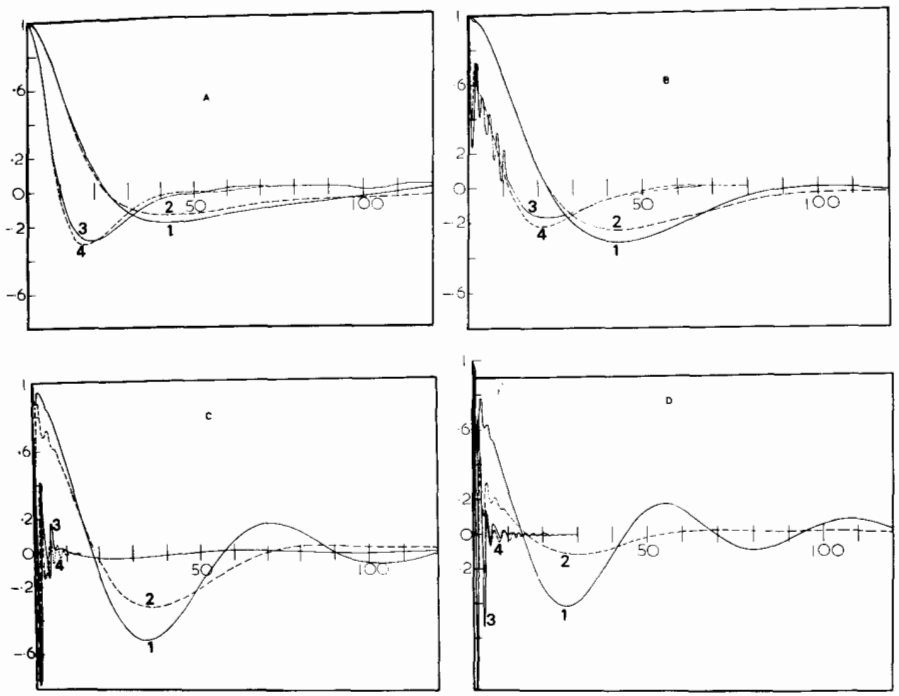

Figure 1.9.2.1 Molecular dynamical simulation by the authors of the torque a.c.f. and the torque derivative a.c.f. in liquid nitrogen. Figs. A–D represent the effect of increasing temperature. (1) Torque a.c.f. (3) Torque derivative a.c.f. (2) Force a.c.f. (4) Force derivative a.c.f. Abscissae: time steps in reduced units.

4. The mean square torque $\langle N_1^2 \rangle$ depends not only on the rotation of molecules *but also on their center of mass translation.* The orientational and angular momentum a.c.f.'s therefore contain information on the mutual interaction of these modes, and should therefore be evaluated with a *matrix* continued fraction (see Chapter 5).

1.9.3 Sum Rules

Equation 1.9.2.1 may therefore be written, for a symmetrical top,

$$C_{\mathbf{u}}(t) \equiv \langle \mathbf{u}(t) \cdot \mathbf{u}(0) \rangle = 1 - \frac{kT}{I} t^2 + \left[2\left(\frac{2kT}{I}\right)^2 \left(1 + \frac{I'}{4I}\right) + \frac{\langle N_1^2 \rangle}{I^2} \right] \frac{t^4}{4!} - \cdots \tag{1.9.3.1}$$

Using Eq. 1.8.1.8b, we have

$$\int_{-\infty}^{\infty} \omega^2 C_{\mathbf{u}}(\omega)\, d\omega = 2\frac{kT}{I} \tag{1.9.3.2}$$

This type of relation is known as a *sum rule.* It turns out (Chapter 3) that $C_{\mathbf{u}}(\omega)$ is related to the power absorption coefficient $\alpha(\omega)$ (measured in Np cm^{-1}), which is related in turn by Maxwell's equations to the complex dielectric permittivity. Equation 1.9.3.2 therefore measures how successfully we have managed to relate $\alpha(\omega)$ and $\omega^2 C_{\mathbf{u}}(\omega)$, that is, what is macroscopically observable and what happens on the molecular scale. This problem is absent in molecular dynamics simulations, but in relating spectra and *actual* molecular dynamics must be considered very carefully, and is the subject of Chapter 3.

Note

The sum rule (Eq. 1.9.3.2) for asymmetric tops has been derived classically by Brot (and quantum mechanically by Gordon):

$$\int_{-\infty}^{\infty} \omega^2 C_{\mathbf{u}}(\omega)\, d\omega \propto \left[\frac{u_y^2 + u_z^2}{I_x} + \frac{u_z^2 + u_x^2}{I_y} + \frac{u_x^2 + u_y^2}{I_z} \right] kT \tag{1.9.3.3}$$

Here u_x, u_y, and u_z are components of the dipole unit vector $\mathbf{u}$ along the x, y, and z direction of the frame of reference defining the principal moments of inertia I_x, I_y, and I_z.

REFERENCES

Atkins, P. W., *Physical Chemistry*, Oxford University Press, Oxford (1978).

Balescu, R., *Equilibrium and Non-Equilibrium Statistical Mechanics*, Wiley, New York (1975).

Berne, B. J. and Harp, G. D., *Adv. Chem. Phys.*, **17**, 63 (1970).

Berne, B. J. and Pecora, R., *Dynamic Light Scattering with Applications to Chemistry, Biology and Physics*, Wiley-Interscience, New York (1976).

Calderwood, J. H. and Coffey, W. T., *Proc. R. Soc. London* **A356**, 269 (1977).

Coffey, W. T. and Evans, M. W., *Mol. Phys.* **35**, 935 (1978).

de Gennes, P. G., *The Physics of Liquid Crystals*, Oxford University Press, Oxford (1974).

Debye, P., *Polar Molecules*, Chemical Catalog Co., New York (1929); reprinted by Dover, New York.

Doob, J. L., (1942), reprinted in Wax (1954).

Jaeger, J. C., *Laplace Transformation*, Methuen, London (1949).

Klein, O., *Ark. Mat. Astron. Fys.* **16** (1921).

Kramers, H. A., *Physica* **7**, 284 (1940).

Kubo, R., *Statistical Mechanics of Equilibrium and Non-Equilibrium*, North-Holland, Amsterdam (1965).

MacDonald, I. R. and Hansen, J. P., *Theory of Simple Liquids*, Academic Press, New York (1976).

McQuarrie, P. A., *Statistical Mechanics*, Harper and Row, New York (1975).

Mori, H., *Prog. Theor. Phys.* **33**(3), 423 (1965).

Nelson, E., *Dynamical Theories of Brownian Motion*, Princeton University Press, Princeton, N.J. (1967).

Pitt, H. R., *Integration, Measure and Probability*, Oliver and Boyd, Edinburgh (1963).

Sack, R. A., *Proc. Phys. Soc. London* **B70**, 402 (1957).

Scaife, B. K. P., E.R.A. Report L/T 392, Electrical Research Association, Leatherhead, Surrey (1959), *Dispersion and Fluctuation in Dielectrics*, in *Progress in Dielectrics*, Vol. 5, Heywood, London (1963).

Titchmarsh, E. C., *Theory of Fourier Integrals*, Oxford University Press, Oxford (1937).

Tolman, R. C., *The Principles of Statistical Mechanics*, Oxford University Press, Oxford (1938).

Wax, N. (Ed.), *Selected Papers on Noise and Stochastic Processes*, Dover, New York (1954).

2

Models for the Translational and Rotational Motion of Molecules

LIST OF SYMBOLS

a	Particle radius
$a(t)$	Response function
$\mathfrak{A}(\omega)$	The power absorption coefficient
$\alpha(\omega)$	The complex polarisability
$b(t)$	After effect function
$B(t)$	Wiener process
β	Friction coefficient
$C(t)$	The angular velocity correlation function
$\mathbf{D}$	Diffusion coefficient
$\mathbf{E}$	External electric field
ϵ	Energy
η	Viscosity coefficient
f	Probability density function
F_s	Intermediate scattering function
$\phi(t)$	Memory function
ϕ	Azimuthal angle of the spherical polar coordinate system
Φ	Characteristic function of the random variable
γ	Coefficient of the Sack continued fraction
G	Green's function
G_s	Van Hove self-correlation function
$\Gamma_s(\boldsymbol{\kappa}, \omega)$	Dynamic structure factor
$\mathbf{H}$	Angular momentum vector of the Euler/Langevin equation
D_n	Weber function
$\mathbf{I}$	Moment of inertia tensor
J	The Smoluchowski current operator
$\boldsymbol{\kappa}$	Scattering vector
m	Molecular mass
$\boldsymbol{\mu}$	Dipole moment vector
$\mathbf{N}$	Torque vector
P_n	nth Legendre polynomial
$\mathbf{r}$	Position vector
ρ	The density function in phase space
σ^2	The variance
θ	Colatitudinal angular displacement

τ_i	Relaxation times of the asymmetric top
τ_2	Characteristic time for the relaxation of Kerr birefringence
$\mathbf{u}$	The dipole unit vector
$\mathbf{v}$	Velocity vector of the center of mass
V	External potential in the Smoluchowski equation
ω	Angular frequency
x	Scalar displacement coordinate
ζ	Friction coefficients of the asymmetric top

2.1 INTRODUCTION

In Chapter 1 in the course of our introduction to fundamental statistical principles we showed how the Kramers equation for the time evolution of probability densities could be derived from the Langevin equation. We went on to show how the Liouville equation could be rewritten as an integral equation and we mentioned that the Liouville equation contains on the average 10^{20} variables. Because of the large number of variables involved, it is clear that no further progress toward a discussion of relaxation problems and their associated spectra can be made unless we introduce specific models for the rotational and translational motions of molecules. We begin by studying models based on the Smoluchowski equation because that equation is the simplest of all probability density diffusion equations.

2.1.1 Solutions of the Smoluchowski Equation

The simplest form of the Smoluchowski equation was originally derived by Einstein in 1905 in the context of his theory of the Brownian movement of a particle in one dimension under no external forces. We have seen in Chapter 1 that this equation is

$$\frac{\partial f}{\partial t} = \frac{kT}{m\beta}\frac{\partial^2 f}{\partial x^2} \qquad (-\infty < x < \infty) \qquad [f = f(x,t)] \tag{2.1.1.1}$$

or

$$\frac{\partial f}{\partial t} = D\frac{\partial^2 f}{\partial x^2} \qquad (-\infty < x < \infty)$$

where $D = kT/m\beta$ is termed the diffusion coefficient. Mathematically our problem is to solve Eq. 2.1.1.1 subject to the initial condition

$$f(x,0) = \delta(x) \tag{2.1.1.2}$$

where $\delta(x)$ denotes the Dirac delta function. The physical meaning of this condition is that the particles are initially squashed together in a narrow clump which is symmetric about the origin and which may be approximated by Dirac's function. The solution of Eq. 2.1.1.1 corresponding to the initial condition, Eq. 2.1.1.2 is called the *fundamental* solution of that equation, and mathematically speaking this solution is the *Green's function* of Eq. 2.1.1.1. For reasons that will become apparent later we write $f(x,t) = G(x,t)$ in all that follows.

We thus have to solve

$$\frac{\partial G}{\partial t} = D\frac{\partial^2 G}{\partial x^2} \qquad (-\infty < x < \infty) \tag{2.1.1.3}$$

subject to

$$G(x,0) = \delta(x) \tag{2.1.1.4}$$

The solution is best effected with the aid of Fourier transforms. On taking the Fourier transform over the space variable x, we have

$$\tilde{G}(\xi,t) = \int_{-\infty}^{\infty} G(x,t)e^{i\xi x}\,dx$$

whence

$$\frac{\partial \tilde{G}(\xi,t)}{\partial t} = -D\xi^2\tilde{G}(\xi,t)$$

and thus

$$\tilde{G}(\xi,t) = A(\xi)e^{-D\xi^2 t} \qquad (t>0)$$

The initial condition is

$$\tilde{G}(\xi,0) = \int_{-\infty}^{\infty}\delta(x)e^{i\xi x}\,dx = 1$$

whence $A(\xi) = 1$ and we have

$$\tilde{G}(\xi,t) = e^{-D\xi^2 t} \qquad (t>0) \tag{2.1.1.5}$$

On inverting Eq. 2.1.1.5 we find that

$$G(x,t) = \frac{1}{2\pi}\int_{-\infty}^{\infty} e^{-D\xi^2 t}e^{-i\xi x}\,d\xi$$

In order to evaluate this integral we make use of the formula

$$\int_0^{\infty} e^{-a^2u^2}\cos 2pu\,du(a^2>0) = \frac{\sqrt{\pi}}{2a}e^{-p^2/a^2}$$

Thus

$$G(x,t) = \frac{1}{(4\pi Dt)^{1/2}}e^{-x^2/4Dt} \tag{2.1.1.6}$$

Equation 2.1.1.6 is a Gaussian distribution with mean zero and variance

$$\sigma^2 = 2Dt \qquad (t>0)$$

Thus (Perrin, 1908)

$$\langle x^2 \rangle = 2Dt \qquad (t > 0)$$

or

$$\langle x^2 \rangle = \frac{2kTt}{m\beta} = \frac{kTt}{3\pi\eta a} \qquad (t > 0)$$

The function $G(x, t)$ or in general $G(\mathbf{r}, t)$ which we have calculated here for the very simplest case of a freely diffusing Brownian particle is of fundamental importance in several fields of physics. In particular $G(\mathbf{r}, t)$ is the *probability per unit volume* of finding a Brownian particle at position $\mathbf{r}$ at time t *given that* it was *initially* at the origin. We mention the field of slow neutron scattering, where Van Hove (1954) has shown that the differential cross sections $d^2\Sigma/d\Omega\, d\epsilon$ per atom for the incoherent scattering of neutrons from a system of atoms into unit solid angle and unit range of energy ϵ may be calculated by means of the formula [in the Born approximation (Van Hove, 1954)]

$$\frac{h\kappa_0}{a_{\text{inc}}^2 \kappa_1} \frac{d^2\Sigma}{d\Omega\, d\epsilon} = \int\int G_s(\mathbf{r}, t) \exp[i(\boldsymbol{\kappa} \cdot \mathbf{r} - \omega t)]\, d\mathbf{r}\, dt \qquad (2.1.1.7)$$

In Eq. 2.1.1.7 $G_s(\mathbf{r}, t)$ is a function which is, in the *classical* limit (Vineyard, 1958), the probability per unit volume of finding the atom at position $\mathbf{r}$ at time t given that it was initially at the origin; a_{inc} is the bound incoherent scattering length per atom; the incident neutrons have wave number $\boldsymbol{\kappa}_0$ and energy ϵ_0; the outgoing neutrons have wave number $\boldsymbol{\kappa}_1$ and energy ϵ; $\boldsymbol{\kappa}_0 - \boldsymbol{\kappa}_1 = \boldsymbol{\kappa}$ is the scattering vector. h is the Planck constant and $d\epsilon = \hbar\, d\omega$, where $\hbar\omega$ is the energy loss of the neutron on scattering. Thus we see that in the classical limit $G_s(\mathbf{r}, t) = G(\mathbf{r}, t)$. We further note that the result of integrating Eq. 2.1.1.7 over the $\mathbf{r}$ variables only is to yield the *characteristic function* of the random variable $\mathbf{r}(t)$. This function is, in the present application, the intermediate scattering function $F_s(\boldsymbol{\kappa}, t)$. For example, for the simple model treated in the earlier part of this section,

$$F_s(\boldsymbol{\kappa}, t) = \exp\left(-\kappa^2 \frac{kT}{m\beta} t\right)$$

while the incoherent scattering cross section $\Gamma_s(\boldsymbol{\kappa}, \omega)$ is simply the Lorentzian

$$\Gamma_s(\boldsymbol{\kappa}, \omega) = \frac{2\gamma\beta\kappa^2}{(\gamma\beta\kappa^2)^2 + \omega^2} \qquad (2.1.1.8)$$

where we have written

$$\gamma = \frac{kT}{m\beta^2} \qquad (2.1.1.9)$$

We now go on to discuss briefly how the one-dimensional Smoluchowski equation may be treated in the presence of an external potential.

2.1.2 Solution of the Smoluchowski Equation in the Presence of an External Potential

The form of the Smoluchowski equation appropriate to the Brownian movement of a particle moving in one dimension under the influence of an external potential $V(x)$ is, from Chapter 1,

$$\frac{\partial f}{\partial t} = \frac{kT}{m\beta} \frac{\partial^2 f}{\partial x^2} + \frac{1}{\beta} \frac{\partial}{\partial x} \left(\frac{\partial V(x)}{\partial x} f \right) \qquad (2.1.2.1)$$

and as before we seek the fundamental solution $G(x, t)$ of this equation, so we have to solve

$$\frac{\partial G}{\partial t} = \frac{kT}{m\beta} \frac{\partial^2 G}{\partial x^2} + \frac{1}{\beta} \frac{\partial}{\partial x} \left(\frac{\partial V(x)}{\partial x} G \right) \qquad (2.1.2.2)$$

subject to the initial condition $G(x, 0) = \delta(x - x_0)$ and by way of application of the results we shall calculate the scattering cross section (or dynamic structure factor) $\Gamma_s(\boldsymbol{\kappa}, \omega)$. In order to proceed with the solution we follow closely a method given by Dieterich et al. (1977). The method we are about to discuss has also been used by Mörsch et al. (1979), by Budó (1949), and by Coffey (1979) in connection with the solution of a number of problems related to the one at hand. The theory has been used to describe the results of computer simulations, exemplified in Fig. 2.1.2.1, which are clearly not reproducible with the simplest kind of Brownian motion theory where the velocity a.c.f. is a purely exponential decay. By means of the ansatz that the complete set of eigensolutions, ψ_n, of the stationary equation may be expressed as

$$\psi_n = e^{-V(x)/2kT} \varphi_n(x)$$

One sees our Smoluchowski equation degenerates into a Schrödinger equation with a temperature-dependent potential

$$\left[-\frac{\partial^2}{\partial x^2} + U(x) \right] \varphi_n(x) = \frac{\lambda_n}{D} \varphi_n(x)$$

where the potential $U(x)$ is given by

$$U(x) = \frac{-V''(x)}{2kT} + \left(\frac{V'(x)}{2kT} \right)^2$$

and where the primes denote differentiation with respect to x. The eigenfunctions φ_n are thus labeled by a wave vector κ (restricted to the first Brillouin zone) and a band index ν: $n = (\kappa, \nu)$. The ground state has eigenvalue $\lambda_0 = 0$. Its wave function is given by

$$\varphi_0 = C \exp\left(-\frac{V(x)}{2kT} \right)$$

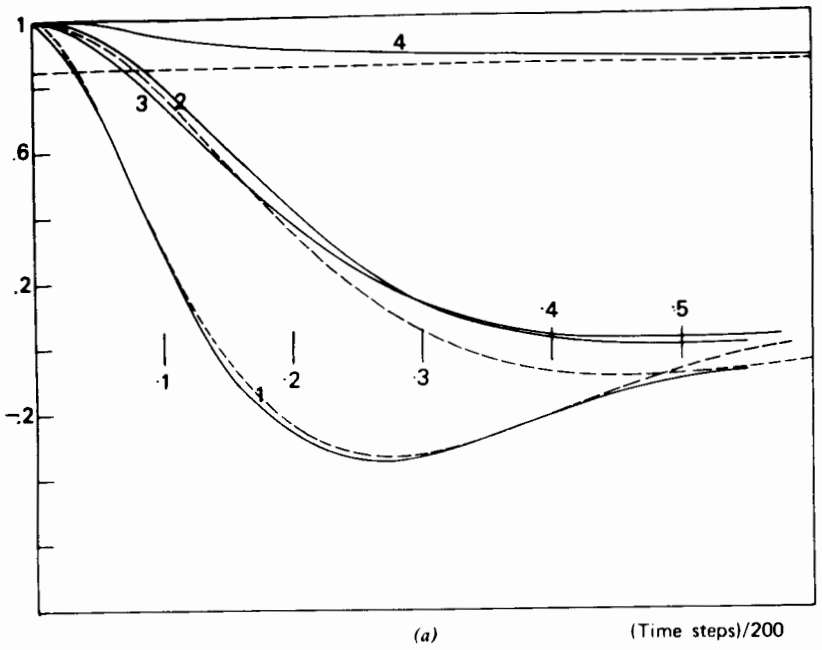

(a) (Time steps)/200

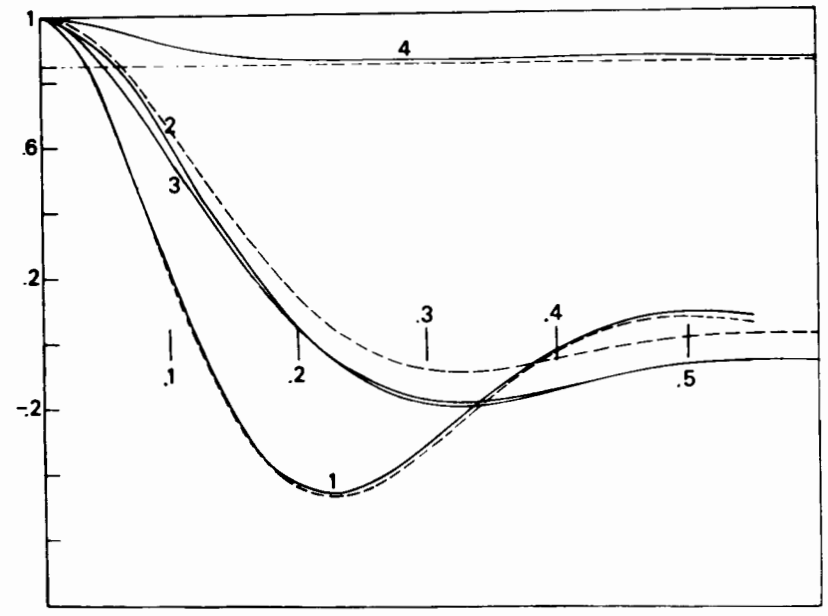

(c) (Time steps)/200

Figure 2.1.2.1 (*a*) (1) Atom–atom simulation of the force a.c.f. $C_F(t)$ in a diatomic molecule for a reduced interatomic separation L^* of 0.1 units. Solid lines: (2) simulated velocity a.c.f., (3) direction of velocity a.c.f., (4) simulated speed a.c.f. The horizontal line is $8/(3\pi)$. Dashed lines: (1) least mean squares fit, Mori approximant. (2) theoretical velocity a.c.f. calculated with the parameters used in l.m.s. fitting (1). (*b*) $L^* = 0.3$. (*c*) $L^* = 0.5$. (*d*) $L^* = 0.7$. [Reproduced by permission from M.W. Evans et al., *J. Mol. Structure* **46**, 395 (1978).]

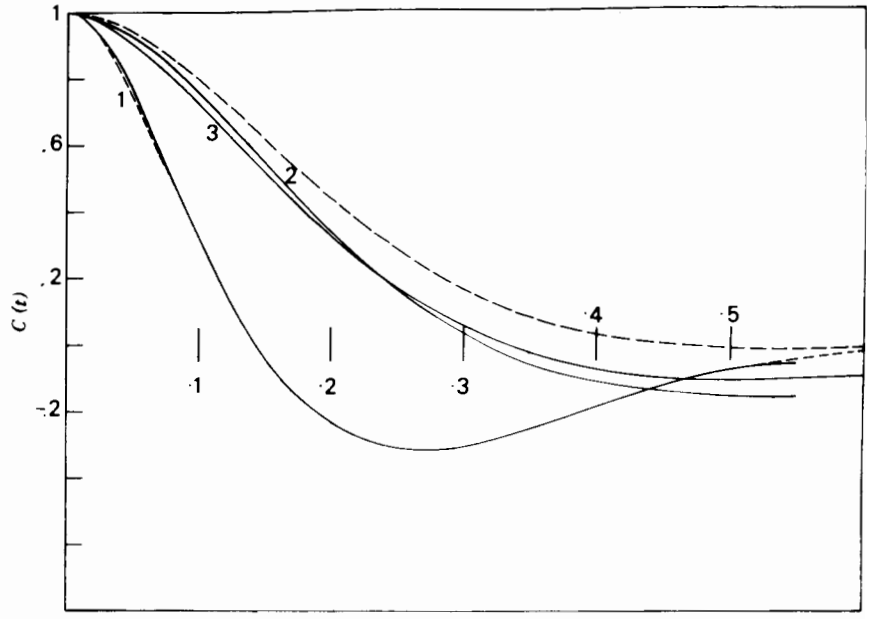

(b)

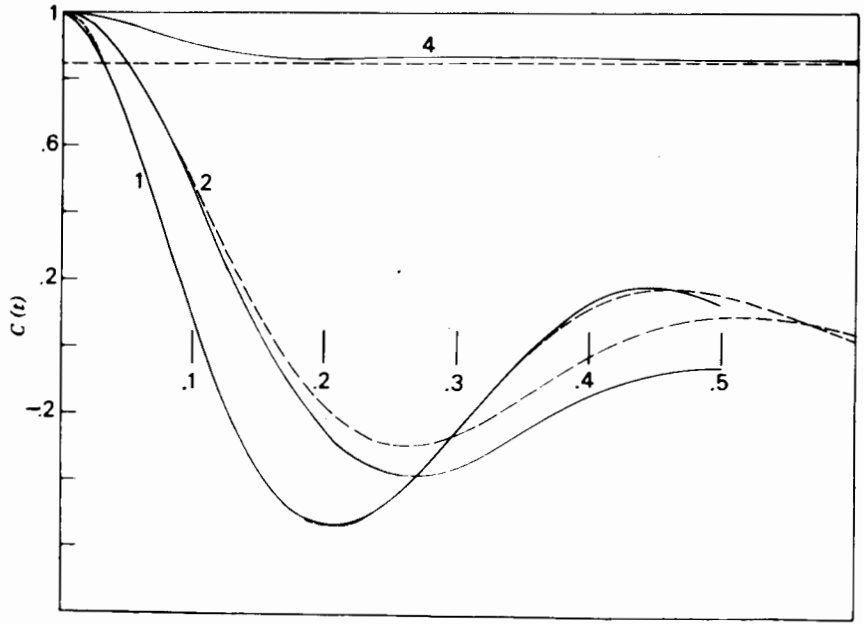

(d)

Figure 2.1.2.1 (*Continued*)

We now restrict ourselves to *periodic* functions $V(x)$ of x so that we may impose *periodic* boundary conditions. Thus $\varphi_0(x)$ is now normalized within the length of the system and the corresponding eigenfunction $\psi_0(x)$ is directly proportional to the equilibrium distribution. The probability density G may now be written in terms of the so-called biorthogonal expansion given by Morse and Feschbach (1953):

$$G(x, t) = \sum_{\kappa, \nu} \varphi_{\kappa, \nu}(x)\varphi_0(x)\varphi^*_{\kappa, \nu}(x)\varphi_0(x_0)^{-1}e^{-\lambda_\nu(\kappa)t}$$

Substituting this equation into our expression for $\Gamma_s(\boldsymbol{\kappa}, \omega)$, one then obtains the dynamic structure factor as a *sum* of Lorentzians:

$$\Gamma_s(\boldsymbol{\kappa}, \omega) = \sum_{\nu=0}^{\infty} \frac{|M_\nu(\kappa^2)|^2\lambda_\nu(\tilde{\kappa})}{\omega^2 + [\lambda_\nu(\tilde{\kappa})]^2} \qquad (2.1.2.3)$$

where

$$M_\nu(\kappa) = \int dx e^{i\kappa x}\varphi_{\kappa, \nu}(x)\varphi_0(x)$$

and $\tilde{\kappa}$ is the wave vector κ reduced to the first Brillouin zone. The most striking consequence of introducing the periodic or indeed any type of potential $V(x)$, then, is the appearance of a *discrete set* of Lorentzian spectra rather than just a single one as in the case of the free Brownian particle. This discrete set of Lorentzians will always be present *whatever* the form of V (always excluding the trivial case where $V = 0$) because the Sturm–Liouville equation (Ince, 1927), will always possess a discrete set of eigenvalues λ_n whenever $V \neq 0$. We thus have seen that, for the greater part, the problem of solving the Smoluchowski equation can be reduced to the solution of a known Sturm–Liouville problem in quantum mechanics. Notwithstanding this, the eigenvalues λ_n and the corresponding eigenfunctions φ_n of the Sturm–Liouville equation can usually be found only by using numerical techniques. We remark on two cases where it is possible to find exact solutions: (*a*) the case where $V(x) \sim x^2$ so that $V' \sim x$ (the parabolic potential); and (*b*) the case where $V'(x) \sim -x + x^{-1}$. In case (*a*) the governing Sturm–Liouville equation reduces to Hermite's equation, whereas in case (*b*) it has been shown by Stratonovitch (1963) that the Sturm–Liouville equation reduces to a form of Laguerre's equation. Finally Mörsch et al. (1979) have recently considered a number of problems in which the potential has the form of a square wave. Again an exact solution is possible in these cases.

A further discussion of physical problems to which structural factors, etc., calculated from the Smoluchowski equation may be applied is given by Dieterich et al. (1977) and by Risken and Vollmer (1978). We now discuss the problem of solving the Fokker–Planck equation for probability distributions in velocity space.

2.2 SOLUTION OF THE FOKKER–PLANCK EQUATION

We start by considering the simplest possible case of the Fokker–Planck equation, namely, the form of that equation which governs the time evolution of the velocity distribution for a free particle moving along the x axis. The Fokker–Planck equation for this problem is

$$\frac{\partial \rho_v}{\partial t} = \frac{\partial}{\partial v}(\beta v \rho_v) + \frac{D}{2}\frac{\partial^2 \rho_v}{\partial v^2} \qquad (2.2.1)$$

This equation may be solved by expanding the function $\rho_v(v, t)$ as follows:

$$\rho_v(v, t) = \sum_{n=0}^{\infty} \varphi_n(t) D_n\left(\sqrt{\frac{m}{kT}}\, v\right) e^{-mv^2/4kT}$$

where the D_n are the Weber functions (Whittaker and Watson, 1927) and we proceed as in the original work of Uhlenbeck and Ornstein. A more transparent method of arriving at the solution, however, is to calculate the characteristic function $\tilde{\rho}_v(\xi, t)$ rather than ρ_v directly; that is, we proceed in the same manner as we did for the Smoluchowski equation in the previous section. Thus, on writing

$$\tilde{\rho}_v(\xi, t) = \int_{-\infty}^{\infty} \rho_v(v, t) e^{-i\xi v}\, dv$$

we have

$$\int_{-\infty}^{\infty} \frac{\partial}{\partial v}(\beta v \rho_v) e^{-i\xi v}\, dv \; - \beta\xi \frac{\partial \tilde{\rho}_v}{\partial \xi}$$

and

$$\int_{-\infty}^{\infty} \frac{\partial^2 \rho_v}{\partial v^2} e^{-i\xi v}\, dv = -\xi^2 \tilde{\rho}_v$$

So our original Fokker–Planck equation is transformed into the *first-order* linear partial differential equation

$$\frac{\partial \tilde{\rho}_v(\xi, t)}{\partial t} = -\frac{D}{2}\xi^2 \tilde{\rho}_v(\xi, t) - \beta\xi \frac{\partial \tilde{\rho}_v(\xi, t)}{\partial \xi}$$

or

$$\frac{\partial \tilde{\rho}_v(\xi, t)}{\partial t} + \beta\xi \frac{\partial \tilde{\rho}_v}{\partial \xi} = -\frac{D}{2}\xi^2 \tilde{\rho}_v \qquad (2.2.2)$$

We make a small aside here concerning the solution of first-order linear partial differential equations such as Eq. 2.2.2. An equation of the form

$$P(x, y, z)\frac{\partial z}{\partial x} + Q(x, y, z)\frac{\partial z}{\partial y} = R(x, y, z)$$

is satisfied by the function defined by the equation

$$\Phi(x, y, z) = 0$$

if (Margenau and Murphy, 1956)

$$P\frac{\partial\Phi}{\partial x}+Q\frac{\partial\Phi}{\partial y}+R\frac{\partial\Phi}{\partial z}=0$$

To solve the equation we form the subsidiary system (Bateman, 1956)

$$\frac{d\Phi}{O}=\frac{dx}{P(x,y,z)}=\frac{dy}{Q(x,y,z)}=\frac{dz}{R(x,y,z)}$$

In the problem at hand, $P=1$, $Q=\beta\xi$, $R=(-D/2)\xi^2\tilde{\rho}_v$: hence our subsidiary system is

$$\frac{dt}{1}=\frac{d\xi}{\beta\xi}=-\frac{d\tilde{\rho}}{\frac{1}{2}D\xi^2\tilde{\rho}_v}$$

and the general solution of this system is

$$\Phi\left\{\xi e^{-\beta t},\left[\exp\left(-\frac{D\xi^2}{4\beta}\right)\right]\tilde{\rho}_v\right\}=0 \tag{2.2.3}$$

which may be written as

$$\tilde{\rho}_v(\xi,t)=\psi(\xi e^{-\beta t})e^{D\xi^2/4\beta}$$

where ψ is an arbitrary function, the value of which for the present problem is found as follows.

Since the initial distribution of velocities has the form

$$\rho_v(v,0)=\delta(v-v_0)$$

then

$$\tilde{\rho}_v(\xi,0)=e^{-i\xi v_0}$$

and on setting $t=0$ in Eq. 2.2.3

$$e^{-i\xi v_0}=\psi(\xi)e^{D\xi^2/4\beta}$$

and therefore

$$\psi(\xi)=e^{-i\xi v_0}e^{-D\xi^2/4\beta}$$

Hence it follows that

$$\psi(\xi e^{-\beta t})=\exp(-iv_0\xi e^{-\beta t})\exp\left[-\frac{D\xi^2}{4\beta}e^{-2\beta t}\right]$$

whence

$$\tilde{\rho}_v(\xi,t)=\exp\left[-iv_0\xi e^{-\beta t}+\frac{D\xi^2}{4\beta}(1-e^{-2\beta t})\right] \tag{2.2.4}$$

Equation 2.2.4 is the characteristic function of a *Gaussian* random variable having mean

$$\langle v(t)\rangle=v_0e^{-\beta t} \tag{2.2.5}$$

and variance σ^2, where

$$\sigma^2=\langle[v(t)-\langle v(t)\rangle]^2\rangle=\frac{D}{2\beta}(1-e^{-2\beta t}) \tag{2.2.6}$$

Thus the probability distribution of the velocities in the Ornstein–Uhlenbeck process is

$$\rho_v(v,t)=\frac{1}{\sigma\sqrt{2\pi}}\exp\left[-\frac{(v(t)-\langle v(t)\rangle)^2}{2\sigma^2}\right]$$

with these quantities given by Eqs. 2.2.5 and 2.2.6. Wang and Uhlenbeck in 1945 (see Wax, 1954) showed how the solution procedure just outlined may be applied to the more general Fokker–Planck equation pertaining to an electric circuit having n meshes, each mesh being driven by a white noise voltage. Their form of the Fokker–Planck equation is

$$\frac{\partial\rho_v(\mathbf{y},t)}{\partial t}=-\sum_{i=1}^{n}\lambda_i\frac{\partial}{\partial y_i}[y_i\rho_v(\mathbf{y},t)]+\frac{1}{2}\sum_{i,j=1}^{n}\sigma_{ij}\frac{\partial^2\rho_v(\mathbf{y},t)}{\partial y_i\partial y_j} \tag{2.2.7}$$

of which it is required to find that solution (λ_i and σ_{ij} are parameters) which for $t=0$ becomes

$$\rho_v(\mathbf{y},0)=\delta(y_1-y_{10})\delta(y_2-y_{20})\cdots\delta(y_n-y_{n0})$$

$\mathbf{y}$ is the vector $\mathbf{y}=(y,\ldots,y_n)$ in $\mathfrak{R}^n$. Again we introduce instead of ρ_v its Fourier transform

$$\tilde{\rho}_v(\boldsymbol{\xi},t)=\int_{\mathfrak{R}^n}\rho_v(\mathbf{y},t)\exp(-i\boldsymbol{\xi}\cdot\mathbf{y})\,d\mathbf{y}$$

from which it follows (in exactly the same manner as we outlined for the one dimensional case above) that $\tilde{\rho}_v(\boldsymbol{\xi},t)$ must satisfy the linear, first-order partial differential equation:

$$\frac{\partial\tilde{\rho}_v}{\partial t}(\boldsymbol{\xi},t)-\sum_{i=1}^{n}\lambda_i\xi_i\frac{\partial\tilde{\rho}_v}{\partial\xi_i}(\boldsymbol{\xi},t)=-\frac{1}{2}\sum_{i,j}\xi_i\xi_j\tilde{\rho}_v(\boldsymbol{\xi},t)$$

The subsidiary equations are

$$\frac{dt}{1}=-\frac{d\xi_1}{\lambda_1\xi_1}=-\frac{d\xi_2}{\lambda_2\xi_2}\cdots=-\frac{d\xi_n}{\lambda_n\xi_n}=-\frac{d\tilde{\rho}_v}{\frac{1}{2}\sum_{i,j}\sigma_{ij}\xi_i\xi_j\tilde{\rho}_v}$$

These may be integrated in exactly the same manner as before and one finds that the general solution is

$$\tilde{\rho}_v(\boldsymbol{\xi},t)=\psi(\xi_1e^{\lambda_1t},\xi_2e^{\lambda_2t},\ldots,\xi_ne^{\lambda_nt})\exp\left(\frac{1}{2}\sum_{i,j}\frac{\sigma_{ij}\xi_i\xi_j}{\lambda_i+\lambda_j}\right)$$

where again ψ is an arbitrary function. Again for $t=0$ with the initial conditions given, we have

$$\tilde{\rho}_v(\boldsymbol{\xi},0)=\exp(-i\boldsymbol{\xi}\cdot\mathbf{y}_0)$$

Therefore our arbitrary function ψ must be

$$\psi(\xi, 0) = \exp\left(-\frac{1}{2}\sum_{i,j}\frac{\sigma_{ij}\xi_i\xi_j}{\lambda_i+\lambda_j} - i\sum_j \xi_j y_{j0}\right)$$

and we obtain for $\tilde{\rho}_v(\xi, t)$

$$\tilde{\rho}_v(\xi, t) = \exp\left(-i\sum_j \xi_j y_{j0}\exp(\lambda_j t) + \frac{1}{2}\sum_{i,j}\frac{\sigma_{ij}\xi_i\xi_j}{\lambda_i+\lambda_j}[1-\exp(\lambda_i+\lambda_j)t]\right) \tag{2.2.8}$$

This is the Fourier transform of an n-dimensional Gaussian distribution with the mean values

$$\langle y_i\rangle = y_{i0}\exp(\lambda_i t)$$

and the variances

$$\langle (y_i - \langle y_i\rangle)(y_j - \langle y_j\rangle)\rangle = \frac{-\sigma_{ij}}{\lambda_i+\lambda_j}[1-\exp(\lambda_i+\lambda_j)t]$$

This solution obtained by Wang and Uhlenbeck is of considerable help in solving the Kramers equation for a particle in a parabolic potential. Since, for that particular problem, the Kramers equation can be transformed into an equation similar to Eq. 2.2.7, we proceed to consider the progress that has been made in calculating probability distributions from the Kramers equation.

2.3 SOLUTIONS OF THE KRAMERS EQUATION

In this section we are faced with the most difficult question in the theory of the translational Brownian movement, namely, how to determine the probability distribution $f(\mathbf{r}, t)$ in configuration space when the Smoluchowski approximation no longer applies and the velocity dependence of the density in phase space must be taken into account. Thus $\rho(\mathbf{r}, \mathbf{v}, t)$ will satisfy the Kramers equation:

$$\frac{\partial\rho}{\partial t} + \mathbf{v}\cdot\nabla_r\rho - \frac{(\nabla_r V)}{m}\cdot\nabla_v\rho = \beta\nabla_v\cdot\rho\mathbf{v} + \frac{\beta kT}{m}\nabla_v^2\rho \tag{2.3.1}$$

Little progress was made toward answering this question, which had originally been posed by Kramers in 1940, until the work of Brinkman in 1956. Before the publication of Brinkman's work and more recently that of Risken and Vollmer (1978) the only cases in which the distribution $f(\mathbf{r}, t)$ had been determined when $\rho(\mathbf{r}, \mathbf{v}, t)$ obeys Eq. 2.3.1 were those of the free Brownian particle when $V = 0$ and the case of the Brownian particle moving in a parabolic potential well. In both these problems the task of solving Eq. 2.3.1, and thus determining $f(\mathbf{r}, t)$, reduces to that of solving a Fokker–Planck type of equation having the form of Eq. 2.2.7. The steps

required to reduce Eq. 2.3.1. to the Fokker–Planck equation are reasonably elementary and have been given in some detail by Wang and Uhlenbeck (1945) (see Wax, 1954), so we merely write the results for $f(\mathbf{r}, t)$ [where $f(\mathbf{r}, t)$ means $f(\mathbf{r}, t \mid \mathbf{r}, 0)$ or if $f(\mathbf{r}, 0) = \delta(\mathbf{r}-\mathbf{r}_0)$ then $f(\mathbf{r}, t) = G(\mathbf{r}, t)$] in each of the two problems under consideration. Thus for a Brownian particle free to move in three dimensions so that its motion is governed by the Langevin equation:

$$m\frac{d\mathbf{v}(t)}{dt} + m\beta\mathbf{v}(t) = m\frac{d\mathbf{B}(t)}{dt}$$

$$\frac{d\mathbf{r}(t)}{dt} = \mathbf{v}(t)$$

We find that the probability distribution $G(\mathbf{r}, t)$ is

$$G(\mathbf{r}, t) = \left(\frac{m\beta^2}{2\pi kT(2\beta t - 3 + 4e^{-\beta t} - e^{-2\beta t})}\right)^{3/2} \times \exp\left[-\frac{m\beta^2\left(\left|\mathbf{r}-\mathbf{r}_0-\frac{\mathbf{u}_0}{\beta}(1-e^{-\beta t})\right|\right)^2}{2kT(2\beta t - 3 + 4e^{-\beta t} - e^{-2\beta t})}\right] \tag{2.3.2}$$

For very short times this reduces to the Dirac delta function $\delta(\mathbf{r}-\mathbf{r}_0)$ as it must, while for $t \gg \beta^{-1}$,

$$G(\mathbf{r}, t) \simeq \frac{1}{(4\pi Dt)^{3/2}}\exp\left(-\frac{|\mathbf{r}-\mathbf{r}_0|^2}{4Dt}\right)$$

which is the result of Einstein (based on the Smoluchowski equation) generalized to a particle moving in three dimensions. The distribution function given by Eq. 2.3.2 is got from the Kramers equation by integrating the density function in phase space namely, $\rho(\mathbf{r}, \mathbf{v}, t) = \rho(\mathbf{r}, \mathbf{v}, t \mid \mathbf{r}_0, \mathbf{v}_0, 0)$ over the velocities. $\rho(\mathbf{r}, \mathbf{v}, t)$; $t > 0$, is got by solving the Kramers equation subject to the initial condition

$$\rho(\mathbf{r}, \mathbf{v}, 0) = \delta(\mathbf{r}-\mathbf{r}_0)\delta(\mathbf{v}-\mathbf{v}_0) \tag{2.3.3}$$

We could write ρ explicitly but there is little point in doing this because the expression involved is extremely cumbersome and has already been given by Chandrasekhar (see Wax, 1954). We now refer to the second soluble problem where the particle moves in a one-dimensional parabolic potential well. Here we find, in the same manner as before,

$$f(x, t) = \left[\frac{m}{4\pi\beta kT\int_0^t \psi^2(\xi)\,d\xi}\right]^{1/2} \times \exp - \left(\frac{[x - x_0e^{-\beta t}(\cosh\frac{1}{2}\beta_1 t + (\beta/\beta_1)\sinh\frac{1}{2}\beta_1 t) - 2(v_0/\beta_1)e^{-\beta t/2}\sinh(\beta_1 t/2)]^2}{(2kT/m\omega_0^2)[1-e^{-\beta t}((2\beta^2/\beta_1^2)\sinh^2\frac{1}{2}\beta_1 t + (\beta/\beta_1)\sinh\beta_1 t + 1)]}\right)$$

where

$$\int_0^t \psi^2(\xi)\,d\xi = \frac{1}{2\omega_0^2\beta} - \frac{e^{-\beta t}}{2\omega_0^2\beta_1^2\beta}\,(2\beta^2 \sin^2\!\text{h}\,\tfrac{1}{2}\beta_1 t + \beta\beta_1 \sinh\beta_1 t + \beta_1^2) \tag{2.3.4}$$

We have written the results for the overdamped case where the quantity β_1, given by

$$\beta_1 = (\beta^2 - 4\omega_0^2)^{1/2}$$

is entirely real. Equation 2.3.4 is thus the probability distribution of the displacement for the system governed by the Langevin equation

$$m\ddot{x} + m\beta\dot{x} + m\omega_0^2 x = m\dot{B}(t)$$

The probability distributions appropriate to the periodic (β_1 imaginary) and the aperiodic (β_1 zero) case can be readily written down by replacing

$$\cosh\frac{\beta_1 t}{2}, \qquad \beta_1^{-1}\sinh\frac{\beta_1 t}{2}, \qquad \beta_1^{-1}\sinh\beta_1 t$$

respectively, by

$$\cos\omega_1 t, \qquad \frac{1}{2\omega_1}\sin\omega_1 t, \qquad \frac{1}{2\omega_1}\sin 2\omega_1 t$$

where

$$\omega_1^2 = \omega_0^2 - \frac{\beta^2}{4}$$

in the periodic case and by

$$1, \qquad \frac{t}{2}, \qquad t$$

in the aperiodic case.

A third situation where the problem of determining the probability distributions from the Kramers equation may be reduced to that of solving the Fokker–Planck equation given by Wang and Uhlenbeck is that of the itinerant oscillator model. These distributions have recently been given by Coffey and Evans (1978) so it is unnecessary to give them here because nothing new is involved beyond the move from considering a stochastic process in $\mathfrak{R}^2$ to one in $\mathfrak{R}^N$. Indeed it is worth noting here that the Kramers equation corresponding to the N-dimensional Langevin equation

$$\dot{\mathbf{X}}(t) = \mathbf{A}\mathbf{X}(t) + \mathbf{B}\boldsymbol{\Lambda}(t)$$

where $\mathbf{X}(t)$ is a column vector in $\mathfrak{R}^N$, $\mathbf{A}$ is an N by N constant matrix, and $\mathbf{B}\boldsymbol{\Lambda}(t)$ is a white noise driving force, may always be reduced to a Fokker–Planck equation corresponding to that given by Wang and Uhlenbeck. Thus the Kramers equation for any system whose behavior is governed by

linear stochastic differential equations with *constant* coefficients may always be solved. Furthermore, the fundamental solution of that equation will *always* be the N-dimensional Gaussian distribution. Finally we remark that once the *fundamental* solution or Green's function $G(\mathbf{r}, \dot{\mathbf{r}}, t)$ of the Kramers equation is known, then the solution corresponding to an *arbitrary* initial distribution may always be found by integration. For example, in the Ornstein–Uhlenbeck process the fundamental solution for the velocity distribution is

$$G(\mathbf{v}, t) = \left(\frac{m}{2\pi kT(1-e^{-2\beta t})}\right)^{3/2} \exp\left[-\frac{m}{2kT}\frac{|\mathbf{v}-\mathbf{v}_0 e^{-\beta t}|^2}{(1-e^{-2\beta t})}\right]$$

Then the solution corresponding to an arbitrary initial distribution of velocities $H(\mathbf{v}_0)$, say, is

$$\rho_v(\mathbf{v}, t) = \int_{-\infty}^{\infty} H(\mathbf{v}_0)G(\mathbf{v}, \mathbf{v}_0, t)\,d\mathbf{v}_0$$

We now leave the relatively easy task of solving the Kramers equation for a linear system and go on to review the methods of solution which have been proposed for the general cases of that equation. We start with the fundamental work of Brinkman.

2.4 REVIEW OF BRINKMAN'S PROCEDURE FOR THE SOLUTION OF KRAMERS' EQUATION

The origins of Brinkman's work lie in the important (1940) paper of Kramers. In that paper Kramers was concerned with a study of the passage of particles over potential barriers due to the shuttling action of the Brownian movement. In the phraseology of Brinkman's paper the following model was studied. "A particle moves in an external field of force, but—in addition to this—is subject to the irregular forces of a surrounding medium in thermal equilibrium (Brownian movement). Originally the particle is caught in a potential hole, but it may escape in the course of time by passing over a potential barrier." Kramers calculated the probability of escape under the assumption of a stationary diffusion current and obtained the result that for such a situation the transition state method (as it is called) has a limited range of applicability.

The basic problem of Kramers' treatment—the Brownian movement of a particle in a field of force—was attacked as a diffusion problem in phase space. Assuming the validity of Einstein's theory of the Brownian motion, Kramers derived a diffusion equation in phase space (as we have done in the preceding section). This equation, however, presented a very difficult mathematical problem and Kramers limited his treatment to two extreme cases, namely, Brownian forces that are much larger or, on the other hand, much smaller than the external force. In the first case Kramers showed that

Smoluchowski's diffusion equation in configuration space may be derived from Kramers' equation with the introduction of certain approximations. For the second problem Kramers considered the probability of escape of a particle over a potential barrier under the assumption of a stationary diffusion current. Brinkman reconsiders the problem when this assumption is abandoned. He further sets out to delineate a region of validity in the time domain for the Smoluchowski equation. Both these questions he proposes may be answered if a general formalism for the treatment of Kramers' equation were available. In this review we describe in detail his treatment of the problem and discuss some criticisms of this treatment that have been advanced recently by Wilemski (1976), by Skinner and Wolynes (1979), and by Titulaer (1978). We also describe some extensions and variations on his treatment that have been proposed by Blomberg (1977) and by Risken and Vollmer (1978). Having said this we now proceed to write the Kramers equation for a particle moving in one dimension under the influence of a potential $V(x)$ where x is the displacement of the particle from the origin. Thus the Langevin equation for the motion of the particle is

$$m\ddot{x} + m\beta\dot{x} + \frac{\partial V(x)}{\partial x} = m\dot{B}(t) \tag{2.4.1}$$

where $B(t)$ is again a Wiener process. Using the methods we have already outlined we are led to the Kramers equation corresponding to Eq. 2.4.1:

$$\frac{\partial \rho}{\partial t} + v\frac{\partial \rho}{\partial x} - \frac{1}{m}\frac{\partial V}{\partial x}\frac{\partial \rho}{\partial v} = \beta\frac{\partial}{\partial v}\left(v\rho + \frac{kT}{m}\frac{\partial \rho}{\partial v}\right) \tag{2.4.2}$$

As we have seen, $\rho = \rho(x, v, t)$ is the particle density in the phase space $\Re^2$; the task that now remains is to solve Eq. 2.4.2, subject to the initial condition proposed by Brinkman, namely,

$$\rho(x, v, 0) = \rho_0 = e^{-mv^2/2kT} f_0(x) \tag{2.4.3}$$

In writing Eq. 2.4.3, Brinkman assumes that initially the velocities of the particles have the Maxwell–Boltzmann distribution, which assumption is valid for most physical problems of interest. In Eq. 2.4.3 $f_0(x)$ represents the initial distribution in configuration space, and in what follows we denote the time-dependent distribution in configuration space by $f(x, t)$. The next step is to take the Laplace transform of Eq. 2.4.2 according to the formula,

$$\mathcal{L}[\rho(x, v, t)] = \tilde{\rho}(x, v, s) = \int_0^\infty e^{-st}\rho(x, v, t)\, dt$$

This yields the transformed Kramers equation

$$\beta\frac{kT}{m}\frac{\partial^2 \tilde{\rho}}{\partial v^2} + \left(\beta v - \frac{F}{m}\right)\frac{\partial \tilde{\rho}}{\partial v} - v\frac{\partial \tilde{\rho}}{\partial x} + (\beta - s)\tilde{\rho} = -\rho_0$$

in which the quantity

$$F(x) = -\frac{\partial V(x)}{\partial x}$$

is the force acting on the particle. Our next step is to attempt to solve this transformed equation. Following Brinkman, then, we assume that $\tilde{\rho}$ may be written as follows:

$$\tilde{\rho}(x, v, s) = e^{-mv^2/4kT}\sum_{n=0}^{\infty} D_n\left(\sqrt{\frac{m}{kT}}\, v\right)\tilde{\varphi}_n(x, s) \tag{2.4.4}$$

where the D_n are the Weber functions (Whittaker and Watson, 1927). These functions satisfy the recurrence relations:

$$D_{n+1}(x) - xD_n(x) + nD_{n-1}(x) = 0$$

$$\frac{dD_n}{dx}(x) + \frac{x}{2}D_n(x) - nD_{n-1}(x) = 0$$

$$\frac{dD_n}{dx}(x) - \frac{x}{2}D_n(x) + D_{n+1}(x) = 0$$

They satisfy the differential equation

$$\frac{d^2D_n}{dx^2}(x) + \left(n + \frac{1}{2} - \frac{x^2}{4}\right)D_n(x) = 0 \tag{2.4.5}$$

They are related to the Hermite polynomials (Margenau and Murphy, 1956) via

$$D_n(x) = 2^{-n/2}e^{-x^2/4}H_n\left(\frac{x}{\sqrt{2}}\right)$$

and have the orthogonality property

$$\int_{-\infty}^{\infty} D_n(x)D_m(x)\, dx = n!\sqrt{2\pi}\,\delta_{m,n}$$

where $\delta_{m,n}$ denotes Kronecker's delta.

On substituting Eq. 2.4.4 into Eq. 2.4.3 and making use of the above recurrence relations and the orthogonality property of the D_n, we find, after considerable algebra, the following set of differential-difference equations for the several functions $\tilde{\varphi}_n(x, s)$:

$$s\tilde{\varphi}_0 = f_0 - \sqrt{\frac{kT}{m}}\frac{\partial \tilde{\varphi}_1}{\partial x}$$

and for $n > 0$

$$\left(\frac{n}{\tau} + s\right)\tilde{\varphi}_n = \frac{F}{\sqrt{mkT}}\tilde{\varphi}_{n-1} - \sqrt{\frac{kT}{m}}\frac{\partial \tilde{\varphi}_{n-1}}{\partial x} - (n+1)\sqrt{\frac{kT}{m}}\frac{\partial \tilde{\varphi}_{n+1}}{\partial x} \tag{2.4.6}$$

It is now necessary to find a systematic method of solving the set of Eqs.

2.4.6. The problem may be simplified somewhat if we stop to consider the meaning of $\tilde{\varphi}_0$ and $\tilde{\varphi}_1$. The quantities that are of the most interest in physical problems are the density, $f(x, t)$, in configuration space and the current flowing along the x axis. We may interpret these in terms of the first two of the φ's in the above equations for, on inspection of Eq. 2.4.4, we see that the only term in that equation which is independent of the velocity variable v is that for which $n = 0$, thus $\tilde{\varphi}_0(x, s)$ must be directly proportional to the Laplace transform of the density in configuration space. That this is so may be seen by integrating Eq. 2.4.4 over the velocities. We then find (on utilizing the orthogonality properties of the D_n) the transformed density

$$\tilde{f}(x, s) = \int_{-\infty}^{\infty} \tilde{\rho}\, dv \propto \tilde{\varphi}_0(x, s)$$

and for the transformed current, we have

$$\tilde{\gamma}_1(x, s) = \int_{-\infty}^{\infty} v\tilde{\rho}\, dv \propto \tilde{\varphi}_1(x, s)$$

Thus the calculation of these two important physical quantities apparently requires only the determination of $\tilde{\varphi}_0$ and $\tilde{\varphi}_1$. In practice, however, owing to the *coupled* nature of the set of differential Eqs. 2.4.6 *all* the $\tilde{\varphi}_n$ have to be calculated in order to determine $\tilde{\varphi}_0$ and $\tilde{\varphi}_1$ to any given accuracy. The following section illustrates how Brinkman tackled the problem and discusses the criticisms that have been leveled at his procedure.

2.4.1 Brinkman's Method of Solving Equations 2.4.6

In order to implement his solution procedure Brinkman defines higher-order probability currents by means of the equation

$$\tilde{\gamma}_n(x, s) = \sqrt{2\pi} kT \tilde{\varphi}_n(x, s) \tag{2.4.1.1}$$

and introduces the Smoluchowski current operator

$$J_S = -\frac{kT}{m\beta}\frac{\partial}{\partial x} + \frac{F}{m\beta} \tag{2.4.1.2}$$

together with the following *dimensionless* operators

$$J = \left(\frac{m}{kT}\right)^{1/2} J_S$$

$$J_D = -\left(\frac{kT}{m}\right)^{1/2} \beta^{-1}\frac{\partial}{\partial x}$$

$$J_F = \frac{F}{\beta\sqrt{mkT}}$$

In the foregoing equations the operator $J = J_D + J_F$ is the Smoluchowski current operator divided by the gas kinetic velocity $\sqrt{kT/m}$. Introducing all

these operators into the system of Brinkman (Eqs. 2.4.6) now gives the following recursion system for the currents:

$$s\tilde{f}(x, s) = f_0(x) - \frac{\partial\tilde{\gamma}_1}{\partial x}(x, s)$$

$$\left(1 + \frac{s}{\beta}\right)\tilde{\gamma}_1(x, s) = \sqrt{\frac{kT}{m}}\, J\tilde{\gamma}_1(x, s) + 2J_D\tilde{\gamma}_2(x, s)$$

and for $n > 1$

$$\left(n + \frac{s}{\beta}\right)\tilde{\gamma}_n(x, s) = J\tilde{\gamma}_{n-1}(x, s) + (n+1)J_D\tilde{\gamma}_{n+1}(x, s)$$

According to Brinkman this recursion system may be solved in nth approximation by neglecting all $\tilde{\gamma}_k(x, s)$ for $k > n$. In this case the system consists of $n + 1$ equations for the functions $\tilde{\gamma}_n(x, s)$.

Again according to Brinkman, sufficient conditions for this procedure to be valid are that the Smoluchowski currents be small in comparison with the gas kinetic currents; in other words,

$$|J\tilde{\gamma}_0(x, s)| \ll |\tilde{\gamma}_0(x, s)|, \qquad |J\tilde{\gamma}_n(x, s)| \ll |\tilde{\gamma}_n(x, s)|, \qquad \tilde{\gamma}_0(x, s) = \tilde{f}(x, s)$$

whereas the diffusion currents are not larger than the gas kinetic currents, that is

$$J_D\tilde{f}(x, s) \leqslant |\tilde{f}(x, s)| \qquad |J_D\tilde{\gamma}_n(x, s)| \leqslant |\tilde{\gamma}_n(x, s)|$$

Then the $\tilde{\gamma}_n(x, s)$ for $k \leqslant n$ are of the order

$$\tilde{\gamma}_k(x, s) \simeq \frac{1}{k!} J_{k-1}\tilde{\gamma}_1(x, s)$$

In the third approximation the elimination of $\tilde{\gamma}_1(x, s)$, $\tilde{\gamma}_2(x, s)$, and $\tilde{\gamma}_3(x, s)$ yields the following equation for $\tilde{f}(x, s)$:

$$\begin{aligned} s\tilde{f}(x, s) - f_0(x, 0) = &\left[\beta\left(1 + \frac{s}{\beta}\right)^{-1} J_D J\tilde{f}(x, s)\right] \\ &+ \left[2\beta\left(1 + \frac{s}{\beta}\right)^{-2}\left(2 + \frac{s}{\beta}\right)^{-1} J_D^2 J^2\tilde{f}(x, s)\right] \\ &+ \left[4\beta\left(1 + \frac{s}{\beta}\right)^{-3}\left(2 + \frac{s}{\beta}\right)^{-2} J_D^2 J J_D J^2\tilde{f}(x, s)\right] \\ &+ \left[6\beta\left(1 + \frac{s}{\beta}\right)^{-2}\left(2 + \frac{s}{\beta}\right)^{-2}\left(3 + \frac{s}{\beta}\right)^{-1} J_D^3 J^3\tilde{f}(x, s)\right] \\ &+ \cdots \end{aligned} \tag{2.4.1.3}$$

Thus the determination of $\tilde{f}(x, s)$ is reduced to solving the ordinary differential Eq. 2.4.1.3. This is exceedingly difficult in practice owing to the high-order derivatives arising from the powers of the operators J_D and J. Further, there has been considerable controversy over the powers of J_D and J at which the solution of Eq. 2.4.1.3 should be terminated. This is discussed below, when we come to describe this controversy. In the

meantime it is appropriate here to mention a paper of Davies (1957) in which a solution procedure, similar to that of Brinkman but somewhat easier to implement, is given. Davies' starting point is again the transformed Kramers equation, namely, (see Coffey, 1981):

$$\beta \frac{kT}{m}\frac{\partial^2 \tilde{\rho}}{\partial v^2} + \left(\beta v - \frac{F}{m}\right)\frac{\partial \tilde{\rho}}{\partial v} - v\frac{\partial \tilde{\rho}}{\partial x} + (\beta - s)\tilde{\rho} = -\rho_0 \qquad (2.4.1.4)$$

He now departs from Brinkman's procedure of developing $\tilde{\rho}$ in Weber functions, by introducing the *characteristic function* of the velocity variables, namely,

$$\tilde{\Phi}(x, u, s) = \int_{-\infty}^{\infty} e^{-iuv}\tilde{\rho}(x, v, s)\, dv \qquad (2.4.1.5)$$

Before proceeding we note that this transformation applied to the equilibrium solution

$$\rho = \text{const} \exp\left[-\left(V(x) + \frac{mv^2}{2kT}\right)\right]$$

transforms this solution into

$$\tilde{\Phi}_0 = \text{const} \exp\left[-\left(V(x) + \frac{u^2 kT}{2m}\right)\right]$$

Hence on writing (following Brinkman)

$$\tilde{\rho}(x, v, 0) = \rho_0 = \exp\left(-\frac{mv^2}{2kT}\right) f_0(x)$$

where $f_0(x)$ is the density in phase space. We find that

$$\tilde{\Phi}(x, u, 0) = \exp\left(-\frac{u^2 kT}{2m}\right) f_0(x)$$

This equation suggests the transformation

$$\tilde{\Phi}(x, u, s) = \tilde{\Psi} \exp\left(-\frac{kTu^2}{2m}\right)$$

which leads us to the following partial differential equation for $\tilde{\Psi}$:

$$s\tilde{\Psi} - f_0(x) + i\frac{\partial^2 \tilde{\Psi}}{\partial x \partial u} - \frac{iu}{m}\left[kT\frac{\partial \tilde{\Psi}}{\partial x} - \tilde{\Psi}F\right] = -\beta u\frac{\partial \tilde{\Psi}}{\partial u}$$

Now on writing

$$D = \frac{\partial}{\partial x}$$

this equation becomes

$$(\beta u + iD)\frac{\partial \tilde{\Psi}}{\partial u} + \left[s - \frac{iu}{m}(kTD - F)\right]\tilde{\Psi} = f_0(x) \qquad (2.4.1.6)$$

According to Davies the solution of Eq. 2.4.1.6 can be found as a power series in u by writing

$$\tilde{\Psi} = \sum_{n=0}^{\infty} \tilde{j}_n(x, s)(iu)^n \qquad (2.4.1.7)$$

(This procedure had already been used by Sack (1957) in a discussion of rotational Brownian movement.) The notation used in Eq. 2.4.1.7 is justified by noting that j_0 is the density and j_1 is the current. In fact, the transformed density is simply

$$\int_{-\infty}^{\infty} \tilde{\rho}(x, v, s)\, dv$$

which is

$$\tilde{\Phi}(x, u, s)|_{u=0} = \tilde{\Psi}(x, u, s)|_{u=0} = \tilde{j}_0$$

Similarly, the transformed current is

$$\int_{-\infty}^{\infty} v\tilde{\rho}(x, v, s)\, dv = i\left.\frac{\partial \tilde{\Phi}}{\partial u}\right|_{u=0} = i\left.\frac{\partial \tilde{\Psi}}{\partial u}\right|_{u=0} = \tilde{j}_1$$

On substituting Eq. 2.4.1.7 into Eq. 2.4.1.6 we now find the recurrence relations

$$s\tilde{j}_0(x, s) + D\tilde{j}_1(x, s) = f_0(x) \qquad n = 0$$

$$(D - F)\tilde{j}_{n-1}(x, s) + (s + n)\tilde{j}_n(x, s) + (n + 1)D\tilde{j}_{n+1}(x, s) = 0 \qquad (n > 0)$$

It is apparent from inspection of these equations and the relation derived by Brinkman (Eq. 2.4.1.3) that the latter equations have the *same structure* as the Brinkman relations and that Brinkman's discussion applies to these equations. Thus the method used by Davies is equivalent to that used by Brinkman, the explanation being that the *moment generating* operation of taking Fourier transforms *converts* the Weber functions of Brinkman into *powers* of u. The advantage of Davies' method over that of Brinkman is that it is much more direct and does not require *any* knowledge of the properties of the Weber functions.* It is now appropriate to mention the work of Blomberg (1977), who has shown that for certain types of potential (e.g., the piecewise parabolic potential) the solution of the recurrence relations of Brinkman can be found as a series of parabolic cylinder functions. The manipulations required to obtain this solution are rather complicated; thus we refrain from discussing this paper any further here and the reader is referred to the original. Before going on to review some recent comments on the papers of Brinkman, Davies, and Sack, it is necessary to discuss the work of Risken and Vollmer (1978), who have

*Brinkman's formulae may be related to those of Davies by using the relation

$$\int_{-\infty}^{\infty} e^{iu\xi} e^{-\xi^2/2} H_n\left(\frac{\xi}{\sqrt{2}}\right) d\xi = \sqrt{2\pi}\, 2^{1/2} e^{-u^2/2}(iu)^n$$

recently carried the method of Brinkman a stage further and shown how his procedure may be adapted to provide a numerical solution of the Kramers equation for a particle moving in a periodic potential.

2.4.2 The Method of Risken and Vollmer

The starting point of Risken and Vollmer (1978) is again the Langevin equation, namely,

$$m\ddot{x} + m\beta\dot{x} + \frac{\partial V(x)}{\partial x} = m\dot{B}(t)$$

which again leads to the Kramers equation

$$\frac{\partial \rho}{\partial t} + v\frac{\partial \rho}{\partial x} - \frac{1}{m}\frac{\partial V(x)}{\partial x}\frac{\partial \rho}{\partial v} = \beta\frac{\partial}{\partial v}\left(v\rho + \frac{kT}{m}\frac{\partial \rho}{\partial v}\right) \tag{2.4.2.1}$$

Brinkman at this stage takes the Laplace transform of Eq. 2.4.2.1. This is not done by Risken and Vollmer; rather they choose to work in the time domain entirely. This leads in the usual manner, on the assumption that

$$\rho(x, v, t) = A\exp\left(-\frac{mv^2}{4kT}\right)\sum_{n=0}^{\infty} D_n\left(\sqrt{\frac{m}{kT}}\,v\right)\psi_n(x, t)$$

to the following set of equations:

$$\frac{\partial \psi_n}{\partial t} + n\beta\psi_n + \frac{1}{\sqrt{mkT}}\frac{\partial V(x)}{\partial x}\psi_{n-1} + \sqrt{\frac{kT}{m}}\left(\frac{\partial \psi_{n-1}}{\partial x} + (n+1)\frac{\partial \psi_{n+1}}{\partial x}\right) = 0 \tag{2.4.2.2}$$

The next step is to assume that *both* the potential and the ψ_n may be *expanded* in Fourier series [we implicitly assume by doing this that $V(x)$ is *periodic* in x, as will be true in many physical situations]. Thus

$$\psi_n(x, t) = \sum_{p=-\infty}^{p=\infty} A_p^n(t)e^{ipx} \tag{2.4.2.3}$$

$$V(x) = \sum_{r=-\infty}^{r=\infty} V_r e^{irx} \tag{2.4.2.4}$$

On substituting Eqs. 2.4.2.3 and 2.4.2.4 into Eq. 2.4.2.2 we then find that the A^n satisfy the following ordinary differential equations (Coffey, 1981)

$$\frac{dA_p^n(t)}{dt} + \beta n A_p^n(t) + \frac{1}{\sqrt{mkT}}\sum_{r=-\infty}^{r=\infty} irV_r A_{p-r}^{n-1}(t) + ip\sqrt{\frac{kT}{m}}\{(n+1)A_p^{n+1}(t) + A_p^{n-1}(t)\} = 0 \tag{2.4.2.5}$$

two particular cases of Eq. 2.4.2.5 are of interest: (1) the case of the cosine potential where

$$V(x) = -V_0\cos x = -\frac{V_0}{2}(e^{ix} + e^{-ix}) \tag{2.4.2.6}$$

and (2) the case of the free particle where $V(x) = 0$. For the cosine potential the equations reduce to

$$\frac{dA_p^n(t)}{dt} + n\beta A_p^n(t) - \frac{iV_0}{2\sqrt{mkT}}[A_{p-1}^{n-1}(t) - A_{p+1}^{n-1}(t)] + ip\sqrt{\frac{kT}{m}}[(n+1)A_p^{n+1}(t) + A_p^{n-1}(t)] = 0 \tag{2.4.2.7}$$

These equations have been solved numerically by Risken and Vollmer and we may calculate the results for several values of the parameters m, β, etc. occurring in the initial Langevin equation. The spectral density $\tilde{A}_p^n(\omega)$ associated with Eq. 2.4.2.5 may be found by simply taking the Laplace transform of that equation and putting $s = i\omega$. (Note that if this is done the task of solving Eq. 2.4.2.5 is reduced to finding the solution of algebraic difference equations.) For the case of the free particle the solution of Eq. 2.4.2.5 may be found in closed form. This seems to have been originally accomplished by Gross (1955). It is instructive to give the derivation here. Equation 2.4.2.5 in the presence of no external forces except those due to the Brownian movement becomes

$$\frac{dA_p^n(t)}{dt} + n\beta A_p^n(t) = -ip\sqrt{\frac{kT}{m}}[(n+1)A_p^{n+1}(t) + A_p^{n-1}(t)] \tag{2.4.2.8}$$

We assume for convenience that our initial density has the form

$$\rho(x, v, 0) = A\exp\left(-\frac{mv^2}{2kT}\right)(1 + d\cos x) \tag{2.4.2.9}$$

where A and d are constants. (This type of initial density commonly occurs in problems in the theory of dielectrics). Equation 2.4.2.9 means that

$$A_p^n(0) = A_p^0(0)\delta_{n,0}$$

where δ again denotes Kronecker's delta. The formal solution of equation 2.4.2.9 subject to the initial condition is

$$A_p^n(t) = \delta_{n,0}A_p^0(0)e^{-n\beta t} - ip\sqrt{\frac{kT}{m}}\int_0^t e^{-n\beta(t-u)}[(n+1)A_p^{n+1}(u) + A_p^{n-1}(u)]\,du \tag{2.4.2.10}$$

Equation 2.4.2.10 may be solved for $A_1^0(t)$ and all the higher $A_p^n(t)$ by means of Picards' method of successive approximations. In order to demonstrate this we write Eq. 2.4.2.10 explicitly for the first few values of n:

$$A_1^0(0), \tag{2.4.2.11}$$

$$A_1^0(t) = A_1^0 - i\sqrt{\frac{kT}{m}}\int_0^t A_1^1(u)\,du \tag{2.4.2.12}$$

$$A_1^1(t) = -i\sqrt{\frac{kT}{m}}\int_0^t e^{-\beta(t-u)}[2A_1^2(u) + A_1^0(u)]\,du \tag{2.4.2.13}$$

$$A_1^2(t) = -i\sqrt{\frac{kT}{m}}\int_0^t e^{-2\beta(t-u)}[3A_1^3(u) + A_1^1(u)]\,du \qquad (2.4.2.14)$$

To a first approximation the solution of Eq. 2.4.2.12 is

$$A_1^0(t) = A_1^1(0) \qquad (2.4.2.15)$$

In order to obtain a second approximation, we write, from Eqs. 2.4.2.13 and 2.4.2.15,

$$A_1^1(t) = -i\sqrt{\frac{kT}{m}}\int_0^t e^{-\beta(t-u)}A_1^0(0)\,du \qquad (2.4.2.16)$$

and substitute this into Eq. 2.4.2.12 to get

$$A_1^0(t) = A_1^0(0) - \frac{kT}{m}\int_0^t du \int_0^u e^{-\beta(u-u_1)}A_1^0(0)\,du_1$$

or

$$A_1^0(t) = A_1^1(0)\left[1 - \frac{kT}{m}\int\int_{0\le u_1\le u\le t} e^{-\beta(u-u_1)}\,du_1\,du\right] \qquad (2.4.2.17)$$

and to the next degree of approximation

$$A_1^0(t) = A_1^0(0)\left[1 - \frac{kT}{m}\int\int_{0\le u_1\le u\le t} e^{-\beta(u-u_1)}\,du_1\,du - \left(\frac{kT}{m}\right)^2\int\int\int\int_{0<u_3\le u_2\le u_1\le u\le t} \times e^{-\beta(u_3-u_2)}e^{-2\beta(u-u_1)}e^{-\beta(u_1-u_2)}\,du_3\,du_2\,du_1\,du\cdots\right] \qquad (2.4.2.18)$$

and so on.

On evaluating these integrals we have

$$A_1^0(t) = A_1^0(0)\left[1 - \frac{kT}{m\beta^2}(\beta t - 1 + e^{-\beta t}) + \frac{1}{2!}\left(\frac{kT}{m\beta^2}\right)^2(\beta t - 1 + e^{-\beta t})^2\cdots\right]$$

which clearly may be written as

$$A_1^0(t) = A_1^0(0)\exp\left(-\frac{kT}{m\beta^2}(\beta t - 1 + e^{-\beta t})\right) \qquad (t>0) \qquad (2.4.2.19)$$

The result embodied in Eq. 2.4.2.19 is of particular interest in the theory of dielectrics. Figures 2.4.2.1 and 2.4.2.2 illustrate some a.c.f.'s of the itinerant librator (Chapter 4); these are closely dependent on the form of Kramers equation chosen for solution. One may show that the Kramers equation describing the evolution of the probability density $\rho(\theta, \dot\theta, t)$ underlying the *reorientational motion*, following on the removal of an electric field **E** (which had been steady up to the time $t = 0$) from an assembly of non electrically interacting two-dimensional dipolar rotators, is,

$$\frac{\partial\rho}{\partial t} + \dot\theta\frac{\partial\rho}{\partial\theta} = \beta\frac{\partial}{\partial\dot\theta}\left(\dot\theta\rho + \frac{kT}{I}\frac{\partial\rho}{\partial\dot\theta}\right) \qquad (t>0) \qquad (2.4.2.20)$$

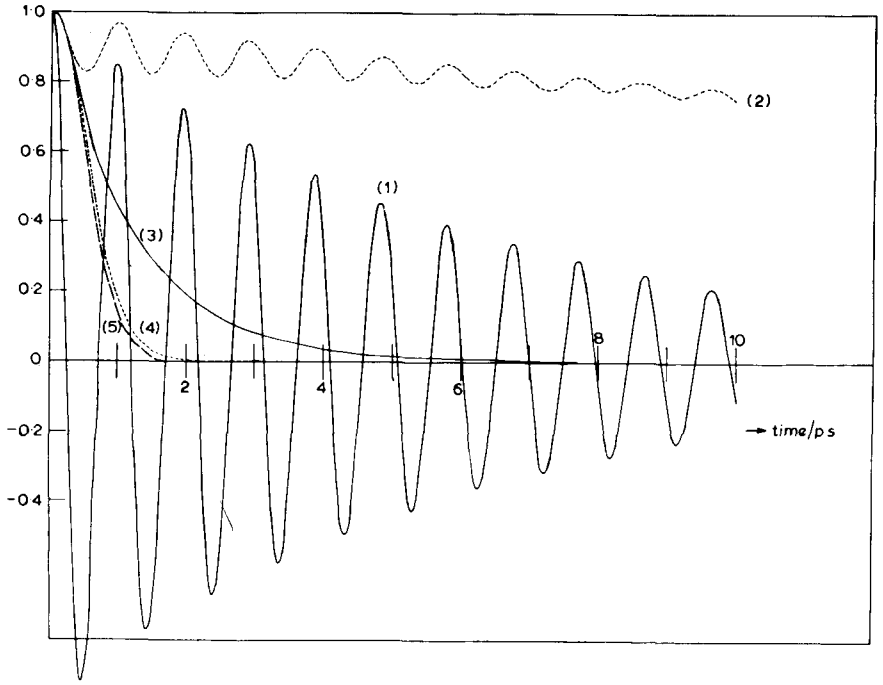

Figure 2.4.2.1 Angular velocity and orientational a.c.f.'s for motion in two dimensions of the itinerant oscillator. Solid line, $\langle\omega(t)\omega(0)\rangle$; (1) $\phi_0(0) = 10\,\phi_1(0) = 10\,kT/I\ \text{sec}^{-2}$, $\gamma = 4(kT/I)^{1/2}\ \text{sec}^{-1}$; (3) $\phi_1(0) = 10\phi_0(0) = 10\,kT/I\ \text{sec}^{-2}$: $\gamma = 4(kT/I)^{1/2}\ \text{sec}^{-1}$. Dashed lines, $\langle\mathbf{u}(t)\cdot\mathbf{u}(0)\rangle$ where (2) is calculated using the same value of the parameters as in (1); (4) is calculated using the same value of the parameters as in (3); (5) $\exp(-kTt^2/2I)$, the orientational a.c.f. for free rotation of a Boltzmann ensemble in a plane. For (1)–(5), $T = 296°\text{K}$; $I = 10^{-38}\,\text{g cm}^2$. [Reproduced by permission from M. Evans, *Mol. Phys.*, **34**, 963 (1977).]

In this equation θ is the angle which the rotator (having a dipole moment $\boldsymbol{\mu}$) makes with **e**, the direction which **E** had at any time $t < 0$, and I is the moment of inertia of the rotator about an axis through its center normal to the plane containing **E**. It is apparent from inspection of Eqs. 2.4.2 and 2.4.2.1 that these equations are *identical* if the space coordinate x is replaced by the angular coordinate θ and if the mass m is replaced by the moment of inertia I. We note that for the problem at hand the potential energy $V(\theta)$ is set equal to zero as the dipoles are not allowed to interact electrically. Furthermore, the *range of variation* of the coordinate θ will be $(0, 2\pi)$ rather than $(-\infty, \infty)$ as in the translational problem. Thus in the notation of the theory of dielectrics Eq. (2.4.2.9) becomes

$$\rho(\theta, \dot\theta, 0) = Ae^{-I\dot\theta^2/2kT}\left(1 + \frac{\mu E}{kT}\cos\theta\right)$$

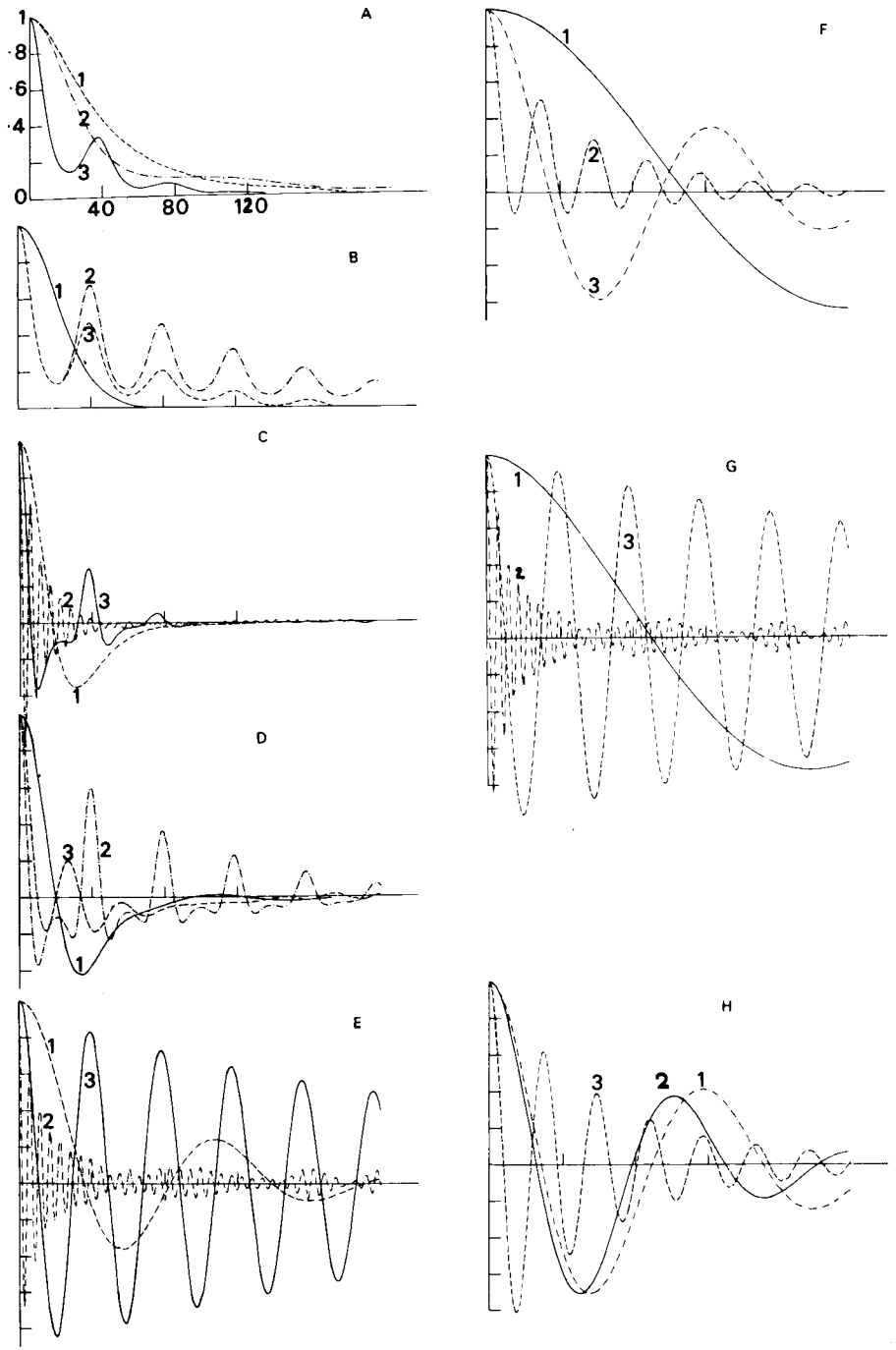

Figure 2.4.2.2 Various a.c.f.'s from a molecular dynamics simulation of the planar itinerant librator. [Reproduced by permission from J. Kestemont et al., *Chem. Phys. Lett.* **58**, 521 (1978).]

and thus Eq. 2.4.2.9 is

$$A_1^0(t) = \frac{\mu E}{2kT} \exp\left(-\frac{kT}{I\beta^2}(\beta t - 1 + e^{-\beta t})\right)$$

or with $I\beta = \zeta$,

$$A_1^0(t) = \frac{\mu E}{2kT} \exp\left[-\frac{kTI}{\zeta^2}\left(\frac{\zeta t}{I} - 1 + e^{-\zeta t/I}\right)\right]$$

It is of particular importance to calculate the mean dipole moment in the direction of the field. One has

$$\langle \boldsymbol{\mu} \cdot \mathbf{e} \rangle = \langle \mu \cos\theta \rangle = \frac{\int_0^{2\pi} \int_{-\infty}^{\infty} \mu \rho(\theta, \dot{\theta}, t) \cos\theta \, d\theta \, d\dot{\theta}}{\int_0^{2\pi} \int_{-\infty}^{\infty} \rho(\theta, \dot{\theta}, t) \, d\theta \, d\dot{\theta}}$$

which with the orthogonality properties of the D_n reduces to

$$\langle \mu \cos\theta \rangle = \frac{\mu \int_0^{2\pi} \psi_0(\theta, t) \cos\theta \, d\theta}{\int_0^{2\pi} \psi_0(\theta, t) \, d\theta}$$

Our Fourier series expansion for the A_n^s allows us to simplify this equation even further so that it now reads

$$\langle \mu \cos\theta \rangle = \frac{\mu}{2} \frac{[A_1^0(t) + A_{-1}^0(t)]}{A_0^0(0)} \tag{2.4.2.21}$$

Furthermore, by symmetry, we have

$$A_1^0(t) = A_{-1}^0(t)$$

and from the initial condition

$$A = A_0^0(0)$$

so that Eq. 2.4.2.21 finally becomes

$$\langle \mu \cos\theta \rangle = \mu \frac{A_1^0(t)}{A}$$

$$\langle \mu \cos\theta \rangle = \frac{\mu^2 E}{2kT} \exp\left[-\frac{kTI}{\zeta^2}\left(\frac{\zeta}{I} t - 1 + e^{-(\zeta/I)t}\right)\right] \tag{2.4.2.22}$$

Before concluding this section we remark that the method based on the Brinkman equations (may also be used to calculate the scattering functions $F_s(\boldsymbol{\kappa}, t)$ and $\Gamma_s(\boldsymbol{\kappa}, \omega)$ for the incoherent scattering of slow neutrons. For example, for the free particle model whose equation of motion is in the usual notation

$$m\ddot{\mathbf{r}}(t) + m\beta\dot{\mathbf{r}}(t) = m\mathbf{A}(t)$$

one finds that the intermediate scattering function is

$$F_s(\kappa, t) = \exp[-\kappa^2\gamma(\beta t - 1 + e^{-\beta t})]$$

This is $A_p^0(t)$ in the set of Eqs. 2.9.2.5 with $p = \kappa$, where this time the initial density has the form

$$\rho(\mathbf{r}, \dot{\mathbf{r}}, 0) = \delta(\mathbf{r} - \mathbf{r}_0)\delta(\mathbf{v} - \mathbf{v}_0), \quad \dot{\mathbf{r}} = \mathbf{v}$$

where δ denotes Dirac's function. Further, on utilizing the fact that Eq. 2.4.2.19 is an even function of the time we find that the scattering function $\Gamma_s(\kappa, \omega)$, where

$$\Gamma_s(\kappa, \omega) = \frac{h\kappa_0}{a_{mc}^2\kappa_1}\frac{d^2\Sigma}{d\Omega\, d\epsilon} = 2\,\mathrm{Re}\int_0^\infty F_s(\kappa, t)\exp(-i\omega t)\,dt$$

has the value

$$\mathrm{Re}\frac{2}{\beta}\left[\frac{1}{|i\omega/\beta} + \frac{\gamma\kappa^2}{|1 + i\omega/\beta} + \frac{2\gamma\kappa^2}{|2 + i\omega/\beta} + \frac{3\gamma\kappa^2}{|3 + i\omega/\beta} + \cdots\right. \tag{2.4.2.23}$$

where the symbol γ denotes $kT/m\beta^2$. We note that if γ is set equal to zero, which is tantamount to putting $m = 0$ in the equation of motion (thus ignoring inertial effects), we regain the result given in Eqs. 2.1.1.8 and 2.1.1.9, which were derived from the Smoluchowski equation. The value of $\Gamma_s(\kappa, \omega)$ correct to any order in γ may be found by computing successive convergents of Eq. 2.4.2.23. For example, taking the first convergent, one finds

$$\Gamma_s(\kappa, \omega) = \frac{2\gamma\beta\kappa^2}{(\gamma\beta\kappa^2)^2 + \omega^2}$$

Taking this approximation to the continued fraction is equivalent to ignoring completely the effect of the inertia of the particle on its own dynamical behavior. On computing the second convergent of Eq. 2.4.2.23, we find that

$$\Gamma_s(\kappa, \omega) = \frac{2\gamma\beta\kappa^2}{\left(\gamma\beta\kappa^2 - \dfrac{\omega^2}{\beta}\right)^2 + \omega^2} \tag{2.4.2.24}$$

Equation 2.4.2.24 includes the effect of inertia to first order in γ and is a close approximation to Eq. 2.4.2.23 provided that $\gamma \lesssim 0.05$. For larger values of γ the effect of the higher order terms in γ becomes important and the departure from the Lorentzian spectrum becomes more and more pronounced. This free particle model is the only one for which the set of Brinkman equations may be solved in any simple fashion. We now mention the harmonic oscillator model, namely,

$$m\ddot{x} + m\beta\dot{x} + m\omega_0^2 x = m\dot{B}(t)$$

Here the potential V is not periodic; hence the Fourier series expansion, Eq. 2.4.2.24, *may no longer be used* and the method breaks down. This will indeed be true of any case where the potential is *not* a periodic function of

x. In such a situation it may often be possible to simplify the problem by taking the Fourier transform over the time variables and then solving the resultant set of ordinary differential equations in x for the $\tilde{\psi}_n(x, \omega)$. Indeed, in the case of the harmonic oscillator, this method of finding the solution may be simplified even further by taking the Fourier transform over *both* space and time variables, that is, calculating $\tilde{\tilde{\psi}}_n(u, \omega)$. The set of Brinkman equations is then reduced to a set of difference equations which may be readily solved.

We now mention some recent papers dealing with the problem of solving the set of Brinkman equations. We also review some criticisms of Brinkman's solution procedure.

2.5 CRITICISMS OF THE BRINKMAN PROCEDURE

The primary purpose of the 1956 paper by Brinkman was to attempt to delineate rigorously a *region of validity* for the Smoluchowski equation and to find a reasonably rigorous way of *reducing* the problem of calculating the configuration space probability density, in the limit of *large* friction constants and *long* times, from that of solving the Kramers equation to that of solving the simpler Smoluchowski equation. In order to do this, Brinkman, as we have seen, derived a set of equations for the Laplace transform $\tilde{f}(x, s)$ of the density in configuration space. Further if all terms on the right-hand side of this set of equations *except the first one* are ignored then the Laplace transform of a Smoluchowski equation *with* corrections, namely,

$$s\tilde{f}(x, s) - f(x, 0) = \frac{\beta}{1 + (s/\beta)} J_D J\tilde{f}(x, s) \tag{2.5.1}$$

is obtained. The obvious step to take from here is then to invert formally this equation back into the time domain in order to obtain a so-called modified Smoluchowski equation for the density in configuration space, namely,

$$\frac{\partial f(x, t)}{\partial t} + \frac{1}{\beta}\frac{\partial^2 f(x, t)}{\partial t^2} = \frac{kT}{m\beta}\frac{\partial^2 f(x, t)}{\partial x^2} \tag{2.5.2}$$

This equation was also derived, using a Fourier transform method similar to that of Davies (1957), by Sack (1956), and it was advocated that this equation (a form of the telegraph equation) should be used to extend the region of validity of the Smoluchowski equation to earlier times. The genesis of the objections to Brinkman's procedure lies in this *suggestion* of extending the validity of the Smoluchowski equation.

An inkling that something might be amiss, if one used the telegraph equation, was provided by Hemmer in 1961. He showed that for a free particle with the initial condition

$$f(x, 0) = \delta(x - x_0)$$

then at *short times* the probability density $f(x, t)$ calculated from the Smoluchowski equation approximates more closely the *exact* $f(x, t)$ calculated from the Kramers equation than the $f(x, t)$ calculated from the modified Smoluchowski equation. However, it should be noted in fairness to the original investigators that Sack himself pointed out (1956) that for the *delta function type* of initial condition, the modified Smoluchowski equation or telegraph equation is *not valid* at short times, and higher-order terms in Brinkman's expansion *must* be included. Wilemski (1976) and Titulaer (1978) in their recent criticism of the work of Brinkman and Sack do not mention this restriction on the use of the modified Smoluchowski equation. They go on to derive new corrections to the Smoluchowski equation *in the time domain* in reciprocal powers of the friction constant, which according to Skinner and Wolynes (1979) are correct. They do not, however, in the opinion of Skinner and Wolynes, "clear up the confusion created by Brinkman's original derivation." Skinner and Wolynes (1979) go some distance toward dispelling this confusion. Using a projection operator derivation of the Smoluchowski equation based on recent work by G. Evans (1976) they show that Brinkman's equations *as obtained* in the frequency (s) domain *are correct*. They also show that what is incorrect in Brinkman's procedure is his *method of inverting* the Laplace transforms in his equation, our equation 2.4.6, to produce a diffusion equation in configuration space. They then perform a *consistent* calculation (in the sense that terms of the *same order* in the reciprocal of the friction constant in the set of Brinkman equations are *all* included in the inversion to the time domain) and find that the corrections in the time domain agree with those obtained by Wilemski and Titulaer. This effectively disposes of the suggestion that Brinkman's method of expanding the velocity dependent portion of $\tilde{\rho}(x, v, s)$ in Weber's functions and so obtaining a set of differential difference equations is fundamentally incorrect. All we have to do is invert his equation into the time domain in such a way that all terms of the *same order* in the reciprocal of the friction constant are given equal weight. In the inversion procedure proposing the modified Smoluchowski equation this has not been done, hence the confusion arising out of the use of that equation. We now proceed to the second part of this chapter, which deals with the rotational Brownian movement and its application to molecular orientational motion.

2.6 ROTATIONAL BROWNIAN MOVEMENT BASED ON THE SMOLUCHOWSKI EQUATION

2.6.1 Rotational Brownian Movement about a Fixed Axis

Debye seems to have been the first person to consider the problem of the rotational Brownian movement. In 1913, in a discussion of the origin of the observed anomalous dispersion at radio frequencies, he adopted Einstein's

theory of the Brownian movement in an attempt to explain the observed dispersion.

In his first model of the phenomenon Debye considered an assembly of molecules, each carrying a permanent dipole moment, with each molecule compelled to rotate about an axis normal to itself. He supposed further that the electrical interaction between each member of the assembly may be ignored so that *on the average* all molecules of the assembly behave in the same way. Thus it suffices to consider the behavior of *one* molecule only. Hence the problem is reduced to considering the rotational Brownian movement in two dimensions of a dipole or rigid rotator subjected to an external time varying electric field **E**. The distribution function f used by Debye is defined as follows: $f(\theta, t)\, d\theta$ which is the number of dipoles whose axes lie in an element of angle $d\theta$ on the circumference of a circle. Since the field **E** is time varying, f is a function both of the time and of the angle θ between the dipole and the field. It now follows that the Smoluchowski equation for the problem can be written from Eq. 2.1.2.1 simply by replacing the x-coordinate by the angular coordinate θ; thus we have the differential equation for f

$$\frac{\partial f(\theta, t)}{\partial t} = \frac{\partial}{\partial \theta}\left(\frac{kT}{\zeta}\frac{\partial f(\theta, t)}{\partial \theta} + \frac{1}{\zeta}\frac{\partial V(\theta, t)}{\partial \theta} f(\theta, t)\right) \tag{2.6.1.1}$$

In Eq. 2.6.1.1 t is the time, k is the Boltzmann constant, T is the absolute temperature, and ζ is the friction coefficient arising from Brownian movement of the surroundings. Equation 2.6.1.1 corresponds to the Langevin equation

$$\zeta\dot{\theta}(t) + \frac{\partial V(\theta, t)}{\partial \theta} = \lambda(t) \tag{2.6.1.2}$$

where $\lambda(t)$ is the random torque again arising from the Brownian movement of the surroundings. $\lambda(t)$ is again represented by a Wiener process as in the translational case. We immediately see from Eq. 2.6.1.2 that the inertial term $I\ddot{\theta}$ arising from the finite mass of the dipole is ignored so that the distribution functions calculated from Eq. 2.6.1.1 will again be in error at high frequencies (short times).

The potential energy due to the external field is (in the absence of induced dipole moments)

$$V = -\mu E \cos\theta = -\boldsymbol{\mu} \cdot \mathbf{E}$$

Thus Eq. 2.6.1 is reduced to

$$\frac{\partial f(\theta, t)}{\partial t} = \frac{\partial}{\partial \theta}\left(\frac{kT}{\zeta}\frac{\partial f(\theta, t)}{\partial \theta} + \frac{\mu E}{\zeta}\sin\theta f(\theta, t)\right) \tag{2.6.1.3}$$

Before proceeding we remark that the angle θ (or the coordinate r) in a diffusion equation such as Eq. 2.6.1.3 is actually an *ensemble average* of the angles. If this were not so Eq. 2.6.1.3 would contain a white noise (Wiener process type) term on its right-hand side. We go on to describe the original

work of Debye. Debye obtained two particular solutions for Eq. 2.6.1.3. The first type of solution he obtained is the so-called aftereffect solution, which may be described as follows. We suppose that the dielectric consisting of the assembly of noninteracting dipolar molecules has been influenced for a *long time* by a steady external field; thus on the average the axes of the dipoles are oriented mainly in the direction of the field. Let us now suddenly switch the field off; then the axes of the dipoles revert to their original random orientations. This phenomenon of returning from the polarized state to the original chaotic state or vice versa is called dielectric relaxation. This effect may be studied by solving Eq. 2.6.1.3 for the following situation. Suppose that the constant field $\mathbf{E} = \mathbf{E}_0$ had been acting for a long time up to $t = 0$; thus for $t > 0$ the potential energy term in Eq. 2.6.1 vanishes and that equation is reduced to

$$\frac{\partial f(\theta, t)}{\partial t} = \frac{kT}{\zeta} \frac{\partial^2 f(\theta, t)}{\partial \theta^2} \tag{2.6.1.4}$$

Furthermore, since $\mathbf{E}_0$ had been acting for a long time up to $t = 0$, the distribution at that time must be the Maxwell–Boltzmann distribution so that

$$f(\theta, 0) = A \exp\left(\frac{\mu E_0 \cos\theta}{kT}\right) \tag{2.6.1.5}$$

and to terms linear in the field strength this expression is approximated by

$$f(\theta, 0) = A\left(1 + \frac{\mu E_0}{kT} \cos\theta\right) \tag{2.6.1.6}$$

where A is a given constant. This holds true if $\mu E_0/kT \sim 10^{-4}$.

Equation 2.6.1.6 is the linear approximation to the distribution function. If higher-order terms are included we are taking account of the nonlinear behavior of the dielectric. This is discussed later, because it is not relevant in the present case. The form of the initial condition now suggests that we seek a solution of Eq. 2.6.1.4 of the form

$$f(\theta, t) = A\left(1 + \frac{\mu E_0}{kT} g(t) \cos\theta\right) \tag{2.6.1.7}$$

On substituting this equation into Eq. 2.6.1.4 and solving the resulting ordinary differential equation for $g(t)$, which is simply

$$\frac{dg(t)}{dt} = -\frac{kT}{\zeta} g(t)$$

we find that $f(\theta, t)$ is given by

$$f = A\left(1 + \frac{\mu E_0}{kT} e^{-(kT/\zeta)t} \cos\theta\right)$$

We note that as $t \to \infty$, f is independent of θ while the variable part of f

decays away with time. The time constant of the decay is

$$\tau_0 = \frac{\zeta}{kT} \tag{2.6.1.8}$$

which is called the *Debye relaxation time.* We now calculate the mean dipole moment, that is, the dipole moment averaged over the ensemble. We have

$$m_{E_0} = \mu\langle\cos\theta\rangle = \frac{\int_0^{2\pi} \mu f \cos\theta \, d\theta}{\int_0^{2\pi} f \, d\theta} = \frac{\mu^2 E_0}{2kT} e^{-t/\tau_0} \tag{2.6.1.9}$$

This is the *mean* component of the electric moment in the direction of the field. This component decays exponentially with decay constant τ_0. We now discuss the second problem posed by Debye, namely, the behavior of f when an *alternating* electric field is applied. We suppose that an alternating field has been applied to the dielectric for a long time so that the transient effect associated with the switching on of the field may be neglected. If we express the field in complex notation as $\mathbf{E}_m e^{i\omega t}$, then

$$\frac{\partial f(\theta, t)}{\partial t} = \frac{\partial}{\partial \theta}\left(\frac{kT}{\zeta} \frac{\partial f(\theta, t)}{\partial \theta} + \frac{\mu E_m}{\zeta} e^{i\omega t} \sin\theta\right) \tag{2.6.1.10}$$

In writing down Eq. 2.6.1.10 we assume that the linear approximation for f still holds; otherwise we cannot use the complex notation for the field. Debye now assumes that the solution of Eq. 2.6.1.10 may be written

$$f(\theta, t) = A\left(1 + B \frac{\mu E_m}{kT} e^{i\omega t} \cos\theta\right) \tag{2.6.1.11}$$

where B must be equal to unity for $t = 0$. On substituting this equation into Eq. 2.6.1.10 we readily find the value of B, and thus f, to be

$$f = A\left(1 + \frac{e^{i\omega t}}{1 + i\omega\tau_0} \frac{\mu E_m}{kT} \cos\theta\right) \tag{2.6.1.12}$$

whence with Eq. 2.6.1.9 the mean dipole moment is

$$\langle\mu \cos\theta\rangle = \frac{\mu^2}{2kT} \frac{E_m e^{i\omega t}}{1 + i\omega\tau_0} \tag{2.6.1.13}$$

or

$$\langle\mu \cos\theta\rangle = \frac{\mu^2}{2kT} \frac{E_m[(\cos\omega t + \omega\tau_0 \sin\omega t) + i(\sin\omega t - \omega\tau_0 \cos\omega t)]}{1 + \omega^2\tau_0^2}$$

Thus we see at once that there is a *difference* in phase between $\langle\mu \cos\theta\rangle$ and E. This phase difference persists if in place of $E_m e^{i\omega t}$ we take its real or imaginary parts $E_m \cos\omega t$ or $E_m \sin\omega t$. We now describe the second model given by Debye (1929).

2.6.2 Rotational Brownian Movement in Space Based on the Smoluchowski Equation

The analysis given in the preceding section pertains to rotators free to rotate about *fixed* axes only. Debye in his analysis also considered a model where the dipoles are free to rotate in space. More specifically each dipole is supposed to be fixed in a rigid sphere which is free to rotate in space, the sphere being subjected both to random noise couples about its axis of rotation, having no preferential direction, and to the action of a time varying electric field applied in a fixed direction. The distribution function f for the problem is defined as follows. f is the number of dipoles whose axes point into an element of solid angle $d\Omega$; thus f is a function of both the time and the angle ϑ between the axis of a dipole and the applied field. Again it is implicitly assumed that the inertia of the dipoles may be neglected and further that the electrical dipole–dipole coupling between them may also be ignored so that *on the average* each dipole behaves in the *same* way. Thus with the aid of our Smoluchowski equation written in coordinate free notation (Chapter 1) we find that

$$\frac{\partial f(\vartheta, t)}{\partial t} = \frac{1}{\sin\vartheta}\frac{\partial}{\partial\vartheta}\left[\sin\vartheta\left(\frac{kT}{\zeta}\frac{\partial f(\vartheta, t)}{\partial\vartheta} + \frac{\mu E}{\zeta}\sin\vartheta f(\vartheta, t)\right)\right] \qquad (2.6.2.1)$$

which is simply the ordinary Smoluchowski equation written in spherical polar coordinates. It is worth noting that Eq. 2.6.2.1 is also the correct form of the Smoluchowski equation for bodies having the shape of *prolate* or *oblate* spheroids as may be seen by writing out the Smoluchowski operator in these coordinates (for a good description of these coordinates see Macrobert (1967) or Hobson (1931)). The general solution of Eq. 2.6.2.1 is of the form

$$f(\vartheta, t) = \sum_{n=0}^{\infty} a_n(t)P_n(\cos\vartheta) \qquad (n = 0, 1, 2, \ldots) \qquad (2.6.2.2)$$

where the P_n are the Legendre polynomials (Hobson, 1931) and the $a_n(t)$ are functions to be determined. However, as far as dielectric relaxation is concerned we are generally only interested in the linear approximation to the solution. Thus for the aftereffect solution in which a steady field is suddenly switched off at time $t = 0$ we may again assume that f has the form

$$f(\vartheta, t) = A\left(1 + \frac{\mu E_0}{kT}g(t)\cos\vartheta\right)$$

which with the aid of Eq. 2.6.2.1 immediately yields

$$f(\vartheta, t) = A\left(1 + \frac{\mu E_0}{kT}e^{-(2kT/\zeta)t}\cos\vartheta\right) \qquad (2.6.2.3)$$

while the mean dipole moment is, taking account of the azimuthal angle φ,

$$\mu\langle\cos\vartheta\rangle = \frac{\int_0^{2\pi}\int_0^{\pi}\mu f\cos\vartheta\sin\vartheta\,d\vartheta\,d\varphi}{\int_0^{2\pi}\int_0^{\pi}f\sin\vartheta\,d\vartheta\,d\varphi} = \frac{\mu^2E_0}{3kT}e^{-t/\tau} \qquad (2.6.2.4)$$

where this time τ, the Debye relaxation time, is

$$\tau = \frac{\zeta}{2kT} \qquad (2.6.2.5)$$

Thus the dynamic behavior of the sphere model in the Smoluchowski approximation differs from that of the disk model *only* in the value of the relaxation time, the relaxation time for the sphere model being *half* that for the disk model. In the same way we may deduce that when the field $\mathbf{E}$ is alternating so that

$$\mathbf{E} = \mathbf{E}_m e^{i\omega t}$$

the value of the mean dipole moment is

$$\mu\langle\cos\vartheta\rangle = \frac{\mu^2}{3kT}\frac{E_m}{1+\omega^2\tau^2}[(\cos\omega t + \omega\tau\sin\omega t) + i(\sin\omega t - \omega\tau\cos\omega t)] \qquad (2.6.2.6)$$

The solutions obtained by Debye are for a body of *arbitrary* shape constrained to rotate in a plane and for a body having spherical symmetry free to rotate in three dimensions. In 1934 F. Perrin generalized the Debye theory to obtain an expression for the mean dipole moment for an asymmetric body rotating in three dimensions. His result for the mean dipole moment is

$$\langle\boldsymbol{\mu}\cdot\mathbf{e}\rangle = \langle\mu\cos\delta\rangle = \left(\frac{\mu_1^2}{1+i\omega\tau_1} + \frac{\mu_2^2}{1+i\omega\tau_2} + \frac{\mu_3^2}{1+i\omega\tau_3}\right)\frac{E_m e^{i\omega t}}{3kT} \qquad (2.6.2.7)$$

where δ is the angle which the moment of the dipole $\boldsymbol{\mu}$ [having components μ_1, μ_2, μ_3 along the principal axes 1, 2, 3 (Goldstein, 1950) of the body] embedded in the body makes with the field. τ_1, τ_2, and τ_3 are relaxation times given by

$$\tau_1 = \frac{1}{kT\left(\frac{1}{\zeta_2}+\frac{1}{\zeta_3}\right)}, \qquad \tau_2 = \frac{1}{kT\left(\frac{1}{\zeta_1}+\frac{1}{\zeta_3}\right)}, \qquad \tau_3 = \frac{1}{kT\left(\frac{1}{\zeta_1}+\frac{1}{\zeta_2}\right)} \qquad (2.6.2.8)$$

where the ζ_i are the friction coefficients for motion about the three principal axes fixed in the body. Thus the departure from spherical symmetry gives rise to three *separate* relaxation mechanisms each of the Debye type. However, if the dipole has a moment only in the direction of one of the principal axes ($\mu_1 = \mu_3 = 0$) then the frequency dependence may be expressed by a *single* relaxation mechanism. Further, if the body has an

axis of symmetry, that is, if the body is a prolate or oblate spheroid, then there are only two distinct relaxation mechanisms. We remark on a curious observation made by Perrin (1934), that the time of relaxation for the component of the dipole moment along any one of the principal axes is a function of the *harmonic mean* of the coefficients of friction about the other two axes. This problem has been investigated by Ford et al. (1979), who regain Perrin's results using rotation operators.

It is now of interest to see how the aftereffect and alternating field solutions may be related in the linear approximation. In order to do this we must describe linear response theory.

2.6.3 Linear Response Theory

In this section we show how the aftereffect and alternating field solution may be related by means of a method which has been described by Scaife (1959, 1971). Let us suppose that at a time $t = 0$, say, a unit electric field is applied to a dielectric body; then an electric dipole moment $a(t)$ is induced in that body. This quantity $a(t)$ is called the *response function* of the body. Let us now suppose that the inducing electric field at time t is $\mathbf{E}(t)$ and $0 \leqslant t' \leqslant t$; then the increase in the field intensity in an infinitesimal time $\delta t'$ is $(d\mathbf{E}/dt')\delta t'$ and this in its turn contributes $\dot{\mathbf{E}}(t')\,\delta t' a(t-t')$ to the induced moment at time t. Thus at time t the instantaneous dipole moment of the body is

$$\mathbf{m}(t) = \int_0^t \frac{d\mathbf{E}(t')}{dt'}\,dt' a(t-t') \tag{2.6.3.1}$$

Now on integrating Eq. 2.6.3.1 by parts

$$\mathbf{m}(t) = \mathbf{E}(t')a(t-t')\Big|_{t'=0}^{t} - \int_0^t \mathbf{E}(t')\frac{da}{dt'}(t-t')\,dt' \tag{2.6.3.2}$$

We now suppose that $\mathbf{E}(t')$ vanishes for $t' \leqslant 0$ and so $\mathbf{E}(0) = 0$. Also we suppose that when a field is switched on there is no instantaneous response so that $a(0) = 0$; thus the first term on the right of Eq. 2.6.2.2 vanishes and we may write with $t - t' = x$

$$\mathbf{m}(t) = \int_0^t \mathbf{E}(t-x)\frac{da(x)}{dx}\,dx \tag{2.6.3.3}$$

Our discussion so far refers to the case where the field is being switched on. Let us now go to the opposite case where a field of unit intensity had been operative for a long time so that the induced moment is $a(\infty)$ and let us suppose that $\mathbf{E}(t)$ is switched off at time $t = 0$. For $t > 0$ the induced moment is $a(\infty) - a(t)$. This leads us to define the *aftereffect function* $b(t)$ by the relation

$$\begin{aligned} b(t) &= a(\infty) - a(t) \qquad (t > 0) \\ &= 0 \qquad\qquad\quad (t < 0) \end{aligned} \tag{2.6.3.4}$$

whence

$$\frac{db(t)}{dt} = -\frac{da(t)}{dt}$$

Let us now put

$$\begin{aligned} \mathbf{E}(t) &= \mathbf{E}_m \cos\omega t \qquad (t > 0) \\ &= 0 \qquad\qquad\quad (t < 0) \end{aligned} \equiv \mathbf{E}_m U(t) \cos\omega t$$

whence

$$\begin{aligned} \mathbf{m}(t) &= \int_0^t \mathbf{E}_m \cos\omega(t-x)\frac{da(x)}{dx}\,dx \\ &= \mathbf{E}_m \cos\omega t \int_0^t \cos\omega x \frac{da(x)}{dx}\,dx + \mathbf{E}_m \sin\omega t \int_0^t \sin\omega x \frac{da(x)}{dx}\,dx \end{aligned}$$

Now if t is very large, $da(x)/dx$, $t \leqslant x \leqslant \infty$, is negligibly small and thus the integrals $\int_t^\infty [da(x)/dx] \cos\omega x\,dx$, $\int_t^\infty [da(x)/dx] \sin\omega x\,dx$ are also negligible.

Thus we may write

$$\mathbf{m}(t) = \mathbf{E}_m \alpha'(\omega)\cos\omega t + \mathbf{E}_m \alpha''(\omega)\sin\omega t$$

where

$$\alpha'(\omega) = \int_0^\infty \frac{da(x)}{dx}\cos\omega x\,dx; \qquad \alpha''(x) = \int_0^\infty \frac{da(x)}{dx}\sin\omega x\,dx$$

both being real functions of ω. We now define the *complex polarizability* $\alpha(\omega)$ by

$$\alpha(\omega) = \alpha'(\omega) - i\alpha''(\omega)$$

and we see that

$$\alpha(-\omega) = \alpha'(\omega) + i\alpha''(\omega)$$

we may also write

$$\alpha(\omega) = \int_0^\infty \frac{da(x)}{dx} e^{-i\omega x}\,dx = \int_0^\infty \frac{da(t)}{dt} e^{-i\omega t}\,dt = -\int_0^\infty \frac{db(t)}{dt} e^{-i\omega t}\,dt$$

which on integrating by parts becomes

$$\begin{aligned} \alpha(\omega) &= -b(t)e^{-i\omega t}\Big|_0^\infty - i\omega \int_0^\infty b(t)e^{-i\omega t}\,dt \\ &= a(\infty) - a(0) - i\omega \int_0^\infty b(t)e^{-i\omega t}\,dt \end{aligned} \tag{2.6.3.5}$$

But

$$a(\infty) - a(0) = \int_0^\infty \frac{da(x)}{dx}\,dx = \alpha'(0) = \alpha(0)$$

Setting $\omega = 0$ we see that $\alpha(0)$ is the static polarizability due to field $\mathbf{E}$ so

we denote it by α_s and we express Eq. 2.6.3.5 as

$$\alpha(\omega) = \alpha_s - i\omega \int_0^\infty b(t)e^{-i\omega t}\, dt$$

or

$$\frac{\alpha(\omega)}{\alpha'(0)} = 1 - i\omega \int_0^\infty R(t)e^{-i\omega t}\, dt \qquad \left(R(t) = \frac{b(t)}{b(0)}\right) \tag{2.6.3.6}$$

This equation effectively *connects* the alternating and aftereffect solutions *provided the response is linear.* We make much use of the above equation in what follows.

2.7 BREAKDOWN OF THE DEBYE THEORY AT HIGH FREQUENCIES

As we have pointed out, the Debye theory (and the generalization of it due to Perrin) of dielectric relaxation takes *no account* of the inertia of the rotating dipoles. Thus, as has been said repeatedly, that theory breaks down at very short periods. (The discussion that follows is largely due to Sack (1957)). In order to achieve maximum clarity in what is to come we now summarize the main findings of the Debye theory. First of all, we see from the preceding discussion that if a system is subject to a sinusoidally alternating field

$$\mathbf{E}_m \cos \omega t = \mathbf{E}_m \operatorname{Re}(e^{i\omega t}) \tag{2.7.1}$$

which is not so large as to cause saturation effects, then the steady-state response may be described by a complex polarizability depending on frequency

$$\alpha(\omega) = \alpha'(\omega) - i\alpha''(\omega)$$

such that the time-dependent dipole moment $\mathbf{m}(t)$ is

$$\mathbf{m}(t) = \mathbf{E}_m(\alpha'(\omega) \cos \omega t + \alpha''(\omega) \sin \omega t) \tag{2.7.2}$$

The coefficient $\alpha''(\omega)$ is a measure of the energy loss per cycle for a constant amplitude E_m. For a system obeying the Debye equations the frequency dependence of $\alpha(\omega)$ is given by

$$\alpha(\omega) = \frac{\alpha'(0)}{1 + i\omega\tau} \tag{2.7.3}$$

$$\alpha'(\omega) = \frac{\alpha'(0)}{1 + \omega^2\tau^2} \tag{2.7.4}$$

$$\alpha''(\omega) = \frac{\omega\tau\alpha'(0)}{1 + \omega^2\tau^2} \tag{2.7.5}$$

The quantity $\alpha''(\omega)$ has a maximum for $\omega\tau = 1$. Experimental curves of $\alpha''(\omega)$ versus $\log \omega$ usually show an absorption peak broader than predicted by Eq. 2.7.5. This can be explained by a *distribution*, $\alpha(\log \tau)$, of relaxation times so that we have for the frequency-dependent response coefficient

$$\alpha(\omega) = \int \frac{\alpha(\log \tau)d(\log \tau)}{1 + i\omega\tau} \tag{2.7.6}$$

We illustrate later how this distribution of relaxation times may arise naturally. Whatever the mechanism for the relaxation, however, the Debye equations Eqs. (2.7.4 and 2.7.5) must break down at very short times. They predict, for example, that in a dielectric a relaxation absorption in the audio or radio frequency range would entail a finite absorption coefficient for visible light with complete opacity in some extreme cases such as water (Debye, 1934) and an infinite rate of energy loss for an electron traveling through the material. They are also unable to account for the resonance or Poley (1955) absorption peak occurring in the far infrared or terahertz band of frequencies. This peak is illustrated using the *J*-diffusion model (Gordon, 1968) in Fig. 2.7.1. This model is considerably more flexible than Debye's but cannot reproduce the most characteristic and fundamental property of the far infrared absorption, the frequency dependence of the peak power absorption (in Np/cm). Note that one limit of this model is rotational diffusion, and the figure illustrates the development of the Debye plateau.

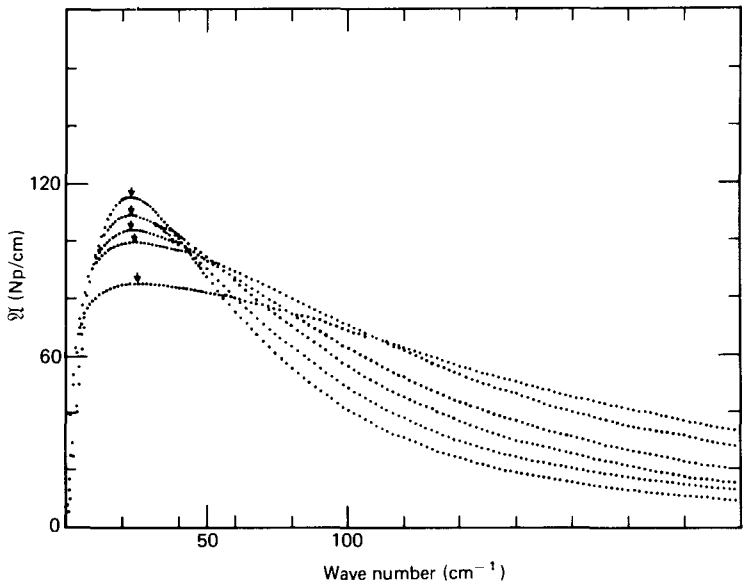

Figure 2.7.1 Some far infrared curves as a function of the time between collisions of the *J*-diffusion model. Note that the peak position of the power absorption coefficient does not move as a function of the mean time between collisions. 1–6 Decreasing time between collisions. [Reproduced by permission from M. W. Evans et al., *J. Chim. Phys.* **75**, 522 (1978).]

In the time domain the Debye equations imply that an abrupt change in the field **E** would produce an instantaneous finite alteration of the rate of change $(d\mathbf{m}(t)/dt)$ of the dipole moment which is impossible in view of the finite rotational inertia of the dipoles. The consequence of this is the Debye plateau of Fig. 1.2.2. In general, the product $\omega\alpha''(\omega)$ *must tend to zero* in the limit of high frequencies, which means that in the frequency range in which $\alpha(\omega)$ can be expanded in negative powers of ω, that is,

$$\alpha(\omega) = a_0 + \frac{a_1}{i\omega} + \frac{a_2}{(i\omega)^2} + \cdots$$

the coefficient a_1 *must* vanish. This is compatible with a distribution of relaxation times of the type given in Eq. 2.7.6 only if the function $\alpha(\log \tau)$ can take on negative as well as positive values, (Gross, 1955; Sack, 1957). In the time domain the stipulation that $\omega\alpha''(\omega)$ must vanish means that the Taylor expansion of the aftereffect function must not contain terms of the order of $|t|$.

The above considerations show that in all relaxation processes inertial effects become important at sufficiently high frequencies. Consequently there have been many attempts to include them in the Debye theory. The earliest attempt to include them was that of Rocard (1933), followed by Dmitriev and Gurevich (1946) and Powles (1948). These attempts were all based in one way or another on the inclusion of an extra term in the Smoluchowski equation, thus rendering them only partially correct. Indeed inertial effects can be consistently treated only on the basis of the generalized Liouville equation (Kramers equation) which considers distributions in configuration-angular velocity space where both angular positions and angular momenta (or angular velocities) are taken as independent variables. The first investigator to adopt this approach based on the generalized Liouville equation was Gross, who in 1955 considered the behavior of rigid dipoles rotating about fixed axes in a viscous medium. The paper of Gross, however, does not include a detailed description of how his results were obtained; indeed, his results were all derived at about the same time by Sack (1957), so in what follows we review the treatment of Sack.

2.7.1 Sack's Treatment of Inertial Effects

As we have already seen in Chapter 1 the statistical behavior of a classical macroscopic assembly under the action of external and internal forces is described by the Liouville equation

$$\frac{D\rho}{Dt} = \frac{\partial\rho}{\partial t} + \{H, \rho\} \qquad (2.7.1.1)$$

Further, because this equation contains a number of variables of the order of 10^{20} it is necessary to modify this equation by both reducing it and generalizing it, reducing by limiting the number of degrees of freedom to a small representative set, and generalizing by the addition of terms on the right-hand side of Eq. 2.7.1.1 to account for the mean interaction between this set and the remaining degrees of freedom (the background or heat bath).

In the case of statistical equilibrium $D\rho/Dt$ will vanish for the generalized Liouville equation since this equilibrium is independent of the nature of the interaction between the set considered and the background. According to Sack (1957), of the various possible types of interactions, the ones mostly investigated belong to the class of *adiabatic* collisions, which are of such *short* duration compared to other explicitly considered time intervals, such as periods of oscillation or rotation, that they can be treated as *instantaneous*. These are the only types of collision that Sack considers. He lists the following types of collisions (on the assumption that the background is always in thermal equilibrium).

1. Small collisions (Brownian movement) in which the position of the particles are unchanged and their velocities are altered by such small amounts that they can be treated as infinitesimal. Correlation between successive collisions is negligible. Under the simplest assumptions the *effect* of such collisions appears as a *viscous retardation*,

$$\frac{d\boldsymbol{\omega}}{dt} = -\beta\boldsymbol{\omega}$$

   superimposed on which are random fluctuations which are governed by a *Wiener process*; $\boldsymbol{\omega}$ denotes the angular velocity vector.
2. Large collisions in which the positions of the particles *remain unaltered* on impact, but all coherence between their *initial* and *final* velocities is destroyed; after each collision a particle may have any velocity with a probability according to Boltzmann's law for the given temperature.
3. Very large collisions which *destroy coherence of positions* as well as *momentum*; after each impact a particle may be found anywhere in phase space according to the Boltzmann distribution corresponding to the momentary Hamiltonian.

The physical explanation of these limiting and some intermediary cases has been given by Gross (1955). Sack summarizes the three cases as follows. Assumption 1 corresponds to the case of the explicitly considered particles being surrounded by a heat bath formed by much smaller particles; in case 2 the molecules of the heat bath are heavier, whereas assumption 3 is strictly speaking contrary to the laws of impact, but can sometimes be taken to be a useful approximation in the case of disproportionately heavier particles forming the background.

Finally Sack notes that the collision rates can, in principle, be functions of the positions and velocities but are treated in this paper as constants of the system as is usually done. Sack then goes on to incorporate inertial effects in the first Debye model described in Section 2.6. The Kramers equation for this model is the same as that for the particle moving along the x-axis; the only alteration is that the coordinates $(x, \dot{x})$ are replaced by the angular equivalents $(\theta, \dot{\theta})$. Thus the Kramers equation is

$$\frac{D\rho}{Dt} = \frac{\partial \rho}{\partial t} + \dot{\theta}\frac{\partial \rho}{\partial \theta} - \frac{1}{I}\frac{\partial V(\theta)}{\partial \theta}\frac{\partial \rho}{\partial \dot{\theta}} = \beta \frac{\partial}{\partial \dot{\theta}}\left(\dot{\theta}\rho + \frac{kT}{I}\frac{\partial \rho}{\partial \dot{\theta}}\right) \tag{2.7.1.2}$$

where V, the potential energy, is given by

$$V(\theta) = -\mu E \cos\theta$$

Furthermore, since we are interested in the aftereffect solution of Eq. 2.7.1.2, V vanishes for $t > 0$ so that Eq. 2.7.1.2 becomes

$$\frac{D\rho}{Dt} = \frac{\partial \rho}{\partial t} + \dot{\theta}\frac{\partial \rho}{\partial \theta} = \frac{\partial}{\partial \dot{\theta}}\left[\dot{\theta}\rho + \frac{kT}{I}\frac{\partial \rho}{\partial \dot{\theta}}\right] \tag{2.7.1.3}$$

Equation 2.7.1.3 must be solved subject to the initial condition

$$\rho(\theta, \dot{\theta}, 0) = A \exp\left(\frac{\mu E}{kT}\cos\theta\right) = A\left(1 + \frac{\mu E}{kT}\cos\theta + \cdots\right) \tag{2.7.1.4}$$

in the linear approximation. A is an irrelevant constant. Figure 2.7.1.1 illustrates angular velocity probability density functions typical of the Kramers equation (specifically those for the planar itinerant librator). The problem now is to calculate the mean dipole moment as a function of time, namely,

$$\langle \boldsymbol{\mu}(t) \cdot \mathbf{e} \rangle = \mu \frac{\int_0^{2\pi}\int_{-\infty}^{\infty} \rho(\theta, \dot{\theta}, t)\cos\theta \, d\dot{\theta}\, d\theta}{\int_0^{2\pi}\int_{-\infty}^{\infty} \rho(\theta, \dot{\theta}, t)\, d\dot{\theta}\, d\theta} \tag{2.7.1.5}$$

In order to calculate $\langle \boldsymbol{\mu}(t) \cdot \mathbf{e} \rangle$ Sack finds it convenient to construct the *characteristic function* of the random variable $\dot{\theta}$ by means of the equation

$$\Phi_{\dot{\theta}}(\theta, u, t) \equiv \Phi(\theta, u, t) = \int_{-\infty}^{\infty} \rho(\theta, \dot{\theta}, t) e^{-iu\dot{\theta}}\, d\dot{\theta} \tag{2.7.1.6}$$

which, with the Kramers equation, gives the following equation for Φ:

$$\frac{\partial \Phi}{\partial t} + i\frac{\partial^2 \Phi}{\partial \theta\, \partial u} = -\beta u\left(\frac{kT}{I}u\Phi + \frac{\partial \Phi}{\partial u}\right) \tag{2.7.1.7}$$

Equation 2.7.1.7 may be further simplified by defining a quantity Ψ where

$$\Psi = \left(\exp\frac{kTu^2}{2I}\right)\Phi$$

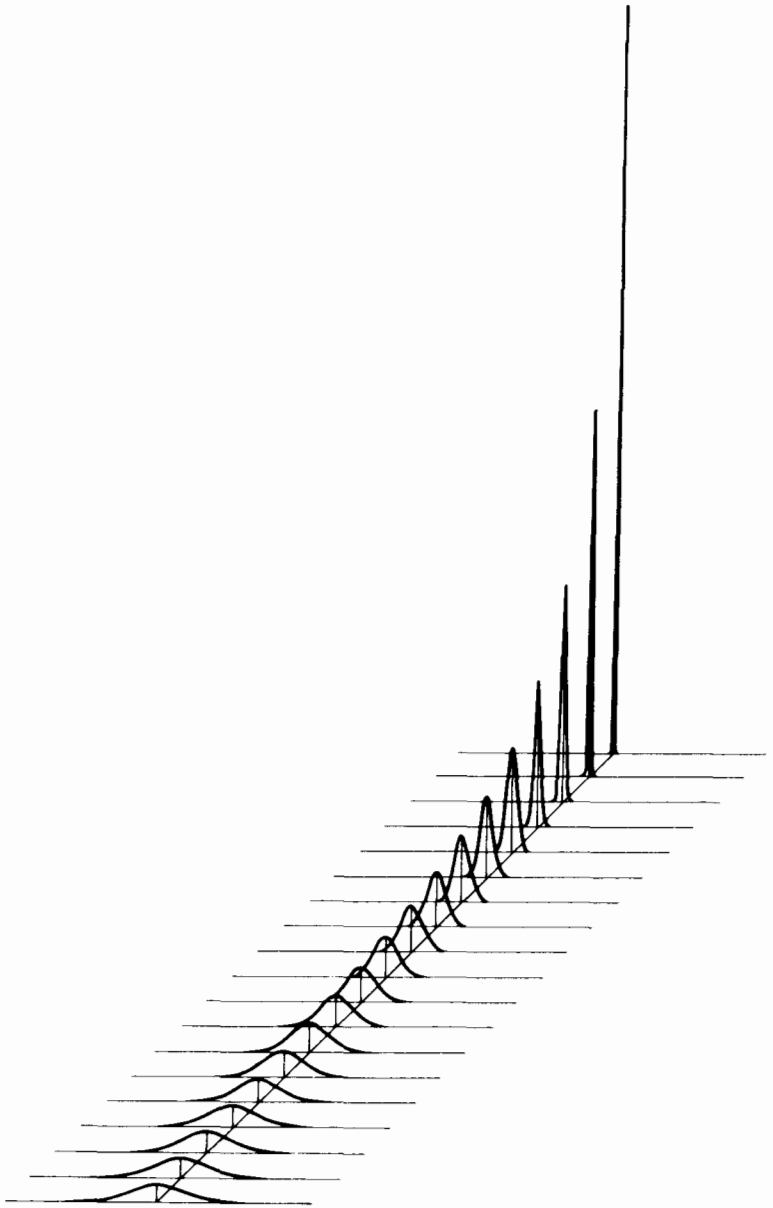

Figure 2.7.1.1 Probability density functions of angular velocity: itinerant libration in a plane. [Reproduced by permission from A. R. Davies and M. W. Evans, *Mol. Phys.* **35**, 864 (1978).]

This results in the following differential equation for Ψ:

$$\frac{\partial \Psi}{\partial t} + i\frac{\partial^2 \Psi}{\partial \theta\, \partial u} - \frac{iu}{I} kT \frac{\partial \Psi}{\partial \theta} = -\beta u \frac{\partial \Psi}{\partial u} \tag{2.7.1.8}$$

It should be noted that Eq. 2.7.1.8 is entirely similar to that obtained by Davies (1957) in his treatment of the one-dimensional translational problem. The next step made by Sack is to express the function Ψ as a Fourier series in θ, namely,

$$\Psi(\theta, u, t) = \sum_k e^{ik\theta} \psi_k(u, t) \tag{2.7.1.9}$$

On putting $t = 0$ in Eq. 2.7.1.9 and comparing the coefficients of $e^{ik\theta}$ to those in Eq. 2.7.1.4 one finds that the linear approximation to $\Psi(\theta, u, t)$ will involve only ψ_1 and ψ_{-1} apart from the constant term $\psi_0 = 1$. Further, in view of Eq. 2.7.1.4, we must have

$$\psi_{-1}(u, t) = \psi_1(-u, t)$$

Thus we have for the mean dipole moment

$$\langle \boldsymbol{\mu}(t) \cdot \mathbf{e} \rangle = \mu \frac{[\psi_1(0, t)]}{\psi_0(0, t)} \tag{2.7.1.10}$$

The next step is to calculate $\psi_1(u, t)$. To this end we substitute Eq. 2.7.1.9 into Eq. 2.7.1.8 and take the $k = 1$ terms only; this gives us the following first-order partial differential equation for $\psi_1(u, t)$:

$$\frac{\partial \psi_1(u, t)}{\partial t} - \frac{\partial \psi_1(u, t)}{\partial u} + u \frac{kT}{I} \psi_1(u, t) = -\beta u \frac{\partial \psi_1(u, t)}{\partial u}$$

which is solved subject to the initial condition (derived by inspection)

$$\psi_1(u, 0) = \frac{\mu E}{2kT}$$

This equation is solved by the methods we have described for dealing with such equations and we easily find that

$$\psi_1(u, t) = \frac{\mu E}{2kT} \exp\left\{\left(-\frac{kT}{I\beta}\right)[t + (u - \beta^{-1})(1 - e^{-\beta t})]\right\}$$

and thus with Eq. 2.7.1.10

$$\langle \boldsymbol{\mu}(t) \cdot \mathbf{e} \rangle = \frac{\mu^2 E}{2kT} \exp\left[-\frac{kT}{I\beta^2}(\beta t - 1 + e^{-\beta t})\right] \qquad (t > 0) \tag{2.7.1.11}$$

The complex polarizability α may now be calculated by means of the equation

$$\frac{\alpha(\omega)}{\alpha'(0)} = 1 - i\omega \int_0^\infty R(t)\, e^{-i\omega t}\, dt \tag{2.7.1.12}$$

where

$$\alpha'(0) = \frac{\mu^2}{2kT}, \qquad R(t) = \frac{\langle \boldsymbol{\mu}(t) \cdot \mathbf{e} \rangle}{\langle \boldsymbol{\mu}(0) \cdot \mathbf{e} \rangle}$$

On substituting Eq. 2.7.1.11 into Eq. 2.7.1.12 and performing the integration, we find that the result may be represented by the following continued fraction:

$$\frac{\alpha(\omega)}{\alpha'(0)} = 1 - \frac{i\omega}{\beta}\left[\frac{1}{|i\omega/\beta} + \frac{\gamma}{|1 + i\omega/\beta} + \frac{2\gamma}{|2 + i\omega/\beta} + \frac{3\gamma}{|3 + i\omega/\beta} + \cdots\right. \tag{2.7.1.13}$$

where

$$\gamma = \frac{kT}{I\beta^2}$$

The first convergent of this yields the Debye relaxation formula, namely,

$$\frac{\alpha'(\omega)}{\alpha(0)} = \frac{1}{1 + i\omega\tau_0}$$

where

$$\tau_0 = \frac{\zeta}{kT} = \frac{I\beta}{kT}$$

while the second convergent gives

$$\frac{\alpha(\omega)}{\alpha'(0)} = \frac{1}{1 + i\omega\tau_0 - \dfrac{\omega^2 \tau_0}{\beta}} \tag{2.7.1.14}$$

We now discuss the physical meaning of these equations. First of all we note that our expression for $\langle \boldsymbol{\mu}(t) \cdot \mathbf{e} \rangle$ may be expanded to give

$$\langle \boldsymbol{\mu}(t) \cdot \mathbf{e} \rangle = \frac{\mu^2 E}{2kT}\left\{\exp\left(-\frac{t}{\tau_0}\right) - \frac{\gamma}{1!}\exp\left(-\frac{t}{\tau_1}\right) + \cdots\right\} e^{\gamma}, \quad \tau_n = \left(\frac{kT}{I\beta} + n\beta\right)^{-1}$$

Thus the first effect of inertia is to give rise to a *discrete set* of relaxation times instead of just a *single* one as in the case of the simple Debye theory. Further, for long times such that $t \gg \beta^{-1}$, one finds that

$$\langle \boldsymbol{\mu}(t) \cdot \mathbf{e} \rangle = \frac{\mu^2 E}{2kT} \exp\left(-\frac{t}{\tau_0}\right)$$

which is the Debye result. On the other hand, one finds for very short times such that $t \ll \beta^{-1}$,

$$\langle \boldsymbol{\mu}(t) \cdot \mathbf{e} \rangle = \frac{\mu^2 E}{2kT} \exp\left(-\frac{kT}{2I} t^2\right)$$

a result which may be deduced from kinetic theory considerations. Returning to our results in the frequency domain, we see that the first convergent of our continued fraction yields the Debye equations as one would expect while the

second convergent yields a response function akin to that of an *overdamped* oscillator. The word overdamped is stressed since this second convergent is only a valid approximation to the continued fraction when $\gamma \ll 1$ which automatically prevents Eq. 2.7.1.14 from exhibiting resonance phenomena. According to Sack, Eq. 2.7.1.14 will be a very good approximation to the continued fraction provided

$$\gamma \leqslant 0.05$$

For larger values of γ the higher order terms in the continued fraction became progressively more important, but according to Gross (1955) the classical model, is then no longer a good approximation in view of the discrete spacing of rotational levels and a quantum-mechanical treatment must be used. The most important point to note from this analysis is that Eq. 2.7.1.14 decays like ω^{-2} as $\omega \to \infty$ thus the objectionable behavior of the Debye equations in the high frequency region is corrected on the other hand, however, Eq. 2.7.1.14 or indeed the continued fraction expansion do not exhibit resonance behavior hence they cannot account for the Poley absorption. A much more extensive discussion of Eq. 2.7.1.13 has been given by Scaife (1971).

Solutions of the problem for collision mechanisms of types (2) and (3) have also been given by Sack. For the collisions of type 2 the generalised Liouville equation takes the form

$$\frac{D\rho}{Dt} = \frac{\partial \rho}{\partial t} + \dot{\theta}\frac{\partial \rho}{\partial \theta} = \left\{\beta_1 \left(\frac{I}{2\pi kT}\right)^{1/2} \exp\left(\frac{-I\dot{\theta}^2}{2kT}\right) \int \rho \, d\dot{\theta} - \beta_1 \rho\right\}$$

which results in the transformed function

$$\frac{D'\Psi}{D't} = \beta_1 \Psi(\theta, 0, t) - \beta_1 \Psi(\theta, u, t)$$

while for the very large collisions of type 3 we have

$$\frac{D'\Psi}{D't} = -\beta_1 \Psi(\theta, u, t) + \beta_1 \Phi_0(\theta, 0) \frac{\int \Psi(\theta, 0, t)\, d\theta}{\int \Phi_0(\theta, 0)\, d\theta}$$

These equations may be solved in substantially the same way as that given in the Brownian motion case. For case 2 one finds that

$$\langle \boldsymbol{\mu}(t) \cdot \mathbf{e} \rangle = \frac{\mu^2 E}{2kT} \left\{ \exp[Z_1(0, t)] + \beta_1 \int_0^t \exp[Z_1(0, \tau)] \psi_1(0, t - \tau)\, d\tau \right\}$$

This equation may be solved by Picard's method of successive approximations; the solution is cumbersome and more insight is gained from the expressions for $\alpha(\omega)$, namely,

$$\frac{\alpha(\omega)}{\alpha'(0)} = 1 - \frac{i\omega}{\beta_1} \frac{\exp \xi^2 \operatorname{erfc} \xi}{(\frac{1}{2}\gamma_1)^{1/2} - \exp \xi^2 \operatorname{erfc} \xi}, \quad Z_1(0, t) = -\beta_1 t - \frac{1}{2}\gamma_1^2 \beta_1^2 t^2$$

$$\gamma_1 = \frac{kT}{I\beta_1^2}, \quad \xi^2 = \left[\left(1 + \frac{i\omega}{\beta_1}\right)^2 \Big/ 2\gamma_1\right]$$

which with use of the asymptotic expansion of the complementary error function erfc ξ (Sack, 1957) (for large ξ, i.e., small γ_1),

$$2\xi \exp \xi^2 \operatorname{erfc} \xi = 1 - \frac{\xi^2}{2} + \frac{1 \cdot 3}{4}\xi^4 - \frac{1 \cdot 3 \cdot 5}{8}\xi^6 \cdots$$

shows that the behavior of the model for small γ_1 follows closely the equation

$$\frac{1}{1 + i\omega\tau_0 - \dfrac{\omega^2 \tau_0}{\beta_1}} \tag{2.7.1.15}$$

Thus for small γ_1, the only case of physical interest, there is little difference between the model of case 2 and the Brownian movement model. For case 3 the expression for $\langle \boldsymbol{\mu}(t) \cdot \mathbf{e} \rangle$ may be given in closed form as follows:

$$\langle \boldsymbol{\mu}(t) \cdot \mathbf{e} \rangle = \frac{\mu^2 E}{2kT} \exp(-\beta_1 t - \tfrac{1}{2}\gamma_1^2 \beta_1^2 t^2)$$

which gives

$$\frac{\alpha(\omega)}{\alpha'(0)} = 1 - \frac{i\omega}{\beta_1}\left(\frac{2}{\gamma_1}\right)^{1/2} \exp \xi^2 \operatorname{erfc} \xi$$

with ξ and erfc ξ defined as before. With our asymptotic expansion this yields for small γ_1

$$\frac{\alpha(\omega)}{\alpha'(0)} = \frac{1}{1 + i\omega/\beta_1} - \frac{i\omega\gamma_1}{(1 + i\omega/\beta_1)^3} + \frac{1 \cdot 3 i\omega\gamma_1^2}{(1 + i\omega/\beta_1)^5} \cdots$$

On inspection of this equation it is seen that again the material behaves approximately as a Debye dielectric for $\gamma_1 \ll 1$, the approximate Debye response, according to Sack, persisting up to the highest frequencies. In conclusion it should be noted that all the results of the section may be obtained by expanding the velocity-dependent portion of the solution of the Kramers equation in Weber functions. This was done in Section 2.4.2 for the Brownian motion type of collisions, and it was seen that $A_p^{n^s}$ calculated by means of the Brinkman method agree entirely with the ψ_k^s of Sack's method. We now go on to review the work on rotational Brownian movement of free rotators in space.

2.8 FREE ROTATION IN SPACE

The previous section dealt with the rotational motion of a system of two-dimensional dipolar rotators. A more satisfactory model for the description of real gases or liquids is a system of dipoles which may rotate

freely in space. We see that in the *Debye approximation* both the two- and the three-dimensional rotators behave *alike* except for the magnitude of the relaxation times, which for identical moments of inertia and frictional constants differ by a factor of 2. In this section we review the results of including inertial effects in the reorientational motion *in space* of an assembly of dipolar rotators which are again supposed to rotate without any electrical interaction with each other. The starting point of such a discussion is always the Euler–Langevin equation of motion,

$$\frac{d\mathbf{H}}{dt} + \boldsymbol{\omega} \times \mathbf{H} + \mathbf{F}\boldsymbol{\omega} = \boldsymbol{\Gamma}(t) \tag{2.8.1}$$

where $\mathbf{H}$ is the angular momentum and $\boldsymbol{\omega}$ is the angular velocity, both referred to a body fixed coordinate frame. $\mathbf{H}$ is related to $\boldsymbol{\omega}$ via the inertia tensor $\mathbf{I}$ (Goldstein, 1950):

$$\mathbf{H} = \mathbf{I}\boldsymbol{\omega}$$

The vector equation 2.8.1 represents simply the *Euler equations* (Goldstein, 1950) for the components of the angular velocity of a rigid body referred to a coordinate frame *fixed* in the body. The Euler equations as represented by Eq. 2.8.1 are supplemented by a frictional torque $\mathbf{F}\boldsymbol{\omega}$ and an external torque $\boldsymbol{\Gamma}(t)$ where

$$\boldsymbol{\Gamma}(t) = \boldsymbol{\Lambda}(t) + \mathbf{N}(\theta, \varphi, \psi, t) \tag{2.8.2}$$

$\boldsymbol{\Lambda}(t)$ is Gaussian white noise which may be discussed using the Wiener process, $\mathbf{N}(\theta, \varphi, \psi, t)$ is an external nonstochastic torque, and θ, φ, ψ are the Eulerian angles. It is assumed that the inertia tensor $\mathbf{I}$ and the friction tensor $\mathbf{F}$ are both positive definite symmetric quadratic forms which are *simultaneously* diagonalizable. Thus the set of Eqs. 2.8.1 may be written

$$A\dot{\omega}_1 - (B - C)\omega_2\omega_3 = -A\beta_1\omega_1 + A\dot{W}_1(t) + N_1(\theta, \varphi, \psi, t)$$

$$B\dot{\omega}_2 - (C - A)\omega_3\omega_1 = -B\beta_2\omega_2 + B\dot{W}_2(t) + N_2(\theta, \varphi, \psi, t)$$

$$C\dot{\omega}_3 - (A - B)\omega_1\omega_2 = -C\beta_3\omega_3 + C\dot{W}_3(t) + N_3(\theta, \varphi, \psi, t)$$

In these equations A, B, C are the moments of inertia referred to principal axes 1, 2, 3 fixed in the body, $\omega_1, \omega_2, \omega_3$ are the components of $\boldsymbol{\omega}$ about these axes, W_1, W_2, W_3 are Wiener processes, all independent of one another, and the Eulerian angles θ, φ, ψ specifying the orientation of the body [notation follows that of Goldstein (1950)] are related to the components of $\boldsymbol{\omega}$ by the following equations:

$$\dot{\theta} = \omega_1 \cos\psi - \omega_2 \sin\psi$$

$$\dot{\varphi} = \frac{1}{\sin\theta}(\omega_1 \sin\psi + \omega_2 \cos\psi)$$

$$\dot{\psi} = \omega_3 - \cot\theta(\omega_1 \sin\psi + \omega_2 \cos\psi)$$

The six foregoing equations are perfectly general and hold for any rigid

body of *arbitrary* shape subjected to both torques arising from the Brownian movement of the surroundings and an external torque $\mathbf{N}$ having components N_1, N_2, and N_3. The first discussion of rotational Brownian movement in space utilizing these Euler–Langevin equations was by Sack (1957); he considered two limiting cases, first, the dumbbell or rotating needle model where $C = 0$ and $A = B$, so that the equations of motion after the external field has been switched off take the form

$$A\dot{\omega}_1 = -A\beta\omega_1 + A\dot{W}_1$$

$$A\dot{\omega}_2 = -A\beta\omega_2 + A\dot{W}_2$$

Second, Sack considered the rotating sphere model where all the moments of inertia are equal, so that the equations of motion reduce to (after the external field has been switched off)

$$I\frac{d\boldsymbol{\omega}}{dt} + I\beta\boldsymbol{\omega} = I\frac{d\mathbf{W}}{dt}$$

$$I = A = B = C$$

Sack studied these models by constructing the appropriate Kramers equation in configuration-angular velocity space. It is easier to study both models by means of the Langevin equation. This has been recently done by Lewis et al. (1976) for the sphere and by McConnell (1978) for the needle. Before proceeding we mention the work of Furry (1957), Favro (1960), Steele (1963), and Hubbard (1972), who have studied the rotational Brownian movement by means of rotational operators.

Morita (1976) has given a comprehensive study of the rotational Brownian movement of the general rigid body (when inertial effects are included) where *all* the moments of inertia are unequal. In his paper he shows how the c.p.d.f. in angular velocity space for a body having an axis of symmetry may be obtained exactly from both the Euler–Langevin equation and the Fokker–Planck equation. Further, he shows how the Laplace transform of the angular velocity correlation function for the general ellipsoid may be calculated from the Fokker–Planck equation. Next he describes how the Laplace transform of the aftereffect function for a body having an axis of symmetry may be calculated both from a stochastic integro-differential equation and the appropriate Kramers equation (termed by him the Fokker–Planck–Kramers equation). Also he shows how the Laplace transform of the aftereffect function for the general ellipsoid may be calculated from the Kramers equation; his results extend the work of Perrin (1934) (who as we have seen studied the rotational Brownian movement of the general ellipsoid in the Smoluchowski approximation) to include inertial effects. All the calculations we have described, starting with the work of Sack, are extremely lengthy so we consider only one case in detail here, namely, the treatment of the rotational-Brownian movement of the spherical body given by Lewis et al. (1976). We also briefly summarize the calculations of Morita (1976, 1978). Before going on it is necessary to

mention some general conclusions that one may draw from the Euler–Langevin equation without doing any calculations. The simplest possible case of rotational motion is that which we have considered in detail in the last section, namely, the disk model where

$$\omega_1 = \omega_2 = 0 \qquad \omega_3 = \dot{\psi}$$

Thus the model is completely described by the equation

$$C\frac{d\omega_3}{dt} + C\beta\omega_3 = C\dot{W}_3 \tag{2.8.3}$$

Equation 2.8.3 is simply the linear stochastic differential equation of the Ornstein–Uhlenbeck theory and so the distribution of ω_3 is Gaussian, as is also the distribution of ψ because of the linear relation connecting ω_3 and ψ. In the sphere model the Euler–Langevin equation is

$$I\frac{d\boldsymbol{\omega}}{dt} + I\beta\boldsymbol{\omega} = I\dot{\mathbf{W}}(t) \tag{2.8.4}$$

This is simply the vector form of the equation used by Ornstein and Uhlenbeck; thus the distribution of the angular velocities is also Gaussian, but this is *not true* of the distribution of the orientations (θ, φ, ψ) since the equations connecting the $\omega_1, \omega_2, \omega_3$ with these are *not linear*. This is *always true* of any body that is allowed to rotate in three dimensions and is the *fundamental reason* why the rotational Brownian movement in three dimensions is difficult to discuss. We illustrate the difficulties by considering in detail the sphere model.

2.9 THE ROTATIONAL BROWNIAN MOVEMENT OF THE SPHERE AND NEEDLE

We first study, following Lewis et al. (1976), the rotational Brownian movement of the sphere which is supposed homogeneous, the motion being due entirely to random couples that have no preferential direction. The sphere contains a rigid electric dipole $\boldsymbol{\mu}$. We take through the center of the sphere a unit vector $\mathbf{u}(t)$ in the direction of $\boldsymbol{\mu}$. Then the rate of change of $\mathbf{u}(t)$ is (Milne, 1948)

$$\frac{d\mathbf{u}(t)}{dt} = \boldsymbol{\omega}(t) \times \mathbf{u}(t) \qquad \left(\mathbf{u}(t) = \frac{\boldsymbol{\mu}(t)}{|\boldsymbol{\mu}|}\right) \tag{2.9.1}$$

where $\boldsymbol{\omega}(t)$ is the angular velocity of the body. It should be noted that Eq. 2.9.1 is a *purely kinematic* relation with no particular reference either to the *Brownian movement* or to the *shape* of the body. Equation 2.9.1 may be solved for $\mathbf{u}(t)$ by means of the Picard method as follows. An integral of Eq. 2.9.1 is

$$\mathbf{u}(t) \equiv \mathbf{u}_0 + \int_0^t \boldsymbol{\omega}(t_1) \times \mathbf{u}(t_1)\, dt_1 \qquad [\mathbf{u}_0(t) \equiv \mathbf{u}(0)] \tag{2.9.2}$$

To a first approximation a solution of Eq. 2.9.2 is

$$\mathbf{u}(t) = \mathbf{u}_0 + \int_0^t \boldsymbol{\omega}_1 \times \mathbf{u}_0\, dt_1 \qquad [\boldsymbol{\omega}_1 = \boldsymbol{\omega}(t_1)] \tag{2.9.3}$$

to obtain a second approximation we write, from Eqs. 2.9.2 and 2.9.3,

$$\mathbf{u}(t) = \mathbf{u}_0 + \int_0^t [\boldsymbol{\omega}_2 \times \mathbf{u}(t_2)]\, dt_2 \qquad [\boldsymbol{\omega}_i = \boldsymbol{\omega}(t_i)]$$

$$\mathbf{u}(t_2) = \mathbf{u}_0 + \int_0^{t_2} (\boldsymbol{\omega}_1 \times \mathbf{u}_0)\, dt_1$$

and deduce that

$$\mathbf{u}(t_2) = \mathbf{u}_0 + \int_0^t (\boldsymbol{\omega}_2 \times \mathbf{u}_0)\, dt_2 + \int_0^t dt_2 \int_0^{t_2} [\boldsymbol{\omega}_2 \times (\boldsymbol{\omega}_1 \times \mathbf{u}_0)]\, dt_1 \tag{2.9.4}$$

We next write $\mathbf{u}(t_3)$ from this and substitute into

$$\mathbf{u}(t) = \mathbf{u}_0 + \int_0^t [\boldsymbol{\omega}_3 \times \mathbf{u}(t_3)]\, dt_3 \tag{2.9.5}$$

Continuing in this way we then find that

$$\begin{aligned}\mathbf{u}(t) = \mathbf{u}_0 &+ \int_0^t (\boldsymbol{\omega}_1 \times \mathbf{u}_0)\, dt_1 + \int\int_{0\le t_1\le t_2\le t} [\boldsymbol{\omega}_2 \times (\boldsymbol{\omega}_1 \times \mathbf{u}_0)]\, dt_1\, dt_2 \\ &+ \int\int\int_{0\le t_1\le t_2\le t_3\le t} \{\boldsymbol{\omega}_3 \times [\boldsymbol{\omega}_2 \times (\boldsymbol{\omega}_1 \times \mathbf{u}_0)]\}\, dt_1\, dt_2\, dt_3 \\ &+ \int\int\int\int_{0\le t_1\le t_2\le t_3\le t_4\le t} (\boldsymbol{\omega}_4 \times \{\boldsymbol{\omega}_3 \times [\boldsymbol{\omega}_2 \times (\boldsymbol{\omega}_1 \times \mathbf{u}_0)]\})\, dt_1 \cdots dt_4 \\ &+ \cdots .\end{aligned} \tag{2.9.6}$$

Provided $\boldsymbol{\omega}(t)$ is a continuous function of t this series will converge to the unique solution of Eq. 2.9.1 with the initial condition $\mathbf{u}(0) = \mathbf{u}_0$ (Ince, 1927).

Now since at any time t after switching off a steady field

$$I\frac{d\boldsymbol{\omega}}{dt} + I\beta\boldsymbol{\omega} = I\dot{\mathbf{W}} \tag{2.9.7}$$

the ω's are *Gaussian* random variables. This leads us to make the following aside concerning a property of Gaussian random variables. If $(x_1, \ldots, x_m)$ are *centered Gaussian* random variables, then

$$\langle x_1 \cdots x_{2n-1}\rangle = 0 \qquad \langle x_1 \cdots x_{2n}\rangle = \sum_{\substack{i_1<\cdots<i_n \\ i_1<j_1\cdots i_n<j_n}} \{\langle x_{i_1}, x_{j_1}\rangle \cdots \langle x_{i_n}, x_{j_n}\rangle\} \tag{2.9.8}$$

We may readily prove the relations given above. We have already seen that if $(x_1 \cdots x_m)$ are centered Gaussian random variables then so also is a linear combination of them:

where the c's are given scalars. Thus the characteristic function $\langle e^{ix}\rangle$ of x is

$$\langle e^{ix}\rangle = \exp[-\tfrac{1}{2}\langle x^2\rangle]$$

and thus

$$\sum_{r=0}^{\infty} \frac{i^r}{r!}\langle x^r\rangle = \sum_{s=0}^{\infty} \frac{(-1)^s}{2^s s!}\langle x^2\rangle^s \tag{2.9.9}$$

Now

$$x^r = (c_1x_1 + \cdots + c_mx_m)^r$$

On comparing the coefficients of $c_1 \cdots c_m$ in Eq. 2.9.9 we have Eq. 2.9.8. The second equation in Eq. 2.9.8 may also be written

$$\langle x_1 \cdots x_{2n}\rangle = \sum_{i_r>i_s} \pi\langle x_{i_r}x_{i_s}\rangle$$

We now return to Eq. 2.9.6 and take mean values; this gives with Eq. 2.9.8

$$\langle \mathbf{u}(t)\rangle = \mathbf{u}_0 + \int\int_{0\leqslant t_1\leqslant t_2\leqslant t} \langle \boldsymbol{\omega}_2 \times (\boldsymbol{\omega}_1 \times \mathbf{u}_0)\rangle\, dt_1\, dt_2 + \int \cdots \int_{0\leqslant t_1 \cdots t_4\leqslant t} \langle (\boldsymbol{\omega}_4 \times \{\boldsymbol{\omega}_3 \times [\boldsymbol{\omega}_2 \times (\boldsymbol{\omega}_1 \times \mathbf{u}_0)]\})\rangle\, dt \cdots dt_4 \tag{2.9.10}$$

Equation 2.9.10 may be written in more compact form by adopting, following Lewis et al., the original bracket notation of Dirac. If we write $|0)$ for the three-dimensional vector $\mathbf{u}_0$ and $|i)$ for ω_i, then (Milne, 1948)

$$\begin{aligned}\boldsymbol{\omega}_2 \times (\boldsymbol{\omega}_1 \times \mathbf{u}_0) &= \boldsymbol{\omega}_1(\boldsymbol{\omega}_2 \cdot \mathbf{u}_0) - (\boldsymbol{\omega}_2 \cdot \boldsymbol{\omega}_1)\mathbf{u}_0 \\ &= (|1)(2| - (2|1))|0)\end{aligned}$$

and thus Eq. 2.9.10 may be expressed as

$$\langle \mathbf{u}(t)\rangle = \mathbf{u}_0 + \int\int_{0\leqslant t_1\leqslant t_2\leqslant t} \langle (|1)(2| - (2|1))|0\rangle\, dt_1\, dt_2 + \int \cdots \int_{0\leqslant t_1\leqslant \cdots t_4\leqslant t} \langle (|3)(4| - (4|3))(|1)(2| - (2|1))|0\rangle\, dt_1 \cdots dt_4$$

We now return to the calculation of $\boldsymbol{\omega}(t)$.

First we note that Eq. 2.9.7 is simply the vector Ornstein–Uhlenbeck equation and we further note that the vector Wiener process satisfies

$$\langle \mathbf{W}(t)\rangle = 0 \qquad \langle (\mathbf{W}(t)\cdot \mathbf{e}_i)(\mathbf{W}(t')\cdot \mathbf{e}_j)\rangle = c^2 \min(t, t')\delta_{ij} \tag{2.9.11}$$

where

$$c^2 = 2\beta\frac{kT}{I}$$

and $\mathbf{e}_i, \mathbf{e}_j$ are members of a triad of mutually orthogonal unit vectors in three-dimensional space. If we write

then we may immediately write in the usual way

$$\langle \boldsymbol{\xi}(\Delta)\rangle = 0 \qquad \langle (\boldsymbol{\xi}(\Delta)\cdot \mathbf{e}_i)(\boldsymbol{\xi}(\Delta')\cdot \mathbf{e}_j)\rangle = c^2\delta_{ij}|\Delta \cap \Delta'|$$

and from the results of the Ornstein–Uhlenbeck theory given earlier,

$$\langle \omega^{(i)}(t_k)\omega^{(j)}(t_l)\rangle = \frac{c^2}{2\beta}\,\delta_{ij}e^{-\beta|t_k - t_l|} \tag{2.9.12}$$

or

$$\langle \boldsymbol{\omega}_k \cdot \boldsymbol{\omega}_l\rangle = \frac{c^2}{2\beta}\, e^{-\beta|t_k - t_l|} = C(t)$$

where δ_{ij} denotes Kronecker's delta. We are now in a position to evaluate the integrals in $\langle \mathbf{u}(t)\rangle$. Following Lewis et al., we calculate

$$\int\int_{0\leqslant t_1\leqslant t_2\leqslant t} \langle (|1)(2| - (2|1))|0)\rangle\, dt_1\, dt_2 \tag{2.9.13}$$

To do this we consider the first component $\langle u^{(1)}(t)\rangle$ of $\langle \mathbf{u}(t)\rangle$; we write the contribution to it as

$$\int\int_{0\leqslant t_1\leqslant t_2\leqslant t} \langle (\boldsymbol{\omega}_2 \cdot \mathbf{u}_0)\omega_1^{(1)} - (\boldsymbol{\omega}_2 \cdot \boldsymbol{\omega}_1)u_0^{(1)}\rangle\, dt_1\, dt_2$$

Now

$$\begin{aligned}\langle (\boldsymbol{\omega}_2 \cdot \mathbf{u}_0)\omega_1^{(1)}\rangle &= \langle \omega_2^{(1)}u_0^{(1)}\omega_1^{(1)}\rangle + \langle \omega_2^{(2)}u_0^{(2)}\omega_1^{(1)}\rangle + \langle \omega_2^{(3)}u_0^{(3)}\omega_1^{(1)}\rangle \\ &= \frac{c^2}{2\beta}\, e^{-\beta(t_2 - t_1)}u_0^{(1)}\end{aligned} \tag{2.9.14}$$

by Eq. 2.9.12. Since $t_1 \leqslant t_2$ and

$$\langle (\boldsymbol{\omega}_2 \cdot \boldsymbol{\omega}_1)\mathbf{u}_0^{(1)}\rangle = \frac{3c^2}{2\beta}\, e^{-\beta(t_2 - t_1)}u_0^{(1)}$$

by Eq. 2.9.12, so that Eq. 2.9.13 is equal to

$$-2\left(\frac{c^2}{2\beta}\right)u_0^{(1)}\int\int_{0\leqslant t_1\leqslant t_2\leqslant t} e^{-\beta(t_2 - t_1)}\, dt_1\, dt_2$$

the contribution to $\langle \mathbf{u}(t)\rangle$ is therefore

$$-2\left(\frac{c^2}{2\beta}\right)\mathbf{u}_0\int\int_{0\leqslant t_1\leqslant t_2\leqslant t} e^{-\beta(t_2 - t_1)}\, dt_1\, dt_2$$

Lewis et al. found the value of this integral to be

$$-2\left(\frac{c^2}{2\beta}\right)\mathbf{u}_0\beta^{-2}(\beta t - 1 + e^{-\beta t})$$

They next consider the third term in the expansion, namely,

$$\int \cdots \int_{0\leqslant t_1\leqslant \cdots t_4\leqslant t} \langle (|3(4| - (4|3))(|1)(2| - (2|1))|0)\rangle\, dt_1 \cdots dt_4 \tag{2.9.15}$$

invoked in order to pair off the ω's in a suitable way. The details of the calculation will be found in their paper. They find for the value of Eq. 2.9.15

$$\left(\frac{c^2}{2\beta}\right)^2 (2\beta^2t^2 - 5\beta t + \tfrac{9}{2} + e^{-\beta t}(2\beta t - 6) + \tfrac{3}{2}e^{-2\beta t})$$

They finally carry their calculation as far as terms in $(c^2/2\beta)^3$ and deduce that

$$\begin{aligned}\langle \mathbf{u}(t)\rangle = \mathbf{u}_0 \Big[& 1 - \left(\frac{\tau_2}{\tau_1}\right)^2 (2\beta t - 2 + 2e^{-\beta t}) \\ & + \left(\frac{\tau_2}{\tau_1}\right)^4 (2\beta^2t^2 - 5\beta t + \tfrac{9}{2} + e^{-\beta t}(2\beta t - 6) + \tfrac{3}{2}e^{-2\beta t}) \\ & - \left(\frac{\tau_2}{\tau_1}\right)^6 (\tfrac{4}{3}\beta^3t^3 - 6\beta^2t^2 + \tfrac{73}{6}\beta t - \tfrac{95}{9} + e^{-\beta t}(\beta^2t^2 - 6\beta t + 15) \\ & + e^{-2\beta t}(\tfrac{1}{2}\beta t - 5) + \tfrac{5}{9}e^{-3\beta t}) + \cdots \end{aligned} \tag{2.9.16}$$

where

$$\tau_1 = \left(\frac{I}{kT}\right)^{1/2} \qquad \frac{1}{\beta} = \tau_2$$

and

$$\frac{\tau_2}{\tau_1} = \left(\frac{c^2}{2\beta}\right)^2$$

They now go on to show that in the limit of short times such that $\beta t \ll 1$ Eq. 2.9.16 becomes (see Eq. 2.15.6)

$$\langle \mathbf{u}(t)\rangle = \mathbf{u}_0 \left[1 - \frac{kT}{I}t^2 + \frac{5}{12}\left(\frac{kT}{I}\right)^2 t^4 \cdots\right] = \frac{1}{3} + \frac{2}{3}\left(1 - \frac{kT}{I}t^2\right)\exp\left(-\frac{kT}{2I}t^2\right)$$

which is *independent* of β, while for very long times such that $t \gg \beta^{-1}$, Eq. 2.9.16 becomes

$$\langle \mathbf{u}(t)\rangle = \mathbf{u}_0 \exp\left(-2\frac{\tau_2 t}{\tau_1^2}\right)$$

which may be written

$$\langle \mathbf{u}(t)\rangle = \mathbf{u}_0 \exp\left(-\frac{t}{\tau_0}\right)$$

where

$$\tau_0 = \left(\frac{\tau_1^2}{2\tau_2}\right) = \left(\frac{I\beta}{2kT}\right) = \frac{\zeta}{2kT}$$

is the Debye relaxation time. Thus in the *limit of long times* the Debye result is recovered. The normalized aftereffect function in the Debye theory is

$$\frac{\langle \boldsymbol{\mu}(t)\cdot\mathbf{e}\rangle}{\langle \boldsymbol{\mu}(0)\cdot\mathbf{e}\rangle} = \frac{b(t)}{b(0)} = \langle \mathbf{u}(t)\cdot\mathbf{u}(0)\rangle = e^{-2(kT/\zeta)t}$$

model *cannot be expressed in closed form.* If, however, the sphere is constrained to rotate in a plane so that

$$\boldsymbol{\omega}(t) = \omega(t)\mathbf{k}$$

Then Eq. 2.9.6 becomes

$$\begin{aligned}\mathbf{u}(t) = \mathbf{u}_0 & + \mathbf{k}\times\mathbf{u}_0\int_0^t \omega_1\,dt - \mathbf{u}_0\int\int_{0\le t_1\le t_2\le t} \omega_2\omega_1\,dt_1\,dt_2 \\ & - \mathbf{k}\times\mathbf{u}_0\int\int\int_{0\le t_1\le t_2\le t_3\le t} \omega_3\omega_2\omega_1\,dt_1\,dt_2\,dt_3 \\ & + \mathbf{u}_0\int\cdots\int_{0\le t_1\le t_2\le t_3\le t_4\le t} \omega_4\omega_3\omega_2\omega_1\,dt_1\cdots dt_4\end{aligned}$$

while we have

$$\begin{aligned}\langle \mathbf{u}(t)\rangle = \mathbf{u}_0 \Big(1 & - \int\int_{0\le t_1\le t_2\le t} \langle\omega_2\omega_1\rangle\,dt_1\,dt_2 \\ & + \int\int\int\int_{0\le t_1\le t_2\cdots\le t} \langle\omega_4\omega_3\omega_2\omega_1\rangle\,dt_1\cdots dt_4\cdots\Big)\end{aligned}$$

On evaluating these integrals they find that $\langle \mathbf{u}_0\cdot\mathbf{u}\rangle$ may be expressed in *closed* form as

$$\begin{aligned}\langle \mathbf{u}(0)\cdot\mathbf{u}(t)\rangle &= \exp\left[-\left(\frac{\tau_2}{\tau_1}\right)^2\left(\frac{t}{\tau_2} - 1 + e^{-t/\tau_2}\right)\right] \\ &= \exp\left[-\frac{1}{2}\int\int_{0\le t_1\le t_2\le t}\langle\omega_1\omega_2\rangle\,dt_1\,dt_2\right] \\ &= \exp\left[-\int_0^t (t-u)\langle\omega(0)\omega(u)\rangle\,du\right]\end{aligned} \tag{2.9.17}$$

as we found earlier for $A_1^0(t)$ from the Kramers equation. In fact the Picard series for $A_1^0(t)$, which is got by solving the equation

$$\frac{dA_p^n}{dt}(t) + n\beta A_p^n(t) = -ip\sqrt{\frac{kT}{I}}[(n+1)A_p^{n+1}(t) + A_p^{n-1}(t)]$$

by successive approximations *corresponds exactly* term by term to Eq. 2.9.17. Steele in 1963 wrote the following expression for $\langle \mathbf{u}(0)\cdot\mathbf{u}(t)\rangle$ for the sphere model

$$\exp\left[-2\frac{kTI}{\zeta^2}\left(\frac{\zeta t}{I} - 1 + e^{-\zeta t/I}\right)\right]$$

Agreement with Eq. 2.9.16 cannot be found after the $(\tau_2/\tau_1)^2$ term. Moreover, as we shall see, the result of Lewis et al. agrees entirely with Sack, who obtained his results using a completely different approach. It would seem that only in the case $I = 0$ (the Debye approximation) can the result for the sphere be obtained in closed form. Why is the result for the sphere model not expressible in closed form? The answer is contained in the equation

$$\frac{d\mathbf{u}(t)}{dt} = \boldsymbol{\omega}(t)\times\mathbf{u}(t) \tag{2.9.18}$$

If $\boldsymbol{\omega} = \omega\mathbf{k}$ this equation becomes, when written in terms of its components,

$$\frac{du_x(t)}{dt} = -\omega_z u_y$$

$$\frac{du_y(t)}{dt} = \omega_z u_x$$

This is a set of *linear* differential equations; hence if ω_z is a Gaussian random variable, so too will be the components u_x, u_y of $\mathbf{u}$. In the three-dimensional case, however, the differential equations for u_x and u_y, u_z obtained by writing Eq. 2.9.18 and making appropriate substitutions are *not linear*; hence, *even* if $\boldsymbol{\omega}$ is a Gaussian random variable, $\mathbf{u}$ *is not*. Thus every term in the series for $\langle \mathbf{u}_0 \cdot \mathbf{u} \rangle$ must be calculated. The argument may be clarified if we write $\langle \mathbf{u}_0 \cdot \mathbf{u} \rangle$ as follows. By definition [If Θ is the angle between $\mathbf{u}_0$ and $\mathbf{u}(t)$]

$$\langle \mathbf{u}_0 \cdot \mathbf{u} \rangle = \langle \mathbf{u}(0) \cdot \mathbf{u}(t) \rangle = \langle \cos\Theta \rangle = \mathrm{Re}\,\langle e^{i\Theta} \rangle \tag{2.9.19}$$

at any time t. If $\Theta(t)$ is a *Gaussian random variable*, Eq. 2.9.19 reduces to (by the properties of the characteristic function)

$$\langle \mathbf{u}(0) \cdot \mathbf{u}(t) \rangle = \langle \cos\Theta \rangle = e^{-\langle\Theta^2\rangle/2} = e^{-\int\int \langle\omega_1\omega_2\rangle\, dt_1\, dt_2/2}$$

This is precisely the situation that is satisfied in the disk model where

$$\boldsymbol{\omega}(t) = \omega(t)\mathbf{k}$$

and where the solution of

$$\frac{d\mathbf{u}}{dt} = \boldsymbol{\omega} \times \mathbf{u}$$

reduces to a matter of solving *linear* scalar differential equations. In the three-dimensional models, however,

$$\langle \mathbf{u}(0) \cdot \mathbf{u}(t) \rangle = \langle \cos\Theta \rangle = \mathrm{Re}\langle e^{i\Theta} \rangle$$

$$= \sum_{n=0}^{\infty} \frac{(-1)^n}{2n!} \langle \Theta^{2n} \rangle$$

and the relation

$$\langle \Theta^{2n} \rangle \propto \langle \Theta^2 \rangle^n$$

is not satisfied because of Eq. 2.9.18, so $\langle \mathbf{u}_0 \cdot \mathbf{u} \rangle$ can *never be expressed in closed exponential form*; that result is *peculiar* to the two-dimensional model and is the reason why rotation in two dimensions is easy to discuss. Lewis et al. now compare their work with Sack, who (just as he did for the disk model) based his work on the Kramers equation. He found that (note $R(t) = b(t)/b(0)$)

$$\int_0^\infty R(t)e^{-i\omega t}\,dt = \cfrac{1/\beta}{i\omega' + \cfrac{2a}{1 + i\omega' + (a/2)(2 + i\omega')^{-1} \pm \cfrac{(3-\frac{1}{2})a}{\quad} \pm \cfrac{4a}{\quad} \pm \cfrac{(5-\frac{1}{3})a}{\quad} \pm \cdots}}$$

with

$$\omega' = \frac{\omega}{\beta}, \qquad a = \left(\frac{\tau_2}{\tau_1}\right)^2 = \left(\frac{c^2}{2\beta^3}\right) = \frac{kT}{I\beta^2}$$

On the other hand, Lewis et al. find from their series for $\langle \mathbf{u} \rangle$ (Eq. 2.9.16) that

$$\int_0^\infty R(t)e^{-st}\,dt = \frac{1}{s} - \frac{c^2}{2\beta}\frac{2}{s^2(s+\beta)} + \left(\frac{c^2}{2\beta}\right)^2 \left(\frac{4}{s^3(s+\beta)^2} + \frac{6}{s^2(s+\beta)^2(s+2\beta)}\right)$$
$$- \left(\frac{c^2}{2\beta}\right)^3 \left(\frac{8}{s^4(s+\beta)^3} + \frac{24}{s^3(s+\beta)^3(s+2\beta)}\right.$$
$$\left. + \frac{18}{s^2(s+\beta)^3(s+2\beta)^2} + \frac{20}{s^2(s+\beta)^2(s+2\beta)^2(s+3\beta)}\right) + \cdots \tag{2.9.21}$$

in which $s = i\omega$. The value of the right-hand side of Eq. 2.9.20 may be found to any order of approximation by calculating successive convergents.

Exact agreement between the result of Lewis et al. up to the order which they have calculated in $(c^2/2\beta)$ and that of Sack is obtained. McConnell (1978) has also shown how Sack's original treatment based on the Kramers equation may be simplified. Again exact agreement with Sack's original treatment is reached.

In his 1957 paper we have mentioned that Sack also discussed the rotational Brownian motion with inclusion of inertial effects of the linear model of a polar molecule. He constructed a Kramers equation in the space of the two angles specifying the orientation of the molecule and of their related angular velocities. He expressed the steady-state linear response to an alternating field as a continued fraction (just as in the sphere model) which is a function of the frequency, the friction constant $I\beta$, and the moment of inertia I of the molecule about a line perpendicular to it through its middle point. Sack's result for the polarizability $\alpha(\omega)$ in continued fraction form is

$$\frac{\alpha(\omega)}{\alpha'(0)} = 1 - \cfrac{i\omega'}{i\omega' + \cfrac{2a}{1 + i\omega' + \cfrac{2a}{2 + i\omega' + \cfrac{4a}{3 + i\omega' + \cfrac{4a}{4 + i\omega' + \cdots}}}}} \tag{2.9.22}$$

As indicated above, this result was obtained using the Kramers equation. McConnell (1978) treated the problem using the Langevin equation. He finds exact agreement with Sack's continued fraction up to the order in $kT/I\beta^2$ to which he has carried his calculation.

The results of this section may be summarized as follows:

For the Disk Model

1. The distribution of *both* the angular velocity $\boldsymbol{\omega}(t)$ and the components of the dipole vector $\mathbf{u}(t)$ is of the Gaussian type.
2. The angular velocity correlation function may be expressed as

3. The normalized aftereffect function may be expressed in *closed form* as

$$\langle \cos\Theta \rangle = \langle \mathbf{u}(0)\cdot\mathbf{u}(t)\rangle = \frac{\langle \boldsymbol{\mu}(t)\cdot\mathbf{e}\rangle}{\langle \boldsymbol{\mu}(0)\cdot\mathbf{e}\rangle} = \exp\left[-\frac{kTI}{\zeta^2}\left(\frac{\zeta}{I}t - 1 + e^{-(\zeta/I)t}\right)\right]$$

4. The correlation functions $\langle \cos n\Theta \rangle$ may be written, $n = 0, 1, 2, 3,$

$$\langle \cos n\Theta \rangle = \exp\left[-n^2\frac{kTI}{\zeta^2}\left(\frac{\zeta}{I}t - 1 + e^{-(\zeta/I)t}\right)\right]$$

5. The relaxation time for the disk in the *Debye approximation* is *twice* that for a sphere with the same moment of inertia and drag coefficient.
6. The relation

$$\langle \mathbf{u}(0)\cdot\mathbf{u}(t)\rangle = \exp\left(-\frac{1}{2}\int\int_{0\le t_1\le t_2\le t}\langle\omega_1\omega_2\rangle\, dt_1\, dt_2\right)$$
$$= \exp\left(-\int_0^t (t-u)\langle\omega(0)\omega(u)\rangle\, du\right)$$

is satisfied, thus providing a simple way of calculating orientational a.c.f.'s from angular velocity a.c.f.'s. The above relation has also been given by Kubo (1965).

7. The normalized polarizability (to terms linear in the field strength) for the disk model may be expressed by the following continued fraction:

$$\frac{\alpha(\omega)}{\alpha'(0)} = 1 - \frac{i\omega}{\beta}\left(\cfrac{1}{i\omega/\beta} + \cfrac{a}{1 + i\omega/\beta} + \cfrac{2a}{2 + i\omega/\beta} + \cfrac{3a}{3 + i\omega/\beta}\cdots\right)$$

For the Sphere Model

1. The distribution of the components of the angular velocity vector $\boldsymbol{\omega}(t)$ is *Gaussian*. The distribution of the components of $\mathbf{u}(t)$ is *not*.
2. The angular velocity correlation functions may be expressed as

$$\langle \omega^{(i)}(t_1)\omega^{(j)}(t_2)\rangle = \frac{kT}{I}\delta_{ij}\exp\left[-\frac{\zeta}{I}|t_1 - t_2|\right] = C(t) \qquad (t = t_1 - t_2)$$

3. The normalized aftereffect function *cannot* be expressed in closed form except in the Debye approximation.
4. The correlation functions $\langle P_n(\cos\Theta)\rangle$ cannot be expressed in closed form except in the inertia free case where

$$\langle P_n(\cos\Theta)\rangle \propto \exp\left(-n(n+1)\frac{kT}{\zeta}t\right)$$

5. The normalized polarizability (in the linear approximation) for the sphere model may be expressed by the continued fraction

$$\frac{\alpha(\omega)}{\alpha'(0)} = 1 - \cfrac{i\omega'}{i\omega' + \cfrac{2a}{1 + i\omega' + \cfrac{a}{2}(2 + i\omega')^{-1} + \cfrac{(3-\frac{1}{2})a}{2 + i\omega' + \cfrac{4a}{3 + i\omega' + \left(\frac{a}{3}\right)(2 + i\omega')^{-1}} + \cdots}}}$$

For the Needle Model

1. The distribution of the components of the angular velocity vector is *Gaussian*. The distribution of the angles specifying the orientation of the needle is *not*.
2. The angular velocity correlation functions may be expressed as

$$\langle \omega_i(t_1)\omega_j(t_2)\rangle = \frac{kT}{I}\delta_{ij}e^{-(\zeta/I)|t_1 - t_2|} = C(t) \qquad (t = t_1 - t_2)$$

3. The normalized aftereffect function cannot be expressed in *closed* form, nor can the higher-order angular correlation functions.
4. The normalized polarizability for the needle model may be expressed by the continued fraction

$$\frac{\alpha(\omega)}{\alpha'(0)} = 1 - \cfrac{i\omega'}{i\omega'} + \cfrac{2a}{1 + i\omega'} + \cfrac{2a}{2 + i\omega'} + \cfrac{4a}{3 + i\omega'} + \cfrac{4a}{4 + i\omega'} + \cfrac{6a}{5 + i\omega'} + \cdots$$

The following conclusions can be drawn for all three models:

1. The approaches based on the Langevin and the Kramers equations appear to be in exact agreement.
2. For values of the factor $kT/I\beta^2 \leqslant 0.05$ (Sack, 1957) the function

$$\frac{\alpha(\omega)}{\alpha'(0)} = \frac{1}{1 + i\omega\tau_0 - \omega^2\tau_0\beta^{-1}}$$

provides an *adequate approximation* to the continued fraction expansions for all three models. This equation is substantially the same as that given earlier by Rocard (1933) (there is a misprint in the original Rocard equation that is corrected by Sack). *This equation shows no sign of resonant behavior in the far infrared.*

3. Each model predicts a *denumerable set* of relaxation times and a *corresponding denumerable set* of relaxation mechanisms for the polarization. In the case of the disk model each mechanism is *exponential.*
4. Each model corrects the bad behavior of the Debye equation at high frequencies but *none of them predict the observed Poley absorption in the terahertz band of frequencies. They all simply produce skewed*

5. The two-dimensional model is the only one for which the angular correlation functions may be expressed in closed form *and is the only one for which there is a simple relation between the angular velocity and the orientational a.c.f.'s.*
6. We have given the results only for the sphere and needle models for the *Brownian movement* type of collisions, that is, type A collisions in the nomenclature of Sack (1957). Sack also deduced continued fraction expansions for both sphere and needle models when collision mechanisms of types B and C are supposed to operate. We have given the results of all three types of collision mechanism for the disk model. The conclusions to be drawn from using mechanisms of types B and C for the needle and sphere model are the same as already given for the disk model with these types of collisions.
7. In all models the decay of the polarization is *essentially exponential* in the limit of long times. *Thus they are unable to explain the hydrodynamic tails found in computer simulations.*

We now proceed to review the work on the Brownian movement of an asymmetric body.

2.10 THE ROTATIONAL BROWNIAN MOVEMENT OF NONSPHERICAL BODIES. EVALUATION OF ANGULAR VELOCITY CORRELATION FUNCTIONS

The most comprehensive treatment of the rotational Brownian movement of nonspherical bodies (including inertial effects) has been given by Morita (1978). He commences his treatment by considering the rotational Brownian movement of a body having an axis of symmetry so that the Euler–Langevin equations become

$$\begin{aligned} A\dot{\omega}_1 - (A-C)\omega_2\omega_3 &= -\zeta_1\dot{\omega}_1 + A\dot{W}_1 + N_1(\theta,\varphi,\psi,t) \\ A\dot{\omega}_2 - (C-A)\omega_1\omega_3 &= -\zeta_1\dot{\omega}_2 + A\dot{W}_1 + N_2(\theta,\varphi,\psi,t) \\ C\dot{\omega}_3 &= -\zeta_3\dot{\omega}_3 + C\dot{W}_3 + N_3(\theta,\varphi,\psi,t) \end{aligned} \qquad (2.10.1)$$

where (θ, φ, ψ) denote the Eulerian angles and $\mathbf{N}$ again is an external mechanical torque which is in general generated by the impressed electric field at any time t. On making the assumptions that the torques $A\dot{W}_1$, $A\dot{W}_2$, and $C\dot{W}_3$ are each independent of one another, that the body carries electric dipoles of moments μ_1, μ_2, and μ_3 along the principal axes 1, 2, and 3, respectively, and that an electric field $\mathbf{E} = \mathbf{e}E$, giving rise to a potential

$$\begin{aligned} V &= -\boldsymbol{\mu}\cdot\mathbf{e}E \qquad t<0 \\ &= 0 \qquad\qquad t>0 \end{aligned}$$

angular velocity correlation functions at any time $t_i > 0$:

$$\langle\omega(t_1)\omega(t_2)\rangle = \langle\omega_2(t_2)\omega_2(t_1)\rangle$$
$$= \frac{kT}{A}\,e^{-\beta_1|t_1-t_2|}\exp\left[-\frac{kT}{C}\left(\frac{d}{\beta_3}\right)(\beta_3|t_1-t_2| - 1 + e^{-\beta_3|t_2-t_1|})\right] = C_1(t)$$

$$\langle\omega_3(t_1)\omega_3(t_2)\rangle = \frac{kT}{C}\,e^{-\beta_3|t_1-t_2|} = C_3(t)$$

$$\langle\omega_i(t_1)\omega_j(t_2)\rangle = 0 \qquad i \neq j$$

where

$$\beta_1 = \frac{\zeta_1}{A}, \qquad \beta_3 = \frac{\zeta_3}{C}, \qquad d = \left(1 - \frac{C}{A}\right)$$

We should note that if $C = A$ in these equations, then the results for the sphere are recovered. The results embodied in the above equations were obtained in two ways. The first is directly from the Euler–Langevin equations, which for $t > 0$ become

$$\begin{aligned} A\dot{\omega}_1 - (A-C)\omega_2\omega_3 &= -A\beta_1\dot{\omega}_1 + A\dot{W}_1(t) \\ A\dot{\omega}_2 - (C-A)\omega_1\omega_3 &= -A\beta_1\dot{\omega}_2 + A\dot{W}_2(t) \\ C\dot{\omega}_3 &= -C\beta_3\dot{\omega}_3 + C\dot{W}_3(t) \end{aligned} \qquad (2.10.2)$$

These equations may be integrated after considerable labor to give *closed form* expressions for ω_1 and ω_2, ω_3, hence the required averages may be evaluated by means of the properties of Wiener integrals and the results given above are obtained. The second method used by Morita is that of evaluating the *characteristic function* of the angular velocity distribution. In order to do this he constructs, using the methods we described earlier, the Fokker–Planck equation in angular velocity space for the time evolution of the probability distribution of angular velocities. He obtains an exact expression for the characteristic function from the Fokker–Planck equation. This is *not* the characteristic function of a Gaussian distribution except in the special case of the sphere where $A = C$, a result already given by Hubbard in 1972. The correlation functions of the angular velocities may be evaluated in the usual way by differentiation of the characteristic function (as we showed in the section on probability) to yield again the angular velocity correlation functions. Thus it is possible to evaluate in *closed form* the angular velocity correlation functions for a body having an *axis of symmetry*. It is also shown (Morita, 1978) how the angular velocity correlation functions may be calculated for the general rigid body. Here the Euler–Langevin equations have the form, for $t > 0$,

$$\begin{aligned} A\dot{\omega}_1 - (B-C)\omega_2\omega_3 &= -\zeta_1\dot{\omega}_1 + A\dot{W}_1 \\ B\dot{\omega}_2 - (C-A)\omega_1\omega_3 &= -\zeta_2\dot{\omega}_2 + B\dot{W}_2 \\ C\dot{\omega}_3 - (B-A)\omega_2\omega_1 &= -\zeta_3\dot{\omega}_3 + C\dot{W}_3 \end{aligned} \qquad (2.10.3)$$

than those describing the body having an axis of symmetry. Their solution for $(\omega_1, \omega_2, \omega_3)$ even in the case where the Brownian torques are zero will *always* require the use of the Jacobian elliptic functions [for a discussion of this solution see Whittaker (1917) or Routh (1892)]. Thus an approach based on direct integration of the Euler–Langevin equations is not in general fruitful, and recourse must be made to the Fokker–Planck equation which at least has the virtue of being linear. Accordingly we may proceed to write the Fokker–Planck equation in angular velocity space for the evolution of the probability distribution of the ω's in Eq. 2.10.3. On utilizing what are essentially the methods of Sack (1957) we find the following approximate expression for the Laplace transform of the angular velocity correlation function

$$\mathscr{L}[\langle\omega_i(0)\omega_i(t)\rangle] = \frac{kT}{I_i}\left[\frac{1}{s+\beta_i} + \frac{\alpha_i\gamma_i}{(s+\beta_i)^2(s+\beta_j+\beta_k)} + \frac{2\alpha_i\gamma_i}{(s+\beta_i)^2(s+\beta_j+\beta_k)^2}\left(\frac{\alpha_j\gamma_j}{s+\beta_i+2\beta_k} + \frac{\alpha_k\gamma_k}{s+\beta_i+2\beta_j}\right)\right] \tag{2.10.4}$$

where i, j, k each equal 1, 2, or 3, and where I_i denotes A, B, or C depending on whether $i = 1, 2$, or 3.

Equation 2.10.4 may be inverted to give

$$\langle\omega_i(0)\omega_i(t)\rangle = \frac{kT}{I_i}e^{-\beta_i t}\left[1 + \frac{\alpha_i\gamma_i[(\beta_j+\beta_k-\beta_i)t - 1 + e^{-(\beta_j+\beta_k-\beta_i)t}]}{(\beta_j+\beta_k-\beta_i)^2} + 2\alpha_i\alpha_j\gamma_i\gamma_j\left(\frac{e^{-2\beta_k t}}{4\beta_k^2(\beta_j-\beta_i-\beta_k)^2} + \frac{2\beta_i(\beta_j+\beta_k-\beta_i)t + \beta_i - 5\beta_j - \beta_k}{4\beta_j^2(\beta_j+\beta_k-\beta_i)^3} + \frac{(\beta_i-\beta_j-\beta_k)(\beta_i+\beta_j-\beta_k)t - (3\beta_i+\beta_j-3\beta_k)}{(\beta_i-\beta_j-\beta_k)^3(\beta_i+\beta_j-\beta_k)^2}e^{-(\beta_j+\beta_k-\beta_i)t}\right)\right] \tag{2.10.5}$$

Also the analysis gives

$$\langle\omega_i(0)\omega_i(t)\rangle = 0 \qquad (i \neq j)$$

In the equations above, the quantity

$$\alpha_i = \frac{I_j - I_k}{I_i}$$

while

$$\gamma_i = \frac{kT}{I_i I_j}(I_j - I_i)$$

For example,

$$\alpha_1 = \frac{B-C}{A} \qquad \gamma_1 = \frac{kT}{AB}(B-A)$$

Morita's analysis also gives a more accurate expression for $\mathscr{L}[\langle\omega_i(0)\omega_i(t)\rangle]$, which is got by calculating more terms in a continued fraction expansion. Equation 2.10.4 in fact represents the second convergent in the general continued fraction for $\mathscr{L}[\langle\omega_i(0)\omega_i(t)\rangle]$. The expression for $\mathscr{L}[\langle\omega_i(0)\omega_i(t)\rangle]$ agrees exactly with the expression for this quantity when $A = B$ so that the body has axial symmetry. This provides a useful check on the accuracy of the calculations. Equation 2.10.5 may also be compared with the work of Hubbard, who in 1977 obtained the following approximate expression for $\langle\omega_i(0)\omega_i(t)\rangle$ for an ellipsoid:

$$C(t) = \langle\omega_i(0)\omega_i(t)\rangle = \frac{kT}{I_i}e^{-\beta_i t}\left(1 + \frac{\alpha_i\gamma_i[(\beta_j+\beta_k-\beta_i) - 1 + e^{-(\beta_j+\beta_k-\beta_i)t}]}{(\beta_j+\beta_k-\beta_i)^2}\right) \tag{2.10.6}$$

It is easily seen that Eq. 2.10.6 is in full agreement with Eq. 2.10.5 when terms in $\alpha_i\gamma_i$ of higher order than the first are omitted. This equation has also been rederived by Ford et al. (1979) using rotation operators.

2.10.1 Calculation of the Aftereffect Functions

First we outline the treatment for the body having an axis of symmetry. As we have seen, the Brownian movement of a rigid body is described by the set of Eqs. 2.9.3, which give the angular velocity vector $\boldsymbol{\omega}(t)$. The orientation of the body as a function of the time is then completely specified if we solve for the Eulerian angles (θ, φ, ψ) as a function of the time. It is evident from our general discussion of the Kramers equation that the set of stochastic differential equations for the angular velocities and the Eulerian angles may be written in the form

$$d\mathbf{X}(t) = \mathbf{a}(t, \mathbf{X})\,dt + B\,d\mathbf{W}(t)$$

whence the Kramers equation for the evolution of the probability density $\rho(\omega_1, \omega_2, \omega_3, \theta, \varphi, \psi, t)$ in the configuration-angular velocity space may be written. This equation is (Morita, 1978)

$$\left\{\frac{\partial}{\partial t} + \sum_{j=1,2,3}\left[i\omega_j L_j - \beta_j\frac{\partial}{\partial\omega_j}\left(\omega_j + \frac{kT}{I_j}\frac{\partial}{\partial\omega_j}\right)\right] + \sum_{i,j,k}\frac{1}{I_i}[\omega_j\omega_k(I_j - I_k) + N_i]\frac{\partial}{\partial\omega_i}\right\}\rho = 0 \tag{2.10.1.1}$$

by the usual method, which we have given in Chapter 1 for the derivation of the Kramers equation from the Langevin equation. In Eq. 2.10.1.1, i, j, k are cyclic indexes and *for convenience*, (A, B, C) are denoted by (I_1, I_2, I_3). Further, L_i is the angular momentum operator defined by

$$L_1 = \frac{1}{i}\left(\cos\psi\frac{\partial}{\partial\theta} + \frac{\sin\psi}{\sin\theta}\frac{\partial}{\partial\varphi} - \cot\theta\sin\psi\frac{\partial}{\partial\psi}\right)$$

$$L_2 = \frac{1}{i}\left(-\sin\psi\frac{\partial}{\partial\theta} + \frac{\cos\psi}{\sin\theta}\frac{\partial}{\partial\varphi} - \cot\theta\cos\psi\frac{\partial}{\partial\psi}\right)$$

$$L_3 = \frac{1}{i}\frac{\partial}{\partial\psi}$$

The dipole moment $\langle \boldsymbol{\mu} \cdot \mathbf{e} \rangle$ induced by an electric field **E** is (after integration over the velocities)

$$\langle \boldsymbol{\mu}(t) \cdot \mathbf{e} \rangle = \frac{\int_0^{\pi} d\theta \int_0^{2\pi} d\varphi \int_0^{2\pi} d\psi \boldsymbol{\mu} \cdot \mathbf{e} f(\theta, \varphi, \psi, t)}{\int_0^{\pi} d\theta \int_0^{2\pi} d\varphi \int_0^{2\pi} d\psi f(\theta, \varphi, \psi, t)} \tag{2.10.1.2}$$

Morita now specializes this equation to the case of a body having an axis of symmetry and having a dipole *only* along the axis of symmetry as is usual in symmetric top molecules. Further, by means of the transformations

$$v_\theta = \dot{\theta} = \omega_1 \cos\psi - \omega_2 \sin\psi$$

$$v_\phi = \dot{\phi} \sin\theta = \omega_1 \sin\psi + \omega_2 \cos\psi$$

$$v_z = \omega_z$$

He finds that Eq. 2.10.1.1 becomes (indirectly assuming that the potential giving rise to **N** in the Euler–Langevin equation is a function of θ only corresponding to $\boldsymbol{\mu}$ lying along the axis of symmetry)

$$\left[\frac{\partial}{\partial t} + v_\theta \frac{\partial}{\partial \theta} + \left(\frac{C}{A} v_z - v_\varphi \cot\theta\right)\left(v_\theta \frac{\partial}{\partial v_\varphi} - v_\varphi \frac{\partial}{\partial v_\theta}\right) - \frac{1}{A}\frac{\partial V}{\partial \theta}\frac{\partial}{\partial v_\theta} - \frac{\zeta_1}{A}\sum_{i=\theta,\varphi} \frac{\partial}{\partial v_i}\left(v_i + \frac{kT}{A}\frac{\partial}{\partial v_i}\right) - \frac{\zeta_3}{C}\frac{\partial}{\partial v_z}\left(v_z + \frac{kT}{C}\frac{\partial}{\partial v_z}\right)\right]\rho_\varphi = 0 \tag{2.10.1.3}$$

where ρ_φ denotes the quantity

$$\rho_\varphi(v_\theta, v_\varphi, v_z, \theta, t) = \int_0^{2\pi}\int_0^{2\pi} \rho \, d\varphi \, d\psi$$

and the quantity $\langle \boldsymbol{\mu}(t) \cdot \mathbf{e} \rangle$ is now

$$\langle \boldsymbol{\mu}(t) \cdot \mathbf{e} \rangle = \frac{\mu_z \int_0^{\pi} \sin\theta \, d\theta \int_{-\infty}^{\infty} dv_\theta \int_{-\infty}^{\infty} dv_\varphi \int_{-\infty}^{\infty} dv_z \cos\theta \rho_\varphi}{\int_0^{\pi} \sin\theta \, d\theta \int_{-\infty}^{\infty} dv_\theta \int_{-\infty}^{\infty} dv_\varphi \int_{-\infty}^{\infty} dv_z \rho_\varphi}$$

Equation 2.10.1.3 closely resembles that given by Sack in his discussion of the rotational Brownian movement of the sphere. Sack's equation is slightly simpler because in his discussion all the moments of inertia are equal. Morita closely follows the method given by Sack for the sphere.

Thus Morita deduces a set of three term recurrence relations for the Laplace-transform of the aftereffect function. He then solves this by means of a continued fraction expansion to get (the result is given in terms of the dipole a.c.f. $R(t)$)

$$\int_0^{\infty} R(t) e^{-st} dt = \cfrac{1}{s + \cfrac{2kT/A}{s + \beta_1 + \cfrac{2kT/A}{s + 2\beta_1 + \cfrac{4kT/A}{s + 3\beta_1}} + \cfrac{(kT/A)(C/A)}{s + \beta_1 + \beta_3 + \cfrac{(2kT/A)(C/A)}{s + \beta_1 + 2\beta_3 + \cfrac{2kT/A}{s + 2\beta_3}}}}} \cdot \tag{2.10.1.4}$$

This expansion may be carried on to give the Laplace transform of the dipole autocorrelation function correct to any desired order in kT/A. Having thus obtained the Laplace transform of the a.c.f. in continued fraction form, Morita now proceeds to show how an equation for it may be obtained from his earlier expressions for the angular velocity correlation functions when combined with the solution by successive approximations of the equation

$$\frac{d\mathbf{u}}{dt} = \boldsymbol{\omega} \times \mathbf{u}$$

He finds from this approach the following expressions for $\mathcal{L}\{R(t)\}$ (again for a dipole lying along the axis of symmetry only)

$$\mathcal{L}\{R(t)\} = \left\{\frac{1}{s} - \frac{2kT}{A}\frac{1}{s^2}\cfrac{1}{s + \beta_1 + \cfrac{(kT/A)(C/A)}{s + \beta_1 + \beta_3 + \cfrac{2kT/A(C/A)}{s + \beta_1 + 2\beta_2}}} + 8\left(\frac{kT}{A}\right)^2 \frac{1}{s^2}(\cdots)\right\} \tag{2.10.1.5}$$

Equation 2.10.1.4 is in agreement with Eq. 2.10.1.5 up to the order in kT/A to which it is carried.

In conclusion of this review of Morita's treatment of the calculation of the aftereffect function for the symmetrical body it should be noted that if one allows the ratio $C/A \to 0$ in the results of his calculation, one finds that

$$\int_0^{\infty} R(t) e^{-\omega t} dt = \cfrac{1/\beta|}{|i\omega'} + \cfrac{2a}{|1 + i\omega'} + \cfrac{2a}{|2 + i\omega'} \cdots$$

where

$$\omega' = \frac{\omega}{\beta_1}, \qquad a = \frac{kT}{A\beta_1^2}$$

which is precisely the result given by Sack for the needle molecule; thus the limit serves as a check on Morita's calculations.

In the last part of his analysis Morita proceeds to give an expression for

the Laplace transform of the aftereffect function for the general ellipsoid (the asymmetric body). He finds from the Kramers equation (after very considerable algebra) the following approximate expression:

$$\Pi(s) = \int_0^\infty \langle \boldsymbol{\mu}_3'(0) \cdot \boldsymbol{\mu}_3'(t) \rangle e^{-st} = \sum_{i=1,2,3} \frac{1}{3} \mu_i^2 a^{(i)}(s) \qquad (2.10.1.6)$$

where

$$\mu_3'(t) = \mu_1 \sin\theta \sin\psi + \mu_2 \sin\theta \cos\psi + \mu_3 \cos\theta$$

$$a^{(i)}(s) = \left[s + \frac{p_2^{(i)}(q_1^{(i)} + r_1^{(i)}) - p_1^{(i)}(q_2^{(i)} + r_2^{(i)})}{q_1^{(i)} r_2^{(i)} - r_1^{(i)} q_2^{(i)}} \right]^{-1}$$

in which

$$p_1^{(i)} = -\frac{4k_BT}{I_j}(s + 2\beta_j)(s + \beta_i + \beta_j)(s + \beta_i + \beta_j)$$

$$p_2^{(i)} = \frac{4k_BT}{I_k}(s + 2\beta_k)(s + \beta_i + \beta_j)(s + \beta_i + \beta_k)$$

$$q_1^{(i)} = 4(s + \beta_j)(s + 2\beta_j)(s + \beta_i + \beta_j)(s + \beta_i + \beta_k) + \frac{8k_BT}{I_j}(s + \beta_i + \beta_j)(s + \beta_i + \beta_k) + \frac{4k_BT}{I_i}(s + 2\beta_j)(s + \beta_i + \beta_k) + \frac{4k_BT}{I_iI_jI_k}(I_i - I_k)^2(s + 2\beta_j)(s + \beta_i + \beta_j)$$

$$q_2^{(i)} = \frac{4k_BT}{I_iI_k}(s + 2\beta_k)[(I_k - I_i)(s + \beta_i + \beta_j) + (I_j - I_i)(s + \beta_i + \beta_k)]$$

$$r_1^{(i)} = \frac{4k_BT}{I_iI_j}(s + 2\beta_j)[(I_j - I_i)(s + \beta_i + \beta_j) + (I_k - I_i)(s + \beta_i + \beta_k)]$$

$$r_2^{(i)} = 4(s + \beta_k)(s + 2\beta_k)(s + \beta_i + \beta_j)(s + \beta_i + \beta_k) + \frac{8k_BT}{I_k}(s + \beta_i + \beta_j)(s + \beta_i + \beta_k) + \frac{4k_BT}{I_iI_jI_k}(I_j - I_i)^2(s + 2\beta_k)(s + \beta_i + \beta_k) + \frac{4k_BT}{I_i}(s + 2\beta_k)(s + \beta_i + \beta_j)$$

In the foregoing, $(i = 1, j = 2, k = 3)$, $(i = 2, j = 3, k = 1)$, and $(i = 3, j = 2, k = 1)$ i, j, k are cyclic indexes.

This equation represents the generalization of the earlier work of Perrin, based on the Smoluchowski approximation, to include *inertial* effects in the rotational Brownian movement of the ellipsoid. Just as we did for the disk, sphere, and needle models we now summarize concisely the chief results of Morita's investigation.

For the Body Having an Axis of Symmetry

1. The distribution of the angular velocity components and the components of the dipole vector $\boldsymbol{\mu}(t)$ are not Gaussian.

2. The angular velocity correlation functions may be written in *closed form* as

$$C_1(t) = \langle \omega_1(t_1)\omega_1(t_2) \rangle = \langle \omega_2(t_2)\omega_2(t_1) \rangle = \frac{kT}{A} e^{-\beta|t_1 - t_2|} \exp\left[-\frac{kT}{C}\left(\frac{d}{\beta_3}\right)(\beta_3|t_1 - t_2| - 1 + e^{-\beta_3|t_2 - t_1|}) \right]$$

$$C_3(t) = \langle \omega_3(t_1)\omega_3(t_2) \rangle = \frac{kT}{C} e^{-\beta_3|t_1 - t_2|}$$

$$\langle \omega_i(t_1)\omega_j(t_2) \rangle = 0 \qquad i \neq j$$

3. These results may be obtained both from the Langevin equation and from the Fokker–Planck equation in velocity space. In the special case $A = C$ they yield the results for the sphere and in the case $C/A \to 0$ they give the result for the needle as already obtained by Sack (1957).
4. The normalized aftereffect function when the body carries a dipole along the axis of symmetry may be calculated both from the linear approximation (aftereffect solution) to the solution of the Kramers equation and by solution of the equation

$$\frac{d\mathbf{u}}{dt} = \boldsymbol{\omega} \times \mathbf{u}$$

5. The polarizability for the model does not show resonance behavior.

For the Asymmetrical Body

1. The distributions of the angular velocity vector and the dipole vector are *not* Gaussian.
3. The angular velocity correlation functions *cannot* be expressed in *closed form* and moreover are not readily calculable from the Langevin equation. They can, however, be calculated to any order of accuracy from a continued fraction arising from the Fokker–Planck equation. The results for the body with an axis of symmetry are immediately obtained when two of the moments of inertia are equal.
3. Morita's results for the angular velocity a.c.f.'s agree with Hubbard (1977) to the order to which Hubbard has calculated.
   An approximate expression for the Laplace transform of the aftereffect function may be obtained from the Kramers equation. This represents the generalization to include inertial effects of the work of Perrin (1934).
4. Ford et al. (1979) have also treated the problem using a perturbation series approximation to the stationary solution of the Euler–Langevin equation and rotation operators. They find that the polarizability for the ellipsoid (when it carries a dipole $\mathbf{m}$ whose components are m_x, m_y, m_z along principal axes x, y, z fixed in the body) is given

approximately by (*in their notation*)

$$\alpha(\omega) = \frac{1}{3kT} \sum_{x,y,z} \frac{m_x^2}{(D_y + D_z + i\omega)} \left[\frac{D_y(D_y + D_z + B_y)}{D_y + D_z + B_y + i\omega} + \frac{D_z(D_y + D_z + B_z)}{D_y + D_z + B_z + i\omega} \right] \tag{2.10.1.7}$$

in which $B_y = \zeta_y / I_y$ (ζ_2/β_2 in our notation) and where (to a first approximation) $D_y = kT/I_y B_y$, etc.

5. *Neither this equation nor that given by Morita shows any sign of resonance behavior; a fortiore none of the equations account for the Poley absorption.*
6. If the body has an axis of symmetry and the dipole lies along this axis then Eq. 2.10.1.7 effectively reduces to the Rocard (1933) equation:

$$\frac{\alpha(\omega)}{\alpha'(0)} = \frac{1}{1 + i\omega\tau - \omega^2 \tau_0 \beta^{-1}}$$

2.11 FREE ROTATIONAL MODELS UNDER THE INFLUENCE OF LARGE EXTERNAL FIELDS

The calculation we have so far presented are valid only for fields so small that terms of the order

$$\left(\frac{\mu E}{kT}\right)^2$$

where E is the magnitude of the impressed field, can be neglected. The upshot of this is that the important relation

$$\alpha(\omega) = \alpha'(0) - i\omega \int_0^\infty b(t) e^{-i\omega t} dt \tag{2.11.1}$$

between the response to an alternating electric field and the response following on the sudden removal of a constant field is satisfied. If the restriction to terms linear in the applied field strength is now relaxed then Eq. 2.11.1 no longer applies and there is *no longer* any simple relation between the aftereffect and steady-state responses. There has lately been considerable interest in the relaxation behavior when the restriction to small fields is lifted. The problem of calculating the response to large fields (in the Debye or Smoluchowski approximation) has been considered by Benoit (1951), Kielich (1966), Beevers et al. (1976), Coffey and Paranjape (1978), Coffey (1978), Morita (1978, 1979), and Morita and Watanabe (1979). The treatment to be given here makes use of the method of successive approximations to calculate the response to an electric field in the form of a rectangular pulse applied at a time $t = 0$. Morita (1978) has shown that the Laplace transform of the polarization following on the application of

such a field may be obtained *exactly* in terms of an infinite continued fraction. The calculation carried out here is in full agreement with the exact solution to the order in the field strength to which the calculation is carried.

2.11.1 The Debye Theory for Large Fields

On the basis of the Debye theory we have seen that the variation, in configuration space of the probability density function, $f(\vartheta, t)$ for a sphere carrying a rigid dipole of moment μ undergoing rotational Brownian motion at absolute temperature T and under the influence of an external time varying electric field $\mathbf{E}(t)$ is governed by the equation

$$2\tau \frac{\partial f(\vartheta, t)}{\partial t} = \frac{1}{\sin\vartheta} \frac{\partial}{\partial \vartheta} \left[\sin\vartheta \left(\frac{\partial f(\vartheta, t)}{\partial \vartheta} - \frac{f(\vartheta, t)}{kT} M(\vartheta, t) \right) \right] \tag{2.11.1.1}$$

in which $f(\vartheta, t) \sin\vartheta \, d\vartheta$ is the probability that at time t the dipole has an orientation between ϑ and $\vartheta + d\vartheta$ relative to the direction of $\mathbf{E}(t)$; $M(\vartheta, t) = -\mu E \sin\vartheta$ is the magnitude of the torque acting on the dipole due to $\mathbf{E}(t)$; k is the Boltzmann constant; and τ is the Debye relaxation time (ζ times its angular velocity is the frictional torque acting on the dipole). Equation 2.11.1.1 although originally derived by Debye for the case of spherical symmetry, also applies *without change of form* to both prolate and oblate spheroids having a dipole along the axis of symmetry. This is easily seen on remembering that Eq. 2.11.1.1 is simply a special case of the Smoluchowski equation, namely,

$$2\tau \frac{\partial f}{\partial t} = \operatorname{div} \left[\operatorname{grad} f + \frac{f}{kT} \operatorname{grad} V \right]$$

(V is the potential of the torque due to the impressed field), then writing out the operator divgrad in prolate or oblate spheroidal coordinates (Macrobert, 1967), and finally considering the special case where f depends on the colatitude ϑ only.

In order to illustrate the method of solution at hand we confine ourselves (as we have mentioned above) to the particular case where the impressed field has the form of a rectangular pulse of length t_1. Thus

$$\mathbf{E}(t) = \mathbf{E}_0[U(t) - U(t - t_1)] = \mathbf{E}_0 e(t)$$

where $U(t)$ denotes the unit step function. With these preliminaries we may proceed with the solution, which is of the form

$$f(\vartheta, t) = \sum_{n=0}^{\infty} a_n(t) P_n(\cos\vartheta)$$

where the $a_n(t)$ are functions to be determined. On substituting this expression into Eq. 2.11.1.1 and making use of well-known recurrence

relations for the Legendre polynomials, $P_n(\cos\vartheta)$, and the orthogonality property

$$\int_{-1}^{+1} P_n(x)P_m(x)\,dx = \frac{2}{2n+1}\,\delta_{m,n}$$

we find that the a_n must satisfy the differential equation

$$\frac{da_n}{dt} = -\frac{n(n+1)}{2\tau}\left[a_n(t) - \frac{\mu E(t)}{kT}\left(\frac{a_{n-1}(t)}{2n-1} - \frac{a_{n+1}(t)}{2n+3}\right)\right] \qquad (2.11.1.2)$$

The solution of this equation is

$$a_n(t) = A\exp\left(-\frac{n(n+1)t}{2\tau}\right) + \frac{n(n+1)\gamma}{2\tau}\int_0^t \exp\left[-\frac{n(n+1)(t-u)}{2\tau}\right] e(u)\left[\frac{a_{n-1}(u)}{2n-1} - \frac{a_{n+1}(u)}{2n+3}\right] du \qquad (2.11.1.3)$$

where this time $\gamma = \mu E_0/kT$; e is defined above; and A is a constant to be determined from the initial conditions of the problem. A is easily found, for in view of the orthogonality property of the P_n, we must have for the ensemble averages

$$\langle P_n(\cos\vartheta)\rangle = \frac{\int_{-1}^{+1} f(\vartheta,t)P_n(\cos\vartheta)d(\cos\vartheta)}{\int_{-1}^{+1} f(\vartheta,t)d(\cos\vartheta)} = \frac{a_n(t)}{a_0(2n+1)}$$

Further, in the absence of an applied field (the circumstance prevailing at $t = 0$), we have

$$\langle P_n(\cos\vartheta)\rangle = 0 \qquad (t \leqslant 0,\ n = 1, 2)$$

whence

$$A = 0$$

and thus

$$a_n(t) = \frac{n(n+1)\gamma}{2\tau}\int_0^t \exp\left[\frac{n(n+1)(t-u)}{2\tau}\right] e(u)\left[\frac{a_{n-1}(u)}{2n-1} - \frac{a_{n+1}(u)}{2n+3}\right] du \qquad (2.11.1.4)$$

Equation 2.11.1.4 is an integral equation for the unknown functions a_n and may be solved to yield the solution as a convergent power series in γ by means of Picard's method of successive approximations. The procedure here is entirely analogous (since Eq. 2.11.1.4 is of the *same* mathematical form) to that used in solving the Brinkman equation for the two-dimensional rotator considered above; thus we content ourselves with merely writing the results for the ensemble averages,

$$\langle P_1(\cos\vartheta)\rangle = \langle\cos\vartheta\rangle, \qquad \langle P_2(\cos\vartheta)\rangle = \tfrac{1}{2}\langle(3\cos^2\vartheta - 1)\rangle$$

appropriate to dielectric and Kerr effect relaxations, respectively. We have

by Picard's method

$$\langle P_1(\cos\vartheta)\rangle = \frac{1}{3}\left[\frac{\gamma}{\tau}\int_0^t \exp\left(-\frac{t-u}{\tau}\right) e(u)\,du - \frac{\gamma^3}{5\tau^3}\int\int\int_{0\leqslant u_1\leqslant u_2\leqslant t} \exp\left(-\frac{t-u}{\tau}\right) \times \exp\left(-3\frac{u-u_1}{\tau}\right)\exp\left(-\frac{u_1-u_2}{\tau}\right) e(u_2)e(u_1)e(u)\,du_2\,du_1\,du\cdots\right]$$

$$\langle P_2(\cos\vartheta)\rangle = \frac{1}{5}\left[\frac{\gamma^2}{\tau^2}\int\int_{0\leqslant u_1\leqslant u<1} \exp\left(-3\frac{t-u}{\tau}\right) \times \exp\left(-\frac{u-u_1}{\tau}\right) e(u_1)e(u)\,du_1\,du\cdots\right]$$

These equations allow us to calculate $\langle P_1\rangle$ and $\langle P_2\rangle$ correct to any order in γ. In practice, we need go only as far as terms in γ^3 in the first equation and as far as terms in γ^2 in the second one since the higher-order terms in γ make negligible contributions to $\langle P_1\rangle$ and $\langle P_2\rangle$. Note that the term linear in γ represents the approximation obtained by Debye to the solution of Eq. 2.11.1.4. All the other terms are the contribution to the ensemble averages due to the nonlinear behavior of $f(\vartheta, t)$. On substituting for $e(u)$ explicitly and evaluating the integrals we find, after considerable algebra, that

$$\langle P_1\rangle = \frac{1}{3}\left\{\gamma[1-e^{-t/\tau}]U(t) - [1-e^{-(t-t_1)/\tau}]U(t-t_1) - \frac{1}{5}\gamma^3\left[\left(\frac{1}{3} - \frac{te^{-t/\tau}}{2\tau} - \frac{1}{12}e^{-2t/\tau} - \frac{1}{4}e^{-t/\tau}\right)U(t) - \left(\frac{1}{3} - \frac{1}{3}e^{-(t-t_1)/\tau} - \frac{(t-t_1)}{2\tau}e^{-t/\tau} - \frac{1}{12}e^{-2t/\tau} + \frac{1}{12}e^{-t_1/\tau}e^{-(t-t_1)/\tau}\right)U(t-t_1)\right]\cdots\right\} + O(\gamma^5)$$

$$\langle P_2\rangle = \frac{1}{5}\gamma^2\left[\left(\frac{1}{3} - \frac{1}{2}e^{-t/\tau} + \frac{1}{6}e^{-3t/\tau}\right)U(t) - \left(\frac{1}{3} - \frac{1}{2}e^{-t/\tau} - \frac{1}{3}e^{-3(t-t_1)/\tau} + \frac{1}{2}e^{-t/\tau}e^{-2(t-t_1)/\tau}\right)U(t-t_1)\right] + O(\gamma^4)$$

Before proceeding any further it is instructive to make some comments on these equations. Let us suppose that $t < t_1$; thus we have

$$\langle P_1\rangle = \frac{1}{3}\left[\gamma(1-e^{-t/\tau}) - \frac{1}{5}\gamma^3\left(\frac{1}{3} - \frac{te^{-t/\tau}}{2\tau} - e^{-2t/\tau} - \frac{1}{4}e^{-t/\tau}\right) + O(\gamma^5), \qquad t < t_1\right.$$

$$\langle P_2\rangle = \tfrac{1}{5}\gamma^2[(\tfrac{1}{3} - \tfrac{1}{2}e^{-t/\tau} + \tfrac{1}{6}e^{-3t/\tau})] + O(\gamma^4)$$

On the other hand for $t > t_1$, we find that

$$\langle P_1(\cos\vartheta)\rangle = \frac{1}{3}\left[\gamma(e^{-(t-t_1)/\tau} - e^{-t/\tau}) - \frac{1}{5}\gamma^3\left(\frac{1}{3}e^{-(t-t_1)/\tau} - \frac{t_1}{2\tau}e^{-t/\tau} - \frac{1}{4}e^{-t/\tau} - \frac{1}{12}e^{-(t-t_1)/\tau}\right) + O(\gamma^5)\right]$$

$$\langle P_2(\cos\vartheta)\rangle = \frac{1}{5}\gamma^2\left[\frac{1}{3}e^{-3(t-t_1)/\tau} + \frac{1}{6}e^{-3t/\tau} - \frac{1}{2}e^{-t/\tau}e^{-2(t-t_1)/\tau}\right] + O(\gamma^4)$$

If we now assume that the times t and t_1 are both very much greater than the Debye relaxation time τ while the quantity $t - t_1$ remains finite, then the above equations reduce to

$$\langle P_1 \rangle = \tfrac{1}{3}[\gamma e^{-(t-t_1)/\tau} - \tfrac{1}{15}\gamma^3 e^{-(t-t_1)/\tau} + O(\gamma^5)] \qquad (t > t_1 \gg \tau)$$

and

$$\langle P_2 \rangle = \tfrac{1}{15}\gamma^2 e^{-3(t-t_1)/\tau} + O(\gamma^4)$$

It should be noted that the terms arising from the application of $U(t)$ do not mirror the terms arising from the application of $-U(t - t_1)$; thus in general the rise transients are not the *mirror images* of the decay transients. An exception to this is in the linear approximation to $\langle P_1 \rangle$ when terms $O(\gamma)$ are retained only. In this special case the rise and decay curves are *mirror images* of one another.

Furthermore it should be noted that in the rise transient the time constants are now functions of the field strength. This is not immediately apparent from the above analysis since that treatment essentially involves expanding $\langle P_n(\cos \vartheta) \rangle$ in powers of γ and consequently any terms of the form $\exp[f(E, t)]$ will also have to be expanded in powers of γ. The term $\gamma^2 t e^{-t/\tau}$ arises as a result of expanding a term like $\exp[f(E, t)]$ as a power series in γ. The exact treatment of Morita (1978, 1979) (of which the above treatment is a limiting case) shows clearly this field dependence of the decay "constants."

The solution appropriate to the case where the applied field is an alternating one has been carried out to third order in the field strength by Coffey and Paranjape (1978). In particular, they consider the case of a constant field superimposed on which is a weak alternating field. It is then possible to calculate the small phase shift produced by the strong constant field interacting with the alternating one. In conclusion of this section we note the experimental work of Hellemans and de Maeyer (1975), and we summarize the principle results of the theoretical investigation as follows:

1. It is possible to obtain an exact solution of Eq. 2.11.1.1 (i.e., a solution correct to any desired order in the field strength) by computing the inverse Laplace transform of a continued fraction.
2. This solution applies to both *spherical* and *symmetrical* top molecules.
3. There is no connection between the aftereffect and alternating field solution as there is in the linear case.
4. The rise and decay transients resulting from the application of a rectangular pulse to the dielectric do not bear a simple relation to each other when nonlinear effects are taken into consideration.
5. Induced moments and thus anisotropy of the polarization may be readily taken into account by including an extra potential energy term in the Smoluchowski equation, as was done by Beevers et al. (1976).
6. Inertial effects may be included by adopting some of the methods we have outlined for the linear case. In particular the process of including these is greatly complicated by the lack of any simple relation between the aftereffect and alternating field solutions. It should be possible, however, to take account of them exactly for the disk model when the applied field has the form of a rectangular pulse. All that is involved is the calculation of higher order ψ_n^s in Sack's solution of the Kramers equation for that model. In fact we may easily write $\langle \cos n\theta \rangle$ (corresponding to $\langle P_n(\cos \vartheta) \rangle$ in the three-dimensional case) for the situation where a *strong* constant field has been applied for a long time and is suddenly switched off. One finds that

$$\Phi(t) = \frac{\langle \cos n\theta(t) \rangle}{\langle \cos n\theta(0) \rangle} = \exp\left[-\frac{n^2 kTI}{\zeta^2}\left(\frac{\zeta t}{I} - 1 + e^{-(\zeta/I)t}\right)\right]$$

This brings to an end our discussion of the Debye theory and the various modifications and additions made to it. *Even with all these modifications the theory still fails to explain many features of the observed spectra.* In accordance with our discussion in Chapter 1 we must now see how memory effects may be included in the theory; to do this we introduce the generalized Langevin equation given by Kubo (1965) and Mori (1965).

2.12 THE GENERALIZED LANGEVIN EQUATION—MEMORY EFFECTS

In what follows we adhere closely to a discussion of the generalized Langevin equation given by Evans (1976).

As we have seen in Chapter 1 Kubo (1965) and Mori (1965) have presented a general form of the classical Langevin equation. (The rigorous theory is described in Chapters 9 and 10.) This is now written for a body constrained to rotate in a plane (or for a sphere if $\boldsymbol{\omega}$ is regarded as a vector quantity):

$$\dot{\omega}(t) = -\int_0^t \phi(t - \tau)\omega(\tau)\, d\tau + \Gamma(t) \qquad (2.12.1)$$

where ϕ (written as K in Chapter 4) is a time-dependent friction coefficient known (Chapter 1) as the memory function. $I\Gamma(t)$ is the fluctuating part of the torque on a molecule of inertia I. It follows from Eq. 2.12.1 on averaging

$$\frac{d\langle \omega(0)\omega(t) \rangle}{dt} = -\int_0^t \phi(t - \tau)\langle \omega(0)\omega(\tau) \rangle\, d\tau + \langle \omega(0)\Gamma(t) \rangle \qquad (2.12.2)$$

The last term is zero since $\omega(0)$ and $\Gamma(t)$ are *assumed* to be *uncorrelated* statistically.

Mori (1965) has shown that the set of memory functions $\phi_0(t) \cdots \phi_m(t)$ obey the set of coupled Volterra integral equations such that

$$\frac{\partial \phi_{n-1}(t)}{\partial t} = -\int_0^t \phi_n(t-\tau)\phi_{n-1}(\tau)\, d\tau \tag{2.12.3}$$

Solving by Laplace transformation (into s space) we have the following continued fraction:

$$\tilde{C}(s) = \frac{C(0)}{s + \tilde{\phi}(s)} = \cfrac{C(0)}{s + \cfrac{\phi_0(0)}{s + \tilde{\phi}_1(s)}} \tag{2.12.4}$$

with $\tilde{C}(s)$ as the Laplace transform of $C(t) = \langle \omega(0)\omega(t)\rangle$. Truncating this continued fraction, using simple forms of $\tilde{\phi}(s)$, can be used to derive complicated but more realistic forms of $C(t)$ (and its Fourier transform) than the simple exponential form of the Ornstein–Uhlenbeck theory.

The equilibrium averages $\phi_0(0)$, $\phi_1(0)$, etc., are related to the terms in the Taylor expansion of $C(t)$, so that if we write (in the manner given in general in Chapter 1)

$$\frac{\langle \omega(0)\omega(t)\rangle}{\langle \omega^2(0)\rangle} = \frac{\sum_n a_n t^{2n}}{(2n)!} \tag{2.12.5}$$

with a_n alternatively positive and negative, we have

$$\phi_0(0) = -a_1 = \{\langle \dot{\omega}^2(0)\rangle / \langle \omega^2(0)\rangle\} \tag{2.12.6}$$

$$\phi_1(0) = a_1 - \frac{a_2}{a_1} = \{[\langle \ddot{\omega}^2(0)\rangle / \langle \dot{\omega}^2(0)\rangle] - [\langle \dot{\omega}^2(0)\rangle / \langle \omega^2(0)\rangle]\} \tag{2.12.7}$$

and so on.

Let us suppose that we may now *truncate* the series with $\phi_1(t) = \phi_1(0)\exp(-\gamma t)$, where γ^{-1} is an empirical correlation time; we then find for the Laplace transform of $C(t)$

$$\mathcal{L}\{C(t)\} = \tilde{C}(s) = \frac{\langle \omega^2(0)\rangle [s(s+\gamma) + \phi_1(0)]}{s^3 + \gamma s^2 + [\phi_0(0) + \phi_1(0)]s + \phi_0(0)} \tag{2.12.8}$$

Equation 2.12.8 may be inverted to give $C(t)$ (the underdamped solution is given):

$$\frac{C(t)}{C(0)} = \left[\cos \omega_1 t + \frac{1}{\omega_1}(\sigma_1 + \Lambda\sigma_2)\sin \omega_1 t\right]\frac{e^{-\sigma_1 t}}{1+\Lambda} + \frac{\Lambda}{1+\Lambda}e^{-\sigma_2 t} \tag{2.12.9}$$

where

$$\Lambda = \frac{-2\sigma_1(\sigma_1^2 + \omega_1^2)}{\sigma_2(3\sigma_1^2 - \omega_1^2 - \sigma_2^2)}$$

$$\sigma_1 = \tfrac{1}{2}(s_1 + s_2) + \tfrac{1}{3}\gamma$$

$$\sigma_2 = -\tfrac{1}{2}(s_1 + s_2) + \tfrac{1}{3}\gamma$$

$$\omega_1 = \frac{\sqrt{3}}{2}(s_1 - s_2)$$

$$s_1 = [-\tfrac{1}{2}B + (\tfrac{1}{27}A^3 + \tfrac{1}{4}B^2)^{1/2}]^{1/3}$$

$$s_2 = [-\tfrac{1}{2}B - (\tfrac{1}{27}A^3 + \tfrac{1}{4}B^2)^{1/2}]^{1/3}$$

with

$$A = \phi_0(0) + \phi_1(0) - \tfrac{1}{3}\gamma^2, \qquad B = \tfrac{1}{3}\gamma[\tfrac{2}{9}\gamma^2 + 2\phi_0(0) - \phi_1(0)]$$

$$\langle \omega^2(0)\rangle = \frac{2kT}{I} \quad \text{(in three dimensions)}$$

$$\langle \omega^2(0)\rangle = \frac{kT}{I} \quad \text{(in two dimensions)} \tag{2.12.10}$$

Thus our introduction of the memory function and truncation as indicated immediately allows of an *oscillatory* angular velocity a.c.f. unlike the simple *exponential* decay of the Ornstein–Uhlenbeck theory. This is much more in accord with the experimental data (Chapter 4).

If the body is *constrained* to rotate in a *plane* we may make use of the Kubo relation (Chapters 9 and 10), namely,

$$\langle \mathbf{u}(0)\cdot\mathbf{u}(t)\rangle = e^{-\int_0^t (t-t')\langle \omega(0)\omega(t')\rangle\, dt'} \tag{2.12.11}$$

to write the orientational a.c.f. $\langle \mathbf{u}(0)\cdot\mathbf{u}(t)\rangle$ we have, with Eq. 2.12.10, in two dimensions:

$$\langle \mathbf{u}(0)\cdot\mathbf{u}(t)\rangle = e^{-y(t)} \tag{2.12.12}$$

where $y(t)$ is given by

$$y(t) = \frac{kT}{I}(1+\Lambda)^{-1}\left[\left(\frac{2\sigma_1\sigma_2 + \Lambda(\sigma_1^2 + \sigma_2^2 + \omega_1^2)}{\sigma_2(\sigma_1^2 + \omega_1^2)}\right)t + \left(\frac{\Lambda}{\sigma_2^2} + \frac{3\sigma_1^2 + 2\sigma_1\sigma_2\Lambda - \omega_1^2}{(\sigma_1^2 + \omega_1^2)^2}\right) + \frac{\Lambda}{\sigma_2^2}e^{-\sigma_2 t} + \left(\frac{3\sigma_1^2 + 2\sigma_1\sigma_2\Lambda - \omega_1^2}{(\sigma_1^2 + \omega_1^2)^2}\right) \times \left(\cos \omega_1 t + \frac{[\sigma_1^3 - 3\sigma_1\omega_1^2 + \sigma_2\Lambda(\sigma_1^2 - \omega_1^2)]}{\omega_1(3\sigma_1^2 + 2\sigma_1\sigma_2\Lambda - \omega_1^2)}\sin \omega_1 t\right)e^{-\sigma_1 t}\right] \tag{2.12.13}$$

Equation 2.12.8 holds for both the sphere and planar rotator (disk) but Eq. 2.12.13 is valid *only* for the rotational motion of a dipole embedded in an asymmetric top, provided that the dipole axis u moves in a *plane* about the fixed axis $\mathbf{k}$ (so that ω in Eq. 2.12.2 is always a *scalar*, often denoted by $\dot{\theta}$). Making use of Eqs. 2.12.8 and 2.12.9 for $\langle \omega(0)\omega(t)\rangle$ provides the results

illustrated in Fig. 2.4.2.1 for various values of γ; $\phi_0(0)$ and $\phi_1(0)$ which may be interpreted physically as in Chapter 4. These equations may be computer-simulated in turn using the Newton equations for the motion of (for example) 120 *rough disks constrained to a plane* (Fig. 2.4.2.2). The simulated and theoretical curves are in perfect agreement. This use of molecular dynamics simulation is a very convenient way of evaluating the usefulness, in interpreting experimental data, of Eq. 2.12.1 when truncated at a particular ϕ. The ideal method is to simulate the averages $\phi_1(0)$ and $\phi_0(0)$ and the a.c.f. $\langle\omega(t)\omega(0)\rangle$ and to regard γ as an adjustable variable. Alternatively, γ, $\phi_0(0)$, and $\phi_1(0)$ may be regarded as variables and a least mean squares iteration procedure used to fit the simulation results for $\langle\omega(0)\omega(t)\rangle$, preferably for spherical tops.

The applicability of such a procedure is limited (strictly) to the spherical geometry assumption compounded with the assumption that one may truncate the continued fraction in the manner given. However, the simulated $\phi_0(0)$ and the theoretical $\phi_0(0)$ have similar trends, despite the fact that we apply Eq. 2.12.2 to nonspherical geometries in the simulation.

Illustration

The approximation (Eq. 2.12.9) to Eq. 2.12.2 described here is an example of creating a theory to respond to new experimental facts (Chapter 4). However, the structure of the Mori equation is such that it may be used *predictively*; for example, we can see from it that Eq. 2.12.2 is not applicable at very long times because of the *mode–mode coupling* of the angular velocity to the hydrodynamic linear velocity field, creating a vortex (Fig. 1.2.1). This means that the angular velocity a.c.f. does not decay exponentially at very long times, but roughly as $t^{-5/2}$. *This is called the hydrodynamic long time tail* (Chapter 5).

The mathematical truncation of the continued fraction corresponds in a molecular dynamics simulation to interaction between rough disks, which may be described in dynamic terms as follows. When a collision occurs, transfer of momentum takes place between rotational and translational degrees of freedom depending on the value of the dimensionless quantity: $\tau = 4I_1/mD^2$, where m is the mass of the rough disk and D its diameter. Each disk is surrounded by a ring of moment of inertia I_1, which represents the collective motion of its nearest neighbors. The motion of the ring is perturbed by collisions, between which the center of each disk/ring system moves along a straight line at constant velocity. The ring and disk are bound together by a harmonic torque, with a restoring constant γ_0. A typical system is described by the differential equations

$$I_1\ddot{\theta}_1(t) = -\gamma_0[\theta_1(t) - \theta_2(t)]$$
$$I_2\ddot{\theta}_2(t) = \gamma_0[\theta_1(t) - \theta_2(t)]$$

$$\mathbf{v}'_A = \mathbf{v}_A + \left[\frac{\tau}{1+\tau}\right]\left[\mathbf{v} + \left(\frac{1}{\tau}\right)\boldsymbol{\kappa}(\boldsymbol{\kappa}\cdot\mathbf{v})\right]$$
$$\mathbf{v}'_B = \mathbf{v}_B - \left[\frac{\tau}{1+\tau}\right]\left[\mathbf{v} + \left(\frac{1}{\tau}\right)\boldsymbol{\kappa}(\boldsymbol{\kappa}\cdot\mathbf{v})\right]$$
$$\boldsymbol{\omega}'_A = \boldsymbol{\omega}_A - \left[\frac{2}{(1+\tau)D}\right]\boldsymbol{\kappa}\times\mathbf{v}$$
$$\boldsymbol{\omega}'_B = \boldsymbol{\omega}_B - \left[\frac{2}{(1+\tau)D}\right]\boldsymbol{\kappa}\times v \qquad (2.12.14)$$

Here, $\mathbf{v}_A$ and $\mathbf{v}_B$ are the translational velocities and $\boldsymbol{\omega}_A$ and $\boldsymbol{\omega}_B$ are the angular velocities of the ring, that of the inner disk being unaffected directly by the collisions. The primed variables correspond to the situation just after the collision. $\boldsymbol{\kappa}$ is the unit vector directed from the center of the B disk to that of A at the time of collision. $\mathbf{v}$ is the *relative velocity* of the points in contact:

$$\mathbf{v} = \mathbf{v}_B - \mathbf{v}_A - \tfrac{1}{2}D\boldsymbol{\kappa}\times(\boldsymbol{\omega}_A + \boldsymbol{\omega}_B)$$

Finally, θ_1 and θ_2 specify the position of a point on the rim of the ring and the position of the dipole vector on the disk, respectively.

We again note that the simulator Eqs. 2.12.14 are *deterministic* whereas Eq. 2.12.1 is *stochastic*. The two systems may be compared by considering the *average* behavior of the ensemble of rough disks (as we described in Chapter 1). Figure 2.4.2.2 illustrates the behavior of $\langle\dot{\boldsymbol{\omega}}(t)\cdot\dot{\boldsymbol{\omega}}(0)\rangle$, for example, which as we have just seen is related to ϕ_0 of Eq. 2.12.3 at $t = 0$. Also illustrated is the simulated $\langle\dot{\mathbf{u}}(t)\cdot\dot{\mathbf{u}}(0)\rangle$, which is proportional to the Fourier transform of the far infrared power absorption coefficient. Figure 1.7.4.1 illustrates the behavior of the itinerant librator when compared with data for a solution of CH_2Cl_2 (Chapter 4). The mismatch emphasizes the fact that the theoretical model is still simplistic in concept though mathematically involved.

We emphasize that this particular computer calculation is designed to simulate, from the *average* behavior of a large number of deterministic systems, a particular stochastic model, not a real *molecular sample*. Nevertheless it illustrates the potential power of the computer method to carry on where the mathematical analysis becomes laborious and eventually, intractable.

Finally we note that Eq. 2.12.9 is also the solution to the set:

$$\dot{\omega}(t) + \int_0^t \phi_0(t-\tau)\omega(\tau)\,d\tau = \Gamma_0(t)$$
$$\dot{\Gamma}_0(t) + \int_0^t \phi_1(t-\tau)\Gamma_0(\tau)\,d\tau = \Gamma_1(t)$$
$$\dot{\Gamma}_1(t) + \gamma\Gamma_1(t) = \Gamma_2(t) \qquad (2.12.15)$$

The last equation is Markovian, and $\Gamma_2(t)$ is a Wiener process. The series 2.12.15 is equivalent to replacing the original non-Markovian equation Eq. 2.12.1 by a set of equations involving a Markov assumption. In this sense Eqs. 2.12.15 form a *multidimensional Markov* system.

Equation 2.12.9 is inconsistent with the general theorem that classical a.c.f.'s have no odd moments. This is simply because of the arbitrary Markov assumption embodied in the truncation.

2.13 MULTIDIMENSIONAL MARKOV EQUATION FOR ANGULAR VELOCITY

In this section we demonstrate by mathematical induction that Eq. 2.12.1 can be written in the matrix form (Chapters 9 and 10):

$$\dot{\mathbf{w}}(t) + \mathbf{\Phi w}(t) + \mathbf{S w}(t) = \mathbf{F}(t) \tag{2.13.1}$$

where $\mathbf{w}(t)$, $\mathbf{\Phi}$, $\mathbf{S}$, and $\mathbf{F}(t)$ are matrices. In particular, the vectors $\mathbf{w}$ and $\mathbf{F}$ are column matrices defined by

$$\mathbf{w} = \begin{bmatrix} w_1 \\ w_2 \\ \vdots \\ \cdot \\ w_n \end{bmatrix}; \qquad \mathbf{F} = \begin{bmatrix} F_1(t) \\ \vdots \\ \cdot \end{bmatrix}$$

In general w_i and F_i may be vectors, but here we confine the proof to the scalar case of planar rotation. The matrix $\mathbf{\Phi}$ is defined as follows (Chapter 10):

$$\mathbf{\Phi} = \begin{bmatrix} 0 & \Phi_{12} & 0 & 0 & \cdots & & 0 & 0 \\ \Phi_{21} & 0 & \Phi_{23} & 0 & \cdots & & 0 & 0 \\ 0 & \Phi_{32} & 0 & \Phi_{34} & \cdots & & 0 & 0 \\ \vdots & \vdots & \vdots & \vdots & & & \vdots & \vdots \\ 0 & 0 & 0 & 0 & \cdots & \Phi_{n-1n-2} & 0 & \Phi_{n-1n} \\ 0 & 0 & 0 & 0 & \cdots & 0 & \Phi_{nn-1} & 0 \end{bmatrix}$$

and $\mathbf{S}$ is null except for the (1, 1) element, which is γ, related to F_1 by the fluctuation-dissipation theorem:

$$\langle F_1(t) F_1(t_1) \rangle = 2\gamma \frac{kT}{I} \delta(t - t_1)$$

or

$$\langle \mathbf{F}_1(t) \mathbf{F}_1^T(t_1) \rangle = \frac{2kT}{I} \mathbf{S} \delta(t - t_1) \qquad \text{for matrix } \mathbf{F}_1$$

The equivalence of Eqs. 2.13.1 and 2.12.1 may be demonstrated by mathematical induction. By this method the theorem (Eq. 2.13.1) is assumed to be true for $n-1$ (of $\mathbf{w}$ and $\mathbf{\Phi}$). It is then proved rigorously that

it must also be true for n. When $n = 1$, we may rewrite Eq. 2.12.1 as

$$\dot{w}_1(t) = -\int_0^t \beta_1(t-\tau) w_1(\tau)\, d\tau + f_1(t)$$

with

$$\tilde{\beta}_1(s) = \gamma$$

The symbol $\tilde{\beta}_n(s)$, $n = 1, 2, \ldots$ is used to denote the value of $\tilde{\phi}(s)$ obtained by replacing $\tilde{\beta}_n(s)$ with the constant value γ. In the $(n-1)$ case we assume that

$$\dot{w}_{n-1} = -\int_0^t \beta_{n-1}(t-\tau) w_{n-1}(\tau)\, d\tau + f_{n-1}(t) \tag{2.13.2}$$

We now have to show that such a property is true also in the nth case. If we assume that Eq. 2.13.1 holds for $n-1$, then it must follow that

$$\begin{aligned} \dot{w}_{n-1} &= -\int_0^t \beta_{n-1}(t-\tau) w_{n-1}(\tau)\, d\tau - \Phi_{n-1n} w_n + f_{n-1}(t) \\ \dot{w}_n &= -\Phi_{nn-1} w_{n-1} \end{aligned} \tag{2.13.3}$$

Taking the Laplace transform of Eq. 2.13.3 and eliminating the variable $\tilde{w}_{n-1}(s)$,

$$-w_n(0) + \frac{(s - \Phi_{nn-1}\Phi_{n-1n})\tilde{w}_n(s)}{s + \tilde{\beta}_{n-1}(s)} = \frac{-\Phi_{nn-1}}{s + \tilde{\beta}_{n-1}(s)} [w_{n-1}(0) + \tilde{f}_{n-1}(s)]$$

This is the Laplace transform of Eq. 2.13.2 with $n-1$ replaced by n, thus proving the theorem 2.13.1, provided that

$$\tilde{\beta}_n(s) = -\frac{\Phi_{nn-1}\Phi_{n-1n}}{s + \tilde{\beta}_{n-1}(s)}$$

and

$$\tilde{f}_n(s) = -\frac{\Phi_{nn-1}}{s + \tilde{\beta}_{n-1}(s)} [w_{n-1}(0) + \tilde{f}_{n-1}(s)]$$

Therefore, the expression of β in terms of continued fractions is equivalent to regarding the non-Markovian process as a "contraction" of a Markov process with higher dimensionality. The variables $w_1, w_2, \ldots, w_{n-1}$ can be regarded as a "reduced" thermal bath for our variables of interest, w_n, the last in the chain. *Therefore any order of approximant may be interpreted in terms of a physical model.* The replacement of the Mori equation (Equation 1.7.1.4) by a matrix equation such as Eq. 2.13.1 is also possible, and this is a powerful aid to interpretation.

2.13.1 Physical Models

1. The first approximant of Eq. 2.12.1 corresponds to Eq. 2.13.1 in the form ($n = 1$):

$$\dot{w}_1(t) = -\Phi_{12} w_2(t) - \gamma w_1(t) + F_1(t) \tag{2.13.1.1}$$

$$\dot{w}_2(t) = 0$$

This is the Langevin equation for rotational Brownian movement of a dipole in a plane,

$$w_1 \equiv \dot{\theta}, \qquad F_1 \equiv \Gamma$$

and

$$\ddot{\theta}(t) = -\gamma\dot{\theta}(t) + \Gamma(t)$$

2. When $n = 2$, we have

$$\begin{aligned} \dot{w}_1(t) &= -\Phi_{12}w_2(t) - \gamma w_1(t) + F_1(t) \\ \dot{w}_2(t) &= -\Phi_{21}w_1(t) - \Phi_{23}w_2(t) \\ \dot{w}_3(t) &= 0 \end{aligned} \tag{2.13.1.2}$$

This describes the rotational Brownian movement of a dipole in a plane under the influence of a restoring torque proportional to the angular displacement of the dipole from a fixed direction, that is,

$$\ddot{\theta}(t) = -\gamma\dot{\theta}(t) - \gamma_0\theta(t) + \Gamma(t)$$

where γ_0 is the torque constant. Figure 2.13.1.1 illustrates some orientational a.c.f.'s of a three-dimensional model (J-diffusion) which behaves very similarly to this two-dimensional system. This is recovered from Eqs. 2.13.2 provided that the following identities are made.

$$w_1 \equiv \dot{\theta}; \qquad w_2 \equiv \theta; \qquad -\Phi_{21}\Phi_{12} \equiv \gamma_0$$

3. With $n = 3$ we recover the model known as the planar itinerant oscillator or librator:

$$\begin{aligned} \dot{w}_1(t) &= -\Phi_{12}w_2(t) - \gamma w_1(t) + F_1(t) \\ \dot{w}_2(t) &= -\Phi_{21}w_1(t) - \Phi_{23}w_3(t) \\ \dot{w}_3(t) &= -\Phi_{32}w_2(t) - \Phi_{34}w_4(t) \\ \dot{w}_4(t) &= 0 \end{aligned} \tag{2.13.1.3}$$

This may be linked with the set of Eq. 2.12.15 by making the following identities:

$$\begin{aligned} \frac{\gamma_0}{I_1} &\equiv -\Phi_{32}\Phi_{23} \\ w_3 &\equiv \dot{\theta} \\ w_2 &\equiv \gamma_0(\theta_1 - \theta_2) \\ w_1 &\equiv \frac{\Phi_{32}\Phi_{23}\dot{\theta}_2}{\Phi_{21}\Phi_{12}} \end{aligned}$$

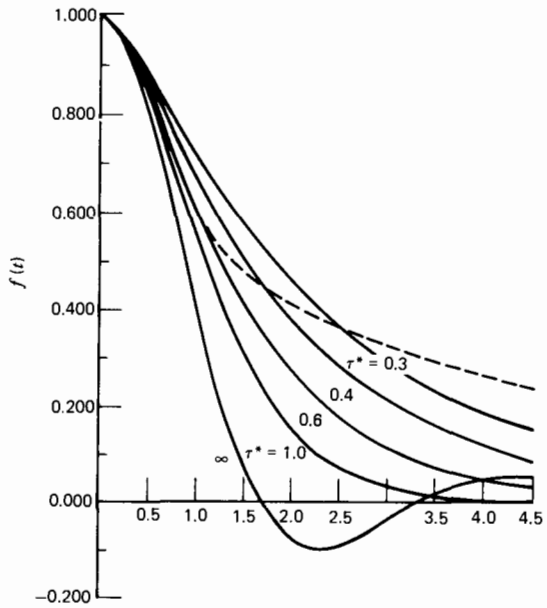

Figure 2.13.1.1 Solid lines, $\langle \mathbf{u}(t) \cdot \mathbf{u}(0) \rangle$, calculated for liquid CHF_3 at 298°K from McClung's J-diffusion model for symmetrical tops. From the top: $\tau^* = 0.3$ psec, 0.4 psec, 0.6 psec, and 1.0 psec and the free rotor, where $\tau^* = \tau(kT/I_x)^{1/2}$, τ being the mean time between collisions and I_x the moment of inertia about an axis perpendicular to that of the permanent molecular dipole. Dashed line, experimental result computed from the far infrared band in the liquid at 298°K. Computed assuming a Debye behavior at low frequencies with a critical relaxation time of 2.9 psec. [Reproduced by permission from M. W. Evans, *J. Chem. Soc. Faraday Trans. II* **71**, 843 (1975).]

Taking cognizance of the fact that this model is also represented in Eqs. 2.12.8, we may further identify

$$\begin{aligned} \phi_0(0) &\equiv \frac{\gamma_0}{I_1} \\ \phi_1(0) &\equiv -\Phi_{21}\Phi_{12} \end{aligned}$$

2.14 EXTENDED DIFFUSION OR COLLISION INTERRUPTED ROTATION

Imagine the assumption leading to Eq. 2.12.8 modified to

$$\phi_0(t) = \phi_{FR}(t)e^{-|t|/\tau} \tag{2.14.1}$$

where $\phi_{FR}(t)$ is a memory function defined by

$$\frac{d}{dt}\langle \mathbf{u}(0) \cdot \mathbf{u}(t) \rangle_{FR} = \dot{\mathcal{R}}_{FR}(t) = -\int_0^t \phi_{FR}(t-\tau)\mathcal{R}_{FR}(\tau)\, d\tau \tag{2.14.2}$$

Here $\mathcal{R}_{FR}(t)$ is the a.c.f. describing the "free rotation" of an ensemble of *linear* molecules. We are assuming physically that the reorientation of the angular momentum is *instantaneous* and *randomized* at each collision according to a Poisson distribution:

$$f_n(t) = \frac{(\omega_0 t)^n}{n!} e^{-\omega_0 t}$$

where ω_0 is the collision frequency ($= 1/\tau$, where τ is the *average* time between collisions).

The memory function $\phi_0(t)$ is related to the correlation function $\mathcal{R}(t)$ of the *collision interrupted* free rotation by the usual integro-differential relation, namely,

$$\langle \mathbf{u}(0) \cdot \mathbf{u}(t) \rangle = \mathcal{R}(t) = \int_0^t \phi_0(t-\tau)\mathcal{R}(\tau)\, d\tau$$

so that

$$\tilde{\mathcal{R}}(s) = \frac{1}{s + \tilde{\phi}_0(s)}$$

since $\mathcal{R}(0) = 1$, by definition, whence with Eq. 2.14.1 and the shifting property of Laplace transforms,

$$\begin{aligned}\tilde{\mathcal{R}}(s) &= \left[s + \tilde{\phi}_{FR}\left(s + \frac{1}{\tau}\right)\right]^{-1} \\ &= \frac{\tilde{\mathcal{R}}_{FR}(s + 1/\tau)}{1 - \tau^{-1}\tilde{\mathcal{R}}_{FR}(s + 1/\tau)} \\ &= \sum_{n=0}^{\infty} \frac{1}{\tau^n} \tilde{\mathcal{R}}_{FR}^{(n+1)}(s + 1/\tau) \qquad (2.14.3)\end{aligned}$$

using Taylor's theorem. Inverting Eq. 2.14.3 term by term gives

$$\begin{aligned}\mathcal{R}(t) &= \langle \mathbf{u}(t) \cdot \mathbf{u}(0) \rangle \\ &= e^{-t/\tau}\left[\mathcal{R}_{FR}(t) + \frac{1}{\tau}\int_0^t \mathcal{R}_{FR}(t - t_1)\mathcal{R}_{FR}(t_1)\, dt_1 \right. \\ &\quad \frac{1}{\tau^2}\int_0^t \mathcal{R}_{FR}(t - t_1)\, dt_1 \int_0^{t_1} \mathcal{R}_{FR}(t_1 - t_2)\mathcal{R}_{FR}(t_2)\, dt_2 + \cdots \\ &\quad + \frac{1}{\tau^n}\int_0^t \mathcal{R}_{FR}(t - t_1)\, dt_1 \int_0^{t_1} \mathcal{R}_{FR}(t_1 - t_2)\, dt_2 \cdots \\ &\quad \left. \cdots \int_0^{t_{n-1}} \mathcal{R}_{FR}(t_{n-1} - t_n)\mathcal{R}_{FR}(t_n)\, dt_n \right. \qquad (2.14.4)\end{aligned}$$

It has been shown in many articles (e.g., Berne and Pecora, 1976) that this is the orientational a.c.f. of the *Gordon J-diffusion model* for *linear* molecules. This is a Mori approximant of the form 2.14.1. The model assumptions are as follows:

1. A molecule undergoes *free rotational motion* until it is interrupted by a hard-core (i.e., adiabatic) collision of zero duration.
2. Each collision randomizes onto a Poisson distribution the angular momentum in both magnitude and direction.
3. Successive collisions are uncorrelated; that is, the instants at which the collisions occur form a purely random process, and the angular momentum changes are uncorrelated.
4. Collisions change the molecule's rotational velocity but do not change its orientation.

The mean square torque in this model is therefore not defined, and its limitations are clearly revealed in the far infrared. However, its shortcomings are revealed precisely in a computer simulation, which indicates that successive collisions are correlated. The memory function governing this correlation may also be simulated exactly (e.g., Singer et al., 1977).

2.15 FREE ROTATION (by Mauro Ferrario)

Equation 2.9.1 may now be solved exactly for each particle

$$\frac{d\mathbf{u}^{(i)}}{dt} = \boldsymbol{\omega}^{(i)} \times \mathbf{u}^{(i)} \qquad (i = 1, \ldots, N) \qquad (2.15.1)$$

or in matrix notation,

$$\frac{d\mathbf{u}^{(i)}}{dt} = \mathbf{A}^{(i)}\mathbf{u}^{(i)} \qquad (2.15.2)$$

where N is the total number of molecules of the liquid. The solution of Eq. 2.15.2 for each molecule i is

$$\mathbf{u}^{(i)}(t) = \exp(\mathbf{A}^{(i)}t)\mathbf{u}^{(i)}(0) \qquad (2.15.3)$$

The correlation function of interest is

$$\begin{aligned}\langle P_1(\cos\theta) \rangle &= \sum_{i=1}^{N} \mathbf{u}^{(i)}(0) \cdot \mathbf{u}^{(i)}(t) \\ &= \frac{1}{N}\sum_{i=1}^{N} (\mathbf{u}^{(i)}(0))^T \exp(\mathbf{A}^{(i)}t)\mathbf{u}^{(i)}(0) \qquad (2.15.4)\end{aligned}$$

We may explicitly calculate the matrix exponential by finding its eigenvalues; that is, we transform it to a coordinate set where the matrix $\mathbf{A}^{(i)}$ is diagonal. The characteristic equation of $\mathbf{A}$ is

$$\lambda^3 + \lambda(\omega_1^2 + \omega_2^2 + \omega_3^2) = 0 \qquad (2.15.5)$$

whose roots are

$$\lambda_1^{(i)} = 0$$
$$\lambda_2^{(i)} = i\sqrt{\omega_1^{(i)2} + \omega_2^{(i)2} + \omega_3^{(i)2}} = i\omega^{(i)} \tag{2.15.6}$$
$$\lambda_3^{(i)} = -i\sqrt{\omega_1^{(i)2} + \omega_2^{(i)2} + \omega_3^{(i)2}} = -i\omega^{(i)}$$

where

$$\omega^{(i)2} = \boldsymbol{\omega}^{(i)} \cdot \boldsymbol{\omega}^{(i)}$$

Let $\tilde{\mathbf{A}}^{(i)}$ be the diagonal matrix whose nonzero elements are the eigenvalues $\lambda_1, \lambda_2, \lambda_3$. This matrix is related to the matrix $\mathbf{A}^{(i)}$ by the transformation

$$\mathbf{C}^{(i)T}\mathbf{A}^{(i)}\mathbf{C}^{(i)} = \tilde{\mathbf{A}}^{(i)} \tag{2.15.7}$$

where $\mathbf{C}^{(i)}$ is the orthogonal matrix which defines the transformation. The transformed vectors $\tilde{\mathbf{u}}^{(i)}(t)$ are given by

$$\tilde{\mathbf{u}}^{(i)}(t) = \mathbf{C}\mathbf{u}^{(i)}(t) \tag{2.15.8}$$

We use Eq. 2.15.7 in Eq. 2.15.3 to get

$$\langle P_l[\cos\theta(t)]\rangle = \sum_{i=1}^{N} [\mathbf{u}^{(i)}(0)]^T[\mathbf{C}^{(i)}\mathbf{C}^{(i)T}\exp(\mathbf{A}^{(i)}t)\mathbf{C}^{(i)}\mathbf{C}^{(i)T}\mathbf{u}^{(i)}(0)]$$
$$= \frac{1}{N}\sum_{i=1}^{N}[(\tilde{\mathbf{u}}^{(i)}(0))^T\exp(\tilde{\mathbf{A}}^{(i)}t)\tilde{\mathbf{u}}^{(i)}(0)] \tag{2.15.9}$$

The advantage of Eq. 2.15.9 is that now we know the elements of the matrix exponential defined by

$$\exp(\tilde{\mathbf{A}}^{(i)}t) = \begin{pmatrix} \exp(\lambda_1^{(i)}t) & 0 & 0 \\ 0 & \exp(\lambda_2^{(i)}t) & 0 \\ 0 & 0 & \exp(\lambda_3^{(i)}t) \end{pmatrix} \tag{2.15.10}$$

We now replace the summation in Eq. 2.15.9 above by an integral over the probability density. Two types of averaging are implied; the first over the initial orientations of the dipoles $\mathbf{u}^{(i)}(0)$ and the second over the angular velocity probability distribution $P(\omega)$, which we assume to be of the Maxwell–Boltzmann type; that is,

$$P(\omega) = Z\exp\left[-\frac{1}{2kT}(A\omega_1^2 + B\omega_2^2 + C\omega_3^2)\right] \tag{2.15.11}$$

where Z is the normalization constant and A, B, C are the principal moments of inertia of the body; then

$$\frac{1}{Z} = \int_{-\infty}^{\infty}\int\int d^3\omega P(\omega) \tag{2.15.12}$$

We now have

$$\langle P_l[\cos\theta(t)]\rangle = \int d^3\omega P(\omega)\langle\tilde{\mathbf{u}}(0)^T\exp(\tilde{\mathbf{A}}t)\tilde{\mathbf{u}}(0)\rangle_{\mathrm{Av}}^0 \tag{2.15.13}$$

The brackets $\langle\ \rangle_{\mathrm{Av}}^0$ mean an average over the initial conditions. For isotropic fluids we can assume without loss of generality that the equilibrium orientations of the single molecule are isotropically distributed so that for any orientation of the equilibrium frame

$$\langle\tilde{u}_k(0)\tilde{u}_k(0)\rangle_{\mathrm{Av}}^0 = \tfrac{1}{3} \tag{2.15.14}$$

with

$$\tilde{\mathbf{u}}^{(i)}(0)\cdot\tilde{\mathbf{u}}^{(i)}(0) = 1$$

That is, the length of the dipole is fixed. With these considerations Eq. 2.15.13 reduces to

$$\langle P_l[\cos\theta(t)]\rangle = \frac{1}{3}\int d^3\omega P(\omega)\,\mathrm{Tr}(e^{\tilde{\mathbf{A}}t})$$
$$= \frac{1}{3}\int d^3\boldsymbol{\omega}P(\boldsymbol{\omega})(1 + e^{i\omega t} + e^{-i\omega t}) \tag{2.15.15}$$

The integral in Eq. 2.15.15 is very easy to compute. For the case of the spherical top we have (as in section 2.9)

$$\langle P_l[\cos\theta(t)]\rangle = \frac{1}{3}\int_{-\infty}^{\infty} d\omega\left\{\omega^2 Z\exp\left(-\frac{I\omega^2}{2kT}\right)[1 + e^{i\omega t} + e^{-i\omega t}]\right\}$$
$$= \frac{1}{3} + \frac{2}{3}\left(1 - \frac{kT}{I}t^2\right)\exp\left(-\frac{kT}{2I}t^2\right) \tag{2.15.16}$$

where we have used the facts that

$$\int_{-\infty}^{\infty} d\omega\left[\omega^2 Z\exp\left(-\frac{I\omega^2}{2kT}\right)e^{i\omega t}\right] = -\frac{d^2}{dt^2}\mathscr{L}^{-1}Z\exp\left(-\frac{I\omega^2}{2kT}\right) \tag{2.15.17}$$

and that the inverse Fourier transform of the Gaussian form in Eq. 2.15.17 is

$$\mathscr{L}^{-1}\left[Z\exp\left(-\frac{I\omega^2}{2kT}\right)\right] = \exp\left(-\frac{kT}{2I}t^2\right)$$

APPENDIX. The Euler Angles
by Mauro Ferrario

The most common and useful set of parameters which are employed to describe the orientation of a rigid body, such as a molecule is assumed to be, are the Eulerian angles. The orientation of a rigid body with respect to a fixed laboratory frame S is described by the direction of the axis of a

coordinate frame S^1 attached to the rigid body with the origin in its center of mass.

We can superimpose these two coordinate frames first with a translation of the frame S^1 in such a way that the center of mass of the body coincides with the origin of the laboratory frame S. This coordinate transformation affects only the position of the body and it allows us to deal with the orientation in a straightforward manner.

Now the two frames can be superimposed by means of three successive counterclockwise rotations (see Fig. 2.A.1). The first one is a rotation through an angle φ around the Z' axis. We call ξ, η, ζ the new axis and perform the second rotation around the η axis through an angle θ.

Let ξ', η', ζ' be the new axis; a rotation around ζ' of the angle ψ completes the transformation.

The orientation of the rigid body is determined by the three angular coordinates φ, θ, ψ, which are called the Eulerian angles. This definition is not unique, however; sometimes in the literature the second rotation is performed around the ξ instead of the η axis, in such a way as to define three different angles.

The generator of infinitesimal rotation is the angular momentum. This means that if we are rotating an infinitesimal angle $d\alpha$ around the axis denoted by the vector $\mathbf{n}$, the relative change $d\mathbf{F}$ of the function of the coordinate F is in general given by

$$d\mathbf{F} = d\alpha[\mathbf{F}, \mathbf{L}\cdot\mathbf{n}] = d\alpha\hat{\mathbf{L}}\cdot\mathbf{n}\mathbf{F} \tag{2.A.1}$$

where [,] means the Poisson brackets. In particular it can be noted that if F is a scalar function its change in a rotation is null; that is,

$$[\mathbf{F}, \mathbf{L}\cdot\mathbf{n}] = 0 \tag{2.A.2}$$

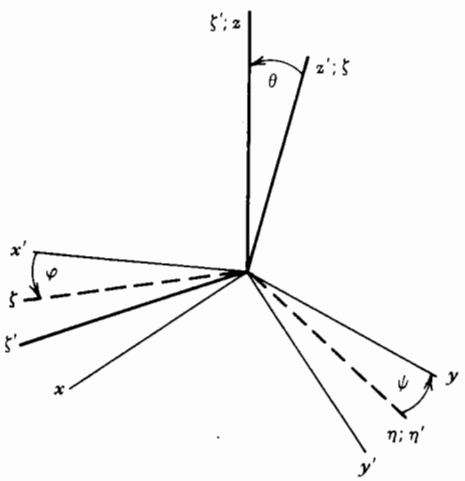

Figure 2.A.1 The Eulerian angles.

and if a vector function $\mathbf{G}$ is taken, then its change is

$$d\mathbf{G} = d\alpha\,\mathbf{n}\times\mathbf{G} \tag{2.A.3}$$

from which it follows that

$$[\mathbf{G}, \mathbf{L}\cdot\mathbf{n}] = \mathbf{n}\times\mathbf{G} \tag{2.A.4}$$

From Eq. 2.A.4 the general relations of commutation for the angular momentum can be simply extracted by taking $\mathbf{L}$ itself as a vector function and $\mathbf{L}^2$ as a scalar function.

$$[\mathbf{L}^2, \mathbf{n}\cdot\mathbf{L}] = 0 \tag{2.A.5}$$

$$[\mathbf{L}, \mathbf{L}\cdot\mathbf{n}] = \mathbf{n}\times\mathbf{L} \tag{2.A.6}$$

which can be written as the tensorial expression

$$[L_i, L_j] = \epsilon_{ijk}L_k \tag{2.A.7}$$

The properties of the operator $\mathbf{L}$ in Eq. 2.A.1 can be easily exploited for a single point particle. In this case $F = F(\mathbf{r})$ and $L = \mathbf{r}\times\mathbf{p}$ so that

$$\begin{aligned}[\mathbf{F}, \mathbf{L}] &= \sum_i \frac{\partial\mathbf{F}}{\partial r_i}\frac{\partial\mathbf{L}}{\partial p_i} - \frac{\partial\mathbf{F}}{\partial p_i}\frac{\partial\mathbf{L}}{\partial r_i} \\ &= \left(\mathbf{r}\times\frac{\partial}{\partial\mathbf{r}}\right)\mathbf{F}\end{aligned} \tag{2.A.8}$$

The formal solution to Eq. 2.A.1 can be given as follows. From

$$\frac{d}{d\alpha}\mathbf{F}(\mathbf{r}, \alpha) = \hat{\mathbf{L}}\cdot\mathbf{n}\mathbf{F}(\mathbf{r}, \alpha) \tag{2.A.9}$$

we get

$$\mathbf{F}(\mathbf{r}, \alpha) = \exp(\hat{\mathbf{L}}\cdot\mathbf{n}\alpha)\mathbf{F}(\mathbf{r}, 0) \tag{2.A.10}$$

The three rotations defining the Eulerian angles are embodied in the operator $R(\varphi, \theta, \psi)$

$$\begin{aligned}R(\varphi, \theta, \psi) &= \exp(\hat{L}_\zeta, \psi)\exp(\hat{L}_\eta\theta)\exp(\hat{L}_{Z'}\varphi) \\ &= \exp(\hat{L}_{Z'}\varphi)\exp(\hat{L}_{Y'}\theta)\exp(\hat{L}_{Z'}\psi) \\ &= \exp(-\hat{L}_Z\varphi)\exp(-\hat{L}_Y\theta)\exp(-\hat{L}_Z\psi)\end{aligned} \tag{2.A.11}$$

The second equality can be justified on the basis that, as the axis η is defined from the axis y' by means of the rotation around the axis z', we have from the transformation properties of operators

$$e^{\hat{L}_\eta\theta} = e^{\hat{L}_{Z'}\varphi}e^{\hat{L}_{Y'}\theta}e^{-\hat{L}_{Z'}\varphi} \tag{2.A.12}$$

The last step is to express the result in the laboratory frame coordinates using the basic idea of inversion of transformations which is achieved by just changing the sign of rotation angles.

It is worth remembering that the operators $\hat{L}_i$ may be expressed as

Poisson brackets if and only if they are acting on a function of the coordinates alone.

Let us now introduce the spherical harmonics Y^l_m as that set of functions which are the eigenfunctions of both operators $\hat{\mathbf{L}}^2$, $\hat{L}_Z$ for a point particle. In fact

$$\hat{\mathbf{L}}^2 Y^l_m(\alpha, \beta) = l(l+1) Y^l_m(\alpha, \beta)$$

$$\hat{L}_Z Y^l_m(\alpha, \beta) = im Y^l_m(\alpha, \beta) \qquad \begin{pmatrix} l = 0, 1, 2, \dots \\ m = -l, -l+1, \dots, 0, 1, \dots, l \end{pmatrix} \tag{2.A.13}$$

These functions are suitable for the description of the orientational motion of a tensor, as the direction of a permanent dipole is, because it is completely defined by the pair of angles α, β (see Fig. 2.A.2).

We are interested in the transformation properties of such functions under rotations of the coordinate frame defined by the Eulerian angles (φ, θ, ψ).

Because the spherical harmonics are a complete set in the $\{\alpha, \beta\}$ space, we can write

$$R(\varphi, \theta, \psi) Y^l_m(\alpha, \beta) = \sum_{m'} \mathcal{D}^l_{m'm}(\varphi, \theta, \psi) Y^l_{m'}(\alpha, \beta) \tag{2.A.14}$$

The function $\mathcal{D}^l_{m'm}$ are the so-called Wigner matrices. In Eq. 2.A.14 the sum over different indices l is not needed because the rotation operator itself, $R(\varphi, \theta, \psi)$ commutes with the operator $\hat{\mathbf{L}}^2$, which means that the rotated functions are still eigenfunctions of $\hat{\mathbf{L}}^2$ with the same eigenvalue $l(l+1)$.

$$\hat{\mathbf{L}}^2 R(\varphi, \theta, \psi) Y^l_m(\alpha, \beta) = R(\varphi, \theta, \psi) \hat{\mathbf{L}}^2 Y^l_m(\alpha, \beta) = l(l+1) R(\varphi, \theta, \psi) Y^l_m(\alpha, \beta). \tag{2.A.15}$$

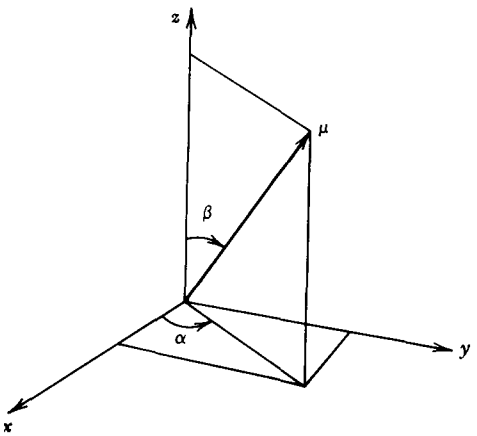

Figure 2.A.2 Angles α and β specifying the orientation of a dipole.

The spherical harmonics are an orthonormal set, and the following relation holds:

$$\int_0^{2\pi} d\alpha \int_{-1}^{1} d(\cos\beta) Y^{l*}_m(\alpha, \beta) Y^{l'}_{m'}(\alpha, \beta) = \delta_{ll'} \delta_{mm'} \tag{2.A.16}$$

where the asterisk means complex conjugation.

To get an expression for the $\mathcal{D}^l_{m'm}(\varphi, \theta, \psi)$ we now use Eq. 2.A.16. Multiplying by $Y^{l*}_m(\alpha, \beta)$ (Eq. 2.A.14) and integrating on the solid angle $d\Omega = d\alpha\, d\cos\beta$, we get

$$\mathcal{D}^l_{m'm}(\varphi, \theta, \psi) = \int d\Omega Y^{l*}_{m'}(\alpha, \beta) R(\varphi, \theta, \psi) Y^l_m(\alpha, \beta) \tag{2.A.17}$$

where the expression of the operator $R(\varphi, \theta, \psi)$ is given in Eq. 2.16.11.

By using the properties given in Eq. 2.A.13,

$$\mathcal{D}^l_{m'm}(\varphi, \theta, \psi) = e^{-im'\varphi} d^l_{m'm}(\theta) e^{-im\psi} \tag{2.A.18}$$

Wigner gave the following expression for the functions $d^l_{m'm}(\theta)$:

$$\begin{aligned} d^l_{m'm}(\theta) = {} & [(l+m')!(l-m)!(l+m')!(l-m)!]^{1/2} \\ & \times \sum_n (-1)^n \frac{1}{(l-m-n)!(l+m'-n)!(n+m-m')!n!} \\ & \times \left(\cos\frac{\theta}{2}\right)^{2l+m'-m-2n} \left(\sin\frac{\theta}{2}\right)^{m-m'+2n} \end{aligned} \tag{2.A.19}$$

The sum is over the values of the integer n for which the factorial arguments involving n are not negative. For example, the first reduced matrix $d^1(\theta)$ is given by

$$d^1(\theta) = \begin{pmatrix} \frac{1+\cos\theta}{2} & -\frac{1}{\sqrt{2}}\sin\theta & \frac{1-\cos\theta}{2} \\ \frac{1}{\sqrt{2}}\sin\theta & \cos\theta & -\frac{1}{\sqrt{2}}\sin\theta \\ \frac{1-\cos\theta}{2} & \frac{1}{\sqrt{2}}\sin\theta & \frac{1+\cos\theta}{2} \end{pmatrix} \tag{2.A.20}$$

The Wigner matrices are an orthogonal set of functions in the space of the three angles (φ, θ, ψ). The normalization is given by

$$\int_0^{2\pi} d\varphi \int_0^{2\pi} d\psi \int_{-1}^{1} d\cos\theta\, \mathcal{D}^{l*}_{m'm}(\varphi, \theta, \psi) \mathcal{D}^j_{n'n}(\varphi, \theta, \psi) = \frac{8\pi^2}{2l+1} \delta_{lj} \delta_{m'n'} \delta_{mn} \tag{2.A.21}$$

A useful property is the rule which involves the Clebsch–Gordan coefficients, and it is well-known as the Clebsch–Gordan series:

$$\mathcal{D}^{j_1}_{m_1 n_1} \mathcal{D}^{j_2}_{m_2 n_2} = \sum_j C(j_1, j_1, j; n_1, n_2) C(j_1, j_2, j; m_1, m_2) \mathcal{D}^j_{m_1+m_2, n_1+n_2} \tag{2.A.22}$$

The sum is over the values of j between the absolute value of the difference $|j_1 - j_2|$ and the sum $j_1 + j_2$. Sometimes the inverse relation

$$\mathscr{D}^j_{mn} = \sum_{m_1 n_1} C(j_1, j_2, j; m, m - m_1) C(j_1, j_2, j; n_1, n - n_1) \mathscr{D}^{j_1}_{m_1 n_1} \mathscr{D}^{j_2}_{m-m_1, n-n_1} \tag{2.A.23}$$

is also useful. Using the relation between spherical harmonics and the Wigner matrices, which is

$$\mathscr{D}^l_{m0}(\varphi, \theta, 0) = \left(\frac{4\pi}{2l+1}\right)^{1/2} Y^l_m(\varphi, \theta) \tag{2.A.24}$$

it is possible to obtain a similar sum rule for the former:

$$Y^{l_1}_{m_1} Y^{l_2}_{m_2} = \sum_j \left[\frac{(2l_1+1)(2l_2+1)}{4\pi(2j+1)}\right]^{1/2} \times C(l_1, l_2, j; m_1, m_2) C(l_1, l_2, j; 0, 0) Y^j_{m_1+m_2} \tag{2.A.25}$$

The Clebsch–Gordan coefficients arise in quantum mechanics from the coupling of two angular momenta and they satisfy the relation

$$Y^l_m = \sum_{m_1} C(l, l_1, l_2; m_1, m - m_1) Y^{l_1}_{m_1} Y^{l_2}_{m-m_1} \tag{2.A.26}$$

The general expression for them is very complicated indeed and we give it here, only for the sake of completeness, in the form used by Wigner:

$$C(l_1, l_2, l_3; m_1, m_2) = C(l_1, l_2, l_3; m_1, m_2, m_3)$$
$$= \delta_{m_3, m_1+m_2} \left[(2l_3+1) \frac{(l_3+l_1-l_2)!(l_3-l_1+l_2)!(l_1+l_2-l_3)!(l_3+m_3)!(l_3-m_3)!}{(l_1+l_2+l_3+1)!(l_1-m_1)!(l_1+m_1)!(l_2-m_2)!(l_2+m_2)!}\right]^{1/2}$$
$$\times \sum_n \frac{(-1)^{n+l_2+m_2}}{n!} \frac{(l_2+l_3+m_1-n)!(l_1-m_1+n)!}{(l_3-l_1+l_2-n)!(l_3+m_3-n)!(n+l_1-l_2-m_3)!} \tag{2.A.27}$$

The sum is over the integer n such that none of the factorial arguments involving n are negative (see Chapter 11).

REFERENCES

Bateman, H., *Differential Equations*, Chelsea, New York (1956).

Beevers, M. S., Crossley, J., Garrington, D. C., and Williams, G., *J. Chem. Soc. Faraday Trans. II* 72, 1482 (1976).

Benoit, H., *Ann. Phys.* 6, 561 (1951).

Berne, B. J. and Pecora, R., *Dynamic Light Scattering with Applications to Chemistry, Biology and Physics*, Wiley-Interscience, New York (1976).

Blomberg, C., *Physica* 86A, 49 (1977).

Brinkman, H. C., Physica 22, 29 (1956).

Budó, A., *J. Chem. Phys.* 17, 686 (1949).

Coffey, W. T., *Chem. Phys. Lett.* 54, 519 (1978).

Coffey, W. T., *Mol. Phys.* 37, 437 (1979).

Coffey, W. T. and Evans, M. W., *Mol. Phys.* 35, 975 (1978).

Coffey, W. T. and Paranjape, B. V., *Proc. R. Ir. Acad.*, 78A, 17 (1978).

Coffey, W. T., in proceedings of NASECODE II Conference, Trinity College, Dublin, ed. J. J. H. Miller and B. Browne, Boole Press, Dublin (1981).

Davies, R. O., *Physica* 23, 1067 (1957).

Debye, P., *Polar Molecules*, Chemical Catalog Co., New York (1929).

Debye, P., *Phys. Z.* 35, 101 (1934).

Dieterich, W., Peschel, I., and Schneider, W., *Z. Phys. B.* 27, 177 (1977).

Dmitriev, V. A. and Gurevich, C. B., *Zh. Eksp. Teor. Fiz.* 16, 937 (1946).

Evans, G. T., *J. Chem. Phys.* 65, 3030 (1976).

Evans, M. W., *Chem. Phys. Lett.* 39, 601 (1976).

Favro, L. D., *Phys. Rev.* 53, 119 (1960).

Ford, G. W., Lewis, J. T., and McConnell, J. R., *Phys. Rev. A* 19, 907 (1979).

Furry, W. H., *Phys. Rev.* 107, 7 (1957).

Goldstein, H., *Classical Mechanics*, Addison Wesley, Reading, Mass. (1950).

Gross, E. P., *J. Chem. Phys.* 23, 1415 (1955).

Hellemans, L. and de Maeyer, B., *J. Chem. Phys.* 63, 3490 (1975).

Hemmer, P. C., *Physica* 27, 79 (1961).

Hubbard, P. S., *Phys. Rev.* A6, 2421 (1972).

Hubbard, P. S., *Phys. Rev.* A15, 329 (1977).

Hobson, E. W., *Spherical and Ellipsoidal Harmonics*, Cambridge University Press, Cambridge (1931); reprinted Chelsea, New York (1955).

Ince, E. L., *Ordinary Differential Equations*, Longmans Green, London (1927), reprinted Dover, New York.

Kielich, S., *Acta Phys. Pol.* 30, 393 (1966).

Kubo, R., *Statistical Mechanics of Equilibrium and Non-equilibrium*, North-Holland, Amsterdam (1965).

Kramers, H. A., *Physica* 7, 284 (1940).

Lewis, J. T., McConnell, J. R. and Scaife, B. K. P., *Proc. R. Ir. Acad.*, 76A, 43 (1976).

Macrobert, T. M., *Spherical Harmonics*, Pergamon (1967).

Margenau, H. and Murphy, G. M., *The Mathematics of Physics and Chemistry*, 2nd ed., Van Nostrand, Princeton, N.J. (1956).

McConnell, J., *Proc. R. Ir. Acad.* 78A, 87 (1978).

Milne, E. A., *Vectorial Mechanics*, Methuen, London (1948).

Mori, H., *Prog. Theor. Phys.* 33, 423 (1965).

Morita, A., Conference on Brownian Motion, School of Theoretical Physics, Dublin

Institute for Advanced Studies (1976); *J. Phys. D., Appl. Phys.* **11**, L9, L1 (1978).

Morita, A., *J. Phys. D, Appl. Phys.* **11**, 1357 (1978).

Morita, A., *J. Phys. A, Math. Gen.* **12**, 991 (1979).

Morita, A. and Watanabe, H., *J. Chem. Phys.*, **70**, 4708 (1979).

Mörsch, M., Risken, H., and Vollmer, H. D., *Z. Phys. B.*, **32**, 245 (1979).

Morse, M. and Feschbach, H., *Methods of Theoretical Physics*, McGraw-Hill, New York (1953).

Perrin, F., *J. Phys. Radium*, **5**, 497 (1934).

Perrin, J., *Compt. Rend.*, **146**, 967 (1908); **147**, 530 (1908).

Poley, J. P., *Appl. Sci. Res. B.* 336 (1955).

Powles, J. G., *Trans. Faraday Soc.* **44**, 802 (1948).

Risken, H. and Vollmer, H. D., *Z. Phys. B* **31**, 209 (1978).

Rocard, Y., *J. Phys. Radium* **4**, 247 (1933).

Routh, E. J., *Advanced Rigid Dynamics*, Vol. II, Macmillan, London (1892); reprinted Dover, New York.

Sack, R. A., *Physica* **22**, 917 (1956).

Sack, R. A., *Proc. Phys. Soc. London B* **70**, 402, 414 (1957).

Scaife, B. K. P., E.R.A. Report L/T392, Electrical Research Association, Leatherhead, Surrey (1959).

Scaife, B. K. P., *Complex Permittivity*, The English Universities Press, London (1971).

Singer, K., Taylor, A., and Singer, J. V. L., Mol. Phys. **33**, 1757 (1977).

Skinner, J. L. and Wolynes, P. G., *Physica* **96A**, 561 (1979).

Steele, W. A., *J. Chem. Phys.* **38**, 2411 (1963).

Stratonovitch, R. L., *Topics in the Theory of Random Noise*, Vol. 1, Gordon and Breach, New York (1963).

Titulaer, U. M., *Physica* **91A**, 123 (1978).

Van Hove, L., *Phys. Rev.* **95**, 249 (1954).

Vineyard, G. H., *Phys. Rev.* **110**, 999 (1958).

Wax, N., Ed., *Selected Papers on Noise and Stochastic Processes*, Dover, New York (1954).

Whittaker, Sir E. T., *Analytical Dynamics*, 2nd. ed., Cambridge University Press, Cambridge (1917).

Whittaker, Sir E. T. and Watson, G. N., *Modern Analysis*, 4th Edition, Cambridge University Press, Cambridge (1927).

Wilemski, G. J., *Stat. Phys.*, **14**, 153 (1976).

3

The Relation of Molecular Motions to Spectral Band Shapes: Electrical Interactions

LIST OF SYMBOLS

$a(t)$	The response function
α	Polarizability (scalar)
$\mathfrak{A}$	Power absorption coefficient
$b(t)$	Aftereffect function
β	$= 1/kT$
$\langle \cos \gamma \rangle$	Average of the cosine of the angle between neighboring dipoles
$\mathbf{e}$	Unit vector
e_i	The ith charge of Fröhlich's cavity
ϵ_s	Relative permittivity of a dielectric at zero frequency
ϵ_∞	Relative permittivity of a dielectric at frequencies at which the orientational mechanism of polarization has ceased to operate. The high frequency cutoff of the real axis of a semicircular Cole–Cole plot
$\mathbf{E}$	Uniform negative potential gradient
$\mathbf{f}$	Field acting on a molecule due to all sources except the molecule itself
$\mathbf{G}$	The cavity field
$L(a)$	Langevin's function
$\mathbf{u}$	Dipole moment vector
$\mathbf{m}$	Total resultant dipole moment of a molecule of a dielectric
$\mathbf{M}$	Total instantaneous dipole moment of a macroscopic spherical region of dielectric
$\mathfrak{M}$	Spectral density of fluctuations
N/V	The molecular number density
$P(\theta)$	Orientational probability
$\mathbf{P}$	Polarization vector
$\mathbf{r}_i$	Displacement of charge
$\mathbf{R}$	The homogenous reaction field of Onsager's spherical cavity
$\mathbf{u}$	Dipole unit vector
V	Potential energy
$\mathbf{X}$	Collective displacement of charge
χ_s	Susceptibility of a dielectric at zero frequency

Having determined the method by which the Liouville equation is to be approximated rationally, we have the problem of relating the calculated correlation functions to spectral data such as those which may be derived from spectroscopy in the 0–THz range of frequencies. There is a variety of experimental techniques used in covering this spectral range. It is essential to be familiar with these techniques and further to ascertain exactly what quantity is measured in a dielectrics experiment and *how* that quantity is being measured. The resolution of these problems is still far from clear, but much progress has been made in the last decade, with the aid of molecular dynamics simulations and the general improvements in far infrared spectroscopy (Appendix). This chapter is concerned with relating the complex susceptibility and dielectric permittivity to correlation functions of molecular quantities. The first step toward this is to consider the classical theory of dielectrics at zero frequency.

3.1 DEBYE'S THEORY

Debye (1912) (see Debye, 1929), following Langevin's (1905) treatment of paramagnetism, was the first investigator to give a relation between the susceptibility χ_s of a polar substance and the permanent dipole moment, μ, of a molecule of the substance. For completeness and in order to preserve continuity of the argument the derivation of Debye's equation is given here.

3.1.1 The Influence of an Imposed Potential Gradient on a Dipolar Molecule

We select from a macroscopic specimen of dielectric of relative permittivity ϵ_s [this specimen could, for example, be taken as a slab of dielectric between the plates of a capacitor (Fig. 3.1.1.1)], a spherical region which is just large enough to have the same physical properties as the macroscopic specimen. We now produce a constant negative potential gradient within the macroscopic specimen. This influences a dipolar molecule inside the spherical region in two ways:

1. It perturbs the rotational motion of the molecule and causes it to have a preferred orientation in the direction of the imposed potential gradient.
2. It *enlarges* the dipole moment of the molecule by elastic displacement of the constituent charges. This induced dipole moment is denoted by $\alpha\mathbf{f}$, where α is termed the polarizability of the molecule and $\mathbf{f}$ is the field acting on the molecule *due to all sources except the molecule itself.*

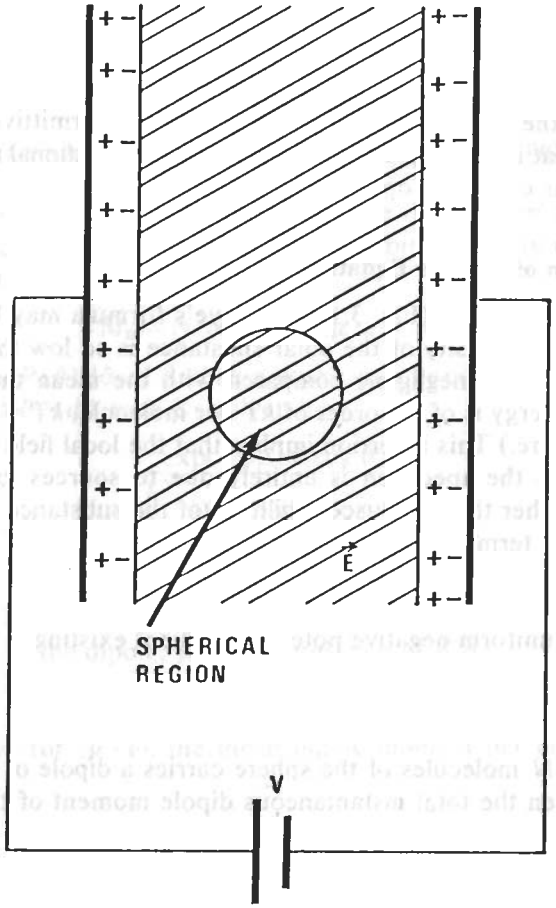

Figure 3.1.1.1 Spherical region in a dielectric sample.

3.1.2 The Lorenz–Lorentz Relation

The total dipole moment of a molecule of the substance may, in view of the preceding section, be written

$$\mathbf{m} = \boldsymbol{\mu} + \alpha\mathbf{f} \tag{3.1.2.1}$$

where $\boldsymbol{\mu}$ is the permanent moment of the molecule when isolated. We now suppose that the molecules are isotropic (i.e., the polarizability α of a molecule can then be described by a scalar quantity); then α is given by the Lorenz–Lorentz relation (Lorentz, 1909):

$$\alpha = \frac{3V}{4\pi N}\left(\frac{\epsilon_\infty - 1}{\epsilon_\infty + 2}\right) \tag{3.1.2.2}$$

$$\frac{4}{3}\pi a^3 = \frac{V}{N} \tag{3.1.2.3}$$

where $\frac{4}{3}\pi a^3$ is the mean volume per molecule, N is the number of molecules in the sphere, and ϵ_∞ is the relative permittivity at optical frequencies, that is, at frequencies at which the orientational mechanism of polarization has ceased to operate.

3.1.3 Derivation of Debye's Equation

With these preliminaries (Fig. 3.1.3.1) Debye's formula may be derived by assuming that the density of the polar substance is so low that the dipolar interaction energy is negligible compared with the mean thermal energy. (The thermal energy is of the order of kT per molecule, $kT = 4.2 \times 10^{-21}$ J at room temperature.) This assertion implies that the local field acting on any molecule within the specimen is entirely due to sources *external* to the sphere, and further that the susceptibility χ of the substance is small. Thus in mathematical terms

$$\mathbf{f} = \mathbf{E} \tag{3.1.3.1}$$

where $\mathbf{E}$ is the uniform negative potential gradient existing in the specimen, and

$$(\epsilon_s - 1) \ll 1 \tag{3.1.3.2}$$

If each of the N molecules of the sphere carries a dipole of instantaneous moment $\mathbf{m}_i$, then the total instantaneous dipole moment of the sphere, $\mathbf{M}$,

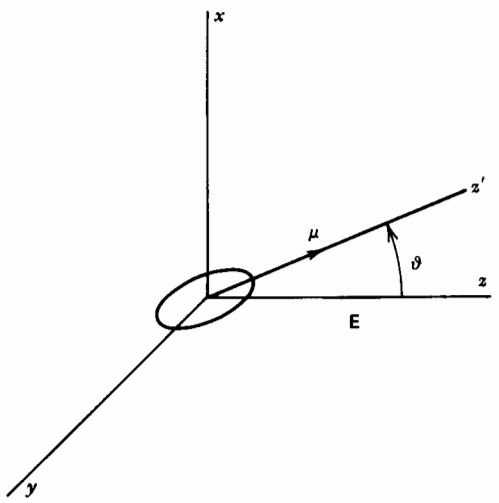

Figure 3.1.3.1 Notation for molecule with permanent moment μ in presence of E.

say, is

$$\mathbf{M} = \sum_{i=1}^{N} \mathbf{m}_i, \tag{3.1.3.3}$$

that is, $\mathbf{M}$ is the vector sum of the dipole moments of the molecules of the sphere.

The mean moment, M_E, of the sphere in the direction of $\mathbf{E}$ is (since on the average each molecule of the sphere contributes equally to the average dipole moment of the sphere)

$$M_E = N\langle \mathbf{m} \cdot \mathbf{e} \rangle = N\langle \boldsymbol{\mu} \cdot \mathbf{e} \rangle + \alpha E \tag{3.1.3.4}$$

The probability $P(\vartheta)\,d\vartheta$ of finding a dipole in a direction making an angle between ϑ and $\vartheta + d\vartheta$ with $\mathbf{E}$ is given by

$$\frac{\exp(-U\beta)d(\cos\vartheta)}{\int_{-1}^{+1} \exp(-U\beta)d(\cos\vartheta)} \tag{3.1.3.5}$$

where

$$\beta = (kT)^{-1}$$

The energy U of the dipole, $\boldsymbol{\mu}$, in the presence of $\mathbf{E}$ is

$$U = -\mu E \cos\vartheta \tag{3.1.3.6}$$

Hence we have for $\langle \boldsymbol{\mu} \cdot \mathbf{e} \rangle$, the mean dipole moment per molecule in the direction of $\mathbf{E}$,

$$\langle \boldsymbol{\mu} \cdot \mathbf{e} \rangle = \frac{\int_{-1}^{+1} \boldsymbol{\mu} \cdot \mathbf{e} \exp(\beta \boldsymbol{\mu} \cdot \mathbf{E})\, d(\cos\vartheta)}{\int_{-1}^{+1} \exp(\beta \boldsymbol{\mu} \cdot \mathbf{E})\, d(\cos\vartheta)} \tag{3.1.3.7}$$

Writing $\mu E\beta = a$ and evaluating the above integral, we obtain

$$\langle \boldsymbol{\mu} \cdot \mathbf{e} \rangle = \mu L(a) = \mu\left(\coth a - \frac{1}{a}\right) \tag{3.1.3.8}$$

The function $L(a)$ is termed Langevin's function (Fig. 3.1.3.2) (Langevin, 1905). $L(a)$ has the following Taylor series expansion (Abramowitz and Stegun, 1965):

$$L(a) = \frac{1}{3}a - \frac{1}{45}a^3 + \frac{2}{945}a^5 - \frac{2}{9450}a^7 + \cdots \tag{3.1.3.9}$$

This function may be approximated by its first term provided that $a < 0{\cdot}1$, that is, as long as

$$E < \frac{0{\cdot}1\,kT}{\mu} \tag{3.1.3.10}$$

At a room temperature of 300 K, this gives for a dipole of moment 1 debye,

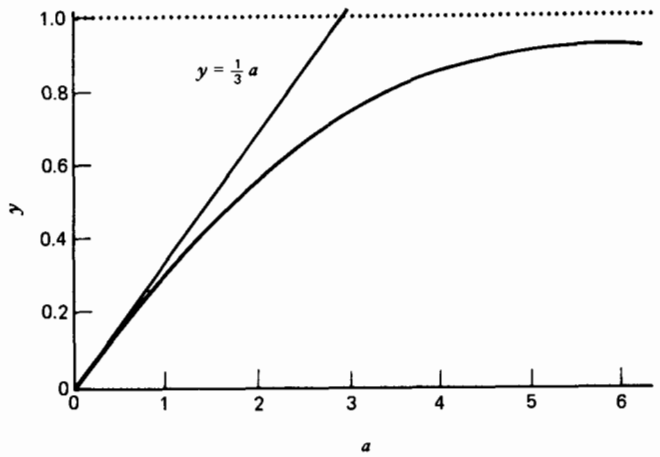

Figure 3.1.3.2 Langevin's function.

$E < 1.2 \times 10^8$ V/m. Usually in dielectric measurements, E is much smaller than 10^8 V/m and hence the approximation

$$L(a) = \frac{a}{3} \tag{3.1.3.11}$$

is quite adequate. We then obtain

$$N\langle \boldsymbol{\mu} \cdot \mathbf{e} \rangle = N\left(\frac{\mu^2 E}{3kT} + \alpha E\right) \tag{3.1.3.12}$$

This must be equal to the macroscopic dipole moment of the spherical region, which is

$$M_E = PV = \chi_s EV \tag{3.1.3.13}$$

and thus with Eq. 3.1.3.12

$$\chi_s = n\left(\frac{\mu^2}{3kT} + \alpha\right) \tag{3.1.3.14}$$

where $n = N/V$ is the molecular number density. Equation 3.1.3.14 is the Debye formula for the susceptibility, χ_s, of a polar substance.

If we write $\chi_\infty = n\alpha$ for the susceptibility of the substance at frequencies so high that the dipoles are unable to respond to the applied field, Eq. 3.1.3.10 may be written

$$(\chi_s - \chi_\infty) = \epsilon_0(\epsilon_s - \epsilon_\infty) = \frac{n\mu^2}{3kT} \tag{3.1.3.15}$$

or

$$(\epsilon_s - \epsilon_\infty) = \frac{N}{V\epsilon_0}\frac{\mu^2}{3kT} \tag{3.1.3.16}$$

which is the contribution to the susceptibility due to orientation of the dipoles.

3.1.4 Onsager's Theory of the Relative Permittivity of Dipolar Fluids

In view of the assumptions made in deriving it, the Debye formula holds only for polar gases at low densities and cannot be applied to liquids.

Onsager (1936) was the first worker to make a successful calculation of the permittivity of a polar liquid. It will be remembered that one of the consequences of the assumption that the interaction energy of the molecules could be neglected in comparison to the mean thermal energy was that the local field acting on a molecule was equal to the negative potential gradient imposed on the dielectric. Onsager modified the above assumption to take account of the effect of the *surroundings* of a molecule on the local field at a molecule. The model used by Onsager effectively takes into account one component of the molecular interaction, namely, the long range dipolar interaction. In order to calculate the relative permittivity of the liquid, Onsager used a model originally proposed by Bell (1931) for a spherical dipolar molecule. This model of a dipolar molecule in a dielectric is a point dipole situated at the center of an empty spherical cavity in a continuous dielectric with permittivity equal to the bulk permittivity ϵ_s of the dielectric (Fig. 3.1.4.1). The radius a of the cavity is determined from the relation

$$\frac{4}{3}\pi n a^3 = 1 \tag{3.1.4.1}$$

where n is the molecular number density. Thus the volume of the cavity is the volume available to each molecule. The field of the dipole, $\boldsymbol{\mu}$, in the cavity polarizes its surroundings. The resulting polarization of the surroundings then induces a homogeneous field in the cavity which is called the reaction field **R**. Since the cavity is spherical **R** has the same direction as $\boldsymbol{\mu}$. This is not so when the cavity is nonspherical (Abbott and Bolton,

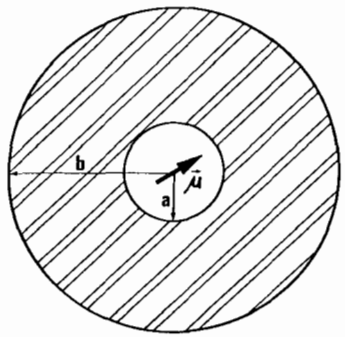

Figure 3.1.4.1 Onsager's model.

1952). If the dipole is polarizable and possesses a polarizability α, the reaction field polarizes the dipole and thus alters the dipole moment. The assumptions made by Onsager have been stated succintly by Fröhlich (1949).

1. A molecule occupies a sphere of radius a, its polarizability is isotropic, and no saturation effects can take place.
2. The *short range molecular interaction energy is negligible compared with kT.*

The second assumption means that the *surroundings* of the molecule are treated as a continuous dielectric of relative permittivity ϵ_s equal to the bulk relative permittivity of the liquid because *long range forces* only are considered. In other words, Onsager's method of calculating ϵ_s is a self-consistent one.

3.1.5 The Cavity Field

If a macroscopic uniform negative potential gradient $\mathbf{E}_0$ is imposed on the dielectric by *external* sources, then a calculation in electrostatics shows that the field, $\mathbf{G}$, in an empty cavity in the dielectric will not be equal to $\mathbf{E}_0$. This field $\mathbf{G}$ is called the cavity field.

3.1.6 Derivation of the Onsager Formula

In order to derive Onsager's formula it is convenient for us to imagine the dipole with its cavity of radius a to be placed at the center of a very large dielectric sphere of outer radius b and relative permittivity ϵ_s. The field within the cavity of such a sphere when subjected to both a uniform external field $\mathscr{E}_0$, parallel to the z axis, and to the field of a polarizable point dipole $\mathbf{m}$, situated at the center of the cavity and making an angle ϑ with the z axis (Fig. 3.1.6.1) consists (Coffey and Scaife, 1975; Scaife, 1971) of a uniform field,

$$\mathbf{f} = \mathbf{G} + \mathbf{R} = \frac{9\epsilon_s \mathscr{E}_0 c}{(2\epsilon_s + 1)(\epsilon_s + 2)} + \frac{2(\epsilon_s - 1)}{(2\epsilon_s + 1)} \frac{\mathbf{m}c}{4\pi\epsilon_0 a^3} \tag{3.1.6.1}$$

and the field of the dipole $\mathbf{m}$ itself which we denote by $\mathbf{D}(\mathbf{m})$

$$\left[c^{-1} = \left(1 - \frac{2(\epsilon_s - 1)^2 a^3}{b^3(\epsilon_s + 2)(2\epsilon_s + 1)}\right)\right]$$

The field $\mathbf{f}$ may be written in terms of the uniform negative potential gradient $\mathbf{E}_0$, at points in the shell far from the cavity; thus

$$\mathbf{f} = \frac{3\epsilon_s \mathbf{E}_0 c}{2\epsilon_s + 1} + \frac{2(\epsilon_s - 1)}{(2\epsilon_s + 1)} \frac{\mathbf{m}c}{4\pi\epsilon_0 a^3} \tag{3.1.6.2}$$

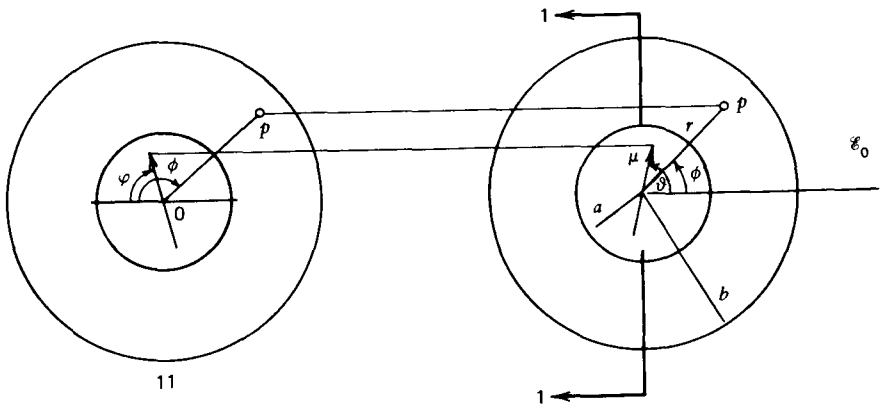

Figure 3.1.6.1 Dipole in a spherical cavity.

On taking the negative gradient of the potential in the shell ($a \leq r \leq b$), we find that it represents:

1. A dipolar field, $\mathbf{F}_d$, due to a dipole of moment

$$\frac{3c}{2\epsilon_s + 1}\left[m\cos\vartheta - 4\pi\epsilon_0 a^3 \left(\frac{\epsilon_s - 1}{\epsilon_s + 2}\right)\mathscr{E}_0\right] \tag{3.1.6.3}$$

   lying parallel to the z axis.
2. A uniform field, $\mathbf{F}_u$, of magnitude

$$\frac{3c}{(\epsilon_s + 2)}\left[\mathscr{E}_0 - \frac{2(\epsilon_s - 1)}{(2\epsilon_s + 1)} \frac{m\cos\vartheta}{4\pi\epsilon_0 b^3}\right] \tag{3.1.6.4}$$

   applied parallel to the z axis.
3. A dipolar field, $\mathbf{H}_d$, due to a dipole of moment

$$\frac{3mc\sin\vartheta}{2\epsilon_s + 1} \tag{3.1.6.5}$$

   lying perpendicular to the z axis.
4. A uniform field, $\mathbf{H}_u$, of magnitude

$$\frac{6(\epsilon_s - 1)mc\sin\vartheta}{(2\epsilon_s + 1)(\epsilon_s + 2)4\pi\epsilon_0 b^3} \tag{3.1.6.6}$$

   applied perpendicular to the z axis.

Equation 3.1.6.2 may be written

$$\mathbf{f} = \mathbf{G} + g\mathbf{m} \tag{3.1.6.7}$$

where

$$g = \frac{2(\epsilon_s - 1)}{(2\epsilon_s + 1)} \frac{1}{4\pi\epsilon_0 a^3} \tag{3.1.6.8}$$

Also from Eq. 3.1.2.1

$$\mathbf{m} = \boldsymbol{\mu} + \alpha\mathbf{f} \tag{3.1.6.9}$$

which, with Eq. 3.1.6.7 yields

$$\mathbf{m} = \boldsymbol{\mu} + \alpha(\mathbf{G} + g\mathbf{m}) \tag{3.1.6.10}$$

Thus

$$\mathbf{m} = \frac{\boldsymbol{\mu}}{(1 - \alpha g)} + \frac{\alpha\mathbf{G}}{(1 - \alpha g)} \tag{3.1.6.11}$$

whence, for the average component of the dipole moment of a molecule parallel to **E**, we obtain

$$\langle \mathbf{m} \cdot \mathbf{e} \rangle = \frac{\langle \boldsymbol{\mu} \cdot \mathbf{e} \rangle}{(1 - \alpha g)} + \frac{\alpha\mathbf{G}}{(1 - \alpha g)} \tag{3.1.6.12}$$

where

$$\langle \boldsymbol{\mu} \cdot \mathbf{e} \rangle = \frac{\int_{-1}^{+1} \boldsymbol{\mu} \cdot \mathbf{e} \exp(-\beta U) d(\cos\vartheta)}{\int_{-1}^{+1} \exp(-\beta U) d(\cos\vartheta)} \tag{3.1.6.13}$$

U is the electrostatic energy stored in the system consisting of the dipole and its surrounding shell when placed in the external field $\mathscr{E}_0$. U may be divided into three parts (Davies and Scaife, 1954):

1. The energy U_1 required to create the dipole $\alpha\mathbf{f}$.
2. The energy U_2 of the dipole **m** in the external field $\mathscr{E}_0$.
3. The energy U_3 required to assemble the dielectric shell around **m** in the presence of $\mathscr{E}_0$.

It may be shown (Coffey, 1975) that

$$U_1 = \frac{1}{2}\alpha f^2 \tag{3.1.6.14}$$

$$U_2 = -\mathbf{m} \cdot \mathscr{E}_0 \tag{3.1.6.15}$$

$$U_3 = -\frac{1}{2}\epsilon_0(\epsilon_s - 1)\int_{v_1} \mathbf{E}_1 \cdot \mathbf{E}_2 \, dV \tag{3.1.6.16}$$

where $\mathbf{E}_1$ and $\mathbf{E}_2$ are the fields before and after the introduction of the dielectric shell and the integral is taken through the volume of the dielectric shell.

We first evaluate the integral in Eq. 3.1.6.16. We have clearly

$$\mathbf{E}_1 = \mathscr{E}_0 + \mathbf{D}(\mathbf{m}) \tag{3.1.6.17}$$

Also

$$\mathbf{E}_2 = \mathbf{F}_u + \mathbf{F}_d + \mathbf{H}_d + \mathbf{H}_v \tag{3.1.6.18}$$

Hence from Eq. 3.1.6.16, together with Eqs. 3.1.6.17 and 3.1.6.18,

$$U_3 = \frac{1}{2}\epsilon_0(\epsilon_s - 1)\left[\int_{v_1} \mathbf{F}_u \cdot \mathscr{E}_0 \, dV + \int_{v_1} \mathbf{F}_d \cdot \mathbf{D}(\mathbf{m}) \, dV + \int_{v_1} \mathbf{H}_d \cdot \mathbf{D}(\mathbf{m}) \, dV\right] \tag{3.1.6.19}$$

Substituting for $\mathbf{F}_u$, $\mathbf{F}_d$, and $\mathbf{H}_d$, from Eqs. 3.1.6.3 and 3.1.6.4, evaluating these integrals (Coffey, 1975), and allowing c to tend to 1, we are led to

$$U_3 = -2\pi b^3 \mathscr{E}_0^2 \epsilon_0 \frac{(\epsilon_s - 1)}{(\epsilon_s + 2)} + \frac{2(\epsilon_s - 1)^2 \mathbf{m} \cdot \mathscr{E}_0}{2(\epsilon_s + 1)(\epsilon_s + 2)} - \frac{(\epsilon_s - 1)}{(2\epsilon_s + 1)} \frac{m^2}{4\pi\epsilon_0 a^3} \tag{3.1.6.20}$$

Substituting for **m** from Eq. 3.1.6.11, then adding Eqs. 3.1.6.14 and 3.1.6.15 to 3.1.6.20, and writing explicitly only those terms which depend on the orientation ϑ gives

$$U = -\frac{9\epsilon_s\left(\frac{\epsilon_\infty + 2}{3}\right)\boldsymbol{\mu} \cdot \mathscr{E}_0}{(\epsilon_s + 2)(2\epsilon_s + \epsilon_\infty)} + \text{terms independent of orientation} \tag{3.1.6.21}$$

(The Lorenz–Lorentz relation has been used to eliminate α.)

On writing Eq. 3.1.6.21 in terms of $\mathbf{E}_0$, then substituting the result into the distribution function (Eq. 3.1.6.13), evaluating the integrals, and retaining only those terms which are linear in $\mathbf{E}_0$, we have with Eq. 3.1.6.12

$$\langle \mathbf{m} \cdot \mathbf{e} \rangle = \frac{3\epsilon_s}{2\epsilon_s + \epsilon_\infty}\left[\frac{\mu^2}{3kT}\left(\frac{\epsilon_\infty + 2}{3}\right)^2 \frac{(2\epsilon_s + 1)}{2\epsilon_s + \epsilon_\infty} + \frac{4\pi}{3}\epsilon_0 a^3(\epsilon_\infty - 1)\right]E_0 \tag{3.1.6.22}$$

Also

$$\langle \mathbf{m} \cdot \mathbf{e} \rangle = \frac{4}{3}\pi a^3 \epsilon_0(\epsilon_s - 1)E_0 \tag{3.1.6.23}$$

We find, on equating Eqs. 3.1.6.22 and 3.1.6.23 and using Eq. 3.1.4.1, that

$$(\epsilon_s - \epsilon_\infty) = \left(\frac{3\epsilon_s}{2\epsilon_s + \epsilon_\infty}\right)\left(\frac{\epsilon_\infty + 2}{3}\right)^2 \frac{N}{V\epsilon_0}\frac{\mu^2}{3kT} \tag{3.1.6.24}$$

which is Onsager's (1936) equation.

3.1.7 The Consistency of Onsager's Equation

In Onsager's model of a polar dielectric, we replace the inner sphere of dielectric (Fig. 3.1.4.1) by a dipole $\boldsymbol{\mu}$ which resides at the center of an empty spherical cavity of radius a equal to the radius of the inner sphere.

Conversely, when in the expression for the negative potential gradient in the shell (Eqs. 3.1.6.3) the dipole $\boldsymbol{\mu}$ is replaced by its mean moment in the direction of the external field, we must retrieve the expression for the negative potential gradient in a solid dielectric sphere. In other words, the system must appear to possess no cavity at all. We now determine whether or not this proposition is true.

From Eq. 3.1.6.22 we conclude that

$$\langle \boldsymbol{\mu} \cdot \mathbf{e} \rangle = \frac{\mu^2 G}{3kT} \tag{3.1.7.1}$$

The potential at points in the shell $a < r < b$ with $\boldsymbol{\mu}$ replaced by $\boldsymbol{\mu} \cdot \mathbf{e}$ is

$$V_2 = \left[\frac{-3\mathscr{E}_0 c}{\epsilon_s + 2} + \frac{6(\epsilon_s - 1)\langle \boldsymbol{\mu} \cdot \mathbf{e} \rangle c}{(2\epsilon_s + 1)(\epsilon_s + 2)4\pi\epsilon_0 b^3}\right] r P_1(\cos\theta) + \left[\frac{3\langle \boldsymbol{\mu} \cdot \mathbf{e} \rangle}{(2\epsilon_s + 1)(4\pi\epsilon_0)} - \frac{3(\epsilon_s - 1)\mathscr{E}_0 a^3 c}{(2\epsilon_s + 1)(\epsilon_s + 2)}\right] \frac{P_1(\cos\theta)}{r^2} \tag{3.1.7.2}$$

Now from Onsager's equation

$$\frac{4\pi\epsilon_0 a^3}{3} \frac{(\epsilon_s - 1)(2\epsilon_s + 1)}{3\epsilon_s} = \frac{\mu^2}{3kT} \tag{3.1.7.3}$$

whence

$$\frac{3\langle \boldsymbol{\mu} \cdot \mathbf{e} \rangle}{(2\epsilon_s + 1)(4\pi\epsilon_0)} = \frac{3(\epsilon_s - 1)\mathscr{E}_0 a^3 c}{(2\epsilon_s + 1)(\epsilon_s + 2)} \tag{3.1.7.4}$$

which shows that the dipolar term in Eq. 3.1.7.2 is zero. Further, on letting $(a/b)^3 \to 0$ in Eq. 3.1.7.2, we have

$$V_2 = -\frac{3\mathscr{E}_0 r P_1(\cos\theta)}{(\epsilon_s + 2)} \tag{3.1.7.5}$$

which is the potential at points in a solid dielectric sphere. Thus Onsager's equation (Eq. 3.1.6.24) is consistent. (Note that ϵ_∞ has been set equal to one throughout in order to make the analysis as simple as possible.)

3.1.8 Kirkwood's Formula

Kirkwood (1939) obtained a general formula for the relative permittivity of a polar liquid by treating the interactions between the molecules of a large sphere of dielectric by the methods of classical statistical mechanics. Kirkwood's results are not derived here since they are more easily obtained from the work of Fröhlich (1949), who gave general expressions for the relative permittivity of any substance that is not permanently polarized.

3.2 FRÖHLICH'S THEORY

Fröhlich's general expression for the relative permittivity of a polar substance may be derived by again taking as our macroscopic specimen a very large sphere and selecting from it a smaller sphere of radius a. This small sphere must be just large enough to have the same properties as the large sphere and at the same time must be far removed from the boundaries of the large sphere. Thus if b is the radius of the large sphere then the ratio $(a/b)^3 \ll 1$. The inner sphere is treated on a discrete basis, whereas the surrounding shell is treated as a continuous dielectric medium. The system consisting of the inner sphere and its surrounding shell is assumed to obey the laws of classical statistical mechanics.

We suppose that the inner sphere contains N charges and we denote the ith charge by e_i. In any given energy state of the system, other than the ground state, all the charges of the system are displaced from the positions they occupied in the ground state. The displacements of the charges in the inner sphere are collectively denoted by $\mathbf{X}$, where $\mathbf{X}$ is the set

$$\{\mathbf{r}_1, \ldots, \mathbf{r}_i, \ldots, \mathbf{r}_N\} = \{\mathbf{r}_i\}_{i=1}^N$$

and $\mathbf{r}_i$ is the displacement of the ith charge. If we assume that the dipole moment of the substance vanishes in the lowest energy state, then the dipole moment of the inner sphere when its charges undergo a set of displacements $\mathbf{X}$ is

$$\mathbf{M}(\mathbf{X}) = \sum_{i=1}^{N} e_i \mathbf{r}_i \tag{3.2.1}$$

An atom or molecule contains several elementary charges. Following Fröhlich, we term an atom or a molecule a cell and label such a cell j. If the cell j contains, say, s elementary charges, we denote them by the set

$$\{e_{jk}\}_{k=1}^{s} \tag{3.2.2}$$

and we denote the collective displacements of these charges by the set

$$\mathbf{x}_j = \{\mathbf{r}_{jk}\}_{k=1}^{s} \tag{3.2.3}$$

The dipole moment of the cell j is

$$\mathbf{m}(\mathbf{x}_j) = \sum_{k=1}^{s} e_{jk} \mathbf{r}_{jk}$$

and the total dipole moment of the inner sphere is

$$\mathbf{M}(\mathbf{X}) = \sum_j \mathbf{m}(\mathbf{x}_j) = \sum_j \sum_{k=1}^{s} e_{jk} \mathbf{r}_{jk} \tag{3.2.4}$$

The probability of finding the charges of the inner sphere with a set of displacements lying between $\mathbf{X}$ and $\mathbf{X} + d\mathbf{X}$, in the presence of a potential

gradient $-\mathbf{E}$ imposed on the system from external sources, is

$$\frac{\exp[-\beta U(\mathbf{X},\mathbf{E})]\,d\mathbf{X}\,d(\cos\vartheta)}{\int_{-1}^{+1}\int_N \exp[-\beta U(\mathbf{X},\mathbf{E})]\,d\mathbf{X}\,d(\cos\vartheta)} \tag{3.2.5}$$

where $U(\mathbf{X},\mathbf{E})$ is the potential energy of the system in the presence of $\mathbf{E}$ and

$$d\mathbf{X} = d\mathbf{r}_1\,d\mathbf{r}_2\cdots d\mathbf{r}_i\cdots d\mathbf{r}_N \tag{3.2.6}$$

The integration must be carried out over all the possible values of the $\mathbf{r}_i$.

If ϑ denotes the angle between the dipole moment, $\mathbf{M}(\mathbf{X})$, of the inner sphere and $\mathbf{E}$, then we have for the *mean* dipole moment of the inner sphere in the direction parallel to $\mathbf{E}$

$$M_E = \langle \mathbf{M}\cdot\mathbf{e}\rangle = \frac{\int_{-1}^{+1}\int_N \mathbf{M}(\mathbf{X})\cdot\mathbf{e}\exp[-\beta U(\mathbf{X},\mathbf{E})]d\mathbf{X}\,d(\cos\vartheta)}{\int_{-1}^{+1}\int_N \exp[-\beta U(\mathbf{X},\mathbf{E})]\,d\mathbf{X}\,d(\cos\vartheta)} \tag{3.2.7}$$

where the symbol

$$\int_N d\mathbf{X} = \int\cdots\int(d\mathbf{r}_1\cdots d\mathbf{r}_N) \tag{3.2.8}$$

denotes an integration over all the position coordinates of all the molecules in the sphere. Equation 3.2.7 may be written in a more compact form by defining a quantity J, given by

$$J^{-1} = \int_N \exp[-\beta U(\mathbf{X})]\,d\mathbf{X} \tag{3.2.9}$$

We denote the value of the potential energy in the absence of $\mathbf{E}$ by the symbol

$$U(\mathbf{X},0) = U(\mathbf{X}) \tag{3.2.10}$$

$U(\mathbf{X})$ may be divided into two parts:

1. The energy of interaction between the particles of the inner sphere themselves which we term $U_i(\mathbf{X})$.
2. The energy of interaction between the particles of the inner sphere and the surrounding shell, namely, $U_e(\mathbf{X})$.

Thus

$$U(\mathbf{X}) = U_i(\mathbf{X}) + U_e(\mathbf{X}) \tag{3.2.11}$$

We now determine $U(\mathbf{X},\mathbf{E})$ (notice that the application of $\mathbf{E}$ alters the displacements $\mathbf{X}$). $U(\mathbf{X},\mathbf{E})$ may be decomposed into three parts:

1. $U_i(\mathbf{X})$, the energy of interaction of the particles of the inner sphere.

2. The energy of interaction of the particles of the inner sphere and the field $\mathscr{E}_0$ outside the sphere before the introduction of the shell; this is $-\mathbf{M}(\mathbf{X})\cdot\mathscr{E}_0$.
3. The energy $U_2(\mathbf{X},\mathscr{E}_0)$, required to polarize the outer shell in the presence of the inner sphere. Proceeding in a manner exactly similar to that described in the discussion of the Onsager model, we are led to the following expression for the mean dipole moment of the inner sphere:

$$M_E = \frac{3\epsilon_s}{2\epsilon_s+1}\frac{\langle M^2(\mathbf{X})\rangle_0 E}{3kT} \tag{3.2.12}$$

where

$$\langle M^2(\mathbf{X})\rangle_0 = \frac{\int_N M^2(\mathbf{X})e^{-\beta U(\mathbf{X})}\,d\mathbf{X}}{\int_N e^{-\beta U(\mathbf{X})}\,d\mathbf{X}} \tag{3.2.13}$$

Equation 3.2.13 is the *mean square value of the instantaneous dipole moment* of the inner sphere in the *absence* of $\mathbf{E}$. In arriving at Eq. 3.2.12 we have made use of the result

$$\int_{-1}^{+1}\int_N (\mathbf{M}(\mathbf{X})\cdot\mathbf{e})e^{-\beta U_i(\mathbf{X})}\,d\mathbf{X}\,d(\cos\vartheta) = 0$$

and we have assumed that $\mathbf{E}$ is sufficiently weak to prevent nonlinear effects occurring. The subscript zero on the angular brackets indicates that the average is to be taken in the absence of $\mathbf{E}$.

$$M_E = Pv = \epsilon_0(\epsilon_s - 1)Ev \tag{3.2.14}$$

where v is the volume of the inner sphere and P its average polarization, whence with Eq. 3.2.12,

$$(\epsilon_s - 1) = \left(\frac{3\epsilon_s}{2\epsilon_s+1}\right)\left(\frac{1}{v\epsilon_0}\right)\frac{\langle M^2\rangle_0}{3kT} \tag{3.2.15}$$

Equation 3.2.15 is a perfectly general result; it expresses the relative permittivity of the specimen in terms of the *mean square fluctuations* in the instantaneous dipole moment $\mathbf{M}(\mathbf{X})$ of a spherical specimen of the dielectric *embedded* in a large volume of the same dielectric. These fluctuations in the instantaneous dipole moment are the *total fluctuations* in the dipole moment *from all causes*, because in a dielectric several mechanisms of polarization may be operative (Scaife, 1957).

3.2.1 Fröhlich's Treatment of Displacement Polarization

Fröhlich separates the contribution to the polarization due to elastic displacement of the constituent charges of the inner sphere by treating this

contribution to the polarization of the inner sphere on a continuous basis. He obtains this component of the polarization by assuming that the space occupied by the inner sphere is filled with material of static relative permittivity ϵ_∞. The charges, e_i, referred to above are embedded in this material and are treated on a discrete basis, whereas the material of relative permittivity ϵ_∞ is treated by means of electrostatics (Fig. 3.2.1.1).

The field in the inner sphere is

$$\mathbf{f} = \frac{9\epsilon_s \mathscr{E}_0}{(2\epsilon_s + \epsilon_\infty)(\epsilon_s + 2)} + \frac{2(\epsilon_s - \epsilon_\infty)\mathbf{M}}{(2\epsilon_s + \epsilon_\infty)4\pi\epsilon_0 a^3} \tag{3.2.1.1}$$

plus the field of the dipole **M**. Proceeding in the manner described for the Onsager model, we obtain for the energy of the system

$$U = -3\epsilon_s \frac{\mathbf{M}(\mathbf{X})\cdot\mathbf{E}}{(2\epsilon_s + \epsilon_\infty)} + \text{terms independent of orientation} \tag{3.2.1.2}$$

In deriving the above expression the following points should be noted:

1. The set **X** of displacements refers to nonelectronic displacements only. **M(X)** is the dipole moment of the inner sphere for a given set **X** of displacements.
2. $U_1 = -\dfrac{3\mathbf{M}\cdot\mathscr{E}_0}{\epsilon_\infty + 2} + \text{terms independent of orientation}$ (3.2.1.3)
3. In expression 3.1.6.17 for the energy required to polarize the shell,

$$\mathbf{E}_1 = \mathscr{E}_0 + D(\mathbf{m}, \mathscr{E}_0) \tag{3.2.1.4}$$

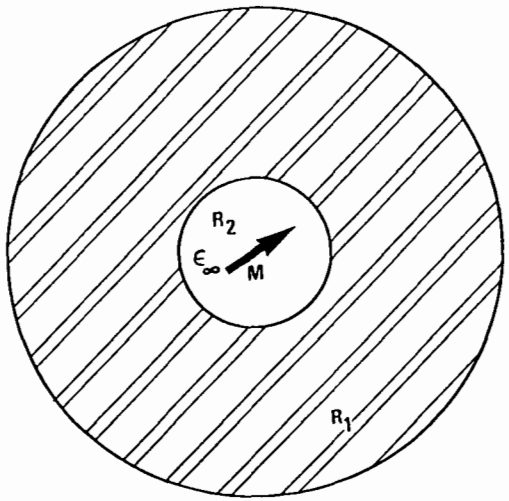

Figure 3.2.1.1 Fröhlich's treatment of displacement polarization.

where $\mathbf{D}(\mathbf{m}, \mathscr{E}_0)$ is a dipolar field of moment

$$\frac{3\mathbf{M}}{(\epsilon_\infty + 2)} + 4\pi\epsilon_0 \frac{(\epsilon_\infty - 1)}{(\epsilon_\infty + 2)} \mathscr{E}_0 a^3 \tag{3.2.1.5}$$

The instantaneous dipole moment, **m**, say, of the inner sphere is the moment **M(X)**, plus the moment *induced in the material of permittivity* ϵ_∞ by **M(X)** and the outer shell, that is,

$$\mathbf{m} = \mathbf{M}(\mathbf{X}) + \int_v \mathbf{P}\, dv \tag{3.2.1.6}$$

where v is the volume of the inner sphere and **P** its polarization. The component of **m** in the direction of the z axis is

$$m_z = \mathbf{m}\cdot\mathbf{e} = \mathbf{M}(\mathbf{X})\cdot\mathbf{e} + \int_v P_z\, dv \tag{3.2.1.7}$$

The integral occurring in this equation is indeterminate due to the presence of the dipole **m** at the origin. However, this difficulty may be circumvented by using the following modified form of Green's theorem (Stratton, 1941):

$$\int_v \nabla V\, dv = \int_S V\mathbf{n}\, dS \tag{3.2.1.8}$$

where V is the potential and **n** is the unit outward drawn normal to the surface S bounding the volume v. Thus we have, with Eq. 3.2.1.7, if $V_1(a, \theta, \phi)$ is the potential at points on the bounding surface S of the sphere, then

$$\int_v P_z\, dv = -\epsilon_0(\epsilon_\infty - 1)\int_S V_1(a, \theta, \phi)(\mathbf{n}\cdot\mathbf{e})\, dS \tag{3.2.1.9}$$

The potential $V_1(r, \theta, \phi)$ at points in the sphere may be obtained by replacing ϵ_s by $\epsilon_s/\epsilon_\infty$ in the expression for the potential for $\epsilon_\infty = 1$. Substituting the potential so obtained in Eq. 3.2.1.9 and evaluating the integral, we conclude that

$$\mathbf{m}\cdot\mathbf{e} = \frac{4\pi\epsilon_0 a^3}{3}\frac{3\epsilon_s(\epsilon_\infty - 1)E}{2\epsilon_s + \epsilon_\infty} - \frac{(\epsilon_\infty - 1)}{2\epsilon_s + \epsilon_\infty}\mathbf{M}\cdot\mathbf{e} \tag{3.2.1.10}$$

Substituting this expression into Eq. 3.2.7, together with Eq. 3.2.1.2 and evaluating the integrals to first order in E, yields

$$\langle\mathbf{m}\cdot\mathbf{e}\rangle = \frac{4\pi\epsilon_0 a^3}{3}\frac{3\epsilon_s(\epsilon_\infty - 1)E}{2\epsilon_s + \epsilon_\infty} + \frac{3\epsilon_s(2\epsilon_s + 1)}{(2\epsilon_s + \epsilon_\infty)^2}\frac{\langle M^2\rangle_0 E}{3kT} \tag{3.2.1.11}$$

The dipole moment of the sphere when it is treated on a macroscopic basis is

$$M_E = \frac{4\pi\epsilon_0 a^3}{3}(\epsilon_s - 1)E \tag{3.2.1.12}$$

Thus from Eqs. 3.2.1.11 and 3.2.1.12 we have

$$(\epsilon_s - \epsilon_\infty) = \frac{3\epsilon_s}{2\epsilon_s + \epsilon_\infty} \frac{1}{v\epsilon_0} \frac{\langle M^2 \rangle_0}{3kT} \tag{3.2.1.13}$$

which is Fröhlich's equation *when the displacement mechanism of polarization is treated on a macroscopic basis.*

3.2.2 A Test of the Consistency of Fröhlich's Equation (3.2.1.13)

Einstein (1910) (see Fröhlich, 1949; and Tolman, 1938) has given a formula connecting *the probability of a fluctuation in a macroscopic variable* describing the condition of a system with a corresponding increase in the Helmholtz free energy of the system *associated with that variable.* Einstein expressed the probability, dP, of finding a fluctuating macroscopic variable within the definite range x to $x + dx$, in the form

$$dP = f(x)\exp\{-\beta[F(x) - F(x_0)]\} \tag{3.2.2.1}$$

where $f(x)$ is the function of x required to make the above equation valid. $F(x)$ is the Helmholtz free energy associated with the variable x and x_0 is the mean value of x.

Fröhlich states the theorem in the following form. If the Helmholtz free energy, $F(\varphi_1, \ldots, \varphi_n)$, of a system depends on n *macroscopic* variables $(\varphi_1, \ldots, \varphi_n)$ of the system, then the probability of finding the variables $(\varphi_1, \ldots, \varphi_n)$ in the range $(\varphi_1, \varphi_1 + d\varphi_1, \ldots, \varphi_n, \varphi_n + d\varphi_n)$ is

$$\frac{\exp[-\beta F(\varphi_1, \ldots, \varphi_n)]\, d\varphi_1 \cdots d\varphi_n}{\int_n \exp[-\beta F(\varphi_1, \ldots, \varphi_n)]\, d\varphi_1 \cdots d\varphi_n} \tag{3.2.2.2}$$

The macroscopic parameter characterizing the inner sphere (Figs. (3.2.2.1) and (3.2.2.2)) is its instantaneous dipole moment, $\mathbf{M}(\mathbf{X})$; hence on applying Eq. 3.2.2.2 to this system we obtain for the probability, dP, of finding the dipole moment, M, of the sphere in the range M to $M + dM$

$$dP = \frac{\exp[-\beta F(M)]M^2\, dM}{\int_0^\infty \exp[-\beta F(M)]M^2\, dM} \tag{3.2.2.3}$$

and

$$\langle M^2 \rangle_0 = \frac{\int_0^\infty M^4 \exp[-\beta F(M)]\, dM}{\int_0^\infty \exp[-\beta F(M)]M^2\, dM} \tag{3.2.2.4}$$

The Helmholtz free energy, $F(M)$, consists of the following:

1. The energy required to induce the moment $\mathbf{M}$ in the inner sphere, termed the internal free energy, $F_i(M)$.

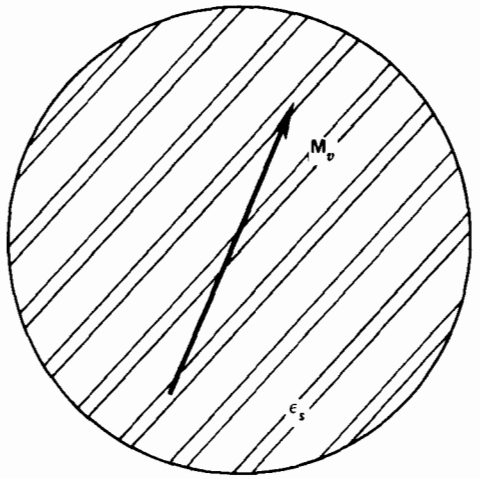

Figure 3.2.2.1 Dielectric sphere in vacuo.

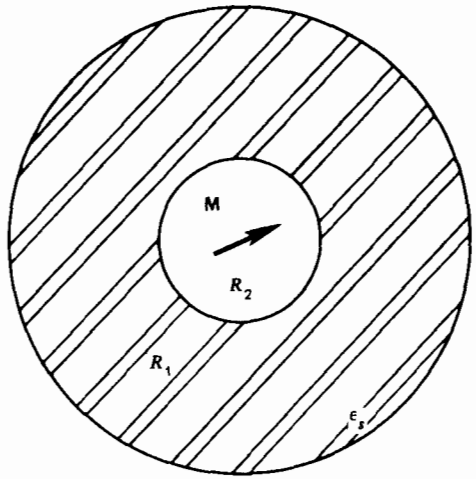

Figure 3.2.2.2 Dielectric shell with central dipole.

2. The energy required to surround the inner sphere with the dielectric shell in the presence of $\mathbf{M}$, termed the external free energy, $F_\epsilon(M)$.

Now, according to Fröhlich (1949),

$$F_i(M) = \frac{1}{2}\frac{M^2}{\alpha} \tag{3.2.2.5}$$

which for an isolated dielectric sphere of volume v becomes

$$\frac{1}{2}\frac{M^2}{\epsilon_0 v}\frac{3\epsilon_s}{(\epsilon_s-1)(2\epsilon_s+1)} \tag{3.2.2.6}$$

$F_e(M)$ is given by the last term of Eq. 3.1.6.20 with m^2 replaced by M^2; thus

$$F_e(M) = -\frac{M^2}{3v\epsilon_0}\left(\frac{\epsilon_s-1}{2\epsilon_s+1}\right) \tag{3.2.2.7}$$

Hence on adding Eqs. 3.2.2.6 and 3.2.2.7 we have, for an *immersed* sphere,

$$F(M) = F_i(M) + F_e(M) = \frac{1}{2}\frac{M^2}{\epsilon_0 v}\frac{3\epsilon_s}{(\epsilon_s-1)(2\epsilon_s+1)} \tag{3.2.2.8}$$

Substituting Eqs. 3.2.2.8 into 3.2.2.4, evaluating the integral, and ignoring terms $O(M^4)$ lead to the relation

$$(\epsilon_s - 1) = \frac{3\epsilon_s}{2\epsilon_s+1}\frac{1}{v\epsilon_0}\frac{\langle M^2\rangle_0}{3kT} \tag{3.2.2.9}$$

Equation 3.2.2.9 is identical to Eq. 3.2.15, and has been obtained via Einstein's theorem from purely *macroscopic* considerations, in contrast to Eq. 3.2.15, which has been obtained by treating the particles of the inner sphere on a *microscopic* basis. Thus we have shown that Fröhlich's results are consistent since the same answers are obtained irrespective of whether the system is treated on a macroscopic or microscopic basis.

A general formula for $(\epsilon_s - 1)$ can also be derived by considering a large sphere of dielectric in vacuo and treating it macroscopically. For a sphere *in vacuo*,

$$F(M) = F_i(M) = \frac{1}{2}\frac{M^2}{3\epsilon_0 v}\left(\frac{\epsilon_s+2}{\epsilon_s-1}\right) \tag{3.2.2.10}$$

which, with the Einstein formula, yields

$$(\epsilon_s - 1) = \left(\frac{\epsilon_s+2}{3}\right)\frac{1}{\epsilon_0 v}\frac{\langle M^2\rangle^0_{\text{vac}}}{3kT}$$

that is,

$$\alpha_s = \frac{\langle M^2\rangle^0_{\text{vac}}}{3kT}$$

where $\langle M^2\rangle^0_{\text{vac}}$ is the mean square value of the instantaneous (3.2.2.11) dipole moment of the large sphere in vacuo.

3.2.3 Evaluation of $\langle M^2\rangle_0$

Fröhlich (1949) obtains an expression for $\langle M^2\rangle_0$ by developing a method first given by Kirkwood (1939) for the calculation of the relative permittivity of a liquid consisting of rigid dipoles. Fröhlich's method may be described as follows:

1. Divide the sphere into N units each of which makes the same contribution to M_E.
2. Let $\{r_{ji}\}_{i=1}^{N}$ denote the displacements of the k elementary charges of the jth cell and let us denote these displacements collectively by the set

$$\mathbf{x}_j = \{\mathbf{r}_{jk}\}_k \tag{3.2.3.1}$$

Then the set of displacements, $\mathbf{X}$, of all the elementary charges of the sphere is

$$\mathbf{X} = \{\mathbf{x}_j\}_{j=1}^{j=N}$$

Let $\mathbf{m}(\mathbf{x}_j)$ be the dipole moment of the jth cell; then

$$\mathbf{M}(\mathbf{X}) = \sum_{j=1}^{N}\mathbf{m}(\mathbf{x}_j) \tag{3.2.3.2}$$

whence

$$\langle M^2(\mathbf{X})\rangle_0 = \sum_{j=1}^{N} J\int_N \mathbf{m}(\mathbf{x}_j)\cdot\mathbf{M}(\mathbf{X})e^{-\beta U(\mathbf{X})}\,d\mathbf{X} \tag{3.2.3.3}$$

where

$$J^{-1} = \int_N e^{-\beta U(\mathbf{X})}\,d\mathbf{X} \tag{3.2.3.4}$$

and

$$d\mathbf{X} = d\mathbf{x}_1\,d\mathbf{x}_2\cdots d\mathbf{x}_j\cdots d\mathbf{x}_N \tag{3.2.3.5}$$

Let us define

$$d\mathbf{X}_j = d\mathbf{x}_1\cdots d\mathbf{x}_{j-1}\,d\mathbf{x}_{j+1}\cdots d\mathbf{x}_N \tag{3.2.3.6}$$

Thus

$$d\mathbf{X} = d\mathbf{X}_j\,d\mathbf{x}_j$$

We now carry out the integrations in Eq. 3.2.3.3 in two parts; first we integrate Eq. 3.2.3.3 over the whole sphere except the jth unit, and second, over the jth unit only. Following this procedure we find that

$$J\int_N \mathbf{m}(\mathbf{x}_j)\cdot\mathbf{M}(\mathbf{X})e^{-\beta U(\mathbf{X})}\,d\mathbf{X} = J\int_j \mathbf{m}(\mathbf{x}_j)\,d\mathbf{x}_j\cdot\int_{N-1}\mathbf{M}(\mathbf{X})e^{-\beta U(X)}\,d\mathbf{X}_j \tag{3.2.3.7}$$

The subscript j denotes an integration over the jth cell only. The right-hand side of Eq. 3.2.3.7 may be written:

$$\int_j \mathbf{m}(\mathbf{x}_j)\cdot\left[\left(\frac{\int_{N-1}\mathbf{M}(\mathbf{X})e^{-\beta U(\mathbf{X})}\,d\mathbf{X}_j}{\int_{N-1}e^{-\beta U(\mathbf{X})}\,d\mathbf{X}_j}\right)\left(\frac{\int_{N-1}e^{-\beta U(\mathbf{X})}\,d\mathbf{X}_j}{\int_N e^{-\beta U(\mathbf{X})}\,d\mathbf{X}}\right)\right]d\mathbf{x}_j \tag{3.2.3.8}$$

The first part of the term in square brackets in Eq. 3.2.3.8 is a function of the set of displacements, $\mathbf{x}_j$, of the jth cell only. We label this term $\mathbf{m}^*(\mathbf{x}_j)$. The same is true for the second term, which is the probability, $p(\mathbf{x}_j)$, of finding the jth cell with the set of displacements $\mathbf{x}_j$.

The quantity $\mathbf{m}^*(\mathbf{x}_j)$ is the *mean moment* of the sphere given that its jth cell has a *fixed set* $\mathbf{x}_j$ of displacements, which give rise to a dipole moment for this cell of $\mathbf{m}(\mathbf{x}_j)$.

Hence with Eq. 3.2.3.7

$$J \int_N \mathbf{m}(\mathbf{x}_j) \cdot \mathbf{M}(\mathbf{X}) e^{-\beta U(\mathbf{X})}\, d\mathbf{X} = \int_j \mathbf{m}(\mathbf{x}_j) \cdot \mathbf{m}^*(\mathbf{x}_j) p(\mathbf{x}_j)\, d\mathbf{x}_j \qquad (3.2.3.9)$$

We have, on using Eq. 3.2.3.3,

$$\langle M^2 \rangle_0 = \sum_{j=1}^{N} \int_j \mathbf{m}(\mathbf{x}_j) \cdot \mathbf{m}^*(\mathbf{x}_j) p(\mathbf{x}_j)\, d\mathbf{x}_j \qquad (3.2.3.10)$$

Thus $\langle M^2 \rangle_0$ has been expressed as a *sum of integrals* over the *jth cell only.*

It may be shown from electrostatics (Scaife, 1971) that the dipole moment induced in a sphere by a dipole residing in a cavity in the sphere is independent of the size of the sphere. This result is true even if the cavity containing the dipole is not concentric with the sphere. Hence if m_s^* (the moment that is induced in any sphere surrounding the jth unit) can be obtained by treating the jth unit as a point dipole, then (Figs. 3.2.3.1 and 3.2.3.2)

$$\mathbf{m}_s^* = \mathbf{m}^* \qquad (3.2.3.11)$$

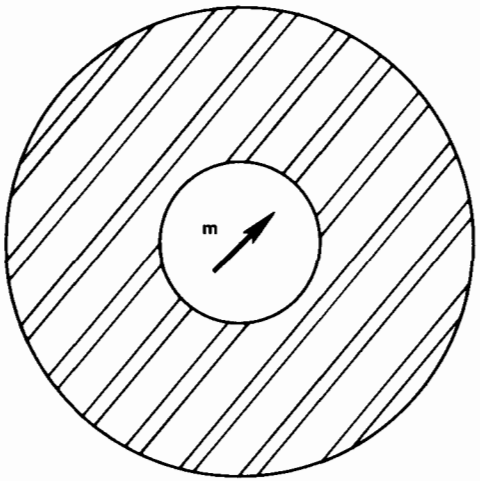

Figure 3.2.3.1 Moment induced in a spherical shell by a central dipole $\mathbf{m}^* = 9\epsilon_s \mathbf{m}/(2\epsilon_s + 1)(\epsilon_s + 2)$.

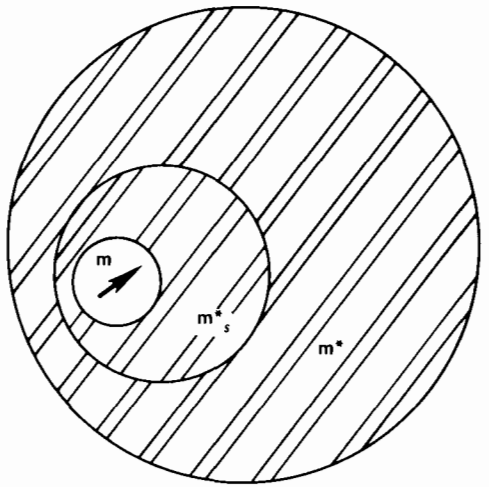

Figure 3.2.3.2 Moment induced in a spherical shell by a noncentral dipole.

where $\mathbf{m}^*$ is the moment of the whole sphere. It also follows from this that

$$\mathbf{m}^* = \mathbf{m} \qquad (3.2.3.12)$$

since we have supposed that each cell makes the same contribution to the dipole moment of the sphere.

If $\mathbf{m}^*$ is not equal to $\mathbf{m}$, it follows from the analysis above that $\mathbf{m}^*$ cannot be obtained by treating the jth unit as a point dipole in a spherical cavity surrounded by a continuous dielectric. Hence $\mathbf{m}^*$ can differ from $\mathbf{m}$ if and only if

1. The shape of the jth cell differs from that of a sphere.
2. The region surrounding the jth cell cannot be treated on a *macroscopic* basis.

The important consequence of the theorem in electrostatics used above is that $\mathbf{m}^*$ is *independent* of the *position* of the jth cell as long as the jth cell is sufficiently far from the surface of the sphere to allow its interactions with the outside to be treated on a macroscopic basis. The number of cells for which this condition does not hold is negligibly small in comparison with the total number of cells and thus Eq. 3.2.3.10 may be written

$$\langle M^2 \rangle_0 = N \langle \mathbf{m} \cdot \mathbf{m}^* \rangle_0 \qquad (3.2.3.13)$$

Thus with Eq. 3.2.15 we are led to

$$(\epsilon_s - 1) = \frac{3\epsilon_s}{(2\epsilon_s + 1)} \frac{N}{\epsilon_0 v} \frac{\langle \mathbf{m} \cdot \mathbf{m}^* \rangle_0}{3kT} \qquad (3.2.3.14)$$

where $\langle \mathbf{m} \cdot \mathbf{m}^* \rangle$ is the average dipole moment of the sphere when one of its cells is held in a fixed configuration, which leads to a dipole moment $\mathbf{m}^*$ for this cell. Similarly Eq. 3.2.1.13 becomes

$$(\epsilon_s - \epsilon_\infty) = \frac{3\epsilon_s}{2\epsilon_s + \epsilon_\infty} \frac{N}{\epsilon_0 v} \frac{\langle \mathbf{m} \cdot \mathbf{m}^* \rangle_0}{3kT} \tag{3.2.3.15}$$

where m and m^* now refer to nonelectronic displacements.

3.2.4 The Kirkwood–Fröhlich Equation

This equation gives us a general expression for the relative permittivity of liquids consisting of polar molecules possessing a permanent dipole moment, μ, and a polarizability, α, where α is given by the Lorenz–Lorentz relation; that is, the effect of α is accounted for by considering the liquid as a continuous dielectric of relative permittivity ϵ_∞ in which are embedded dipoles with permanent dipole moments μ.

3.2.5 Derivation of the Kirkwood–Fröhlich Equation

We choose the cell j (discussed in Section 3.2.3) so that it contains just *one* dipolar molecule; hence the moment $\mathbf{m}$ of the cell is μ. The orientations of the dipoles are then the only variables. We now define

$$\mathbf{m}^* = \mu^* \tag{3.2.5.1}$$

where μ^* is the average moment of the sphere when the dipole μ is held in a *fixed orientation.* Thus if we write

$$\langle \mathbf{m} \cdot \mathbf{m}^* \rangle_0 = \langle \mu \cdot \mu^* \rangle_0 \tag{3.2.5.2}$$

then in a liquid in the absence of an applied field all dipolar directions are equivalent and

$$\langle \mu \cdot \mu^* \rangle_0 = \mu \cdot \mu^* \tag{3.2.5.3}$$

so that with Eq. 3.2.3.15 we have

$$(\epsilon_s - \epsilon_\infty) = \frac{3\epsilon_s}{2\epsilon_s + \epsilon_\infty} \frac{N}{\epsilon_0 v} \frac{\mu \cdot \mu^*}{3kT} \tag{3.2.5.4}$$

If the interactions between μ and its nearest neighbors only are considered then μ^* is the sum of the moment μ of the central dipole when this dipole is held in a fixed direction *relative to its neighbors* and the *average* of the sum of the moments of its nearest neighbors. Hence if z is the *average* number of nearest neighbors we may write

$$\mu \cdot \mu^* = \mu^2(1 + z\langle \cos \gamma \rangle) \tag{3.2.5.5}$$

where $\langle \cos \gamma \rangle$ is the average of the cosine of the angle between *neighboring dipoles.*

From Section 3.2.3,

$$\mathbf{m}^*(\mathbf{x}_j) = \frac{\int_{N-1} \mathbf{M}(\mathbf{X}) e^{-\beta U(\mathbf{X})}\, d\mathbf{X}_j}{\int_{N-1} e^{-\beta U(\mathbf{X})}\, d\mathbf{X}_j} \tag{3.2.5.6}$$

It then follows that

$$\langle \cos \gamma \rangle = \frac{\int \cos \gamma\, e^{-\beta U}\, d\omega_1\, d\omega_2}{\int e^{-\beta U}\, d\omega_1\, d\omega_2} \tag{3.2.5.7}$$

where 1 and 2, refer to two neighboring dipoles, $d\omega_1, d\omega_2$ are the solid angles of the two dipoles, and U is the part of the energy of interaction of the dipoles which depends on the angle γ between them. Substituting Eq. 3.2.5.7 into Eq. 3.2.5.4 and writing μ in terms of μ_v, we are led to

$$(\epsilon_s - \epsilon_\infty) = \frac{3\epsilon_s}{2\epsilon_s + \epsilon_\infty} \left(\frac{\epsilon_\infty + 2}{3}\right)^2 \left(\frac{N}{v\epsilon_0}\right) \frac{\mu_v^2}{3kT} (1 + z\langle \cos \gamma \rangle) \tag{3.2.5.8}$$

The equation is called the Kirkwood–Fröhlich equation. It is often written:

$$\epsilon_s - \epsilon_\infty = \frac{3\epsilon_s}{2\epsilon_s + \epsilon_\infty} \left(\frac{\epsilon_\infty + 2}{3}\right)^2 \frac{N}{v\epsilon_0} g\mu_v^2$$

where g is the Kirkwood correlation factor $g = 1 + z\langle \cos \gamma \rangle$.

3.3 THE FREQUENCY DEPENDENCE OF THE PERMITTIVITY

In Chapter 2 we saw that the dipole moment $\mathbf{M}(t)$ induced in a dielectric body by an external field $\mathbf{E}(t)$ could be calculated by means of the equation (throughout it is assumed that quasi-electrostatics applies; i.e., the dimensions of the body are smaller than any wavelength of significance)

$$\mathbf{M}(t) = \int_0^t \mathbf{E}(t - x) \frac{da(x)}{dx}\, dx \tag{3.3.1}$$

where $a(t)$ is the response of the body to a unit step function and $\mathbf{E}(t) = 0$, $t < 0$. Furthermore, if one introduces the aftereffect function

$$\begin{matrix} b(t) = a(\infty) - a(t) & (t > 0) \\ = 0 & (t < 0) \end{matrix}$$

then one finds for the polarizability $\alpha(\omega)$ of the body

$$\alpha(\omega) = \int_0^\infty \dot{a}(t) e^{-i\omega t}\, dt = -\int_0^\infty \dot{b}(t) e^{-i\omega t}\, dt \tag{3.3.2}$$

or

$$\alpha(\omega) = \alpha_s - i\omega \int_0^\infty b(t) e^{-i\omega t}\, dt \tag{3.3.3}$$

where

$$\alpha(\omega) = \alpha'(\omega) - i\alpha''(\omega) \tag{3.3.4}$$

From Eq. 3.3.2 we may write

$$\alpha'(\omega) = \int_0^\infty \dot{a}(t) \cos \omega t\, dt \tag{3.3.5}$$

$$\alpha''(\omega) = \int_0^\infty \dot{a}(t) \sin \omega t\, dt \tag{3.3.6}$$

We may now make use of the Kramers–Kronig dispersion relations (Scaife, 1959, 1971) to rewrite these equations as

$$\alpha'(\omega) = \frac{2}{\pi} \mathfrak{P} \int_0^\infty \frac{\alpha''(\mu)\mu\, d\mu}{(\mu^2 - \omega^2)} \tag{3.3.7}$$

$$\alpha''(\omega) = \frac{2}{\pi} \mathfrak{P} \int_0^\infty \frac{\alpha'(\mu)\omega\, d\mu}{\omega^2 - \mu^2} \tag{3.3.8}$$

where the $\mathfrak{P}$ indicates that the Cauchy principal value (Jeffreys and Jeffreys, 1950, Art. 12.02) of the integral is to be taken. Let us put $\omega = 0$ in Eq. 3.3.7, and since ω and μ may be interchanged, we must have

$$\alpha'(0) = \alpha_s = \frac{2}{\pi} \int_0^\infty \frac{\alpha''(\omega)\, d\omega}{\omega} \tag{3.3.9}$$

This is a most interesting and important relation since it connects the *equilibrium* polarizability α_s with the *dissipative* part of the *frequency-dependent* polarizability; in other words, it provides a link between the equilibrium and the nonequilibrium properties of the body. We now go on to describe a most important theorem known as the fluctuation–dissipation theorem, of which Eq..3.3.9 is one form:

3.3.1 The Fluctuation–Dissipation Theorem

The method we now describe follows closely that of Scaife (1959, 1971). We have shown in Section 3.2 that the polarizability of a dielectric body may be written (c.f. Eqs. 2.2.2.9 and 3.2.2.11)

$$\alpha_s = \frac{\langle M^2 \rangle_0}{3kT} \tag{3.3.1.1}$$

where $\langle M^2 \rangle_0 = \langle \mathbf{M} \cdot \mathbf{M} \rangle_0$ is the ensemble average of the square of the fluctuating dipole moment $\mathbf{M}$ of the body in the absence of an external field. By the ergodic hypothesis we must have

$$\langle M^2 \rangle_0 = \overline{\mathbf{M} \cdot \mathbf{M}} = \overline{M^2} = \lim_{T \to \infty} \frac{1}{T} \int_{-T/2}^{T/2} \mathbf{M}(t) \cdot \mathbf{M}(t)\, dt$$

Let us now write the Fourier transform pair:

$$\tilde{\mathbf{M}}(\omega) = \int_{-T/2}^{T/2} \mathbf{M}(t) e^{-i\omega t}\, dt \qquad (T \to \infty) \tag{3.3.1.3}$$

$$\mathbf{M}(t) = \frac{1}{2\pi} \int_{-\infty}^{\infty} \tilde{\mathbf{M}}(\omega) e^{i\omega t}\, d\omega \tag{3.3.1.4}$$

Inserting Eq. 3.3.1.4 into Eq. 3.3.1.2 then leads after a short calculation (or immediately from Parseval's theorem; Titchmarsh, 1937) to

$$\langle M^2 \rangle_0 = \overline{M^2} = \frac{1}{2\pi} \int_{-\infty}^{\infty} \lim_{T \to \infty} \frac{|\tilde{\mathbf{M}}(\omega) \cdot \tilde{\mathbf{M}}^*(-\omega)|}{T}\, d\omega$$
$$= \frac{1}{2\pi} \int_{-\infty}^{\infty} \mathfrak{M}(\omega)\, d\omega \tag{3.3.1.5}$$

where

$$\mathfrak{M}(\omega) = \lim_{T \to \infty} \frac{|\tilde{\mathbf{M}}(\omega) \cdot \tilde{\mathbf{M}}^*(-\omega)|}{T} = \lim_{T \to \infty} \frac{|\tilde{\mathbf{M}}(\omega)|^2}{T} \tag{3.3.1.6}$$

is the *spectral density* of the fluctuations in $\mathbf{M}(t)$. Then we have as a *direct* consequence of the Parseval theorem and the ergodic hypothesis

$$\langle M^2 \rangle_0 = \overline{M^2} = \frac{1}{2\pi} \int_{-\infty}^{\infty} \mathfrak{M}(\omega)\, d\omega \tag{3.3.1.7}$$

With the aid of Eq. (3.3.9)

$$\alpha_s = \frac{2}{\pi} \int_0^\infty \frac{\alpha''(\omega)}{\omega}\, d\omega = \frac{1}{3kT} \frac{1}{2\pi} \int_{-\infty}^{\infty} \mathfrak{M}(\omega)\, d\omega$$
$$= \frac{1}{3kT} \frac{1}{\pi} \int_0^\infty \mathfrak{M}(\omega)\, d\omega \tag{3.3.1.8}$$

since $\mathfrak{M}(\omega)$ is an even function of ω, from which it follows that

$$6kT\alpha''(\omega) = \omega \mathfrak{M}(\omega) \tag{3.3.1.9}$$

We have related the *dissipative part* of the *frequency-dependent* complex polarizability to the *spectral density* of the spontaneous fluctuations in the dipole moment at *equilibrium* of the body. This is the fluctuation–dissipation theorem (Callen and Welton, 1951; Greene and Callen, 1951). In identifying the integrals in Eq. 3.3.1.8 we have asserted that *macroscopic fluctuations* decay according to *macroscopic* laws.

3.3.2 Generalization of Fröhlich's Equations to the Frequency-Dependent Case

Let us now introduce again the concept of the autocorrelation function (a.c.f.), which in this case is the time average of $\mathbf{M}(t)$ with $\mathbf{M}(t+t')$ or $\mathbf{M}(t-t')$, that is,

$$C_{\mathbf{M}}(t) = \overline{\mathbf{M}(t')\cdot\mathbf{M}(t+t')} = \overline{\mathbf{M}(t-t')\cdot\mathbf{M}(t')}$$

The reader will recall from Chapter 1 the Wiener–Khintchin theorem; namely, the a.c.f. and the spectral density are each other's Fourier cosine transform. Thus

$$C_{\mathbf{M}}(t) = \frac{1}{\pi}\int_0^\infty \mathfrak{M}(\omega)\cos\omega t\, d\omega \tag{3.3.2.1}$$

which with Eq. 3.3.1.9 gives

$$C_{\mathbf{M}}(t) = \frac{6kT}{\pi}\int_0^\infty \frac{\alpha''(\omega)}{\omega}\cos\omega t\, d\omega \tag{3.3.2.2}$$

This on inversion gives

$$\alpha''(\omega) = \omega\left(\frac{\pi}{6kT}\right)\left(\frac{2}{\pi}\right)\int_0^\infty C_{\mathbf{M}}(t)\cos\omega t\, dt$$

$$= \omega\int_0^\infty b(t)\cos\omega t\, dt \tag{3.3.2.3}$$

from Eq. 3.3.3 and thus

$$3b(t) = \frac{1}{kT}C_{\mathbf{M}}(t) \tag{3.3.2.4}$$

Hence

$$\alpha(\omega) = \alpha_s - \frac{i\omega}{kT}\int_0^\infty C_{\mathbf{M}}(t)e^{-i\omega t}\, dt \tag{3.3.2.5}$$

or

$$\alpha(\omega) = \frac{1}{3kT}\left(\overline{\mathbf{M}\cdot\mathbf{M}} - i\omega\int_0^\infty \overline{\mathbf{M}(t')\cdot\mathbf{M}(t'+t)}\, e^{-i\omega t}\, dt\right)$$

$$= \frac{1}{3kT}\left[\langle\mathbf{M}\cdot\mathbf{M}\rangle_0 - i\omega\int_0^\infty \langle\mathbf{M}(t')\cdot\mathbf{M}(t'+t)\rangle_0\, e^{-i\omega t}\, dt\right] \tag{3.3.2.6}$$

This is the Kubo relation, and is the generalization of the Fröhlich relation,

$$\alpha_s = \frac{\langle M^2\rangle_0}{3kT} \tag{3.3.2.7}$$

to cover the dynamical behavior of the dielectric. Either the Kubo relation or the fluctuation–dissipation theorem (3.3.1.9) (Scaife, 1971) may be used to calculate $\alpha(\omega)$; that is, either $C_{\mathbf{M}}(t)$ or $\mathfrak{M}(\omega)$ provide the same information. Equation 3.3.2.6 may be written in the manner of Eq. 3.2.2.11 for an isolated spherical body as

$$\alpha_{\text{isph}}(\omega) = 3\epsilon_0 v\,\frac{\epsilon(\omega)-1}{\epsilon(\omega)+2} = \frac{1}{3kT}\left[\langle M^2\rangle^0_{\text{vac}} - i\omega\int_0^\infty \langle\mathbf{M}(t')\cdot\mathbf{M}(t'+t)\rangle^0_{\text{vac}}\, e^{-i\omega t}\, dt\right] \tag{3.3.2.8}$$

or in terms of the dispersion relations as (Scaife, 1971)

$$\alpha'_{\text{isph}}(\omega) = \frac{1}{3kT}\frac{1}{\pi}\mathfrak{P}\int_0^\infty \frac{\mathfrak{M}_{\text{vac}}(\omega)}{1-(\omega^2/\mu^2)}\, d\mu \tag{3.3.2.9}$$

$$\alpha''_{\text{isph}}(\omega) = \frac{\omega\mathfrak{M}_{\text{vac}}(\omega)}{6kT} \tag{3.3.2.10}$$

where $\mathfrak{M}_{\text{vac}}$ is the spectral density of the fluctuations in $\mathbf{M}(t)$ for an isolated spherical body. Scaife (1971) has shown that for a sphere of volume v immersed in an infinite volume of its own material

$$\alpha_{\text{imsph}}(\omega) = \frac{v\epsilon_0[\epsilon(\omega)-1][2\epsilon(\omega)+1]}{3\epsilon(\omega)}$$

$$= \frac{1}{3kT}\left[\langle M^2\rangle^0_{\text{med}} - i\omega\int_0^\infty \langle\mathbf{M}(t')\cdot\mathbf{M}(t+t')\rangle^0_{\text{med}}\, e^{-i\omega t}\, dt\right] \tag{3.3.2.11}$$

$$\alpha'_{\text{imsph}}(\omega) = \frac{1}{3kT}\frac{1}{\pi}\mathfrak{P}\int_0^\infty \frac{\mathfrak{M}_{\text{med}}(\mu)\, d\mu}{1-(\omega^2/\mu^2)} \tag{3.3.2.12}$$

$$\alpha''_{\text{imsph}}(\omega) = \frac{\omega\mathfrak{M}_{\text{med}}(\omega)}{6kT} \tag{3.3.2.13}$$

where $\mathfrak{M}_{\text{med}}(\omega)$ is the spectral density of the fluctuations in dipole moment of the *immersed* macroscopic sphere. Any calculation of either $\mathfrak{M}_{\text{vac}}(\omega)$ or $\mathfrak{M}_{\text{med}}(\omega)$ necessitates a detailed investigation of the dynamics of the fluctuation phenomena from a microscopic point of view.

3.3.3 Debye Type Theories

Equation 3.3.2.8 for the polarizability for an isolated macroscopic sphere is

$$\alpha(\omega) = \frac{3v\epsilon_0[\epsilon(\omega)-1]}{\epsilon(\omega)+2} = \frac{1}{3kT}\left[-\int_0^\infty \frac{d}{dt}C_{\mathbf{M}}(t)e^{-i\omega t}\, dt\right] \tag{3.3.4.1}$$

where

$$C_{\mathbf{M}}(t) = \langle\mathbf{M}(0)\cdot\mathbf{M}(t)\rangle^0_{\text{vac}} = \sum_{i,j}\langle\boldsymbol{\mu}_i(0)\cdot\boldsymbol{\mu}_j(t)\rangle \tag{3.3.4.5}$$

where $\boldsymbol{\mu}_i$, $\boldsymbol{\mu}_j$ are typical microscopic dipoles inside the sphere. This equation contains both dipolar auto- and cross-correlation functions, the cross-correlation functions being those for which $i \neq j$ and the a.c.f.'s the remainder. Let us now make the drastic assumption that all cross cor-

relations may be rejected so that

$$\langle \boldsymbol{\mu}_i(0) \cdot \boldsymbol{\mu}_j(t) \rangle = 0 \qquad i \neq j$$

This is tantamount to saying that all *electrical* interactions between the molecules may be ignored. Thus if N is the number of dipoles inside the sphere

$$\sum_{i,j} \langle \boldsymbol{\mu}_i(0) \cdot \boldsymbol{\mu}_j(t) \rangle = N \langle \boldsymbol{\mu}(0) \cdot \boldsymbol{\mu}(t) \rangle \tag{3.3.4.3}$$

This is the original assumption made by Debye (1913) in his (Debye, 1929) theory of dielectric relaxation. $\langle \boldsymbol{\mu}(0) \cdot \boldsymbol{\mu}(t) \rangle$ is the single dipole a.c.f. and thus Eq. 3.3.4.1 becomes

$$\alpha(\omega) = 3v\epsilon_0 \frac{\epsilon(\omega) - 1}{\epsilon(\omega) + 2} = -\frac{N\mu^2}{3kT} \int_0^\infty \frac{d}{dt} [\langle \mathbf{u}(0) \cdot \mathbf{u}(t) \rangle] e^{-i\omega t}\, dt \tag{3.3.4.4}$$

where $\langle \mathbf{u}(0) \cdot \mathbf{u}(t) \rangle$ is the dipole unit vector a.c.f. This is the equation that forms the basis of all the simple models for molecular reorientation described in Chapter 2. Under the assumption we have used to get Eq. 3.3.4.4 it is permissible to set $\epsilon(\omega) + 2 \simeq 3$ in that equation, which then becomes, on separating it into its real and imaginary parts,

$$\epsilon'(\omega) - 1 = \frac{N\mu^2}{3kTv\epsilon_0} \left[1 - \omega \int_0^\infty C_u(t) \sin \omega t\, dt \right] \tag{3.3.4.5}$$

$$\epsilon''(\omega) = \frac{N\mu^2 \omega}{3kTv\epsilon_0} \int_0^\infty C_u(t) \cos \omega t\, dt \tag{3.3.4.6}$$

where we have written $C_u(t) = C(t)$ in the notation of Chapter 2:

$$C_u(t) = \langle \mathbf{u}(0) \cdot \mathbf{u}(t) \rangle$$

In terms of the spectral density $\mathfrak{M}_{vac}(\omega)$ of the moment $\mathbf{M}(t)$ of the body the assumption involved in writing Eq. 3.3.4.4 is tantamount to writing

$$\mathfrak{M}_{vac}(\omega) = N \mathfrak{M}_\mu(\omega)$$

where $\mathfrak{M}_\mu(\omega)$ is the spectral density associated with a *single* fluctuating dipole.

Accepting the assumptions that led to Eqs. 3.3.4.5 and 3.3.4.6 we may link $C_u(t)$ directly to the power absorption coefficient $\mathfrak{A}(\omega)$ (Scaife, 1972):

$$\mathfrak{A}(\omega) = \frac{\omega \epsilon''(\omega)}{n(\omega) c} \tag{3.3.4.7}$$

Here $n(\omega)$ is the real part of the refractive index, given by

$$n(\omega) = \frac{\{[\epsilon'(\omega)^2 + \epsilon''(\omega)^2]^{1/2} + \epsilon'(\omega)]\}^{1/2}}{\sqrt{2}}$$

The behavior of $\mathfrak{A}(\omega)$, $\epsilon''(\omega)$, and $\epsilon''(\omega)/\omega$ [the intensity (approximately) of depolarized scattered light] is shown in Fig. 3.3.4.1. Note that $\mathfrak{A}(\omega)$ and

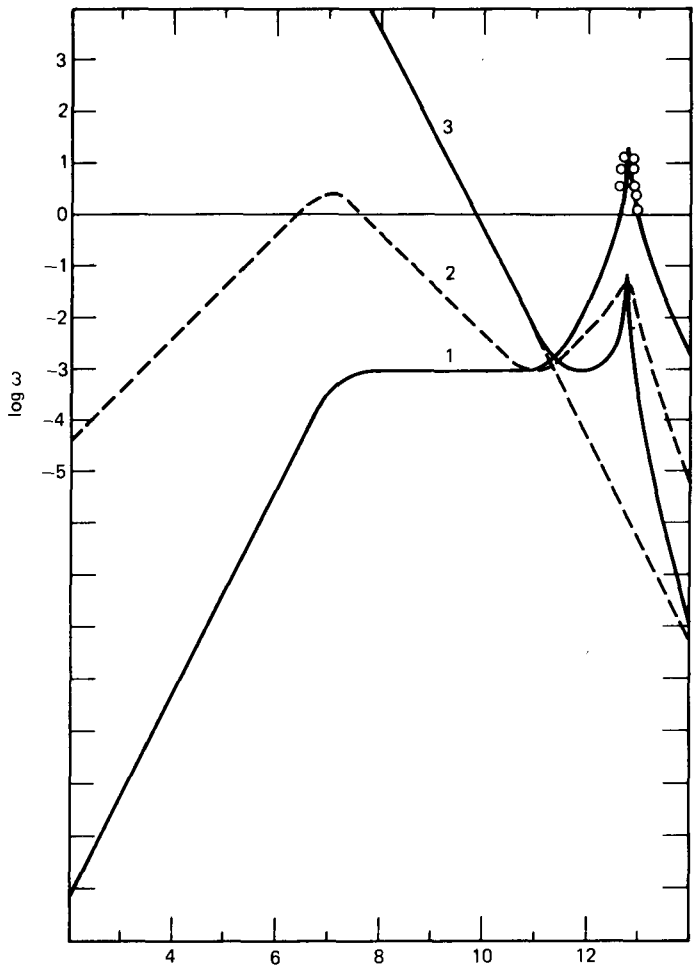

Figure 3.3.4.1 A schematic of (1) $\mathfrak{A}(\omega)$, the power absorption coefficient (in Np/cm), (2) the dielectric loss $\epsilon''(\omega)$, and (3) $\epsilon''(\omega)/\omega$, (approximately the intensity of depolarized, scattered light) over about eight decades of frequency. [Reproduced by permission from C. J. Reid and M. W. Evans, *J. Chem. Soc. Faraday Trans. II*, **75**, 1213 (1979).]

$\epsilon''(\omega)$ contain the same information, but weight different frequency regions rather heavily, so that it is *essential* to plot both when attempting to obtain an overall view of the dynamical evolution.

Note that Eqs. 3.3.4.5 and 3.3.4.6 are valid only when we may neglect completely the internal, or reaction, field correction, when the macroscopic sample is spherical, and when dynamical cross correlations are vanishingly small, that is, in a dilute solution of weakly polarizable molecules in a nondipolar medium at a relatively low molecular number density (Coffey and

Vij, 1982). It is worth noting that the quantum mechanical version* of Eq. 3.3.4.6 *under these conditions* is (Gordon, 1965)

$$\epsilon''(\omega) = \frac{\pi N}{3\hbar v \epsilon_0}(1 - e^{-\hbar\omega/kT})\,\mu^2 \tilde{C}_u^{qm}(\omega) \tag{3.3.4.8}$$

where $C_u^{qm}(t)$ is the nonsymmetrical quantum mechanical a.c.f. Alternatively, if one prefers the symmetrical correlation function,

$$\hat{C}_u(t) = \tfrac{1}{2}\langle \hat{u}(t)\cdot\hat{u}(0) + \hat{u}(t)\cdot\hat{u}(0)\rangle$$

then

$$\epsilon''(\omega) = \frac{N^2\mu^2}{3\hbar v\epsilon_0}\tanh\left(\frac{\hbar\omega}{2kT}\right)\int_{-\infty}^{\infty} e^{i\omega t}\,\hat{C}_u(t)\,dt$$

If the correlation function in the integrand is replaced by its classical equivalent then we obtain the *first-order quantum correction* for the classical spectral profile.

3.4 THE INTERNAL FIELD

Consider now the case of a dielectric sample consisting of weakly dipolar but polarizable molecules in a nondipolar but polarizable solvent. Let n^2 be the permittivity (or square of the refractive index) at a frequency which is very rapid compared with the orientational velocity of the molecules, but negligibly small compared with those of intramolecular vibrations. Generally speaking, we may take n^2 at about 50 to about 300 cm^{-1} in the far infrared. If the molecules are only weakly dipolar and if the vectors μ_i are mutually independent, $\epsilon'(\omega)$ will be only slightly greater than n^2. Taking account of the Maxwell relations (Scaife, 1972),

$$\epsilon(\omega) = n_c(\omega)^2 \equiv [n(\omega) - ik(\omega)]^2$$

$$\mathfrak{A}(\omega)\dagger = \frac{2\omega k(\omega)}{c} \tag{3.4.1}$$

then

$$\frac{\epsilon'(\omega) - n^2}{\epsilon_s - n^2} \doteq 1 - \omega\int_0^{\infty} C_u(t)\sin\omega t\,dt \tag{3.4.2}$$

Note that the square of the refractive index, n^2, differs from the permittivity ϵ_∞ defined by the Debye theory (see Figs. 1.1.1 and 1.1.2). The difference $\epsilon_\infty - n^2$ was first used by Poley in 1955 to predict the characteristic far infrared absorption band of all dipolar molecules in the liquid, plastic, and related phases of matter. Some values of ϵ_∞ and n^2 are tabulated in Table 3.4.1.

*M. K. S. units are used.

†$\mathfrak{A}(\omega)$ is often denoted in the literature as $\alpha(\omega)$. We retain the notation $\mathfrak{A}(\omega)$ in order to avoid confusion with the polarizability.

Table 3.4.1 Comparison of Dipole Moments from Microwave (μ_{ons}) and Far-Infrared Data (μ_z)

Liquid	ϵ_s	n_{ir}^2 (at $\bar{\nu}$ = 100 cm^{-1})	$\epsilon_\infty - n_{ir}^2$ experimental	ϵ_∞	$\epsilon_s - n_{ir}^2$	$10^{30}\mu_{ons}$ (C m)	10^{20} xA_1/N (cm)*	A_2	$10^{30}\mu_z$ (C m)	$10^{30}\chi$ $(\mu_z - \mu_{ons})$ (C m)*	$10^{30}\chi$ μ_{gas} (C m)*
1,1,1-Trichloroethane	7.11				4.65	6.17	24.1	7.3	6.34	0.17	5.94
t-Butyl chloride	9.87				11.5	7.84	54	18.1	7.87	0.03	7.10
2,2-Dichloro propane	11.5			2.3	9.49	7.74	44.5	14.9	7.61	−0.10	7.57
2-Chloro-2-nitro-propane	24.0			3.0		12.44	100		12.38	−0.07	
Chloroform	4.806			2.22		4.00	15.4		4.30	0.30	3.37
Chlorobenzene	5.60	2.22	0.23	2.55	3.37	5.00	14.1	5.30	6.30	1.30	5.64
Bromobenzene	5.39					4.34	8.6		6.94	2.54	5.67
Iodobenzene	4.64					3.60	4.9		6.90	3.30	5.67
o-Difluorobenzene						8.01	35.8		9.04	1.03	
o-Dichlorobenzene						7.54	22.3		8.91	1.37	8.34
o-Dibromobenzene						7.14	16.8		9.57	2.44	
m-Difluorobenzene						5.27	28.3		5.94	0.67	5.27
m-Dichlorobenzene						4.97	15.5		5.84	0.87	5.74
m-Dibromobenzene						5.20	12.2		6.24	1.03	
Toluene	2.3837	2.211	0.056	2.2670		1.28	9.1		3.17	1.90	1.20
Benzonitrile	25.57	2.27	1.48	3.85	25.2	12.14	107	39.6	16.34	4.54	13.94
SO_2/cyclohexane						5.37	316		6.04	0.67	5.44
Bromoethane	9.20					6.10	43		7.61	1.50	6.77

*$\chi = 9n_{ir}/(n_{ir}^2 + 2)^2$. Temperature = 296°K except where stated.

The small differences $\epsilon_\infty - n^2$, when translated into dynamical terms, represent the Debye plateau phenomenon of Chapters 1 and 2.

Consider now the dielectric to be composed of undiluted strongly dipolar molecules which are polarizable. Each molecular dipole polarizes its neighbors, which in turn react. As we have already pointed out, there is no general method formulated yet of relating $\mathfrak{A}(\omega)$ to $C_u(t)$. Most of the theories developed to deal with this problem contain some kind of strong assumption that restricts their validity. A careful discussion of the problem is available in a volume edited by Scaife (1971) and in articles by Brot (1975) and Deutch (1976). Greffe et al. (1973) have made a numerical comparison of the various theories and according to them the results are not significantly different. Recently (see Appendix) the technique of molecular dynamics simulation has shed some light on the problem. In this section we illustrate the difficulties of the problem by considering the Onsager model in the dynamic case. We adhere closely to a treatment given by Scaife (1964, 1966, 1971).

3.4.1 Frequency Dependence in Onsager's Model

For clarity we recall the main points of the Debye theory. The molecule is regarded as a small sphere situated in a spherical cavity in a dielectric medium. The *surroundings* are described in terms of the *macroscopic* dielectric properties of the medium. The sphere containing the dipole is not assumed to interact with its neighbors. This leads to the formula (in the usual notation)

$$\epsilon(\omega) - 1 = \frac{\epsilon(\omega)+2}{3}\frac{N}{\epsilon_0 v}\frac{\mu^2}{3kT}\frac{1}{1+i\omega\tau_\mu} \qquad \tau_\mu = \frac{\zeta}{2kT} \tag{3.4.1.1}$$

where τ_μ is the relaxation time associated with the dipole carried in the sphere. Aside from any consideration of inertial effects this formula is deficient in two most important ways:

1. The formula for the static permittivity, namely,

$$(\epsilon_s - 1) = \left(\frac{\epsilon_s + 2}{3}\right)\frac{N}{\epsilon_0 v}\frac{\mu^2}{3kT}$$

   is not in agreement with experiment.

2. Equation 3.4.1.1 does not allow for a *distribution* of *macroscopic relaxations*. This is because we may write from Eq. 3.4.1.1 the explicit formula

$$3v\epsilon_0\frac{\epsilon(\omega)-1}{\epsilon(\omega)+2} = \frac{N\mu^2}{3kT}\frac{1}{1+i\omega\tau_\mu} \tag{3.4.1.2}$$

   which clearly shows that the *macroscopic* dielectric relaxation process is characterized by a *single* relaxation time.

Onsager, as we have seen, removed the first defect in 1936 by showing that the correct cavity field should be

$$\mathbf{G} = \frac{3\epsilon_s \mathbf{E}}{2\epsilon_s + 1}$$

and not

$$\frac{(\epsilon_s + 2)\mathbf{E}}{3}$$

(where $\mathbf{E}$ is the field in the dielectric outside the cavity). The resulting equation

$$\epsilon_s - 1 = \frac{3\epsilon_s}{2\epsilon_s + 1}\frac{N}{\epsilon_0 v}\frac{\mu^2}{3kT}$$

(displacement polarization is ignored for convenience) gives reasonable agreement with experiment. It is also exact for the Debye model. Let us suppose that we retain Debye's value for τ_μ but use Onsager's expression for the local field; then the last equation becomes

$$\epsilon(\omega) - 1 = \frac{3\epsilon(\omega)}{2\epsilon(\omega)+1}\frac{N}{\epsilon_0 v}\frac{\mu^2}{3kT}\frac{1}{1+i\omega\tau_\mu} \tag{3.4.1.3}$$

Equation 3.4.1.3 now clearly shows that $\epsilon(\omega)$, the macroscopic permittivity, can no longer be described by a *single* macroscopic relaxation time in accordance with experiment. One might think at this stage that Eq. 3.4.1.3 represents *without any further investigation* the generalization of Onsager's equation to the frequency-dependent case. This is not so, as the following discussion will show. Let us consider, following Onsager (1936) and Scaife (1971), the dipole in a cavity in a polar dielectric medium. The field acting on the dipole at any time t is

$$\mathbf{F}(t) = \mathbf{G}(t) + \mathbf{R}(t)$$

where $\mathbf{G}(t)$ is the cavity field arising from the impressed electric field in the dielectric outside the cavity and $\mathbf{R}(t)$ is the reaction field arising from interaction of the dipole $\boldsymbol{\mu}$ with its surroundings. The Euler–Langevin equation for the motion of $\boldsymbol{\mu}$ (considered as a sphere) is (Chapter 2):

$$I\frac{d\boldsymbol{\omega}}{dt} + \zeta\boldsymbol{\omega} - \boldsymbol{\mu}\times\mathbf{F} = \boldsymbol{\lambda}(t) \tag{3.4.1.4}$$

where as usual $\boldsymbol{\lambda}(t)$ is the white noise driving torque arising from the Brownian movement of the surroundings. I is the moment of inertia of $\boldsymbol{\mu}$. In view of the formidable calculations associated with the spherical model even in the absence of dipole–dipole coupling, we specialize the three-dimensional equation above to the case of the two-dimensional rotator so that it reduces to

$$I\ddot{\theta} + \zeta\dot{\theta} - \mu F(t)\sin(\psi - \theta) = \lambda(t) \tag{3.4.1.5}$$

Further, we set $I = 0$ so that our final equation reads

$$\zeta\dot{\theta} - \mu F(t)\sin(\psi - \theta) = \lambda(t) \tag{3.4.1.6}$$

In Eq. 3.4.1.6 $F(t)$ is, as before, the electric field acting on $\boldsymbol{\mu}$, ψ is the angle between $F(t)$ and a particular direction, and θ is the angle between this direction and that of the dipole. Even with the simplification that $I = 0$ it is impossible to calculate exactly the mean dipole moment from Eq. 3.4.1.6. This is because Eq. 3.4.1.6, owing to the term in $F(t)$, contains the complex permittivity $\epsilon(\omega)$, which is proportional to the Fourier transform of the quantity we are trying to calculate. Scaife (1964, 1966) postulated a way out of this difficulty by making the observation that a dipole $\boldsymbol{\mu}$ rotating with uniform angular velocity $\dot{\theta}$ about an axis through its center creates a rotating reaction field which, if the surrounding medium is not loss free, lags behind the dipole. This field may be resolved into two components: $\mu g'(\dot{\theta})$ parallel to the dipole and $\mu g''(\dot{\theta})$ perpendicular to the dipole. This latter field produces a torque $\mu^2 g''(\dot{\theta})$ on the dipole that tends to slow it down. Thus on Scaife's suggestion Eq. 3.4.1.6 is to be replaced by the expression

$$\zeta\dot{\theta} + \mu^2 g''(\dot{\theta}) = \lambda(t) \tag{3.4.1.7}$$

where

$$g(\dot{\theta}) = g'(\dot{\theta}) - ig''(\dot{\theta}) = 2\left(\frac{\epsilon(\dot{\theta}) - 1}{2\epsilon(\dot{\theta}) + 1}\right)\frac{N}{3v\epsilon_0} \tag{3.4.1.8}$$

Further, if $\dot{\theta}$ is small Eq. 3.4.1.7 may be written in the *linear* form

$$6\mu^2\frac{\epsilon'(0) - 1}{(2\epsilon'(0) + 1)^2}\left(\frac{N}{3v\epsilon_0}\right)\bar{\tau}_m\dot{\theta} = a\theta$$

say, where

$$\bar{\tau}_m = \frac{1}{\epsilon'(0) - 1}\left(\frac{\partial\epsilon''(\omega)}{\partial\omega}\right)_{\omega=0}$$

This immediately leads (with the aid of Eq. 3.4.1.7 and the properties of $\lambda(t)$) to the following generalization of Onsager's equation:

$$\epsilon(\omega) - 1 = \frac{3\epsilon(\omega)}{2\epsilon(\omega) + 1}\frac{N}{v\epsilon_0}\frac{\mu^2}{3kT}\frac{1}{1 + i\omega\tau'_\mu} \tag{3.4.1.9}$$

in which the Debye *microscopic* relaxation time τ_μ in Eq. 3.4.1.1 is replaced by

$$\tau'_\mu = \tau_\mu + \frac{[\epsilon'(0) - 1]^2\bar{\tau}_m}{\epsilon'(0)[2\epsilon'(0) + 1]} \tag{3.4.1.10}$$

In reviewing the derivation of Eq. 3.4.1.9 we have assumed that displacement polarization may be neglected, that is

$$\epsilon_\infty = 1$$

Scaife (1964) and later Fatuzzo and Mason (1967) included the effect of displacement polarization in their calculations. The results of both calcalculations reduce to Eq. 3.4.1.9 when $\epsilon_\infty = 1$. If $\epsilon_\infty \neq 1$ Eq. 3.4.1.9 becomes

$$\frac{[\epsilon(\omega) - \epsilon_\infty][2\epsilon(\omega) + 1][2\epsilon^*(\omega) + \epsilon_\infty]}{3\epsilon(\omega)[2\epsilon^*(\omega) + 1]} = \frac{N\mu^2}{3kTv\epsilon_0}\frac{(\epsilon_\infty + 2)^2}{9}\frac{1}{1 + i\omega\tau'_\mu} \tag{3.4.1.11}$$

$$\tau'_\mu = \tau_\mu + \frac{[\epsilon'(0) - \epsilon_\infty]^2\bar{\tau}_m}{\epsilon'(0)[2\epsilon'(0) + \epsilon_\infty]} \tag{3.4.1.12}$$

in which $\epsilon^*(\omega)$ denotes the complex conjugate of $\epsilon(\omega)$. Thus the effect of the surroundings immediately alters the microscopic relaxation time. Equations 3.4.1.9 ff. are as far as we can go toward generalizing the Onsager model to the frequency-dependent case. This is entirely due to the mathematical difficulties associated with the nonlinear equation (Eq. 3.4.1.5). In particular, it should be noted that Eqs. 3.4.1.9 ff., although producing a *distribution* of *macroscopic* relaxation times, merely predict a *single microscopic* relaxation time. For as far as Eq. 3.4.1.9 is concerned, the indication is that dipole–dipole coupling only gives rise to a shift in the microscopic relaxation time. This is at variance with the results obtained from calculations of Budó (1949) and Zwanzig (1963). In view of the difficulties associated with the generalization of even the simple Onsager model we are more or less thrown back on the Debye theory in order to obtain any relationship between the absorption coefficient and the single dipole correlation function.

3.4.2 The Relation between $\mathfrak{A}(\omega)$ and $\epsilon''(\omega)$ from the Debye Theory

Assuming that the Debye theory holds (this may be approximately true for dilute solutions), we may write

$$\epsilon'(\omega) - 1 = \frac{N\mu^2}{3kT}\frac{1}{v\epsilon_0}\left[1 - \omega\int_0^\infty C_u(t)\sin\omega t\,dt\right] \tag{3.4.2.1}$$

$$\epsilon''(\omega) = \frac{N\mu^2}{3kT}\frac{\omega}{v\epsilon_0}\int_0^\infty C_u(t)\cos\omega t\,dt \tag{3.2.4.2}$$

$$\mathfrak{A}(\omega) = \frac{2\omega\epsilon''(\omega)}{c} \tag{3.4.2.3}$$

$$\frac{c\mathfrak{A}(\omega)}{\omega} = \frac{N\mu^2\omega}{3kT\epsilon_0 v}\int_0^\infty C_u(t)\cos\omega t\,dt \tag{3.4.2.4}$$

$$C_u(t) = \frac{2}{\pi}\frac{3kTv\epsilon_0 c}{N\mu^2}\int_0^\infty\frac{\mathfrak{A}(\omega)}{\omega^2}\cos\omega t\,d\omega \tag{3.4.2.5}$$

In terms of the wave number $\bar{\nu} = \lambda^{-1}$, this is

$$C_u(t) = \frac{3kT\epsilon_0 v}{\pi^2 N\mu^2} \int_0^\infty c \frac{\mathfrak{A}(\bar{\nu})\cos 2\pi\bar{\nu} ct\, d\bar{\nu}}{\bar{\nu}^2} \qquad (3.4.2.6)$$

Equation 3.4.2.5 may also be written in terms of the second derivative of C_u as

$$-\ddot{C}_u(t) = \frac{2}{\pi}\frac{3kTv\epsilon_0}{N\mu^2} c \int_0^\infty \mathfrak{A}(\omega)\cos \omega t\, d\omega \qquad (3.4.2.7)$$

This is the relationship between the *single* dipole correlation function and the absorption coefficient on the basis of the Debye theory. It has been the practice to write instead of $C_u(t)$ in Eq. 3.4.2.7

$$C_u(t) = \left\langle \mathbf{u}_1(0) \cdot \sum_{i=1}^{N} \mathbf{u}_i(t) \right\rangle = g(t)$$

where $g(t)$ is the dynamic analogue of the Kirkwood–Fröhlich g factor. Clearly this expression can be true only if we neglect entirely all cross correlations between dipoles. Also in practice Eq. 3.4.2.6 is written

$$\frac{3kT\epsilon_0 v}{N\mu^2\pi^2}\left(\frac{9n}{(n^2+2)^2}\right) c \int_0^\infty \frac{\mathfrak{A}(\bar{\nu})\cos 2\pi\bar{\nu}ct\, d\bar{\nu}}{\bar{\nu}^2}$$

where the parentheses enclose the Polo–Wilson nondispersive correction (Davies, 1971).

3.4.3 An Approximate Expression for $\ddot{g}$ in Terms of the Absorption Coefficient

Brot (1975), using cavity theories, has derived various expressions for the dynamic g factors which in the far infrared region [where $\epsilon'(\omega)$ is of the order of n^2 (Table 3.4.1) and where $\epsilon''(\omega)^2$ is small with respect to $\epsilon'(\omega)^2 \doteqdot n^2$ and thus is approximately constant] reduce to:

$$-\ddot{g}(t) \doteqdot \frac{2}{\pi}\frac{3kTv\epsilon_0}{N\mu_v^2}\left(\frac{3}{n^2+2}\right)^2 nc \int_0^\infty \mathfrak{A}(\omega)\cos \omega t\, d\omega \qquad (3.4.3.1)$$

This appears to be a good approximation in liquids in the far infrared region and has been used in Fig. 1.3.1.3. It is the same as Eq. 3.4.2.7 derived from the Debye theory. It is not a good approximation at long times (low frequencies), but in this region $-\ddot{g}(t)$ is in any case very small. *By using the far infrared power absorption coefficient $\mathfrak{A}(\omega)$, not only is there a great deal of information obtained about the molecular dynamics, but also the problems of cavity theory are minimized.* The problem still remains, however (just as in the static case), of relating the multimolecular correlation function $g(t)$ (or its second derivative) to the single molecule autocorrelation function $C_u(t)$.

3.4.4 Collective Motions and Computer Simulations

The correlation function $g(t)$ contains the cross correlations produced both by short range forces (e.g., higher multipoles, anisotropy of repulsive forces) and by the dipolar forces in the "inner sphere." It is through the latter that such phenomena as tendency to antiferroelectricity (i.e., to antiparallel arrangement of the molecules at low temperature) may be accounted for. The Onsager formula makes the static dielectric constant increase at low temperatures but a simulation of $g(0)$ or $g(t)$ by molecular dynamics and Monte Carlo methods (Brot and Darmon, 1971) may often yield a $g(0)$ or $g(t)$ whose magnitudes are well below unity at low temperatures. This is the case in disordered molecular crystals, such as the hexasubstituted benzenes, which are constrained to librate about an axis perpendicular to the plane of the benzene rings. A detailed semistochastic Monte Carlo simulation of such a system has been carried out by Brot and Darmon (1971) and compared with the results of dielectric spectroscopy on the same system. In order to carry out such calculations the Boltzmann factor relevant to each configuration must be known, that is, the change of energy that figures in each time step of the Monte Carlo simulation. This involves the energy of the configuration within the inner sphere together with the interaction energy with the outer continuum. The proper manner of accounting for this interaction energy depends on the representation adopted for the outer continuum. The energy within the inner sphere is easier to calculate, because it is equal to the sum of the mutual energy of pairs of nonpolarizable dipoles embedded in a medium of dielectric permittivity n^2. However, in any real liquid the contribution to the energy due to short range forces must be added. Direct comparison of $g(t)$ with its single-particle equivalent is possible from an experiment such as that illustrated for CH_2Cl_2 in Fig. 3.4.4.1, where the effect of dilution is marked. In dilute solution the $\mathfrak{A}(\omega)$ spectral profile is a good approximation to $C_u(t)$ although vortex effects, for example, could still be transmitted through the solvent molecules. Wolynes and Deutch (1977) have recently discussed such long ranged effects in the context of rototranslation motion.

The semistochastic Monte Carlo simulation of Brot and Darmon is a fine example of how this technique may be used to monitor the progressive orientational decorrelation in a well defined dipolar system as the temperature is raised. It illustrates the techniques developed in this chapter and we recount it here in some detail. In these systems (which are strongly dipolar chloromethyl hexasubstituted benzenes) the molecules exhibit a one-axis sixfold disorder at high temperatures. The static permittivity ϵ_s decreases on cooling, indicating the development of orientational order, that is, of significant cross correlation. The energy that governs the ordering is essentially electrostatic in origin, and antiferroelectric. Using an intermolecular potential consisting of Coulomb interactions between the atoms of each molecule, Brot and Darmon carried out a dynamic simula-

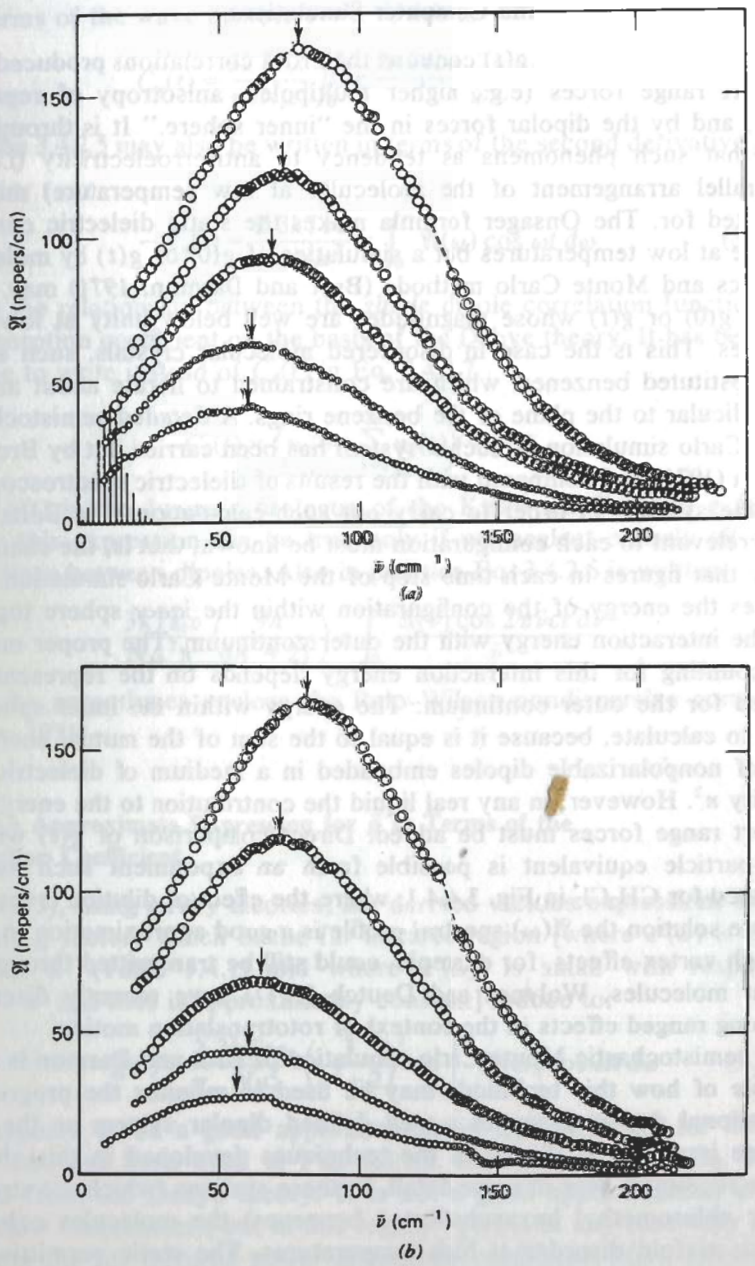

Figure 3.4.4.1 (*a*) Absorption of dichloromethane in CCl_4 at 298°K, corrected for solvent absorption. From top to bottom: pure CH_2Cl_2 ($N = 9.4\times10^{21}$, 7.22×10^{21}, 4.93×10^{21}, 3.25×10^{21}, and 1.97×10^{21} molecules/cm^3. (*b*) The same in decalin. The stick spectrum represents some $J\rightarrow J+1$ ($\Delta K = 0$) lines for quantized free rotation of CH_2Cl_2, an accidental near-symmetric top. [Reproduced by permission from M. W. Evans et al., *J. Chem. Soc. Faraday Trans. II* **74**, 2143 (1978).]

tion of the complex permittivity over a range of temperatures, obtaining quite good agreement with the dielectric results. The rotational freedom remaining to these molecules in the crystalline condition is temperature dependent via *higher-order thermodynamic transitions*, which means that there is a progressive evolution of cooperative effects. The system is therefore well adapted for the study of dipole cross correlations. Figure 3.4.4.2 illustrates the arrangement of the molecules in trichlorotrimethylbenzene at high and low temperatures. The orientational freedom arises from the molecules being sterically very symmetrical. The heights of the barriers between allowed orientations may be associated with the dielectric *activation enthalpy*, which is shown in Fig. 3.4.4.3 as a plot of reciprocal temperature against the peak of the low frequency dielectric loss $\epsilon''(\omega)$. (Note that this peaks again in the far infrared.)

The onset of orientational ordering in TCTMB and DCTMB (1,2-dichloro-3,4,5,6-tetramethylbenzene) may be monitored by X-ray analysis. At 300°K each chlorine or methyl group is distributed with equal probability among six substituent sites. However, as the temperature is decreased an ordered "superstructure" sets in *reversibly*. The molecular centers and orientation of the aromatic planes remain the same as in the structure at 300°K, but the dipoles are antiparallel along the crystal axes *b* and *c*, and parallel along *a*. This structure is termed antiferroelectric (Fig. 3.4.4.2). The superstructure appears as *domains* with noncorresponding families of molecules. There is no fundamental change of structure such as that which occurs in the *plastic crystals* where *first-order* thermodynamic transitions are observable. In the disk-like benzene derivatives the molecules occupy only those orientations corresponding to their own steric symmetry. Since the volume of each substituent group is very nearly the same, no volume increase with respect to the ordered phase occurs when a chlorine is

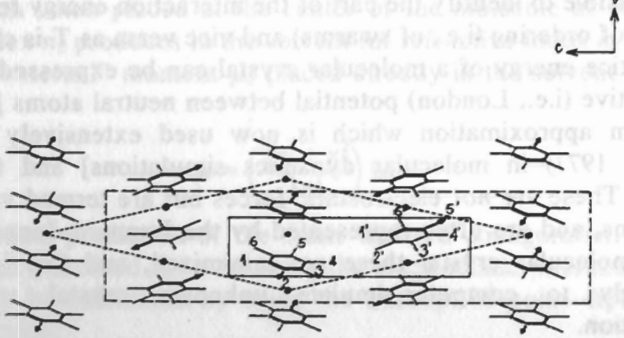

Figure 3.4.4.2 Crystal structures of TCTMB. Solid line: high temperature unit cell $P2_1/c$, $Z = 2$ (suppress the arrows). Dashed line: low temperature pseudo-monoclinic cell, $Z = 8$. Dotted line: low temperature crystallographic unit cell PT, $Z = 2\times2$. [Reproduced by permission from C. Brot and I. Darmon, *J. Chem. Phys.* **53**, 2271 (1970).]

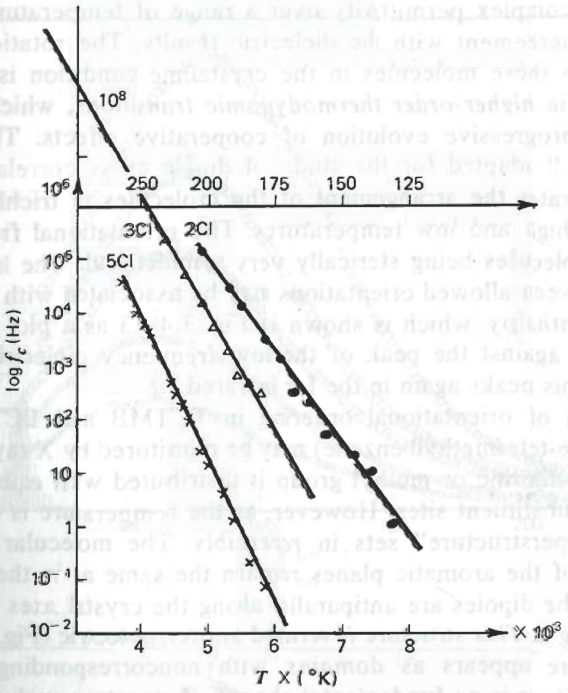

Figure 3.4.4.3 Logarithms of dielectric critical frequencies versus reciprocal temperature. Enthalpies of activation. ● $E' = 7.7$ kcal/mole; △ $E' = 10.2$ kcal/mole; × $E' = 12.1$ kcal/mole. [Reproduced by permission from C. Brot and I. Darmon, *J. Chem. Phys.* **53**, 2271 (1970).]

replaced by a methyl and vice versa. Eliminating the volume change eliminates the *discontinuity* in the cohesive (or attractive) energy associated with a *first-order* thermodynamic transition.

It is possible to identify the part of the interaction energy responsible for the onset of ordering (i.e., of swarms) and vice versa as T is changed. Most of the lattice energy of a molecular crystal can be expressed by summing the attractive (i.e., London) potential between neutral atoms [the so-called atom–atom approximation which is now used extensively (Streett and Tildesley, 1977) in molecular dynamics simulations] and the repulsive potential. These are *not* electrostatic forces but are termed van der Waals interactions, and are often represented by the Lennard-Jones form. In an ordered molecular crystal these are minimized, and this is being used increasingly to computer-simulate unknown crystal structures by extrapolation.

The electrostatic energy (e.g., dipole–dipole, or quadrupole–quadrupole) is usually relatively small in comparison, *but* when the van der Waals forces impose several almost equivalent *potential wells* (as in sterically symmetrical molecules), the electrostatic part of the overall potential

energy becomes important and *governs the orientational transition*. This is because the governing factor is the *difference* in energy between the wells. The van der Waals energy differences between Cl—Cl, Cl—CH_3, and CH_3—CH_3 pairs in neighboring molecules is <60 cal/mole at the equilibrium separation, whereas for the Cl—Cl and CH_3—CH_3 pairs (assumed to carry a net charge), the Coulomb potential amounts to 1760 cal/mole.

The calculation of the electrostatic energy must be made by taking into account both the permanent charge of the molecules and their *polarizability*. Two approaches are used by Brot and Darmon: (1) the "molecular" method, which treats the molecules as distinct entities in the crystal, and then calculates the interaction energy between their charges and the polarization energy, and (2) the continuum method, which considers the crystal as a polarizable continuum in which permanent charges are immersed.

The *absolute* electrostatic energy in the crystal may be calculated in principle using method 1, but for nonspherical molecules the potential equation cannot be solved. Also, because the molecules are anisotropic and larger than the spatial variations of the local electric fields, the approximation of a single molecular *scalar* polarizability is very rough. The second method is easier because one can use the electrostatic formulas for a material medium, provided the electric charges (or alternatively, multipole moments) are chosen correctly. This method automatically includes the polarization but the absolute value of the electrostatic energy is not defined. However, only differences in potential energy are of interest, and the latter method was adopted by Brot and Darmon.

The charges to be immersed in the medium must induce the same field as a molecule inserted in a "cavity" of the continuum. We wish to construct a spatial arrangement of dipoles μ surrounded by molecular volumes of refractive index n_2, which may be approximated by using the same dipoles μ immersed in a continuum of refractive index n_2. Here μ is a rigid dipole moment which when placed at the center of the molecule of solute with refractive index n_2 produces in the solvent (of refractive index n_1) the same field as the "external" moment μ_e placed directly in the solvent (Fröhlich, 1958), that is,

$$\mu = \left(\frac{2n_1^2 + n_2^2}{3n_1^2}\right)\mu_e$$

The theoretical prediction of the *static* ordered configuration may now proceed, given a method for evaluating the electrostatic interaction potential. This may be calculated by using the concept of point-dipole–point-dipole interaction:

$$E_1 = \frac{1}{2}\frac{\mu^2}{n_2^2}\sum_m \left(\frac{\mathbf{u}_0 \cdot \mathbf{u}_m}{r^3} - \frac{3(\mathbf{u}_0 \cdot \mathbf{r})(\mathbf{u}_m \cdot \mathbf{r})}{r^5}\right)$$

Here $\mathbf{u}_m$ and $\mathbf{u}_0$ are unit vectors along the dipole m and the reference

dipole, respectively, and **r** is the vector joining them; n_2^2 is the high frequency permittivity of the crystal (i.e., the square of the refractive index at about 200 cm^{-1}). This, and *not* the static permittivity ϵ_s, should be used because we are computing the energy of independent, (supposedly) fixed, configurations in the static case. If the same expression is taken for the second molecule in the unit cell, and the half-sum of the two r's taken, then this gives the energy per molecule in the superstructure (or domain) under consideration. Brot and Darmon perform the lattice sum up to a cutoff radius sufficient to ensure a convergence of better than 0.5%. It is found that this method does *not* ultimately give the correct stable configuration at low temperature. This is because the dipolar character of each molecule is distributed among several atoms which are localized far from the molecular center.

To improve the calculation there is a choice between a multipole expression (see Chapter 11) and a direct evaluation of the Coulomb energy between *discrete charges* correctly localized on the molecule. The latter is much more straightforward to carry out for molecules of relatively low symmetry. The total molecular dipole moment is decomposed into bond moments, taking into account mesomeric and induction effects. In the continuum approach these are scaled by the factor μ/μ_v where μ_v is the dipole moment of the isolated molecule in a vacuum. The Coulomb interaction energy is for a reference molecule:

$$E_1 = \frac{1}{2}\frac{(\mu/\mu_v)^2}{n_2^2}\sum_m \sum_{i,j} \frac{q_i q_{jm}}{r_{ijm}} \qquad (3.4.4.1)$$

where i and j refer to atoms in the reference molecule and in molecule m, respectively. The electrostatic energy per molecule is then the half-sum of this expression computed for the two molecules in the *high temperature* unit cell. This was computed for 288 separate configurations. The one with minimum energy is precisely that which may be observed by X-ray crystallography at low temperature. This configuration is fourfold degenerate because of the symmetry of the domain superstructure.

The mean interaction energy in the disordered phase was calculated along the same lines using 400 randomly disordered configurations. The energy is positive, owing to the constraints imposed by molecular shapes, and not zero as in isotropic crystals, that is, the plastic rotator phases.

3.4.4.1 Monte Carlo Simulations, Static and Dynamic Correlations

There are many textbooks and reviews available on the Monte Carlo technique (see Brot and Darmon, 1970, 1971) whose purpose is to estimate the Boltzmann average of the parameters of an interacting system by randomly generating representative, correctly weighted states of the system. The method may be illustrated by the use to which it is put by Brot and Darmon in computing the mean electrostatic energy of the TCTMB

crystal and also its mean electric moment. The method is usually regarded as applicable to equilibrium properties, but with a few small changes the dipole correlation function may also be simulated. This method represents one of the most powerful ways we have at present of dealing with the long range dipole interactions in the condensed phase. It is to be hoped that the coming generation of faster computers will ease the economic problem of computer time, so that the method may be extended to liquids (as in the appendix of this chapter).

The Brot–Darmon calculation was made for a molecular block of 240 molecules with edges $6a$, $10b$, and $2c$ (where a, b, and c are the parameters of the monoclinic unit cell in the high temperature phase). The customary periodic boundary conditions of this technique were used. At a given temperature T some initial configuration is set up, either ordered or disordered, to which corresponds an energy E_i of the molecular block. Each molecule has a well-defined initial orientation $N_i (1 \leqslant N_i \leqslant 6)$. A molecule J is chosen at random, as is its final orientation N_f, after the jump (not necessarily into the adjacent potential well). The energy increment of the molecular system is now

$$\Delta E_{N_i \to N_f} = \sum_{M=1}^{12} [Q(M, N_f) - Q(M, N_i)] V(J, M)$$

where $V(J, M)$ is the potential created at each atomic site M of the molecule J by the 239 other molecules of the block, and $Q(M, N_f)$ and $Q(M, N_i)$ are the final and initial charges on the site M. If $\Delta E \leqslant 0$, the new orientation of the molecule becomes N_f and the total energy of the block $(E_i + \Delta E)$. If $\Delta E > 0$, a random number P between zero and one is generated and compared with $\exp(-\Delta E/kT)$. If $P \leqslant \exp(-\Delta E/kT)$, the new orientation N_f is accepted, but otherwise the molecule keeps its original position, N_i, and the system remains with energy E_i. If the trial is "successful", that is, the molecule has moved, the new potential is recomputed at each of the 239×12 undisturbed atomic sites. After each trial, whether successful or not, the total electric moment and energy of the block are recorded. After every few thousand trials, they are averaged. The convergence from both a completely ordered and a completely disordered starting point is shown in Fig. 3.4.4.1.1.

At low temperatures, when starting from the ordered phase which corresponds to the minimum energy, the molecules stay ordered in the relatively deep potential wells until about 80°K. At 50°K only about 1 in 10,000 of the trials produces movement, and this only to and fro from an adjacent well. These are "lattice defect" type transitions and the disorder is not cooperative. Figure 3.4.4.1.2 shows the variation with temperature of the mean square value of the total dipole moment of the block of $N = 240$ molecules divided by N times the square of the dipole moment. This factor g is defined as

$$gN\mu^2 = \langle M^2 \rangle = N\langle \boldsymbol{\mu} \cdot (\boldsymbol{\mu}_1 + \boldsymbol{\mu}_2 + \cdots + \boldsymbol{\mu}_N) \rangle$$

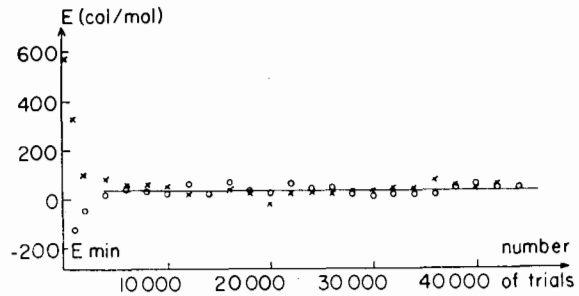

Figure 3.4.4.1.1 TCTMB. Convergence of the mean interaction energy starting the Monte Carlo calculation from ordered and disordered states. [Reproduced by permission from C. Brot and I. Darmon, *J. Chem. Phys.* **53**, 2271 (1970).]

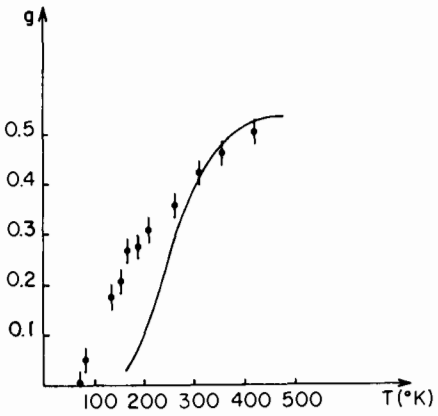

Figure 3.4.4.1.2 TCTMB. Kirkwood g factor. Solid line, experimental; ● computed, Monte Carlo simulation. [Reproduced by permission from C. Brot and I. Darmon, *J. Chem. Phys.* **53**, 2271 (1970).]

The experimental Kirkwood factor g is

$$g = \frac{\boldsymbol{\mu} \cdot \boldsymbol{\mu}^*}{\mu^2}$$

where $\boldsymbol{\mu}^*$ is the average of $\boldsymbol{\mu}$ (kept fixed in a certain direction) and all its neighbors.

To evaluate the correlation function of the total moment **M** a potential barrier which hinders the orientational jumps is introduced into the simulation. The frequency of trials is then given by the weighting factor of the Arrhenius *rate* equation:

$$f_c = A \exp\left(-\frac{V - E_i}{kT}\right)$$

where $V - E_i$ is the actual well depth of the molecule in the orientation i. The computation is carried out in the same way as in the static case, and the results are shown in Fig. 3.4.1.1.3. At high temperatures, owing to the

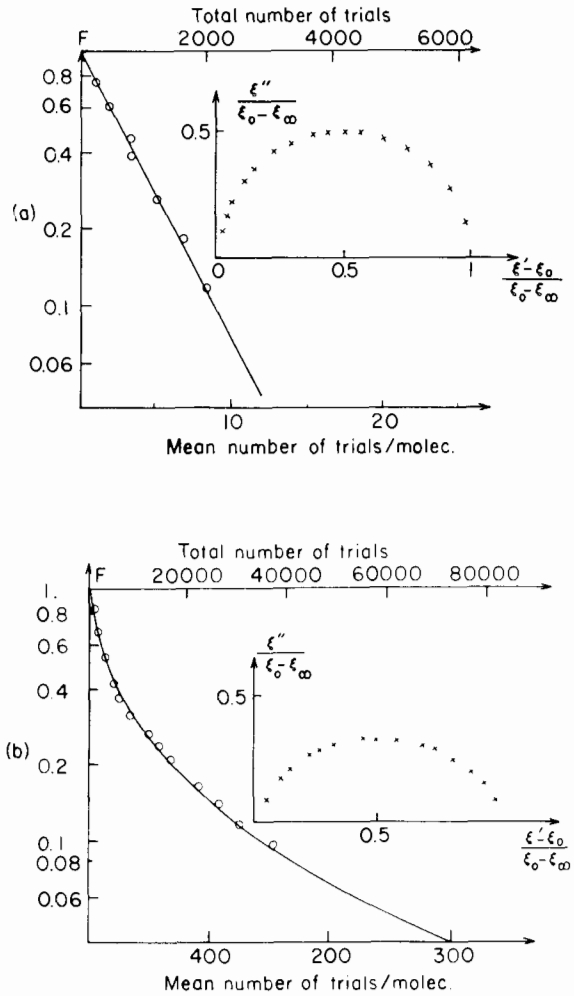

Figure 3.4.4.1.3 TCTMB. Dipolar correlation functions and Cole–Cole plots. Top, 300°K; bottom, 170°K. [Reproduced by permission from C. Brot and I. Darmon, *J. Chem. Phys.* **53**, 2271 (1970).] (Note ξ_0 in the figures above means ϵ_s.)

amount of orientational disorder in the neighboring molecules, the differences in depth of the potential wells cancel out and are $< kT$, producing a constant probability of making a jump. In consequence (Chapter 1), the correlation function,

$$F(t) = \frac{\langle \mathbf{M}(t_0) \cdot \mathbf{M}(t + t_0) \rangle}{\langle M(t_0)^2 \rangle}$$

is almost an exponential. At low temperatures the few disoriented molecules produce potential differences of opposite signs for different neigh-

bors, and there is a wide spread in the probability of making a jump. This produces a markedly nonexponential $F(t)$ (Fig. 3.4.1.1.3) and is an extreme example of the influence of cross correlations on the total correlation function. The agreement with dielectric measurements is good. This leads us to stress that the method used by Brot and Darmon may be used where the time scale of the molecular motions is too slow for the use of conventional molecular dynamics techniques.

3.4.4.2 A Diffusion Equation for the Motions of Interacting Dipoles

The solid-state lattice dynamics of TCTMB provide us with an opportunity to pursue an analytical solution by taking advantage of the simplifications offered by the fixed centers of mass. There can be no vorticity, but the solid will support phonon or shearing modes; these broaden the far infrared part of the loss. Let us assume that the center of mass of each molecule on a lattice is fixed and that they may interact *pairwise* via the site–site model of Brot and Darmon; then let us ask how well does the analytical model agree with either the experimental results or those of computer simulations? This is a question of fundamental importance because if pairwise interaction is not a close approximation in the disordered molecular solid state, then it is not so in the liquid state. Thus the only tractable method of dealing with the electrostatic interactions in a liquid of strongly dipolar molecules is simulation using large ensembles of molecules in order to circumvent the problem of the long range potentials.

In this section we take the TCTMB lattice and assume that the rotational motions of each molecule may be described by a Smoluchowski equation with a superimposed potential. This is made up of charge–charge interactions of a type given by Eq. 3.4.4.1, except that *the summation over m is neglected.* Pairwise interaction in this context thus means that nearest neighbor pairs of molecules are assumed to undergo a rotational motion locked together by a strong electrostatic interaction.

We may discuss the idea as follows. Let us choose for convenience an axis joining the centers of each benzene ring in the crystal lattice. In order to write the Smoluchowski equation (Chapter 2) for the variation in configuration space of the probability distribution function f associated with the orientation of the molecule under the influence of a time varying field, let us suppose as usual that each molecule experiences a frictional drag ζ_1 arising from the thermal energy of the surroundings. Further, let us denote by μ_1 and μ_2 the dipole vectors of each molecule. These remain in planes perpendicular to the axis of centers (axis 1). If we denote by V the intermolecular electrostatic potential (due to charge–charge Coulomb interactions), then the system is governed by the following differential equation (first derived by Budó in the context of a theory of dielectric relaxation of molecules containing rotating polar groups) for the variation in configuration space of f at time t after the sudden removal at $t = 0$ of a

unidirectional field of magnitude E:

$$\frac{\partial f}{\partial t} = \frac{kT}{\zeta_1}\left[\frac{\partial^2 f}{\partial \theta^2} + \cot\theta\,\frac{\partial f}{\partial \theta} + (1+\cot^2\theta)\left(\frac{\partial^2 f}{\partial \phi_1^2} + \frac{\partial^2 f}{\partial \phi_2^2}\right) + 2\cot^2\theta\,\frac{\partial^2 f}{\partial \phi_1 \partial \phi_2}\right]$$
$$+ \frac{\partial}{\partial \phi_1}\left(f\,\frac{\sin\theta}{\zeta_1}\,\frac{\partial V}{\partial \phi_1}\right) + \frac{\partial}{\partial \phi_2}\left(f\,\frac{\sin\theta}{\zeta_1}\,\frac{\partial V}{\partial \phi_2}\right) \qquad t > 0$$

The geometry for the derivation of this equation is illustrated in Fig. 3.4.4.2.1. The angles θ and ψ are polar angles which specify the direction of axis 1 relative to that of **E**, and ϕ_1 and ϕ_2 are the azimuthal angles of μ_1 and μ_2 measured from the plane containing **E** and axis 1. If we introduce the variables $\chi = (\phi_1 + \phi_2)/2$ and $\eta = (\phi_1 - \phi_2)/2$, the solution may be expressed in the form

$$f(\theta, \chi, \eta, t) = Ae^{-\beta V(2\eta)} \sum_{n=0}^{\infty} \sum_{m=0}^{n} [A_{nm} X_n^m(\theta, \chi) F_{nm}(\eta, t) + B_{nm} Y_n^m(\theta, \chi) G_{nm}(\eta, t)]$$

where

$$X_n^m(\theta, \chi) = P_n^m(\cos\theta)\cos m\chi; \qquad Y_n^m(\theta, \chi) = P_n^m(\cos\theta)\sin m\chi$$

are spherical harmonics and where the functions $F_{nm}(\eta, t)$ and $G_{nm}(\eta, t)$ are

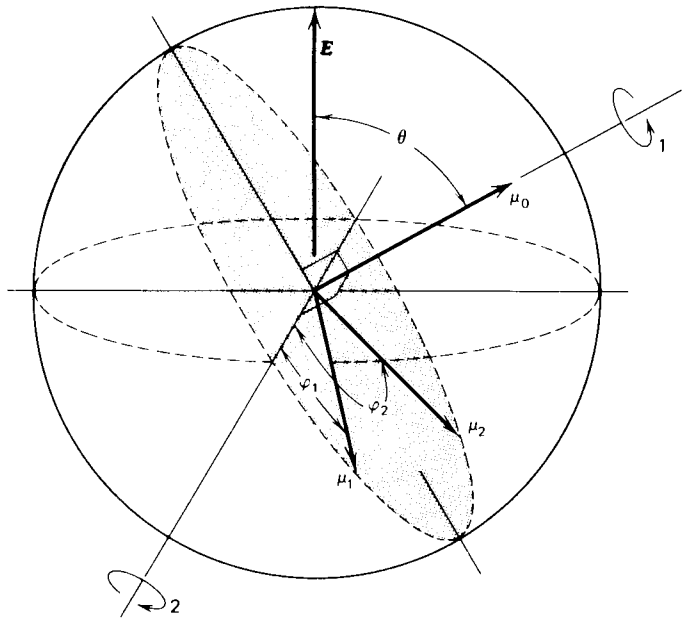

Figure 3.4.4.2.1 Schematic of dipole–dipole interaction, azimuthal and polar angles. [Reproduced by permission from W. T. Coffey, *Mol. Phys.* **37**, 437 (1979).]

to be determined. The initial condition is

$$f(\phi_1, \phi_2, \theta, 0) = A \exp[-\beta(\mu_1 \sin\theta \cos\phi_1 + \mu_2 \sin\theta \cos\phi_2)E - \beta V(\phi_1 - \phi_2)]$$

where $\beta = 1/kT$, and A is an irrelevant constant. The mathematical process of solution is lengthy. Basically the task is to calculate the eigenvalues λ and eigenfunctions $Z_\lambda(\eta)$ of the Sturm–Liouville equation (Coffey, 1979):

$$\frac{d^2 Z_\lambda(\eta)}{d\eta^2} - 2\phi(\eta)\frac{dZ_\lambda(\eta)}{d\eta} + \lambda Z_\lambda(\eta) = 0$$

Here, where $\phi(\eta) = V'(2\eta)/kT$. Given these, the complex polarizability is expressible as a summation over the spectrum of eigenvalues λ, namely:

$$\alpha(\omega) = \frac{\beta E}{3}\sum_\lambda \frac{J_\lambda}{1 + i\omega\tau_\lambda}$$

where:

$$J_\lambda = \sum_\lambda e^{-t/\tau_\lambda}\int_{-\pi}^{\pi} e^{-\beta V(2\eta)} Z_\lambda(\eta)[C_\lambda(\mu_1 + \mu_2)^2 \cos\eta + C'_\lambda(\mu_1 - \mu_2)^2 \sin\eta]\, d\eta$$

where

$$C_\lambda = \frac{\int_{-\pi}^{\pi} g(\eta) Z_\lambda(\eta)\cos\eta\, d\eta}{\int_{-\pi}^{\pi} g(\eta) Z_\lambda^2(\eta)\, d\eta}$$

$$C'_\lambda = \frac{\int_{-\pi}^{\pi} g(\eta) Z_\lambda(\eta)\sin\eta\, d\eta}{\int_{-\pi}^{\pi} g(\eta) Z_\lambda^2(\eta)\, d\eta}$$

and the weighting function $g(\eta)$ is defined by

$$g(\eta) = \exp\left[-2\int_0^\eta \phi(\eta_1)\, d\eta_1\right]$$

A first-order inertial correction is, for planar rotation (Coffey, 1980):

$$\alpha(\omega) = \frac{\beta E}{2}\sum_\lambda \frac{J_\lambda}{1 + i\omega\tau_\lambda - (\omega^2\tau_\lambda I/\zeta_1)}$$

where I is the molecular inertia component about an axis perpendicular to that of μ_1 or μ_2. The complex polarizability $\alpha(\omega)$ is related to the complex permittivity by the methods we have described in the earlier part of this chapter.

An extension of this treatment has been considered by Zwanzig (1963) using point dipoles placed on a rigid lattice, the interdipole field effects being represented by external torque terms in the Smoluchowski equation. The solution of the problem to *first order*, resulting in a second, faster relaxation mechanism in addition to the Debye relaxation. The appearance of

a second relaxation mechanism in Zwanzig's lattice is consistent to first order with the *infinite* number in the above equation for $\alpha(\omega)$, [whatever the form of $V(2\eta)$], where the relaxation times are inversely proportional to the eigenvalues of the Sturm–Liouville equation. Zwanzig's initial equation is a multidimensional Smoluchowski equation for the Brownian rotations, at the lattice sites, of dipoles in a rigid cubic lattice in a spherical sample in vacuo.

The theoretical conclusions of the above paragraph are bolstered somewhat by the experimental and Monte Carlo results for TCTMB (Fig. 3.4.4.1.3), which show a clear symmetric broadening at low temperatures in the Cole–Cole arc and total dipole correlation function. In pentachlorotoluene the presence of many shorter relaxation times is indicated by a Cole–Davidson type of distribution (i.e., a skewed Cole–Cole plot). Using Eq. 3.4.4.1 for $V(2\eta)$, without the m summation, we have

$$\phi(\eta) = \frac{dV(2\eta)}{d(2\eta)}$$

$$= -\frac{1}{n_2^2}\left(\frac{\mu}{\mu_V}\right)^2 \sum_{ij} \frac{r_i r_j q_i q_j \sin(2\eta)}{[R_0^2 + r_i^2 + r_j^2 - 2r_i r_j \cos(2\eta)]^{3/2}}$$

where R_0 is the intercenter distance between TCTMB rings and r_i that from the ring center to each atom on molecule i. The Sturm–Liouville equation is then

$$\frac{d^2 y}{d\eta^2} + y\left(\lambda - \phi^2(\eta) + \frac{d\phi(\eta)}{d\eta}\right) = 0$$

where $Z = y \exp[-\int \phi(\eta)\, d\eta]$.

This equation may be solved numerically, but not analytically, for the complex polarizability $\alpha(\omega)$. To relate $\alpha(\omega)$ to the complex permittivity $\epsilon(\omega)$ requires cavity theory, and by implication an a priori solution to the very problem we have to solve. However, the cavity problems may be bypassed by comparing $\alpha(\omega)$ as calculated from the Sturm–Liouville equation with that calculated from the Monte Carlo simulation, because both approaches are molecular. The simulation takes account of all charge–charge interactions in a block of 240 molecules. The equivalent of the friction coefficient ζ_1 is introduced in the simulation by setting up repulsive potential barriers to hinder orientational jumps between one molecular site and the next. In the Smoluchowski approach the friction coefficient at 300°K is many orders of magnitude less than that at low temperatures because the low frequency loss peaks at much higher frequencies. However, the variation in the electric potential energy is *small*. Here the experimental data, simulation, and model produce results in close accord (a slightly flattened Cole–Cole arc, Fig. 3.4.4.2.2). As the temperature is lowered (as R_0 becomes progressively a little smaller and ζ_1 increases enormously) the flattening of the Cole–Cole arc is not followed (Fig. 3.4.4.2.2) by the pair interaction model, even when the lattice spacing is reduced to an unrealistically small value of $R_0 = 2.50$ Å. The analytical

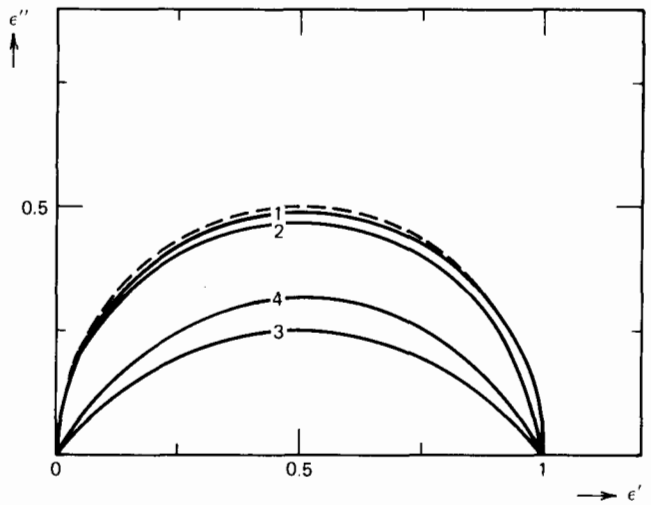

Figure 3.4.4.2.2 Cole–Cole plot, Smoluchowski equation, simulation and experimental data. 1–2: increasing strength of interaction. [Reproduced by permission from M. W. Evans, *J. Chem. Soc. Faraday Trans. II* **75**, 1442 (1979).

technique based on the Smoluchowski equation is not therefore a good representation of the overall molecular dynamic process of TCTMB, which relies on cooperative phenomena, especially at low temperatures. In fact the Monte Carlo simulations were performed with a virtually constant R_0, so that in both high and low temperature configurations the Brownian motion model plus pair interactions would yield the same type of slightly flattened Cole–Cole arc.

A self-consistent approach to the problem of rotational diffusion in the presence of electrostatic potentials has many interesting consequences, especially if the equations are modified to take into account both inertial and memory effects, so that the far infrared region could also be described satisfactorily. The results have recently been extended to spheroids by Warchol and Vaughan (1977).

However, these results are essentially based on the Cole method of treating the Zwanzig lattice, and none of these is capable of producing the symmetric broadening of the Cole–Cole arc observed experimentally in TCTMB and disordered molecular crystals of this type. The analytical methods tend to produce a series of shorter relaxation times and not the observed symmetrical flattening of the arc. This is an area where computer simulation is more revealing, and we illustrate this in the next section.

3.4.4.3 Molecular Dynamics Simulation of Weakly Interacting Dipoles on a Rigid Lattice

It is possible to discuss this problem within the context of the statistical theory of irreversible processes developed by the Prigogine school, in particular through the molecular dynamics simulations of Bellemans and

Kohler (1967). The approach to equilibrium of an assembly of dipoles on a lattice is a direct case of the application of the fluctuation–dissipation theorem, and is therefore of interest in the theory of dielectric relaxation. Each dipole is located on a particular site of a rigid lattice and is allowed only to rotate. The Hamiltonian is then

$$H = \sum_j \frac{J_j^2}{2I} - 2\mu^2 \sum_{\substack{j<k \\ j\neq k}} \sum \frac{\cos(\phi_j + \phi_k - 2\alpha_{jk})}{r_{jk}^2} \qquad (3.4.4.3.1)$$

(see Fig. 3.4.4.3.1) where J_j, ϕ_j are, respectively, the angular momentum and coordinate of the jth dipole, μ is the dipole moment, I is the moment of inertia, and r_{jk}, α_{jk} are the polar coordinates of site k relative to site j. It may be shown analytically using the Prigogine formalism that *a weak interaction involving two dipoles only cannot drive the system to equilibrium*. The true equilibrium state,

$$f_{eq} \doteq \exp\left(-\frac{\sum_j J_j^2}{2IkT}\right)$$

is attained by means of processes involving *at least three interacting dipoles*. These conclusions spring directly from the nature of the dipolar forces themselves. If one considers a weakly coupled system such that the potential energy is only a small fraction of the total energy (i.e., almost free rotation), then the second moment $\langle J^2 \rangle$ of the angular momentum is almost constant, since the mean square torque is small. Because of the relation between angular momentum and dipole orientation discussed in Chapters 1 and 2, the *nonequilibrium* average $\langle \mathbf{J}(t) \rangle$ should regress to zero with a characteristic time $= \mu^{-4}$ while $\langle J^4 \rangle$ should relax to about $3\langle J^2 \rangle$ with a characteristic time of $\sim \mu^{-8}$.

Bellemans and Kohler (1967) have used the molecular dynamics technique to investigate directly the approach to equilibrium of $\langle \mathbf{J}(t) \rangle$ and $\langle J^4(t) \rangle$, the kinetic energy, the potential energy, and the Hamiltonian of Eq. 3.4.4.3.1 using the canonical equation of motion:

$$\dot{\phi}_j = \frac{J_j}{I} \qquad (j = 1, \ldots, N)$$

$$\dot{J}_j = -\sum_{k(\neq j)} \left(\frac{2\mu^2}{r_{jk}^2}\right) \sin(\phi_j + \phi_k - 2\alpha_{jk})$$

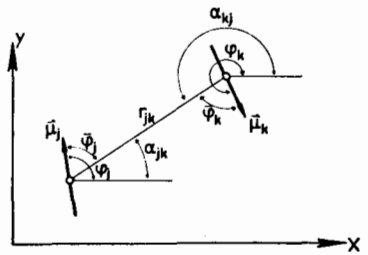

Figure 3.4.4.3.1 Coordinate system of two interacting dipoles (or generally two axially symmetrical molecules). [Reproduced by permission from A. Bellemans et al., *J. Chem. Phys.* **51**, 2578 (1969).]

for a two-dimensional lattice of 400 rotating dipoles located on the sites of a square lattice. These differential equations were solved using the standard numerical integrator methods of the molecular dynamics technique, described, for example, by Streett and Tildesley (1976, 1977). The equilibrium value of the mean potential energy per dipole is obtained by taking a Boltzmann average. The final equilibrium value for the Hamiltonian is therefore derived using a canonical average, although strictly speaking the simulation technique deals with a microcanonical surface. In the limit of infinitely weak interaction (free rotation) the microcanonical entropy of the system at equilibrium is given by

$$\log_e \left\{ \frac{(\pi E)^{n/2}}{\Gamma(N/2+1)} \right\}$$

where E is the total energy. This would introduce a correction of $(2N)^{-1}$ $\log_e(\pi N)$ to the molecular dynamics results for a canonical ensemble. For $N = 400$ this is small. Periodic boundary conditions were used in the computation. Initial conditions were taken as follows:

1. All angular velocities are set equal in magnitude.
2. All the polar angles ϕ are randomly distributed between 0 and 2π, so that V_0 nearly averages to zero.

Only interactions between neighboring dipoles were retained (i.e., each dipole interacts with only four others), since the medium being simulated is *unpolarized.* No qualitative difference then exists in the mechanism of approach to equilibrium. Consideration of all the terms would result in a faster decay to equilibrium than that shown in Fig. 3.4.4.3.2, which illustrates the situation when all the dipoles are initially set rotating in the same

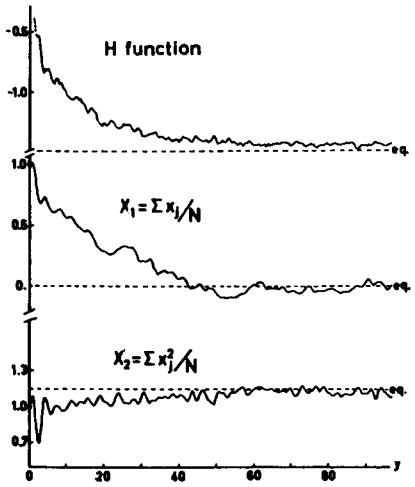

Figure 3.4.4.3.2 Evolution of H, the computer-simulated Hamiltonian, X_1 and X_2, with time for a given dipole–dipole coupling strength. [Reproduced by permission from A. Bellemans and F. Kohler, *J. Chem. Phys.* **47**, 1261 (1967).]

direction. After a rapid initial fall, the Hamiltonian slowly decreases to just above the equilibrium value. The kinetic energy (denoted by X_2) *increases* by about 15% and fluctuates around the equilibrium value. X_1 on the figure is proportional to $\langle J(t) \rangle$, and X_4 (not shown) to $\langle J^4(t) \rangle$. The potential energy (not drawn), initially zero, becomes negative because of the creation of orientational correlations. Both X_1 and X_4 go to their expected equilibrium values.

The relaxation times for X_1 and X_4 are not easy to extract, but it may be shown that they do in fact corroborate the analytical result that the true equilibrium state is attained by processes which must involve *more* than *two* interacting dipoles. If the friction term and stochastic force term were left out of the Smoluchowski equation in the preceding section *then there would be no possibility of the system attaining equilibrium.* This illustrates the difficulty of using analytical theories with only pairs of interacting dipoles.

The same molecular dynamics simulation may be used to elucidate the following very important information concerning the *dielectric response function.*

1. The form of the dielectric response function is strongly related to the nature of the orientational interactions between the molecules.
2. If this interaction is *purely dipolar* in nature the response function is not very different from its limiting form at zero coupling *even if the dipolar interaction is quite strong.*
3. The *long range* part of the dipolar interaction seems to play only a very limited role in the response function, as anticipated by Zwanzig (1963) and Scaife (1971).

These conclusions were reached in a simulation by Bellemans and Kohler of the correlation function and response function of the total moment $\mathbf{M}(t)$ of dipoles located in a plane on the sites of a rigid square lattice involving 101, 193, and 421 entities, respectively. This work, carried out more than a decade ago, still represents one of the most penetrating views we have of the separate role of dipole–dipole interaction in dielectric relaxation. The Brot–Darmon paper was based on this work, and all these workers have powerfully illustrated the use to which the molecular dynamics method can be put given the computer time and facilities. The correlation function is defined by

$$C_{\mathbf{M}}(t) = \frac{\langle \mathbf{M}(t) \cdot \mathbf{M}(0) \rangle}{\langle M^2 \rangle}$$

for a spherical, homogeneous and isotropic specimen. (Otherwise, e.g., in a molecular crystal or mesophase, it is *tensor* $\langle \mathbf{M}(t)\mathbf{M}^T(0) \rangle$.) The macroscopic response function $\Phi_{\mathbf{M}}(t)$ is

$$\Phi_{\mathbf{M}}(t) = -\dot{C}_{\mathbf{M}}(t) = -\frac{\langle \mathbf{M}(0) \cdot \dot{\mathbf{M}}(t) \rangle}{\langle M^2 \rangle}$$

The problem of relating $\Phi_M(t)$ to the observable complex permittivity $\epsilon(\omega)$ still involves cavity theories, however, and we follow Bellemans and Kohler in using *two-dimensional electrostatics*:

$$\frac{\epsilon(\omega)-1}{\epsilon(\omega)+1}=\frac{\epsilon_s-1}{\epsilon_s+1}\int_0^\infty \Phi_M(t)e^{-i\omega t}\,dt$$

that is, assuming that the medium is weakly polarizable and that the dipole–dipole interactions are relatively weak.

Equation 3.4.4.3.1 represents the effect of dipole–dipole interactions *only* on the free rotation. *These alone are enough to produce dielectric relaxation—without the inclusion of stochastic forces and hydrodynamical friction.* The form of Eq. 3.4.4.3.1 ensures inertial corrections automatically, and also the even-time properties of the classical correlation function. This is because we are solving the Liouville equation exactly for a specified Hamiltonian in a molecular dynamics simulation. In a "real" fluid, of course, we also have to consider short range orientational interactions of the Lennard–Jones type. In two dimensions the most general representation of the interaction between two axially symmetrical molecules (ellipsoids) i and k is

$$U(r_{jk},\bar{\phi}_j,\bar{\phi}_k)=\sum_{m=-\infty}^{\infty}\sum_{m'=-\infty}^{\infty}U_{mm'}(r_{jk})\exp[i(m\bar{\phi}_j+m'\bar{\phi}_k)]$$

(see Fig. 3.4.4.3.1).

The first term U_{00} of this representation corresponds to *central* forces (angle independent). Terms involving U_{10} and U_{20} vanish on the rigid square lattice by symmetry. The first nonvanishing *angle-dependent* terms are

$$2U_{11}\cos(\bar{\phi}_j+\bar{\phi}_k)+2U_{1,-1}\cos(\bar{\phi}_j-\phi_k)$$

The first term corresponds to dipole–dipole interactions if we put $U_{11}=\mu^2/r_{jk}^2$. The second one is the *classical analogue of the spin–spin exchange interaction of Heisenberg.* According to the sign of $U_{1,-1}$ this favors parallel or antiparallel alignment of neighboring molecules. It is possible to simulate the correlation function $C_M(t)$[and $\Phi_M(t)$] using *exchange interaction* instead of *dipole–dipole interaction.* This provides a direct insight into the importance of short range interactions in the evolution of $C_M(t)$. The Hamiltonian in this case is

$$H=\sum_j\frac{J_i^2}{2I}-v\sum_{j\neq k}\sum\cos(\phi_j-\phi_k)$$

where v is a constant. Note that the exchange interaction appears in *addition* to the usual central forces (van der Waals). The exchange interaction in this case is a constant, and does not appear in the Hamiltonian since the molecules are translationally fixed. However, this interaction could very well play an important role in the formation of a mesophase,

where the molecules are roughly axially symmetrical and the potential is *strongly angle* dependent. Such a simulation would be informative.

The x and y components of $\mathbf{M}$ are, respectively, $\mu\,\Sigma_j\cos\phi_j$ and $\mu\,\Sigma_j\sin\phi_j$, so that

$$M^2=N\mu^2+\mu^2\sum_{j\neq k}\sum\cos(\phi_j-\phi_k)$$

$$\mathbf{M}(t)\cdot\mathbf{M}(0)=\mu^2\sum_j\cos[\phi_j(t)-\phi_j(0)]+\mu^2\sum_{j\neq k}\sum\cos[\phi_j(t)-\phi_k(0)]$$

In the limit of infinitely weak coupling (i.e., free rotation in a plane), we have (see Chapter 2)

$$\langle\mathbf{M}(t)\cdot\mathbf{M}(0)\rangle\to N\mu^2\left\langle\cos\frac{Jt}{I}\right\rangle=N\mu^2\exp\left(-\frac{t^2kT}{2I}\right)$$

This well-known form will be modified by (1) dipole–dipole interaction and (2) exchange interaction.

In the simulation $C_M(t)$ and $\Phi(t)$ are calculated using *time averages*, not phase space averages, that is, by assuming that the system is ergodic (Chapter 1). The error caused by this is of the order N^{-1}, where N is the number of molecules (i.e., the difference between the microcanonical and canonical ensembles). Starting from randomly oriented dipoles with random angular momenta *correlations grow within the system* so that its potential energy becomes slightly negative with respect to that prevailing at the start of the process.

In the case of *dipolar interaction* the Kirkwood factor is proportional to

$$\frac{\langle M^2\rangle}{N\mu^2}=1-B_2\gamma^2-B_4\gamma^4\cdots$$

where $\gamma=\mu^2/a^2kT=\rho\mu^2/kT$, a is the distance between nearest neighbors, and ρ is the density. The forms B_2 and B_4 are N dependent and shape dependent, that is, angle dependent. To go into this in more detail, each dipole is directly coupled to all others with a *long range* (r^{-2}) potential. The computation is only practical then with $N=101$. In order to treat larger systems of 193 and 421 dipoles the problem is simplified by retaining nearest neighbor interactions only; that is, the long range part of the potential is truncated as described above.

Figure 3.4.4.3.3 demonstrates, however, that (1) the long range part of the potential is ineffective for $\gamma\leq 0.342$; (2) the dependence of the molecular dynamics results upon the size of the systems is very small; (3) the difference from the free rotor response function is *very small* despite the fact that $\gamma=0.342$ represents quite strong interaction; (4) *the results are not capable of producing the exponentially decaying response function of the Debye theory*; and (5) there is a tendency for the response function to be oscillatory, which is tentative evidence for a dipole–dipole origin for those oscillations observed in related functions using far infrared data.

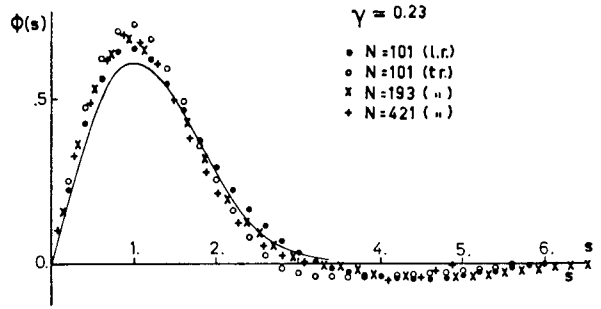

Figure 3.4.4.3.3 Response functions $\phi_r(t) = \langle \dot{\mathbf{M}}(\tau) \cdot \mathbf{M}(\tau + t) \rangle / \langle M^2(\tau) \rangle$ for computer-simulated dipolar interactions. The solid line corresponds to free rotation (l.r. signifies long range and t.r. truncated interaction; see text). [Reproduced by permission from A. Bellemans et al., *J. Chem. Phys.* **51**, 2578 (1969).]

Exchange interactions, on the other hand, produce response functions typified in Fig. 3.4.4.3.4 in terms of a coupling parameter $\delta = v/kT > 0$, and in Fig. 3.4.4.3.5 for $\delta < 0$ (antiparallel alignment). A positive value of δ favors a *parallel* alignment of the dipoles so that $\langle M^2 \rangle / N\mu^2$ is larger than one. In consequence $\Phi(t)$ must deviate negatively from the free rotor function. For $\delta > 0$ there appears *a new characteristic time related to the interactions, and* $\Phi(t)$ *eventually resembles an exponential* at relatively long times. For $\delta < 0$ the response function is oscillatory, any deviations from free rotor behavior being pronounced for relatively weak coupling.

3.4.5 Dipole–Dipole Coupling and Far Infrared Spectroscopy

It seems, therefore, that except in the case of parallel Heisenberg exchange interaction, the dipole–dipole interaction contribution to $\langle \mathbf{M}(0) \cdot \mathbf{M}(t) \rangle$ is

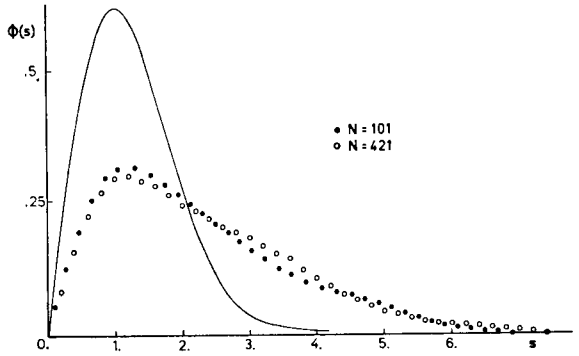

Figure 3.4.4.3.4 Computer-simulated response functions $\phi_r(t)$ for exchange interactions favoring parallel alignment ($\delta > 0$). The solid line is for free rotation. [Reproduced by permission from A. Bellemans et al., *J. Chem. Phys.* **51**, 2578 (1969).]

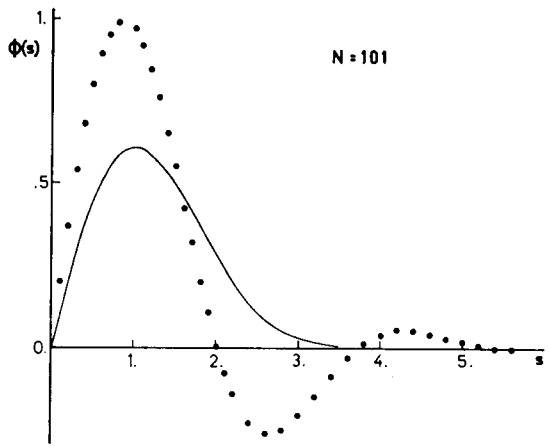

Figure 3.4.4.3.5 As for Fig. 3.4.4.3.4, classical analogue of antiparallel Heisenberg exchange ($\delta < 0$). [Reproduced by permission from A. Bellemans et al., *J. Chem. Phys.* **51**, 2578 (1969).]

small. *It would not be correct to infer from this that*

$$\langle \mathbf{M}(0) \cdot \mathbf{M}(t) \rangle = \sum_i \sum_j \langle \boldsymbol{\mu}_i(0) \cdot \boldsymbol{\mu}_j(t) \rangle$$
$$= N \langle \boldsymbol{\mu}(0) \cdot \boldsymbol{\mu}(t) \rangle$$

even in the complete absence of dipole–dipole interaction, because the relation between $\langle \mathbf{M}(0) \cdot \mathbf{M}(t) \rangle$ *and* $\langle \boldsymbol{\mu}(0) \cdot \boldsymbol{\mu}(t) \rangle$ *is determined by the structure of Mori theory, through a macro–micro correlation theorem.* This is discussed in Section 3.5. In general, the electrostatic forces in a system may be less important than the van der Waals forces, but in TCTMB this is not the case, and *will not be the case* when there are factors such as hydrogen bonding to take into account, since this may be regarded as an extreme instance of the effects of dipole–dipole interaction. In this section we illustrate how the far infrared may be used to detect the effect of electric forces on the overall ensemble motion. The effect is obvious in a case such as HF dissolved SF_6, whose first multipole moment is the very *short* ranged *hexadecapole* (Chapter 1); the $\Delta J = 1$ rotational structure is already resolved (Fig. 1.2.4). However, in *pure* HF liquid there is no sign of structure, despite the fact that the peak frequency is roughly in the same position for both cases (so that the total mean square torques due to *central* forces are roughly commensurate). The electrostatic effect on the motion of water molecules (Fig. 1.2.2) is of course obvious, but in strongly dipolar liquids the total dipole correlation function $\langle \mathbf{M}(0) \cdot \mathbf{M}(t) \rangle$ is also strongly affected.

In liquids where electrostatic forces are relatively important, such as the very strongly dipolar molecules CHF_3, CH_3F, and CH_3Cl, the mean square torque (obtained by the admittedly crude and self-defeating ap-

proximation that $\langle \mathbf{M}(0)\cdot\mathbf{M}(t)\rangle$ is simply proportional to $\langle \mathbf{u}(0)\cdot\mathbf{u}(t)\rangle$) seems to be unusually high; that is, *there is a large shift away on dilution from the neat liquid value* of the far infrared power absorption coefficient. Such is also the case in CH_2Cl_2 (Fig. 3.4.4.1), and in pure liquid HF, HCl, and HBr. This is all the more remarkable because these molecules are very fast rotors even in the vicinity of the triple point. The anisotropy (or angle dependence) of the total intermolecular potential strongly depends on the contributions of multipole–multipole interactions (see Chapter 11). Another sign of electrostatic influence is a *weak density dependence* of the torques, arising from the fact that the dipole interactions are long-ranged, and in consequence are not sensitive to the mean intermolecular separation.

Experimental measurements of the mean square torque provide therefore a direct and unambiguous measure of the strength of angle-dependent intermolecular forces, and nowhere is this more evident than in the far infrared, which provides us with one of the most sensitive means of evaluating the analytical form of the intermolecular potential in a dynamic context. (In the static context virial measurements are better.) In order to obtain unambiguous information on the mean square torque the relationship between $\langle \mathbf{M}(t)\cdot\mathbf{M}(0)\rangle$ and $\langle \mathbf{u}(t)\cdot\mathbf{u}(0)\rangle$ and between $\langle \mathbf{M}(t)\cdot\mathbf{M}(0)\rangle$ and the observable power absorption coefficient must be refined. By definition, when electrostatic effects are present, $\langle \mathbf{M}(t)\cdot\mathbf{M}(0)\rangle$ contains cross correlations, so that collective molecular motions (or coherent dynamics) are relatively important. The Mori formalism may allow us to take into account the coupling of the single and multiparticle motions without going into the details of the analytical form of the intermolecular potential. From this the mean square torque can be extracted and thereafter related to an integral over the anisotropic part of the pair potential.

The problem of cavity theory in relating $\langle \mathbf{M}(t)\cdot\mathbf{M}(0)\rangle$ and the power absorption coefficient is minimal numerically, as Fig. 3.4.5.1 illustrates for the intensely dipolar liquid fluoroform. The corresponding correlation functions are shown in Fig. 3.4.5.2. Despite the fact that there is a considerable amplitude of dispersion and absorption in these compounds there is little appreciable difference between the various cavity corrections derived by Brot (1975) (cf. Section 3.4.3 above). We now consider a case that epitomizes the influence of multipole–multipole interaction on the molecular dynamics—water in the liquid state.

3.4.6 Dipole–Dipole Correlation in Liquid Water—Molecular Dynamics Simulation

Using an effective pairwise interaction potential energy (but with no reaction field) Rahman and Stillinger (1971) have simulated the motions and interactions of pure liquid water molecules. They were able to extract the static correlation factor: $\langle M^2\rangle/N$, where $\mathbf{M} = \sum_{i=1}^{N} \boldsymbol{\mu}_i$ ($N = 216$ molecules). If the dipole directions were entirely uncorrelated then $\langle M^2\rangle/N = 1$, but for

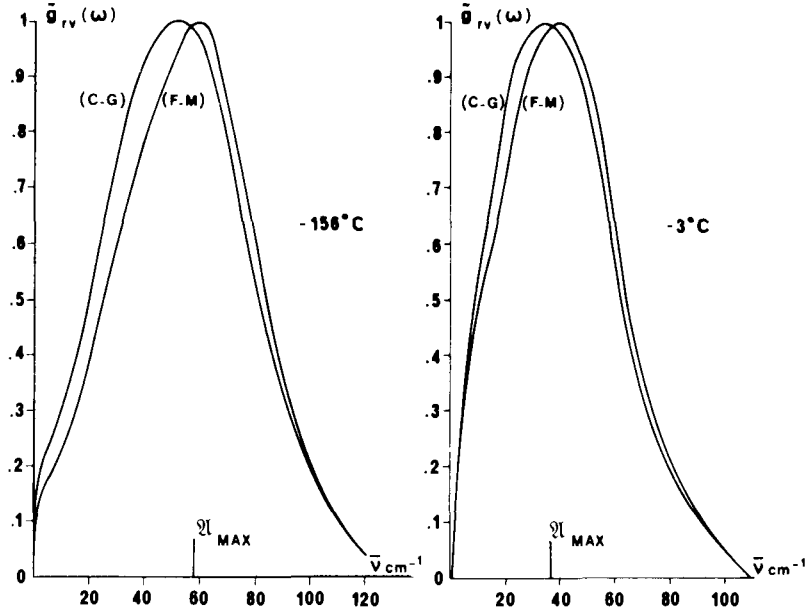

Figure 3.4.5.1 Power spectra in the far infrared, the effect of internal field corrections using microscopic cavities. F–M, Fatuzzo/Mason theory; C–G, Cole/Glarum theory. $\mathfrak{A}_{max}$ indicates the maximum of the raw data, in this case for the intensely dipolar liquid fluoroform. [Reproduced by permission from A. Gerschel et al., *Mol. Phys.* **33**, 527 (1977).]

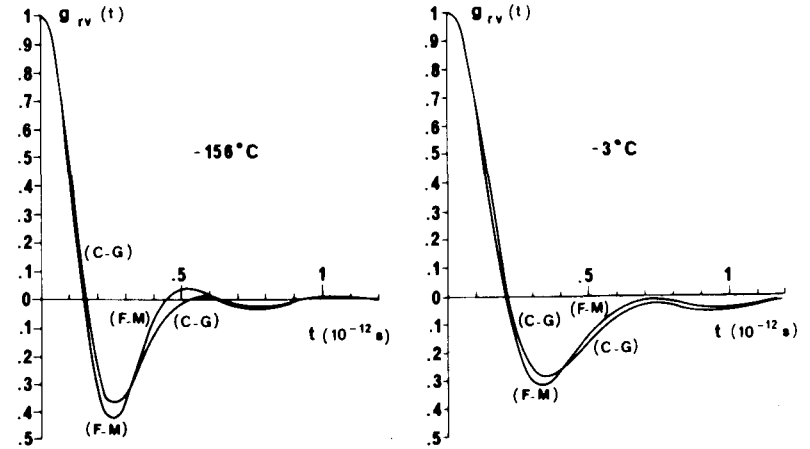

Figure 3.4.5.2 Fourier transforms of the curves of Fig. 3.4.5.2. [Reproduced by permission from A. Gerschel et al., *Mol. Phys.* **33**, 527 (1977).]

water,

$$G_K \equiv \frac{\langle M^2 \rangle}{N} = 0.171$$

at a density of 1 g/ml. This is an apparent Kirkwood correlation factor linked to the true factor by the relation

$$G_K = \left(\frac{9\epsilon_s}{[\epsilon_s + 2][2\epsilon_s + 1]}\right) g_K$$

That is to say that the relation between G_K and g_K is precisely that between the local moment **m** of a fixed molecule and the macroscopic moment **M** of the spherical cavity c. The quantity G_K is the same for the molecular dynamics simulation as it is for a spherical dielectric sample in vacuo. Not surprisingly, therefore, the molecular dynamics simulations produce strong interaction effects usually attributed to *hydrogen bonding*. This is represented by the effective pair potential:

$$V_{\text{eff}}(\mathbf{x}_i, \mathbf{x}_j) = V_{\text{LJ}}(r_{ij}) + S(r_{ij}) V_{\text{el}}(\mathbf{x}_i, \mathbf{x}_j)$$

Here $\mathbf{x}_i, \ldots, \mathbf{x}_N$ are configurational vectors (center of mass position and the three Euler angles), r_{ij} denotes oxygen–oxygen separation, and V_{LJ} is *the Lennard–Jones potential*:

$$V_{\text{LJ}}(r_{ij}) = 4\epsilon \left[\left(\frac{\sigma}{r_{ij}}\right)^{12} - \left(\frac{\sigma}{r_{ij}}\right)^{6}\right]$$

where ϵ and σ are the Lennard–Jones parameters. The part V_{el} of the overall potential depends sensitively on orientations about the oxygen nuclei. It is produced by four *point charges*, each 1 Å from the oxygen nucleus arranged so as to form the vertices of a regular tetrahedron. Two of them are positive ($0.19e$, where e is the electron charge), in order to simulate partially shielded protons, while the remaining two ($-0.19e$) act as unshared electron pairs. The 16 charge–charge interactions from V_{el}:

$$V_{\text{el}}(\mathbf{x}_i, \mathbf{x}_j) = (0.19e)^2 \sum_{\alpha_i, \alpha_j = 1}^{4} \frac{(-1)^{\alpha_i + \alpha_j}}{d_{\alpha_i \alpha_j}(\mathbf{x}_i, \mathbf{x}_j)}$$

The switching function $S(r_{ij})$ suppresses the possibility of divergence caused by d becoming vanishingly small. The absolute minimum of this potential (Fig. 3.4.6.1) agrees satisfactorily with the stable dimer geometry predicted by ab initio quantum mechanical calculations. *Note that this type of potential can be transferred almost intact to describe by molecular dynamics simulation the motion of CH_2Cl_2*, as described in Chapter 12.

The diffusion (both rotational and translational) of the water molecule is slowed very much by the electrostatic V_{el} potential. Indeed, during the whole time allotted to the run (1 psec) the proton had not been able to complete a rotation on average. This is in strong contrast to the situation in dilute organic solvents, where the rotational velocity correlation function

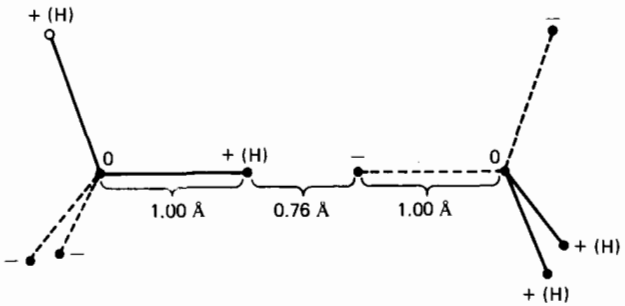

Figure 3.4.6.1 Minimal energy configuration for two water molecules according to the molecular dynamics potential used by Rahman and Stillinger. Each oxygen nucleus is symmetrically surrounded by a tetrad of four point charges ($\pm 0.19e$), the positive members of which represent partially shielded protons. The configuration has a plane of symmetry and incorporates a single linear hydrogen bond. [Reproduced by permission from A. Rahman and F. H. Stillinger, *J. Chem. Phys.* **55**, 3336 (1971).]

of the far infrared decays to zero in ~0.2 psec (cf. Chapter 1). In sharp contrast to liquid argon, the velocity a.c.f. is oscillatory (Fig. 3.4.6.2), in a manner reminiscent of the *angular* velocity correlation functions of Fig. 1.3.1.3. In liquid argon the simulated velocity a.c.f. has only a single, well-defined, long-lived, negative minimum, followed by a positive long-time tail due to coupling with collective (hydrodynamic) modes. The oscillatory motion (due to structural rigidity) is of direct electrostatic origin. There is no evidence for a hopping process but, rather, translational diffusion proceeds via individual molecules participating in the continual restructuring of the labile, random, hydrogen bond network.

The simulated dipole a.c.f. $\langle \boldsymbol{\mu}(t) \cdot \boldsymbol{\mu}(0) \rangle$ shows an initial rapid falloff (compared directly with the far infrared solution result, free of hydrogen bonding, in Fig. 3.4.6.3) followed by a severe retardation as the latter takes effect. The decay is never exponential, since the rotational motion (from stereoscopic motion pictures) corresponds to a sequence of finite turns rather than the infinitely rapid infinitesimal turns of the Wiener process in the classical theory of the Brownian movement. Only rotations about two out of three Cartesian axes affect the direction of $\boldsymbol{\mu}_j(t)$ in molecule j so that the a.c.f. $\langle \boldsymbol{\mu}(t) \cdot \boldsymbol{\mu}(0) \rangle$ is a combination of these motions. The angular velocity a.c.f.'s about each axis are oscillatory (Fig. 3.4.6.4), and reflect a degree of cooperative behavior, the molecular motion depending strongly on the form of the hydrogen bonding in the liquid.

In supercooled liquid water at 265°K the diffusions are markedly slower because the hydrogen bonding is markedly stronger. In contrast, as the temperature is raised G_K increases. The conditions used in the simulation by Rahman and Stillinger of water at different temperatures were as follows: T_1, supercooled water at 265°K; T_2, 307.5°K; T_3, 588°K (6 kbar), all at 1 g/cm^3. These lead to the static Kirkwood correlation: $G_K(T_1) = 0.20$;

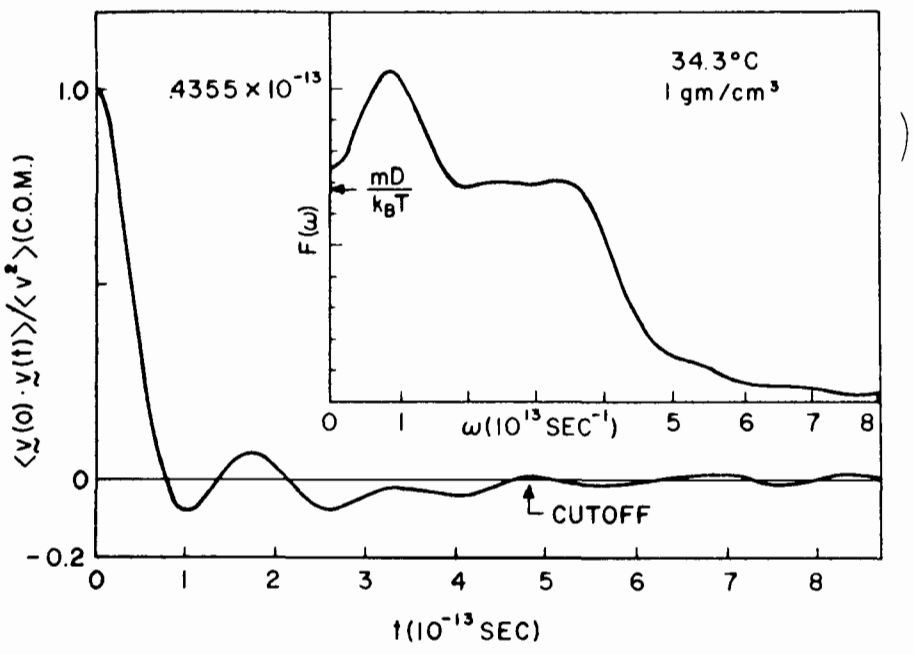

(a)

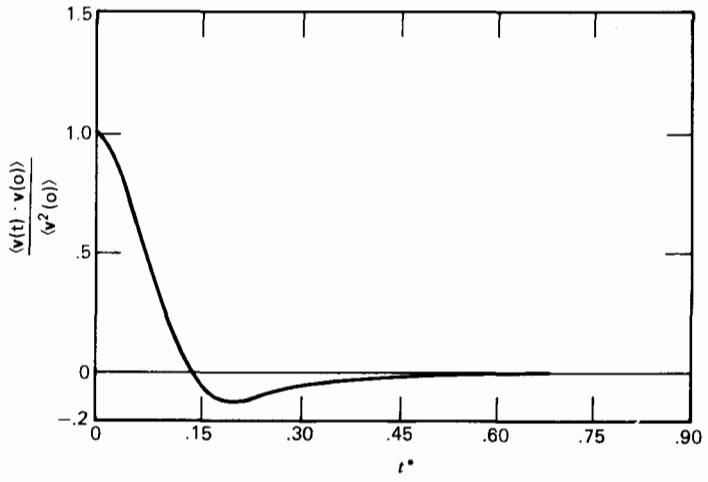

(b)

Figure 3.4.6.2 (*a*) Center of mass velocity a.c.f. for liquid water and its Fourier cosine transform (inset) obtained by a molecular dynamics simulation. Electrostatic interactions are predominant. (*b*) The same for liquid argon, where electrostatic interactions are minimal. [Reproduced by permission from A. Rahman and F. H. Stillinger, *J. Chem. Phys.* **55**, 3336 (1971).]

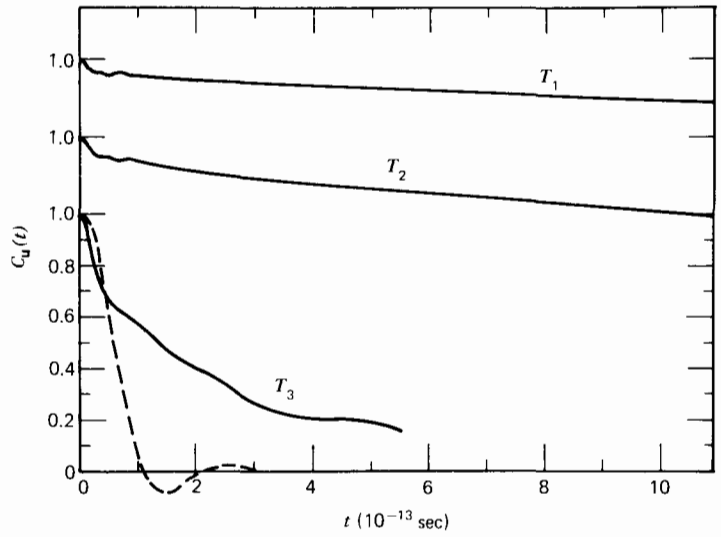

Figure 3.4.6.3 Autocorrelation functions $C_u(t)$ computer simulated for liquid water at $T_1 = 265°K$, $T_2 = 307.5°K$, and $T_3 = 588°K$ (6 kbar). Superimposed on the curve at T_3 is a schematic of that obtained by Evans from far infrared spectroscopy of a dilute solution of water in cyclohexane at 296°K, effectively free of all hydrogen bonds (dashed curve). [Computer results reproduced by permission from A. Rahman and F. H. Stillinger, *J. Chem. Phys.* **57**, 1281 (1972).]

$G_K(T_2) = 0.171$; $G_K(T_3) = 0.278$. This means that even under the conditions represented by T_3, there is very strong dipole cross correlation *so that the collective correlation function* $\langle \mathbf{M}(0) \cdot \mathbf{M}(t) \rangle$ will never be proportional to the a.c.f. $\langle \boldsymbol{\mu}(0) \cdot \boldsymbol{\mu}(t) \rangle$. On the other hand, the linear velocity a.c.f.'s are markedly different at T_1 and T_3, (Figs. 3.4.6.5 and 3.4.6.6), but neither is exponential in nature. Evidently, the orientation–dependent part of the pair interaction continuously loses effectiveness as the temperature increases, compared with the van der Waals forces. Figure 3.4.6.3 and 3.4.6.6 epitomize the effect of *molecular* electric forces on *particle* dynamics.

Rotational motion proceeds much more freely at the higher temperatures (Fig. 3.4.6.6); at T_3 the motion is very similar to that of a dilute solution of water in benzene, albeit a little more hindered. However, the value of $G_K(T_3) < 1$ emphasizes how correlation may arise *even when hydrogen bonding is not a dominant factor.* The shift in the first maximum of the angular momentum a.c.f.'s (at the three temperatures about the axis of least moment of inertia; Fig. 3.4.6.4) means that the thermal disruption moves neighbors out of the optimal positions and orientations that are needed to firmly bind the central molecule.

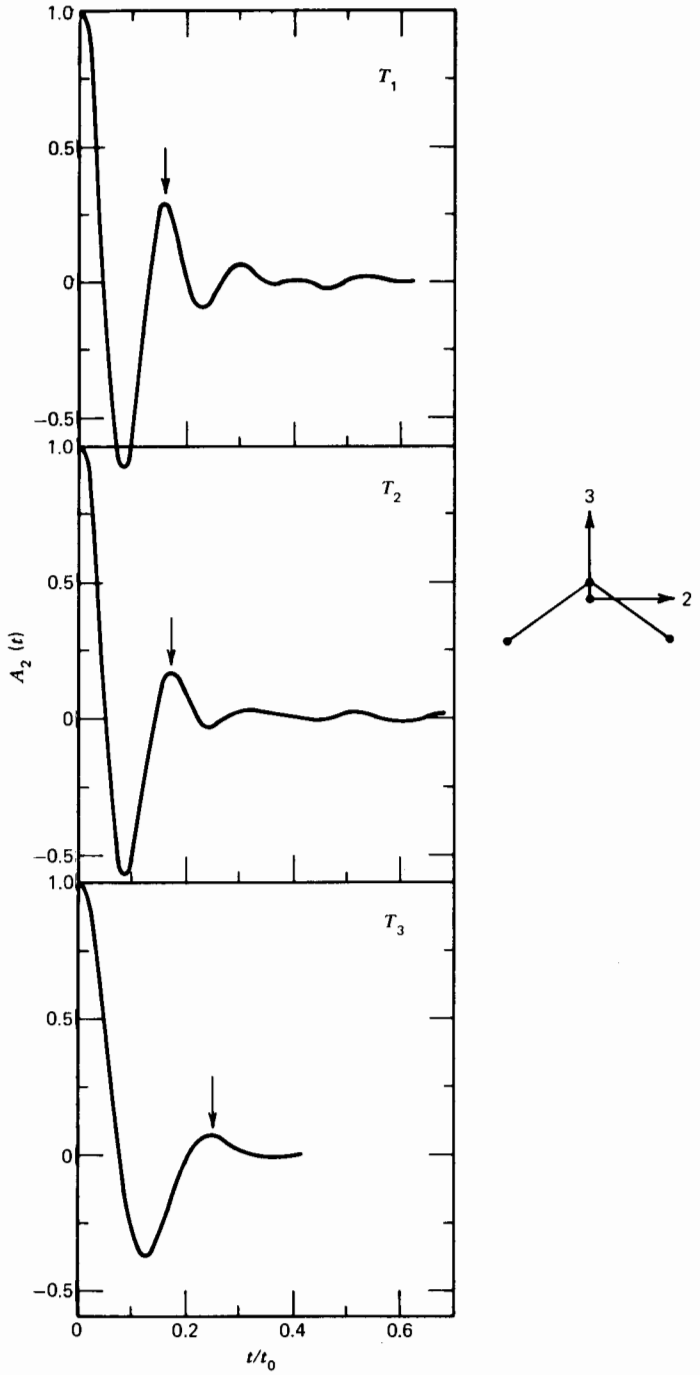

Figure 3.4.6.4 Computer-simulated normalized angular momentum a.c.f.'s. The rotation axis lies in the molecular plane, perpendicular to the dipole axis, and corresponds to the smallest of the inertial moments. $t_0 = 2.18 \times 10^{-13}$ sec. [Reproduced by permission from A. Rahman and F. H. Stillinger, *J. Chem. Phys.* **57**, 1281 (1972).]

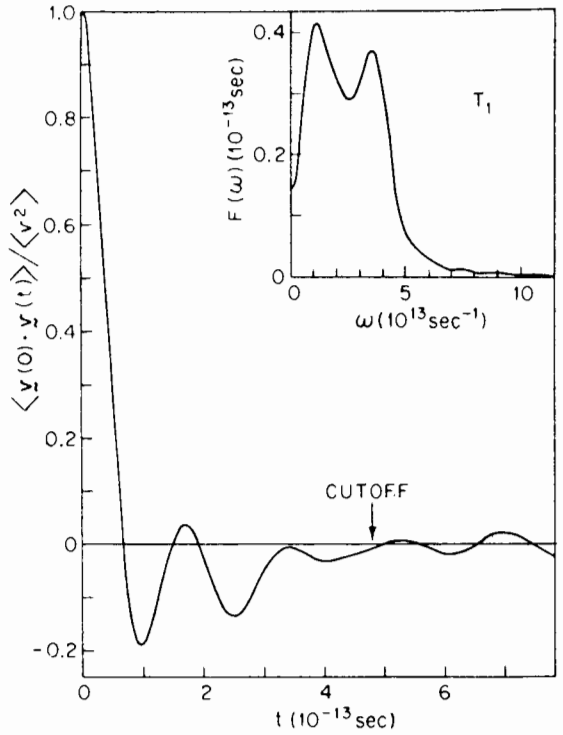

Figure 3.4.6.5 Computer-simulated center of mass velocity a.c.f. for water at $T_1 = 265°K$ (supercooled liquid). The Fourier transform is inset. [Reproduced by permission from A. Rahman and F. H. Stillinger, *J. Chem. Phys.* **57**, 1281 (1972).]

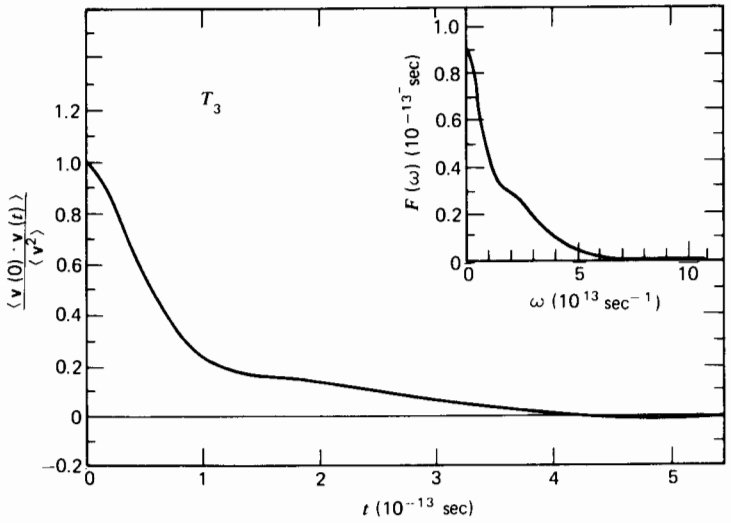

Figure 3.4.6.6 As in Fig. 3.4.6.5, for $T_3 = 588°K$ (6 kbar). [Reproduced by permission from A Rahman and F. H. Stillinger, *J. Chem. Phys.* **57**, 1281 (1972).]

3.4.7 Dielectric Friction

The reaction field, as mentioned in Section 3.3 above, follows the motion of the dipole, not instantaneously but in a "retarded" fashion, owing to what has been termed dielectric friction (see Appendix). In a model of this, formulated by Nee and Zwanzig (1970) a dipolar molecule is represented by a permanent dipole embedded in a small sphere which has a dielectric *constant* ϵ_∞ (or n^2 in the far infrared when the high frequency absorption is accounted for). They find for $\epsilon(\omega)$ the equation

$$\epsilon(\omega) - n^2 = \frac{3\epsilon(\omega)}{2\epsilon(\omega)+n^2}\frac{(N/V)\mu^2}{3kT\epsilon_0}\mathscr{L}_a[-\dot{C}_u(t)] \qquad (3.4.7.1)$$

where

$$C_u(t) = \frac{\langle \mathbf{u}(t)\cdot\mathbf{u}(0)\rangle}{\langle \mathbf{u}(0)\cdot\mathbf{u}(0)\rangle}$$

is the unit vector dipole a.c.f. Furthermore,

$$\mathscr{L}_a[-\dot{C}_u(t)] = \left[1 - i\omega\tau_0 - \left(1-\frac{n^2}{\epsilon_s}\right)\left(\frac{\epsilon(\omega)-\epsilon_s}{2\epsilon(\omega)+n^2}\right)\right]^{-1}$$

where τ_0 is the microscopic relaxation time inversely proportional to the rotational-diffusion constant (or friction coefficient). Equation 3.4.7.1 includes the effect of the reaction field, that is, takes into account the effect of long range, instantaneous (i.e., dipolar) interactions. However, their derivation of these equations is open to serious objection. Thus we explain only the concept of dielectric friction here and the problems associated with it.

1. When a dipole rotates, it produces a time-varying electric field outside the cavity, and energy is dissipated to the surroundings because of the dielectric loss. This energy dissipation has the effect of slowing down the rotation of the dipole. This is termed dielectric friction. This frictional effect is in addition to the local effects of van der Waals forces, which are usually represented by the frictional term in the Langevin equation.
2. The problem is to determine how dielectric friction interacts with the van der Waals friction of the Brownian movement. Some indication of the combined effect of these two frictions has been given in the section dealing with the attempts to generalize Onsager's equation.

3.5 MACRO–MICRO CORRELATION THEOREMS

The feature common to all cavity models is the physical assumption that the dipole of interest is in a cavity embedded in a dielectric continuum. Information on the permittivity $\epsilon(\omega)$ then leads to a multimolecular correlation function $\langle \mathbf{M}(t)\cdot\mathbf{M}(0)\rangle$, not to a single molecule a.c.f. $\langle \mathbf{u}(t)\cdot\mathbf{u}(0)\rangle$.

Deutch (1976) has recently suggested that in this area molecular dynamics simulations will be important in computing more directly $\langle \mathbf{M}(t)\cdot\mathbf{M}(0)\rangle$ and $\langle \mathbf{u}(t)\cdot\mathbf{u}(0)\rangle$. At present this is uneconomical but the great power of the new-generation computers such as the Cray computer should ease the difficulties considerably. (see Appendix).

Kivelson and Madden (1975) made the first attempt to determine the relation between $\langle \mathbf{M}(t)\cdot\mathbf{M}(0)\rangle$ and $\langle \mathbf{u}(t)\cdot\mathbf{u}(0)\rangle$ using Mori theory. They term the result a macro–micro correlation theorem. As we have seen, the microscopic, or autocorrelation, function $C_u(t)$ is obtained usually by cavity techniques, the cavity being shrunk to the size of one molecule, while macroscopic field equations are still employed.

A detailed account of the relationship between macroscopic and microscopic field equations is given by Van Vleck (1932) and Scaife (1972).

The final result of the macro–micro theorem is that if $C_u(t)$ can be expanded as a sum of (complex) exponentials, then $C_M(t)$ takes the same form with *scaled* parameters. The derivation according to Kivelson and Madden (1975) makes no use of microscopic cavity fields, and in this manner apparently circumvents the problem of the reaction field. If we take a spectrum of the form 2.12.8, as used by Evans and co-workers, then this will not be changed essentially, but only scaled if we work with $C_M(t)$ rather than $C_u(t)$. This is true however strongly dipolar the liquid with which we are working. We briefly sketch the work of Kivelson and Madden below. The notation follows closely that of the original paper.

The Hamiltonian for N interacting molecules placed in a uniform electric field $E_0(t)$ is, in general, for terms to second order in field strength:

$$\mathbf{H} = \mathbf{H}_0 - \int d\mathbf{R}\mathbf{m}(R)\cdot\mathbf{E}_0(t) - \frac{1}{2}\int d\mathbf{R}\mathbf{E}_0(t)\cdot\mathbf{a}(R)\cdot\mathbf{E}_0(t)$$

Here R is a *space point* (i.e., a coordinate) so that $d\mathbf{R}$ is the three-dimensional volume element corresponding to $\mathbf{R}$. The integrals are taken over the volume of the sample (V). $\mathbf{m}(\mathbf{R})$ is the *dipole density* and $\mathbf{a}(\mathbf{R})$ is the corresponding polarizability density tensor; $\mathbf{m}$ and $\mathbf{a}$ are defined by

$$\begin{aligned}\mathbf{m}(\mathbf{R}) = \sum_j \mathbf{m}_j(\mathbf{R}) &= \boldsymbol{\mu}_j\delta(\mathbf{R}-\mathbf{q}_j) \\ &\quad - \sum_k \boldsymbol{\mu}_k\cdot\mathbf{T}_{kj}\cdot\boldsymbol{\alpha}_j\delta(\mathbf{R}-\mathbf{q}_j) \\ &\quad + \sum_{k,l}\boldsymbol{\mu}_k\cdot\mathbf{T}_{kl}\cdot\boldsymbol{\alpha}_l\cdot\mathbf{T}_{lj}\cdot\boldsymbol{\alpha}_j\delta(\mathbf{R}-\mathbf{q}_j)+\cdots \qquad (3.5.1)\end{aligned}$$

$$\begin{aligned}\mathbf{a}_j(\mathbf{R}) &= \boldsymbol{\alpha}_j\delta(\mathbf{R}-\mathbf{q}_j) - \frac{1}{2}\sum_k \boldsymbol{\alpha}_k\cdot\mathbf{T}_{kj}\cdot\boldsymbol{\alpha}_j\delta(\mathbf{R}-\mathbf{q}_j) \\ &\quad + \frac{1}{6}\sum_{k,l}\boldsymbol{\alpha}_k\cdot\mathbf{T}_{kl}\cdot\boldsymbol{\alpha}_l\cdot\mathbf{T}_{lj}\cdot\boldsymbol{\alpha}_j\delta(\mathbf{R}-\mathbf{q}_j)+\cdots \qquad (3.5.2)\end{aligned}$$

Here $\mathbf{T}_{jk}$ is the *dipole–dipole interaction tensor* for interactions between molecules j and k. $\boldsymbol{\mu}_j$ and $\boldsymbol{\alpha}_j$ are the molecular dipole moment and

polarizability tensor, respectively. The dipolar interaction terms dependent on $\mathbf{E}_0$ are shown explicitly; other types of intermolecular interaction are incorporated in $\boldsymbol{\mu}_j$, $\boldsymbol{\alpha}_j$, and $\mathbf{H}_0$. These include *collision-induced* effects (see Chapter 11).

The polarization per unit volume $\mathbf{P}(\mathbf{R}, \omega)$ at point $\mathbf{R}$ is then

$$\mathbf{P}(\mathbf{R}, \omega) = \int_0^\infty dt \exp(i\omega t)[\overline{\mathbf{m}(\mathbf{R}, t)} + \overline{\mathbf{a}(\mathbf{R}, t)} \cdot \mathbf{E}_0(t)]$$

where the bar denotes an instantaneous ensemble average at time t and position $\mathbf{R}$ in the presence of the electric field $\mathbf{E}_0(t)$. By means of linear response theory, (Chapter 2):

$$\mathbf{P}(\mathbf{R}, \omega) = \left[-(kT)^{-1}\left(\int d\mathbf{R}'\langle \mathbf{m}(\mathbf{R}, 0)\mathbf{m}(\mathbf{R}', 0)\rangle + i\omega \int_0^\infty dt \int dR'\langle \mathbf{m}(\mathbf{R}, t)\mathbf{m}(\mathbf{R}', 0)\rangle \exp(i\omega t)\right) - \langle \mathbf{a}(\mathbf{R}, t)\rangle\right] \cdot \tilde{\mathbf{E}}_0(\omega)$$

Here $\langle\ \rangle$ indicates an ensemble average in the absence of the field $\mathbf{E}_0$, and $\tilde{\mathbf{E}}_0(\omega)$ is the Fourier transform of $\mathbf{E}_0(t)$. The average is over phase points, the coordinates of molecules, and not over the space points $[\mathbf{R}, \mathbf{R}']$. In uniform fields, $\mathbf{P}(\mathbf{R}, \omega)$ is independent of $\mathbf{R}$. In this case $\int d\mathbf{R}'\langle \mathbf{m}(0), t)\mathbf{m}(\mathbf{R}', 0)\rangle$ is proportional to $(N/V)C_{\mathbf{m}}(t)$.

The component of $\mathbf{m}(\mathbf{R})$ in the direction of $\mathbf{E}_0$ can be rewritten as

$$m_{E_0}(\mathbf{R}) = \sum_j [\langle \mu \rangle \cos \theta_j + \Delta\mu_{E_{0,j}}]\delta(\mathbf{R} - \mathbf{q}_j)$$

where $\langle \mu \rangle$ is the average value of the dipole moment in the molecular frame (the magnitude of the permanent molecular dipole moment in the liquid). θ_j is the angle between the permanent molecular dipole moment of the jth molecule and the field $\mathbf{E}_0$, and $\Delta\mu_{E_{0,j}}$ represents all the other contributions to the component of the dipole moment along $\mathbf{E}_0$ arising from intermolecular effects.

Note that the dipole interaction tensor has the following properties: (1) $T_{jj} = 0$; and (2) if $k \neq j$, T_{kj} is proportional to r_{kj}^{-3}, where r_{kj} is the distance between the jth and kth molecules. The quantity $\langle \mu \rangle$ is the ensemble average of $\mathbf{m}_j$ in the jth molecular frame. The only terms in Eq. 3.5.1 that are nonvanishing in this average are those for which $k = j$, because, viewed from the coordinate system on the jth molecule, the kth molecule is randomly distributed. Thus $\langle \mu \rangle$ comes from the first term in Eq. 3.5.1, and from "short range" terms that vary as r_{jk}^{-n} with $n \geq 6$. These latter depend on the molecular shape. Consequently, $\langle \mu \rangle$ in liquids differs from $\langle \mu \rangle$ in gases. Kivelson and Madden assume that the major contributor to $\Delta\mu_{E_{0,j}}$ is the second term in Eq. 3.5.1. The ensemble average $\langle \mathbf{a}(\mathbf{R}) \rangle$ in our expression for $P(\mathbf{R}, \omega)$ may be written

$$\langle \mathbf{a}(\mathbf{R}) \rangle = \frac{N}{V}[1 + NF]\langle \alpha \rangle$$

where N is the number of molecules, $\langle \alpha \rangle$ is the mean polarizability and

$$\langle \alpha \rangle = \frac{1}{3} \mathrm{Tr}\langle \boldsymbol{\alpha}_j(t) \rangle$$

and F is a correlation factor which measures the dipole-induced dipole effect:

$$NF = \frac{1}{6} \mathrm{Tr} \sum_{k \neq j} \frac{\langle \boldsymbol{\alpha}_k \cdot \mathbf{T}_{k_j} \cdot \boldsymbol{\alpha}_j \rangle}{\langle \alpha \rangle} + \cdots$$

Intermolecular interactions affect $\langle \alpha \rangle$, but these are short range. The long range dipole fields are accounted for separately by the F factor, which depends on the shape of the dielectric sample. The polarization can be reexpressed as:

$$P(\omega) = \sum_{n,m} \left\{ \frac{N}{kTV} \sum \langle A_i^{(n)} A_j^{(m)} \rangle [1 + i\omega \tilde{C}_{\mathrm{M}}^{(n,m)}(\omega)] \right\} \cdot \mathbf{E}_0(\omega) + \frac{N}{V} \langle \alpha \rangle (1 + NF)\mathbf{E}_0(\omega)$$

where

$$\tilde{C}_{\mathrm{M}}^{(n,m)}(\omega) = \int_0^\infty dt \exp(i\omega t) C_{\mathrm{M}}^{(n,m)}(t)$$

and

$$A_j^{(n)} = \langle \mu \rangle \cos \theta_j$$

for $n = 1$; and

$$A_j^{(n)} = \Delta\mu_{E_{j0}}$$

for $n = 2$. Here, Kivelson and Madden write the macroscopic correlation function $C_{\mathrm{M}}(t)$ as a weighted sum of the four $C_{\mathrm{M}}^{(n,m)}(t)$ functions. $C_{\mathrm{M}}^{(11)}(t)$, $C_{\mathrm{M}}^{(22)}(t)$, and $C_{\mathrm{M}}^{(12)}(t)$ express the time dependence of the macroscopic correlation functions owing to reorientation of the molecules, to intra- and intermolecular effects, and to cross correlations between the two, respectively.

They also postulate that:

1. $C_{\mathrm{M}}^{(22)}(t)$ decays very rapidly compared with $C_{\mathrm{M}}^{(11)}(t)$ because $\Delta\mu_{E_{0j}}(t)$ contains many high frequency components due to intramolecular vibrations and molecular interactions.
2. The correlation functions $C_{\mathrm{M}}^{(12)}(t)$ may be slowly varying, but need not be included in the analysis if molecular polarizability is neglected.
3. The factors $C_{\mathrm{M}}^{(12)}(t)$ and $C_{\mathrm{M}}^{(21)}(t)$ may be described qualitatively with reference to Eq. 3.5.1. For instance, the dominant nonvanishing contribution to $\langle \Delta\mu_{E_{0i}} \cos \theta_j \rangle$ is a factor which is of long-range and is shape-dependent. This is supposed to have a very slow time dependence, and therefore the behavior of $C_{\mathrm{M}}^{(21)}(t)$ is determined principally by that of $\langle \cos \theta_j(t) \cos \theta_j \rangle$, which is that of $C_{\mathrm{u}}^{(11)}(t)$, the single-particle a.c.f.

At low frequencies, setting $C_M^{(22)} = 0 = C_M^{(21)} = C_M^{(12)}$ means that the effects of molecular polarizability are neglected. Let us now define a susceptibility $\chi^0(\omega)$ such that

$$\mathbf{P}(\omega) = \chi^0(\omega)\mathbf{E}_0(\omega)$$

Then if

$$\chi^0 = \chi_R^0 + i\chi_I^0$$

we have

$$\chi_R^0(\omega) = \frac{N\langle\mu\rangle^2}{3kTV}(1+Nf)[1-\omega\hat{I}C_M^{(11)}(\omega)] + \frac{N}{V}\left[\langle\alpha\rangle(1+NF) + \frac{B}{kT}\right]$$

where

$$B = \sum_j \langle\Delta\mu_{E_{0i}}\Delta\mu_{E_{0j}}\rangle + 2\sum_j \langle\Delta\mu_{E_{0i}}\cos\theta_j\rangle\langle\mu\rangle$$

and

$$\chi_I^0(\omega) = \frac{N\langle\mu\rangle^2}{3kTV}(1+Nf)\omega\hat{R}C_M^{(11)}(\omega)$$

and

$$f = 3\langle\cos\theta_1(0)\cos\theta_2(0)\rangle$$

The factor f is a dimensionless equilibrium structure factor which measures the correlations in the orientations of the dipoles. If the dipoles are all in the same direction, then $f = 1$; if there is no correlation, then $Nf = 0$. The quantity $1 + Nf$ is the Kirkwood factor at equilibrium. As $\omega \to 0$ and $\omega \to \infty$, χ_I^0 vanishes so that

$$1 + Nf = \frac{3kTV}{(N\langle\mu\rangle^2)}(\chi_R^0(0) - \chi_{R\infty}^0)$$

For a rectangular slab of dielectric material,

$$\chi^{(0)}(\omega) = \frac{\epsilon_0[\epsilon(\omega)-1]}{\epsilon(\omega)}$$

For a spherical sample in vacuo

$$\chi^0(\omega) = \frac{3\epsilon_0[\epsilon(\omega)-1]}{[\epsilon(\omega)+2]}$$

For a spherical sample embedded in an infinite continuum of dielectric material with the same dielectric constant as the sphere

$$\chi^0(\omega) = \frac{\epsilon_0[\epsilon(\omega)-1][2\epsilon(\omega)+1]}{3\epsilon(\omega)}$$

Therefore, provided that the sample is small compared with the measuring

wavelength, these are the equations that measure the shape dependence of the macroscopic correlation functions as we saw in our section dealing with the static permittivity.

Using these expressions for the spherical sample embedded in a continuous medium of the same dielectric constant, we have

$$\frac{\chi^0(\omega) - \chi_s^0}{\chi_s^0 - \chi_\infty^0} = i\omega C_M^{(11)}(\omega) \tag{3.5.3}$$

$$= \frac{\epsilon_\infty[\epsilon_s - \epsilon(\omega)][1 + 2\epsilon_s\epsilon(\omega)]}{\epsilon(\omega)[1 + 2\epsilon_s\epsilon_\infty][\epsilon_s - \epsilon_\infty]}$$

an equation derived by Fatuzzo and Mason (1967). These authors neglect the molecular polarizability embodied in the decay of $C_M^{(22)}(t)$, $C_M^{(12)}(t)$, and $C_M^{(21)}(t)$. In other words, although $\langle\alpha\rangle$ and $\langle\mu\rangle$ are both time independent and the same for all molecules in the system, they are equilibrium averages which may differ from the corresponding values in gases because of the distortion of the molecules due to intermolecular interactions.

3.5.1 Relation of $C_M^{(11)}(t)$ and $C_u^{(11)}(t)$

If the molecules are undergoing Debye-type rotational diffusion then "dielectric friction" is neglected and so are all intramolecular and intermolecular fluctuation details; that is, $\Delta\mu_{E_{0j}} = 0$ and $B = 0$. In this case,

$$C_u^{(11)}(t) = \exp\left(-\frac{t}{\tau_{s\theta}}\right)$$

The macro–micro theorem (Keyes and Kivelson, 1972) in this case provides us with the corresponding

$$C_M(t) = \exp\left(-\frac{t}{\tau_{M\theta}}\right)$$

where $\tau_{M\theta}$ is the macroscopic correlation time. The relationship between $\tau_{s\theta}$ and $\tau_{M\theta}$ is

$$\tau_{M\theta} = \tau_{s\theta}\frac{1+Nf}{1+N\dot{f}}$$

where

$$\dot{f} = \frac{\int_0^\infty dt\left\langle\frac{d}{dt}\cos\theta_1(t_p)\frac{d}{dt}\cos\theta_2(0)\right\rangle}{\int_0^\infty dt\left\langle\frac{d}{dt}\cos\theta_1(t_p)\frac{d}{dt}\cos\theta_1(0)\right\rangle}$$

is known as a dynamic orientational correlation factor. Here θ_j is the angle between the jth dipole and the applied field, and t_p indicates that the time dependence involves a projection operator (see Chapter 1). According to Kivelson and Madden (1975) the theories that make use of the microscopic

internal field implicitly set $\dot{f} = 0$. This is because the interrelationships obtained between the correlation times in these theories depend only upon ϵ_s and ϵ_∞ and so must be independent of dynamic terms such as $\dot{f}$.

If the above calculations are carried out correctly they must yield $\epsilon(\omega)$ independent of sample shape. This implies that $C_u^{(11)}(t)$ and $C_M^{(11)}(t)$ are both sample dependent.

In general, the dynamic models of Chapters 1 and 2 must be used to evaluate $C_u^{(11)}(t)$ and in this case the micro–macro theorems indicate that the multiparticle functions $C_M^{(11)}(t)$ have the same mathematical structure as the single-particle one.

In this way we suppose that we may approximate the Liouville equation as follows. Define as "primary variables" those that can be observed directly. Select a "complete set of slow variables" made up of the primary and secondary variables directly coupled to them. This is equivalent to truncating the continued fraction at a certain stage, or alternatively to choosing for the column vector **A** of Chapter 1 the required number of variables in the complete set. The secondary variables which decay rapidly compared with the times of observation are equivalent to random forces, the remaining slow variables being incorporated within **A** (Hansen and McDonald, 1976). For measurements at higher frequencies the secondary variables themselves can no longer be regarded as random; that is, their correlation functions start to resemble those of a deterministic system. The greater the frequency range to be studied, the larger the number of variables needed to complete the "slow" set and the larger the number (Q) of integro-differential Langevin equations. The solutions for $C_u(t)$ can be expressed as a sum of Q complex exponentials, or in the s domain, as a polynomial in s of order $Q-1$ over one of order Q. In the frequency domain they appear as a sum of generalized Lorentzians.

According to Kivelson and Madden the Mori continued fraction may be described in this way as being a prescription for adding derivatives to the set of primary variables $\mathbf{A} = [A_i]$. For a one-variable set, the second moment of the spectrum is finite but the fourth is infinite. For the set $[A, \dot{A}, \ddot{A}]$, the second and fourth are finite but the sixth is infinite. This process is continued as described in Chapter 1. The thermodynamic averages described as $\phi_0(0)$, $\phi_1(0)$, etc. are often transport coefficients.

Kivelson and Madden (1975) point out a useful analogy with perturbation theory. According to them the number of variables used in the Mori theory is analogous to the number of zeroth-order states in quantum mechanics (see Chapter 9). Perturbation theory works well if the state to be studied is the ground state and if the dominant interacting states are well below the infinite manifold of other states. The Mori theory is useful when the variable A to be studied is the *slowest* relevant variable. It is also useful if the first few derivatives are slower than the infinite manifold of processes of comparable rapidity described by the derivatives of A. In general, as Fig. 3.5.1.1 shows, $\langle \dot{\mathbf{u}}(t) \cdot \dot{\mathbf{u}}(0) \rangle$ does decay much more rapidly than

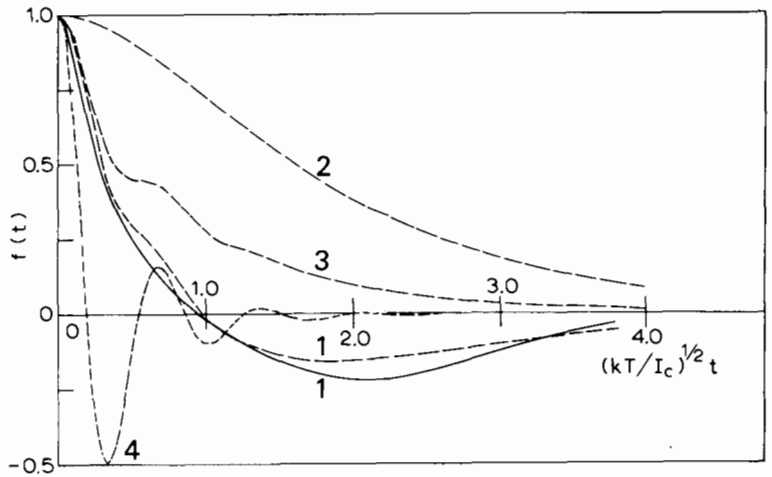

Figure 3.5.1.1 Solid line, experimental $\langle \dot{\mathbf{u}}(t) \cdot \dot{\mathbf{u}}(0) \rangle$ for liquid CH_2Cl_2, 1.97×10^{21} molecules/cm^3 in CCl_4. Dashed lines, (1) best fit, planar itinerant librator; (2) $\langle \mathbf{u}(t) \cdot \mathbf{u}(0) \rangle$, theoretical; (3) angular velocity a.c.f., theoretical; (4) torque a.c.f., theoretical. [Reproduced by permission from W. T. Coffey et al., *J. Chem. Soc. Faraday Trans. II* **74**, 310 (1978).]

$\langle \mathbf{u}(t) \cdot \mathbf{u}(0) \rangle$, but the simulation of Fig. 3.5.1.2 shows that this is by no means always the case.

The derivation of the macro–micro correlation theorem for the two-variable set and three-variable set depends on choosing for A the direction cosine $\cos\theta_1$ and its derivatives, where θ_1 is the angle between the applied field and dipole 1. The complete set of primary variables in the simplest case is

$$\mathbf{A} = \left[\cos\theta_1, \sum_{j=2}^{N} \cos\theta_j \right] \tag{3.5.1.1}$$

so that

$$C_u^{11}(t) = \langle \cos\theta_1(t) \cos\theta_1(0) \rangle$$

and

$$C_M^{11}(t) = \sum_{j=1} \langle \cos\theta_1(t) \cos\theta_j(0) \rangle$$

are both simple exponentials. If the angular velocity decays slowly but the torques decay rapidly, then we can take the set

$$\mathbf{A} = \left[\cos\theta_1, \frac{d}{dt}(\cos\theta_1), \sum_{j=2} \cos\theta_j, \sum_{j=2} \frac{d}{dt}(\cos\theta_j) \right]$$

In this case both $C_u(t)$ and $C_M(t)$ are sums of two complex exponentials. The easiest way of looking at this is to take the continued fraction for

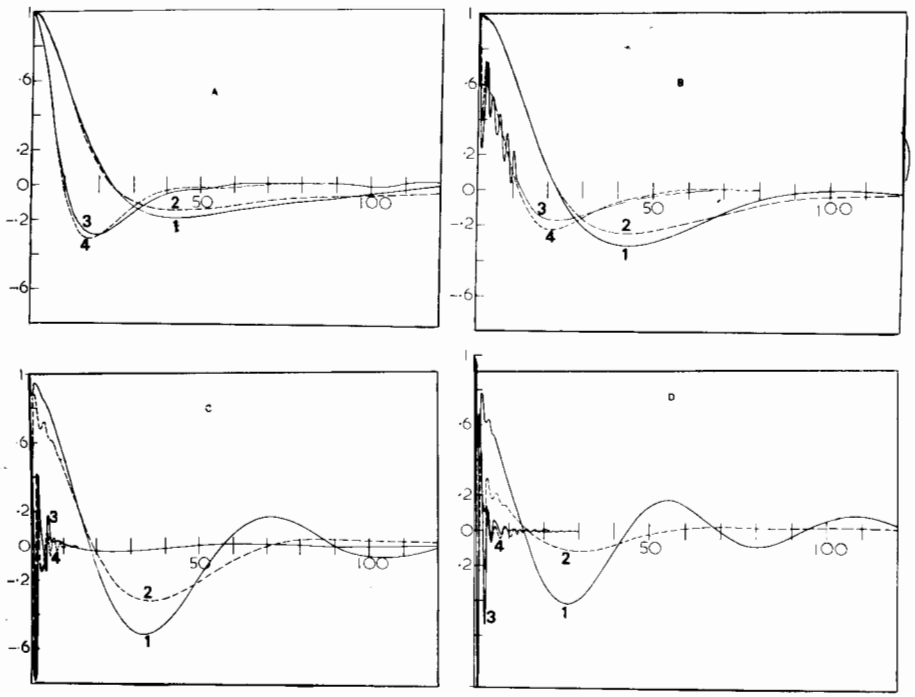

Figure 3.5.1.2 Computer simulation of a.c.f.'s for liquid nitrogen using a purely van der Waals type of potential (atom–atom Lennard-Jones).

1—$C_1(t) = \langle \dot{\mathbf{v}}(t) \cdot \dot{\mathbf{v}}(0) \rangle$; 2—$C_2(t) = \langle \ddot{\mathbf{v}}(t) \cdot \ddot{\mathbf{v}}(0) \rangle$;
3—$C_3(t) = \langle \dot{\boldsymbol{\omega}}(t) \cdot \dot{\boldsymbol{\omega}}(0) \rangle$; 4—$C_4(t) = \langle \ddot{\boldsymbol{\omega}}(t) \cdot \ddot{\boldsymbol{\omega}}(0) \rangle$

(*A–D*) increasing temperature. [Reproduced by permission from G. Wegdam et al., *Mol. Phys.* **33**, 1805 (1977).]

$C_u^{11}(t)$ and truncate so that

$$\tilde{C}_u^{11}(s) = \frac{C_u^{11}(0)}{s + \dfrac{\phi_0(0)}{s + \tilde{\phi}_1(s)}} = \frac{1}{s + \dfrac{\phi_0(0)}{s + \gamma_1}} = \frac{(s + \gamma_1)}{s(s + \gamma_1) + \phi_0(0)}$$

where γ is a constant defined by

$$\phi_0(t) = \phi_0(0) \exp(-\gamma t)$$

It follows that the spectrum $C_u^{11}(i\omega)$ is obtained by replacing s by $-i\omega$, so that

$$\tilde{C}_u^{11}(i\omega) = \frac{\gamma_1 \phi_0(0) + i\omega(\gamma_1^2 - \phi_0(0) + \omega^2)}{[\phi_0(0) - \omega^2]^2 + \omega^2 \gamma_1^2} \tag{3.5.1.2}$$

This is identical with the expression used by Kivelson and Madden; that is,

$$\tilde{C}_u^{11}(i\omega) = \frac{\tau_{s\theta} + i\omega^* \tau_{s\theta}[1 - \omega_\theta^{*-2} + \omega^{*2}\omega_\theta^{*-1}]}{(1 - \omega^{*2}\omega_\theta^{*-2})^2 + \omega^{*2}} \tag{3.5.1.3}$$

provided we identify the variables as follows:

$$\phi_0(0) = \frac{kT}{I} = 3\left\langle \left(\frac{d \cos \theta_1}{dt} \right)^2 \right\rangle_{t=0}$$

$$\tau_{s\theta} = \frac{\gamma}{\phi_0(0)} = \frac{I\gamma_1}{kT}$$

$$\omega^* = \tau_{s\theta}\omega$$

and finally

$$\omega_\theta^{*2} = \frac{kT}{I}\,\tau_{s\theta}^2$$

Here I is an effective moment of inertia, and $\tau_{s\theta}$ an effective single particle orientational correlation time.

The Mori equation is now written in the tensor form:

$$\frac{d}{dt}\langle \mathbf{A}(t)\mathbf{A}^T(0) \rangle = [i\hat{\Omega} - \hat{\phi}]\langle \mathbf{A}(t)\mathbf{A}^T(0) \rangle \tag{3.5.1.4}$$

with **A** defined by Eq. 3.5.1.1. Note that the resonance operator $\hat{\Omega}$ is no longer necessarily null because we are now dealing with collective motions. $\hat{\phi}$ and $\hat{\Omega}$ are as defined in Chapter 1. After some mathematics we find that $C_M^{(11)}(i\omega)$ is also given by an equation of the form of Eq. 3.5.1.3 but with the all-important difference that

$$\begin{aligned} \tau_{s\theta} \text{ is replaced by } \tau_{M\theta} &= \frac{(1 + Nf)\tau_{s\theta}}{1 + N\dot{f}} \\ \omega^* \text{ is replaced by } \Omega &= \omega\tau_{M\theta} \\ \omega_\theta^{*2} \text{ is replaced by } \Omega_\theta^2 &= \frac{(1 + Nf)\omega_\theta^{*2}}{(1 + N\dot{f})^2} \end{aligned} \tag{3.5.1.5}$$

This result is valid under the following conditions. Introduce the correlation time $\tau_\omega^{-1} = \omega_T^2 \tau_{sT}$ where ω_T is the equilibrium average:

$$\omega_T^2 = \frac{3}{\omega_s^2}\left\langle \left((\hat{1} - \hat{P})\frac{d^2}{dt^2}\cos\theta_1 \right)^2 \right\rangle_{t=0}$$

The time τ_{sT} is that of the correlation of intermolecular torques. This must be short compared with all other times. Furthermore, $\tau_\omega \omega_s \ll 1$, where τ_ω is an angular velocity correlation time. We have already mentioned that the fourth spectral moment is not defined in this approach, so that there is no definable mean square torque. The consequences in the far infrared are clearly seen in Fig. 3.5.1.3. They also manifest themselves as a failure to move the peak position away from the value defined by the root mean square angular velocity in the gas phase. This is quite a severe shortcoming which does not show up on a Cole–Cole plot (Fig. 1.1.1), Chapter 1, because this tends to underestimate the significance of the far infrared information. The correlation functions of this model are identical with those derived from the Bocard equation derived in Chapter 2. These are illustrated in Fig.

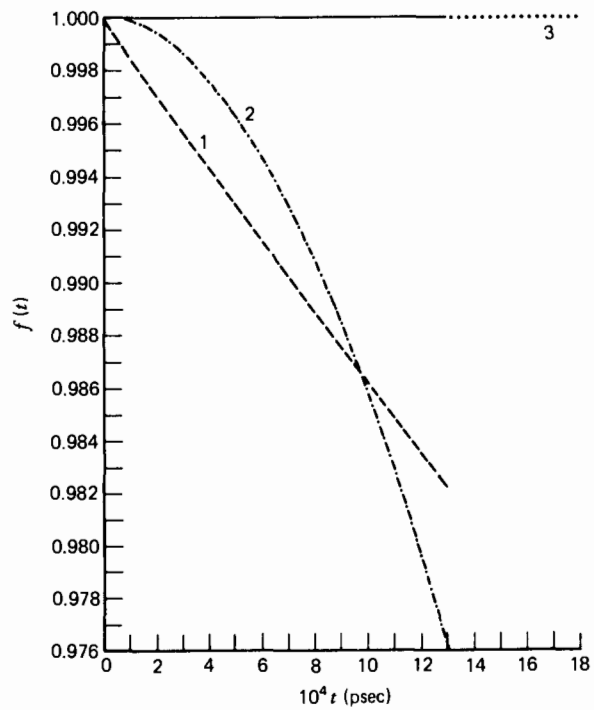

Figure 3.5.1.3 Behavior of models at short times. Solid line, experimental; ---- (1) rotational diffusion, (2) –·–·–·– two-variable Mori theory, and (3) free rotor for *tert*-butyl chloride (rotator phase) at 238°K. [Reproduced by permission from M. W. Evans, *J. Chem. Soc. Faraday Trans. II* **71** 2051, (1975).]

1.3.1.3 for several liquids and plastic crystals. The failure at short times is obvious, and is exemplified by Fig. 3.5.1.3. We have:

$$C_u^{11}(t) = \frac{\lambda_+}{\lambda_+ - \lambda_-}\exp(-\lambda_- t) - \frac{\lambda_-}{\lambda_+ - \lambda_-}\exp(-\lambda_+ t)$$

where

$$\tau_{s\theta}\lambda_\pm = \tfrac{1}{2}(\omega_\theta^*)^2[1 \pm (1 - 4(\omega_\theta^*)^{-2})^{1/2}]$$

which is again identical with the form used by Brot (1975) for a model of libration in potential wells. This is valid only for $\omega_\theta^{*2} \gg 1$, that is, for $\gamma_I^2/kT \gg 1$ ($kT/I\beta^2 \ll 1$ in the notation of Chapter 2), for large moments of inertia and low temperatures as discussed in Chapter 2. It will be helpful to the reader to see the exact steps involved in comparing this Mori approximant with the Rocard equation. From Chapter 2 the normalized complex polarizability is

$$\frac{\alpha(s)}{\alpha'(0)} = 1 - s\mathscr{L}C_u(t) = 1 - s\tilde{C}_u(s)$$

Now from the Rocard equation

$$\frac{\alpha(s)}{\alpha'(0)} = \frac{1}{1 + s\tau_0 + s^2(\tau_0/\beta)}$$

and thus $\tilde{C}_u(s)$ is given by

$$\tilde{C}_u(s) = \frac{s + \beta}{s^2 + \beta s + \beta/\tau_0}$$

which is identical with our Mori approximant.

A formula extensively tested by Evans and co-workers (1980) is obtained if we extend the macro–micro correlation theory to three variables. This means that the mean square torque is defined and the characteristic far infrared shift of the peak frequency (e.g., Figs. 3.4.4.1 and 1.2.3) may be followed more successfully. It is doubly advantageous to use the far infrared in this context since we have already seen that here the cavity corrections have little numerical effect, and that it is exactly at these frequencies that the collective motions (embodied in $C_M^{11}(t)$, and termed "plasmons" by Lobo et al., 1973) are likely to be effective. There is tremendous scope for further development here since none of the present theories (see Fig. 1.7.4.1) are very satisfactory when the complete 0–THz range is taken into account.

The easiest way of handling the initial stages of the three-variable theory is to take the following Mori approximant (Chapters 2 and 4):

$$\tilde{C}_u^{11}(s) = \frac{C_u^{11}(0)}{s + \dfrac{\phi_0(0)}{s + \tilde{\phi}_1(s)}} = \frac{1}{s + \dfrac{\phi_0(0)}{s + \dfrac{\phi_1(0)}{s + \gamma_2}}} = \frac{s(s + \gamma_2) + \phi_1(0)}{s^3 + \gamma_2 s^2 + [\phi_1(0) + \phi_0(0)]s + \phi_0(0)\gamma_2}$$

so that

$$\hat{R}\tilde{C}_u''(i\omega) = \frac{\gamma_2\phi_0(0)\phi_1(0)}{\gamma_2^2[\phi_0(0) - \omega^2]^2 + \omega^2\{\omega^2 - [\phi_0(0) + \phi_1(0)]\}^2} \qquad (3.5.1.6)$$

is the absorption spectrum. The form used by Kivelson and Madden (1975) is

$$\hat{R}\tilde{C}_u^{11}(i\omega) = \tau_{s\theta}\left\{1 + \left(\frac{\omega^*}{\omega_\theta^*}\right)^2[(\omega_\theta^* + \omega_I^*)^2 - 2] + \left(\frac{\omega^*}{\omega_\theta^*}\right)^4[1 - 2\omega_I^*(\omega_\theta^* + \omega_I^*)] + \left(\frac{\omega^*}{\omega_\theta^*}\right)^6\omega_I^{*2}\right\}^{-1} \qquad (3.5.1.7)$$

Equations 3.5.1.6 and 3.5.1.7 are equivalent provided that we make the identities

$$\frac{\phi_0(0)}{\phi_1(0)}\gamma_2 \equiv \frac{1}{\tau_{s\theta}}$$

$$\left(\frac{\omega^*}{\omega_\theta^*}\right)^6\frac{\omega_I^{*2}}{\tau_{s\theta}} \equiv \frac{\omega^6}{\gamma_2\phi_0(0)\phi_1(0)}$$

$$\omega^2\left[\left(\frac{\phi_0(0)}{\phi_1(0)}+\frac{\phi_1(0)}{\phi_0(0)}+2\right)\frac{1}{\gamma}-\frac{2\gamma_2}{\phi_1(0)}\right]\equiv\left(\frac{\omega^*}{\omega_\theta^*}\right)^2\frac{[(\omega_\theta^*+\omega_T^*)^2-2]}{\tau_{s\theta}}$$

$$\frac{[1-2\omega_T^*(\omega_\theta^*+\omega_T^*)]}{\tau_{s\theta}}\left(\frac{\omega^*}{\omega_\theta^*}\right)^4\equiv\frac{\omega^4}{\phi_0(0)\phi_1(0)}\left(\gamma_2-\frac{2[\phi_0(0)+\phi_1(0)]}{\gamma_2}\right)$$

The ability of this type of equation to reproduce far infrared/microwave data has been illustrated in Fig. 1.7.4.1. The parameters of Eq. 3.5.1.7 are defined as follows. The frequency ω_T^* is defined as

$$\omega_T^*=\left(\frac{kT}{T}\right)^{1/2}\tau_{sT}$$

where τ_{sT} is a single-particle correlation time associated with intermolecular torques. The single-particle orientational correlation time is now

$$\tau_{s\theta}=\left[\frac{\langle(d^2\cos\theta_1/dt^2)^2\rangle}{(kT/I)^2}-1\right]\tau_{sT}$$

which is $\tilde{C}_u(0)$. Using now the relations $\omega_\theta^{*2}=(kT/I)\tau_{s\theta}^2=\phi_0(0)\tau_{s\theta}^2$, $\omega^*=\tau_{s\theta}\omega$, and $\omega_T^{*2}=\phi_0(0)\tau_{sT}^2$, then it follows that

$$\frac{\phi_1(0)}{\phi_0(0)}=\frac{\langle(d^2\cos\theta_1/dt^2)^2\rangle}{(kT/I)^2-1}\qquad(3.5.1.8)$$

and

$$\gamma_2=\frac{1}{\tau_{sT}}$$

Given these relations, Eq. 3.5.1.7 may be rewritten exactly as Eq. 3.5.1.6. By comparing this again with Eq. 3.4.7.1 we can see that the correlation time τ of Nee and Zwanzig is:

$$\tau=\tau_{sT}=\gamma_2^{-1}\qquad(3.5.1.9)$$

The mean square torque $\langle N_T^2\rangle$ used by these authors is:

$$\frac{\langle N_T^2\rangle}{2(kT)^2}=\left[\frac{\langle(d^2\cos\theta_1/dt^2)^2\rangle}{(kT/I)^2}-1\right]\qquad(3.5.1.10)$$

We thus see that the three-variable continued fraction accounts for the presence of mean square torque via the torque correlation frequency γ_2 and via $\phi_1(0)/\phi_0(0)$. It is a very useful representation of some of the single-particle models in the literature, and using a micro–macro correlation theorem allows us to extend the models to include cooperative behavior without microscopic cavities.

If we now define $\omega_s=(kT/I)^{1/2}$, then $\tau_{s\theta}=(\omega_T^2/\omega_s^2)\tau_{sT}$. The conditions under which Eqs. 3.5.1.6 and 3.5.1.7 are valid may now be clarified. The factor ω_T^* is associated with the rate of fluctuation of intermolecular torque, since $(d^2\cos\theta_1/dt^2)$ is very nearly a torque (Eq. 3.5.1.10). If $\omega_T^*\ll 1$, that is, if $\phi_0^{1/2}(0)=(kT/I)^{1/2}\ll\gamma_2$, then the motion is diffusional, or extended

diffusional (along the lines of the J- or m-diffusion models). If $\gamma_2\lesssim\phi_0(0)$, then the torques are long acting and the molecule "jumps" from orientational site to site with a long time between the jumps. This is the situation expected in TCTMB at fairly high temperatures or in a plastic crystalline (rotator) phase. There is an obvious analogy with the jump models of Ivanov (1964). Whereas $\omega_T^*=\phi_0^{1/2}/\gamma_2$ is the time (in units of free rotational periods $1/\phi_0^{1/2}$) at an orientational site or the time between the start of successive jumps, $\omega_\theta^*=\phi_0^{1/2}\tau_{s\theta}$ is related to the time required to reorient molecules in the liquid, that is, the orientational relaxational time. We have

$$\omega_\theta^*=\frac{\phi_1(0)}{\phi_0^{1/2}(0)\gamma_2}$$

The ratio $\omega_T^*/\omega_\theta^*$ is given by

$$\frac{\omega_T^*}{\omega_\theta^*}=\left[\frac{\langle(d^2\cos\theta_1/dt^2)\rangle}{(kT/I)^2}-1\right]^{-1}=\frac{2(kT)^2}{\langle N_T^2\rangle}=\frac{\phi_0(0)}{\phi_1(0)}$$

The larger the torque, the smaller $(\omega_T^*/\omega_\theta^*)$, which is a measure of the "angle" covered in a jump, that is, when $\langle N_T^2\rangle\to 0$ (free rotation), the "angle" $\omega_T^*/\omega_\theta^*$ is effectively infinite. There are a number of limitations in this theory, some of which have already been discussed. In all cases we must have $\omega_\theta^*\gg 1$, that is,

$$\phi_1(0)\gg\gamma_2\left(\frac{kT}{I}\right)^{1/2}$$

otherwise the molecule would perform almost free rotation for a period commensurate with $(I/kT)^{1/2}$, and this would require primary orientation variables for each angular momentum state J. The limit of free rotation is therefore not correctly approached. The intermolecular torques must decay sufficiently rapidly so that their effects on the primary variables are required for each site in the liquid, described by a distinct intermolecular torque. This means that

$$\frac{\Delta(N_T)}{I\gamma_2}\ll 1$$

where $\Delta(N_T)$ is the standard deviation in the intermolecular torques. In the one- and two-variable theories the torques must change rapidly, that is, $\omega_\theta^*\omega_T^*\ll 1$ and $\gamma_2^2\gg\phi_1(0)$, but in three-variable theory this is not necessarily so and is very rarely the case in practice.

The macroscopic function $\tilde{C}_M^{11}(i\omega)$ is very conveniently given by a relation identical with Eqs. 3.5.1.6 or 3.5.1.7 but with ω^*, ω_θ^*, and ω_T^* replaced by the dimensionless quantities Ω, Ω_θ, and Ω_T, respectively, and $\tau_{s\theta}$ by $\tau_{M\theta}$. These are defined in Eqs. 3.5.1.5 except for Ω_T, which is defined by

$$\Omega_T^2=\frac{(1+\ddot{f}N)^2}{1+fN}\omega_T^{*2}=\frac{(1+\ddot{f}N)^2}{1+fN}\frac{\phi_0(0)}{\gamma_2^2}$$

where $\ddot{f}$ is an equilibrium coupling parameter defined by

$$\ddot{f} = \frac{\langle (d^2/dt^2)\cos\theta_1 (d^2/dt^2)\cos\theta_2\rangle + (kT/I)^2 f(1+fN)^{-1}}{\langle (d^2\cos\theta_1/dt^2)^2\rangle - (kT/I)^2}$$

To fit experimental data in a highly dipolar liquid over the whole 0–THz range the following procedure has been recommended by Evans:

1. Firstly use an equation such as Eq. 3.5.3 to relate $C_M^{(1)}(\omega)$ and $\epsilon(\omega)$, the complex permittivity. Replace ϵ_∞ by n^2 taken at the end of the far infrared dispersion.
2. Introduce $C_M^{(1)}(\omega)$ through Eq. 3.5.1.4 with Γ_2 substituted for γ_2, $\Phi_0(0)$ for $\phi_0(0)$, and $\Phi_1(0)$ for $\phi_1(0)$. These are defined by

$$\Gamma_2 = \frac{1}{\tau_{MT}}$$

where

$$\tau_{MT} = \frac{\tau_{sT}}{(1+\dot{f}N)/(1+\ddot{f}N)}$$

that is,

$$\Gamma_2 = \gamma_2(1+\dot{f}N)(1+\ddot{f}N) \qquad (3.5.1.11)$$

$$\Phi_0(0) = \frac{\Omega_\theta^{*2}}{\tau_{M\theta}^2} = \frac{kT}{I}(1+Nf)^{-1} = \frac{kT}{Ig} \qquad (3.5.1.12)$$

where g is the Kirkwood factor. Finally,

$$\Phi_1(0) = \frac{kT}{I}(1+\ddot{f}N)\left[\frac{\langle (d^2\cos\theta_1/dt^2)^2\rangle}{(kT/I)^2} - 1\right] = \frac{1+\ddot{f}N}{2kTI}\langle N_T^2\rangle \qquad (3.5.1.13)$$

3. Use a least mean squares best fitting algorithm to fit the power absorption coefficient $\mathfrak{A}(\omega)$, the loss $\epsilon''(\omega)$, the permittivity $\epsilon'(\omega)$, and the frequency-dependent refractive index $n(\omega)$.

Summary

The complete set of equations that have been found useful in relating the observables to $C_M^{(1)}(i\omega)$ and then to the molecular averages are as follows:

$$\frac{\chi^0(\omega)-\chi_s^0}{\chi_s^0-\chi_\infty^0} = i\omega C_M^{(1)}(i\omega)$$

$$C_M^{(1)}(i\omega) = \tilde{C}_M^{(1)}(s) = \frac{s^2+\Gamma_2 s+\Phi_1(0)}{s^3+\Gamma_2 s^2+[\Phi_0(0)+\Phi_1(0)]s+\Gamma_2\Phi_0(0)}$$

with $s = -i\omega$.

$\epsilon'(\omega)$ and $\epsilon''(\omega)$ are then obtained for a given macroscopic sample shape. Finally these are related to the power absorption coefficient $\mathfrak{A}(\omega)$ by a least mean squares iteration on Γ_2, $\Phi_0(0)$, and $\Phi_1(0)$; and Eqs. 3.5.1.11 to 3.5.1.13 are used to obtain information on f, $\dot{f}$, and $\ddot{f}$, the correlation time γ_2, the Kirkwood factor g, and the effective molecular mean square torque.

The relative magnitudes of $\Phi_0^{1/2}(0)$ and Γ_2 are used to obtain information about the nature of the molecular dynamics; that is, if $\Phi(0)^{1/2} \ll \Gamma_2$, the motion is diffusional. If $\Gamma_2 \leqslant \Phi_0^{1/2}(0)$ torques are long-lived. If $\Phi_1(0)/\Phi_0(0)$ is large, then so is the effective torque, and the mean "angle" covered in a "jump" is small.

In the three variable equations given above internal field corrections and cross correlations are treated with a macro–micro correlation theorem linking $C_M(t)$ and $C_u(t)$. It is essential to use the complete 0–THz spectrum in evaluating this formula; otherwise it will be impossible to calculate the various parameters for lack of discriminatory, short time, high frequency data. An example of its use is given in the next section. Finally note that $C_M''(i\omega)$ is relevant to rigid molecules with zero polarizability. For all but the simplest of liquids, multiple relaxation processes may occur. If the intermolecular torques do not relax rapidly enough for the rotational motion to be averaged over all different molecular sites, then each site, distinguished by an appreciably different local environment, must be treated separately. This would give a skewed Cole–Cole arc (i.e., Cole–Davidson) in the complex plane defined by ϵ' and ϵ''.

3.6 EVALUATION IN THE FAR INFRARED

To end this chapter we exemplify the methods used to evaluate the orientational Mori three-variable theory of Section 3.5 in the far infrared, using referential low frequency loss data. In Chapter 4 we deal with angular velocity formalism (Evans, 1976). Initially, note that the correlation functions $C_M(t)$ and $C_u(t)$ are both given by an equation of the following kind (in the notation of section 2.12):

$$C(t) = (1+\Lambda)^{-1}\{[\cos\omega_1 t + (\sigma_1+\Lambda\sigma_2)^{-1}\omega_1^{-1}\sin\omega_1 t)e^{-\sigma_1 t}] + \Lambda e^{-\sigma_2 t}\}$$

$$\Lambda = \frac{-2\sigma_1(\sigma_1^2+\omega_1^2)}{\sigma_2(3\sigma_1^2-\sigma_2^2-\omega_1^2)} \qquad (3.6.1)$$

where

$$\sigma_2 = -\frac{1}{2}(s_1+s_2)+\frac{\Gamma_2}{3}; \qquad \sigma_1 = \frac{1}{2}(s_1+s_2)+\frac{\Gamma_2}{3}$$

with

$$\omega_1 = \frac{\sqrt{3}}{2}(s_1-s_2)$$

The parameters s_1 and s_2 are defined by

$$s_1 = \left[-\frac{B}{2} + \left(\frac{A^3}{27} + \frac{B^2}{4}\right)^{1/2}\right]^{1/3}$$

$$s_2 = \left[-\frac{B}{2} - \left(\frac{A^3}{27} + \frac{B^2}{4}\right)^{1/2}\right]^{1/3}$$

where

$$A = \Phi_0(0) + \Phi_1(0) - \frac{\Gamma_2^2}{3}$$

$$B = \frac{\Gamma_2}{3}\left(\frac{2\Gamma_2^2}{9} + 2\Phi_0(0) - \Phi_1(0)\right)$$

Note: This orientational a.c.f. has the same form as the *angular velocity* correlation function for the itinerant oscillator model (Calderwood and Coffey, 1977) discussed in Chapter 4.

We may replace Γ_2 by γ, $\Phi_0(0)$ by $\phi_0(0)$, and $\Phi_1(0)$ by $\phi_1(0)$ using the three-variable macro–micro theorem. The Taylor series of Eq. 3.6.1 is even up to t^4, but it has a term in t^5, and all odd terms thereafter are also nonzero. Equation 3.6.1 is the one used in Fig. 3.4.6.3 to describe the motions of water in very dilute solution. In this case and in all cases where the factors f, $\dot{f}$, and $\ddot{f}$ are vanishingly small [when $\epsilon_s - n^2$ is small] we may use the theory in its simplest form; that is,

$$\epsilon''(\omega) = \frac{[\epsilon_s - n^2]\gamma\phi_0(0)\phi_1(0)}{\gamma^2[\phi_0(0) - \omega^2]^2 + \omega^2\{\omega^2 - [\phi_0(0) + \phi_1(0)]\}^2}$$

$$\epsilon'(\omega) = \epsilon_s - [\epsilon_s - n^2]\omega^2 \times \left(\frac{\gamma^2[\omega^2 - \phi_0(0)] + [\omega^2 - \phi_1(0)]\{\omega^2 - [\phi_0(0) + \phi_1(0)]\}}{\gamma^2[\omega^2 - \phi_0(0)]^2 + \omega^2\{\omega^2 - [\phi_0(0) + \phi_1(0)]\}^2}\right)$$

The far infrared power absorption coefficient as a function of wave number, $\bar{\nu}(\omega = 2\pi\bar{\nu}c)$, is now

$$\mathfrak{A}(\bar{\nu}) = \frac{2\sqrt{2}\pi\epsilon''(\bar{\nu})\bar{\nu}}{\{[\epsilon'(\bar{\nu})^2 + \epsilon''(\bar{\nu})^2]^{1/2} + \epsilon'(\bar{\nu})\}^{1/2}} \tag{3.6.2}$$

It is convenient to normalize the factors appearing in these equations with the scheme

$$\gamma^* = \gamma\left(\frac{I}{2kT}\right)^{1/2}$$

$$\phi_0^*(0) = \phi_0(0)\left(\frac{I}{2kT}\right)$$

$$\phi_1^*(0) = \phi_1(0)\left(\frac{I}{2kT}\right)$$

where the moment of inertia used is defined as follows:

1. In a linear molecule or symmetrical top, use the moment of inertia perpendicular to the dipole.
2. In an asymmetric top use the normalizing factor:

$$\langle\dot{u}^2\rangle^{1/2} = \left[kT\left(\frac{1}{I_x} + \frac{1}{I_y}\right)\right]^{1/2}$$

if the dipole lies in the axis of I_z. Otherwise use

$$\langle\dot{u}^2\rangle^{1/2} = \left[\frac{u_y^2 + u_z^2}{I_x} + \frac{u_z^2 + u_x^2}{I_y} + \frac{u_x^2 + u_y^2}{I_z}\right]kT$$

Note again carefully, however, that the three-variable theory is strictly valid only for rotation in a plane and as a crude approximation to the spherical top. This may be seen most clearly by writing the effective Debye relaxation time of this theory

$$\tau_D = \left(\frac{[\phi_0(0) + \phi_1(0)]^2 - 2\phi_0(0)\gamma^2}{\phi_0^2(0)\gamma^2}\right)^{1/2}$$

that is, the inverse peak frequency ω_{max} of $\epsilon''(\omega)$. There is only one τ_D, whereas the theory of Chapter 2 demands three for the asymmetric top and two for the symmetrical top. Note lastly that the spherical top with embedded dipole does not exist naturally except in some very special cases such as 1,1,1-trifluoroethane. A spread of primary relaxation times needs a spread of primary variables as mentioned already.

3.6.1 Molecular Motion in the Gas Phase

In this section we use Eq. 3.6.2 to describe the molecular orientations in a compressed dipolar gas before proceeding to the liquid state as embodied in such a species as CH_2Cl_2 (see Chapter 6). We have chosen for experimental convenience the symmetrical top CH_3Cl and the asymmetric planar top CH_2CF_2. In the limit of free rotation the infinite continued fraction reduces to the classical free rotor functions (when these are known) for $C_u(t)$, but the three variable theory does not. A typical least mean squares fit of $\mathfrak{A}(\bar{\nu})$ (Eq. 3.6.2) to the CH_3Cl compressed gas is shown in Fig. 3.6.1.1, together with that for a gaseous mixture of CH_3Cl in ethylene (to remove cross correlations). The fit for pure liquid CH_3Cl is good with $\phi_1(0)$ considerably increased. In this fitting an internal field correction was not used in the sense that $\epsilon_s - n^2$ is still small enough for Eq. 3.6.2 to be valid, and the Kirkwood factor $1 + Nf$ was set at unity, so that $\phi_0(0)$ was not iterated upon. A more accurate fitting would involve an equation such as Eq. 3.5.3 and all three parameters Γ, $\Phi_0(0)$, and $\Phi_1(0)$. In a mixture with ethane in the liquid state $\phi_1(0)$ is small and the observed band is narrow (reflected in a small γ). The mean square torque is small and the torque itself is long-lived; that is, the reorientation is inertia dominated and

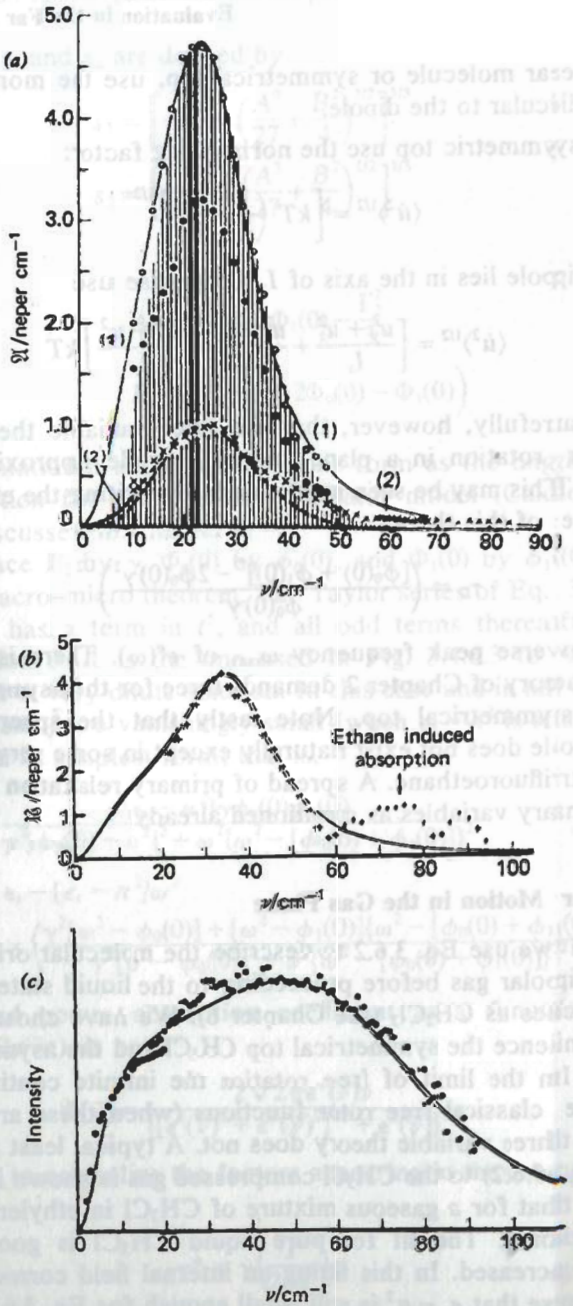

Figure 3.6.1.1 (*a*) ○ Absorption of CH_3Cl at 5.8 bar, 296°K; ● 4.4 bar, 296°K; × CH_3Cl/ethane at a total pressure of 33.5 bar, 296°K. Vertical lines, set of $\Delta J = 1$ lines for quantized free rotation. (1) Solid line, best fitted using $\phi_0(0)$, $\phi_1(0)$, and γ. (2) Best least mean squares fit to the ××× data. Dashed line, contour of the $J \rightarrow J+1$ lines. (*b*) Absorption of CH_3Cl/ethane (liquid) at 296°K. Solid line, best fit using $\phi_0(0)$, $\phi_1(0)$, and γ. (*c*) Absorption of liquid CH_3Cl at 296°K. Solid line, best fit Mori three-variable theory. [Reproduced by permission from G. J. Evans et al., *J. Chem. Soc. Faraday Trans. II*, 72, 1901 (1976).]

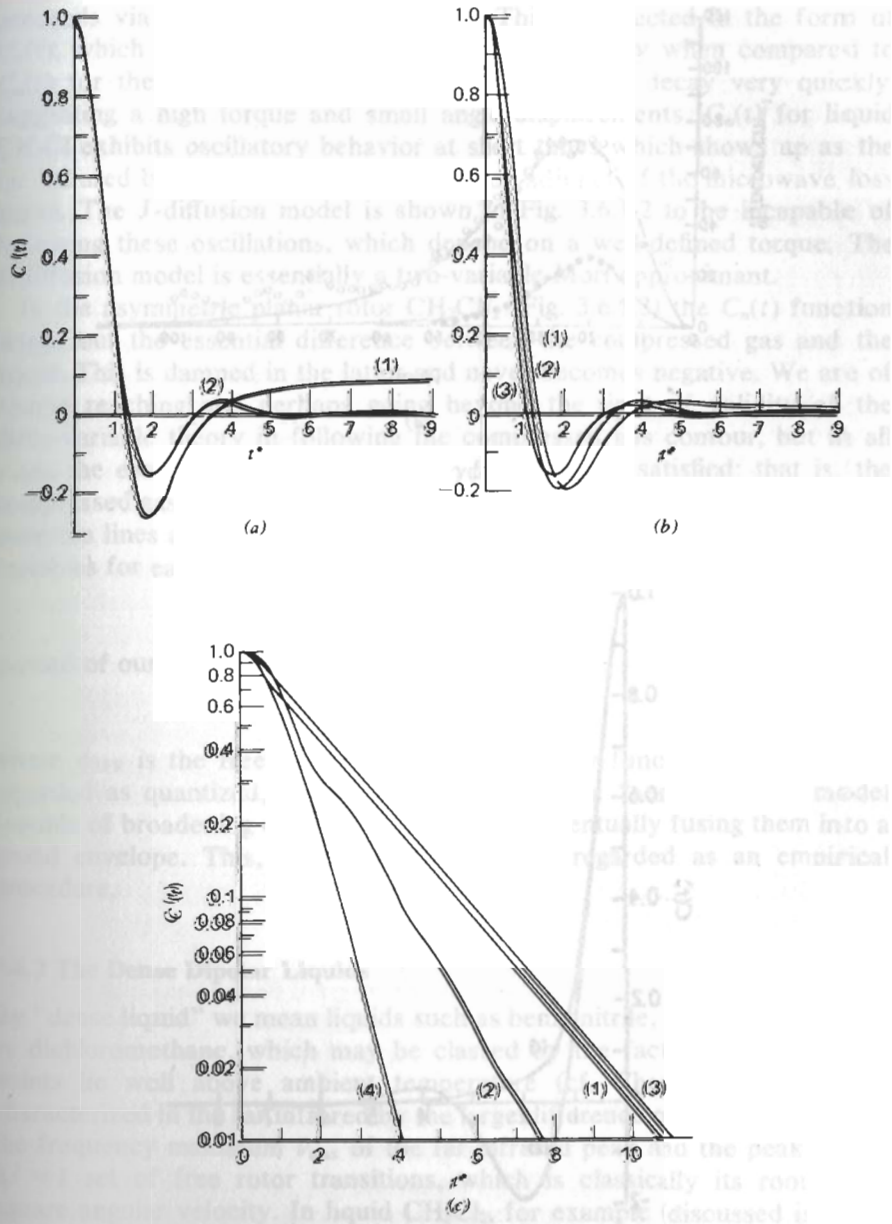

Figure 3.6.1.2 (*a*) $t^* = (kT/I_B)^{1/2}t$. (1) True free rotor orientational a.c.f. for CH_3Cl at 296°K; (2) best fit of Mori three-variable theory to the $J \rightarrow J+1$ contour. (*b*) (1) $C_n(t)$ for gaseous CH_3Cl at 5.8 bar, 296°K; (2) J-diffusion model with $\tau^* = (kT/I_B)^{1/2}\tau = 4.0$, the mean time between elastic collisions; (3) $C_n(t)$ for CH_3Cl/ethane (gas) at 33.5 bar, 296°K. (*c*) (1) $C_n(t)$ for CH_3Cl (liquid) at 296°K; (2) $C_n(t)$ for CH_3Cl/ethane (liquid) at 296°K; (3) J-diffusion model with $\tau^* = 0.2$; (4) $\tau^* = 0.5$. [Reproduced by permission from G. J. Evans et al. *J. Chem. Soc. Faraday Trans. II* 72, 1901 (1976).]

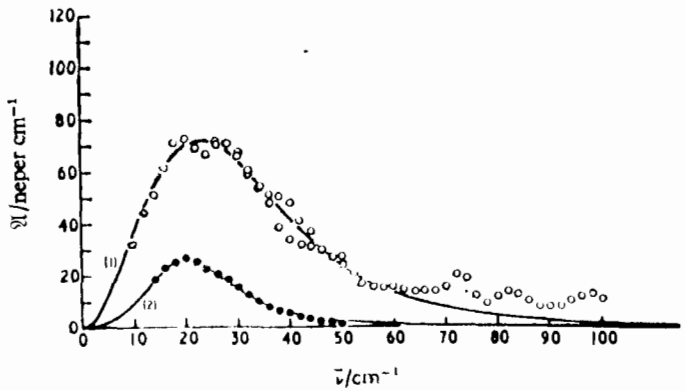

(a)

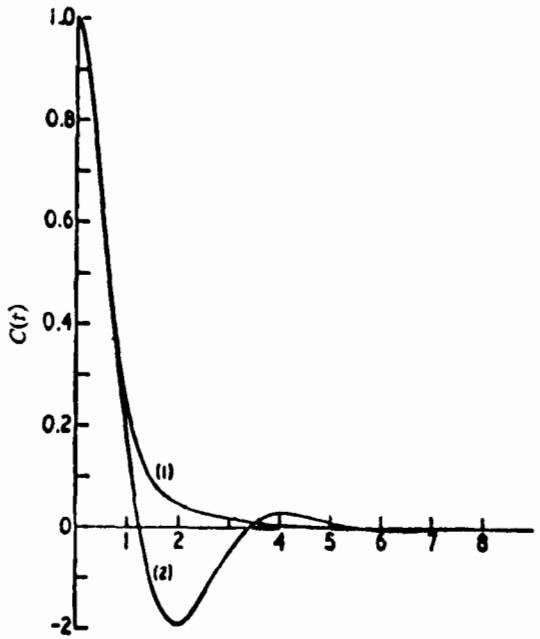

(b)

Figure 3.6.1.3 (*a*) ○ Absorption in the far infrared of CH_2CF_2 liquid at 296°K; ● absorption of CH_2CF_2 gas at 35.2 bar, 296°K. Curves 1 and 2, Mori three-variable theory, best fit, iterating on three variables. (*b*) (1) $C_u(t)$ from (*a*), liquid CH_2CF_2; (2) gas at 35.2 bar. [Reproduced by permission from G. J. Evans, *J. Chem. Soc. Faraday Trans. II* **72**, 1901 (1976).]

proceeds via large angle displacements. This is reflected in the form of $C_u(t)$, which becomes exponential at long times only when compared to $C_u(t)$ for the pure liquid. This exhibits logarithmic decay very quickly, suggesting a high torque and small angle displacements. $C_u(t)$ for liquid CH_3Cl exhibits oscillatory behavior at short times which shows up as the far infrared broad band, the high frequency adjunct of the microwave loss curve. The J-diffusion model is shown in Fig. 3.6.1.2 to be incapable of following these oscillations, which depend on a well-defined torque. The J-diffusion model is essentially a two-variable Mori approximant.

In the asymmetric planar rotor CH_2CF_2 (Fig. 3.6.1.3) the $C_u(t)$ function brings out the essential difference between the compressed gas and the liquid. This is damped in the latter and never becomes negative. We are of course reaching and perhaps going beyond the limit of validity of the three-variable theory in following the compressed gas contour, but in all cases the essential constraint $\phi_1(0) > \gamma\phi_0^{1/2}(0)$ is still satisfied; that is, the compressed gas absorption is the classical envelope of the set of the $\Delta J = 1$ quantum lines and it is not essential to construct a separate set of primary variables for each J. However, this could be done by using

$$\phi_1(t) = \phi_{1FR}(t)\exp(-\gamma|t|)$$

instead of our

$$\phi_1(t) = \phi_1(0)\exp(-\gamma t)$$

where ϕ_{1FR} is the free rotational second memory function. This may be regarded as quantized, so that we can build up a "semiclassical" model capable of broadening each $J \to J+1$ line and eventually fusing them into a broad envelope. This, however, must yet be regarded as an empirical procedure.

3.6.2 The Dense Dipolar Liquids

By "dense liquid" we mean liquids such as benzonitrile, *tert*-butyl chloride, or dichloromethane, which may be classed by the fact that their critical points lie well above ambient temperature (cf. Chapter 4). They are characterized in the far infrared by the large difference observable between the frequency maximum $\tilde{\nu}_{max}$ of the far infrared peak and the peak of the $\Delta J = 1$ set of free rotor transitions, which is classically its root mean square angular velocity. In liquid CH_2Cl_2, for example (discussed in great detail in Chapter 12), the complete 0–THz band shape is available and accurate to within a few percent of $\mathfrak{A}(\tilde{\nu})$. At a long enough time after the initial $t = 0$ the molecular interactions and motions in the densely packed N molecule ensemble evolve in such a way that the decay in the correlation functions $\langle A_j(t)A_j(0)\rangle$ is exponential. After many interruptions in its trajectory the probability of finding a molecule with, for example, an orientation $\mathbf{u}(t)$, given an initial $\mathbf{u}(0)$, is a time-dependent Gaussian distribution.

In consequence, the low frequency loss curve should be modeled accurately and $\mathfrak{A}(\bar{\nu})$ of the terahertz region extrapolated therefrom. In the pure liquid state a three-variable fitting should be used with $\Phi_0(0)$, $\Phi_1(0)$, and Γ_2. The motion of CH_2Cl_2 molecules in the pure liquid has been monitored by sweep frequency microwave klystron and interferometric techniques (see Chapter 6), and the absorption in the far infrared is intense. In consequence, there is little discernible effect of induced absorption (Chapter 11), although this is always present if the molecules are taken as polarizable; that is, if $C_M^{(12)}(t)$ and $C_M^{(22)}(t)$ are finite. CH_2Cl_2 has also been used as a probe into the mesophase and glassy environments—this is discussed in Chapter 7.

If cross-correlation effects and those of the internal field are ignored (i.e., if Eq. 3.6.2 is applied directly) the result is fairly satisfactory (Fig. 1.7.4.1) if $\phi_1(0)$ and γ are adjusted for best fit. However, iterating on Γ_2, $\Phi_0(0)$, and $\Phi_1(0)$ would produce an almost perfect result, in the sense that the liquid phase data could be produced over a broad range of frequency at room temperature. The validity of some Mori approximants at the three- and four-variable level has been investigated for the monohalogenobenzenes (Fig. 3.6.2.1). A fairly realistic result is obtained for an exponential $\phi_1(t)$ which gives an integrated absorption intensity of about half that observed in the far infrared. This suggests that the experimental data are heavily influenced, in this case by the collision-induced temporary dipoles. The extent of this induction may be measured against the observation of a broad absorption in the nondipolar benzene molecule, which is entirely collision induced (see Chapter 11).

APPENDIX: MOLECULAR DYNAMICS AND THE INTERNAL FIELD PROBLEM

Some of the major problems posed by the internal field have been resolved recently by use of *molecular dynamics simulation.* This work was carried out by Brot et al. (1980). Their main conclusions are reproduced in this appendix.

The system used was two-dimensional, consisting of 313 molecules represented by a Stockmayer type potential (Lennard–Jones plus strong dipole–dipole interaction). The dipole–dipole interaction strength is measured through a coupling parameter γ, and two simulations were completed with $\gamma = 1$ and $\gamma = 2$.

The dielectric system is illustrated in Fig. 3.A.1 and consists of concentric areas whose resultant dipole moments are respectively **m**, **X**, and **M**. In essence the simulation evaluates the complete time correlations of these areas and compares these with the true single-particle a.c.f. of a centrally placed dipole unit vector **u**.

The Scaife or Fatuzzo–Mason relation linking the whole disk (or sphere)

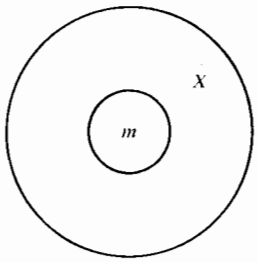

Figure 3.A.1 Dipole system of Brot et al. [Reproduced by permission from *Mol. Phys.* **40**, 1053 (1980).]

time-correlation function to that of the small inner disk or sphere is capable of describing the results of the computer simulation. For strongly dipolar potentials of the Stockmayer type the single-particle time a.c.f. differs considerably in shape from the complete correlation function of the inner area whose resultant dipole moment is **m**. This means of course that the Madden–Kivelson theorem is not a good description of the macro–micro relation in this case. Neither the static nor the dynamic Onsager picture is a good approximation here.

For strong anisotropic forces of dipolar origin at medium to high densities the picture of itinerant oscillation (Chapter 4) appears to be broadly acceptable. The librations of the molecular dipole can be seen clearly in Fig. 3.A.2.

The idea of dielectric friction as formulated by both Nee and Zwanzig and by Fatuzzo and Mason is an oversimplification because it is assumed that the reaction field is that produced by a homogeneous and isotropic

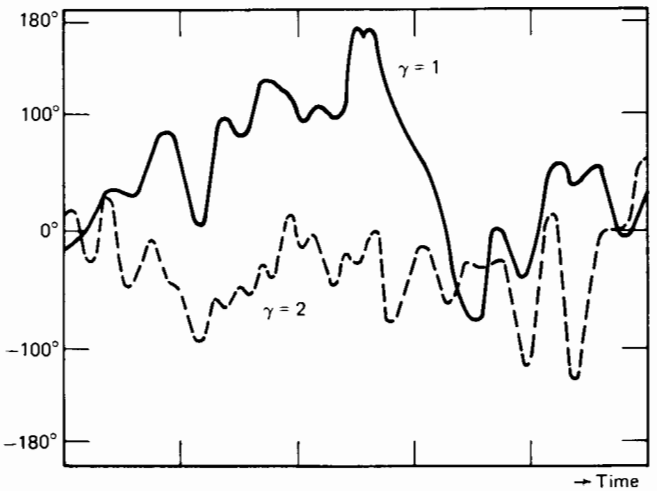

Figure 3.A.2 Time evolution of the orientation of the molecule dipole of Brot et al. [Reproduced by permission from *Mol. Phys.* **40**, 1053 (1980).]

environment, which is not the case in even the simplest of molecular dynamics simulations involving strong electrical forces.

The Quentrec–Bezot (Brot et al., 1980) or the Mori formulation (Evans et al., 1980) of orientational memory functions provides an acceptable description of the correlation function of the region labeled **m**. This is probably because the random torques acting on the total resultant **m** are numerous and less correlated than for a single molecule, whose a.c.f. is subject to a more oscillatory behavior. As we have shown in Chapters 1–3 the zero time value of the zeroth and first-order memory functions are expressible in terms of equilibrium averages which can be extracted from the simulation. The best fit values are in agreement with the theoretical expressions.

The a.c.f. of **u** is reminiscent of itinerant libration, being oscillatory at short times and diffusive at long times. The a.c.f. is shorter lived than the total correlation function of **m**.

Finally, this seems to be a clear demonstration of the fact that with a few hundred molecules it is possible to obtain realistic values of the complex permittivity of highly dipolar fluids despite the long range nature of the electrostatic interaction.

REFERENCES

Abbott, J. A. and Bolton, H. C. *Trans. Faraday Soc.* **48**, 422 (1952).

Abramowitz, M. and Stegun, I. A., Eds., *Handbook of Mathematical Functions*, Dover, New York (1965).

Bell, R. P., *Trans. Faraday Soc.* **27**, 797 (1931).

Bellemans, A. and Kohler, F., *J. Chem. Phys.* **47**, 1261 (1967).

Brot, C., in *Dielectric and Related Molecular Relaxation Processes*, Vol. II Specialist Periodic Reports, The Chemical Society, London (1975).

Brot, C., Bossis, G., and Hesse-Bezot, C., *Mol. Phys.* **40**, 1053 (1980).

Brot, C. and Darmon, I., *J. Chem. Phys.* **53**, 2271 (1970).

Brot, C. and Darmon, I., *Mol. Phys.* **21**, 785 (1971).

Budó, A., *J. Chem. Phys.* **17**, 686 (1949).

Calderwood, J. H. and Coffey, W. T., *Proc. R. Soc. London A*, **356**, 269 (1977).

Callen, H. B. and Welton, J. A., *Phys. Rev.*, **83**, 34 (1951)

Coffey, W. T., Ph.D. Thesis, University of Dublin (1975).

Coffey, W. T. and Scaife, B. K. P., *J. Electrostat.* **1**, 193 (1975).

Coffey, W. T. and Vij, J. K., (1982) *Mol. Phys.*, in press.

Coffey, W. T., *Molec. Phys.*, **37**, 437 (1979).

Coffey, W. T., *Molec. Phys.*, **39**, 227 (1980).

Coffey, W. T., *Adv. in Molec. Rel. Int. Proc.*, **17**, 169 (1980).

Davies, G. J., Thesis, University of Wales (1971).

Davies, R. O. and Scaife, B. K. P., *J. Chem. Phys.*, **22**, 148 (1954).

Debye, P., *Polar Molecules*, Chemical Catalog Co., New York (1929).

Deutch, J. M., in *Faraday Symp. Chem. Soc.*, **11**, 51 (1976).

Deutch, J. M. and Wolynes, P. G., *J. Chem. Phys.*, **67**, 633 (1977).

Evans, M. W., Evans, G. J., and Davies, A. R., *Adv. Chem. Phys.* **44**, 255 (1980).

Fatuzzo, E. and Mason, P. R., *Proc. Phys. Soc. London* **90**, 729 (1967).

Fröhlich, H., *Theory of Dielectrics*, Oxford University Press, Oxford (1949); 2nd ed. (1958).

Gordon, R. G., *J. Chem. Phys.* **44**, 1830 (1960).

Gordon, R. G., *Adv. Mag. Res.* **3**, 1 (1965).

Greene, R. F. and Callen, H. B., *Phys. Rev.* **83**, 1231 (1951).

Greffe, J. L., Goulon, J., Brondeau, J. and Rivail, J. L., *J. Chim. Phys.* **70**, 282 (1973).

Hansen, J. P. and McDonald, I. R., *Theory of Simple Liquids*, Academic Press (1976).

Ivanov, E. N., *Sov. Phys., J.E.T.P.* **18**, 1041 (1964).

Jeffreys, Sir H. and Jeffreys, Lady B. S., *Mathematical Physics*, Cambridge University Press, Cambridge (1950).

Keyes, T. and Kivelson, *J. Chem. Phys.* **57**, 4599 (1972).

Kirkwood, J. G., *J. Chem. Phys.* **7**, 911 (1939).

Kivelson, D. and Madden, P., *Mol. Phys.* **30**, 1749 (1975).

Kohler, F., *The Liquid State*, Verlag Chemie, Göttingen, (1972).

Langevin, P., *J. Phys.* **4**, 678 (1905).

Lobo, R., Robinson, J. E., and Rodriguez, P., *J. Chem. Phys.* **59**, 5992 (1973).

Lorentz, H. A., *The Theory of Electrons*, Teubner, Leipzig (1909); reprinted Dover, New York (1952).

Nee, T. W. and Zwanzig, R., *J. Chem. Phys.* **52**, 6353 (1970).

Onsager, L., *J. Am. Chem. Soc.* **58**, 1486 (1936)

Prigogine, I., *Non-Equilibrium Statistical Mechanics*, Wiley-Interscience, New York (1962).

Rahman, A. and Stillinger, F. H., *J. Chem. Phys.* **58**, 3336 (1971); **57**, 1281 (1972).

Scaife, B. K. P., *Proc. Phys. Soc. London* **70B**, 314 (1957).

Scaife, B. K. P., E.R.A. Report L/T 392, E.R.A. Leatherhead, Surrey (1959).

Scaife, B. K. P., *Proc. Phys. Soc. London* **84**, 616 (1964).

Scaife, B. K. P., *Molecular Relaxation Processes*, Chemical Society Special Publication No. 20, Academic Press (1966).

Scaife, B. K. P., *Complex Permittivity*, English Universities Press, London (1971).

Scaife, B. K. P., in *Dielectric and Related Molecular Relaxation Processes*, Vol. I Specialist Periodic Reports, The Chemical Society, London (1972).

Stratton, J. A., *Electromagnetic Theory*, McGraw-Hill, New York (1941).

Streett, W. B. and Tildesley, D. J., *Proc. R. Soc. London A* **348**, 485 (1976); **355A**, 239 (1977).

Titchmarsh, E. C., *Introduction to the Theory of Fourier Integrals*, Oxford University Press, Oxford (1937).

Tolman, R. C., *The Principles of Statistical Mechanics*, Oxford University Press, Oxford (1938).

Twu, C. H., Evans, C., and Gubbins, K. F., *Mol. Phys.* **27**, 1601 (1974).

Van Vleck, J. H., *The Theory of Electric and Magnetic Susceptibilities*, Oxford University Press, Oxford (1932).

Warchol, M. P., and Vaughan, W. E., *J. Chem. Phys.* **67**, 476 (1977).

Wolynes, P. G., and Deutch, J. M., *J. Chem. Phys.* **67**, 733 (1977).

Zwanzig, R., *J. Chem. Phys.* **38**, 2766 (1963).

4

Evaluation of Models in the Far Infrared*

LIST OF SYMBOLS

a	Least principal moment of inertia axis
α	Absorption coefficient, nepers cm^{-1}
α_1, α_2	Coefficients in the angular velocity autocorrelation function of the i.o.
α_μ	Complex polarizability
b	Principal intermediate moment of inertia axis
β	Angular frequency in the angular velocity a.c.f.
c	Greatest principal moment of inertia axis
$C_\omega(t)$	Angular velocity autocorrelation function
$C_u(t)$	Orientational autocorrelation function
θ	Colatitudinal displacement
γ	Characteristic frequency (of $K_1(t)$)
$\langle\Gamma^2(0)\rangle$	Mean square torque
ϵ_s	Static permittivity
ϵ''	Dielectric loss
ϵ_0	Permittivity of free space
I	Moment of inertia of the spherically isotropic rotator
I_1	Moment of the inertia of the ring of the planar itinerant librator
I_2	Moment of inertia of the disk of the planar itinerant librator
I_r	Reduced moment of inertia
I_a	Least principal moment of inertia
I_b	Intermediate principal moment of inertia
I_c	Greatest principal moment of inertia
$K_\omega(t)$	Angular velocity memory function
K_0	First memory function
K_1	Second memory function
$\boldsymbol{\mu}$	Dipole moment vector
μ_a	Dipole moment components along the **a** axis
μ_b	Dipole moment component along the **b** axis
μ_c	Dipole moment component along the **c** axis
$\bar{\nu}_{max}$	Far infrared peak frequency (cm^{-1})
$P(0)$	Mean square torque per unit volume of rotation
ϕ	Fixes the orientation of the ring with respect to the disk in the itinera librator

*In joint authorship with C. J. Reid.

T_q	Torque factor
$\mathbf{T}_q$	Projected torque
τ_D	Debye relaxation time
τ_{exp}	Inverse of the loss peak angular frequency
$\mathbf{u}$	Dipole unit vector ($\boldsymbol{\mu}/\lvert\boldsymbol{\mu}\rvert$)
V	Solute volume of rotation
$\boldsymbol{\omega}$	Angular velocity
ω_0	Resonance frequency of the planar itinerant librator
W	Wiener process
Ω_0	$= (I_2/I_1)^{1/2}\omega_0$
ζ	Friction coefficient

In Chapters 1 to 3 we have outlined the theoretical basis of the description in molecular terms of broad band spectroscopy. In this chapter we describe how models compare with spectral data in the 0–THz range of frequencies. The fundamental aim of a theory of the liquid state must evolve from a narrow consideration of specific features to take into view the expanded horizon provided by the continuing advances in spectroscopy. It is no longer valid to analyze low frequency (dielectric) spectral information in isolation from the far infrared. We have mentioned this in earlier chapters and develop the theme further in Chapters 6 and 12. Here we describe how one specific model, described in 1976 by Evans, stands up to analysis using a broad range of spectra in the 0–THz region. We confine ourselves to the liquid phase of dilute solutions of dipolar molecules in nondipolar solvents in order to minimize the problems of interpretation arising from electrostatic sources as considered in Chapter 3. The simplest form of another type of model—the itinerant librator—is essentially kinematic in concept and we aim to isolate this aspect insofar as is experimentally practical. The theme is developed for glasses in Chapter 7. It will become clear after a reading of Chapters 6 and 12 that a theory of molecular diffusion must be made to reproduce a much wider variety than hitherto of experimental data with simplicity and objectivity. Because the itinerant librator, for example, is neither simple nor objective it should be regarded as a stopgap prior to the fuller development of molecular dynamics simulation or a more complete treatment of existing models. Experimentally it is still often the case that a technique such as low frequency dielectric spectroscopy is used in isolation when the aim of the investigation is to shed light on molecular dynamics and interaction. By implication the investigation is then taking place over too limited a range of frequencies, excluding totally the individualistic features observable in the far infrared. When this happens it is often possible to match the data with the Debye model of rotational diffusion developed in Chapter 2. Unfortunately this is also the result with virtually every other type of model envisaged since Debye, including that of 180° rotational jumping from one potential energy minimum into another. In the absence of far infrared information we can either conclude that the molecule is rotating through infinitesimally small angles infinitely quickly (Debye's model) or by jumps

of 180°. If we consider the far infrared part of the spectrum both these models fail qualitatively to reproduce the additional high frequency features. Both result in a plateau (Chapters 1 and 2) in the power absorption coefficient. Taking together the far infrared and dielectric data (which are obtained with quite different pieces of equipment), the situation is turned on its head, and it becomes very difficult indeed to reproduce the complete range of data even with the most powerful theoretical technique now available, molecular dynamics simulation.

The range of complementary techniques is also increasing (Chapters 6 and 12). Information about molecular motion and interaction can be obtained by an analysis of the way in which electromagnetic or neutron radiation is scattered from a liquid, by using the shape of infrared or Raman bands, from nuclear magnetic resonance, from the features of transiently induced birefringence (e.g., Kerr effect), and from a number of other sources. It is clearly desirable to use the dynamic data simultaneously from all these techniques on one convenient specimen and to see how well the computer simulates them in terms of the interaction of molecular potentials in a temporal context. This theme is developed in Chapter 12.

Ideally one should determine what is meant by molecular potential energy (from sources such as molecular orbital theory) and use this mathematical facsimile in the Liouville equation of motion, incorporating, if we must, reasonable approximations such as pairwise additivity. To handle hundreds of such facsimiles requires enormous computing power, and Chapters 1–3 attempt to describe this complicated problem in terms of only a few thermodynamic averages, accessible through the intermediacy of an increasingly abstract type of statistical mechanics. Subjective ideas therefore abound (e.g., holes, clusters, hypernetted chains, liquid lattices) which are often inconsistent with the basic thermodynamic facts and are destined to be disregarded when they have served their purpose as deliberate oversimplifications thrown up in the face of limited computational power. The objective truths remain, the time correlation function and frequency spectrum remain Fourier transform pairs, and the shape of spectral bands remain a source of statistical information concerning the motion and interaction of the molecular entity. No one spectroscopic technique has a monopoly of the view, but a careful selection of pertinent spectroscopic facts can be made that will ultimately sharpen immeasurably our picture of the liquid state of matter wherein most of our chemistry takes place. It is therefore clear that this chapter is concerned with the experimental evaluation by one technique alone (0–THz spectroscopy) of one or two specific models.

4.1 BACKGROUND

The modern version of the planar itinerant librator (Calderwood and Coffey, 1977) produces an angular velocity a.c.f. which corresponds

exactly in mathematical form with an approximant of the Mori continued fraction first derived by Evans (1976). In two dimensions the a.c.f. may be written as $\langle\dot{\theta}(t)\dot{\theta}(0)\rangle$, where θ is the angular displacement. If we apply the three-variable Mori theory described for *orientation* at the end of Chapter 3 instead to *angular velocity* we are essentially solving the usual integro-differential equation (Section 2.12):

$$\dot{\boldsymbol{\omega}}(t) = -\int_0^t K_\omega(t-\tau)\boldsymbol{\omega}(\tau)\,d\tau + \mathbf{T}_q(t)/I \tag{4.1.1}$$

for the motion of the angular velocity vector $\boldsymbol{\omega}$. This equation can be solved by expanding the memory kernel (as described in Chapter 3 for the orientational vector **u**). It is linear in the angular velocity, however, and involves a scalar moment of inertia which we denote by I. The memory kernel of this equation is also a scalar quantity and therefore the frictional resistance to rotational diffusion is assumed to be isotropic. The equation is therefore strictly applicable only to spherically isotropic diffusion involving an averaged effective moment of inertia. Memory effects may also be incorporated in the equation of motion of an asymmetrical body given in Chapter 2. However consideration of these effects becomes extremely complicated because of the non-linear character of the Euler equations for a general rotating body (Chapter 2).

This particular truncation can be given physical significance from the observation that the expression it yields for $C_\omega(t)$ appears to be identical, except for a factor in the moment of inertia, with the angular velocity a.c.f. of a simple model which may be described with the aid of Fig. 4.1.1. It is assumed that a dipolar molecule and its nearest neighbors may be represented by a mechanical system consisting of the cage of nearest neighbors (assumed rigid) and the encaged dipolar molecule. In the experimental work described in this chapter we use dilute solutions, so the cage of molecules consists of

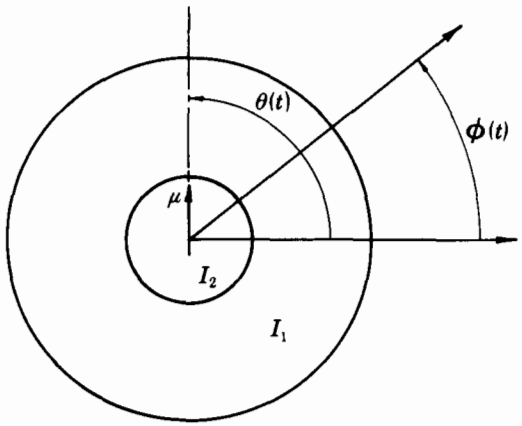

Figure 4.1.1 Itinerant librator model.

nondipolar entities. This limits the problem essentially to kinematics. The encaged molecule is in general an asymmetric top, but the angular motion of the dipole moment is either assumed to be isotropic (Evans, 1976), or constrained to two dimensions in order to make the analysis mathematically tractable. The itinerant librator is dynamically equivalent to a mechanical system consisting of a disk of moment of inertia I_2 surrounded by a ring of moment of inertia I_1, that of the nearest neighbor cage. The torques from Brownian motion of the surroundings act only on the cage so that the Langevin equation for the complete molecule/cage system may be written (assuming that a constant steady field applied at $t = -\infty$ is switched off at $t = 0$ as)

$$I_2\ddot{\theta}(t) + I_2\omega_0^2 \sin[\theta(t) - \phi(t)] = I_2\dot{W}(t) \tag{4.1.2}$$

$$I_1\ddot{\phi}(t) + \zeta\dot{\phi}(t) - I_2\omega_0^2 \sin[\theta(t) - \phi(t)] = I_1\dot{W}(t) \quad t > 0 \tag{4.1.3}$$

Here $\zeta\dot{\phi}(t)$ is the frictional couple acting on the cage and $W(t)$ is a Wiener process as in earlier chapters. These are nonlinear stochastic differential equations and essentially are those describing a coupled pendulum driven by random torques. They can be solved analytically only if we restrict the amplitude of oscillation, i.e. when

$$\sin[\theta(t) - \phi(t)] \doteq \theta(t) - \phi(t)$$

This is the case considered by Calderwood and Coffey where

$$I_2\ddot{\theta}(t) + I_2\omega_0^2[\theta(t) - \phi(t)] = I_2\dot{W}(t) \tag{4.1.4}$$

$$I_1\ddot{\phi}(t) + \zeta\dot{\phi}(t) - I_2\omega_0^2[\theta(t) - \phi(t)] = I_1\dot{W}(t) \tag{4.1.5}$$

After a rather difficult but clearly explained mathematical exercise (Calderwood and Coffey, 1977) these authors obtain the angular velocity a.c.f. in the by now familiar form (Coffey et al., 1981):

$$C_\theta(t) = (1+\Gamma)^{-1}\left(\cos\beta t + \frac{(\alpha_1 + \Gamma\alpha_2)}{\beta}\sin\beta t\right)e^{-\alpha_1 t} + \frac{\Gamma}{1+\Gamma}e^{-\alpha_2 t} \tag{4.1.6}$$

where α_1, α_2, β, and Γ are defined as in Eq. 3.6.1. The linearized two dimensional equations of motion (4.1.4) and (4.1.5) allow us to make use of the theorem. ($\alpha_1 = \sigma_1$, $\alpha_2 = \sigma_2$, $\beta = \omega_1$, $\Gamma = \Lambda$ in Eq. 3.6.1.)

$$C_u(t) = \exp\left[-\frac{kT}{I_2}\int_0^t (t-\tau)C_\theta(\tau)\,d\tau\right]$$

for the orientational a.c.f. $C_u(t)$. For three-dimensional isotropic diffusion it is assumed that the result is modified to

$$C_u(t) = \exp\left[-\frac{2kT}{I}\int_0^t (t-\tau)C_\omega(\tau)\,d\tau\right]$$

Note. This expression is written down by supposing that the orientational a.c.f. for the sphere model is sufficiently approximated by the exponential

form above. This is not in fact true as may be seen from the results of the calculations for the disk and sphere models given in Chapter 2. However numerical computation suggests that in many cases the exponential may provide a good approximation to $\langle \mathbf{u}(0) \cdot \mathbf{u}(t) \rangle$. We can obtain from this last equation, apart from the orientational a.c.f. and its second derivative, the rotational velocity a.c.f., whose Fourier transform is essentially the far infrared power absorption coefficient. Specifically, for three-dimensional diffusion (where it is assumed that the last equation above is valid):

$$C_u(t) = \exp\left[-\frac{2kT}{I}\left(A_1(e^{-\alpha_1 t}\cos\beta t - 1) - B_1 e^{-\alpha_1 t}\sin\beta t + \frac{\Gamma}{\alpha_2^2}\frac{(e^{-\alpha_2 t}-1)}{1+\Gamma} + C_1 t\right)\right] \tag{4.1.7}$$

where

$$A_1 = \frac{3\alpha_1^2 + 2\alpha_1\alpha_2\Gamma - \beta^2}{(1+\Gamma)(\alpha_1^2+\beta^2)^2}$$

$$B_1 = \frac{2\beta^2\alpha_1 + (\alpha_1 + \Gamma\alpha_2)(\beta^2 - \alpha_1^2)}{\beta(1+\Gamma)(\alpha_1^2+\beta^2)^2}$$

$$C_1 = \frac{2\alpha_1\alpha_2 + \Gamma(\alpha_1^2+\beta^2+\alpha_2^2)}{\alpha_2(1+\Gamma)(\alpha_1^2+\beta^2)}$$

which reduces in the limit of free rotation in three dimensions (Chapter 2), to (compare this with the exact result on pages 140 and 167)

$$\exp\left[-\frac{kTt^2}{2I}\right]$$

From a consideration of the physical aspects of the itinerant librator model ω_0 may be taken for didactic purposes as the far infrared peak frequency ($2\pi c\bar{\nu}_{max}$). Values of I_1 and I_2 may be estimated for a particular system and $\zeta = kT\tau_D$, where τ_D is the Debye relaxation time. In dilute solution the numerical value of the latter is close to the inverse of the peak frequency of the dielectric loss. From the Mori type treatment of Evans (1976) the zero-time intercepts of the first and second memory functions of angular velocity, K_0 and K_1, are (see Section 2.12)

$$K_0(0) = \frac{\langle \dot{\omega}^2 \rangle}{\langle \omega^2 \rangle}$$

$$K_1(0) = \frac{\langle \ddot{\omega}^2 \rangle}{\langle \dot{\omega}^2 \rangle} - \frac{\langle \dot{\omega}^2 \rangle}{\langle \omega^2 \rangle}$$

This important result indicates that the librational peak position depends on the mean square torque exerted on the librator by the environment. Further use of this is made in this chapter and also in Chapter 7.

The expression for the theoretical spectrum can be obtained from the linear response theory formula:

$$\alpha_\mu(\omega) = -\int_0^\infty e^{-i\omega t}\frac{\mu^2}{2kT}\frac{d}{dt}\langle \mathbf{u}(t)\cdot\mathbf{u}(0)\rangle\, dt$$

where $\alpha_\mu(\omega)$ is the complex polarizability and $\mathbf{u}$ the dipole unit vector. This equation applies strictly to a system where cross correlations (Chapter 3) are negligible and where $\langle \mathbf{u}(0) \rangle$ vanishes. It applies only when the external and Maxwell fields are identical so that

$$\alpha''_\mu(\omega) = \epsilon_0[\epsilon''(\omega) - 1]$$

Calderwood and Coffey (1977) find that:

$$\frac{\alpha_\mu(p)}{\alpha'_\mu(0)} = 1 - p\left(\frac{1}{p+\frac{kT}{\zeta}} - \frac{\frac{kT}{I_2}\left\{-\frac{I_2}{\zeta}\left(p+\frac{kT}{\zeta}\right)^2 + \left(p+\frac{kT}{\zeta}\right)\left(1-\frac{I_2}{I_1}\right) + \frac{\zeta}{I_1}\left[1 - \frac{\eta}{\zeta^2}(I_1+I_2)\right]\right\}}{\left(p+\frac{kT}{\zeta}\right)\left[\left(p+\frac{kT}{\zeta}\right)^3 + \frac{\zeta}{I_1}\left(p+\frac{kT}{\zeta}\right)^2 + \eta\frac{(I_1+I_2)}{I_1I_2}\left(p+\frac{kT}{\zeta}\right) + \frac{\zeta\eta}{I_1I_2}\right]} + \cdots\right)$$

where $I_2\omega_0^2 = \eta$, a spring constant.

If all the terms inside the braces are ignored except the first (unity), one obtains the Debye equations. It follows therefore that

$$\tau_D = \zeta(kT)^{-1} = K_2^{-1}$$

As a first approximation we can consider the first two terms and ignore the contribution of K_2 in each term $p + K_2$. This leads to:

$$\frac{\alpha_\mu(p)}{\alpha'_\mu(0)} = \frac{kT[p(I_1p+\zeta)+\eta]}{[I_1I_2p^3 + I_2\zeta p^2 + \eta(I_1+I_2)p + \eta\zeta](p+K_2)}$$

and separating real and imaginary parts we have the required spectral details theoretically. This set of relations can be used to generate the theoretical loss and far infrared spectrum from the input parameters ω_0, I_1, I_2, ζ, T, ϵ_s, and ϵ_∞.

Mori's continued or recurrent fraction expression for the solution of the generalized Langevin equation is a very general theorem (Chapters 1, 9, and 10) but one which to be of use must be closed in a manner which makes some physical sense. The truncation $K_1(t) = K_1(0)e^{-\gamma t}$ gives the simplest realistic approximation to molecular behavior in a liquid phase because the mean square torque is clearly defined (Evans, 1976) and the bare essentials of the far infrared absorption are reproduced; that is, we have theoretically a peak in the power absorption coefficient and not a plateau, and what is more, a peak whose frequency is theoretically adjustable, and a measure of the mean square torque itself. The simpler closure or approximant $K_0(t) = K_0(0)e^{-\gamma_0 t}$, through its relation with the extended diffusion concept of Gordon (1965), corresponds with unrealistic impulsive torques and in effect an inability to follow the shifts observed experimentally in the far infrared peak frequency.

4.2 COMPARISON WITH DATA

In this section we are concerned with the position and shape of the spectral bands observable in dilute solutions of dipolar molecules primarily in the far infrared and then over the complete range of lower frequencies to static. The electrodynamic factors in pure dipolar liquids complicate the model analysis in two ways. Firstly, the dynamic internal field problem outlined in Chapter 3 can be tackled satisfactorily only with computer simulation. Secondly, even in the absence of such a complication the mean square torque determined from the peak positions of pure liquids would relate to the interaction between like molecules, as opposed to the interaction of a solute with a common environment, which is the case when we dissolve a series of dipolar solutes in a solvent such as decalin.

For example, consider two liquids such as dichloromethane (CH_2Cl_2) and nitrobenzene. In their pure state their far infrared absorptions are intense and peak respectively at about 80 and 40 cm^{-1}. One might easily be led to infer some empirical relation between $\bar{\nu}_{max}$ and the solute volume of rotation (V) which we use later on. In dilute decalin solution, however, the peaks are now centered around 53 and 39 cm^{-1}, respectively. There is in one case a characteristically large far infrared solvent shift, reflecting the basic fact that this type of absorption is intermolecular in origin. Whether such solvent shifts are due primarily to the kinematic or to the electrodynamic environment is the essential problem.

Therefore the systems chosen for study (Reid, 1979) should be those of rigid dipolar molecules in dilute nondipolar solution. Decalin is a convenient solvent because the scope of the work can be extended to viscous and vitreous media (Chapter 7) by supercooling. Some aspects are conveniently left until then with respect to detailed description. The effect of viscosity is in some instances dramatic and provides a stringent test for theoretical analysis. The concentration normally chosen (10% v/v) is sufficiently dilute to minimize the electrodynamic interaction between the fields of dipolar solute molecules while still permitting accurate measurement with (in our case) up to five different pieces of apparatus over a very wide range of frequency. In all cases the contribution of the solvent absorption (See Chapter 11) can be eliminated by the relevant subtraction process, using volume to volume concentrations. The resulting spectrum is then considered to be a signature of the behavior of the solute molecule in a decalin environment. In principle the total absorption should be considered, with the correlation function being compounded of terms involving $\langle \boldsymbol{\mu}(t) \cdot \boldsymbol{\mu}(0) \rangle$ and also $\langle \boldsymbol{\mu}'(0) \cdot \Sigma_i \boldsymbol{\mu}_i'(t) \rangle$, where $\boldsymbol{\mu}_i'$ is the collision-induced dipole (Chapter 11) of the ith decalin molecule, as well as the solute-solvent correlations $\langle \boldsymbol{\mu}(0) \cdot \Sigma_i \boldsymbol{\mu}_i'(t) \rangle$. The correction for solvent used in this chapter is made on the assumption that the solvent spectrum component is not affected by the presence of the solute. This is an excellent approximation except for weakly dipolar solutes such as toluene, where the solvent contribution is about 50% of the spectral intensity. The same procedure must be adopted at all lower frequencies in order to provide ourselves with a consistent means of testing the theoretical model.

In Section 4.2.1 we present the far infrared data for about 40 systems classified according to the type and size of the solute molecules. This classification is primarily one of convenience; the data, in particular the peak positions, are discussed together with structural and other relevant data. An attempt is made in Section 4.2.2 to quantify these results in terms of a solute volume of rotation (see also Chapter 7) and to ensure that the (Evans, 1976) analysis is internally consistent. In Section 4.2.3 we consider the spectral behavior of the theoretical model. By fitting only the high frequency data (20–220 cm^{-1}) the fitting parameters K_0, K_1, and γ can be determined adequately and the analytic expression so obtained may be used to extrapolate the far infrared band over the 0–20 cm^{-1} region, thus producing the microwave behavior and that at lower frequencies. The values of the loss peak frequency so obtained can then be compared with their experimental counterparts. In Section 4.2.4 a brief discussion of absolute intensities is developed.

The far infrared peak frequency depends inversely on the root of the (reduced) moment of inertia (I_r) and is proportional to the torque or barrier height to activated rotation. A useful empirical parameter for data comparison therefore is $I_r\bar{\nu}_{max}^2$. To avoid the use of small numbers the normalization $T_q = I_r\bar{\nu}_{max}^2 \times 10^{38}$ is used which has the unit of grams and is referred to as the "torque factor" (Reid, 1979).

4.2.1 Qualitative Description of the Data

In this section we classify the far infrared spectra of a wide range of small molecules according to the *solute structure* in decalin solvent. The factor T_q is to some extent characteristic of the grouping. For phenyl derivatives and heterocyclic molecules a subdivision is made according to substituents. For each division the far infrared peak positions ($\bar{\nu}_{max}$), calculated moments of inertia, dipole moment components, reduced inertia, and torque factor are tabulated (e.g., Table 4.2.1.1). Each spectrum is the result of at least three separate investigations spread over a period of 12 months. The spectral variations result in an uncertainty of typically 5% in absolute intensity (scale error) or in some cases a constant (additive) error over the whole band (zero error). To represent such errors, the bands have been given error bars at points along the frequency axis. The band distortion is such as to put a maximum probable error on the values of $\bar{\nu}_{max}$ quoted here of ± 2 cm^{-1}. For weak absorbers where solvent subtraction is important or for systems whose spectra peak below 30 cm^{-1} the error is estimated to be ± 3 cm^{-1}; for spectra with interfering high frequency proper modes quoted errors may be larger than this. The latter are compounded in some instances by the process of proper mode subtraction where because of the

Table 4.2.1.1 Structural and Spectral Data for Groups A1 and A2

Solute	Z (Å)	I_a*	I_b*	I_c*	μ (D)[a]	I_r*	$\tilde{\nu}_{max}$ (cm^{-1})[b]	T_q (g)[c]
A1								
Pyridine	0	1.40	1.45	2.85	2.23	0.96	45	1858
Thiopyran	0.28	1.47	2.00	3.47	?	1.27	—	—
Pyrimidine	0	1.47	1.47	2.93	2.44	0.96	—	—
A2								
Fluorobenzene	0.44	1.47	3.24(5)	4.71(5)	1.40	1.92	39	2923
Chlorobenzene	0.96	1.47	5.30	6.77	1.58	2.97	34	3433
Bromobenzene	1.63	1.47	8.20	9.67	1.56	4.43	24(±3)	2551(±25%)

*Unit: 10^{-38} g cm^2.
[a] 1 Debye(D) = 3.33×10^{-30} C m.
[b] Uncertainty of ±2 cm^{-1} or as parenthesis.
[c] Uncertainty of 10% or as parenthesis.

uncertainty of peak position and intensity in the region above about 180 cm^{-1} a Lorentzian curve of the form $a/[(\bar{\nu} - \bar{\nu}_{max}^{(p.m.)})^2 + b^2]$, where a/b^2 is the maximum absorption and $2b$ is the half-width, cannot be fitted with certainty.

The decalin solvent is an isomeric mixture of cis and trans forms of density 0.886 g cm^{-3}. The solvent absorption itself (Fig. 4.2.1.1) reveals a

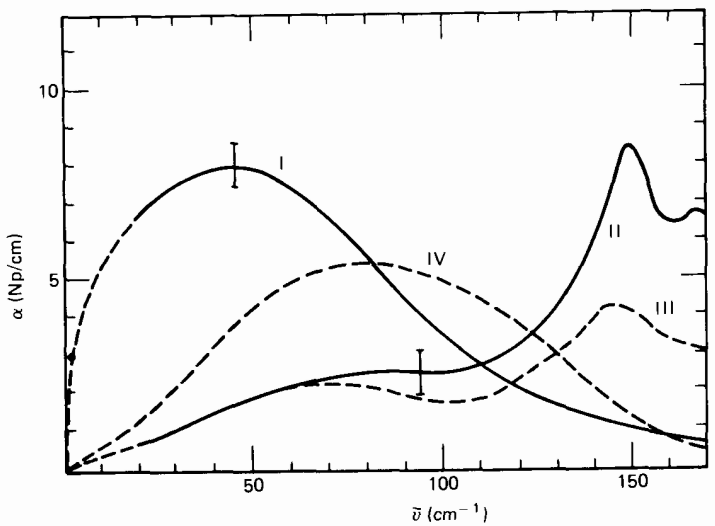

Figure 4.2.1.1 Absorption spectra for decalin solutions at 293°K (10% v/v except where stated). I Pyridine ● = microwave point; II decalin solvent ×5; III *trans*-decalin ×5 (ref. *l*); IV pure benzene.

broad shoulder of *induced* absorption around 70 cm^{-1}, headed by a proper mode at 150 cm^{-1}.

4.2.1.1 Group A1, Benzene Ring Structures, and A2, Single-Atom Derivatives

These are sketched in Fig. 4.2.1.1.1 (bond lengths in Å). All C—H bond lengths are represented by 1.08 Å. The italic letters in parentheses refer to table references, listed at the end of the chapter.

The parent structure, benzene, is nondipolar but strongly quadrupolar, and absorbs relatively intensely in the far infrared (Chapter 11). The presence of electronegative substituents creates a dipolar charge distribution (e.g., chlorobenzene) so that multipole moments are presumably smaller, although no experimental evidence is available to corroborate this point. Therefore, although induced absorptions contribute to the spectra of substituted benzenes in the far infrared as in every case, the cross section is expected to be smaller than that of benzene.

Pyridine has a large dipole moment (2.12 D) due to its highly electronegative nitrogen atom, resulting in shorter C—N bonds compared with the C—C bonds in the same molecule. When referring to moments of inertia in the case of pyridine and all other molecules we use principal axes such that I_a is the principal moment of inertia about axis **a**, and is the lowest obtainable for the molecule in question. I_c, about axis **c**, is the greatest. Axis **b** is mutually perpendicular and has an associated moment of inertia I_b. The three axes intersect at the center of mass. For pyridine (as an example) the three moments of inertia have been computed from the above structures to be (in units of 10^{-38} g cm^2) $I_a = 1.41$, $I_b = 1.45$, $I_c = 2.86$. Because all mass points have been assumed to be on the **a–b** plane, $I_a + I_b = I_c$. The moments of inertia of the benzene molecule are notably larger ($I_a = I_b = 1.47$, $I_c = 2.96$) and are indicative of the contraction caused by the replacement of carbon with nitrogen.

The presence of two nitrogen atoms in the ring (pyrimidine) creates a larger net dipole moment of 2.44 D and a greater contraction of ring size together with more angular distortions. If we now define a parameter Z as

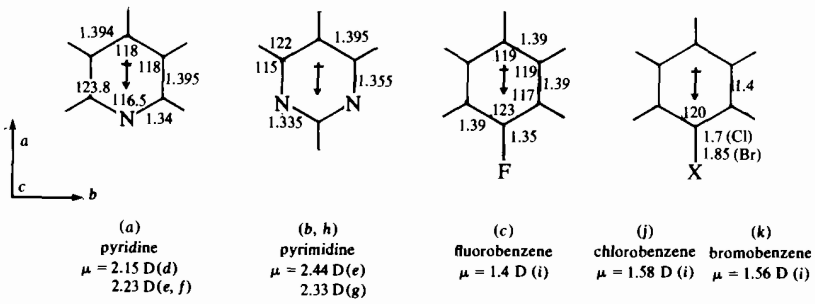

Figure 4.2.1.1.1 Group A1, benzene and its analogues, and group A2, single atom derivatives.

the center of mass coordinate along the symmetry axis and such that the ring carbon opposite the substituent has a position relative to this of -1.4 Å, then $Z = 0$ for benzene, pyridine, and pyrimidine, but for fluorobenzene $Z = 0.44$ Å; that is, there is a center of mass displacement. This means that the moments of inertia are calculated about axes through this mass center point using the structural data. The replacement of fluorine by chlorine results in $Z = 0.96$ Å; consideration of bromobenzene means that the mass center must lie almost midway along the C—Br bond ($Z = 1.63$ Å). Therefore in these three molecules, the halogenobenzenes, one has a series where the solute is increasingly hindered rotationally by the increasing volume and mass of the substituent atom and by an increasing Z.

The spectrum of pyridine in decalin (10% v/v) at 293°K is shown in Fig. 4.2.1.1 to be a typically broad band, peaking in this case at $45 \pm 2\,\text{cm}^{-1}$ with a maximum absorption intensity of 8 Np/cm. We note in passing that only Fourier transform spectroscopy (Chamberlain, 1977) allows us our required *ordinate* accuracy (in Np/cm). This is not usually available with grating spectrometers, and in conventional infrared spectroscopy is not usually considered with enough care. This inevitably leads to gross error (Chapter 12) when considering band shape as opposed to band position unless Fourier transform techniques are implemented as in this work. A single microwave point, obtained with a separate piece of equipment (in this case based on a klystron generator), is drawn in at $2.3\,\text{cm}^{-1}$ to indicate how in general the low frequency side of the observed band can be extrapolated smoothly below $20\,\text{cm}^{-1}$ before a characteristically steeper drop to zero power absorption occurs in the microwave range below about $3\,\text{cm}^{-1}$ (90 GHz). In Section 4.2.3 we illustrate the relationship between microwave and far infrared spectra in more detail. It is sometimes useful to note that at very high frequencies (equivalent to very short time scales) the power absorption coefficient of the far infrared falls approximately as $\bar{\nu}^{-3}$ or, almost equivalently, as $\bar{\nu}^3 \exp(-\bar{\nu}^2/a)$; $a = kT/(2\pi^2 c^2 I)$, which is the form taken by the free rotor Kummer function of a rodlike molecule (Chapter 2).

Figure 4.2.1.1.2 illustrates the spectra of the three halogenobenzene solutions, with fluoro, chloro-, and bromobenzene peaking at 39, 34, and $24\,\text{cm}^{-1}$, respectively. Although these molecules have similar dipole moments, the area of the absorption band (the so-called integrated intensity) decreases with increasing moment of inertia, measured by the effective or reduced inertia, which for these molecules, where $\boldsymbol{\mu}$ is exactly on the **a** axis, is

$$\frac{1}{I_r} = \frac{1}{I_b} + \frac{1}{I_c}$$

(Eq. 1.9.3.3).

The torque factor for pyridine is observed to be lower than in the halogenobenzenes and reflects a smaller hindrance to rotation. The T_q

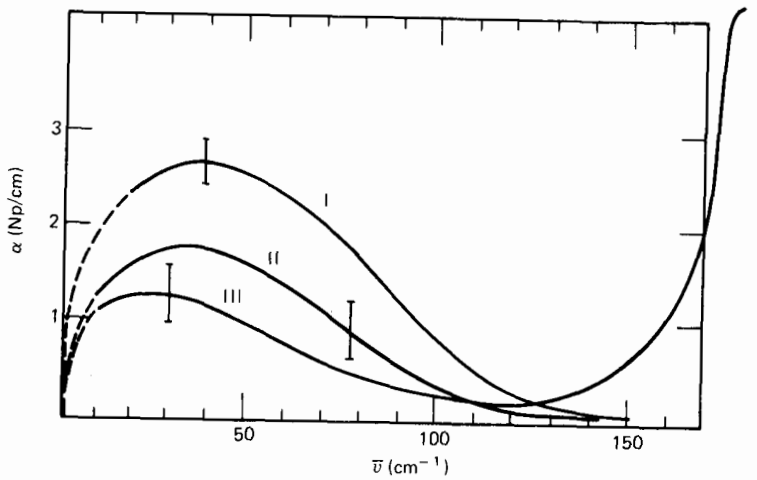

Figure 4.2.1.1.2 Absorption spectra for decalin solutions at 293°K (10% v/v). I Fluorobenzene; II chlorobenzene; III bromobenzene.

values for the A2 compounds are such as to indicate an apparently smaller hindrance to rotation for bromobenzene than for either chloro- or fluorobenzene. This reflects a change in the essential nature of the molecular dynamics between the almost disklike pyridine or fluorobenzene (zero or small Z parameter) to the elongated bromobenzene molecule. The symmetry of incident torques is such that pyridine and fluorobenzene undergo preferential in-plane rotation about I_c. As we shall see in Section 4.2.2, this is an indication of the role of translation/rotation coupling (Chapter 5).

4.2.1.2 Group A3—Six-Membered Aromatics with Bulky Substituents

These are sketched in Fig. 4.2.1.2.1*b*. In nitrobenzene the NO_2 group is coplanar with the aromatic ring but aniline is not planar because the nitrogen lone pair forces the NH_2 plane to make an angle of 37° with the **a**–**b** plane when looking along the **b** axis. For α-picoline we have estimated the molecular dipole moment by group dipole vector addition (Hill et al., 1969) to be 2.04 D ($\mu_a = 0.74$ D, $\mu_b = 1.9$ D). The inertial data are tabulated in Table 4.2.1.2.1.

The far infrared data for 20% v/v solutions of toluene and *o*-xylene are also shown in Fig. 4.2.1.2.2. In each case the librational absorption is so weak that resolution from the proper mode absorptions (CH_3 torsions) peaking above $200\,\text{cm}^{-1}$ is difficult and uncertain. However, the CH_3 group substituent is of special interest because it presents a mean volume similar to that of the bromine atom with a mass smaller by more than five times, so that it is worth describing the process of determining $\tilde{\nu}_{max}$ for toluene and *o*-xylene with some care. The overlapping mode on the toluene spectrum has its origins in a peak observed at $216\,\text{cm}^{-1}$, of maximum absorption

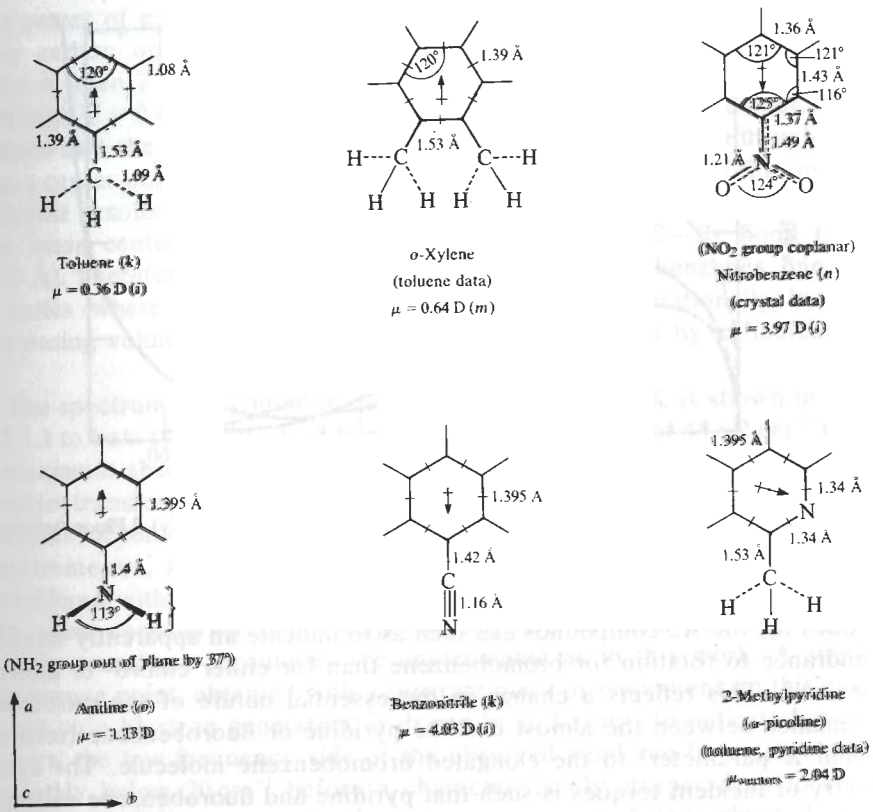

Figure 4.2.1.2.1 Group A3. Six-membered aromatics with bulky substituents.

Table 4.2.1.2.1 Structural and Spectral Data for Group A3[a]

Solute	Z (Å)	I_a	I_b (10^{-38} g cm^2)	I_c	μ (D)	I_r (10^{-38} g cm^2)	$\bar{\nu}_{max}$ (cm^{-1})	T_q (g)
A3								
20% Toluene	0.46	1.52	3.25	4.77	0.36	1.92	60 ± 4	6912(16%)
20% o-xylene	0.66	2.56	3.67	6.19	0.64	2.3	65 ± 5	9717(16%)
α-Picoline	0.46	1.52	3.25	4.77	2.04	1.22	60	4392
					$\mu_a = 0.74$			
					$\mu_b = 1.9$			
Nitrobenzene	1.21	2.08	6.9	8.98	3.97	3.9	39	5932
5% aniline	0.465	1.49	3.23	4.72	1.13	1.92	(64)	(7864)
5% Benzonitrile	0.855	1.47	5.5	6.97	4.03	3.87	47	6781
Pentafluorobenzene	0.30	6.29	8.32	14.6	1.4	4.4	30 ± 4	3960(25%)

[a] See footnotes of table 4.2.1.1.

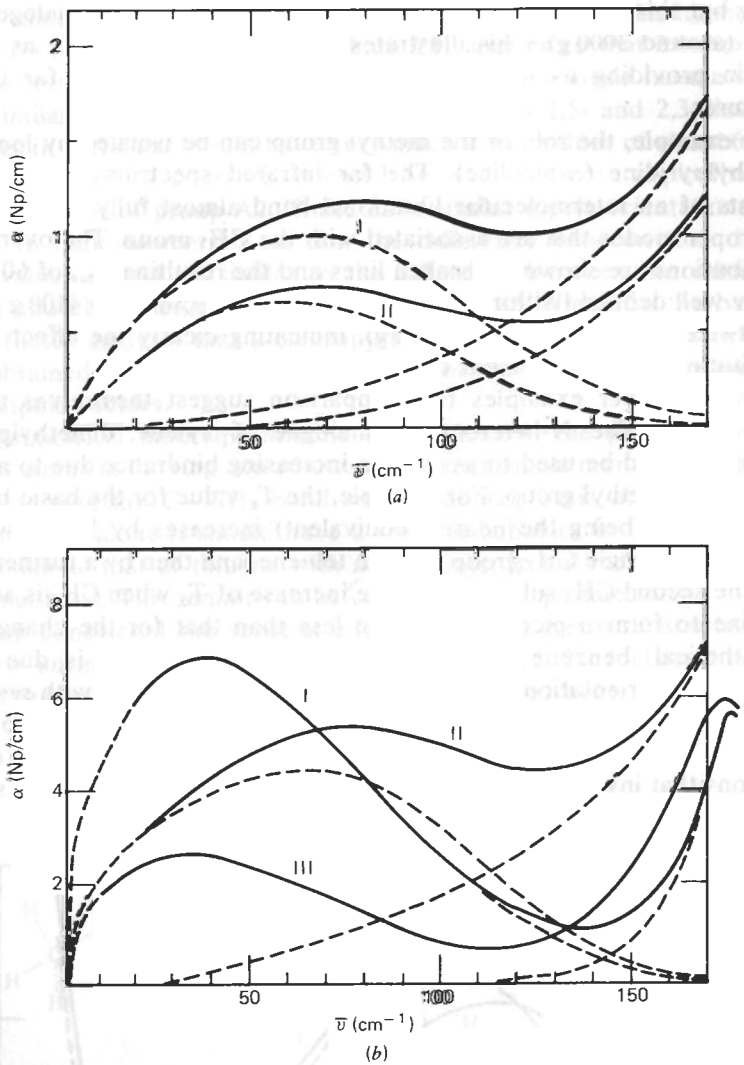

Figure 4.2.1.2.2 Absorption spectra. (*a*) I 20% *o*-xylene; II 20% toluene. (*b*) I Nitrobenzene; II 5% aniline; III pentafluorobenzene. Solid lines, as observed (corrected for solvent); dashed lines, components.

3.4 Np/cm and half-width 32 cm^{-1}. Its shape can be fitted to a Lorentzian allowing the resolution of the librational band with $\bar{\nu}_{max} = 60 \pm 4$ cm^{-1}. The corresponding proper mode features for *o*-xylene appear at a higher mid-infrared frequency than for toluene because of intramolecular interaction between the neighboring CH_3 groups. This information allows us to use the same procedure to resolve for *o*-xylene $\bar{\nu}_{max} = 65 \pm 5$ cm^{-1}, giving a solute torque factor of $T_q = 9717$ g. Toluene has the lower value of $T_q =$

7380 g but this is already very large in comparison with the halogenobenzenes (around 3000 g). This illustrates the role of solute *shape* as well as bulk in providing us with the observable band shapes, or far infrared signatures.

For example, the role of the methyl group can be isolated by looking at 2-methylpyridine (α-picoline). The far infrared spectrum (Fig. 4.2.1.2.3) consists of an intermolecular librational band almost fully resolved from the proper modes that are associated with the CH_3 group. The overlapping contributions are shown by broken lines and the resulting $\bar{\nu}_{max}$ of 60 cm^{-1} is clearly well defined (within ±2 cm^{-1}). The torque factor $T_q = 4100$ g is more than twice that for pyridine (1860 g), indicating clearly the effect of CH_3 substitution on the molecular dynamics.

Several further examples for comparison suggest themselves and are made below. The *N*-heterocyclic analogue of xylene, dimethylpyridine (lutidine), could be used to assess the increasing hindrance due to addition of a second methyl group. For example, the T_q value for the basic benzene ring (pyridine being the nearest equivalent) increases by 5522 g with the addition of a single CH_3 group to form toluene, and then by a further 2337 g with the second CH_3 substitution. The increase of T_q when CH_3 is added to pyridine to form α-picoline is 2240 g less than that for the change from (hypothetical) benzene (pyridine value) to toluene. This is due to the difference in orientation of the dipole vectors in both cases with respect to the position of CH_3 attachment. The α-picoline can relax by rotation along its long axis (containing the CH_3 group), whereas toluene can relax only by rotations that involve the movement of the CH_3 group through the solvent.

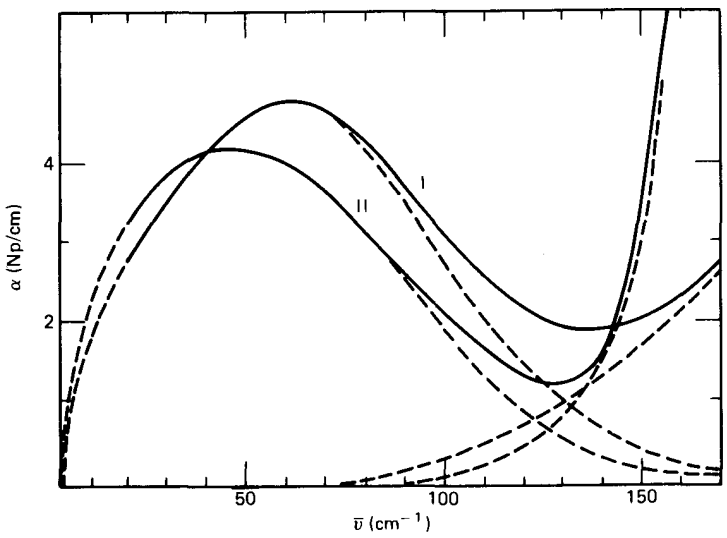

Figure 4.2.1.2.3 Absorption spectra. I α-Picoline; II 5% benzonitrile.

The T_q value for the dimethylpyridine would, according to this hypothesis, depend on the relative positions of both CH_3 groups so that 2,6-dimethylpyridine (essentially the same geometry as *o*-xylene) would have a torque value similar to that of *o*-xylene (9700 g), whereas 2,5- and 2,3-dimethylpyridines in particular would have very much lower values of about 6000 g.

A similar type of comparison could be made between α-picoline and 2-chloropyridine of group A2. These have similar dipole orientations with respect to their geometries so that the difference between their torque factor values should be similar to the difference between the values for toluene and chlorobenzene. One can therefore anticipate on the basis of torque factor analysis that 2-chloropyridine would have T_q less than the value obtained for chlorobenzene by virtue of the difference in orientation of the dipole vectors.

In symmetrical methylpyridimine (Fig. 4.2.1.2.4) the presence of two nitrogen atoms in the ring contributes a large net dipole moment along the a axis containing the C—CH_3 bond so that on the basis of torque factor considerations alone it should have a spectral behavior in the far infrared very similar to that of toluene with a more intense but more "resolvable" librational band. This remains to be corroborated experimentally.

Having considered the spectral effect of methyl group substitution, we can now surmise whether the difference between T_q for pyridine and fluorobenzene can be regarded as a measure of hindrance due to a single

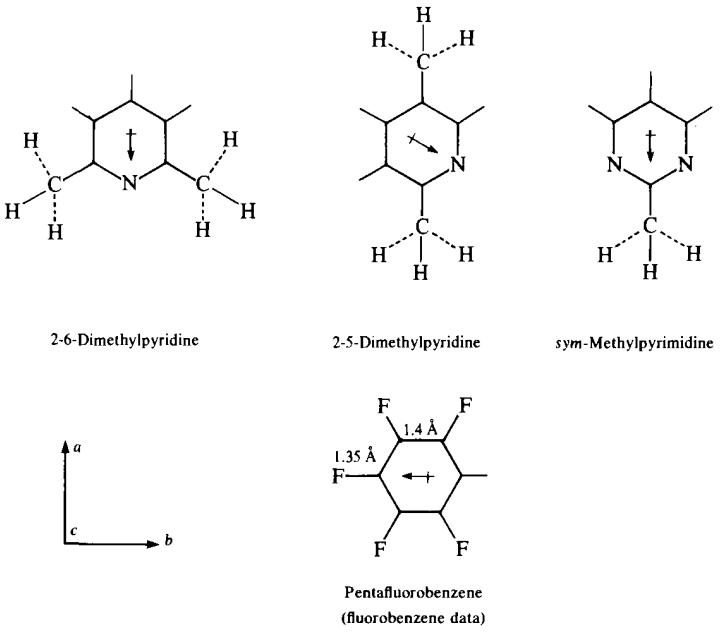

Figure 4.2.1.2.4

fluorine atom and whether T_q for pentafluorobenzene will be greater than that of pyridine by five times this value. The far infrared spectrum of C_6F_5H (Figure 4.2.1.2.2) reveals a librational band peaking at $30 \pm 4\,cm^{-1}$ and weaker in intensity by a factor of about three compared with the spectrum of fluorobenzene. The T_q factor is $3960 \pm 25\%$, which is only 1040 g above that of fluorobenzene or 2100 g above pyridine. It appears that additional substituents do not hinder the rotation/libration as much as the one substituent in isolation.

Of the remaining solutes in this section nitrobenzene (Fig. 4.2.1.2.2) has a libration band that is suitably intense and sufficiently resolved from proper modes, the lowest of which peaks at $176\,cm^{-1}$. The peak frequency produces a value of $T_q = 5901$ g, intermediate between the values for the halogeno- and methylbenzenes.

Aniline is a nonplanar solute with the *N*-hydrogens above the ring plane. Similarly as in ammonia, nitrogen inversion may occur to place the *n*-hydrogens below the plane, and this involves a small degree of relaxation (reversal of the component). The inversion frequency of ammonia is 23.8 GHz ($<1\,cm^{-1}$) so at far infrared frequencies an aniline inversion at a similar frequency would mean that the molecule behaves as a rigid entity. The vibrational levels associated with inversion are separated by large energy levels associated with infrared frequencies. However, because of the central barrier to inversion (energy 24.5 kJ/mole for ammonia), each level is split into two, separated by energies that may correspond to far infrared frequencies (one such separation for ammonia corresponds to $36\,cm^{-1}$). Transitions, between such levels may be infrared active.

The spectrum for a 5% solution of aniline is shown in Fig. 4.2.1.2.2. Upon subtraction of the proper mode wings, a broad band remains centered at $64\,cm^{-1}$ which is probably librational. The factor T_q then takes a value of 8100 g, implying that rotation of aniline in solution is highly hindered, which cannot be rationalized in terms of the solute size alone (aniline having a geometry and mass distribution similar to those of fluorobenzene). The high T_q value could perhaps indicate that the peak at $64\,cm^{-1}$ is compounded of a librational component at lower frequency and a further band possibly having to do with the inversion mechanism or molecule association due to pairwise hydrogens bonding in solution. This means that the behavior of aniline in decalin is anomalous and may be reasonably excluded for our present purposes.

Finally the spectrum of 5% benzonitrile solution (Fig. 4.2.1.2.3) exhibits a proper mode of $166\,cm^{-1}$, but this is narrow enough to allow an accurate separation of peaks. The librational band thereafter peaks at $47\,cm^{-1}$, providing a T_q of 6780 g, a large value, but not inconsistent with the solute size, because with $Z = 0.855$ Å the infrared active rotation/libration motion of this molecule involves the extreme nitrogen atom sweeping out a sphere of 3.16 Å (from center of mass to nitrogen center).

With the exception of aniline the T_q values increase with increasing

anisotropy of solute (Table 4.2.1.2.1). Thus pentafluorobenzene, which is a borderline case between groups A2 and A3, is massive but not obtrusive, and has a low torque factor. α-Picoline, hindered by a methyl group, nevertheless relaxes easily about the a axis. Nitrobenzene and benzonitrile have increasingly bulky substituents, whereas methyl substituents give rise to high T_q coefficients in toluene and *o*-xylene.

4.2.1.3 Group B, The Halogenonaphthalenes

In this group the principal moments of inertia change direction with the size and position of the substituent (Fig. 4.2.1.3.1). The center of mass positions can be described in terms of component shifts (Z_x and Z_y) from an origin centered on the midpoint of the C_9—C_{10} bond. By varying the substituent the orientation of the resultant dipole vector with respect to the principal inertia system can be changed by many degrees. Thus 1-fluoronaphthalene would have μ almost perpendicular to the **a**-axis, whereas the 2-fluoronaphthalene has μ almost parallel to **a**. The far infrared spectra of 10% decalin solutions of halogenonaphthalenes (Fig. 4.2.1.3.2) show the relevant intermolecular librational absorptions almost resolved from the proper mode higher frequency spectra, represented by broken lines in the region of overlap, and allow values of 38 and $48\,cm^{-1}$ to be fixed for $\bar{\nu}_{max}$ of 1-bromo- and 1-chloronaphthalene, respectively. Both solutes have similar dipole moments and the sum rule (Chapter 1) therefore dictates that the integrated intensities vary inversely with the inertia, as is indeed the case experimentally. The structural and spectral data are summarized in Table 4.2.1.3.1.

The empirical T_q factor for 1-bromonaphthalene is the lesser. The T_q values in general are larger than those of the corresponding halogenobenzenes by a factor of almost three. As discussed in the next section there is appreciable translation/rotation coupling involved in determining this ratio.

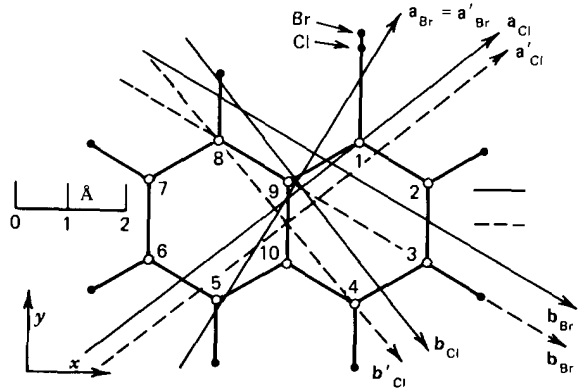

Figure 4.2.1.3.1 Structural diagram for the α-halogenonaphthalenes. Solid lines, center of mass axes; dashed lines, assumed center of volume axes.

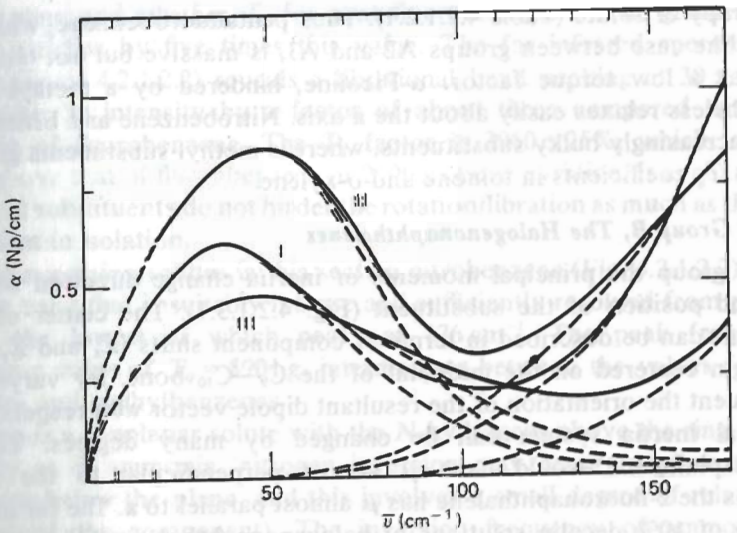

Figure 4.2.1.3.2 Absorption spectra. I 1-Bromonaphthalene; II 1-chloronaphthalene; III thiophene $\times\frac{1}{2}$.

Table 4.2.1.3.1 Structural and Spectral Data, Halogenonaphthalenes

Solute	Z (Å)	I_a	I_b (10^{-38} g cm²)	I_c	μ (D)	I_r (10^{-38} g cm²)	$\bar{\nu}_{max}$ (cm⁻¹)	T_q (g)
1-Chloro-naphthalene	$Z_x = 0.25$ $Z_y = 0.65$	5.5	8.5	14.0	$\mu = 1.58$ $\mu_a = 1.05$ $\mu_b = 1.17$	4.43	47	9786
1-Bromo-naphthalene	$Z_x = 0.46$ $Z_y = 1.24$	5.97	13.23	19.2	$\mu = 1.56$ $\mu_a = 1.34$ $\mu_b = 0.80$	5.17	38	7465

4.2.1.4 *Group C1, Five-Membered Aromatic Heterocyclics*

The five-membered heterocyclics provide a useful series of solutes where the hetero atoms N, O, and S increase in mass, while the ring shape remains fairly constant (Fig. 4.2.1.4.1). For the solutes displayed in the figure the moments of inertia have been calculated about center of mass axes intersecting at a distance Z from the C—C bond opposite the heteroatom; they are tabulated in Table 4.2.1.4.1. The spectra for furan (Fig. 4.2.1.4.2) and thiophene (Fig. 4.2.1.3.2) reveal for the former a libration band centered at 51 cm^{-1} and for the latter an imperfectly resolved band peaking at 46 cm^{-1}. The calculated torque factors are respectively 1560 and 2040 g, reflecting the increase of solute size with carbon to hetero atom bond length. Pyrrole has a reduced moment of inertia very similar to

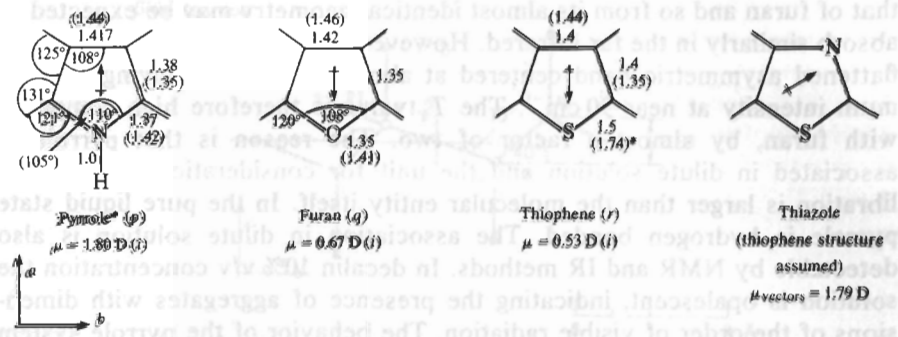

Figure 4.2.1.4.1 Group C1. Five-membered aromatic heterocyclics. C—H = 1.08 Å. All lengths in Å; lengths in parentheses (not used except *) are from reference *k*. (Italic letters in parentheses refer to table reference listed at end of chapter.)

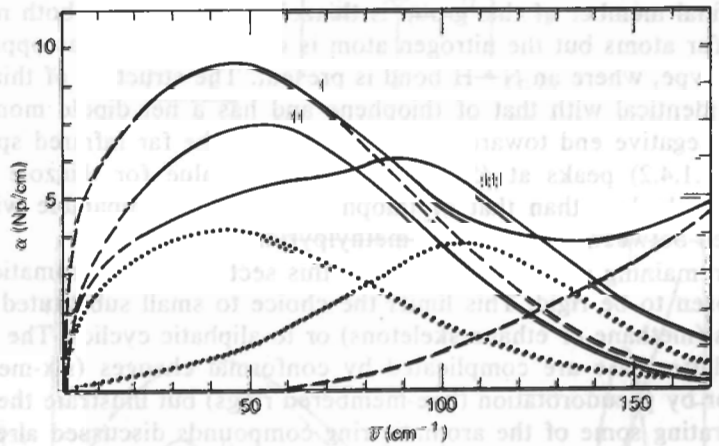

Figure 4.2.1.4.2 Absorption spectra. I Thiazole; II furan ×3; III pyrrole/cyclohexane. Dotted lines, component bands.

Table 4.2.1.4.1 Structural and Spectral Data for Group C1

Solute	$Z^{a a}$ (Å)	I_a*	I_b*	I_c*	μ (D)	I_r (10^{-38} g cm²)	$\bar{\nu}_{max}$ (cm⁻¹)	T_q (g)
C1								
Pyrrole	0.96	0.88	0.92	1.80	1.80	0.61	(65)	(2577)
Furan	1.0	0.88	0.907	1.787	0.6	0.6	51	1560
Thiophen	1.3	1.04	1.54	2.58	0.53	0.964	46	2040
Thiazole	1.3	1.04	1.54	2.58	1.79	0.833[b]	45	1687

*Unit: 10^{-38} g cm².
[a]'Z' for C_5H_5 = 0.96 (hypothetical).
[b]Value depends on vector directions (see text).

that of furan and so from its almost identical geometry may be expected to absorb similarly in the far infrared. However, as Fig. 4.2.1.4.2 shows, it is a flattened asymmetric band centered at about 65 cm^{-1} but having a maximum intensity at near 90 cm^{-1}. The T_q value is therefore high compared with furan, by almost a factor of two. The reason is that pyrrole is associated in dilute solution and the unit for consideration in terms of libration is larger than the molecular entity itself. In the pure liquid state pyrrole is hydrogen bonded. The association in dilute solution is also detectable by NMR and IR methods. In decalin 10% v/v concentration the solution is opalescent, indicating the presence of aggregates with dimensions of the order of visible radiation. The behavior of the pyrrole system strongly resembles that of aniline in decalin in failing to conform with the pattern discernible in similarly shaped solute molecules. Pure aniline is well known to be strongly hydrogen bonded and the far infrared results strongly suggest that this persists in dilute solution.

The final member of this group is thiazole. This contains both nitrogen and sulfur atoms but the nitrogen atom is of pyridine type as opposed to pyrrole type, where an N—H bond is present. The structure of thiazole is almost identical with that of thiophene and has a net dipole moment of 1.79 D, negative end towards the hetero atom. The far infrared spectrum (Fig. 4.2.1.4.2) peaks at 45 cm^{-1}, and the T_q value for thiazole is correspondingly less than that of thiophene, a result comparable with that observed between toluene and 2-methylpyridine.

The remaining solutes considered in this section are nonaromatic. They are chosen to be rigid. This limits the choice to small substituted hydrocarbons (methane or ethane skeletons) or to aliphatic cyclics. The spectra in the latter case are complicated by conformal changes (six-membered rings) or by pseudorotation (five-membered rings) but illustrate the effects of saturating some of the aromatic ring compounds discussed already. In this context it might be expected that the libration spectra of saturated aliphatic cyclics should peak at higher frequencies than their unsaturated aromatic equivalents owing to an increase in bulk but not in inertia.

4.2.1.5 Groups D1 and D2, Nonaromatic Six-Membered Rings and Their Derivatives

The basic structure is the cyclohexane ring whose side and front elevations (Fig. 4.2.1.5.1*a*) can be used to determine the centers of mass, axial directions, and moments of inertia of several dipolar derivatives and analogues. The molecules considered are tetrahydropyran (oxane), where the CH_2 segment at R is replaced by O; 1,3-dioxane (*Q* and *Q'* segments replaced by O's); 1,4-thioxane (segments, R replaced by S, R′ replaced by O); piperidine (CH_2 at R replaced by NH); morpholine (R replaced by NH, R′ by O); chlorocyclohexane; N-methylmorpholine and *N*-methylpiperazine (R replaced by N—Me, R′ by NH). In addition cyclohexanol and

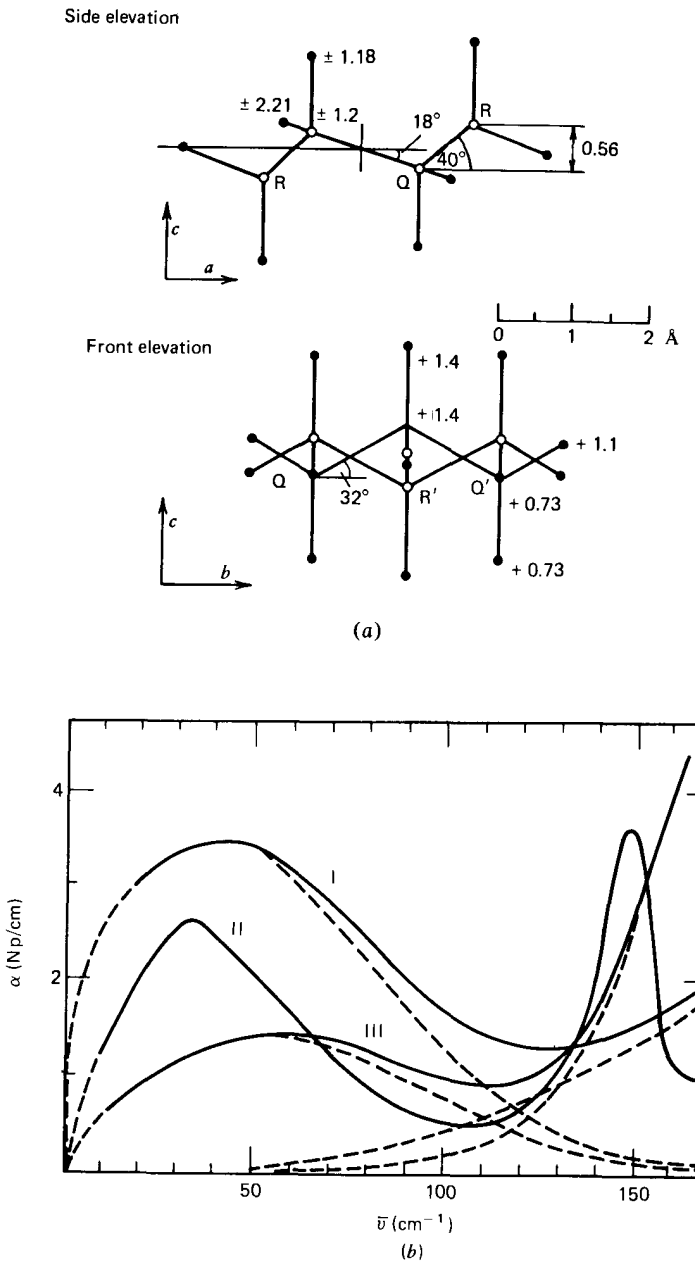

Figure 4.2.1.5.1 (*a*) Side and front elevations of cyclohexane ring. (*b*) Absorption spec Tetrahydropyran; II chlorocyclohexane; III thioxane.

cyclohexanone were studied as examples of relaxation occurring by internal rotation, at least in principle (the ketone via its enol). The moments of inertia and centers of mass shift factors (Z) are tabulated in Table 4.2.1.5.1. The former can be determined by finding the coordinates of each atom. For tetrahydropyran, 1,3-dioxane, piperidine, and morpholine these can be compared with known microwave rotational constants, but in general the principal moments of inertia for these molecules are less well known, giving greater uncertainty in I_r. In addition these molecules may have

Table 4.2.1.5.1 Heterocyclics

Solute	Z (Å)	I_a* [μ_a]	I_b*	I_c* [μ_c]	μ (D)	I_r (10^{-38} g cm^2)	$\bar{\nu}_{max}$ (cm^{-1})	T_q (g)
Tetra-hydropyran	0	1.8 [a][1.53] [1.05]	1.8	3.12 [0.82] [0.84]	1.6(solution)[b] 1.74 1.34	1.14 1.04	41	1832
1-3-Dioxane	0	1.68 [b][1.29] [0.93]	1.74	3.04 [1.61] [1.88]	2.14(solution)[b] 2.06 2.09	0.99 0.9	40	1520
Thioxane	0.24	1.87 [0.22]	2.37	3.67 [0.1]	0.24	1.36	50 ± 8	3400 (±35%)
Piperidine	0 axial	1.87 [a][0.2] [0.58]	1.91	3.31 [0.78] [0.86]	1.18(solution)[b] 0.8 1.04	(0.95) 1.2		
	equat.	[a][0.63] [0.66]		[0.5] [0.85]	0.8 1.08	(1.08) 1.2	65 ± 5	5070
Morpholine	0	[a] 1.7	1.81	3.12				
	equat.	[a][1.68] [1.72]		[0.3] [0]	1.71 1.72	1.14		
	axial	[0.47]		[1.7]	1.76	0.9		
Chloro-cyclohexane	equat. $z = 0.93$	1.85 [1.8]	5.71	7.03 [0.45]	1.86	2.94	32	2560
	axial $z = 0.75$	2.68 [1.55]	4.37	4.86 [1.0]	1.86	2.07		
N-methyl morpholine	equat. $z = 0.44$	1.88 [1.04]	3.56	4.88 [0.21]	1.06	2.0	56 ± 5	5582
	axial $z = 0.36$	2.6 [1.08]	2.89	3.46 [0.185]	1.09	1.56		
N-methyl piperazine	equat.	1.88 [0.67] [0.57]	3.56 H. eq H. ax	4.88 [0.22] [1.49]	0.71 1.6	1.93 1.21		
	axial	2.6 [1.25]	2.89 H. eq	3.46 [1.0]	1.6	1.49	76	8666
	$z = 0.36$	[0]	H. ax	[0.71]	0.71	1.37		

*Unit: 10^{-38} g cm^2.
[a]References (*s*, *t*, *u*, and *v*).
[b]References (*w*, *t*, *x*, and *y*).

different conformal isomers, but at short times each species is effectively rigid.

In cyclohexane the chair form is about 20 kJ/mole more stable than the "flexible" form, with interconversion between chair forms via the "boat" form transition state (eclipsed ethylenes), a barrier of 42 kJ/mole. In the hetero rings, interconversion involves redirection of the dipole vector and results in low frequency infrared proper modes.

Tetrahydropyran undergoes rapid ring inversion but only chair form spectral contributions can be expected on the grounds of microwave spectroscopic results. The gas phase dipole components give $\mu = 1.74$ D, which is larger than measured solution values (1.58–1.63 D), whereas dipole components from bond moments provide an even smaller value of 1.34 D. The far infrared spectrum in decalin peaks at 41 cm^{-1}, slightly overlapping with the proper modes at higher frequency. The T_q value of 1832 g is similar to that for pyridine.

1,3-Dioxane has two oxygen atoms in the ring and moments of inertia that are smaller than for cyclohexane, indicating a decreasing size in the saturated ring with oxygen substitution. Dipole component calculations result in $\mu = 2.06$ D, consistent with solution values, and the resulting I_r multiplied with $\bar{\nu}^2_{max}$ obtained from the spectrum gives a relatively small T_q of 1520 g.

Thioxane can be modeled with a C—S bond length of 1.77 Å intermediate between thiophene (1.7 Å) and dimethyl sulfoxide (1.86 Å) and a C—S—C angle of 103° (as in SCl_2). The far infrared spectrum (Fig. 4.2.1.5.1) reveals a small librational absorption and an intense proper mode at 185 cm^{-1}, the latter being a ring torsion shifted to a lower frequency compared with a similar mode of tetrahydropyran by virtue of increasing ring inertia. The weak librational intensity is in accord with the small dipole moment (0.24 D) from bond moments. A value of 50 ± 8 cm^{-1} is obtained for the librational peak frequency, after correcting for the proper mode, resulting in a relatively high $T_q = 3400$ g.

Piperidine (Fig. 4.2.1.5.2) on size considerations alone should provide us with a T_q value intermediate in the hetero-atom series. The presence of the single imino hydrogen allows two possible conformers (axial and equatorial) with almost identical inertial values but different dipole directions. The dipole components calculated from bond moments based on the cyclohexane geometry are not in good agreement with experimental microwave estimates but the inertia estimates are in good agreement. Depending on which set of dipole data is accepted the T_q values for the two conformers are either identical (microwave data) or else the axial conformer has the smallest value (bond moments). The solution moment is experimentally 1.18 D. Piperidine is known to be hydrogen bonded in the pure liquid state, and it is likely that association might be a factor in proton acceptor solvents. It is insoluble in decalin, but a 10% solution in cyclohexane provides a far infrared spectrum which consists of the ascending

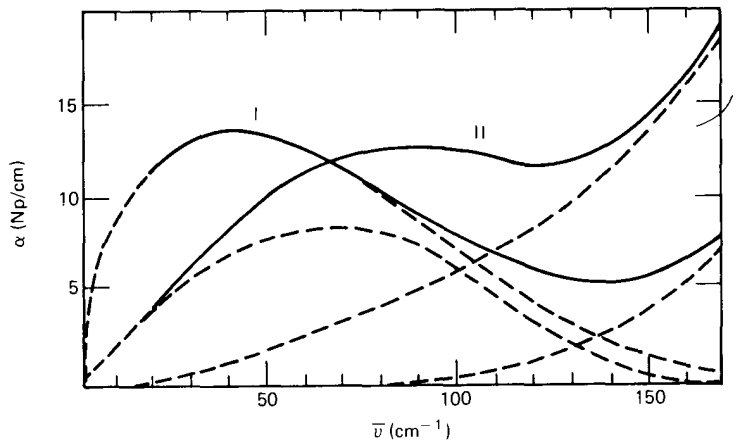

Figure 4.2.1.5.2 Absorption spectra. Dashed lines represent resolved spectra. I 1, 3-Dioxane ×2; II piperidine/cyclohexane.

wing of a proper mode absorption with a libration component appearing as a shoulder at 80 cm^{-1}. After correction the librational band is found to peak at 65 ± 5 cm^{-1}, giving $T_q = 5070$ g, a high value indicating association in the manner of aniline and pyrrole solutions. A systematic study of the role of the N—H bond in this context would be of interest because of the possibility that cyclic imines may undergo nitrogen inversion as in ammonia. A useful solute would be morpholine, which is extensively hydrogen bonded in the pure liquid state and whose dipole moment of 1.71 D is oriented almost precisely along the inertial **a** axis of the molecule.

The structure of chlorocyclohexane is basically that of cyclohexane with one hydrogen on carbon R replaced by chlorine at a C—Cl distance of 1.77 Å. The I_r values for conformers differ markedly. The spectrum peaking at 32 cm^{-1} is almost fully resolved from a proper mode at 146 cm^{-1}. This results in a mean for both conformers of $T_q = 2560$ g, which is larger than the value obtained for tetrahydropyran but lower than expected from a direct comparison of the effective doubling of T_q in chlorobenzene measured against pyridine.

The role of methyl group substitution in these ring compounds may be delineated with sufficiently polar solutes such as *N*-methylmorpholine ($\mu = 1.06$ D), whose far infrared spectrum (Fig. 4.2.1.5.3) in decalin is a low intensity librational band on the wing of a large proper mode peaking above 200 cm^{-1}. The librational peak frequency is estimated at $\bar{\nu}_{max} = 56$ cm^{-1}, and $T_q = 5582$ g, again indicating a relatively large resistance to rotational motion caused by methyl group substitution.

If a solute molecule is chosen so as to be rotationally hindered both by virtue of methyl substitution and also through the associating effect of NH as in *N*-methylpiperazine (Fig. 4.2.1.5.3) then T_q increases as expected to

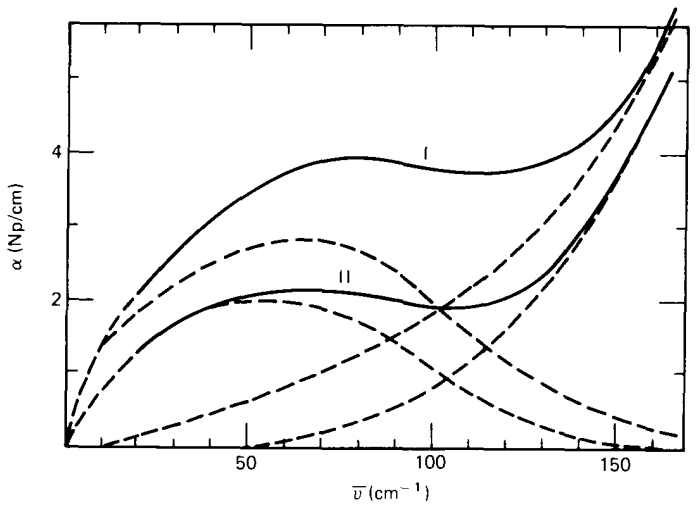

Figure 4.2.1.5.3 Absorption spectra. I *N*-Methylpiperazine/CCl_4; II *N*-methylmorpholine.

the relatively large value of 8666 g, corresponding to a far infrared peak at 76 cm^{-1}. The carbonyl and hydroxyl groups are strongly dipolar and liquids containing them are usually hydrogen bonded or associated. The hydroxyl group is one of many substituents that can relax appreciably by internal rotation and so has a dielectric absorption at microwave frequencies (rotation frequency) and an associated vibrational mode in the infrared of appreciable intensity.

The far infrared spectrum of cyclohexanol, for example (in cyclohexane), consists of a shoulder of librational origin on an intense proper mode (Fig. 4.2.1.5.4). The former may be estimated to peak at 55 cm^{-1}. If it is assumed that the librating species has an averaged dipole along the C—O bond of 0.75 D then the appropriate T_q value is 6588 g, typical of associated systems in dilute solution. The spectrum of cyclohexanone in decalin (Fig. 4.2.1.5.4) peaks at 110 cm^{-1} and shoulders at 50 cm^{-1}, implying the existence of two distinct relaxing species in solution. As is well known, a ketone can exist in its tautomeric form (an enolate) by virtue of a hydrogen atom from an adjacent carbon transferring to C=O to form the hydroxyl group and leaving a C=C double bond. The enolate form (cyclohex-1-enol) would have a spectrum very similar to that of cyclohexanol. There is therefore a possibility that the keto and enol tautomers exist in solution as a complex species which by virtue of their larger size would contribute a librational absorption at higher frequency compared with the uncomplexed cyclohexanone.

Table 4.2.1.5.1 summarizes the variety of T_q values obtained and these can be compared with values for the corresponding six-membered aromatic rings. Thus tetrahydropyran and 1,3-dioxane, representing the smallest

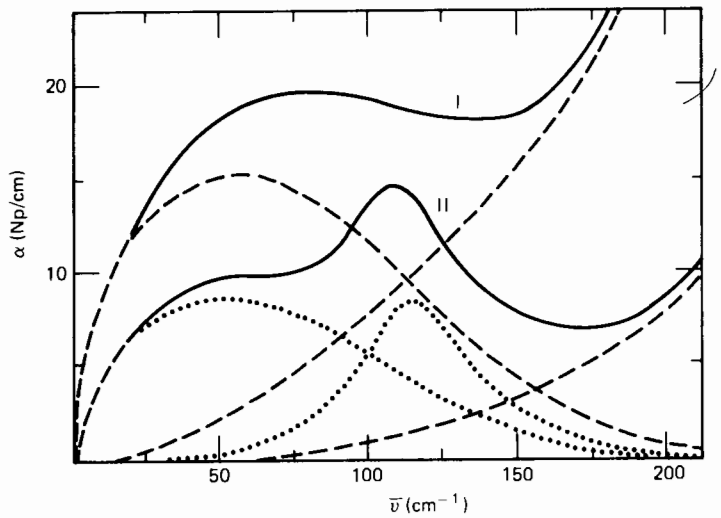

Figure 4.2.1.5.4 Absorption spectra. I 5% Cyclohexanol/C_6H_{12} ×3; II cyclohexanone. Dotted lines, components.

six-membered rings, have T_q values lower than that obtained for pyridine. Thioxane, containing a more massive sulfur atom (atomic volume 17 Å^3 compared with that of carbon, 8 Å^3), is a larger solute and has a larger T_q. The chloro derivative has a lower T_q value than does chlorobenzene, and *N*-methylmorpholine has a value comparable to that of toluene. In general, ring saturation decreases T_q which is contrary to expectations based purely on ring expansion. This may be explained through the observation that although inertially these molecules are almost oblate symmetrical tops, geometrically they are almost spherical, so that the molecule does not have to displace volume upon rotation. Independent evidence for the isotropic rotational behavior of cyclohexane comes from the fact that it forms a soft low density rotator phase solid with a face-centered cubic structure typical of the most isotropic rotators. There is very little interlocking of molecules in the solid. Benzene, on the other hand, has an orthohombic rotator phase structure, and the available experimental evidence (Chapter 3) indicates planar movement through large angles. Even in the liquid phase the rotational movement of benzene is anisotropic and is preferential about the axis of least hindrance. It may be shown (Ford et al., 1976) that the average rate of diffusion of a dipole constrained to a plane is twice as slow as the equivalent motion in space, so that the lower T_q values of saturated six-membered rings may be explained on the basis of the fact that the phenyl compounds, being planar, preferentially undergo in-plane librations. Motions about any axis perpendicular to the c axis (normal to the ring plane) are consequently exposed to large torques. The saturated rings under the same environmental conditions experience a more isotropic distribution of

torques (i.e., less extreme) and the mean square torque is consequently lower. In other words, the phenyls rotating preferentially in a plane produce a lower frequency Debye peak than do the saturated rings of similar moment of inertia rotating isotropically. Owing to the fact that the Debye and librational processes are linked by causality, the phenyl compounds peak at a higher frequency in the far infrared and so have a higher T_q value.

Despite the complications within this group the hypothesis that the mean square torque (or T_q) on a solute molecule is linked to shape anisotropy appears to be verifiable experimentally.

4.2.1.6 Group E1, Five-Membered Saturated Rings, and Group E2, Their Derivatives

The molecules are sketched in Fig. 4.2.1.6.1. The parent cyclopentane molecule can adopt the tetrahedral geometry of sp^3 carbon by forming a planar pentagonal structure. Present understanding indicates that the equilibrium structure is nonplanar and of either a twist or a bend form (Fig. 4.2.1.6.2). These forms are interconvertible so that the prow atom of the bend form rotates around the ring in a manner first considered by Kilpatrick et al. (1947) and referred to as pseudorotation. For polar derivatives

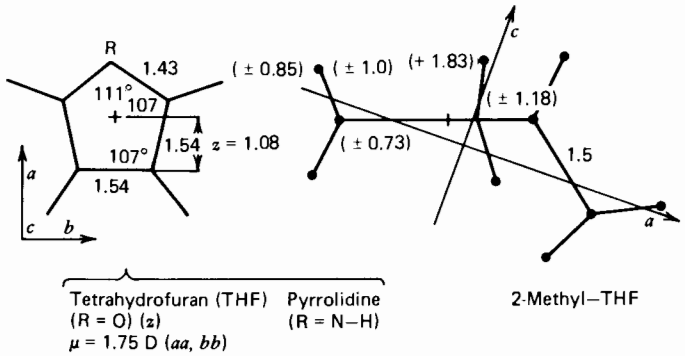

Figure 4.2.1.6.1 Group E1 and E2 molecules.

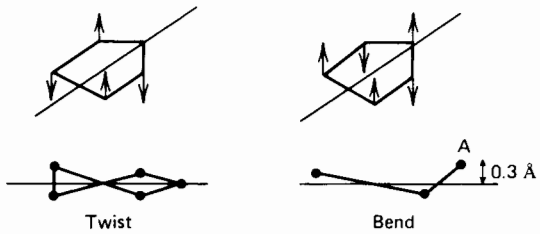

Figure 4.2.1.6.2 Twist and bend forms of pentagonal molecules.

of cyclopentane this motion is observable as a series of absorptions in the far infrared. In consequence the librational bands of tetrahydrofuran and other analogues may be significantly distorted by pseudorotation.

Nevertheless, in contrast to such asymmetric probe molecules as CH_2Cl_2, CH_3CN, or pyridine, a molecule such as tetrahydrofuran (THF) has an almost spherical geometry and is soluble in decalin at low temperatures in the viscous and vitreous conditions (Chapter 7). The empirical parameter T_q allows us to distinguish the effects of pseudorotation from those of libration. In Table 4.2.1.6.1 the I_r value calculated for THF is derived on the basis of microwave data. The far infrared spectrum is illustrated in Fig. 4.2.1.6.3, together with the gas phase spectrum scaled to the same number density. The solution spectrum peaks at 52 cm^{-1}, resulting in $T_q = 2264$ g, which compares with 1560 g for furan, a five-membered aromatic, and tetrahydropyran (1832 g), a six-membered saturated cyclic. This is evidence that pseudorotation persists in THF in the condensed phase. If the gas phase spectrum is decomposed into its rotation and pseudorotation components (Fig. 4.2.1.6.3) and the latter subtracted from the solution spectrum, the residual librational band has its maximum at 40 cm^{-1}. This results in $T_q = 1340$ g. This is a lower limit because of the probability of pseudorotational features remaining in the spectrum.

The radial pseudorotatory transition of pyrrolidine (Fig. 4.2.1.6.4) is centered at about 200 cm^{-1}. Upon subtraction of this component the librational mode of pyrrolidine remains at 60 cm^{-1}, with an intensity appreciably less than that of THF, although the solution dipole moment of 1.58 D is only 10% less than that of THF. The reduced inertia of pyrrolidine is calculated at 2–4% larger than for THF. A permanent μ_c component is also expected to be present, the simplest assumption for the direction of the resultant dipole μ being that pyrrolidine has the same moment as dimethylamine (1.17 D), which gives components $\mu_a = 0.34$ D

Table 4.2.1.6.1 Saturated Heterocyclics

Solute	Z (Å)	I_a* [μ_a]	I_b*	I_c* [μ_c]	μ (D)	I_r (10^{-38} g cm^2)	$\bar{\nu}_{max}$ (cm^{-1})	T_q (g)
Tetra hydrofuran		[a] 1.30	1.32	2.29	$\mu_a = 1.76$	0.84	52 (observed)	2271
(T.H.F.)	1.06	[b] 1.21	1.27	2.21	$\mu_{soln} = 1.75$[c]		40 (corrected)	1344
Pyrrolidine	1.08	[b] 1.32	1.36	2.32	$\mu_{soln} = 1.58$[c]	0.71	60 (observed)	2556
		[d][0.34]		[1.08]	⟶ 1.13		46 (corrected)	1500
2-methyl T.H.F.	0.48 From T.H.F. ring center	[b] 1.34 [d][1.72]	2.7	3.42 [0.3]	⟶ 1.76	1.48	50 (observed)	3700

*Unit: 10^{-38} g cm^2.
[a] Microwave data.
[b] Determined from model.
[c] References *aa*, *bb*, and *i*.
[d] Bond moment analysis.

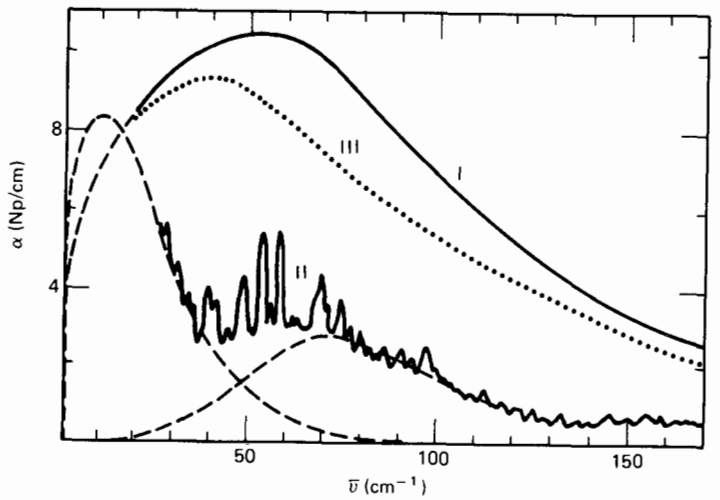

Figure 4.2.1.6.3 Absorption spectra of THF. I Solution spectra (observed); II scaled gas spectrum (refs. *ss*, *dd*) (dashed lines represent resolved spectra); III corrected solution spectra.

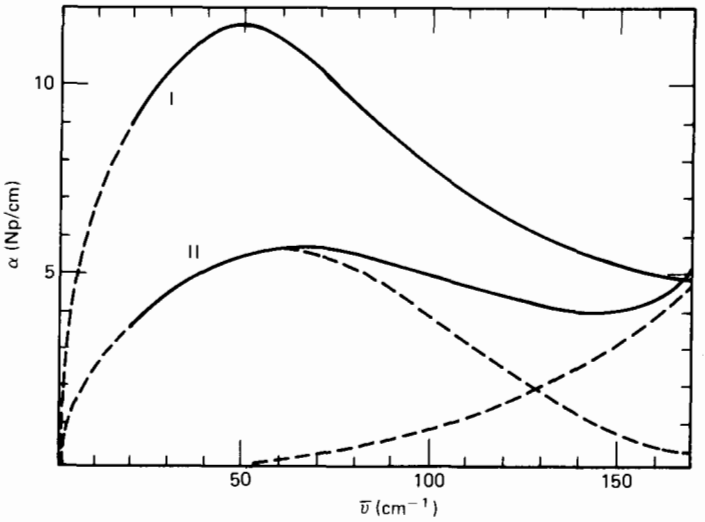

Figure 4.2.1.6.4 Absorption spectra. I 2-Methyltetrahydrofuran; II pyrrolidine.

Table 4.2.1.6.2 Classification Scheme Based on T_q Values for Cyclic Solutes in Decalin (293°K)

Solute	μ (D)	I_a*	I_b*	I_c*	I_r*	$\bar{\nu}_{max}$ (cm^{-1})	T_q g ± %
A1							
Pyridine	2.23	1.4	1.45	2.85	0.96	45 ± 2	1858 ± 9
A2							
Fluorobenzene	1.4	1.47	3.24	4.71	1.92	39 ± 2	2923 ± 10
Chlorobenzene	1.58	1.47	5.3	6.77	2.97	34 ± 2	3433 ± 12
Bromobenzene	1.56	1.47	8.2	9.67	4.43	24 ± 3	2551 ± 25
Pentafluorobenzene	1.4	6.29	8.32	14.6	4.4	30 ± 4	3960 ± 26
A3							
α-Picoline	2.04	1.52	3.25	4.77	1.22	60 ± 2	4393 ± 7
Nitrobenzene	3.97	2.08	6.9	8.98	3.9	39 ± 2	5932 ± 9
Benzonitrile	4.03	1.47	5.5	6.97	3.07	47 ± 2	6781 ± 8
Toluene (20%)	0.36	1.52	3.25	4.77	1.92	60 ± 4	6912 ± 16
o-Xylene (20%)	0.64	2.56	3.67	6.19	2.3	65 ± 5	9717 ± 16
B2							
1-Chloronaphthalene	1.58	5.5	8.5	14.0	4.43	47 ± 2	9786 ± 8
1-Bromonaphthalene	1.56	5.97	13.2	19.2	5.17	38 ± 3	7465 ± 16
C1							
Furan	0.67	0.88	0.9	1.79	0.6	51 ± 2	1560 ± 8
Thiazole	1.79	1.04	1.54	2.58	0.83	45 ± 3	1687 ± 13
Thiophene	0.53	1.04	1.54	2.58	0.96	46 ± 3	2040 ± 13
D1							
Tetrahydropyran	1.6	1.8	1.8	3.12	1.09	41 ± 2	1832 ± 8
1,3-Dioxane	2.14	1.68	1.74	3.04	0.95	40 ± 2	1520 ± 8
Thioxane	0.24	1.87	2.37	3.67	1.36	50 ± 4	3400 ± 16
D2							
Chlorocyclohexane	1.86	1.85	5.71	7.03	2.94	32 ± 3	2560 ± 20
	1.86	2.68	4.37	4.86	2.07		
N-Methylmorpholine	1.06	1.88	3.56	4.88	2.0	56 ± 5	5582 ± 20
		2.6	2.89	3.46	1.56		
E1							
THF	1.75	1.3	1.32	2.29	0.84	46 ± 6	1777
Pyrrolidine	1.58	1.32	1.36	2.32	0.71	53 ± 6	1994
2-Methyl-THF	1.76	1.34	2.7	3.42	1.48	50 ± ?	3700
Associated Species							
Aniline	1.13	1.49	3.23	4.72	1.92	64	7864
Pyrrole	1.8	0.88	0.92	1.8	0.6	65	2577
Piperidine	1.0	1.87	1.91	3.3	1.2	65	5070

*Unit: 10^{-38} g cm^2.

and $\mu_c = 1.05$ D. These moments give an I_r and a torque value (2556 g) similar to that of THF. Unlike the associated species already considered pyrrolidine is readily soluble in decalin and the far infrared spectrum shows no sign of association.

The far infrared spectrum of 2-methyltetrahydrofuran is very similar in shape and intensity to tetrahydrofuran itself. If a planar ring structure with the dipole in this plane is assumed, the center of mass and principal axes can be determined to yield an I_r value larger than that for tetrahydrofuran and in consequence $T_q = 3710$ g, in line with the expectation of rotational hindrance created by the CH_3 group. Pseudorotational motion in the condensed phase is reduced by methylation to an almost negligible intensity. To corroborate these conclusions we would need more exact microwave structural data for five-membered rings and their methyl derivatives.

A summary of the data for cyclic molecules is given in Table 4.2.1.6.2.

4.2.1.7 Group F; Noncyclic Molecules

These are subgrouped for ease of discussion according to size.

4.2.1.7.1 Group F1, Pseudospherical Methane Derivatives

These are illustrated in Fig. 4.2.1.7.1.1. The dipole moment for *tert*-butyl chloride is directed along the **a** axis. For 2-chloro-2-nitropropane, tabulated bond lengths may be used to fix the **a** axis. This is almost parallel to the line joining the chlorine and nitrogen centers, and neither **a** nor **b** axes pass through the central carbon. The dipole moment from group vector addition is 3.69 D, in agreement with the experimentally determined value in solution. Chloroform is the most massive solute of the three molecules in this subgroup with the **c** axis along the threefold axis containing the dipole of value 1.11 D. The **a** and **b** axes are equivalent and chloroform is an oblate symmetrical top. *Tert*-butyl chloride is the opposite extreme of a prolate symmetrical top. The far infrared solution spectra are illustrated in Fig. 4.2.1.7.1.2. There are no proper modes below 200 cm^{-1} so only the undistorted librational bands are present, and these at comparatively low frequencies, 22–33 cm^{-1}. The integrated intensities are in the same order as the respective dipole moments. The T_q values are tabulated in Table 4.2.1.7.1.1.

Both *tert*-butyl chloride and 2-chloro-2-nitropropane are geometrically spherical enough to allow for the existence of face-centered cubic rotator phases in the pure states at low temperatures. However, the T_q value for the latter is much the greater. The internal rotation of the nitro group creates around it a large effective volume, however, and thereby increases the resistance to rotation. A second and probably more significant consideration concerns the relative directions of the dipoles. In *tert*-butyl chloride the slightly smaller van der Waals radius of chlorine and the almost tetrahedral symmetry result in a flattened distribution of volume

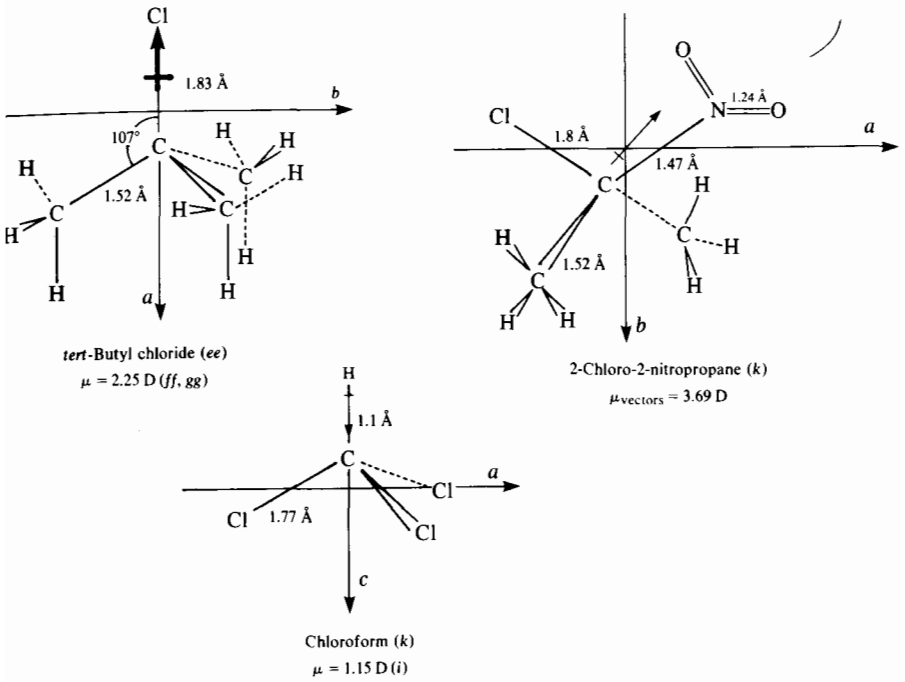

Figure 4.2.1.7.1.1 Group F1. Large spherical molecules. C—H = 1.1 Å.

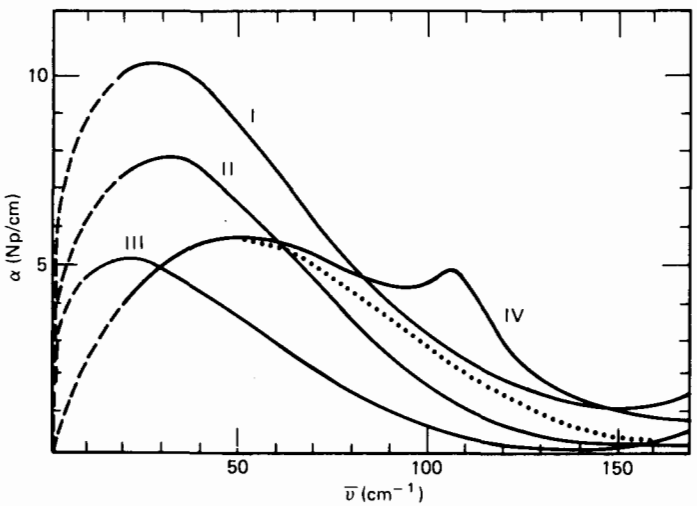

Figure 4.2.1.7.1.2 Absorption spectra. I Chloroform ×5; II 2-chloro-2-nitropropane; III *tert*-butyl chloride: IV sulfur dichloride ×2.

Table 4.2.1.7.1.1 Spherical Acyclics

Solute	Z^a (Å)	I_a* [μ_a]	I_b* [μ_b]	I_c* [μ_c]	μ (D)	I_r (10^{-38} g cm^2)	$\bar{\nu}_{max}$ (cm^{-1})	T_q (g)
t-Butyl chloride	0.47	1.91 [2.15]	2.86	2.86	2.15	1.43	24 ± 2	823
2-Chloro-2-nitropropane	0.48	3.06 [1.56]	4.41 [3.35]	4.97	3.69	1.96	33 ± 2	1915
Chloroform	0.25	2.52	2.52	5.0 [1.1]	1.1	1.26	30 ± 2	990

*Units: 10^{-38} g cm^2.
[a]Center of mass distance from central atom.

with the dipole along the shortened axis. For 2-chloro-2-nitropropane the molecule is slightly elongated (prolate) along the C—N bond or approximately along the **a** axis, which is also the approximate dipole direction. This means that rotation of the dipole in this case requires rotation about an axis perpendicular to the axis of elongation, which is more hindered than the active motions of *tert*-butyl chloride.

In effect chloroform has an almost planar (highly oblate) geometry and thus its behavior compared with the more spherical *tert*-butyl chloride produces a larger T_q in a fashion analogous to the difference between six-membered aromatic and saturated rings. It would be of interest to compare a much larger variety of these pseudospherical solutes by sequentially replacing CH_3 with larger groups (e.g., NO_2 or Br). However, these three molecules illustrate how T_q varies with the ellipsoidal solute geometry and with the direction of the net dipole moment with respect to this geometry. In the next subgroup we consider a set of solute molecules chosen to represent a very different geometry in relation to the dipole vector.

4.2.1.7.2 Group F2, Disubstituted Methanes and Sulfur Analogues

These are illustrated in Fig. 4.2.1.7.2.1 and form a collection of some of the smallest nonlinear molecules that contain two substituent atoms other than hydrogen attached to a centrally placed carbon or sulfur atom. Their centers of mass and moments of inertia can be calculated from available structural data and are listed in Table 4.2.1.7.2.1. The dipole moments all lie along the **b** axis.

The far infrared spectra of dichloro- and dibromomethane at 10% volume/volume concentration in decalin are shown in Fig. 4.2.1.7.2.2. We have referred to the former molecule in Chapter 1 as ideal for many purposes connected with the study of molecular dynamics, and the theme is developed further in Chapters 6 to 12. Its librational band in decalin peaks at 54 cm^{-1} and is uncomplicated by proper modes. Dibromomethane has

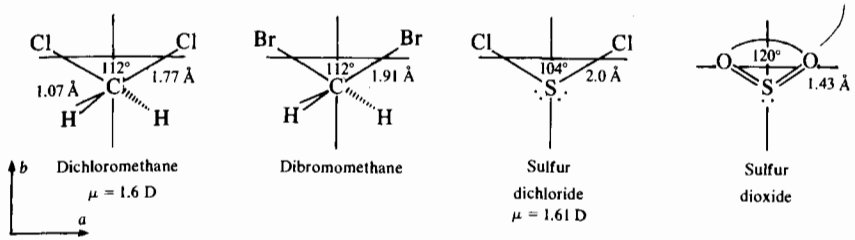

Figure 4.2.1.7.2.1 Group F2. Disubstituted methanes and sulfur analogues. Data from references *k* and *i*.

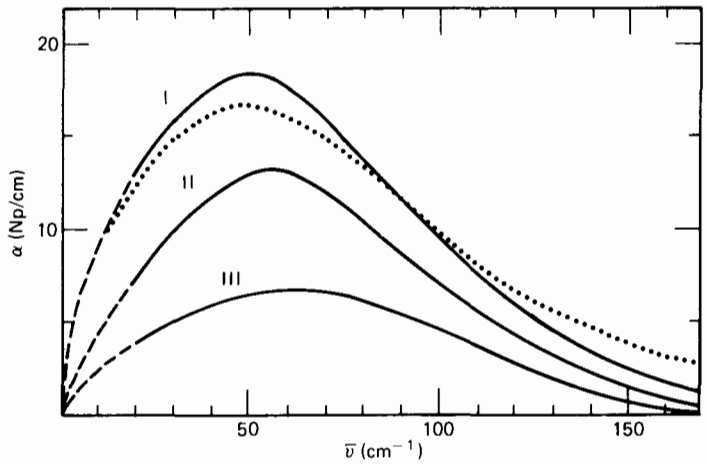

Figure 4.2.1.7.2.2 Absorption spectra. I Dichloromethane (solid line, mean of seven runs; dotted line, most extreme run); II dibromomethane; III iodomethane.

Table 4.2.1.7.2.1 Group F2

Solute	*Z* (Å)	I_a	I_b (10^{-38} g cm^2)	I_c	μ_b (D)	I_r (10^{-38} g cm^2)	$\bar{\nu}_{max}$ (cm^{-1})	T_q (g)
Dichloromethane	0.81	0.26	2.56	2.77	1.6	0.24	53	674
Dibromomethane	0.975	0.32	6.67	6.92	—	0.3	55	925
Sulfur dichloride	0.85	(0.55)	(2.93)	(3.48)	1.61	(0.475)	50	(1187)
		0.26[a]	3.82	4.39		0.245		612
Sulfur dioxide (cyclohexane)	0.36	0.136	0.81	0.946		0.119	50	300

[a] (Cl—S—Cl angle of 130° assumed.)

a similar but less intense librational band peaking at 55 cm^{-1}. The drop in intensity is qualitatively explicable on the basis of the sum rule (Chapter 1).

The spectrum of purified sulfur dichloride (Fig. 4.2.1.7.1.2) peaks at 50 cm^{-1} with a mode at 106 cm^{-1} due probably to traces of S_2Cl_2. Sulfur dioxide has been found by Pardoe (1969) to peak at 50 cm^{-1} with a possible error margin of 4 cm^{-1}.

Table 4.2.1.7.2.1 reveals a range of T_q from 500 to 1200 g, these extremes being the two sulfur compounds. In general, the T_q values are much lower than those of the F1 group, which is the opposite to what is expected on the grounds of geometric anisotropy alone. This must be considered also in the light that T_q values for propyne and acetonitrile in the next subgroup are again around 2400 g. The maximum length of these molecules are respectively 5.86 and 6.1 Å, whereas the greatest dimension of CH_2Cl_2 is actually larger at 6.5 Å. These findings are explicable, however, on the grounds that dichloro- and dibromomethane have their dipole moments directed perpendicularly to an axis of very low moment of inertia, the **a** axis. In fact, I_c/I_a for the four molecules in this subgroup are all very large (e.g., 7 for SO_2, 10 for CH_2Cl_2, and over 20 for CH_2Br_2). In subgroup F1 the equivalent values are all below 2. Of course the ratios are also large in propyne and acetonitrile, but in these cases the dipole moment is parallel to the axis of lowest inertia and the process of dipole relaxation correspondingly more hindered. In contrast, CH_2Cl_2 may relax about its long axis, as is the case also in SO_2, this molecular being quasi-linear. SCl_2 is less elongated, however, and its T_q coefficient is intermediate between CH_2Cl_2 or SO_2 (dipole perpendicular to the long axis) and CH_3CN (parallel).

4.2.1.7.3 Group F3, Monosubstituted Methanes and Planar Acyclics

These are illustrated in Fig. 4.2.1.7.3.1. In the top row of this figure the long axis containing the dipole is the **a** axis, whereas in the second row the **a** and

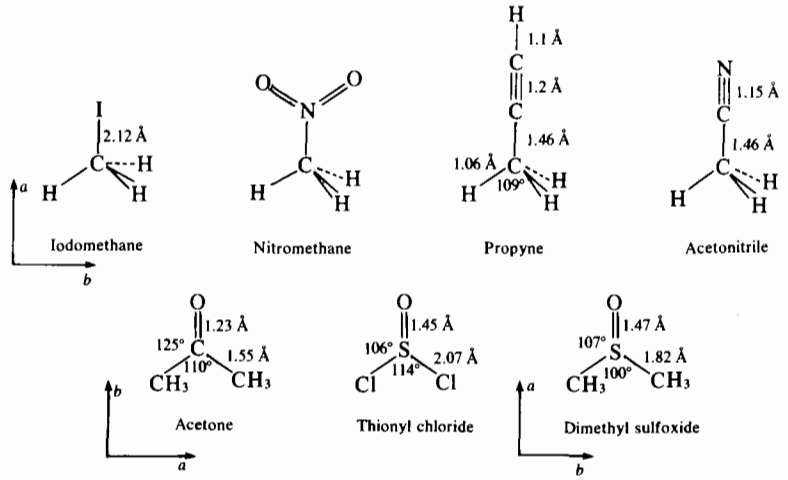

Figure 4.2.1.7.3.1 Group F3. Monosubstituted methanes and "planar" acyclics

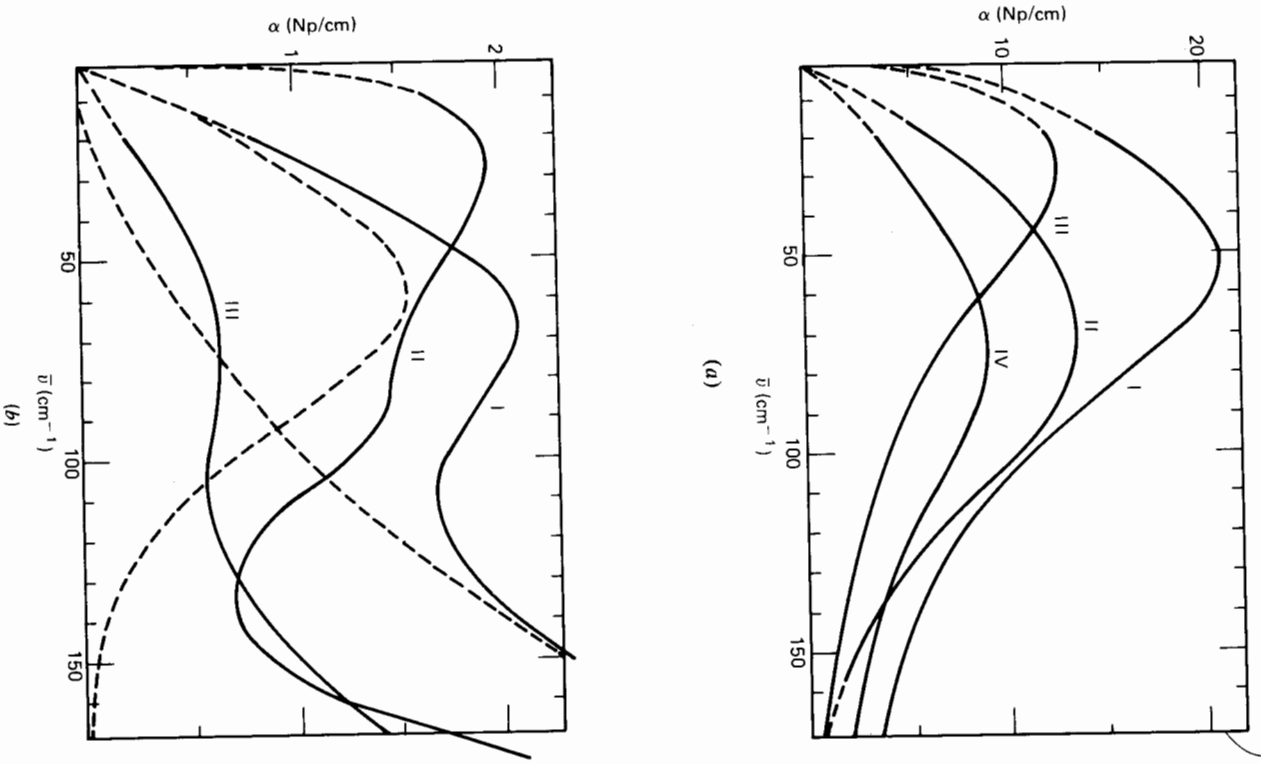

Figure 4.2.1.7.3.2 Absorption spectra. I Acetone; II 8% propyne in CCl_4 (adapted from reference *hh*); III thionyl chloride ×6; IV 4.3% acetonitrile/CCl_4. (*b*) Some nonrigid solutions. I 5% diphenylamine; II diphenylether; III diphenylmethane.

Table 4.2.1.7.3.1 Group F

Solute	Z (Å)	I_a	I_b (10^{-38} g cm^2)	I_c	μ (D)	I_r (10^{-38} g cm^2)	$\bar{\nu}_{max}$ (cm^{-1})	T_q (g)
Iodomethane	1.89	0.05	1.1	1.1		0.55	60	1980
Chloromethane	1.24	0.05	0.55	0.55		0.275	37 (Ref. *ii*)	(376)
Propyne/CCl_4	1.31	0.05	0.94	0.94	2.07	0.47	75 (Ref. *hh*)	(2643)
Acetonitrile/CCl_4	1.3	0.05	0.87	0.87	3.39	0.435	70 (Ref. *jj*)	(2131)
Acetone	0.13	0.79	0.84	1.63		0.53	53	1495
Thionylchloride	$Z_b = 0.45$[a]	1.6	3.7	4.7	0.76[b]	1.19	32	1218
	$Z_c = 0.44$		$\mu_b = 0.73$	$\mu_c = 0.23$				
Dimethylsulfoxide	$Z_a = 0.15$[a]	1.05	1.23	2.1	1.16[b]	0.75	68 (Ref. *kk*)	3482?
	$Z_c = 0.3$	$\mu_a = 1.1$		$\mu_c = 0.35$				

[a] Mass center distance from S atom.
[b] Bond moment analysis.

b axes are interchanged. The sulfur-containing molecules are pyramidal, owing to the lone pair which gives $SOCl_2$ its powerful reactivity and basicity. The center of mass therefore lies below the plane of the paper, the sulfur atom being in this plane. The nonplanar geometry also provides us with nonzero μ_b and μ_c dipole vector components calculable from bond moments. Absorption spectra for this group are shown in Fig. 4.2.1.7.3.2 and spectral data are summarized in Table 4.2.1.7.3.1.

The spectrum of iodomethane is very similar to that of dichloromethane (Fig. 4.2.1.7.2.2) but peaking instead at 60 cm^{-1} with a lower intensity. This molecule is considered in much greater detail in Chapters 6 and 12.

The linear type molecules in this subgroup have high T_q values ranging from 1980 g (CH_3I) to 2643 g (propyne), increasing with molecular length. Note that T_q in propyne and acetonitrile are similar despite the very large difference in dipole moment. This means that the dilution method has effectively insulated the kinematics of the problem from the electrical interactions (e.g., dipole–dipole).

Acetone and thionyl chloride are similar to dichloromethane in that the dipole is perpendicular to the axis of least inertia so that the volume displacement on rotation is minimized. Their T_q coefficients are consequently smaller.

4.2.1.7.4 Group F4, Small Molecules

These are illustrated in Fig. 4.2.1.7.4.1 and tabulated in Table 4.2.1.7.4.1. The torque coefficients T_q are very low, reflecting the approach to free rotation, in some cases (Chapter 1) quantized (e.g., HF and NH_3).

For 39 solutes in nondipolar environments (in the great majority of cases, decalin) the coefficient T_q (Evans, Reid, 1980) is an effective empirical measure of the far infrared spectral features. It takes values from 200 to 10,000 g across the series of molecules considered. The acyclics show that T_q depends markedly on the shape of the solute (Table 4.2.1.7.4.2).

Table 4.2.1.7.4.1 Small Molecules

Solute	Solvent	T (°K)	Reference	μ (D) (gas)	I_r (10^{-40} g cm^2)	$\bar{\nu}_{max}$ (cm^{-1})	T_q (g)
HCl	Cyclohexane	293	Datta, Barrow (*ll, mm*)	1.08		122	190
HCl	Cyclohexane		Morita (*nn*)	—	2.68	125	200
HCl	Argon	105	Aalst, Elsken (*oo*)	—		75	75
DCl	SF_6	273	Birnbaum (*pp*)		5.19	84	183
HBr	SF_6	296	Evans, Wegdam (*qq*)	0.82	4.8	108	280
H_2O	Cyclohexane	296	Evans (*rr*)	1.85	I_a 1.18, I_b 2.1, I_c 3.28, I_r 0.87	150	196
	CCl_4	300	Evans (*xx*)	—		170	250
	Benzene	300	Evans (*rr*)	—		210	383
NH_3	SF_6	273	Birnbaum (*ss*)	1.47	$I_a = I_b$ 2.8, $I_c = 4.4$ $I_r = 1.4$	138	266

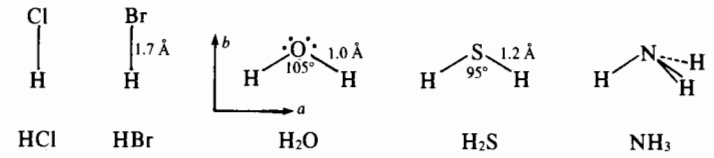

Figure 4.2.1.7.4.1 Group F4. Small molecules.

Table 4.2.1.7.4.2 Classification Scheme for some Acyclic Molecules in Decalin (293°K)

Group	Solute	μ (D)	I_a*	I_b*	I_c*	I_r*	$\bar{\nu}_{max}$ (cm^{-1})	T_q (g)
F1	2Cl—$2NO_2$ propane	3.69	3.06	4.41	4.97	1.96	33 ± 2	1915
	t-butyl-chloride	2.15	1.91	2.86	2.86	1.43	24 ± 2	823
	Chloroform	1.1	2.52	2.52	5.0	1.26	30 ± 2	990
F2	Dichloro methane	1.6	0.26	2.56	2.77	0.24	53 ± 2	674
	Dibromomethane	1.43[a]	0.32	6.67	6.92	0.3	55 ± 2	925
	Sulfur dichloride	1.61	0.55	2.93	3.48	0.48	50 ± 5	1187
	Sulfur dioxide cyclohexane	1.63[a]	0.14	0.81	0.95	0.12	50 (Ref. *tt*)	(300)
F3	Methyl iodide	1.62[a]	0.05	1.1	1.1	0.55	60 ± 2	1980
	Methyl chloride/ (ethane)	1.87[a]	0.05	0.55	0.55	0.28	37 (Ref. *ii*)	(376)
	Propyne (CCl_4)	2.07	0.05	0.94	0.94	0.47	75 (Ref. *hh*)	(2643)
	Acetonitrile (CCl_4)	3.39	0.05	0.87	0.87	0.435	70 (Ref. *jj*)	(2131)
	Acetone	2.88[a]	0.79	0.84	1.63	0.53	53	1495
	Thionyl chloride	1.45[a]	1.6	3.7	4.7	1.19	32 ± 2	1218
	Dimethyl sulfoxide (liquid)	3.96[a]	1.05	1.23	2.1	0.75	68 (Ref. *uu*)	(3482)
F4	HCl (cyclohexane)	1.08[a]	0	0.027	0.027	0.0134	125 (Ref. *ll, mm*)	(200)
	HBr (SF_6)	0.82[a]	0	0.048	0.048	0.024	108 (Ref. *qq*)	(280)
	H_2O (cyclohexane)	1.85[a]	0.012	0.021	0.033	0.009	150 (Ref. *rr*)	(196)
	$NH_3(SF_6)$	1.47[a]	0.028	0.028	0.044	0.014	138 (Ref. *ss*)	(266)

*Unit: 10^{-38} g cm^2.
[a]Gas values (Ref. *kk*).

In Section 4.2.2 the torque factor is related to the Mori/itinerant librator description of the molecular dynamics. The empirical correlation exercise outlined in this section lends support to the initial hypothesis on T_q, that is, that the far infrared librational peak frequency $\bar{\nu}_{max}$ is directly related to the mean square torque exerted on a dipolar diffuser by its surroundings, in this instance nondipolar solvent molecules. The correlation between T_q and molecular geometry which we have discussed in terms of the hindrance to dipolar libration implies that some relation also exists between T_q and the Debye relaxation frequency of classical dielectric spectroscopy. This is developed in Section 4.2.3.

4.2.2 Molecular Description of the above Equations

The basis of this section rests on the hypothesis that the far infrared peak frequency bears some direct relation to the mean square molecular torque. This theme is developed for liquids here and for glasses and related viscous media in Chapter 7. We may relate our data to the molecular dynamics either in the (Evans, 1976) context (using the coefficients K_0, K_1, and γ) or in that of the planar itinerant librator model as outlined already earlier in this chapter.

At the outset there are several points which must be considered before entering into the details of the molecular dynamics.

1. When the itinerant librator is used to represent a molecular spectrum the parameters involved in the model, that is, ζ, ω_0^2, and Ω_0^2, may be given numerical values for a given ratio I_2/I_1 by measurement of the dielectric loss peak frequency (whose inverse in the absence of an internal field correction is the Debye relaxation time) and by measurement of the far infrared peak frequency. In this way the model may be made to reproduce the essential features of the spectrum *but* it is always necessary to assume that I_1 is *smaller* than I_2 in order to reproduce the breadth of the far infrared absorption. This is only partly consequential upon the fact that we use the equations of motion of the itinerant librator in their harmonic form. Preliminary numerical analysis of the model where the harmonic approximation is not used indicates that the cosine potential considerably broadens the theoretical spectrum.
2. If we use the more "abstract" (Evans, 1976) approach a set of (K_0, K_1, γ) parameters may be obtained to fit the spectral data over *both* far infrared *and* microwave frequencies. It is this latter set of values that, given the continued fraction approximant used, best represents the statistical means of the torques and torque derivatives present in the system under consideration. It is typically the case that to reproduce the experimental profile we must have $K_1 > K_0$ and $K_0 > \gamma$ for the 40 or so solute/solvent systems of Section 4.2.1. This means that in the itinerant librator picture we must have $I_2 > I_1$ and $\Omega_0^2 > \omega_0^2$, which differs considerably from the physical expectations at the base of the formal representation embodied in the equations of motion (Eq. 4.1.4 and 4.1.5). These are, of course, that the moment of inertia of the cage should be greater than that of the encaged molecule (i.e., $I_1 > I_2$) and that $\omega_0^2 > \Omega_0^2$. If the restriction $I_1 > I_2$ is not lifted then the resonance in the far infrared, about the frequency ω_0, is far too sharp (Fig. 4.2.2.1). This defect might be removed by using a cosine potential instead of a harmonic potential. A possible way out is to suppose, for example, that the cage is not in reality a rigid entity. Rather, it is composed on average of loosely coupled

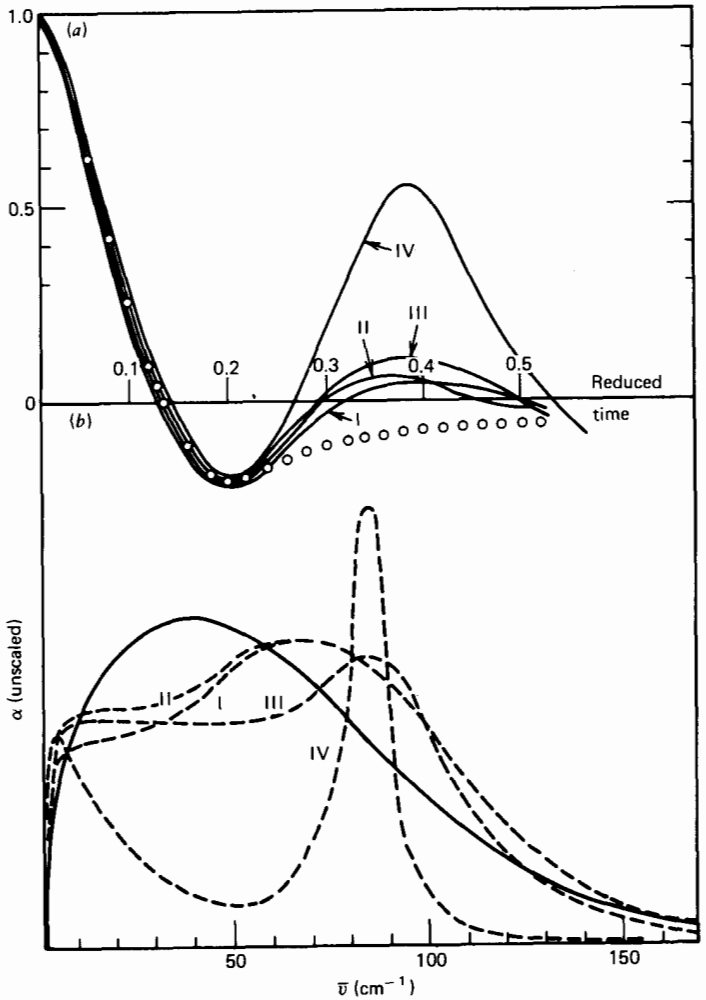

Figure 4.2.2.1 Effect of α_2 on best fit in time and spectral domains by reference to nitrobenzene/decalin (293°K) data. (*a*) Short time domain. Dotted line, experimental curve (transform of spectrum). Solid lines, possible model fits. (*b*) Spectral domain. Solid line, experimental spectrum. Dashed lines, transforms of I–IV in (*a*).

solvent molecules so that I_1 is an effective annulus inertia much smaller than that of the rigid entity. One must be careful to note, however, that although this statement is a reasonable one it does *not* remove the fact that in the actual equations of motion used (Eqs. 4.1.4 and 4.1.5) the cage is assumed to be *rigid*. The Mori type continued fraction, although seemingly the more abstract, is nevertheless an approach to the problem that does not contradict the basic physics in the manner just described. In the Mori type approach it

is perfectly possible that the numerical value of the thermodynamic average K_1 may exceed K_0. Note finally that the Mori type model, within the constraints imposed by Eq. (4.1.1) et seq., namely spherical geometry and the assumption that the equation following (4.1.6) holds, is three dimensional in nature. The itinerant oscillator model is further weakened by the fact that representing spatial libration by a planar model involves two degrees of freedom condensed into one, and a factor of two becomes involved in the equivalency relation. This means that $2\pi\bar{\nu}_{max}c$ is not necessarily equal to ω_0 but that the latter is greater. Taking a mean of all 40 systems it turns out that K_0 is larger than $(2\pi\bar{\nu}_{max}c)^2$ by a factor of approximately 2.5; that is, observation indicates that K_0 of the Mori type model is not numerically equal to $(2\pi\bar{\nu}_{max}c)^2$, but is rather proportional.

With these caveats we can proceed to relate the torque factor T_q to a volume of rotation as described more fully in Chapter 7. In considering the physical validity of the Mori itinerant librator parameters the relevant meaningful thermodynamic averages are always K_0, K_1, and γ of the Mori continued fraction and not ζ, Ω_0^2, and ω_0^2 of the planar itinerant librator.

4.2.2.1 Volume of Rotation and Rotation/Translation Interaction (Reid, 1979a)

The first consideration is the correct choice of inertia for a spatially librating asymmetric top. The expression for the orientational a.c.f. derived by Ford et al. (1976) on the basis of a cumulant expansion and used for spherically isotropic diffusion by Evans (1976) is of asymptotic validity for spherical top molecules of inertia I. For planar libration the factor of two disappears. For asymmetric tops, which form the great majority of the molecules we have considered, we have replaced $I/2$ by I_r, the reduced moment of inertia. This mean measure of molecular inertia allows the Mori type parameters K_0, K_1, and γ, obtained from best fitting high frequency (far infrared) data of liquid solutions, to predict correctly the low frequency data, including Debye relaxation times measured afresh and presented in Section 4.2.3. I_r is the only measure of inertia which succeeds in this respect. It reduced to $I/2$ for the spherical top, providing the result $2kT/I$ for the mean square angular velocity. Note that in order to use the planar itinerant librator in three dimensions a factor of two must be included twice, once in the exponent of the a.c.f. for orientation to double the rate of Debye relaxation at long times and once with respect to the libration frequency of the solute. The itinerant oscillator and Mori type models are not equivalent without these factors.

Introducing the torque as $\Gamma = I_r\dot{\omega}$ and using the Mori expression for $K_0(0)$, we have

$$K_0(0) = \frac{\langle\Gamma(0)^2\rangle}{I_r kT} \qquad (4.2.2.1.1)$$

Using now the "equivalence relation," or approximation,

$$K_0(0) \propto (2\pi c\bar{\nu}_{max})^2$$

we obtain

$$\langle\Gamma(0)^2\rangle \propto I_r\bar{\nu}_{max}^2 \qquad (4.2.2.1.2)$$

which is a relation between T_q, the torque factor, and the thermodynamic mean square torque. This relation is of course a way of putting the basic empirical hypothesis of Section 4.2.1 into molecular terms.

For didactic reasons we use the relation between $\langle\Gamma(0)^2\rangle$ and V, the volume of rotation, again in Section 7.2.4. This is the volume generated by the 2π rotation of all surface elements on the advancing surfaces of the molecular body. The mean square torque depends not only on the volume of a particular molecule but also on its shape. Thus, for example, pyridine and *tert*-butyl chloride have similar van der Waals volumes (85 Å^3) and similar values for I_r (0.98×10^{-38} and 1.25×10^{-38} g cm^2, respectively), but T_q for pyridine is fully 2.5 times larger owing to the far greater shape anisotropy of the latter. Therefore the most significant molecular shape parameters are the volumes swept out on rotation, not the molecular volumes themselves, which are the parameters usually taken to be of importance in dielectric relaxation studies. To relate the mean square torque $\langle\Gamma^2(0)\rangle$ to this measure of the volume of rotation we consider the motion of the asymmetric top about a body fixed axis. The infinitesimal surface area element $\delta\mathbf{A}_j$ is fixed at a distance $\mathbf{r}_j$ from this axis. The interaction with the environment at any instant results in a force per unit area $\mathbf{P}_j(t, \mathbf{r}_j)$ parallel to the instantaneous linear velocity $\mathbf{v}_j$ of the element $\delta\mathbf{A}_j$ considered. This assumption means that we specifically ignore forces perpendicular to the $\mathbf{v}_j$ vector irrespective of whether such forces cancel on averaging over the surface or whether they combine to produce translation of the whole molecule or alternatively combine to tilt the rotating molecule out of the plane perpendicular to our body fixed axis. For a rigid impenetrable body the spatial variation of $\mathbf{P}_j(t, \mathbf{r}_j)$ is cancelled by forces that maintain rigidity, so that the interaction with the environment may in consequence be represented by an effective force per unit normal surface area, which we denote by $\mathbf{P}^{(i)}(t)$. At any instant this is the mean value of the elemental forces. We may now specify the total torque for the body fixed axis in question as

$$\Gamma^{(i)}(t) = \sum_j |\mathbf{P}^{(i)}(t)|(\delta\mathbf{A}_j \times \mathbf{r}_j)$$

The volume of rotation for 2π rotation of all surface elements is now

$$V^{(i)} = \sum_j 2\pi\delta S_j r_j$$

where δS_j is the projection of $\delta\mathbf{A}_j$ in a plane perpendicular to $\mathbf{P}^{(i)}(t)$ and the

summation is taken over all elements $\delta \mathbf{A}_j$ that give $\delta \mathbf{A}_j \cdot \boldsymbol{v}_j > 0$. The magnitude of the torque is then

$$\Gamma^{(i)}(t) = \sum_j |\mathbf{P}^{(i)}(t)|\delta S_j r_j = \pi^{-1} P^{(i)}(t) V^{(i)}$$

where the superscript (i) designates this motion as uniaxial. Assuming again that a molecule may be considered as a rigid body with an impenetrable surface, then for an ensemble of such molecules the torque correlation function with respect to the i-axis is

$$\langle \boldsymbol{\Gamma}_i(t) \cdot \boldsymbol{\Gamma}_i(0) \rangle = \pi^{-2} V_i^2 \langle \mathbf{P}_i(t) \cdot \mathbf{P}_i(0) \rangle$$

where i has been relegated now to subscript status. If the molecule under consideration is geometrically anisotropic (e.g., planar or linear) then the mean square value of $\mathbf{P}_i(t)$ and also its evolution depend on the axis chosen for consideration. In this case the correlation of $\mathbf{P}_i(t)$ retains some dependence on the molecular shape through mutual shielding of adjacent surfaces. Initially we assume that $\langle \mathbf{P}_i(t) \cdot \mathbf{P}_i(0) \rangle$ is independent of shape and hence axis, and account for the shielding in a manner to be described shortly.

We now wish to form a relation between the torque correlation function and the force per unit area correlation function for molecules rotating about their three mutually perpendicular (principal) axes. For simplicity it is proposed that the three-dimensional torque correlation function can be related to an axis-independent force correlation function

$$P(t) = \pi^{-2} \langle \mathbf{P}_{Av}(t) \cdot \mathbf{P}_{Av}(0) \rangle$$

by a relation similar to that already described; that is,

$$\langle \boldsymbol{\Gamma}(t) \cdot \boldsymbol{\Gamma}(0) \rangle = VP(t)$$

where V is some appropriate average of the three respective molecular volumes of rotation V_i ($i = a, b$, and c).

To describe V analytically consider a molecule containing a dipole along its **a**-axis, which can therefore librate in two perpendicular planes corresponding to small rotations about **b** and **c**. Suppose that over times of the order of a period of libration these motions may be treated independently. Thus the far infrared spectrum is a superposition of contributions from both librations, each of which has an intensity proportional to the mean amplitude θ_i. If the energy of this mode (kT on average) is divided between potential and kinetic forms as

$$E = \tfrac{1}{2} I_i \dot{\theta}_i(t)^2 + \theta_i(t)^2 k_i$$

where k_i is the "force constant" giving rise to a potential energy proportional to the angular displacement $\theta_i(t)$, then the maximum displacement, that is, amplitude of the motion is on average $\theta_i^2 = kT/k_i$. The force constant, which is the mean slope of the potential energy curve, is taken to

be proportional to the root mean square torque relevant to this direction. Therefore θ_i^2 is proportional to V_i^{-1}. The spectral components are additive; therefore the behavior of the total spectrum must depend on the reciprocal average:

$$V^{-1} = V_b^{-1} + V_c^{-1}$$

This means that V approaches the numerically smallest V_i component when the spectrum is at its most intense.

The similarity between this average and the relation for the reduced moment of inertia

$$I_r^{-1} = I_b^{-1} + I_c^{-1}$$

(in this case for μ_a) suggests that in general the expression for V when $\boldsymbol{\mu}$ does not lie on a principal axis (as it generally does not), is

$$\mu^2 V^{-1} = (\mu_b^2 + \mu_c^2) V_a^{-1} + (\mu_a^2 + \mu_c^2) V_b^{-1} + (\mu_c^2 + \mu_b^2) V_c^{-1}$$

We therefore arrive at the relation

$$I_r \bar{\nu}_{max}^2 \propto V^2 P(0)$$

with $P(0) = \pi^{-2} \langle P_{Av}^2(0) \rangle$, the mean square torque per unit volume of rotation defined by

$$\langle \Gamma^2(0) \rangle = V^2 P(0)$$

This quantity is assumed to be independent of the molecular shape and size provided some account of shielding effects is taken in deducing values for V_i. Essentially, therefore, it is possible to factorize $\langle \Gamma^2(0) \rangle$ into a solute–dependent parameter V^2, and a parameter $P(0)$ which should then, to a good approximation, depend only on the solvent and the temperature.

To estimate the components V_i the relevant definition of a molecular surface we have used is that created by the covalent radii of the constituent atoms. The spheres thus defined do not overlap to a significant extent so that their volumes of rotation may be obtained independently and summed to provide V_i. An often used definition of a molecular surface is that formed when each atom is allocated a van der Waals radius. However, this is abandoned for the following reasons.

1. The van der Waals volume (which is also similar to the mean volume occupied by the solute, as deduced from the density of a close packed liquid), is a thermodynamic (averaged) volume and not a dynamic one, so does not represent the "nonimpenetrable" (hard sphere) surface. If one considers two interacting molecules in a liquid close to its boiling point then their kinetic energy increases at the expense of pair potential energy. At the point of lowest energy (the van der Waals separation), the pair have sufficient kinetic energy to continue their approach, although the reaction is now repulsive.

The minimum distance of separation then corresponds to that of the covalent radii separation, rather than to the position of the minima on the van der Waals contour. Only at very low temperatures would the former separation become more relevant, whereas the latter represents a hard sphere surface at all temperatures.

2. In some cases it may be shown experimentally that molecular rotation about a certain axis is preferred. These findings may be rationalized in terms of volume swept out by rotation only by using covalent radii. The use of van der Waals radii sometimes produces the reverse of the experimental indication.
3. Covalent sphere radii may be more accurately determined and are corroborated theoretically, as we shall see later.

To account for intramolecular shielding in estimating volumes of rotation we may consider the volume swept out by a given sphere and then subtract the volumes of any parts of the molecule which also lie on this toroid of generated volume. Thus an atom such as the nitrogen of benzonitrile of radius r and rotating at a distance d from the center of mass has a volume of rotation contribution (Appendix B) amounting to $2\pi^2 r^2 d$. This rotation path does not include any other part of the molecule; hence only the volume of the nitrogen atom ($\frac{4}{3}\pi r^3$) need be subtracted. However, if we consider that the hydrogen atoms of benzonitrile are also rotating in the plane under consideration then we would have to subtract six times the volume of each hydrogen atom from each $2\pi^2 r^2 d$ term.

In this context the benzene ring of six carbon atoms represents an extreme of shielding when rotation in the plane is considered. Such a ring does not contribute to the V component of benzene. However, in benzonitrile the same kind of motion would take place epicyclically about the **c**-axis because the Z factor (Section 4.2.1) is no longer zero; in other words the center of mass is not at the ring center. In such a case the volume of rotation contribution would be a volume generated by a disk of thickness L (whose circumferential surface is a distance d from the rotation center) minus the volume of the benzene disk. The volume of the benzene disk is taken as seven times the volume of the carbon atom; that is, a seventh carbon atom is centrally placed in the ring center to account for this area being inaccessible to the surrounding solvent.

If we wish to consider the nonplanar rotations (about the **a** and **b** axes) then each atom of the carbon ring is taken in turn, including the hypothetical central atom.

In what follows (see also Section 7.2.4) the atomic radii are taken as H = 0.5 Å (half the bond length of H), C(acyclic) = 0.77 Å, N = 0.70 Å, O = 0.65 Å, F = 0.6 Å, and Cl = 0.9 Å, Br = 1.0 Å. The dimensions of the benzene ring carbons are taken as C = 0.7 Å in the ring plane and 0.75 Å perpendicular to this direction. This gives a thickness of 1.5 Å for the benzene ring (or disk).

For example, if we take the **c**-axis rotation of pyridine ($Z = 0$) there are contributions from the ring and the five hydrogen atoms. Considering the nitrogen atom as roughly equivalent to a carbon atom, then the radius of the ring is 2.1 Å (i.e., 1.4 Å from the ring center to a carbon center plus 0.7 Å, the radius of carbon), and the ring contribution is therefore $1.5\pi(2.1)^2 - 7.\frac{4}{3}\pi(0.7)^2(0.75)$. For **b** axis rotation the distances of this axis to each atom center are calculated and the overlap volumes estimated and subtracted. (These may be determined for any solute by reference to the structure diagrams of Section 4.2.1). In fluorobenzene, the ring contribution to V now involves the distance $(2.1 + Z)$ Å, whereas for toluene the presence of a rapidly rotating methyl group introduces another complication. Such groups can be accounted for by taking a cross section chosen so as to represent the greatest hindrance to motion for the axis concerned. Thus for the **c**-axis of toluene it is assumed that the effect of CH_3 can be approximated by having two hydrogens set permanently above and below the ring plane. For the **b**-axis rotation, however, these two atoms are set permanently in the ring plane as in Fig. 4.2.2.1.1.

When molecules as complicated as the halogenonaphthalenes are dealt with, scaled constructions are used containing the positions of the principal axes. Using these methods the displacement of each atom from the axis considered can be obtained together with estimates of the subtraction terms. The ring contribution is again calculated assuming the carbon skeleton to behave as an epicentric rotating disk of volume $12V_{CR}$.

The values of V_a, V_b, and V_c and their averages V for 20 solutes are listed in Table 4.2.2.1.1, together with the torque coefficients. The values in parentheses refer to those obtained by using an even larger hydrogen covalent radius of 0.55 Å. Figure 4.2.2.1.2 is the plot of the torque coefficient versus V^2. All the points lying appreciably below the line drawn through the data correspond to molecules for which the factor Z is largest. In these molecules the center of mass is well away from the center of "volume." Two

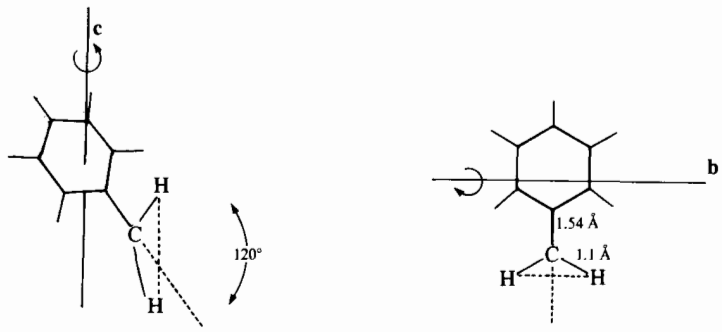

Figure 4.2.2.1.1 Approximation made for toluene CH_3 contribution to V_i using CH_2 fixed in the orientations shown.

Table 4.2.2.1.1 Volumes of Rotation

Solute	Z (Å)	V_b (Å^3)		V_c (Å^3)	V^2 (Å^6)	T_q (g)
1 Pyridine	0	69(76.5)		59(66)	1011(1263)	1858
2 Fluorobenzene	0.44	98(100)		83(91)	2019(2265)	2923
3 Chlorobenzene	0.96	126(133)		106(119)	3314(3958)	3433
4 Bromobenzene	1.66	170(181)		123(129)	5093(5700)	2551
5 Penta-fluorobenzene	0.3	106(133)		95(99.4)	2510(3227)	3960
6 Toluene	0.46	129(142)		115(132)	3697(4680)	6912
7 o-Xylene	0.66	156(176)		150(158)	5848(6932)	9717
8 Nitrobenzene	1.22	164(173)		128(136)	5168(5800)	5932
9 Benzonitrile	0.85	141(151)		124(138)	4353(5200)	6781
10 (Aniline)	0.46	131		106	3433	(7864) Associated
			V_a			
11 α-Picoline	0.46	129(142)	73(81)	115(132)	2144(2764)	4392
12 1-Chloro-naphthalene	0.69	223(235)	V_a 197(205)	161(177)	8216(9510)	9786
13 1-Bromo-naphthalene	1.32	256(269)	V_a 201(218)	192(199)	11,320(12,420)	7465
14 Furan	0	48(54)		46(51.5)	552(678)	1560
15 T.H.F.	0	76(84)		76(84.6)	1444(1778)	1777
			V_a			
16 Dichloromethane	—		25(27.5)	43(43)	250(280)	674
17 t-butylchloride	—	70(80)		70(80)	1225(1600)	823
			V_a			
18 Chloroform	—	47(50)	47(50)		552(625)	990
19 2-Chloro-2-nitropropane		113	V_a 109	122	3326	1915
20 (Acetonitrile)		36		36	324	(2131) Associated

Values in parenthesis are for H = 0.55 Å.

points (10 and 20) lie well above the straight line. These correspond to aniline and acetonitrile, respectively, which are associated in dilute decalin solution. The bulk of the data corroborate our interpretation in terms of the relation between the empirical torque factor and the square of the effective molecular volume of rotation.

The behavior of the large Z molecules may be rationalized as follows in terms of rotation/translation coupling. We have already mentioned briefly that molecules may rotate in condensed media about some point other than the center of mass, because as pointed out by Steele (1976), the principal axes of a molecule in solution will be torque determined rather than inertia determined. To illustrate how this effects the distribution (Fig. 4.2.2.1.2), the volumes of rotation for molecules with Z greater than 0.46 Å were determined about axes intersecting at what we term the "center of volume." This can be taken for present purposes (of comparison) at the ring centers and the torque-determined principal axes chosen parallel to the former inertial axes. The volumes of rotation can then be recalculated on the basis of taking the volume of rotation component of the ring to be that

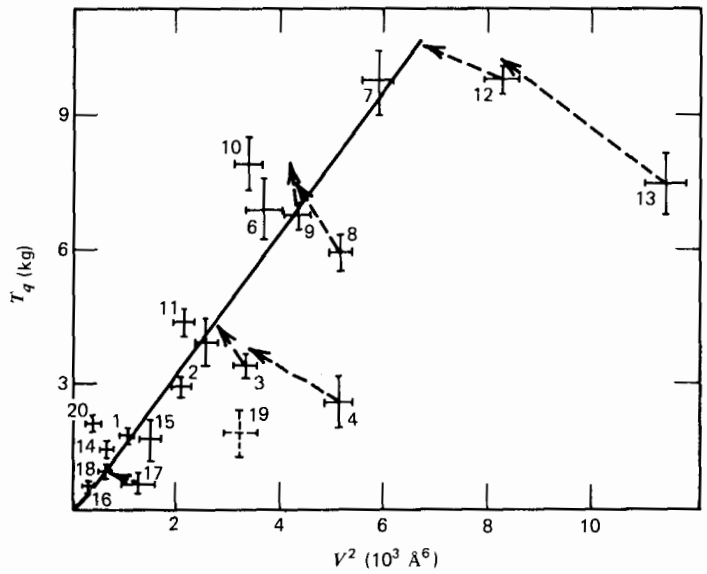

Figure 4.2.2.1.2 Torque factor versus solute volume of rotation squared for decalin solutions at 293°K.

1 pyridine	6 PhMe	11 α-Picoline	16 CH_2Cl_2
2 PhF	7 $Ph(Me)_2$	12 $C_{10}H_7Cl$	17 $CCl(Me)_3$
3 PhCl	8 $PhNO_2$	13 $C_{10}H_7Br$	18 $CHCl_3$
4 PhBr	9 PhCN	14 Furan	19 $NO_2CCl(Me)_2$
5 C_6F_5H	10 $PhNH_2$	15 THF	20 CH_3CN

Numbers 3, 4, 8, 12 and 13 are rotation/translation coupled (arrowheads). Number 19 is rotation/vibration coupled. Numbers 10 and 20 are associated. Solid line, best line through data.

of pyridine for each solute. These new axes are illustrated for the halogenonaphthalenes in Fig. 4.2.1.3.1. In *tert*-butyl chloride the central carbon atom may be chosen as the new center of rotation. The V_i components would be minimized if calculated about the center of least hindrance. The recalculated T_q and V values are listed in Table 4.2.2.1.2. For molecules such as bromobenzene and 1-chloronaphthalene, a very large drop in V results from rotation about the center of volume. Despite the implied increases in moment of inertia components it is likely that this is the preferred motion in condensed media, not the least because the adjustment brings the molecules with large Z on to the line (Fig. 4.2.2.1.2).

This is evidence for the fact that such molecules rototranslate (Chapter 5) rather than rotate in decalin solution, that is, rotate like a flywheel about the "center of volume." A discussion of this type of motion in connection with the HCl molecule has been given by Ewing (1969), who considers the rotation as being within a rigid cage; thus for HCl to rotate it must continually translate so as to keep its center of volume in the center of the cage. This is

Table 4.2.2.1.2 Rototranslating Molecules

Solute	Center of Mass				Center of Volume					
	Z (Å)	I_r (10^{-38} g cm^2)	V^2 (Å^6)	T_q (g)	V_b (Å^3)	V_c (Å^3)	V^2 (Å^6)	I_r (10^{-38} g cm^2)	T_q (g)	$\Delta T_q/\Delta V^2$
Bromobenzene	1.66	4.43	5093	2551	127	108	3406	6.57	3784	0.73
Chlorobenzene	0.98	2.97	3314	3433	115	96	2737	3.83	4427	1.72
Benzonitrile	0.85	3.07	4353	6781	141	123	4304	3.7	8173	26
Nitrobenzene	1.22	3.9	5168	5932	155	109	4109	5.18	7878	1.84
1-Bromonaphthalene	1.32	5.17	11,320	7465	199	165	8150	7.06	10,194	0.86
					$V_a = 201$					
1-Chloronaphthalene	0.69	4.43	8216	9786	199	137	6496	4.82	10,647	0.5
					$V_a = 194$					
o-Xylene	0.66	2.3	5848	9717	156	150	5840	2.7	11,406	≈ 200
t-butyl chloride	0.47	1.43	1225	823	49	49	600	1.78	1,028	0.33

discussed further in Chapter 6. In much the same way 2-chloro-2-nitropropane (point 19) rotovibrates.

Generally the analysis corroborates the general picture of molecular dynamics incorporated in the Mori type continued fraction and the empirical (Reid, 1979) torque factor T_q. The basic features of the itinerant oscillator model are in conflict with the spectral evidence, insofar as the model produces for $I_2 > I_1$ a far infrared peak that is too sharp, but it is nevertheless of interest because of the interrelations discussed already. The validity of the Mori type continued fraction analysis extends with reservations to viscous and vitreous media as discussed in Chapter 7.

4.2.3 Band Shape Analysis in the Far Infrared and Microwave

Having therefore shown that there exists a pattern in the variety of spectra considered in the far infrared, we go on to incorporate the low frequency adjunct of the far infrared data and extend our analysis to the complete 0–THz range available to us. For the first time we turn our attention fully on the band shape and therefore the time domain correlation function.

The far infrared data of 23 systems have been analyzed by Reid (1979) in this context in the time domain. Using this information the Debye relaxation times (Chapter 3) can be calculated theoretically on the basis of the Mori style equations for the orientational a.c.f. (Eq. 4.1.7) and its second derivative, which (Chapter 1) is the direct Fourier transform of the far infrared power absorption coefficient with due regard for the internal field correction. For numerical convenience the reduced units $\bar{K}_0 = (kT/I_r)K_0$, etc., $\bar{t} = (kT/I_r)^{1/2}t$ are used, so that the Mori style rotational velocity correlation function may be expressed in the form

$$\ddot{C}_u(\bar{t}) = \Bigg[[2\alpha_1\beta A_1 - (\alpha_1^2 - \beta^2)B_1]\sin(\beta\bar{t})e^{-\alpha_1\bar{t}} + [2\alpha_1\beta B_1 + (\alpha_1^2 - \beta^2)A_1] \times \cos(\beta t)e^{-\alpha_1\bar{t}} + \frac{\Gamma}{1+\Gamma}e^{-\alpha_2\bar{t}} - \Big((\alpha_1 B_1 - \beta A_1)\sin\beta\bar{t}e^{-\alpha_1\bar{t}} - (\beta B_1 + \alpha_1 A_1)\cos(\beta\bar{t})e^{-\alpha_1 t} - \frac{\Gamma}{(1+\Gamma)\alpha_2}e^{-\alpha_2\bar{t}} + C_1\Big)^2\Bigg] C_u(\bar{t}) \quad (4.2.3.1)$$

In Appendix A to this chapter we analyze this complicated equation with a view to easing the problems of data fitting in both frequency and time domains. The coefficients appearing in Eq. 4.2.3.1 can each be written out in terms of K_0, K_1, and γ, the Mori type coefficients. In principle, therefore, we require three spot frequencies only to determine them unambiguously. In practice, of course, we aim always to make use of the complete range of loss and power absorption data available at all frequencies up to the terahertz (or far infrared). The behavior of the model versus nitrobenzene in decalin is illustrated in Fig. 4.2.2.1. Four sets of model parameters are seen to produce theoretical curves which behave similarly

to 0.2 units of reduced time and which follow the far infrared data Fourier transformed to the time domain. Beyond this the four theoretical curves go their own ways. If we were to use only short time data they would be indistinguishable. Over the complete time range of the rotational velocity a.c.f. the best behaved curve by least mean squares analysis is II. The situation is the same when we Fourier transform into the frequency domain to regenerate the far infrared spectra. We may, however, extend the range of available frequencies even further by using microwave experimental methods in the well-known manner of dielectric spectroscopists, who present the attenuation in terms of dielectric loss, which peaks usually in the range of frequencies from megahertz to gigahertz, that is, below 1 cm^{-1}. In Chapter 7 we show that the loss sometimes peaks in vitreous media at kilohertz frequencies and below so that the spectrum we have to attempt to interpret extends over a range of many octaves in one continuous sweep. In liquid solutions, however, the dielectric loss peaks normally in the microwave range. If this peak frequency is expressed in radians per second the inverse of this number is the experimental relaxation times τ_{exp}. After correcting this for the internal field (Chapter 3), we finally obtain the so-called Debye relaxation time τ_D. The analysis illustrated in Fig. 4.2.2.1 must aim to reproduce this accurately because it is an integral feature of the complete experimental spectrum.

The Debye relaxation time may be expressed as

$$\tau_D = \left(\frac{I_r}{kT}\right)^{1/2} \bar{\gamma} \frac{\bar{K}_0}{\bar{K}_1}$$

The relation is derived in the appendix from Mori (1965) theory and is a convenient measure of how well the far infrared spectrum may be made to behave in the microwave and lower frequencies. For the curves of Fig. 4.2.2.1 the results are summarized in Table 4.2.3.1, where the model parameters are expressed in reduced time units with $(I_r/kT)^{1/2} = 1.5$ psec. The experimentally available Debye relaxation time in dilute decalin at 293°K is, after correction for the internal field using Cole's equation,

$$\tau_D = \left[\frac{3\epsilon_\infty}{2\epsilon_\infty + \epsilon_s}\right] \tau_{exp} \qquad (4.2.3.2)$$

20 ± 3 psec. From the table it is clear that set 2 is the best.

This kind of exercise is therefore one approach to the problem of comparing what is after all a complicated set of experimental data with a complicated theoretical analysis. To extend the analysis to other solutes we minimize uncertainty by choosing spectra (1) with well-defined librational band shapes free of proper modes over most of the relevant far infrared range; (2) with moderate to intense spectral intensity in the far infrared for ordinate accuracy, to minimize uncertainties due to solvent absorption and induced absorption (Chapter 11); and (3) free of any signs of association in

Table 4.2.3.1 Best Fit Parameters of Fig. 4.2.2.1

Curve	β	α_1	α_2	$\bar{\gamma}$	$\bar{K}_0$	$\bar{K}_1$	τ_D (psec)
I	17	8	40	56	252	741	22
II	18	6.7	18	31.4	221	398	19
III	18	4.8	11	20.6	185.3	267	16.4
IV	16	1	2.7	4.7	147.6	115	7.2

solution. Our results on toluene, aniline, and acetone solutions illustrate the effects of these factors on our analysis of the theoretical model.

Figure 4.2.3.1 illustrates the procedure for 10% volume/volume solutions in decalin at 293°K of pyridine, methylene chloride, chlorobenzene, and chloroform. The rotational velocity a.c.f. is defined from fitting the far infrared data Fourier transformed into the time domain. The Mori type parameters are thereby fixed and can then be used to produce the theoretical orientation, angular velocity, and torque a.c.f.'s illustrated in Fig. 4.2.3.1. These statistical functions are all capable of revealing something new about the nature of the molecular dynamics, in solution the kinematics of the diffusing dipolar solute molecule. These same functions of time can be simulated by computer-based molecular dynamics, which produces the exciting new possibilities outlined in Chapter 12.

The angular velocity a.c.f. behaves in a similar way to the rotational velocity a.c.f. but is by no means identical, except at short times. The orientational (or dipole unit vector) a.c.f. oscillates at short times before developing the familiar exponential form at longer times (lower, microwave frequencies). On a logarithmic scale the linear (exponential) decay extrapolates back to cross the $t = 0$ axis close to unity on the ordinate in almost every case. The torque (or more accurately the angular acceleration) a.c.f. is also well defined by Mori's theory and behaves in a similar way to the first memory function, which is a correlation function of projected random torques as defined by Mori and discussed at length in Chapters 9 and 10 in the context of nonlinear electrooptics and picosecond fluorescence spectroscopy.

The effect of experimental uncertainty is illustrated in Fig. 4.2.3.1 where two different spectra for methylene chloride have been processed. One of these is the mean of seven different runs, each consisting of the mean of three individual interferograms of an N.P.L./Grubb Parsons cube interferometer. The other is the extremum. The extremum uncertainty in the Mori type parameters is 22%. It is unlikely that the root mean square deviation in the majority of cases exceeds the range 5–10%. As we have mentioned already each spectrum and thus each set of a.c.f.'s is the result of averaging at least four high quality interferograms. The uncertainty

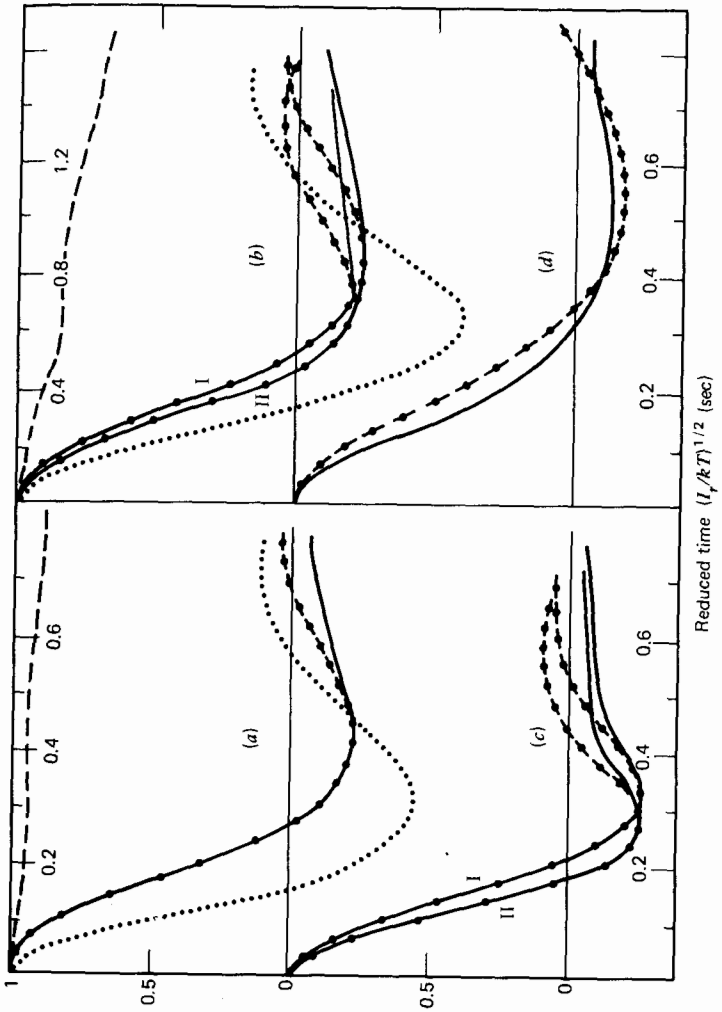

Figure 4.2.3.1 Rotational velocity correlation functions, each indicating points of consideration in the curve-matching analysis. (*a*) Pyridine (spectrum in Fig. 4.2.1.1). (*b*) CH_2Cl_2. $C_\mu(t)_{exp}$ from (I) mean spectrum (Fig. 4.2.1.7.2.2) and (II) extreme spectrum. (*c*) Chlorobenzene. I_r taken for (I) center of mass axes and (II) torque-determined axes. (*d*) Chloroform. ——, Experimental $C_\mu(t)$, and · · · ·, its analytical fit; · · · · · ·, derived $C_\theta(t)$; - - - -, derived $C_\mu(t)$.

analysis illustrated in Fig. 4.2.3.1 reveals the importance of knowing the band shape accurately in the high frequency region. In unfavorable cases the uncertainty in the Mori type parameters is unacceptably high for various reasons, and for these solutes the details of the molecular dynamics are obscured. We make no further use of these data in this section.

An additional source of uncertainty present in molecules such as chloroform is that due to induced absorption (Chapter 11) accentuating the high frequency spectral wings.

Finally the calculation of the reduced moment of inertia I_r (center of mass determined or torque determined) will affect the numerical value of the Mori type parameters for such molecules as bromobenzene, nitrobenzene, and bromonaphthalene.

Table 4.2.3.2 lists the Mori type parameters of 23 suitable solutes in decalin. The K_0 parameter is related to the mean square torque by

$$\langle \Gamma^2(0) \rangle = I_r k T K_0$$

so that CH_2Cl_2 and CH_2Br_2, for example, have the lowest values, and bromonaphthalene and nitrobenzene close to the highest of mean square torque.

The limitations of the itinerant librator are brought out most clearly by a plot such as that in Fig. 4.2.3.2. The ratio $K_0/(2\pi c\bar{\nu}_{max})^2$ should be constant if the Evans (1976) and itinerant-oscillator theories were strictly equivalent, but this is not the case. For the 23 systems it takes values from 1.7 to 3.7, which fall into a pattern. The reasons for this are that it is difficult to justify the use of a

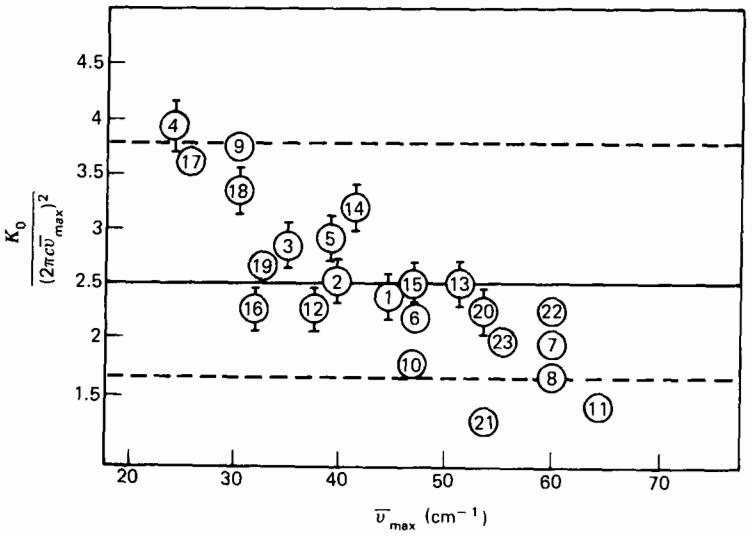

Figure 4.2.3.2 Variation of "mean square torque to peak" ratio with peak frequency ($\bar{\nu}_{max}$) for decalin systems at 293°K. (Numbered as Table 4.2.3.2.)

Table 4.2.3.2 Mori Theory Equations: Best-Fit Data for Decalin Systems at 293°K

	Solute	$(I_i/kT)^{1/2}$ (psec)	α_1	β (reduced time units)	$\bar{K}_0$	$\bar{K}_1$	$\bar{\gamma}$	K_0 $(\text{psec})^{-2}$	$\bar{\nu}_{max}$ (cm^{-1})	K_0/ω_{max}
1	Pyridine	0.48	3.1	8.0	41.5	81.8	14.2	180	45	2.5
2	Fluorobenzene	0.69	3.7	9.7	61	118	17.1	128	39	2.37
3	Chlorobenzene	0.85	3.6	10.8	77.7	130	18	108	34	2.6
		0.97	4.1	12.8	110	176	21	117		2.84
4	Bromobenzene	1.04	6.0	11.5	82	224	23.5	76	24	(3.7)
		1.27	6.7	15.2	147	333	28.6	91		(4.4)
5	Nitrobenzene	0.98	5.6	15	147	277	26.2	153	39	2.8
		1.15	6.7	18	211	398	31.4	159		2.94
6	Benzonitrile	0.87	4.6	14.2	135	218	23.4	178	47	2.26
7	α-picoline	0.55	2.75	10	69.4	93	15.5	230	60	1.8
8	Toluene	0.69	2.75	11.8	100	112	17.3	210	60	1.64
9	Pentafluorobenzene	1.04	5	14	129	232	24	119	30	3.7
10	Chloronaphthalene	1.0	4	14.3	141	193	22.3	136	47	1.73
11	Aniline	0.69	2.3	12.3	94.5	94.3	11.6	198	64	(1.35)
				$(\alpha_2 = 7)$						
12	Bromonaphthalene	1.13	4.8	14.9	149	239	24.5	117	38	2.27
		1.32	5.5	17.5	207	322	28.5	118.6		2.3
13	Furan	0.38	2.5	7.2	34.3	60	12.2	237	51	2.56
14	Tetrahydropyran	0.53	3.5	9.1	53.7	105	16.1	191	41	3.2
15	Thiazole	0.45	2.7	7.4	35.9	66	12.8	177	45	2.46
16	Chlorocyclohexane	0.78	3.0	8.8	51.4	87.8	14.8	84.5	32	2.32
17	t-Butylchloride	0.59	3.2	6.5	26.4	67.6	12.9	76	24	3.7
18	Chloroform	0.55	3.6	7.0	32.6	27	15.2	108	30	3.36
				$(\alpha_2 = 8)$						
19	2-chloro-2-nitropropane	0.7	3.6	8.8	49.7	104	16	101.4	33	2.6
20	CH_2Cl_2	0.24	1.6	4.8	13.4	23.4	6.7	232	52	2.6
				$(\alpha_2 = 3.5)$						
21	Acetone	0.53	2.5	7.2	34.3	60	12.2	122	53	(1.2)
22	Methyl-iodide	0.37	2.3	7.3	35.9	56.2	11.9	262	60	2.05
23	CH_2Br_2	0.27	1.45	5	15.7	23	6.9	215	55	2.0
				$(\alpha_2 = 4)$						

planar model in a three-dimensional context and that there is no clear a priori reason why the frequency ω_0 of the itinerant-oscillator model should lie exactly under $2\pi\bar{\nu}_{max}c$ of the far infrared.

The pattern revealed in Fig. 4.2.3.2 also has consequences that are model independent. For example, the basic hypothesis behind the introduction of a factor T_q is approximately verified in Fig. 4.2.3.2 but the ratio is obviously not exactly constant. This just means, of course, that the far infrared peak frequency contains information about the higher derivatives of angular velocity, for example, the derivative of torque. The Mori (1965) equations themselves imply this. In terms of the Mori (1965) type of continued fraction the situation could be improved by taking further approximants. This is at the root of exciting new developments such as semi-stochastic molecular dynamics simulation (C.E.C.A.M., 1980).

Another contribution to the pattern of Fig. 4.2.3.2 is collision-induced absorption (Chapter 11). Molecular dynamics simulation is the only reasonable way of treating this in detail, but on a simple basis we may obtain the following indications. These absorptions come from the induction effect of temporary fluctuations in proximate molecular fields of force. Electromagnetic radiation is modulated by collision-induced dipoles, which in dipolar molecules enhance in a more or less complicated way the absorption of the permanent molecular dipole itself. The induced absorption bands (Chapter 11) of most nondipolar liquids peak at a relatively high frequency (70 cm^{-1} in decalin, 80 cm^{-1} in benzene). It is therefore reasonable to assume as a first approximation that induced absorption distorts the far infrared spectrum of the permanent dipole on the high frequency side, especially when we recall that each dipolar solute molecule is surrounded generally by decalin molecules. If the spectrum of 10% bromobenzene in decalin, for example, is corrected in a simple way by subtraction of a fraction (less than 10%) of the pure benzene spectrum, a narrower band results. The fitting parameters are affected in such a way as to reduce the ratio in Fig. 4.2.3.2 for bromobenzene to 3.6. In this respect, however, the easily polarizable bromobenzene still represents the extremum deviation from the mean ratio for 23 solutes of 2.5. Finally we must not overemphasize the role of collision-induced absorption because a plot of integrated absorption intensity against solute number density in these systems is almost always linear. This cannot be the case if induced absorption is comparable in intensity with permanent dipolar absorption, because the former is in the dynamical picture a multibody effect. Decalin is one of the most weakly absorbing materials in the far infrared (which is one reason for its use as solvent) and in consequence is not a strong inducer of temporary dipoles. The only remaining source of induced absorption is long range dipole interaction between solute molecules, but we have already seen by comparing acetonitrile and propyne that the kinematics have been effectively isolated from the electrostatics except in clearly anomalous instances of molecular association in dilute solution.

Having dealt with the far infrared part of the spectrum we now turn our attention to the microwave loss data and Debye relaxation times. These have been measured afresh for this purpose by Reid and Evans (1980) for 16 of the solutes in decalin. Loss and dispersion points are now available for these at 4, 10, 18, 37, and 69 GHz (i.e. up to about 2 cm^{-1}. The dispersion of the permittivity is less than 0.4 except for pyridine, picoline, nitrobenzene, and benzonitrile solutes.

To measure the loss peak frequency with sufficient accuracy it is necessary to consider the well-known analysis of Fuoss and Kirkwood afresh, as described in the original paper by Reid and Evans and in greater detail by Reid (1979). This is because for systems with fast relaxation times the dielectric loss curve is distorted to a considerable degree by the far infrared (higher frequency) side in the sense that Debye's symmetrical theoretical curve no longer follows the experimental data. The CH_2Cl_2 system is a good example of this (Fig. 4.2.3.3) and the traditional Fuoss–Kirkwood approach is inapplicable.

In Table 4.2.3.3 are listed the experimental relaxation times τ_{exp} together with the Fuoss–Kirkwood parameter β and static permittivities ϵ_s. Some

Table 4.2.3.3 Microwave Data for 10% v/v Solutes in Decalin at 293°K

Solute	ϵ_s	τ_{exp} (psec)	β	τ_{lit} (293 + 5°K) (psec)†	τ_{Mori} (psec)	V^2 (Å^6)
1 CH_2Cl_2	2.59	1.2 ± 0.3 (1.1)*	0.9	—	0.95	280
2 Chloroform	2.36	4.3 ± 0.3 (4.2)	0.9	3.2cy; 5.0cl(*a*)	3.1	625
3 Furan	2.25	2.0 ± 0.3 (2.0)	0.9	1.9(*b*)	2.6	678
4 Pyridine	2.92	3.4 ± 0.3 (3.1)	0.8	3.1cy; 4.6b(*b*)	3.35	1263
5 2-Methyl-pyridine	2.66	9.0 ± 1 (8.5)	0.7	—	6.5	2724
6 THF	2.59	2.0 ± 0.5 (1.8)	0.9	—		1400
7 Fluorobenzene	2.47	4.0? (3.9)	0.74	5.4*b*(*a*); 6.8(*d*)	6.0	2265
8 Pentafluoro-benzene	2.4	10 ± 1 (9.8)	0.76	—	13.8	3227
9 Bromobenzene	2.5	16.7 ± 1 (16.2)	0.82	12cl(*a*); 14(*d*)	8.5	5700
					16‡	3840†
10 Chlorobenzene	2.46	11.2 ± 1 (10.7)	0.8	8.6cl(*a*); 10.2(*d*)	9.2	3958
					12.7‡	3117†
11 (20%) Toluene	2.2	9.0 ± 2 (9.0)	—	14cl(*e*)	10.7	4680
12 (20%) *o*-Xylene	2.27	12 ± 1 (12)	0.8	9cl(*a*)	—	—
13 Nitrobenzene	4.18	24 ± 3 (20)	0.9	15.2cl(*a*)	13.6	5800
					19‡	5020†
14 (5%) Benzonitrile	3.0	30 ± 5 (27)	0.7	17cl(*a*); 40(*d*)	12.6	—
15 1-Chloro-naphthalene	2.43	30 ± 5 (29)	0.9	18cl(*a*); 21(*f*)	16.6	—
16 *t*-Butylchloride	2.62	3.6 ± 0.3 (3.4)	0.85	3.2cl(*a*)	3.0	1600

*Values in parenthesis are field corrected.
‡Torque-determined inertial axes.
†References (*a*) = *vv*; (*b*) = *ww*; (*c*) = *xx*; (*d*) = yy in *p*-xylene at 288°K; (*e*) = *zz*; (*f*) = *aaa* in decalin at 293°K.
cy = cyclohexane; cl = CCl_4; b = benzene.

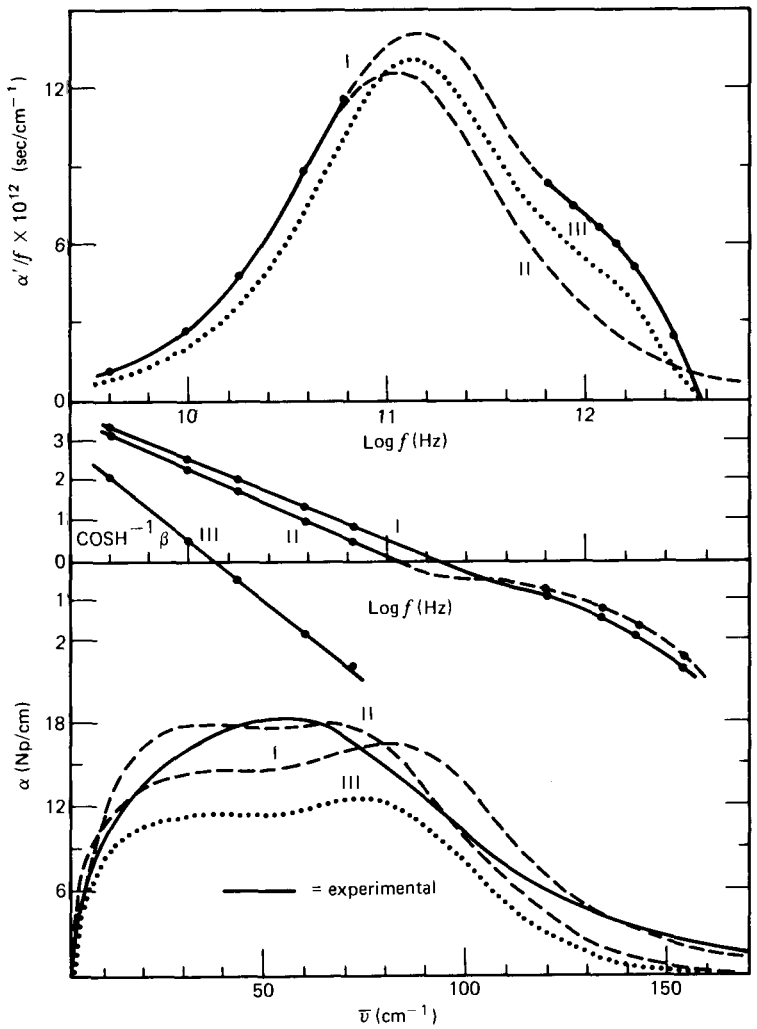

Figure 4.2.3.3 Microwave and far infrared data for CH_2Cl_2/decalin: Fuoss–Kirkwood curves and analytical fits. (*a*) α'_f (or ϵ'') representation (microwave): I best Fuoss–Kirkwood curve through data; II Debye curve through low frequency data; III itinerant librator fit (see part *c*). (*b*) Fuoss–Kirkwood (β) plots of curves I and II above; III plot for 10% v/v phCl/decalin for comparison (ordinate scale doubled). (*c*) Absorption representation (far infrared): I Mori fit (best short time fit), parameters as Table 4.2.3.2, arbitrary scale; II best spectral fit, parameters $\bar{K}_0 = 10$, $\bar{K}_1 = 21$, $\bar{\gamma} = 6.5$, arbitrary scale; III itinerant librator fit, parameters as II above with $\epsilon_s = 2.59$, $\epsilon_\infty = 2.2$.

literature values are listed where available. Before an attempt is made to reproduce these theoretically, an internal field correction is made in each case using the factor derived by Cole (Eq. 4.2.3.2). The choice of internal field factor is not critical as the table shows. The correction is small in the majority of cases, which is consistent with our earlier assertion that the kinematics of the problem have been effectively isolated from the elec-

trodynamics. The Mori theory estimate of relaxation time is, from appendix A,

$$\tau_M = \left(\frac{I_r}{kT}\right)^{1/2} \frac{\bar{K}_0 \bar{\gamma}}{\bar{K}_1}$$

and is almost always within 30% of the Debye time defined in Eq. 4.2.3.2. The individual results are listed in Table 4.2.3.3. Torque-determined I_r values produce significantly longer and more realistic values of τ_M.

4.2.4 Conclusions and Intensity Analysis

The Mori theory model is a useful representation of the data available in the liquid phase of decalin but its essentially oversimplified nature is easily exposed by extending the range of investigation to the vitreous state of matter as described in Chapter 7. The planar itinerant librator is at odds with the basic spectral features of the far infrared despite the fact that it is an appealingly concrete model bearing some resemblance to the Mori angular velocity a.c.f.

In the frequency domain Mori (1965) theory produces on the whole analytical power absorption spectra which tend to be twin-peaked (e.g., curve II of Fig. 4.2.2.1 for nitrobenzene and curve I of Fig. 4.2.3.3 for dichloromethane). The theory is of course the simplest possible approach to the problem that is just capable of maintaining a modicum of effectiveness over a restricted range of conditions. The major approximations involved includes the spherical top assumption implicit in the use of the integro-differential equation (Eq. 4.1.1). The Mori continued fraction expansion of Eq. 4.1.1 was applied by Evans to the angular velocity a.c.f. in this limit and truncated at a stage designed to maximize the effectiveness of the final equations while maintaining a minimum of adjustable variables. The appendix is a discussion of the methods employed to control the use of these parameters with broad ranging spectral data. The proper use of Mori type theory means that the asymmetric top must be represented by a reduced moment of inertia I_r. The effect of these approximations is most clearly manifest in the mid-spectral region of 10–80 cm^{-1} because at long times the orientational a.c.f. is as usual exponential and at very short times the molecular motion is essentially free. The Mori type equations reproduce these limits correctly for the sphere (rotational diffusion). The abruptness of the truncation, designed to minimize the number of parameters, has the effect of hurrying the transition from deterministic to stochastic regimes in the range 10–80 cm^{-1}. In addition there is a need to clarify the role of rotation/translation coupling, which is the subject and object of Chapter 5.

The spectral behavior of the itinerant librator is illustrated in Fig. 4.2.4.1. If we relate ζ of this model to the Debye relaxation time, ω_0 to the far infrared peak frequency $\bar{\nu}_{max}$, and use $I_1 > I_2$ for fluorobenzene in decalin, the resulting spectrum is unrealistic in that the far infrared resonance is far too narrow. By

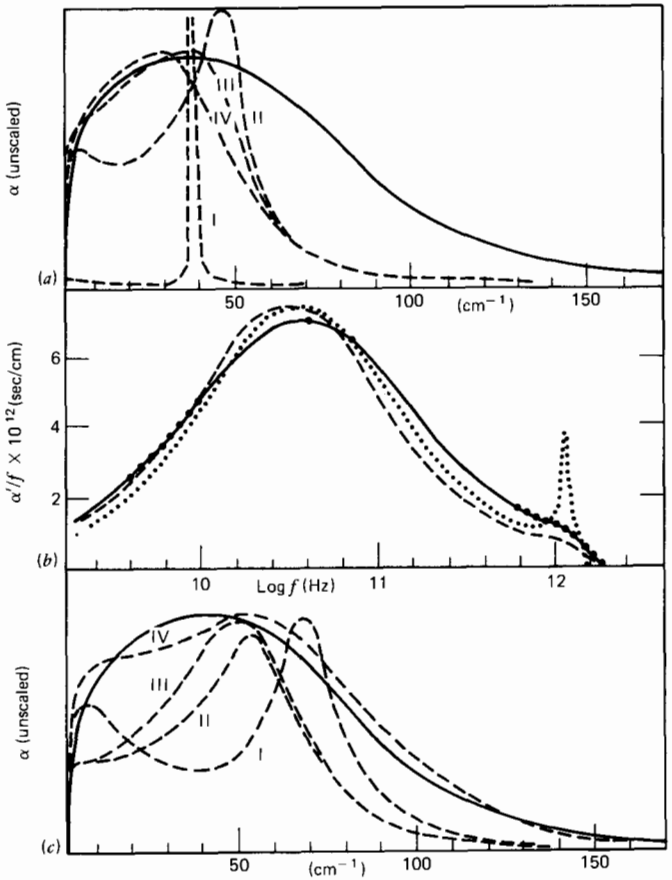

Figure 4.2.4.1 Illustrating spectral form of itinerant oscillator model for various parameter sets, with reference to PhF/decalin at 293°K. (*a*) Absorption curves with $\omega_0 = 2\pi c\bar{\nu}_{max}$ ($\bar{\nu}_{max}$ for PhF = 39 cm^{-1}, $I_2 = 1.92 \times 10^{-38}$ g cm^2).

	ζ/I_1	ω_0^2	Ω_0^2	I_1/I_2 (time units 10^{-12} sec)
I	0.82	54	5.4	10
II	8.2	54	54	1
III	16.4	54	108	0.5
IV	32.8	54	216	0.25

Solid line, experimental. (*b*) "Loss" representation. –·–·–, Experimental (microwave and far infrared); ·····, itinerant oscillator model for curve I of part *a*; – – – –, Mori analytical fit with parameters of Table 4.2.3.2 (curve IV of part *c*). Both fits scaled using $\epsilon_s = 2.47$ and $\epsilon_\infty = 2.2$. (*c*) Absorption curves with ω_0 variable.

	ζ/I_1	ω_0^2	Ω_0^2	I_1/I_2 (time units 10^{-12} sec)
I	8.2	108	108	1
II	16.4	108	216	0.5
III	32.8	108	432	0.25
IV	24.7	128	249	0.51

IV corresponds to a Mori fit (Table 4.2.3.2), $\omega_0^2 = 2.37(2\pi c\bar{\nu}_{max})^2$. Solid line, experimental.

artificially reducing the ratio I_1/I_2 the absorption curve widens, but this means that ω_0 must be readjusted to keep the far infrared peak at its experimental value. This process is illustrated in Fig. 4.2.4.1. The parameters of curve IV of this figure are equivalent to those of the Mori type equations only in the strictly limited sense that they produce the same spectrum. In terms of dielectric loss the same spectrum looks like the dotted curve of Fig. (4.2.4.1*b*).

4.2.4.1 Intensity Analysis

The intensity of the far infrared spectrum depends theoretically on the value chosen for $\epsilon_s - \epsilon_\infty$. The static permittivity is accurately measurable but ϵ_∞ is not an experimentally accessible parameter. It is defined mathematically as the value of permittivity fixed by the high frequency intercept of the Cole–Cole semicircle with the abscissa. It is important to note that the loss spectrum is accurately determined in the case of Debye behavior by the well-known relation $\epsilon''_{max} = \frac{1}{2}(\epsilon_s - \epsilon_\infty)$, but as with many other traditional methods this is no longer true when we extend our thinking to include the far infrared. A measure of the ϵ_∞ parameter sometimes used in the literature is the square of the measurable (?) refractive index at a far infrared frequency just above that at which "all traces of the librational absorption have disappeared." The far infrared integrated intensity is acutely sensitive to the numerical value of ϵ_∞ and in consequence it is important to devote some theoretical effort in the future to a development of a fundamental method for calculating this parameter (as outlined in Chapter 3). This is a problem of fundamental equilibrium thermodynamics which seems not to have been considered. The obvious method to use would be Monte Carlo simulation. In the absence of such a calculation we devote this subsection to a consideration based on the Gordon sum rule.

In Table 4.2.4.1.1 we list the measured (A_{exp}) and calculated (A_G) (i.e., Gordon sum rule) far infrared integrated intensities as defined by Eq.

Table 4.2.4.1.1 Illustrating Failure of Gordon's Rule for Decalin Systems[a]

Solute	A_{exp}	A_G	A_G/A_{exp} (%)	Solute	A_{exp}	A_G	A_G/A_{exp} (%)
phF	214	100	47(47)	2.9% CH_3CN (CCl_3)	1400	1300	93
phCl	125	76	61(50)	CH_2Cl_2	1800	1580	88
phBr	82	47	57(56)	*t*-butylchloride	325	266	82(77)
$phNO_2$	600	356	59(58)	2-chloro-2-nitro-propane	571		
5% phCN	349	231	66(62)	chloroform	147	108	73(88)
Furan	210	95	45	MeI	680		(85)
Pyridine	728			thiazole	784		
THF	1300	408	31	chloro-cyclohexane	155		
THP	293	191	65	2-3-dihydro-pyran	273	240	88

[a]Units of A are cm^{-2}, bracketed values, Ref. (*bbb*).

1.9.3.3. The aromatic ring compounds are associated with ratios A_G/A_{exp} below 65%, where A_G is the Gordon sum rule integrated absorption intensity and A_{exp} the measured absorption intensity (or area of the far infrared librational band). In THF the A_{exp} is more than three times greater than A_G. The ratios in dilute decalin solution are very similar to their equivalents in the pure solutes (in parentheses in Table 4.2.4.1.1) where available. This illustrates very well the fact that upon dilution A_{exp} varies linearly with solute number density, so that there is in fact little direct evidence for collision-induced effects. This brings into question whether the use of the Gordon sum rule is valid in the condensed phases of matter.

The instantaneous value of molecular dipole moment responsible for far infrared absorption is by a comparison of A_G and A_{exp} larger than that of the gas phase, which is a root mean square average. The idea of an effective dipole at short times has been considered by Evans (1975), who used the Gordon sum rule to obtain values to compare with Onsager moments. The origin of this effective moment lies in the fact that at far infrared frequencies the modulation of electromagnetic radiation depends critically on the detailed mechanism of dipole fluctuation. Not only is this true with regard to the solute dipole itself but also with regard to the distribution of nearest neighbors. For present purposes these solvent molecules are essentially not only nondipolar but also weakly multipolar (i.e., decalin). There is furthermore a symmetry of inducing fields (Chapter 11) in the liquid phase of matter, which means that any tendency to induce a dipole by one solvent molecule is counterbalanced electrically by the symmetrical disposition of other nearest neighbors. It is difficult to see, therefore, how the excess over Gordon's sum rule can be generated on electrostatic grounds alone.

However, it is well known that the half-width of a far infrared collision-induced band such as that of nitrogen, for example, is a measure of the inverse of a collision time. Evans (1975a) has shown that in oxygen it is likely that the far infrared spectral evidence can be used to support the existence of a long-lived dimer complex in the gas phase. The forces responsible for the creation of this O_4 molecule are very short range, and include the "O_2 hexadecapole" and (what is more relevant in the present context) short range overlap forces causing distortion of the monomer framework. These short range forces are of course instantaneously very large because the repulsion fields of the interacting molecules have been forced to overlap, thus distorting the framework. If the distortion is in any way asymmetric, as is probably the case with big dipolar molecules, the dilute gas phase root mean square dipole moment is increased for time scales corresponding to that for which the molecular framework is distorted, in other words for time scales over which a pair of molecules may be said to collide. These time scales correspond with far infrared frequencies as evidenced vividly for oxygen. The range of such forces is so restricted falling off as R^{-12} (for example, in the hexadecapole, Chapter 11)

that they rapidly vanish over distances smaller even than the mean intermolecular separation and are to a large degree unaffected by the symmetry with which a given molecule is oriented with respect to the instantaneous disposition of nearest neighbors. That these forces enhance the far infrared intensity rather than the reverse is of course evidenced by the available broad band data for O_2, N_2, SF_6, and a whole range of other nondipolar species in both gas and liquid states. We elaborate in Chapter 11.

If we add to these considerations of the enhanced dipole the fact that Gordon based the derivation of his sum rule on a gas phase treatment then we can begin to shed some light on the experimental evidence in what is necessarily a semiqualitative manner. In principle this kind of argument can lead to a significant improvement in our understanding of the molecular potential at short and intermediate range, and should be a target for molecular dynamics simulation in future work.

4.3 DEBYE RELAXATION TIMES

Finally in this chapter we consider a practical approach to the new questions and problems posed by the meaning of the Debye relaxation time when taken in the context of advances in far infrared spectroscopy. The dielectric loss peak and the far infrared power absorption peak are linked, and their frequency separation depends on the value of the mean square torque. This is illustrated in Fig. 4.3.1, where we have plotted the square root of the torque, T_q, factor obtainable from first the loss peak frequency and second the far infrared. On a logarithmic scale the separation of peaks is a good empirical measure of the degree to which the librational motion of a molecule is hindered by factors over and above the molecular inertia itself. In the free rotor limit there is no separation because the effective intermolecular torque is vanishingly small whereas in the vitreous state of matter at the other extreme, the separation is many orders of magnitude greater for any given solute. We can now attempt to derive a direct relation between the Debye relaxation time and the far infrared peak frequency.

We observe that the position of the minimum of the rotational velocity a.c.f. is governed to a significant degree solely by the far infrared peak

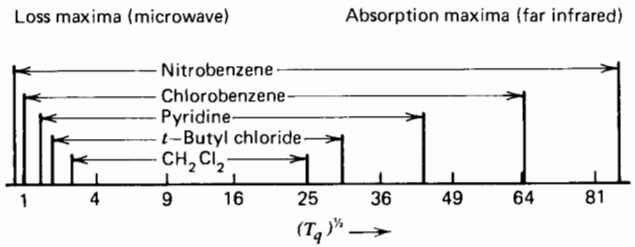

Figure 4.3.1

frequency, whereas the value of the minimum is governed by the width of the frequency domain far infrared absorption. Using these relations it is possible to see that the relaxation time for a particular solute molecule is proportional to the square of its volume of rotation. Equivalently,

$$\tau_D \propto \frac{(I_r/kT)^{1/2}\bar{\beta}^2}{4\bar{\alpha}_1} \tag{4.3.1}$$

These relationships are based on the fact that far infrared band shapes do not vary appreciably from solute to solute if scaled on both ordinate and abscissa.

If the well-known Einstein relation (Chapters 1 and 2) of traditional dielectric spectroscopy is used, it is possible to show that the Debye relaxation time must be approximately the time for a molecule to have rotated on average through an angle of 1.2 rad from its position at any arbitrarily chosen $t = 0$. In Mori (1965) theory the friction coefficient is defined through the Kubo relation (cf. Eq. 4.1.1):

$$K_0 = (2kT)^{-1} \int_0^\infty \langle \mathbf{\Gamma}_q(0) \cdot \mathbf{\Gamma}_q(t) \rangle \, dt$$

but at long times (microwave frequencies) this reduces to a form which implies the relation

$$\tau_D \propto V^2(kT)^{-2} \int_0^\infty P(t) \, dt$$

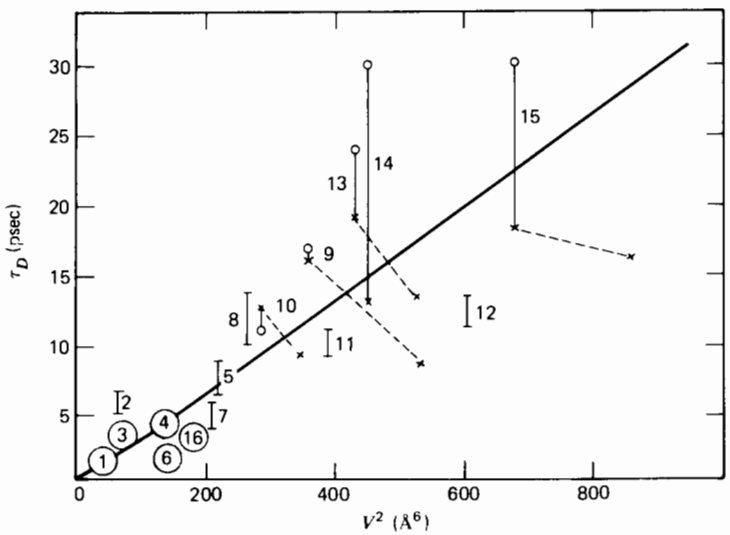

Figure 4.3.2 Predicted and observed Debye times and their correlation with V^2. × = Mori predictions from far infrared data; ○ = observed microscopic relaxation times. Numbers as in Table 4.2.3.3.

between the Debye relaxation time and $P(t)$. This means approximately that $\tau_D \propto V^2$ provided that $P(t)$, the mean square torque per unit volume of rotation, evolves similarly in all solutes. This empirical relation is followed fairly closely (Fig. 4.3.2), although the correlation is not as good as that between the torque coefficient and V^2. It is possible to use such a correlation to produce the Debye relaxation time from a consideration of volume of rotation (Section 4.2.2.1). This is a more realistic approach than that based on the Stokes law and was used by Debye to produce the well-known equation

$$\tau_D = 4\pi a^3 \eta (kT)^{-1}$$

where η is the macroscopic solvent viscosity.

APPENDIX A: FITTING MORI THEORY TO EXPERIMENTAL DATA: MATHEMATICAL DETAILS (REID (1979))

The Mori continued fraction for angular velocity is truncated to produce in the frequency domain ($p = -i\omega$):

$$\tilde{C}_\omega(p) = \frac{p^2 + \gamma p + K_1}{p^3 + \gamma p^2 + (K_0 + K_1)p + \gamma K_0}$$

The inverse transform of this function produces the angular velocity a.c.f. in the time domain. To find the roots of this cubic equation we define a new variable S and let p take the form

$$p = S - A(3S)^{-1} - C$$

so that the S^2 and S terms vanish. This happens when $A = K_0 + K_1 - \gamma^2/3$ and $C = \gamma/3$ leaving $S^3 + B - (A/3S)^3 = 0$, which is a quadratic in S^3 with roots

$$\begin{bmatrix} p_a \\ p_b \end{bmatrix} - \frac{B}{2}\begin{bmatrix} - \\ + \end{bmatrix}\left(\frac{B^2}{4} + \left(\frac{A}{3}\right)^3\right)^{1/2}$$

where $B = (\gamma/3)[(2\gamma^2/9) + 2K_0 - K_1]$. If the bracket is positive then p_a and p_b are real and S takes the form dictated by the solutions

$$-|p_a|^{1/3}; \qquad -|p_a|^{1/3}\left(\cos\frac{\pi}{3} + i\sin\frac{\pi}{3}\right); \qquad \text{and } |p_a|^{1/3}\left(\cos\frac{\pi}{3} - i\sin\frac{\pi}{3}\right)$$

with a similar set for p_b. Only one root p_a or p_b need be used to generate all three roots of the cubic, which are thereby

$$p_1 = -p_a^{1/3}\left(\cos\frac{\pi}{3} + i\sin\frac{\pi}{3}\right) + \frac{A}{3p_a^{1/3}}\left(\cos\frac{\pi}{3} - i\sin\frac{\pi}{3}\right) - \frac{\gamma}{3}, \text{ etc.}$$

These may be rewritten as

$$p_1 = -\frac{1}{2}(p_a^{1/3} + p_b^{1/3}) + \frac{i\sqrt{3}}{2}(p_a^{1/3} - p_b^{1/3}) - \frac{\gamma}{3}$$

$$p_2 = -\frac{1}{2}(p_a^{1/3} + p_b^{1/3}) - \frac{i\sqrt{3}}{2}(p_a^{1/3} - p_b^{1/3}) - \frac{\gamma}{3}$$

$$p_3 = (p_a^{1/3} + p_b^{1/3}) - \frac{\gamma}{3}$$

That is, they take the general form $-\alpha_1 - i\beta$, $-\alpha_1 + i\beta$, and $-\alpha_2$, with

$$\begin{bmatrix} p_a \\ p_b \end{bmatrix} = -\frac{B}{2}\begin{bmatrix} + \\ - \end{bmatrix}\left(\frac{A^3}{27} + \frac{B^2}{4}\right)^{1/2}$$

If the square root bracket is negative then p_a and p_b are complex conjugates. S now takes the values $|p_a|^{1/3}e^{i\theta/3}$, $|p_a|^{1/3}e^{(\theta+\pi)i/3}$, and $|p_a|^{1/3}e^{(\theta+2\pi)i/3}$ where

$$|p_a|^2 = \left(\frac{B}{2}\right)^2 + \left(-\frac{B^2}{4} - \frac{A^3}{27}\right)$$

and

$$\theta = \cos^{-1}\left(\frac{B}{2}\left(-\frac{A^3}{27}\right)^{1/2}\right)$$

The roots of the cubic are now $p_n = |p_a|^{1/3}\cos(\theta/3 + n\pi/3) - \gamma/3$, where $n = 1, 2$, and 3. In this case, therefore, all three roots are real and negative.

In practice the condition $A^3/27 > B^2/4$ is almost always met when matching experimental data. In this case the cubic denominator factorizes as

$$(p + \alpha_1 + i\beta)(p + \alpha_1 - i\beta)(p + \alpha_2)$$

which implies the further relations

$$\begin{aligned} \gamma &= 2\alpha_1 + \alpha_2 \\ K_0 + K_1 &= 2\alpha_1\alpha_2 + \beta^2 + \alpha_1^2 \\ \gamma K_0 &= (\alpha_1^2 + \beta^2)\alpha_2 \end{aligned} \tag{4.A.1}$$

The inverse Laplace transformation may now be carried out using the method of partial fractions or using Heaviside's theorem to produce the angular velocity a.c.f. in the form

$$\begin{aligned} C_\omega(t) = {} & \frac{\alpha_2^2 - \gamma\alpha_2 + K_1}{3\alpha_2^2 - 2\alpha_2\gamma + K_0 + K_1} e^{-\alpha_2 t} \\ & + \frac{(\alpha_1 + i\beta)^2 - \gamma(\alpha_1 + i\beta) + K_1}{3(\alpha_1 + i\beta)^2 - 2\gamma(\alpha_1 + i\beta) + K_0 + K_1} e^{-(\alpha_1 + i\beta)t} \\ & + \frac{(\alpha_1 - i\beta)^2 - \gamma(\alpha_1 - i\beta) + K_1}{3(\alpha_1 - i\beta)^2 - 2\gamma(\alpha_1 - i\beta) + K_0 + K_1} e^{-(\alpha_1 - i\beta)t} \end{aligned}$$

or equivalently,

$$C_\omega(t) = Ze^{-\alpha_2 t} + (X+iY)e^{-(\alpha_1+i\beta)t} + (X-iY)e^{-(\alpha_1-i\beta)t}$$
$$= Ze^{-\alpha_2 t} + [2X\cos(\beta t) + 2Y\sin(\beta t)]e^{-\alpha_1 t}$$

where

$$Z = \Gamma(1+\Gamma)^{-1}$$
$$X = \tfrac{1}{2}(1+\Gamma)^{-1}$$
$$Y = (\alpha_1 + \alpha_2\Gamma)(1+\Gamma)^{-1}(2\beta)^{-1}$$
$$\Gamma = \frac{2\alpha_1(\alpha_1^2+\beta^2)}{\alpha_2(\beta^2+\alpha_2^2-3\alpha_1^2)}$$

Note that the Maclaurin series in time is time even up to t^4.

When the roots of the cubic are all real the expression for $\tilde{C}_\omega(p)$ in the frequency becomes

$$\tilde{C}_\omega(p) = \frac{p(p-p_1-p_2-p_3) + \dfrac{p_1^2(p_2+p_3)+p_2^2(p_3+p_1)+p_3^2(p_2+p_1)+2p_1p_2p_3}{p_1+p_2+p_3}}{(p-p_1)(p-p_2)(p-p_3)}$$

which is identical in mathematical structure with the equivalent expression obtained by Coffey and Calderwood (1977, 1981). Note that there is an error in Eq. 39 of that paper, whose second term denominator coefficient $(\lambda_3^2-\lambda_1^2)$ should read $(\lambda_3^2-\lambda_2^2)$.

Using the Shimizu expansion in terms of cumulants it is possible to relate the orientational (dipole) a.c.f. of the isotropic space diffuser to the angular velocity a.c.f. as in the text. This equation was used by Evans in 1976 to produce the result of Eq. 4.1.7.†

The rotational velocity a.c.f. is the negative of the second derivative of this equation. In terms of the numerically convenient reduced units of the text we obtain Eq. 4.2.3.1.

The Fourier transform of this function is the far infrared spectrum after accounting for the relevant proportionality factors, which may include an internal field correction. Reid (1979) has analyzed the algebraic construction of this equation and has simplified it to the point where data comparison can be carried out on a pocket calculator. Reid's method is first to define $L = (\beta A_1 - \alpha_1 B_1)(1+\Gamma)$ and $M = (\beta B_1 + \alpha_1 A_1)(1+\Gamma)$ so that

$$L = \frac{\alpha_1\alpha_2\beta^2\Gamma - \beta^4 + \alpha_1^2(\alpha_1^2+\alpha_1\alpha_2\Gamma)}{\beta(\alpha_1^2+\beta^2)^2}$$

$$M = \frac{2\alpha_1+\alpha_2\Gamma}{\alpha_1^2+\beta^2}$$

†Note it is explicitly assumed in writing this equation that the equation following 4.1.6 is also valid for the sphere model.

This allows us to replace $2\alpha_1\beta A_1 - (\alpha_1^2-\beta^2)B_1$ by $(\beta M + \alpha_1 L)(1+\Gamma)^{-1}$ and $2\alpha_1\beta B_1 + (\alpha_1^2-\beta^2)A_1$ by $(\beta L - \alpha_1 M)(1+\Gamma)^{-1}$. Reid notes that $\beta L - \alpha_1 M = -1$ so L is defined more simply by $L = (\alpha_1 M - 1)/\beta$. Also $C_1 = [M + \Gamma/\alpha_2](1+\Gamma)$. The rotational velocity a.c.f. is therefore

$$\ddot{C}_u(\bar{t}) = \frac{(\cos\beta\bar{t} + (\beta M + \alpha_1 L)\sin\beta\bar{t})e^{-\alpha_1\bar{t}}}{1+\Gamma} + \frac{\Gamma e^{-\alpha_2\bar{t}}}{1+\Gamma}$$
$$-(1+\Gamma)^{-2}\left[(L\sin\beta\bar{t} + M\cos\beta\bar{t})e^{-\alpha_1\bar{t}} + \frac{\Gamma}{\alpha_2}(e^{-\alpha_2\bar{t}}-1) - M\right]^2$$

where Reid uses the further useful approximation $C_u(t) \doteqdot 1$ in the short time region where $\ddot{C}_u(t)$ is still significantly different from zero.

This expression can now be used on a programmable calculator to determine the form of the analytical $\ddot{C}_u(t)$ for a given set of α_1, α_2, and β (uniquely related to the set K_0, K_1, and γ). A program suitable for an SR56 Texas calculator (100 step program capacity, 10 memories) is given below:

Load Program (Radian Mode)

rcl 0 sin x rcl 4 + rcl 0 cos x rcl 3
$= x$ rcl $1e^x$ + rcl $7x$ (rcl $2e^x - 1$) − rcl 3
$= x^2 \div$ rcl 6 − rcl $5x$ rcl $2e^x$ − (rcl 0 cos + rcl $8x$ rcl 0 sin) x rcl $1e^x$
= R/S rcl 0 sbr 9 0 sum 0 rcl 1 sbr 9 0 sum 1 rcl 2 sbr 9 0 sum 2
.02 sum 9 RST ÷ rcl $9x$. 02 = rtn

Now compute the following parameters and insert into memories:

Memory		Memory	
0	0.02β	5	Γ
1	$-0.02\alpha_1$	6	$(1+\Gamma)$
2	$-0.02\alpha_1$	7	Γ/α_2
3	M	8	$\beta M + \alpha_1 L$
4	L	9	$t = 0.02$

This program produces an initial value of $(1+\Gamma)\ddot{C}_u(t)$ corresponding to 0.02 units of reduced time. Restarting (R/S key), the value 0.02β is called from memory 0 and divided by $t = 0.02$ from memory 9 to give β, then the value 0.02β is summed into memory 0 to give 0.04β overall. This process is repeated for memories 1 and 2; then finally t in memory 9 is incremented by 0.02. The next value displayed corresponds to $(1+\Gamma)\ddot{C}_u(t)$ at 0.04 time units. By reinitiating the program after each readout the sequence of $\ddot{C}_u(t)$ values at 0.02 unit intervals is generated, the corresponding time for each readout being held in memory 9. By using test sets of α_1, α_2, and β the experimental correlation function obtained by direct Fourier transfor-

mation of the far infrared spectrum, and normalized to unity at $t = 0$ on a reduced time scale, can be matched over the first half-period of its oscillation to any degree of accuracy by simple trial and error. The whole procedure can then be refined if necessary on a main-frame computer with a nonlinear least mean squares iteration procedure, using the full equations.

With K_0, K_1, and γ, the Mori type parameters, determined in this way, the orientational a.c.f. itself is defined. At long times (microwave frequencies and below) the largest term in the exponent is $-(kT/I)C_1 t$. Therefore the C_1 factor is related to the Debye relaxation time by

$$\tau_D = \left(\frac{I}{kT}\right)^{1/2} \frac{\alpha_2(1+\Gamma)(\alpha_1^2+\beta^2)}{2\alpha_1\alpha_2+\Gamma(\alpha_1^2+\alpha_2^2+\beta^2)} = \left(\frac{I}{kT}\right)^{1/2} C_1^{-1}$$

Numerically the value taken by α_2 is always similar to that taken by β. To a good approximation $\alpha_2 = \beta$. If we then define f as the ratio α_1/α_2, then Γ becomes $(2f^3+2f)/(2-3f^2)$ and C_1 becomes $(8f+2f^5)/(2+2f-f^2+4f^3-3f^4+2f^5)\beta$. Because f is typically between 0.2 and 0.5, then ignoring f^2 terms one obtains $\tau_D = (I/kT)^{1/2}(1+f)\beta/4f$. This in turn leads to an even simpler relation between τ_D and K_0, K_1, and γ.

It is also possible to produce a relatively simple theoretical far infrared spectrum following Reid's use of the relation (Chapter 2)

$$\frac{\chi(\omega)}{\chi(0)} = 1 - i\omega \int_0^\infty e^{-i\omega t} C_u(t)\, dt \qquad (4.A.2)$$

derived by Scaife between the complex susceptibility $\chi(\omega)$ and the orientational a.c.f. This equation takes no account of internal field corrections. The complex susceptibility is proportional to ϵ for a spherical sample in this case. To obtain the far infrared power absorption coefficient from this equation the most convenient expression for $C_u(t)$ is

$$\exp\left[-\left(\frac{kT}{I}\right)(C_1 t + A_0 e^{-(\alpha_1 - i\beta)t} + B_0 e^{-(\alpha_1+i\beta)t} + C_0 e^{-\alpha_2 t} + D_0)\right]$$

where $A_0 = \frac{1}{2}(A_1 - iB_1)$, $B_0 = \frac{1}{2}(A_1 + iB_1)$, $C_0 = (\Gamma/\alpha_2^2)(1+\Gamma)^{-1}$, and $D_0 = -A_0 - B_0 - C_0$. Factorizing out the $-C_1 t$ term and expanding the other exponential to first order in kT/I, one has

$$C_u(\bar{t}) = \exp(-C_1\bar{t})(1 - A_0 e^{-(\alpha_1 - i\beta)\bar{t}} - B_0 e^{-(\alpha_1+i\beta)\bar{t}} - C_0 e^{-\alpha_2\bar{t}} - D_0 + \text{higher terms})$$

with all parameters in reduced units. Substituting in Eq. 4.A.2 and integrating with the approximations $\alpha_1 \doteq \alpha_2 \gg C_1$, $A_0 \doteq B_0 \doteq C_0 \ll 1$, one obtains

$$\frac{\chi(\omega)}{\chi(0)} = 1 - i\omega[(C_1 + i\omega)^{-1} - A_0(\alpha_1 + i\omega - i\beta)^{-1} - B_0(\alpha_1 + i\omega + i\beta)^{-1} - C_0(\alpha_2 + i\omega)^{-1}]$$

Separating real and imaginary parts and multiplying the imaginary part by ω, the angular frequency produces a good approximation to the far infrared power absorption coefficient. One may always use a main frame to obtain the spectrum to any degree of accuracy by numerical Fourier transformation.

APPENDIX B: VOLUME OF ROTATION (REID, 1979)

The volume of rotation of an isolated sphere, radius r and distance d from axis, is determined as follows.

1. *Case where $d > r$.* The cross-sectional area of such a sphere is a circle (of radius r) which generates a volume of rotation upon rotation through 2π of

$$V = 2\pi \int_0^r (f_1(x))^2\, dx - 2\pi \int_0^r (f_2(x))^2\, dx$$

where $f_1(x)$ is the equation of the outer semicircle and $f_2(x)$ that of the inner semicircle. Thus

$$V = 2\pi \int_0^r (d + (r^2 - x^2)^{1/2})^2\, dx - 2\pi \int_0^r (d - (r^2 - x^2)^{1/2}]^2\, dx$$

or

$$V = 8\pi d \int_0^r (r^2 - x^2)^{1/2}\, dx$$

Substituting $x = r \sin\theta$ and integrating by parts

$$V = 8\pi\, dr^2 \int_0^r \cos^2\theta\, d\theta = 8\pi\, dr^2 |\tfrac{1}{2}(\cos\theta \sin\theta + \theta)|_0^r$$

so that

$$V = 2\pi^2\, dr^2.$$

2. *Case where $d < r$.* Spheres that have the axis passing through them may be sectioned across into circles of thickness Δx.

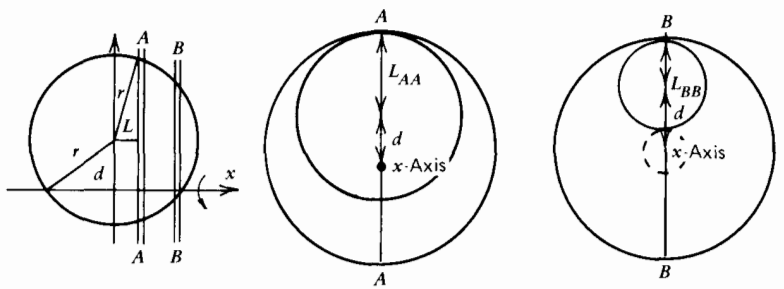

The volume of rotation of cross section AA in the figure is then $2\pi\Delta c$ times its extreme distance from circumference to center of rotation, minus its volume. Because the radius is $1_{AA} = (r^2 - x^2)^{1/2}$, the volume of rotation of section AA is $\Delta x(1_{AA} + d)^2 - \Delta x\pi 1_{AA}^2$.

Similarly, the volume of rotation of a section BB is the volume of the toroid generated minus the volume of the section: $\Delta x\pi[(1_{BB}+d)^2-(1_{BB}-d)^2]-\Delta x\pi 1_{BB}^2$.

TABLE REFERENCES

a Bak, B., Hansen-Nygaard, L., and Rastrup-Anderson, J., *J. Mol. Spectrosc.* **2**, 361 (1958).

b Wheatley, P. J., *Acta Cryst.* **13**, 80 (1960).

c Nygaard, L., Bojesen, I., Pederson, T., and Rastrup-Anderson, T., *J. Mol. Struct.* **2**, 209 (1968).

d de More, B., Wilcox, W., and Goldstein, J., *J. Chem. Phys.* **22**, 876 (1954).

e Rein, R., Adams S., Shlomo, N., and Swissler, T., *Chem. Phys. Lett.* **21**, 483 (1973).

f Jonas Pederson, E., Vold, R. R., and Vold, R. L., *Mol. Phys.* **35**, 997 (1978).

g Blackman, G. L., Brown, R. D., and Burden, F. D., *Mol. Spectrosc.* **35**, 444 (1970).

h Sharma, Y., *Spectrochim. Acta.* **30A**, 1802 (1974).

i McLellan, A. L., *Tables of Experimental Dipole Moments*, Freeman, San Francisco (1963).

j *Handbook of Physics and Chemistry*, Chemical Rubber Company, 59th ed.

k Sutton, L. E., *Tables of Interatomic Distances*, Chemical Society, London, (1958) p. 11.

l Davies, G. J., and Evans, M. W., *J. Chem. Soc. Faraday Trans. II*, **72**, 1194 (1976).

m Rudolph, H. D., Walzer, K., and Krurtzig, L., *J. Mol. Spectrosc.* **47**, 314 (1973).

n Trotter, J., *Acta Cryst.* **12**, 884 (1959).

o Lister, D. G., Taylor, J. K., Hoeg, J. M., and Larsen, W., *J. Mol. Struct.* **23**, 253 (1974).

p Sutter, D. and Flygare, W., *J. Am. Chem. Soc.* **91**, 6895 (1969).

q Bak, B., Christensen, D., Dixon, W., Hansen-Nygaard, L., Rastrup-Anderson, J., and Schottlander, M., *J. Mol. Spectrosc.* **9**, 124 (1962).

r Bak, B., Christensen, D., Hansen-Nygaard, L., and Rastrup-Anderson, J., *J. Mol. Spectrosc.* **7**, 58 (1961).

s Rao, V. M., and Kewley, R., *Can. J. Chem.* **50**, 1690 (1972).

t Kewley, R., *Can. J. Chem.* **50**, 1690 (1972).

u Buckley, P. J., *J. Chem. Soc. Chem. Commun.* **1968**, 668.

v Slone, J. J. and Kewley, R., *Can. J. Chem.* **47**, 3453 (1969).

w Pellicia-Galland, F., *C. R. Acad. Sci.* **277c**, 137 (1973).

x Aroney, N. J., and LeFevre, R. J. W., *J. Chem. Soc.* **1958**, 3002.

y Rao, M. and Narayanaswany, E. N., *Z. Phys. Chem.* **26B**, 23 (1934).

z Eyster, J. M. and Prohofsky, E. W., *Spectrochim. Acta* **30a**, 2041 (1974).

aa Marchal, J. P., Bonnet, P., and Barriol, J., *J. Chim. Phys.* **71**, 1285 (1974).

bb Cumper, C. and Vogel, A., *J. Chem. Soc.* **1959**, 3521.

cc Lafferty, W., Robinson, B., St Louis, R., Russe, J., and Strauss, L., *J. Chem. Phys.* **42**, 2915 (1965).

dd Greenhouse, J. A. and Strauss, H. L., *J. Chem. Phys.* **50** 124 (1969).

ee Hiderbront, R. L. and Weiser, J. D., *J. Chem. Phys.* **56**, 1142 (1972).

ff Lassier, R. and Brot, C., *Chim. Phys.* **65**, 1723 (1968).

gg Evans, M., *Spectrochim. Acta* **31A**, 609 (1975).

hh Evans, M. W., *Spectrochim. Acta*, **30A**, 79 (1974).

ii Davies, G. J., Evans, G. J., and Evans, M. W., *J. Chem. Soc. Faraday Trans. II*, **72**, 1901 (1976).

jj Reid, C. J., M.Sc. Thesis, University of Wales (1977).

kk *Handbook of Physics and Chemistry*, Chemical Rubber Company, 61st ed.

ll Datta, P. and Barrow, G. M., *J. Chem. Phys.*, **43**, 2137 (1965).

mm *Ibid.*, **48**, 4662 (1968).

nn van Aalst, R. M. and van der Elsken, J., *Chem. Phys. Lett.* **13**, 631 (1972).

oo Morita, A., Walker, S., and Calderwood, J. H., *J. Phys. D* **9**, 2485 (1976).

pp Birnbaum, G. and Ho, W., *Chem. Phys. Lett.* **5**, 334 (1970).

qq Evans, G. J., Wegdam, G., and Evans, M. W., *Chem. Phys. Lett.* **42**, 331 (1976).

rr Evans, M. W., *J. Chem. Soc. Faraday Trans. II*, **72**, 2138 (1976).

ss Birnbaum, G., *Mol. Phys.*, **25**, 241 (1973).

tt Gordon, R. G., *J. Chem. Phys.* **44**, 1830 (1966).

uu Bulkin, B. J., *Helv. Chim. Acta.* **52**, 1348 (1962).

vv *N.B.S. Circ.* 501 (1957).

ww Crossley, J. and Hassel, W., *Can J. Chem.* **46**, 218 (1969).

xx *Dielectrics*, 29 (1970).

yy Tucker, S. and Walker, S., *Trans. Faraday Soc.*, **62**, 2690 (1966).

zz Hassel, W. F. and Walker, S., *Trans. Faraday Soc.*, **62**, 861 (1966).

aaa Grubb, E. and Smyth, C. P., *J. Am. Chem. Soc.*, **83**, 4122 (1961).

bbb Hindle, P., Walker, S., and Warren, J., *J. Chem. Phys.* **62**, 3230 (1975).

TEXT REFERENCES

Calderwood, J. H. and Coffey, W. T., *Proc. R. Soc. A* **356**, 269 (1977).

Chamberlain, J., *The Principles of Interferometric Spectroscopy*, Wiley, New York (1977).

Coffey, W. T., Pearce, J. G., and Calderwood, J. H., *Adv. Mol. Rel. Int. Proc.*, **20**, 27 (1981).

Evans, M. W., *Spectrochim. Acta*, **31A**, 609 (1975).

Evans, M. W., *Mol. Phys.* **29**, 1345 (1975).

Evans, M. W., *Chem. Phys. Lett.* **39**, 601 (1976).

Evans, M. W. and Reid, C. J., *J. Chem. Soc. Faraday Trans. II*, **76**, 286 (1980).

Ewing, G. E., *Acc. Chem. Res.* **2**, 168 (1969).

Ford, G. W., Lewis, J. T., and McConnell, J., *Proc. R. Ir. Acad.* **76**, 122 (1976).

Gordon, R. G., *J. Chem. Phys.*, **43**, 1307 (1965).

Hill, N., Vaughan, W., Price, A., and Davies, M., *Dielectric Properties and Molecular Behaviour*, Van Nostrand, Princeton, N. J. (1969).

Kilpatrick, J. E., Pitzer, K. S., and Pitzer, R., *J. Am. Chem. Soc.* **69**, 2483 (1947).

Pardoe, G. W. F., Ph.D. Thesis, University of Wales (1969).

Reid, C., Ph.D. Thesis, University of Wales (1979).

Reid, C. J. and Evans, M. W., *Mol. Phys.*, **40**, 1357 (1980).

Reid, C. J., *Chem. Phys. Lett.*, **66**, 517 (1979a).

Rocard, M., *J. Phys. Radium* **4**, 247 (1933).

Steele, W. A., *Adv. Chem. Phys.* **34**, 1 (1976).

5

The Interaction of Rotation with Translation

LIST OF SYMBOLS

α_l, α_ω, α_v	Constants in the hydrodynamic (long time) tail behavior of some simulated autocorrelation functions
$C_u(t)$	Single particle autocorrelation function of orientation
$C_M(t)$	Multiparticle equivalent
d	Dimensionality
D	Self-diffusion coefficient
γ	Friction supermatrix
G	Rigidity modulus
$\mathbf{G}$	Force/torque tensor
I	Molecular moment of inertia
κ	Loading parameter
$\hat{\mathscr{L}}_0$	Ideal gas Liouville operator
m	Molecular mass
n	Number density
ν	Kinematic shear viscosity
P_l	Legendre polynomial of order l
q	Particle charge
ρ	Fluid density
σ_k^{xz}	Component of the microscopic stress tensor
τ	Time between collisions
$\hat{T}_{21}$	Collision operator of rototranslational motion
$\mathbf{v}_a$	Resultant atomic velocity of a diatomic molecule
$\boldsymbol{\omega}$	Molecular angular velocity vector
ω_p	Plasma frequency
$\zeta(s)$	Memory function in s space
ζ_R	Rotational friction coefficient

The orientational a.c.f.'s $C_u(t)$ and $C_M(t)$ are constructed by averaging over an ensemble of molecules whose dipole unit vectors $\mathbf{u}$ depend on the mutual interaction of rotation and translation, on both macroscopic and molecular levels. If the rotation of a labeled molecule is to set up a vortex in the surrounding ensemble (as was intimated in Chapter 3), the outer

molecules of the vortex must be translating in a coherent fashion; there is a marked degree of correlation between molecular center of mass linear velocities. This leads to the molecular dynamics results simulated in Fig. 1.2.1. The exponential behavior of the angular velocity a.c.f. is replaced by one which goes roughly as $t^{-5/2}$. The more elongated the rotating molecule, the more pronounced is the deviation from logarithmic decay. A simulation such as that shown in Fig. 5.1 illustrates this fairly clearly. There are tails of this nature in the linear and angular velocity a.c.f.'s and in the orientational a.c.f. $\langle \mathbf{u}(t)\cdot\mathbf{u}(0)\rangle$.

In this area the hydrodynamic approach has proved to be revealing when used in combination with the results of molecular scale computer simulations. The consequences of the long time tails in 0–THz low frequency spectroscopy have hardly been explored, but in Chapter 7, which deals with the behavior of viscous liquids and glasses, we shall see that the macroscopic viscosity has an enormous effect on the characteristics of the

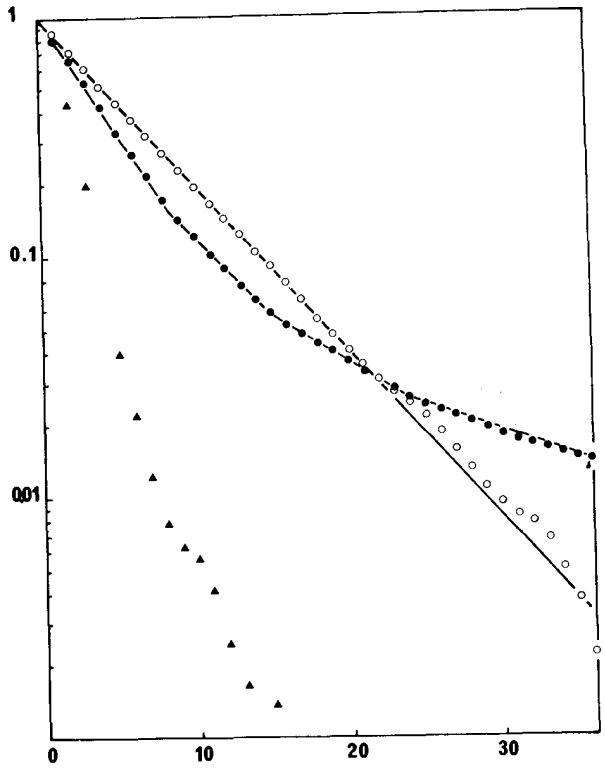

Figure 5.1 Semilogarithmic plot of ▲ the orientational a.c.f., ● the velocity a.c.f., and ○ the angular velocity a.c.f. from a molecular dynamics simulation of a two-dimensional system of 1600 diatomic molecules with periodic boundary conditions, atom–atom potential. [Reproduced by permission from G. S. Tresser et al., *J. Phys.* **38**, 267L (1977).

low frequency dielectric loss. Low frequency dielectric spectroscopy provides us in principle with a photographic "enlargement" of the nature of these tails. Berne (1976) has pointed out the attempts made to apply hydrodynamic modeling on the molecular level to account for observations such as illustrated in Figs. 1.2.1 and 5.1. From generalized hydrodynamics the normalized angular velocity correlation function $\langle \boldsymbol{\omega}(t)\cdot\boldsymbol{\omega}(0)\rangle/\langle\omega^2\rangle$ has been shown by Ailawadi and Berne (1976) to decay asymptotically as

$$C_\omega(t) = \frac{d\pi I}{2mn}[4\pi(D+\nu)]^{-(d+2)/2}t^{-(d+2)/2} \tag{5.1}$$

where I, m, n, ν, D, and d are respectively the molecular moment of inertia, molecular mass, number density, kinematic shear viscosity ($\nu = \eta/mn$), self-diffusion coefficient, and dimensionality of the system. For planar motion $d = 2$ and in space $d = 3$. It follows that the orientational correlation functions,

$$C_l(t) \equiv \langle P_l[\mathbf{u}(t)\cdot\mathbf{u}(0)]\rangle$$

also behave asymptotically as $t^{-(d+2)/2}$, if we take account of the effect of molecular translation on rotation. If we use the simple relation for planar movement (holding only when ω is a Gaussian r.v.)

$$\langle \mathbf{u}(t)\cdot\mathbf{u}(0)\rangle = \exp\left[-\frac{kT}{I}\int_0^t (t-\tau)\langle\omega(\tau)\omega(0)\rangle d\tau\right]$$

(Chapter 2), then, in two dimensions (if ω is Gaussian)

$$\langle\omega(t)\omega(0)\rangle \propto t^{-2}$$

in the region of interest. The asymptotic behavior of $C_l(t)$ was calculated from the "hydrodynamic equations" used to describe a feature of depolarized light scattering called "the shear doublet" observable at low frequency. We shall return to this later, but in Section 5.1 we consider the implications of the long time tail on dielectric spectroscopy at low frequencies, especially in viscous media, which can support very long-lived vortex phenomena.

5.1 LONG TIME TAILS

By simulating the function $C_u(t) = \langle \mathbf{u}(t)\cdot\mathbf{u}(0)\rangle$ using computer molecular dynamics, it is possible to pinpoint deviations from the Debye-like exponential decay at long times. Figure 5.1.1 is a plot of $C_u(t)$ against $1/t^2$ for a two-dimensional system of 1296 ellipsoidal particles arranged in a plane. This is the work of Berne and Nady (1976), each pair of ellipses interacting according to a Lennard–Jones 12-6 potential, with parameters ϵ and σ which are noncentral, that is, dependent on the relative orientations of the ellipses. The results show clearly that at long enough times after the

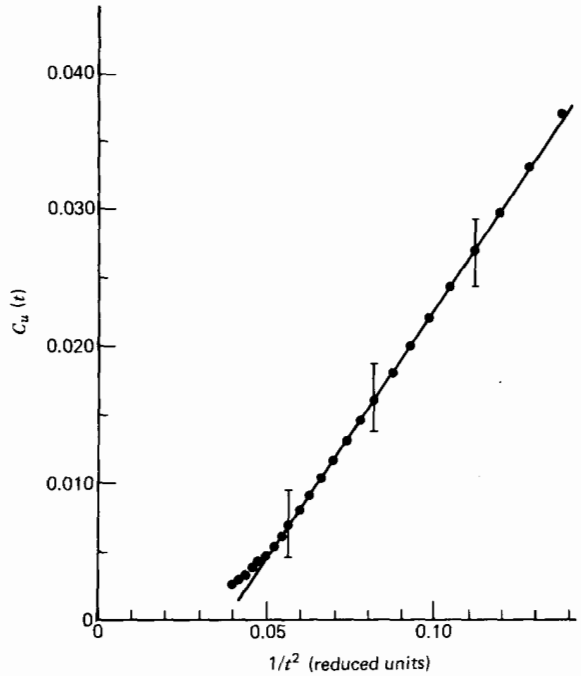

Figure 5.1.1 Orientational correlation function $C_u(t)$ from a simulation of 1296 Lennard–Jones ellipses in a plane; long time t^{-2} dependence. [Reproduced by permission from B. J. Berne, *Faraday Symposium No. 11* (1976).]

arbitrary initial time $t = 0$

$$C_u(t) = \alpha_1 t^{-2}$$

(or $\rightarrow \alpha_1 t^{-2}$ asymptotically). Figure 5.1.2 from the same simulation shows that the angular velocity a.c.f. behaves similarly at t^{-2}; that is,

$$C_\omega(t) = \alpha_\omega t^{-2}$$

The theoretical value of the constant α_ω as estimated from hydrodynamic theory (e.g., Eq. 5.1) is two orders of magnitude smaller than the simulated α_ω. This implies that the angular velocity long time tail is much longer than that expected on the basis of the hydrodynamic theory. This means in turn that the vortex motion set up by the rotating reference molecule is more effective in determining the decay of the angular velocity a.c.f. itself. This result is corroborated by similar simulations in hard disks. In contrast the constant α_v, defined for the linear velocity a.c.f.,

$$C_v(t) \rightarrow \alpha_v t^{-1}$$

agrees well with the kinetic theory.

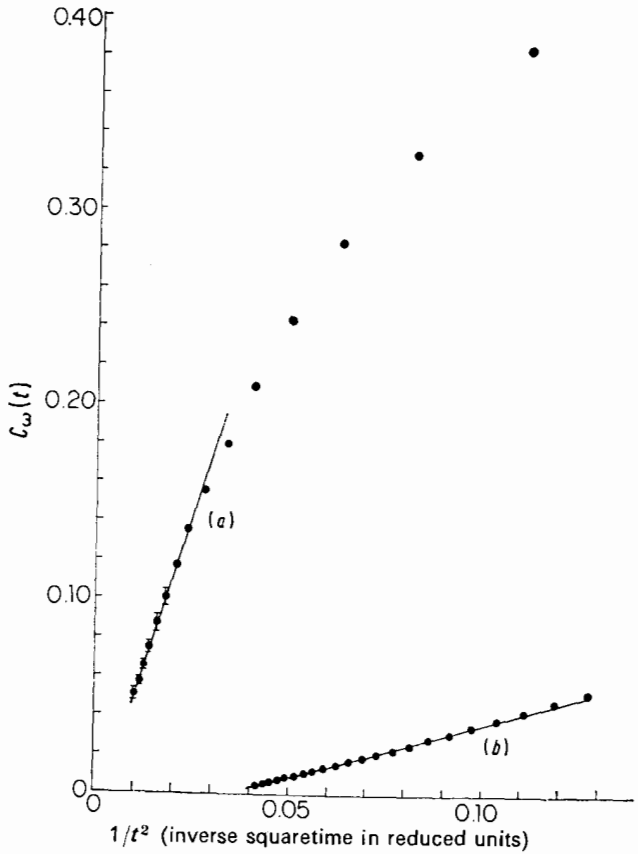

Figure 5.1.2 Dependence of the t^{-2} tail in the angular velocity a.c.f. on molecular anisotropy. The longer the ellipsoid (curve *b*), the earlier seems to be the onset. Reproduced by permission from B. J. Berne, *Faraday Symposium No. 11* 1976).]

As $t \rightarrow \infty$, however, the plot of $C_\omega(t)$ against t^{-2} does not extrapolate to zero, which is a result of the periodic boundary conditions imposed in the simulation. These give rise to the so-called sound kink due to an artificial recurrence in the longitudinal velocity, and also imply that $C_\omega(t)$ should decay faster in a periodic system than in the real infinite system. The advent of newer and much more powerful computers should enable this type of problem to be investigated with many more molecules than used at present. However, simulations from different sources and with different potentials have proved conclusively the existence of these tails in the simplest of molecular fluids, at relatively low viscosities. In more viscous liquids nonexponential tails should be more pronounced, and in our opinion have already been studied under a different guise as the (α, β) processes of the viscous liquid dielectric loss, which is treated at length in Chapter 7. To open this chapter we give a rough preliminary treatment of the effect these

time dependencies would have on the dielectric permittivity, as calculated in the absence of an internal field correction through Eq. 3.1.1.5.

To recover the dielectric spectrum from Eq. 5.1 requires a Laplace transform, followed by a replacement of the Laplace variable s by $i\omega$, where ω is the frequency. If $C_u(t)$ is an exponential, then

$$\frac{\epsilon(\omega)-\epsilon_\infty}{\epsilon_s-\epsilon_\infty}=\frac{1}{1+i\omega\tau} \tag{5.1.1}$$

in the simplest of cases where the internal field is neglected. The experimental low frequency dispersion and absorption curves in viscous liquids do not obey Eq. 5.1.1 but rather an empirical relation

$$\frac{\epsilon(\omega)-\epsilon_\infty}{\epsilon_s-\epsilon_\infty}=(1+i\omega t)^{-\beta} \qquad (0<\beta\leq 1)$$

or an alternative,

$$C_u(t)=\exp\left[-\left(\frac{t}{\tau_1}\right)^{\bar{\beta}}\right]$$

where $\bar{\beta}$ is a factor introduced by Williams and Watts (1970). We note that the Williams–Watts factor $\bar{\beta}$ is defined such that $0<\bar{\beta}\leq 1$ and has found successful application in *o*-terphenyl solutions and for solid polymers where the α process (or long time tail) is also clearly discernible with the appropriate dielectric apparatus. From the point of view of the theory of dielectrics, the effect of the viscous medium is to skew the Cole–Cole plot and broaden the dielectric loss, as illustrated in Fig. 5.1.3 for poly(ethylene terephthalate) and in Fig. 5.1.4, where $\bar{\beta}=0.50$ for benzophenone, 0.475 for cyclohexanone, and 0.45 for fenchone in supercooled *o*-terphenyl. This is the so-called α process which accounts for about one-half of the total dispersion (i.e., there is some relaxation process taking place at high frequencies). The *o*-terphenyl solute is geometrically rather flat so that a type of shearing leading to a modification of Eq. 5.1 would not be out of place. Note that the long time α process appears as a very broad, asymmetric loss curve in the hertz to kilohertz frequency range. Note also (Fig. 1.2.8) that the α process is only the long time part of the total $C_u(t)$ or total dielectric dispersion, which involves the β and γ processes (Chapter 7). These are essentially noncooperative in nature and correspond to the short time oscillations (Fig. 5.1) of the simulated $C_u(t)$.

The α and β processes fuse as the viscosity decreases to its value at ambient temperature (some orders of magnitude smaller than that in the supercooled solution) and the broadening in the loss curve is hardly discernible within the experimental uncertainty. Therefore multidecade dielectric spectroscopy of this nature is a beautiful and powerful way of studying mode–mode coupling as embodied in shearing and viscosity. Up to now, however, most attention has been focused on the zero-frequency splitting of depolarized light scattering, a technique that to date has neither the range nor the accuracy of dielectric spectroscopy.

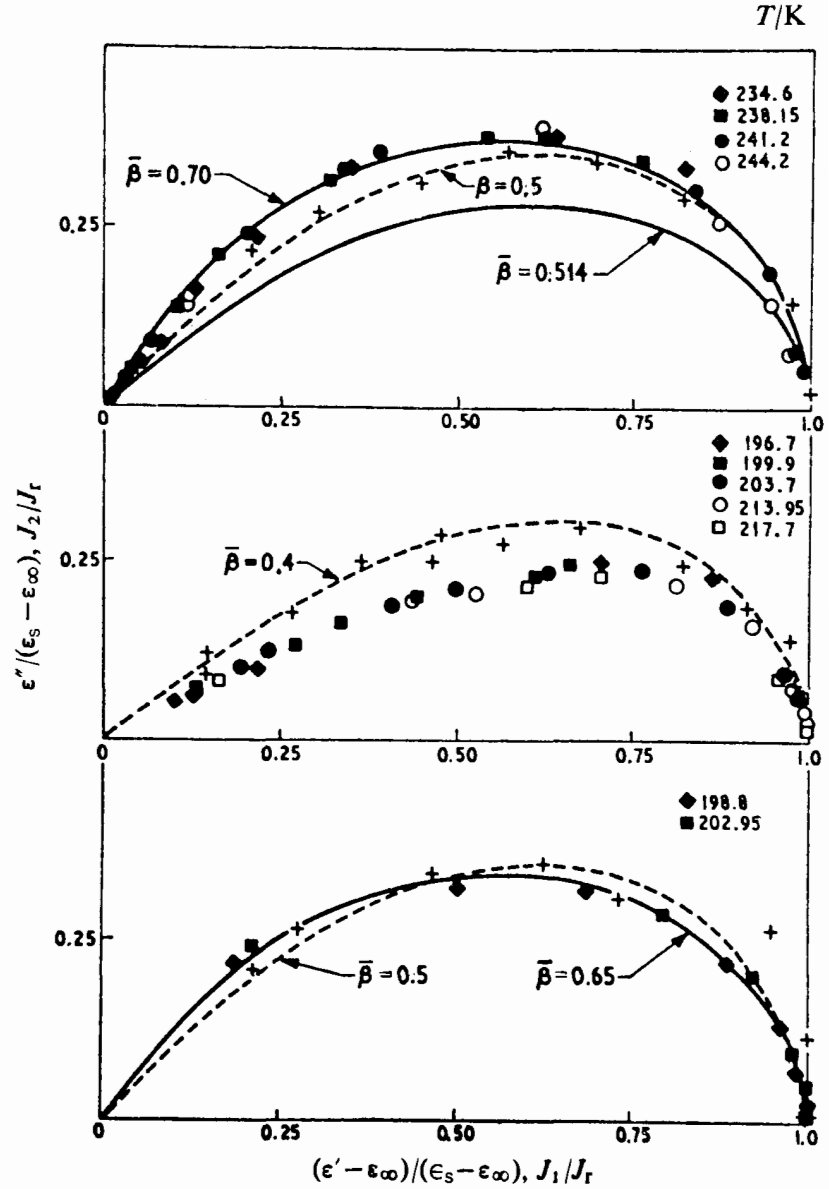

Figure 5.1.3 Comparison of dielectric relaxation data and viscoelastic retardation data at different temperatures for (*a*) tri-*O*-tolyl phosphate, (*b*) tri-2-chloroethyl phosphate, and (*c*) di-*n*-butyl phthalate. Points + are viscoelastic compliance data of Barlow and Erginsav. The dielectric data for tri-*O*-tolyl phosphate and di-*n*-butyl phthalate are fitted by the solid curves based upon the Williams–Watts distribution functions. The viscoelastic data are fitted by the Davidson–Cole equation shown by the dashed curves. The Williams–Watts curve for $\bar{\beta}=0.514$ is that which gives agreement with a stress relaxation function, based upon a defect-diffusion model (see Chapter 7). [Reproduced by permission from M. Shears et al., *J. Chem. Soc. Faraday Trans. II*, **1974**, 1783.]

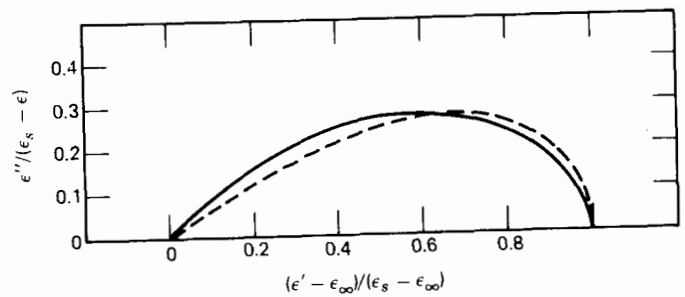

Figure 5.1.4 The α process for polyethyl acrylate at different pressures, fitted with a Williams–Watts function (solid line) and Davidson–Cole function (dashed line). [Reproduced by permission from G. Williams et al., *Trans. Faraday Soc.* **66**, 80 (1970).]

In Fig. 5.1.5 we plot the Williams–Watts function and $t^{-5/2}$ tail in $C_u(t)$. At short times the latter form is invalid but the asymptotic behavior of $\exp[-(t/\tau)^{1/2}]$, for example, is very nearly that of the hydrodynamic function. If the $t^{-5/2}$ tail in $C_u(t)$ were properly extrapolated to the origin (using a technique discussed below) the empirical and hydrodynamic functions would behave very similarly. The broad α process appearing at low frequency can therefore be described in terms of the hydrodynamic mechanism which gives rise to this type of $C_u(t)$ function. The theory is

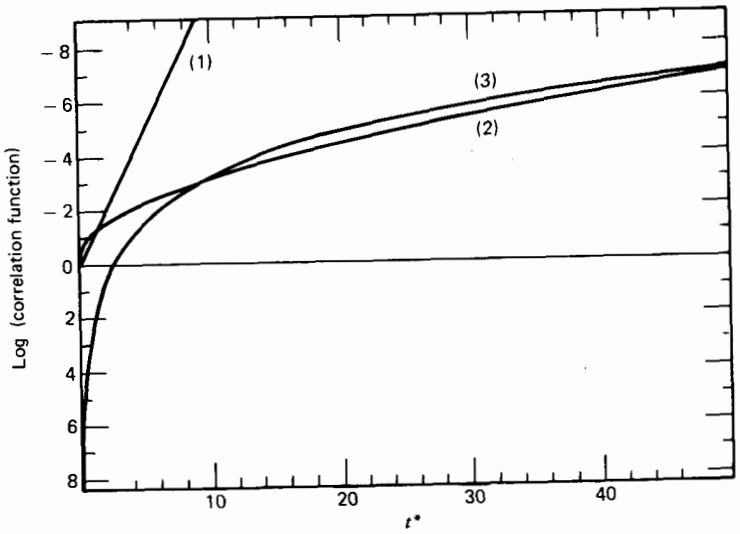

Figure 5.1.5 Comparison of the $t^{-5/2}$ tail and the Williams–Watts function at very long times. Note that the extrapolation of the $t^{-5/2}$ tail back to the $t = 0$ axis is physically meaningless. Both curves are compared with an exponential decay. (1) Exponential, (2) $\exp(-t^{*1/2})$, and (3) $A/t^{*5/2}$, where $t^* = t/\tau$.

oversimplified, and crude, however, depending as it does on the motion of spheres in a viscoelastic medium, but it has several attractive features which could be elaborated upon to produce all three α, β, and γ loss peaks observable over the complete 0–THz range of about 12 decades (see Fig. 1.2.8). However, Eq. 5.1 for the angular velocity shows that the greater the value of ν, the kinematic shear viscosity, the less pronounced is the effect of the tail; that is, the more able is the highly viscous medium to support shearing in the liquid phase, but the less able to propagate a vortex which is long-lived. In Chapter 7 we discuss the many theories formulated to explain the equivalent manifestation in depolarized light scattering spectroscopy—the splitting of the intensity spectrum [roughly $\epsilon''(\omega)/\omega$] around $\omega = 0$. All these theories are transferable to 0–THz spectroscopy.

5.1.1 Viscoelastic Theory of the Angular Velocity Autocorrelation Function

This is a means by which the $t^{-5/2}$ asymptotic behavior in the angular velocity a.c.f. may be derived from the use of viscosity as an interpretation of the memory function, and is the work of Berne and Montgomery (1976). The theory essentially depends on regarding the friction coefficient of the Langevin equation, for example, in terms of the viscosity of the surrounding medium. There is nothing new in this but it is a remarkable fact that the interpretation in terms of the hydrodynamic Navier–Stokes equation of the incompressible viscous medium (continuum fluid) works very well, or seems to do so, at the molecular level. Alder and Wainright (1958) have shown by the use of computer simulation of the motion of smooth spheres that the computed translational friction coefficient is precisely the Stokes result $4\pi\eta a$, where η is the shear viscosity and a is the sphere radius. The application of the hydrodynamic theory to light scattering is discussed at length by Berne and Pecora (1976), and also by McDonald and Hansen (1976).

The Navier–Stokes equation is built up on the principles of conservation of mass, momentum, and energy, together with some simplifying, linearizing assumptions. If this equation is solved for a rotating sphere for the hydrodynamic drag upon it when executing rotational oscillations in a compressible viscoelastic (frequency-dependent) fluid, it follows that for "stick" boundary conditions (corresponding to transfer of angular momentum), the frequency-dependent rotational friction coefficient is given by

$$\tilde{\zeta}(s) = \zeta_R \left[1 + \frac{\alpha^2 s}{3(1 + \alpha\sqrt{s})} \right]$$

where α^2 is the time required for transverse momentum to diffuse a distance equal to the radius of the sphere. This is $\alpha^2 = \rho_s R^2/\eta$ where ρ_s is the fluid density and η is related to the static rotational friction coefficient ζ_R by $\zeta_R = 8\pi\eta R^3$, where R is the radius of the sphere. We have seen in Chapters 1 and 2 that the normalized angular velocity a.c.f. may be written

as

$$\tilde{C}_\omega(s) = \frac{1}{s + \zeta(s)/I}$$

where $\zeta(s)$ is the memory function.

A loading parameter κ may be defined for rotating spheres by $\kappa = I/mR^2$, where I is the moment of inertia and m is the mass of the sphere. The parameter κ measures the rotational inertia and varies between $\kappa = 0$ and $\frac{2}{3}$ depending on whether the mass is completely concentrated in the center or entirely at the surface. Using this we may define a parameter λ, which embodies the effects of both buoyancy (in the hydrodynamic fluid) and inertia, so that $\lambda = \kappa\rho/\rho_s$, where ρ/ρ_s is the mass density of the sphere relative to ρ_s, the mass density of the fluid. With these definitions,

$$\tilde{C}(s) = (1 + s^{1/2}) \Big/ \left[s^{3/2} + \left[\left(\lambda + \frac{2}{\lambda} \right) s + \left(\frac{6}{\lambda} \right) s^{1/2} + \frac{6}{\lambda} \right] \right] \qquad (5.1.1.1)$$

where $s(\equiv s\alpha^2)$ is measured in units of α^{-2}. This may be written

$$\tilde{C}(s) = \frac{1 + s^{1/2}}{(s^{1/2} + a)(s^{1/2} + b)(s^{1/2} + b^*)}$$

where $-a$, $-b$, and b^* are the roots of the cubic equation

$$x^3 + \left(\frac{\lambda + 2}{\lambda} \right) x^2 + \frac{6x}{\lambda} + \frac{6}{\lambda} = 0$$

The angular velocity a.c.f. is now

$$C_\omega(t) = \frac{a(a-1)}{(b-a)(b^*-a)} \exp(a^2 t) \operatorname{erfc}(a\sqrt{t}) + \frac{2 \operatorname{Re} b(b-1)}{(b-b^*)(b-a)} \exp(b^2 t) \operatorname{erfc}(b\sqrt{t}) \qquad (5.1.1.2)$$

where erfc is the complementary error function. As $t \to \infty$ this equation reduces to

$$C(t) \to \frac{\lambda t^{-5/2}}{24\sqrt{\pi}}$$

(remember that t is now dimensionless, being in units of α^2, which depends on the viscosity λ).

If now the memory function $\eta(s)$ is given a frequency dependence, then the concept of viscoelasticity may be introduced in a rational manner. If, for example, we choose to close the Mori continued fraction by $\eta(s) = \eta/(1 + \gamma s)$, where γ is the viscoelastic relaxation time (in units of α^2), then

$$C_\omega(s) = \frac{\lambda(1 + \gamma s)(1 + \sqrt{A})}{\lambda A^{3/2} + (\lambda + 2)A + 6A^{1/2} + 6} \qquad (5.1.1.3)$$

where $A = s(1 + \gamma s)$. Equation 5.1.1.3 may be inverted analytically to give

the result

$$C_\omega(t) = \left(\frac{1 - (1 + 4\gamma a^2)^{1/2}}{(1 + 4\gamma a^2)^{1/2}} \right) \exp\left(- \frac{1 + (1 + 4\gamma a^2)^{1/2} t}{2\gamma} \right) + 2 \operatorname{Re} \left(\frac{1 - (1 + 4\gamma b^2)^{1/2}}{(1 + 4\gamma b^2)^{1/2}} \right) \exp\left(- \frac{1 + (1 + 4\gamma b^2)^{1/2}}{2\gamma} t \right) + \frac{2\lambda}{\pi} \int_0^{1/\gamma} \frac{e^{-xt}(1 - \gamma x)[x(1 - \gamma x)]^{3/2}\, dx}{[6 - (\lambda + 2)x(1 - \gamma x)^2 + x(1 - \gamma x)[6 - \lambda x(1 - \gamma x)]^2}$$

which again reduces to the $t^{-5/2}$ tail as $t \to \infty$. The function $C_u(t)$ is related to $C_\omega(t)$ as in Chapter 2, and it may be verified that the former also decays as $t^{-5/2}$ as $t \to \infty$. For $t \ll 1$:

$$C_\omega(t) \to 1 - \frac{2}{\lambda\sqrt{\gamma}} t + O(t^2) \qquad (5.1.1.5)$$

which is linear in t and therefore violates the classical laws governing the behavior of $C_\omega(t)$. This is characteristic of "hard" systems, that is, where the dispersion and electrostatic part of the potential is neglected (see, for example, Fig. 1.2.1). If viscoelasticity is also neglected, then, for $t \ll 1$,

$$C_\omega(t) \to 1 - \frac{4}{\lambda\sqrt{\pi}} \sqrt{t} + O(t)$$

which is a faster decay than an exponential and which has an infinite slope at $t \to 0$.

The initial decay of the angular velocity a.c.f. is governed by molecular encounters, which may be approximated by binary collisions between rough spheres. This kind of fluid may be treated exactly, from which it follows that an equation such as Eq. 5.1.1.5 is expected at short times. [Note that the initial linear decay can be avoided (e.g., Chapter 4) by encaging the inner disk by a ring. Only the rings interact.] The two free parameters (the viscosity and viscoelastic relaxation time) may now be determined, and also the parameter that characterizes the viscosity in the rough sphere fluid. There is a good agreement between the exact and viscosity results for the elastic parameter γ but not for the viscosity parameter of the exact (Enskog) theory. This is hardly surprising since we are comparing directly two theories which represent the opposite poles of the theoretical approaches to liquid state dynamics, the viscoelastic theory being essentially an elaboration of the Langevin equation where the friction coefficient is treated in depth, the hard collision theory being essentially adopted from the kinetic theory of gases. Neither is asymptotically correct for $t \ll 1$. The interest of the viscoelastic approach lies in the behavior at long times (Fig. 5.1.6, where the complete evolution of $C_\omega(t)$ of the viscoelastic theory is plotted). Clearly a theory is needed whereby $C_u(t)$ of Eq. 3.1.1.5 is related directly to the long time hydrodynamic tail. Only then does it become possible, although extremely laborious, to obtain

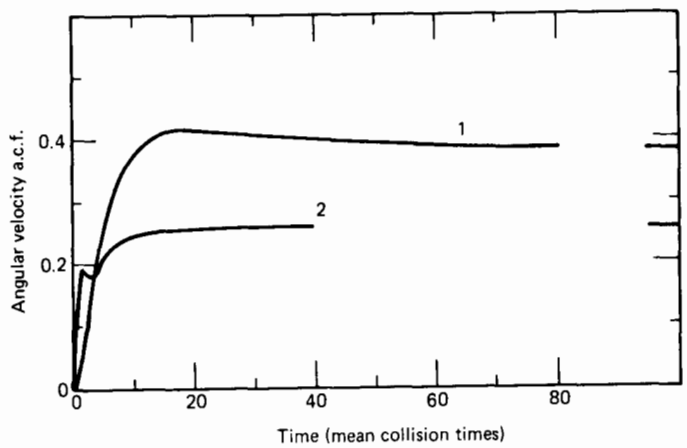

Figure 5.1.6 Dependence of the angular velocity and linear velocity a.c.f.'s, calculated from viscoelastic theory. (1) Angular velocity a.c.f. $\times 10 \times t^{5/2}$. (2) Linear velocity a.c.f. $\times t^{3/2}$. [Reproduced by permission from B. J. Berne and J. A. Montgomery, *J. Chem. Phys.* **66**, 2161 (1977).]

an expression for the empirical Williams–Watts function using Eq. 5.1.1.4 and the purely kinematic relation between $C_u(t)$ and $C_\omega(t)$.

Using the complex number identities

$$s^{1/2} = \left(\frac{\omega}{2}\right)^{1/2}(1-i)$$

and

$$(1+\gamma s)^{1/2} = \{\tfrac{1}{2}[1+(1+\omega^2\gamma^2)^{1/2}]\}^{1/2} - i\{\tfrac{1}{2}[(1+\omega^2\gamma^2)^{1/2}-1]\}^{1/2}$$

it may be seen that the spectrum corresponding to Eq. 5.1.1.3 is far from Lorentzian. In the absence of viscoelastic effects the asymptotic low frequency falloff of the dielectric loss is

$$\hat{\mathcal{J}}\{-i\omega + 2D_r[1+\sqrt{2}\lambda^3 i(i\omega)^{3/2}]\}$$

where D_r is the rotational diffusion coefficient $[kT/(8\pi\eta a^3)]$ and $\lambda = [a^2\rho/(2\eta)]^{1/2}$. As $\omega \to 0$ (i.e., as $t \to \infty$), the dielectric loss decays as

$$\epsilon''(\omega) = \frac{\omega + \sqrt{2}/2\lambda^3\omega^{3/2}l(l+1)D_r}{\left(\omega + \frac{\sqrt{2}}{2}\lambda^3\omega^{3/2}l(l+1)D_r\right)^2 + l^2(l+1)^2D_r^2\left(1-\frac{\sqrt{2}}{2}\lambda^3\omega^{3/2}\right)^2}$$

where $l = 1$. This is again markedly different from Lorentzian behavior. Note that in the case where the α, β, and γ processes of the viscous liquid dielectric loss are present, the major feature of the dielectric frequency dependence of $\epsilon''(\omega)$ is well removed from the value $l(l+1)D_R$, and is found at regions corresponding to the $t^{-5/2}$ tail in $C_u(t)$.

The importance of the long time tail in the context of rotation/translation interaction is that it represents the coupling of the molecular angular momentum to the transverse velocity fluctuations or shear modes of the liquid. As the latter becomes more and more viscous, the tail becomes predominant so that the whole decay of the orientational a.c.f. is dominated by the low frequency process, owing to the fact that $C_u(t)$ is essentially the Fourier transform of $\epsilon''(\omega)/\omega$. The α process may sometimes decay on the time scale of years as the viscous liquid gives way to the glassy state. Such a process may only be cooperative (on the molecular scale) and in the viscoelastic model depends only on the ratio of the density of the sphere (or particle) to that of the surrounding medium. In a liquid or gas consisting of polyatomic molecules, the angular momentum associated with each molecule can be decomposed into two parts: an orbital part, representing the angular momentum due to the motion of the molecular center of mass about an origin fixed in the laboratory frame, and an intrinsic part, representing the angular momentum of the molecule about its own center of mass. The latter is what we have been concerned with in Chapters 1–3. If a molecule is given an initial intrinsic angular momentum, this will decay, but since the total angular momentum (orbital plus intrinsic) is conserved, it follows that the orbital part must grow. The orbital angular momentum is a vortex field. The intrinsic angular momentum of a molecule rapidly comes to equilibrium with the vortex field which it creates. This vortex inevitably involves molecular translation. The long time tail in the orientational a.c.f. is therefore a direct measure of the extent of interaction between molecular rotation and translation. As the vortex field decays away slowly the intrinsic angular momentum persists for times that are very long compared with a period of free rotation.

5.1.2 Shear Waves and Viscoelasticity

If we define a current density of particles at a position $\mathbf{r}$ by

$$\mathbf{j}(\mathbf{r}, t) = \sum_{i=1}^{N} \mathbf{v}_i(t)\delta[\mathbf{r} - \mathbf{r}_i(t)] \tag{5.1.2.1}$$

where $\mathbf{v}_i$ is the velocity of the particle (in the simplest case an atom), this may be Fourier transformed to give the Fourier components

$$\mathbf{j}_\mathbf{k}(t) = \sum_{i=1}^{N} \mathbf{v}_i(t)\exp[-i\mathbf{k}\cdot\mathbf{r}_i(t)] \tag{5.1.2.2}$$

The meaning of the delta function $\delta[\mathbf{r} - \mathbf{r}_i(t)]$ is that the density of particles at a point $\mathbf{r}$ is given by

$$\rho(\mathbf{r}) = \sum_{i=1}^{N} \delta(\mathbf{r} - \mathbf{r}_i)$$

The quantity $\mathbf{k}$ has the units of inverse distance and is known as a wave

vector. It is convenient to define a longitudinal and transverse component of $\mathbf{k}$ parallel and perpendicular to $\mathbf{j}_{\mathbf{k}}(t)$. In atomic liquids, molecular dynamics calculations provide the only information on the transverse component, and show that at high wave numbers the liquid is capable of supporting shear waves which appear for values of $\mathbf{k}$ for which the rigidity of the liquid can no longer be neglected. The appearance of shear waves can be accounted for by incorporating viscoelastic concepts, as discussed in the previous section. The shear waves are analogous to transverse phonons in a crystal. The "frequency–dependent viscosity" or memory function used in Section 5.1.1 may be written in the form

$$\eta(\omega) = G\left(-i\omega + \frac{G}{\eta}\right)^{-1} \tag{5.1.2.3}$$

as used by McDonald and Hansen (1976) so that by relating $\eta(\omega)$ in a structured molecular fluid it is possible to obtain experimental information on the shearing processes. Qualitative description of the onset of shear waves (which are propagative) may be given in terms of an equation such as Eq. 5.1.2.3 (McDonald and Hansen, 1976). The constant η/G is the Maxwell relaxation time; the limit $\omega\tau_M \ll 1$ corresponds to the hydrodynamic description of Section 5.1.1, but when $\omega\tau_M \gg 1$ corresponds to solidlike propagation. Here G is a rigidity modulus.

The situation in molecular fluids is much more complex than that embodied in the simple viscoelastic (or memory function) approximation (Eq. 5.1.2.3), but it seems that shear waves in computer simulations of atomic liquids become effective at values of the wave vector $|\mathbf{k}|$ above a critical $\mathbf{k}_c$. For finite $\mathbf{k}$ Eq. 5.1.2.3 must be rewritten as

$$\eta(\mathbf{k}, \omega) = \frac{\beta}{v}\int_0^\infty \langle \sigma_{\mathbf{k}}^{xz}(t)\sigma_{-\mathbf{k}}^{xz}(0)\rangle \exp(i\omega t)\, dt$$

where β/v is a constant and $\sigma_{\mathbf{k}}^{xz}$ is the xz component of the microscopic stress tensor. In this limit $\mathbf{k}\to\mathbf{0}$ a long tail appears in the atomic velocity a.c.f. and the molecular angular velocity and velocity a.c.f.'s, as discussed in the previous section. The transverse current fluctuations at small wave vectors can be adequately represented only if a long tail is incorporated in the transverse current memory function $\phi_t(\mathbf{k}, t)$, which is identical with the stress a.c.f. (i.e., frequency–dependent shear viscosity) $\eta(\mathbf{k}, t)$ when $\mathbf{k}\to\mathbf{0}$, the hydrodynamic limit. In molecular liquids the stress tensor develops an antisymmetric part which can be traced directly to the coupling between rotation and translation. It follows then that the latter mechanism is also important for the description of the shear doublet observable in depolarized light scattering.

At this stage it is relevant to discuss the role of the wave vector $\mathbf{k}$ in a 0–THz spectrum. If for some reason this remains finite in such an experiment then the spectrum would be capable of giving us information of density fluctuations. If we deal with a Kirkwood correlation sphere containing a large number of molecules the relevant 0–THz correlation function is in fact (Lobo et al., 1973)

$$\frac{1}{k^2\mu^2}\left\langle \mathbf{k}\cdot\boldsymbol{\mu}_1(t)e^{i\mathbf{k}\cdot\mathbf{r}_1(t)}\sum_j \mathbf{k}\cdot\boldsymbol{\mu}_j(0)e^{-i\mathbf{k}\cdot\mathbf{r}_j(0)}\right\rangle \tag{5.1.2.4}$$

where the sums run over all the molecules within the Kirkwood sphere (Chapter 3) centered on $\mathbf{r}_1(0)$. The $\mathbf{k}\cdot\boldsymbol{\mu}$ signifies that it is the polarization charge density that responds to a scalar probe, not the polarization, as was tacitly assumed throughout Chapter 3. Reduction to the Kirkwood result is possibly only for $\mathbf{k}\to\mathbf{0}$, the hydrodynamic limit, where Eq. 5.1.2.4 reduces to the familiar Kirkwood factor

$$\frac{1}{3\mu^2}\langle \boldsymbol{\mu}_1(t)\cdot\sum_j \boldsymbol{\mu}_j(0)\rangle$$

of Chapter 3.

In a fluid made up of ions we may define a charge density via the Poisson equation (in c.g.s. units)

$$\nabla\cdot\mathbf{E} = 4\pi q\delta\rho$$

where q is the particle charge and $\mathbf{E}$ an external applied field. A term proportional to $\mathbf{E}(\mathbf{r}, t)$ must be added to the Navier–Stokes equation. When solved this leads directly to a plasma frequency

$$\omega_p^2 = \frac{4\pi\rho q^2}{m}$$

where m is the particle mass. The frequency of collective oscillations does not vanish as $|\mathbf{k}|\to 0$ in this case, but $\to\omega_p$. This collective oscillation in the ionic fluid is called the plasmon and may be simulated by molecular dynamics. If we substitute for the charge density the polarization charge density then it is clear that 0–THz spectroscopy with finite $\mathbf{k}$ leads to information on plasmons appearing, according to Lobo et al., in the far infrared. As in an ionic fluid the density fluctuations are dominated by the plasma oscillations. In some cases (e.g., molten salts) it is possible to separate and identify the fluctuations in density and those in charge density. The former determine sound wave propagation and the latter the plasmons, or plasma oscillations. These are liquid state analogues of the acoustic and optic longitudinal phonons in an ionic crystal. These show up in the far infrared for both ionic and molecular crystals, and have been identified, for example, by Wegdam and co-workers (1971) in $NaNO_2$. Obviously the plasmon frequency of polarization charge density fluctuations in a molecular liquid is the liquid–state analogue of the longitudinal optical phonon mode in the far infrared of the molecular crystal. Needless to say, all these propagative modes depend strongly on the mutual interaction of the translation and rotation of each individual molecule. The molecular crystal phonon modes are of course classifiable into those of translational origin and of rotational.

Summary

1. The appearance of the α, β, and γ loss processes in viscous molecular liquids cannot be explained purely by viscoelasticity, although there are certain resemblances between the empirical function of Williams and Watts (1970) and the $t^{-5/2}$ tail in $C_u(t)$ caused by the vorticity (or backflow) set up by a rotating reference molecule. The time scale of the α relaxation process is vastly different from that envisaged by the $t^{-5/2}$ effect, but is nevertheless cooperative in nature.
2. If 0–THz spectra were to be regarded in the light of polarization charge density $\mathbf{k}\cdot\boldsymbol{\mu}$, it follows that cooperative density fluctuations (the liquid state analogue of the molecular solid plasmon modes) would determine the band shape in the high frequency region. These are expected to be strongly dependent on translation/rotation interaction through, for example, an antisymmetric part of the microscopic stress tensor of structured (as opposed to atomic) centers of hydrodynamic flow.

5.2 TRANSLATION/ROTATION ON THE MOLECULAR SCALE

In this section we consider a simple example of the interaction between the rotational and translational dynamics of a diatomic molecule, this being one of the simplest cases (apart from the loaded rough sphere) in which this kind of interaction can occur.

5.2.1 Linear Diatomics

In this case let $\boldsymbol{\mu}$ denote a dipole of unit length; then the total velocity $\mathbf{v}_a$ of an atom is

$$\mathbf{v}_a = \mathbf{v} + \tfrac{1}{2}\boldsymbol{\omega}\times\boldsymbol{\mu} \tag{5.2.1.1}$$

where $\mathbf{v}$ denotes the center of mass velocity and $\boldsymbol{\omega}$ the angular velocity. Thus the a.c.f. of $\mathbf{v}_a$ contains information on both linear and angular velocities. The relation between the a.c.f.'s of $\mathbf{v}_a$ and $\mathbf{v}$ can easily be found if $\boldsymbol{\omega}$ is constrained to lie in a fixed direction, that is, planar rotation. In general, from Eq. 5.2.1.1,

$$\begin{aligned}\langle \mathbf{v}_a(t)\cdot\mathbf{v}_a(0)\rangle &= \langle \mathbf{v}(t)\cdot\mathbf{v}(0)\rangle + \langle \mathbf{v}(t)\cdot\boldsymbol{\omega}(0)\times\boldsymbol{\mu}(0)\rangle \\ &\quad + \tfrac{1}{4}\langle \boldsymbol{\mu}(t)\cdot\boldsymbol{\mu}(0)\boldsymbol{\omega}(t)\cdot\boldsymbol{\omega}(0)\rangle\end{aligned} \tag{5.2.1.2}$$

since

$$\langle \boldsymbol{\omega}(t)\times\boldsymbol{\mu}(t)\cdot\mathbf{v}(0)\rangle = \langle \mathbf{v}(t)\cdot\boldsymbol{\omega}(0)\times\boldsymbol{\mu}(0)\rangle$$

The central term on the right describes the effect of rotation/translation interaction and would vanish in a decoupled approximation, that is, if the two types of motion were to be describable separately. The third term vanishes in the limit $t\to\infty$. The functions $\langle \mathbf{v}(t)\cdot\mathbf{v}(0)\rangle$, $\langle \boldsymbol{\omega}(t)\cdot\boldsymbol{\omega}(0)\rangle$, and $\langle \boldsymbol{\mu}(t)\cdot\boldsymbol{\mu}(0)\rangle$ can be calculated from an itinerant oscillator/librator model, that is, a Mori three-variable theory with $\boldsymbol{\omega}$ fixed in direction. This may be extended fairly straightforwardly to calculate $\langle \boldsymbol{\mu}(t)\cdot\boldsymbol{\mu}(0)\boldsymbol{\omega}(t)\cdot\boldsymbol{\omega}(0)\rangle$, but an evaluation of the coupling term $\langle \mathbf{v}(t)\cdot\boldsymbol{\omega}(0)\times\boldsymbol{\mu}(0)\rangle$ would involve calculating in detail the collisional dynamics. Simulation is the best choice for this problem. In the decoupled approximation

$$\langle \mathbf{v}_a(t)\cdot\mathbf{v}_a(0)\rangle \doteq \langle \mathbf{v}(t)\cdot\mathbf{v}(0)\rangle + \tfrac{1}{4}\langle \boldsymbol{\mu}(t)\cdot\boldsymbol{\mu}(0)\boldsymbol{\omega}(t)\cdot\boldsymbol{\omega}(0)\rangle$$

The evaluation of $\langle \boldsymbol{\mu}(t)\cdot\boldsymbol{\mu}(0)\boldsymbol{\omega}(t)\cdot\boldsymbol{\omega}(0)\rangle$ provides us with an opportunity for illustrating the statistical principles of molecular dynamics, although it may be calculated more easily from the kinematic relation

$$\dot{\boldsymbol{\mu}} = \boldsymbol{\omega}\times\boldsymbol{\mu}$$

We leave this as an exercise for the interested reader.

Since $\boldsymbol{\mu}(t)\cdot\boldsymbol{\mu}(0) = \cos[\theta(t)-\theta(0)]$ where $\theta(t)$ denotes the angular orientation of the dipole at time t, the required correlation function is defined by

$$\begin{aligned}&\langle \boldsymbol{\mu}(t)\cdot\boldsymbol{\mu}(0)\boldsymbol{\omega}(t)\cdot\boldsymbol{\omega}(0)\rangle \\ &\quad = \int_{-\infty}^{\infty}\int_{-\infty}^{\infty}\int_{-\pi}^{\pi}\int_{-\pi}^{\pi} \omega\omega_0\cos(\theta-\theta_0) f(\omega,\theta;t\mid\omega_0,\theta_0) f(\omega_0,\theta_0)\,d\omega\,d\omega_0\,d\theta\,d\theta_0\end{aligned} \tag{5.2.1.3}$$

where $f(\omega,\theta;t\mid\omega_0,\theta_0)$ denotes the joint conditional probability function for $\omega(t)$ and $\theta(t)$ at time t, given that $\omega(0)=\omega_0$, $\theta(0)=\theta_0$, and $f(\omega_0,\theta_0)$ is the joint density for the initial distribution of ω and θ at time $t=0$. Since ω and θ are statistically independent variables and the initial distribution of ω may be assumed Maxwellian, we have

$$f(\omega_0,\theta_0) = \left(\frac{2\pi kT}{I}\right)^{-1/2}\exp\left[-\frac{\omega_0^2}{(2kT/I)}\right] f(\theta_0)$$

where the initial distribution $f(\theta_0)$ satisfies

$$\int_{-\pi}^{\pi} f(\theta_0)\,d\theta_0 = 1$$

but otherwise need not be specified for the present calculation. The problem is to specify the joint conditional density in Eq. 5.2.1.3 remembering that we are calculating the rotational motion in the laboratory frame. If $\theta(t)$ were the total angle swept out in time t then the joint conditional distribution could be taken as bivariate normal (see Chapter 1). Since $\theta(t)$ is restricted (Chapter 2) to the range $-\pi\leq\theta\leq\pi$, however, we require a cylindrical distribution whose marginal distribution is normal for ω and wrapped normal for θ. We achieve this by generalizing a well-known result in the theory of wrapped distributions (Evans et al., 1978). If x is a normally distributed random variable with mean $\langle x\rangle$ and variance $\sigma_x^2 =$

$\langle (x-\langle x\rangle)^2\rangle$ then the corresponding wrapped variate $\tilde{x} = x(\mathrm{mod}\, 2\pi)$ has a density

$$f(\tilde{x}) = \frac{1}{2\pi}\left[1 + 2\sum_{n=1}^{\infty}[\cos(n\langle x\rangle)\cos(n\tilde{x}) + \sin(n\langle x\rangle)\sin(n\tilde{x})]e^{(-n^2/2)\sigma_x^2}\right]$$

This result has already been used in Chapter 2. Extending this to the case of two normal (Gaussian) variables, only one of which is wrapped, we obtain

$$\begin{aligned} f(\omega, \theta; t \mid \omega_0, \theta_0) = \frac{1}{(2\pi)^2}\int_{-\infty}^{\infty}\Big[& e^{is\langle\omega\rangle - s^2\sigma_\omega^2/2}e^{-is\omega} \\ & + 2\sum_{n=1}^{\infty}[\cos(s\langle\omega\rangle + n\langle\theta\rangle)\cos(s\omega + n\theta) \\ & + \sin(s\langle\omega\rangle + n\langle\theta\rangle)\sin(s\omega + n\theta)] \\ & \times \exp[-\tfrac{1}{2}(s^2\sigma_\omega^2 + 2ns\ \mathrm{Cov} + n^2\sigma_\theta^2)]\Big]\, ds \end{aligned} \qquad (5.2.1.4)$$

where the covariance is $\mathrm{Cov} = \langle(\omega - \langle\omega\rangle)(\theta - \langle\theta\rangle)\rangle$. If $C_v(t)$, $C_\omega(t)$, and $C_\mu(t)$ denote the normalized a.c.f.'s for $\mathbf{v}$, $\boldsymbol{\omega}$, and $\boldsymbol{\mu}$, then we have seen in Chapter 3 that in terms of Mori three-variable theory,

$$\begin{aligned} C_v(t) &= \frac{m}{3kT}\langle \mathbf{v}(t)\cdot\mathbf{v}(0)\rangle \\ &= \frac{1}{1+\Gamma_v}\left[\left(\cos\beta_v t + \left(\frac{\alpha_{v_1} + \Gamma_v\alpha_{v_2}}{\beta_v}\right)\sin\beta_v t\right)e^{-\alpha_{v_1}t} + \Gamma_v\exp(-\alpha_{v_2}t)\right] \\ C_\omega(t) &= \frac{I}{kT}\langle\boldsymbol{\omega}(t)\cdot\boldsymbol{\omega}(0)\rangle \\ &= \frac{1}{1+\Gamma_\omega}\left[\left(\cos\beta_\omega t + \left(\frac{\alpha_{\omega_1} + \Gamma_\omega\alpha_{\omega_2}}{\beta_\omega}\right)\sin\beta_\omega t\right]e^{-\alpha_{\omega_1}t} + \Gamma_\omega\exp(-\alpha_{\omega_2}t)\right] \end{aligned}$$

and

$$C_\mu(t) = \langle\boldsymbol{\mu}(t)\cdot\boldsymbol{\mu}(0)\rangle = \exp\left[-\frac{kT}{I}\int_0^t X_\omega(\tau)\, d\tau\right]$$

where

$$X_\omega(t) = \int_0^t C_\omega(\tau)\, d\tau$$

In terms of these functions, therefore,

$$\begin{aligned} \langle\omega\rangle &= C_\omega(t)\omega_0 \\ \langle\theta\rangle &= \theta_0 + X_\omega(t)\omega_0 \\ \sigma_\omega^2 &= \frac{kT}{I}[1 - C_\omega^2(t)] \\ \sigma_\theta^2 &= \frac{kT}{I}\left[2\int_0^t X_\omega(\tau)\, d\tau - X_\omega^2(t)\right] \\ \mathrm{Cov} &= \frac{kT}{I}X_\omega(t)[1 - C_\omega(t)] \end{aligned} \qquad (5.2.1.5)$$

The integration of Eq. 5.2.1.3 must be carried out taking into account Eq. 5.2.1.5. This is complicated and the integrals must be taken in a certain order. Firstly,

$$\begin{aligned} &\int_{-\infty}^{\infty}\cos(\alpha s + \beta)\exp[-\tfrac{1}{2}(as^2 + 2bs + c)]\, ds \\ &\quad = \sqrt{\frac{2\pi}{a}}\cos\left(\beta - \frac{\alpha b}{a}\right)\exp\left[-\frac{1}{2}\left(c - \frac{\alpha^2 - b^2}{a}\right)\right] \end{aligned}$$

Equation 5.2.1.4 may be written

$$\begin{aligned} f(\omega, \theta; t \mid \omega_0, \theta_0) = {} & \frac{1}{(2\pi)^{3/2}\sigma_\omega}\exp\left[-\frac{(\omega - \langle\omega\rangle)^2}{2\sigma_\omega^2}\right] \\ & \times\left[1 + 2\sum_{n=1}^{\infty}\cos n\left[(\theta - \langle\theta\rangle) - \frac{\mathrm{Cov}}{\sigma_\omega^2}(\omega - \langle\omega\rangle)\right]\right] \\ & \times\left[\exp\left(-\frac{n^2\sigma_\theta^2(1-p^2)}{2}\right)\right] \end{aligned}$$

where

$$p = \frac{\mathrm{Cov}}{\sigma_\omega\sigma_\theta}$$

Since

$$2\int_{-\pi}^{\pi}\cos(\theta - \alpha)\cos n(\theta - \beta)\, d\theta = \begin{bmatrix} 0 & (n > 1) \\ 2\pi\cos(\beta - \alpha) & (n = 1) \end{bmatrix}$$

it follows that

$$\begin{aligned} &\int_{-\pi}^{\pi}\cos(\theta - \theta_0)f(\omega, \theta; t \mid \omega_0, \theta_0)\, d\theta \\ &\quad = \frac{1}{\sqrt{2\pi}\sigma_\omega}\exp\left[-\frac{(\omega - \langle\omega\rangle)^2}{2\sigma_\omega^2}\right]\cos\left[\frac{\mathrm{Cov}}{\sigma_\omega^2}(\omega + \omega_0)\right]e^{-\sigma_\theta^2(1-p^2)/2} \end{aligned}$$

which is independent of θ_0. Next, using the standard integral,

$$\begin{aligned} &\int_{-\infty}^{\infty}\omega\cos(\alpha\omega + \beta)\exp\left[-\frac{(\omega - \mu)^2}{2\sigma^2}\right]d\omega \\ &\quad = \sqrt{2\pi}\,\sigma[\mu\cos(\alpha\mu + \beta) - \alpha\sigma^2\sin(\alpha\mu + \beta)]e^{-\alpha^2\sigma^2/2} \end{aligned}$$

We obtain

$$\begin{aligned} &\int_{-\infty}^{\infty}\int_{-\pi}^{\pi}\omega\cos(\theta - \theta_0)f(\omega, \theta; t \mid \omega_0, \theta_0)\, d\omega\, d\theta \\ &\quad = [C_\omega(t)\omega_0\cos(X_\omega(t)\omega_0) - \mathrm{Cov}\sin(X_\omega(t)\omega_0)]e^{-\sigma_\theta^2/2} \end{aligned}$$

Finally we integrate with respect to ω_0, using the results

$$\left(\frac{2\pi kT}{I}\right)^{-1/2}\int_{-\infty}^{\infty}\omega_0^2\cos(X\omega_0)\exp\left[-\frac{\omega_0^2}{2kT/I}\right]d\omega_0 = \frac{kT}{I}\left(1 - \frac{kT}{I}X^2\right)e^{-kTX^2/(2I)}$$

and

$$\left(\frac{2\pi kT}{I}\right)^{-1/2}\int_{-\infty}^{\infty}\omega_0\sin(X\omega_0)\exp\left(-\frac{\omega_0^2}{2kT/I}\right)d\omega_0=\frac{kT}{I}X\exp\left(-\frac{kT}{2I}X^2\right)$$

to obtain finally

$$\langle\boldsymbol{\mu}(t)\cdot\boldsymbol{\mu}(0)\boldsymbol{\omega}(t)\cdot\boldsymbol{\omega}(0)\rangle=\frac{kT}{I}\left(C_\omega(t)-\frac{kT}{I}X_\omega^2(t)\right)\exp\left(-\frac{kT}{I}\int_0^t X_\omega(\tau)\,d\tau\right)$$
$$=\langle\boldsymbol{\mu}(t)\cdot\boldsymbol{\mu}(0)\rangle\left[\langle\boldsymbol{\omega}(t)\cdot\boldsymbol{\omega}(0)\rangle-\left(\frac{kT}{I}X_\omega(t)\right)^2\right]$$

The methods used in deriving this result may be extended to a molecule containing many atoms, but at the cost of laborious mathematical analysis. It is advantageous, therefore, to search for methods that give us the maximum insight into the mutual effect of translation and rotation on the molecular level, both analytical and experimental. One of the most incisive techniques is via the use of molecular dynamics simulation, and the most direct approach is to investigate directly the normalized mixed a.c.f. of linear and angular momentum: $\langle\mathbf{p}(0)\cdot\mathbf{J}(t)\rangle$ which in a linear molecule is the normalized mixed a.c.f. of velocities. Before proceeding it is as well to check that the a.c.f. we wish to simulate is not disallowed by considerations of symmetry. There are at least three symmetry operations that may be performed to determine this. These are time reversal, parity, and reflection (Berne and Pecora, 1976).

5.2.1.1 Time Reversal Symmetry

Consider the column vector of linear and angular momentum $\mathbf{A}=\begin{bmatrix}\mathbf{p}\\ \mathbf{J}\end{bmatrix}$ for the space reorientation of the asymmetric top. The mixed a.c.f. of angular and linear momentum vanishes for all t if $\mathbf{p}$ and $\mathbf{J}$ have different time reversal symmetry. This means that both $\mathbf{p}$ and $\mathbf{J}$ must change under the transformation of phase space $(\mathbf{q},\mathbf{p})\rightarrow(\mathbf{q},-\mathbf{p})$. It may also be proved that if $\mathbf{p}$ and $\mathbf{J}$ have the same time reversal symmetry the resonance matrix of the Mori equation (denoted $\hat{\Omega}$) vanishes. $\mathbf{J}$ may always be written at the same instant in time as $\mathbf{R}\times\mathbf{p}$ where $\mathbf{R}$ is a position vector invariant under time reversal symmetry. The mixed a.c.f. $\langle\mathbf{p}(0)\cdot\mathbf{J}(0)\rangle$ vanishes but $\langle\mathbf{p}(0)\cdot\mathbf{J}(t)\rangle$ does not.

5.2.1.2 Parity

This transformation inverts all atomic positions and molecular momenta, and $\langle\mathbf{p}(0)\cdot\mathbf{J}(t)\rangle$ vanishes for all t if $\mathbf{p}$ and $\mathbf{J}$ have different parity, *provided the total Hamiltonian is parity invariant and the molecules have a center of symmetry.* We sometimes deal in this chapter with the rototranslation of the asymmetric top whose rotational motion is constrained about the laboratory z-axis, but whose center of mass translation is through three-dimensional space. $\mathbf{J}(t)$ therefore reduces to $I\omega_z\mathbf{k}$. In general the asymmetric top has no center of symmetry and there is no analytical relation between $\mathbf{v}(0)$ and $\omega_z(t)$, which is not complicated. Consequently it is not possible on the grounds of symmetry alone to relate the parity of $\mathbf{J}(t)$ and $\mathbf{v}(0)$, and there is no reason why the mixed a.c.f.'s should not exist for $t>0$, in for example, optically active molecules or such states of matter as the liquid crystalline, where there is a symmetry-breaking macroscopic order.

5.2.1.3 Reflection Symmetry

In a system with reflection symmetry, properties that transform under reflection are uncorrelated for all t. The transformation reflects all linear positions and momenta coordinates through the (x, z) plane.

If a system contains optically active molecules (with no inversion symmetry) none of these rules apply. The same is true if a symmetry-breaking field is applied to the molecular ensemble, such as an electric field, which induces a polarization $-\mathbf{P}\cdot\mathbf{E}$. The Hamiltonian is then $H=H_0-\mathbf{P}\cdot\mathbf{E}$; that is, it loses its own parity since $\mathbf{P}$ itself is odd in parity. Since we are always dealing with this case in dielectric spectroscopy, that is, since the fluctuation-dissipation theorem is derived on the assumption that H_0 is perturbed by a quantity $H'=-\mathbf{P}\cdot\mathbf{E}$, then the above rules must be taken with caution. We proceed on the assumption that the mixed a.c.f. of linear and angular momentum exists for a dipolar molecule.

In the nondipolar nitrogen molecule the polarization field is no longer applied, but computer simulation may be used to investigate in great detail the mixed momentum a.c.f.'s. It is more convenient to look at the associated functions:

1. $\langle|\mathbf{v}(0)||\boldsymbol{\omega}(t)|\rangle$, the linear/angular speed a.c.f.'s.
2. The kinetic/rotational-kinetic energy a.c.f.'s, $\langle v^2(0)\omega^2(t)\rangle$, and even moments, that is, $\langle v^{2n}(0)\omega^{2n}(t)\rangle$ $(n=2,4,\ldots)$.

These functions reflect the survival on the molecular level of the mode–mode coupling between spin and current density, the multimolecular "analogues". If these functions survive in as simple a symmetry as that of nitrogen then they are direct indications of the general effect of center of mass translation on the angular velocity and vice versa. This means of course that angular and linear Brownian motion are not mutually exclusive. In particular for dipolar molecules in parity breaking fields the mixed functions $\langle\mathbf{v}(0)\cdot\boldsymbol{\omega}(t)\rangle$ and $\langle\boldsymbol{\omega}(t)\cdot\mathbf{v}(0)\rangle$ may exist and Mori approximants of the column vector $\mathbf{A}=\begin{bmatrix}\mathbf{p}(t)\\ \mathbf{J}(t)\end{bmatrix}$ should be considered as in the next section.

Having investigated the problem at a single molecule level, we can more easily understand the simulation of multiparticle mode–mode coupling. A particular type of micro–macro correlation may then be used to link the multi- and single-particle functions.

Figure 1.4.9.1 illustrates functions 1 and 2 given above for diatomics of different interatomic separation which have been computer simulated using an algorithm in which each atomic interaction was approximated using a Lennard–Jones form. The algorithm reproduces satisfactorily most of the available thermodynamic data for nitrogen. The usual periodic boundary conditions were employed, the diatomics being initially deployed on an α-nitrogen lattice. Running time averages were built up according to Fig. 1.3.1.1 over a total period of about 10 psec (a limit imposed economically). Figure 1.4.9.1 illustrates clearly the surges of interaction that develop with increasing shape anisotropy. These are represented by peaks in the mixed a.c.f.'s which become more or less clearly defined for molecules respectively longer or shorter than N_2. The simulation was carried out at a reduced density of $\rho^* = 0.643$, a reduced temperature $T^* = 2.32$, and for reduced bond lengths of $L^* = 0.20$, 0.33 (N_2), and 0.50. This means that the shape of the molecule varies from almost spherical to pronouncedly dumbbell. The surges of translation/rotation interaction mean that periodically it becomes increasingly probable that the correlation between angular and linear speed and the corresponding kinetic energies is sharply increased after the arbitrary initial $t = 0$ in the more elongated molecules. Note that these a.c.f.'s (normalized just after the origin) can become greater than unity. In the near spherical molecule the correlation rises to a plateau level and remains beyond the limit of the simulation time. This appears to be related to the fact that the a.c.f.'s $\langle \boldsymbol{\omega}(t) \cdot \boldsymbol{\omega}(0) \rangle$ and $\langle \mathbf{v}(t) \cdot \mathbf{v}(0) \rangle$ themselves are longer lived. For the cases $L^* = 0.33$ and 0.50 the Fourier cosine transforms of the mixed a.c.f.'s are illustrated in Fig. 5.2.1.1, together with the power spectra of rotation/translation speed and energy. These spectra are finite at $\omega = 0$ and thereafter decay similarly to the usual exponential behavior of the a.c.f.'s in the time domain. The negative regions in the mixed kinetic energy power spectrum arise from the narrow half-width in time of the a.c.f. peaks. They may be thought of physically as emission details rather than absorption, that is, surges of rototranslational time correlation giving rise to "emission" spectra in the frequency domain. An increase in computer speed and power is needed to investigate these features for more interesting symmetries such as that of the propeller. A gradual extension of the methodology to mode–mode coupling on the hydrodynamic level produces features discernible spectroscopically. In Section 5.2.3 we solve the Mori equation for Eq. 1.7.4.1 for a column vector of linear and angular momentum. In this way it is possible to account for mutual rototranslational effects in the theory of the Brownian motion.

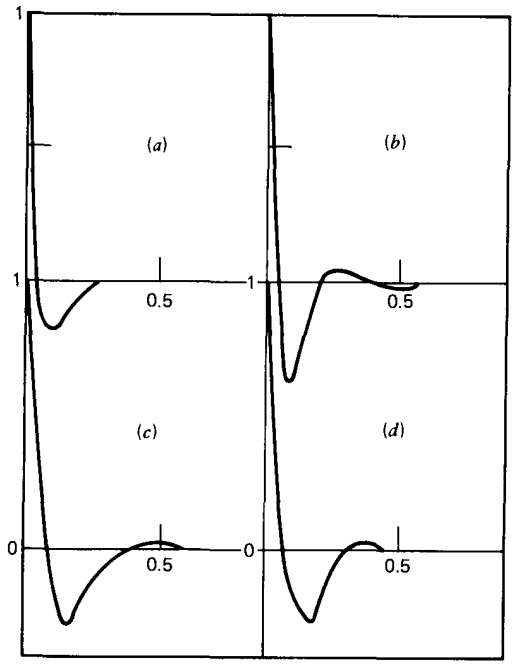

Figure 5.2.1.1 Power spectra of mixed a.c.f.'s computer simulated for nitrogen. Abscissa: Frequency in reduced units.

(*a*) $\int_0^\infty \left[\frac{\langle v^4(0)\omega^4(t)\rangle}{\langle v^4(0)\omega^4(t)\rangle} - 1\right] \cos \omega t \, dt$

(*b*) $\int_0^\infty \left[\frac{\langle \mathbf{v}(0)\|\boldsymbol{\omega}(t)\|\rangle}{\langle |\mathbf{v}(0)\|\boldsymbol{\omega}(0)|\rangle} - 1\right] \cos \omega t \, dt$ for N_2 ($d^* = 0.33$)

(*c*) $\int_0^\infty \left[\frac{\langle v^4(0)\omega^4(t)\rangle}{\langle v^4(0)\omega^4(0)\rangle} - 1\right] \cos \omega t \, dt$, $d^* = 0.5$

(*d*) As for (*b*), $d^* = 0.5$.

5.2.2 Rototranslation of Loaded Rough Spheres

The "classical" theory (Brownian movement for instance) overestimates the rotational drag on a body by neglecting translational motions that can partially relieve the torque. Similarly, stochastic rotations reduce translational drag. This diminution is set against the expectation that rotation/translation coupling has the net effect of strongly enhancing the overall frictional drag. By using a theory of loaded rough hard sphere motions, Chandler (1974) has shown that the diffusion coefficient (the area, essentially, beneath the velocity a.c.f.) is decreased by a factor of two by rototranslational interaction owing to the fact that when two slightly aspherical hard core particles collide, their angular momenta are changed

by the inelastic nature of the collision. The rototranslational interactions in this kind of rough sphere fluid (where electrodynamic potentials are neglected) has the effect of lowering the diffusion coefficient for linear center of mass translation. This is because the coupling provides an additional mechanism for the relaxation of the velocity of the particle in the fluid. As a result the velocity a.c.f. decays to zero more rapidly if the coupling exists than otherwise. The amount of coupling is measured by Chandler through the average $\langle \mathbf{v} \cdot \hat{T}_{21}\boldsymbol{\omega} \rangle$ and $\langle \boldsymbol{\omega} \cdot \hat{T}_{21}\mathbf{v} \rangle$ where $\hat{T}_{21}$ is a collision operator that approximates the dynamics in such a way that after a collision (which is elastic) two hard spheres move away from each other and never recollide unless other particles cause them to do so. In general, in a fluid of rough hard spheres the Laplace transform of the velocity a.c.f. is

$$\tilde{C}_v(s) = \frac{\left\langle \mathbf{v} \cdot \left(s - \hat{\mathcal{L}}_0 + \sum_{j>i=1}^{N} \hat{T}_{ji} \right)^{-1} \mathbf{v} \right\rangle}{\langle v^2 \rangle}$$

where $\hat{\mathcal{L}}_0$ is Liouville's operator for the ideal gas (free particle) and $\hat{T}_{ji}$ is the binary collision operator for the pair of particles i and j. When this type of theory is applied to the orientational a.c.f. $C_u(t)$, one finds

$$\tilde{C}_u(s) = \frac{\tilde{C}_l^{(0)}(s + \tau^{-1})}{1 - \tau^{-1}\tilde{C}_l^{(0)}(s + \tau^{-1})} \tag{5.2.2.1}$$

which is the J-diffusion model of Gordon (Chapter 2) if τ is the time between collisions, expressed in terms of the operator $\hat{T}_{21}$ as

$$\tau^{-1} = \frac{(N-1)\langle \dot{\mathbf{u}} \cdot [\hat{T}_{21}\dot{\mathbf{u}}] \rangle}{\langle \dot{u}^2 \rangle} = \frac{(N-1)\langle \boldsymbol{\omega} \cdot [\hat{T}_{21}\boldsymbol{\omega}] \rangle}{\langle \omega^2 \rangle}$$

Provided $\tau_\omega = \tilde{C}_J(s = 0)$ where C_J is the angular momentum a.c.f., Eqs. 5.2.2.1 and 2.14.3 are exactly similar. This means that the dynamic events contributing to $C_v(t)$ can be approximated by sequences of uncorrelated binary collisions as mentioned in Chapter 2. Chandler neglects all electrodynamic interactions in deriving this theory. We have already seen that in the J-diffusion limit this cannot reproduce the characteristic far infrared shift of ω_{max} as observed in real liquids. This shift is large (1) when highly dipolar liquids are diluted in nondipolar solvents (Fig. 3.4.4.1); (2) along the gas-liquid coexistence curve (Fig. 1.2.3); and (3) enormously so between the glassy and liquid states (Fig. 1.2.8). It is interesting to note that the theory is expected to work best at high densities where in reality it fails completely when tested against data over an adequate range of frequency, density, and other variables, notably macroscopic viscosity (Chapter 7). Even when electrostatic effects are minimized, that is, in dilute solution, Fig. 3.4.4.1 demonstrates clearly that there is a need to consider correlated

collisions, because as the far infrared data vividly show, the J-diffusion model produces a curve that remains at the gas phase $\Delta J = 1$ peak, as much as 50 or 100 cm^{-1} below the experimental. This is true for a pseudospherical molecule such as *tert*-butyl chloride or chloroform (Chapter 4) in a pseudospherical solvent such as CCl_4. The trouble with all such collision theories is that the molecules in a liquid are continuously in contact, via short range van der Waals potentials and longer range electrodynamic potentials, and in consequence the very idea of collision is ill-defined.

Although the loaded rough hard sphere fluid is analytically tractable and provides us with valuable insight into rototranslational coupling it has defects that can sometimes lead to bizarre results. We illustrate this as follows, using the hard sphere correlation function:

$$C_l(\mathbf{q}, t) = \langle P_l(\mathbf{u}(t) \cdot \mathbf{u}(0)) \exp[i\mathbf{q} \cdot \Delta\mathbf{r}(t)] \rangle$$

Here $\mathbf{q}$ denotes a wave vector, $\mathbf{r}$ the position of a particle of the rough hard sphere fluid, and P_l the Legendre polynomials. If we choose dimensionless units we may denote the dimensionless wave vector by $\mathbf{Q}$, take s as the Laplace variable in units of $(kT/I)^{1/2}$, and express C_l in the form

$$\tilde{C}_l(\mathbf{Q}, s) = \frac{\tilde{C}_l^{(0)}[\mathbf{Q}, s + \beta_l(\mathbf{Q})]}{1 - \beta_l(\mathbf{Q})\tilde{C}_l^{(0)}[\mathbf{Q}, s + \beta_l(\mathbf{Q})]} \tag{5.2.2.2}$$

generalizing Eq. 5.2.2.1. Here $C_l^{(0)}$ is the a.c.f. of an ensemble of noninteracting rough spheres which are assumed to rotate and translate freely in this limit. The usual assumption made in theories of, for example, inelastic neutron scattering is that $C_l(\mathbf{q}, t)$ may be factorized into an orientational component $C_l(\mathbf{0}, t)$ and a translational component $C_0(\mathbf{Q}, t)$, so that

$$C_l^{(\text{unc})}(\mathbf{Q}, t) = C_l(\mathbf{0}, t)C_0(\mathbf{Q}, t) \tag{5.2.2.3}$$

Note that in theories of the 0–THz absorption which take $\mathbf{Q} \to \mathbf{0}$, the spectrum may be evaluated from Eq. 5.2.2.2 in this limit by replacing s by $-i\omega$ in the usual way. Otherwise the 0–THz spectrum depends on the full Eq. 5.2.2.2. The factorization in Eq. 5.2.2.3 may have strange consequences within the context of rough hard sphere dynamics as we now demonstrate. The free rotor correlation function is given by (Berne and Montgomery, 1976)

$$C_l^{(0)}(\mathbf{Q}, t) = \left\langle \frac{1}{2l+1} \sum_{m=-l}^{l} [i(m\omega + Qv_z)t] \right\rangle \tag{5.2.2.4}$$

for the rototranslation of noninteracting rough spheres. Here ω is the angular velocity, v_z the linear velocity, and t is the time, all in reduced units. To second order in Laplace space,

$$\tilde{C}_l^{(0)}[\mathbf{Q}, s + \beta_l(\mathbf{Q})] = \frac{1}{s + \beta_l(\mathbf{Q})} - \frac{l(l+1) + Q^2}{[s + \beta_l(\mathbf{Q})]^3} \tag{5.2.2.5}$$

The question arises whether or not Eq. 5.2.2.5 is a sufficiently good

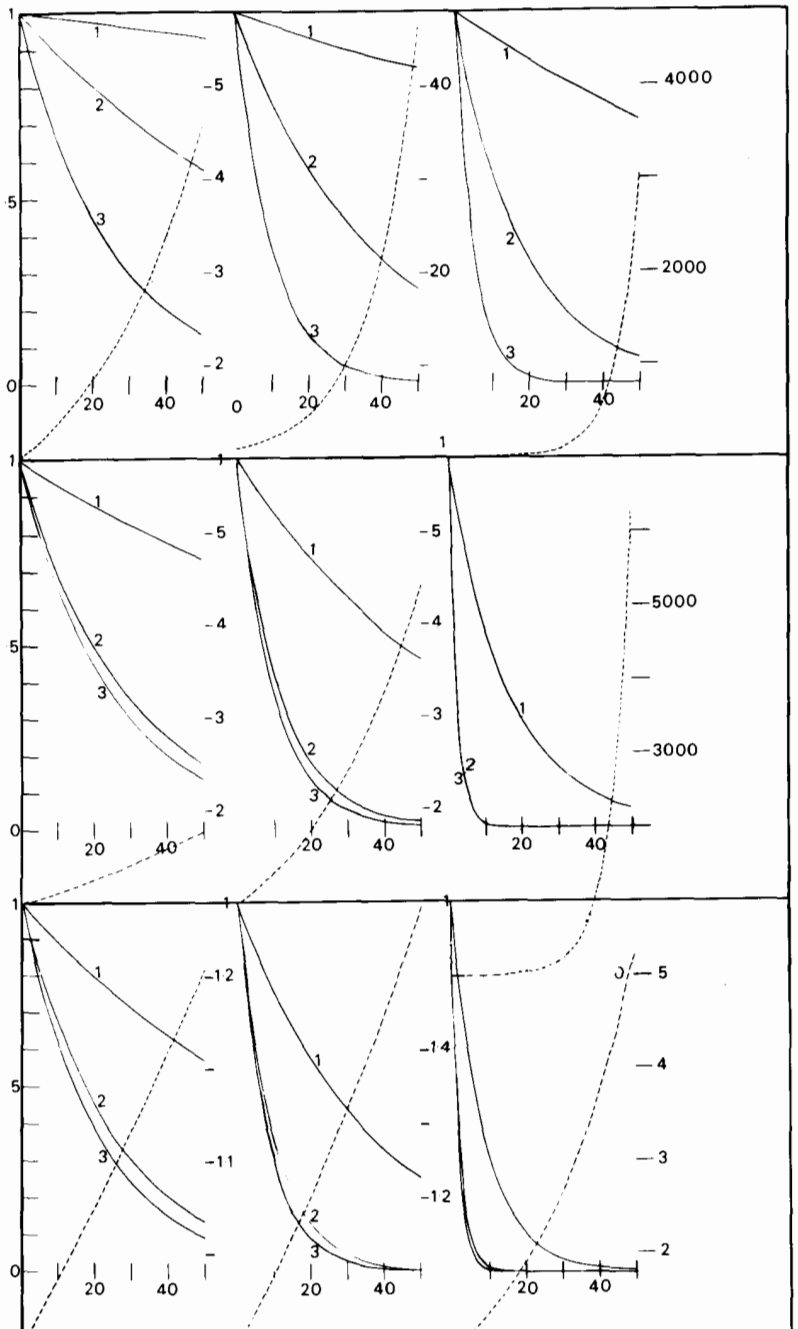

Figure 5.2.2.1 (1) $C_0(\mathbf{Q}, t)$; (2) $C_1(\mathbf{Q}, t)$; (3) $C_1(\mathbf{0}, t)$. Dashed lines, the ratio $C_1(\mathbf{Q}, t)/C_1^{(unc)}(\mathbf{Q}, t)$ for $|\mathbf{Q}| = 1$, $\kappa = 0.4$. [The superscript (*unc*) denotes factored, or uncoupled.] (*a*) $\lambda = 0.1$, $\beta_\omega = 50$; (*b*) $\lambda = 0.1$, $\beta_\omega = 20$; (*c*) $\lambda = 0.1$, $\beta_\omega = 10$; (*d*) $\lambda = 0.5$, $\beta_\omega = 50$; (*e*) $\lambda = 0.5$, $\beta_\omega = 20$; (*f*) $\lambda = 0.5$, $\beta_\omega = 5$; (*g*) $\lambda = 1.0$, $\beta_\omega = 50$; (*h*) $\lambda = 1.0$, $\beta_\omega = 20$; (*i*) $\lambda = 1.0$, $\beta_\omega = 5$. [Reproduced by permission from M. W. Evans et al., *Faraday Disc.* (1978).]

approximation to the exact Eq. 5.2.2.4. This may be answered easily in the $\mathbf{Q} \rightarrow \mathbf{0}$ limit (below) where we recover the characteristic rotational frequency β_ω as

$$\beta_\omega = \frac{(I/kT)^{1/2}}{\tau_\omega}$$

the dimensionless angular velocity relaxation rate. If $\beta_l(\mathbf{Q})$ is typically greater than unity, then

$$\tilde{C}_l(\mathbf{Q}, s) = \frac{s^2 + 2\beta_l(\mathbf{Q})s + (\beta_l^2(\mathbf{Q}) - l(l+1) - Q^2)}{s^3 + 2\beta_l(\mathbf{Q})s^2 + \beta_l^2(\mathbf{Q})s + \beta_l(\mathbf{Q})[Q^2 + l(l+1)]}$$

The ratio $C_l(\mathbf{Q}, t)/C_l^{(unc)}(\mathbf{Q}, t)$ may now be evaluated for various values of $\beta_l(\mathbf{Q})$. This is illustrated in Fig. 5.2.2.1. In all cases $\beta_l(\mathbf{Q}) \gg 1$ so that Eq. 5.2.2.5 is valid, but clearly the ratio $C_l(\mathbf{Q}, t)/C_l^{(unc)}(\mathbf{Q}, t)$ becomes unphysically large. We seek a more realistic way of measuring analytically the mutual interaction of rotation and translation by systematically approximating the Mori continued fraction for a column vector **A** consisting of linear and angular momentum components.

5.2.3 Mori Approximants for Rototranslation

If we take the Mori equation with a column vector **A** defined by $\mathbf{A} = [{}^{m\mathbf{v}}_{I\boldsymbol{\omega}}]$, a null resonance operator and delta memory function, then the resulting pair of equations describe the rototranslation of an asymmetric top whose dipole is constrained to librate in a plane but whose centers of mass may move in space. The question now arises as to how the memory function should be written. In general, since ϕ is a time-independent matrix the symmetry of the situation strongly suggests that the correct form is $\hat{\phi} = \begin{bmatrix} \gamma_t & \gamma_{tr} \\ \gamma_{rt} & \gamma_r \end{bmatrix}$. Were the off-diagonal elements of $\hat{\phi}$ to disappear, then the separate translational and planar reorientational Langevin equations would result. Using this form for $\hat{\phi}$ results in the rototranslational Langevin equations:

$$\begin{aligned} m\dot{\mathbf{v}} &= -m\gamma_t \mathbf{v} - \gamma_{tr} I\boldsymbol{\omega} + \mathbf{F} \\ I\dot{\boldsymbol{\omega}} &= -I\gamma_r \boldsymbol{\omega} - \gamma_{rt} m\mathbf{v} + \mathbf{N} \end{aligned} \tag{5.2.3.1}$$

The Langevin equations in this form are extendable to asymmetric top rototranslation under the following conditions.

1. The center of mass velocity is $\mathbf{v} = \begin{bmatrix} \mathbf{v}_x \\ \mathbf{v}_y \\ \mathbf{v}_z \end{bmatrix}$
2. The angular velocity is $\boldsymbol{\omega} = \begin{bmatrix} 0 \\ 0 \\ \omega_z \end{bmatrix}$ (planar).

3. γ_t is regarded here as a scalar, the mean translational friction coefficient. Using all three coefficients (tensor $\boldsymbol{\gamma}_t$) complicates the comparisons with experimental data.
4. In general $\boldsymbol{\gamma}_r$ is a 3×3 matrix (assumed to be diagonal), so that

$$\boldsymbol{\gamma}_r = \begin{bmatrix} \gamma_r^{(xx)} & 0 & 0 \\ 0 & \gamma_r^{(yy)} & 0 \\ 0 & 0 & \gamma_r^{(zz)} \end{bmatrix}$$

5. $\boldsymbol{\gamma}_{rt}$ and $\boldsymbol{\gamma}_{tr}$ are diagonal matrices defined similarly.

The solution of Eqs. 5.2.3.1 in terms of a.c.f.'s may be written in terms of the matrix:

$$\mathbf{C}(t) = \begin{bmatrix} \langle \mathbf{v}(t)\mathbf{v}^T(0)\rangle\langle \mathbf{v}(0)\mathbf{v}^T(0)\rangle^{-1} & \langle \mathbf{v}(t)\boldsymbol{\omega}^T(0)\rangle\langle \boldsymbol{\omega}(0)\boldsymbol{\omega}^T(0)\rangle^{-1} \\ \langle \boldsymbol{\omega}(t)\mathbf{v}^T(0)\rangle\langle \mathbf{v}(0)\mathbf{v}^T(0)\rangle^{-1} & \langle \boldsymbol{\omega}(t)\boldsymbol{\omega}^T(0)\rangle\langle \boldsymbol{\omega}(0)\boldsymbol{\omega}^T(0)\rangle^{-1} \end{bmatrix}$$

In Laplace space

$$\begin{aligned} \tilde{\mathbf{C}}(s) &= [\mathbf{1}s + \tilde{\mathbf{C}}_1(s)\cdot\boldsymbol{\phi}_1(0)]^{-1} \\ &= [\mathbf{1}s + [\mathbf{1}s + \tilde{\mathbf{C}}_2(s)\cdot\boldsymbol{\phi}_2(0)]^{-1}]^{-1}\cdot\boldsymbol{\phi}_1(0) \end{aligned}$$

where $\boldsymbol{\phi}_1(s) = \tilde{\mathbf{C}}_1(s)\cdot\boldsymbol{\phi}_1(0)$ and $\tilde{\boldsymbol{\phi}}(s) = \tilde{\mathbf{C}}_2(s)\cdot\boldsymbol{\phi}_2(0)$ etc., are the Laplace transforms of the first and second memory matrices, and the $\boldsymbol{\phi}_j(0)$ are defined by

$$\boldsymbol{\phi}_j(0) = \langle \mathbf{f}_j\cdot\mathbf{f}_j^T\rangle\langle \mathbf{f}_{j-1}\cdot\mathbf{f}_{j-1}^T\rangle^{-1}$$

with

$$\mathbf{f}_0 = \begin{bmatrix} \mathbf{v}(0) \\ \boldsymbol{\omega}(0) \end{bmatrix}$$

$$\mathbf{f}_1 = \begin{bmatrix} \dot{\mathbf{v}}(0) \\ \dot{\boldsymbol{\omega}}(0) \end{bmatrix}$$

and

$$\mathbf{f}_2 = \begin{bmatrix} \ddot{\mathbf{v}}(0) + \dfrac{\langle \dot{v}^2(0)\rangle \mathbf{v}(0)}{\langle v^2(0)\rangle} \\ \ddot{\boldsymbol{\omega}}(0) + \dfrac{\langle \dot{\omega}^2(0)\rangle \boldsymbol{\omega}(0)}{\langle \omega^2(0)\rangle} \end{bmatrix}$$

We find that

$$\boldsymbol{\phi}_j(0) = \begin{bmatrix} \phi_{t_j} & 0 \\ 0 & \phi_{r_j} \end{bmatrix}$$

where

$$\phi_{t_2} = \frac{\langle \ddot{v}^2(0)\rangle}{\langle \dot{v}^2(0)\rangle} - \frac{\langle \dot{v}^2(0)\rangle}{\langle v^2(0)\rangle}; \qquad \phi_{r_2} = \frac{\langle \ddot{\omega}^2(0)\rangle}{\langle \dot{\omega}^2(0)\rangle} - \frac{\langle \dot{\omega}^2(0)\rangle}{\langle \omega^2(0)\rangle}$$

As we shall see, these latter terms are identical with the corresponding ones in the individual Mori style equations (Chapter 4) for each type of motion. The solution for Langevin rototranslation may be found if we define

$$\tilde{\mathbf{C}}_1(s)\cdot\boldsymbol{\phi}_1(0) = \begin{bmatrix} \lambda_t & \lambda_{tr} \\ \lambda_{rt} & \lambda_r \end{bmatrix}$$

where the λ's have frequency dimensions. It follows that

$$\tilde{\mathbf{C}}(s) = \begin{bmatrix} s+\lambda_t & \lambda_{tr} \\ \lambda_{rt} & s+\lambda_r \end{bmatrix}^{-1}$$

for each component of $\mathbf{v}$ or $\boldsymbol{\omega}$:

$$\begin{aligned} \langle v(t)v(0)\rangle &= \langle v^2(0)\rangle \exp(-bt)\left[\cos(c-b^2)^{1/2}t + \frac{\lambda_r - b}{(c-b^2)^{1/2}}\sin(c-b^2)^{1/2}t\right] \\ &\qquad (c > b^2) \\ &= \langle v^2(0)\rangle \exp(-bt)\left[\cosh(b^2-c)^{1/2}t + \frac{\lambda_r - b}{(b^2-c)^{1/2}}\sinh(b^2-c)^{1/2}t\right] \\ &\qquad (c < b^2) \\ \langle \omega(t)v(0)\rangle &= -\frac{\langle \omega^2(0)\rangle}{(c-b^2)^{1/2}}\lambda_{tr}\exp(-bt)\sin(c-b^2)^{1/2}t \qquad (c > b^2) \\ &= -\frac{\langle \omega^2(0)\rangle}{(b^2-c)^{1/2}}\lambda_{rt}\exp(-bt)\sinh(b^2-c)^{1/2}t \qquad (b^2 < c) \end{aligned}$$

with similar expressions for $\langle \omega(t)\omega(0)\rangle$ and $\langle \omega(t)v(0)\rangle$. Since $\langle v(t)\omega(0)\rangle = \langle \omega(t)v(0)\rangle$ it follows that

$$\lambda_{tr}\langle \omega^2(0)\rangle = \lambda_{rt}\langle v^2(0)\rangle$$

In these equations $b = 2(\lambda_t + \lambda_r)$; $c = \lambda_t\lambda_r - \lambda_{tr}\lambda_{rt}$. It can be seen that the angular velocity a.c.f. $\langle \boldsymbol{\omega}(t)\cdot\boldsymbol{\omega}(0)\rangle$ depends on λ_t, λ_r, λ_{tr}, and λ_{rt}, as does the velocity a.c.f.:

$$\langle \mathbf{v}(t)\cdot\mathbf{v}(0)\rangle = 3\langle v(t)v(0)\rangle$$

When $\lambda_{tr} = \lambda_{rt} = 0$ the dependence reduces to one parameter (classical Brownian motion) and the mixed a.c.f.'s vanish at all times. When $\lambda_{tr} \neq 0$ the mixed a.c.f.'s vanish as they should at $t = 0$ and as $t \to \infty$. A computer simulation of the mixed angular momentum/linear momentum a.c.f. for a C_{2v} symmetry triatomic is shown in Fig. 5.2.3.2. The existence of this function would imply the existence of λ_{tr} and λ_{rt} of the rototranslational Langevin equation and that the "classical" theory of purely rotational Brownian motion is incomplete.

We consider some specific cases.

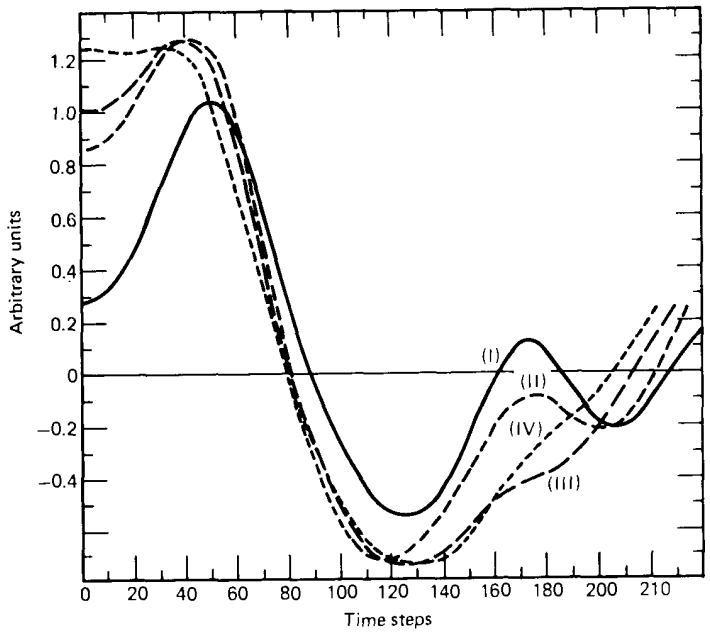

Figure 5.2.3.2 C_{2v} triatomic, computer simulation of the mixed momentum a.c.f. $\langle \mathbf{P}(0)\cdot\mathbf{J}(t)\rangle$ for various time steps. The convergence to the final curve is not complete because of the economic limit imposed on the run time. (i) 1000 time steps; (ii) 800 time steps; (iii) 600 time steps; (iv) 500 time steps.

The Asymmetric Top with Dipole Librating in a Plane

In this case the unnormalized off-diagonal mixed terms are given by

$$\langle \mathbf{v}(t)\boldsymbol{\omega}^T(0)\rangle = \begin{bmatrix} 0 & 0 & \langle v_x(t)\omega_z(0)\rangle \\ 0 & 0 & \langle v_y(t)\omega_z(0)\rangle \\ 0 & 0 & \langle v_z(t)\omega_z(0)\rangle \end{bmatrix}$$

$$\langle \boldsymbol{\omega}(t)\mathbf{v}^T(0)\rangle = \begin{bmatrix} 0 & 0 & 0 \\ 0 & 0 & 0 \\ \langle \omega_z(t)v_x(0)\rangle & \langle \omega_z(t)v_y(0)\rangle & \langle \omega_z(t)v_z(0)\rangle \end{bmatrix}$$

The translation/libration interaction manifests itself through the mixed a.c.f.'s $\langle v_z(t)\omega_z(0)\rangle$ and $\langle \omega_z(t)v_z(0)\rangle$. By comparison of matrix elements,

$$\mathcal{L}_a[\langle v_z(t)\omega_z(0)\rangle\langle \omega_z(0)\omega_z(0)\rangle^{-1}] = -\frac{\gamma_{rt}^{(zz)}}{(s+\gamma_r^{(zz)})(s+\gamma_t)-\gamma_{rt}^{(zz)}\gamma_{tr}^{(zz)}}$$

$$\mathcal{L}_a[\langle v_x(t)v_x(0)\rangle\langle v_x(0)v_x(0)\rangle^{-1}] = \frac{1}{s+\gamma_t}$$

$$\mathcal{L}_a[\langle v_y(t)v_y(0)\rangle\langle v_y(0)v_y(0)\rangle^{-1}] = \frac{1}{s+\gamma_t}$$

$$\mathcal{L}_a[\langle v_z(t)v_z(0)\rangle\langle v_z(0)v_z(0)\rangle^{-1}] = \frac{s+\gamma_t}{(s+\gamma_t)(s+\gamma_r^{(zz)})-\gamma_{rt}^{(zz)}\gamma_{tr}^{(zz)}}$$

$$\mathcal{L}_a[\langle \omega_z(t)\omega_z(0)\rangle\langle \omega_z(0)\omega_z(0)\rangle^{-1}] = \frac{s+\gamma_r^{(zz)}}{(s+\gamma_r^{(zz)})(s+\gamma_t^{zz})-\gamma_{rt}^{(zz)}\gamma_{tr}^{(zz)}}$$

If the translation is not spatial (i.e., if it is always in the plane of rotation of $\boldsymbol{\omega}$) there is no mutual effect of rotation and translation since $\boldsymbol{\omega}$ is always perpendicular to $\mathbf{v}$. Unless $\gamma_{rt}^{(zz)}$ is zero, the angular velocity a.c.f. is no longer exponential. We note that a propeller is a body constrained to rotate in a plane but free to translate in three dimensions. In the case of the propeller there is, according to everyday experience, a strong rototranslational interaction.

Far Infrared Power Absorption ($\alpha(\omega)$)

In the absence of internal field effects this is related to the rotational velocity a.c.f., $\langle \dot{\mathbf{u}}(t)\cdot\dot{\mathbf{u}}(0)\rangle$, as we have seen in earlier chapters. In certain circumstances this is similar to $\langle \boldsymbol{\omega}(t)\cdot\boldsymbol{\omega}(0)\rangle$ in time dependence. Approximately, therefore,

$$\alpha(\omega) \propto \int_0^\infty \frac{\langle \boldsymbol{\omega}(t)\cdot\boldsymbol{\omega}(0)\rangle}{\langle \boldsymbol{\omega}(0)\cdot\boldsymbol{\omega}(0)\rangle}\cos\omega t\, dt = \frac{\omega(\omega^2+\gamma_r^2+\gamma_{tr}\gamma_{rt})}{(\gamma_r\gamma_t-\gamma_{rt}\gamma_{tr}-\omega^2)^2+(\gamma_t+\gamma_r)^2\omega^2}$$

when the γ's are scalar. At low frequencies we extract the effective Debye relaxation time as

$$\tau_D \sim \frac{(\gamma_t+\gamma_r)^2-2(\gamma_r\gamma_t-\gamma_{rt}\gamma_{tr})}{(\gamma_r\gamma_t-\gamma_{rt}\gamma_{tr})}$$

which diverges when $\gamma_r\gamma_t = \gamma_{rt}\gamma_{tr}$ (i.e., in the limit of strong coupling). Some curves are plotted in Fig. 5.2.3.3 which show the pronounced effects of the off-diagonal terms γ_{rt} and γ_{tr} should these ever be comparable with γ_t and γ_r, as is likely in liquid crystals.

Molecular Dynamics Simulation in the Presence of a Parity Breaking Field

This method provides an exact set of rotational and translational trajectories for the 3×3 Lennard–Jones atom–atom potential used to simulate a C_{2v} triatomic. We may see directly whether the mixed momentum a.c.f.'s $\langle \mathbf{p}(t)\cdot\mathbf{L}(0)\rangle$ or $\langle \mathbf{L}(t)\cdot\mathbf{p}(0)\rangle$ exist for this kind of asymmetric top, and using the simulator, we may attempt to describe in a self-consistent theoretical fashion $\langle \mathbf{p}(t)\cdot\mathbf{p}(0)\rangle$, $\langle \mathbf{L}(t)\cdot\mathbf{L}(0)\rangle$ and the mixed functions themselves. Here $\mathbf{L}$ denotes the net angular momentum. Figure 5.2.3.2 shows the result of some runs carried out at 220°K with the Lennard–Jones parameters $\epsilon/k = 173.5$°K, $\sigma = 3\times10^{-10}$ m. Some conventional a.c.f.'s are displayed in Fig. 5.2.3.4. Unlike these, the mixed a.c.f.'s have a relatively high built-in uncertainty in absolute value but exhibit the same kind of overall form for all averaging runs.

As a first approximation we may attempt to match the simulation data

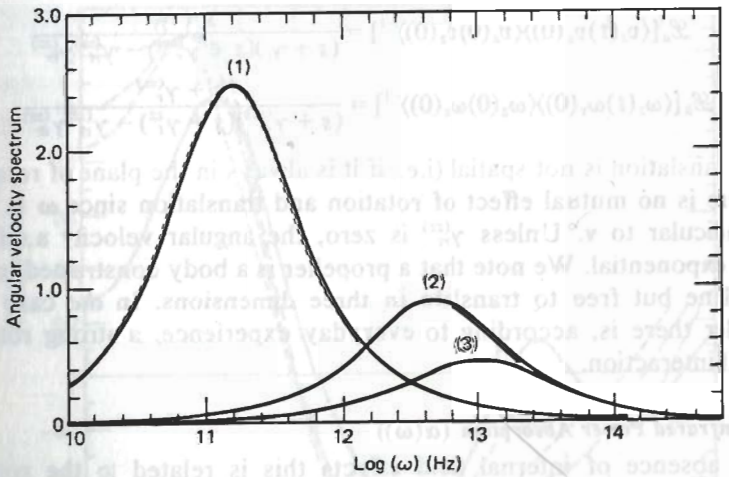

Figure 5.2.3.3 The effect of very strong translation/rotation coupling on the dielectric loss. Curves 1–3, increasing translation/rotation coupling.

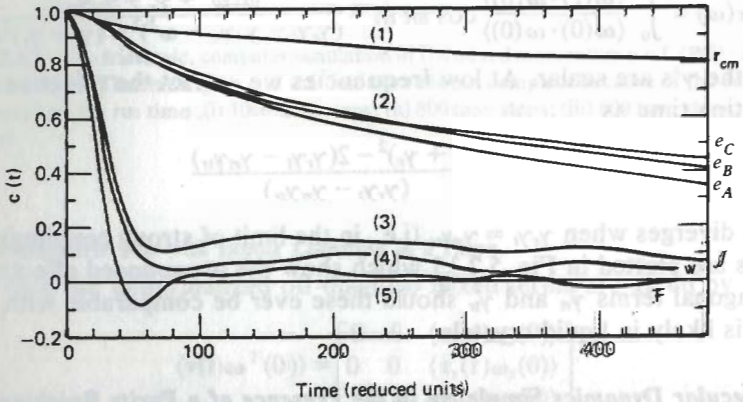

Figure 5.2.3.4 Some correlation functions from a computer simulation of a C_{2v} triatomic. It is much easier to obtain than the curves of Fig. 5.2.3.2. (1) Position of center of mass a.c.f.; (2) orientational a.c.f.; (3) angular velocity a.c.f.; (4) velocity a.c.f.; (5) force a.c.f.

with the rototranslational Langevin equations (5.2.3.1). The easiest way to make this comparison is to regard λ_t, λ_r, and the product $\lambda_{tr}\lambda_{rt}$ as variables and carry out a nonlinear least mean squares minimization on the difference:

$$\frac{\langle \omega(t)\cdot\omega(0)\rangle}{\langle \omega(0)\cdot\omega(0)\rangle} - \frac{\langle \mathbf{v}(t)\cdot\mathbf{v}(0)\rangle}{\langle \mathbf{v}(0)\cdot\mathbf{v}(0)\rangle} = \frac{(\lambda_t-\lambda_r)}{(c-b^2)^{1/2}}\, e^{-bt}\sin(c-b^2)^{1/2}t \qquad (c>b^2)$$

$$= \frac{(\lambda_t-\lambda_r)}{(c-b^2)^{1/2}}\, e^{-bt}\sinh(b^2-c)^{1/2}t \qquad (b^2>c)$$

The result shows the need for a higher Mori approximant for the behavior of A. The effect of rototranslational interaction in terms of the Langevin equation of molecular motion may be rationalized as follows. Hydrodynamically the origin of the coupled "drag coefficients" γ_{rt} and γ_{tr} lies in the fact that the translational or rotational motion of one Brownian particle causes a flow in the surrounding solvent. The moving solvent then exerts forces and torques on the other Brownian solute particles. It seems that even for rough sphere symmetries the mixed a.c.f.'s, and therefore the drag coefficients γ_{rt} and γ_{tr}, do not vanish. The problem is to gauge the extent of the rototranslational interaction by measurement of γ_{rt} and γ_{tr}, or more correctly, their equivalents in a higher approximant. It is always possible to extract a Debye relaxation time from the peak frequency of the dielectric loss but if translation and rotation mutually interact then this is defined in terms of rotational/translational and mixed drag coefficients. Data from three separate experimental sources, or alternatively over the complete 0–THz range of in a variety of conditions, are needed before progress can be made.

However, we can discuss analytically the role of γ_{tr} and γ_{rt} as follows. Consider the simplest form of the rototranslational Langevin equation:

$$\dot{\mathbf{v}} = -\gamma_t\mathbf{v} - \gamma_{tr}\boldsymbol{\omega} + \mathbf{F}(t)$$
$$\dot{\boldsymbol{\omega}} = -\gamma_{rt}\mathbf{v} - \gamma_r\boldsymbol{\omega} + \mathbf{N}(t)$$

We may express these equations in terms of the linear velocity as follows. By Laplace transformation,

$$-\mathbf{v}(0) + s\tilde{\mathbf{v}}(s) = -\gamma_t\tilde{\mathbf{v}}(s) - \gamma_{tr}\tilde{\boldsymbol{\omega}}(s) + \tilde{\mathbf{F}}(s)$$
$$-\boldsymbol{\omega}(0) + s\tilde{\boldsymbol{\omega}}(s) = -\gamma_r\tilde{\boldsymbol{\omega}}(s) - \gamma_{rt}\tilde{\mathbf{v}}(s) + \mathbf{N}(s)$$

so that

$$-\mathbf{v}(0) + s\tilde{\mathbf{v}}(s) = \left[-\gamma_t + \frac{\gamma_{tr}\gamma_{rt}}{s+\gamma_r}\right]\tilde{\mathbf{v}}(s) + \tilde{\mathbf{F}}'(s)$$
$$\equiv -\tilde{\beta}_v(s)\tilde{\mathbf{v}}(s) + \tilde{\mathbf{F}}'(s) \qquad (5.2.3.2)$$

where

$$\tilde{\mathbf{F}}'(s) \equiv \tilde{\mathbf{F}}(s) + \frac{(\tilde{\mathbf{T}}(s) + \boldsymbol{\omega}(0))}{s+\gamma_r}$$

Examine now the Laplace transform of the memory kernel $\tilde{\beta}(s)$ in Eq. 5.2.3.2 in the case:

$$|\gamma_{tr}|, |\gamma_{rt}| \ll \gamma_r, \gamma_t$$

We may approximate it with the Markovian idea:

$$\tilde{\beta}_v(s) = \gamma_t - \frac{\gamma_{rt}\gamma_{tr}}{s+\gamma_r} \doteq \gamma_t\left(1 - \frac{\gamma_{rt}\gamma_{tr}}{\gamma_r\gamma_t}\right) \qquad (5.2.3.3)$$

A similar approach may be made to obtain

$$\tilde{\beta}_\omega(s) \doteq \gamma_r\left(1 - \frac{\gamma_{rt}\gamma_{tr}}{\gamma_r\gamma_t}\right) \tag{5.2.3.4}$$

Equations 5.2.3.3 and 5.2.3.4 imply that in the absence of off-diagonal elements of $\boldsymbol{\gamma}$ translational and rotational frictions are diminished if γ_{rt} and γ_{tr} have the same signs. Otherwise the translation/rotation interaction increases both the rotational and translational frictions separately considered. It is preferable to call $\boldsymbol{\gamma}$ a dissipative matrix rather than a frictional matrix. It seems possible then that its off-diagonal elements may differ in sign. This is a question that must be settled with the aid of far infrared data and careful statistical analysis of the data from more than one experiment.

In Chapter 4 we have discussed the properties of the planar itinerant librator and oscillator. In the case of rototranslation we may write this as the multidimensional matrix equation (Chapters 9 and 10):

$$\begin{aligned}
\dot{\mathbf{A}}_1 &= -\boldsymbol{\omega}_{12}\cdot\mathbf{A}_2 - \boldsymbol{\gamma}\cdot\mathbf{A}_1 + \mathbf{F}(t)\\
\dot{\mathbf{A}}_2 &= -\boldsymbol{\omega}_{21}\cdot\mathbf{A}_1 - \boldsymbol{\omega}_{23}\cdot\mathbf{A}_3\\
\dot{\mathbf{A}}_3 &= -\boldsymbol{\omega}_{32}\cdot\mathbf{A}_2 - \boldsymbol{\omega}_{34}\cdot\mathbf{A}_4\\
\mathbf{A}_4 &= \mathbf{0}
\end{aligned} \tag{5.2.3.5}$$

where the column vectors are defined as follows:

$$\mathbf{A}_1 = \begin{bmatrix} \left(\frac{\Delta_2^{(t)}}{\Delta_1^{(t)}}\right)\dot{x} \\ \left(\frac{\Delta_2^{(r)}}{\Delta_1^{(r)}}\right)\dot{\psi} \end{bmatrix}$$

$$\mathbf{A}_2 = \begin{bmatrix} \Delta_2^{(t)}(X - x) \\ \Delta_2^{(r)}(\theta - \psi) \end{bmatrix}$$

$$\mathbf{A}_3 = \begin{bmatrix} \dot{X} \\ \dot{\theta} \end{bmatrix}$$

Here x is the component of the center of mass velocity of the cage, X of the molecule, and (θ, ψ) are angles defined in Chapter 4 which describe the rotational itinerant oscillator. Here

$$\Delta_2^{(t)} = \phi_0^{(t)}(0); \qquad \Delta_1^{(t)} = \phi_1^{(t)}(0); \qquad \text{etc.}$$

Substituting in Eq. 5.2.3.5 we have

$$\left(\frac{\Delta_2^{(t)}}{\Delta_1^{(t)}}\right)\ddot{x} = \Delta_1^{(t)}\Delta_2^{(t)}(X - x) - \left(\frac{\Delta_2^{(t)}}{\Delta_1^{(t)}}\right)\gamma^{(t)}\dot{x} - \gamma^{(tr)}\left(\frac{\Delta_2^{(r)}}{\Delta_1^{(r)}}\right)\dot{\psi} + F_x$$

$$\left(\frac{\Delta_2^{(r)}}{\Delta_1^{(r)}}\right)\ddot{\psi} = \Delta_1^{(r)}\Delta_2^{(r)}(\theta - \psi) - \left(\frac{\Delta_2^{(t)}}{\Delta_1^{(t)}}\right)\gamma^{(rt)}\dot{x} - \gamma^{(r)}\left(\frac{\Delta_2^{(r)}}{\Delta_1^{(r)}}\right)\dot{\psi} + N$$

$$\ddot{X} = -\Delta_2^{(t)}\Delta_2^{(t)}(X - x)$$

$$\ddot{\theta} = -\Delta_2^{(r)}\Delta_2^{(r)}(\theta - \psi)$$

which decouple in the absence of rotation/translation interaction to those for itinerant planar libration and space itinerant oscillation. These may be solved for the autocorrelation matrix by using their equivalence to the Mori approximant. If we define the third memory matrix by

$$\tilde{\mathbf{C}}_3(s)\cdot\boldsymbol{\phi}_3(0) = \begin{bmatrix} \lambda_t & \lambda_{tr} \\ \lambda_{rt} & \lambda_r \end{bmatrix}$$

we find

$$\tilde{\mathbf{C}}(s) = \frac{1}{D_2(s)}\begin{bmatrix} s + \left[s + (s + \lambda_r)\frac{\phi_{t_2}}{D(s)}\right]\frac{\phi_{r_1}}{D_1(s)}; & -\frac{\lambda_{tr}\phi_{r_2}\phi_{r_1}}{D(s)D_1(s)} \\ -\frac{\lambda_{rt}\phi_{t_2}\phi_{t_1}}{D(s)D_1(s)}; & s + \left[s + (s + \lambda_t)\frac{\phi_{r_2}}{D(s)}\right]\frac{\phi_{t_1}}{D_1(s)} \end{bmatrix}$$

where

$$D_1(s) = \left[s + (s + \lambda_t)\frac{\phi_{r_2}}{D(s)}\right]\left[s + (s + \lambda_r)\frac{\phi_{t_2}}{D(s)}\right] - \frac{\lambda_{tr}\lambda_{rt}\phi_{t_2}\phi_{r_2}}{D^2(s)}$$

and

$$D_2(s) = \left[s + \left(s + (s + \lambda_t)\frac{\phi_{r_2}}{D(s)}\right)\frac{\phi_{t_1}}{D_1(s)}\right]\left[s + \left(s + (s + \lambda_r)\frac{\phi_{t_2}}{D(s)}\right)\frac{\phi_{r_1}}{D_1(s)}\right]$$
$$- \frac{\lambda_{tr}\lambda_{rt}\phi_{t_2}\phi_{t_1}\phi_{r_2}\phi_{r_1}}{D^2(s)D_1^2(s)}$$

$$D(s) = (s + \lambda_t)(s + \lambda_r) - \lambda_{tr}\lambda_{rt}$$

We now have the relation

$$\lambda_{tr}\phi_{r_2}\phi_{r_1} = \lambda_{rt}\phi_{t_2}\phi_{t_1}$$

and all the a.c.f.'s involve the seven phenomenological variables ϕ_{t_1}, ϕ_{t_2}, ϕ_{r_1}, ϕ_{r_2}, λ_t, λ_r, and $\lambda_{tr}\lambda_{rt}$. It is possible to evaluate the first four using computer molecular dynamics and the general properties of correlation functions argued in Chapter 1.

Three-dimensional rototranslation of the asymmetric top is insoluble analytically. This is due to the nonlinear terms in the Euler–Langevin rototranslational equation. The angular velocity components cannot be related to the orientation vector in an analytical, linear fashion. Using Euler angles to define the orientational time dependence it is preferable to express the dynamic equations in the molecule fixed frame. A precessional contribution has then to be added to the dynamical equations. When the vector variable $\mathbf{A}$ contains an angular momentum component such as $\mathbf{I}\cdot\boldsymbol{\omega}$ it is convenient to make the transformation by replacing Eq. 5.2.3.1 with rigorous equations modified by the inclusion of precessional terms which are nonlinear in nature. Such a modification does not circumvent the difficulty of the

problem, and in the Markov limit,

$$\dot{\omega}_i = \frac{(I_j - I_k)\omega_j\omega_k}{I_i} - \sum_{l=1}^{3} (\gamma_{il}^{(r)}\omega_l + \gamma_{il}^{(rt)}v_l) + T_i(t)$$

$$\dot{v}_i = -\sum_{l=1}^{3} (\gamma_{il}^{(t)}v_l + \gamma_{il}^{(tr)}\omega_l) + F_i(t)$$

where i, j, and k permute 1, 2, and 3 cyclically. The presence of the nonlinear terms prevent the use of Laplace inversion but the corresponding Fokker–Planck equation is soluble numerically for the p.d.f. $f(\mathbf{v}, \boldsymbol{\omega}, t \mid \mathbf{v}_0, \boldsymbol{\omega}_0, t_0)$. For f we may write

$$\begin{aligned}\frac{\partial f}{\partial t} = \sum_{i=1}^{3} \Bigg\{ &- \left(\frac{\partial}{\partial \omega_i}\left[\frac{I_j - I_k}{I_i}\right]\omega_j\omega_k f\right) \\ &+ \sum_{l=1}^{3}\left[\frac{\partial}{\partial\omega_i}(\gamma_{il}^{(r)}\omega_l + \gamma_{il}^{(rt)}v_l) + \frac{\partial}{\partial v_i}(\gamma_{il}^{(t)}v_l + \gamma_{il}^{(tr)}\omega_l)\right]f \\ &+ \sum_{l=1}^{3}\left[\frac{\partial}{\partial\omega_i}\left(\gamma_{il}^{(r)}\frac{kT}{I_i}\frac{\partial}{\partial\omega_l}\right) + \frac{1}{2}\left(\gamma_{il}^{(tr)}\frac{kT}{I_i} + \gamma_{il}^{(rt)}\frac{kT}{m}\right)\frac{\partial}{\partial v_l}\right]f \\ &+ \sum_{l=1}^{3}\frac{\partial}{\partial v_i}\left[\gamma_{il}^{(t)}\frac{kT}{m}\frac{\partial}{\partial v_l} + \frac{1}{2}\left(\gamma_{il}^{(rt)}\frac{kT}{m} + \gamma_{il}^{(tr)}\frac{kT}{I_i}\right)\frac{\partial}{\partial\omega_l}\right]f\Bigg\} \end{aligned} \tag{5.2.3.6}$$

where i, j, and k permute 1, 2, and 3 cyclically.

5.2.4 Wiener Algebra of Rototranslation

The solution of Eq. 5.2.3.1 is that of the matrix equation

$$\dot{\mathbf{X}}(t) = \mathbf{A}\cdot\mathbf{X}(t) + \mathbf{B}\cdot\dot{\mathbf{W}}_i(t) \tag{5.2.4.1}$$

which is

$$\mathbf{X}(t) = \exp(\mathbf{A}t)\cdot\mathbf{X}(0) + \int_0^t \exp[\mathbf{A}(t-\tau)]\cdot\mathbf{B}\cdot\boldsymbol{\xi}\,(d\tau) \tag{5.2.4.2}$$

where ξ_i denotes a column vector whose elements are differences of Wiener processes governing the random force and torque. The maximum of information may be extracted from Eq. 5.2.4.2 if they are identified with $\mathbf{X}$, $\mathbf{A}$, and $\dot{\mathbf{W}}_i$, the Wiener process, as follows:

$$\mathbf{X} = \begin{bmatrix}\theta\\ R\\ \omega\\ v\end{bmatrix}; \qquad \mathbf{A} = \begin{bmatrix}0 & 0 & 1 & 0\\ 0 & 0 & 0 & 1\\ 0 & 0 & -\gamma_r & -\gamma_{rt}^*\\ 0 & 0 & -\gamma_{tr}^* & \gamma_t\end{bmatrix}$$

$$\mathbf{B} = \begin{bmatrix}0 & 0 & 0 & 0\\ 0 & 0 & 0 & 0\\ 0 & 0 & 1 & 0\\ 0 & 0 & 0 & 1\end{bmatrix}; \qquad \dot{\mathbf{W}} = \begin{bmatrix}0\\ 0\\ \dot{W}_3\\ \dot{W}_4\end{bmatrix}$$

Here $\gamma_{rt}^* = \gamma_{rt}(m/I)$; $\gamma_{tr}^* = (I/m)\gamma_{tr}$; θ denotes the total angle through which the molecule has rotated since the arbitrary initial $t = 0$ and R is a component of the center of mass position vector. As we have seen it is now convenient to make the Laplace transform:

$$\tilde{\mathbf{X}}(s) = \mathscr{L}_a[\mathbf{X}(t)] = \int_0^\infty \exp(-st)\mathbf{X}(t)\,dt$$

so that

$$\mathscr{L}_a^{-1}[(s\mathbf{1} - \mathbf{A})^{-1}] = \exp(\mathbf{A}t)$$

$$\mathscr{L}_a^{-1}[s\mathbf{1} - \mathbf{A})^{-1}\cdot\mathbf{B}\cdot\boldsymbol{\xi}] = \int_0^t \exp[\mathbf{A}(t-\tau)]\cdot\mathbf{B}\cdot\boldsymbol{\xi}(d\tau)$$

$$\langle\mathbf{X}(t)\rangle = \exp(\mathbf{A}t)\mathbf{X}_0.$$

and

$$\mathbf{Y}(t) = \mathbf{X}(t) - \langle\mathbf{X}(t)\rangle = \int_0^t \exp[\mathbf{A}(t-\tau)]\cdot\mathbf{B}\cdot\boldsymbol{\xi}(d\tau)$$

In these equations $\langle\,\rangle$ denotes a nonequilibrium, transient time average. Note that in some cases at equilibrium

$$\langle\mathbf{X}(t)\rangle \xrightarrow{t\to\infty} \mathbf{0}$$

It is possible therefore to obtain expressions for the nonequilibrium average of θ, R, ω, and v, for their moments and mixed moments. Further analytical averaging is then possible for the purpose of comparison with observables. The influence of rotation on, for example, the mean square displacement may then be given analytical form in terms of these averages explicitly. The matrix $\exp(\mathbf{A}t)$ is the inverse Laplace transform of

$$(s\mathbf{1} - \mathbf{A})^{-1} = \{s^2[(s+\gamma_t)(s+\gamma_r) - \gamma_{tr}^*\gamma_{rt}^*]\}^{-1}$$

$$\times\begin{bmatrix} s[(s+\gamma_r)(s+\gamma_t) - \gamma_{rt}^*\gamma_{tr}^*]; & 0; & s(s+\gamma_t); & -\gamma_{rt}^*s\\ 0; & s[(s+\gamma_r)(s+\gamma_t) - \gamma_{rt}^*\gamma_{tr}^*]; & -\gamma_{tr}^*s; & (s+\gamma_r)s\\ 0; & 0; & s^2(s+\gamma_t); & -\gamma_{rt}^*s^2\\ 0; & 0; & -\gamma_{tr}^*s^2; & (s+\gamma_r)s^2\end{bmatrix}$$

Denoting the elements of this matrix by α_{ij}, we may write the averages:

$$\langle\theta(t)\rangle = \alpha_{11}(t)\theta(0) + \alpha_{13}(t)\omega(0) + \alpha_{14}(t)v(0)$$

$$\langle R(t)\rangle = \alpha_{22}(t)R(0) + \alpha_{23}(t)\omega(0) + \alpha_{24}(t)v(0)$$

$$\langle\omega(t)\rangle = \alpha_{33}(t)\omega(0) + \alpha_{34}(t)v(0)$$

$$\langle v(t)\rangle = \alpha_{43}(t)\omega(0) + \alpha_{44}(t)v(0)$$

at time t given $\theta(0)$, $R(0)$, $\omega(0)$, and $v(0)$.

Illustration

At this stage it is convenient to consider the method of building up observable averages from the rotational equation

$$I\ddot{\theta} + I\beta\dot{\theta}(t) = I\dot{B}(t)$$

that is, that of the plane rotor. It is important to note that $\theta(t)$ is the total angle turned through since $t = 0$ and is not restricted to the range $-\pi$ to π. This means that for the purposes of illustration we can regard $\theta(t)$ as a Gaussian and not a wrapped Gaussian in nature. Taking the state variables $X_1 = \theta(t)$; $X_2 = \dot{\theta}(t)$, then

$$\begin{bmatrix}\theta(t)\\ \dot{\theta}(t)\end{bmatrix} = \begin{bmatrix}1 & (1-e^{-\beta t})/\beta\\ 0 & e^{-\beta t}\end{bmatrix}\begin{bmatrix}\theta_0\\ \dot{\theta}_0\end{bmatrix} + \int_0^t \begin{bmatrix}1 & (1-e^{-\beta t})/\beta\\ 0 & e^{-\beta(t-\tau)}\end{bmatrix}\begin{bmatrix}0\\ 1\end{bmatrix}\xi(d\tau)$$

so that

$$\theta(t) = \theta_0 + \frac{\dot{\theta}_0}{\beta}(1-e^{-\beta t}) + \frac{1}{\beta}\int_0^t (1-e^{-\beta(t-\tau)})\xi(d\tau)$$

$$\dot{\theta}(t) = \dot{\theta}_0 e^{-\beta t} + \int_0^t e^{-\beta(t-\tau)}\xi(d\tau)$$

Here θ_0 and $\dot{\theta}_0$ are the initial values of $\theta(t)$ and $\dot{\theta}(t)$. Since $\langle\xi(1-e^{-\beta(t-\tau)})\rangle = \langle\xi(e^{-\beta(t-\tau)})\rangle = 0$ we have

$$\langle\theta(t)\rangle = \theta_0 + \frac{\dot{\theta}_0}{\beta}(1-e^{-\beta t})$$

or

$$\langle\theta(t)-\theta(0)\rangle = \frac{\dot{\theta}_0}{\beta}(1-e^{-\beta t}); \qquad \langle\dot{\theta}(t)\rangle = \dot{\theta}_0 e^{-\beta t}$$

The experimentally observable average is the equilibrium mean square displacement, denoted by $\langle[\theta(t)-\theta(0)]^2\rangle = \langle(\Delta\theta)^2\rangle$. However, since we regard $\Delta\theta$ as the total angular displacement this is observable only in a carefully controlled computer simulation. If, however, we replace θ by the linear x coordinate and I by the mass m, then the linear mean square displacement $\langle\Delta x^2\rangle$ is directly observable, for example, by using a microscope on a colloidal suspension. Evaluating the square we have

$$\begin{aligned}\langle(\Delta\theta)^2\rangle &= \left\langle\left[\frac{\dot{\theta}_0}{\beta}(1-e^{-\beta t}) + \frac{1}{\beta}\int_0^t (1-e^{-\beta(t-\tau)})\xi(d\tau)\right]^2\right\rangle\\ &= \left\langle\left[\frac{\dot{\theta}_0^2}{\beta^2}(1-e^{-\beta t})^2 + \frac{2\dot{\theta}_0}{\beta^2}\int_0^t (1-e^{-\beta(t-\tau)})\xi(d\tau)\right.\right.\\ &\quad \left.\left. + \frac{1}{\beta^2}\left[\int_0^t (1-e^{-\beta(t-\tau)}\xi(d\tau))\right]^2\right\rangle\\ &= \frac{\langle\dot{\theta}_0^2\rangle}{\beta^2}(1-e^{-\beta t})^2 + \frac{1}{\beta^2}\left\langle\left[\int_0^t [1-e^{-\beta(t-\tau)}\xi(d\tau)]\right]^2\right\rangle\end{aligned}$$

Using the properties of the Wiener process, the integral may now be evaluated explicitly:

$$\begin{aligned}\langle\Delta\theta^2\rangle &= \frac{\langle\dot{\theta}_0^2\rangle}{\beta^2}(1-e^{-\beta t})^2 + \frac{c^2}{\beta^2}\int_0^t (1-2e^{-\beta(t-\tau)} + e^{-2\beta(t-\tau)})\,d\tau\\ &= \frac{c^2 t}{\beta^2} + \frac{\langle\dot{\theta}_0^2\rangle}{\beta^2}(1-e^{-\beta t})^2 + \frac{c^2}{2\beta^3}(4e^{-\beta t} - e^{-2\beta t} - 3)\end{aligned}$$

(see Chapter 2). In exactly the same way we find that

$$\langle\dot{\theta}^2\rangle = \frac{c^2}{2\beta} + \left(\dot{\theta}_0^2 - \frac{c^2}{2\beta}\right)e^{-2\beta t}$$

To evaluate the constant c^2 we assume that the Maxwell–Boltzmann distribution for $\dot{\theta}(t)$ as $t\to\infty$, so that $\frac{1}{2}I\lim_{t\to\infty}\langle\dot{\theta}^2(t)\rangle = \frac{1}{2}kT$, and $c^2 = 2\beta kT/I$. Taking a second average over $\dot{\theta}_0$, remembering that $\langle\dot{\theta}_0^2\rangle = kT/I$, we find

$$\langle\langle\Delta\theta\rangle\rangle = 0$$

$$\langle\langle(\Delta\theta)^2\rangle\rangle = \frac{2kT}{I\beta^2}(\beta t - 1 + e^{-\beta t})$$

$$\langle\dot{\theta}(t)\rangle = 0$$

For $\beta t \gg 1$

$$\langle\langle\Delta\theta^2\rangle\rangle = \frac{2kT}{I\beta^2}\beta t = \frac{2kTt}{I\beta}$$

which is the Einstein relation.

In the same way the mean square linear and angular displacement of a pollen particle may be calculated from the mean square of

$$R(t) - R(0) - \int_0^t \alpha_{43}(t)\omega(0)\,dt - \int_0^t \alpha_{44}(t)v(0)\,dt$$

The result is that

$$\begin{aligned}\langle\langle[R(t)-R(0)]^2\rangle\rangle = \frac{kT}{m}\left(\frac{(1+y)}{(b-x)^2}((b-x)t\right.\\ \left. + \exp[-(b-x)t-1]) + \frac{(1-y)}{(b+x)^2}\{(b+x)t + \exp[-(b+x)t] - 1\}\right)\end{aligned}$$

where

$$y = \frac{(\lambda_r - b)}{(b^2-c)^{1/2}}; \qquad x = (b^2-c)^{1/2}$$

As $t\to\infty$ we recover the rototranslational equivalent of Einstein's result:

$$\langle\langle[R(t)-R(0)]^2\rangle\rangle \xrightarrow[t\to\infty]{} \frac{2kTt}{m}\left(\frac{\gamma_r}{\gamma_t\gamma_r - \gamma_{tr}^*\gamma_{rt}^*}\right)$$

We note that $\gamma_r/(\gamma_t\gamma_r - \gamma_{tr}^*\gamma_{rt}^*) \to 1/\gamma_t$ in the decoupled limit, producing Einstein's relation for translational Brownian motion. Similarly,

$$\langle\langle[\theta(t)-\theta(0)]^2\rangle\rangle \xrightarrow[t\to\infty]{} \frac{2kTt}{I}\left(\frac{\gamma_t}{\gamma_t\gamma_r - \gamma_{tr}^*\gamma_{rt}^*}\right) \longrightarrow \left(\frac{2kT}{I}\right)\gamma_r^{-1}$$

in the decoupled limit. In the case $c > b^2$, the result may be expressed as

$$\begin{aligned}\langle\langle[R(t)-R(0)]^2\rangle\rangle = \frac{2kT}{m}\Bigg[&\left(t - \frac{b+xy}{x^2+b^2}\right)\left(e^{-bt}\frac{x\sin xt - b\cos xt}{x^2+b^2} + \frac{b}{x^2+b^2}\right)\\ &- \left(yt - \frac{yb-x}{x^2+b^2}\right)\left(e^{-bt}\frac{b\sin xt + x\cos xt}{x^2+b^2} - \frac{x}{x^2+b^2}\right)\\ &+ te^{-bt}\left(\frac{(yb-x)\sin xt + (yx+b)\cos xt}{x^2+b^2}\right)\Bigg]\end{aligned}$$

with $y = (\lambda_r - b)/(c-b^2)^{1/2}$; $x = (c-b^2)^{1/2}$. Again, as $t \to \infty$ we recover the Einstein type relations.

In the same way it is possible to evaluate the mean square velocities and angular velocities:

$$\langle(\omega(t) - \langle\omega(t)\rangle)^2\rangle \xrightarrow[t\to\infty]{} \frac{kT}{I} \qquad \text{(for planar rotation)}$$

$$\langle[v(t) - \langle v(t)\rangle]^2\rangle \xrightarrow[t\to\infty]{} \frac{kT}{m} \qquad \text{(for each component of } \mathbf{v})$$

$$\langle[\omega(t) - \langle\omega(t)\rangle][v(t) - \langle v(t)\rangle]\rangle \xrightarrow[t\to\infty]{} 0$$

The method of Wiener matrix algebra may be generalized to the non-Markov regime by expressing Eqs. 5.2.3.5 in the matrix form (5.2.4.1). In this case we have

$$\dot{\mathbf{X}}_0(t) = \mathbf{A}_0 \cdot \mathbf{X}_0(t) + \mathbf{B}_0 \cdot \mathbf{W}_0(t)$$

where

$$\mathbf{A}_0 = \begin{bmatrix} 0 & 0 & 0 & 0 & 1 & 0 & 0 & 0 \\ 0 & 0 & 0 & 0 & 0 & 1 & 0 & 0 \\ 0 & 0 & 0 & 0 & 0 & 0 & 1 & 0 \\ 0 & 0 & 0 & 0 & 0 & 0 & 0 & 1 \\ \Delta_2^{(t)2} & \Delta_2^{(t)2} & 0 & 0 & 0 & 0 & 0 & 0 \\ \Delta_1^{(t)2} & -\Delta_1^{(t)2} & 0 & 0 & 0 & -\gamma^{(t)} & 0 & \dfrac{-\Delta_2^{(r)}\Delta_1^{(t)}\gamma^{(tr)}}{\Delta_1^{(r)}\Delta_2^{(t)}} \\ 0 & 0 & -\Delta_2^{(r)2} & \Delta_2^{(r)2} & 0 & 0 & 0 & 0 \\ 0 & 0 & \Delta_1^{(r)2} & -\Delta_1^{(r)2} & 0 & \dfrac{-\Delta_2^{(t)}\Delta_1^{(r)}\gamma^{(rt)}}{\Delta_2^{(r)}\Delta_1^{(t)}} & 0 & -\gamma^{(r)} \end{bmatrix} \qquad (5.2.4.3)$$

Here the matrices $\mathbf{X}_0(t)$ and $\mathbf{W}_0(t)$ are defined by

$$\mathbf{X}_0(t) = \begin{bmatrix} X(t) \\ x(t) \\ \theta(t) \\ \psi(t) \\ \dot{X}(t) \\ \dot{x}(t) \\ \dot{\theta}(t) \\ \dot{\psi}(t) \end{bmatrix}; \qquad \mathbf{W}_0(t) = \begin{bmatrix} 0 \\ 0 \\ 0 \\ 0 \\ 0 \\ W_1(t) \\ 0 \\ W_2(t) \end{bmatrix}$$

and B_0 is an 8×8 matrix which is null except for the (6, 6) and (8, 8) elements, which are 1. In these matrices x is a component of the center of mass of the itinerant oscillator cage, X of the encaged molecule, and θ and ψ are the angles defined in Chapter 4 for the planar itinerant librator. $\Delta_2^{(t)2}$ is the mean square linear force of the encaged molecule and $\Delta_2^{(r)2}$ is its angular counterpart. $\Delta_1^{(t)2}$ and $\Delta_1^{(r)2}$ are similarly equilibrium averages involving the mean square force (or torque) and its derivative. $\gamma^{(t)}$, $\gamma^{(r)}$, $\gamma^{(tr)}$, and $\gamma^{(rt)}$ are elements of the matrix γ of Eq. 5.2.3.5. Obviously it is advisable to solve Eq. 5.2.4.3 numerically, but the analytical form of the associated secular equation is of interest, since it tells something about the physical nature of the model we have constructed. This is the determinantal equation of $[s\mathbf{1} - \mathbf{A}_0]^{-1}$, that is,

$$\begin{aligned} s^2G(s) \equiv s^2\{&(s^2+\Delta_2^{(t)2})(s^2+\Delta_2^{(r)2})[(s+\gamma^{(t)})(s+\gamma^{(r)}) - \gamma_{rt}\gamma_{tr}]\\ &+ s[(s+\gamma^{(t)})\Delta_2^{(t)2}\Delta_1^{(r)2} + (s+\gamma^{(r)})\Delta_1^{(t)2}\Delta_2^{(r)2}]\\ &+ s^3[\Delta_1^{(r)2}(s+\gamma^{(t)}) + \Delta_1^{(t)2}(s+\gamma^{(r)})]\} = 0 \end{aligned} \qquad (5.2.4.4)$$

We obtain the known equations governing the purely translational itinerant oscillator or purely rotational planar librator, that is,

$$s^4[s^3 + s^2\gamma^{(t)} + s(\Delta_1^{(t)2} + \Delta_2^{(t)2}) + \Delta_2^{(t)2}\gamma^{(t)}](s+\gamma^{(r)}) = 0 \qquad (5.2.4.5)$$

$$s^4[s^3 + s^2\gamma^{(r)} + s(\Delta_1^{(r)2} + \Delta_2^{(r)2}) + \Delta_2^{(r)2}\gamma^{(r)}](s+\gamma^{(t)}) = 0 \qquad (5.2.4.6)$$

if the following associated conditions are obeyed:

(*a*) For Eq. 5.2.4.5: $\Delta_1^{(r)2} = \Delta_2^{(r)2} = 0$; $\quad \gamma^{(tr)}\gamma^{(rt)} = 0$

(*b*) For Eq. 5.2.4.6: $\Delta_1^{(t)2} = \Delta_2^{(t)2} = 0$; $\quad \gamma^{(tr)}\gamma^{(rt)} = 0$

We are now in a position to extract some physical information about rototranslation in the Markov limit. This may be summarized as follows:

1. Then only natural instance of mutually exclusive translational or rotational motion occurs when torques or forces (respectively) are absent. This is the case also for space rototranslation and is expected intuitively.

2. Taking note of the structure within the braces of the above equation allows us to identify the factors γ_r, γ_t, γ_{rt}, and γ_{tr} in terms of the model in hand. γ_r is the purely rotational part of the dissipative frequency matrix of the central molecule relative to the stationary cage. γ_{rt} and γ_{tr} are off-diagonal elements of this matrix.
3. The truncated form of Eq. 1.7.4.1 resulting in Eq. 5.2.4.3, 5.2.4.5, and 5.2.4.6 is fully consistent with equations of motion which are separately Markovian (i.e., represented in Eq. 5.2.3.5). The truncated Mori continued fraction is therefore fully consistent with the physical model of constrained itinerant oscillation/libration.
4. It is self-consistent to use a dissipative matrix of the form $\begin{bmatrix} \gamma_t & \gamma_{tr} \\ \gamma_{rt} & \gamma_r \end{bmatrix}$. Physically, however, the motion of the molecule/cage system depends only on the product $\gamma_{tr}\gamma_{rt}$ so that individually their sign is irrelevant provided it is the same for γ_{rt} and γ_{tr}.

The linear velocity a.c.f. can be calculated from the (5, 5) element of $(s\mathbf{1} - \mathbf{A}_0)^{-1}$, and is

$$F^{(t)}(s) = \mathscr{L}_a \frac{\langle \dot{X}(t)\dot{X}(0)\rangle}{\langle \dot{X}(0)\dot{X}(0)\rangle}$$
$$= \{s[s^2 + \Delta_2^{(r)2}][(s + \gamma^{(t)})(s + \gamma^{(r)}) - \gamma^{(rt)}\gamma^{(tr)}]$$
$$+ s^2[\Delta_1^{(t)2}(s + \gamma^{(r)}) + \Delta_1^{(r)2}(s + \gamma^{(t)})] + \Delta_1^{(t)2}(s\Delta_1^{(r)2} + (s + \gamma^{(r)})\Delta_2^{(r)2}\}/G(s)$$

which in the decoupled limit reduces to

$$\frac{s^2 + \gamma^{(t)}s + \Delta_1^{(t)2}}{s^3 + \gamma^{(t)}s^2 + (\Delta_1^{(t)2} + \Delta_2^{(t)2})s + \Delta_2^{(t)2}\gamma^{(t)}}$$

This is exactly the expression for the purely translational itinerant oscillator. Similarly the angular velocity a.c.f. is

$$F^{(r)}(s) = \frac{\mathscr{L}_a\langle \dot{\theta}(t)\dot{\theta}(0)\rangle}{\langle \dot{\theta}(0)\dot{\theta}(0)\rangle}$$
$$= \{s[s^2 + \Delta_2^{(t)2}][(s + \gamma^{(r)})(s + \gamma^{(t)}) - \gamma^{(tr)}\gamma^{(rt)}]$$
$$+ s^2[\Delta_1^{(r)2}(s + \gamma^{(t)}) + \Delta_1^{(t)2}(s + \gamma^{(r)})] + \Delta_1^{(r)2}[s\Delta_1^{(t)2} + (s + \gamma^{(t)})\Delta_2^{(t)2}]\}/G(s)$$

which reduces to

$$\frac{s^2 + \gamma^{(r)}s + \Delta_1^{(r)2}}{s^3 + \gamma^{(r)}s^2 + (\Delta_1^{(r)2} + \Delta_2^{(r)2})s + \Delta_2^{(r)2}\gamma^{(r)}}$$

in the decoupled limit. The mixed a.c.f.'s can be extracted similarly as

$$\mathscr{L}_a[\langle \dot{\theta}(t)\dot{X}(0)\rangle] = \langle \dot{X}(0)\dot{X}(0)\rangle\left[s^3(s + \gamma^{(t)})\Delta_2^{(r)}\Delta_2^{(t)}\frac{\Delta_1^{(r)}}{\Delta_1^{(t)}}\gamma^{(rt)}/G(s)\right]$$

$$\mathscr{L}_a[\langle \dot{X}(t)\dot{\theta}(0)\rangle] = \langle \dot{\theta}(0)\dot{\theta}(0)\rangle\left[s^3(s + \gamma^{(r)})\Delta_2^{(t)}\Delta_2^{(r)}\frac{\Delta_1^{(t)}}{\Delta_1^{(r)}}\gamma^{(tr)}/G(s)\right]$$

which vanish in the decoupled limit. It is clear that we may autocorrelate θ, ψ, X, and x in 16 ways and that all 16 a.c.f.'s may be both calculated analytically and computer simulated.

5.2.4.1 Rototranslation of the Asymmetric Top

The multidimensional Markov equation (Eq. 5.2.3.5) may be used to consider this general problem of single-particle translation/rotation dynamics. In general, for a finite Mori approximant of order n the relaxation process affecting the first variable of the chain, the nth memory function, must be defined. This is not possible in the context of Eq. 1.7.4.1 because the Mori equation does not allow us to define physically the meaning of the memory kernel when the rotational part of the motion involves the three Euler angles.

However, a general theory of asymmetric top rototranslation may be developed using the Markovian set of Eq. 5.2.3.5. For example, we consider the simple instance where the $(n + 1)$th matrix is

$$\mathbf{A}_{n+1} = \begin{bmatrix} v_z \\ \omega_z \end{bmatrix}$$

In the multidimensional Markov representation a rotranslational coupling exhibited by the friction or dissipative matrix γ (Eq. 5.2.3.5) would be transmitted through the chain of "virtual" matrices (see Chapters 9 and 10) $\mathbf{A}_1, \ldots, \mathbf{A}_n$ to the real $\mathbf{A}_{n+1}$. As a consequence we may take $\mathbf{A}_1$ to $\mathbf{A}_n$ as diagonal. This implies the following.

1. The multidimensional Markov chain (Eq. 5.2.3.5) removes the abstract memory kernel not only when dealing with the theory of single-particle motion but also in the extensively developed field of hydrodynamics. We may therefore relate conceptually the single-particle and multiparticle theories within a Markovian framework for molecules of any symmetry moving in three dimensions. The extension of Eq. 5.2.3.5 to higher n may be interpreted physically for planar reorientation in terms of the addition of more cages, or annuli which naturally become larger in comparison with a molecular diameter. Eventually the outer cages are macroscopic entities whose movement is equivalent to cooperative translation/rotation of groups of molecules. This is conceptually similar to vorticity, the translational part of the hydrodynamic spin density. By analogy, therefore, we may use Eq. 5.2.3.5 to construct a generalized hydrodynamic formalism without assuming, for example, a frequency-dependent viscosity. This would be equivalent to taking the Navier–Stokes equation and solving without first linearizing, as is the usual practice. It may therefore be possible to build up a powerful theory of bulk phenomena from molecular considerations. One of the first tasks of such a theory would be to describe the vorticity and long

time tails on a purely molecular basis as in computer simulation, where there is no continuum.

2. Our interpretation in terms of a mechanical model such as the itinerant oscillator/librator eases the intuitive difficulty of understanding in single molecule terms the meaning of $\gamma^{(rt)}\gamma^{(tr)}$. By regarding Eq. 5.2.3.5 as a Markovian approximation to physical reality involving multimolecular ensembles we may describe the action of a propeller in terms of a macroscopic model corresponding to a higher-order Mori approximant. Development of the asymmetric top formalism allows us to consider also the motion of a single molecule shaped like a propeller where there is no difficulty in imagining translation at a time t in terms of a rotation at $t = 0$.

To remove all planar constraint on the motion of a dipole embedded in the asymmetric top it is necessary to use an iterative method of solution of the multi-Markovian system using a basis set representation of the diffusion equation. The solution set of the Fokker–Planck equation in this terminology is the set of Hermite polynomials. For the last variable in the chain, denoted by

$$\mathbf{A}_n = (A_1^{(n)}, A_2^{(n)}, \ldots, A_m^{(n)})$$

the basis set consists of the eigenstates (eigenkets or vectors)

$$\langle H_m(\mathbf{A}_n)\exp(-\tfrac{1}{2}\|\mathbf{A}_n\|^2)\rangle$$

where

$$H_m(\mathbf{A}_n) = H_{m_1}(A_1^{(n)})H_{m_2}(A_2^{(n)})\cdots H_{m_n}(A_m^{(n)})$$

Here H denotes the Hermite polynomials. Consequently the whole diffusion operator of the Fokker–Planck equation may be described by the basis set of Hermite polynomials, and consequently by the basis set spanned by the direct products:

$$\langle H_{m_1}(\mathbf{A}_1)\exp(-\tfrac{1}{2}\|\mathbf{A}_1\|)\cdots H_{\mathbf{m}_n}(\mathbf{A}_n)\exp(-\tfrac{1}{2}\|\mathbf{A}_1\|^2)\rangle$$

When inertial effects are negligible our generalized Fokker–Planck equation, through integration over the velocity variables, should provide a diffusion equation identical with the one by Favro (1960).

For the primary angular momentum variables the set of Wigner rotation matrices (see appendix to Chapter 2) is the standard. In the most general case, therefore, of an asymmetric top rotation and translation in space the latter must be used in combination with the eigenkets of the Hermite polynomials described above. The rotation/translation Fokker–Planck equation is put into the matrix form:

$$\mathbf{X} = \mathbf{B}\mathbf{X}$$

where $\mathbf{X}$ is a vector whose components are provided by the direct products

of eigenkets described above. The matrix equation is solved numerically, truncating the basis set in order to deal with the finite memory size of the computer. The end products of the computation are spectra, correlation functions, and probability density functions, demonstrating the effects of asymmetry and finite rotation/translation interaction on spectral features which are experimentally observable.

5.2.5 Comparison with Experimental Data

This is not an easy matter when theories as elaborate as those in Section 5.2.4 are to be considered. This is where computer simulation again plays an important role in bridging the gap between abstract formulation and experimental results. It is a truism that every function that can be calculated experimentally can also be computer simulated provided we stay with classical mechanics, but the reverse is not always true. The only way to check multiparameter models effectively is with a combination of experimental and computer techniques. This is a major undertaking involving close cooperation between laboratories. Chapters 6 and 12 illustrate the state of present efforts along these lines for the molecules CH_2Cl_2, CH_3CN, CH_3F, and CH_3I. The rototranslational theories, for example, may be evaluated with data from the far infrared (line broadening), the multidecade regions of frequency up to the far infrared, Raman and Rayleigh scattering, neutron scattering, NMR relaxation, time-dependent Kerr effect measurements, stimulated emission, and many more techniques of increasing complexity. The only fairly satisfactory method of evaluation is to use these techniques in combination over as wide a range of conditions as possible. At the same time a molecular dynamics simulation (with well-defined interaction potentials) may be used to illuminate these aspects of the molecular dynamics which are experimentally inaccessible. The shortcomings of our analytical approach could then be explored in a constructive way.

When dealing with the rotation/translation Langevin equations (5.2.3.1) it is sufficient just to use the 0–THz data to define the defects in the analytical approach. Modern methods of computer-aided least mean squares fitting are powerful enough to create a false impression of the meaning of any multiparameter theory. The final opinion on any liquid state theory must be a balance of uncertainties—those inherent in the original hypothesis of the experimental data and in the technique of molecular dynamics simulation. The modeling of a liquid is only a transient stage between empiricism and predictive theorems. It is inevitable that the description of the condensed phase in terms of interacting molecules will become abstract in the manner of wave and quantum mechanics.

It is probable that the constrained itinerant librator/oscillator will be no match for 0–THz data with an adequate variety of thermodynamic conditions especially when the apparently independent parameters $\Delta_1^{(t)2}$, $\Delta_2^{(t)2}$,

$\Delta_1^{(r)2}$, $\Delta_2^{(r)2}$, $\gamma^{(t)}$, $\gamma^{(r)}$, and $\gamma^{(tr)}\gamma^{(rt)}$ are interrelated by molecular dynamics simulation. The problem is not so much over flexibility as knowing how to bring out subtle effects such as those of rotation/translation interaction in a fairly clear way. Collision-induced far infrared absorption is one such method, but analytically the results are often unexpected as we show in the next section.

5.3 SOME EFFECTS OF ROTATION/TRANSLATION INTERACTION

Recent work on this topic has been concentrated on hydrodynamic and multiparticle theories rather than single-molecule rototranslation as discussed above. Evans (1978) has, however, derived a rototranslational Fokker–Planck equation for Brownian motion in terms of the diffusion coefficients D. The coupling in this theory is based on a nonvanishing force/torque mixed a.c.f. and its basis is the splitting of the Liouville operator $\hat{\mathscr{L}}$ into a streaming and collisional part. The streaming operator $i\hat{\mathscr{L}}_S$ then consists of a translational part $i\hat{\mathscr{L}}_{S,T}$ and a rotational part $i\hat{\mathscr{L}}_{S,R}$:

$$i\hat{\mathscr{L}}_S = i\hat{\mathscr{L}}_{S,T} + i\hat{\mathscr{L}}_{S,R}$$

with

$$i\hat{\mathscr{L}}_{S,T} = \mathbf{v}\cdot\hat{\nabla}_r + \langle\mathbf{F}\rangle\cdot\hat{\nabla}_p$$
$$i\hat{\mathscr{L}}_{S,R} = i\boldsymbol{\omega}\cdot\mathbf{J} + \mathbf{L}\times\boldsymbol{\omega}\cdot\hat{\nabla}_L + \langle\mathbf{N}\rangle\cdot\hat{\nabla}_L$$

where $\mathbf{r}$ is the spatial coordinate of the center of mass, $\mathbf{v}$ and $\mathbf{p}$ are the linear velocity and linear momentum, respectively, and $\langle\mathbf{F}\rangle$ is the ensemble-averaged force on the body. The rotational part of the streaming operator is defined by reference to a principal body fixed coordinate system of the rigid body in which the inertia tensor $\mathbf{I}$ is diagonal. With respect to this frame $\boldsymbol{\omega}$ and $\mathbf{L}$ are the angular velocity and angular momentum, respectively, and $\langle\mathbf{N}\rangle$ is the ensemble-averaged torque. If $\mathbf{u}$ is the vector fixed along the dipole moment direction then $\hat{J}(\equiv -i\mathbf{u}\times\hat{\nabla}_u)$ is the rotation operator for the orientation of the body. The collision operator $i\hat{\mathscr{L}}_c$ represents the disruptive effect exerted by its surrounding fluid on the otherwise free translational and precessional motion of the rigid Brownian particle. The collisional term takes the form

$$-i\hat{\mathscr{L}}_c(t)[\hat{\nabla}_p\hat{\nabla}_L]\begin{bmatrix}\mathbf{G}_{TT}(t) & \mathbf{G}_{TR}(t)\\ \mathbf{G}_{RT}(t) & \mathbf{G}_{RR}(t)\end{bmatrix}\begin{bmatrix}\hat{\nabla}_p+\beta\mathbf{v}\\ \hat{\nabla}_L+\beta\boldsymbol{\omega}\end{bmatrix}$$

where $\beta \equiv 1/kT$. $\mathbf{G}$ is a tensor which is made up of the a.c.f. of fluctuating force $[\mathbf{G}_{TT}(t)]$, torques, and mixed terms.

Solving this type of Liouville equation allows us to consider among other factors the effect of a nonvanishing single-particle torque-force a.c.f. on the time dependence of the orientational a.c.f., $C_{\mathbf{u}}(t)$, and its second rank equivalent $\frac{1}{2}\langle 3[\mathbf{u}(t)\cdot\mathbf{u}(0)]^2 - 1\rangle \equiv C_{\mathbf{u}}^{(2)}(t)$. The coupling in this type of theory is

like that experienced by Brownian particles in a dilute fluid that obeys hydrodynamical equations of motion. The distribution function for the orientation of the rigid body is then obtained from a non-Markov rotation/translation Smoluchowski equation by an integration over the center of mass coordinates, finally giving

$$\frac{\partial f}{\partial t}(\Omega, t) = \int_0^t i\mathbf{J}\cdot\mathbf{D}_{RR}(t')\cdot i\mathbf{J}f(\Omega, t-t')\,dt' \tag{5.3.1}$$

This equation has no explicit translational variables but the diffusion coefficient $\mathbf{D}_{RR}$ is expressed in terms of the correlation function $\mathbf{G}$ of these random intermolecular torques and forces that act on the labeled particle. The structure of the $\mathbf{G}$ tensors may be inferred from a hydrodynamic analysis of rotation/translation coupled Langevin equations. When using Langevin equations the form of $\mathbf{G}$ is neglected and then it is convenient to take the vectors

$$\mathbf{v}(t) = \exp(-i\hat{\mathscr{L}}_C t)\mathbf{v}f_{eq}(\mathbf{p}, \mathbf{L})$$
$$\boldsymbol{\omega}(t) = \exp(-i\hat{\mathscr{L}}_C t)\boldsymbol{\omega}f_{eq}(\mathbf{p}, \mathbf{L})$$

which satisfy the relations

$$\frac{d}{dt}[m\mathbf{v}(t), \mathbf{I}\cdot\boldsymbol{\omega}(t)] = -\beta[\mathbf{v}(t), \boldsymbol{\omega}(t)]\cdot\mathbf{G}$$

Dotting into this the column vector of Section 5.2 gives a scalar denoted by E:

$$E = \left(\frac{d}{dt}[m\mathbf{v}(t), \mathbf{I}\cdot\boldsymbol{\omega}(t)]\right)\cdot\begin{bmatrix}\mathbf{v}(t)\\ \boldsymbol{\omega}(t)\end{bmatrix}$$
$$= -\beta[\mathbf{v}(t)\cdot\mathbf{G}_{TT}\cdot\mathbf{v}(t) + 2\boldsymbol{\omega}(t)\cdot\mathbf{G}_{RT}\cdot\mathbf{v}(t) + \boldsymbol{\omega}(t)\cdot\mathbf{G}_{RR}\cdot\boldsymbol{\omega}(t)]$$

where we have made use of the symmetry relations $\mathbf{G}_{RT} = \mathbf{G}_{TR}$, which follows from the Hermitian property of the $\mathbf{G}$ factors and the reality of these correlation functions. The scalar E is invariant to rotations and reflections of the coordinate system. If the matrix $\mathbf{A}$ is then the symmetry operation of the group of the molecule then the invariance of E requires that the elements of $\mathbf{G}$ transform as

$$\mathbf{G}_{TT} = \mathbf{A}^T\cdot\mathbf{G}_{TT}\cdot\mathbf{A}; \qquad \mathbf{G}_{RR} = \mathbf{A}^T\cdot\mathbf{G}_{RR}\cdot\mathbf{A}$$

and in particular

$$\mathbf{G}_{RT} = \det[\mathbf{A}]\mathbf{A}^T\cdot\mathbf{G}_{RT}\cdot\mathbf{A}$$

On the basis of symmetry arguments alone it is then possible to say that $\mathbf{G}_{RT}$ vanishes for certain symmetries such as $C_{\infty v}$ or $D_{\infty h}$, and in general for most molecules having a C_n axis and a few mirror planes. That this is not the case in a rough sphere fluid is easy to see, and the symmetry arguments will not apply when the system is perturbed by an external field. However, even in very dilute solution, rotation/translation interaction is possible for a

molecule of D_2 symmetry, which is a symmetrical top propeller where the eigenfunctions of $i\mathbf{J}\cdot\mathbf{D}_{RR}(t)$ are the Wigner functions. In contrast to the result for rough spheres put forward by Chandler and discussed in Section 5.2 the effect of rotation/translation coupling in a dilute hydrodynamic medium seems to be small even for D_2 (propeller) symmetry. The effect of the coupling in this case is to decrease the correlation time and to increase the rate of decay of the correlations.

The same author (Evans, 1978) has considered rototranslation in a bath of diatomic molecules. If we label, or tag, one molecule, the problem is then to reduce the N-particle Liouville equation for the fluid to an equation of motion for the tagged-particle distribution function. This may be accomplished by the use of projection operators for taking into account the mutual effects of translation/rotation. A Fokker–Planck equation may then be derived from the microscopic molecular dynamics as opposed to the stochastic theory of Chapter 1. This was first accomplished for a fluid of spherical particles by Resibois (1966) for translational motions and later by Hwang and Freed (1975) for rotational motions. Evans extended these results to rototranslation using a novel type of collision operator. The rotational and translational diffusion coefficients have contributions from rototranslational interaction which cannot appear if the motions are analyzed separately.

In deriving this type of Fokker–Planck equation a reduction of the Liouville equation for the whole system is required to an equation for the p.d.f. in the phase space of the single test particle. Projection operators are used to project the density in the whole phase space into this subspace. The unwanted variables are integrated out. By considering a single test molecule we reject information about correlation in the motion of neighboring molecules. Such information is to be had in principle by projecting into the broader subspace of a test system of two or three particles and is essential for the calculation of such properties as the dielectric response of a concentrated solution or of a pure dipolar fluid. There are few analytical results in this area of many body effects and not many from numerical molecular dynamics. The approach is broadly similar to that used in deriving a macro–micro correlation theorem. To illustrate the methodology we use some clarifying remarks by Wyllie, (1981).

Consider a sample of N solvent molecules and one test molecule—all may, but need not, be identical. Consider only two body interactions. Hwang and Freed (1975) take angular momenta rather than angular velocities as arguments and reduce the Liouville equation to the form

$$\frac{\partial}{\partial t} f_{N+1} = -(\hat{\mathscr{L}}_0 + \hat{\mathscr{L}}) f_{N+1}$$

where

$$\hat{\mathscr{L}}_0 = \sum_{k=1}^{N} (i\boldsymbol{\omega}_k \cdot \mathbf{J}_k + \mathbf{N}_k \cdot \hat{\nabla}_{L_k} + \hat{\mathbf{L}}_k \cdot \hat{\nabla}_{L_k})$$

$$\hat{\mathscr{L}} = i\boldsymbol{\omega} \cdot \mathbf{J} + \mathbf{N} \cdot \hat{\nabla}_L + \hat{\mathbf{L}} \cdot \hat{\nabla}_L$$

The sum $\hat{\mathscr{L}}_0$ refers to the coordinates and momenta of the solvent, $\hat{\mathscr{L}}$ refers to the test particle, and the precession terms $\hat{\mathbf{L}}$ have components $\hat{L}_{a,b,c}$ given by

$$\hat{L}_a = L_b L_c (I_c^{-1} - I_b^{-1}) \epsilon_{abc}$$

in the principal axis frame. ϵ_{abc} defines the cyclic permutations in standard fashion.

The torques $\mathbf{N}$ depend on the configuration of the system and may be written

$$\mathbf{N} = -i\mathbf{J} \sum_{i=1}^{N} U(\mathbf{r} - \mathbf{r}_i, \Omega, \Omega_i)$$

$$\mathbf{N}_k = -i\mathbf{J}_k [U(\mathbf{r} - \mathbf{r}_k, \Omega, \Omega_k) + \sum_{i \neq k} V(\mathbf{r}_i - \mathbf{r}_k, \Omega_i, \Omega_k)$$

If H is the total Hamiltonian of the system and K the kinetic energy of the test particle, the function

$$f_{\text{eq}} = \frac{\exp[-(H-K)/kT]}{\int d\Gamma_s \exp[-(H-K)/kT]}$$

would be the equilibrium solvent density function in the presence of the test particle. Γ_s is the phase space of the solvent molecules. A suitable projection operator $\hat{P}$ is then defined by

$$\hat{P}A = f_{\text{eq}} \int d\Gamma_s A$$

where A is any function of the phase variables. In particular,

$$\hat{P} f_{N+1} = f_{\text{eq}} f_1(\Omega, \mathbf{L}, t)$$

where f_1 is the one-particle density function for the test particle. Provided f_{N+1} and its derivatives vanish as any angular momentum components tend to infinity,

$$\hat{P}\hat{\mathscr{L}}_0 f_{N+1} = 0$$

so

$$-f_{\text{eq}} \frac{\partial f_1}{\partial t} = \hat{P}\hat{\mathscr{L}}(\hat{1} - \hat{P}) f_{N+1} + \hat{P}\hat{\mathscr{L}}\hat{P} f_{N+1}$$

which reduces to

$$\left(\frac{\partial}{\partial t} + i\boldsymbol{\omega} \cdot \mathbf{J} + \hat{\mathbf{L}} \cdot \hat{\nabla}_L + \langle \mathbf{N} \rangle \cdot \hat{\nabla}_L\right) f_1 = -f_{\text{eq}}^{-1} \hat{P}\mathbf{N} \cdot \hat{\nabla}_L (\hat{1} - \hat{P}) f_{N+1}$$

The assumption of the initial condition,

$$f_{N+1}(t=0) = f_{\text{eq}} f_1 \qquad (t=0)$$

gives

$$\left(\frac{\partial}{\partial t} + i\boldsymbol{\omega} \cdot \mathbf{J} + \hat{\mathbf{L}} \cdot \hat{\nabla}_L + \langle \mathbf{N} \rangle \cdot \hat{\nabla}_L\right) f = \hat{\nabla}_L \int_0^t d\tau \mathbf{G}(t-\tau) \cdot \left(\frac{\boldsymbol{\omega}}{kT} + \hat{\nabla}_L\right) f_1(\tau)$$

where

$$\langle \mathbf{N} \rangle = \int d\Gamma_s N f_{eq} f_1$$

is the average torque acting on the fixed test particle and the effective torque correlation tensor $\mathbf{G}$ is

$$\mathbf{G}(t) = \langle \mathbf{R} \exp[(\hat{P} - \hat{1})(\hat{\mathscr{L}}_0 + \hat{\mathscr{L}})t]\mathbf{R} \rangle$$

with

$$\mathbf{R} = \mathbf{N} - \langle \mathbf{N} \rangle$$

In an isotropic fluid $\langle \mathbf{N} \rangle$ is zero and the Fokker–Planck equation takes the form

$$\frac{\partial}{\partial t} f_1(\Omega, \mathbf{L}, t) = -i\hat{\mathscr{L}}_s f_1(t) - i \int_0^t d\tau \hat{\mathscr{L}}_c(\tau) f_1(t - \tau)$$

with streaming operator

$$i\hat{\mathscr{L}}_s = i\boldsymbol{\omega} \cdot \mathbf{J} + (\mathbf{L} \times \boldsymbol{\omega}) \cdot \hat{\nabla}_L$$

and collision operator

$$i\hat{\mathscr{L}}_c(\tau) = -\hat{\nabla}_L \cdot \mathbf{G}(t) \cdot (\hat{\nabla}_L + \beta\boldsymbol{\omega})$$

Evans (1978) has shown that on introducing the new projection operator

$$\hat{P} = \frac{f'_{eq}(\mathbf{L})}{d\mathbf{L}(\ldots)}$$

where

$$f'_{eq}(\mathbf{L}) = \frac{\left(\frac{\beta}{2\pi}\right)^{3/2} \exp(-\beta \mathbf{L} \cdot \boldsymbol{\omega}/2)}{(I_1 I_2 I_3)^{1/2}}$$

the evolution equation for the orientational density function $f_u(\Omega, t)$ may be expressed as

$$f_u(\Omega, s) = \frac{1}{z - \theta(s)} \delta(\Omega - \Omega_0)$$

where $f_u(\Omega, s)$ is the Laplace transform of $f_u(\Omega, t)$ and the function $\theta(s)$ is defined by

$$\theta(s) = \int d\mathbf{L} i\hat{\mathscr{L}}_s [s + i(\hat{1} - \hat{P})\hat{\mathscr{L}}_s + i\hat{\mathscr{L}}_c(s)]^{-1} i\hat{\mathscr{L}}_s f'_{eq}(\mathbf{L})$$

which reduces to

$$\theta(s) = \langle i\boldsymbol{\omega} \cdot \mathbf{J}[s + i(\hat{1} - \hat{P})\hat{\mathscr{L}}_s + i\hat{\mathscr{L}}_c(s)]^{-1} i\boldsymbol{\omega} \cdot \mathbf{J} \rangle$$

the angle brackets representing the expectation value over $f'_{eq}(\mathbf{L})$. These

results are exact, but at this point the dynamic approximation is introduced that the projected (or orthogonalized) streaming operator may be treated by perturbation theory. This is probably true when the mean free angle of rotation is small. In this case:

$$\theta(s) = \theta_2(s) + \theta_4(s) + \cdots$$

where

$$\theta_2(s) = \langle i\boldsymbol{\omega} \cdot \mathbf{J} \psi(s) i\boldsymbol{\omega} \cdot \mathbf{J} \rangle$$

and

$$\theta_4(s) = \langle i\boldsymbol{\omega} \cdot \mathbf{J} \psi(s) i\hat{\mathscr{L}}_s \psi(s) i\hat{\mathscr{L}}_s \psi(s) i\boldsymbol{\omega} \cdot \mathbf{J} \rangle - \frac{\theta_2^2(s)}{s}$$

with

$$\psi(s) = [s + i\hat{\mathscr{L}}_c(s)]^{-1}$$

Expansion of f_u in terms of the Wigner functions in the form

$$f_u(\Omega, s) = \sum_{l,m,n} \left(\frac{2l+1}{8\pi^2}\right) \mathscr{D}^l_{mn}(\Omega) \mathscr{D}^{*l}_{mn}(\Omega_0) C^l_{mn}(s)$$

implies that the matrix elements of θ_2 and θ_4 are, for the symmetric top, respectively linear in q_x and cubic in q_{xy}, where

$$q_x(s) = \left[s + \frac{\beta G_x(s)}{I_x}\right]^{-1}$$

$$q_{xy}(s) = \left[s + \frac{\beta G_x(s)}{I_x} + \frac{\beta G_y(s)}{I_y}\right]^{-1}$$

and x, y denote principal axes of inertia of the top. To the order of approximation $\theta \doteq \theta_2 + \theta_4$ there is no point in an elaborate treatment of $G(s)$, and the crudest hypothesis that $G_x = I_x/\beta\tau_x$ gives interesting results.

For the symmetric top, the correlation functions $C(t)$ are independent of m, and Evans obtains for short times

$$C^l_n(t) \doteq 1 - \frac{kT}{2I_\perp} t^2 \left(l(l+1) + \frac{n^2(I_\perp - I_\parallel)}{I_\parallel}\right)$$

and for long times

$$C^l_n(t) \doteq \left[1 - kT\left(\frac{x^2\tau_\perp^2}{I_\perp} + \frac{n^2\tau_\parallel^2}{I_\parallel}\right)\right]^{-1} e^{-t/\tau_{ln}}$$

where

$$x^2 = l(l+1) - n^2$$

$$\frac{\beta I_\perp}{\tau_{ln}} = x^2\tau_\perp^2 + n^2\tau_\parallel^2\left(\frac{I_\perp}{I_\parallel}\right) + \beta I_\perp Q_{ln}$$

$$\beta^2 I_\perp^2 Q_{ln} = \left[2n^2\left(\tau_\parallel - \frac{3\tau_\parallel}{4}\right) + \frac{x^2\tau_\perp[1 - (I_\parallel/I_\perp)]\tau_\parallel}{\tau_\perp + \tau_\parallel}\right]\tau_\perp$$

It is clear that this type of microscopic or particle theory produces no long time hydrodynamic tail but simply the exponential. Doubtless a form for G could be found where the tail is in fact of the $t^{-5/2}$ form. The long time exponential extrapolates back (see Fig. 1.1.2) to an initial value greater than unity. This has been found to be true also when certain types of Fokker–Planck equations are solved numerically, and is a useful criterion when deciding whether a real system must be modeled by a Fokker–Planck equation or can be represented by a simpler model, for example, of the Gordon type. Random walk models generally extrapolate back to an initial value less than one. It is less than one in Gordon's m-diffusion model and less than 1.1 in his J-diffusion model.

When dealing with rototranslation the physical content of the G tensor may be clarified by separating the rotational (R) and translational (T) Liouville operators into bath (superscript 0) and tagged (superscript 1) parts.

$$i\hat{\mathscr{L}}_T = i\hat{\mathscr{L}}_T^{(0)} + i\hat{\mathscr{L}}_T^{(1)}; \qquad i\hat{\mathscr{L}}_R = i\hat{\mathscr{L}}_R^{(0)} + i\hat{\mathscr{L}}_R^{(1)}$$

If we define f_{eq} by

$$f_{eq} = \exp\left(-\beta \frac{H - L_1^2}{2I_1}\right)$$

where L_1^2 refers to the angular momentum of particle 1, then

$$f_{eq}\mathbf{G}(s) = \hat{P}[\mathbf{I}(s + i\hat{\mathscr{L}}_0 + i\hat{\mathscr{L}}_1)^{-1}\mathbf{I}f_{eq}]^{-1} \tag{5.3.1}$$

where $\mathbf{T}$ is the torque tensor on the diatomic molecule under consideration. Here

$$i\hat{\mathscr{L}}_0 = i\hat{\mathscr{L}}_T^{(0)} + i\hat{\mathscr{L}}_R^{(0)}; \qquad i\hat{\mathscr{L}}_1 = i\hat{\mathscr{L}}_T^{(1)} + i(\hat{1} - \hat{P})\hat{\mathscr{L}}_R^{(1)} \tag{5.3.2}$$

The $i\hat{\mathscr{L}}_0$ term describes a tagged particle which neither rotates nor translates but nevertheless interacts with the surrounding fluid. If $i\hat{\mathscr{L}}_1$ were to be neglected in the denominator of Eq. 5.3.1 then we would obtain the hydrodynamic torque correlation function for a fixed obstacle in a moving fluid or vice versa. The inclusion of $i\hat{\mathscr{L}}_1$ means that the angular momentum operators and generators of tagged particle translational motion are taken into account. If the extrarotational and angular momentum operators in G are ignored by removing the $i(\hat{1} - \hat{P})\hat{\mathscr{L}}_R^{(1)}$ term in Eq. 5.3.2 then the G correlation function depicts the motion of a stochastically translating nonrotating molecule. This is not the same as that obtained from the hydrodynamic model. It turns out that

$$\mathbf{G}(s) = \exp(i\hat{\mathscr{L}}_s\partial_z)\langle \mathbf{T}\Phi(s)\mathbf{T}\rangle + \mathbf{G}_{2,T}(s) + \mathbf{G}_{2,L}(s)$$

where

$$\Phi(s) = (s + i\hat{\mathscr{L}}_0)^{-1}$$

The three contributions to $\mathbf{G}(s)$ may be described as follows. The streaming collision part (the first term on the right side) depicts collisions that change the orientation of the molecule as well as its angular momentum. In the classical Langevin equation the latter is changed infinitesimally at each collision. The angular momentum relaxation is no longer consistent with the latter type of formalism. The $\mathbf{G}_{2,T}(s)$ term has no angular momentum or orientation dependence and modifies the value of the torque correlation function by allowing the particle to translate. The motion of the tagged particle partially relieves the torque and thereby decreases the value of the torque correlation function. At high frequencies (in the far infrared) $\mathbf{G}_{2,T}(s)$ behaves as

$$\mathbf{G}_{2,T}(s) \doteqdot -\mathbf{1}\frac{\sum_\alpha \langle(\hat{\nabla}_{R,\alpha}\mathbf{T})\cdot(\hat{\nabla}_{R,\alpha}\mathbf{T})\rangle}{3\beta m s^3}$$

where m is the particle mass. This clearly diminishes the effective total torque $\mathbf{G}(s)$.

The term $\mathbf{G}_{2,L}(s)$ includes momentum derivatives and powers and is inconsistent with the linear Langevin approach and the traditional Fokker–Planck collision operator. Slow, orientation-dependent operators are accommodated in the streaming collision part of $\mathbf{G}(s)$ and the faster, angular momentum operators in $\mathbf{G}_{2,L}(s)$.

The cumulant expression up to θ_4 is now repeated and $\mathbf{G}_{2,L}(s)$ neglected, to obtain finally an expression for the correlation functions of orientation

$$C_l(s) = [s + D_R(l, s)l(l+1)]^{-1}$$

with

$$D_R(l, s) = \frac{q_1(s)}{I\beta}[1 + q_1(s)q_2(s)[2l(l+1) - 1] \times \left[1 + \frac{(\beta a_1(s)/I)^2}{I\beta} - \frac{l(l+1)a_2(s)q_1(s)}{s^2}\right]^{-1}$$

for spherical tops and with $2l(l+1)^{-2}$ for linear molecules. In this equation

$$q_n(s) = 1\left(s + \frac{n\beta a_0(s)}{I}\right)$$

$$a_0(s) = \langle TT(s)\rangle - \frac{1}{9}\sum_\alpha \langle \hat{\nabla}_{R,\alpha}[\mathbf{T}\Phi(s)]\cdot\Phi(s)\hat{\nabla}_{R,\alpha}[\Phi(s)\mathbf{T}]\rangle$$

The effect of the term $G_{2,T}(s)$ of the collision operator on the correlation times τ_l is to decrease it by decreasing the effective drag on the object. The effect is in the same sense as that asserted in Section 5.2 with the Mori continued fraction approach, that is, in that language rotational and translational frictions are separately diminished by their mutual interaction.

1. Note that $G_{2,T}(s)$ is a part of the rotational friction constant which has received no attention experimentally. The rototranslational $C_l(t)$

correlation functions again exhibit quadratic curvature at short times and become exponential at long times. The factor $G_{2,T}(s)$ is a measure of the importance of translational motion in determining the rotational friction constant, which at long times is effectively the inverse correlation time of the exponential decay of $C_l(t)$.

2. The only natural method of incorporating rototranslation within the framework of a single-particle Mori continued fraction is to postulate that the mixed a.c.f.'s of linear and angular momentum do not vanish; otherwise the system decouples completely into separate translation and rotation. For dilute Brownian rototranslation these vanish in a linear molecule by symmetry. In the microscopic Fokker–Planck approach just described the $G_{2,T}(s)$ term exists and the far infrared/microwave spectrum is affected by rototranslational interaction. Accurate computer simulations are needed to evaluate further the analytical theories. It seems that in the language of the continued fraction, rototranslation enters strongly in the presence of memory effects. In other words, γ_{rt} and γ_{tr} of Section 5.2 are always frequency dependent, since the whole matrix $\underline{\gamma}$ is frequency dependent in the presence of dynamical memory.

Perhaps these questions are best resolved by reference to the paper by Condiff and Dahler (1966) on classical Brownian rototranslation. We recount this in detail in the next section.

5.3.1 Phenomenological, Microscopic, and "Dilute Gas" Theories of Brownian Rototranslation

The phenomenological approach consists of deriving the Fokker–Planck equation and has already been mentioned in the context of multidimensional Markov processes and the associated Langevin type of equations. However, the statistical-mechanical treatment of the problem leads to formally identical results and provides precise definitions for the cross terms γ_{rt} and γ_{tr} in terms of the potential of molecular interaction and the p.d.f. In the limit of a dilute gas of perfectly rough spheres and symmetrical spherocylinders the coupling vanishes, but never otherwise. Therefore it is generally essential to take account of this correlation in any dielectric experiment with real dipolar molecules. It turns out that the rototranslational coupling is particularly strong when the dipole–dipole coupling is strong. The only part of the phenomenological theory we have not already covered is embodied in the equations

$$\dot{\mathbf{p}} = -\frac{\boldsymbol{\gamma}_t \cdot \mathbf{p}}{m} - \boldsymbol{\gamma}_{tr} \cdot \mathbf{I}^{-1} \cdot \mathbf{L} + \mathbf{F}'$$

$$\dot{\mathbf{L}} = -\frac{\boldsymbol{\gamma}_{rt} \cdot \mathbf{p}}{m} - \boldsymbol{\gamma}_r \cdot \mathbf{I}^{-1} \cdot \mathbf{L} + \mathbf{N}'$$

which are the rotation/translation Langevin equations for the asymmetric top in three-dimensional space with all the constraints removed. In this case the γ's are all tensors. $\mathbf{I}$ is the inertia tensor, $\mathbf{L}$ is the angular momentum, and $\mathbf{F}'$ and $\mathbf{N}'$ the force and torque due to a stochastic external bath acting on and about the molecular center of mass. These equations are in complete accord also with a general hydrodynamic theory for the Stokes resistance acting on the arbitrarily shaped rigid particle termed an "arbiton." For low Reynolds number flows γ_{rt} is the transpose of γ_{tr}. This same Onsager relation may be obtained as a consequence of microscopic reversibility using statistical mechanics first developed by Kirkwood. The quantities

$$\frac{\langle \Delta \mathbf{p} \rangle}{\tau}, \quad \frac{\langle \Delta \mathbf{L} \rangle}{\tau}, \quad \frac{\langle \Delta \mathbf{p} \Delta \mathbf{p} \rangle'}{2\tau}, \quad \frac{\langle \Delta \mathbf{L} \Delta \mathbf{L} \rangle'}{2\tau}$$

and $\langle \Delta p \Delta L \rangle'/2\tau$ appearing in the Fokker–Planck equation may now be evaluated by integration over the interval τ, keeping the molecular orientation fixed throughout the averaging interval as in Chapter 1. Thus

$$\frac{\langle \Delta \mathbf{p} \rangle}{\tau} = -\frac{\boldsymbol{\gamma}_t \cdot \mathbf{p}}{m} - \boldsymbol{\gamma}_{tr} \cdot \mathbf{I}^{-1} \cdot \mathbf{L} + 0(\tau)$$

$$\frac{\langle \Delta \mathbf{L} \rangle}{\tau} = -\frac{\boldsymbol{\gamma}_{rt} \cdot \mathbf{p}}{m} - \boldsymbol{\gamma}_r \cdot \mathbf{I}^{-1} \cdot \mathbf{L} + 0(\tau)$$

$$\frac{\langle \Delta \mathbf{p} \Delta \mathbf{p} \rangle'}{2\tau} = kT\boldsymbol{\zeta}_t \qquad (\boldsymbol{\zeta}_t = \boldsymbol{\gamma}_t)$$

$$\frac{\langle \Delta \mathbf{L} \Delta \mathbf{L} \rangle}{2\tau} = kT\boldsymbol{\zeta}_r \qquad (\boldsymbol{\zeta}_r = \boldsymbol{\gamma}_r)$$

$$\frac{\langle \Delta \mathbf{p} \Delta \mathbf{L} \rangle'}{2\tau} = kT\boldsymbol{\zeta}_I \qquad (\boldsymbol{\zeta}_I = \boldsymbol{\gamma}_{tr} = \boldsymbol{\gamma}_{rt}^T)$$

The Fokker–Planck equation can be written in the very simple form

$$\frac{\partial_r f}{\partial t} = \frac{\partial}{\partial \mathbf{p}} \cdot \mathbf{J}_p + \frac{\partial}{\partial \mathbf{L}} \cdot \mathbf{J}_L$$

where

$$\mathbf{J}_p = \boldsymbol{\gamma}_t \cdot \left[\frac{f\mathbf{p}}{m} + kT\left(\frac{\partial}{\partial \mathbf{p}}\right) f \right] + \boldsymbol{\gamma}_{tr} \cdot \left[f\mathbf{I}^{-1} \cdot \mathbf{L} + kT\left(\frac{\partial}{\partial \mathbf{L}}\right) f \right]$$

$$\mathbf{J}_L = \boldsymbol{\gamma}_{rt} \cdot \left[\frac{f\mathbf{p}}{m} + kT\left(\frac{\partial}{\partial \mathbf{p}}\right) f \right] + \boldsymbol{\gamma}_r \cdot \left[f\mathbf{I}^{-1} \cdot \mathbf{L} + kT\left(\frac{\partial}{\partial \mathbf{L}}\right) f \right]$$

which is directly comparable with Eq. 5.2.3.6. Using the definitions

$$(\Delta \mathbf{p})' = \int_0^\tau \mathbf{F}'(s)\, da; \qquad (\Delta \mathbf{L})' = \int_0^\tau \mathbf{N}'(s)\, ds$$

the friction tensors are

$$\gamma_t = \frac{1}{2\tau kT}\int_0^\tau ds \int_0^\tau du \langle \mathbf{F}'(s)\mathbf{F}'^T(u)\rangle_1$$

$$\gamma_r = \frac{1}{2\tau kT}\int_0^\tau ds \int_0^\tau du \langle \mathbf{N}'(s)\mathbf{N}'^T(u)\rangle_1$$

$$\gamma_{tr} = \frac{1}{2\tau kT}\int_0^\tau ds \int_0^\tau du \langle \mathbf{F}'(s)\mathbf{N}'^T(u)\rangle_1$$

the subscript 1 meaning that the average refers only to the bath and does not extend to the dynamical variables of the rotor.

We have:

$$\mathbf{F}'(s) = -\frac{\partial V}{\partial \mathbf{R}}$$

$$\mathbf{N}'(s) = -\mathbf{e}\times\frac{\partial v(s)}{\partial \mathbf{e}} - (\boldsymbol{\theta}\cot\theta + \mathbf{e})\frac{\partial V(s)}{\partial \psi}$$

If $\mathbf{e}$ is an axis of symmetry with regard to an external potential V, then the latter is independent of ψ, the third Euler angle. The torque $\mathbf{N}'$ has no component in the $\mathbf{e}$ direction. The rotational tensor γ_r has no components in the $\mathbf{e}$ direction and $\gamma_{tr}\cdot\mathbf{e}$ vanishes.

The microscopic approach to the problem is via the Liouville equation for f, the N-particle distribution function:

$$\left[\frac{\partial}{\partial t} + i\hat{\mathscr{L}}\right] f(\Gamma, t) = 0$$

We have:

$$i\hat{\mathscr{L}}f = \sum_j \left[\frac{\partial}{\partial \mathbf{p}_j}\cdot(\mathbf{F}_j f) + \frac{\partial}{\partial \mathbf{L}_j}\cdot(\mathbf{N}_j f) + \frac{\partial}{\partial \mathbf{R}_j}\cdot\frac{(\mathbf{p}_j f)}{m} + \frac{\partial}{\partial \boldsymbol{\alpha}_j}\cdot(\dot{\boldsymbol{\alpha}}_j f)\right]$$

This equation is then integrated over the dynamic states of all the molecules except one to obtain the first member of what is called the BBGKY hierarchy (McDonald and Hansen, 1976). This equation is then "time-smoothed" to obtain the time-averaged distribution function. In order to proceed, several assumptions are made:

1. The statistical probability density has only a weak dependence on position and orientation.
2. The instantaneous departures from equilibrium are small.
3. For purposes of estimating correlations and/or torques the particles of the system are taken to be free and noninteracting, that is,

$$\Delta\mathbf{p}_1 = \Delta\mathbf{L}_1 = \mathbf{0}.$$

This amounts to replacing $\hat{\mathscr{L}}$ by the sum of free streaming Liouville operators for the individual molecules; that is, cross correlations are ignored.

The first constraint has been removed by G. T. Evans (Section 5.3) and is a kind of quasi-Markov approximation. It is also therefore removed by introducing memory functions in a Mori continued fraction and is very closely akin to the assumption of instantaneous changes of force/torque at each collision.

By time reversal symmetry,

$$(\mathbf{R}_i, \mathbf{p}_i, \boldsymbol{\alpha}_i, \mathbf{L}_i) \to (\mathbf{R}_i, -\mathbf{p}_i, \boldsymbol{\alpha}_i, -\mathbf{L}_i)$$

and

$$\hat{\mathscr{L}}_0 \to -\hat{\mathscr{L}}_0$$

This implies the Onsager–Casimir relations

$$\begin{bmatrix}\gamma_t & \gamma_{tr}\\ \gamma_{rt} & \gamma_r\end{bmatrix} \to \begin{bmatrix}\gamma_t^T & \gamma_{tr}^T\\ \gamma_{rt}^T & \gamma_r^T\end{bmatrix}$$

In particular, when these tensors are even functions of the momenta $\mathbf{p}_l$ and $\mathbf{L}_l$, the grand matrix is symmetrical and

$$\gamma_{tr} = \gamma_{rt}^T$$

Each element of γ, the grand friction matrix, in turn has off-diagonal elements only if there is a dissipative gyrostatic frictional force and/or torque acting on the particle. Otherwise γ_t, γ_r, γ_{tr}, and γ_{rt} are each diagonal matrices.

If it is assumed now that the potential energy of the system is unchanged by rotation of the individual molecules about body-fixed dipole axes whose directions are indicated by the unit vectors $\boldsymbol{\xi}_i$, then

$$\mathbf{F} = -\frac{\partial U}{\partial \mathbf{R}_i}; \quad \mathbf{N}_i = -\boldsymbol{\xi}_i \times \left(\frac{\partial U}{\partial \boldsymbol{\xi}_i}\right)$$

Assume also that the interaction energy is the sum of pair potentials $U_{ij} = U(\mathbf{R}_i - \mathbf{R}_j, \boldsymbol{\xi}_i, \boldsymbol{\xi}_j)$ and that U_{12} can be separated into the sum of a central dipole potential $U_c(|\mathbf{R}_2 - \mathbf{R}_1|)$ and of a dipole–dipole interaction:

$$U_d(\mathbf{R}_{21}, \boldsymbol{\xi}_1, \boldsymbol{\xi}_2) = -3R_{21}^{-5}\mathbf{R}_{21}^0\mathbf{R}_{21} : \boldsymbol{\mu}_1\boldsymbol{\mu}_2$$

where

$$\mathbf{R}^0\mathbf{R} = \mathbf{R}\mathbf{R} - \tfrac{1}{3}R^2\mathbf{U}$$

and

$$\boldsymbol{\mu}_i = \mu\boldsymbol{\xi}_i\cdot\mathbf{U}$$

is the unit dyadic. Since the idealization of the point dipole is inadequate for small separations a lower cutoff is imposed on the angle-dependent potential U_d; that is, $U_d = 0$ for $R_{12} \leqslant \epsilon$. It results that the rotational and coupling tensors γ_r, γ_{tr}, and γ_{rt} depend on the degree to which the dipole–dipole interactions distort the function $g(\mathbf{r}, \mathbf{e}_1, \mathbf{e}_2)$ from the orientational-independent radial distribution characteristic of the central poten-

tial $U_c = U_c(r)$. This suggests that rotation/translation effects are long range.

5.3.1.1 *Rotation/Translation in Perfectly Rough Spheres and Loaded Spherocylinders*

The dynamic state of a perfectly rough hard sphere is described completely by the position of its center of mass $\mathbf{R}_i$, by its linear momentum $\mathbf{p}_i \equiv m_i\mathbf{v}_i$ and by its internal angular momentum $\mathbf{L}_i \equiv I_i\boldsymbol{\omega}_i$. Here m_i is the mass of the particle and I_i its moment of inertia. The internal mass distribution is isotropic, so that: $\mathbf{I}_i = I_i\mathbf{1}$. The distribution of mass is characterized by the dimensionless moment of inertia $\kappa_i = 4I_i/m_i\sigma_i^2$, where σ_i denotes the diameter of the sphere.

To evaluate rototranslational coupling the following assumptions are made:

1. The medium is a dilute gaseous solution with solute and solvent species denoted by 1 and 2, respectively.
2. The solute molecules are much more massive than those of the solvent and they also have much larger moments of inertia.
3. The state of the system departs very little from a condition of thermodynamic equilibrium characterized by an uniform density n_2 and an absolute temperature T.

The equations governing the collisional-induced alterations of linear and angular momentum are

$$\mathbf{p}_1' - \mathbf{p}_1 = \mathbf{J}; \qquad \mathbf{L}_1' - \mathbf{L}_1 = \sigma_1\mathbf{k}\times\mathbf{J}$$

and permit us to express the collisional alterations of linear and angular velocity in terms of the momentum impulse:

$$\mathbf{J} = 2m(\kappa+1)^{-1}(\kappa\mathbf{g}_{21} + \mathbf{k}\mathbf{k}\cdot\mathbf{g}_{21})$$

where

$$\mathbf{g}_{21} = \mathbf{v}_{21} + \tfrac{1}{2}\mathbf{k}\times(\sigma_1\boldsymbol{\omega}_1 + \sigma_2\boldsymbol{\omega}_2)$$

is the relative velocity of the contact points on the two colliding spheres,

$$m = \frac{m_1m_2}{m_1+m_2}$$

and

$$\kappa = \left(\frac{4}{m}\right)\left(\frac{\sigma_1^2}{I_1} + \frac{\sigma_2^2}{I_2}\right)^{-1}$$

We assume that $|\sigma_1\boldsymbol{\omega}_1| = 0(|\mathbf{v}_1|)$, which is valid only near equilibrium, provided only that

$$I_1 = 0(m, \sigma_1^2)$$

As m_2/m_2 and I_2/I_1 both approach zero, the friction term

$$\gamma_{tr} = \left[\frac{64}{3}\sigma^4(2\pi m_2kT)\sigma_1\left(\frac{m}{m_2}\right)^2 \Big/ 32m_1\sigma^2\right]\kappa(\kappa+1)^{-2}\times\left(1-\frac{\kappa}{\kappa_2}\right)$$

tends to zero. In a dilute gas of massive, perfectly rough hard spheres there is no translation/rotation coupling, as we have mentioned earlier in Section 5.2. For this very artificial model the rotational friction coefficient is finite even though every direction is a symmetry axis for the molecular interaction. This is because of the gripping between two of the surfaces of the rough spheres. The rotational friction exists for much the same reason that there is a Stokes resistance to the rotation of the macroscopic sphere immersed in a viscous fluid. The latter is a consequence of environmental correlations or disturbances which are introduced by the "no-slip boundary conditions" of hydrodynamics.

The loaded spherocylinder is a composite of the loaded sphere and of the spherocylinder. It is assumed that each of these molecules has a rigid and smooth spherocylindrical surface and a cylindrically symmetrical internal distribution of mass. The inertial tensor of one such particle is therefore of the form

$$\mathbf{I}(\mathbf{e}) = \Gamma(\mathbf{u} - \mathbf{e}\mathbf{e}) + \Gamma'\mathbf{e}\mathbf{e}$$

where $\mathbf{e}$ denotes a unit vector that lies parallel to the axis of the cylinder and that is directed from its center of mass toward its center of symmetry. A dilute solution of such bodies in a solvent of smooth spheres is considered by Condiff and Dahler (1966). The spherocylinders are very much more massive than their collision partners and the state of the system is not significantly altered by the presence of a few such spherocylinders. If the speed of a point z along the cylinder axis is low compared with the speed of sound in a solvent gas, then we arrive at the following result. The coupling tensor $\boldsymbol{\gamma}^{tr}$ vanishes for symmetric spherocylinders, that is, where the centers of mass and symmetry coincide. If we denote by $\boldsymbol{\xi}_s = \xi_s\mathbf{e}$ the displacement vector from the center of mass to the center of symmetry, then

$$\boldsymbol{\gamma}_{tr} = -\boldsymbol{\gamma}_t\times\boldsymbol{\xi}_s$$
$$\boldsymbol{\gamma}_r = -\boldsymbol{\xi}_s\times\boldsymbol{\gamma}_t\times\boldsymbol{\gamma}_s$$

so that in this case the rotational friction vanishes also if vanishes. This is the result for the loaded spherocylinder (e.g., a dipolar diatomic).

In general, therefore, it is quite clear that for molecules that are dipolar there will always be a mutual effect of rotation and translation. The 0–THz spectra must accordingly be reinterpreted. We suggest how the mutual interaction may be evaluated in Section 5.4.

5.3.1.2 *Einstein Relations: The Oseen Tensors*

In Section 5.2 we have derived some Einstein relations for the special case of constrained asymmetric top rototranslation. To produce a generalized

relation of this kind, a constitutive relation, it is fruitful to categorize the collisions into the brief but violent events involving the short range repulsive interactions and the smaller exchanges of momentum and energy caused by the long range, slowly varying part of the intermolecular forces. In a dense gas or liquid the "free path length," if meaningful, is the same order of magnitude as these long range forces, and it is necessary to adopt a many-body or collective description of this second category as embodied in the Fokker–Planck equation and friction coefficients. If the collisions of the first category are two-body type, they can be represented by binary collision operators of the kind that appear in Enskog theory. A theory that allows for both categories has been developed by Rice and Gray (1965), and it allows us to look at the effect of molecular motion on the diffusive motions of massive Brownian particles. In this type of theory the friction tensors for the heavy solute molecules are rigorously independent of the momenta **p** and **L**. It is possible to obtain some interesting hydrodynamical type of results from the Fokker–Planck equations by the method of moments. An example is the equation of particle conservation:

$$\frac{\partial n^*}{\partial t} + \frac{\partial}{\partial \mathbf{r}} \cdot \mathbf{j}r + \frac{\partial}{\partial \boldsymbol{\alpha}} \cdot \mathbf{j}_\alpha = 0$$

where

$$n^*(\mathbf{r}, \boldsymbol{\alpha}) = \int f \, d\mathbf{p} \, d\mathbf{L}; \qquad \int n^* \, d\boldsymbol{\alpha} = n(\mathbf{r})$$

We have used the notation

$$n^*\langle\psi\rangle = \int f\psi \, d\mathbf{p} \, d\mathbf{L}; \qquad \mathbf{j}_r(\mathbf{r}, \boldsymbol{\alpha}) = n^*\langle \mathbf{v} \rangle;$$

and

$$\mathbf{j}_\alpha(\mathbf{r}, \boldsymbol{\alpha}) = n^*\langle \dot{\mathbf{a}} \rangle$$

where **a** denotes angular displacement. The **j** factors are therefore currents or fluxes. The total particle flux is given by $\mathbf{j} = \int \mathbf{j}_r \, \alpha\alpha$. The flux $\mathbf{j}_\omega = n^*\langle\boldsymbol{\omega}\rangle$ is conveniently defined by the relation

$$\mathbf{j}_\alpha = \boldsymbol{\Lambda}(\boldsymbol{\alpha}) \cdot \mathbf{j}_\omega$$

where

$$\dot{\mathbf{a}} = \boldsymbol{\Lambda}(\boldsymbol{\alpha}) \cdot \boldsymbol{\omega}$$

With ψ taken equal to **p** and **L**, we obtain the steady-state constitutive relations:

$$\begin{bmatrix} \mathbf{j}_r \\ \mathbf{j}_\omega \end{bmatrix} = -kT \begin{bmatrix} \mathbf{D}_t & \mathbf{D}_{tr} \\ \mathbf{D}_{rt} & \mathbf{D}_r \end{bmatrix} \begin{bmatrix} \left(\frac{\partial}{\partial \mathbf{r}}\right) \cdot (mn\langle \mathbf{vv} \rangle) + \left(\frac{\partial}{\partial \boldsymbol{\alpha}}\right) \cdot (n^*\langle \dot{\mathbf{a}}\mathbf{p} \rangle) - n^*\mathbf{F}_e(\mathbf{r}, \boldsymbol{\alpha}) \\ \left(\frac{\partial}{\partial \mathbf{r}}\right) \cdot (n^*\langle \mathbf{vL} \rangle) + \left(\frac{\partial}{\partial \boldsymbol{\alpha}}\right) \cdot (n^*\langle \dot{\mathbf{a}}\mathbf{L} \rangle) - n^*\mathbf{N}_e(\mathbf{r}, \boldsymbol{\alpha}) \end{bmatrix}$$

where the grand diffusion tensor is

$$\begin{bmatrix} \mathbf{D}_t & \mathbf{D}_{tr} \\ \mathbf{D}_{rt} & \mathbf{D}_r \end{bmatrix} = (kT)^{-1} \begin{bmatrix} \boldsymbol{\gamma}_t & \boldsymbol{\gamma}_{tr} \\ \boldsymbol{\gamma}_{rt} & \boldsymbol{\gamma}_r \end{bmatrix}^{-1}$$

which is a general form of the Einstein relation. The currents or fluxes $\mathbf{j}_r$ and $\mathbf{j}_\omega$ generally depend on gradients with respect to the position and orientation coordinates. The constitutive equations also provide a means of predicting the effects on diffusion of external fields which tend to alter the orientations of individual molecules embodied in the external force $\mathbf{F}_e$ and torque $\mathbf{N}_e$. In the general case the alignment of the molecular axes is involved in the diffusion process and it is only to the extent that such polarization may be neglected that simple Stokes–Einstein relations obtain.

For a symmetrical top molecule with

$$\mathbf{I} = \Gamma(\mathbf{1} - \mathbf{ee}) + \Gamma'\mathbf{ee}$$

we have

$$\begin{bmatrix} \boldsymbol{\gamma}_t & \boldsymbol{\gamma}_{tr} \\ \boldsymbol{\gamma}_{rt} & \boldsymbol{\gamma}_r \end{bmatrix} = \begin{bmatrix} \gamma_1(\mathbf{1} - \mathbf{ee}) + \gamma_2\mathbf{ee} & \gamma_3\mathbf{e} \times \mathbf{1} \\ -\gamma_3\mathbf{e} \times \mathbf{1} & \gamma_4(\mathbf{1} - \mathbf{ee}) + \gamma_5\mathbf{ee} \end{bmatrix}$$

All the friction coefficients γ_1–γ_4 are independent of ψ, the angle of rotation round the body axis defined by **e**, the unit vector. the inverse is then

$$\begin{bmatrix} \boldsymbol{\gamma}_t & \boldsymbol{\gamma}_{tr} \\ \boldsymbol{\gamma}_{rt} & \boldsymbol{\gamma}_r \end{bmatrix} = (\gamma_1\gamma_4 - \gamma_3^2)^{-1} \begin{bmatrix} \gamma_4(\mathbf{1} - \mathbf{ee}) + (\gamma_1\gamma_4 - \gamma_3^2)\mathbf{ee}\gamma_2^{-1}; & -\gamma_3\mathbf{e} \times \mathbf{1} \\ \gamma_3\mathbf{e} \times \mathbf{1}; & \gamma_1(\mathbf{1} - \mathbf{ee}) + (\gamma_1\gamma_4 - \gamma_3^2)\mathbf{ee}\gamma_5^{-1} \end{bmatrix}$$

The effects of rotation/translation coupling are quite clear when expressed in terms of these constitutive relations. If we consider a model of rotational relaxation in solution making the assumption that the velocities of all the particles are zero (i.e., in a lattice of rotors), the rotational self-diffusion tensor satisfying stick boundary conditions is to lowest order in **r** the interparticle separation

$$(\mathbf{D}_r)_{11} = \frac{kT}{\gamma_{r_1}} \left[\mathbf{1} - \frac{3a_1^3a_2}{4r^4}(\mathbf{1} - \mathbf{rr})\right] \qquad \gamma_{r_1} = 8\pi\eta a_1^3 \qquad (5.3.1.2.1)$$

In the opposite case (slip boundary conditions)

$$(\mathbf{D}_t)_{11} = \frac{kT}{\gamma_{t_1}} \left[\mathbf{1} - \frac{3a_1a_2^3}{4r^4}(\mathbf{1} + 4\mathbf{rr})\right], \qquad \gamma_{t_1} = 6\pi\eta a_1 \qquad (5.3.1.2.2)$$

In contrast the hydrodynamic solution for two bodies simultaneously rotating and translating gives

$$(\mathbf{D}_t)_{11} = \frac{kT}{\gamma_{t_1}} \left[\mathbf{1} - \frac{15a_1a_2^3}{4r^4}\mathbf{rr}\right] \qquad (5.3.1.2.3)$$

$$(\mathbf{D}_r)_{11} = \frac{kT}{\gamma_{r_1}} \left[\mathbf{1} - \frac{15a_1^3a_2^3}{4r^6}(\mathbf{1} - \mathbf{rr})\right] \qquad (5.3.1.2.4)$$

The distance-dependent corrections to the Stokes–Einstein relations are

therefore wholly different owing to the hydrodynamic coupling between rotational and translational motions. Equations 5.3.1.2.3 and 5.3.1.2.4 satisfy the grand matrix relation provided that

$$\mathbf{D}_t = kT(\boldsymbol{\gamma}_t - \boldsymbol{\gamma}_{tr}\boldsymbol{\gamma}_r^{-1}\boldsymbol{\gamma}_{rt})^{-1}$$
$$\mathbf{D}_r = kT(\boldsymbol{\gamma}_r - \boldsymbol{\gamma}_{rt}\boldsymbol{\gamma}_t^{-1}\boldsymbol{\gamma}_{tr})^{-1}$$

The above two sets of equations, Eqs. 5.3.1.2.1–5.3.1.2.4, correspond and are obtained only when the coupling tensors $\boldsymbol{\gamma}_{tr}$ and $\boldsymbol{\gamma}_{rt}$ are neglected. In this case the interactions between translating particles are governed by the Oseen tensors.

Wolynes and Deutch (1977) have considered a many-particle coupled rotation/translation diffusion model pertinent to single-particle and collective orientational correlation functions. In this model they consider the coupled Brownian motion of solute particles interacting with anisotropic potentials in a continuum solvent, the motion of which is described hydrodynamically. This gives rise to long range dynamical orientation correlation, which manifests itself in the appearance of long range off-diagonal coupled diffusion constants in the complete diffusion equation describing the system. Current densities **j** are used as described above and the diffusion tensors **D** are functions of the Brownian particles' configuration. If it is assumed that the time scales of momentum and configurational change may be separated in a dense fluid, then the **D** tensors are integrals over time-correlation function tensor products:

$$\mathbf{D}_{ij}^{XX}(Q) = \int_0^\infty \langle \mathbf{v}_i(0)\mathbf{v}_j^T(t)\rangle_Q$$
$$\mathbf{D}_{ij}^{X\Omega}(Q) = \int_0^\infty \langle \mathbf{v}_i(0)\boldsymbol{\omega}_j^T(t)\rangle_Q$$
$$\mathbf{D}_{ij}^{\Omega X}(Q) = \int_0^\infty \langle \boldsymbol{\omega}_i(0)\mathbf{v}_j^T(t)\rangle_Q$$
$$\mathbf{D}_{ij}^{\Omega\Omega}(Q) = \int_0^\infty \langle \boldsymbol{\omega}_i(0)\boldsymbol{\omega}_j^T(t)\rangle_Q$$

The Langevin equations now read

$$m_i\dot{\mathbf{v}}_i = -\sum_j [\boldsymbol{\gamma}_{ij}^{XX}\cdot\mathbf{v}_j + \boldsymbol{\gamma}_{ij}^{X\Omega}\cdot\boldsymbol{\omega}_j] + \mathbf{F}_i(t)$$

$$I_i\dot{\boldsymbol{\omega}}_i = -\sum_j [\boldsymbol{\gamma}_{ij}^{\Omega X}\cdot\mathbf{v}_j + \boldsymbol{\gamma}_{ij}^{\Omega\Omega}\cdot\boldsymbol{\omega}_j] + \mathbf{N}_i(t)$$

The friction tensors $\boldsymbol{\gamma}$ originate from the forces and torques on the solute molecules caused by the translational and rotational movement of a reference point source. The exact treatment of low Reynolds number hydrodynamic interaction for any arbitrary configuration of finite sized bodies is extremely difficult, but Wolynes and Deutch have developed such a formalism for well separated Brownian particles, the outcome of which is

that the diffusion tensors **D** are directly related to the hydrodynamic interaction tensors or Oseen tensors. These are Green's functions of the steady-state linearized, incompressible fluid Navier–Stokes equations. Thus

$$\mathbf{D}_{ij}^{XX} = kT[(\boldsymbol{\gamma}_0^{XX})^{-1}\delta_{ij} + (1-\delta_{ij})\mathbf{T}_{ij}^{XX}]$$
$$\mathbf{D}_{ij}^{X\Omega} = kT(1-\delta_{ij})\mathbf{T}_{ij}^{X\Omega}$$
$$\mathbf{D}_{ij}^{\Omega X} = kT(1-\delta_{ij})\mathbf{T}_{ij}^{\Omega T}$$
$$\mathbf{D}_{ij}^{\Omega\Omega} = kT[(\boldsymbol{\gamma}_0^{\Omega\Omega})^{-1}\delta_{ij} + (1-\delta_{ij})\mathbf{T}_{ij}^{\Omega\Omega}]$$

where **T** denotes the Oseen tensor. The "rotation/rotation" Oseen tensor $\mathbf{T}^{\Omega\Omega}$ is particularly simple, and takes precisely the same form as the tensorial interaction between dipoles in a fluid, and is therefore long range in nature. Collective hydrodynamic effects lead to a correlation of the angular velocities of distant solute molecules. The other tensors $\mathbf{T}_{ij}^{X\Omega}$ and $\mathbf{T}_{ij}^{\Omega X}$ similarly reflect the presence of long range contributions of the rotation and translation of different solute particles.

5.4 EXPERIMENTAL METHOD FOR DETECTING ROTATION/TRANSLATION INTERACTION

It is advantageous to pick a pseudospherical molecular geometry to minimize the number of free friction parameters appearing in the grand matrix. This may be self-defeating, however, in the sense that the rotation/translation interaction might be minimized in consequence. However, a computer simulation of the mixed a.c.f.'s and especially their moments, as in Section 5.2, help to determine this. Data over a complete 0–THz frequency range can be used as follows:

1. Choose a rotator phase or plastic crystalline phase where molecular rotation is as free in the liquid, yet translation is almost absent. The far infrared spectrum of such a rotator phase liquid system is shown in Fig. 5.4.1. In the plastic crystalline phase there is for practical purposes no translation, so that the traditional rotational approach is probably adequate. Smyth has tabulated the rotator phase molecules.

   In systems such as $(CH_3)_2CCl_2$, CCl_3CH_3, $(CH_3)_3CNO_2$, and $(CH_3)_2CClNO_2$, the relaxation times (the inverse of the main loss peak) are almost identical just above and below the freezing point, whereas when no rotator phase exists there is practically no rotation in the solid at all (i.e., the loss peak moves to zero frequency). Reid (1980) has lately produced an example of the use of rotator phase benzene as a solvent for the study of purely rotational motions in a disk-shaped dipolar molecule such as fluorobenzene.
2. The change in shape of the far infrared part of the total 0–THz spectrum between the liquid and plastic crystalline phase is a clear

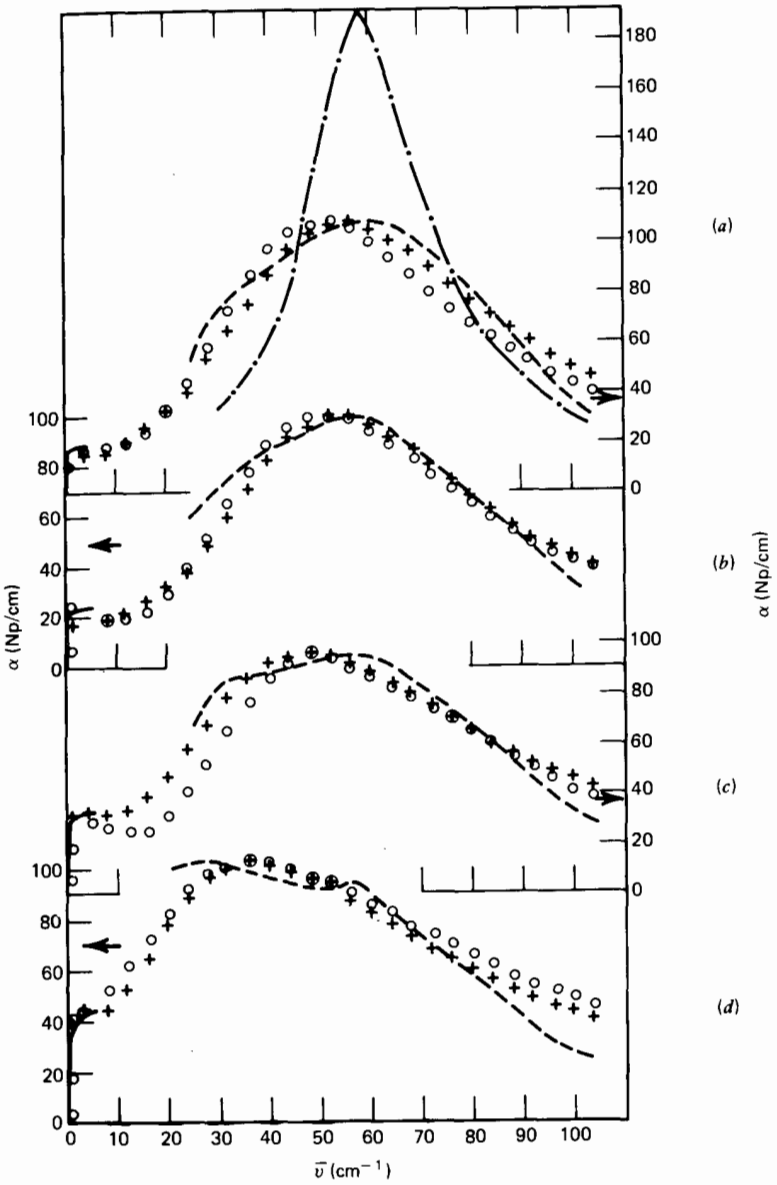

Figure 5.4.1 The effect of rototranslation as embodied in rotator phase and liquid data for 2-chloro-2-nitropropane. ----, Rotator phase at 209°K; – · –, non rotation at 193°K. (*b*) Rotation phase at 233°K. (*c*) Liquid at 253°K. (*d*) Liquid at 293°K.

indication of the effect of rotation/translation coupling (Fig. 5.4.1). By making analogous comparisons with another two or three experimental probes, such as depolarized light scattering, and perhaps inelastic neutron scattering, the efficacy of the rototranslational theory may be evaluated in detail.

3. The system chosen can be simulated at the same time with a molecular dynamics run with a convenient intermolecular potential. Strong mutual effects of rotation and translation have recently been brought to light by Steele and Streett (1980) in computer nitrogen.
4. The "opposite pole" of purely translational absorption in the absence of rotation is observable in the far infrared when considering collision-induced absorptions (Chapter 11).

Finally, it seems clear that with the advent of adequate theoretical methods the 0–THz region is not only richer in detail about mode–mode coupling than we have hitherto imagined, but also in the long run seems a likely candidate for "the richer-than-we-can-imagine" tag.

Mode–mode coupling is discussed in further detail in Chapter 7.

REFERENCES

Ailawadi, N. K. and Berne, B. J., *Faraday Symposium No. 11* (1976).

Alder, B. J. and Wainwright, T., *Nuovo Cimento Suppl.* **9**, 116 (1958).

Berne, B. J. *Faraday Symposium No. 11* (1976).

Berne, B. J. and Montgomery, J. A., *Mol. Phys.* **32**, 363 (1976).

Berne, B. J. and Nady, L. D., *Faraday Symposium No. 11* (1976).

Berne, B. J. and Pecora, R., *Dynamic Light Scattering with Applications to Chemistry, Biology and Physics*, Wiley-Interscience, New York (1976).

Chandler, D., *J. Chem. Phys.* **60**, 3508 (1974).

Condiff, D. W. and Dahler, J. S., *J. Chem. Phys.* **44**, 3988 (1966).

Enskog theory: see, for example, Berne, B. J. and O'Dell, J., *J. Chem. Phys.* **62**, 2376 (1975).

Evans, G. T., *Mol. Phys.* **36**, 1199 (1978).

Evans, M. W., Evans, G. J., and Davies, A. R., *Faraday Disc.* **66**, 231 (1978).

Evans, M. W. and Reid, C. J., *Mol. Phys.*, in press (1981).

Favro, L. D., *Phys. Rev.* **53**, 119 (1960).

Hwang, L.-P. and Freed, J. H., *J. Chem. Phys.* **63**, 118, 4017 (1975).

Lobo, R., Robinson, J. E., and Rodriguez, S., *J. Chem. Phys.* **58**, 5995 (1973).

McDonald, I. R. and Hansen, J.-P., *Theory of Simple Liquids, Academic*, New York (1976).

Resibois, P., *Physics of Many Particle Systems*, E. Meeron, Ed., Gordon and Breach, New York (1966).

Rice, S. A. and Gray, P., *The Statistical Mechanics of Simple Liquids*, Wiley-Interscience, New York (1965).

Rosato, V., work in progress, University of Wales.

Steele, W. A. and Streett, W. R., personal communication (1980).

Streett, W. B. and Gubbins, K. E., *Ann. Rev. Phys. Chem.* **28**, 373 (1977).

Wegdam, G.and van der Elsken, J., *Phonons, Proc. Int. Conf.*, M. A. Nusimovici, Ed., Flammarion Sci., Paris, 469–473 (1971).

Williams, G. and Watts, B., *Trans. Faraday Soc.* **66**, 80 (1970).

Wolynes, P. G. and Deutch, J. M., *J. Chem. Phys.*, **67**, 733 (1977).

Wyllie, G., *Phys. Rep.*, in press (1981).

6

Experimental Considerations. An Evaluation of Models and Interexperimental Comparison

LIST OF SYMBOLS

A	Integrated absorption intensity
$\mathfrak{A}$	Absorption coefficient (neper cm^{-1})
$a_0^{(l)}$	Molecular scattering factors
$\underline{\alpha}(A, t)$	Polarizability tensor of light scattering
b_α, b_β	Scattering lengths of respective molecular nuclei
γ_1, γ_2	Memory function characteristic frequencies
$C_1(t)$	First rank orientational autocorrelation function
$C_2(t)$	Second rank orientational autocorrelation function
$C_{DRS}(t)$	Correlation function of depolarized Rayleigh scattering
$C_{LS}(t)$	Total light scattering correlation function
$C_{RB}(t)$	Correlation function of Rayleigh/Brillouin scattering
$\delta\theta_{ij}(t)$	Angle between dipole directions of molecule i (at t) and j
$\boldsymbol{\epsilon}_0$	Incident electric field strength vector of the light scattering experiment
ϵ_s	Static permittivity scalar
$\boldsymbol{\epsilon}_s$	Scattered field strength vector
ϵ_∞	High frequency permittivity
$g_{00}^{(1)}$	First rank of the tensor structure factor (or Kirkwood factor)
$g_{00}^{(2)}$	Second rank structure factor
$g_{\alpha\beta}(r)$	Atomic pair correlation function
$\mathbf{H}^s$	Magnetic shielding field
$\mathbf{H}_0$	Applied magnetic field strength vector
I	Spin quantum number
I_B	Molecular moment of inertia about the B axis
$I(0)$	Intensity distribution in X ray scattering
J	Molecular rotational quantum number
$\mathbf{k}_0$	Incident wave vector of the light scattering experiment
$\mathbf{k}_s$	Scattered wave vector
$\mu_{x,y,z}$	Components of the molecular dipole vector
$\boldsymbol{\mu}(A, t)$	Dipole moment induced in the light scattering process
$\mathbf{n}_0$	Incident polarization vector of the light scattering experiment
$\mathbf{n}_s$	Polarization vector of scattered light

$\bar{\nu}$	Wavenumber in cm^{-1}
P_1	Legendre polynomial of order 1
P_2	Legendre polynomial of order 2
$\hat{\phi}_u(t)$	Orientational memory function
$\phi_u^{(1)}(t)$	First memory function
$\phi_u^{(2)}(t)$	Second memory function
q	Magnitude of the non-zero component of the electric field gradient
Q	Nuclear quadrupole moment
Q	Normalizing factor of eq. (6.2.2.4)
σ	Shielding tensor
$d^2\sigma/d\Omega\, dE$	Number of neutrons scattered per unit solid angle and (per) energy interval
$d\sigma/d\Omega$	Diffraction cross section per unit angle
θ	Scattering angle
τ_2	Correlation time for the spin–spin vector
τ_D	Debye relaxation time
τ_H	Spin rotation correlation time
$\mathbf{u}$	Molecular dipole unit vector
$\mathbf{v}$	Field gradient direction of N.M.R. relaxation
$\omega_M^{(1)}$	Far infrared peak angular frequency
ω_0	Frequency of the incident beam of the light scattering experiment
ω_s	Angular frequency of scattered light
$\hat{\Omega}_u$	Resonance frequency operator
Ω	Unit of solid angle

In this chapter we collate the results from a series of experiments for a few carefully selected dipolar systems. In so doing we comment on complications involved in applying the models to actual experimental conditions and on the significance of the experimental results. We see that it is not always a straightforward matter to relate measurable quantities to variables involving molecular dynamics. Indeed it is not always straightforward to assign the measured quantities to a particular relaxation mechanism without making simplifying assumptions.

Dynamic data are available using the techniques of infrared absorption, NMR relaxation, light scattering, neutron scattering, and the experiment with which we are primarily concerned, namely, 0–THz spectroscopy. Several types of relaxation can contribute to the decay of correlations in those experiments. Furthermore, these mechanisms contribute differently to correlation functions determined from different experiments, so we must proceed with the utmost care. It is our considered opinion that the safest approach is through a careful comparison of measurements from all the techniques available (Chapter 12). Only in this way will we acquire a better understanding of the relative importance of the relaxation mechanisms operative for a particular molecule in the liquid or dense gas, and only then will theories emerge that enable us to advance from this model building era

to one of a more predictive nature. We consider here the progress already made in this direction, mainly through the intercomparison of "experimental" correlation times.

Since the theory of translation/rotation coupling is still in its infancy (Chapter 5) we consider only the molecular rotation. Molecular rotation was studied extensively in the past by dielectric relaxation methods. Debye's pioneering work had a profound influence on the development of the field. Debye's philosophy was a simple one, as outlined in a Biographical Memoir of the Royal Society:

> He knew that physical phenomena must have simple explanations; he took complexity to be lack of understanding. If a theory was not yet simple then it was not yet right—it was unfinished and imperfect. To achieve simplicity one must identify the essentials and isolate the irrelevancies. To recognize the essentials, to express them clearly and pictorially and then to pursue their consequences with superb technical facility was Debye's style. He had a deep distrust of overly mathematical theories, and dismissed as "mere mathematics" any explanation of a physical phenomena that lacked visualizable basis.

Theoreticians still develop abstract theories far removed from physical reality or with numerous adjustable parameters that make nonsense of attempted experimental comparisons. Experimentalists, on the other hand, are still too often content using old and oversimplistic models. As we shall see, absurd situations then arise where data, with large associated uncertainties, are analyzed, often in the quantitative fashion, using unrealistic theories. The conclusions drawn are meaningless and of little value.

There is a need to coordinate research so that a better balance between theory and experiment is obtained. In this chapter the most we can do is to outline the state of the art as it stands. We suggest likely courses for profitable future study in Chapter 12.

6.1 SOME FACTORS THAT COMPLICATE THE STUDY OF THE ROTARY DYNAMICS

The dipole time correlation function determined by Fourier transforming infrared or 0–THz spectral profiles is given classically by

$$C_1(t) = \langle P_1[\mathbf{u}(0)\cdot\mathbf{u}(t)]\rangle = \langle \mathbf{u}(0)\cdot\mathbf{u}(t)\rangle \tag{6.1.1}$$

where P_1 is the first Legendre polynomial and $\mathbf{u}$ is a unit vector along the direction of the dipole transition moment. The inverse Fourier transformation of a Raman (or light scattering) band yields correlation functions of the type

$$C_2(t) = \langle P_2[\mathbf{u}(0)\cdot\mathbf{u}(t)]\rangle = \tfrac{1}{2}\langle 3[\mathbf{u}(0)\cdot\mathbf{u}(t)]^2 - 1\rangle \tag{6.1.2}$$

These depend on the reorientation of a second rank molecule—fixed tensor. In Eq. 6.1.2 P_2 is the second Legendre polynomial and **u** is a unit vector along the symmetry axis of the linear or symmetrical top molecule at time t (which is also the axis of the polarizability anisotropy that gives rise to the depolarized wing). In principle, neutron scattering data are the most informative, being dependent on the rotation of all the molecule fixed tensors.

If $C_1(t)$ and $C_2(t)$ were determined solely by rotational relaxation, we could proceed directly to the comparison of the experiment with a reorientational model. However, they are in fact a complex convolution of various contributory factors which severely complicate the analyses.

6.1.1 The Problem of Collision-Induced Contributions

Weak depolarized light scattering exists for a number of spherical and tetrahedral molecules in dense gases and liquids. This is interpreted as being collision induced; that is, a fluctuating distortion of the symmetrical polarizability tensors of the isolated molecules is caused by the strong intermolecular interactions in the fluids. The interactions result in induced dipole moments as well as asymmetry in the polarizability; consequently, these collision-induced spectra are observed as excess intensity in the far infrared spectra (Figure 6.1.1.1) as well as in depolarized light scattering. Obviously, induced distortions are present to some extent in all liquids, and may give rise to measurable intensity in the depolarized Rayleigh wings, vibrations rotation bands, or far infrared spectra of any molecule (Chapter 11).

Using the theories of orientational motion given in Chapters 2–4, we can estimate the induced absorption contribution to the total far infrared intensity, for a dipolar liquid, by a simple subtraction of the theoretical

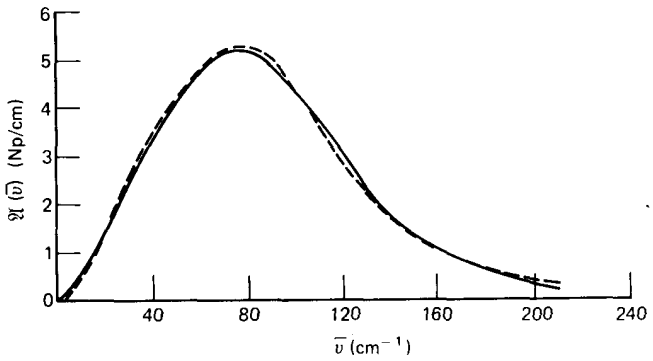

Figure 6.1.1.1 The far infrared induced absorption (298°K) of benzene. Solid line, experimental; dashed line, theoretical, after M. W. Evans.

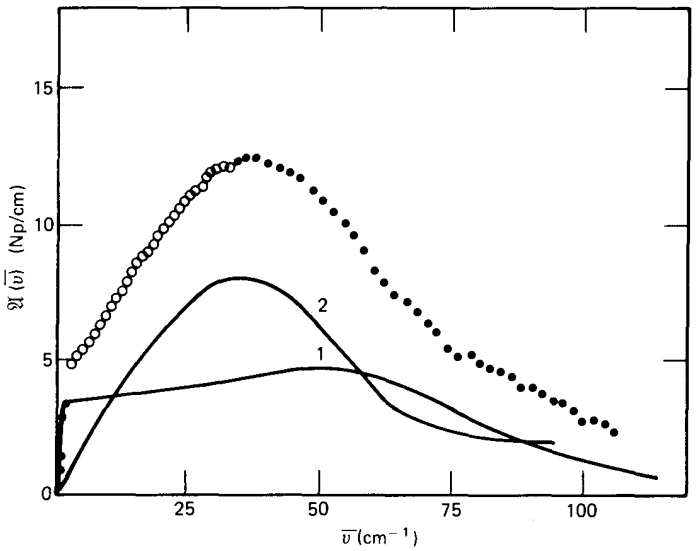

Figure 6.1.1.2 The estimated induced absorption for bromobenzene. ● Klystron results; ○ polarizing interferometer; · phase modulated interferometer. 1, Theoretical (exponential memory function, Chapter 2); 2, the estimated induced absorption.

curve from the experimental (assuming of course that no other relaxation process contributes to the spectrum). Two examples are shown for bromobenzene and methyl fluoride in Figs. 6.1.1.2 and 6.1.1.3, respectively. For bromobenzene the integrated intensity of the induced absorption closely resembles the estimates of Pardoe (1969) using the sum rule for the integrated intensity expected from the permanent dipole alone, and is approximately 50% of the total intensity. This is consistent for all the halogenobenzenes where the loosely bonded, highly mobile π electron clouds are easily distorted by the electrostatic fields of neighboring molecules. The contribution of induced absorption in methyl fluoride is seen to be much less significant.

In the infrared and Raman experiments the presence of induced absorptions provides a reasonable explanation for the deviation of the experimental second moments from theory. Rothschild (1970) established a deviation of approximately 20% between the calculated second moments of his infrared bands and those evaluated using the general expression of Gordon (1965).

Clearly, collision-induced contributions, if present, prove to be a major obstacle in the interpretation of either the $l = 1$ or $l = 2$ correlation functions. However, it has been suggested that at long times correlation functions are devoid of collision-induced behavior, the exponential decay reflecting only a loss of memory by the system of the initial molecular trajectories (van Konynenburg, 1972). Thus, this problem may be by-

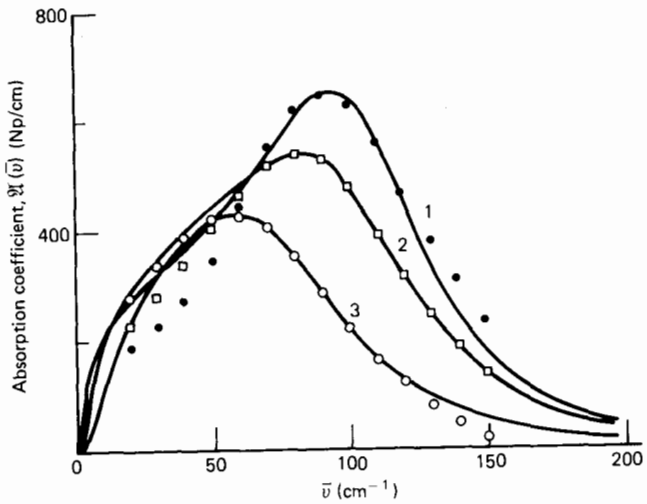

Figure 6.1.1.3 The induced absorption for CH_3F is very small using the estimation as for bromobenzene in Fig. 6.1.1.2. ● Absorption at 133°K; 1, least mean squares best fit to the data. Subtraction of this from the experimental curve gives an estimate of the induced absorption. □ Absorption at 173°K; 2, least mean square best fit to the data. ○ Absorption at 270°K; 3, least mean square best fit to the data (M. W. Evans).

passed, in principle, by fitting the correlation function at long times when the rotational contribution $[C_{rot}(t)]$ is predominant. Alternatively, in the frequency domain, by fitting the pair (ϵ', ϵ'') on an Argand diagram for $\bar{\nu} < 2\,\text{cm}^{-1}$, say (as in 0–THz spectroscopy, for example). The $C_{rot}(t)$ is then extrapolated through to the time origin and the far infrared rotational profile predicted. This approach was adopted in Figs. 6.1.1.2 and 6.1.1.3 and is the only acceptable one when molecular models have phenomenological parameters associated with them and recourse to fitting is essential.

6.1.2 The Problem of Rotation/Translation Coupling

A feature in the depolarized scattering spectrum of liquids such as aniline, quinoline, and nitrobenzene that has been attributed to the presence of rotation/translation coupling (Chapters 4, 5, 7) appears as a deviation from a simple Lorentzian of the depolarized spectra and the emergence of a dip in VH and HV geometries, commonly called the Rytov or "shear wave dip" (Fig. 6.1.2.1). This shear dip does not appear to be related to a specific microscopic structure. Indeed it has now been observed in a number of molecular liquids including polar and nondipolar liquids, planar and non-planar molecules, and both large and small molecules. Consequently, it is proposed that its origin resides in local strains set up by transverse shear waves that are relieved by collective reorientations.

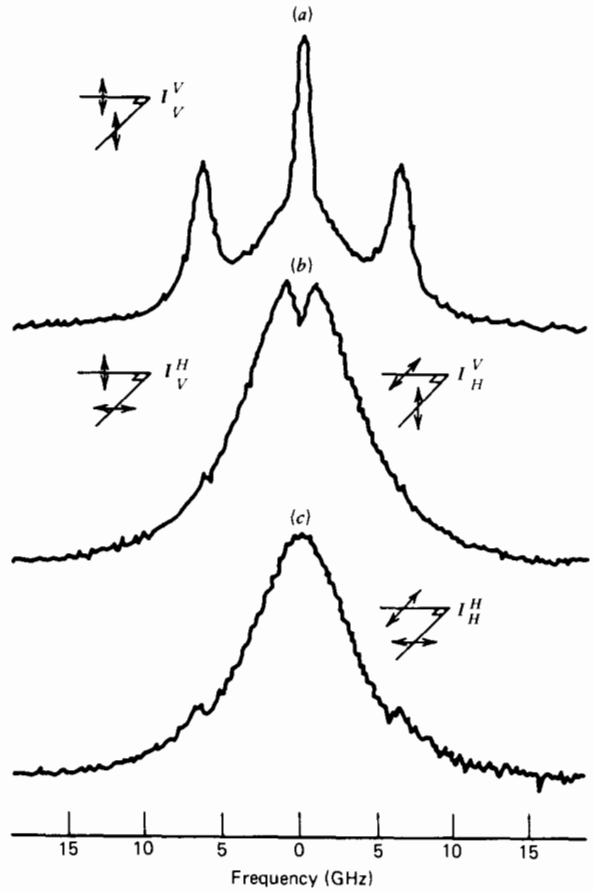

Figure 6.1.2.1 High resolution polarized and depolarized spectra of quinoline showing (*b* and *c*) deviation from a simple Lorentzian and the emergence of (*b*) a "shear wave" or "Rytov" *dip* in VH and HV spectra. [Reproduced by permission from G. I. A. Stegeman et al., *Phys. Rev.* **A7**, 1160 (1973).]

This is a well-known phenomenon. However, it is not so well realized that the effects of translational rotational coupling are also observable in the far infrared spectra of small molecular liquids. Ewing et al. (1966) reported spectra for dilute solutions of H_2, D_2, and HD in liquid argon. The rotational and translational transitions of these light molecules are easily distinguished so that complications normally associated with the liquid phase are reduced. We must comment on the origin of the observed absorptions. They are a consequence of the molecular quadrupole moment which induces a dipole in the surrounding liquid environment. This induced dipole is modulated as the molecule rotates so that transitions involving changes in these energies can be effected in the far infrared. In H_2 and D_2

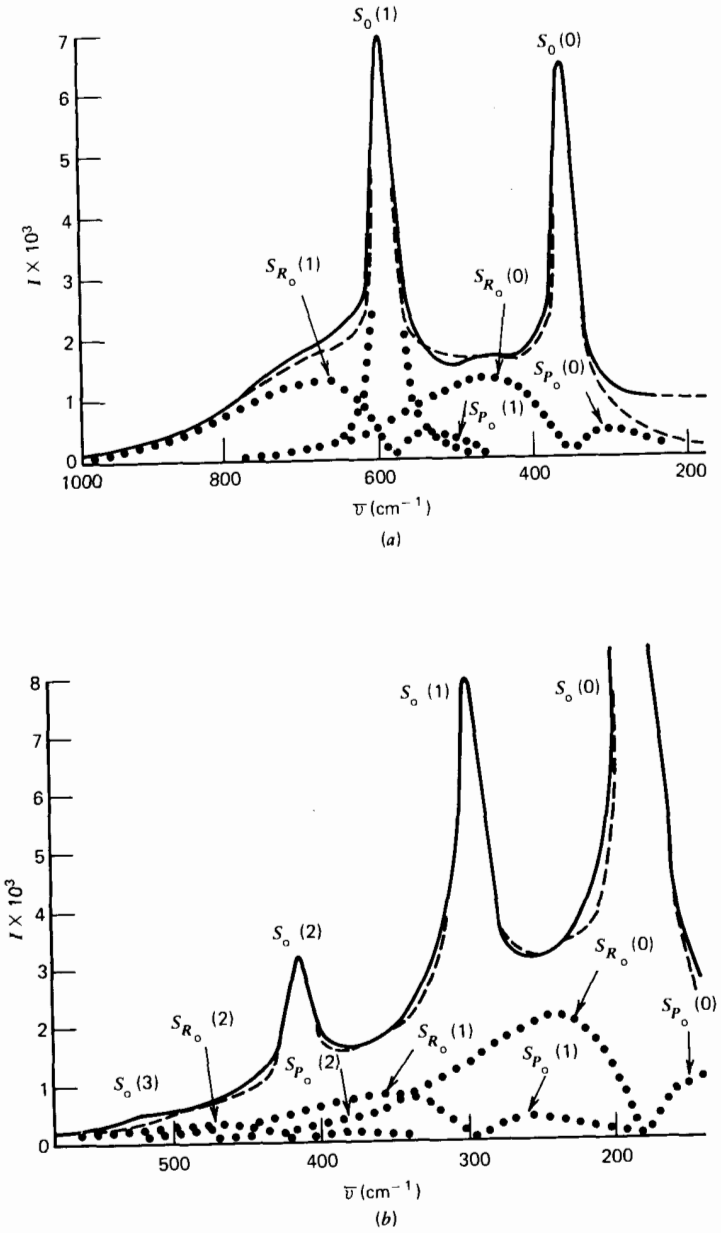

Figure 6.1.2.2 (*a*) Rotation/translation spectrum of H_2 in liquid argon. Solid line, experimental results. Dotted line, Lorentzian and four-parameter equations fitted to the data [only the $S_0(1)$ Lorentzian is shown]. Dashed line, the sum of the Lorentzian and four-parameter curves. (*b*) Rotation/translation spectrum of D_2 in liquid argon. Solid line, experimental results. Dotted line, four-parameter equations fitted to the data. Dashed line, the sum of Lorentzian and four-parameter curves. [Reproduced by permission from G. E. Ewing, *Acc. Chem. Res.* **2**(6), 168 (1969).]

the frequencies of the rotational transitions do not differ from those calculated for the unperturbed gas phase molecule within experimental error (Fig. 6.1.2.2). The lines are broadened because of the uncertainty effect, analogous to the situation present in gas phase induced spectra where the broadening arises because the dipole moment lasts only for the duration of a collision complex. In the liquid the broadening arises from the diffusive motions of solute molecules from short-lived molecular cages.

The far infrared spectrum of HD in liquid argon (Fig. 6.1.2.3) shows even larger half-widths, erratic frequency shifts, and additional absorptions arising from the relaxation of the rotational selection rules. The mechanism most able to account for these anomalous characteristics follows from a consideration of rotation/translation coupling. Transitions corresponding to $\Delta J = +2$, $+3$, and $+4$ become allowed through the mixing of rotational wave functions, a direct consequence of the rotation/translation coupling perturbation. A given J level acquires $(J + 1)$ and $(J - 1)$ characteristics and thereby the dipole moment operator responsible for $\Delta J = +2$ transitions in the H_2 and D_2 liquid systems causes interactions between the HD $(J = 0)$ state and the $(J = 2)$ character of the $(J = 3)$ state, thus allowing the observed $T_0(0)$ (rototranslational) feature. Likewise the $(J = 1)$ character of the $(J = 0)$ state combines with the $(J = 3)$ character of the $(J = 4)$ state to give the $U_0(0)$ transition. The perturbation theory of Friedmann and Kimel (1967) gives the rotation/translation interaction a quantitative form. Their results are consistent with the observed selection rules, frequency shifts, and linewidths in the spectrum of HD in liquid argon.

Nor are these observations restricted solely to the HD/argon system, where they are pronounced because of the asymmetric mass distribution of HD. Weaker coupling effects are even observed in the H_2/argon solution. A closer examination of Fig. 6.1.2.2 reveals a feature of the high frequency side of the $J = 3 \leftarrow J = 1$ transition that is assigned to a rotation/translation absorption in which the rotational transition is accompanied by the $n = 1 \leftarrow n = 0$ translational transition. A weaker transition in the low frequency side of each rotational absorption corresponds to a "hot band" in which translational deexcitation, $n = 0 \leftarrow n = 1$, accompanies the rotational transition.

Since translation/rotation coupling effects are so pronounced in these most simple systems they must also be present in other liquids. However, they are not easily distinguished *if individual fine structure is not resolved.* In the liquid phase, of course, the spacings of rotational energy levels (except for H_2) are smaller than the intermolecular potentials and so are greatly perturbed. Expressed in classical terms, since rotational and translational frequencies in the liquid are usually comparable, these motions become easily coupled. The net results of these interactions is to smear out individual rotational fine structure. The only instances known where structure persists in the liquid phase are systems composed of hydrogen containing molecules or its isotopes. In some cases only a few transitions

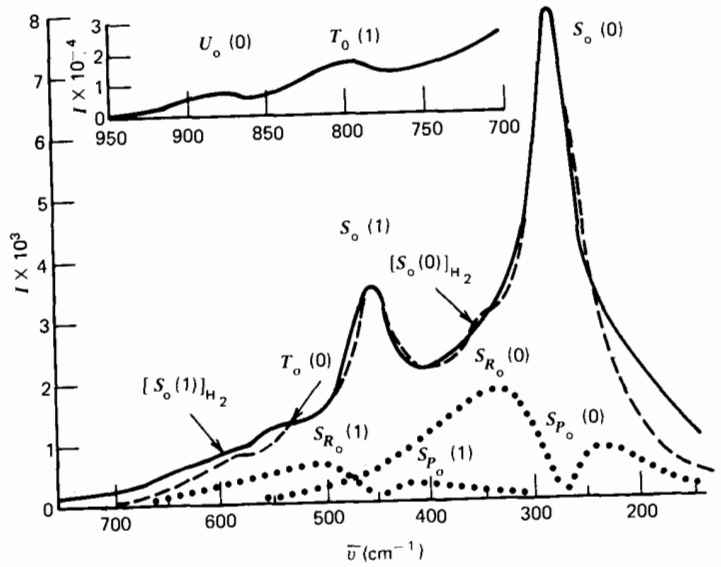

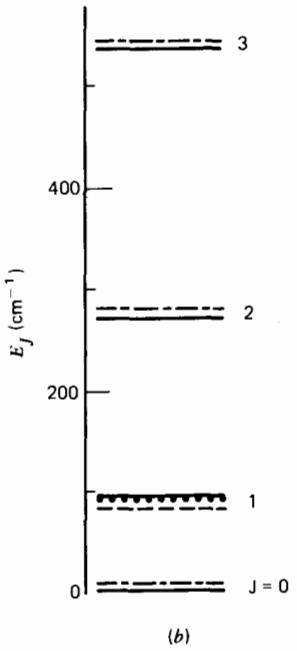

Figure 6.1.2.3 (*a*) Rotation translation spectrum of HD in liquid argon. Solid line, experimental results. Dotted line, four-parameter equations fitted to the data. Dashed line, the sum of Lorentzian and four-parameter curves. (*b*) Energy level diagram displaying translation/rotation coupling of HD in liquid argon. Solid lines, unperturbed rotatory levels. Dotted lines, theoretical HD levels after coupling of translational and rotational motions. Dashed lines, experimental levels. [Reproduced by permission from G. E. Ewing, *Acc. Chem. Res.*

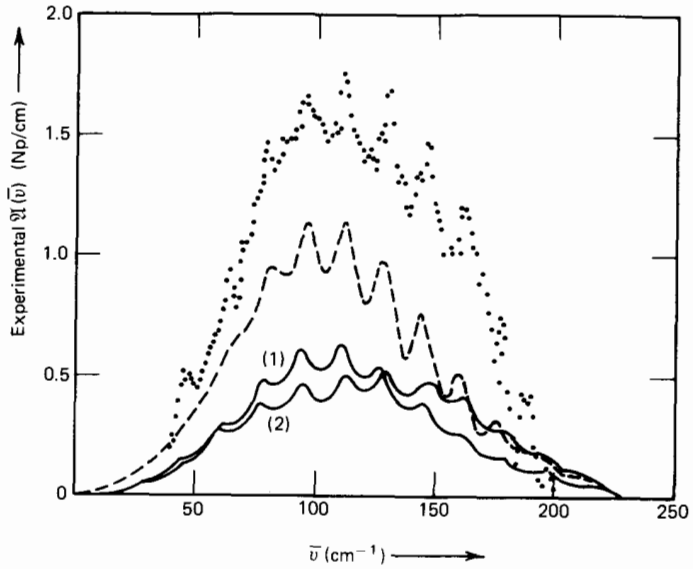

Figure 6.1.2.4 Experimental absorption of HBr/SF_6 liquid mixture at 296°K. ●, Experimental absorption at 296°K. ---, Frenkel/Wegdam formalism, ordinate scale unnormalized. (1) and (2), Truncated Mori formalism of Bliot et al., (1) $\beta_2 = 1$; (2) $\beta_2 = 1.2$. Both curves are unnormalized to the experimental data on the ordinate scale. [Evans, G. J., Ph.D Thesis (Wales), 1977.]

are observed (Fig. 6.1.2.4). The first few rotational levels in this instance are beneath the barrier height to rotation and are consequently not resolved. In most other liquids the far infrared spectrum is a broad band. It reflects a superposition over different local environments and fluctuations of these environments which also contribute to the broadening. However, evidence is still available that testifies to their rotation/translation origin.

Figure 6.1.2.5 shows the absorption of nitrobenzene, nitromethane, acetonitrile, and benzonitrile in dilute solutions of *n*-heptane, and acetonitrile in various solvents. Two features of the bands are prominent and give information concerning their origin. The first is the much lower absorption intensity (per molecule) for the phenyl compounds as compared with the methyl compounds. The band intensity depends on the molecular moment of inertia, suggesting strongly a rotational origin. The second feature, and the most striking, is the strong influence of the solvent on the position of the band. In the more polarizable solvents the entire band shifts to shorter wavelengths. Furthermore, the band intensity for one solute depends strongly on the solvent, so that mechanisms other than rotation must also be contributing to the total cross section. We can proceed further and estimate the extent of these contributions.

The band intensity of a pure rotation spectrum is given theoretically

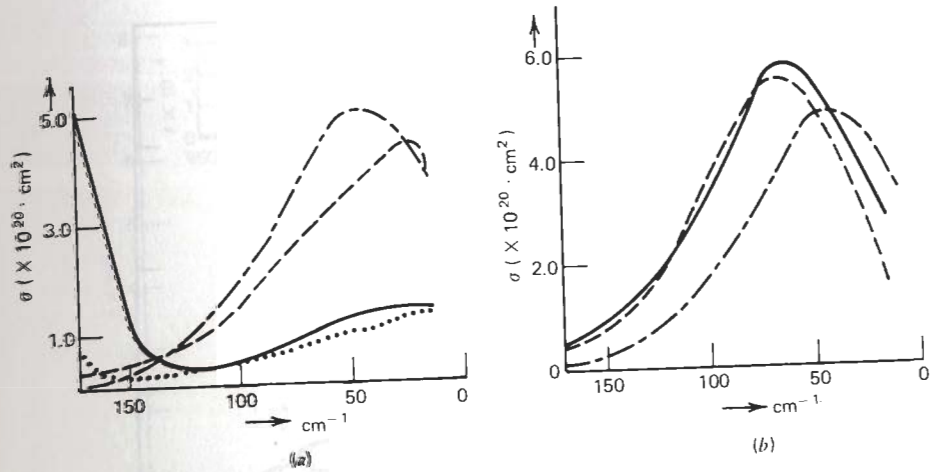

Figure 6.1.2.5 (*a*) The absorption cross section in the far infrared region of some polar solutes in *n*-heptane. –·–, CH_3CN; – – –, CH_3NO_2; ———, C_6H_5CN; · · · ·, $C_6H_5NO_2$. (*b*) The absorption cross section of acetonitrile in different solvents. – – –, *n*-heptane (4%), – – – –, CCl_4(3%); ———, CS_2(3%). [Reproduced by permission from S. G. Kroon et al., *Chem. Phys. Lett.* **1**, 285 (1967).]

(Chapters 1 and 4) by

$$A = \int \mathfrak{A}(\bar{\nu})\, d\bar{\nu} = \frac{2\pi^2}{c} \sum_k \left(\frac{I_k^2}{M_k} + \frac{(\mu_y^k)^2 + (\mu_z^k)^2}{3I_x^k} + \frac{(\mu_x^k)^2 + (\mu_z^k)^2}{3I_y^k} + \frac{(\mu_x^k)^2 + (\mu_y^k)^2}{3I_z^k} \right) \tag{6.1.2.1}$$

where the sum is over all molecules. μ_i is a component of the dipole moment and I_i the respective moments of inertia. This assumes only that the molecules are rigid, that relativistic effects are negligible, and that the wavelengths are long compared to the molecular dimensions (which they are in the far infrared). It applies both classically and quantum mechanically. By subtracting this pure rotational component from the total experimental integrated intensity it is estimated that for the *n*-heptane solutions 10% of the band intensity for the methyl compounds or 30% for the phenyl compounds is an excess intensity. The percentage is even larger for solutions of acetonitrile in polarizable solvents. Of course, in these instances contribution to the band intensity can be expected from terms arising from the changes of the dipoles induced in the surrounding molecules, with changes of intermolecular distance and orientation. These contributions, however, arise from intermolecular interactions and also have a translational as well as a rotational origin.

The effect of temperature on a polar liquid gives another clear indication of a rototranslation origin. Figure 6.1.2.6 shows the influence of temperature on a solution of acetonitrile in *n*-heptane and Fig. 6.1.2.7 the variation of peak $[\mathfrak{A}(\bar{\nu})_{max}]$ position with temperature for dichloromethane.

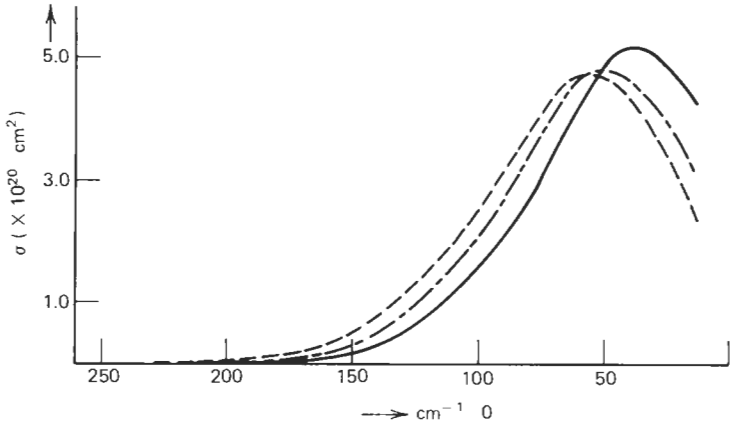

Figure 6.1.2.6 The effect of the temperature on the absorption cross section of acetonitrile (4%) in *n*-heptane. – – – –, Experimental data at 248°K; ——–——, experimental data at 277°K; ———, experimental data at 345°K. [Reproduced by permission from S. G. Kroon et al., *Chem. Phys. Lett.* **1**, 285 (1967).]

A clear band shift to shorter wavelengths occurs with decreasing temperatures though the band intensity remains approximately constant. This is contrary to that anticipated for a purely rotational band and is a consequence of the translational character. When the density increases, the pure rotational motion, as is found in the dilute gas, passes gradually over into a motion where translation and rotation are strongly coupled.

Recently computer simulation studies have brought to the fore the extent of rotation/translation coupling. Wolynes and Deutch (1977) and Berne and Montgomery (1976) have observed that in dilute solutions of spherical Brownian particles strong rotation/translation interactions exist and play a significant role in determining the dynamics of the *N*-particle system.

It appears, therefore, that the extent of rotation/translation coupling in molecular liquids is considerable. The consequences of this cannot be over-emphasized. Neutron scattering experimentalists, for example, work with the severe assumption of complete decoupling of rotation from translation and their conclusions concerning the details of the dynamics are true only within this approximation. It should be judged in the light of the fact that the analytical roto/translational neutron scattering spectrum of a rough sphere fluid is different from that of a smooth hard sphere fluid. Since the assignment of low frequency, far infrared bands to a rotation/translation origin seems justified it is probably also the case for depolarized light scattering and other techniques that have hitherto been assumed to be of purely rotational origin. Features of the spectra, such as the frequency of maximum absorption ($\mathfrak{A}_{max}$), then have no special *rotational* significance.

We have outlined the situation, as it stands, concerning the development

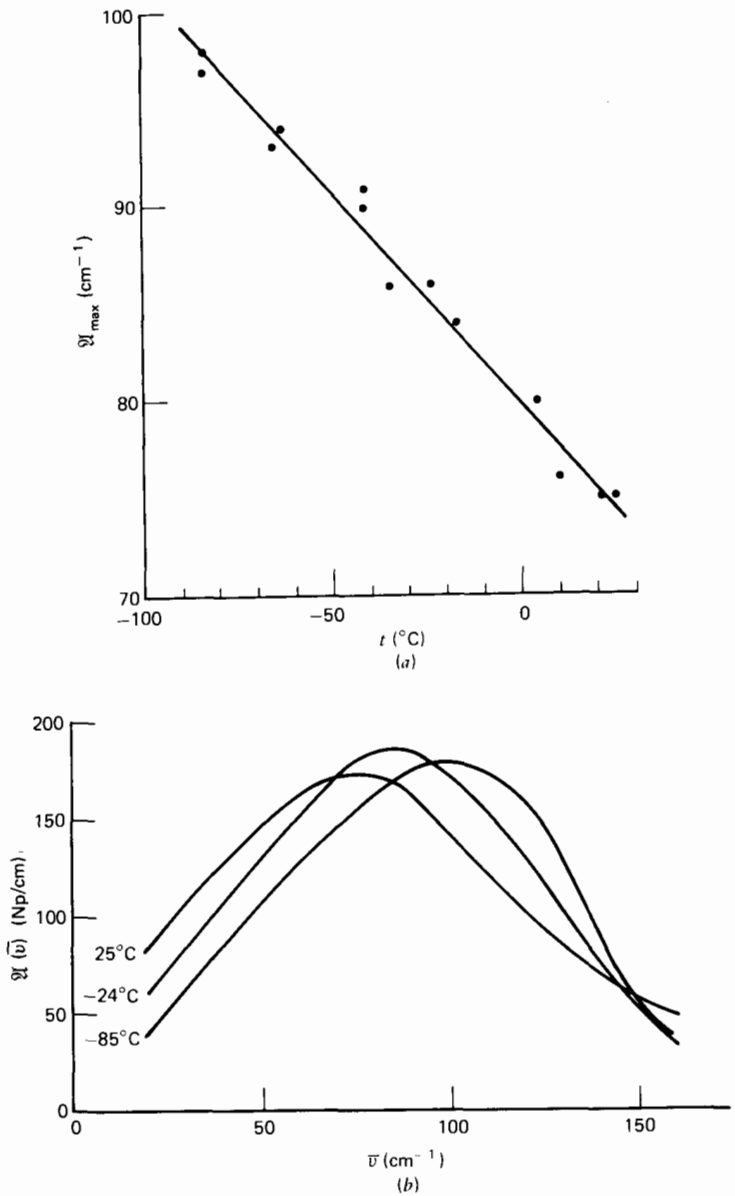

Figure 6.1.2.7 (*a*) Variation of peak position ($\mathfrak{A}_{max}$) with temperature for CH_2Cl_2. (*b*) Some typical absorption contours of CH_2Cl_2 at various temperatures.

of a full roto/translational theory (Chapter 5). There is still considerable progress required to formulate this theory in a way that will enable a complete evaluation with spectroscopic techniques and for the present, therefore, we are restricted to using the rotational models that are available.

6.1.3 The Problem of Rotational/Vibration Coupling

Infrared and anisotropic Raman profiles are obtained by the convolution of a rotational profile with a vibrational profile. It is customary to assume that coupling between the internal vibrations of a molecule and other degrees of freedom of the system is negligible, thus enabling, in principle, the deconvolution of the isotropic Raman spectrum with the infrared or depolarized Raman spectrum to yield "pure" rotational band shapes.

It is questionable if such an assumption is justifiable. Consider the infrared and isotropic Raman spectra of HCl dissolved in SF_6 (Fig. 6.1.3.1). The very sharp Raman profile suggests a small vibrational component and an infrared profile arising essentially from fast angular fluctuations of the molecules in solution. However, the subtle effects of molecular vibration are apparent in the far infrared profile of the $0 \rightarrow 2$ transition for the same system (Fig. 6.1.3.2). The vibrational fluctuations are large enough to scramble the rotational fine structure, making it barely visible in the $0 \rightarrow 1$ transition profile and distinct in the $0 \rightarrow 2$ vibrational transition.

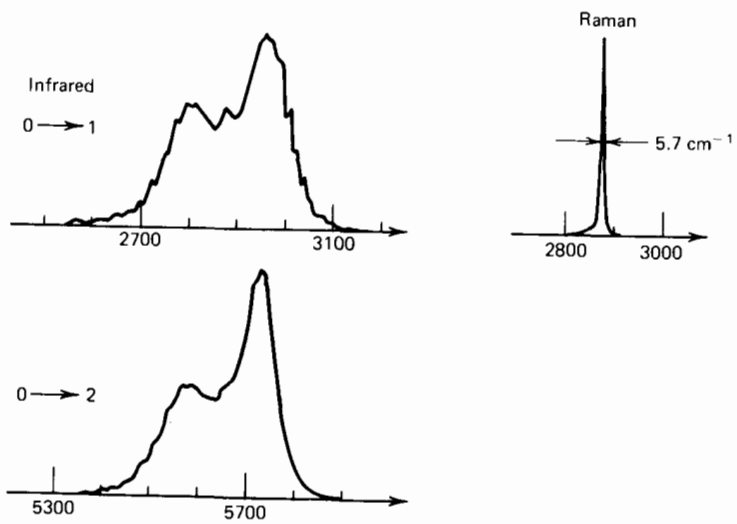

Figure 6.1.3.1 Infrared and isotropic Raman spectra of HCl/SF_6 solutions. Ordinate, absorption coefficient; abscissa, $\tilde{\nu}$ (cm^{-1}). [Reproduced by permission from M. Perrot, *J. Chem. Phys.* **70** (1973).]

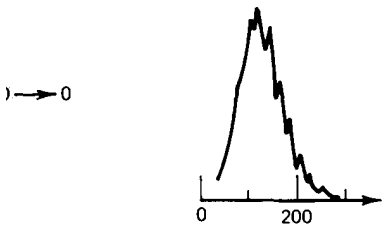

Figure 6.1.3.2 Far infrared spectrum of HCl/SF_6. Ordinate absorption coefficient (Np/cm); abscissa, $\bar{\nu}$ (cm^{-1}). [Reproduced by permission, M. Perrot, *J. Chem. Phys.* **70**, 1486 (1973).]

An increasing vibrational character is discerned in solvents that cause greater perturbations, such as CCl_4 or SO_2 (Fig. 6.1.3.3). The Raman profiles are now appreciably broadened and very different infrared profiles are observed for $0 \rightarrow 1$, $0 \rightarrow 2$, and $0 \rightarrow 3$ vibrational transitions.

In addition to complications already discussed, infrared and Raman profiles, therefore, suffer from the complication of vibration/rotation coupling. Van Woerkom et al. (1974) were the first to question the separation of vibration and reorientation functions. Lynden-Bell (1977), reexamining the problem, showed theoretically that in many instances the line shape is Lorentzian with a width equal to the sum of the vibrational and reorientational parts, but sometimes these components become coupled to give complex, non-Lorentzian line shapes, sometimes broader, sometimes narrower than expected, and on occasion showing a central dip (Fig. 6.1.3.4). She found that when the solute motion was faster than the solvent the vibrational "line widths" were sometimes negative and varied with l. Figure 6.1.3.5 shows a comparison of the ratio of vibrational half-widths at half peak height for infrared and depolarized Raman spectra. If there was no coupling between vibrational and reorientational relaxation the ratio would be unity. In the figure $l = 0$ corresponds to the isotropic Raman, $l = 1$ to the infrared, and $l = 2$ to the depolarized Raman experiments. The infrared half-widths are too large and the Raman widths too small. Such a situation may physically correspond to the case of a small dipolar molecule dissolved in a glass (Chapter 7) or liquid crystal (Chapter 8). However, studies reported to date on these systems are confined to 0–THz spectroscopy.

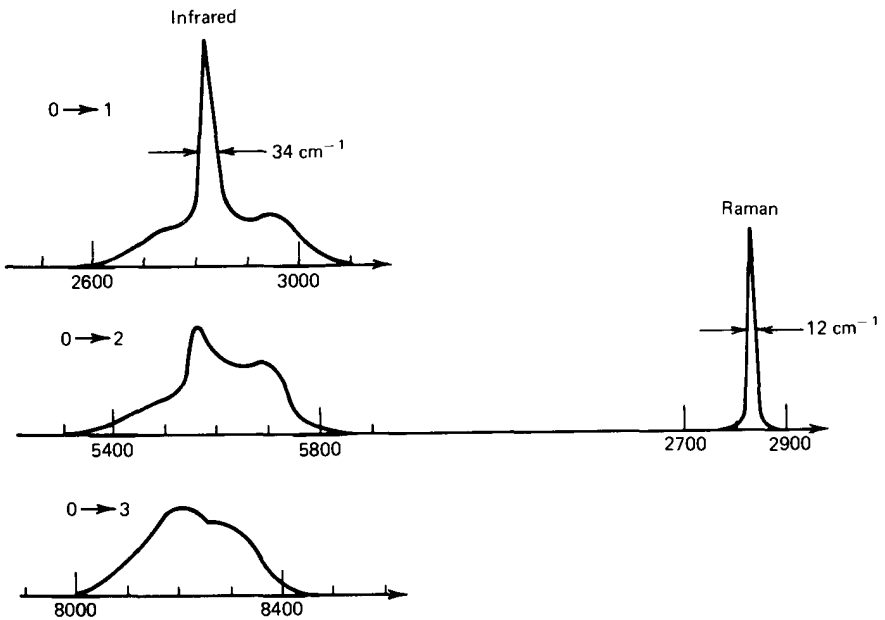

Figure 6.1.3.3 Infrared and isotropic Raman spectra of HCl/CCl_4 solutions. Ordinate, absorption coefficient; abscissa $\bar{\nu}$ (cm^{-1}). [Reproduced by permission from M. Perrot, *J. Chem. Phys.* **70**, 1486 (1973).]

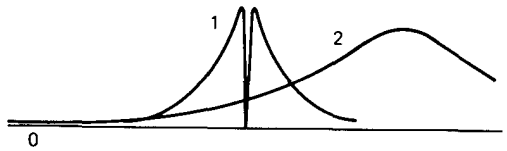

Figure 6.1.3.4 The line shape for infrared (1) and depolarized Raman (2) spectra for dipole–dipole vibrational modulation. The ratio of the rates of solvent motion to solute reorientation is zero. Note that the dip in the infrared spectrum is the instance where the solute molecules are reorienting about a fixed point in a rigid solvent lattice. [Reproduced by permission from R. M. Lynden-Bell, *Mol. Phys.* **33**, 907 (1977).]

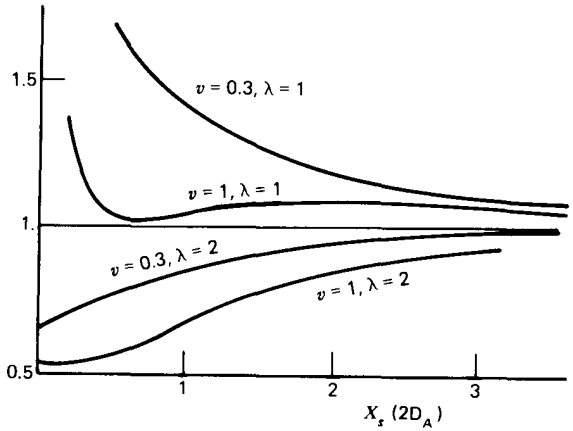

Figure 6.1.3.5 The ratio of vibrational half-widths at the half-height for infrared and depolarized Raman spectra to half-widths of the isotropic Raman spectra. Reproduced by permission from R. M. Lynden-Bell, *Mol. Phys.* **33**, 907 (1977).]

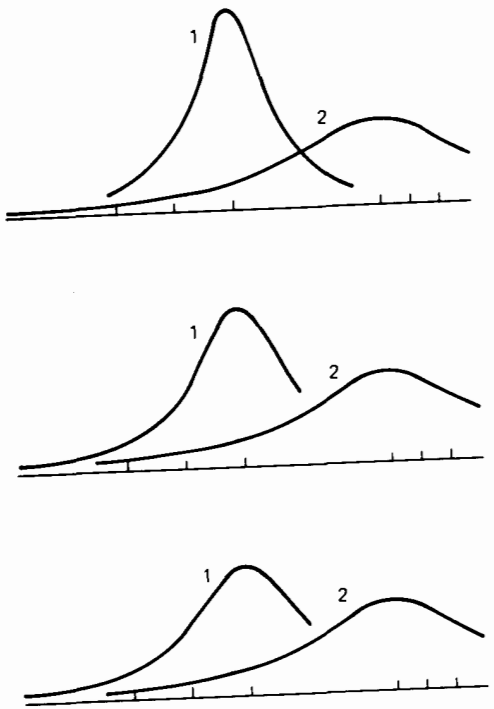

Figure 6.1.3.6 The line shapes for infrared (1) and depolarized Raman (2) spectra for dipole–dipole vibrational modulation. From top to bottom the rate of solvent motion to solute reorientation is 1, 2, and 3, respectively. [Reproduced by permission from R. M. Lynden-Bell, *Mol. Phys.* **33**, 907 (1977).]

The physical situation in isotropic liquid systems corresponds to one in which the rates of solvent and solute reorientation are comparable. Figure 6.1.3.6 shows the line shapes for infrared and depolarized Raman spectra where the ratio of the rates of the solvent motion to solute reorientation is 1, 2, and 3, respectively. The tops of the spectra are flattened and the half-widths vary with the type of experiment, the $l = 2$ spectra tending to be too narrow and the $l = 1$ spectra too broad.

In conclusion, when the time scale of the modulation of vibrational frequency by solute reorientation is faster than or comparable with the time scale of modulation by solvent reorientation, the vibrational line widths and line shapes depend on the type of spectrum observed.

6.1.4 The Problem of Cooperative Behavior

It has been established that depolarized light scattering and 0–THz spectra contain contributions from correlated mutual dipole moments. A comparison of the depolarized Rayleigh and depolarized Raman profiles of a Σ_g^+

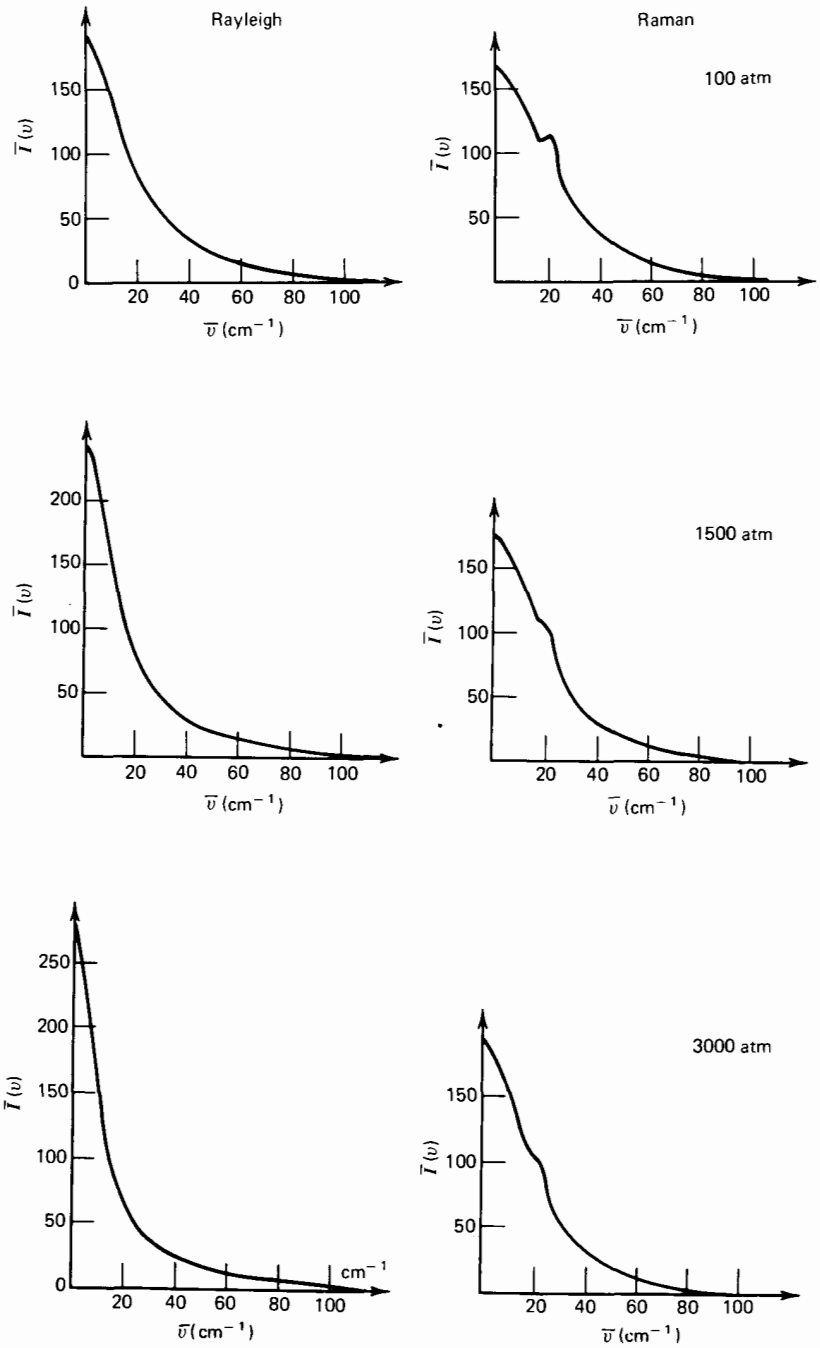

Figure 6.1.4.1 Normalized depolarized Rayleigh and Raman profiles of liquid CO_2 at various pressures. [Reproduced by permission from M. Perrot, *Mol. Phys.* **30**, 97 (1975).]

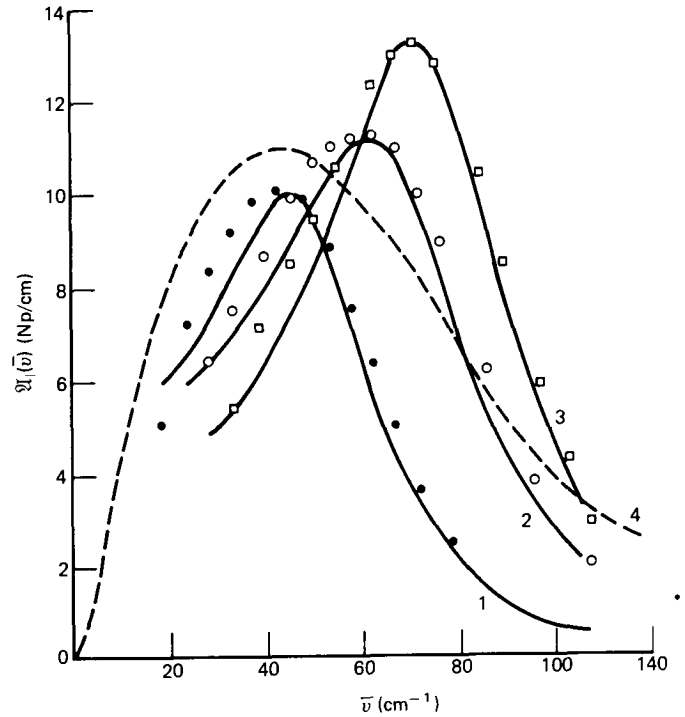

Figure 6.1.4.2 The far infrared absorption of liquid chlorobenzene under external pressure. (1) 0.6 kbar; (2) 2.3 kbar; (3) 4.4 kbar; (4) estimated induced absorption for chlorobenzene as for bromobenzene; see Fig. 6.1.1.2. Solid lines, least mean square best-fit results using Mori three-variable formalism (after M. W. Evans). Note that unlike the extended diffusion models it successfully follows the shift of $\bar{\nu}_{max}$ to higher frequencies with increasing pressure.

transition of liquid CO_2 under varying external pressures emphasizes the extent of the effect (Fig. 6.1.4.1). The isotropic Raman component is very narrow and remains relatively unaffected by increasing pressure. The Rayleigh profiles have very different evolution with increasing pressure. The corresponding increasing values of the correlation time indicate an increasing orientational correlation between the CO_2 molecules.

A similar situation exists in far infrared spectra. As external pressure is applied to liquid chlorobenzene a large shift of the frequency of maximum absorption to higher wave numbers is observed (Fig. 6.1.4.2), and dilution of a dipolar liquid in a nondipolar solvent causes a shift of $\mathfrak{A}_{max}$ to lower wave numbers as the extent of cross correlations is reduced (Fig. 6.1.4.3).

6.1.5 Some General Remarks

From the foregoing it is clear that molecular liquids pose significant problems in deciphering the dynamic motions. Since one is dealing with an

entity, the molecule, there exists both intra- and intermolecular terms. Ideally we should consider these separately. However, this is not always possible, as we saw in the last section (6.1.3). Intra- and intermolecular motions may become coupled and may severely distort infrared or Raman band shapes. Even if these processes were separable further complications arise because the molecular center of mass motion (translation), and

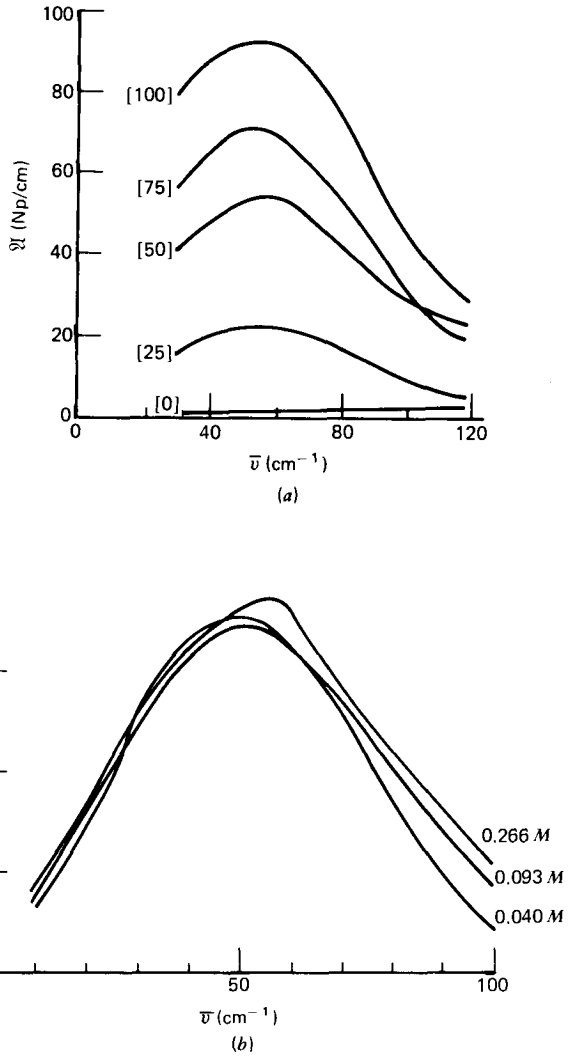

Figure 6.1.4.3 (*a*) Absorption coefficient for solutions of benzonitrile in cyclohexane at the indicated volume percent concentrations. (*b*) Solutions of sulfur dioxide in cyclohexane. $\mathfrak{A}' = \mathfrak{A}(\bar{\nu})_{solution} - \mathfrak{A}(\bar{\nu})_{solvent}$. (*c*) Absorption coefficient and refractive index for solutes of chlorobenzene in *p*-xylene at the indicated volume percent concentration.

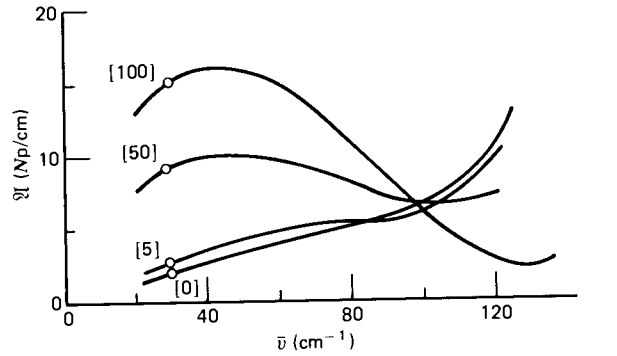

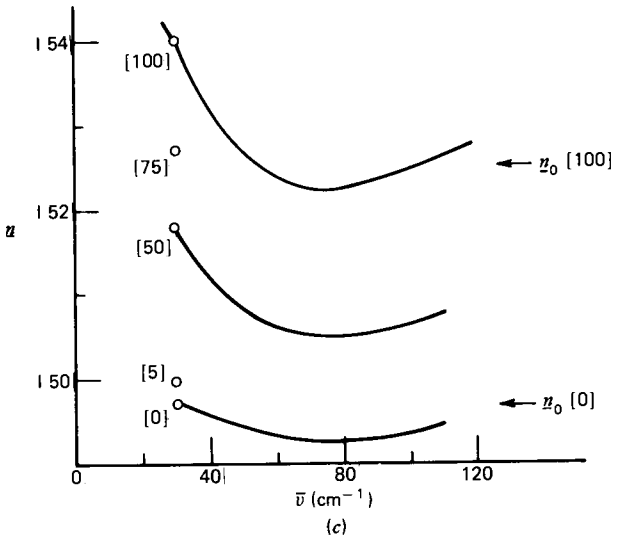

Figure 6.1.4.3 (*Continued*)

motions around the center of mass (rotations) are not always dynamically independent. They may become coupled and contribute significantly to the correlation functions, contributions that again vary with the experimental technique.

The experimental situation is complex and there is considerable uncertainty associated with all the measured data. No one technique yields a complete picture of the dynamic process because each projects a particular aspect of the motions of molecules in the fluid. Until the complications discussed above are better understood none of the experiments should be

used in isolation. The safest approach is to consider the results from several techniques simultaneously or to limit one's studies to simple liquid systems or those showing the extremes of molecular motion, for example, rotator phase studies where translational contributions are absent. We consider other such extremes (the glass and liquid crystalline states) in ensuing chapters.

6.2 THE EXPERIMENTAL TECHNIQUES

Here we describe very briefly the experimental techniques of current interest. We reproduce the equations that show how rotational motion is related to the observable quantities. We do not attempt any derivation of these equations. These are fully discussed elsewhere in the literature. We consider only the role played by single molecule motion and ignore correlated affects. These may be bypassed by considering systems of a solute dissolved in an "inert" solvent, Chapter 4. The proposed models we use later are only applicable to single molecule motion. No complete theory for correlated effects is available at present.

6.2.1 Magnetic Relaxation Experiments

Spin resonance spectra, in principle, provide a useful tool for investigating molecular dynamics. By comparing correlation times for different nuclei in the same molecule we can obtain information about the degree of anisotropy of the molecular motion and internal motions. A drawback is that in normal organic liquids the viscosity is low and spin-resonance spectra are motionally narrowed. The frequencies involved are generally small with respect to those representative of molecular motions in liquids. In these circumstances the experiment gives only the zero frequency component, or the correlation time, of the correlation functions involved. Macromolecules or viscous solutions of small molecules (Chapter 7) may have slow motion spectra which contain much more information about the molecular dynamics. However, this is difficult to extract.

The physical process under study is the relaxation of nuclear magnetization. The relaxation is caused by magnetic interactions randomly modulated by molecular motion. The simplest system is that of a sample containing many identical molecules each with a single spin $\frac{1}{2}$ in an external magnetic field. Such a two-level system has two distinct relaxation times, T_1 and T_2. T_1 is the longitudinal or spin-lattice relaxation time and can be calculated using time-dependent perturbation theory. The other spin-relaxation time, T_2, measures the rate of decay of magnetization perpendicular to the applied field and is known as the transverse or spin–spin relaxation time.

A number of relaxation mechanisms can be exploited to give information

about the dynamics of liquids. These include the following:

1. *Dipole–dipole interaction.* This is the most common interaction for spin $= \frac{1}{2}$ nuclei. The nuclear spins are associated with magnetic dipole moments; therefore other nuclei of the sample produce a magnetic field at the site of a given nucleus. Both translational and rotational motions may contribute to the relaxation process. To see this, consider two nuclear spins associated with the same molecule; then the angle between the internuclear vector γ_{12} and the external field is clearly made time dependent by molecular reorientations. If the two spins belong to different models then the internuclear distance γ_{12} also becomes time dependent so that translational and rotational motions of molecules relative to each other may in this case be studied. This relaxation method also suffers from the complication of cooperative behavior. The complication may be overcome experimentally by dilution in a nonmagnetic solvent, or by choosing the relaxing spin such that the entire relaxation is due to a few nearby spins in the same molecule (e.g., relaxation of the ^{13}C nucleus in a hydrocarbon is generally dominated by the protons that are bonded to the carbon atom).

   In the simplest case of two equivalent nuclear dipoles of spin quantum number I, the rotational relaxation times, in the case where the time required for attainment of a random distribution of reorientations in a fluid is much shorter than the Larmor period $2\pi/\omega$, are given by (Abragam, 1961)

$$\frac{1}{T_1^{DD}} = \frac{1}{T_2^{DD}} = \frac{2\gamma^4\hbar^2(I+1)I}{b^6}\tau_2 \qquad (6.2.1.1)$$

   where τ_2 is the correlation time for the spin–spin vector associated with spherical harmonics with $l = 2$ and $b = r_{12}(0) = r_{12}(t)$ and is the separation of a pair of spins in the same rigid molecule.

   The magnitude of the correlation time depends on the orientation of the spin–spin vector relative to the molecular frame except for molecules with tetrahedral or higher symmetry.

2. *Electric quadrupole-field gradient interactions.* In the extreme narrowing case for reorientational contributions (Abragam, 1961),

$$\frac{1}{T_1^{Q}} = \frac{1}{T_2^{Q}} = \frac{3(2I+3)}{40I^2(2I-1)}\left(\frac{e^2qQ}{h}\right)^2 \tau_2(\mathbf{v}) \qquad (6.2.1.2)$$

   where Q is the nuclear quadrupole moment and q is the magnitude of the only nonzero component of the field gradient. The direction of this gradient relative to the molecular axes is given by the vector $\mathbf{v}$.

3. *Spin-rotation interaction.* Because a moving charge produces a magnetic field the atomic nuclei of molecules in certain rotational states experience additional magnetic fields. Making the assumptions that the decay of the correlations involved is rapid and the fluid is isotropic, then the spin-rotation relaxation rate is given by (Abragam, 1961)

$$\frac{1}{T_1^{SR}} = \frac{1}{T_2^{SR}} = \frac{8\gamma^2 I(I+1)\langle H^2\rangle}{9\hbar^2}\tau_H \qquad (6.2.1.3)$$

   where the spin-rotational correlation time τ_H involves not only the reorientational motions but also the change in angular momentum due to torques exerted on a molecule in the dense phase.

4. *Anisotropic chemical shift.* Consider a nucleus on a symmetry axis of at least threefold symmetry, for which the shielding tensor σ is axially symmetrical. Then the shielding field $\mathbf{H}^{CS}$ depends on the angle between the applied field $\mathbf{H}_0$ and this symmetry axis. As with dipole–dipole interaction the time dependence is introduced through the angle which changes during a molecular rotation. It might be expected, therefore, that no further information is available from this mechanism that is not also extractable from the dipole–dipole case. However, this is not in fact the case because the unique directions, whose orientations relative to the applied field are monitored by the spins, can be different in both cases. This means that in a planar molecule, for example, all the internuclear vectors pertinent to the dipole–dipole coupling are in the molecular plane. The unique axis of the shielding tensor for ^{13}C and ^{15}N (when it exists) is perpendicular to the molecular plane.

The relaxation rate is given by

$$\frac{1}{T_1^{CS}} = \frac{2}{15}\gamma^2 H_0^2(\Delta\sigma^2)\tau^{CS} \qquad (6.2.1.4)$$

so that the relaxation rate depends on the square of the external field strength and thus on the square frequency, whereas all the other relaxation rates discussed are independent of this frequency in the extreme narrowing case. To observe this relaxation mechanism it is necessary to use as high a magnetic field as possible. Its contribution is too small to compete with dipolar coupling using ordinary electromagnets where fields of typically 20 kG are employed. Indeed, $\Delta\sigma$ is so small for covalently bound hydrogens that this mechanism is too small to make a contribution even using some of the newest generation of superconducting magnets with capacities for generating fields up to 85 kG.

In proton relaxation dipole–dipole interaction usually dominates in liquids. Quadrupole relaxation is overwhelmingly predominant in the relaxation of nuclei with spin greater than $\frac{1}{2}$. For $I = \frac{1}{2}$ nuclei, such as ^{12}C and ^{15}N, the anisotropic chemical shift and spin-rotation interaction may give appreciable contributions to the relaxation rates because shielding

effects are larger than for protons by at least an order of magnitude and spin-rotation interaction is also significantly greater.

6.2.2 Light Scattering

In a light scattering experiment the incident beam is described by the electric field strength $\boldsymbol{\epsilon}_0$, polarization vector $\mathbf{n}_0$, frequency ω_0, and wave vector $\mathbf{k}_0$. The scattered component is similarly characterized by $\boldsymbol{\epsilon}_s$, $\boldsymbol{\omega}_s$, $\mathbf{n}_s$, and $\mathbf{k}_s$. For 90° scattering geometry four experimental arrangements are of interest, differing only in the polarization of the incident and scattered light. These are commonly described by the combination of letters VV, VH, HH, and HV, where V stands for vertically and H for horizontally polarized light.

If the scattering only arises from the dipole moments $\boldsymbol{\mu}(A, t)$ induced in a particle A by the applied field $\mathbf{n}_0$, $\boldsymbol{\epsilon}_0$, we can write

$$\boldsymbol{\mu}(A, t) = \underline{\boldsymbol{\alpha}}(A, t) \cdot \mathbf{n}_0 \cdot \boldsymbol{\epsilon}_0$$

There are several resulting macroscopic scattering components that are best classified according to the rotational symmetry of the polarizability tensor $\underline{\boldsymbol{\alpha}}$. This is displayed schematically below.

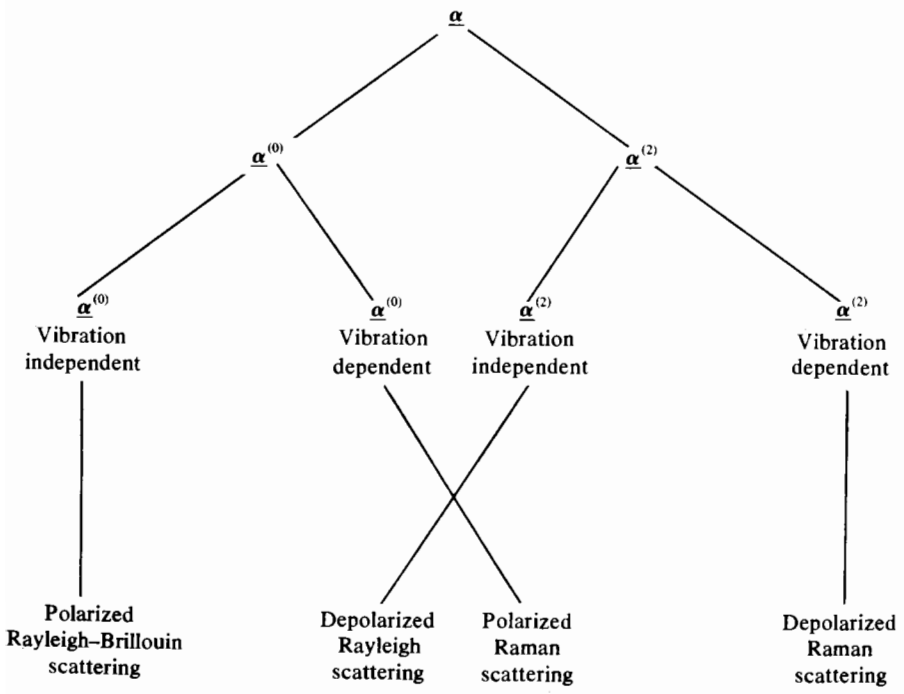

A decomposition of $\underline{\boldsymbol{\alpha}}$ into its spherical tensor components shows that (for optically inactive molecules) the polarizability has components of rank zero and rank two. Both these components are further subdivided into a permanent (vibration-independent) and a vibration-dependent part. The two vibration-dependent contributions give rise to the polarized and depolarized Raman scattering experiments. The vibration-independent parts give rise to polarized Rayleigh–Brillouin scattering (which is not influenced by the orientation of individual molecules) and to depolarized Rayleigh scattering (which is strongly influenced by the orientational behavior of the individual scattering centers).

Raman scattering suffers from the disadvantage of having a convoluted vibrational component: Rayleigh scattering from the contributions of correlated mutual dipole moments. Polarized Raman scattering is used to deconvolute infrared or depolarized Raman spectra to obtain "pure" rotational spectra. Bratos and Marechal (1971) derived the following set of equations for the band profiles of infrared and Raman spectra:

1. Infrared

$$I_{0\to n}(\omega) \propto \int_{-\infty}^{+\infty} \exp(i\omega t) C_{V0\to n}(t) C_R(t)\, dt \qquad (6.2.2.1)$$

2. Polarized Raman component

$$I_{0\to 1}(\omega) \propto \int_{-\infty}^{+\infty} \exp(i\omega t) C_{V0\to 1}(t)\, dt \qquad (6.2.2.2)$$

3. Depolarized Raman component

$$I_{0\to 1}(\omega) \propto \int_{-\infty}^{+\infty} \exp(i\omega t) C_{V0\to 1}(t) C_{2R}(t)\, dt \qquad (6.2.2.3)$$

where $C_R(t)$ and $C_{2R}(t)$ are the correlation functions of the first and second Legendre polynomials associated with the orientation of the unit vector $\mathbf{u}$ along the molecular axis. Analysis proceeds by recording an isolated $0 \to n$ infrared band and the corresponding Raman bands in both VV and VH scattering geometries. It depends on the assumptions that no interaction between rotation and vibrations exists and that induced polarizability or dipole moments are absent. It is confined to a study of dilute solutions. This is because as the molecule rotates the polarizability tensor varies with time, giving rise to a rotational band centered on the vibrational frequency. The vibrational and rotational character of the depolarized component generates a partially chaotic time variation of the polarizability tensor, causing the bands to be significantly broadened. As a rule, rotational broadening effects predominate for small molecules dissolved in very inert solvents and vibrational broadening effects are decisive in the case of heavy polatomic and associated liquids. Other factors may contribute to

the Raman experiment, including isotopic splitting, anharmonic hot bands, and spectral slit width, making analysis and the extraction of rotational detail anything but trivial. The calculated correlation time $[J_R = \int_{-\infty}^{\infty} C_{2R}(t)\,dt]$ is the same as that which appears in the usual treatments of nuclear spin relaxation by electric quadrupole coupling and intramolecular dipole–dipole coupling. However, the Raman experiment, in principle, contains the most information, the entire P_2 correlation function being extractable.

Rayleigh–Brillouin and depolarized Rayleigh scattering occur at lower frequencies than the Raman experiments. Because a small frequency shift is to be associated with a relatively slow molecular motion the time variation of the light scattering correlation function is associated with fluctuations in both the orientations and positions of molecules which may become coupled. The former arise from the anisotropy of the molecular polarizabilities, the latter from local disturbances of the density or from the creation and destruction of sound waves (phonons).

There is the added complication of cross correlations which to some degree determine the low frequency scattered intensities. It is a common supposition that molecular interaction effects are more significant in depolarized light scattering (and 0–THz) spectra than in infrared and Raman spectra. Vibrational motions are assumed to completely quench rotational interference effects in the latter two, in this way reducing their role. However, this assumption still has no firm experimental grounding.

The light scattering correlation function is written as

$$C_{LS}(t) = \frac{1}{Q}[C_{RB}(t) + C^{1}_{DRS}(t)] \qquad (6.2.2.4)$$

where Q is a normalizing factor.

$C_{RB}(t)$ when Fourier transformed gives Rayleigh–Brillouin scattering. It is observed in VV geometry. However, these spectra are not influenced by the orientation of individual molecules. Depolarized Rayleigh scattering spectra are. They are observed when the polarized vectors of the incident and scattered light are perpendicular (VH or HV geometry). Ignoring the effects of cross correlations, a rotational correlation function is extractable from $C^{1}_{DRS}(t)$ and values for the second-rank correlation factor $g^{(2)}_{00}$ obtained. (The first-rank tensor factor $g^{(1)}_{00}$ is the extensively studied Kirkwood factor for polar liquids.)

6.2.3 The Infrared Experiment

Much of our discussion of the Raman experiment applies to the infrared. Equation 6.2.2.1 shows that this again arises from a convolution of rotational and vibrational motions. However, the infrared experiment gives the P_1 correlation function. It must again be assumed that vibration/rotational coupling and coupling between vibrations of different molecules are small.

Infrared bands can be appreciably broadened by the presence of isotropic species or hot bands. The latter arise because molecules may exist in excited vibrational levels and are slightly displaced from the fundamental band by anharmonicity. The existence of these hot bands are well established in, for example, the vibrational Raman spectra (Chapter 12) of liquid CH_3I (Doge, 1973) at 525 cm^{-1}. Similar hot bands must be present in the infrared but cannot be resolved because they underly the rotational bands.

All these considerations are of extreme importance if accurate time correlation functions are to be obtained from infrared measurements.

6.2.4 Neutron Scattering

Neutron scattering is in principle one of the most powerful techniques. The wavelength of a neutron is of the order of the interatomic or intermolecular distances (0.5–10 Å) and the energy of the neutron is of the order of intermolecular interactions (1–100 MeV). Consequently it can give information about the space and time intervals of molecular motion.

However, for molecular systems, in particular organic liquids, the situation is complex. Both intra- and intermolecular properties are observable including translational, rotational, and vibrational motion, as well as different forms of collective motion. The successful and acceptable deconvolution of such a conglomerate has still to be mastered. Further, the structural information for the intermolecular properties is contained at low scattering angle and the dynamical information appears mainly at small energy transfer. Both studies require high resolution instruments (and consequently the signal intensity is often low), together with a number of independent experiments on isotope-substituted samples. We shall see this in the diffraction studies of acetonitrile reported in Section 6.3.2.

Neutron scattering is a random process controlled phenomenon, the scattered neutron wave containing an incoherent and a coherent component. This provides us with a means for studying monomolecular and collective motions separately, presupposing, however, that coherent and incoherent waves are experimentally separable. This is not always so but the problem does not exist for hydrogenated compounds where the hydrogen nuclei have a large spin incoherent cross section. Whereas oxygen, carbon, and nitrogen are almost purely coherent scatterers, hydrogen is a very strong, almost purely incoherent scatterer. Incoherent scattering involves single-particle motion only. Coherent scattering involves collective reorientations. The theoretical problems associated with the latter have not yet been solved and this source of information has not been exploited.

Unlike the other spectroscopic techniques there are no selection rules governing the values of l [in $P_l(\cos\theta)$] that contribute to the rotational scattering. The partial wave expansion involves a weighted sum of angular

correlations functions of spherical harmonics of *all orders*. Their weight can, in principle, be modulated by varying the scattering vector k. Expressions are available for computation of the higher-order functions of the set only in the limiting cases of free rotation and small step diffusion. For this reason, a Gaussian approximation involving only the first-order function is almost universally adopted. Also invoked in the theory of neutron scattering is the assumption that translation and rotational motions are uncoupled.

6.2.5 Zero–Terahertz Spectroscopy

Zero–terahertz spectroscopy is analogous to depolarized light scattering and contains contributions from correlated mutual dipole moments

$$C_{ZT} = \frac{1}{D}\left\{\left\langle \cos \delta\Omega(t) + \left\langle \sum_j \cos \delta\theta_{ij}(t) \right\rangle \right\rangle\right\} \qquad (6.2.5.1)$$

where

$$D = 1 + \sum_j \cos \delta\theta_{ij}(0)\rangle$$

and $\delta\theta_{ij}(t)$ is the angle between the permanent dipole on molecule i at time t and that on molecule j at time 0.

This spectroscopy covers the whole frequency range from static up to terahertz. We emphasize that the frequency range up to about $2\,cm^{-1}$ (the start of the conventional far infrared region) measures the absorption due to dipole motion over about 56 octaves of frequency. The whole of this region is scanned nowadays using only four (sometimes five) instruments operating simultaneously.

Recently there has been a flurry of activity to improve existing and develop new instrumentation for spectroscopy in the far infrared (2–$300\,cm^{-1}$) region. The result is that 0–THz spectra are obtained quickly and inexpensively. As an entity they provide discriminating tests for models of the fluid state (see Chapter 4).

The development of the far infrared region has been slow for a number of reasons. Firstly, the only readily available (and practical) source for many years was an almost black body heated to a convenient temperature. Most of the radiation from such a source is concentrated in the near infrared. The power radiated in the far infrared region up to $100\,cm^{-1}$ is only of the order of $4 \times 10^{-4}\,cm^{-2}$ so that only 1 part in 10^4 of the total radiation emitted by a black body lies in the submillimeter band. Raising the temperature of the source causes more submillimeter radiation to be produced but vastly more so in the near infrared region.

Secondly, there are problems associated with the detector system. There is no detector available in the infrared region to match the extreme sensitivity of the photomultiplier in the visible region. And there is no far infrared detector able to match the sensitivity of some of the better near

infrared detectors. The Golay pneumatic cell is most commonly used. It operates at ambient temperature. More sensitive detectors are available but are necessarily operated at lower temperatures. Room temperature corresponds to a frequency of about $200\,cm^{-1}$ so that, if a submillimeter photon is to have an energy much larger than that of the electrons in the detecting material, the temperature must be very low. Furthermore, the submillimeter region is a detector noise limited case (the signal to noise ratio is directly proportional to the incident power).

It is clearly desirable to choose a spectroscopic system giving an optimum transfer of energy from the source to the detector. Such a system is a two-beam interferometer which, though suffering from the disadvantage of providing, to the eye at least, unintelligible displays, has the highest throughput of any spectroscopic system. This is so because it records all parts of the spectrum of interest simultaneously. The interferogram produced by the interferometer and the spectral distribution of the radiation are Fourier cosine transforms.

The spectrometer (Fig. 6.2.5.1) consists of a Michelson two-beam interferometer connected to a digital computer which selects the component frequencies from the interference record observed by the detector as the path difference X between the two partial beams of the interferometer is varied.

The aperiodically scanned interferogram is modulated by means of a rotating chopper blade (amplitude modulation, A.M.), by a superimposed periodic displacement of one of the interferometer mirrors through a distance of the order of the mean wavelength (phase modulation, P.M.), or by rotating a polarizing grid (square function modulation).

In amplitude modulation the maximum magnitude of the interference fluctuations is little more than half the total signal but the detector is required to record all the signal. Phase modulation overcomes this disadvantage. It allows the detector to record only that part of the signal that is varying with path difference, thereby eliminating a constant and unwanted background contribution (which occupies and wastes part of the dynamic range of the amplifier). In this way electronic noise is reduced and source noise superimposed on the extraneous background is also removed. Stray rays transmitted by the interferometer are similarly discarded. Furthermore, the rotating chopper in amplitude modulation cuts off the radiation for half the duration of the measurement. There is a significant increase in signal level in phase modulation because of the elimination of this periodic shutter.

Phase modulation both discriminates in favor of the interferogram and utilizes all the radiation passing through the source aperture. The periodic displacement of one of the mirrors is achieved, at far infrared wavelengths where the magnitude of the oscillations and tolerance on the quality of the motion are such that a relatively simple vibrator may be used, by sinusoidally vibrating the fixed mirror using an electrically driven loud speaker

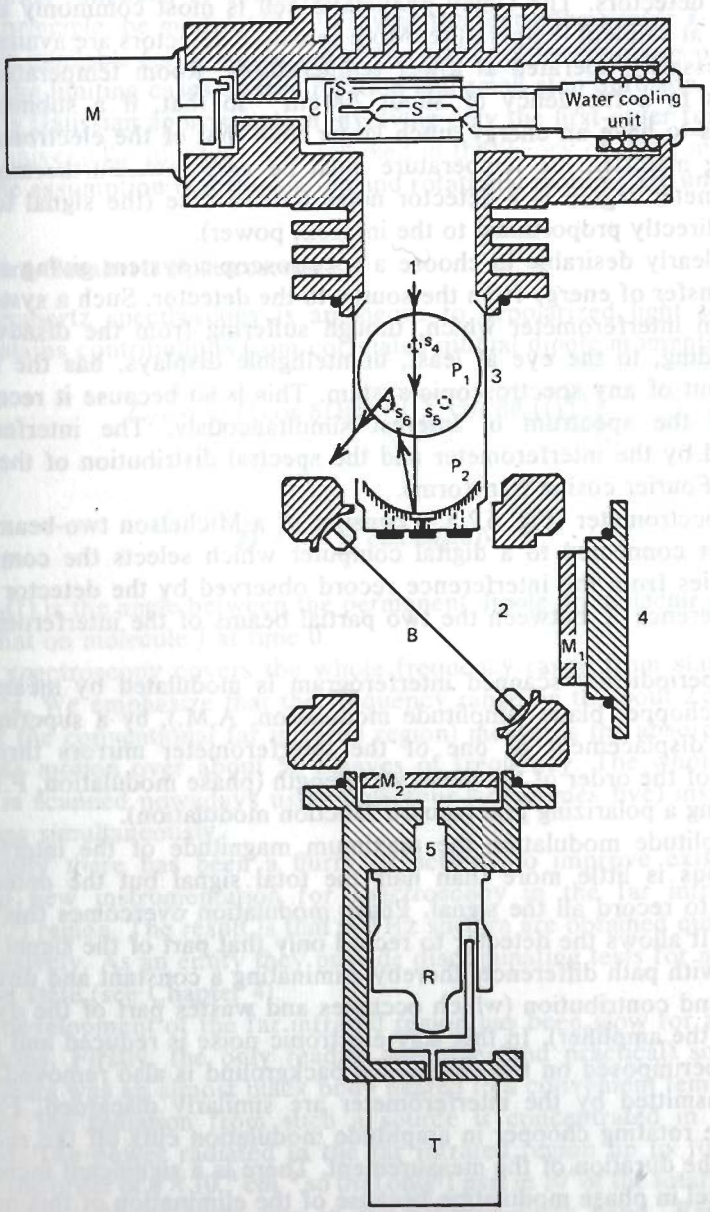

Figure 6.2.5.1 Schematic diagram of a modular design Grubb–Parsons/N.P.L. Far Infrared Cube Interferometer. 1, Source chamber; 2, interferometer; 3, collimator; 4, plane mirror (mounted on loud speaker coil providing phase modulation of detected signal); S, movable mirror; B, beam divider; S, source; C, chopper; M, chopper motor; R, micrometer; T, micrometer motor; P, plane mirro; P_2, paraboloid mirror. S_1, S_2, and S_3 and s_4, s_5, and s_6 are adjusting screws; S_1, water cooling sheath; M_1, plane mirror of interferometer: M_2, movable plane mirror of interferometer.

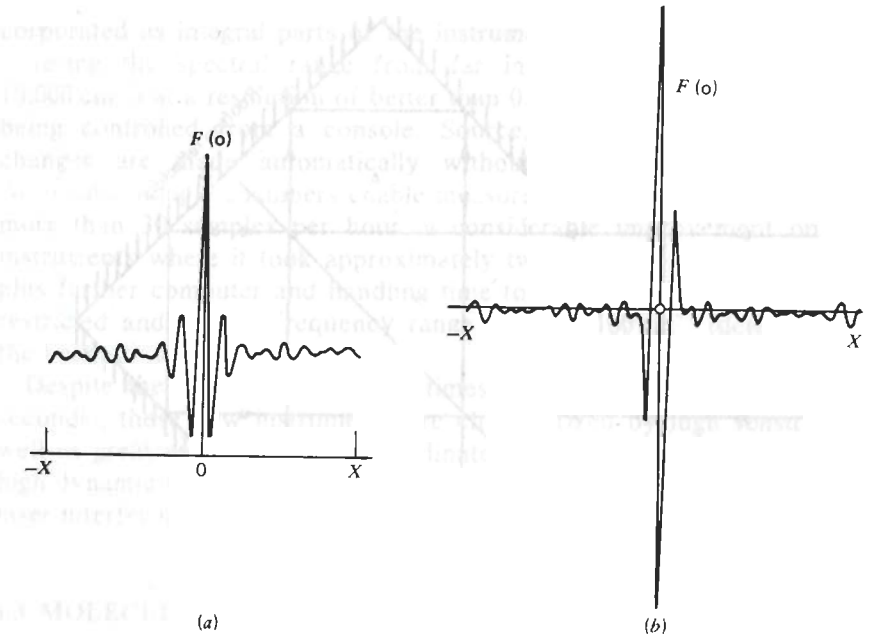

Figure 6.2.5.2 (*a*) An amplitude modulated interferogram. (*b*) A phase modulated interferogram.

coil. This provides a voltage interference record resembling the first derivatives of the usual (A.M.) interferogram and which, under ideal conditions, is an antisymmetric function (Fig. 6.2.5.2). Square function modulation, as used in the polarizing interferometer, can be shown to give a superior spectrum to both the sinusoidal amplitude and phase modulation techniques commonly in use. This new generation of interferometer, as originally developed by Martin and Puplett (1970), uses retroreflectors and wire grid beam dividers. Difficulties associated with thin film dielectric beam splitters are overcome by using these polarizing films. The beam splitter has an efficiency from well below $2\,cm^{-1}$ to above $100\,cm^{-1}$ and suppresses the background level. However, it does become necessary to use similar films as polarizer and analyzer. Figure 6.2.5.3 shows a sketch of Martin's polarizing interferometer. The wire grid polarizers used can have reflection and transmission coefficients close to 100% for their respective planes of polarization from frequencies close to zero to $1/2d\ cm^{-1}$, where $1/d$ is the spatial frequencies of the wires.

Modern-day instruments are completely automated. The digital interface gives the minicomputer control over the optics as well as many automatic accessories. The interface also provides the computer with extensive status information, allowing the computer to detect, and often correct, instrument malfunctions. Data systems of word length as large as 24 bits are in-

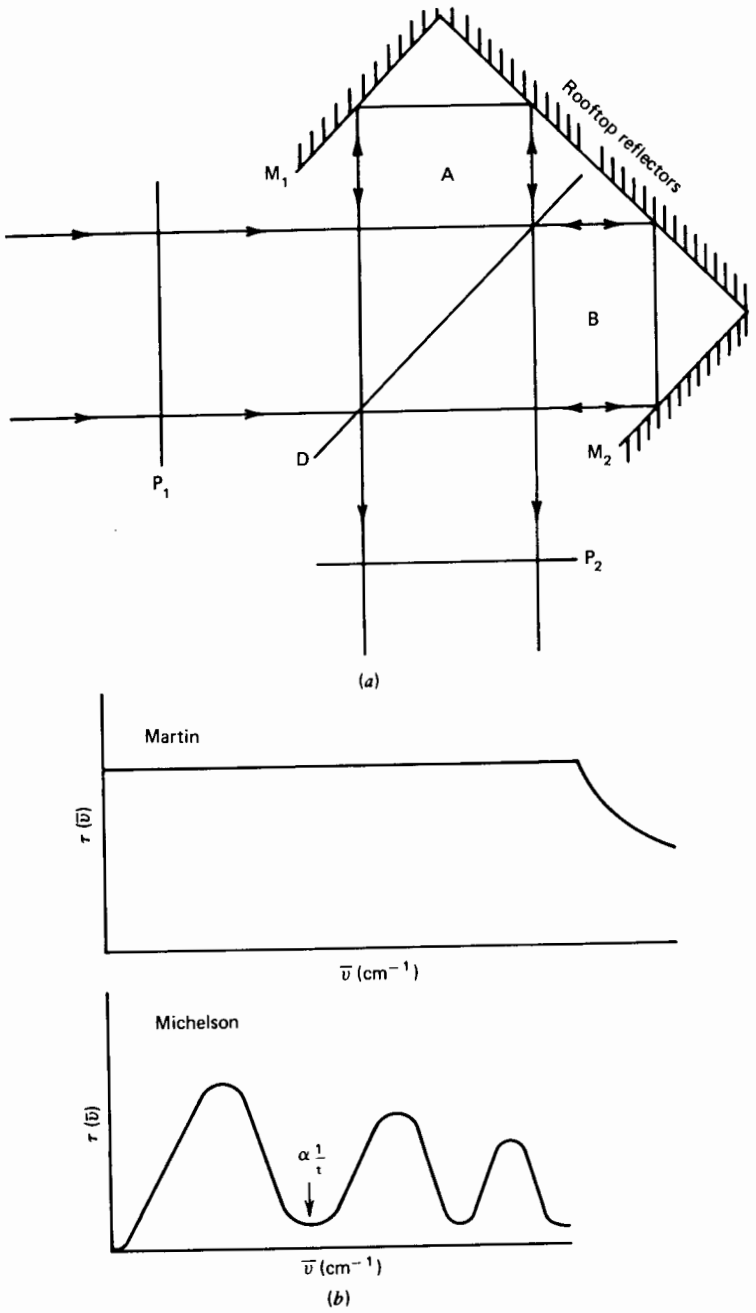

Figure 6.2.5.3 (*a*) Sketch of Martin's polarizing interferometer. (*b*) Comparison of the transmissivities of a Michelson and polarizing interferometer. P_1 is a polarizing grid, D a beam splitter, P_2 an analyzing grid, M_1 and M_2 rooftop reflector mirrors. A and B are the paths of the reflected and transmitted beams through the beam divides respectively.

corporated as integral parts of the instrumentation. Some are capable of covering the spectral range from far infrared to near infrared (20–10,000 cm^{-1}) at a resolution of better than 0.05 cm^{-1}, the whole experiment being controlled from a console. Source, beam splitter, and detector changes are made automatically without dismantling the apparatus. Automatic sample chambers enable measurements to be made at a rate of more than 30 samples per hour, a considerable improvement on older instruments where it took approximately two hours of experimental time plus further computer and handling time to obtain a spectrum covering a restricted and narrow frequency range, say, 10–100 cm^{-1} (determined by the beam divider being used).

Despite the short measurement times (spectra are surveyed in a few seconds), these new instruments are characterized by high sensitivity as well as great wave number and ordinate accuracy, a consequence of the high dynamic range of the computer in conjunction with the precision of a laser interferometer and the high focal ratio of the instrument.

6.3 MOLECULAR DYNAMICS STUDIES

We discuss results for iodomethane (CH_3I), acetonitrile (CH_3CN), and dichloromethane (CH_2Cl_2), three molecules providing a range of molecular polarizabilities, moments of inertia, and dipole moments. In addition a variety of spectroscopic data has been reported for them. We supplement the results with those available for other liquid systems where it helps to clarify certain features of the discussions.

We outline the state of the art as it stands and consider inferences about the molecular dynamics, available from the experimental data directly and from approaches based on modeling procedures and comparisons of various "experimental" correlation times.

Throughout it is assumed that cross correlations do not significantly affect the measured data and that the coupling of mutual correlations with translational modes and their resulting contribution to the spectral band shapes may be ignored. Also, it is assumed that vibrational relaxation is too slow to contribute significantly to the rotational relaxation.

6.3.1 Iodomethane

Iodomethane is almost linear if we take moments of inertia as a criterion (Chapter 4). It is representative, therefore, of one of the simplest systems available for study. Accordingly, it might be anticipated that good agreement would exist between theory and experiment and between the experimental results from different techniques.

Studies of the reorientation of liquid CH_3I are among the most detailed and painstaking of any to be found in the literature (Chapter 12).

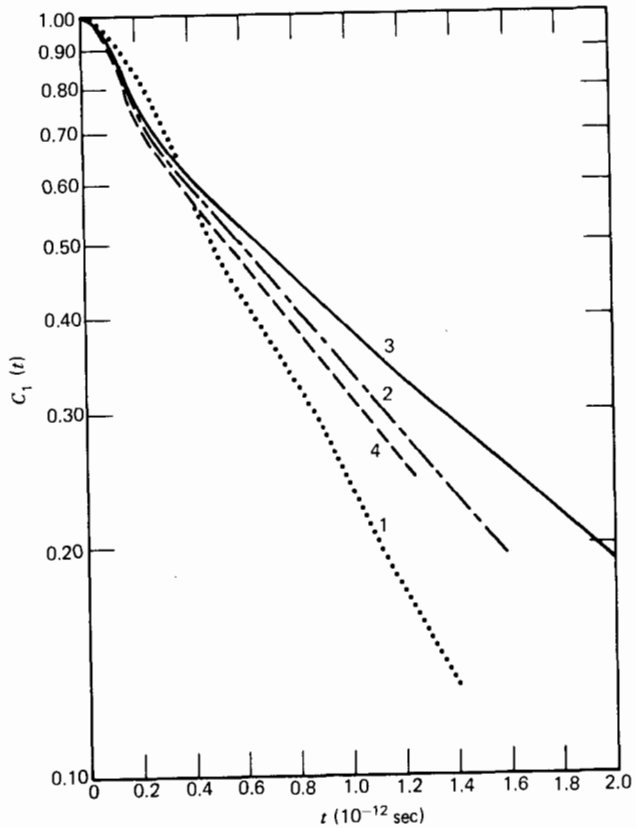

Figure 6.3.1.1 Infrared correlation functions calculated from the ν_3 band. The curves show changes of the angular correlation function as various corrections discussed in the text are applied. Curve 1: Rothschild (1970). Curve 2: Fulton (1970). Curve 3: Fulton's results further corrected for hot bands and the presence of isotopes. Curve 4: Favelukes et al. (1968). [Reproduced by permission from P. van Konynenburg and W. A. Steele, *J. Chem. Phys.* **56**, 5776 (1972).]

The infrared experimentalist studying CH_3I is faced with a number of problems. Figure 6.3.1.1 shows the correlation functions, calculated from the ν_3 band of CH_3I in the infrared. They change appreciably as various corrections are applied to the data. Curve 1 is the unmodified work of Rothschild (1970). Curve 2 is the result corrected for variation of refractive index by Fulton, and curve 3 is Fulton's results further corrected for hot bands and the presence of isotopes. The results of Favelukes et al. (1968) (curve 4) include corrections made by Crawford (1969) for dielectric effects, that is, corrections applied to the apparent absorption coefficient because of the frequency dependence of the local susceptibility. The corrections are substantial and should not be neglected if any insight into the molecular dynamics is to be obtained from the infrared experiment.

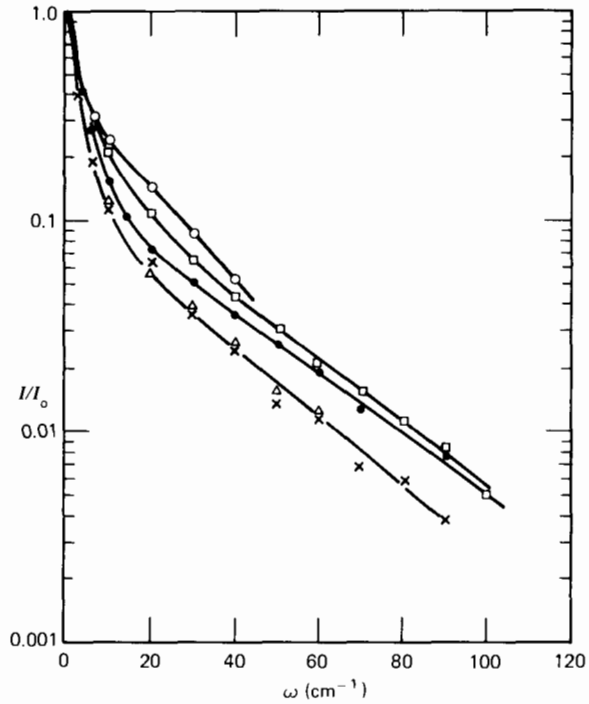

Figure 6.3.1.2 Depolarized Rayleigh wing spectra plotted on a logarithmic intensity scale for ● CH_3I ($\Delta = 30\,cm^{-1}$), □ CH_3I/CCl_4 ($\Delta = 30\,cm^{-1}$), X $CHCl_3$ ($\Delta = 27\,cm^{-1}$), △ CH_2Cl_2 ($\Delta = 25\,cm^{-1}$), and ○ CCl_4 ($\Delta = 20\,cm^{-1}$). [Reproduced by permission from P. van Konynenburg and W. A. Steele, *J. Chem. Phys.* **56**, 5776 (1972).]

Van Konynenburg and Steele (1972) reported infrared and depolarized Rayleigh scattering results for CH_3I. They corrected the infrared data for band shape changes due to variable refractive index, isotope splitting, and hot bands. They measured depolarized Rayleigh spectra for CH_3I and CH_3I in CCl_4 (0.3 mole fraction). The spectra are shown in Fig. 6.3.1.2. From zero frequency up to about the half-width they are very close to Lorentzians; at frequencies beyond $20\,cm^{-1}$ for CH_3I the spectra are exponential. For the mixture CH_3I/CCl_4 exponential behavior is attained only after $50\,cm^{-1}$ and in this region has the same slope as pure CH_3I. The intensity due to CCl_4 was estimated at less than 10% of the total.

Figure 6.3.1.3 shows the experimental time correlation functions for liquid CH_3I at room temperature. In CCl_4 the correlation function decays somewhat faster, reflecting the more isotropic environment and the decrease of angular correlations between neighboring molecules. The simple rotation diffusion model (Chapter 2) predicts that the rotational diffusion constant is inversely proportional to the viscosity of the fluid. It fails here because the viscosity of the mixture is a factor of ~1.7 greater

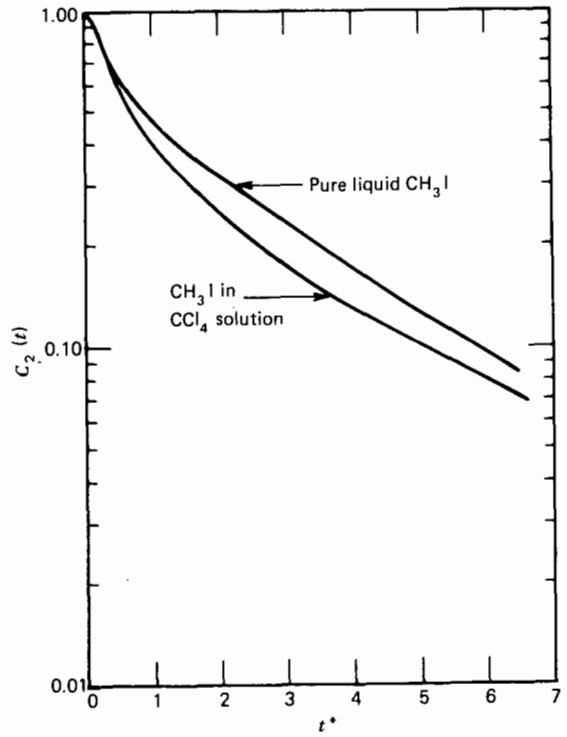

Figure 6.3.1.3 A comparison of the $l = 2$ correlation functions for the molecules in pure CH_3I, in CCl_4. The orientational correlations decrease more rapidly for the molecules in solution than in the pure liquid, presumably because hindrance to motion is less when the neighboring molecules are more nearly spherical. Abscissa: time units. [Reproduced by permission from P. van Konynenburg and W. A. Steele, *J. Chem. Phys.* **56**, 10 (1972).]

than that for pure CH_3I. A large value for the relaxation time of the mixture, and thus a slower exponential decay of the correlation function, would have been anticipated.

CH_3I possesses three vibrational modes of symmetry A_1 and three doubly degenerate modes of E symmetry. All are active in both the Raman and infrared. However:

1. There is a lack of information concerning the values of the polarizabilities so that it is hard to envisage how any quantitative information can be obtained from the Raman E bands.
2. There are difficulties associated with the interpretation of correlation functions obtained from the A_1 Raman bands and infrared data. Consider the Raman bands for CH_3I (Fig. 6.3.1.4). There is a considerable overlap between many of the bands in the depolarized spectrum so that accurate estimates of bandwidths are far from

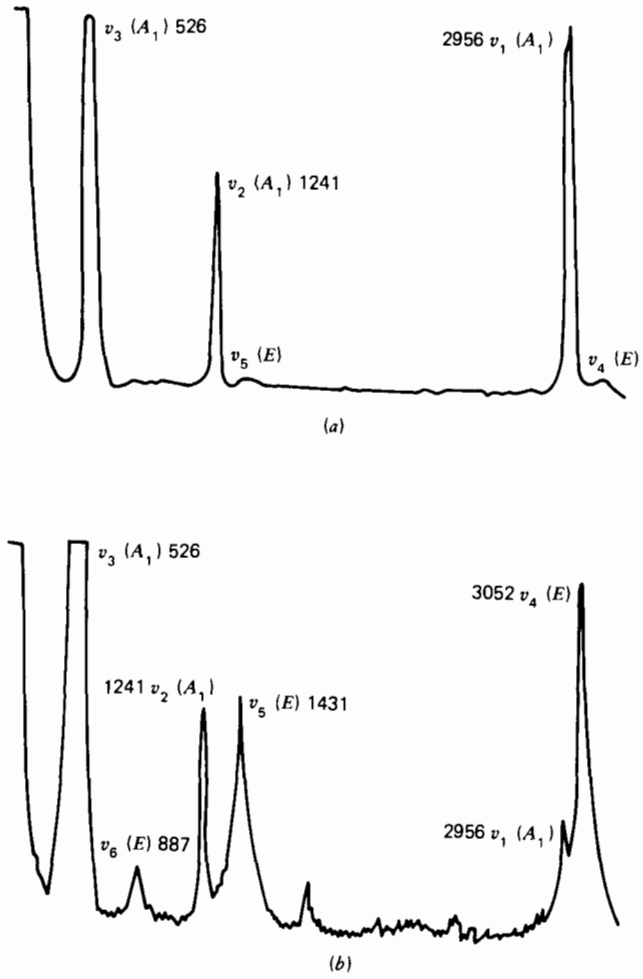

Figure 6.3.1.4 Raman spectra for liquid CH_3I: (*a*) polarized, (*b*) depolarized. Ordinate: intensity (arbitrary unit). Abscissa; wave number (cm^{-1}). [Reproduced by permission W. A. Steele, *Adv. in Chem. Phys.* **34**, 1 (1976).]

trivial. Since the E bands are noticeably broader than the A_1 bands, qualitatively at least, we can say that the rotation about the molecular axis is noticeably faster than reorientation of this axis.

The ν_3 band is by far the strongest of the depolarized A_1 bands and as such should yield the most reliable bandwidth data. From this the correlation time ($\tau_{2,0}$) is estimated at 1.5 ± 0.2 psec for CH_3I at room temperature. The same correlation time for CD_3I is some 10% longer.

Data from depolarized Rayleigh light scattering measurements are sufficiently detailed to give the correlation function as well as the

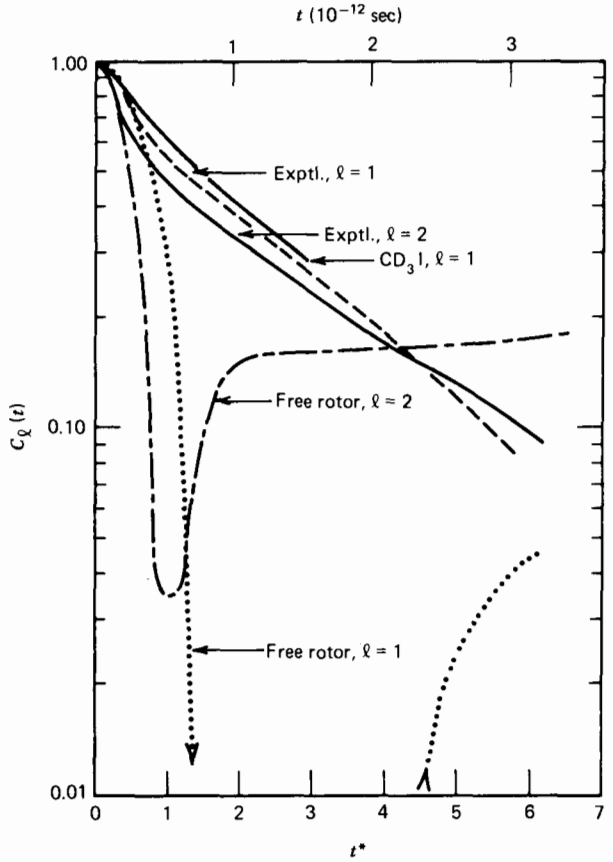

Figure 6.3.1.5 Experimental time correlation functions of CH_3I at room temperature. The $l = 1$ correlation function is the corrected curve of Fig. 6.3.1.1. The $l = 1$ curve for CD_3I has not been corrected. The vertical lines along the $l = 2$ correlation function indicate the estimated uncertainty of this result. Also displayed are the calculated correlation functions for a classical ensemble of freely rotating CH_3I molecules. [Reproduced by permission from W. A. Steele, *Adv. in Chem. Phys.* **34**, 1 (1976).]

correlation time. Figure 6.3.1.5 shows the correlation function ($l = 2$), which is exponential for $t^* > 1$ but oscillatory and different from the free rotor for $t^* > 0.5$. Correlated rotational motions in this instance seem to be unimportant. They do not appear to contribute to the depolarized Rayleigh spectrum at frequencies where they are expected to predominate.

3. A paradox emerges when we compare the infrared data for the A_1 and E bands. The respective correlation functions are shown in Fig. 6.3.1.4. The $l = 2$ and $l = 1$ (near infrared) correlation times ($\tau^*_{2,0}$ and $\tau^*_{1,0}$, respectively) have values $\tau^*_{2,0} = 3$ and $\tau^*_{1,0} = 2$. As we show later

for small step diffusion, the ratio $\tau^*_{2,0}/\tau^*_{1,0}$ is $\frac{1}{3}$ so it appears that here small step diffusion does not provide an adequate description of the molecular dynamics. However, $\tau_{1,0}$ from the infrared data predicts a ratio of $\tau^*_{2,0}/\tau_{1,0}$ approximately $\frac{1}{3}$ and in accord with that anticipated for rotational diffusion. It is tempting to explain the discrepancy in terms of correlated motions which contribute to the far infrared. However, this then contradicts the conclusions already drawn from a comparison of Raman and depolarized scattering results. Some of the discrepancy must surely arise from extraneous factors that affect the spectral measurements. The omission of vibrational broadening in the analysis of the infrared band shapes is undoubtedly important, as emphasized by Steele (1976). In addition there is the problem of collision-induced absorption or scattering and the estimation of their relative importance.

Further discrepancies are apparent when we consider the NMR results available. Nuclear quadrupolar relaxation times (of CD_3I), ^{13}C relaxation times, and the intramolecular part of the proton relaxation times have all been measured. Measurements of the nuclear Overhauser effect show that the last two are affected by a nondipolar relaxation mechanism which is spin rotational in origin. The first gives

$$\tau_D = 0.13\tau_{2,0} + 0.25\tau_{2,1} + 0.62\tau_{2,2} \qquad (6.3.1.1)$$

where τ_D is the Debye time. The third gives

$$\tau_{2,0} + 3\tau_{2,2} = (1.8 \pm 0.5)\ \text{psec} \qquad (6.3.1.2)$$

Since the ^{13}C—H vector, which dominates the ^{13}C dipolar relaxation, has the same orientation in the molecular frame as the C—D vector, the first two relaxation processes give rise to identical relaxation times.

Using $\tau_{2,0}$ (from Raman measurements above), $\tau_{2,2}$ is calculable from Eq. 6.3.1.2, and thereby $\tau_{2,1}$ is evaluated knowing the Debye relaxation time (the infrared experiment) from Eq. 6.3.1.1. As we have seen, large uncertainties are associated with the experimental determination of $\tau_{2,0}$ so that unequivocal values of the NMR correlation times cannot be calculated. The estimated values are for $\tau_{2,2}$ 0.1 psec, with an uncertainty of at least 0.3 psec and for $\tau_{2,1}$ between 0.5 and 1 psec.

A study of the temperature dependence of $\tau_{2,0}$ suggests that reorientation of the symmetry axis is governed by small step diffusion. However, we arrive at the result only at the expense of ignoring the fact that the estimated ratio of $\tau_{2,0}/\tau_{1,0}$ from Raman/infrared differs greatly from the value of $\frac{1}{3}$ necessary for rotational diffusion. The temperature dependence of the relaxation times for rotation about the symmetry axis, on the other hand, is quite small. Several authors (Griffiths, 1973; Steele, 1976) have suggested, therefore, that motion about this axis is governed by inertial effects and almost free. However, we must be skeptical of such hypotheses

based on the interpretation of experimental results with such large associated uncertainties.

No satisfactory overall viewpoint is obtained from these studies concerning the molecular dynamics. The calculated correlation times are certainly disparate and must be regarded as subject to revision until methods are available for estimating the nonrotational spectral intensities which are clearly contributing, to measurements made on the liquid system.

6.3.2 Acetonitrile

In acetonitrile light scattering and nuclear magnetic ^{14}N relaxation probe the tumbling motion of the C_3 axis. In this instance Keyes and Kivelson (1972) have shown that

$$\tau_{LS} = g_{00}^{(2)}\tau_S \qquad (6.3.2.1)$$

where τ_S is the single-particle orientational time and $g_{00}^{(2)}$ is the second-rank structure factor. Like the Kirkwood $g_{00}^{(1)}$ factor (Chapter 3), $g_{00}^{(2)}$ contains information concerning the orientational order in liquids. The value $g_{00}^{(2)} = 0.8$ for benzene, for example, indicates that there is preferred relative orientation in the range between 54° (the well-known "magic angle" of a magnetic relaxation) and 126°. The small deviation of $g_{00}^{(2)}$ from unity does not imply

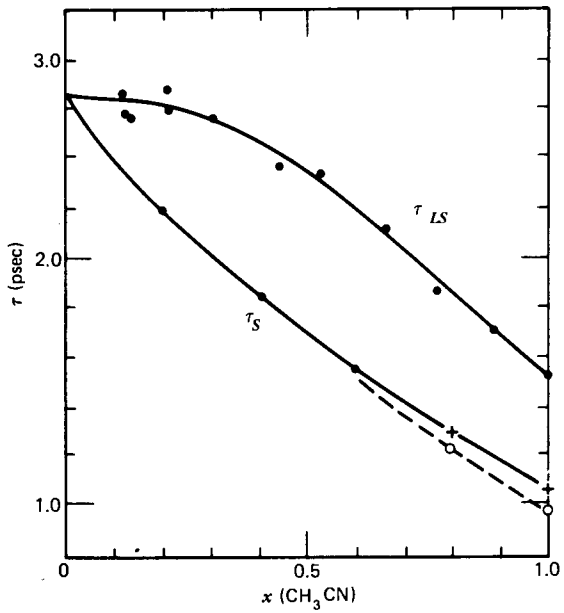

Figure 6.3.2.1 τ_{LS} and τ_S calculated from depolarized Rayleigh scattering and ^{14}N nuclear magnetic relaxation studies in mixture of CH_3CN with CCl_4 at 25°C. [Reproduced by permission from H. Versmold.]

that there is almost no orientational order, but indicates that the most probable relative arrangement is close to the magic angle.

CH_3CN is of particular interest because there exists significant evidence indicating a strongly oriented structure of the pure liquid (on the local level at least). If we study τ_{LS} and τ_S in a solution of acetonitrile in a solvent which shows weak depolarized scattering and further does not form complexes with acetonitrile, τ_{LS} and τ_S should become equal at infinite dilution, when pair correlations are negligible. Figure 6.3.2.1 gives τ_S, obtained from magnetic relaxation, and τ_{LS} in solutions of CH_3CN in CCl_4 as a function of the mole fraction at 25°C. The full circles represent low frequency light scattering, the crosses show ^{14}N results, and the open circles are obtained by normalizing the viscosity of the solutes to the limiting values of τ_{LS} and τ_S. At high concentration there is a moderate deviation between this relative viscosity and the magnetic relaxation results. From Eq. 6.3.2.1 the ratio τ_{LS}/τ_S gives the factor $g_{00}^{(2)}$, shown in Fig. 6.3.2.2. At lower concentrations pair correlations vanish, $g_{00}^{(2)} = 1$. On the other hand, in pure acetonitrile $g_{00}^{(2)}$ reaches a value of 1.4.

Figure 6.3.2.3 shows the temperature dependence of τ_{LS} and τ_S. The activation energy for τ_{LS} was found to be $E_A = 1.92$ kcal/mole; the activation energy for the ^{14}N results is reported to be $E_A = 1.7$ kcal/mole; that is, $g_{00}^{(2)}$ increases slightly with decreasing temperature.

What do we learn from these static correlation functions? Figure 6.3.2.4 shows a plot of $P_1(\cos\theta) = \cos\theta$ and $P_2(\cos\theta) = \frac{1}{2}(3\cos^2\theta - 1)$ in the angular range between 0 and 180°. The value of $g_{00}^{(2)} = 1.4$ at 25°C indicates that a more parallel or antiparallel configuration is favored (since $g_{00}^{(2)}$ is symmetrical with respect to 90° it is impossible to distinguish between the two cases). Further information comes from the ordinary $g_{00}^{(1)}$ factor, which

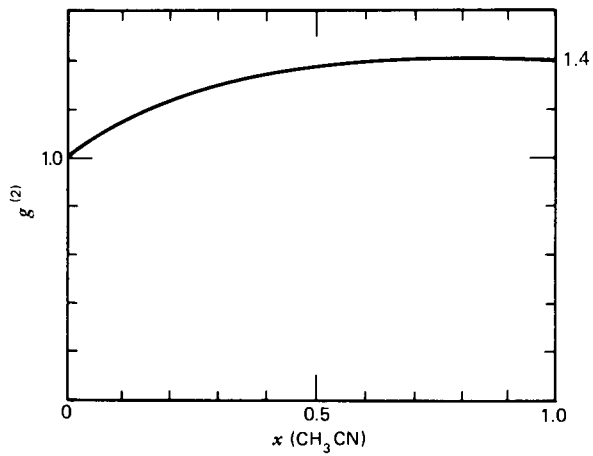

Figure 6.3.2.2 Second-rank Kirkwood g factors for mixtures of CH_3CN in CCl_4 at 295°K. [Reproduced by permission from H. Versmold.]

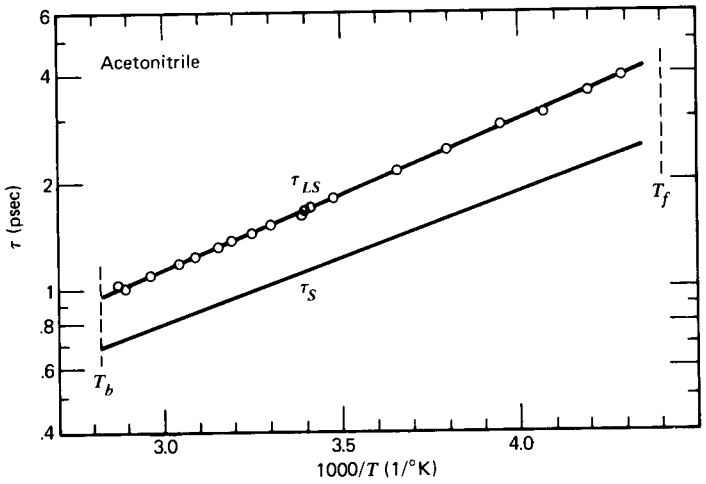

Figure 6.3.2.3 Temperature dependence of τ_{LS} and τ_S. [Reproduced by permission from T. T. Bopp, *J. Chem. Phys.* **47**, 3621 (1967).]

for acetonitrile at room temperature equals 0.78. This negative deviation of $g_{00}^{(1)}$ from unity shows according to Fig. 6.3.2.4 that antiparallel alignment is the most likely structure. The fact that $g_{00}^{(2)}$ deviates more from unity than $g_{00}^{(1)}$ can be understood if pair ordering extends to neighbors that do not belong to the first shell of reference particles. These second neighbors are oriented parallel to the reference particle and therefore contribute with positive sign to both $g_{00}^{(1)}$ and $g_{00}^{(2)}$. In this way the negative deviation of $g_{00}^{(1)}$ from unity is diminished whereas $g_{00}^{(2)}$ is further increased.

This is consistent with diffraction results. Indeed, thermodynamic (Put-

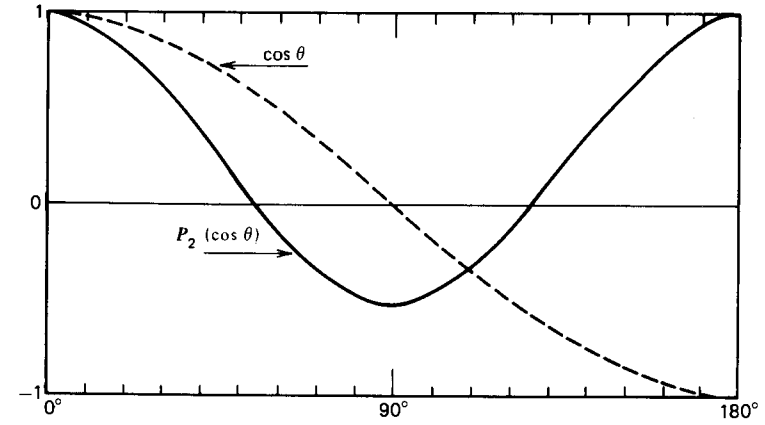

Figure 6.3.2.4 The first and second Legendre polynomials $P_n(\cos\theta)$ for $0° \leq \theta \leq 180°$.

nam et al., 1965), dielectric (Krishnaji and Mansingh, 1964), spectroscopic (Lippert et al., 1972), X-ray and neutron diffraction experiments reflect a strongly oriented structure of the pure liquid CH_3CN. In a neutron scattering experiment a double differential scattering cross section $d^2\sigma/d\Omega\, dE$ is measured. It represents the number of neutrons scattered per unit solid angle and unit energy interval. In a diffraction experiment, the scattered neutrons are collected for each scattering angle θ but no energy analysis is performed. The relevant experimental quantity is then the diffraction cross section,

$$\left(\frac{d\sigma}{d\Omega}\right)_\theta = \int_{-\infty}^{\theta_0} \frac{d^2\sigma}{d\Omega\, dE}\bigg|_{\text{constant }\theta} \tag{6.3.2.2}$$

which may be split into coherent and incoherent contributions. The coherent term is further split into a self-term and a distinct term. The probability of finding a nucleus β at a separation r from a nucleus α is called the atomic pair correlation function $g_{\alpha\beta}(r)$. This is related to the coherent distinct differential cross section in the following manner:

$$\left(\frac{d\sigma}{d\Omega}\right)_{\text{coh}}^{\text{dis}} = \frac{4\pi\rho}{\kappa} \sum_{\substack{\alpha,\beta=1 \\ \alpha\neq\beta}}^{m} \langle b_\alpha\rangle\langle b_\beta\rangle \int_0^\infty [g_{\alpha\beta}(\gamma) - 1] \sin(\kappa r) r\, dr \tag{6.3.2.3}$$

where $\kappa = 4\pi \sin\theta/\lambda$ is the length of scattering vector in the case of elastic scattering, $\rho = N/V$, the molecular number density of the liquid, and b_α, b_β are scattering lengths of the respective nuclei. By Fourier transformation we obtain a weighted sum of pair correlation functions:

$$D(r) = 4\pi\rho r^2 = \sum_{\substack{\alpha,\beta=1 \\ \alpha\neq\beta}}^{m} \langle b_\alpha\rangle\langle b_\beta\rangle g_{\alpha\beta}(r)$$

$$= 4\pi\rho r^2 \left[\sum_{\alpha=1}^{m} \langle b_\alpha\rangle\right]^2 + \frac{2r}{\pi}\int_0^\infty \left(\frac{d\sigma}{d\Omega}\right)_{\text{coh}}^{\text{dis}} \sin(\kappa r)\kappa\, d\kappa \tag{6.3.2.4}$$

where $(d\sigma/d\Omega)_{\text{coh}}^{\text{dis}}$ is the differential cross section after elimination of forward scattering.

In order to obtain information about the pair correlation functions the maximum number of diffraction experiments must be carried out. Neutron experiments on different isotopes of the substance must be investigated together with X-ray diffraction analysis. The latter experiment is the same as that employed in X-ray crystallography. However, the intensity distribution, $I(\theta)$, where θ is the scattering angle, differs from the diffraction pattern in crystals in that no sharp reflections obeying Bragg's law are observed because no long range order is present. Instead $I(\theta)$ is composed essentially of one broad peak with perhaps some inflections in the direction of increasing scattering angle.

The theoretical relations required for the evaluation of X-ray diffraction data are similar to those for neutron diffraction. However, since the

scattering centers for X-rays are electrons instead of nuclei, the nuclear scattering length b is replaced by an atomic scattering length $f(\kappa)$ which depends on the scattering vector κ because of the comparable size of atoms and the radiation wavelength.

In molecular liquids it is more appropriate to interpret the coherent differential cross section in terms of molecular pair correlations. The molecular pair distribution function can be written as a series expansion in the complete set of orthogonal polynomials in the orientation variables, the coefficients of such a series being a function of the intermolecular distance only. The coherent distinct differential cross section contains contributions from intra- and intermolecular terms. The latter, for a molecule of C_{3v} symmetry (acetonitrile) may be written as (Bertagnoli et al., 1978):

$$\left(\frac{d\sigma}{d\Omega}\right)_{\text{inter}} = a_0^{(0)}a_0^{(0)*}h_{00}^{(000)} + 0.385a_0^{(1)}a_0^{(0)*}h_{000}^{(101)} + 0.179a_0^{(2)}a_0^{(0)*}h_{000}^{(202)} \quad (6.3.2.5)$$

where $a_0^{(l)}$ are molecular scattering factors that can be calculated from the atomic scattering lengths and the atomic positions within the molecule, $h_{m_i m_j}^{(l_i l_j l)}$ is the Fourier–Bessel transform of the coefficients of the molecular pair correlation, and the termination $l_i = l_j = 2$ is made. This is acceptable because of the experimental limitation that the intermolecular coherent cross section is unobtainable at small intermolecular distances or large κ (for $|\kappa| > 3.5$ Å^{-1}). Higher terms in the expansion which correspond to sharper angle-dependent correlations are important only at those smaller intermolecular distances. The first three terms only are considered because for X-rays as well as neutron scattering they dominate the series expansion. The coefficients $h_{00}^{(000)}$, $h_{00}^{(101)}$, and $h_{00}^{(202)}$ are determined by carrying out three experiments and thereby solving three simultaneous equations. X-ray data are available for CH_3CN and neutron diffraction data for CD_3, $C^{14}N$, and $CD_3C^{15}N$. These data allow us to calculate the following three coefficients of the molecular pair correlation function:

1. $g_{00}^{(000)}$, the center–center correlation terms. For acetonitrile these are related to two fluctuations at 4.7 Å corresponding to a first nearest neighbor peak and a second at 8.5 Å corresponding to a second neighbor peak.
2. $g_{00}^{(101)}$ and $g_{00}^{(202)}$ orientational correlation terms, which give information concerning the orientation of a molecule relative to the center–center system irrespective of the orientation of the partner molecules. For $0 \leq \gamma \leq 90°$, $g_{00}^{(101)}$ is negative, and for $90° \leq \gamma \leq 180°$, $g_{00}^{(101)}$ is positive. Also, for $0 \leq \gamma \leq 54.7°$ and $125.3° \leq \beta \leq 180°$, $g_{00}^{(202)}$ is positive, but for $54.7° \leq \gamma \leq 125.3°$ it is negative. Thus, below 4.4 Å preferred orientations of the dipole axis relative to the center–center line are found in the range $90° \leq \beta \leq 125.3°$, whereas from about 5.2 Å preferred orientations $0° \leq \beta \leq 54.7°$ dominate. A second reversal is observed at 6.8 Å which restores the initial situation.

The more interesting dipole–dipole terms $g_{00}^{(110)}$, which give information about the relative orientation of two dipoles, are indeterminable for this liquid system because only three sets of diffraction data are available. However, $g_{00}^{(110)}$ is calculable in a system such as chloroform, where four diffraction experiments are possible. They are X-ray data for $CH^{35}Cl_3$ and neutron diffraction data for $CH^{35}Cl_3$, $CD^{35}Cl_3$, and $CD^{37}Cl_3$. Four expansion coefficients of the molecular pair correlation function are extractable. The symmetry is again C_{3v} so that Eq. 6.3.2.5 is still valid except that the first four terms are now retained:

$$\left(\frac{d\sigma}{d\Omega}\right)_{\text{inter}} = a^{(0)}a^{(0)}h_{00}^{(000)} + 0.385a_0^{(1)}a_0^{(0)}h_{00}^{(101)} + 0.179a_0^{(2)}a_0^{(0)}h_{00}^{(202)} - 0.064a_0^{(1)}a_0^{(1)}h_{00}^{(110)} \cdots \quad (6.3.2.6)$$

$g_{00}^{(000)}$ shows a peak at 4.8 Å with an area corresponding to six nearest neighbors. Above 4Å $g_{00}^{(101)}$ is negative and $g_{00}^{(202)}$ is positive. Consequently stronger parallel alignment of the molecular C_3 axis along the center–center line must be present ($0° \leq \beta \leq 54.7°$). If the z-axis of the system is chosen to coincide with the C_3 axis of one chloroform molecule and to be the angle between this axis and either the line joining the centers of the two molecules or the C_3 axis of a second molecule, then it can be shown that (a) for $\beta < 90°$ (parallel alignment of the C_3 axis) a negative $g_{00}^{(110)}$ results; and (b) for $\beta > 90°$ (antiparallel alignment) a positive $g_{00}^{(110)}$ results. Thus Fig. 6.3.2.5 shows how parallel and antiparallel alignment changes from one coordinate sphere to another.

In dielectric and light scattering experiments the correlation parameters $g_{00}^{(l)}$ (where $l = 1$ and $l = 2$, respectively) occur. These are related to the dipole–dipole coefficient $g_{00}^{(l10)}$ of the molecular pair correlation function by

$$g_{00}^{(l)} - 1 = (-1)^l(2l+1)^{-3/2}\rho \int_0^\infty g_{00}^{(l10)} 4\pi R^2 \, dR = (-1)^l(2l+1)^{-3/2}h_{00}^{(l10)} \qquad (\kappa = 0) \quad (6.3.2.7)$$

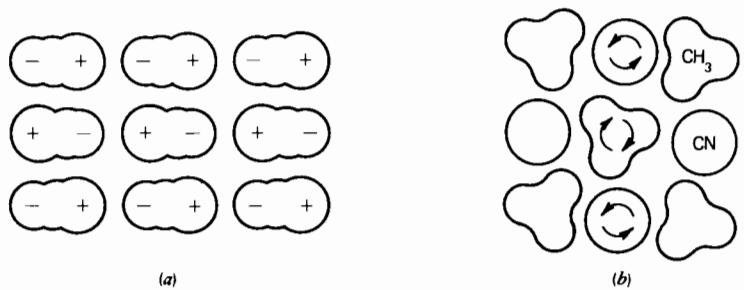

Figure 6.3.2.5 (a) Axial and antiparallel orientation of the molecular dipoles of acetonitrile—libration perpendicular to the axis. (b) Antiparallel orientation—free rotation around the axis.

whence for chloroform for $l = 1$, $g_{00}^{(1)} = 0.05 \pm 0.4$ from diffraction results. An estimation of $g_{00}^{(1)}$ from the Kirkwood–Fröhlich theory (Chapter 3) yields $g_{00}^{(1)} = 1.33 \pm 0.07$. However, it seems certain from neutron and X-ray diffraction data that $h_{00}^{(110)}$ must be larger than 0 at low κ values so that $g_{00}^{(1)}$ must lie below one. A discrepancy is present which Bertragnoli suggests is a consequence of incorrect estimates of the dielectric constants or dipole moments in the fluid state. However, we should bear in mind that there are also considerable uncertainties associated with the diffraction study. There is a fundamental limitation to the information that can be obtained from a diffraction experiment on a liquid. This is because diffraction data represent a one-dimensional quantity which is the *average* of a number of quantities. In general these vary with the three dimensions of the system, with the relative orientations within the system and with time. The diffraction experiment cannot give the full angular dependence of the structure function, the function depending on six variables, namely, one distance between the molecules, two angles to point the direction of the second molecule, and three Euler angles that determine the orientation of the second molecule relative to the first. A one-dimensional experiment cannot map a six-dimensional function. The situation is similar to the analysis of a powder crystal pattern in which one sees an angular average of all different configurations.

In addition to this intrinsic limitation there are numerous sources of systematic error in the intricate process of going from the experimentally observed function to the distribution function describing the liquid structure. Diffraction data of high accuracy are necessary. It is now generally believed that the overall precision of $\sim 1\%$, which is obtainable with present-day instrumentation, is barely adequate. Data prior to 1960 (when systematic errors of 10% and more were the rule rather than the exception) are of little use in obtaining information about the molecular distribution functions.

For this reason another approach to analyze the diffraction results has been used. Here diffraction functions are simulated using modeling techniques and compared with the experimental diffraction results. As in all modeling procedures the approach is not without criticism. However, if used with care it may prove successful, as a study by Kratochwill et al. (1973) on methyl cyanide has shown.

Their X-ray analysis revealed a short range structure given by a bundle of five molecules in which a central molecule is surrounded by four antiparallel neighbors. Between these five molecules a pronounced correlation is observed, $D = 4.4$ Å. Cluster diameters amount to $D \triangleq 11$ Å. Each cluster has eight molecules occupying sites in an orthorhombic unit cell with 95% site occupancy. This is in good agreement with a cluster diameter $D = 13$ Å estimated using a theory of Losche (1952) based on dipolar interactions in liquids.

This information on the short range structure is invaluable to the molecular dynamicist attempting computer simulations of the time evolution of the molecular motions. It also aids our understanding of the interrelation of micro- and macroscopic properties of the liquid state (discussed in Chapter 3) and, in instances where coefficients of the molecular pair correlation function are estimable, provides an additional test for the consistency of measurements from various experimental techniques through a comparison of the correlation parameters.

There is a need to use such data in conjunction with other experimental results. However, until a concerted effort is made to study one liquid system carefully, using all the experimental techniques available, under the same thermodynamic conditions, spectroscopists are confined to the tedious task of sifting out as many of the details of the complex molecular dynamics as are available from their solitary experiment. A popular approach is to use results to evaluate models of the fluid state. In particular, 0–THz spectroscopy has proved to be most discriminating in this respect.

Dilute solutions of CH_3CN in various solvents have been used to test the various analytical models available for the rotational motions of a symmetrical top molecule. Results for CH_3CN in CCl_4 are available over a mole fraction range 0.018–0.37 at temperatures between 252 and 343°K. Some typical power absorption spectra are shown in Fig. 6.3.2.6 and refractive index data in Figs. 6.3.2.7 and 6.3.2.8, where a comparison of the $\mathfrak{A}(\bar{\nu})$ and $\epsilon''(\bar{\nu})$ curves at two concentrations and 318°K are also displayed. Comparison with models are restricted to the lower concentration data in order to avoid the problem of the internal field and to eliminate cross-correlation effects. All models are fitted in such a way that the microwave dielectric loss curve is reproduced accurately, that is, at long times where the orientational anticorrelation function decays exponentially, as described in Chapter 4.

The models we consider have already been described in general terms as truncations of the Mori expansion of the Liouville equation of motion and listed in the order in which they succeed in defining the potential energy of the total hamiltonian of the system (Chapter 2). When using these models we avoid, if possible, and certainly limit, the use of adjustable parameters to produce the absorption contours for comparison with experiment. It is the intention here to explain how we have attempted this and to describe the observations and inferences that can be made.

For ease of reference we again write down the basic equation, the Mori relation

$$\dot{\mathbf{A}}(t) = i\hat{\Omega}_A \mathbf{A}(t) - \int_0^t \bar{\phi}_A(t-\tau)\mathbf{A}(\tau) + \mathbf{F}_A(t)\, d\tau \qquad (6.3.2.8)$$

The first approximation produces the Langevin equation for the angular Brownian motion of an asymmetric top, our model *I*. This includes inertia unlike Perrin's equations. It corresponds to the solution of Eq. 6.3.2.8 using a friction tensor with delta function elements in time and a small resonance

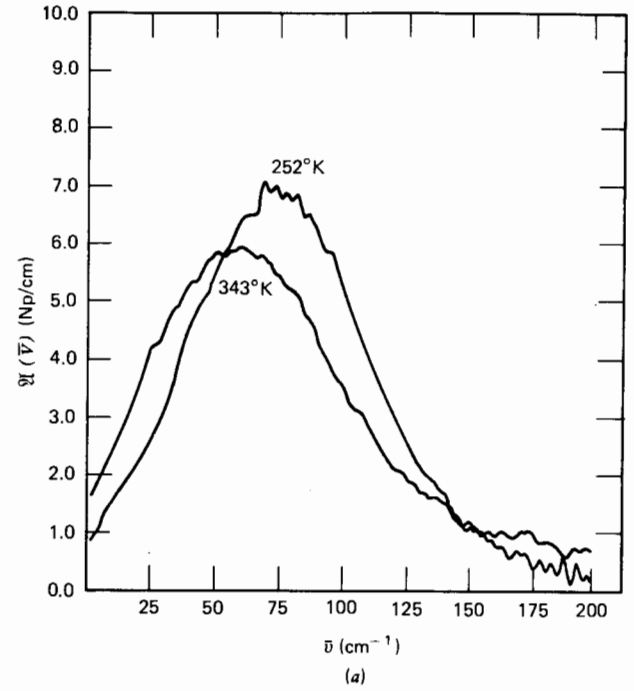

Figure 6.3.2.6 (*a*) Comparison of observed data for a mole fraction of 0.02 for CH_3CN in CCl_4 at two temperatures. (*b*) Comparison of observed data for CH_3CN in an isotropic phase (CCl_4) (1) and a mesomeric phase (cholesteryl oleyl carbonate, COC) (2) at comparable concentration and the same temperature.

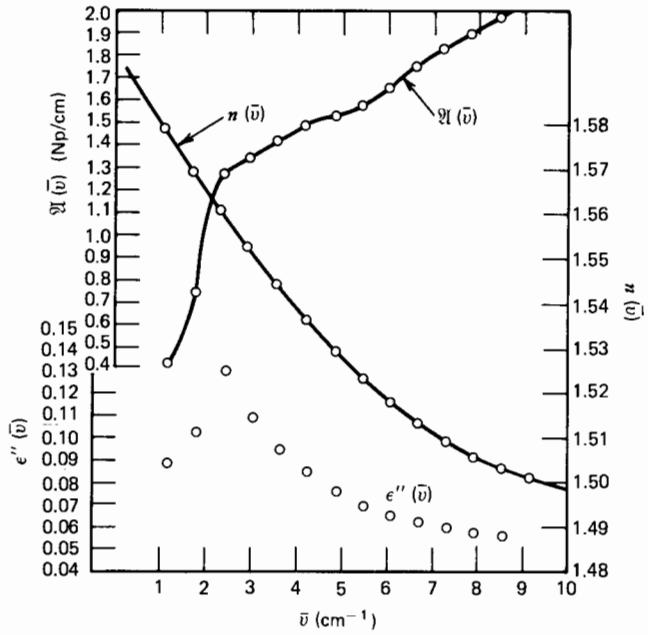

Figure 6.3.2.7 Low frequency observed $\mathfrak{A}(\bar{\nu})$, $n(\bar{\nu})$, and $\epsilon''(\bar{\nu})$ data for a mole fraction of 0.02 for CH_3CN in CCl_4 at 318°K.

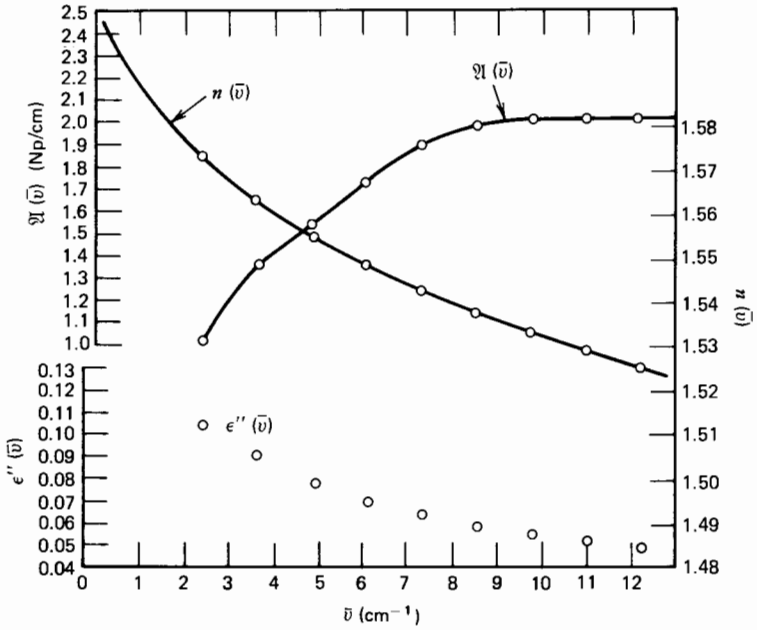

Figure 6.3.2.8 Low frequency observed $\mathfrak{A}(\bar{\nu})$, $n(\bar{\nu})$, and $\epsilon''(\bar{\nu})$ data for a mole fraction of 0.06 for CH_3CN in CCl_4 at 318°K.

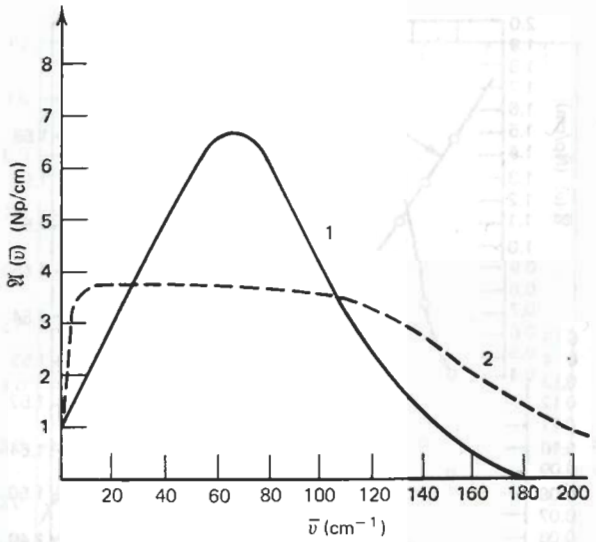

Figure 6.3.2.9 A comparison of the delta function memory of model I with experimental data. 1, Experimental; 2, curve predicted using model I.

operator $\hat{\Omega}_J$. The solutions involve the friction coefficients β_x, β_y and β_z along the inertial principal axes, x, y, and z. These may be estimated using the ellipsoidal shape factor analysis of Budó et al. (1938). There are no parameters adjusted to best fit to the observed spectrum other than these, which are fixed by observation of the loss frequency maximum. Thereby it is possible to calculate the far infrared spectra that deviate considerably from the observed experimental curve, Fig. 6.3.2.9.

The solution of Eq. 6.3.2.8 for the spherical top with the assumption that the memory kernel obeys an equation of the form

$$\phi_t = \phi_{FR}(0)\exp(-t/\tau_\omega)$$

where τ_ω is the characteristic time of the dynamical system and $\phi_{FR}(0)$ is the memory kernel for a gaussian ensemble of noninteracting rotors, gives a resulting spectrum analytically identical with that from the Gordon J diffusion model, and the Chandler collision operator theory, where binary events only are considered (model II). Then one parameter τ_ω is adjustable for best fit or may be roughly estimated from kinetic theory. The result is shown in Fig. 6.3.2.10 where it is compared with the observed spectrum at the lowest concentration. The theoretical curve peaks at the position predicted by the average rotational energy and makes no allowance for torques which shift the far infrared spectrum to higher frequency.

Next consider Eq. 6.3.2.8 where A contains one element $\mathbf{u}$, the dipole unit vector, corresponds to the orientational Mori series (model III). The resonance frequency operator $\hat{\Omega}_u$ is null and $\hat{\phi}_u(t-\tau)$ is an orientational

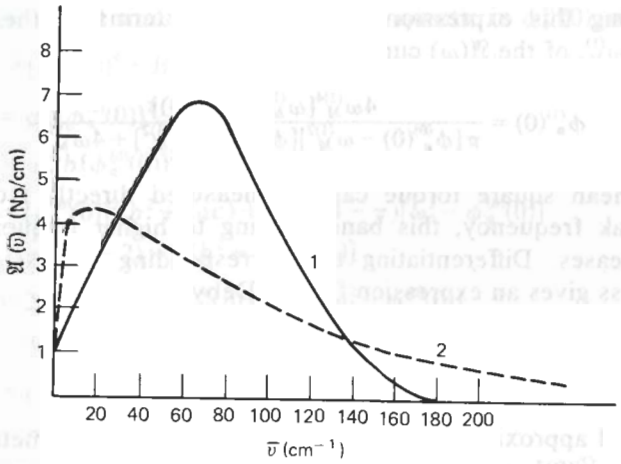

Figure 6.3.2.10 A comparison of the binary collision (J-diffusion) model with experimental data. 1, Experimental; 2, curve calculated using model II.

memory function. The vector $\mathbf{u}$ is embedded in the asymmetric top reorienting in space. If we truncate the series expansion at various levels the formalisms represent rigorous and tractable approximations to the equation of motion of $\mathbf{u}$:

$$\dot{\mathbf{u}} = i\tilde{\mathcal{L}}\mathbf{u}(t)$$

This is recovered by taking the orientational continued fraction to infinity, convergence being discussed by Tokuyama and Mori (1976). We consider the second and third order approximations using the truncating functions

$$\phi_u^{(1)}(t) = \phi_u^{(1)}(0)e^{-\gamma_1 t}$$

and

$$\phi_u^{(2)}(t) = \phi_u^{(2)}(0)e^{-\gamma_2 t} \qquad \text{respectively.}$$

The first corresponds to a Gaussian memory function $\phi_u(t)$ and implies the following relation between γ_1 and $\phi_u^{(1)}(0)$

$$\gamma_1 = \left[\frac{\pi}{2}\phi_u^{(1)}(0)\right]^{1/2}$$

The remaining parameter $\phi_u^{(1)}(0)$ may be estimated by differentiating the model absorption coefficient with respect to ω_1 whereupon $\phi_u^{(1)}(0)$ can be obtained from the measured peak frequency of the far infrared $\omega_M^{(1)}$. The analytical expression for the power absorption coefficient of the two-variable approximant is approximately, from Chapter 3,

$$\mathfrak{A}(\omega) = \frac{A\omega^2\phi_u^{(0)}(0)\phi_u^{(1)}(0)\gamma_1}{\gamma_1^2[\phi_u^{(0)}(0)-\omega^2]^2 + \omega^2\{\omega^2 - [\phi_u^{(0)}(0)+\phi_u^{(1)}(0)]\}^2} \qquad (6.3.2.9)$$

Differentiating this expression gives $\phi_u^{(1)}(0)$ in terms of the maximum frequency, $\omega_M^{(1)}$, of the $\mathfrak{A}(\omega)$ curve, namely,

$$\phi_u^{(1)}(0) = \frac{4\omega_M^{(1)4}[\omega_M^{(1)2} - \phi_u^{(0)}(0)]}{\pi[\phi_u^{(0)}(0) - \omega_M^{(1)2}][\phi_u^{(0)}(0) + \omega_M^{(1)2}] + 4\omega_M^{(1)4}} \qquad (6.3.2.10)$$

Thus the mean square torque can be measured directly from the far infrared peak frequency, this band shifting to higher frequency as the torque increases. Differentiating the corresponding expression for the dielectric loss gives an expression for the Debye time

$$\tau_D = \frac{I_B}{2kT}\left(\frac{2\phi_u^{(1)}(0)}{\pi}\right)^{1/2}$$

The second approximation contains three adjustable parameters $[\phi_u^{(0)}(0)$, $\phi_u^{(1)}(0)$, and $\phi_u^{(2)}(0)]$, which may be estimated using a fitting procedure or again calculated from the maxima of the dielectric loss and power absorption curves. $\phi_u^{(0)}(0)$ is now proportional to the orientational second moment ($2kT/I_B$ for a symmetrical top molecule), $\phi_u^{(1)}(0)$ to the mean square torque $\langle 0(V)^2\rangle$, and $\phi_u^{(2)}(0)$ to the torque and its mean square derivative. The loss is given by

$$\epsilon''(\omega) = \frac{(\epsilon_s - \epsilon_\infty)\omega\phi_u^{(0)}(0)\phi_u^{(1)}(0)\phi_u^{(2)}(0)[\pi\phi_u^{(2)}(0)/2]^{1/2}}{D} \qquad (6.3.2.11)$$

where

$$D = \frac{\pi}{2}\phi_u^{(2)}(0)\omega^2\{\omega^2 - [\phi_u^{(0)}(0) + \phi_u^{(2)}(0)]\}^2$$

$$+ \{\omega^4 - \omega^2[\phi_u^{(0)} + \phi_u^{(1)}(0) + \phi_u^{(2)}(0)] + \phi_u^{(2)}(0)\phi_u^{(2)}(0)\}^2$$

and

$$\mathfrak{A}(\omega) = \frac{\omega\epsilon''(\omega)}{n(\omega)c} \qquad (6.3.2.12)$$

In the region where $\mathfrak{A}(\omega)$ reaches a maximum, the refractive index $n(\omega)$ is constant to within a few percent so that differentiation of the equations above yields the expression

$$\phi_u^{(2)}(0) = \frac{\pi}{2}\omega_0^2\frac{[\phi_u^{(0)}(0) + \phi_u^{(1)}(0)]^2 - 2\omega_0^2\phi_u^{(0)}(0)[\phi_u^{(0)}(0) + \phi_u^{(1)}(0)]}{\phi_u^{(0)}(0)[\phi_u^{(0)}(0) + 2\omega_0^2]}$$

and

$$[\phi_u^{(2)}(0)]^2\{([\phi_u^{(0)}(0)]^2 - \omega_1^4) + \omega_1^4\}\phi_u^{(0)}(0)[\omega_1^2(4-\pi) + \phi_u^{(0)}(0)(\pi - 4)$$
$$+ \phi_u^{(1)}(0)(\pi - 2)] + \{\omega_1^4 - \omega_1^2[\phi_u^{(0)}(0) + \phi_u^{(1)}(0)]\}\{\omega_1^2[\phi_u^{(0)}(0) + \phi_u^{(1)}(0) - 3\omega_1^4\} = 0$$

which, when solved simultaneously, yield a quartic in $\phi_u^{(1)}(0)$, namely,

$$A[\phi_u^{(1)}(0)]^4 + B[\phi_u^{(1)}(0)]^3 + C[\phi_u^{(1)}(0)]^2 + D\phi_u^{(1)}(0) + E = 0$$

where
$$A = a^2\{[\phi_u^{(0)}(0)]^2 - \omega_1^4\}$$
$$B = a\{2b[\phi_u^{(0)}(0)]^2 + \omega_1^4[\pi - 2(1+b)]\}$$
$$C = [\phi_u^{(0)}(0)]^2(b^2 + 2ac) + \omega_1^4\{a(4-\pi)[\omega_1^2 - \phi_u^{(0)}(0)]$$
$$+ b(\pi - 2) - b(b^2 + 2ac + 1)\}$$
$$D = 2bc[\phi_u^{(0)}(0)^2 + \omega_1^4\{b(4-\pi)[\omega_1^2 - \phi_u^{(0)}(0)]$$
$$+ c[\pi - 2(1+b)] + 4\omega_1^2 - 2\phi_u^{(0)}(0)\}$$
$$E = c^2[\phi_u^{(0)}(0)]^2 + \omega_1^4\{(4-\pi)[\omega_1^2 - \phi_u^{(0)}(0)]c - c^2$$
$$- \{3\omega_1^4 - 4\omega_1^2\phi_u^{(0)}(0) + [\phi_u^{(0)}(0)]^2\}$$

and

$$a = \frac{\omega_0^2\pi}{2\phi_u^{(0)}(0)[\phi_u^{(0)}(0) + 2\omega_0^2]}$$

$$b = \frac{(\pi - 2)\omega_0^2}{\phi_u^{(0)}(0) + 2\omega_0^2}$$

$$c = \frac{\phi_u^{(0)}(0)\omega_0^2[(\pi/2) - 2]}{\phi_u^{(0)}(0) + 2\omega_0^2}$$

The quartic equation is solved numerically and the appropriate real root of the equation then gives $\phi_u^{(1)}(0)$ and hence $\phi_u^{(2)}(0)$.

Figure 6.3.2.11 shows a number of curves including, for the second approximant, those using the following:

1. The expression $\mathfrak{A}(\omega) = \sqrt{(2)}\epsilon'(\omega)\omega/c[(\epsilon'(\omega)^2 + \epsilon''(\omega)^2)^{1/2} + \epsilon'(\omega)]^{1/2}$ (curve 1). Here the maximum frequency is somewhat higher than that observed. $(\epsilon_s - \epsilon_\infty)$ is fixed at the experimental value.
2. The same expression but without recourse to fitting the data (curve 2). Clearly this fitting procedure is more satisfactory.
3. Experimental refractive index data and the expression $\mathfrak{A}(\omega) = \omega\epsilon''(\omega)/(cn(\omega))$. This is used as a check on the internal consistency of the model. A best fit was achieved allowing both $(\epsilon_s - \epsilon_\infty)$ and $\phi_u^{(0)}(0)$ to vary. Although this fitted curve is in general agreement with experimental data it is achieved with an unrealistic value for $(\epsilon_s - \epsilon_\infty)$ of 0.55 compared with the observed value 0.21. This implies a τ_D of 0.66 psec and calculated $\epsilon''(\omega)$ curve peaking at 8 cm^{-1}. Using the observed $n(\omega)$ results, any attempts to fix $\phi_u^{(0)}(0)$ and/or $(\epsilon_s - \epsilon_\infty)$ results in unreasonably low values of γ and an extremely narrow band profile. The lack of consistency reflects either the inadequacy

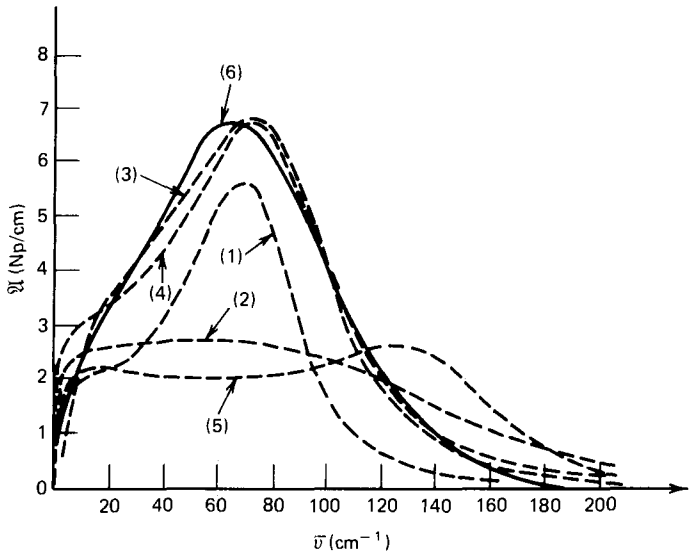

Figure 6.3.2.11 A comparison of second- and third-order Mori truncations with experiment. 1, Second-order Mori truncation, best fit with $\epsilon_0 - \epsilon_\infty = 0.21$. 2, Second-order Mori truncation without recourse to fitting (see text for details). 3, Second-order Mori truncation with $\phi_u^{(0)}(0)$ and $\epsilon_s - \epsilon_\infty$ variable (see text for details). 4, Second-order Mori truncation with $\phi_u^{(0)}(0)$ variable, $\phi_u^{(1)}(0) = 27.5$, $\gamma = 3.9$, $\epsilon_s - \epsilon_\infty = 0.33$. 5, Third-order Mori truncation. 6, Experimental.

of the model based on the second-order truncation and/or uncertainties associated with the experimental $\mathfrak{A}(\omega)$ and $n(\omega)$ results (e.g., uncertainties associated with the persistence of cross correlation).

4. A higher-order approximant was used to obtained $\phi_u^{(1)}(0)$, $\phi_u^{(2)}(0)$, and γ as outlined. Again there is significant deviation between observed and calculated data and convergence is clearly not yet attained. This is reflected in the fact that $\phi_u^{(1)}(0) = 21.0\phi_u^{(0)}(0)$ for the first approximant and $\phi_u^{(1)}(0) = 43.2\phi_u^{(0)}(0)$ for the second approximant.

We make a brief comment concerning the forms of the truncating functions used. A simple exponential implies a correlation function containing odd powers of time, whereas theoretically it should be devoid of them (an even time expansion). To remedy this we considered (Evans, 1977) the following truncations which produce even time expansions:

$$\phi_u^{(1)}(t) = \phi_u^{(1)}(0)\exp(-\gamma_2^2 t^2) \tag{6.3.2.13}$$

$$\phi_u^{(1)}(t) = \frac{\phi_u^{(1)}(0)}{1+\gamma_3^2 t^2} \tag{6.3.2.14}$$

$$\phi_u^{(1)}(t) = \frac{\phi_u^{(1)}(0)}{1-(1+\gamma_4^2 t^2)^{1/2}} \tag{6.3.2.15}$$

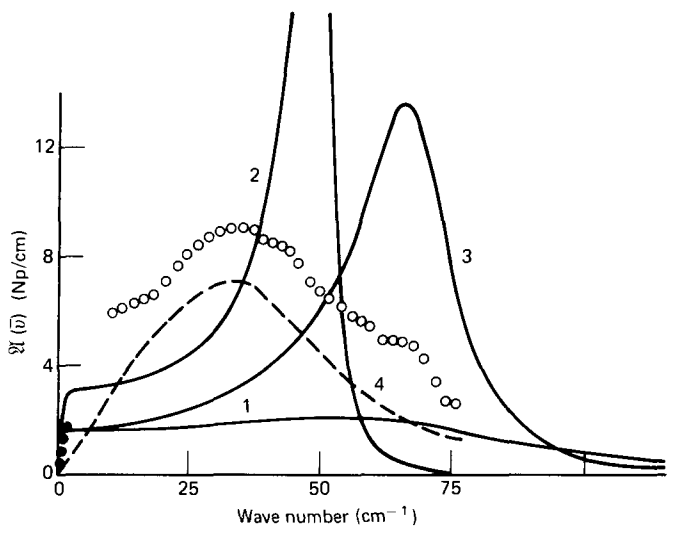

Figure 6.3.2.12 Theoretical fitting of even time Lorentzian and Gaussian functions to the experimental data for iodobenzene. ● Poley's low frequency data for iodobenzene (*J. Appl. Sci. B*, **4**, 337 (1955)]; ○ polarizing interferometer results. 1, Exponential truncating function; 2, Gaussian truncating function; 3, Lorentzian truncating function; 4, experimental data with curve 1 subtracted—an estimation of the induced absorption contribution.

The resulting expressions were compared with the experimental results for a series of liquids. The Gaussian and Lorentzian functions (Eqs. 6.3.2.13 and 6.3.2.14 respectively) are particularly unrealistic, producing curves much too sharp in comparison with experiment (Fig. 6.3.2.12). It may be considered a paradox that a simple exponential, at least for methyl fluoride, is more realistic than the even time function produced by Eq. 6.3.2.15 (Fig. 6.3.2.13). This spectrum provides a particularly severe test for any model of the fluid state because a pair of absorption processes are clearly resolved in the liquid at 133°K. Usually these two processes are superimposed, forming one continuous profile. The simple exponential truncation of the Mori series is the only one tested to date that reproduces the two absorption processes to any acceptable degree of precision.

Lastly we consider the model of planar oscillation (Chapter 4) (model IV). The dynamic system evolves according to Eq. 6.3.2.8. I_1 and I_2 are the moments of inertia of the annulus and inner ring, respectively. As we have already seen the simple planar itinerant oscillator model with β_1 set at 0 corresponds exactly with the Mori type approximant to the dipole angular velocity a.c.f. function (in model III the orientational a.c.f. is considered). The Mori type approximant is to the equation of motion of $\boldsymbol{\omega}$, namely,

$$\dot{\boldsymbol{\omega}} = i\hat{\mathscr{L}}\boldsymbol{\omega}(t)$$

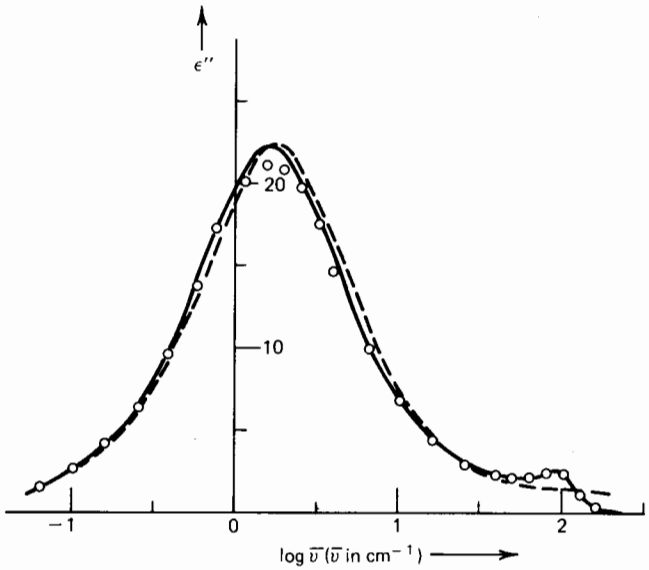

Figure 6.3.2.13 Theoretical fitting to the whole of the microwave and far infrared region for CH_3F. ○ Experimental data at 133°K (note the resolution of low and high frequency peaks at this temperature. At room temperature these coalesce, forming one broad continuum). Solid line, the theoretical curve that coincides throughout the whole of the frequency range (exponential first-order truncation of Mori series; see text). Dashed line, the theoretical curve using a Lorentzian truncating function (note the failure of this truncation at far infrared frequencies):

$$\phi_u^{(1)}(t) = \phi_u^{(1)}(0)\exp[1-(1+\gamma_2^2 t^2)^{1/2}]$$

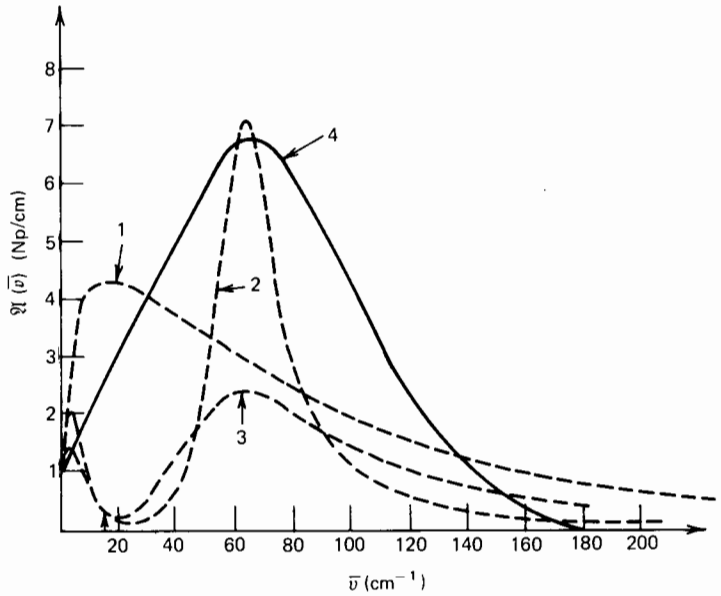

Figure 6.3.2.14 Comparison of experimental and theoretical results for CH_3CN in CCl_4 (0.02 mole fraction at 318°K). Solid line, observed data. 1, Symmetrical top itinerant oscillator model with $I_1 = 10I_2$, $\beta_2 = 5$ THz. 2, Symmetrical top itinerant oscillator model with $I_1 = 10I_2$, $\beta_2 = 15$ THz. 3, Binary collision model for comparison with $\beta_1 = 20$ THz. (Note that this zero-order Mori truncation is unable to shift the frequency of maximum absorption to observed experimental frequencies. The itinerant oscillator model, on the other hand, produces two distinct peaks corresponding to the low and high frequency absorptions but is unable to produce one continuous profile matching the experimental observation.)

It might be anticipated to be a better approximation because the mean intermolecular potential is better defined.

Figure 6.3.2.14 shows the result of using the planar oscillator model with $I_1 > I_2$. It produces a far infrared spectral distribution which is too narrow (see also Chapter 4) even for large values of the molecular annulus friction parameter β_2.

From the foregoing it is clear that none of the models satisfactorily describe the experimental data. It is important in every experiment to bear in mind the uncertainties associated with the measured data and the ability of the data to reflect the short time details of the molecular rotation. The far infrared is both sensitive and discriminating and demonstrates well the most obvious deficiencies of the models. It is true that infrared and Raman spectra in principle contain the same information. However, in practice, the bands must be carefully chosen to avoid the numerous features that may complicate the spectra, and it is rarely possible to achieve high enough signal-to-noise ratios in the high frequency region. Likewise, since the far wings of the depolarized Rayleigh scattering measure approximately the factor $\epsilon''(\omega)/\omega$, the short time details are concealed and resolved only with the most careful intensity control.

The models we use should be restricted to those that successfully describe the short time details of the motion. The rotational diffusion model used to calculate NMR correlation times is unacceptable because it obscures these features, giving artificial experimental correlation times.

The intercomparison of results from different experiments for this molecule proves inconsistent. In his review of the data available, Griffiths (1973) concludes that the best values for the $l = 1$ and $l = 2$ correlation times $\tau_{1R}(\perp)$ and $\tau_{2R}(\perp)$ are 3.3 and 1.1 psec, respectively, at 298°K, which (conveniently) is exactly the ratio expected for rotational diffusion. There is evidence, however (Chapter 12), that both these values may be incorrect. The τ_{1R} value is obtained from microwave data on the liquid and includes the effects of cross correlations but still has a large uncertainty associated with it. Data on τ_{2R} obtained from more recent measurements on ν_2 and ν_3 modes of CH_3CN suggest a value nearer 1.4 psec at 298°K. This lack of agreement may be a consequence of the strongly oriented local structure of

the liquid acetonitrile and the fact that all the models used are of purely orientational origin. In such a strongly oriented liquid structure it is difficult to conceive of a molecular rotation without a simultaneous translation so that the pronounced effects rotation/translation interaction must also be explained.

6.3.3 Dichloromethane

Lastly we consider dichloromethane (see also Chapters 4 and 12). Its molecular structure is depicted in Fig. 6.3.3.1. Mechanically it is nearly a prolate symmetrical top with C_{2v} point group symmetry. Hence, there are infrared active vibrations with transition moment vectors parallel to any one of the axes of inertia. By evaluating the band shapes of different vibrational modes one is, in principle, able to discern whether or not the

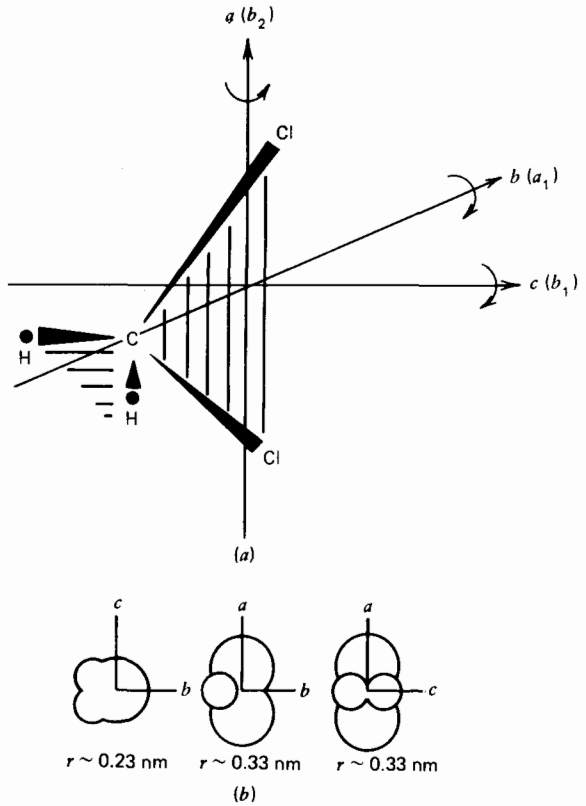

Figure 6.3.3.1 (*a*) The structure of CH_2Cl_2 where *a*, *b*, and *c* are the axes of inertia and b_2, a_1, and b_1 are the symmetry species (point group C_{2v}) parallel to the same. Moments of inertia are $I_a \sim 26 \times 10^{-47}\,\mathrm{kg\,m^2}$; $I_b \sim I_c \sim 260 \times 10^{-47}\,\mathrm{kg\,m^2}$. (*b*) Shape and effective radii of CH_2Cl_2. [Reproduced by permission from P. N. Brier, *Adv. Mol. Rel. Inter. Proc.* **13**, 1 (1978).]

rotational motion reflects the asymmetry of the moments of inertia and also the nature of the diffusion (Debye type or not). In choosing a set of axes for a molecule of arbitrary geometry, the principal axes of the rotational diffusion tensor are not necessarily related to those of the inertia tensor. However, the C_{2v} symmetry of CH_2Cl_2 ensures that these directions coincide. It is therefore a particularly favorable molecule for study. In addition, it has a predominantly incoherent scattering cross-section due to the presence of the (equivalent) hydrogen atoms and there are no low frequency vibrational modes to give vibrational inelastic features in a low energy neutron scattering experiment or to seriously distort the 0–THz absorption band shapes.

Either inertial or molecular shape considerations would predict symmetrical top behavior but the complex nature of the intermolecular interactions including the effects of the dipole moment along the **b**-axis may invalidate such simple arguments (Chapter 4). However, infrared evidence suggests that the angular motion may be axially symmetrical so that dynamic models valid for symmetrical tops may be evaluated with the data. This is significant since, as we saw in Chapter 2, only a few models are available for the asymmetric top where the mathematics often become intractable.

In the infrared experiment the correlation functions of the rotational motion of the transition moment vector are studied. Since it is always parallel to only one of the inertial axis of the molecules the rotational motion of each axis may be studied by choosing an appropriate vibrational band. Figure 6.3.3.2 shows the motions of inertial axes *a*, *b*, and *c*, respectively. It is seen that the correlation functions decay more slowly for motion occurring around the larger axis of inertia. In addition the decay at short times is not exponential, indicating that a non-Debye type diffusion process is occurring. Agreement using various different vibrational modes is displayed in Fig. 6.3.3.3. The effective angles of "free rotation" are estimated by comparison with the free rotor function and are of the order of 30° and 40° for motion around the **c**-, **a**- and **b**-axes, respectively. Also the rotational motion in the liquid displays about the same degree of anisotropy as the motion of freely rotating molecules. It appears that although dichloromethane has a strong dipole moment in a direction parallel to the inertial axis μ_b (1.6 D), the components of the forces that tend to twist this axis are not very different from those acting on axes **a** and **c**.

In comparing these results with NMR measurements care must be taken because of the anisotropy of the rotational motion. A drawback of the nuclear magnetic relaxation technique is the assumption that the rotational motions proceed through random angular steps which are short in comparison with the mean period of rotation of the free rotor. In this way the experimental reciprocal spin-lattice relaxation times of the equivalent protons of CH_2Cl_2, extrapolated to zero proton concentration, may be equated with the rotational spin-lattice relaxation time of a single CH_2Cl_2 molecule

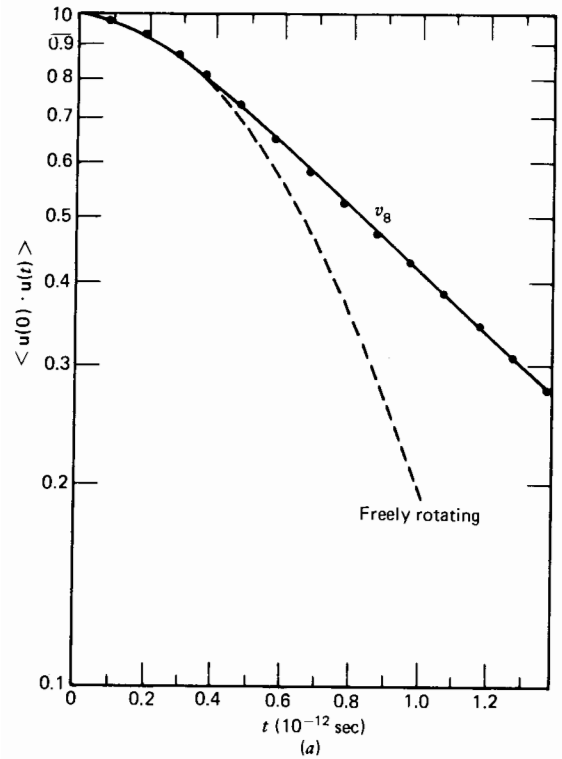

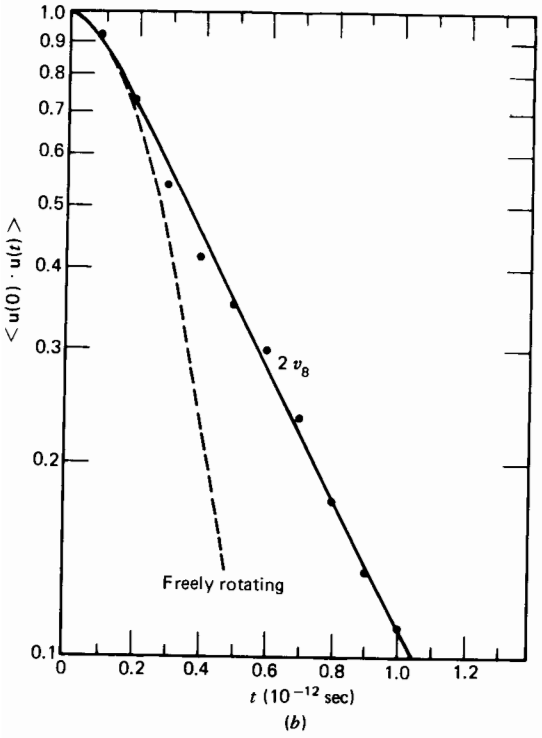

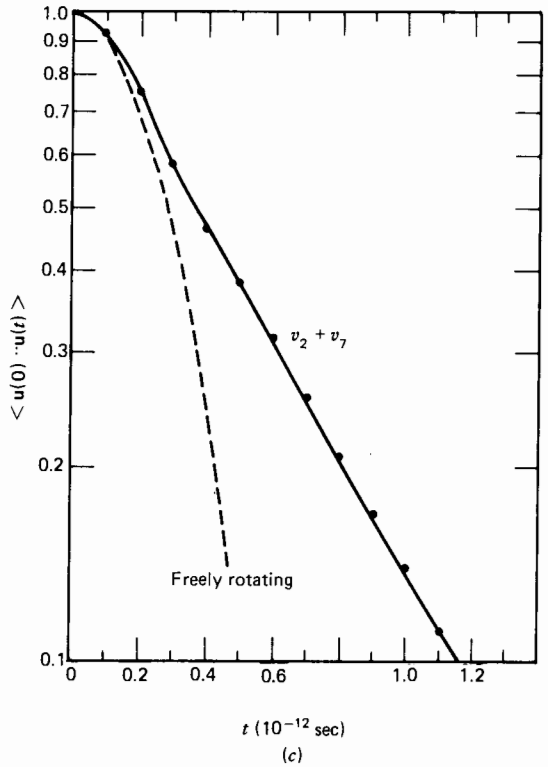

Figure 6.3.3.2 Correlation functions of the motion of inertial axes *a*, *b*, and *c*, respectively, of the freely rotating and liquid phase CH_2Cl_2 molecules. (*a*) Rotational motion of axis *a* (symmetry species b_2). (*b*) Rotational motion of axis *b* (symmetry species a_1). (*c*) Rotational motion of axis *c* (symmetry species b_1). [Reproduced by permission from W. G. Rothschild, *J. Chem. Phys.* **53**, 990, 3265 (1970).]

in the liquid using a simple expression. For CH_2Cl_2 in CD_2Cl_2 solution the relaxation time calculated in this way is estimated as $\tau_2^{(0)} \sim 0.5$ psec, where the subscript indicates the axis whose orientational motion is observed in the experiment when the molecule rotates around the other two axes. The infrared experimental gives a correlation time $\tau_{ir} = 1.1$ psec and there is now an obvious discrepancy. If indeed the rotational process is Debye-like, τ_{ir} should equal $3\tau_2^{(a)}$, which is clearly not the case. It is conceivable, of course, that if the NMR data were reevaluated in terms of a model allowing "free rotation" through relatively large angles, closer agreement would be found between the nuclear magnetic and infrared results.

Van Konynenburg and Steele (1972) calculated rotational correlation functions from both depolarized Rayleigh wing scattering and infrared absorption experiments. The appropriate infrared bands for comparison with the depolarized wing scattering are those involving parallel vibrational

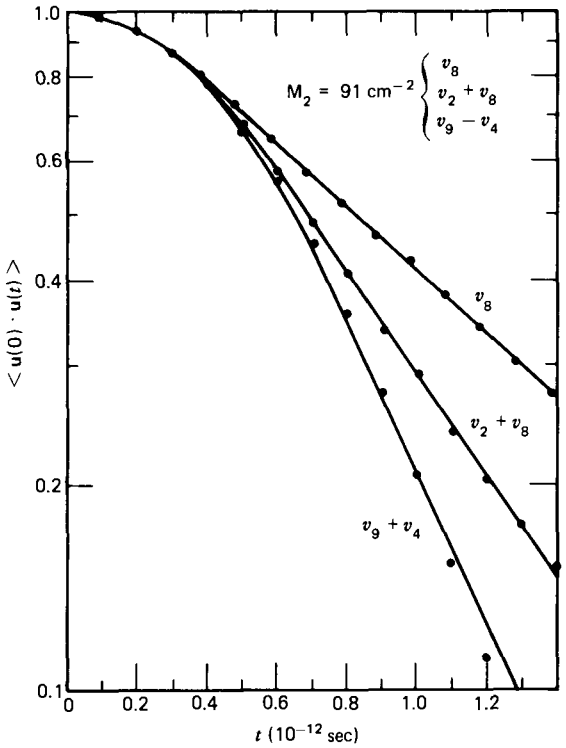

Figure 6.3.3.3 Correlation functions of the orientational motion of inertial axis a for the ν_8, $\nu_2 + \nu_8$, and $\nu_9 - \nu_4$ modes. The spread of the curves gives an indication of experimental uncertainties and the effect of contributions such as rotation/vibration coupling. Rotation about axes b and c (symmetry species b_2). M_2(theoretical) = 88 cm^{-2}. [Reproduced by permission from W. G. Rothschild, *J. Chem. Phys.* **53**, 990, 3265 (1970).]

transitions. Figure 6.3.3.4 shows the comparison of the respective correlation functions together with the free rotor correlation functions calculated using the gas phase moments of inertia. Corrections have been made for contributions from induced spectral intensity but isotopic broadening has been neglected since this appears negligible compared with the other sources of uncertainty.

In the same study van Konynenburg and Steele reported depolarized Rayleigh scattering results for chloroform. These we can compare with the results of Bucaro and Litovitz (1971) (Fig. 6.3.3.5), where the spectra show considerable deviation even though their general shapes are quite similar. In this instance perfect agreement exists between depolarized Rayleigh relaxation times and those calculated from the NMR experiment, a result that is more probably fortuitous than meaningful when we consider that, in general, agreement between correlation times is extremely difficult to find.

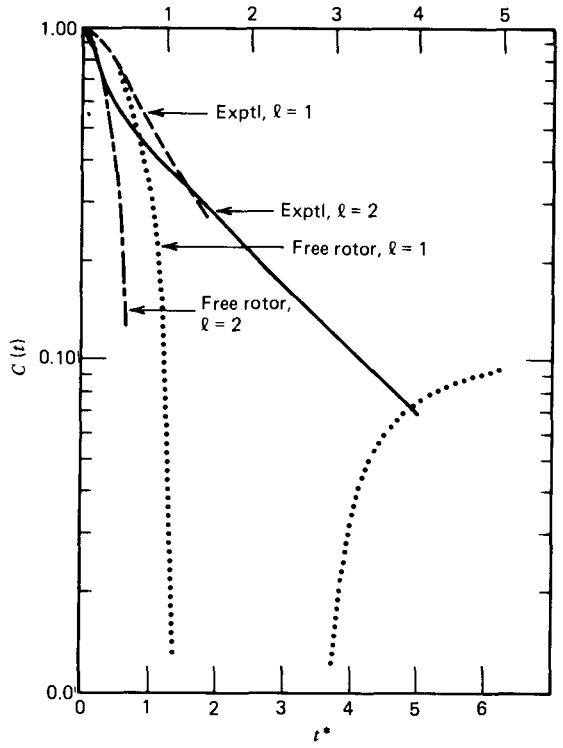

Figure 6.3.3.4 Rotational correlation functions for CH_2Cl_2 from depolarized Rayleigh wing scattering and infrared absorption experiments. Free rotor curves are shown for comparison. [Reproduced by permission from P. van Konynenburg and W. A. Steele, *J. Chem. Phys.* **56**, 4776 (1972).]

Results for CH_2Cl_2 considered below emphasize this point. Part of the reason for the discrepancy lies in the fact that correlation times from the NMR experiment, as already emphasized, are model dependent. In addition we should remember that all correlation times are integrals over a correlation function. It is conceivable that such a summation process is weighted in a manner that "flattens out" important aspects of the rotational motion.

The vibrational relaxation contribution may be estimated from measurements of the isotopic (polarized) component of the corresponding Raman band. This is for totally symmetrical A_1 vibrations. In CH_2Cl_2 no additional information is available from the Raman experiment because the low symmetry of the molecule implies that the Raman band shapes are not related to the reorientational motion of the molecular axes in any simple manner. The corresponding correlation functions describe some combination of the reorientational motions about the three different molecular axes. It is certain that vibrational relaxation contributions to the infrared

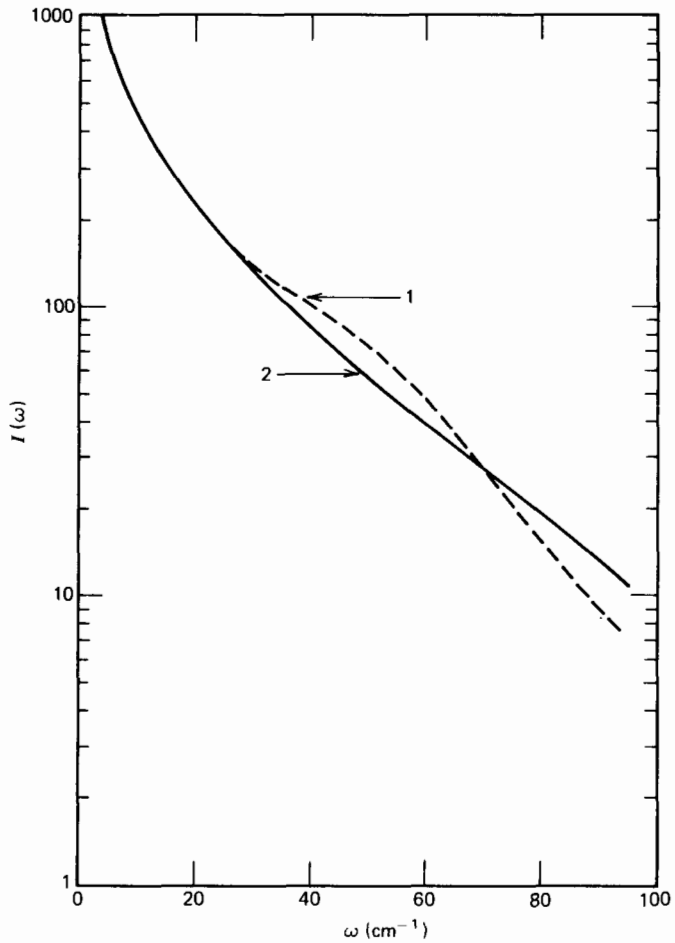

Figure 6.3.3.5 A comparison of the results for chloroform of Bucaro and Litovitz (1) and van Konynenburg and Steele (2), where the intensity scales have been adjusted to give equality at $\omega = 10\,cm^{-1}$. The agreement is imprecise enough for the data to be used to discriminate satisfactorily between models of the liquid state. [Reproduced by permission from P. van Konynenburg and W. A. Steele, *J. Chem. Phys.* **56**, 10, 4776 (1972).]

band contours differ quite markedly from one (A_1) vibration to another. However, for some of the bands these effects are minimized by virtue of their high vibrational frequencies, their predominantly C–H motions, and their weak intensities.

Lyerla et al. (1971) have reported the NMR correlation time τ_2 for the reorientation of the C—H vector [$\tau_2(^{13}C)$]. This is calculated from the ^{13}C spin-lattice relaxation times and C—H nuclear Overhauser enhancement factors for CH_2Cl_2. The latter allows the separation of the proton ^{13}C

dipolar relaxation time from the measured ^{13}C time, giving the correlation time τ_2 for the reorientation of the C—H vector. The disappointing result is that the available NMR data do not support the theory of axial symmetry of the angular motion as implied by the infrared experiment because $\tau_2(H—H) \neq \tau_2(C—H)$.

We should bear in mind that there is significant uncertainty associated with the NMR results. Estimated errors are of the order of at least 10%, which is sufficient to ensure that results cannot easily distinguish between models of the liquid state, not even between a stochastic model for large angular steps and small step theory [unless the angular steps exceed something like 30° (Heatley, 1974)]. O'Reilly et al. (1972) attempted an interpretation of their data using a model based on rotational motion occurring during the period a molecule is excited to an "interstitial site" in the liquid "lattice" by a "hard" collision. During this time it was specifically assumed that the anisotropy of the reorientational motion was determined entirely by the inertial properties of the molecule. The model predicts a ratio for $\tau_2(^{13}C)/\tau_2(D)$ for the C—H/C—D vector in CH_2Cl_2 and CD_2Cl_2 of 0.87, which compares favorably with a value of 0.88 ± 0.14 estimated experimentally. However, within experimental error, the measured ratio also agrees with the predictions of stochastic models for which the correlation times are independent of the inertial changes produced by deuteration.

As an academic exercise, Brier and Perry (1978) considered the anisotropy implied by the NMR results of $\tau_2(H—H) = 0.53 \pm 0.06$ psec, $\tau_2(C—H) = 0.75 \pm 0.07$ psec and $\tau_2(C—Cl) = 1.2 \pm 0.1$ psec. This they did within the framework of small step rotational diffusion. No single set of values for the three adjustable parameters in the model would produce the NMR relaxation times simultaneously. The "best fit" values to the $l = 2$ NMR data predicted an anisotropy completely different to that implied by the infrared data and the $l = 1$ NMR data.

The only conclusion to be drawn is that no clear picture of the rotational dynamics, even of a semiquantitative nature, emerges from an intercomparison of "experimental" correlation times. The times are insufficiently discriminating to make a critical test of any model of the liquid state dynamics. At present this is partly a consequence of uncertainties associated with the experimental results themselves.

van Konynenburg and Steele also use the *full experimental correlation function* to evaluate three models of the fluid state. These are Debye's diffusion model, Ivanov's jump model, and Gordon's extended diffusion model. The first two fail to reproduce the observed results. Debye's model gives a correlation function which is Gaussian at small times and predicts exponentially decaying correlation functions at longer times with a slope for $l = 2$ three times that for $l = 1$.

Ivanov's model is a large step version of the diffusion model where it is assumed that molecules make occasional large reorientations about a

randomly oriented axis. The time dependence of the correlation function is entirely determined by the jump frequency β. The l dependence of the exponential decay is much smaller in the model but the observed short time Gaussian decay of the correlation functions is not reproduced. This feature is common to all jump models and is a consequence of the neglect of free rotation at times short enough to minimize the effects of collisions or unbalanced torques in the fluid.

Of the three models the Gordon diffusion model produced the best result. Here the molecules undergo a type of random walk in momentum space, rather than in coordinate space as assumed in the other two models. It allows for a long time exponential decay, with a slope relatively insensitive to l and a logarithmic extrapolation back to $t = 0$ giving an intercept different from unity, in agreement with experiment.

Neutron scattering results for CH_2Cl_2 have also been used to distinguish between different models and to assess the extent to which the measurements are sensitive to the degree of anisotropy of the angular motion. Brier and Perry (1978) considered four dynamic models including again the extended diffusion models of Gordon. In their experiment they asssumed that rotational and translational motions are decoupled. For the translational component they considered only the Egelstaff-Schofield (E-S) modification of the simple diffusion model. Though this has the correct short time behavior ($\sim t^2$), in contrast to the simple Fick's law it predicts a velocity a.c.f. which monotonically decreases to zero. This is not in accord with molecular dynamics results, which show that the correlation function has a negative overshoot.

For rotational motion Brier and Perry considered four models. The first two were empirical, allowing for axial symmetry about the a-axis. No detailed physical interpretation of the reorientational dynamics or even an estimate of the degree of anisotropy of the motion can be obtained from an empirical approach. They considered also, therefore, models based on specific physical assumptions, namely, the extended diffusion models for a symmetrical top molecule. The predictions of each of the four models in conjunction with the E-S model for the translational motion are shown in Fig. 6.3.3.6, where the experimental results are shown for comparison.

One of the empirical models gives closest agreement with experiment. The J- and M-diffusion models show considerable deviation. Changing the one adjustable parameter of the models did little to improve the situation, altering the magnitude but not the position of maximum absorption. Figure 6.3.3.7 shows that the positions of all the inelastic maxima calculated in fact deviate to some degree from experiment so that even the "correctness" of the best fit empirical model is far from satisfactory.

There are several possible explanations for the observed deviations:

1. Inadequacies of the dynamical models for both translational and rotational motions.

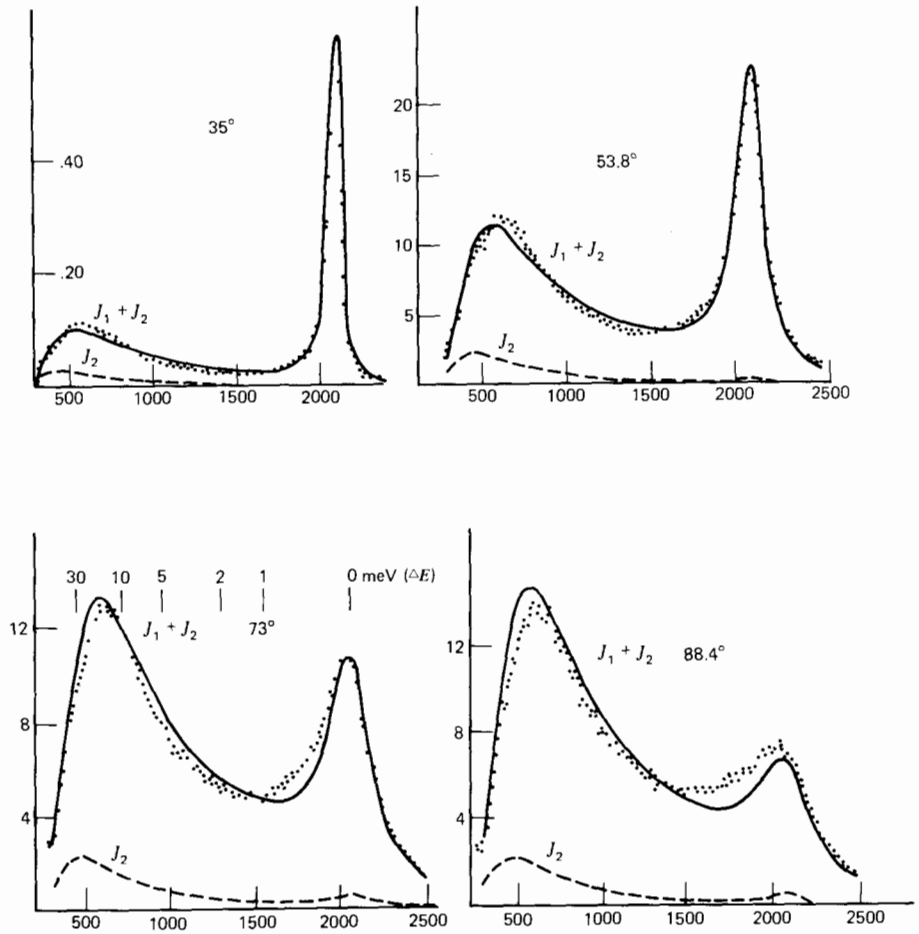

Figure 6.3.3.6 Experimental neutron scattering results for CH_2Cl_2 compared with the model (model II) which gives best agreement with experiment. Dashed lines, experimental; solid lines, model calculations. Scattering angles are (*a*) 35°, (*b*) 53.8°, (*c*) 73°, and (*d*) 88.4°. Ordinate: neutrons $s^{-1}Sr^{-1}$ (μ sec/m)$^{-1} \times 10^6$. Abscissa: time of flight (μ sec/m). [Reproduced by permission from P. N. Brier, *Adv. Mol. Rel. Inter. Proc.* **13**, 1 (1978).]

2. The anisotropy of the reorientational motion may not be axially symmetrical.
3. The experimental results may be insufficiently discriminating and/or have large associated uncertainties.

Brier and Perry considered points 2 and 3 within the context of the rotational diffusion model. They found that agreement with neutron scattering data was only slightly improved when the anisotropy was increased many times. However, this does not necessarily imply that neutron scattering measurements are insensitive to the anisotropy of the angular

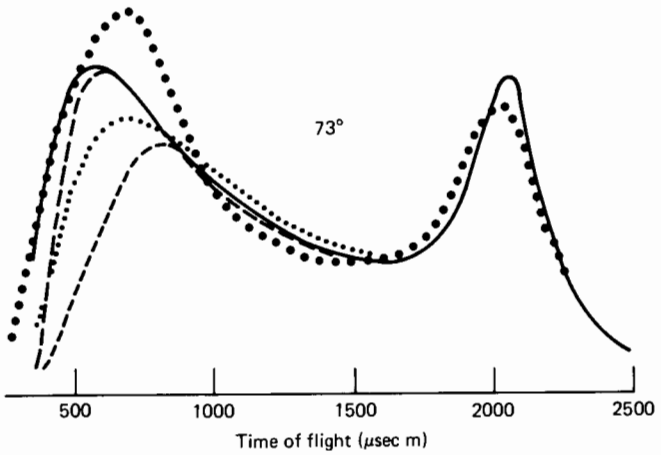

Figure 6.3.3.7 The optimum single scattering predictions of all four rotational models compared with each other and experiment at 73° scattering angle. (All curves calculated using the same translational model.) ●●●●, Experimental; ———, empirical model 1; –·–·– empirical model 2; – – – –, M-diffusion model with $T_j^*(M) = 0.16$; · · · · · ·, J-diffusion model with $T_j^*(J) = 0.16$.

motion. Rather, it may only reflect the inadequacy of the molecular model. Zero–tetrahertz results emphasize this point. Evans et al. (1978) have compared solutions of the Langevin equation for rotational Brownian motion for the asymmetric top, symmetrical top sphere, and needle with experimental results for a series of liquids. Morita in 1976 solved the Euler equations for a diffusing asymmetric top. The complex permittivity is given by (see Chapter 2)

$$\frac{\epsilon(\omega) - \epsilon_\infty}{\epsilon_s - \epsilon_\infty} = 1 - p \sum_{l=x,y,z} \left(\frac{m_i^2}{\mu^2}\right) A^{(i)}(p) \tag{6.3.3.1}$$

where $p = i\omega$ and $\mu^2 = M_x + M_y + M_z$, in which M_i is the permanent dipole moment along the principal axis denoted by i, and β_i is the corresponding frictional component. $A^{(i)}(p)$ is defined by Morita (see Chapter 2 references).

A little later McConnell et al. (1979) studied the problem. They found that the complex polarizability is given by (Chapter 2)

$$\alpha(\omega) = \frac{1}{3kT} \sum_{x,y,z} \left(\frac{D_y(D_y + D_z + \beta_y)}{(D_y + D_z + i\omega)(D_y + D_z + \beta_y + i\omega)} + \frac{D_z(D_y + D_z + \beta_z)}{(D_y + D_z + i\omega)(D_y + D_z + \beta_z + i\omega)} \right) \mu_x^2 \tag{6.3.3.2}$$

Here $D_x = kT/I_x\beta_x$, etc. The frictional couples with respect to the rotating principal axes of inertia are $I_x\beta_x\omega_x$, $I_y\beta_y\omega_y$, and $I_z\beta_z\omega_z$.

Equations 6.3.3.1 and 6.3.3.2 reduce to Perrin's equations when inertial

effects are neglected, where three "Debye times" are defined as

$$\tau_x^{-1} = D_y + D_z$$
$$\tau_y^{-1} = D_x + D_z$$
$$\tau_z^{-1} = D_x + D_y$$

The solutions of McConnell et al. and Morita are consistent with each other and reduce, in appropriate limits, to the results of McConnell et al. for the sphere with an embedded dipole. The correlation times appropriate to dielectric relaxation (τ_1) and to NMR spin–spin relaxation, the dynamic Kerr effect, depolarized Rayleigh scattering, or Raman line broadening (τ_2) are given for the spherical model in this context by

$$\tau_1 = \frac{1}{2\gamma\beta}\left[1 + \tfrac{3}{2}\gamma - \tfrac{5}{6}\gamma^2 + \cdots\right]$$

$$\tau_2 = \frac{1}{6\gamma\beta}\left[1 + \tfrac{11}{2}\gamma - \tfrac{83}{6}\gamma^2 + \cdots\right]$$

so that $\tau_1 = 3\tau_2$ if $\gamma \ll 1$. Here $\gamma = kT/I\beta^2$ and $\beta = 2kT\tau_D/I$.

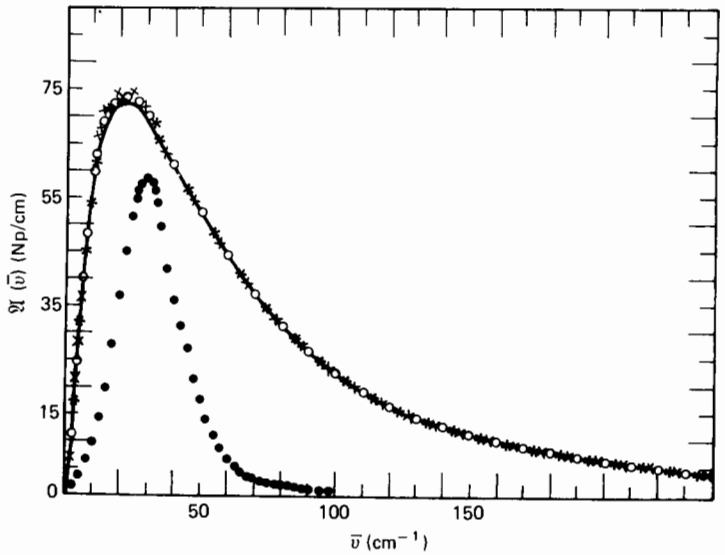

Figure 6.3.3.8 The far infrared absorption spectrum of fluoroform at 293°K which shows up clearly deficiencies of the Langevin equation for the rotary dynamics ●, Experimental [A. Gerschel, *Mol. Phys.* **31**, 209 (1976)]. ———, Morita's model for a symmetrical top, needle, and spherical top [all three coincident, as indeed is the model for the asymmetric top—see text for details and G. J. Evans and M. W. Evans, *J. Chim. Phys.* **75**, 523(5) (1978)]. * * *, McConnell's model for a needle. ○○○, McConnell's model for a spherical top. + + +, Morita's model for an asymmetric top reduced to the symmetrical top.

The point of present interest is that results for the sphere, needle, symmetrical top, and asymmetric top are all, to a high degree of proximity, coincident so that, at 0–THz frequencies, the *model* itself is insensitive to the anisotropy of the motion. In addition it produces a return to spectral transparency which is too slow compared with the observed high frequency part of the far infrared spectrum, and there is a large discrepancy in intensity (Fig. 6.3.3.8). Only additional studies on asymmetric top molecules and the development of more sophisticated molecular models to analyze the data will resolve the problem.

The sensitivity of 0–THz spectra to many of the details of the molecular dynamics is without question. This is seen in dilution studies where, for CH_2Cl_2, the far infrared spectra corrected for solvent absorption (Fig. 6.3.3.9), show a shift on dilution to lower frequency in $\bar{\nu}_{max}$, the band peak frequency (cm^{-1}). Further, this sensitivity is reflected by changes that occur during a transition from the compressed gas to the liquid. Even in the gas phase spectra for "typical" small molecules, organic fluids are broad bands resulting from the perturbation of rotational energy levels and the broadening effects of repeated collisions. No such data are presently available for CH_2Cl_2. However, results for CH_3Cl and CH_2CF_2 emphasize the spectral changes that occur. Figure 6.3.3.10 shows the spectra for CH_3Cl (g) at 5.8 bar and 4.4 bar at 296°K and for CH_3Cl/ethane mixture at a total pressure of 33.5 bar at 296°K, together with the set of $\Delta J = 1$ lines for quantum free rotation of CH_3Cl molecules. The experimental absorption bandwidths exceed that of the $J \rightarrow J + 1$ contour. This is so because the set of $J \rightarrow J + 1$ rotational lines for freely rotating CH_3Cl molecules arise from transitions occurring between the various rotational quantum states. Since rotational energy levels are clearly spaced compared with kT, molecules populate, according to the Maxwell–Boltzmann distribution, many of the lower levels, leading to a maximum in the population at some value of J other than $J = 0$. Collisional interactions cause a change of statistics from that of a Boltzmann distribution and a shift of the frequency of maximum absorption. Also, the closeness of the rotational states means that they are easily perturbed by intermolecular potentials, which are comparatively much larger. This causes the broadening of the absorption spectra observed in the compressed gas phases.

It is noticeable that $\bar{\nu}_{max}$ remains approximately constant in both CH_2CF_2 and the mixture of CH_3Cl/ethane on moving from the compressed gas to the liquid state. However, a shift in $\bar{\nu}_{max}$ of some 25 cm^{-1} occurs during the same transition in CH_3Cl. From the spectral changes alone we deduce the following:

1. Interference by neighboring molecules is more pronounced in CH_3Cl molecules in their own environment than in an ethane environment.
2. The considerable orientational freedom in an ethane environment is retained on passing from the compressed gas to the liquid phase.

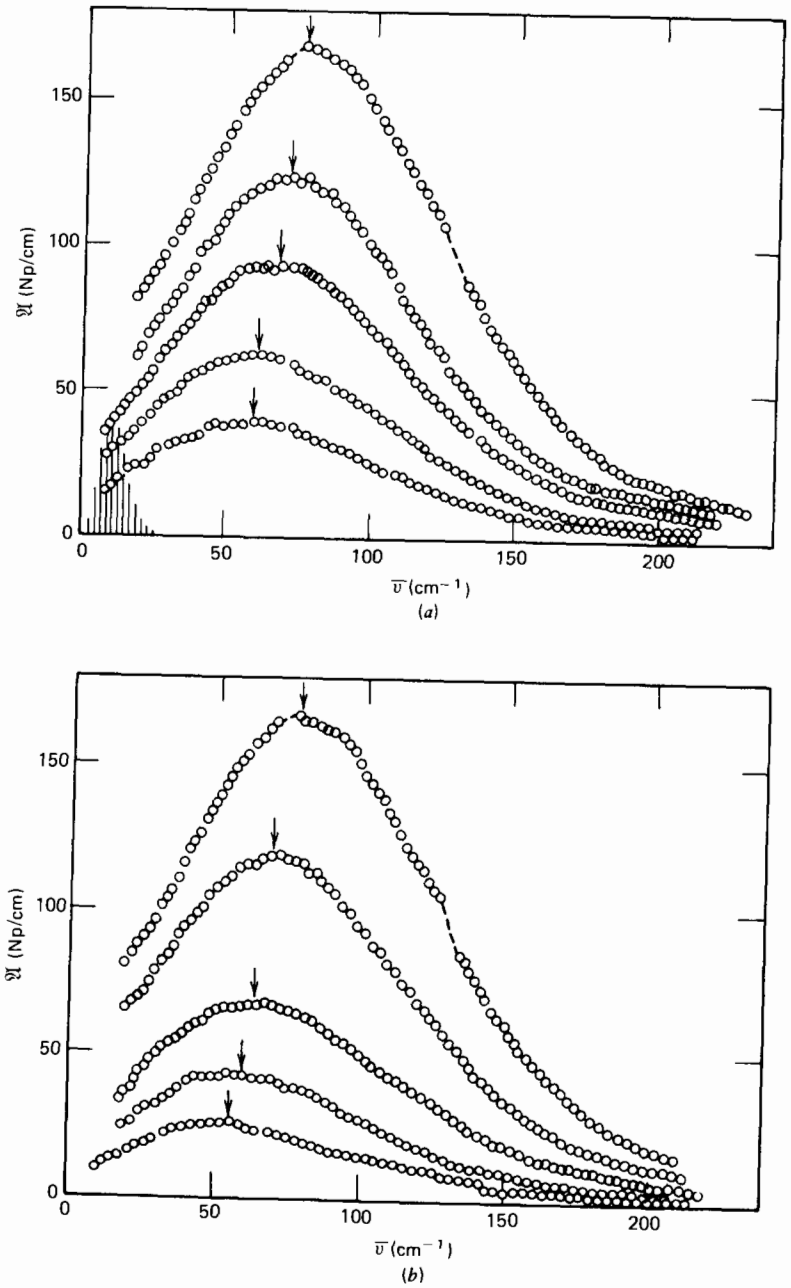

Figure 6.3.3.9 The absorption of CH_2Cl_2 showing a shift on dilution in CCl_4 and decalin. (a) From top to bottom in CCl_4: number density $N = 9.4 \times 10^{21}$ molecules CH_2Cl_2/cm^3; $N = 7.22 \times 10^{21}$ molecules CH_2Cl_2/cm^3; $N = 4.93 \times 10^{21}$ molecules CH_2Cl_2/cm^3; $N = 3.25 \times 10$ molecules CH_2Cl_2/cm^3; $N = 1.97 \times 10^{21}$ molecules CH_2Cl_2/cm^3. The stick spectrum represen some $J \rightarrow J + 1$ ($\Delta K = 0$) lines for quantized free rotation of CH_2Cl_2 (arbitrary intensity). (b) The same in decalin.

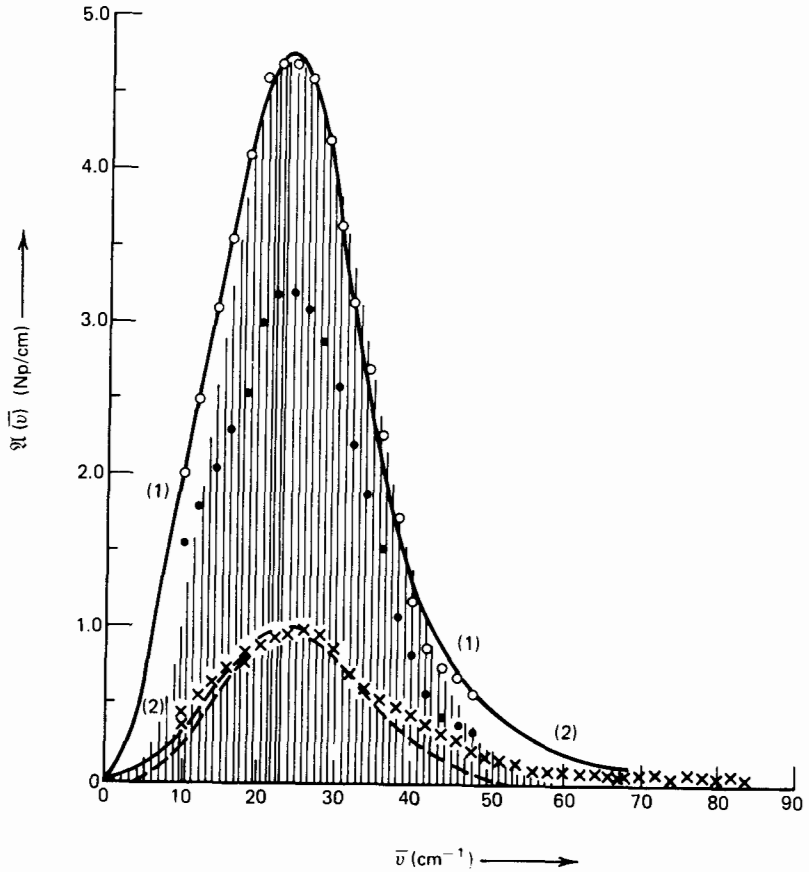

Figure 6.3.3.10 The gas phase absorption of CH_3Cl. ○ Absorption at 5.8 bar, 296°K; ● absorption at 4.4 bar, 296°K; × absorption of CH_3Cl and ethane at a total pressure of 33.5 bar, 296°K. Solid lines: 1, Mori three-variable fit to gas phase data (CH_3Cl at 5.8 bar); 2, Dashed line, Mori three-variable fit to gas phase data (CH_3Cl/ethane at 33.5 bar), contour of the $J \rightarrow J+1$ lines. Vertical lines are the set of $\Delta J = 1$ lines for quantum free rotation.

3. The rotational dynamics of liquid CH_3Cl are significantly different from those occurring in the compressed gas.
4. This is not so in CH_2CF_2, which appears to retain most of its degrees of orientational freedom on passing from the compressed gas to the liquid state.

These observations are reflected in the corresponding corrrelation functions calculated analytically using model III, Section 6.3.2. In the compressed gas state diffusive steps through large angles are indicated by negative minima in the correlation functions. These minima tell us that

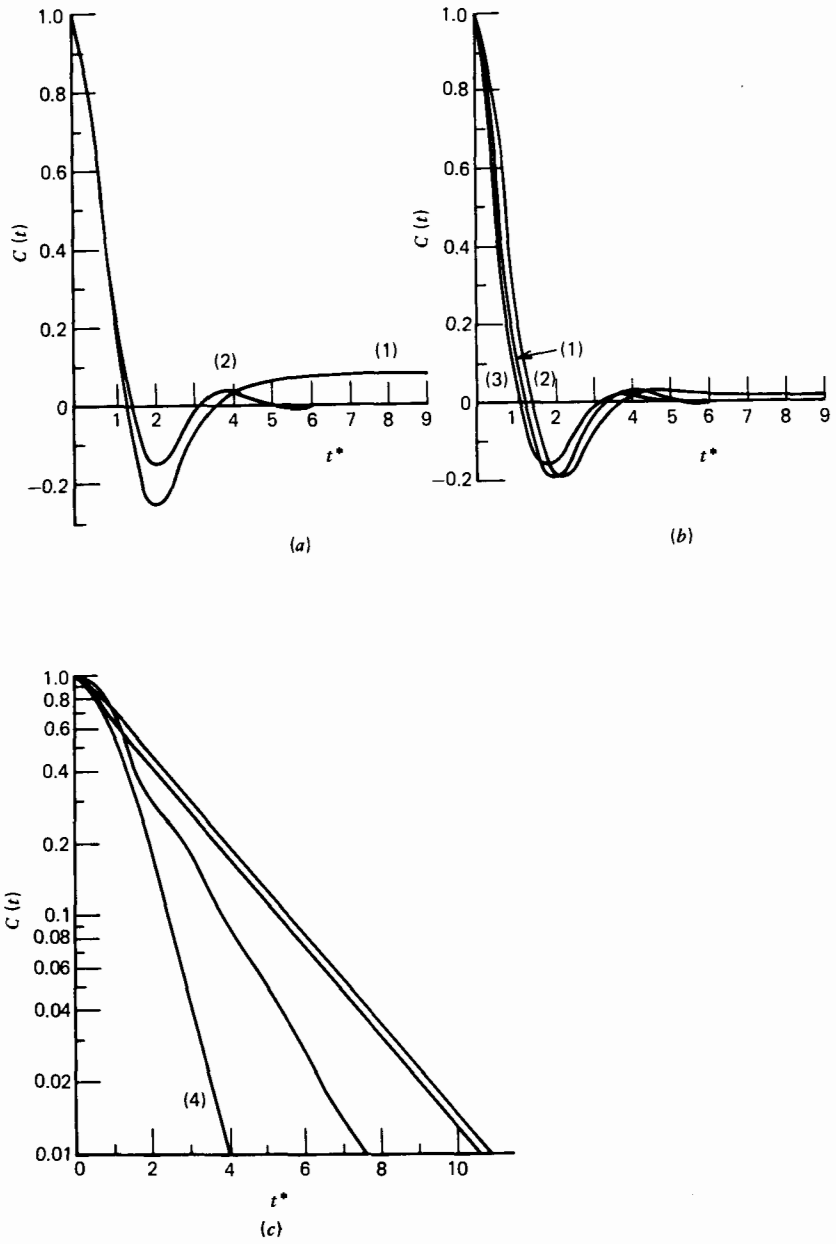

Figure 6.3.3.11 (*a*) $t^* = (kT/I_B)^{1/2}t$. 1, True free rotor orientational a.c.f. for CH_3Cl at 296°K; 2, best fit of Mori three-variable theory to the $J \rightarrow J+1$ contour (Fig. 6.3.3.10), the equivalent correlation function. (*b*) 1, $C(t)$ for CH_3Cl (*g*) at 5.8 bar, 296°K; 2, *J*-diffusion model with $T^*(kT/I_B)^{1/2} = 4$; 3, $C(t)$ for CH_3Cl/ethane at 33.5 bar, 296°K. (*c*) Logarithmic plots of the correlation functions of liquid CH_3Cl and CH_3Cl in ethane. 1, $C(t)$ for CH_3Cl (*l*) at 296°K; 2, $C(t)$ for CH_3Cl/ethane (*l*) at 296°K; 3, *J*-diffusion model with $\tau^* = 0.2$; 4, *J*-diffusion model with $\tau^* = 0.5$.

after a certain time a dipole is more likely to be found in a hemisphere opposite to that in which it started. The logarithmic plots of the correlation functions (Fig. 6.3.3.11) show oscillatory behavior, more pronounced for CH_3Cl/ethane liquid mixture but also present at smaller times ($t^* < 1$) for CH_3Cl. This short time oscillatory behavior reflects the excess or Poley absorption observed at far infrared wavelengths. Two functions derived from the J-diffusion model using various times between collisions are also shown. The model is unable to reproduce oscillations at short times because it cannot reproduce this Poley absorption and shift the frequency of maximum absorption $\bar{\nu}_{max}$ away from the free rotor maximum as experiment demands. The correlation functions, though initially oscillatory, eventually decay exponentially, a decay corresponding to the onset of a stochastic (Markov) process which is described only in terms of the higher moments of a spectrum which, unlike the invarient second moment, are highly complex equilibrium properties (Chapter 1). In dense fluids, therefore, it becomes impractical to follow the dynamics at long times because of the complexity of the molecular trajectories. Thus we understand why Debye's rotation/diffusion model, ignoring all dynamic coherence, is successful in reproducing the long time details of the molecular motion. However, an acceptable model must also reproduce the short time features. In frequency terms it must reproduce the entire 0–THz frequency spectrum. For many substances this spans many decades of frequency, 11, for example, in a disordered solid (Chapter 7) and seven or more in the organized nematic phase of a liquid crystal. These systems show better than any, how markedly environmental sensitive the orientational dynamics and 0–THz spectra are. In a cholesteric environment, for instance, strong anisotropic forces hinder the reorientation of CH_2Cl_2 solute molecules causing a significant decrease in the observed far infrared intensity (Chapter 8). $\bar{\nu}_{max}$ remains approximately constant whereas in a glassy environment large shifts to higher wavenumbers are observed (Chapter 7).

CH_2Cl_2 has also been studied dissolved in highly viscous polymer solutions. The latter showed that the macroscopic viscosity does not influence the mobility of a solute molecule, that is, local intermolecular forces do not reflect the bulk viscosity, in sharp contrast to the far infrared glass state results of Reid (Chapter 7). It might have been anticipated that the polymer (polystyrene, a prototype polymeric medium) would interact with the solute molecules by "nonspecific" intermolecular forces via the benzene rings. In fact, although the polystyrene environment causes the CH_2Cl_2 molecules to slow down, the far infrared experiment shows that the macroscopic viscosity of the solution, which varies over many *orders* of magnitude, is essentially irrelevant to the characteristics of the rotational dynamics of the halide molecule in this instance.

It is this sensitivity to details of the molecular dynamics that makes 0–THz spectra such a discriminating test for molecular models. As for

CH_3CN we use data for dichloromethane in CCl_4 to evaluate the four models considered there. Results for the inertia corrected Langevin equation (model I) have already been considered in Fig. 6.3.3.8. Curve 2 of the same figure shows the results for the extended diffusion model (model II). τ_ω has been optimized for best fit which is poor. This illustrates the most characteristic and discriminating features of the present data, the large shift to lower wavenumbers on dilution, which cannot be followed by the model. Even in model III, where the mean square torque is at least well defined, the calculated band shape with no adjustable parameters is rather too broad compared with the experimental data. Iterating on γ_1, and $\phi_u^{(1)}(0)$ (separately) improves the situation but the agreement is still not satisfactory. Using $I_1 = I_2$, $\beta_1 = \beta_2 = kT\tau_0/I_2$ in the dipole–dipole interpretation of model IV produces a poor fit and iteration on β_1, β_2 and I_1/I_2 is barely an improvement. And using the geometrical relation $I_1 = 10I_2$ for various values of β_2 in the disc-annulus context produces a resonance around ω_0 too narrow in frequency range, Fig. 6.3.3.12. Iteration on I_1 and β_2 rectifies matters though at the expense of physical realism since for a *poor* best fit $I_1 < I_2$.

Using model III we can at least estimate, to a first approximation, the mean square torque contribution to the mean potential energy. This is plotted against the molecular number density of CH_2Cl_2 in CCl_4 in Fig. 6.3.3.13. Results are also shown for fluoroform and methylfluoride, Fig. 6.3.3.14, as a function of density and temperature. The plots show that the torques typically increase with the number density and decrease with temperature, in accord with physical expectation.

All the models above are early approximants of the Mori continued fraction expansion and as such define the potential energy of the total hamiltonian using only one or two terms in the effective Taylor expansion. This situation will remain unless a realistic intermolecular potential is employed, either by direct numerical integration of the equations of motion (molecular dynamics simulation) or by taking a fundamentalist line in employing later approximants of various continued fractions. If this kind of continued fraction is to be physically meaningful (as opposed to useful) and is to acquire a predictive nature, a means of extending it to infinity without introducing more adjustable variables must be found. It has been postulated that it may be possible to extend the set of $\phi_u(0)$ further in the future with the aid of recent mathematical development in the ill-posed problem theory as a method of estimating the statistical information lost by using approximants.

A perusal of the literature has revealed that results are often disparate, confused and sometimes contradictory. It may seem that little real progress has resulted from the extensive experimental and theoretical effort expended in an attempt to elucidate the liquid dynamics. Certainly the time is right to carefully appraise our future course of study. In the words of Berne and Harp (1970), "understanding the liquid state has proven to be a challenge and an embarrassment to generations of outstanding physicists and chemists". This

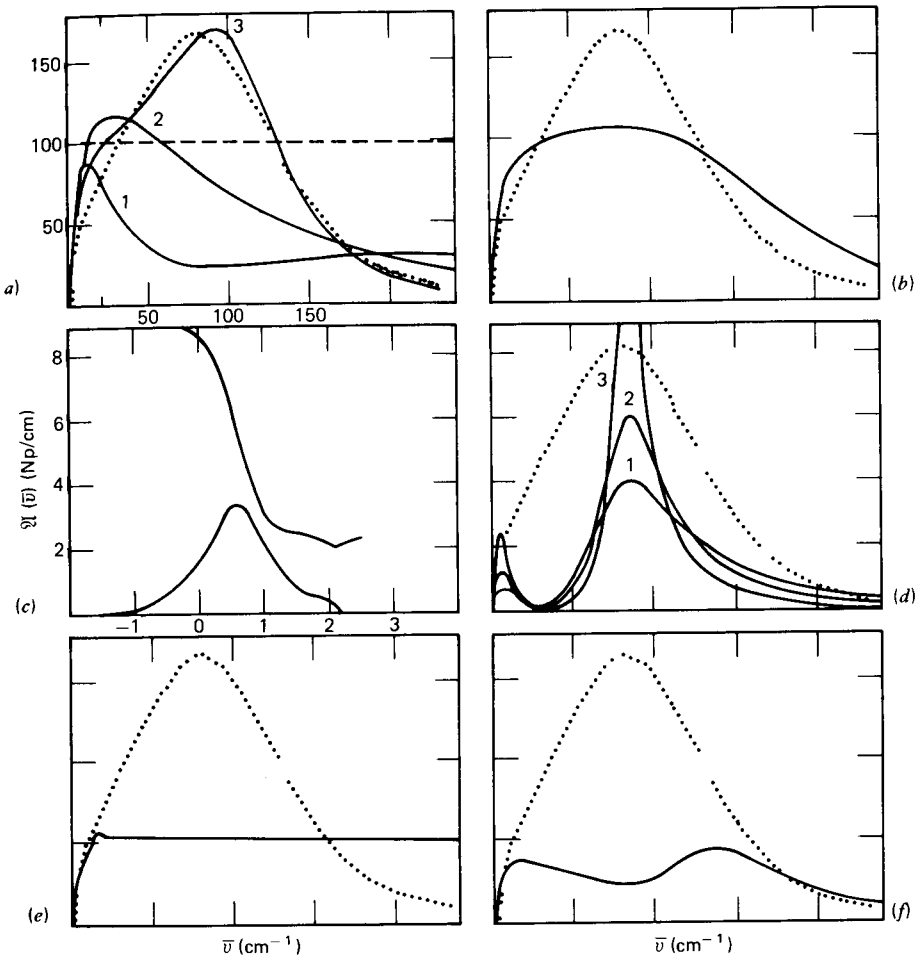

Figure 6.3.3.12 Absorption in terms of $\mathfrak{A}(\bar{\nu})$ of pure CH_2Cl_2 liquid: (*a*) Dashed line, spherical top Debye plateau. (1) Langevin equation, asymmetric top, $\beta_x = 2.0$, $\beta_y = 25.7$, $\beta_z = 2.2$ THz. Inverse of loss peak frequency = 1.45 psec. (2) *J*-Diffusion model, spherical top, best fit, with $\beta_\omega = 7.4$ in units of $[kT(1/I_x + 1/I_y)]^{1/2} = \langle\omega^2\rangle^{1/2}$. (3) Model III Mori approximant of $\mathbf{u} = i\mathcal{L}\mathbf{u}$, iterating separately on $\gamma = 4.9\langle\omega^2\rangle^{1/2}$ for best fit and $\phi_{\mathbf{u}}^{(1)}(0) = 27.8\langle\omega^2\rangle$. (*b*) As for part (*a*); the solid curve is model III with y related as in the text to $\phi_{\mathbf{u}}^{(1)}(0)$ calculated as $58\langle\omega^2\rangle$. The latter can be calculated also as $57.3\langle\omega^2\rangle$ from the loss peak frequency. Further approximants are clearly needed since the calculated curve is too broad. (*c*) Loss curve and dispersion corresponding to curve 3 of part (*a*). (*d*) As for part (*a*), showing the effect of varying β_2 in model IV for $I_1/I_2 = 10$, $\beta_1 = 1.23$ THz (calculable), $\omega_0 = 15.26$ THz (far infrared peak). (1) $\beta_2 = 10$, (2) $\beta_2 = 15$, (3) $\beta_2 = 5$ THz. (*e*) As for part (*a*), iterating on I_1 ($> I_2$ for best fit) and β_2, with β_1 of the disk/annulus interpretation fixed at 1.23 THz. The very poor result illustrates that iteration of this kind is often unhelpful since the system merely tends to rotational diffusion, giving a slow return to high frequency spectral transparency. (*f*) The dipole–dipole interpretation of model IV with $I_1 = I_2 = 4.8 \times 10^{-39}$ g cm^2 (the mean of these perpendicular to $\boldsymbol{\mu}$ of CH_2Cl_2), and with β_1 and $\beta_2 = 1.23$ THz, $\omega_0 = 15.26$ THz.

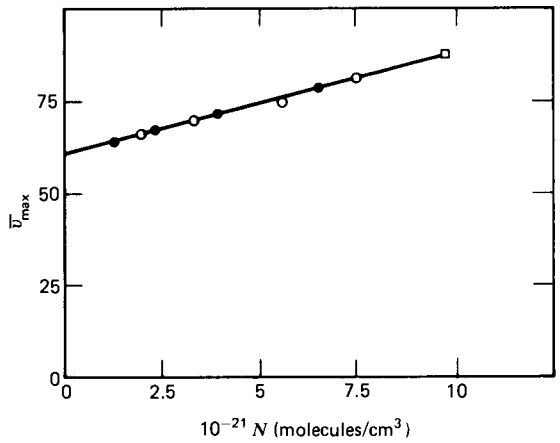

Figure 6.3.3.13 Plot of $\bar{\nu}_{max}$ against number density in CCl_4 and decalin. ○ CCl_4 solution ● decalin solution. □ (N.B. $\bar{\nu}_{max}$ is related to the mean square torque parameter in Mori three-variable theory by Eq. 6.3.2.10.)

is undoubtedly partly a consequence of the large uncertainties associated with the experimental results and the many *ad hoc* assumptions that are still made in both their treatment and subsequent analysis.

There is a clear need for a concerted effort to coordinate research into the relaxation properties of a small number of representative fluids by simultaneous use of all the experimental techniques available. Depolarized Rayleigh wing scattering and 0–THz results, for instance, complement each

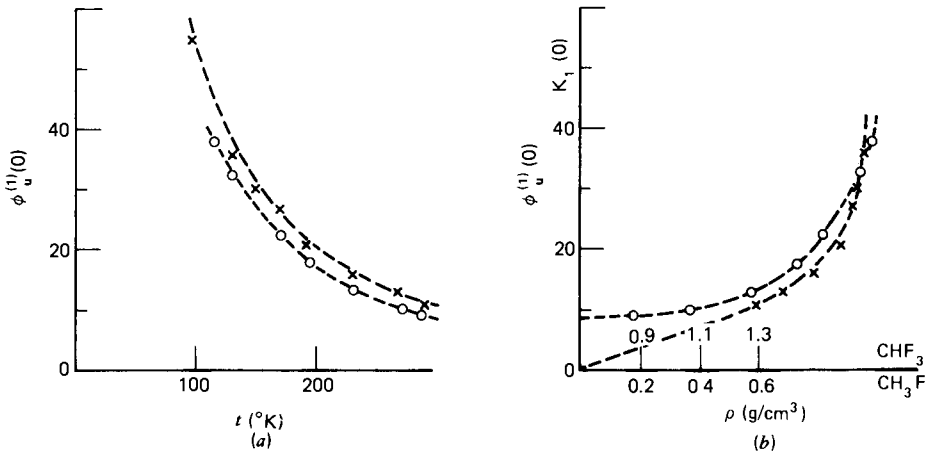

Figure 6.3.3.14 The dependence of the mean square torque term $\phi_{\mathbf{u}}^{(1)}(0)$ on temperature and density for CH_3F and fluoroform. (*a*) Temperature dependence, $\phi_{\mathbf{u}}^{(1)}(0)$ calculated using Eq. 6.3.2.10. (*b*) Density dependence. * CH_3F; ● CHF_3.

other. The former are roughly equivalent to $\epsilon''(\omega)/\omega$, whereas the latter are available as approximately $\omega\epsilon''(\omega)$ and $\epsilon''(\omega)$ and so give better frequency discrimination. These experiments should be used in conjunction with computer simulations and analyzed with the most realistic and sophisticated models available. In evaluating these models we should remember the wise words of one J. H. Hildebrand (1964) "a model should be regarded as suspect if it yields inferences in serious conflict with *any* of the pertinent properties of a system, regardless of how closely it can be made to agree with some, *especially if there are adjustable parameters.* A model that is consistent with all properties, even if only approximately, can probably be made more precise, but if it is in irreconcilable conflict with any part of the evidence, it is destined to be discarded, and in the meantime predictions and extrapolations based on it should be regarded as unreliable. Such a scheme of study has now been proposed in a joint European venture and is discussed in further detail in Chapter 12.

REFERENCES

Abragam, A., *The Principles of Nuclear Magnetism*, Oxford University Press (1961).

Berne, B. J. and Harp, G. D., *Adv. Chem. Phys.* **17**, 63 (1970).

Berne, B. J. and Montgomery, J., *Mol. Phys.* **32**, 363 (1976).

Bertagnoli, H., Leicht, D. O., and Zeidler, M. D., *Mol. Phys.* **35**, 199 (1978).

Bratos, S. and Marechal, E., *Phys. Rev.* **A4**, 1078 (1971).

Brier, P. N. and Perry, A., *Adv. Mol. Rel. Inter. Proc.* **13**, 1 (1978).

Bucaro, J. A. and Litovitz, T. A., *J. Chem. Phys.* **54**, 3846 (1971).

Budó, A., *J. Chem. Phys.* **17**, 686 (1949) (and references therein).

Crawford, B. Jr., Gilby, A. C., Clifford, A. A., and Fujiyama, T., *Pure Appl. Chem.* **18**, 373 (1969).

Doge, G., *Z. Naturforsch. A* **28**, 919 (1973).

Evans, G. J., Ph.D. Thesis, University of Wales (1977).

Evans, G. J. and Evans, M. W., *J. Chim. Phys.*, Paris, **72**, 522 (1978).

Ewing, G. E., *Acc. Chem. Res.* **2**(6), 168 (1979).

Favelukes, C. E., Clifford, A. A., and Crawford, B., *J. Phys. Chem.* **72**, 962 (1968).

Friedmann, M. and Kimel, S., *J. Chem. Phys.* **47**, 589 (1967).

Fujiyama, T. and Crawford, B., Jr., *J. Phys. Chem.* **73**, 4040 (1969).

Fulton, R. L., *J. Chem. Phys.* **55**, 1390 (1970).

Gordon, R. G. *J. Chem. Phys.* **43**, 307 (1965).

Griffiths, S. E., *J. Chem. Phys.* **59**, 751 (1973).

Heatley, F., *J. Chem. Soc. Faraday II* **70**, 148 (1974).

Hildebrand, J. H., *Faraday Disc.* **66** (1978).

Holleman, W. and Ewing, G. E., *J. Chem. Phys.* **44**, 3121 (1966).

Keyes, T. and Kivelson, D., *J. Chem. Phys.* **56**, 1057 (1972).

Kratochwill, A., Weidner, J., and Zimmerman, H. W., *Ber. Bunsenges. Phys. Chem.* **77**, 408 (1973).

Krishnaji and Mansingh, A., *J. Chem. Phys.* **41**, 827 (1964).

Lippert, E., Schröer, W., Mahnke, H., and Michel, H., *International Conference on Hydrogen Bonding*, H. J. Bernstein, Ed., Ottawa, p. 22 (1972).

Losche, A., *Z. Phys. Chem.* **201**, 302 (1952).

Lyerla, J. R., Grant, D. M., and Bertrand, R. O., *J. Phys. Chem.* **75**, 3967 (1971).

Lynden-Bell, R. M., *Mol. Phys.* **33**(4), 907 (1977).

Martin, D. H. and Puplett, E., *Infrared Phys.* **10**, 105 (1970).

McConnell, J., Lewis, J. T., and Scaife, B. K. P., *Proc. R. Ir. Acad.* **76A**, 43 (1976); Ford, G. W., Lewis, J. T., and McConnell, J., *Proc. R. Ir. Acad.* **76A**, 117 (1976), *Phys. Rev.* **A19**, 907 (1979).

Morita, A., Conference on Brownian Motion, Dublin (1976); *J. Phys. D* **11**, L1 (1978); *J. Chem. Phys.* **76**, 3198 (1982).

Pardoe, G. W. F. and Gebbie, H. A., *Symposium on Submillimeter Waves*, Polytechnic Institute of Brooklyn, p. 643 (1970); Pardoe, G. W. F., Thesis, University of Wales (1969).

Putnam, W. E., McEachern, D. M., and Kilpatrick, J. E., *J. Chem. Phys.* **42**, 749 (1965).

O'Reilly, D. E., Peterson, E. M., and Yasaitis, E. L., *J. Chem. Phys.* **57**, 890 (1972).

Rothschild, W. G., *J. Chem. Phys.* **53**, 990, 3265 (1970).

Steele, W. A., *Adv. Chem. Phys.* **34** (1976).

Tokuyama, M. and Mori, H., *Prog. Theor. Phys.* **55**, 411 (1976).

van Konynenburg, P. and Steele, W. A., *J. Chem. Phys.* **56**, 4776 (1972).

van Woerkom, P. C. M., De Bleyser, J., De Zwart, M., and Leyte, J. C., *Chem. Phys.* **4**, 236 (1974).

Wolynes, P. G. and Deutch, J. M., *J. Chem. Phys.* **67**, 733 (1977).

7

The Molecular Dynamics of Supercooled Liquids and Glasses

LIST OF SYMBOLS

α	The ultra-low frequency dielectric relaxation process in supercooled and glassy solutions of dipolar molecules
$\alpha(\omega)$	The complex molecular polarizability
$\mathfrak{A}(\bar{\nu})$	Power absorption coefficient
β	The intermediate frequency dielectric loss peak in glasses and supercooled liquids
β_1	First friction term of the itinerant librator model
β_2	Second friction term of the itinerant librator
$\bar{\beta}$	Empirical factor used by Williams and Watts
γ	The high frequency (far infrared) loss in glasses and supercooled liquids
$\gamma(\tau)$	A constant of the bivariate Gaussian distribution function denoted by f_2
$\langle\Gamma^2\rangle$	Mean square torque
dl	The space interval
D	Diffusivity in inverse time units
$\mathbf{D}$	Diagonal form of the matrix of transition probabilities $\mathbf{I}$
f_{ji}	Intersite probability function
${}^0f_i$	The conditional occupational probability for site i
$\mathbf{f}$	Matrix of probabilities
$F(t)$	Overall correlation function of the Lassier–Brot model
$g(t)$	The decay function for the relaxation of a temporary local environment
$I(\omega)$	Intensity of scattered light
I_r	reduced moment of inertia
$\mathbf{I}$	Matrix of transition probabilities
$J_{5/2}$	Bessel function of order $\frac{5}{2}$
k	(Scalar) transition probability
$\mathbf{k}$	(Vector) propagation vector of the Maxwell field equations
$\xi(t)$	Decay functions
K	The activation energy constant in Kelvin units
$\bar{\nu}_0$	Wavenumber of harmonic libration in the far infrared
n^2	Square of the refractive index in the high frequency part of the far infrared
p	Measure of probability
$p^{(i)}(t)$	Effective force per unit normal surface area
$P(t)$	Elementary polarization
P_2	Second Legendre polynomial

P_{ij}	Site transition rate
r_i	Position vector
r	A radius measure
ρ	Mass density
τ	A measure of time, in general denoted by t
u_c	Critical value of the local strain
$\mathbf{v}$	Current density
ω_0	Resonance frequency of the itinerant librator
Ω_0	Second resonance frequency of the itinerant librator
x	Linear (scalar) coordinate
$Y_{2,m}$	Spherical harmonic function of the azimuthal(θ) and polar(ϕ) angles of the spherical coordinate system

The viscosity of a dipolar liquid may be varied through many orders of magnitude by supercooling, and the resulting effect on the dielectric loss is illustrated in Fig. 1.2.8. To follow the changes from a broadly based theory is one of the most challenging tasks confronting the molecular dynamicist. The motion over the whole of the frequency range up to terahertz frequencies is a compendium of the cooperative and individual motions, the final result being a subtle amalgam of the two. In order to bring out various aspects of the dynamics it is possible in these systems to vary the external pressure as well as the temperature-dependent viscosity, so that a wide range of conditions presents itself to the interested theorist. A comprehensive review of the results in this area has been written by Williams (1975). An important advance of recent years in this field is the discovery that the motions of small, rigid dipolar molecules (such as CH_2Cl_2) can be slowed enormously by supercooling in a solvent such as decalin or *o*-terphenyl. The 0-THz spectrum of molecular motions (rotations and translations) undergoes a startling metamorphosis, as illustrated in Fig. 1.2.8. In some cases in a highly viscous medium at low temperatures the overall dielectric loss peaks three times in the region up to the far infrared. In other words, the time evolution of the orientational a.c.f. spans a corresponding dozen or so *decades* of frequency. These peaks are identified as the low frequency α and β processes, and the far infrared γ process. The terminology is unfortunate because there is at equilibrium only one overall process, which manifests itself in the triad of loss peaks observable in the frequency domain.

The α process is often spoken of as being the large-scale Brownian motions of the liquid and the β process as being primarily the limited motions in the glassy state below the so-called glass transition temperature T_g. This again is a little misleading because both α and β processes are sometimes clearly observable in the supercooled, very viscous, *liquid* state. There is a close parallel between the dielectric behavior of supercooled liquids and solid amorphous polymers. The α process has been characterized as a function of frequency, temperature, and solute concentration

by Williams (1975) and the closely related *viscoelastic relaxation phenomena* have been studied by Barlow, Lamb, and co-workers (see Williams, 1975). We have already mentioned these efforts briefly in Chapter 5, and to begin this chapter we review the theory of the α and β processes. This is in an incomplete and fragmentary condition because memory and inertial effects have not so far been included to account for the far infrared γ process. There would seem to be no difficulty in making this extension in principle. In practice, however, the presence of the β process at intermediate frequencies between those of the α and γ loss peaks provides a much sterner challenge to the theoretician, who will have to develop a strategy capable of accounting for all three peaks on the basis of molecular dynamics and hydrodynamics. In addition, the theory has to account for the breadth and asymmetry of the α process, the extreme breadth of the β peak, and also the characteristics of the γ process, which are brought out best by a representation in power absorption [$\mathfrak{A}(\bar{\nu})$ in Np/cm]. The results for supercooled decalin solutes in particular are fascinating. These are discussed in detail in this chapter in the light of novel data over the complete range of frequency recently acquired by Reid (1979). The α, β, and γ relaxations are a general property of a wide range of small molecule, glass-forming materials and characteristic also of amorphous solid polymers, and polymers in the rubbery condition. In the glassy condition the peak moves to zero frequency but the β process is still clearly observable. There is a corresponding dramatic shift to *higher* frequency in the far infrared γ process (Fig. 1.2.8*b*). The rate of large scale Brownian motion in the glass is therefore extremely slow, although the frequency of molecular libration in a potential well of nearest neighbors (characterized by the γ process) increases to double and even to three times its mean value in the ambient temperature solution. This is despite the fact that the temperature in the glass is very much *lower* in comparison.

The β loss process is observable in the supercooled liquid state but is more usually associated with organic glasses, inorganic glasses, and polymer glasses, and has been treated analytically in terms of a distribution of barrier heights confronting the reorientation of a reference molecule. At low temperatures in the glassy state the probability distribution of reorientation is such that only the lower barriers are surmountable. The β process covers a very wide range of frequency and both it and the α peak may be described theoretically in terms of the partial and total reorientation of dipoles found in a "range of environments." The theory implies that the α and β peaks are of course part of the same overall dynamic evolution, and as the temperature increases the peaks coalesce. If a variable such as pressure reduces the magnitude of the β process there is an identical increase in the magnitude of the α process. The model is one of partial (β) followed by total (α) relaxation. This suggests that in the glass the relaxation is always "partial." Unfortunately, in coming to these conclusions no attempt was made to account for the γ behavior within the same overall framework. It would be advantageous therefore to incorporate the whole theory within the framework of the Mori continued fraction. This is work that is still in the course of evolution, but later on we describe a very crude attempt in terms of three-variable Mori theory.

7.1 THEORY OF DEFECT DIFFUSION RELAXATION

The diffusion and relaxation rates in supercooled liquids, polymers, and glasses vary as $\exp[-K/(T-T_g)]$, where K is a constant (Chapter 5), rather than as $\exp[-K/T]$, as a simple activation (Arrhenius) theory predicts. Glarum (1960) has introduced a theory of relaxation in such systems by assuming that any given molecule relaxes only when it is passed by a mobile structural defect. In one dimension the model may be described as follows.

Suppose that a dipole at a fixed point $x = 0$ is reversed in direction every time a defect diffuses past. The probability that a defect initially at $x = l > 0$ has passed the dipole an odd number of times in time t is the probability that the defect is now in the region $x < 0$. If the defect has a diffusive motion with diffusivity D, this probability is $\frac{1}{2}\operatorname{erfc}[l/(4Dt)^{1/2}]$, where erfc is the complementary error function. Let the probability that the defect started in any space interval dl be dl/a, corresponding to a uniform initial probability density in the interval $0 \leq x \leq a$. One could consider $-a \leq x \leq a$ with an extra factor of 2. The probability that the dipole has reversed in time is now

$$\begin{aligned}
&\frac{1}{2a}\int_0^a \operatorname{erfc}\left(\frac{l}{(4Dt)^{1/2}}\right) dl \\
&\quad = \frac{1}{2} - \frac{\sqrt{Dt}}{a}\left[\frac{a}{\sqrt{4Dt}}\operatorname{erf}\frac{a}{\sqrt{4Dt}} + \frac{1}{\sqrt{\pi}}\exp\left(\frac{-a^2}{4Dt}\right) - \frac{1}{\sqrt{\pi}}\right] \\
&\quad = \frac{1}{a}\sqrt{\frac{Dt}{\pi}} + O(\text{terms with the factor } \exp[-a^2/(4Dt)])
\end{aligned}$$

If we consider a region far from sample boundaries, a can be taken large enough to neglect the Gaussian terms above. Then the probability that the dipole has not been reversed at time t by one particular defect is

$$p = 1 - \frac{1}{a}\left(\frac{Dt}{\pi}\right)^{1/2}$$

The probability that, of N noninteracting defects in the interval, a may have produced a reversal and $(N - M)$ may not have is

$$\frac{N!}{M!(N-M)!}(1-p)^M p^{N-M}$$

and the sum over even M is $\frac{1}{2}[1 + (2p-1)^N]$. If N increases with a as na,

implying a constant numerical density n of defects, the probability that the dipole has its original orientation at time t is $a\ \frac{1}{2}\{1+\exp[-2n(Dt/\pi)^{1/2}]\}$. The probability of the reverse orientation is $\frac{1}{2}\{1-\exp[-2n(Dt/\pi)^{1/2}]\}$ and the average fraction of orientation retained is $\exp[-2n(Dt/\pi)^{1/2}]$, a result identical with that derived by Bordewijk and Böttcher (1979) on the slightly different assumption that each defect produces complete orientation relaxation, rather than direct reversal, as it passes. This correlation function is identical to the empirical form used by Williams and Watts (1970), with their $\bar{\beta} = 0.5$.

In *three-dimensional, isotropic systems* an analysis by Bordewijk and Böttcher (1979) shows that behavior approximating $\exp[-(t/\tau)^{1/2}]$ can be found *only for a defect density so high* that there must be a large, fast component of the relaxation contributed by those defects that are already in the relaxation range of a dipole at $t = 0$. This might possibly be identified with the γ process, but again the form $\exp[-(t/\tau)^{1/2}]$ does not conform with the general time even properties of an a.c.f. Either the slow relaxation involves some other mechanism or defects tend to follow preferred tracks. That would be reasonable in polymer systems but surprising in most supercooled melts. A relaxation that is slower than any single exponential can be represented by a broad distribution of relaxation times. Comparison of Glarum's and Bordewijk's treatment of their diffusion/relaxation model suggests that an essential contribution to this distribution comes from the fluctuations of concentration of the defects which, catalyze the relaxations as pointed out by Wyllie (1981), whose remarks are summarized as follows.

It is interesting to consider (following Wyllie) whether there are consequences of these fluctuations if there are defect concentrations arising from a longer range section of the defects. If the defects are unchanged the first such action arises from whatever strain field surrounds the defect. We consider defects possibly with a wide range of individual size, which constitute a local dilation of the structure. They may not be individually spherically symmetrical, but we suppose that on an average they are. In an elastic medium a local spherical dilatation produces an outflow of volume which is the same across every concentric spherical surface, so that the radial displacement decreases as r^{-2} and the radial strain, which is compressive, as r^{-3}. Outside the central dilatation there is no bulk strain and the resultant strain field is one of pure shear. The corresponding stress field is related to the strain by the shear modulus of the medium.

In a liquid, the stress may relax faster than the strain builds up and the dilatation stores no elastic energy in the surrounding material. It is not obvious that this should be so in a glass. In any event, the buildup of shear strain due to dilatation at some distance may serve to release "jammed" molecules and so permit relaxation. The interaction of dilatation defects with each other is rather small and we shall neglect it, simply regarding the excess volume in the material as a randomly diffusing component with a constant diffusivity D. The fluctuating excess volume around a given point

then relaxes on average according to the ordinary diffusion equation and the interesting part of the relaxing distribution is

$$e(t) = \sum_k e^{-Dk^2t}(kr)^{1/2}J_{5/2}(kr)\sum_m A_{mk}Y_{2,m}(\theta,\phi)$$

where $J_{5/2}$ and $Y_{2,m}$ are defined above (Abramowitz and Stegun, 1965). We have $J_{5/2}(kB) = 0$ and A_{mk} as independent Gaussian variables of determinate mean square value. B is a large radius corresponding to the specimen boundary. We need only the spherical harmonic $Y_{2,m}$ because none of the other terms will give a resultant shear stress at the origin after integrating over θ and ϕ. The individual stress components contain terms proportional to the radial integral of $r^{-1}x^{-n}$ ($n = 1$, 2, or 3) ($\sin x$ or $\cos x$) where $x = kr$, so we require a lower cutoff at one or two molecular diameters, at $r = b$, say. Physically this means that the free volume on a molecule's surface contributes directly to its relaxation. There must be an upper cutoff to k so that we have $0 < kb \leqslant 1$ to avoid the difficulty of having more variables than are needed to determine the configuration of the system. The values of k are to all extents distributed with spacing π/B, so for large B the summation is well represented by an integral $\Sigma_k = B/k \int dk$.

The autocorrelation of the fluctuating shear stress is then the sum of the a.c.f.'s of the individual components. We thus have exponential decays, $\exp(-Dk^2t)$ with uniform distribution in k, weighted with the radial integrals, which are dominated for the smaller k values by $(kb)^2$ [with $(kb)^4$ and an oscillating factor contributing for large k]. Equivalently we have the form $e^{-\beta t}$ weighted with $\beta^{1/2}$, $\beta^{3/2}$, and $\beta^{5/2}$. The distribution of exponentials with weighting toward longer decay times gives a correlation function approximated for times t much longer than b^2/D *by a sum of inverse powers of t. This is of course similar in form to the vortex* t^{-2} *or* $t^{-5/2}$ *decay discussed in Chapter* 5. The importance of these strain fluctuations in promoting relaxation may depend in a very sensitive way on the hardness of the intermolecular forces, since hard molecules join firmly with small overlap and relax with small strains. We may suppose in any case that a given molecule makes a relaxation step when the local strain U passes a critical value U_c. A correlation function with a nonnegative Laplace transform is a sum of exponential decays with positive coefficients and has nonzero slope at zero time, giving infinite mean square derivatives of the sample functions; that is, the spectral moments are not properly defined (see Chapter 1) just as with the simple Einstein or Debye theory of the Brownian movement. We only escape this difficulty by explicit consideration of the correlation function at times $\leqslant b^2/D$ (i.e., at frequencies approaching the far infrared, where the γ process is observable). The simplest way of avoiding difficult analysis is to assume reversal relaxation. We then need to know the *two-time distribution* of U, which is given by

the *bivariate* Gaussian distribution (Chapter 1):

$$f_2(U_1, U_2, \tau) = \{2\pi\sigma^2[1-\gamma^2(\tau)]^{1/2}\}^{-1} \exp\left(\frac{-U_1^2 - 2\gamma(\tau)U_1U_2 + U_2^2}{2\sigma^2[1-\gamma^2(\tau)]}\right)$$

Then the correlation function of the relaxing quantity of interest is $1-2p(t)$, where

$$p(t) = 2\int_0^{U_c} dU_1 \int_{U_c}^{\infty} dU_2 f_2(U_1, U_2, t)$$

This then has to be averaged over a distribution of U_c. With hard repulsions, a rectangular distribution of U_c seems reasonable, but numerical investigation of the distribution over the *whole* 0–THz region (inclusive of α, β, and γ processes) is desirable.

If the α, β, and γ processes are well separated in the time or frequency domain then the orientational correlation function may be written

$$C_u(t) = a_\alpha C_u^{(\alpha)}(t) + a_\beta C_u^{(\beta)}(t) + a_\gamma C_u^{(\gamma)}(t)$$

where $a_\alpha + a_\beta + a_\gamma = 1$. To account for the great range of processes contributing to the overall relaxation (especially the β process, *which is* 10^3 *to* 10^5 *times broader* than a single relaxation process), the following theory has been developed by Cole (1963) and used by Williams (1973, 1977) and others in polymer and glassy environments.

The basic idea is that a dipole of magnitude μ reorients between a number of sites prescribed by a temporary local environment which persists for a time *long* compared with that required for reorientation between sites. The local environment may fluctuate via the large scale Brownian motions of the system which relax the dipole in the temporary barrier system. The dipole a.c.f. is then obtained by Cole as a sum of decay functions:

$$C_u(t) = \mu^{-2}\left[\sum_i {}^0f_i[\boldsymbol{\mu}(t)\cdot\boldsymbol{\mu}(0)]_i\right] g_\alpha(t)$$

Here the sum is taken over all the sites in the barrier system. ${}^0f_i$ is the "equilibrium" occupational probability of site i, and $[\boldsymbol{\mu}(0)\cdot\boldsymbol{\mu}(t)]_i$ is the dipole decay function for a dipole in site i at $t=0$. $g_\alpha(t)$ is the decay function for the relaxation of the temporary local environment, that is, the barrier system. $[\boldsymbol{\mu}(0)\cdot\boldsymbol{\mu}(t)]_i$ is calculated from the conditional probabilities $f_{ji}(t)$, where $f_{ji}(t)$ is the probability of occupation of sites at t given site i occupation at $t=0$. These probabilities are obtained from the solution of *rate equations* governing the occupation of the sites:

$$[\boldsymbol{\mu}(t)\cdot\boldsymbol{\mu}(0)]_i = \sum_j f_{ji}(t)\boldsymbol{\mu}_i\cdot\boldsymbol{\mu}_j$$

These rate equations apply to the classical motions of molecules, ions, or vacancies between equilibrium sites. In the simplest case the orientational

time correlation functions are exponential or weighted sums of exponentials, the inertia of the molecule being neglected. The γ process is not describable in this case. For example, a dipole may occupy two orientations with an included angle π, separated by a barrier, and moving between sites with a transition probability k. The occupational probabilities for site 1 and site 2 are then governed by the differential equations

$$\begin{aligned}\frac{df_1(t)}{dt} &= -kf_1(t) + kf_2(t)\\ \frac{df_2(t)}{dt} &= kf_1(t) - kf_2(t)\end{aligned} \tag{7.1.1}$$

These equations are soluble using matrix algebra, and more complicated versions use a group theoretical method development by Williams and Cook (1972). In matrix form,

$$\dot{\mathbf{f}}(t) = \mathbf{I}\mathbf{f}(t)$$

so that $\mathbf{f}(t) = [\exp \mathbf{I}t]\mathbf{f}(0) = \mathbf{S}[\exp \mathbf{D}t]S^{-1}\mathbf{f}(0)$, where $\mathbf{I} = \begin{bmatrix}-k & k\\ k & -k\end{bmatrix}$. $\mathbf{D}$ is the diagonal form of $\mathbf{I}$, generated using $\mathbf{S}^{-1}\mathbf{T}\mathbf{S} = \mathbf{D}$. The matrix $\mathbf{f}(t)$ follows from the elemental relation $\exp[\text{diag}\,\lambda_m t] = [\text{diag}(\exp\lambda_m t)]$, λ_m being the elements of $\mathbf{D}$.

The introduction of group theory may be effected by introducing an orthogonal matrix $\mathbf{Q}$ using the site symmetry. The matrix $\mathbf{W} = \mathbf{Q}^{-1}\mathbf{T}\mathbf{Q}$ is calculated and its constituent smaller matrices are taken individually as eigenvalues and eigenvectors. This leads to $\mathbf{f}(t) = \mathbf{Q}\mathbf{U}[\exp \mathbf{D}t]\mathbf{U}^{-1}\mathbf{Q}^{-1}\mathbf{f}(0)$, where $\mathbf{U}^{-1}\mathbf{W}\mathbf{U} = \mathbf{D}$. In suitable cases $\mathbf{Q} = \mathbf{S}$ provided that no class appears more than once in the reducible representation generated using the sites as the basis set. For the two-site model, the C_2 character table gives $\Gamma = A + B$, $\mathbf{Q}$ is evaluated from the A and B irreducible representations, and $\mathbf{Q}^{-1}\mathbf{T}\mathbf{Q} = \mathbf{D}$, $\mathbf{U} = \mathbf{E}$, $\mathbf{Q} = \mathbf{S}$. Here $\mathbf{E}$ is the identity matrix. Therefore,

$$\mathbf{S} = \frac{1}{\sqrt{2}}\begin{bmatrix}1 & 1\\ 1 & -1\end{bmatrix}; \qquad \mathbf{D} = \begin{bmatrix}0 & 0\\ 0 & -2k\end{bmatrix}$$

$$\mathbf{f}(t) = \begin{bmatrix}f_1(t)\\ f_2(t)\end{bmatrix} = \frac{1}{2}\begin{bmatrix}1+\psi_2(t), & 1-\psi_2(t)\\ 1-\psi_2(t), & 1+\psi_2(t)\end{bmatrix}\begin{bmatrix}f_1(0)\\ f_2(0)\end{bmatrix}$$

where $\psi_2(t) = \exp(-2kt)$.

The orientational a.c.f. is calculated as the average of the decay functions $\xi_1(t)$ and $\xi_2(t)$ for dipoles starting in sites 1 and 2, respectively, at $t=0$:

$$\langle\boldsymbol{\mu}(0)\cdot\boldsymbol{\mu}(t)\rangle = \mu^2\sum_{i=1}^{2} {}^0f_1\xi_1(t)$$

$$\xi_i(t) = \sum_{i=1}^{2} f_{ji}\boldsymbol{\mu}_i\cdot\boldsymbol{\mu}_j.$$

${}^0f_i$ is the equilibrium occupation probability of site i, and the sum is taken over all sites. $f_{ji}(t)$ is the conditional probability that the dipole is in site j and t given it was in site i at $t=0$. $f_{ji}(t)$ follows from eq. 7.1.1 with $f_1(0)=1$, $f_2(0)=0$, with similar considerations for $f_j^2(t)$. Using $\boldsymbol{\mu}_1 \cdot \boldsymbol{\mu}_1 = \boldsymbol{\mu}_2 \cdot \boldsymbol{\mu}_2 = -\boldsymbol{\mu}_1 \cdot \boldsymbol{\mu}_2$, we have finally

$$\langle \boldsymbol{\mu}(0) \cdot \boldsymbol{\mu}(t) \rangle = \mu^2 \exp(-2kt)$$

For more complicated barrier systems several relaxation times may arise, and also $\langle \boldsymbol{\mu}(t) \cdot \boldsymbol{\mu}(0) \rangle$ does not generally decay to zero for nonequivalent sites. Different experimental techniques may probe different aspects of the motion when this is prescribed completely by the probability rate equations. It is therefore necessary to compare the time-correlation functions from several related experiments in order to establish the detailed mechanism of site relaxation.

An interval of time $\tau_\beta \leqslant t \leqslant \tau_\alpha$ may be chosen where τ_α and τ_β are characteristic times for the α and β processes, respectively, that is, τ_β is for motion in the barrier system, τ_α for the "environment." In this time range $f_{ji}(t) \to {}^0f_j$ and

$$\begin{aligned} C_u(t) &= \mu^{-2}\left[\sum_i {}^0f_i \left(\sum {}^0f_j \boldsymbol{\mu}_i \cdot \boldsymbol{\mu}_j\right)\right] \\ &= \mu^{-2}\left[\sum_i \sum_j ({}^0f_i \boldsymbol{\mu}_i) \cdot ({}^0f_j \boldsymbol{\mu}_j)\right] \\ &= \mu^2 [\langle \boldsymbol{\mu} \rangle]^2 \end{aligned}$$

Here $\langle \boldsymbol{\mu} \rangle = \Sigma_i {}^0f_i \boldsymbol{\mu}_i$ is the average moment remaining in the barrier system after reorientation has occurred between the sites. The α and β processes may now be separately described through the equations

$$a_\alpha = \frac{[\langle \boldsymbol{\mu} \rangle]^2}{\mu^2} \qquad \text{and} \qquad a_\beta = 1 - a_\alpha;$$

$$C_\alpha(t) = g_\alpha(t)$$

$$C_\beta(t) = \frac{\sum_i {}^0f_i \left\{\sum_j [f_{ji}(t) - {}^0f_j]\right\} \boldsymbol{\mu}_i \cdot \boldsymbol{\mu}_j}{\mu^2 - [\langle \boldsymbol{\mu} \rangle]^2}$$

A further generalization of these equations to involve a whole range of local environments has been achieved by Williams and Watts (Williams, 1975). It seems that partial relaxation of μ^2 may occur by fast reorientation in a variety of local environments (β process) and the *residual* mean moment $\langle \boldsymbol{\mu}_r \rangle$ for a given environment is relaxed by the slower α process. For supercooled liquids and some polymers the partial reorientation process may be quite small relative to the α process, but in some systems, (Fig. 1.2.8) it is not. The defect diffusion treatment of the cooperative α process has already been mentioned.

In order to assimilate the far infrared γ process the site models have to be modified to include inertial and memory effects. To describe the related situation in plastic crystals, some models have been devised by Brot (1975) to account for the fact that the rotator is in a crystalline type field with several potential wells fixed in space. During their stays in the wells the rotators are not motionless but are distributed among librational energy levels. The resultant polarization is responsible for the initial part of the overall vector correlation function $C_u(t)$.

This raises the question of treating dynamically the short time details of the mechanism of escape from a given potential well or site, and incorporating memory and inertial effects into the rate equations. When V represents two neighboring potential wells separated by a barrier of finite height, the relevant equation is the Kramers equation described earlier in Chapters 1 and 2. Lassier and Brot (1969) have treated the related question of rotation among a set of potential wells, with the simplifying assumption that velocity correlation is completely lost by the strong collision which provides the energy necessary for crossing each potential hump. If such a collision occurs at time t_j the dipole orientation correlation function is

$$\begin{aligned} \langle \cos\theta(t) \rangle &= \langle \cos\theta(t_j) \rangle \langle \cos\theta(t - t_j) \rangle \\ &= L(t_j) H(t - t_j) \end{aligned}$$

where L is the correlation function for a librating molecule and H is that in the "activated" state of jump. If τ_r^{-1} is the probability per unit time of a strong collision inducing a jump, and angular correlation is completely lost by the conclusion of the jump (so that there is no need to consider several successive jumps), the overall correlation function is

$$F(t) = e^{-t/\tau_r} L(t) + \int_0^t \tau_r^{-1} \exp\left(\frac{-t_j}{\tau_r}\right) L(t_j) H(t - t_j)\, dt_j$$

They assume for L a form previously calculated by Brot (1975) which corresponds to a two-variable Mori theory for orientation (Chapter 2), assuming instantaneous collisions which reduce the preceding velocity by a constant factor and add a random impulse whose mean square value is adjusted to maintain constant temperature. The form of $H(t)$ is arbitrarily taken as

$$H(t) = \exp\left(\frac{-t}{\tau_a}\right)\left(1 + \frac{t}{\tau_a}\right)$$

where τ_a is the mean duration of a jump.

Larkin (1973) has extensively tested this model for rotator phases as mentioned briefly in Chapter 5. Figure 1.3.1.3 shows, however, that the fit at short times is rather poor in the 100-odd cases tested. This is due to the assumption of instantaneous collisions so that the limiting shape of $C_u(t)$ is ill-defined. Also the fitting of this model to the highly discriminating

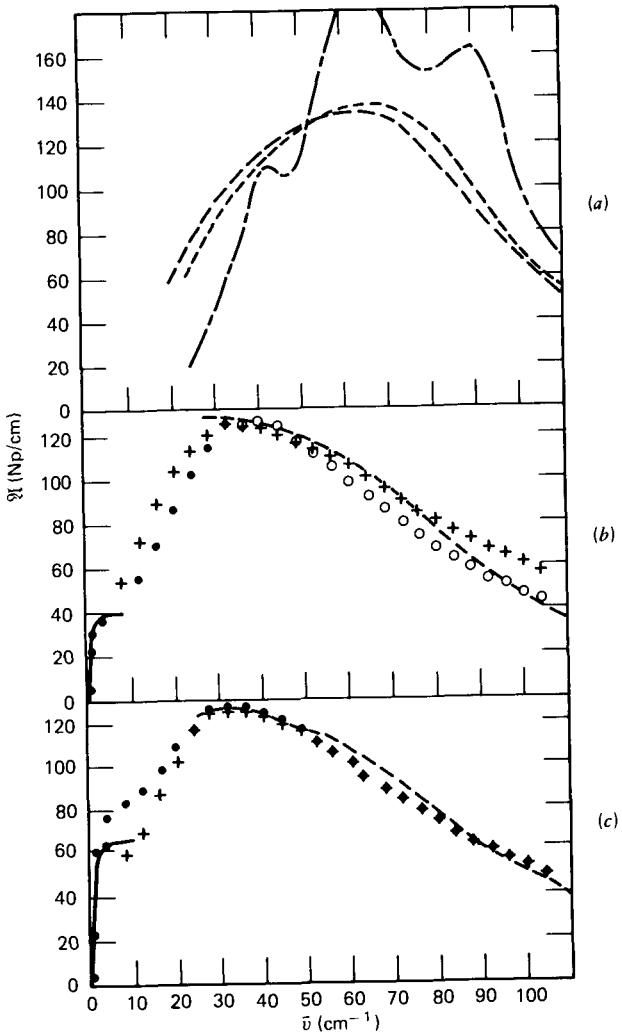

Figure 7.1.1 Far infrared absorption coefficient (denoted by $\mathfrak{A}$ in figure) of 2-methyl-2-nitropropane. Continuous lines are extrapolated microwave observations. Dashed lines are far infrared observations. Open circles and crosses are the results of a well jumping model and an itinerant librator. (*a*) Rotator phase II at 219°K (dotted line) and 244°K (dashed line). Mixed line denotes the crystalline nonrotator phase. (*b*) Phase I rotator at 273°K. (*c*) Liquid at 303°K and phase I at 294°K. [Reproduced by permission from I. W. Larkin, et al., *J. Chem. Soc. Faraday Trans. II* **69**, 1729 (1972).]

microwave/far infrared data brings out the fact that the theoretical power absorption coefficient, as in the planar itinerant librator (Fig. 7.1.1) tends to peak twice whereas the experimental data is a single band.

The difficulty of extending overparameterized models such as these to the viscous liquid state is an order of magnitude greater, and a different line of approach is needed. The most attractive approach seems to be by

incorporating into the Mori column vector **A** suitable modes that couple with each other to produce the overall (α, β, γ) loss profile. It would be preferable to mix the orientational vector **u** with two or three modes and then perhaps form a final average over a variety of local environments to produce the breadth of the β and α loss curve. In the appendix to this chapter we briefly review the various phenomenological viewpoints of this nature devised for the features of depolarized and polarized light scattering.

7.2 MODELS FOR MOLECULAR DYNAMICS IN GLASSES

In making this type of comparison it is advantageous to treat the dynamic system in terms of molecules whose rototranslation is very strongly hindered, but which are still amenable to theoretical treatment in terms of Mori approximants with the inclusion of a strong external potential. The major difficulty in using a three-variable theory directly on the vector **u** is that the breadth and asymmetry of the β process are not reproducible and the separation in frequency between the β and γ features in the glass causes the theoretical γ peak to be very narrow, owing to the very high memory function ratio of $\phi_1(0)$ to $\phi_2(0)$. This is illustrated in Fig. 7.2.1.

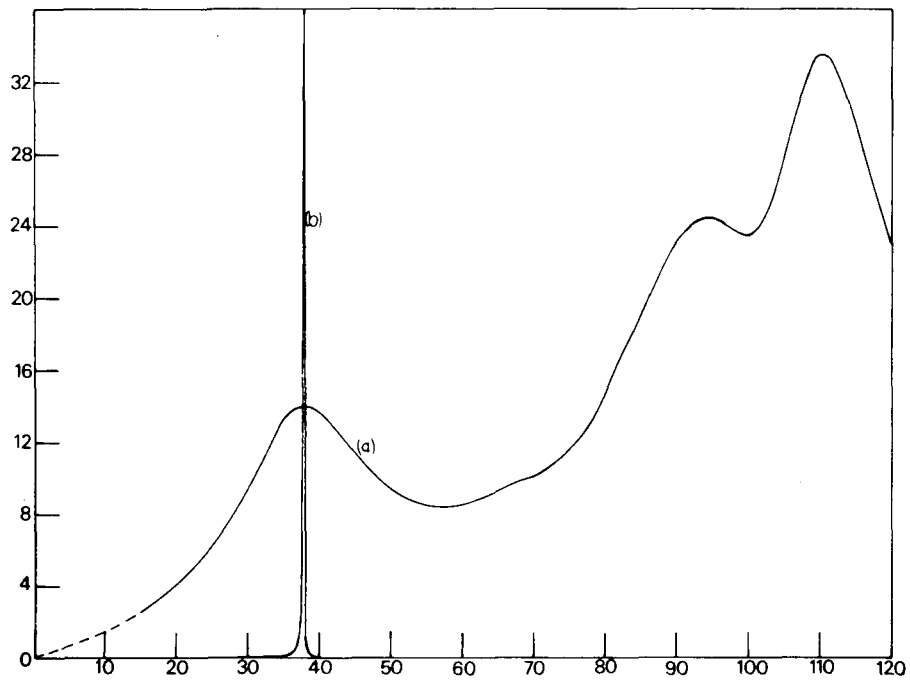

Figure 7.2.1 (*a*) Far infrared spectrum of disordered solid pentachloronitrobenzene at 296°K, 1 bar. (*b*) Theoretical absorption predicted with a simple three-variable Mori theory. Ordinate, $\mathfrak{A}(\omega)$ (Np/cm); abscissa, $\bar{\nu}$(cm^{-1}). [Reproduced by permission from M. W. Evans et al., *Adv. Mol. Rel. Int. Proc.* **12**, 301 (1978).]

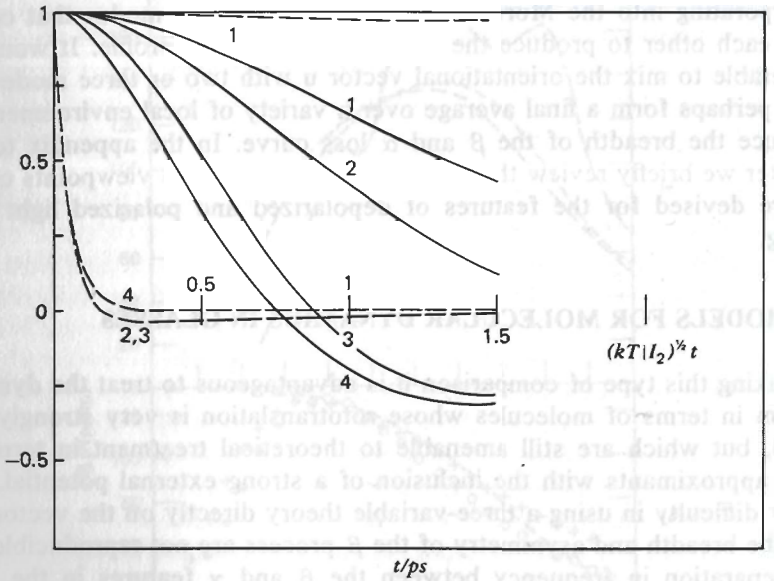

Figure 7.2.2 Glass state a.c.f.'s $C_u(t)$ and $\ddot{C}_u(t)$. (1) Liquid solution, orientational a.c.f. $\langle\cos\theta(t)\cos\theta(0)\rangle$; (2) normalized angular velocity a.c.f., $\langle\dot{\theta}(t)\dot{\theta}(0)\rangle/\langle\dot{\theta}(0)\dot{\theta}(0)\rangle$; (3) normalized rotational velocity a.c.f., $\langle\dot{\theta}(t)\dot{\theta}(0)\rangle/\langle\dot{\theta}(0)\dot{\theta}(0)\rangle$; (3) normalized rotational velocity a.c.f. $\langle(d/dt)\cos\theta(t)[(d/dt)\cos\theta(t)]_{t=0}\rangle$; (4) normalized torque a.c.f. $\langle\ddot{\theta}(t)\ddot{\theta}(0)\rangle\langle\ddot{\theta}(0)\ddot{\theta}(0)\rangle$. --- (1) to (4) as for above but in the glass.

It is clear that an extra averaging or statistical distribution is needed to broaden both the β and γ features. The three-variable Mori theory is capable of reproducing the positions of the γ and β processes, which suggests that for each "site" in the glass for each type of environment, the analytical form of the governing probability diffusion equation might conceivably be structured according to the continued fraction. In terms of the overall $C_u(t)$ the situation in both glassy and viscous liquid environments vividly contrast with $\ddot{C}_u(t)$. The former decays exponentially from about 0.5 psec onwards, taking upwards of milliseconds and sometimes much longer to reach zero asymptotically. The latter is oscillatory, with pronounced negative regions and far from exponential (Fig. 7.2.2).

The planar itinerant librator, or three-variable Mori theory applied to the angular velocity of a two-dimensional rotator, as described in Chapter 4, should be (a priori) particularly well suited to the description of the planar librational reorientations in TCTMB (Chapter 3), with the proviso that the cage diffusion is very slow indeed. In the related species pentachloronitrobenzene (PCNB), the equivalent of the β process is detected at frequencies between 30 Hz and 1 MHz in the temperature range 293–372°K, with a large energy barrier to rotation (Aihara et al., 1970). An entropy difference between the stationary and transitional positions was calculated

on the basis of phase reorientation between two opposite wells, ignoring the effect of molecular inertia. The γ process, which peaks at 38 cm^{-1} in the far infrared, may be treated by assuming that the angular movement of the molecule occurs in a fixed crystalline potential. The libration frequency $\bar{\nu}_0$ is then defined for simple symmetries such as that of benzene by

$$\bar{\nu}_0 = \frac{3}{\pi c}\left(\frac{v}{2I}\right)^{1/2} \tag{7.2.1}$$

where I is the moment of inertia about the hexad axis. Equation 7.2.1 has been used to describe the observed Raman or far infrared peak librational frequencies in plastic crystalline benzene, furan, and some other hexasubstituted benzenes which all lie in the range 30–60 cm^{-1}.

No account is taken in Eq. 7.2.1 of intermolecular interaction or of the fact that the far infrared γ peak is broadened and is the high frequency adjunct of the β process. Direct application of the constrained itinerant librator (i.e., angular velocity three-variable theory), with no attempt made at accounting for interactions in the manner of Chapter 3, produces the result of Fig. 7.2.1 for PCNB. The γ part of the loss (or power absorption coefficient) is too sharply resonant in character (see also Chapter 4). The corresponding "β process" (Fig. 7.2.3) is a little too narrow.

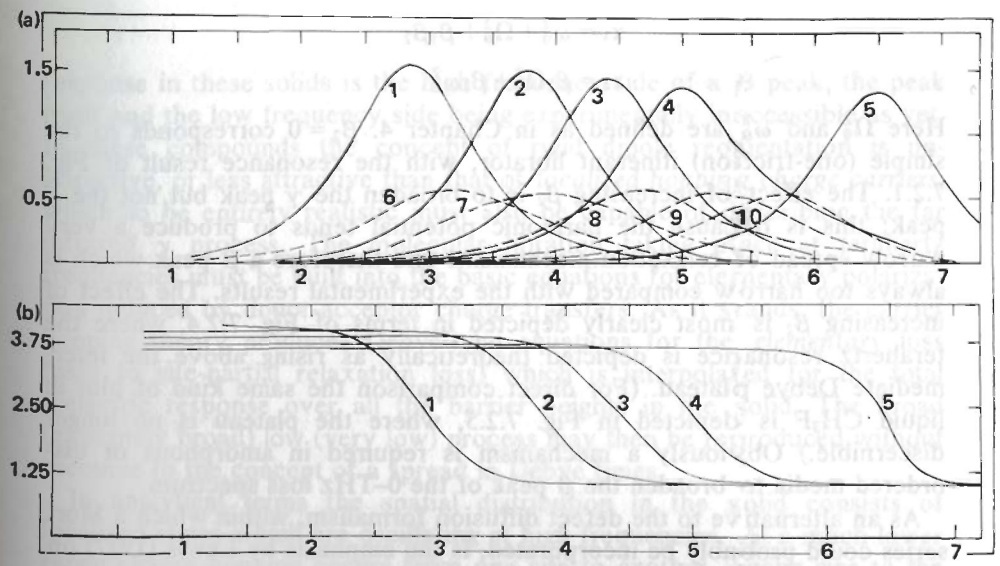

Figure 7.2.3 (*a*) Dashed line, the experimental dielectric absorptions of pentachloronitrobenzene at temperatures (6) 293°K, (7) 313.4°K, (8) 333°K, (9) 353.7°K, (10) 372.1°K. Solid lines, the theoretical absorptions at the same temperatures. Ordinate, ϵ''; abscissa, $\log f$ (Hz). (*b*) The theoretical permitivity ϵ' 1–5. [Reproduced by permission from M. W. Evans et al., *Adv. Mol. Rel. Int. Proc.* **12**, 301 (1978).]

Again the three-variable Mori theory with no applied external potential can be made to describe correctly only the peak positions of the (β, γ) process. Of course this is hardly surprising since a large part of Chapter 3 was devoted to the crucial role of electrostatic interactions in these media. The choice of the systems in the present context is purely for the purpose of illustrating the way in which the simplest possible kind of three-variable theory behaves when confronted with these extremes of the dielectric loss process.

An extra friction term may be incorporated in the planar itinerant librator. If we denote the two frictions by γ_1 and γ_2, then in the limit $kT/I_2\gamma_1^2 < 0.1$ (where I_2 is the moment of inertia of the ring) the complex polarizability is given by

$$\alpha(\omega) = \frac{kT}{I_2}\left(\frac{x(\Omega_0^2 - \omega^2) + \omega\beta_1 y - i[\omega\beta_1 x - y(\Omega_0^2 - \omega^2)]}{x^2 + y^2}\right)$$

$$x = \omega^2(\omega^2 - x_3) + x_1(x_4 - x_2\omega^2)$$

$$y = \omega[x_4 + x_1(x_3 - \omega^2) - x_2\omega^2]$$

with

$$x_1 = \frac{kT}{I_1\beta_1}\left(\frac{\beta_1\omega_0^2}{\beta_1\omega_0^2 + \beta_2\Omega_0^2}\right)$$

$$x_2 = \beta_1 + \beta_2$$

$$x_3 = \omega_0^2 + \Omega_0^2 + \beta_1\beta_2$$

$$x_4 = \beta_2\Omega_0^2 + \beta_1\omega_0^2$$

Here Ω_0^2 and ω_0^2 are defined as in Chapter 4. $\beta_2 = 0$ corresponds to the simple (one-friction) itinerant librator, with the resonance result of Fig. 7.2.1. The effect of increasing β_2 is to broaden the γ peak but not the β peak; this is because the harmonic potential tends to produce a very narrow spread of relaxation mechanisms and therefore a β peak which is always too narrow compared with the experimental results. The effect of increasing β_2 is most clearly depicted in terms of Fig. 7.2.4, where the terahertz resonance is depicted theoretically as rising above the intermediate Debye plateau. (For direct comparison the same kind of plot in liquid CH_3F is depicted in Fig. 7.2.5, where the plateau is no longer discernible.) Obviously a mechanism is required in amorphous or disordered media to broaden the β peak of the 0–THz loss spectrum.

As an alternative to the defect diffusion formalism, within which a Mori series could probably be incorporated, is the emphasis by Lewis (1977) on the apparently simple law of the low frequency conductivity in a wide variety of compounds for which the γ process has not yet been characterized experimentally. These include vanadium phosphate glass, doped silica semiconductors, aluminum oxide, amorphous selenium, organic polymers, and biopolymers such as *trans*-carotene. In dielectric terms the

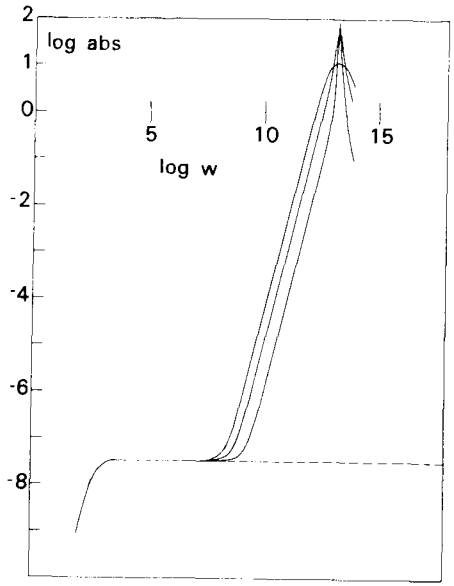

Figure 7.2.4 Log $\mathfrak{A}(\omega)$ versus log (ω) representation of the absorption in glassy CH_2Cl_2/decalin. Note the horizontal Debye plateau which continues as $\omega \to \infty$ for classical theories of Brownian motion. The far infrared resonance rises steeply above this at 90 cm^{-1} (114°K) in itinerant libration. [Reproduced by permission from G. J. Evans et al., *Chem. Phys. Lett.* **56**, 529 (1978).]

response in these solids is the high frequency side of a β peak, the peak itself and the low frequency side being experimentally inaccessible as yet. In these compounds the concept of rigid dipole reorientation is unattractive, or less attractive than that of *localized hopping charge carriers*, which to be entirely realistic must also be capable of describing the far infrared γ process. The molecular libration taking place at terahertz frequencies must be built into the basic equations for elementary polarization induced by donor-acceptor charge transfers. As it stands, the carrier hopping theory produces Debye-type equations for the *elementary* loss (akin to site-partial relaxation loss) which is interpolated for the total dielectric response over all the barrier heights in the solid. The broad (extremely broad) low (very low) process may then be reproduced without recourse to the concept of a spread in Debye times.

In analytical terms the spatial distribution in the solid consists of localized states which are oscillating at high frequencies. At a much lower range charge hopping occurs from one site to another, giving rise to the observed ac conductivity. This may be formulated by considering the *elementary polarization*:

$$P(t) = V^{-1}\left[\sum_D e(1 - f_i)r_i \cos\theta_i - \sum_A e f_i r_i \cos\theta_i\right] \qquad (7.2.2)$$

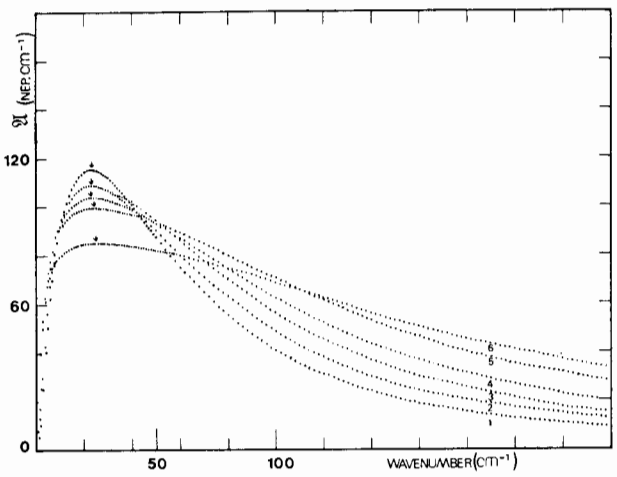

(*a*)

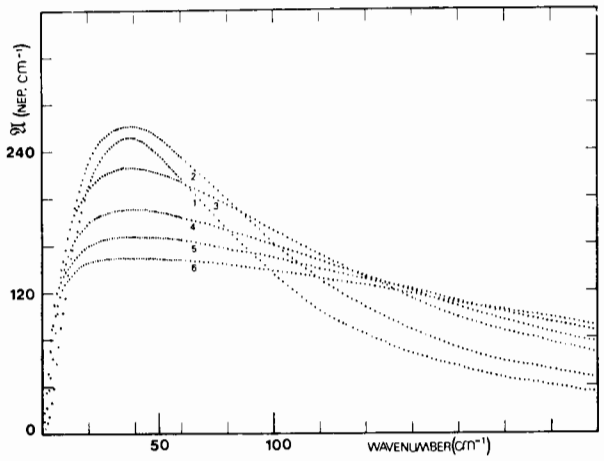

(*b*)

Figure 7.2.5 Variation with temperature of the spectra calculated from the symmetrical top Langevin equation for (*a*) CHF_3 with (1–6) increasing friction. (*b*) CH_3F with (1–6) increasing friction. [Reproduced by permission from G. J. Evans et al., *J. Chim. Phys.* **75**, 527 (1978).]

where e is the electronic charge, f_i is the probability that a state i (donor or acceptor) is occupied by an electron, r_i is the distance of this state from a chosen origin, and θ_i is the angle between $\mathbf{r}_i$ and $\mathbf{F}(t)$, the probe field. If the vector $\mathbf{r}_i$ remains fixed in space, Debye type equations for the elementary loss are obtained after certain simplifying assumptions:

$$\Delta\epsilon''(\omega) = e^2 r_{ij}^2 \frac{\cos^2\theta_i}{kT} \frac{\omega P_{ij} P_{ji}}{\omega_{ij}(\omega^2 + \omega_{ij}^2)}$$

where P_{ij} and P_{ji} are transition *rates* between sites, and $\omega_{ij} = P_{ij} + P_{ji}$ is the characteristic relaxation frequency for the pair element in question. However, the dipole moment determining the polarization is $e\mathbf{r}_{ij}$ which is affected by a torsional oscillation in r_{ij} at far infrared frequencies. Thus in Eq. 7.2.2, if r_{ij} were given a characteristic libration frequency, $\cos\theta_i$ would become time dependent and the γ process more properly accounted for. The overall time correlation function for the reorientation of $e\mathbf{r}_{ij}$ would then be well-defined as $t \to 0$ (see Chapter 1). Certainly librational type absorptions in the far infrared should be observed for all the amorphous solids mentioned in this section as well as in the zeolites and clathrates, where the rototranslation of encaged molecules as opposed to rotation has been found to be all-important. It should be mentioned that in this type of theory we are not necessarily confined to molecular dipole autocorrelations since hopping occurs between different librating molecules. Naturally $\mathbf{r}_{ij}$ does not coincide with the molecular permanent dipole vector $\boldsymbol{\mu}_i$ in general.

7.2.1 Experimental Features for Some Viscous Liquids and Glasses

We have established that the broad band far infrared absorptions that go to make up the γ process are just the high frequency adjuncts of an evolution covering many decades. This is sketched in Fig. 7.2.1.1 in terms of $\mathfrak{A}(\omega)$, $\epsilon''(\omega)$, and $\epsilon''(\omega)/\omega$. It is a measure of the rotational motions of the molecules in the condensed phase but is an outcome of rototranslational dynamics. In this section we present a few of our results for rigid dipolar molecules in decalin at supercooled and room temperature, respectively. These are available at low temperatures (77–153°K) both in the 0.5 to 100 kHz region of the (α, β) processes and in the 20–200 cm^{-1} range of the far infrared. In Chapter 6 and later in Chapter 12 we review the literature fairly comprehensively for CH_2Cl_2, which is soluble in supercooled decalin, toluene-pyridine, and *o*-terphenyl. In Table 7.2.1.1 we summarize our available terahertz data and introduce as in Chapter 4 the torque factor (T_q) of the reduced moment of inertia (I_r) and the square of the far infrared absorption maximum ($\bar{\nu}^2_{max}$). This is a measure of the mean square torque on the solute (or probe) molecule. The data in Table 7.2.1.1 tend to fall into groups according to the shape of the solute molecule, as indicated by $I_r\bar{\nu}^2_{max}$. However, to some extent the peak positions are independent of solvents so that the molecules in dilute solution experience a "spherical force field." Table 7.2.1.2 summarizes some data in the viscous liquid and glass for various types of α, β, and γ processes, in decalin solvent, which is ideal as a medium because its dielectric loss is small throughout the whole frequency range from static to 220 cm^{-1} ($\sim 10^{13}$ Hz).

Three types of processes are generally discernible: (1) prominent (α, β) separation; (2) shoulder; and (3) absence of the β process. The factor $I_r\bar{\nu}^2_{max}$ indicates to what extent the mean square torque has increased in the glass for a given probe as compared with the equivalents in Chapter 4. For

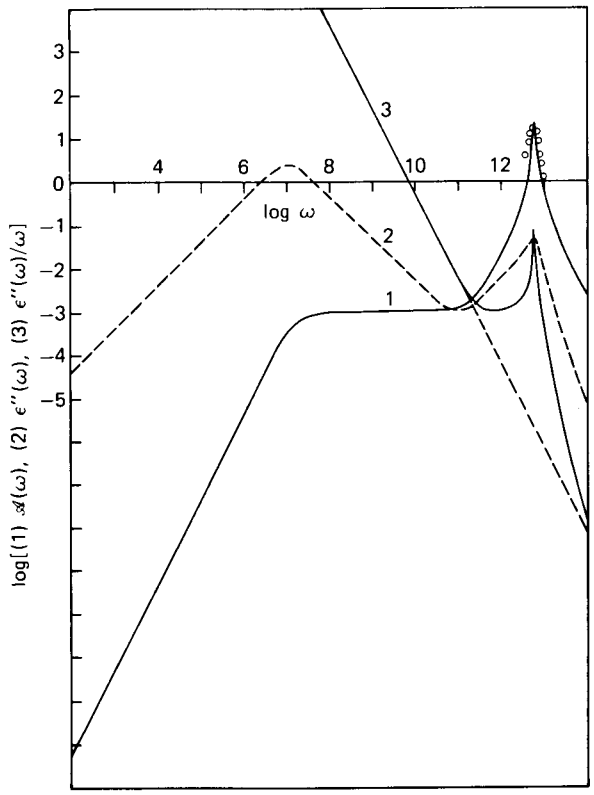

Figure 7.2.1.1 Schematic of the behavior of glassy $\mathfrak{A}(\omega)$, $\epsilon''(\omega)$, and $\epsilon''(\omega)/\omega$ on a log/log scale. [Reproduced by permission from C. J. Reid and G. J. Evans, *J. Chem. Soc. Faraday Trans. II* **75(9)**, 1213 (1979).]

the halogenobenzenes this is large initially and increases by only 50%. The fluorobenzene is slightly less hindered, which is commensurate with the observed low frequency "permittivity decrement" $\Delta\epsilon = [\epsilon_s - \epsilon'(\omega)]/[\epsilon_s - n^2] = 0.55$; that is, *this molecule can still relax fairly easily in the glass.* Toluene becomes appreciably hindered in the glass and yet still possesses a relaxation. Possibly the CH_3 rotation causes a large fluctuation of the hindering potential barrier rototranslationally. To a lesser extent this occurs for tetrahydrofuran. In these cases it is probable that a mechanism of hexad rotation predominates. By using the enthalpy values measured from the slopes in Fig. 7.2.1.2 and the moment of inertia for this C_n-axis we can estimate the terahertz libration frequency using the Brot–Darmon model described already. This produces the discrete set of frequencies recorded in column 2 of Table 7.2.1.2. These are high compared with the experimental value in chlorobenzene and fluorobenzene, but too low for tetrahydrofuran.

Table 7.2.1.1 Probe Molecules in Decalin at 298°K

Solute[a]	Moments of Inertia[b] (10^{-45} kg m^2)		Reduced Inertia (I_r)	$\bar{\nu}_{max}$ FIR peak (298°K)(cm^{-1})	10^{40} $I_r\bar{\nu}^2_{max}$ (gm)	Type
Bromobenzene	9.67	C_6	4.43	24	2551	
(Z = 1.63 Å)	8.2					
	(1.45)					
Chlorobenzene	6.83	C_6	3.05	33	3321	Planar
(z = 0.98 Å)	5.52					6 ring
	(1.45)					
Fluorobenzene	4.71	C_6				
(z = 0.44 Å)	3.24		1.92	39	2920	
	(1.45)					
Toluene	4.77	C_6	1.92	60	6912	Planar
(z = 0.46 Å)	3.25			(shoulder)		6 ring,
	(1.49)					bulky side
Nitrobenzene	8.98	C_6	3.90	40	6240	group
(z = 1.22 Å)	6.90					
	(2.1)					
THF	2.29	C_5	0.82	46 ± 6	1746	"Semirigid"
	1.32					5 ring
	0.91					
Furan	1.88		0.6	51	1560	Planar
	0.94					5 ring
	1.1					
Thiazole	2.58		0.83	45	1680	
	1.54					
	0.97					
CH_2Cl_2	0.26		0.23	54	670	
(approx. prolate	2.65					
symmetric top)	(2.8)					Small
Chloroform	2.53		1.26	28	992	ellipsoids
(oblate	2.53					
symmetrical	(5.0)					
top)						
CH_3CN	0.875					
(CCl_4 solvent)	0.875		0.437	73	2328	Almost
	(0.05)					linear
SCl_2	4.4					
	0.26		0.24	50	612	
	(3.82)					Small
CH_2Br_2	0.32					ellipsoids
	6.79		0.30	54	875	
	(6.9)					

[a] z is displacement of mass center from C_6-ring center.

[b] Moments of inertia are estimated from bond length data, bracketed value being that along dipole axis. I_r in same units.

Table 7.2.1.2 Probe Molecules in Glassy Decalin (107°K)

Solute in decalin	FIR Peak (cm^{-1})	Harmonic Model $\tilde{\nu}_{harm}$ (cm^{-1})	10^{40} $\Delta I_r \tilde{\nu}^2_{max}$ (gm)	Fraction Permittivity Decrement[a] (500 Hz)
10% bromobenzene	42	—	3.06	0.9
10% chlorobenzene	53	58 ($n = 6$)	2.58	0.82
10% fluorobenzene	57	60 ($n = 6$)	2.13	0.55
20% toluene	90	77 ($n = 6$)	2.25	0.65
10% THF	80	50 ($n = 5$)	3.02	0.6
5% furan	80	—	(2.46)	0.55
10% CH_2Cl_2	113	—	4.38	0.8
10% chloroform	51	45 ($n = 3$)	3.31	0.6
10% SCl_2	64	—	1.64	0.55
3% CH_2Br_2	105	—	3.78	0.72

[a]This is defined as $(\epsilon_s - \epsilon')/(\epsilon_s - \epsilon_\infty)$ (see text).

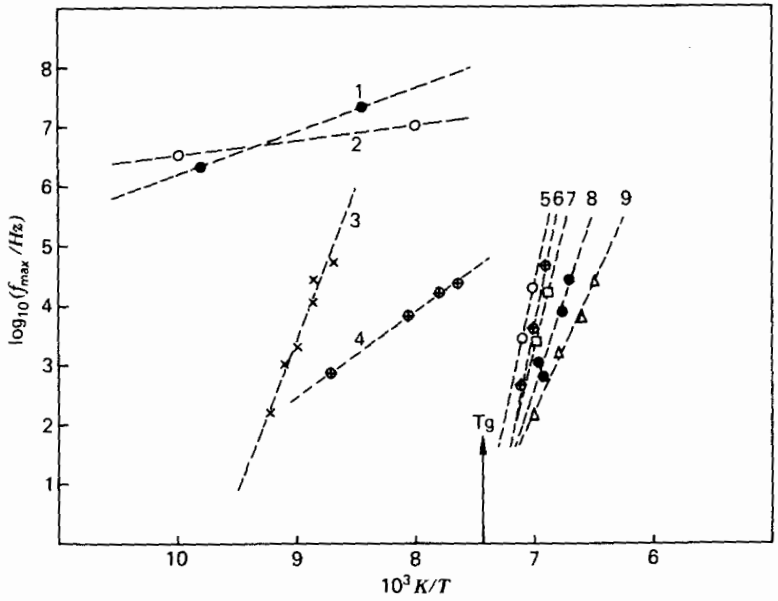

Figure 7.2.1.2 Activation energy plots for α and β processes observed in decalin (10% v/v solutions). (1) Fluorobenzene (β); (2) THF (β); (3) dichloromethane (β); (4) chlorobenzene (β); (5) THF (α); (6) chlorobenzene (α); (7) bromobenzene (α); (8) fluorobenzene (α); (9) 1 bromo-3-methylbutane (α). [Reproduced by permission from C. J. Reid and G. J. Evans, *J. Chem Soc. Faraday Trans. II* **75**, 1369 (1979).]

The high torque factor for furan, for instance, may be explained in that initially at 298°K this probe rotates easily within a decalin cage whose enclosure is larger than furan. As the sample cools the enclosure contracts. There is, however, still appreciable rotation in the glass. In Table 7.2.1.3 we compare some far infrared and dielectric data with those for two weakly dipolar glass-forming solvents, *o*-terphenyl, a large, planar type of molecule, and for a mixture of pyridine and toluene. Decalin, being nondipolar, is a poor solvent for intensely dipolar probes such as CH_3CN and pyridine at low temperature. Conversely, pyridine-toluene is good for weakly dipolar solutes. CH_2Cl_2 and fluorobenzene are compared in all three glasses. In *o*-terphenyl, fluorobenzene has a β peak but CH_2Cl_2 does not. The latter far infrared ($\tilde{\nu}$) peak is also relatively low at 103 cm^{-1}, implying less hindrance than in decalin. In pyridine-toluene there are no appreciable β relaxations in the glass (except that due to the solvent). The γ process has shifted a very long way to higher frequency in the far infrared for the CH_2Cl_2 solution compared with the position in the liquid at 298°K.

It is informative to compare the temperature shifts in the far infrared for dichloromethane in decalin and pyridine-toluene glasses. In decalin the shift was 4 cm^{-1} between 127 and 113°K, a change of 1 cm^{-1} per 3.5°K. This is mirrored in the overall shift from 58 to 110 cm^{-1} between 298°K and 113°K (i.e., 1 cm^{-1} in 3.5°K). The shift remains linear in the glass. In pyridine-toluene a shift of 3 cm^{-1} in 17°K is measured in the low temperature glass (1 cm^{-1} in 3.5°K), but the overall shift is from 62 to 148 cm^{-1} in 193°K. In the glass, the rate of shift is slowed, indicating that CH_2Cl_2 becomes very slightly hindered just below the glass transition temperature (T_g). The linear shift in decalin indicates the continued existence of the β process, which should not be modeled without its far infrared adjunct, the γ process. The nature of the problem may be seen in the fact that the peak sweeps across two decades of frequency in only 4°K, implying an activation enthalpy of 100 ± 15 kJ/mole. The peak also moves dramatically *but in the opposite direction* to the β peak. The two features will merge eventually as the envelope of the *free rotor* (gas phase) absorption in the far infrared. If we were to treat in isolation the γ peak, the physically meaningless result of negative Arrhenius enthalpy would lead us to suspect that this feature is only *a part* of the complete 0–THz evolution. The root mean square angular velocity for a freely rotating ensemble of gaseous CH_2Cl_2 is 21.2 cm^{-1}, so that the change in the far infrared peak frequency $\tilde{\nu}_{max}$ produced by a glassy environment is commensurate with that produced by condensing the infinitely dilute gas into the liquid at 298°K. At the same time the β part of the total loss moves from 180 GHz at 298°K to 5 kHz in the glass at 111°K. It is not possible to induce such large shifts even with the use of kilobars of external pressure!

The situation for CH_2Cl_2-decalin is summarized in Fig. 7.2.1.3. Superimposed on the data is a double loss peak calculated from the two-friction itinerant oscillator. This is a variant of the continued fraction applied to

Table 7.2.1.3 FIR Peak Comparisons for Three Organic Glasses (107°K)[a]

Solute	Decalin			o-Terphenyl			10/90 Pyridine + Toluene		
	FIR Peak (cm^{-1})	$\Delta I_r\bar{\nu}^2_{max}$	$\Delta\epsilon$	FIR Peak (cm^{-1})	$\Delta I\bar{\nu}^2_{max}$	$\Delta\epsilon$	FIR Peak (cm^{-1})	$\Delta I\bar{\nu}^2_{max}$	$\Delta\epsilon$
10% CH_2Cl_2	113	4.38	0.8	103	3.6	(0.8)	140	5.8	0.85
10% fluorobenzene	57	2.13	0.55	56	2.0	0.6	70	3.0	0.88
3% CH_3CN	—	—	—	90	1.52	—	120	2.7	0.85
10% pyridine	—	—	—	—	2.05	0.6	76	2.85	0.85
5% nitrobenzene	—	—	—	—	—	—	48	1.43	0.9
3% benzonitrile	—	—	—	—	—	—	74	—	0.9

[a] $\Delta\epsilon = (\epsilon_s - \epsilon')/(\epsilon_s - \epsilon_\infty)$, $\Delta I_r\bar{\nu}^2_{max}$ in units of 10^{-40} gm.

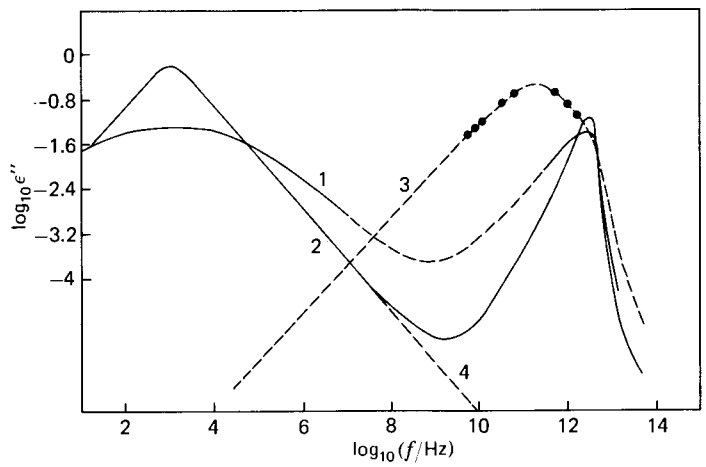

Figure 7.2.1.3 Complete spectrum of 10% v/v CH_2Cl_2/decalin; (1) experimental curve at 110°K; (2) itinerant librator (two-friction version) at 110°K; (3) experimental points (●) on the analytical curve at 300°K; (4) Debye process (no description of the γ peak possible). The defect diffusion model is a combination of these processes. [Reproduced by permission from C. J. Reid and M. W. Evans, *J. Chem. Soc. Faraday Trans. II* **75**, 1369 (1979).]

angular velocity. The concept of planar reorientation of a rigid cage in the glassy state is intuitively unacceptable but this does *not* mean that the phenomenological continued fraction is physically meaningless in this context. On the contrary, the attraction of the Mori formalism is its use for model classification, and it is clear that a variety of situations may be modeled by mathematical forms of the continued fraction type. We are in the "modeling stage" of condensed phase physics, *and a degree of intuition is always required.* The purpose of making the comparison in Fig. 7.2.1.3 is to demonstrate the path along which progress in this area must be made. This is to say that *any apparently successful formalism of liquid state molecular dynamics must also be capable of reproducing the complete* (β, γ) *or* (α, β, γ) *profile of the viscous liquid or glassy state of matter.* This is perhaps overstressing the obvious, but we wish to avoid (Chapter 6) the use of different models for different situations. Some loss curves of the (β, γ) type are illustrated in Figs. 1.2.8 and 7.2.1.4 for fluorobenzene and chlorobenzene in decalin glass. The breadth of the β process in these cases can be seen clearly in comparison with the far infrared γ peak. In Fig. 1.2.8*a* it is clear that at 143°K a 10% v/v solution of fluorobenzene in decalin reveals all three processes if a sufficient frequency range is used in the measurements. On the log/log scale used in that figure the γ process appears as the *least* affected by the enormous changes in viscosity in the 77–293°K range. However, a "blowup" of the far infrared region in terms of power absorption coefficient (Fig. 7.2.1.5) clearly shows the acute sensitivity of the γ process to changes in environment of this nature.

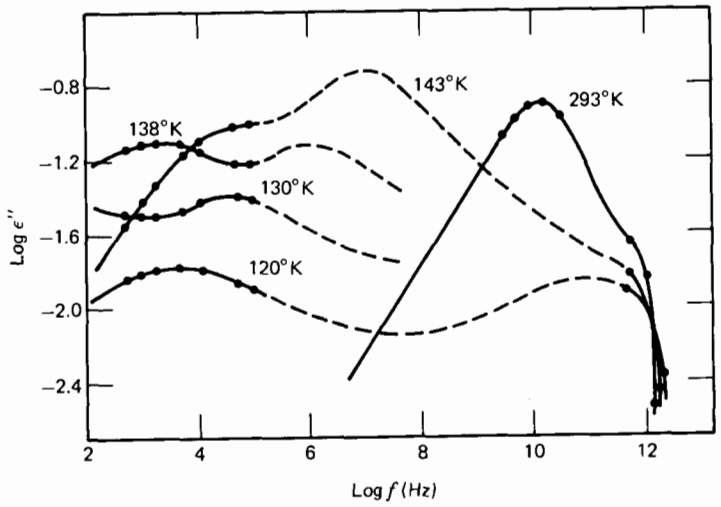

Figure 7.2.1.4 Multidecade loss profile of 10% v/v chlorobenzene-decalin at various temperatures in the liquid, supercooled liquid, and glass (120°K). [Reproduced by permission from C. J. Reid, Ph.D. Thesis, University of Wales (1979).]

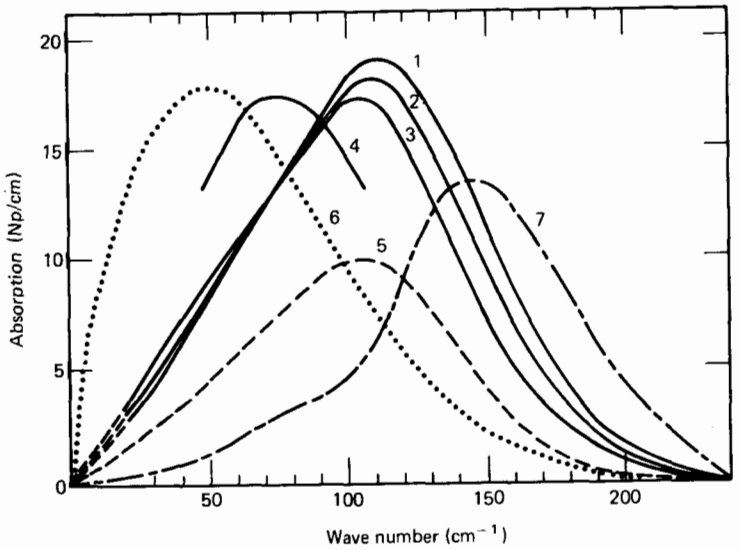

Figure 7.2.1.5 Far infrared spectra for CH_2Cl_2 systems. Variation with temperature of the far infrared γ process for CH_2Cl_2-decalin solutions. (1) 10% v/v CH_2Cl_2-decalin glass at 107°K; (2) 117°K; (3) 127°K; (4) 220°K; (5) 5% v/v solution at 110°K; (6) 10% v/v liquid solution at 293°K; (7) 10% v/v solution in 10% pyridine-toluene. In pyridine-toluene glass the γ peak shifts up to about 150 cm^{-1}. [Reproduced by permission from C. J. Reid, Ph.D. Thesis, University of Wales (1979).]

The extent of these changes can be gauged in comparison with the gas/liquid coexistence data of Gerschel (Fig. 1.2.3), by the effect on liquid chlorobenzene of kilobars of external pressure (Fig. 7.2.1.6), by crystallization (Fig. 7.2.1.7), by dilution (Fig. 3.4.4.1), and by a phase change in a nematic liquid crystal. The influence of viscosity is by far the most pronounced of all of these, and is summarized in (Fig. 7.2.1.8) across the glass transition temperature T_g.

The most involved evolution (of the (α, β, γ) type) is present in flurorbenzene and bromobenzene. At 143°K, the process peaks in the audio frequency region for the viscous liquid. It is interesting (Fig. 7.2.1.9) that bromobenzene does not exhibit a β process, in contrast to the fluoro derivative. The bulky bromo group evidently prohibits partial relaxation within the solute cage. The α peaks of fluorobenzene and bromobenzene disappear just below the glass transition temperature of 130°K, the β peak

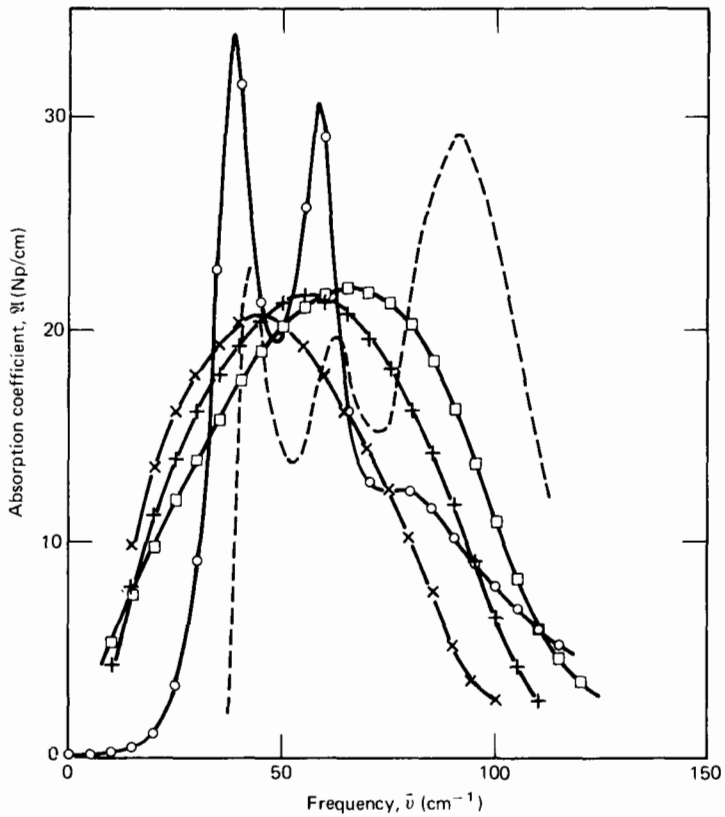

Figure 7.2.1.6 The effect of kbar of hydraulic pressure on the far infrared spectrum of liquid C_6H_5Cl. Curves ×, +, □, ⊙: Effect of increasing pressure. ---: Solid at low temperature. [Reproduced by permission from G. Chantry et al., *Nature*, **211**, 839 (1966).]

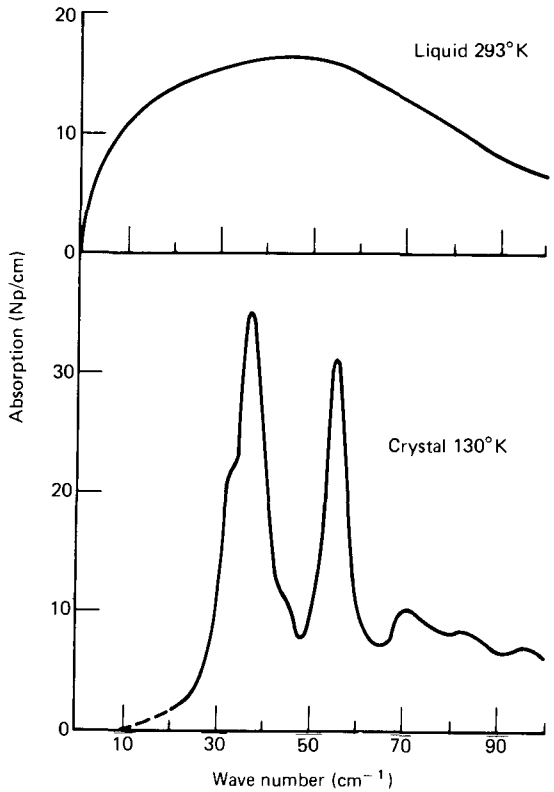

Figure 7.2.1.7 Far infrared absorption spectrum of liquid and polycrystalline chlorobenzene. [Reproduced by permission from Chantry, *Submillimetre Spectroscopy*, Academic Press, London (1971).]

surviving only in fluorobenzene. The high frequency γ peak of bromobenzene in the glass may therefore be considered as being due to libration in "potential wells" so deep that the molecules remain at the minima.

Only the smaller or very symmetrical solutes exhibit a β process. For fluorobenzene and tetrahydrofuran solutes the apparent activation enthalpy of the β process is similar to their values in the liquid state (ΔH = 10–15 kJ/mole). Dichloromethane is unusual in this respect with an enthalpy of 95 kJ/mole. In a solvent made up of smaller molecules (toluene, for example) the β process in CH_2Cl_2 *disappears*. These results are reflected in the behavior of the γ process in that solutes with no β peak have their γ peaks shifted by a factor greater than two in frequency, while systems with β peaks are less affected. The far infrared shift in fluorobenzene is 46% along the frequency scale and 108% in bromobenzene. Another striking example is CH_2Cl_2 in decalin and toluene solvents. In a 10% solution CH_2Cl_2 peaks at 53 cm^{-1} in decalin and 60 cm^{-1} in toluene. At 110°K the CH_2Cl_2-

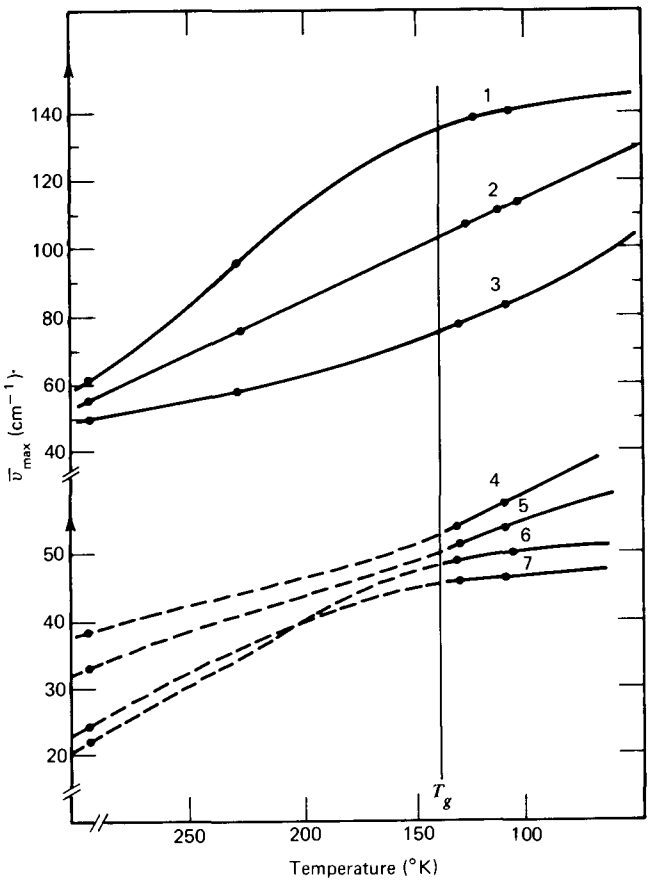

Figure 7.2.1.8 Variation of the γ peak position with temperature. (1) CH_2Cl_2-toluene; (2) CH_2Cl_2-decalin; (3) THF-decalin; (4) fluorobenzene-decalin; (5) chlorobenzene-decalin; (6) *tert*-butyl chloride-decalin; (7) bromobenzene-decalin. [Reproduced by permission from C. J. Reid, Ph.D. Thesis, University of Wales (1979).]

decalin system has a mean librational frequency of 113 cm^{-1} (an increase of 113%) whereas the CH_2Cl_2-toluene system peaks at 147 cm^{-1}, an increase of 145% on the cm^{-1} scale.

7.2.1.1 The Halogenobenzenes

It is convenient to take these as a group, because they represent many of the features of the viscous liquid/glass spectra in a coherent pattern. The absorption spectra of (10% v/v) fluoro-, chloro-, and bromobenzene solutions in decalin at 293°K peak at 39 cm^{-1}, 34, and 23 cm^{-1}, respectively. If these values are squared and multiplied by the respective reduced inertias (computed about axes intersecting at the center of volume as opposed to

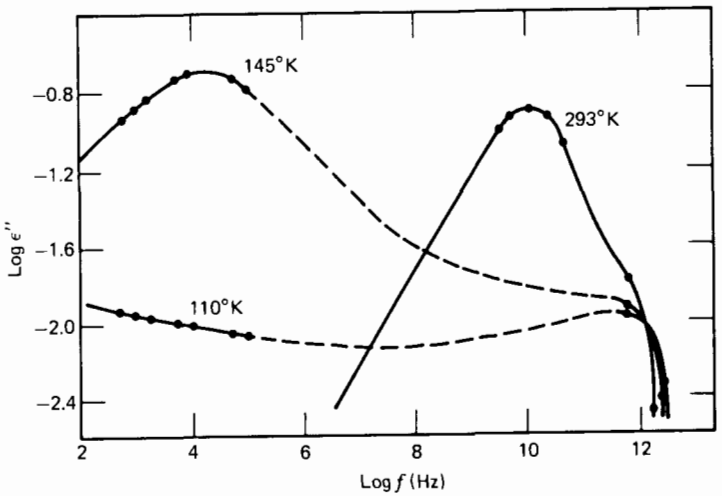

Figure 7.2.1.9 Multidecade loss profile of 10% bromobenzene in decalin over 12 decades. [Reproduced by permission from C. J. Reid, Ph.D. Thesis, University of Wales (1979).]

the inertial axes) the product $I_r\bar{\nu}^2_{max}$ is a measure of the mean square torque. This factor for C_6H_5F, C_6H_5Cl, and C_6H_5Br increases in this order, reflecting the increasing hindrance to rotation with increasing size of substituent group. For these same solutions in the homogeneous glassy state at 110°K the far infrared bands continue to exist and now all peak at higher wave number. There is a 46% increase for C_6H_5F (18 cm^{-1}), 56% for C_6H_5Cl (19 cm^{-1}), and 108% for C_6H_5Br (25 cm^{-1}). This variation is significant as we have already seen. In the spectra at 293°K the proximity of the Debye type *microwave* β peak distorts the γ bandshape significantly on the low frequency side, especially for C_6H_5F, which has a Debye relaxation time (Chapter 3) of 4 psec compared with C_6H_5Cl (10 psec) and C_6H_5Br (17 psec). In contrast, at low temperatures the bands are almost symmetrical owing to the vast difference between the peak frequencies of the β process. The far infrared integrated intensity cross section per molecule decreases significantly because of this shift to low frequencies and in some cases the lower frequency loss disappears.

In the audio frequency range (200 Hz to 100 kHz) at 148°K, some 12°K above the glass transition temperature, the spectrum takes the form of a broad band. This is the α process peak of about $3\frac{1}{2}$ decades width in C_6H_5F solution in decalin. As the temperature is lowered the band rapidly passes to lower frequencies as the β band appears from high frequencies. At the very lowest temperatures used (77°K), the β peak passes into the audio range, indicating that relaxation is still going on 60°K below T_g. The loss and permittivity are conveniently represented (Fig. 7.2.1.1.1) as constant

frequency curves of $\epsilon''(\omega)$ versus T and $\epsilon'(\omega)$ versus T and give some idea of the relative importance of the α and β processes. The intensity of the β process decreases with decreasing temperature or frequency so that at 148°K, the α and β intensities are much larger than those at 77°K. By determining the ratio of shift of peaks with temperature the activation energies may be found and we may reasonably extrapolate the loss curves to yield the complete spectra over 12 decades at a given temperature. The activation energy for the β process is 12 kJ/mole. The ΔH for the α peak at temperatures for which this quantity lies within the range of observation

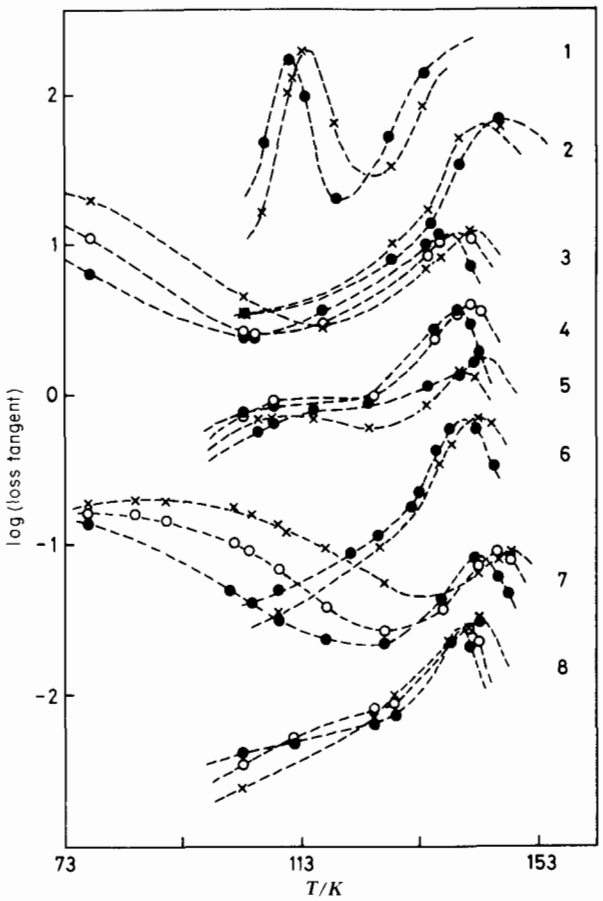

Figure 7.2.1.1.1 Loss tangents for decalin solutions at ● 50 kHz, ○ 5 kHz, × 500 Hz. (1) 10% v/v CH_2Cl_2 (raised by four decades); (2) 3% CH_2Br_2 (raised by four decades); (3) 10% THF (raised by three decades); (4) 20% toluene (raised by two decades); (5) 10% chloroform (raised by two decades); (6) 10% bromobenzene (raised by one decade); (7) 10% fluorobenzene (raised by one decade); (8) 10% chlorobenzene. [Reproduced by permission from C. J. Reid and M. W. Evans, *J. Chem. Soc. Faraday Trans. II*, **75**, 1369 (1979).]

is 90 kJ/mole (±15 kJ/mole). This is very large compared with that of the β peak (Fig. 7.2.1.2), and is also temperature dependent (see Section 7.1), which is indicative of a cooperative process.

Figure 1.2.8 illustrates the complete loss curve on a log–log scale for 10% C_6H_5F-decalin at four temperatures. At 293°K, the far infrared absorption becomes, in this loss representation, a slight shoulder on the main Debye loss peak in the microwave (50 GHz). With cooling the main *loss* peak broadens and at some temperature *above* 143°K (about 180°K where the linearly extrapolated ΔH plots intersect) separates into the α and β peaks, which shift at different rates to lower frequency with decreasing temperature. At 143°K the α peak is at audio frequencies, and the β peak is estimated to be at 10^8 Hz. At the glass transition temperature of 133°K the α peak lies probably below 1 Hz. To state that this process centers on zero frequency at and below T_g is probably an oversimplification and requires the assumption that T_g is a well-defined temperature for a given system where all large angle rotation ceases. The glass transition is rather a small range of temperatures over which the motions of solute and solvent molecules change from being cooperative at short range to highly cooperative over a long range. The presence of regions of low density of occupation (defects) in the solid may then permit further cooperative motions of the α type even below T_g (which is of course a macroscopic property). At 110°K the β process peaks at about 3 MHz but the γ process continues to exist in the 10^{12} Hz region; at 77°K the β peak is in the kilohertz region and is of reduced intensity. The intensity decrease of the loss indicates that ϵ_s is also falling, and implies a gradual freezing in of all large-angled motion.

The total loss spectra for the C_6H_5Cl-decalin solution differs in that the α and β peaks are not fully resolvable at 143°K but become so at lower temperatures because the enthalpy of activation for the α process is again six to seven times greater than that for the β process. At 120°K the β process is very low in intensity and is centered in the kilohertz range. The intensity is less than that of C_6H_5F. In C_6H_5Br-decalin the peak is absent (or else unresolved from the α process). At 110°K, except for possibly some slight relaxation at frequencies below 1 Hz, the only relaxation process that remains is the librational motions in the far infrared. The low intensity losses arising at this temperature in the kilohertz range are due mainly to impurity and inherent dc conduction.

7.2.2 Analysis in Terms of Mean Square Torque

We utilize the property that the γ peak frequency is proportional to the mean square torque (Γ^2) acting on the solute while $\log \omega_{\text{Debye}}$ is roughly proportional to $T/\langle\Gamma^2\rangle$. By considering the variation of $\bar{\nu}_{\max}$ with temperature we may also infer how the torque varies with temperature. We first consider how the α, β, and γ processes may be described within the concept of itinerant libration. In normal solution, each molecule has a mean

volume of occupation determined by the macroscopic density. A given solute molecule may be thought of as surrounded by a sphere of nearest neighbors, effectively a solvation cluster. Because at short range no molecule has a spherical interaction potential, there is an angular dependent force within the cluster urging the solute toward some position of minimum potential. This gives rise to the librational motion observed as the γ peak in the far infrared. The replacement of solvent molecules in the cage due to translational motion continually varies the position of the potential minimum so that the mean orientation of the librating molecule rotates in the laboratory frame. *Mathematically* we must assume that this process occurs in terms of a rigid annulus of perhaps six molecules cooperatively translating about the solute molecule. At low liquid densities or high temperatures replacement generally occurs faster than cooperative translation. In addition the solute molecule may independently surmount a given potential and arrive in another minimum. All three processes contribute in general.

As the liquid density increases with decreasing temperature the degree of translational motion decreases and the cluster becomes more permanent. At this stage cooperative translation is still possible but its rate will have slowed through greater (viscous) interaction with the environment and generally lower available energy. The central solute molecule may continue to "slip" with its cage as this pulsates, and this tends to become the faster process at these temperatures if the solute molecule is small compared with those of the solvent. In such a case the cage rotation gives the α process and the slip motion the β process. In the rigid, glassy phase, cage rotations degenerate to at most small-angled oscillation, so the α process relaxation advances rapidly to zero frequency and loses all its intensity. The process retains a constant rate of progress of $\log \omega_{\max}$ versus $1/T$ until the dimension of the cage is similar to that of the solute, whereupon solute molecules gradually become frozen in.

The mean square torque acting on the solute will have been increasing while the cage was contracting but now, on cessation of rotational, as opposed to librational, motion the rate of change lessens. Superimposed is the thermal effect, which lessens the torque as the temperature decreases. The overall variation of mean square torque with decreasing temperature will be to increase initially but thereafter to decrease at sufficiently low thermal energies. The C_6H_5F-decalin spectrum peaks at 39 cm^{-1} at 293°K and shifts with a slightly increasing rate to about 57 cm^{-1} in the glass. The $\bar{\nu}_{\max}$ of the C_6H_5Cl-decalin system shifts at an almost constant rate with temperature while C_6H_5Br and *tert*-butyl chloride clearly exhibit a slower rate of shift in the glass than in the liquid. Similar extremes of variation are seen for THF-decalin (increasing rate of shift in the glass), CH_2Cl_2-decalin (constant rate), and CH_2Cl_2 in a glass of toluene with 5% pyridine (decreasing rate of shift). This latter solution gives a very large overall shift from 61 to 140 cm^{-1} on cooling into the glass and does not show a β peak. It appears (Fig. 7.2.2.1) that torque curves with concave slopes (positive

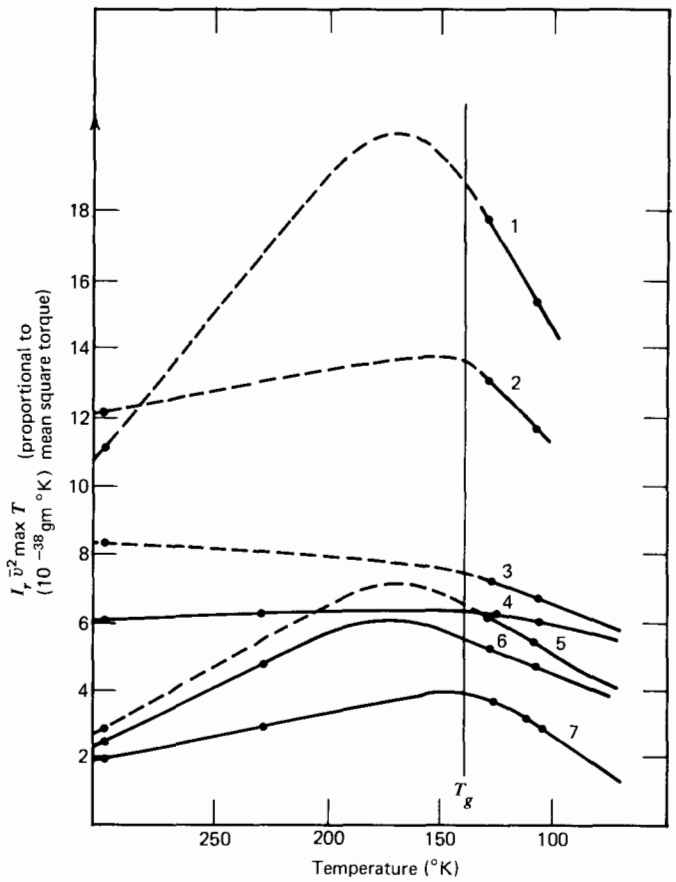

Figure 7.2.2.1 Estimated variation of mean square torque with temperature for several systems. (1) C_6H_5Br-decalin (no β peak); (2) C_6H_5Cl-decalin (small β peak); (3) C_6H_5F-decalin (large β peak); (4) THF-decalin (large β peak); (5) *tert*-butyl chloride-decalin (no β peak); (6) CH_2Cl_2-toluene (no β peak); (7) CH_2Cl_2-decalin (small β peak). T_g = glass transition temperature. [Reproduced by permission from C. J. Reid, Ph.D. Thesis, University of Wales (1979).]

second derivative), that is, THF and C_6H_5F, show β relaxation that persists with high frequency and intensity into the glassy phase. Those with convex shapes (C_6H_5Br-decalin, *tert*-butyl chloride-decalin, and CH_2Cl_2-toluene) do not. In those instances where the slope is fairly constant the β process is poorly resolved, if at all.

The mean square torques generally increase initially and reach a maximum at or before T_g. The fall in temperature causes a rapid increase of $\langle\Gamma^2\rangle$ on the C_6H_5Br molecule, for instance, which soon reduces the β intensity well before T_g. At T_g the cessation of the α (cooperative) process causes a drop in the value of permittivity to a value close to that of the

decalin solvent. The effect of cage contraction on C_6H_5Cl-decalin is less severe and appreciable β relaxation still remains in the upper temperature range of the glassy state. The effect of lowering the temperature in the C_6H_5F-decalin solution is to reduce $\langle\Gamma^2\rangle$. This is possibly due to preferential rotation of C_6H_5F about an axis perpendicular to the ring plane and therefore remaining almost independent of the cage contraction. Evidence for anisotropy of rotation in planar molecules is plentiful (Canet, 1972). Tetrahydrofuran-decalin also exhibits a negligibly small change of $\langle\Gamma^2\rangle$ with lowering temperature. Both C_6H_5F and THF therefore support intense β losses for several tens of degrees below the glass transition temperature.

A decalin solution of *tert*-butyl chloride and CH_2Cl_2-toluene are similar to PhBr/decalin, with all rotation (but not libration) ceasing at T_g. In contrast, CH_2Cl_2 in decalin has a curve similar to C_6H_5Cl-decalin. The lack of a β process for the CH_2Cl_2-toluene system is explained in that toluene solvent molecules are smaller, so that the cage of molecules around a solute molecule may contract sufficiently to prevent rotation of CH_2Cl_2, whereas for CH_2Cl_2-decalin, larger solute size allows a larger cavity for this rotation.

7.2.3 Some Applications of the Mori Theory

Having used the peak positions of the α, β, and γ losses we now consider the whole of the spectral profile in terms of itinerant oscillator parameters ω_0, Ω_0, β_1, and β_2. We have already illustrated a fitting of this nature in Fig. 7.2.1.3 for CH_2Cl_2-decalin at 110°K. The model has been tried and tested over an extreme range of "friction," including at room temperature a situation where the mean libration angle is about 1 rad (Fig. 1.7.4.1). The model has shortcomings, the main fault being an inability, in its simplest form, for producing more than two peaks in the 0–THz range. This is due to a vast oversimplification of the environment confronting any given molecule at any given instant. It is also overparameterized, in the sense that $\beta_1 = (kT/I_1)\tau_D$, where β_1 is the annulus/environment friction, I_1 the annulus moment of inertia, and τ_D the Debye relaxation time. If T is lowered, the cooperative nature of the rotation extends further from the solute molecule. This may be described either as an increase in β_1, the viscous drag on an annulus with constant I_1, or vice versa. The peak frequency of the β process ($1/\tau_D$) will be unable to discriminate. This redundancy is partly the reason why the itinerant oscillator seems to be successful.

Alternatively, application of the three-variable *orientational* Mori expansion of $C_u(t)$, used by Evans et al. and by Kivelson and Madden (Chapter 3; *not* the Mori type theory of Chapter 4) is unsuccessful in the viscous liquid and glass again because of the assumption inherent in this type of approach that the system is not perturbed by a strong potential (or arbitrarily strong driving field). The position (but never the breadth) of the β process can be reproduced in this context only by forcing the γ peak to a

near-delta function half-width. As mentioned already the remedy seems to involve coupling to the velocity field, and averaging over site environments.

7.2.4 Volume of Rotation

By assuming that an inpenetrable molecular surface can be defined, the simple argument of Chapter 4 can be used (Reid, 1979) to factorize the mean square torque $\langle \Gamma^2 \rangle$ into a solute-dependent part V, the volume of rotation of the solute, and (to a good approximation) the solute-independent part $P(0)$. This leads to a linear relation, for a given temperature and solvent, between the product $I_r \bar{\nu}^2_{max}$ and V^2. The molecular volumes of rotation of the solute, and (to a good approximation) the solute-independent (reciprocal) average formed for V. Such values are discussed in this section for a wide variety of glassy decalin solutions.

It is probably possible to predict to within about $\pm 10\%$ the $\bar{\nu}_{max}$ of any rigid solute molecule from its structure using extrapolations of the kind developed in Chapter 4, provided the value of $P(0)$ is known for the solvent and temperature considered, and provided suitable principal axes are chosen. Large or smaller $P(0)$ values are expected for different solvents, which may be found to depend on macroscopic solvent properties, viscosity or density, or the solvent molecular volume of rotation.

In the glass at 110°K a good correlation is obtained between T_g and V^2 when appropriate center of volume axes are chosen. The value of $P(0)$ is

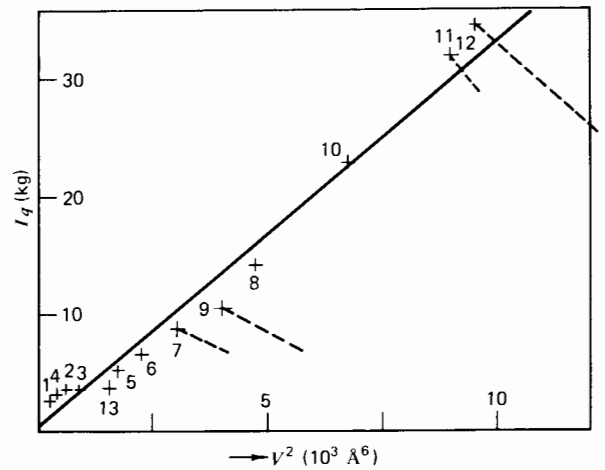

Figure 7.2.4.1 Plot of mean square torque against the volume of rotation squared for decalin glass solutions at 110°K (solid phase). Solid line, best linear line. (1) CH_2Cl_2; (2) chloroform; (3) furan; (4) pyridine; (5) THF; (6) fluorobenzene; (7) chlorobenzene; (8) toluene; (9) bromobenzene; (10) *o*-xylene; (11) 1-chloronaphthalene; (12) 1 bromonaphthalene; (13) *tert*-butyl chloride. [Reproduced by permission from C. J. Reid, Thesis, Univ. of Wales (1979).

identical with the room temperature value (Fig. 7.2.4.1), indicating that the overall mean square torque is identical at both temperatures, 110 and 293°K. If $P(0)$ is temperature independent then the observed increases in $\bar{\nu}_{max}$ with decreasing temperature are due to the $1/T$ dependency and not to changing mean square torque. The far infrared (γ) process of a large number of systems in decalin may be rationalized in terms of a single empirical parameter $P(0)$ representing the solvent interaction, and the methodology can be extended to other systems.

7.3 THERMODYNAMIC EQUILIBRIUM IN VISCOUS AND GLASSY MEDIA: COMPUTER SIMULATIONS

The formation of a glass is experimentally a kinetic process, and the structure and formation of certain glasses has been investigated by computer simulation. Glass formation in hard spheres is a purely kinetic phenomenon with no underlying thermodynamic second-order transition temperature ($T_2 < T_g$) being anticipated in the cooling behavior, in contrast to polymers. Indeed, molecular dynamics simulation of a 500-particle amorphous system of Lennard–Jones particles, used to study the glassy state by rapidly quenching an originally liquid sample, show that the resulting structural properties are those of random close-packed hard spheres, the resulting glassy state being able to support longitudinal and transverse phonon modes at short and long wavelengths, respectively. The strength of computer simulation in this area is that the rapidity of crystal nucleation in pseudospherical molecules presents no special difficulty. The phenomenon of freezing is not normally observed in Monte Carlo or molecular dynamics calculations owing to the short time and small sample size available. Consequently, when a computer run is "quenched," by suddenly dropping the temperature, the resulting system is a highly viscous liquid or an amorphous glass where the reference particle is constrained strongly in such a way as to prevent its center from moving far from its momentary position.

The process of self-diffusion is characterized by the time dependence of the mean square displacement and the velocity a.c.f. $\langle \mathbf{v}(t) \cdot \mathbf{v}(0) \rangle$. There is a characteristic time during which a particle is caged in by its neighbors, allowing a mean square displacement commensurate with the structure of the radial distribution function. The asymptotic behavior of the mean square displacement indicates an extremely viscous fluid with a diffusion constant that is very small indeed (about four orders of magnitude smaller than that near the triple point). In a glass in thermodynamic equilibrium, therefore, the value of D is nonzero; the velocity a.c.f. is detailed at short times but goes to zero very rapidly thereafter. The computer results are especially interesting when dealing with collective motions, and when dealing with transverse phonon modes, unique. Rahman and co-workers

have studied the spectra of mass and current densities given by

$$\rho(\mathbf{k}, t) = N^{-1/2} \sum_{j=1}^{N} \exp[i\mathbf{k} \cdot \mathbf{r}_j(t)]$$
$$\mathbf{v}(\mathbf{k}, t) = N^{-1/2} \sum_{j=1}^{N} \mathbf{v}_j(t) \exp[i\mathbf{k} \cdot \mathbf{r}_j(t)] \tag{7.3.1}$$

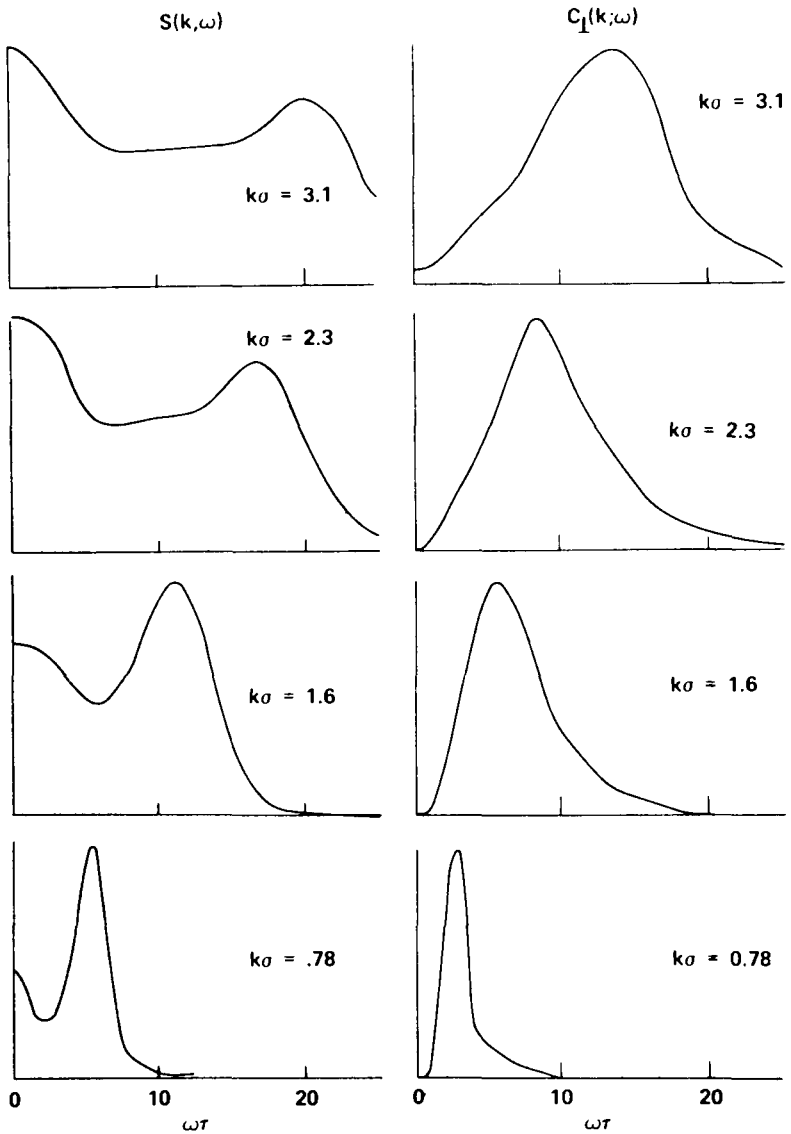

Figure 7.3.1 Scattering functions and transverse current correlation functions for a computer-simulated glass. [Reproduced by permission from A. Rahman et al., *J. Chem. Phys.* **64**, 1564 (1976).]

where $\mathbf{r}_j(t)$ and $\mathbf{v}_j(t)$ are particle positions and velocities. The spectrum is then, for example,

$$S(\mathbf{k}, \omega) = \frac{1}{2\pi} \int_{-\infty}^{\infty} \langle \rho(\mathbf{k}, s)\rho(-\mathbf{k}, t + s) \rangle \cos \omega t \, dt$$

We can show that $\omega^2 S(\mathbf{k}, \omega)$ is the spectrum of the fluctuating *longitudinal current*, and we may similarly define a spectrum of current fluctuations normal to $\mathbf{k}$, that is, $C_\perp(\mathbf{k}, \omega)$.

The spectra $S(\mathbf{k}, \omega)$ and $C_\perp(\mathbf{k}, \omega)$ (Fig. 7.3.1) evidence propagating density fluctuations or *phonons* which have a lifetime decreasing approximately as $1/k$. In the hydrodynamic limit these decrease as $1/k^2$. This behavior is in marked contrast to that observed in the region of the triple point. For example, $C_\perp(k, \omega = 0)$ is zero so that the system is stable against a shear strain, that is, *can support shearing*. The long time tail in the velocity a.c.f. is far too small to be observable owing to the very high viscosity, but doubtless the orientational a.c.f.'s would show pronounced features of this type.

The full discussion of equilibrium phase diagrams is outside the scope of this book but we mention that Rahman and others have conducted some isochoric heating and cooling runs on 108 particles. An abrupt devitrification was observed on heating. Under the same conditions a crystal would not melt until heated to a higher temperature. The radial distribution shows no substantial change. At a lower density the computer system devitrifies at a much lower temperature and at a higher density the glass transition seems to be continuous. With very slow rates of cooling it is possible to crystallize a supercooled Lennard–Jones fluid, and in this way it is useful to regard the molecular dynamics technique as a guide for differentiating between the glass and crystalline solid by reference to molecular dynamics. A nucleation event is sketched in Fig. 7.3.2, the sample becoming crystalline if the following are met:

1. There is an apparent complete absence of diffusion.
2. There are resolved second, third, and fourth neighbor peaks in the radial distribution function (McDonald and Hansen, 1976).
3. The *structure factor*

$$s(\mathbf{k}) = \left| \sum_j e^{i\mathbf{k} \cdot \mathbf{r}_j} \right|^2$$

is of order N^2 with small relative fluctuations for particular vectors. Here N is the number of particles used in the simulation.

The entire freezing event (Fig. 7.3.2) takes only 10^{-11} sec. The most obvious difference between glass and crystalline solid is that in the former the center of mass diffusion constant is *still finite*, whereas in the latter case

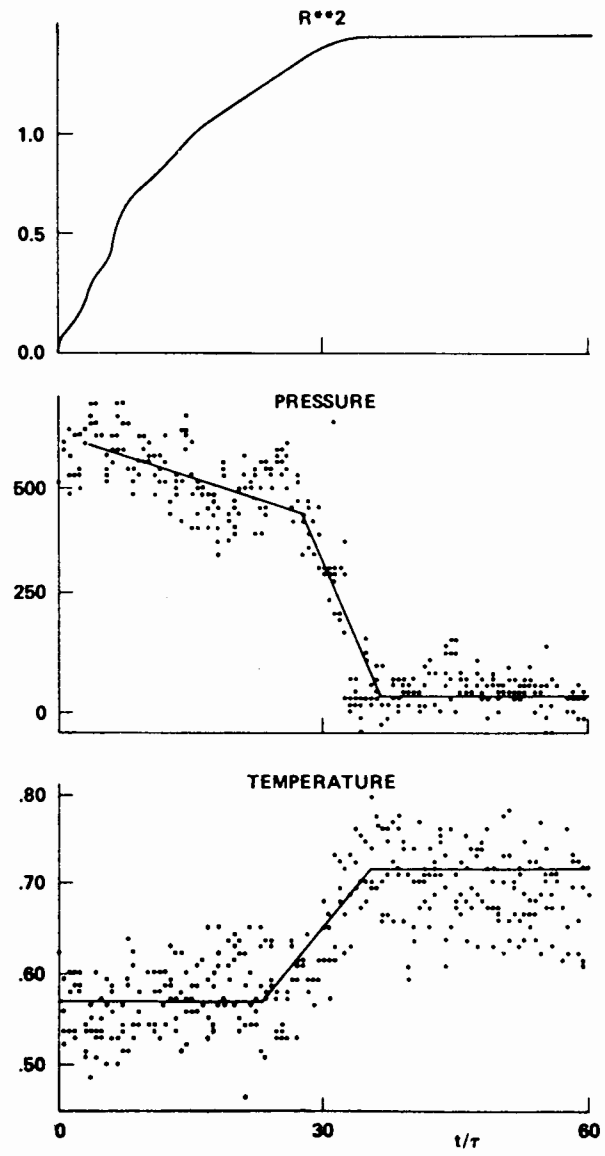

Figure 7.3.2 Temporal development of mean square displacement, pressure, and temperature during crystallization. Molecular dynamics simulation. [Reproduced by permission from Mandell et al., *J. Chem. Phys.* **64**, 3699 (1976).]

(if crystallization were complete), the pressure would drop to zero and all diffusion cease. If crystallization is incomplete the pressure remains finite and the intermediate structures exhibit a *highly non-Gaussian* self-diffusion process with diffusion coefficients an order of magnitude less than that for the liquid. The radial distribution function has shoulders rather than well-defined peaks in this case. If this state is cooled further the

self-diffusion shows rapidly and the second and fourth neighbors' peaks become well-defined. Under these conditions vacancy diffusion is the dominant mechanism of molecular movement.

The computer simulations corroborate the experimental finding that liquid chracteristics are not affected in any apparent way by the condition of metastability. Further, these investigations are just as relevant to the elucidation of the nature of the fluid state as studies of the liquids in the fully stable regime. The computer can be used to simulate glass transitions for simple "molecules" such as hard spheres. These results essentially support the theoretical idea that vitrification is a "kinetic effect"; that is, a substance becomes glassy *when its free volume decreases to a critical value.* This is in broad accord with the results of Reid, quoted in the preceding section. The difficulty is to reconcile this idea with the pressure dependence of the normal glass transition temperature T_g.

Vitrification has also been described in terms of the loss of configurational entropy, in order to explain some experimental results when various curves of equilibrium data were extrapolated to lower temperature to determine what thermodynamic properties would be observable if a liquid could be cooled sufficiently slowly to remain in metastable equilibrium to temperatures below T_g. Energy, enthalpy, entropy, and volume appear on extrapolation to become *smaller* than the corresponding values in the crystalline state. The second-order transition temperature T_2 is that where the configurational entropy S_c (the excess entropy of the liquid relative to that of the crystal) vanishes. In a purely kinetic interpretation of T_g, T_2 has no particular meaning.

For simple liquids, however, the free volume and configurational entropy are related, and in the ultimate case of hard spheres it is possible to investigate by molecular dynamics whether abrupt changes in apparent thermodynamic properties occur over a relatively small temperature range (T_g). The existence of T_2 may be investigated by calculating the configurational entropy as a function of temperature at constant pressure, for simulated hard spheres confirm the presence of abrupt changes and the isothermal compressibility and thermal expansion decrease at the apparent glass transition from the equilibrium liquid to the glass. The extrapolated configurational entropy does not become small relative to the entropy of fusion, and consequently it is not possible for $T_2 \geq 0$; that is, there is no second-order thermodynamic transition.

It must always be remembered when dealing with computer simulations of glasses that the cooling rate of the simulator is many orders of magnitude greater than that achievable in reality. The cooling rate used by Rahman and co-workers was, for example, 7×10^{12} deg/sec! For nonsimple liquids in the laboratory glass formation occurs even with very slow cooling rates, and may be thought of as a consequence of a dramatic increase in relaxation times near T_g. This is correlated with the system's rapidly decreasing configurational entropy. In order to avoid these quenching difficulties Evans et al. (1980) have simulated by computer molecular

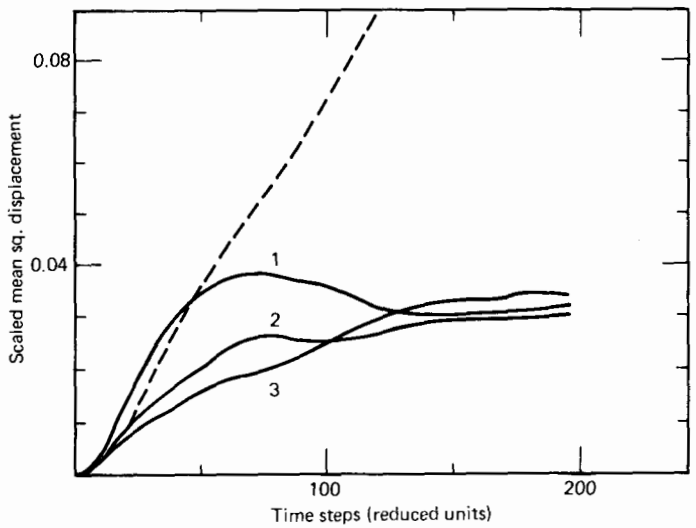

Figure 7.3.3 Mean square displacements in a high temperature, high pressure glass for various diatomics. Computer simulation. (1) Interatomic distance = 0.2 (in reduced units). (2) Interatomic distance = 0.329 (N_2). (3) Interatomic distance = 0.4. Itinerant librator, from a fitting of the force a.c.f.

dynamics the molecule N_2 and similar (but unreal) diatomics in the amorphous state brought about by the use of high temperatures and very high pressures. This is the opposite pole of the supercooled condition and very difficult indeed to study in the laboratory, particularly when fragile spectroscopic window material is a prerequisite. Nevertheless the results are strikingly similar with regard particularly to the behavior of the mean square displacement (Fig. 7.3.3) and the short time behavior of various a.c.f.'s, which is oscillatory. Again there are signs (not surprisingly, because of the logjamming at these extremes) of violent non-Gaussian behavior in the moments of the mean square displacement (Fig. 7.3.4).

In a system such as this we are dealing with a metastable solid state induced by kilobars of external pressure at a temperature beyond the normal melting point. It is possible to attempt to fit the dynamics in this kind of glass with the itinerant librator. The method adopted is to least mean squares fit the force correlation function (Fig. 7.3.5) and then use the optimized parameters to describe analytically the other simulated functions. This procedure clearly overestimates the rate of diffusion because the analytical mean square displacement develops much too rapidly (Fig. 7.3.3). The simulated functions for various diatomics (ranging from spherical to prominantly dumbbell) behave very similarly to those simulated by Rahman et al. in the quenched, low temperature glass. In both the high temperature and low temperature glass the rate of diffusion is much smaller than that in the liquid. The simulated mean square displacement in both

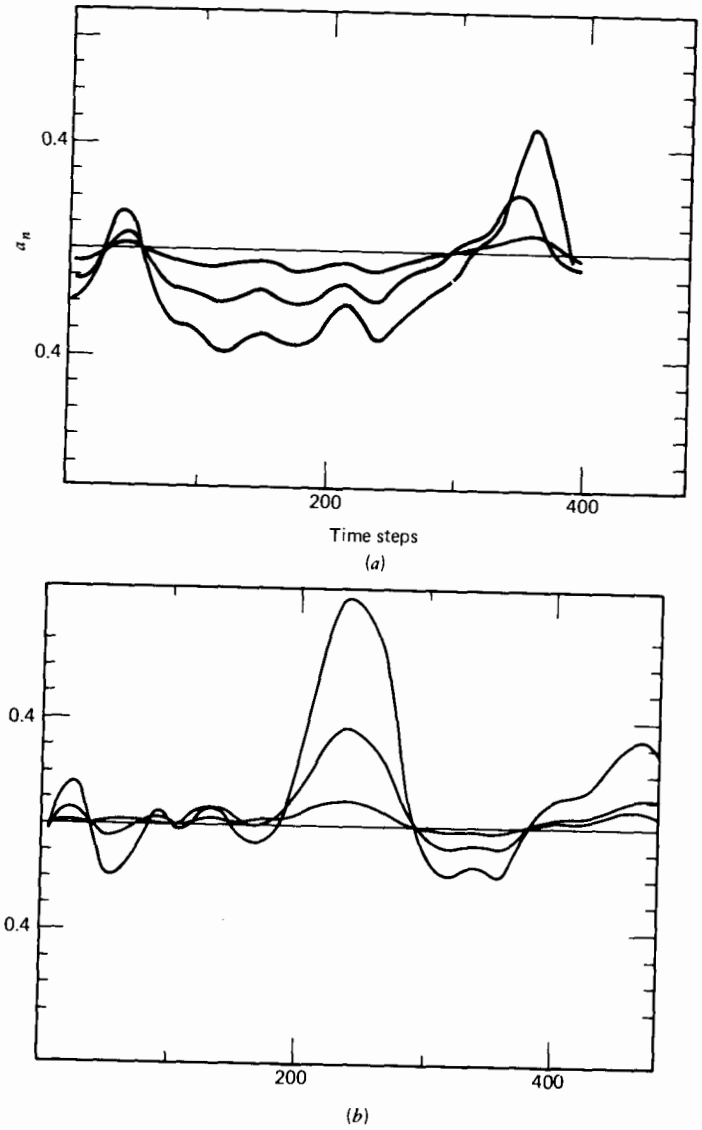

Figure 7.3.4 Non-Gaussian nature of the high temperature glass. Each $a_n(t)$ should be zero for gaussian statistics. (*a*) $n = 2, 3, 4$, $L^* = 0.200$; (*b*) $L^* = 0.3292$.

types of glass flatten out, in marked contrast to the result for Brownian motion, where the function is proportional to t (as it is also in the itinerant librator). The non-Gaussian nature of the high temperature glass is illustrated in Fig. 7.3.4 in terms of moments of the force correlation function. The constant long time limits of Gaussian statistics are reached, with difficulty, if at all, for both the second and fourth moments of velocity and

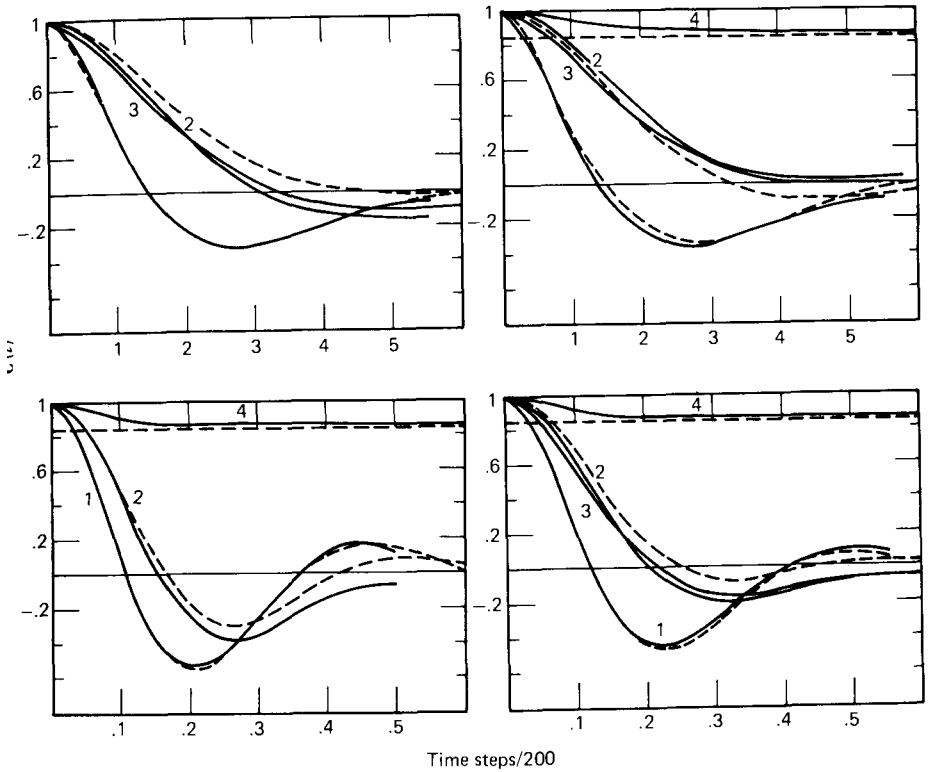

Figure 7.3.5 In figure (*a*) where the interatomic distance $L^* = 0.1$, the curves represent the following: Solid lines: (1) atom–atom simulation of the force a.c.f. $C_F(t)$ for a reduced interatomic separation $L^* = 0.1$, (2) simulated velocity a.c.f.; (3) simulated direction of velocity a.c.f.; (4) simulated speed a.c.f. The horizontal line is at $8/(3\pi)$. Dashed line: (1) least mean squares best fit of the itinerant librator to the simulated $C_F(t)$; (2) $C_v(t)$ calculated theoretically for curve 1 (dashed). (*b*) The same for $L^* = 0.3$; (*c*) $L^* = 0.5$; (*d*) $L^* = 0.7$. [Reproduced by permission from G. J. Davies et al., *J. Mol. Structure* **46**, 395 (1978).]

force. The effect of molecular elongation in the high temperature glass is pronounced (Fig. 7.3.5), but even for almost spherical shapes the mean square displacement becomes a plateau at a very low value. Finally it is clear that a.c.f.'s such as those of molecular speed must be conserved well in any type of system (decaying to only $8/(3\pi)$ of their initial value), but even here there is a discernible effect of elongation on the molecular dynamics, the decay of the speed functions being oscillatory and faster the longer the molecule. The mean square force (both model and simulated) increases steadily as the molecule is elongated (Fig. 7.3.6). Using simulations such as these it would be useful to test out directly some assumptions made about the "local states" in a glass (both high temperature and low

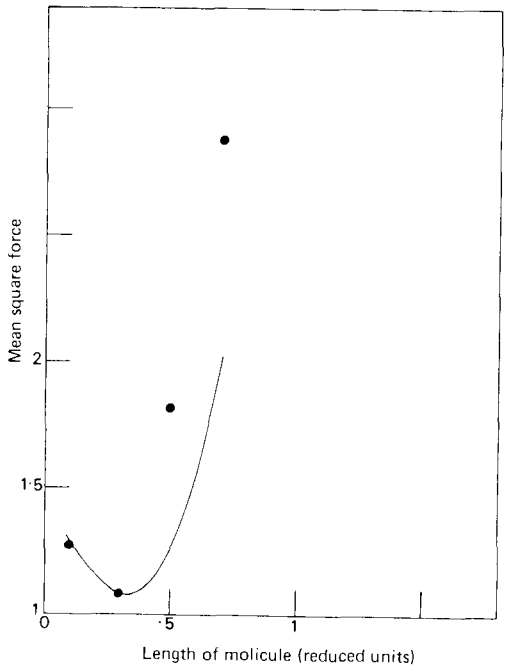

Figure 7.3.6 Plot of simulated (———) and calculated (●) mean square force, itinerant oscillator model. [Reproduced by permission from G. Davies et al., *J. Mol. Struct.* **46**, 395 (1978).]

temperature). The most straightforward method is of course to build up a stereoscopic picture in three dimensions using transparencies as in X-ray analysis. The solidification by pressure of a simple liquid such as chlorobenzene certainly leads to oscillatory behavior at short times in the angular velocity correlation function, and the resulting vitreous solid is an example of a high temperature glass where dielectric relaxation is still possible. Very few studies of these glasses have been made, owing to the kilobars of external pressure needed for solidifying the liquid at ambient temperature. It would be interesting to see if in addition to the clearly observable γ process (Fig. 7.2.1.6) there also appear low frequency α and β relaxations as in the low temperature glass. In this context pressure studies on liquids along the whole of the 0–THz range would be very revealing as to the role played by configurational entropy and free volume. These experiments have the advantage that they are *not* limited to systems where supercooling is easily achievable and can be carried out on CH_2Cl_2, a simple enough asymmetric top for exactly parallel computer simulation (Chapter 12). The resulting data would naturally defy any drastic oversimplification such as modelling the process by the itinerant oscillator.

7.4 DEPOLARIZED LIGHT SCATTERING AND KERR EFFECT RELAXATION IN VISCOUS LIQUIDS AND GLASSES

These techniques prove revealing when used in conjunction with 0–THz spectroscopy and molecular dynamics simulation. The cross correlation of the rapidly increasing bulk of data will be beneficial. The interrelation of these techniques demands a broadly based theoretical treatment such as that described in Chapter 1. The topic of light scattering and molecular dynamics is the subject of a fine monograph by Berne and Pecora (1976), and in this section and in the appendix we wish to deal with the subject from the point of view of 0–THz spectroscopy and to concentrate almost exclusively on depolarized Rayleigh band shapes. The relaxation of the Kerr effect provides us with information, in combinational form, on the dynamics of both molecular dipole moment and the polarizability tensor.

In the viscous liquid just above T_g the intensity of depolarized scattered light is split into a doublet appearing either side of the lowest attainable frequency shifts away from that of the incoming laser light. The appendix to this chapter is devoted to a critique of the different Mori type formalisms used for its explanation. Broadly speaking, the split is explained by propagative transverse modes (discussed in the opening to Chapter 5) supported by the ability of the viscous liquid to shear. There is a close relation between the depolarized Rayleigh scattered intensity spectrum and the 0–THz spectrum. We emphasize this in the next section.

7.4.1 Comparison of Depolarized Rayleigh Intensity and Permittivity

The discussion here is not rigorous and the interested reader is referred to Berne and Pecora for more detail on the intensity of scattered light. The depolarized light scattered from molecules with an anisotropic polarizability is related in the simplest case to the second Legendre function of the orientational correlation function, while the permittivity over 12 decades or so is related to the first. Simply speaking we may write the intensity of the scattered light as

$$I(\omega) \propto (\alpha_{\parallel} - \alpha_{\perp})^2 \int_{-\infty}^{\infty} dt \, \exp(-i\omega t) C_u^{(2)}(t)$$

where

$$C_u^{(2)}(t) = \langle P_2[\cos\theta(t)] P_2[\cos\theta(0)] \rangle$$

Here ω is the angular frequency shift of the scattered light, $\theta(0)$ and $\theta(t)$ are the angles between the axis of the molecule and the direction of the incident electric field at times 0 and t, respectively. $P_2(\cos\theta)$ is the second Legendre polynomial. $\alpha_{\parallel}$ and $\alpha_{\perp}$ are polarizability tensor components for the symmetrical top. With full quantum corrections (Chapter 3) the 0–THz

"equivalent intensity" to $I(\omega)$ is, forgetting about the effect of the internal field,

$$A(\omega) = \frac{\mathfrak{A}(\omega)}{\omega[1 - \exp(-\hbar\omega/kT)]} \propto \mu^2 \int_{-\infty}^{\infty} dt \, \exp(-i\omega t) C_u(t)$$

so that $I(\omega)$ and $\mathfrak{A}(\omega)$ are qualitatively similar. In fact these workers have gone so far as to propose $\mathfrak{A}(\omega) \propto I(\omega)$ in certain cases. If we express the depolarized Rayleigh data in the form $\omega^2 I(\omega)$ we should obtain a form very similar to the far infrared power absorption coefficient $\mathfrak{A}(\omega)$. The resulting function behaves very similarly to $\mathfrak{A}(\omega)$ as the glass transition temperature is approached. Heuristically we can say that $\mathfrak{A}(\omega)$ reflects the same kind of shearing phenomenon as does $\omega^2 I(\omega)$. Furthermore it is possible to say that both $C_u(t)$ and $C_u^{(2)}(t)$ are affected by rotation/translation coupling (Chapter 5). In Section 7.2 we have already seen that defect diffusion is related to dilatation and shear and it seems that before long a unifying theory will emerge. In the $\mathfrak{A}(\omega)$ representation we present some data for viscous halogenobenzenes over the complete 0–THz range in Fig. 7.4.1.1. In future such features might well be discernible in $I(\omega)$ measured very close to the exciting line. There seems to be no a priori reason why the viscous liquid state should be considered for the purposes of light scattering as a medium capable of supporting shear, and for the purposes of 0–THz spectroscopy as a suspension of relaxing defects. These techniques may probe different parts of the species under investigation, but the overall dynamic structure

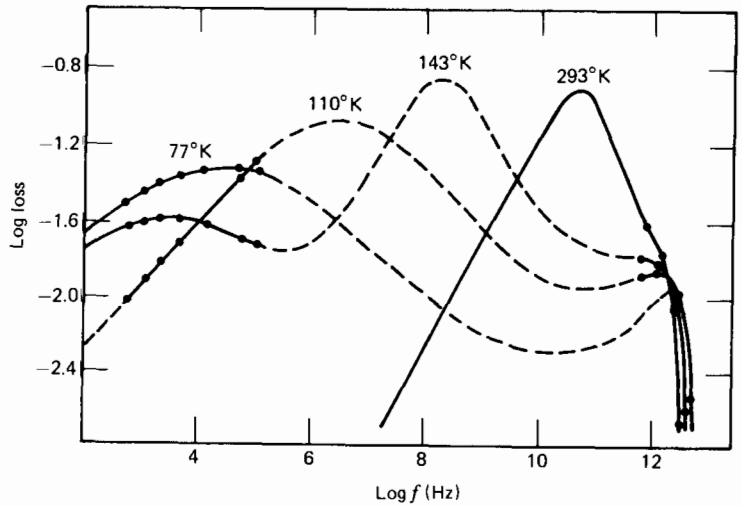

Figure 7.4.1.1 Zero to terahertz loss spectrum for 10% v/v fluorobenzene in decalin representation for halogenobenzene-decalin solutions over the complete 12 decade frequency range. Depolarized light scattered with intensity $I(\omega)$ should resemble this function.

must be recognizably the same. The important question is whether the dipole unit vector $\mathbf{u}(t)$ and a component of the polarizability tensor can be coupled within the column vector A to the same type of collective variables. Some of these are discussed in the appendix.

7.4.2 Kerr Effect and Low Frequency Dielectric Relaxation

This is almost exclusively the work of Williams and colleagues (1977) for solutes in *o*-terphenyl, and for pure liquid tritolyl phosphate and its mixtures with *o*-terphenyl in an attempt to define the mechanism for the α relaxation in these and other glass-forming systems. The transients of the Kerr effect relaxation are discussed again in Chapter 8 in the context of pretransition behavior in liquid crystals. It is helpful to make a comparison of the characteristic times of the Kerr decay transient (τ_{Kerr}) and the inverse of the main loss peak of the 0–THz frequency range (τ_D). For various models the ratio $\tau_{\text{Kerr}}/\tau_D$ is significantly different, ranging from $\frac{1}{3}$ for rotational diffusion to 1 for well jumping of the Ivanov type. There is an obvious need to accommodate the Kerr effect theory within the context of the Mori continued fraction, which, as we have seen in Chapter 3, is capable of covering both these extremes.

Experimentally, for the fluorenone-*o*-terphenyl system the rise and decay Kerr transients were equivalent at a given temperature. They are characterized by the same broad relaxation function and the *same* relaxation time as that obtained from the dielectric region. Williams et al. interpret this as being due to defect diffusion. However, it is much more likely to be a symptom of the uncertainties inherent in both experimental techniques in the sense that both monitor collective fluctuations which are forgotten in a one-molecule theory, that is, when A contains only **u** or alternatively an angular velocity of some type. Rotation/translation coupling is probably pronounced and contributing to the data in both cases; that is, the orientational density is coupling to the transverse velocity field (in the language of hydrodynamics).

Clearly the comparison of Kerr effect relaxation and low frequency dielectric data, both over a restricted frequency range, is relatively unfruitful *in the absence of high frequency data*, such as those which characterize the γ process, the wings of $I(\omega)$, or those simulated by molecular dynamics. It is inadmissible to evaluate any type of theory using low frequency data alone when a wealth of results is already there from the high frequency experiments. Kerr effect relaxation is useful in specialized cases, such as the investigation of pretransition effects in liquid crystals, but is so far limited in scope, since it gives, as does incoherent neutron scattering from liquids, too much information on the rise transient (and too little on the decay). Some well-known contributory second- and multi-order sources of uncertainty in Kerr effect experiments are discussed fully by Bordewijk and Böttcher (1979).

The intercomparison of experimental data can therefore be fruitful but also misleading and (Chapter 6) confusing.

APPENDIX: MODE–MODE INTERACTION AND DEPOLARIZED LIGHT SCATTERING

This appendix is based on the excellent review of developments in this field by Searby et al. (1978). These workers have shown that many of the apparently different theories in this area lead to the same, or very similar, analytical forms for the intensity $I(\omega)$. This means that if experiments are not carried out over a wide enough range of conditions the data from depolarized light scattering cannot discriminate between the theoretical models. It would, of course, be sensible to use this technique as one experimental probe amongst many.

Theoretical Approaches

Depolarized scattered light contains information about the so-called "anisotropic fluctuations" in a molecular fluid which are dependent on reorientations. Leontovich et al. (1967) were the first to predict that the shape of the intensity $I(\omega)$ might be affected by overdamped transverse shear waves. Under certain conditions (such as in the viscous liquid) this results in a dip at close to zero frequency (or what *appears* on a linear scale to be close to zero frequency). If it were possible to obtain data to within kilohertz of the exciting line then the (α, β) equivalent process might be uncovered.

Viscoelastic theories, such as those of Rytov (1958), start from the assumption of a frequency-dependent shear modulus coupling stress and strain tensors. This produces a line shape which reflects the modulation of the strain tensor by shear and longitudinal waves.

There have been numerous theories based on the Mori equations given in Chapter 1. Searby et al. discuss their outward difference and fundamental similarity. The approach is similar to that of Kivelson and Madden described at the end of Chapter 3. Usually the method is to search for variables with which the fluctuating *dielectric tensor* (Berne and Pecora, 1976) can be treated inside the column vector $\mathbf{A}_0$. The primary variable is a tensor describing the orientation characteristics *on the molecular scale* (e.g. the polarizability tensor). The primary variable or variables are then mixed with one or more secondary variables, usually a *momentum density tensor* (current density, Eqn. 7.3.1). Various authors choose different primary and secondary variables. However, owing to the structure of the Mori equations the theories eventually give the same result. The analytical dependence of $I(\omega)$ on ω differs only in that the constant terms have different physical meaning. This is an unsatisfactory state of affairs brought about because the seemingly simple

geometrical shape of $I(\omega)$ can be reproduced analytically in a variety of ways. The very opposite is true of the far infrared power absorption coefficient $\mathfrak{A}(\omega)$, and it might be advantageous to construct a variety of mode–mode theories for 0–THz spectroscopy. It is noticeable that Ailawadi and Berne (1971) have produced a theory which is different in that there are two primary variables, angular momentum and stress, which produce $I(\omega)$ different from all the others, but this does not fit the data. All these theories are for *spherical tops*.

De Gennes (1974) has argued in favor of a theory that produces the same $I(\omega)$ as those just discussed. This theory was developed for the isotropic phase of a liquid crystal. The primary variable is a traceless symmetrical second-rank tensor $\mathbf{Q}_{\alpha\beta}$ describing local orientational order: the tensor order parameter. The secondary variable is hydrodynamic velocity (velocity field), for which de Gennes constructs a tensor describing the *rate of shear* ($\dot{\epsilon}_{\alpha\beta}$). The force conjugate to the shear rate tensor in the stress tensor and the force conjugate to the rate of change of the order parameter are obtained by expanding the free energy as a function of powers of $\mathbf{Q}_{\alpha\beta}$ and then differentiating with respect to $\mathbf{Q}_{\alpha\beta}$. This theory is valid for temperatures near the isotropic-nematic transition point of a liquid crystal, where some physical constants of the system diverge. There are further elements of $\mathbf{Q}_{\alpha\beta}$ which do not interact with hydrodynamic modes and contribute an undisplaced central Lorentzian. Taking this into account the total $I(\omega)$ is the same as in viscoelastic theories. $I(\omega)$ for two-variable theories takes the form

$$I(\omega) \propto \sin^2\left(\frac{\theta}{2}\right)\frac{1/\Gamma_1}{1+\omega^2/\Gamma_1^2} + \frac{B(1/\Gamma_2)\cos^2(\theta/2)[(k^4\eta^2/\rho^2\Gamma_2^2)(1-R)+\omega^2/\Gamma_2^2]}{(k^2\eta/\rho\Gamma_2-\omega^2/\Gamma_2^2)^2+(\omega/\Gamma_2)^2(1+(1-R)k^2\eta/\rho\Gamma_2)^2} \qquad (7.A.1)$$

In general $B = 1$ and $\Gamma_1 = \Gamma_2 = \Gamma$. In this equation θ is the angle at which the light is scattered, k is the scattering wave vector, η the normal shear viscosity, and ρ the density. Γ is a correlation frequency $(1/\tau)$, where τ may be defined as follows:

1. τ = correlation time for the anisotropic part of the polarizability density (Keyes and Kivelson, 1972).
2. τ = correlation time of the orientational order parameter (de Gennes, 1974).
3. τ = correlation time of the angular momentum density (Ailawadi and Berne, 1971).
4. τ = correlation time of a second-rank tensor, identifiable with either an orientational density tensor or a stress tensor (Keyes and Kivelson, 1972).

R is a dimensionless parameter expressing the coupling between the

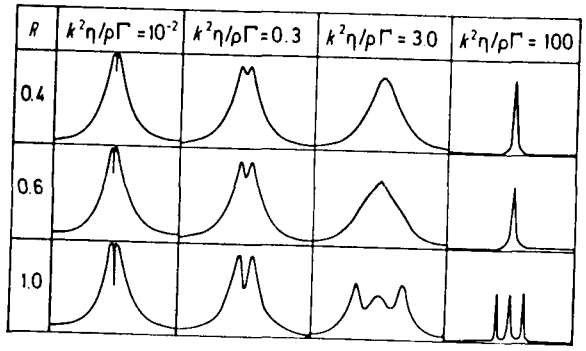

Figure 7.A.1 Depolarized line shapes for values of R and $k^2\eta/\rho\Gamma$. [Reproduced by permission from G. Searby et al., *Faraday Symp. No. 11* (1976).]

hydrodynamic modes and molecular anisotropy. Only the shear waves are able to couple to the primary variable in depolarized (VH) scattering geometry. In HH scattering at $\theta = \pi/2$ transverse velocity gradients cannot contribute but longitudinal gradients now can. For $\theta \neq \pi/2$ isotropic Brillouin scattering is present as well.

Searby and co-workers (1978) point out that in VH geometry the scattering is a function only of R and $k^2\eta/\rho\Gamma$, which are both dimensionless. The second is a ratio of two characteristic times, $1/\Gamma$ and the time $\rho/k^2\eta$. If $R = 1$ in Eq. 7.A.1, Rytov's hydrodynamic theory appears. However, experimental evidence suggests that $R = 0.4$. Moreover, in the Rytov theory τ is identified with the relaxation time of the shear strain tensor and is not a molecular parameter. The ratio of times $k^2\eta/\rho\Gamma$ can be divided into four regions: $(a) \ll 1$; $(b) < 1$; $(c) > 1$; $(d) \gg 1$. A Lorentzian is obtained if $R \to$ or $k^2\eta/\rho\Gamma \to 0$, of half-width $1/\tau$ (Fig. 7.A.1).

In region a Γ is large; the liquid is composed of small, simple molecules and is of low viscosity. The fine structure is very difficult to resolve by light scattering, but using the relation between $A(\omega)$ and $I(\omega)$ this difficulty is surmountable using 0–THz spectroscopy. The central dip seems often not to be observable at all.

Region b may be used to classify the larger molecules and viscous liquids well above their freezing points. It seems that in a variety of liquids $R = 0.4$ produces a good fit to the data, even for molecules as different as CS_2 and ethyl benzoate. This is apparently not understood in terms of molecular light scattering theory.

Region c corresponds to just above the freezing point. The whole line shape is now as narrow as the splitting observed in region a. The shear disturbances are propagative and are less than criticially damped. As the viscosity is increased Eq. 7.A.1 becomes increasingly ineffective, and has to be modified by the introduction of higher-order terms.

In region d the viscosity approaches that of the supercooled liquids

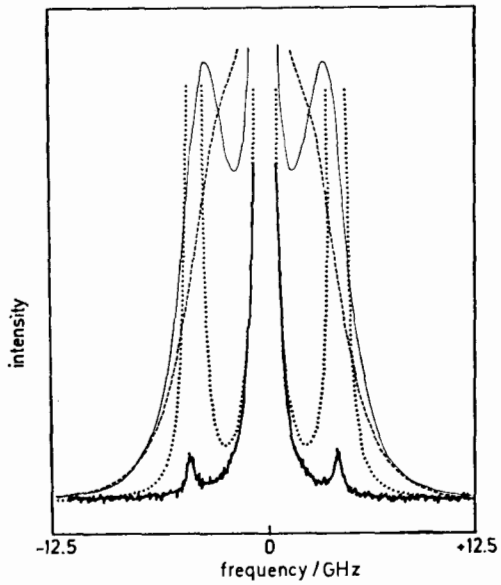

Figure 7.A.2 Depolarized line shape for supercooled benzyl benzoate at 213°K, with attempts at theoretical fitting with a two-variable Mori formalism. [Reproduced by permission from G. Searby et al., *Faraday Symp. No. 11* (1976).]

approaching T_g. Equation 7.A.1 predicts a triplet spectrum for $R = 1$, and for $R < 1$ a central Lorentzian of width $1/\tau$ superimposed on a broader Lorentzian of width $\Gamma/(1-R)$. In the latter case the shear waves are no longer propagative but diffusive. These predictions are contrary to what is found experimentally where at sufficiently low temperatures a very weak doublet appears in the wings of the central line (Fig. 7.A.2), *indicating the presence of well-defined propagating shear waves. The spectra expressed in terms of* $\omega^2 I(\omega)$ *would be similar to those found in terms of* $\mathfrak{A}(\omega)$, *the power absorption coefficient, in the far infrared.* The corresponding polarized spectra show no signs of structure. The doublet was first observed by Leontovich et al. (1967) in supercooled Salol. As the temperature is lowered the intensity of the doublet decreases as the transverse sound velocity increases.

The situation in the viscous liquid therefore is quite similar to that in 0–THz spectroscopy. There is an "α process" very close to the existing line, a "β process," a narrow, weak doublet peak at gigahertz frequencies, and a broad line out in the wings (at far infrared frequencies). The spectra apparently require three-variable theories; a pertinent third variable would be the one describing the translational motion of the molecules.

The polarized light scattered from these systems has certain features in common; there is an intense central Lorentzian of half-width and fine structure at the Brillouin frequencies (ω_B). The calculated intensity of the fine structure tends to zero as $\omega_B/\Gamma \to 0$ and also as $\omega_B/\Gamma \to \infty$. There is often a dip at the Brillouin frequencies in the limit $\omega_B/\Gamma \ll 1$. In the case $\omega_B/\Gamma \gg 1$, however, the dip is replaced by a hump.

REFERENCES

Abramowitz, M. and Stegun, I. A., *Handbook of Mathematical functions*, Dover, New York (1965).

Aihara, H., Kitasawa, C., and Nohara, A., *Bull. Chem. Soc. Jap.* **43**, 3750 (1970).

Ailawadi, N. K. and Berne, B. J., *IUPAC Conference on Statistical Physics*, Chicago (1971).

Ailawadi, N. K. and Harris, S. J., *Chem. Phys.* **56**, 5783 (1972).

Berne, B. J. and Pecora, R., *Dynamic Light Scattering with Applications to Chemistry, Physics and Biology*, Wiley-Interscience, New York (1976).

Bordewijk, P. and Böttcher, C. J. F., *Theory of Electric Polarisation*, Vols. I and II, Elsevier, Amsterdam (1979).

Brot, C., *Dielectric and Related Molecular Processes*, Chem. Soc. Spec. Per. Rep., Vol. 2, Chemical Society, London, p. 1 (1975).

Canet, D., Thèse d'État, University of Nancy (1972).

Cole, R. H. (Ed.), *J. G. Kirkwood—Collected Works*, Gordon/Breach Series: "Documents on Modern Physics" (1963).

De Gennes, P. G., *The Physics of Liquid Crystals*, Oxford University Press, Oxford (1974).

Evans, M. W., Evans, G. J., and Davies, A. R., *Adv. Chem. Phys.* **44**, 255–481 (1980).

Gershon, N. D. and Ben Reuven, A., *J. Chem. Phys.* **51**, 893 (1969).

Glarum, S., *J. Chem. Phys.* **33**, 639 (1960).

Keyes, T. and Kivelson, D., *J. Chem. Phys.* **57**, 4599 (1972).

Kivelson, D. and Madden, P., *Mol. Phys.* **30**, 1749 (1975).

Larkin, I. W., *J. Chem. Soc. Faraday Trans. II* **69**, 1278 (1973).

Lassier, B. and Brot, C., *Chem. Phys. Lett.* **1**, 581 (1968); *Disc. Faraday Soc.* **48**, 39 (1969).

Leontovich, V. S., Tiganov, E. V., and Fabelinskii Z. I., *Zhur. Eksp. Teor. Fiz. Pisma Red.* **5**, 317 (1967).

Lewis, T. J., in *Dielectric and Related Molecular Processes*, Vol. 3, Chemical Society, London (1977).

McDonald, I. R. and Hansen, J-P. *Theory of Simple Liquids*, Academic, New York (1976).

Rahman, A. and Stillinger, F. H., *J. Chem. Phys.* **58**, 3336 (1971).

Reid, C. J., Ph.D. Thesis, University of Wales (1979).

Reid, C. J. and Evans, M. W., *J. Chem. Soc. Faraday Trans. II* **75**(9), 1213 (1979).
Rytov, S. M., *Sov. Phys. J.E.T.P.* **6**, 401, 513 (1958).
Searby, G., Bezot, P., and Sixou, P., *Chem. Soc. Symp. No. 11* (1978).
Steele, W. A., *Adv. Chem. Phys.* **34**, 1 (1976).
Williams, G., *Diel. Rel. Mol. Proc.* **2**, 51 (1975).
Williams, G., *J. Chem. Soc. Faraday Trans. II*, **73**, 458 (1977).
Williams, G. and Hains, P. J., *Chem. Phys. Lett.* **10**, 585 (1971).
Williams, G. and Watts, B., *Trans. Faraday Soc.* **66**, 80 (1970).
Wyllie, G., *Phys. Rep.*, in press (1981).

8
Molecular Dynamics of Mesophases

LIST OF SYMBOLS

$D_\parallel$	Parallel component of the diffusion tensor
$D_\perp$	Perpendicular component of the diffusion tensor
$\mathscr{D}^j_{lm}(\Omega)$	Wigner rotation matrix element
$\epsilon_\parallel$	Component of the permittivity tensor parallel to the aligning field
$\epsilon_\perp$	Perpendicular component
g_2	Orientation parameter
$\mathbf{H}$	Magnetic field strength
$\mathbf{K}$	Matrix of torque correlation functions
Ξ	Stochastic variable associated with the instantaneous orientation of the director relative to a fixed laboratory axis
χ	Dielectric susceptibility
χ_m	Mass susceptibility
$\hat{M}$	Infinitesimal rotation operator
$\mathbf{n}(\omega)$	The liquid crystal depolarization tensor
$\bar{n}$	Mean refractive index
P_n	Legendre polynomial
$\mathbf{R}$	The rotational diffusion tensor
ρ	Number density
V_N or $V(\beta)$	The nematic pseudopotential
$\mathbf{\Omega}$	The space of Euler angles
x, y, z	The molecule-fixed cartesian frame
X, Y, Z	The laboratory fixed cartesian frame
$\mathscr{L}^{lm}_{jk}$	Matrix elements in the solution of the nematic phase diffusion equations

The mesophase of some organic compounds is found beyond the normal melting temperature but before the fluid is recognizably monorefringent. There seems to be a cloudy region over a range of temperature sharply delineated at either end by changes of phase. On microscopic inspection the mesophase may often be classified into subphases such as the nematic, cholesteric, and smectic. There are many articles available to describe these

phases in great detail and an admirable textbook by de Gennes (1974b). Our particular interest is limited to the description of 0–THz spectra, Kerr effect relaxation, and depolarized light scattered intensity in terms of dynamics on the molecular scale. The spectral results are supplemented by a small number of molecular dynamics simulations.

8.1 DIELECTRIC LOSS IN MESOPHASES

The translational motions of molecules in an aligned mesophase (Chapter 1) must be described by a second-rank tensor, because the medium as a whole is no longer isotropic. It follows that the rotational motions are also anisotropic to such a degree that the dielectric permittivity is a tensorial quantity, meaning in turn that the medium is birefringent (Fig. 1.2.5). Molecular reorientation in a liquid crystal must be strongly coupled to the translation and restricted by an external potential (usually called the director) but traceable in reality to the geometric anisotropy of the molecules themselves. To describe the orientational correlation function $C_u(t)$ it is therefore necessary to incorporate both translational and orientational modes of motion in any model used to calculate that a.c.f. Symmetry theorems of time reversal, parity, and reflection no longer apply, and it is possible for a variety of mode–mode couplings to exist that would disappear in the isotropic liquid. Molecular theories that do not account for long range order are inapplicable because of the tensor nature of $\epsilon(\omega)$, the permittivity. One of the first attempts to produce a theory of the dielectric permittivity of mesophases in molecular terms is recounted in the next section.

8.1.1 Theory of Tensor Permittivity

The initial equation from which the permittivity parallel and perpendicular to the orienting external field (electric or magnetic) is calculated is a diffusion equation of the Smoluchowski type with an external potential, which restricts the range of orientations available to a rotationally diffusing molecule. The effect of the restriction may be described as follows. Select an axis for the rotation (z-axis in a spherical polar coordinate system of reference). Then only rotations defined by θ are considered. The term in $\partial/\partial\theta$ in the rotational Laplacian drops out so that $(\mathbf{u}\times\nabla_u)^2 = (\sin^2\theta)^{-1}(\partial^2/\partial\phi^2)$. The z direction is specified by a vector $\mathbf{i}$ and the instantaneous dipole moment has a component in this direction, a component which does not relax, because θ is fixed. The remaining part of the dipole moment is $\boldsymbol{\mu}' = (\mathbf{1} - \mathbf{i}\,\mathbf{i})\cdot\boldsymbol{\mu}$ where $\mathbf{i}\,\mathbf{i}$ is a *tensor product.* This part contains the angle ϕ and relaxes. The dipole a.c.f. then involves the product of the *tensor* quantity $(\mathbf{1} - \mathbf{i}\,\mathbf{i})$ and the tensor quantity

$$\langle\boldsymbol{\mu}(0)\boldsymbol{\mu}^T(0)\rangle.$$

Similarly the diffusion equation for symmetrical top molecules subjected to the orienting potential $V(\beta)$, the nematic "pseudopotential" (Chapter 1), takes the form

$$\nabla_\Omega^2 f + (\sin\phi)^{-1}\frac{\partial}{\partial\phi}\left[\sin\phi f\left(\frac{\partial V}{\partial\beta}\right)\right] = D_\perp^{-1}\left(\frac{\partial f}{\partial t}\right) \qquad (8.1.1.1)$$

where ∇_Ω^2 represents the Laplace operator written in terms of Euler angles. The eigenfunctions of this are the Wigner rotation matrices, denoted by $\mathcal{D}^j_{lm}(\Omega)$, that is, for a symmetrical top,

$$\nabla_\Omega^2\mathcal{D}^j_{lm}(\Omega) = E_{jm}\mathcal{D}^j_{lm}(\Omega)$$
$$\equiv -\left[j(j+1) + \left(\frac{D_\parallel}{D_\perp} - 1\right)m^2\right]\mathcal{D}^j_{lm}(\Omega)$$

Here $D_\parallel$ and $D_\perp$ are coefficients, equal for a spherical top but not otherwise. Nordio and co-workers (1972) have solved this equation analytically by expanding $V(\beta)$ in Legendre polynomials and the solution $f(\Omega, t)$ in a series of eigenfunctions of the Laplace operator.

The interesting quantities are the probability distribution of (Ω) and the conditional probability $f(\Omega, \Omega_0; t)$, from which the relevant tensor a.c.f. may be calculated.

It is known experimentally that the dielectric dispersion and loss in liquid crystals macroscopically oriented by a magnetic field occurs at frequencies that are very different. The solutions to Eq. 8.1.1.1 must therefore reflect this accurately. The activation enthalpy of the "parallel" process is very high, owing to the fact that the relaxation must take place about the short axis of the liquid crystal molecules, which by their very nature are lathlike (not cylindrical) and geometrically anisotropic.

The problem is to relate the p.d.f.'s which are the solutions of Eq. 8.1.1.1 to the observable axially symmetrical second-rank tensor, dielectric susceptibility $\boldsymbol{\chi}(\omega)$. The relation of $\boldsymbol{\chi}(\omega)$ to the tensor permittivity $\boldsymbol{\epsilon}(\omega)$ involves all the factors of Chapter 3 plus the complications introduced by the anisotropy of the medium. This is perhaps the most severe problem when attempting to account for dielectric measurements in terms of the molecular interactions and movements. However, we can take another look at the system using magnetic susceptibility measurements, and these are described later.

The optical axis of the mesophase is the symmetry axis of $\boldsymbol{\chi}(\omega)$, and the dependence of the static principal values of $\boldsymbol{\chi}(\omega)$ upon the degree of order has been described by Maier and Meier (1961) in an often-quoted paper. In precise terms, if we neglect the high frequency memory and inertial effects for the moment, the problem is to evaluate the orientational a.c.f. $C_u(t)$ perpendicular and parallel to the (nematic) director axis.

Let (X, Y, Z) be a laboratory coordinate axis with the Z-axis in the direction of the optical axis of the liquid crystal, and (x, y, z) a system in the molecule frame with z in the long axis, of the lathlike molecule. If $(\theta, \phi,$

χ) are the Euler angles relating the two systems, then the components of $\boldsymbol{\mu}(t)$, the dipole vector in the Z and X direction, are

$$\mu_Z(t) = \sum_p (-1)^p \mathscr{D}^1_{0,-p}(t)\mu'^{(1,p)}$$

$$\mu_X(t) = \frac{1}{\sqrt{2}} \sum_p (-1)^p [\mathscr{D}^1_{-1,-p}(t) - \mathscr{D}^1_{1,-p}(t)]\mu'^{(1,p)}$$

where $\mu'^{(1,p)}$ are *irreducible spherical tensor components*:

$$\mu'^{(1,0)} = \mu_z; \qquad \mu'^{(1,\pm 1)} = \mp \frac{1}{\sqrt{2}}(\mu_x \pm i\mu_y)$$

The problem is therefore reduced to calculating the correlation functions of the Wigner matrices (Chapter 2 appendix):

$$\langle \mathscr{D}^1_{lm}(0)\mathscr{D}^{1*}_{l'm'}(t)\rangle = \int d\Omega_0 \mathscr{D}^1_{lm}(\Omega_0) f(\Omega_0) \int d\Omega\, \mathscr{D}^{1*}_{l'm'}(\Omega) f(\Omega, \Omega_0; t)$$

The diffusion equation is

$$\nabla^2_\Omega f + \frac{1}{kT} \operatorname{div}[f \operatorname{grad} V_N] = Rf \equiv \frac{1}{D_\perp}\frac{\partial f}{\partial t}$$

$$= \nabla^2_\Omega f + \frac{1}{2kT}[\nabla^2_\Omega f V_N + f(\nabla^2_\Omega V_N) - V_N(\nabla^2_\Omega f)]$$

The pseudopotential is expanded, as we have mentioned, in Legendre polynomials (P_n):

$$\frac{V_N}{kT} = \sum \lambda_n P_n(\cos\beta)$$

The general solution of the diffusion equation then is of the form

$$f(\Omega, t) = \sum a_{klm}(0) \exp(D_\perp \alpha^k_{lm} t)\psi_{klm}(\Omega)$$

$$\psi_{klm}(\Omega) = \sum \mathscr{X}^{lm}_{jk} \mathscr{D}^j_{lm}(\Omega)$$

The matrix elements X and the roots α_k are obtained by solving for each set of indices (lm) the eigenvalue problem:

$$\mathbf{X}^{-1}\hat{R}\mathbf{X} = \underline{\alpha}$$

The matrix elements of the operator $\hat{R}$ in the linear space of the Wigner functions are

$$\mathscr{R}^{lm}_{jj'} = -\left[j(j+1) + \left(\frac{D_\parallel}{D_\perp - 1}\right)m^2\right]\delta_{jj'}$$

$$-\frac{1}{2}\sum_n \lambda_n[j(j+1) - j'(j'+1) + n(n+1)]$$

$$\times \mathscr{C}(n, j', j; 0, l)\mathscr{C}(n, j', j; 0, m) \qquad (8.1.1.2)$$

where $\mathscr{C}$ are Clebsch–Gordan coefficients (see Chapter 2 appendix and Chapter 11). The expression for $f(\Omega, \Omega_0; t)$ with the initial condition $f(\Omega, 0) = \delta(\Omega - \Omega_0)$ is now evaluable analytically as

$$f(\Omega, \Omega_0; t) = \sum (2i+1)\mathscr{X}^{lm-1}_{ki}\mathscr{X}^{lm}_{jk} \exp(D_\perp \alpha^k_{lm} t)\, \mathscr{D}^{i*}_{lm}(\Omega_0)\mathscr{D}^i_{lm}(\Omega)$$

The angular distribution function $f(\Omega)$ is

$$f(\Omega) \underset{t\to\infty}{=} f(\Omega, \Omega_0; t)$$

From the structure of the elements $\mathscr{R}^{lm}$, it can be seen that for $l = m = 0$ the lowest root α^0_{00} vanishes for any value of the parameters λ_n. It follows that $\mathscr{X}^{-1}_{0i} = \mathscr{X}^{-1}_{00}\delta_{0i}$. Therefore, $f(\Omega) = \mathscr{X}^{-1}_{00} \Sigma\, \mathscr{X}_{j0}\mathscr{D}^j_{00}(\Omega)$ and it follows that the required correlation functions are

$$\langle \mathscr{D}^1_{lm}(0)\mathscr{D}^{1*}_{lm}(t)\rangle = \frac{1}{3}\sum (2i+1)\mathscr{X}^{lm-1}_{ki}\mathscr{X}^{lm}_{1k} \exp(D_\perp \alpha^k_{lm} t)\, \langle \mathscr{D}^1_{lm}(0)\mathscr{D}^{i*}_{lm}(0)\rangle$$

where

$$\langle \mathscr{D}^1_{lm}(0)\mathscr{D}^{i*}_{lm}(0)\rangle = \langle \mathscr{D}^j_{00}\rangle \mathscr{C}(j, 1, i; 0, l)\mathscr{C}(j, 1, i; 0, m)$$

$$\langle \mathscr{D}^j_{00}\rangle = \frac{\mathscr{X}^{-1}_{00}\mathscr{X}_{j0}}{2j+1}$$

At both $t = 0$ and $t \to \infty$ the correlation function reduces to $\langle|\mathscr{D}^1_{lm}|^2\rangle$. Cross terms vanish due to the orthogonality of the Wigner functions. Furthermore, from the symmetry properties of the Clebsch–Gordan coefficients, the following equalities hold:

$$\langle \mathscr{D}^1_{lm}(0)\mathscr{D}^{1*}_{lm}(t)\rangle = \langle \mathscr{D}^1_{l,-m}(0)\mathscr{D}^{1*}_{l,-m}(t)\rangle = \langle \mathscr{D}^1_{-l-m}(0)\mathscr{D}^{1*}_{-l-m}(t)\rangle$$

For spherical molecules,

$$D_\parallel/D_\perp - 1 = 0$$

and

$$\langle \mathscr{D}^1_{lm}(0)\mathscr{D}^{1*}_{lm}(t)\rangle = \langle \mathscr{D}^1_{ml}(0)\mathscr{D}^{1*}_{ml}(t)\rangle$$

This implies that

$$\langle \mu_Z(0)\mu_Z(t)\rangle = \langle \mathscr{D}^1_{00}(0)\mathscr{D}^{1*}_{00}(t)\rangle \mu_z^2 + \langle \mathscr{D}^1_{01}(0)\mathscr{D}^{1*}_{01}(t)\rangle(\mu_x^2 + \mu_y^2)$$

$$\langle \mu_X(0)\mu_X(t)\rangle = \langle \mathscr{D}^1_{01}(0)\mathscr{D}^{1*}_{10}(t)\rangle \mu_z^2 + \langle \mathscr{D}^1_{11}(0)\mathscr{D}^{1*}_{11}(t)\rangle(\mu_x^2 + \mu_y^2)$$

In much the same way as Favro's theory for unconstrained symmetrical top rotation leads to a sum of two exponentials, the Nordio theory (also for symmetrical tops) produces such a sum for each of the parallel and perpendicular a.c.f.'s. The problems of Chapter 3 must be tackled before the appropriate dielectric loss spectrum may be evaluated. However, V_N must first be constructed from the Legendre polynomials. Experimentally,

only P_2 and, with some difficulty, P_1 can be accessed. In this case we take

$$\frac{V_N}{kT} = \lambda_2 P_2(\cos\phi) + \lambda_4 P_4(\cos\phi)$$
$$= \alpha[\langle P_2\rangle P_2(\cos\phi) + \lambda\langle P_4\rangle P_4(\cos\phi)]$$

following Nordio et al. The parameter α is calculated for any given value of the orientational order $\langle P_2\rangle$ (Fig. 1.2.7) and the parameter λ is obtained from the nematic/isotropic transition point. Internal consistency is then sought between $\langle P_2\rangle$ and $\langle P_4\rangle$ by an iterative procedure. The matrix elements $\mathcal{R}^{lm}$ are then evaluated with λ_2 and λ_4. For increasing values of the order parameters $\langle P_2\rangle$ in the interval of experimental interest (0.3–0.7) only the lowest odd root α^1_{lm} determines the experimental decay of $C_u(t)$. The correlation function $\mathcal{D}^1_{lm}$ is always close to a single exponential (i.e., with a single relaxation time). The anisotropy $D_\parallel/D_\perp - 1$ has the effect of increasing the difference $|\alpha^1_{01} - \alpha^1_{00}|$ and decreasing $|\alpha^1_{01} - \alpha^1_{11}|$.

This theory is basically very simple and runs into difficulties when dealing with details of the behavior of V_N/kT. The Nordio et al. theory effectively deals with long range order, but a considerable amount of short range Kirkwood type correlation (introduced in Chapter 3) remains to be accounted for when relating the tensor susceptibility and permittivity. The short range correlations are embodied in the diffusion tensor. The Nordio theory is a zeroth Mori approximant with superimposed potential. In the far infrared there is of course a "γ process" (Chapter 7) or processes corresponding to each of the low frequency loss curves ($\parallel$ and $\perp$).

The order parameters $\langle P_2\rangle$ *and* $\langle P_4\rangle$ are accessible to experimental measurement and, as mentioned in Chapter 1, computer simulation. At the nematic/isotropic transition $\langle P_2\rangle$ is roughly 0.4, increasing to 0.7 as the temperature falls. A purely repulsive form for the intermolecular potential is inappropriate since this leads to a $\langle P_2\rangle$ at the order-disorder transition, which is theoretically too high. For instance, Monte Carlo simulation of hard spherocylinders produces *no* order-disorder phase transition at a packing density much larger than experimentally expected, suggesting that strongly dipolar molecules form mesophases with greater ease than their nondipolar counterparts. A nondipolar mesophase is quite rare. The most striking properties of the mesophase are electric and magnetic: the ease with which the nematic phase is aligned with very weak electric and magnetic fields testifies to this. It was surely then a little optimistic to expect to simulate such behavior with purely repulsive potentials. There is more to mesophase behavior than molecular shape alone. The molecular dynamics simulation illustrated in Fig. 1.2.7 results in an unrealistically high $\langle P_2\rangle$, and as its authors request, should be regarded as a first foray. The parameter $\langle P_4\rangle$ can be obtained, with difficulty, from the intensity of light scattered in a Raman experiment and from line width variations in an ESR experiment. Very little is known about it up to now.

It is probably wiser to revise the whole approach by using the increasingly available information from molecular dynamics simulations about the efficacy and particular characteristics of model potentials. The long flexible alkyl tails of some mesogens are vitally important in many cases, and it is already possible to simulate simple alkanes with an atom–atom potential. Taking the flexible tail into account, the nematic director potential takes the form

$$V(\theta_i) = -\sum_j V_{ij}\bar{P}_2^{(j)}P_2(\cos\theta_i) \qquad (8.1.1.3)$$

where θ_i is the angle between the director and the supposed symmetry axis of the ith unit in the chain. It is possible to calculate the transition temperature to the isotropic phase using a potential such as this and also more subtle effects such as the alternation with chain length in the entropy of transition. Using the power of modern computers *the complete* 0–THz spectrum may soon be amenable to theoretical description using a potential such as Eq. 8.1.1.3.

8.1.2 The Internal Field Correction

Luckhurst and Zannoni (1975) have approached the problem of the exact relationship between the frequency-dependent permittivity and the dipole moment a.c.f. when the susceptibility is a tensor. These authors have employed linear response theory in the manner of Chapter 3 to produce for the permittivity parallel to the director

$$\frac{[\epsilon_\parallel(\omega)-\epsilon_\parallel(\infty)]\{\epsilon_\parallel(\omega)-n_\parallel(\omega)[\epsilon_\parallel(\omega)-\epsilon_\parallel(\infty)]\}\epsilon_\parallel(0)}{[\epsilon_\parallel(0)-\epsilon_\parallel(\infty)]\{\epsilon_\parallel(0)-n_\parallel(0)[\epsilon_\parallel(0)-\epsilon_\parallel(\infty)]\}\epsilon_\parallel(\omega)} = \int_0^\infty -\dot{\Phi}_\parallel(t)\exp(-i\omega t)\,dt$$

where $\mathbf{n}(\omega)$ is not a refractive index but a depolarization tensor. The matrix $\mathbf{\Phi}(t)$ is defined in terms of the dipole moment of an ellipsoidal cavity embedded in the mesophase. All the drawbacks of cavity theory mentioned in Chapter 3 must therefore be kept in mind. The tensor $\mathbf{\Phi}(t)$ could be related to the single particle $\mathbf{C}_u(t)$ tensor using a macro-micro approach inside a matrix continued fraction. This type of theory is sketched in the appendix to this chapter, the problem being the usual one of minimizing the number of free parameters.

8.1.3 Freed's Theory of the Nematic Phase Dynamics (1977)

The molecular dynamics in the nematic phase is treated in this case by separating the hydrodynamic modes of motion from the short time fluctuations. The latter are described with the Mori type of time-dependent rotational diffusion coefficient for molecules of similar size. This of course introduces a non-Markovian element into the description arising from the fact that the relaxation process is defined by inertial and memory effects. However, the dissipative character of the hydrodynamic modes (which are

described fully by de Gennes, 1974b) means that they are each amenable to a treatment employing Markovian concepts. Fluctuations of the nematic director are describable in this way. The problem reduces to solving a diffusion equation whose orienting Nordio type potential has itself a Markovian stochastic time dependence. In this respect the formulation of the theory is similar to that of Nordio et al. except that the latter does not involve memory effects. The important point is that reorientational motion of *individual* molecules is not *statistically independent* of director fluctuations. It is not physically sound to define the motion of the molecule with reference to the director frame which is fluctuating in time, because this introduces an incorrect statistical dependence of the molecular representation on the director fluctuations. The reorientation is statistically dependent upon the orienting potential fluctuations when and only when the molecule is partially ordered.

Near the nematic to isotropic phase transition the fluctuations in the ordering become quasi-critical, some physically measurable parameters such as the Kerr constant diverge, and this phenomenon may be incorporated within the framework of the Freed theory, although nonrigorously. It is worth describing the initial equations of this treatment since they illustrate the methods of Chapter 2.

The first equation is a Smoluchowski equation describing the reorientational relaxation of a liquid-crystal molecule under the effect of an orienting potential (U)

$$\frac{\partial f}{\partial t}(\Omega, t) = -\hat{M} \cdot \mathbf{R}(\Omega, t) \cdot \left(\hat{M} + \frac{\hat{M}U(\Omega, t)}{kT}\right) f(\Omega, t)$$

Here $f(\Omega, t)$ is the time-dependent probability distribution in orientation of the molecule relative to a fixed coordinate frame. $\hat{M}$ is the infinitesimal rotation operator $\hat{M} = i\mathbf{r} \times (\nabla_r)$ generating the infinitesimal molecular rotation in the three-dimensional space. The rotational diffusion tensor is denoted now by $\mathbf{R}(\Omega, t)$; both $\mathbf{R}$ and $\hat{M}$ are defined in the molecular coordinate frame (x^1, y^1, z^1). The operator $\hat{M}$ then has the following properties:

$$M^2 \phi^L_{KM} = L(L+1)\phi^L_{KM}(\Omega)$$

$$M_{\pm}\phi^L_{KM}(\Omega) = [(L \mp K)(L \pm K + 1)]^{1/2}\phi^L_{K\pm 1, M}(\Omega)$$

$$M_{z'}\phi^L_{KM}(\Omega) = K\phi^L_{KM}(\phi)$$

where $\phi^L_{KM}(\Omega)$ are the eigenfunctions of M^2 and $M_{z'}$. L is the "azimuthal quantum number" and K its component along the z'-axis and $M_{\pm} = M_{x'} \pm iM_{y'}$. The ϕ^L_{KM} functions are simply related to the Wigner matrices:

$$\phi^L_{KM}(\Omega) = \left(\frac{2L+1}{8\pi^2}\right)^{1/2} \mathcal{D}^L_{KM}(\Omega)$$

The (x', y', z') frame is chosen to be the one in which $\mathbf{R}$ is diagonalized. The potential $U(\Omega, t)$ is then that of the mean torque, and the mean orienting torque is

$$\mathbf{T} = i\hat{M}U(\Omega, t)$$

This is then assumed to be slowly varying and to include the fluctuations in the director caused by hydrodynamic effects. There are several approximations implicit in this form of Smoluchowski equation:

1. The angular momentum relaxation is very rapid, so much so that the angular momentum must have relaxed to equilibrium before the reorientation has evolved appreciably. The orienting potential must therefore be small.
2. The torque is rapidly fluctuating and there is no memory in the system. This may be remedied with the Mori form:

$$\frac{\partial f}{\partial t}(\Omega, t) = -\hat{M} \cdot \int_0^t d\tau\, \mathbf{R}(t-\tau) \cdot \left(\hat{M} - \frac{i\mathbf{T}}{kT}\right) f(\Omega, \tau)$$

This now defines a torque correlation function $\mathbf{K}$ through the relation

$$\mathbf{K}(t) = \langle \Delta\mathbf{N}(t)\Delta\mathbf{N}^T(0)\rangle$$

where

$$\Delta\mathbf{N} = \mathbf{N}(t) - \mathbf{T}$$

is the fluctuating part of the total time-dependent torque $\mathbf{N}(t)$. We have, in the frequency domain

$$\mathbf{R}(s) = (kT)^2\mathbf{K}^{-1}(s)$$

The torque fluctuations $\Delta\mathbf{N}$ take place at a rate faster than or comparable with molecular reorientation rates. The time-dependent part of $\mathbf{T}$ fluctuates more slowly. If there are director fluctuations affecting $U(\Omega, t)$, then $f(\Omega, t)$ cannot be independent of these.

Freed (1977) now assumes that the time dependence of $U(\Omega, t)$ lies in its dependence on a set of variables Ξ, describing the instantaneous orientation of the director relative to a fixed laboratory axis. The stochastic behavior of Ξ is stationary and Markovian, so that

$$\frac{\partial f(\Xi, t)}{\partial t} = -\hat{\Gamma}_{\Xi} f(\Xi, t)$$

Here $\hat{\Gamma}_{\Xi}$ is a Markov operator for the distribution function $f(\Xi, t)$. This is the form usually taken by hydrodynamic theories such as those described by de Gennes. *The combined distribution function is now a multidimen-*

sional Markov process, (Chapters 9 and 10)

$$\frac{\partial f(\Omega, \Xi, t)}{\partial t} = -(\hat{\Gamma}_\Omega + \hat{\Gamma}_\Xi) f(\Omega, \Xi, t)$$

$$\hat{\Gamma}_\Omega = \hat{M} \cdot \mathbf{R} \cdot \left(\hat{M} + \frac{\hat{M} U(\Xi)}{kT} \right)$$

Here, $f(\Omega, \Xi, t)$ is the *joint* p.d.f. in both Ω and Ξ and is Markovian. This equation is generally known as the (Kubo) stochastic Liouville equation and is discussed further in Chapters 9 and 10. The problem of describing the molecular dynamics of the nematic phase now depends on choosing $\hat{\Gamma}_\Xi$. The problem is eased analytically by making use of the physical fact that Ξ fluctuates much more slowly than Ω, so that the approximation

$$f(\Omega, \Xi, t) \doteqdot f_\Xi(\Omega, t) f(\Xi, t)$$

is valid. The eigenfunctions and eigenvalues of $f(\Omega, \Xi, t)$ are similar to those discussed in Section 8.1.1. The equilibrium result is

$$f_{eq}(\Omega, \Xi) = f_{eq,\Xi}(\Omega, t) f(\Xi, t)$$

where

$$f_{eq,\Xi}(\Omega) = \frac{\exp[-U(\Omega, \Xi)/kT]}{\int d\Omega \exp[-U(\Omega, \Xi)/kT]}$$

A simple form for $f_{eq,\Xi}(\Omega)$ may now be chosen by defining Ξ through a hydrodynamic model of the director fluctuations. All the hydrodynamic modes, when taken together, make up the Markov process Ξ. This means that a leading term in the expansion of the potential of mean torque is retained, and the Freed theory is not a "mean field" theory such as that of Maier and Saupe (1958). The form taken for U reflects the fact that the molecule reorients towards the instantaneous direction of $\mathbf{n}$, the nematic director vector. The order parameter in Freed's theory is

$$\langle \mathscr{D}^2_{00} \rangle_\Omega = \int \mathscr{D}^2_{00}(\Omega) f_{eq,\Xi_{eq}}(\Omega)\, d\Omega$$

To first order in Ξ, this is unaffected by the director fluctuations as in the hydrodynamic model, where the fluctuation $\delta\mathbf{n}(\mathbf{r})$ of the director is a superposition of plane-wave disturbances:

$$\delta\mathbf{n}(\mathbf{q}) \equiv \frac{1}{V} \int \delta\mathbf{n}(\mathbf{r}) \exp(-i\mathbf{q} \cdot \mathbf{r})\, dV$$

where V is the sample volume. Usually (de Gennes, 1974) the $\mathbf{q}$th hydrodynamic mode relaxes according to the "viscosity" law:

$$\frac{\partial}{\partial t} \delta\mathbf{n}_\alpha(\mathbf{q}) = -\frac{1}{\tau_\alpha(\mathbf{q})} \delta\mathbf{n}_\alpha(\mathbf{q})$$

where various distortions are embodied in the subscript α. The hydrodynamic equations are shown by Freed to be Markovian in nature.

To account for large fluctuations in the ordering near the nematic/isotropic phase transition it becomes necessary to take account of fluctuations in the *magnitude* as well as the *orientation* of the potential U. The Freed theory then is a generalization of the hydrodynamic theory of de Gennes (1974b) for data near the nematic/isotropic transition. Examples for the Kerr effect are described in Section 8.1.4. As the order parameter tends to zero (i.e., as the isotropic phase is approached), the overall correlation functions become independent of any director fluctuations.

8.1.4 Selected Low Frequency Dielectric Results

In the simplest case where the long axis and dipole axis coincide, the nematic phase is characterized by two regions of relaxation (excluding the far infrared). In the gigahertz range the process is attributed to rotations of the molecule about the long axis; the other, in the megahertz range, is associated with the more energetic (strongly hindered) movement about the short axis. This latter is very sensitive to cooperative (macroscopically applied) forces, such as a shear flow. If a shear deformation is applied via a longitudinal motion of one capacitor plate with respect to another, for example, the measured megahertz relaxation time decreases significantly in an aligned mesophase held between the plates. The response to the shear is not immediate.

The systematic work of Price and co-workers (1973 etc.) in this field is recounted in this section, since it illustrates much of the complexity and interest of nematogen behavior. Generally the results are interpreted in terms of the order parameter $\langle P_2 \rangle$, which depends on the strength of the directing field, and the behavior of the $\tau_\parallel$ and $\tau_\perp$ relaxation times, explained in terms of extensions to the Debye theory. This would not of course be valid in the far infrared range of frequencies where the complexity of the nematic phase behavior is fully developed.

The measurement of the electric permittivity and dielectric anisotropy is a delicate business and reproducibility is not easy to come by. However, since interest is centered around the effect of applied magnetic and electric fields it is possible to express results as a difference in dielectric behavior in the presence and absence of the aligning field. For a few typical nematogens the results trend as follows (Moutran, 1975): both $\epsilon_\parallel$ and $\epsilon_\perp$ relax at microwave frequencies and in the far infrared. Similar relaxations are also found in the isotropic phase.

If the molecule under study has a nonzero component of its electric dipole moment in the long axis, there is an additional process at much lower frequencies, which involves only $\epsilon_\parallel$. In materials where the nematic range falls around 375°K (e.g., *p*-azoxyanisole) this occurs in the radio frequency range. The effect was discovered by Maier and Saupe (1958) and

interpreted by Maier and Meier (1961) using their mean field theory. The anisotropy in the static permittivity of *p*-azoxyanisole is typical, amounts to a few percent, and decreases monotonically with increasing temperature. At the nematic/isotropic clearing point it vanishes abruptly and thereafter the scalar permittivity continues to decrease as the temperature is raised.

The work in this field tends to concentrate around a few well characterized molecules. Among these are *p*-methoxybenzylidene-*p'*-*n*-butylaniline (MBBA), which is illustrated in Fig. 8.1.4.1. In the aligned nematic the dielectric anisotropy is negative and considerably larger than that in *p*-azoxyanisole. Its dipole moment has been measured by Maurel and Price (1973). Agarwal and Price (1974) have measured the permittivity and dielectric loss of the magnetically aligned MBBA up to a frequency of 7.93 MHz and for the isotropic phase in the region 0.5–250 MHz. The low frequency measurements in electrode aligned MBBA indicate a considerable antiparallel dipole alignment which persists into the isotropic phase. There is no significant change of the measured Kirkwood *g* factor at the nematic to isotropic transition. The dielectric parameters describing the relaxation behavior of MBBA in benzene solution and in the isotropic phase at microwave frequencies (Table 8.1.4.1) are analyzed empirically with the Fuoss-Kirkwood equation:

$$\cosh^{-1}\left(\frac{\epsilon_m''}{\epsilon''}\right) = \beta \log_e\left(\frac{f_m}{f_r}\right)$$

where β is an empirical factor describing the width of the ϵ'' versus $\log f_r$ curve, where f_r is the frequency in hertz. We have $\beta = 1$ for a single relaxation time and $0 < \beta \leq 1$ for a distribution of relaxation times. The subscript m refers to values of maximum absorption.

The observed relaxation times $[\tau = (2\pi f_m)^{-1}]$ may be compared with those of benzophenone (a molecule of similar shape to MBBA). In benzene solution benzophenone has $\tau = 17.5$ psec at 298°K, while liquid benzophenone at 333°K has $\tau = 82$ psec. The estimated times for MBBA in benzene solution are 47.9 and 20.5 psec for rotational diffusion about axes perpendicular and parallel to the long axis (or optic axis) of the molecule, respectively. The observed value is 30.6 psec. In the isotropic liquid at 340°K the relaxation times are 206 psec ($\perp$) and 88 psec ($\parallel$), the observed

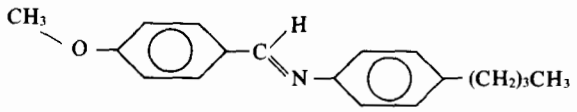

Figure 8.1.4.1 Structure of *p*-methoxybenzylidene-*p'*-*n*-butylaniline (MBBA).

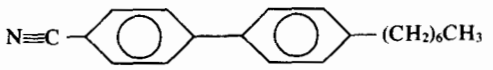

Figure 8.1.4.2 Structure of 4-*n*-heptyl-4'-cyanobiphenyl (HCB).

Table 8.1.4.1 Dielectric Relaxation Parameters for the Nematic Phase of MBBA

	T'(°K)	ϵ_s	ϵ_∞	β	$10^8\tau$ (sec)	$10^{30}\mu$ (C m)
Pure MBBA	300.0	4.61	4.11	0.84	10.1	2.63
	305.0	4.62	4.15	0.85	5.8	2.23
	309.5	4.62	4.14	0.75	3.0	2.30
	313.0	4.63	4.03	0.64	1.8	2.62
1.86% CCl_4	300.0	4.63	4.19	0.98	7.4	2.13
in MBBA	307.0	4.67	4.17	0.84	2.6	2.30

Reproduced from Agarwal and Price, J. Chem. Soc. Faraday Trans. II, **70**, 188 (1974).

relaxation time at 340°K being 76 psec. The width of the microwave absorption suggests that relaxation mechanisms are present simultaneously. The activation energy of 30 kJ/mole is consistent with that of 23 kJ/mole observed for benzophenone, which does not form an observable mesophase.

To remove the interpretive difficulties caused by the misalignment of dipole and long axes in MBBA, Moutran et al. (1975) have made use of the nematogen 4-*n*-heptyl-4'-cyanobiphenyl (HCB) (Fig. 8.1.4.2) whose resultant dipole vector in the molecule frame is conveniently placed for analysis. They have collected dielectric, Kerr effect, and refractive index data for the nematic and isotropic phases and in benzene solution. The permittivity and refractive index temperature variation are shown in Fig. 8.1.4.3. The permittivity and refractive index of benzene solutions of HCB were linear functions of the HCB concentrations up to about 3 mole/dm^3, showing the absence of any significant dipolar association in these solutions. It is significant that the benzene solution itself becomes nematic at room temperature before the pure nematogenic figure of 3.39 mole/dm^3 is reached.

The anisotropy of polarizability in HCB is less than that of benzene, and this in itself is not important in the formation of the nematic phase. This is hardly surprising in view of the fact that the stability of the mesophase is sensitively dependent on the length of the flexible tail, that is, upon intermolecular forces depending on the molecular configuration. To emphasize this de Vries (1978) recently attempted to define precisely the difference between solid crystals and liquid crystals with *three-dimensional* anisotropy. The most significant difference seems to be that in the solid crystal the alkyl chains at the ends of the molecule have very little disorder or no disorder at all, whereas in the (hypothetical) three-dimensional anisotropic liquid crystals the alkyl chains are *slightly* disordered. The anisotropy of polarizability would be the same in each case and play no part. An example of such subtlety is the smectic H-phase of BBEA (4-*n*-butyloxybenzal-4'-

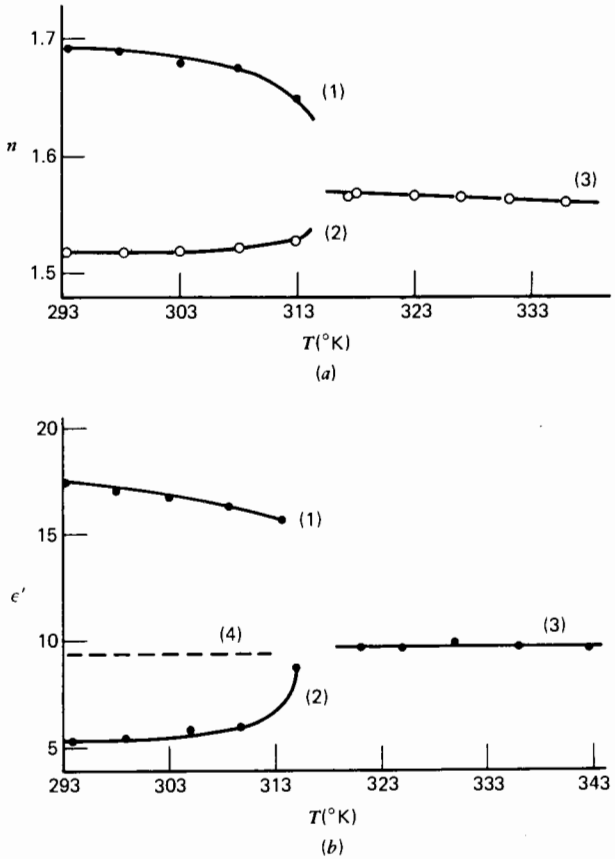

Figure 8.1.4.3 Temperature variation of the refractive index and permittivity of HCB. (*a*) (1) Refractive index n_e of the extraordinary ray in the nematic phase; (2) refractive index n_0 of the ordinary ray in the nematic phase; (3) refractive index n in the isotropic phase. (*b*) (1) permittivity $\epsilon_{\parallel}$ measured with the nematic director parallel to the measuring field; (2) permittivity $\epsilon_{\perp}$ measured with the nematic director perpendicular to the measuring field; (3) permittivity ϵ in the isotropic phase; (4) The mean permittivity in the nematic phase. [Reproduced by permission from R. F. S. Moutran et al., *J. Chem. Soc. Faraday Trans. II* **72**, 1447 (1976).]

ethylaniline), which is a *liquid* crystal (not a molecular crystal) because of the following:

1. There is no supercooling at the transition from the nematic phase to the smectic H-phase.
2. The observed changes in the *microscopic texture* during the formation of the phase from the nematic phase would not be expected for the crystallization of a solid phase.
3. *The phase can be made to flow.*

4. A crystal structure of an optically active compound has a single three-dimensional lattice, but the lattice of a three-dimensional smectic phase becomes twisted if the molecules are optically active.
5. Three-dimensional anisotropic liquid crystals form mixed phases in all proportions whereas mixed molecular crystals very seldom do.

In liquid crystals with three-dimensional order the alkyl chains are only slightly disordered (a few kinks per chain), but this is enough to destroy almost completely the transmission of translational phonon modes through the system. The translational coupling is much weaker than the rotational coupling. Where the two compete, as in structures with optically active molecules, the translational autocorrelation is destroyed so as to achieve a more favorable rotational arrangement. In the cases where the alkyl chains are free to take up many conformations owing to the bulk of the rest of the molecule, translational order disappears and there is no three-dimensional order. At the same time we must not overemphasize the role of chain dynamics, because if the CN group is removed from HCB the nematic phase *disappears* irrespective of the length of the alkyl chain. Clearly, then, the subtleties of chain dynamics play their part only after the system has been brought to order by the presence of strong dipole–dipole interactions.

The Kirkwood factor g as measured in HCB is indicative of antiparallel dipole aggregation similar to that found in benzonitrile at room temperature. However, not much significance can be attached to this purely empirical force-fitting of experimental data. The extension of Kirkwood's ideas to the nematic phase has been undertaken by Maier and Meier and lately by Bordewijk and Böttcher (1979). It follows that the permittivities in the nematic phase should depend critically on $\langle P_2 \rangle (\equiv S)$, but the theoretical and experimental S are at variance. Using the method of Bordewijk and Böttcher there seems to be order parallel to the long axes but not perpendicular. Before too much meaning is read into such statements the reader should consult Chapter 3, and bear in mind that the relation between macroscopic data and molecular parameters in the nematic condition is more complicated. Dielectric parameters for pure HCB in the nematic and isotropic phases are listed in Table 8.1.4.2. We note, however, that these measurements ignore as usual the existence of the far infrared relaxation process and are therefore, in strict terms, uninterpretable. However, this is the traditional approach, and is likely to remain so for a while longer. The data as they stand may be given limited significance by using a director potential theory similar to that of Nordio et al. and Freed sketched above, but this is a case of judging the Parthenon by the frieze alone. The complexity of the situation is brought out only by an adequate study of the *complete* 0–THz range up to about $250\,\mathrm{cm}^{-1}$, and thereafter by intercomparison of techniques. The quasi-critical fluctuations near the isotropic to nematic transition temperature (T_c) are studied conveniently by using

Table 8.1.4.2 Dielectric Parameters for Pure HCB in the Nematic and Isotropic Phases

Measurements made parallel to the nematic director[a]				
T (°K)	ϵ_s	ϵ''_m	ϵ_∞	$10^9\tau_\parallel$ (sec)
293	17.5	7.1	3.3	110
298	17.0	7.1	2.8	71
303	16.7	6.8	3.1	40
308	16.3	6.6	3.1	32

Measurements made perpendicular to the nematic director					
T (°K)	ϵ_s	ϵ''_m	ϵ_∞	β	$10^9\tau_\perp$ (sec)
294	5.40	0.90	2.63	0.65	2.5
299	5.45	0.93	2.63	0.66	2.4
305	5.80	1.01	2.59	0.63	2.2
310	5.95	1.14	2.55	0.67	2.2

Measurements of the isotropic phase[a]				
T (°K)	ϵ_s	ϵ''_m	ϵ_∞	$10^9\tau$ (sec)
315	8.75	2.32	4.13	4.6
321	9.75	3.04	3.67	3.8
325	9.70	3.14	3.42	3.3
330	9.80	3.10	3.60	2.9
336	9.75	3.13	3.49	2.5
342	9.70	3.08	3.54	2.2
349	9.60	3.00	3.60	1.7

Reproduced from M. Davies et al., *J. Chem. Soc. Faraday Trans. II* **72**, 1447 (1976).
[a] $\beta = 1.0$ throughout.

anisotropy of polarizability (i.e., quasi-critical opalescence). This may be expressed as an effective molecular Kerr constant ${}_mK_2$ which increases dramatically at temperatures near T_c and diverges in the nematic proper. The increase is "pretransitional" in the sense of de Gennes (1974a), who has treated it hydrodynamically. The molecular counterpart can be extracted from Freed's theory given above. The process is clearly degraded by dilution (Fig. 8.1.4.4), which suggests the Curie–Weiss type of relaxation:

$$ {}_mK_2 = C(T - T^*)^{-\gamma} $$

where C is a constant and T^* a temperature slightly below T_c. The formal explanation for such sensitivity in ${}_mK_2$ *while still* in the *isotropic phase* may be made in terms of expressions given by Kielich (1972). Such angular

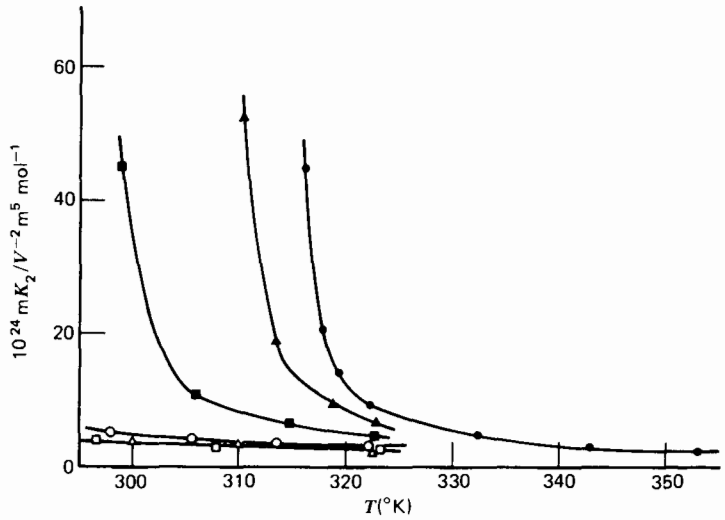

Figure 8.1.4.4 Temperature variation of the molecular Kerr constant of pure HCB and of its solutions in benzene of decreasing concentrations. ●: pure; ▲: 3.34; ■: 3.21; ○: 3.03; △: 2.04; □ 1.05 mol cm^{-3}. [Reproduced by permission from R. F. S. Moutran et al., *J. Chem. Soc. Faraday Trans. II* **72**, 1447 (1976).]

correlations involve the molecular axes, and the molecular dipole directions must therefore be a mixture of terms. The Kerr effect relaxation is dominated by cross terms close to the transition temperature so that hydrodynamic modes rapidly begin to take over from single molecule equations of motion.

8.1.5 Depolarized Rayleigh Scattering

The theory of light scattering from rodlike molecules has been discussed at length by Berne and Pecora (1976), and use of the technique has been made by Gierke and Flygare (1974) in MBBA-CCl_4 solutions. Static and dynamic correlations analogous to those described at the end of Chapter 3 are used, after Keyes and Kivelson (1972). Orientational pair correlations become important above 0.4 mole fraction MBBA and the value of $g_2 = 0.565$ observed for 0.9 mole fraction MBBA at 303°K is an order of magnitude larger than in pure nitrobenzene. In contrast, the dielectric measurements quoted above provide us with g, which is similar in the nematic and isotropic environments. In the hydrodynamic theory of de Gennes we have $g_2 = bT/(T - T^*)$ so that this, as well as the Kerr constant, diverges when $T = T^*$. In molecular terms the factor g_2 is defined by

$$ g_2 = 1 + \sum_{l \neq 1} \frac{\langle \mathcal{D}^2_{00}(\Omega^1)\mathcal{D}^2_{00}(\Omega^l)\rangle}{\langle \mathcal{D}^2_{00}(\Omega^1)\mathcal{D}^2_{00}(\Omega^1)\rangle} $$

which can become very large compared with unity (when there are many contributing terms in the numerator) but cannot diverge. In view of the values attributable to g_2 the average J_2 is surprisingly small (0.8 ± 0.3). This may be rationalized using the relation

$$\mathscr{D}^2_{00}(\Omega^1) = \sqrt{3/2}\left(\sqrt{-1}(\mathscr{D}^2_{0,-1} + \mathscr{D}^2_{01})\frac{J_y}{I_{yy}} - (\mathscr{D}^2_{0,-1} - \mathscr{D}^2_{01})\frac{J_x}{I_{xx}}\right)$$

Using this it may be seen that J_2 measures correlations in the *angular momentum* of MBBA. The small value of J_2 is due to a near cancellation of equally strong parallel and antiparallel pair correlations in the angular momentum of two MBBA molecules. Both these configurations would contribute *additionally* to g_2. Using the empirical relation

$$(g_2 - 1)^{-1} = W(\rho^* - \rho)$$

where ρ^* is a critical number density, it is possible to build up a systematic scheme for the evaluation of factors important in the formation of the

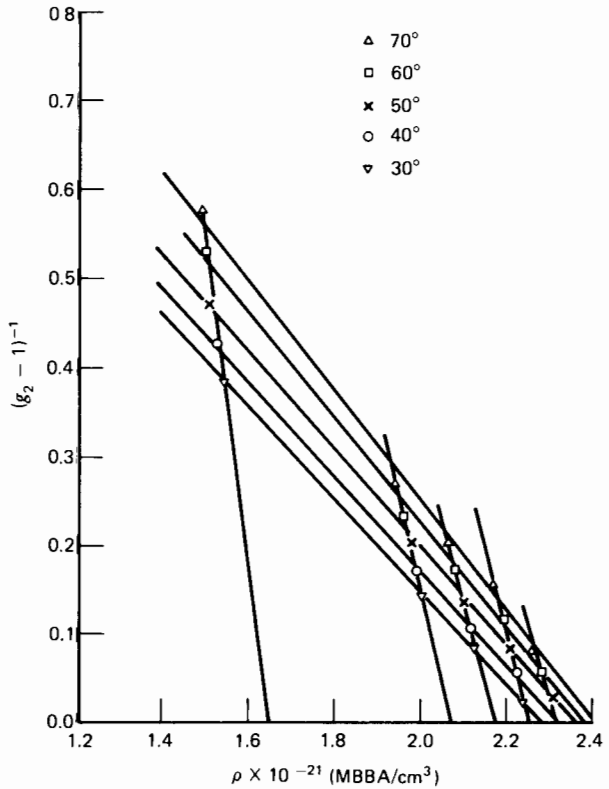

Figure 8.1.5.1 Critical density curve for MBBA. [Reproduced by permission from T. D. Gierke and W. H. Flygare, *J. Chem. Phys.* **61**, 2231 (1974).]

mesophase. Here W is a constant. The critical density is found from g_2 at each temperature or mole function of MBBA. ρ^* is the density of MBBA molecules at which the orientational pair correlation becomes infinite and is connected intimately with the nematic to isotropic transition temperature. If the measured temperature dependence of the density is plotted (Fig. 8.1.5.1) on the critical density curve $T(\rho^*)$, the resulting interactions are very close to the observed nematic/isotropic transition temperatures for each solution in CCl_4.

This suggests that the factors that are important in producing a nematic phase can be quantitatively measured through g_2. For example:

1. The effect of molecular structure and molecular polarity on the pair correlation can be measured quantitatively using depolarized Rayleigh scattering.
2. By measuring the depolarized intensities as a function of temperature and pressure it might be possible to explore the relative importance of hard core repulsive and electric (attractive) forces.

8.1.6 Magnetic Susceptibility Measurements

The magnetic properties of liquid crystals are the most fascinating and the most neglected when it comes to interpreting the susceptibility in terms of molecular dynamics. We are not here referring to the enormous NMR and EPR literature but to the phenomena embodied in the alignment of the nematic director with a very small magnetic field. The interaction energy per molecule is less than $10^{-6}kT$ at ambient temperatures so that well over a million in-phase torques are operative in overcoming the thermal energy.

Moutran (1975) has used the Gouy method for the measurement of magnetic susceptibility in the pure phases and solutions of liquid crystal compounds. The mass susceptibility was calculated using the density ρ so that

$$\chi_m(\text{pure l.c.}) = \frac{\chi(\text{pure l.c.})}{\rho_{\text{l.c.}}}$$

The method probes the effect of alignment at different temperatures and different concentrations. At low values of the magnetic field the mass susceptibility values are constant, but thereafter change (Fig. 8.1.6.1) until another constant value is reached at high magnetic field intensities, indicating complete alignment. There is a noticeable variation of the mass susceptibility at the clearing point when plotted as a function of temperature. As a function of solute concentration in benzene the susceptibility increases with decreasing concentration, suggesting that molecular interactions disappear at a concentration of about 2.4–2.8 mole/dm^3, confirming

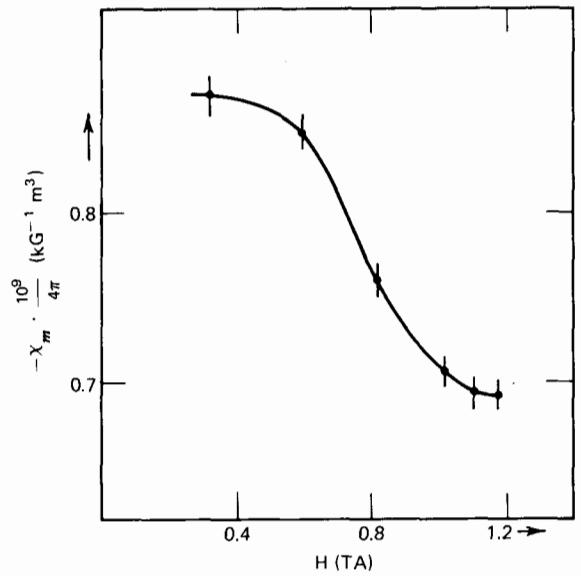

Figure 8.1.6.1 Curve of the magnetic susceptibility versus magnetic field strength for a pure HCB sample at room temperature. [Reproduced by permission from R. Moutran, Ph.D. Thesis, University of Wales (1975).]

the results of other measurements. The usefulness of such measurements has been demonstrated by Moutran (1975), who has calculated the average number of molecules in the swarm. In their theory they postulated that the molecules belonging to one swarm have parallel Z-axes but in the absence of a magnetic field the direction of the Z-axes differ from swarm to swarm and that the Z-axes of the swarm can rotate freely. A magnetic field is able to give a reasonable orientation when the energy corresponding to this orientation of the swarm is of the order of or larger than kT. When the mass of the swarm equals m, this roughly means that

$$\tfrac{1}{2}mH^2\left[\chi_Z - \frac{\chi_X + \chi_Y + \chi_Z}{3}\right] \geqslant kT$$

Whether or not the swarms are oriented by the magnetic field therefore depends on the value of the magnetic field **H**. In a weak magnetic field no orientation occurs at all. The measured susceptibility of the nematic state in weak magnetic fields should not differ markedly from the susceptibility of the isotropic liquid. A more rigorous statistical treatment involving averaging over all possible orientations gives an improvement of about 30% in the value of m calculated. Assuming that

$$\chi_{\text{isotropic}} = \frac{\chi_X + \chi_Y + \chi_Z}{3} \qquad \text{and} \qquad \chi_Z = \chi_{\parallel}$$

the mass susceptibility of the parallel aligned nematic, then on the average there are 17×10^7 HCB molecules and 6.7×10^7 molecules of MBBA in a "swarm" compared with 3×10^{10} for p-azoxyanisole. The magnetic field intensity therefore exerts a torque just enough to overcome kT through the mediation of swarms of this size. There are several methods available therefore (electrooptic and magnetic) that are more sensitive to molecular aggregation than classical dielectric spectroscopy. However, the molecular dynamics are revealingly studied by microwave methods.

8.1.7 Microwave Studies of Liquid Crystals

By extending the frequency range to the higher end of the 0–THz frequency region the details of the molecular dynamics in the nematic and isotropic phases begin to emerge more clearly, and modifications to the memoryless and inertialess equations of motion soon become necessary even for qualitative description. An extension up to 18 GHz for the study of the nematic and isotropic phase of n-heptyl- and n-heptoxycyanobiphenyl has revealed an extra high frequency loss peak in both the nematic phase (parallel alignment) and in the isotropic phase. This multiple loss process requires the use of more sophisticated dynamic models or, alternatively, more realistic forms of the intermolecular superimposed potential in the Nordio or Freed theories.

The problem may be typified analytically by using a very simple form of the Smoluchowski equation originally devised by Budó (1949) for the reorientational Brownian motion of molecules with internal degrees of freedom. This relies on the assumption that on the time scale characterizing the observable dielectric loss (that of the orientational correlation function), the angular velocity is a fast-decaying variable. In other words, to a first approximation, we may describe the high frequency rotational molecular dynamics in terms of a lattice with fixed molecular centers of mass. The extra potential may then be regarded as being electrostatic; for example, dipole–dipole interaction would be appropriate. The positive (repulsion) forces due to shape anisotropy could then be appropriately accounted for through the friction coefficient (tensor) and stochastic part of the Langevin equation governing the Brownian motion. The fictional nematic director can now be replaced by imagining a typical parallel ordering built up on this pairwise basis. The Smoluchowski treatment governing the process is now that of Section 3.4.4.2. It is not sensible to use an overelaborate form for the V in this oversimplified model, and we may conveniently use the form

$$V = -\frac{V_0}{kT}\cos(\phi_1 - \phi_2)$$

as in Chapter 3. The solution may then be solved numerically, as in Chapter 3, through the medium of the Sturm–Liouville equation whose

eigenvalues and eigenfunctions go to make up the theoretical microscopic polarizability and dielectric susceptibility. Using this type of rough modeling the theoretical and experimental curves are matched in Fig. 8.1.7.1. Not surprisingly, the result is better in the isotropic phase since the tensor nature of $\underline{\epsilon}''(\omega)$ in the nematic cannot easily be accommodated within the framework of a scalar friction coefficient as used in the Smoluchowski equation given by Budó.

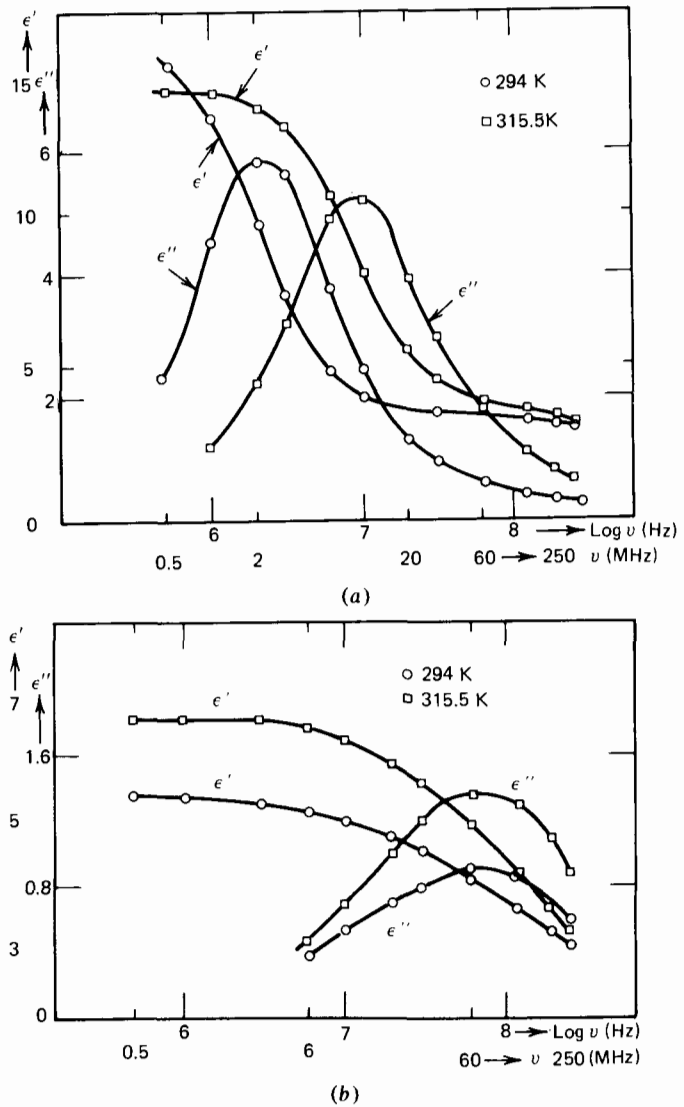

Figure 8.1.7.1 (*a*) Measured dielectric loss of 4-*n*-heptyl-4′-cyanobiphenyl in the isotropic liquid state. (*b*) The same in the nematic state. ○ 294°K; □ 315.5°K. (*c*) At 303°K. (Source as for Fig. (8.1.6.1).)

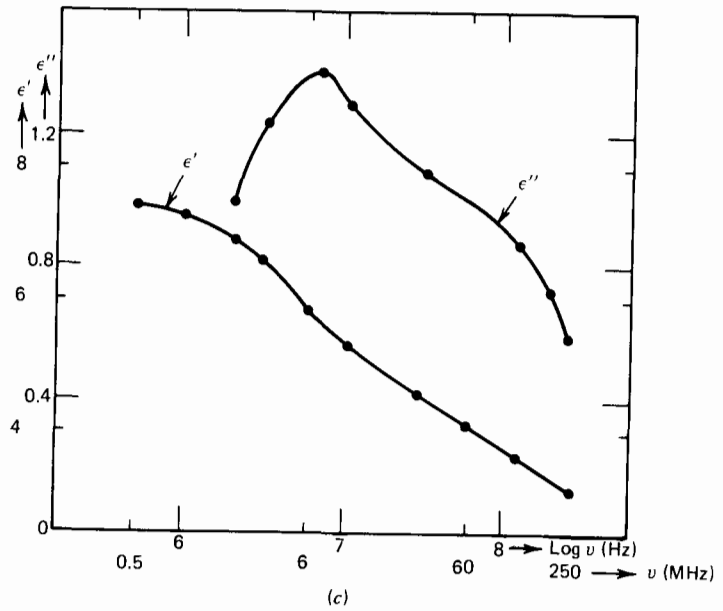

Figure 8.1.7.1 (*Continued*)

The further far infrared loss of Section 8.2 may be described only by using inertial and memory effects. The complete 0–THz spectrum is more complicated than can be accommodated within the dynamic theories of the nematic phase presently available.

8.1.8 Inelastic Neutron Scattering

This is a method of studying fast reorientation in a liquid crystal in the region of energy transfer (or frequency) covered by the far infrared and microwave in electromagnetic absorption and dispersion. Typical are the results of *p*-azoxyanisole (PAA) which are intended to complement those from dielectric relaxation and NMR relaxation (Janik, 1977). In Chapter 6 we have discussed the inconsistencies of this methodology for CH_2Cl_2 and it is hardly to be expected that the situation will be any better in a molecule as complicated as PAA. However, dielectric measurements evidence two relaxation regions in PAA in the nematic phase at 398°K with relaxation times of 4.3×10^{-9} and 2.2×10^{-11} sec. The available NMR data are entirely inconsistent with the dielectric data, because if the observed NMR effect is caused by the molecular reorientations about the short axis, then from the dielectric relaxation time $\tau_1 = 4.3 \times 10^{-9}$ sec, and using the known relation $\tau_2 = \tau_1/4$, it follows that $\tau_2 = 1.0 \times 10^{-9}$ sec, one order of magnitude more than the measured correlation time. If, on the other hand, the NMR

relaxation has been caused by reorientation about the long axis, from the value $\tau_1 = 2.2 \times 10^{-11}$ sec and the $\tau_2 = \tau_1/4$ relation it follows that $\tau_2 = 0.6 \times 10^{-12}$ sec, one order of magnitude less than the measured time.

Despite some insupportable assumptions such as the factorization of rotation and translation the quasi-elastic neutron scattering results on the nematic phase of *p*-azoxyanisole seem to suggest the following:

1. The stochastic dynamics are more complicated than rotational diffusion about the long molecular axis.
2. The observable rotational dynamics are much faster than those connected with the dielectrically measured relaxation time of 2.2×10^{-11} sec. This is a way of saying that the neutron scattering (quasi-elastic) is complementing the far infrared part of the 0–THz data.
3. The neutron scattering data is interpretable in terms of motions about the long molecular axis, but could equally well be referring to fast stochastic fluctuations of the long molecular axes with respect to the nematic director vector **n**. These faster fluctuations are echoed by high microwave frequency relaxations bordering on the far infrared.

However, there are so many model assumptions needed to extract meaningful information from quasi-elastic neutron scattering that any detailed information about rotational mechanisms must be regarded with caution unless they are corroborated by molecular dynamics simulation (Chapter 12). The central problem is the evaluation of the intermediate scattering function (McDonald and Hansen, 1976), which is usually written as a product of scattering functions. It is difficult to evaluate the correlation function except for special situations. If the long molecular axis is fixed and the molecule undergoes rotational diffusion about this axis as in the model for PAA, the correlation function can be evaluated as a series expansion. However, as pointed out by Luckhurst and Faber (1975), the assumptions employed in this derivation are unlikely to be valid in the nematic phase, owing to the neglect of long-axis motion.

8.2 THE FAR INFRARED SPECTRA OF LIQUID CRYSTALS

The first attempts at evaluating the interactions and dynamics associated with the molecules of a mesophase using the far infrared may be dated to around 1972. The difference between the aligned nematic phase and the plastic crystalline or disordered solid mesophase (Chapter 7) is that molecular rototranslation in the former evidently prohibits crystallization or even solidification. This degree of dynamic freedom is propagated by the asymmetric van der Waals contours (constantly fluctuating due to intramolecular motions) of molecules such as MBBA which have liquid

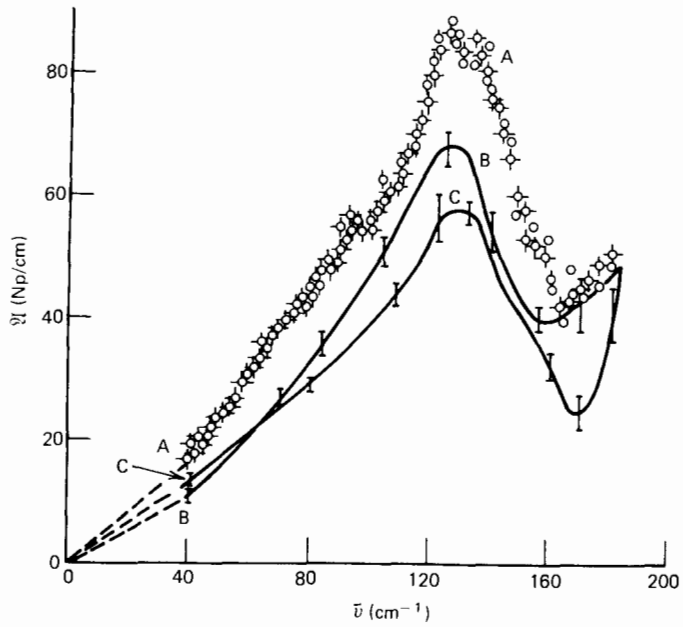

Figure 8.2.1 (*A*) Spectrum of nematic MBBA at 296 ± 0.5°K. -⊙- Mean of three interferograms at a thick pathlength ratioed to the mean of three interferograms at a thin pathlength. ⊙ An individual thick path length interferogram ratioed to the latter mean. (*B*) Spectrum of isotropic MBBA at 341°K; (*C*) at 359°K. [Reproduced by permission from M. Evans et al., *J. Chem. Soc. Faraday Trans. II* **69**, 1013 (1973).]

crystalline properties. It is possible, therefore, to supercool the aligned nematic phase, the sample remaining a viscous fluid. The main feature of the MBBA far infrared spectrum (taken in unaligned, aligned, isotropic solution and solid states) is a strong and broad band peaking at 130 cm^{-1} (Fig. 8.2.1). In the pure isotropic phase this shifts slightly to lower frequencies (123 cm^{-1}). The band seems almost to disappear in very dilute solution and broadens considerably on heating a moderately dilute solution of MBBA in cyclooctane (Fig. 8.2.2). At the same time the peak moves to a lower frequency. Thus the absorption is markedly environment sensitive, the near neighbor interactions involved being strong in the pure nematic phase. It can be concluded therefore that its origin is possibly due to torsional oscillation of the MBBA resultant dipole vector $\boldsymbol{\mu}$ occurring at a higher frequency than is usual for isotropic dipolar liquids, such as the halogenobenzenes or CH_2Cl_2. On this basis, Evans et al. (1973) carried out some model calculations of the MBBA absorptions. The first of these involved the itinerant oscillator and the second the Brot–Lassier formalism mentioned in Chapter 7. Neither is strictly valid for tensor permittivity, but may be applied in the isotropic phase. These models are of course early

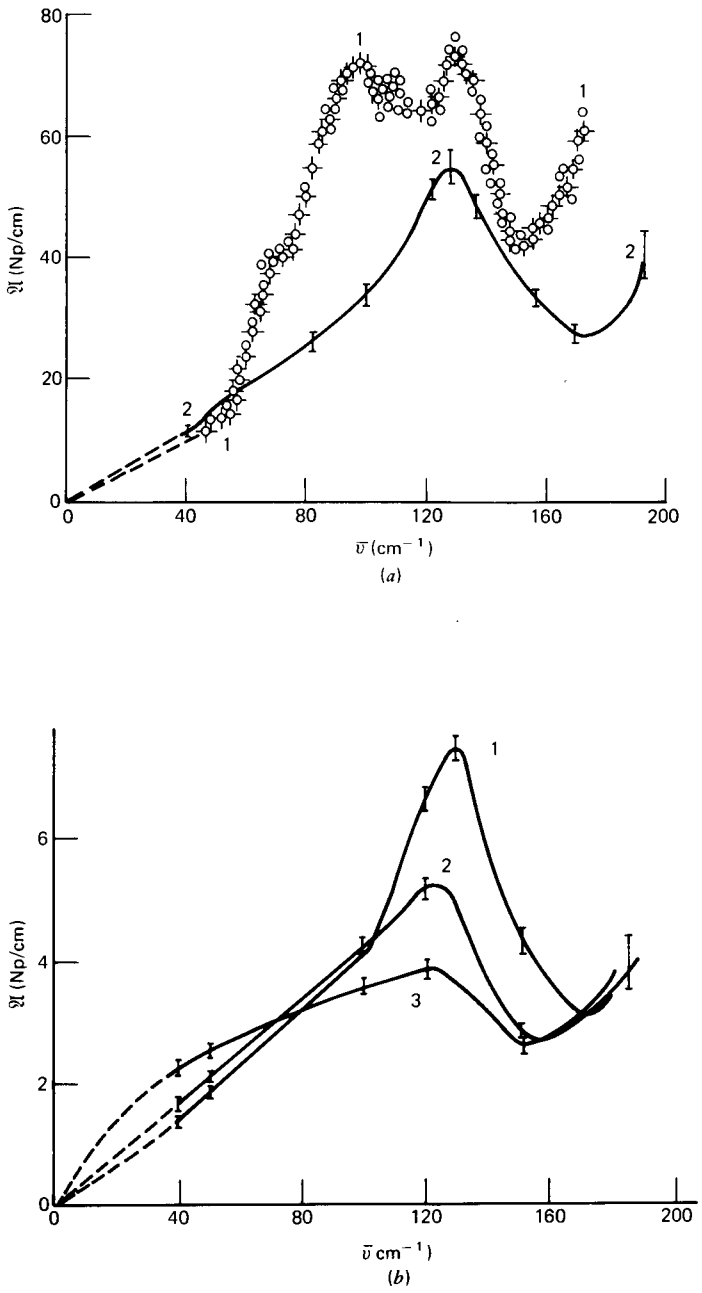

Figure 8.2.2 (*a*) (1) Spectrum of crystalline MBBA at 283 ± 1°K. (2) Spectrum of 67.3% (w/w) solution of MBBA in benzene at 296 ± 0.5°K corrected for solvent absorption. (*b*) (1) Spectrum of a 10.2% (w/w) solution of MBBA in cyclooctane (corrected as in Fig. 8.2.2*a*) for solvent absorption; (2) same at 324°K; (3) same at 338°K. [Reproduced by permission from M. Evans et al., *J. Chem. Soc. Faraday Trans. II* **69**, 1013 (1973).]

approximants of the Mori continued fraction neglecting all rototranslational coupling and mode–mode coupling. In the Brot–Lassier model the torque is not properly defined. To reproduce the observed spectrum it was found that the potential well experienced by an MBBA molecule in the field of its neighbors must be considerably narrower and steeper than that of isotropic phase molecules. The well depth estimated for best fit agreed fortuitously with a rough calculation using a potential of the form

$$V = a \exp(-br) - \frac{c}{r^6}$$

in which the only intermolecular interactions considered were those between the benzene rings of MBBA packed in an idealized geometry.

Each model envisages a central molecule instantaneously surrounded by a certain number of neighbors. This coordination number defines the angular aperture of the energy wells in which the molecule librates; the contour of the supposed identical energy wells and their depth (nkT) providing parameters which have to be chosen to match the observed spectrum. However, each is classifiable or based on a Mori approximant, and it is logical to pursue this methodology applied to $C_u(t)$. Varying γ and $\phi_1(0)$ of that equation gives the results of Fig. 8.2.3 where the theoretical $\mathscr{A}(\omega)$ and loss curves are in fairly satisfactory agreement with experiment for the isotropic phase. $\mathbf{C}_u(t)$ for the nematic is tensorial. The mean square torque term $\phi_1(0)$ takes on a high value compared with those found empirically in fluids such as CH_2Cl_2. Across the series MBBA:propyne:$CBrF_3$:$CClF_3$:CHF_3, for example, the apparent mean square torques decrease roughly in the ratio 200:25:10:10:8. This trend is the one expected on the assumption that the greater the molecular geometrical anisotropy, the greater the barrier to torsional oscillation. For a high mean square torque the microwave and far infrared parts of the 0–THz band must be widely separated, whereas for a low mean square torque (as in CHF_3, for example) the two parts are virtually fused into one.

Despite the apparently good fit obtained with γ and $\phi_1(0)$ it must be emphasized that any modeling as described must of necessity be approximate because mathematical tractability demands the use of rigid whole molecule libration using a very simple representation of the intermolecular potential. The far infrared spectrum of MBBA is environment sensitive but is best described as arising from the librations of a dipole within a flexible framework, the motions of which are determined by and in turn determine the character of the nearest neighbor and less immediate environment. In treating analytically the flexible molecular framework a degree of extra complication is engendered which often leads to overparameterization. The moment of inertia tensor is, for example, time dependent. In addition the long range correlations are important in the mesophase, so that it is likely that collective motions are favored. The continuum theory (de Gennes, 1974) has to be dovetailed accurately with

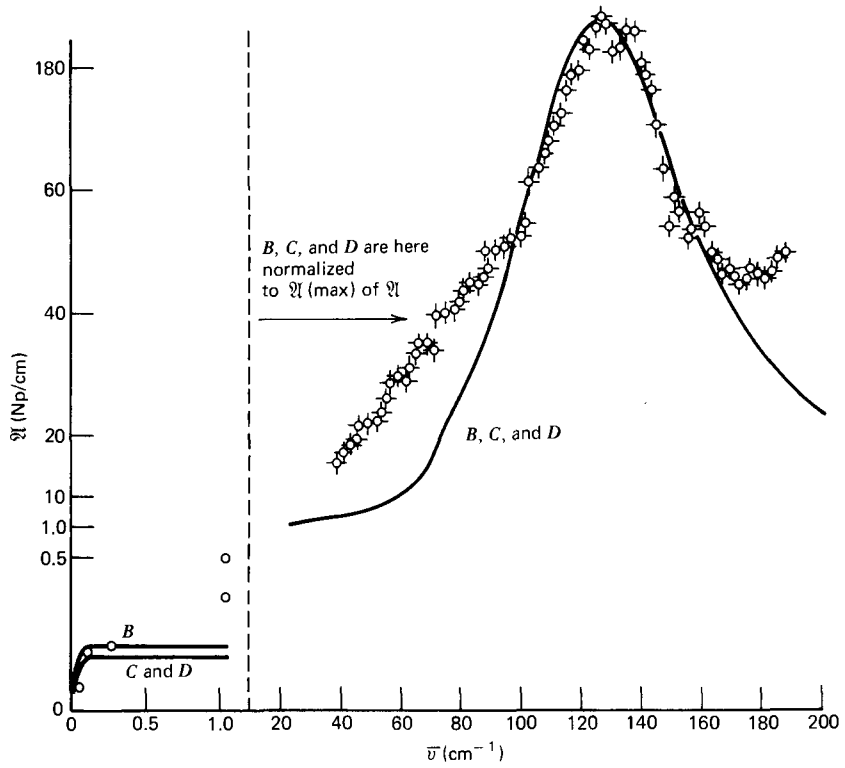

Figure 8.2.3 (*A*) -⊙- Mean of 11 interferograms for nematic MBBA at 296°K. (*B*) Theoretical curve of the Brot–Lassier model of Chapter 7. (*C*) An itinerant librator model of Wyllie and Larkin. ⊙ Experimental microwave data. [Reproduced by permission from M. Evans, *J. Chem. Soc. Faraday Trans. II* **69**, 1013 (1973).]

molecular theories if a cohesive picture is to be built up. Computer simulation runs into difficulties because the swarm sizes to be dealt with are larger than the box of molecules used initially. Finally, it has been observed (Evans, 1973) that in solid MBBA the 130 cm^{-1} band splits into at least four partially resolved peaks so that there is a possibility that, as pointed out by Sciesincka et al. (1973), the torsional vibrations and other low frequency internal modes of the MBBA molecule account for at least some of the absorption below 170 cm^{-1}. They cite evidence of changes in the spectra which they associate with different phases of MBBA solid and in the persistence of the absorption in solution. However, the 130 cm^{-1} band is dilution sensitive as regards its shape and peak position so that intermolecular sensitivity is detectable.

So far we have dealt only with the dynamics of the nematic phase but to extend the 0–THz monitor to phases such as the cholesteric (or cholesteryl oleyl carbonate and cholesteryl linoleate, e.g.) it is more fruitful to look

indirectly at the effect of the environment on small amounts of rigid, intensely absorbing dipolar solute molecules such as CH_2Cl_2 used as dynamic probes. This is the kind of approach used for glasses in the previous chapter. The following advantages accrue.

1. Cross correlation terms between guest molecules (dynamic and electrostatic), not amenable to ready mathematical analysis, are minimized in dilute solution in the cholesteric, nematic, or aligned nematic solvent.
2. The probe can be chosen to be particularly suitable for model simulation of its absorption profile (i.e., to be rigid and intensely absorbing).
3. The influence of a liquid crystalline environment on molecular motion may be measured directly against the equivalent spectra in an isotropic solvent such as CCl_4 or decalin (Chapters 4 and 7).

The far infrared spectra of the mesophases themselves are often rich in detail but consequently very difficult to model. For example, if HCB is treated in the nematic phase with AC and DC electric fields of up to 7 kV/cm or with magnetic fields, extra peaks seem to appear, underlying the structure in the unaligned condition (Fig. 8.2.4). However a crude first

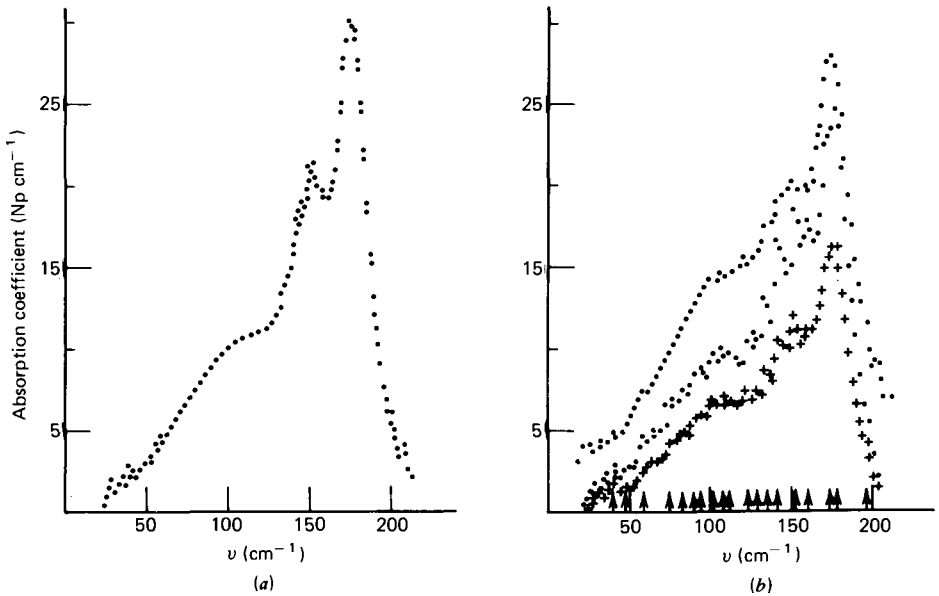

Figure 8.2.4 Electric field effect on the nematic phase of HCB. (*a*) Nematic phase of HCB at 299°K, unaligned. (*b*) Applied fields of ● 2.0 kV/cm; ○ 3.0 kV/cm; + 7.1 kV/cm. [Reproduced by permission from G. J. Evans et al., *J. Chem. Soc. Chem. Commun.* 1978, 267).]

attempt has been made to use the scalar equations of Chapter 3 to fit the data for HCB in the parallel aligned nematic over a broad sweep of 0–THz frequency. The $C_u(t)$ Mori three-variable theory is capable of reproducing only two out of the many peaks observable. The microwave shoulder recently discovered by Price and co-workers (1976, 1979) can be matched only with a superimposed potential so that the Mori equation is affected by an extra linear term as in Freed's theory of Section 8.1. The extra term also introduces tensorial quantities into the final $\mathbf{C}_u(t)$, as is the requirement in the nematic phase. With the simple scalar $C_u(t)$ the peak corresponding to rigid end-over-end torsional oscillation is theoretically very sharp, centered at over $100\,cm^{-1}$ but obviously (in the light of the electric and magnetic field work) one of the many possible such absorptions, all markedly environment sensitive. The effect of applying an increasing dc field to the nematic phase of HCB is shown in Fig. 8.2.4. The overall intensity of the absorption decreases over the whole of the far infrared range and the spectrum is split into peaks hitherto unresolved in the unaligned condition. An intensity decrease on application of an external field has been observed in the Raman bands by Schwartz et al. (1976). In the nematic phase of two compounds striking changes in the relative intensity of several Raman bands were observed as a function of applied electric field strength. An explanation was given in terms of the collective stabilization due to the large ensemble of molecules aligned by the field. The question of what happens to the far infrared torsional oscillatory band is an interesting one, with a direct bearing on single and collective molecular dynamics. However, little experimental work has been completed in this region to date.

The use of probe molecules such as CH_2Cl_2 is designed to avoid for the moment the difficulties of quantitative interpretation associated with the far infrared spectra of pure liquid crystals. The far infrared broad band absorptions of pure CH_2Cl_2 and in isotropic solution have been measured carefully. Whereas the CH_2Cl_2 band maximum ($\bar{\nu}_{max}$) shifts by about $30\,cm^{-1}$ to lower frequency on dilution in both CCl_4 and decalin, there is a smaller corresponding change when CH_2Cl_2 is dissolved in cholesteryl oleyl carbonate and cholesteryl linoleate (Fig. 8.2.5). This may be attributed to a persistence of statistical cross correlations (time-dependent Kirkwood g factors) which vanish gradually in isotropic solvents. The observed integrated absorption intensity per molecule (A/N) of CH_2Cl_2 is decreased significantly compared with that in CCl_4 or decalin. However, the opposite effect is observed in the microscopic region, where the apparent dipole moment increases on dilution in cholesteryl oleyl carbonate. There is an inhibition in intensity of CH_2Cl_2 when dissolved in molecules such as those of the cholesteric phase (the twisted nematic).

The integrated intensity (A) of the far infrared band is plotted against molecular number density (N) in Fig. 8.2.5 for the CH_2Cl_2 Poley band in various solvents at 298°K. These are carbon tetrachloride, decalin, choles-

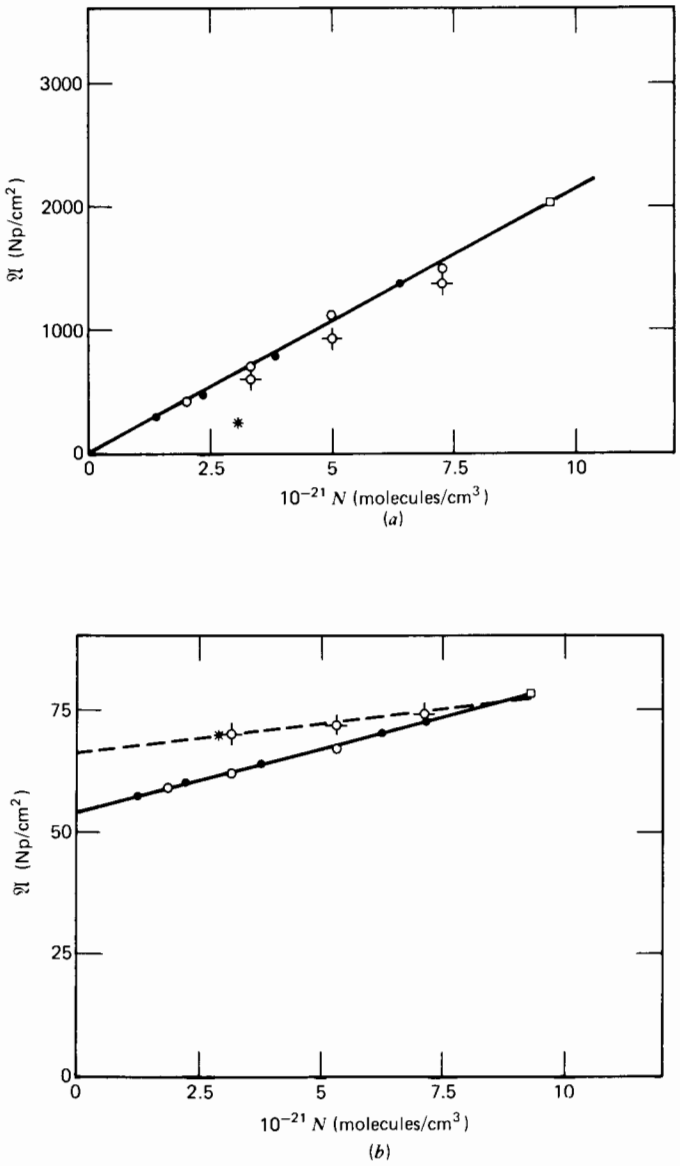

Figure 8.2.5 Variation of $\bar{\nu}_{max}$ and integrated intensity for in all environments. (a) ○ in CCl_4; □ pure CH_2Cl_2: ● in decalin; -⊙- in OCC; * in cholesteryl linoleate. (b) Solid line, best straight line through the CCl_4 and decalin data. Dashed line, best straight line through the cholesteric data. □ Pure CH_2Cl_2; ○ CCl_4 solution; ● decalin solution; -⊙- in OCC; * in cholesteryl linoleate. [Reproduced by permission from G. J. Evans et al., *J. Chem. Soc. Faraday Trans. II* **74**, 343 (1978).]

teryl oleyl carbonate (OCC), and HCB. In CCl_4 and decalin A/N is constant within the experimental uncertainty over the whole range of dilution, while it is clear that dilution in the solvents that have liquid crystal type phases reduces A/N considerably. This reflects an unusual constraint on angular movement (polarization) which persists when the concentrations of CH_2Cl_2 are such that no liquid crystalline properties are apparent on the macroscopic scale, for example, when birefringence has disappeared. This is substantiated by the pretransitional Kerr effects of Section 8.1.4.

In the mesophase itself this type of partial ordering was first observed using NMR methods of studying benzene in a nematic solvent. A spectrum is obtained consisting of broad bands attributable to the solvent, superimposed on which is a series of sharp lines. Benzene acquires a preferential orientation due to solvent-solute interactions and its NMR spectrum is governed by magnetic dipole-magnetic dipole interactions which are uniquely intramolecular in origin. The benzene molecule retains a translational freedom with respect to the nematic solvent, which is an explanation of the sharpness of the NMR lines. The orientation is in the direction of the principal magnetic field. Since this discovery analogous NMR studies have shown that most molecules are preferentially oriented in the nematic phase. The effect of this on its far infrared Poley absorption is retained well into the apparently isotropic condition. Additional dynamic information is of course available in the 0–THz range because the band shape of the Poley absorption contains dynamic information at short times in the orientational a.c.f., while NMR studies give us areas beneath a correlation function and not the details of its time evolution. We have illustrated this point by roughly reproducing the Fourier transform of $\mathfrak{A}(\omega)$ of CH_2Cl_2 in cholesteryl oleyl carbonate, whereupon the following related functions can be calculated analytically:

1. The orientational a.c.f. or dielectric decay function $\langle \cos\theta(t)\cos\theta(0)\rangle$, where θ is the angle between the dipole and a reference field direction,
2. The torque a.c.f. which mirrors the molecular librations by oscillatory behavior about the abscissa (time), that is, $\langle \ddot{\theta}(t)\ddot{\theta}(0)\rangle$.
3. The angular velocity a.c.f., the area beneath which is the NMR spin-rotation relaxation time.

8.2.1 Far Infrared/Megahertz Spectrum of Cholesteryl Oleyl Carbonate in the Cholesteric Phase

The cholesteric phase as distinct from the nematic involves a screw periodicity of the director which produces spectacular optical effects at visible frequencies. To attempt a rigorous description of the dynamics of the large, flexible molecules that make up the phase is well beyond the capabilities of present-day computers, but phenomenologically it is possible to extract some interesting features using the 0–THz range of frequencies.

The refractive index variation in this phase was shown in Fig. 1.2.5. A polarizer inserted in the refractometer eyepiece allows the measurement of the index of both the ordinary (n_o) and extraordinary (n_e) rays. The former is related to the mean polarizability perpendicular to the optic axis, the latter to the polarizability parallel to the optic axis. The calculated mean refractive index $[\bar{n} = \frac{1}{3}(2n_0^2 + n_e^2)^{1/2}]$ in the cholesteric phase extrapolates smoothly to that in the isotropic phase. The molecular polarizability of cholesteryl oleyl carbonate calculated from the refractive index does not show a large anisotropy in comparison with molecules which do not form mesophases. There is an absence of association in isotropic solution as measured from the static permittivity (i.e., that close to zero frequency). Recent Kerr effect studies have revealed also that in this case there are no large pretransition effects in the static Kerr constant (Williams and Crossley, 1977). Dielectric relaxation results in the kilohertz to megahertz range yield the refined data of Table 8.2.1.1 in terms of the empirical Fuoss–Kirkwood equation. The dipole moment of the low frequency process is smaller than that deduced from the low frequency measurement in solution, which implies that there is a second relaxation at higher frequencies above 250 MHz. Part of this must, as always, be in the far infrared, but it is not possible to rule out the presence of a further relaxation process at intermediate frequencies. The temperature variation of the low frequency

Table 8.2.1.1 The Dielectric Relaxation Parameters for OCC (See Text for Key to Symbols)

Phase	T (°K)	$10^3\epsilon''$	$10^8\tau$ (sec)	β	ϵ_s	ϵ_∞	$10^{30}\mu$ (C m)
Smectic	275	29	48.0	0.63	2.46	2.34	2.27
	276	28	33.0	0.82	2.44	2.34	2.00
	283	27	27.0	0.38			
	293	20	13.0	0.70	2.39	2.33	1.90
Cholesteric	296	23	2.1	0.43	2.44	2.33	2.56
	303	24	1.6	0.46	2.40	2.30	2.56
	308	27	1.1	0.50	2.41	2.31	2.63
Isotropic	310	24	1.1	0.41	2.41	2.29	2.77
	313	24	0.8	0.41	2.41	2.29	2.80
	319	28	0.5	0.44	2.41	2.28	2.97

Reproduced from Moutran et al., *J. Chem. Soc. Faraday Trans. II* **71**, 1854 (1975).

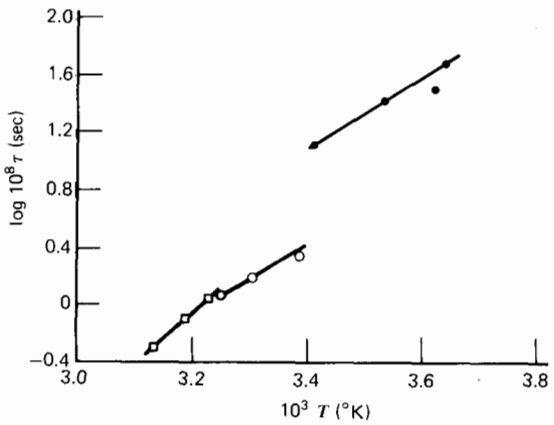

Figure 8.2.1.1 Temperature variation of the relaxation time (τ) of OCC; □ isotropic phase; ○ cholesteric phase; ● smectic phase. [Reproduced by permission from A. H. Price et al., *J. Chem. Soc. Faraday Trans. II* **71**, 1854 (1975).]

relaxation time in the isotropic liquid phase and in the cholesteric and smectic phases is illustrated in Fig. 8.2.1.1. The enthalpy of activation for the relaxation process in the isotropic phase is 70 ± 20 kJ/mole, in the cholesteric phase 44 ± 20 kJ/mole, and in the smectic phase 35 ± 20 kJ/mole. The relaxation times observed in the isotropic and cholesteric phases are very similar despite the difference in viscosity. A simple Stokes–Einstein model is therefore inapplicable. It would be strange if this were not the case.

The far infrared portion of the 0–THz absorption is illustrated for the pure cholesteric phase in Fig. 8.2.1.2. The solid line is the Brot–Lassier–Larkin model of molecular dynamics mentioned in previous chapters. This can be made to fit the data fairly well but serves only to emphasize that the broad band centered at 78 cm^{-1} should be regarded as the high frequency adjunct of the megahertz loss process. In this case it is partly masked by high frequency proper modes. For such an entanglement of inertias as the OCC cholesteric (or smectic) phase presents, the $\bar{\nu}_{max}$ value is rather high, indicating a significant mean square torque contribution to the overall dynamics. This pushes the low frequency adjunct of the 0–THz process to low frequencies and the high to high.

On dilution in cyclohexane there is a slight shift of 8 cm^{-1} to lower frequencies in $\bar{\nu}_{max}$. Such observations may be consistent with the following:

1. The libration in solution is still constrained largely to that about the long axis and the frequency shift indicates that the barrier to this motion has decreased slightly.

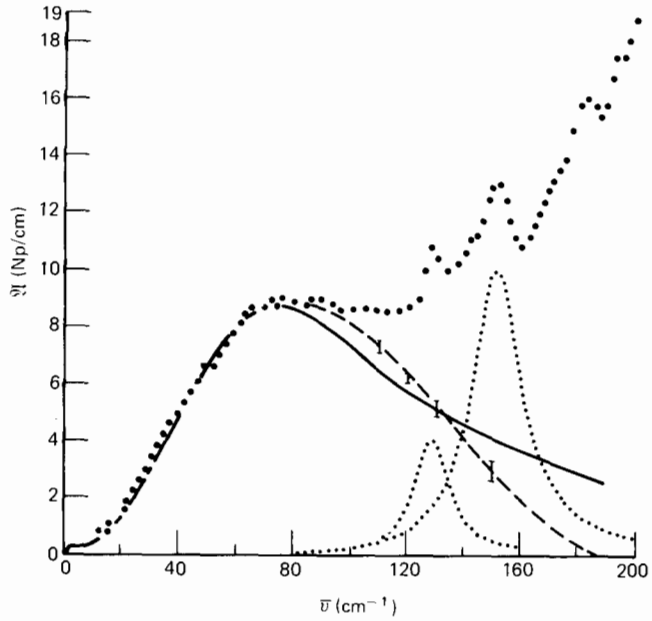

Figure 8.2.1.2 Mean of several determinations of the absorption of OCC at 298°K. The line shapes of the 128 and 151 cm^{-1} bands are idealized Lorentzians. Solid line, a model band shape (first approximation). [Reproduced by permission from A. H. Price et al., *J. Chem. Soc. Faraday Trans. II* **71**, 1854 (1975).]

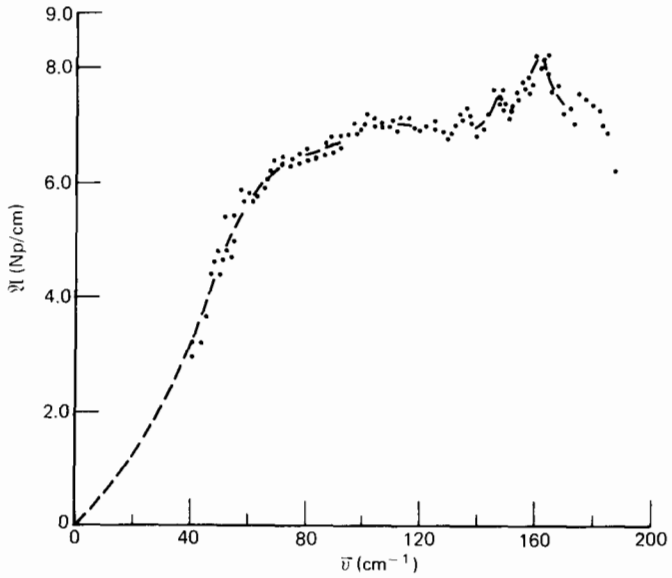

Figure 8.2.1.3 OCC in the far infrared amorphous solid at 111°K. [Reproduced by permission from A. H. Price et al., *J. Chem. Soc. Faraday Trans. II* **71**, 1854 (1975).]

2. As evidenced from Kerr effect studies of MBBA and HCB (Section 8.1.4) molecular aggregation can sometimes persist in the pretransition range, but this is unlikely to be the case in the OCC solutions.

Finally, in the amorphous phase at 111°K (Fig. 8.2.1.3) the $\tilde{\nu}_{max}$ shifts to around 100 cm^{-1}, a little higher than that in the cholesteric phase, so that there is an increased mean square torque.

8.3 COMPUTER SIMULATIONS

These are restricted at present to the study of facsimiles of the liquid crystal-forming molecule using vastly oversimplified intermolecular potential forms. Berne and Kushick (1975) have simulated cylindrically symmetrical molecules with arbitrary eccentricity as a first attempt. However, the swarms of 10^6 or 10^7 molecules are obviously too big to be detectable in a simulation using 100 or 1000 molecules with periodic boundary conditions. The system is initially ordered by a simulated electric field which when removed allows it to relax to equilibrium. The criterion for the existence of the simulated nematic phase is that the order parameter S stabilizes at a value significantly higher than zero with the density of the system still significantly lower than the expected solid density. The trouble is that simulation with molecules of this type often jams in a configurational bottleneck which does not necessarily have physical attributes. These last for a long time so that true equilibrium is difficult to obtain.

The results indicate that a system of ellipses with an axial ratio of 3 might be capable of forming a stable nematic phase in a range of densities intermediate between the solid and the isotropic liquid. Figure 1.2.7 illustrates the loss of ability to sustain ordering with axial ratios which are decreased below about 2 or 3.

The velocity a.c.f. for long ellipsoids behaves significantly since it is clear that the ellipsoid is more mobile when moving parallel to its principal axis than otherwise. This is also true in a state where $\langle P_2 \rangle$ is much lower—the simulated isotropic state. The anisotropy of translation seems to be overestimated in comparison with real systems, but is nevertheless fairly realistic.

An interesting attempt was made by Berne and Kushick to work out the contribution of collective motions to the second Legendre polynomial orientational a.c.f. (P_2) such as the one responsible for the depolarized Rayleigh spectrum. The cross-correlation function was evaluated by labeling the 256 ellipsoids at random and considering only correlations among the labeled molecules. N was then varied so that a sampling of concentrations could be observed. The multiparticle correlation function is shown in Fig. 8.3.1. The correlation time for the collective correlation function decreases as the concentration rises.

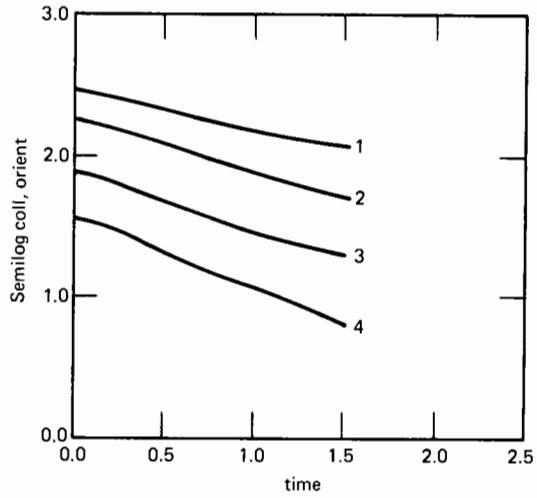

Figure 8.3.1 Multiparticle $C_u^{(N)}(t)$ molecular dynamics simulation of ellipsoids. Curves (1) to (4): decreasing number of particles used in simulation. [Reproduced by permission from J. Kushick and B. J. Berne, *J. Chem. Phys.* **64**, 1362 (1975).]

There are some Monte Carlo simulations of rodlike particles which produce results on the equilibrium properties of the ensemble under study. This is strictly outside the scope of this volume on dynamics but provides useful complementary information. A recent study by Luckhurst and co-workers (1980) is informative. Here the static properties of a linear array of rodlike bodies were simulated for the calculated temperature dependence of the energy and specific heat. The results were in agreement with those attained from thermodynamic considerations. Rotational disorder is correctly simulated only when the number of particles used exceeds 1000. The purpose of this simulation was to test the reliability of the Monte Carlo method for ensembles of anisotropic potentials whose thermodynamic properties are well-defined. The majority of calculations were performed with a sample of 256 particles. Figure 8.3.2 illustrates the analytical and Monte Carlo results for reduced energy per molecule. The agreement is satisfactory. The dependence of the order parameter on the number of particles used is, however, rather pronounced (Table 8.3.1). At a reduced temperature of 0.2, for example, it decreases from an unrealistic value of 0.180 for 256 particles to a value of 0.048 for 2500 particles. The energy and specific heat were independent of the sample size. The order parameter of Fig. 1.2.6 for a C_{2v} triatomic seems, however, to be satisfactorily close to zero with only 108 particles. This was a calculation by the authors using the molecular dynamics method as opposed to Monte Carlo. Because computer power is expected to increase dramatically in the next decade the extension of molecular dynamics will provide us with more detailed information than hitherto on the factors responsible for the exis-

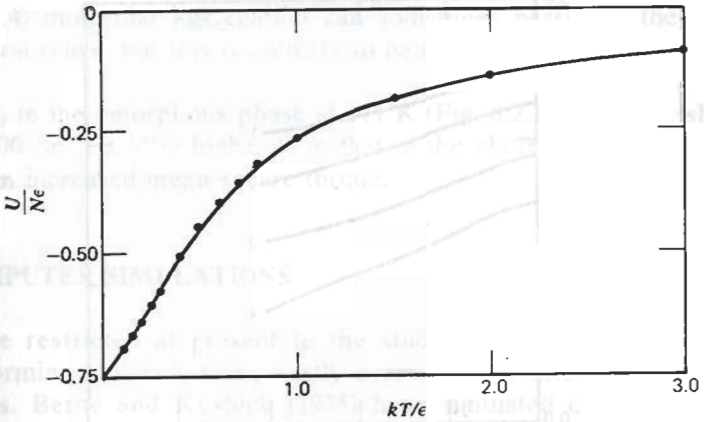

Figure 8.3.2 Analytical and Monte Carlo entropies and free energy per molecule. [Reproduced by permission from G. R. Luckhurst et al., *Mol. Cryst. Liq. Cryst.* **41**, 67 (1977).]

Table 8.3.1 Dependence of the Orientational Order ($\bar{T}_2$) Parameter on Reduced Temperature and Size of the Ensemble

kT/ϵ	$\bar{T}_2$	N	$L/10^6$ [a]
3.0	0.062	256	2.0
2.0	0.071	256	2.0
1.5	0.074	256	2.0
1.0	0.077	256	2.0
0.7	0.093	256	2.0
0.6	0.096	256	2.0
	0.063	576	4.5
0.3	0.158	256	1.0
	0.117	256	2.0
0.25	0.217	256	1.0
	0.129	576	4.5
0.2	0.180 ± 0.07	256	3.0
	0.116 ± 0.05	576	3.0
	0.078 ± 0.02	1156	5.0
	0.048 ± 0.02	2500	7.0
0.1	0.260	256	2.0
	0.127	576	4.5
0.05	0.290	576	4.5

[a] Length of production run.

tence of this state of matter. We might then be able to predict from a molecular basis some physical properties of these compounds without recourse to the crudities of mathematical modeling.

APPENDIX: MACRO-MICRO RELATIONS IN THE PRESENCE OF MODE–MODE COUPLING

If we choose the single-particle column vector to be represented by $\mathbf{A}_S$ and the collective processes by $\mathbf{A}_M$ the problem of correlating $\mathbf{A}_S$ and $\mathbf{A}_M$ may be dealt with within the Mori framework as described in detail by Berne and Pecora (1976). It is convenient to define a vector orthogonal to $\mathbf{A}_S$ by

$$\mathbf{A}_R = \mathbf{A}_M - \langle \mathbf{A}_M \mathbf{A}_S^T \rangle \langle \mathbf{A}_S \mathbf{A}_S^T \rangle^{-1} \mathbf{A}_S$$

where the superscript T denotes transpose. The Mori equation is then solved for the grand matrix:

$$\mathbf{A}_1 = \begin{bmatrix} \mathbf{A}_S \\ \mathbf{A}_R \end{bmatrix}$$

thus giving us a micro-macro relation between $\mathbf{A}_S$ and $\mathbf{A}_M$. To do this it is convenient to make the following definitions:

1. Define $\hat{P} = \hat{1} - \hat{Q}$ as the projection operator onto the subspace $[\mathbf{A}_S, \mathbf{A}_R]$.
2. Define the matrix $\mathbf{F}$ as

$$\mathbf{F} = \langle \mathbf{A}_S^{(2)} \mathbf{A}_S^{T(1)} \rangle \langle \mathbf{A}_S^{(1)} \mathbf{A}_S^{(1)T} \rangle^{-1}$$

where $\mathbf{A}_S^{(2)T}$ refers to the vector of particle 2 and $\mathbf{A}_S^{(1)}$ to that of particle 1. The matrix $\mathbf{F}$ is that of the static pair correlation of distinct particles:

$$\mathbf{G} = \frac{\int_0^\infty dt \langle \dot{\mathbf{A}}_S^{(2)}(0) [e^{i\hat{Q}\hat{\mathcal{L}}t} \dot{\mathbf{A}}_S^{(1)}(0)]^T \rangle}{\int_0^\infty dt \langle \dot{\mathbf{A}}_S^{(1)}(0) [e^{i\hat{Q}\hat{\mathcal{L}}t} \dot{\mathbf{A}}_S^{(1)}(0)]^T \rangle}$$

We have then

$$\langle \mathbf{A}_R \mathbf{A}_R^T \rangle = \langle [\mathbf{A}_M - \langle \mathbf{A}_M \mathbf{A}_S^T \rangle \langle \mathbf{A}_S \mathbf{A}_S^T \rangle^{-1} \mathbf{A}_S][\mathbf{A}_M - \langle \mathbf{A}_M \mathbf{A}_S^T \rangle \langle \mathbf{A}_S \mathbf{A}_S^T \rangle^{-1}]^T \rangle$$

The product $\langle \mathbf{A}_S^{(1)} \mathbf{A}_M^T \rangle$ may be expanded as

$$\langle \mathbf{A}_S \mathbf{A}_M^T \rangle = \langle \mathbf{A}_S^{(1)} \mathbf{A}_S^{(1)T} \rangle + (N-1) \langle \mathbf{A}_S^{(1)} \mathbf{A}_S^{(2)T} \rangle$$

and

$$\langle \mathbf{A}_M \mathbf{A}_S^T \rangle = \langle \mathbf{A}_S^{(1)} \mathbf{A}_S^{(1)T} \rangle + (N-1) \langle \mathbf{A}_S^{(2)} \mathbf{A}_S^{(1)T} \rangle$$

where N is the number of molecules in the system. By definition we have

$$\langle \mathbf{A}_M \mathbf{A}_S^T \rangle = \langle \mathbf{A}_S^{(1)} \mathbf{A}_S^{(1)T} \rangle [\mathbf{1} + N\mathbf{F}]$$

Similarly,

$$\langle \mathbf{A}_M \mathbf{A}_M^T \rangle = N \langle \mathbf{A}_S \mathbf{A}_S^T \rangle [\mathbf{1} + N\mathbf{F}]$$

so that

$$\begin{aligned} \mathbf{A}_R &= \mathbf{A}_M - \mathbf{A}_S(\mathbf{1} + N\mathbf{F}) \\ \langle \mathbf{A}_R \mathbf{A}_R^T \rangle &= N \langle \mathbf{A}_S \mathbf{A}_S^T \rangle (\mathbf{1} + N\mathbf{F}) - \langle \mathbf{A}_S \mathbf{A}_S^T \rangle (\mathbf{1} + N\mathbf{F})^2 \\ &\doteq N \langle \mathbf{A}_S \mathbf{A}_S^T \rangle (\mathbf{1} + N\mathbf{F}) \end{aligned}$$

because $N \sim 10^{23}$ and because intermolecular forces are short range on a microscopic scale so that $N\mathbf{F} \sim \mathbf{1}$. The off-diagonal elements of $\langle \mathbf{A}_R \mathbf{A}_S^T \rangle$ and $\langle \mathbf{A}_S \mathbf{A}_R^T \rangle$ are zero, so that restricting ourselves to Markov processes, the grand column vector $\mathbf{A}$ is governed by

$$\dot{\mathbf{A}}(t) = i\boldsymbol{\Omega} \cdot \dot{\mathbf{A}}(t) - \boldsymbol{\Gamma} \cdot \mathbf{A}(t) + \mathbf{F}(t)$$

where

$$\boldsymbol{\Gamma} = \boldsymbol{\Lambda} \cdot \boldsymbol{\chi}^{-1}$$

$$\boldsymbol{\Lambda} = \begin{bmatrix} \boldsymbol{\lambda}_{11} & N\boldsymbol{\lambda}_{11}(\mathbf{G}_{12} - \mathbf{F}) \\ N\boldsymbol{\lambda}_{11}(\mathbf{G}_{21} - \mathbf{F}) & \boldsymbol{\lambda}_{11} N(\mathbf{1} + N\mathbf{G}) \end{bmatrix}$$

We have assumed that $\mathbf{G}$ has elements of the order of $1/N$ so that $(\mathbf{1} + N\mathbf{F})^2$ is small compared with $N(\mathbf{1} + N\mathbf{G})$. The resonance term $i\boldsymbol{\Omega} \cdot \mathbf{A}(t)$ is defined by

$$\langle \dot{\mathbf{A}}(0) \mathbf{A}^T(0) \rangle \langle \mathbf{A}(0) \mathbf{A}^T(0) \rangle^{-1} \mathbf{A}(t)$$

and the λ terms by $G_{12} = \boldsymbol{\lambda}_{12} \boldsymbol{\lambda}_{11}^{-1}$. The dissipative matrix Γ and column vector $\mathbf{A}$ together yield expressions for the correlation functions of interest so that, for example,

$$\langle \mathbf{A}_S(t) \mathbf{A}_S^T(0) \rangle \langle \mathbf{A}_S(0) \mathbf{A}_S^T(0) \rangle^{-1} = \hat{\mathscr{L}}_a^{-1} \frac{\mathbf{1}s + \underline{\Gamma}_{22}}{(\mathbf{1}s + \underline{\Gamma}_{11})(\mathbf{1}s + \underline{\Gamma}_{22}) - \underline{\Gamma}_{12}\underline{\Gamma}_{21}}$$

$$\langle \mathbf{A}_R(t) \mathbf{A}_R^T(0) \rangle \langle \mathbf{A}_R(0) \mathbf{A}_R^T(0) \rangle^{-1} = \hat{\mathscr{L}}_a^{-1} \frac{\mathbf{1}s + \underline{\Gamma}_{11}}{(\mathbf{1}s + \underline{\Gamma}_{11})(\mathbf{1}s + \underline{\Gamma}_{22}) - \underline{\Gamma}_{12}\underline{\Gamma}_{21}}$$

If we were to concern ourselves with the mixing of spin and current densities we might have, for example,

$$\mathbf{A}_S = \begin{bmatrix} \mathbf{p}(t) \sum_n e^{i\mathbf{k} \cdot \mathbf{r}_n(t)} \\ \boldsymbol{\Omega}(t) \sum_n e^{i\mathbf{k} \cdot \mathbf{r}_n(t)} \end{bmatrix}$$

where $\mathbf{r}_n(t)$ is the position vector of the nth atom of the ith molecule and $\mathbf{p}(t)$ the linear momentum of the ith molecule and $\boldsymbol{\Omega}(t)$ the angular

REFERENCES

Agarwal, V. K., and Price, A. H., *J. Chem. Soc. Faraday Trans II*, **70**, 188 (1974).

Berne, B. J. and Kushick, J., *J. Chem. Phys.* **64**, 1362 (1975).

Berne, B. J. and Pecora, R., *Dynamic Light Scattering with Applications to Physics, Chemistry and Biology*, Wiley-Interscience, New York (1976).

Bordewijk, P. and Böttcher, C. J. F., *Theory of Electric Polarisation*, Vols. I and II, Elsevier, Amsterdam (1973, 1979).

Budó, A., *Phys. Z.* **39**, 706 (1938); *J. Chem. Phys.*, **17**, 686 (1949).

De Gennes, P. G., *J. Phys. (Paris)* **35**, 217 (1974a).

De Gennes, P. G., *The Physics of Liquid Crystals*, Oxford University Press, Oxford, (1974b).

De Vries, A., *Mol. Cryst. Liq. Cryst.* **49**, 19 (1978).

Evans, M. W., Davies, M., and Larkin, I. W., *J. Chem. Soc., Faraday Trans. II* **69**, 1013 (1973).

Freed, J. H., *J. Chem. Phys.* **66**, 3428, (1977).

Gierke, T. D. and Flygare W. H., *J. Chem. Phys.* **61**, 2231 (1974).

Janik, J., *Dielectric and Related Molecular Processes*, Vol. 3, Chem. Soc. p. 53 (1977).

Keyes, T. and Kivelson, D., *J. Chem. Phys.* **57**, 4599 (1972).

Kielich, S., *Dielectric and Related Molecular Processes*, Vol. 1, p. 233 (1972).

Luckhurst, G. R. and Faber, G., *Chem. Soc. An. Rep.* **75**, 40 (1975).

Luckhurst, G. R. and Zannoni, C., *Proc. Roy. Soc.* **343A**, 389 (1975).

Luckhurst, G. R., Denham, J. Y., Zannoni, C., and Lewis, J. W., *Mol. Cryst. Liq. Cryst.*, **60**, 157 (1980).

McDonald, I. R. and Hansen, J-P., *Theory of Simple Liquids*, Academic, New York (1976).

Maier, W. and Meier, G., *Z. Naturforsch.* **16A**, 470 (1961).

Maier, W., and Saupe, A. *Z. Naturforsch.* **13A**, 564 (1958).

Massen et al., see Moutran, R. F. S., Ph.D. Thesis, University of Wales (1975).

Maurel, P. and Price, A. H., *Trans. Faraday Soc.* **69**, 1486 (1973).

Moutran, R. F. S., Ph.D. Thesis, University of Wales (1975).

Moutran, R. F. S., Price, A. H., and Evans, M. W., *J. Chem. Soc. Faraday Trans. II*, **71**, 1854 (1975).

Nordio, P. L., Rigatti, G., and Segre, U., *Mol. Phys.* **56**, 2117 (1972).

Price, A. H. and Maurel, P., *J. Chem. Soc. Faraday Trans. II*, **69**, 1486 (1973).

Price, A. H., Moutran, R. F. S., Davies, M., Beevers, M. S., and Williams, G., *J. Chem. Soc. Faraday Trans. II* **72**, 1447 (1976).

Price, A. H., Buka, A., and Owen, P. G., *Mol. Cryst. Liq. Cryst.* **273**, 295 (1979).

Schwartz et al., see Evans, M. W., *Dielectric and Related Molecular Processes*, Vol. 3, p. 1 (1977).

Sciesincka et al., see Evans, M. W., *ibid.*

9

A Study of Relaxation Phenomena by Equivalent "Reduced" Processes, Nonlinear Phenomena Using Projection Operator Methods

LIST OF SYMBOLS

$\mathbf{A}$	A general column vector of variables
$\|e\rangle$	Quantum-mechanical excited state of a two-level system
$F(t)$	Time shape of the exciting field
$f_{eq}(\Gamma)$	Equilibrium distribution function of the phase space variable Γ
$\hat{\Gamma}_y$	Evolution operator of the stochastic variable y
g	Memory strength of the dissipation system under study. $g \gg 1$ means that the system is largely non-Markovian; $g \ll 1$ means that the system is approximately Markovian
$\|g\rangle$	Quantum-mechanical ground state of a two-level system
H	Intensity of exciting field
$\hat{\mathscr{H}}$	Quantum-mechanical hamiltonian operator for intramolecular processes
$\hat{L}$	Liouville operator
$\{\|m\rangle\}$	Dense set of quantum-mechanical states resulting in the relaxation of the state $\|e\rangle$
$\|M\rangle$	"Virtual" quantum-mechanical state simulating a dissipation quasicontinuum
$\|\psi(t)\rangle$	Quantum-mechanical "wave-function" denoting the state of the system under study at time t
$\hat{P}$	Mori–Zwanzig projection operator
$\hat{P}_S$	Projection operator in the Schrödinger picture
$\Phi_{intra}(t)$	Intramolecular memory kernel
ρ	Quantum-mechanical statistical density matrix
σ	Quantum-mechanical statistical density matrix within the context of the semiclassical Liouville equation
$w(\Gamma)$	Weighting function to be used for defining the Mori scalar product
$\{\ \}_{PB}$	The Poisson bracket operator

9.1 THE FLUCTUATING FORCE

In Chapter 1 it is shown that the equation of motion of a variable $\mathbf{A}$ related to the Liouvillian operator can be replaced by a generalized Langevin equation, whose most striking feature is its non-Markovian nature. This is an expression of the second fluctuation-dissipation theorem, which is related to the first fluctuation-dissipation theorem in the sense that both are expressions of linear response theory.

Mori's theory is based on the assumption that the thermal bath of $\mathbf{A}$ is close to thermodynamic equilibrium. It should not be expected, therefore, that it could be used to describe a system where the thermal bath is far from equilibrium. On the contrary, in this and in the next Chapter, we shall show that Mori theory may be used to describe this physical condition. The Langevin equation may be put in a form that allows us to deal with thermal bath excitations.

The whole problem is made clearer with another derivation of the generalized Langevin equation where better understanding of the excited fluctuating force emerges. A more detailed description of this derivation can be found in the literature (Nordholm and Zwanzig, 1975).

We start from the Liouville equation

$$\frac{\partial}{\partial t} f(t, \Gamma) = -i\hat{L}(t, \Gamma) \tag{9.1.1}$$

where Γ is a multidimensional coordinate summarizing all the positions and momenta of a point particle system, $f(t, \Gamma)$ is a probability density in Γ-space, and $\hat{L}$ is the Liouville operator,

$$\hat{L}B(\Gamma) = -i\{B(\Gamma), \mathscr{H}(\Gamma)\}_{PB} \tag{9.1.2}$$

where $\{\ ,\ \}_{PB}$ is the Poisson bracket and $\mathscr{H}$ is the Hamiltonian. The main difference between the approach by Mori (1965) and the one by Zwanzig is that Mori starts from the equation of motion of the variable of interest itself, $\mathbf{A}$,

$$\frac{\partial}{\partial t}\mathbf{A}(t, \Gamma) = i\hat{L}\mathbf{A}(t,\ \Gamma) \tag{9.1.3}$$

whereas Zwanzig starts from the Liouville equation, Eq. 9.1.1. As stressed in the following chapter, within the context of Mori theory what we must do is define a suitable scalar product between two operators, regarded thereby as quantum mechanical states. A general definition of scalar product could be the following*:

$$(B, C^{\dagger}) = \int d\Gamma\ B(\Gamma)C^{*}(\Gamma)w(\Gamma) \tag{9.1.4}$$

*The symbol † denotes Hermitian conjugation. In the multidimensional case, this involves the replacement of a column vector $\mathbf{V} = (V_1, V_2, \ldots, V_n)$ with the row vector $\mathbf{V}^{\dagger} = [V^{\dagger}_1, V^{\dagger}_2, \ldots]$. The symbol * denotes complex conjugation.

where $w(\Gamma)$ is a real-valued and nonnegative weighting function, for example, the canonical equilibrium distribution, $f_{eq}(\Gamma)$.

In the context of the Zwanzig theory we need a projection operator $\hat{P}$ which defines the part of interest of the distribution function f. According to Zwanzig, irreversibility can appear only as a consequence of the fact that a limited part of the whole universe is directly attainable through the usual experimentation. The signal monitored in an experiment depends only on a part of the whole universe, a part that undergoes an ineluctable interaction with the remainder of the universe.

As a consequence, a suitable physical theory of irreversible processes must be based on the replacement of Eq. 9.1.1 with its *projection* over the subsystem of interest, and, of course, a suitable projection operator $\hat{P}$ has to be defined. If we apply to Eq. 9.1.1 first the projection operator $\hat{P}$ and then the complementary operator, $\hat{1} - \hat{P}$, we obtain

$$\frac{\partial}{\partial t}\hat{P}f(t, \Gamma) = -\hat{P}i\hat{L}\hat{P}f(t, \Gamma) - \hat{P}i\hat{L}(1-\hat{P})f(t, \Gamma) \tag{9.1.5}$$

$$\frac{\partial}{\partial t}(\hat{1}-\hat{P})f(t, \Gamma) = -(\hat{1}-\hat{P})i\hat{L}(1-\hat{P})f(t, \Gamma) - (\hat{1}-\hat{P})i\hat{L}\hat{P}f(t, \Gamma) \tag{9.1.5'}$$

respectively. We can formally solve the second equation:

$$(\hat{1}-\hat{P})f(t, \Gamma) = \exp[-it(\hat{1}-\hat{P})\hat{L}](\hat{1}-\hat{P})f(t, \Gamma) - \int_0^t ds\, \exp[-is(\hat{1}-\hat{P})\hat{L}](1-\hat{P})i\hat{L}\hat{P}f(t-s, \Gamma) \tag{9.1.6}$$

Using Eq. 9.1.6 in Eq. 9.1.5 we have

$$\frac{\partial}{\partial t}\hat{P}f(t, \Gamma) = -\hat{P}i\hat{L}\hat{P}f(t, \Gamma) + \int_0^t ds\, \hat{P}i\hat{L}\exp[-is(\hat{1}-\hat{P})](\hat{1}-\hat{P}) \times i\hat{L}\hat{P}f(t-s, \Gamma) - Pi\hat{L}\exp[-it(\hat{1}-\hat{P})\hat{L}](\hat{1}-\hat{P})f(0, \Gamma) \tag{9.1.7}$$

The preceding equation is a generalized master equation first derived by Zwanzig (1960, 1961). The first term on the right side of Eq. 9.1.7 does not involve dissipation. When the part of interest of the whole universe does not interact with the remaining "irrelevant" part, the closed universe so obtained would exhibit reversible dynamics described by only the first term on the right side of Eq. 9.1.2. Thus only the second term is really significant from the point of view of relaxation. In fact, by a perturbation expansion of the memory kernel (see, for example, Section 9.2) we can show that the nonvanishing contribution of lowest order to this term (the second) can be related with the damping parameter of standard approaches to dissipation phenomena such as the Weisskopf–Wigner theory (1930).

What is the role played by the third term on the right side of Eq. 9.1.7?

Usually, this contribution is disregarded (Platz, 1972) by assuming that at the initial time ($t = 0$) the "irrevelant" part of the distribution function vanishes. A major aim of this chapter, and of the following one, is to demonstrate the important role played by this contribution in overcoming the limitations of the first and second fluctuation–dissipation theorems. According to Kubo (1966), both theorems can be regarded as being expressions of linear response theory.

We now show that the generalized Langevin equation (Chapter 1) can be obtained through the generalized master equation of Zwanzig, that is, by Eq. 9.1.7. The basic idea is that it is possible to choose as projection operator $\hat{P}$ the one defining the space spanned by the variable of interest:

$$\mathbf{A} = \begin{pmatrix} A_1 \\ A_2 \\ A_3 \\ \vdots \end{pmatrix} \tag{9.1.8}$$

We define the average value of the component A_i through the following equation:

$$\langle A_i(t)\rangle = (A_i, f(t)^\dagger) = (A_i, [\hat{P}f(t)]^\dagger) \tag{9.1.9}$$

Both the projection operator $\hat{P}$ and the Liouvillian operator $\hat{L}$ are assumed to be Hermitian with respect to the definition of scalar product given in Eq. 9.1.4. Of course, this implies that $w(\Gamma)$ should be defined accordingly. The Hermitian assumption is also present in the original derivation of the generalized Langevin equation (Mori, 1965a). However, this is not necessary, as is shown in Chapter 10.

The Liouvillian of the total system is often Hermitian as a direct consequence of the definition of a scalar product. If the Liouvillian operator is the classical one defined in Eq. 9.1.2 and the weighting function $w(\Gamma)$ is 1, then $\hat{L}$ can be shown to be Hermitian. However, in several cases, though the total Liouvillian is Hermitian, a large part of the system can be regarded as being a "background thermal bath." The stochastic motion of a dipole is a significant example. The precessional motion of a dipole depends on the stochastic motion of the molecule in which the dipole is embedded. The stochastic motion of the molecule, in turn, depends on a stochastic interaction between the labeled molecule and the other molecules in the liquid sample. The Markovian approximation to this latter interaction, or the truncation of the corresponding Mori chain, means replacing the Hermitian Liouvillian (satisfying the time reversal properties) with an effective one, non-Hermitian in nature.

This replacement can be very fruitful for it allows us to exploit directly a phenomenological description of the complex dynamics of the molecular system. In some cases the molecular dynamics are fairly well described by a Fokker–Planck type equation and one would like to include this information directly in the equation of motion for the dipole itself. This very

requirement resulted in the stochastic Liouville equation of Kubo (Kubo 1969a, b).

The inclusion of this information in the theory implies that the Liouvillian loses its Hermitian nature. This problem is studied in Chapter 10.

Though the approach described in the following makes it possible to deal with the non-Hermitian case, for simplicity we limit this preliminary discussion to the Hermitian. By simply using Eq. 9.1.9 we can exploit the information provided by the generalized Zwanzig equation (Eq. 9.1.7) and write

$$\frac{\partial}{\partial t}\langle A_j\rangle_t = \left(A_j, \left[\frac{\partial}{\partial t}\hat{P}f(t)\right]^\dagger\right) = -(A_j, [\hat{P}i\hat{L}\hat{P}f(t)]^\dagger) + \int_0^t ds(A_j, \{\hat{P}i\hat{L}\exp[-is(\hat{1}-\hat{P})\hat{L}](\hat{1}-\hat{P})i\hat{L}\hat{P}f(t-s)\}^\dagger) - (A_j, \{\hat{P}i\hat{L}\exp[-i(\hat{1}-\hat{P})\hat{L}t](\hat{1}-\hat{P})f(0)\}^\dagger) \quad (9.1.10)$$

The use of the assumption that $\hat{P}$ and $\hat{L}$ are Hermitian operators allows us to replace Eq. 9.1.10 with

$$\frac{\partial}{\partial t}\langle A_j\rangle_t = (\hat{P}i\hat{L}A_j, [f(t)]^\dagger) + \int_0^t ds(\hat{P}i\hat{L}\exp[is(\hat{1}-\hat{P})\hat{L}] \times (\hat{1}-\hat{P})i\hat{L}A_j, [f(t-s)]^\dagger) + (\exp[it(\hat{1}-\hat{P})\hat{L}](\hat{1}-\hat{P})i\hat{L}A_j, [f(0)]^\dagger) \quad (9.1.11)$$

which can be regarded as being just the generalized Langevin equation written in the form of average values for the variable of interest.

Using the property that any operator when projected with $\hat{P}$ can be written as being a suitable linear contribution of the components A_i of the variable $\mathbf{A}$, we obtain

$$\hat{P}i\hat{L}A_j(\mathbf{\Gamma}) = \sum_{l=1}^{M} c_{jl}A_l(\mathbf{\Gamma}) \quad (9.1.12)$$

$$\hat{P}i\hat{L}\exp[is(\hat{1}-\hat{P})\hat{L}](\hat{1}-\hat{P})i\hat{L}A_j(\mathbf{\Gamma}) = \sum_{l=1}^{M} d_{jl}(s)A_l(\mathbf{\Gamma}) \quad (9.1.13)$$

which can be written in a more compact form as follows:

$$\mathbf{c} = (\hat{P}i\hat{L}\mathbf{A}, \mathbf{A}^\dagger)(\mathbf{A}, \mathbf{A}^\dagger)^{-1} \quad (9.1.14)$$

$$\mathbf{d}(s) = (\hat{P}i\hat{L}\exp[is(\hat{1}-\hat{P})\hat{L}](\hat{1}-\hat{P})iL\mathbf{A}, \mathbf{A}^\dagger)(\mathbf{A}, \mathbf{A}^\dagger)^{-1} \quad (9.1.15)$$

Using Eqs. 9.1.14 and 9.1.15 we can write Eq. 9.1.10 in the following form:

$$\frac{\partial}{\partial t}\langle\mathbf{A}\rangle_t = \mathbf{c}\langle\mathbf{A}\rangle_t + \int_0^t ds\,\mathbf{d}(s)\langle\mathbf{A}\rangle_{t-s} + \langle\mathbf{F}(t)\rangle_0 \quad (9.1.16)$$

where

$$\mathbf{F}(t) = \exp[it(\hat{1}-\hat{P})\hat{L}]i\hat{L}\mathbf{A}(\mathbf{\Gamma}) \quad (9.1.17)$$

We can now make a first attempt at understanding the role of the fluctuating force $\mathbf{F}(t)$. It is clear from the present derivation that the instantaneous average value of this force may vanish and that this depends on the third contribution of the right side of Eq. 9.1.7. It is usual to assume that this contribution does vanish. However, in the next sections we consider the effects in a relaxation experiment of exciting the "irrelevant" part. When the relaxation phenomenon under study is not Markovian, the subsequent decay of the "irrelevant" part is fairly slow and can affect the decay of the part of interest of the system under study. In particular we consider effects on intramolecular motion.

The correlation function of the fluctuating force (using the expression for $\mathbf{F}$ provided by Eq. 9.1.17 and the Hermitian properties of $\hat{P}$ and $\hat{L}$) can be written as follows:

$$(\mathbf{F}(t+s), \mathbf{F}(s)^\dagger) = (\exp[i(t+s)(\hat{1}-\hat{P})\hat{L}](\hat{1}-\hat{P})\hat{L}\mathbf{A}, \times\{\exp[is(\hat{1}-\hat{P})\hat{L}]\times(\hat{1}-\hat{P})i\hat{L}\mathbf{A}\}^\dagger) \quad (9.1.18)$$

Through comparison of Eq. 9.1.18 with Eq. 9.1.15, we obtain

$$\mathbf{d}(t) = -(\mathbf{F}(t+s), \mathbf{F}(s)^\dagger)(\mathbf{A}, \mathbf{A}^\dagger)^{-1} \quad (9.1.19)$$

which is the second fluctuation-dissipation theorem already dealt with in Chapter 1. This means that if the correlation function of the stochastic force is not short-lived with respect to the relaxation time (i.e., the time defining the relaxation dynamics of the variable of interest itself), Eq. 9.1.7 cannot lose its non-Markovian structure. In this case, the relaxation process and the excitation process cannot be clearly separated (see Sections 9.2 and 9.4).

It is now clear that Eq. 9.1.19 does not imply that

$$\langle\mathbf{F}(t)\rangle_0 = 0 \quad (9.1.20)$$

The approach developed in Chapters 9 and 10, therefore, applies also to cases where Eq. 9.1.20 is not satisfied.

According to Nordholm and Zwanzig (1975) we can replace Eq. 9.1.16 with

$$\frac{\partial}{\partial t}\mathbf{A} = \mathbf{c}\mathbf{A}(t) + \int_0^t ds\;\mathbf{d}(s)\mathbf{A}(t-s) + \mathbf{F}(t) \quad (9.1.21)$$

which has the same form as the generalized Langevin equation of Mori already dealt with in Chapter 1. Nordholm and Zwanzig assert that Eq. 9.1.21 is valid even in the case where in its averaged counterpart, Eq. 9.1.16, the third term on the right side of Eq. 9.1.21 does not disappear.

The term generalized Langevin equation is more often used to denote the equation by Mori, which is assumed to be valid only when the thermal baths are close to their equilibrium distribution. In the following, however, we extend this denomination to Eq. 9.1.21, which, in a sense, is more general than the equation of Mori. In the next chapter we present further

extensions which are obtained without using the Hermitian properties of the Liouvillian $\hat{L}$.

Even when the thermal bath is supposed to be at equilibrium, the standard treatments require that a further assumption be made. This is the Gaussian assumption (Fox, 1978). It results in a Maxwellian distribution of velocities and is related to the truncation of entropy expansion at second order (de Groot and Mazur, 1962).

Since the central limit theorem has not been proved with sufficient generality, we believe that some attention must be devoted to investigating the Gaussian assumption in this context. Molecular dynamics simulations do not always corroborate equilibrium Gaussian behavior (Evans et al., 1980).

If we focus our attention on the fluctuating force, the first requirement of the Gaussian assumption is expressed by Eq. 9.1.20. Then, it is assumed that any higher-order odd correlation function vanishes; that is, for any generic n,

$$\langle \mathbf{F}(t_1)\mathbf{F}(t_2)\cdots\mathbf{F}(t_{2n+1})\rangle = 0 \tag{9.1.22}$$

whereas any even correlation function can be related to the second-order one, Eq. 9.1.18, through the following expression:

$$\langle \mathbf{F}(t_1)\mathbf{F}(t_2)\cdots\mathbf{F}(t_{2n})\rangle$$

$$= \sum \langle \mathbf{F}(t_{i1})\mathbf{F}(t_{i2})\rangle\langle \mathbf{F}(t_{i3})\mathbf{F}(t_{i4})\rangle\cdots\langle \mathbf{F}(t_{i2n-1})\mathbf{F}(t_{i2n})\rangle \tag{9.1.23}$$

where the sum is over the different ways of splitting the $2n$ variables $t_1,\ldots,t_{2n}$ into n pairs. If the Markovian assumption is no longer satisfied, Eqs. 9.1.22 and 9.1.23 may be invalidated. This makes it necessary that a non-Markovian–non-Gaussian approach be developed. We consider this problem in Chapter 10.

A further problem to be discussed is the relaxation in the presence of external excitation. In such a case the Liouvillian used in Eqs. 9.1.1 and 9.1.23 is replaced by the following one:

$$\hat{L}_T(t) = \hat{L} + \hat{L}_1(t) \tag{9.1.24}$$

The derivation of Eqs. 9.1.7 and 9.1.5 can be repeated. However, since the Liouvillian $\hat{L}_T(t)$ is time dependent and in general $\hat{L}_T(t)$ does not commute with $\hat{L}_T(t')$, we must introduce time-ordered exponential algebra. For an excellent introduction to this subject the reader should consult the paper by Muus (1972). The time-ordered exponentials are denoted by the symbols $\overleftarrow{\exp}$ and $\overrightarrow{\exp}$.

Thus the generalized Zwanzig equation can be replaced by the following one:

$$\frac{\partial}{\partial t}\hat{P}f(t,\Gamma) = -i\hat{P}\hat{L}(t,\Gamma) + \int_0^t ds\, \hat{P}i\hat{L}_T(t) \times \left\{\overleftarrow{\exp}\left[-\int_s^t ds_1(\hat{1}-\hat{P})i\hat{L}_T(s)\right]\right\}(\hat{1}-\hat{P})i\hat{L}(s)\hat{P}f(s,\Gamma) \tag{9.1.25}$$

$$-\hat{P}i\hat{L}_T(t)\left\{\overleftarrow{\exp}\left[-\int_0^t ds(\hat{1}-\hat{P})i\hat{L}_T(s)\right]\right\}(\hat{1}-\hat{P})f(0,\Gamma)$$

In order to obtain this equation we have assumed that the total Liouvillian is Hermitian.

The averaged Langevin equation, in turn, can be written as follows:

$$\frac{\partial}{\partial t}\langle A_k\rangle_t = \langle \hat{P}i\hat{L}_T(t)A_k\rangle_t + \int_0^t ds\langle \hat{P}i\hat{L}_T(s) \times \left\{\overrightarrow{\exp}\left[\int_0^t ds_1(\hat{1}-\hat{P})i\hat{L}_T(s_1)\right]\right\}(\hat{1}-\hat{P})i\hat{L}_T(t)A_k\rangle_s + \langle F_k(t)\rangle_0 \tag{9.1.26}$$

where the average fluctuating force is defined by

$$\langle F_k(t)\rangle_0 = \left\langle \left\{\overrightarrow{\exp}\left[\int_0^t ds(\hat{1}-\hat{P})i\hat{L}_T(s)\right]\right\} \times (\hat{1}-\hat{P})i\hat{L}_T(t)A_k(\Gamma)\right\rangle_0 \tag{9.1.27}$$

Equation 9.1.26 shows clearly that the presence of an external force cannot be taken into account simply by adding to the generalized Langevin equation the contribution $\langle \hat{P}i\hat{L}_1(t)A_k\rangle$, as was done by Kubo himself (1966). In fact, the rigorous derivation described above shows that the "memory kernel" is in general affected by the presence of an external force. Providing a solution to Eqs. 9.1.25 and 9.1.27 is a further important aim of Chapters 9 and 10. This is closely related to the problem of overcoming the limitations of the first fluctuation–dissipation theorem mentioned in the first half of this section.

In this section we have outlined the main problems to be discussed in Chapters 9 and 10. In the following sections of the present chapter we show that a straightforward solution can be obtained by replacing the real thermal bath with a "reduced" one. In Chapter 10 we show that this approach finds in the Mori theory a rigorous justification.

9.2 EXCITATION–RELAXATION PROCESSES IN THE REALM OF QUANTUM MECHANICS: RADIATIONLESS DECAY IN MOLECULES

The purpose of this section is not to describe radiationless transitions in standard terms. It is possible to find many interesting reviews concerning

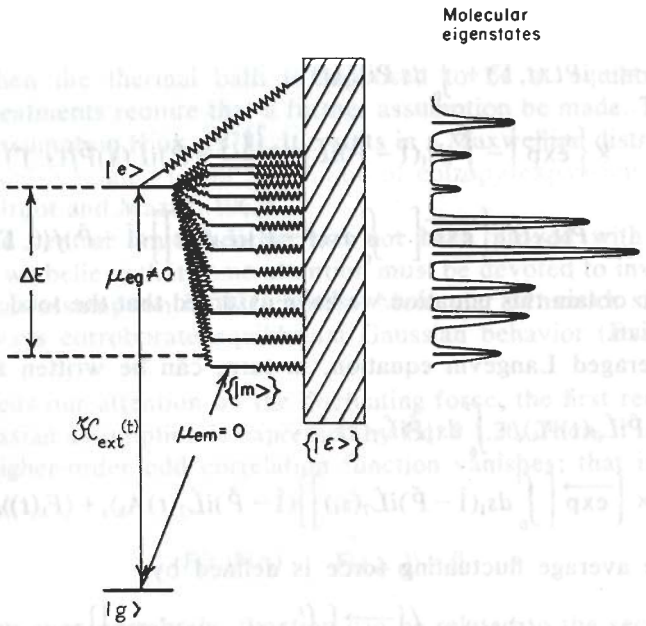

Figure 9.2.1 Schematic of the system described by Eqs. 9.2.1–9.2.5. The n-manifold has been replaced by the ϵ-continuum. This corresponds to the idea of background, which will play an important role in the following.

this problem (Freed, 1972; Jortner and Mukamel, 1974; Rhodes, 1980). The reader is invited to consult these reviews for a more detailed description of this subject.

Our aim, rather, is one of using a simple scheme frequently used in this field of research as a didactic tool to clarify what we mean by a "reduced" model when replacing the more "complex" one of physical reality. The problem of radiationless decay in molecules is too complex for description through the "a priori" methods of quantum mechanical theoretical chemistry. Researchers working in this field are currently relating theoretical approaches to models such as the one described by Fig. 9.2.1, which corresponds to the following quantum mechanical Hamiltonian:

$$\hat{\mathcal{H}} = \hat{\mathcal{H}}_S + \hat{\mathcal{H}}_L + \hat{V} + \hat{\mathcal{H}}_{ext} \tag{9.2.1}$$

$$\hat{\mathcal{H}}_S = |g\rangle\epsilon_g\langle g| + |e\rangle\epsilon_e\langle e| \tag{9.2.2}$$

$$\hat{\mathcal{H}}_L = \sum_m \epsilon_m |m\rangle\langle m| + \sum_{mn} (|m\rangle\langle m|W|n\rangle\langle n| + |n\rangle\langle n|W|m\rangle\langle m|) + \sum_n \epsilon_n |n\rangle\langle n| \tag{9.2.3}$$

$$\hat{V} = \sum_m (|e\rangle\langle m|v_m + |m\rangle\langle e|v_m) + \sum_n (|e\rangle\langle n|v_n + |n\rangle\langle e|v_n) \tag{9.2.4}$$

and

$$\hat{\mathcal{H}}_{ext}(t) = 2F(t)H \cos \omega t[|g\rangle\langle e| + |e\rangle\langle g|] \tag{9.2.5}$$

In the case of electronic relaxation the state of interest $|e\rangle$ can be a low vibronic state belonging to an excited electric potential, whereas the first dissipative quasi-continuum can represent the excited vibronic states belonging to a lower electronic potential.

According to Freed (1976) the n-manifold must be regarded as being a dissipative manifold (ϵ-continuum of Fig. 9.2.1) to take into account the completely isolated nature of the molecular system. For simplicity, first we assume that the interaction between the state $|e\rangle$ and the quasi-continuum $\{|n\rangle\}$ may be neglected. In the next Chapter we shall show how to take into account this interaction.

From an illustrative point of view, the model described by the Hamiltonian of Eq. 9.2.1 is useful. In fact, we can see that unless some significant further assumptions on the coupling $\hat{V}$ are made [such as the constant coupling assumption of the Bixon and Jortner theory (1968)] the description of any excitation–relaxation process requires the diagonalization of quite large matrices (virtually of infinite size). The use of computer diagonalization programs (Gelbart et al., 1975; Grigolini and Lami, 1978) allows us to diagonalize virtually infinite matrices in the sense that it is possible to show that the results can attain a convergence after taking into account a fairly large number of states, N (e.g., $N = 50$).

There is a correspondence between the "complex" model described by Eq. 9.2.1 and the "complex" model of physical reality described in earlier chapters, where a real liquid is simulated by a mathematical box containing a finite number of molecules supposed to be interacting through a Lennard–Jones potential.

In both cases we focus our attention on a "complex" model of physical reality rather than on the real systems themselves. In both cases a mathematical evaluation is made possible by the use of computer programs. In both cases we cannot limit ourselves to the description of such computational results for we need a theoretical discussion which can provide us with an intuitive understanding of the main features of such relaxation processes, simulated through a complex computer calculation. It is a major purpose of this part of the book (Chapters 9 and 10) to show that in both cases we can replace the "complex" model of physical reality with a "reduced" equivalent. We shall refer to this as the "reduced" model theory (RMT).

Before giving a clearer idea of what we really mean by RMT, we may use the model of Fig. 9.2.1 to elucidate the role of the fluctuating force in an excitation–relaxation process.

When no "external" kind of reservoir is present, that is, when from a formal point of view the thermal baths are described as belonging to the same mathematical space as the system of interest, it is better to apply the

Zwanzig approach, described in Section 9.1, not to the classical Liouville equation but to the quantum mechanical Schrödinger equation:

$$i\frac{\partial}{\partial t}|\psi(t)\rangle = \hat{\mathscr{H}}(t)|\psi(t)\rangle \tag{9.2.6}$$

By denoting with $\hat{P}_S$ the projection operator

$$\hat{P}_S = |e\rangle\langle e| + |g\rangle\langle g| \tag{9.2.7}$$

and applying to Eq. 9.2.6 Zwanzig's method, we obtain

$$\begin{aligned} i\frac{\partial}{\partial t}\hat{P}_S|\psi(t)\rangle = {} & \hat{P}_S\hat{\mathscr{H}}(t)P_S|\psi(t)\rangle - i\int_0^t \hat{P}_S\hat{\mathscr{H}}(t) \\ & \times \exp\left(\int_\tau^t dt'(\hat{1}-\hat{P}_S)\hat{\mathscr{H}}(t')\right)(\hat{1}-\hat{P}_S)\hat{\mathscr{H}}(\tau)\hat{P}_S|\psi(\tau)\rangle\, d\tau \\ & + \hat{P}_S\hat{\mathscr{H}}(t)\exp\left[-i(\hat{1}-\hat{P}_S)\int_0^t \hat{\mathscr{H}}(t')\,dt'\right](\hat{1}-\hat{P}_S)|\psi(0)\rangle \end{aligned} \tag{9.2.8}$$

Note that this equation has the same structure as Eq. 9.1.25. However, Eq. 9.2.8 contains an approximation. We have not used the time-ordered exponentials because we assume $[\hat{\mathscr{H}}(t), \hat{\mathscr{H}}(t')] = 0$ for $t \neq t'$.

In the case of both electronic relaxation and intermolecular vibrational relaxation (Freed, 1976; Laubereau and Kaiser, 1978) the low temperature approximation is usually used. Here it is assumed that the system is in a state $|g\rangle$ at $t = 0$; that is, the third term on the right side of Eq. 9.2.8 is neglected.

Though this could be right at $t = 0$, we note that during the excitation process the m-manifold can be populated as a simple result of the excitation of the state, that is, through the radiation pulse described by $\hat{\mathscr{H}}_{ext}$ (Eq. 9.2.5).

If the m-manifold is depopulated owing to its interaction with the n-manifold very quickly with respect to the dynamics of the state $|e\rangle$, the effect of the nonequilibrium "fluctuating force" which depends on the presence of population in the m-manifold can be neglected. From the structure of the third term on the right side of Eq. 9.2.8, we see that the fluctuating force can affect the time evolution of the state $|e\rangle$ when either the m-manifold or the n-manifold is populated. However, the effect of the n-manifold population depends on higher-order interaction. We can thus focus our attention on the fluctuation coming from the m-manifold population. Then we can assert that neglecting the effect of the fluctuating force really means that any excitation affecting the m-manifold is soon lost as an effect of the interaction with the n-manifold.

This assumption is equivalent to saying that the microscopic time (correlation time) is infinitely short with respect to the macroscopic time (relaxation time); that is, it means that our relaxing system is Markovian (Bixon–Jortner assumption).

Only Markovian systems have relaxation properties completely independent of the excitation process used to detect them. When the decay rate of the m-manifold is comparable with the fluctuation dynamics of the state $|e\rangle$, then the m-manifold can be significantly populated during the excitation process. The relaxation process, in turn, depends on the presence of population in the m-manifold. The only way of separating the two processes would be to use infinitely short excitation pulses. This is the usual assumption of standard treatments.

Therefore, non-Markovian processes from both an experimental and a theoretical point of view require more care than Markovian ones, which involve a clear-cut separation of excitation and relaxation.

Neglecting the third term on the right side of Eq. 9.2.8 does not mean that the "nonequilibrium fluctuating force" is disregarded. With reference to the previous section, it is clear in fact that the assumption

$$(\hat{1}-\hat{P}_S)|\psi(0)\rangle = 0 \tag{9.2.9}$$

means that in the absence of external excitation the average value of the fluctuating force is zero.

In order to understand clearly this point we note that the relevant Langevin equation should be the one related to an observable such as

$$\mathbf{A} = (|e\rangle\langle e|, |e\rangle\langle g|, |g\rangle\langle e|, |g\rangle\langle g|)$$

The partner of this equation would then be the Liouville equation governing the statistical density matrix. This is the approach followed by Grigolini and Lami (1978). However, when dealing with an "intramolecular" Hamiltonian such as the one of Eq. 9.1.1, Zwanzig's use of the Schrödinger equation provides us with the same amount of information as his use of the Liouville equation. Furthermore, in the former case significant simplifications can be gained with respect to the latter case. However the reader should keep in his mind the relationship with the Liouville approach. This enables us to interpret relaxation in terms of fluctuating forces. For example, when Eq. 9.2.9 is satisfied and no external excitation is present, the vacuum fluctuations resulting in the decay of the state $|e\rangle$ are pictured as an equilibrium fluctuating force.

By noting that

$$(\hat{1}-\hat{P}_S) = \sum_m |m\rangle\langle m| + \sum_n |n\rangle\langle n| \tag{9.2.10}$$

we see that the only part of the total Hamiltonian appearing in the exponentials of Eq. 9.2.8 is the "intramolecular" thermal bath Hamiltonian defined by Eq. 9.2.3. Equation 9.2.8 can be written as follows:

$$\begin{aligned} i\frac{\partial}{\partial t}\hat{P}_S|\psi(t)\rangle = {} & \hat{\mathscr{H}}_S\hat{P}_S|\psi(t)\rangle + \hat{\mathscr{H}}_{ext}(t)\hat{P}_S|\psi(t)\rangle \\ & - i\int_0^t \Phi_{intra}(t-\tau)\hat{P}_S|\psi(\tau)\rangle\, d\tau \end{aligned} \tag{9.2.11}$$

where

$$\Phi_{\text{intra}}(t) = \langle e|\hat{V}\exp(-i\hat{\mathscr{H}}_L t)\hat{V}|e\rangle = \sum_m |\langle e|\hat{V}|m\rangle|^2\langle m|\exp(-i\hat{\mathscr{H}}_L t)|m\rangle \qquad (9.2.12)$$

The use of the model Hamiltonian of Eq. 9.2.1 therefore simplifies the general result of Eq. 9.1.25. The "memory kernel" is unaffected by the interaction with the external field. The general theory we describe in the following is valid even when this approximation cannot be made. However, this simplification does not mean that the relaxation process, depending on the third term on the right side of Eq. 9.2.11, is really fully separated from the excitation. This statement is valid only when the "memory kernel" Φ_{intra} is a delta function in time. In the more general case the third term on the right side of Eq. 9.2.11 depends on the history to time t of the part of interest of the dynamic system. The history, in turn, is determined both by the dissipative part and the excitation part, $\hat{\mathscr{H}}_{\text{ext}}P|\psi(t)\rangle$ of the same equation.

In order to make clear how a model of "reduced" type can be built up in practice, we take into account two different models of "complex" type used to describe relaxation processes of "intramolecular" kind. Throughout Chapters 9 and 10 we use the term "intramolecular" to denote a type of dissipative coupling such as the one described by the Hamiltonian of Eq. 9.2.1. This term is used in order to emphasize the difference between this and the kind of relaxation processes described in the next section. The first model we study is the one by Morokuma and Freed (1974). Then we study the model introduced by Kushick and Rice (1977) to deal with vibrational decay in liquids.

The former model gives the coupling $\hat{V}$ the following form:

$$\begin{aligned}\langle e|\hat{V}|m\rangle &= w \qquad (m=0)\\ &= \exp(i\delta_m)\frac{w}{|m|} \qquad m\neq 0\end{aligned} \qquad (9.2.13)$$

The Hamiltonian $\hat{\mathscr{H}}_L$ is replaced by the effective one, defined as follows:

$$\hat{\mathscr{H}}_L|m\rangle = (\epsilon_m - i\Gamma)|m\rangle = (\epsilon_M + m\epsilon - i\Gamma)|m\rangle \qquad (9.2.14)$$

By using this model, from Eq. 9.2.12 we obtain (Grigolini, 1977)

$$\Phi_{\text{intra}}(t) = 2\pi^2 w^2 \exp(-\Gamma t + i\epsilon_e t) \times\left[\frac{1}{6}+\pi^{-2}+\left(\frac{\epsilon t}{2\pi}\right)^2-\left(\frac{\epsilon t}{2\pi}\right)\right] \qquad \left(0<t<\frac{2\pi}{\epsilon}\right) \qquad (9.2.15)$$

which in the case where $\epsilon \ll \Gamma$ (statistical limit) becomes

$$\Phi_{\text{intra}}(t) = \frac{g^2}{4\tau_c^2}\exp\left(i\epsilon_e t - \frac{t}{t_c}\right) = v^2\exp(i\epsilon_e t - \gamma t) \qquad (9.2.16)$$

An important point is that the model by Morokuma and Freed introduces a damping Γ to take into account some other dissipative source. The Hamiltonian of Eq. 9.2.14 can be obtained using very drastic assumptions on the interaction of the n-manifold of the model of Fig. 9.2.1 with the remaining part of that physical system. The first assumption is that the state $|e\rangle$ does not interact with the n-manifold. Then we have to assume that the states $|m\rangle$ interact with the n-manifold without giving rise to any interference effect. Whereas the model by Morokuma and Freed is useful in order to emphasize the importance of a background continuum, it is based on a series of assumptions that could be avoided by using the generalized theory of Chapter 10. The effect of a background continuum has been taken into account by Morokuma and Freed by removing the Hermiticity requirement for the Hamiltonian under study.

In Eq. 9.2.16 the correlation time τ_c and the memory strength parameter g are provided by the equations

$$\tau_c = \frac{1}{\gamma} = \frac{1}{\Gamma} \qquad (9.2.17)$$

and

$$g^2 = \frac{8\pi^2 w^2\left(\frac{1}{6}+\frac{1}{2\pi^2}\right)}{\Gamma^2} \qquad (9.2.18)$$

respectively. For simplicity we have also assumed that $\epsilon_M = \epsilon_e$.

The correlation function given by Eq. 9.2.16 has the same form as the correlation function of Friedrich's model (Schieve, 1974), where $g = 1$ is the boundary between the exponential decay region ($g < 1$) and the oscillating decay region ($g > 1$).

Friedrich's model has been used in order to study the decay of unstable elementary particles (Pietenpol, 1967). It emphasizes once again that our description of the dissipation interaction under study in the present section as being "intramolecular" has to be considered *cum grano salis*. In Friedrich's model a state of interest such as $|e\rangle$ is assumed to interact with a dissipation continuum. In order to obtain analytical solutions it is then assumed that this interaction is of Lorentzian kind (Schieve, 1974; Pietenpol, 1967).

The model proposed by Kushick and Rice (1977) is closely related to Friedrich's model. They assume that the first manifold is fairly dense so as to replace the summation appearing through the vehicle of Eq. 9.2.12 with an integration. The coupling between $|e\rangle$ and the m-manifold, furthermore, is assumed to be Lorentzian, with line width γ. Assuming that the interaction between the m-manifold and the n-manifold is random, they succeeded in obtaining a correlation function endowed with the same form as the one of Eq. 9.1.16. In their case, then, the memory strength parameter g is related to the intensity of the relative Lorentzian coupling.

We have been justifying intuitively the fact that the function $\Phi_{\text{intra}}(t)$ of

Eq. 9.2.12 may be described in terms of a few complex circular functions (in the present case, one). A correlation function, such as the one of Eq. 9.2.16, may be the result of different physical features. In fact, in some cases the m-manifold may be dense enough to result directly in dissipation behavior for the state $|e\rangle$ (Friedrich's model, Kushick and Rice model). However, population relaxation may take place without attaining the extreme condition $|v_m| \gg |\epsilon_m - \epsilon_{m\pm1}|$. Clear evidence for this statement has been given through computer calculations by Gelbart et al. (1975). A rough description is enough to show the physical meaning of the constant-coupling assumption present in the Bixon–Jortner model (1968). When the m-manifold is fairly dense the absorption spectrum loses all detailed structure. The summation in Eq. 9.2.12 may then be replaced by an integration. It is then evident that a further assumption such as the one of constant coupling results in replacing Eq. 9.2.12 with a correlation function such as the one of Eq. 9.2.16 with $\tau_c = 0$. Because the modern theory of relaxation processes (Zwanzig, 1960, 1961) shows that Markovian behavior may be recovered intact when the macroscopic time scale is totally separated from the microscopic one, we can assert that the constant-coupling assumption is equivalent to the Markovian assumption.

We can now describe the "reduced" model to be associated with the one of Eq. 9.2.1 (Fig. 9.2.1), in the case where assumptions are made concerning the coupling $\hat{V}$ to obtain the correlation function of Eq. 9.2.16. It is advantageous to define the relaxation properties of "complex" models through their correlation function. Because the latter provides a complete account of the dissipation properties of the corresponding model, we see that different models may have the same dissipation features if they can be related to the same correlation function. As a consequence the "reduced" model to be related to the correlation function of Eq. 9.2.16 is the same for different models of "complex" kind, such as the Morokuma and Freed model, the Bixon and Jortner model, the Kushick and Rice model, and so on. A major aim of Chapter 10 is to show that this property is even more general in the sense that quantum mechanical models such as the ones studied in this section can have the same relaxation properties as the classical physical systems used to study Brownian dynamics in liquids. This similarity should help us in our attempt to generalize the Mori theory, because any suggestions provided by the first field of research can be transferred to the second one.

To build up the "reduced" model corresponding to the correlation function of Eq. 9.2.16 we use the following effective Hamiltonian:

$$\hat{\mathcal{H}}' = \hat{\mathcal{H}}_s + \hat{\mathcal{H}}'_L + \hat{V}' + \hat{\mathcal{H}}_{\text{ext}} \tag{9.2.19}$$

where

$$\hat{\mathcal{H}}'_L = |M\rangle(\epsilon_e - i\gamma)\langle M| \tag{9.2.20}$$

$$\hat{V}' = (|e\rangle\langle M| + |M\rangle\langle e|)v \tag{9.2.21}$$

This could be generalized by assuming that the state $|M\rangle$ could interact dissipatively with a suitable continuum. If this interaction is assumed to be a Lorentzian coupling whose bandwidth is very large, the state $|M\rangle$ would decay exponentially with a rate governed by the parameter γ. Then, by applying to the Hamiltonian of Eq. 9.2.19 the same projection method as that applied to Eq. 9.2.6 with the Hamiltonian of Eq. 9.2.1, we would obtain a "memory kernel" equal to the one of Eq. 9.2.16. This means that Eq. 9.2.19 is exactly the "reduced" model to be associated with the more complex one of Eq. 9.2.1 when the "memory kernel" of the latter model is provided by Eq. 9.2.16.

For the "intramolecular" thermal baths the description of any excitation–relaxation process as consisting of two separate steps, the excitation and the relaxation, is not realistic. As stressed by Rhodes (1974), it is incorrect to assume that, soon after the excitation pulse, the system may be found in the Born–Oppenheimer state $|e\rangle$. This could be attained only by using an infinitely narrow excitation pulse. There is no doubt that the nature of the exciting pulse may affect the subsequent decay behavior. The number of states involved in the problem expressed by Eqs. 9.2.1 and 9.2.6 is overwhelmingly large. The projection operator method of arriving at Eq. 9.2.8 seems to have the effect of significantly reducing the size of the system to be studied. However, the non-Markovian nature of Eq. 9.2.8 generates some further conceptual problems. If the system is not Markovian the relaxation process cannot be separated in a clear-cut way from the excitation one, even when the "memory kernel" is unaffected by the presence of an external perturbation.

We treat in this section the effect of the intensity of the excitation pulse and that of its form and time duration in the relaxation process. In Sections 9.4 and 9.5 we show that the effects described here can be regarded as being a particular case of a more general property of both "intramolecular" and "external" thermal baths. By using a perturbation calculation it has been possible to assess that a non-Markovian system can be decoupled from its thermal bath through excitation by a strong radiation source (Grigolini, 1976). However, owing to the presence of the time convolution (the third term on the right side of Eq. 9.2.8), the perturbation approach results in a very complicated calculation. A simpler theory is desirable for the decoupling resulting from external excitation.

The RMT provides an easy way of making an "exact" calculation. We can focus our attention on the following equation:

$$i\frac{\partial}{\partial t}|\psi'\rangle = \hat{\mathcal{H}}'|\psi(t)\rangle \tag{9.2.22}$$

where $\hat{\mathcal{H}}'$ is the "reduced" effective Hamiltonian given by Eq. 9.2.19. We can now avoid the need for dealing with both the overwhelming number of states involved in Eq. 9.2.1 and the time convolution contribution exhibited by Eq. 9.2.11.

In addition, the RMT enables us to interpret relaxation of non-Markovian kind in terms of quantum mechanical degeneracies. The "real" state $|e\rangle$, in fact, is pictured by the Hamiltonian $\hat{\mathscr{H}}'$ as interacting with the degenerate state $|M\rangle$. The state $|M\rangle$ is Markovian. The rate of its relaxation is provided by the parameter γ. In the absence of the coupling between $|M\rangle$ and its "thermal bath" ($\gamma = 0$), the population time evolution of the state $|e\rangle$ would oscillate with frequency v. When the relaxation affecting the state $|M\rangle$ is very fast with respect to the time period of the harmonic oscillation, no recurrence can be detected and a nearly exponential relaxation is exhibited. In contrast, when the rate γ is comparable to the frequency v a damped oscillating behavior results. In this case, the population of the "virtual" state $|M\rangle$ is not fully lost before the beginning of the back-reaction.

We can easily obtain a quantitative result by noticing that, in the absence of external perturbations Eq. 9.2.22 can be written in the following matrix form:

$$i\frac{d}{dt}\begin{pmatrix}\langle e|\psi'\rangle\\ \langle M|\psi'\rangle\end{pmatrix} = \begin{pmatrix}0 & v\\ v & -i\gamma\end{pmatrix}\begin{pmatrix}\langle e|\psi'\rangle\\ \langle M|\psi'\rangle\end{pmatrix} \tag{9.2.23}$$

Then, by putting $x = \langle e|M\rangle$ and $y = \langle M|y\rangle$, we obtain

$$\dot{x} = -ivy \tag{9.2.24}$$

$$\dot{y} = -ivx - \gamma y \tag{9.2.25}$$

which, through elimination of the variable y, results in

$$\ddot{x} + \gamma\dot{x} + v^2x = 0 \tag{9.2.26}$$

The real and imaginary parts of this equation may be regarded as being the equation of motion of a particle subject to both an elastic restoring force, $-v^2x$, and a friction force, $-\gamma x$. In keeping with the above intuitive remarks, when the restoring force is fairly strong ($g = 2v/\gamma \gg 1$) the system exhibits a damped oscillating behavior.

When the exciting field is a square wave, it is convenient to use as an unperturbed Hamiltonian the operator $\mathscr{H}_0'$, defined as follows:

$$\hat{\mathscr{H}}_0' = \epsilon_e'\{|e\rangle\langle e| + |M\rangle\langle M|\} + \epsilon_g'|g\rangle\langle g| \tag{9.2.27}$$

where $\epsilon_e' - \epsilon_g' = \omega$. As a consequence, the perturbation Hamiltonian must be defined as follows:

$$\mathscr{H}_1' = \mathscr{H}' - \mathscr{H}_0' = \mathscr{H}_{ext} + \Delta\omega|g\rangle\langle g| - i\gamma|M\rangle\langle M| \qquad (\Delta\omega = \omega - \omega_0) \tag{9.2.28}$$

By writing the Schrödinger equation in the corresponding interaction picture (Appendix A), we then obtain

$$i\frac{\partial}{\partial t}|\tilde{\psi}\rangle = \hat{\mathscr{H}}_1'|\tilde{\psi}\rangle(|\tilde{\psi}\rangle = e^{i\hat{\mathscr{H}}_0't},\ \tilde{\hat{\mathscr{H}}}_1' = e^{i\hat{\mathscr{H}}_0't}\hat{\mathscr{H}}_1'e^{-i\hat{\mathscr{H}}_0't} \tag{9.2.29}$$

Using the *rotating wave approximation* (Appendix A) on the *basis set* of the vectors $|g\rangle$, $|e\rangle$, and $|M\rangle$, $\hat{\mathscr{H}}_1'$ can be given the following form:

$$\tilde{\hat{\mathscr{H}}}_1' = \begin{pmatrix}\Delta\omega & H & 0\\ H & 0 & v\\ 0 & v & -i\gamma\end{pmatrix} \tag{9.2.30}$$

Through diagonalization of this matrix one can obtain a complete solution for Eq. 9.2.29. It is equivalent, in turn, to solving Eq. 9.2.11 without approximating either the intensity of exciting radiation or the "memory strength."

As far as the effect of high intensity radiation fields is concerned, this kind of approach complements the perturbation method (Grigolini, 1976). This approximate method enables one to see that non-Markovian dissipation properties *depend significantly on the radiation field intensity*: as the field intensity increases, the effective dissipation damping can decrease markedly. The matrix of Eq. 9.2.30 can be used to explain this result. Assume for simplicity that the excitation experiment is performed at the exact resonance $\Delta\omega = 0$. Assume also that $H \gg v, \gamma$. Then, through a suitable *similarity transformation* the matrix of Eq. 9.2.30 can be written as follows:

$$\hat{\mathscr{H}}_1' = \begin{pmatrix}-H & 0 & -\frac{v}{\sqrt{2}}\\ 0 & H & \frac{v}{\sqrt{2}}\\ -\frac{v}{\sqrt{2}} & \frac{v}{\sqrt{2}} & -i\gamma\end{pmatrix} \tag{9.2.30a}$$

which is a convenient form in the case of a strong excitation field. Note that now we can perform a perturbative calculation of the usual kind (Appendix B), whereas a complex perturbation calculation for time-dependent phenomena has been applied in a previous attempt (Grigolini, 1976). We obtain the result that the part of interest of the system has two complex energy values*:

$$E_1 = -H - \frac{iv^2\gamma}{2(H^2+\gamma^2)} \tag{9.2.30b}$$

$$E_2 = H - \frac{iv^2\gamma}{2(H^2+\gamma^2)} \tag{9.2.30c}$$

It is then evident that for increasing values of H the dissipation rate is weakened.

We discuss now the effect of strong excitation on relaxation. If a

*For $H = 0$ this perturbative result coincides with that of a Weisskopf–Wigner type approach (Weisskopf and Wigner, 1930).

physical system, which is found at the initial time $t = 0$ in the ground state $|g\rangle$ is driven by a monochromatic radiation tuned in to the frequency $\omega_{eg} = \epsilon_e - \epsilon_g$, the population of the state $|e\rangle$ oscillates with a frequency proportional to the excitation field intensity, the Rabi frequency. If the excited state $|e\rangle$ is not a stable one, the oscillations decay with the rate $\lambda/2$, where λ is the free relaxation rate (Markovian case). This standard result can be reproduced as a limit of the more general one.

When $H = 0$ Eq. 9.2.30 describes free relaxation. In such a case, the Markovian assumption $g = 2v/\gamma \ll 1$ allows us to use again the perturbation approach of Appendix B when evaluating the damping of the state $|e\rangle$. This damping is given by

$$\lambda = \frac{v^2}{\gamma} = g^2 \frac{\gamma}{4} \tag{9.2.30d}$$

When $g \ll 1$ we have $\lambda \ll \gamma$. Then for $H \gtrsim \lambda$, from Eqs. 9.2.30b and 9.2.30c, we obtain a damping which is just $\lambda/2$.

When $g \sim 1$, and $H \sim \gamma$, the damping of the Rabi oscillations is significantly weakened as the intensity of the electromagnetic coupling H is increased. In Fig. 9.2.2 we illustrate the result obtained in the case of the model by Morokuma and Freed. We can see that the decay of the Rabi oscillations is weaker than that of the free decay. This results, in part, from the presence of the factor $\frac{1}{2}$ affecting the damping in the presence of external irradiation. As the Rabi frequency increases, however, the decay of the oscillations is weakened. It seems, thus, that the effect of strong excitation pulses on the non-Markovian system is to decouple the part of interest from its "thermal bath." In Section 9.5 we show that this also happens in the case of thermal baths of "external type."

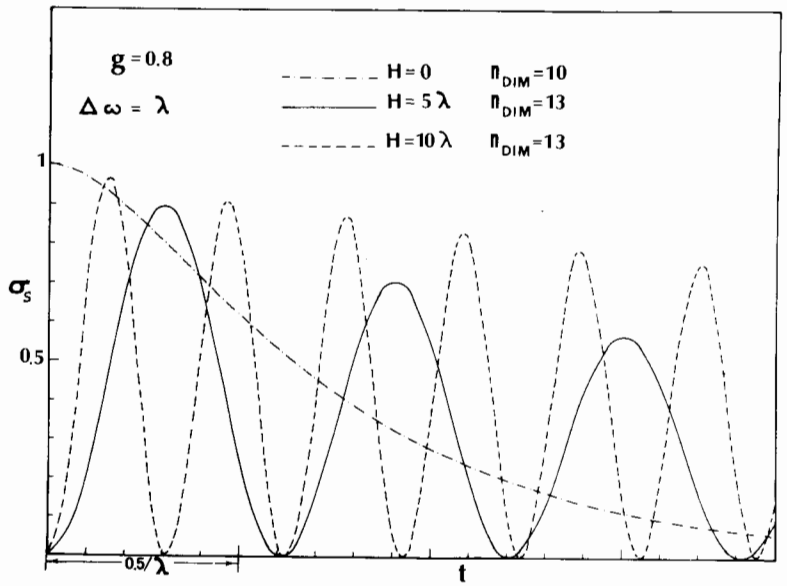

Figure 9.2.2 The population of the state $|e\rangle$, σ_s, as a function of time in the presence of external excitation. We also report the free decay, $H = 0$. In this case the system is in the excited state at the initial time $t = 0$. In the other cases the system at $t = 0$ is in the ground state. The symbol n_D indicates the number of states used to express the Hamiltonian of the model by Morokuma and Freed (1974).

Whereas the diagonalization of Eq. 9.2.30 allows one to examine effects of intense fields, it limits the study of excitation–relaxation process to the case of square pulses. In the case where the exciting field is of low intensity, however, we can also study the effects of realistic quasi-rectangular pulses of the form

$$F(t) = \exp(\gamma_1 t) \qquad (t < 0) \tag{9.2.31}$$

$$= 1 \qquad (0 \leqslant t < T) \tag{9.2.31a}$$

$$= \exp(-\gamma_2 t) \qquad (t \geqslant T) \tag{9.2.31b}$$

When the exciting radiation field is fairly weak we can regard $\hat{\mathcal{H}}_{ext}(t)$ as a small perturbation of the unperturbed Hamiltonian $\hat{\mathcal{H}}_0'' = \hat{\mathcal{H}}' - \hat{\mathcal{H}}_{ext}(t)$. The Schrödinger equation in the relative interaction picture

$$i \frac{\partial}{\partial t} |\tilde{\psi}\rangle = \tilde{\hat{\mathcal{H}}}_{ext}(t) |\tilde{\psi}(t)\rangle \tag{9.2.32}$$

where $\tilde{\hat{\mathcal{H}}}_{ext}(t) = \exp(i\hat{\mathcal{H}}_0'' t)\hat{\mathcal{H}}_{ext}(t)\exp(-i\hat{\mathcal{H}}_0'' t)$ and $|\tilde{\psi}\rangle = \exp(i\hat{\mathcal{H}}_0'' t)|\psi\rangle$, has the formal solution

$$|\tilde{\psi}(t)\rangle = -i \int_0^t \tilde{\hat{\mathcal{H}}}_{ext}(t')|\tilde{\psi}(t')\rangle \, dt' \tag{9.2.33}$$

When the electromagnetic field is fairly weak we can replace $|\psi(t')\rangle$ in Eq. 9.2.33 with $|\tilde{\psi}(0)\rangle$. By assuming, furthermore, that at $t = 0$ our system is found in its ground state, we obtain

$$\langle e|\tilde{\psi}(t)\rangle = -i \int_0^t \langle e|\tilde{\hat{\mathcal{H}}}_{ext}(t')|g\rangle \, dt' \tag{9.2.34}$$

In order to get an analytical expression for $\hat{\mathcal{H}}_{ext}$, we only need to know the eigenstates and the eigenvalues of $\hat{\mathcal{H}}_0''$. This information, in turn, can be obtained simply by diagonalizing the two-dimensional matrix appearing in Eq. 9.2.23.

Then we obtain

$$\langle e|\widetilde{\psi(t)}\rangle = -iH \sum_{\pi} \langle e|\pi\rangle\langle\tilde{\pi}|e\rangle \exp[-i(E_\pi + \Delta\omega)t] F_\pi(t) \tag{9.2.35}$$

where $|\pi\rangle$, $\langle\tilde{\pi}|$, and E_π are right eigenvectors, left eigenvectors (see Appendix

C), and eigenvalues of $\mathcal{H}_0''$, respectively, $\Delta\omega_1 = -\Delta\omega$, and

$$F_\pi(t) = \frac{\exp(\gamma_1 t)\exp[i(E_\pi + \Delta\omega_1)t]}{\gamma_1 + i(E_\pi + \Delta\omega_1)} \qquad (t<0) \tag{9.2.36}$$

$$= \frac{1}{\gamma_1 + i(E_\pi + \Delta\omega_1)} + \frac{i\{\exp[i(E_\pi + \Delta\omega_1)t] - 1\}}{E_\pi + \Delta\omega_1} \qquad (0 \leqslant t < T) \tag{9.2.36a}$$

$$= \frac{1}{\gamma_1 + i(E_\pi + \Delta\omega_1)} + \frac{i\{\exp[i(E_\pi + \Delta\omega_1)T] - 1\}}{E_\pi + \Delta\omega_1} \tag{9.2.37}$$

$$- e^{-\gamma_2 t}\,\frac{\exp\{-[\gamma_2 - i(E_\pi + \Delta\omega)]t\} - \exp\{-[\gamma_2 - i(E_\pi + \Delta\omega_1)]T\}}{\gamma_2 - i(E_\pi + \Delta\omega_1)} \qquad (t \geqslant T)$$

The eigenvalues and eigenstates are defined by the following relations:

$$E_{\pi_1} = -\frac{(G+i)\gamma}{2}, \qquad E_{\pi_2} = \frac{(G-i)\gamma}{2} \tag{9.2.38}$$

$$\langle e|\pi_1\rangle = \left(\frac{G-i}{2G}\right)^{1/2}, \qquad \langle e|\pi_2\rangle = -\left(\frac{G+i}{2G}\right)^{1/2} \tag{9.2.39}$$

where

$$G = (g^2 - 1)^{1/2} \tag{9.2.40}$$

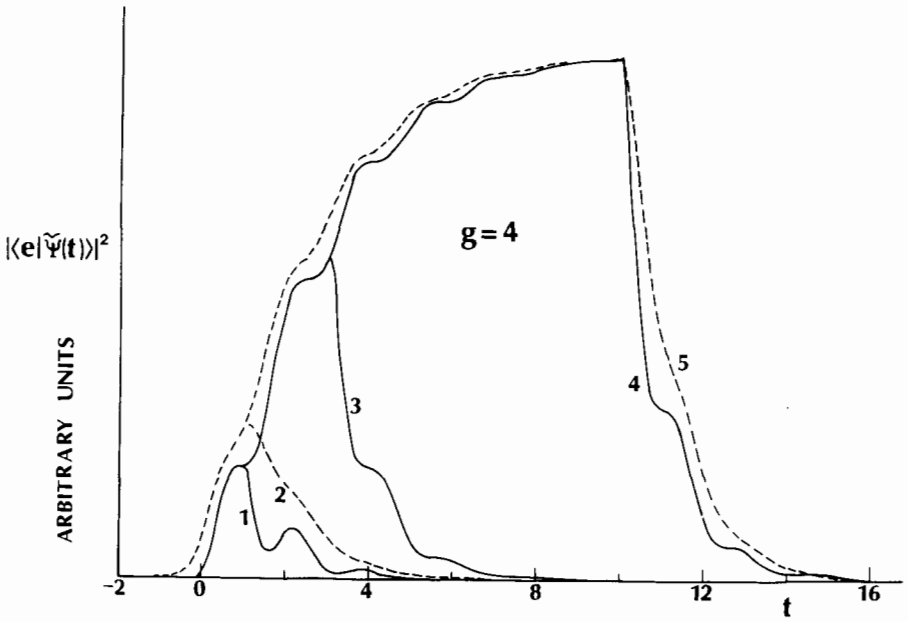

Figure 9.2.3 Time dependence of the population of the excited state $|e\rangle$. The rise and fall time of excitation pulses are provided by the following time constants: $\gamma_1 = \gamma_2 = 2\gamma$(– – –); $\gamma_1 = \gamma_2 = 10\gamma$ (———). The plateau lengths are $T = 1$ (curves 1 and 2); $T = 3$ (curve 3); $T = 10$ (curves 4 and 5). Time is expressed in units of $1/\gamma$. $\Delta\omega_1 = G\gamma/2$.

By using the previous analytical results we can study the effect of the time duration of the excitation pulse on the relaxation process; see Fig. 9.2.3. We see that the oscillations of the non-Markovian decay are significantly washed out as the time duration of the excitation pulse increases. Furthermore, we can see that "realistic" pulses are more effective in making the oscillations disappear.

We have emphasized in this section the usefulness of "reduced" models for studying relaxation phenomena. In the next Chapter we show that this approach can be justified more rigorously. However, first we show that the RMT allows also the treatment of dissipation processes "external" in nature.

9.3 THE RMT FOR "EXTERNAL" THERMAL BATHS

The relaxation processes of the previous section can be studied without the use of the Liouville equation, which is needed only with "external" thermal baths belonging to a vector space different from the states of interest. These are "intermolecular" thermal baths. Though the relaxation resulting from the thermal baths of Section 9.2 is sometimes regarded as being a relaxation of transverse type, its effect on the emission spectra can be shown (Grigolini, 1979) to be quite different from the effects of a genuine "transverse" relaxation.

A genuine "transverse" relaxation is defined as one affecting only the off-diagonal elements of the part of interest of the statistical density matrix, ρ. In order to study this relaxation process, we must replace Eq. 9.2.6 by the following one:

$$i\frac{\partial}{\partial t}\rho = [\hat{\mathcal{H}}, \rho] \tag{9.3.1}$$

where

$$\hat{\mathcal{H}}_0 = \hat{\mathcal{H}}_0 + \hat{\mathcal{H}}_1 \tag{9.3.1a}$$

The unperturbed part of this Hamiltonian and the perturbation are expressed as follows:

$$\hat{\mathcal{H}}_0 = \hat{\mathcal{H}}_S + \hat{\mathcal{H}}_B \tag{9.3.1b}$$

$$\hat{\mathcal{H}}_1 = \hat{\mathcal{H}}_{SB} + \hat{\mathcal{H}}_{ext} \tag{9.3.1c}$$

respectively. Both $\hat{\mathcal{H}}_S$ and $\hat{\mathcal{H}}_{ext}$ have the same form as the corresponding Hamiltonians in Eq. 9.2.1, whereas $\hat{\mathcal{H}}_B$ must now be regarded as the Hamiltonian of a thermal bath B of "external" kind interacting with $\hat{\mathcal{H}}_S$ through $\hat{\mathcal{H}}_{SB}$. As already stressed in the previous section, the space of the whole universe is now to be regarded as spanned by the direct products $|a\,f\rangle$, where $|a\rangle = |e\rangle$, $|g\rangle$, and $|f\rangle$ is a *state* of B.

A convenient projection operator acting on the universal statistical density matrix is then defined as follows (Argyres and Kelley, 1964):

$$\hat{P}_L\rho = \rho_B \operatorname{Tr}_{\{B\}} \rho \tag{9.3.2}$$

where ρ_B expresses the statistical equilibrium of the "external" thermal bath.

The first step of our approach consists in expressing the universal Liouville equation, Eq. 9.3.1, in the interaction picture. Thus we obtain

$$i\frac{\partial}{\partial t}\tilde{\rho} = \tilde{\hat{\mathscr{H}}}_1(t)\tilde{\rho} \tag{9.3.3}$$

where (we recall that $\hat{A}^X\hat{B} = \hat{A}\hat{B} - \hat{B}\hat{A}$ for any arbitrary operator $\hat{B}$)

$$\tilde{\rho} = \exp(i\hat{\mathscr{H}}_0 t)\rho \exp(-i\hat{\mathscr{H}}_0 t) \tag{9.3.4}$$

and

$$\tilde{\mathscr{H}}_{\text{int}} = \exp(i\hat{\mathscr{H}}_0 t)\hat{\mathscr{H}}_1 \exp(-i\hat{\mathscr{H}}_0 t) \tag{9.3.5}$$

This transformation is the corresponding one of that described in Appendix A in the case of the Schrödinger equation.

It is interesting to remark that $\hat{P}_L$ commutes with the transformation from the laboratory reference framework to the interaction one. By applying the Zwanzig projection technique (see Section 9.1) to Eq. 9.3.1, we obtain:

$$i\frac{\partial}{\partial t}\tilde{\rho}_1 = \hat{P}_L\tilde{\hat{\mathscr{H}}}_1^X\tilde{\rho}_1(t) - \int_0^t \tilde{\hat{\Phi}}(t,\tau)\tilde{\rho}_1(\tau)\,d\tau \tag{9.3.6}$$

where

$$\tilde{\rho}_1 = \hat{P}_L\tilde{\rho} \tag{9.3.7}$$

The "memory superoperator" $\tilde{\hat{\Phi}}(t,\tau)$ is defined as follows:

$$\tilde{\hat{\Phi}}(t,\tau) = \hat{P}_L\tilde{\hat{\mathscr{H}}}_1^X(t)\overleftarrow{\exp}\left[-i\int_\tau^t (\hat{1}-\hat{P}_L)\tilde{\hat{\mathscr{H}}}_1^X(t')\,dt\right](\hat{1}-\hat{P}_L)\tilde{\hat{\mathscr{H}}}_1^X(\tau)\hat{P}_L \tag{9.3.8}$$

Since, in the interaction picture, the Hamiltonian is time dependent and $\tilde{\hat{\mathscr{H}}}_1(t)$, in general, does not commute with $\tilde{\hat{\mathscr{H}}}_1(t')$(if $t \neq t'$), we are obliged to introduce the time-ordered exponential. The kind of approach used in order to obtain Eq. 9.3.8 is the same as the one used to derive Eq. 9.1.25.

By expanding the time-ordered exponential $\overleftarrow{\exp}$ in a power series, it is possible to relate the evaluation of $\tilde{\hat{\Phi}}(t,\tau)$ to the calculation of a sum over infinite terms. Any term of this sum, in turn, relies on independent contributions such as ($t_1 \geqslant t_2 \geqslant \cdots \geqslant t_n$)

$$S^{(n)} = \hat{P}\tilde{\hat{\mathscr{H}}}_1^X(t_1)\tilde{\hat{\mathscr{H}}}_1^X(t_2)\cdots\tilde{\hat{\mathscr{H}}}_1^X(t_n)\hat{P} \tag{9.3.9}$$

For simplicity we assume that the interaction between the system of interest and the "external" thermal bath, $\hat{\mathscr{H}}_{SB}$, takes the following form:

$$\hat{\mathscr{H}}_{SB} = \sum_i |r_i\rangle\langle r_i|\hat{F}_{ii} \tag{9.3.10}$$

where

$$|r_1\rangle = |e\rangle \tag{9.3.11}$$

$$|r_2\rangle = |g\rangle \tag{9.3.11a}$$

The previous assumption corresponds to disregarding any longitudinal process. After some algebra, then, $S^{(n)}$ can be expressed in terms of quantities such as ($\tilde{\hat{F}}_{i_\mu i_\nu}(t) = \exp(i\hat{\mathscr{H}}_B t)\hat{F}_{i_\mu i_\nu}\exp(-i\hat{\mathscr{H}}_B t)$)

$$\begin{aligned}\hat{P}_L A[(|r_{i_1}\rangle\langle r_{i_1}|)\tilde{\hat{F}}(t_{i_1})]^X A_{i_1 i_2}[(|r_{i_2}\rangle\langle r_{i_2}|)\tilde{\hat{F}}_{i_2 i_2}(t_{i_2})]^X A_{i_2 i_3}\cdots \\ \times[(|r_{i_{n'}}\rangle\langle r_{i_{n'}}|)\tilde{\hat{F}}_{i_{n'} i_{n'}}(t_{i_{n'}})]^X B\hat{P}_L\end{aligned} \tag{9.3.12}$$

where

$$t_{i_1} \geqslant t_{i_2} \geqslant t_{i_3}\cdots \geqslant t_{i_{n'}};\ 1 \leqslant i_1 \leqslant i_2 \leqslant i_2 \leqslant \cdots \leqslant i_{n'};\quad n' \leqslant n;$$

A, $A_{i_1 i_2}, \ldots, A_{i_{n'-1} i_{n'}}$, and B are c-numbers or superoperators depending only on the interaction between the system of interest and the radiation field.

By assuming that for $\mu \neq \nu$ $[\tilde{\hat{F}}_{i_\mu i_\mu}(t_{i_\mu}),\ \tilde{\hat{F}}_{i_\nu i_\nu}(t_{i_\nu})] = 0$ we obtain that the superoperator of Eq. 9.3.12 when applied to $\rho_B s$ (where s is acting only on the system of interest) results in

$$\begin{aligned}&[A(|r_{i_1}\rangle\langle r_{i_1}|)^X A_{i_1 i_2}(|r_{i_2}\rangle\langle r_{i_2}|)^X A_{i_2 i_3}\cdots(|r_{i_n}\rangle\langle r_{i_{n'}}|)^X Bs] \\ &\times \operatorname{Tr}_{\{B\}}\rho_B\tilde{\hat{F}}_{i_1 i_1}(t)\tilde{\hat{F}}_{i_2 i_2}(t_{i_2})\cdots\tilde{\hat{F}}_{i_{n'} i_{n'}}(t_{i_{n'}}) \\ &(t_{i_1} \geqslant t_{i_2} \geqslant \cdots \geqslant t_{i_{n'}};\quad 1 \leqslant i_1 \leqslant i_2 \leqslant \cdots \cdots \leqslant i_{n'};\ n' \leqslant n)\end{aligned} \tag{9.3.12a}$$

Following the suggestions of the stochastic approach (Freed, 1972) we evaluate the right-hand factor of Eq. 9.3.12a by replacing any quantum mechanical operator $\tilde{F}_{ii}(t)$ with the classical function $f_{ii}(y)$, where y is a stochastic variable. The dynamic behavior of y is defined by the following diffusion equation:

$$\frac{\partial}{\partial t}p(y,t) = \hat{\Gamma}_y p(y,t) \tag{9.3.13}$$

for the corresponding probability density $p(y,t)$. Equation 9.3.13 is assumed to be a complete description of the stochastic dynamics of the thermal bath B. In Section 10.5 we show that the RMT allows one to deal even with the case where the stochastic dynamics of the thermal bath B is not Markovian. In the present section, however, we limit ourselves to taking into account the Markovian dynamics described by Eq. 9.3.13.

In the following we make a distinction between the stochastic variable y

and the variable $\hat{y}$ defined by

$$\frac{d}{dt}\hat{y} = \hat{\Gamma}_y^X \hat{y} = \hat{\Gamma}_y \hat{y} - \hat{y}\hat{\Gamma}_y \tag{9.3.13a}$$

The distinction is that $\hat{y}$ is regarded as being an operator the dynamics of which is determined from $\hat{\Gamma}_y$ instead of a rigorous Liouvillian superoperator (see also Chapter 10, Appendix D).

If we consider the right-hand factor of Eq. 9.3.12a, we can write

$$\begin{aligned}&\mathrm{Tr}_{\{B\}}\rho_B \tilde{\hat{F}}_{i_1 i_1}(t)\tilde{\hat{F}}_{i_2 i_2}(t_{i_2})\cdots\tilde{\hat{F}}_{i_{n'} i_{n'}}(t_{i_{n'}})\\ &\quad = \mathrm{Tr}_{\{B\}}\rho_B e^{i\hat{\mathscr{H}}_B t_1}\hat{F}_{i_1 i_1}e^{-i\hat{\mathscr{H}}_B(t_1-t_2)}\hat{F}_{i_2 i_2}\cdots\hat{F}_{i_{n'} i_{n'}}e^{-i\hat{\mathscr{H}}_B t_{i_{n'}}}\end{aligned} \tag{9.3.14}$$

Equation 9.3.13 allows us to replace the quantum mechanical operator $\hat{F}_{i_r i_r}$ with the $f_{i_r i_r}(\hat{y})$ which are operators on the space of the $|p_n\rangle$'s. The time evolution $\exp(-i\hat{\mathscr{H}}_B t_{i_r})$ is replaced by $\exp(-\hat{\Gamma}t_{i_r})$. As a consequence we obtain (Appendix D)

$$\begin{aligned}&\langle\tilde{p}_0|\exp(-\hat{\Gamma}_y t_{i_1})\hat{f}_{i_1 i_1}\exp[-\hat{\Gamma}_y(t_{i_1}-t_{i_2})]\hat{f}_{i_2 i_2}\cdots\\ &\qquad\times\exp[-\hat{\Gamma}_y(t_{i_{n'-1}}-t_{i_{n'}})]\hat{f}_{i_{n'} i_{n'}}\exp(\hat{\Gamma}_y t_{i_{n'}})|p_0\rangle\\ &\quad = \langle\tilde{p}_0|\hat{f}_{i_1 i_1}\exp[-\hat{\Gamma}_y(t_{i_1}-t_{i_2})]\cdots\exp[-\hat{\Gamma}_y(t_{i_{n'-1}}-t_{i_{n'}})]\hat{f}_{i_{n'} i_{n'}}|p_0\rangle\end{aligned} \tag{9.3.14a}$$

We can show now that this replacement may be justified from a stochastic–probabilistic point of view. First we note that in general the left eigenstates defined by

$$\langle\tilde{\hat{p}}_n|\Gamma_y = E_n\langle\hat{p}_n| \tag{9.3.15}$$

including $\langle\tilde{p}_0|$ of Eq. 9.3.14a are not the usual vectors corresponding to the right eigenstates defined by

$$\hat{\Gamma}_y|p_n\rangle = E_n|p_n\rangle \tag{9.3.16}$$

In fact $\hat{\Gamma}_y$ is in general *a non-Hermitian operator.* So we obtain

$$\langle y \mid p_0\rangle = w_0(y) \tag{9.3.17}$$

where $w_0(y)$ is the equilibrium distribution, and

$$\langle\tilde{p}_0 \mid y\rangle = 1 \tag{9.3.18}$$

as can easily be checked when, for example, the diffusion operator $\hat{\Gamma}_y$ is given by

$$\hat{\Gamma}_y = -\gamma\left(\frac{\partial}{\partial y}y + \Delta^2\frac{\partial^2}{\partial y^2}\right) \tag{9.3.19}$$

It is also clear that

$$\hat{\Gamma}_y|p_0\rangle = 0 \tag{9.3.20}$$

$$\langle\tilde{p}_0|\hat{\Gamma}_y = 0 \tag{9.3.20a}$$

These equations completely justify Eq. 9.3.14a. Of course the scalar product used to define Eq. 9.3.14a is as follows:

$$\langle A \mid B\rangle = \int dy\, A^*(y)B(y) \tag{9.3.21}$$

From the general theory of stochastic processes we have (Freed, 1972):

$$P(y_0 \mid yt) = e^{-\hat{\Gamma}_y t}\delta(y - y_0) \tag{9.3.22}$$

which results in

$$e^{-\hat{\Gamma}_y t}A(y) = \int P(y_i \mid y, t)A(y)\, dy_i \tag{9.3.23}$$

If we make explicit Eq. 9.3.14a by using the scalar product of Eq. 9.3.21 and the definition of right and left eigenvector given by Eq. 9.3.15 and Eq. 9.3.16, respectively, we obtain

$$\begin{aligned}&\langle\tilde{p}_0|\hat{f}_{i_1 i_1}\exp[-\hat{\Gamma}_y(t_{i_1}-t_{i_2})]\hat{f}_{i_2 i_2}\cdots\exp[-\hat{\Gamma}_y(t_{i_{n'-1}}-t_{i_{n'}})]\hat{f}_{i_{n'} i_{n'}}|p_0\rangle\\ &\quad = \int dy\exp(-\hat{\Gamma}_y t_{i_1})f_{i_1 i_1}(y)\exp[-\hat{\Gamma}_y(t_{i_1}-t_{i_2})]\\ &\qquad\times f_{i_2 i_2}(y)\exp[-\hat{\Gamma}_y(t_{i_{n'-1}}-t_{i_{n'}})]f_{i_{n'} i_{n'}}(y)w_0(y)\\ &\quad = \int dy\, dy_1\, dy_2\cdots dy_{n'-1}f_{i_1 i_1}(y_{i_1})P(y_{i_2}t_{i_2} \mid y_{i_1}t_{i_1})f_{i_2 i_2}(y_{i_2})\\ &\qquad\cdots f_{i_{n'-2} i_{n'-2}}(y_{i_{n'-2}})P(y_{i_{n'-1}}t_{i_{n'-1}} \mid y_{i_{n'-2}}t_{i_{n'-2}})f(y_{i_{n'-1}})\\ &\qquad\times P(y, t_{i_{n'}} \mid y_{i_{n'-1}}t_{i_{n'-1}})f_{i_{n'-1} i_{n'-1}}(y)w_0(y)\end{aligned} \tag{9.3.24}$$

The right side of Eq. 9.3.24 could be replaced by the corresponding contribution in Eq. 9.3.12a simply by using a probabilistic–stochastic approach. The fact that it results as a consequence of Eq. 9.3.13a sheds some light on the importance of that equation. We can also regard this as being theoretical support for the use of that equation.

However, still more important is the fact that we are now able to obtain the stochastic Liouville equation (SLE) theory by the same kind of theoretical approach as that of the previous section. The SLE theory is a well-known theory by Kubo (1969), the semiclassical version of which is obtained in the standard way in Appendix E.

With reference to the case being dealt with here, it can be written as follows:

$$i\frac{\partial}{\partial t}\sigma = \hat{\mathscr{H}}_S^X\sigma + \hat{\mathscr{H}}_{\mathrm{ext}}^X(t)\sigma + \hat{h}^X\sigma - i\hat{\Gamma}_y\sigma \tag{9.3.25}$$

where the statistical density matrix also depends on the statistical variable y. It is convenient to expand σ over the eigenstates of as follows:

$$\sigma = \sum_n \sigma_n \mid p_n\rangle \tag{9.3.26}$$

The matrix σ_n is independent of the stochastic variable y. We shall see better in the following that σ_0 and $\sigma_n (n \neq 0)$ can be regarded as being just the counterpart of the part of interest and the "virtual" state of the previous section.

The operators $\hat{\mathcal{H}}_S$ and $\hat{\mathcal{H}}_{ext}$ are the same as those used in Eqs. 9.3.16 and 9.3.10. The operator $\hat{h}$ is obtained by replacing the one of Eq. 9.3.10 with its corresponding counterpart defined by

$$\hat{h} = \sum_i |r_i\rangle\langle r_i| f_i(\hat{y}) \tag{9.3.27}$$

Note that the SLE directly includes the diffusion operator $\hat{\Gamma}_y$ appearing in Eq. 9.3.13 and consequently is very useful. In fact, it can exploit directly any information on the molecular dynamics provided, for example, by a Fokker–Planck equation. We shall regard

$$\hat{\Lambda}_0 = \hat{\mathcal{H}}_0^X - i\hat{\Gamma}_y \tag{9.3.28}$$

as being the unperturbed part of the superoperator appearing in Eq. 9.3.25. Then the perturbation part is given by

$$\hat{\Lambda}_1 = \hat{h}^X + \hat{\mathcal{H}}_{ext}^X(t) \tag{9.3.29}$$

In the interaction picture Eq. 9.3.25 is written as

$$i\frac{\partial}{\partial t}\tilde{\sigma} = \tilde{\hat{\Lambda}}_1 \tilde{\sigma} \tag{9.3.30}$$

where

$$\tilde{\sigma} = \exp(i\hat{\Lambda}_0 t)\sigma \tag{9.3.31}$$

and

$$\tilde{\hat{\Lambda}}_1 = e^{i\hat{\Lambda}_0 t}\hat{\Lambda}_1 e^{-i\hat{\Lambda}_0 t} \tag{9.3.32}$$

We can define now a projection operator $\hat{P}'$ acting on the stochastic statistical density matrix $\sigma(y)$ as follows:

$$\hat{P}'\sigma = \sigma_0 |p_0\rangle \tag{9.3.33}$$

We can then replace Eq. 9.3.30 with its projected counterpart (we can repeat the same approach as that applied to Eq. 9.3.3) and we obtain

$$i\frac{\partial}{\partial t}\hat{P}'\sigma(t) = \hat{P}'\hat{\Lambda}_1(t)\hat{P}'\tilde{\sigma}(t) - \int_0^t \tilde{\hat{\Phi}}'(t,\tau)\hat{P}'\tilde{\sigma}(t)\,d\tau \tag{9.3.34}$$

where

$$\tilde{\hat{\Phi}}'(t,\tau) = P'\hat{\Lambda}_1(t)\overleftarrow{\exp}[-i\int_0^t (\hat{1}-\hat{P}')\hat{\Lambda}_1(t')\,dt'](\hat{1}-\hat{P})\hat{\Lambda}_1(\tau)\hat{P}' \tag{9.3.35}$$

The first term on the right side of Eq. 9.3.34 is the same as the corresponding one in Eq. 9.3.6. We have now to show that the "memory kernel" $\tilde{\hat{\Phi}}'(t,\tau)$ is equivalent to the "memory kernel" $\tilde{\hat{\Phi}}(t,\tau)$ of Eq. 9.3.8.

To do it we can expand $\hat{\Phi}'(t,\tau)$ in the same way as that for $\hat{\Phi}(t,\tau)$. We can then find that independent contributions to $\tilde{\hat{\Phi}}'(t,\tau)$ have the following form:

$$\{|A|r_{i_1}\rangle\langle r_{i_1}|)^X A_{i_2 i_2}(|r_{i_2}\rangle\langle r_{i_2}|)^X A_{i_2 i_3}\cdots(|r_{i_{n'}}\rangle\langle r_{i_{n'}}|)^X Bs\}$$
$$\times\langle\tilde{p}_0|f_{i_1 i_1}\exp[-\hat{\Gamma}_y(t_{i_1}-t_{i_2})]\cdots\times\exp[-\hat{\Gamma}_y(t_{i_{n'-1}}-t_{i_{n'}})]\hat{f}_{i_{n'} i_{n'}}|p_0\rangle \tag{9.3.36}$$

The left factor in Eq. 9.3.36 is the same as the corresponding one of Eq. 9.3.12a. The right factor is just the stochastic expression to be replaced by the corresponding factor of Eq. 9.3.12a. We have therefore completely justified Eq. 9.3.25. A more concise derivation can be found in Appendix E.

This approach shows that Eq. 9.3.25 is the "reduced" model corresponding to the "complex" physical system described by the Hamiltonian of Eq. 9.3.1. The kind of demonstration used to obtain Eq. 9.3.25 is, in fact, the same as that used in the previous section for obtaining, for example, the two-state model from the Friedrich one. Furthermore, there is a profound similarity between the SLE and the "reduced" models introduced in the previous section.

In order to emphasize this similarity, let us recall the well-known case of a two-state jump model (Kubo, 1969). In this model the operator y is assumed to take only two values:

$$\hat{y} = \pm y_1 \quad \text{or} \quad \hat{y} = \begin{pmatrix} y_1 & 0 \\ 0 & -y_1 \end{pmatrix} \tag{9.3.37}$$

corresponding to two states, say, a and b, of the environment. The Markovian master equation of the two-level system is

$$\frac{d}{dt}\rho_a = -\frac{\gamma_m}{2}(\rho_a - \rho_b) \tag{9.3.38}$$

$$\frac{d}{dt}\rho_b = \frac{\gamma_m}{2}(\rho_a - \rho_b), \tag{9.3.38a}$$

which corresponds to the following diffusion operator

$$\hat{\Gamma}_y = \frac{\gamma_m}{2}\begin{pmatrix} -1 & 1 \\ 1 & -1 \end{pmatrix} \tag{9.3.39}$$

The "diffusion" operator of Eq. 9.3.39 has two eigenstates $|p_0\rangle$ and $|p_1\rangle$ with eigenvalues 0 and γ_m, respectively.

We consider now a quantum mechanical state consisting of a ground state, $|g\rangle$, and an excited state, $|e\rangle$. We assume that the energy of the excited state can take in a random way two values, $\epsilon_e \pm y_1$ being driven by the diffusion operator of Eq. 9.3.39. By applying the standard approach of

Appendix F to this case we obtain

$$i\frac{\partial}{\partial t}\langle e|\sigma_0|g\rangle = \omega_{eg}\langle e|\sigma_0|g\rangle + \Delta\langle e|\sigma_1|g\rangle \tag{9.3.40}$$

$$i\frac{\partial}{\partial t}\langle e|\sigma_1|g\rangle = (\omega_{eg} - i\gamma_m)\langle e|\sigma_1|g\rangle + \Delta\langle e|\sigma_0|g\rangle \tag{9.3.40a}$$

where

$$\Delta = \langle e|\hat{h}|e\rangle \tag{9.3.40b}$$

$$\hat{h} = |e\rangle\langle e|\hat{y} \tag{9.3.40c}$$

Denoting by x the matrix element $\langle e|\sigma_0(t)|g\rangle$, from the previous set of differential equations we obtain the following second-order differential equation:

$$\ddot{x} + \Delta^2 x + \gamma_m \dot{x} = 0 \tag{9.3.41}$$

Equation 9.3.41 has the same form as Eq. 9.2.26. It means that the dipole $\langle e|\sigma_0|g\rangle$ has the same time evolution as the coefficient $\langle e \mid \psi\rangle$ of the intramolecular model studied in the previous section, provided that

$$\Delta = v \tag{9.3.42}$$

$$\gamma_m = \gamma \tag{9.3.42a}$$

The physical interpretation is the same. In Section 9.2 a real state $|e\rangle$ could interact nondissipatively with a "virtual" state $|M\rangle$, which in turn was subject to an exponential decay. Here we have a "real" dipole interacting in a nondissipative way with a "virtual" one. The nonvanishing value of such a dipole could be prepared by a coherent excitation pulse. Coherence should not be lost through the nondissipative interaction. However, it is lost with a rate γ_m when attaining the "virtual" part of our system. When the dissipation rate is fairly small, the decay of $\langle e|\sigma_0|g\rangle$ exhibits a damped oscillating behavior.

In the case of the "intramolecular" model of the previous section it is then possible to show that even the off-diagonal element $\langle e|\sigma_0|g\rangle$ follows the same equation of motion as $\langle e \mid \psi\rangle$. In fact, the Liouville equation corresponding to the effective Hamiltonian of Eq. 9.2.19 is (Appendix G)

$$\frac{\partial}{\partial t}\rho = -i\hat{\mathscr{H}}'^{\times}\rho = -i(\hat{\mathscr{H}}'\rho - \rho\hat{\mathscr{H}}'^{+}) \tag{9.3.43}$$

In the absence of external excitation, from the previous equation we obtain:

$$i\frac{\partial}{\partial t}\langle e|\rho|g\rangle = \omega_{eg}\langle e|\rho|g\rangle + v\langle M|\rho|g\rangle \tag{9.3.44}$$

$$i\frac{\partial}{\partial t}\langle M|\rho|g\rangle = (\omega_{Mg} - i\gamma)\langle M|\rho|g\rangle + v\langle e|\rho|g\rangle \tag{9.3.45}$$

If $\omega_{eg} = \omega_{Mg}$ (recall that in the previous section the states $|M\rangle$ and $|e\rangle$ have been assumed to be degenerate), Eqs. 9.3.44 and 9.3.45 can be replaced by the following second-order differential equation:

$$\ddot{x} + v^2 x + \gamma\dot{x} = 0 \tag{9.3.46}$$

where now

$$x = \langle e|\rho|g\rangle \tag{9.3.47}$$

Equation 9.3.46 is equal to 9.2.26. When Eqs. 9.3.42 and 9.3.42a are satisfied, the "intramolecular" coherence satisfies the same equation of motion as the "external" one.

Since in the context of the linear response approximation the absorption spectrum depends only on the free relaxation properties of the off-diagonal elements $\langle e|\rho|g\rangle$ and $\langle e|\sigma_0|g\rangle$, it is evident that the linear response absorption spectrum is the same in the two cases under study.

According to the standard theories [Goldberger and Watson, 1964; Robinson, 1974] the line shape is given by $-Im\langle G|\hat{\mu}\hat{G}\hat{\mu}|g\rangle$ where $\hat{\mu}$ is the dipole operator and $\hat{G} = (\epsilon_g + \omega - \hat{\mathscr{H}}')^{-1}$ is the Green function associated with the Hamiltonian $\hat{\mathscr{H}}'$. When $\hat{\mathscr{H}}'$ is to be related to a relaxation model of "intramolecular" kind such as the complex ones of the previous sections, we obtain

$$Im\langle g|\hat{\mu}\hat{G}\hat{\mu}|g\rangle = Im\hat{G}_{ee} \tag{9.3.48}$$

In order to evaluate $\hat{G}_{ee}$, we can use the well-known Dyson equation (Goldberger and Watson, 1964; Robinson, 1974):

$$\hat{G} = \hat{G}^0 + \hat{G}^0\hat{V}\hat{G} \tag{9.3.49}$$

where $\hat{G}^0$ is the Green's function (see Chapter 2) of the unperturbed Hamiltonian. By taking into account the nature of the "intramolecular" relaxation under study we can write

$$\hat{G}_{ee} = \hat{G}^0_{ee} + \hat{G}^0_{ee}\hat{V}_{em}\hat{G}_{me} \tag{9.3.50}$$

$$\hat{G}_{me} = \hat{G}^0_{mm}\hat{V}_{me}\hat{G}_{ee} \tag{9.3.50a}$$

When the model of "intramolecular" relaxation is the "reduced" one of the previous section, we obtain from Eqs. 9.3.50 and 9.3.50a

$$\hat{G}_{ee} = \frac{1}{(\omega - \epsilon_e + \epsilon_g)}\left(1 - \frac{v^2}{(\omega - \epsilon_e + \epsilon_g)(\omega - \epsilon_e + \epsilon_g + i\gamma)}\right)^{-1} \tag{9.3.51}$$

By using the notation $\Delta\omega = \omega - \epsilon_e + \epsilon_g$ we obtain

$$-Im\hat{G}_{ee} = \frac{\gamma v^2}{(\Delta\omega^2 - v^2)^2 + \Delta\omega^2\gamma^2} \tag{9.3.51a}$$

which is the absorption spectrum of the two-jump model (Kubo, 1969b).

However, this similarity is destroyed when one is using strong excitation

pulses (Grigolini, 1979), as can be shown by using an advantageous property of the RMT: the mathematics behind RMT can in fact be used to avoid the limitations of linear response theory.

We have stressed the similarity between the SLE and the RMT when applied to the standard "intramolecular" model described in the previous section. However, more generally, the two theories differ.

If, instead of using the two-jump model, we had used a more realistic diffusion operator, for example, the one of Eq. 9.3.19, we would have obtained a chain of "virtual" dipole $\langle e|\sigma_1|g\rangle$, $\langle e|\sigma_2|g\rangle, \ldots$ decaying with a rate $\gamma_1, \gamma_2, \ldots$, respectively. The generic damping γ_m would have been provided by the mth eigenvalue of the operator $\hat{\Gamma}_y$. Thus in the SLE theory any term of the chain of "virtual" dipoles is directly undergoing a relaxation process of Markovian type.

As a consequence, the main difference between the RMT theory applied to the model of the previous section and the SLE is not in the fact that in the former the chain consists of off-diagonal elements (dipoles) instead of populations, but rather in the dissipative damping of any term of the chain of "virtual" elements. In fact, when the RMT is given a rigorous theoretical support in terms of the Mori theory, only the last state of the chain is shown to directly undergo a relaxation process.

In the following, we try to clarify the theoretical reasons for this difference (see Sections 10.3 and 10.5).

9.4 EFFECTS OF THE TIME DURATION OF EXCITATION PULSE IN THE CASE OF "EXTERNAL" THERMAL BATHS

After introducing the SLE, we are now able to discuss the effects of the time duration of the excitation pulse on the relaxation in the case of thermal baths of "external" kind. In this case we obtain the same effects as in the "intramolecular" one even though now physical intuition is of little aid.

The effects described in Section 9.2 can be explained in part by intuitive arguments, illustrated by Fig. 9.2.1. We can remark, as already seen in Section 9.2, that the excited state of interest interacts with a dense set of states $\{|m\rangle\}$, which, in turn, interacts with a dissipative continuum, $\{|\epsilon\rangle\}$. We recall that the last dissipative continuum is introduced in order to take into account the fact that even in the gas phase a molecular system can be regarded as isolated only for times less than $\tau_{\max}$ (Freed, 1972).

We note that the true molecular eigenstates

$$|\psi_n\rangle = c_{ne}|e\rangle + \sum_m c_{nm}|m\rangle \tag{9.4.1}$$

spread over a frequency interval whose size is given by ΔE.

Let us suppose now that the radiation excitation pulse is of minimum

duration. For short excitation pulses, then, each molecular eigenstate has an absorption intensity proportional to $|\mu_{eg}|^2|c_{ne}|^2$. Its quantum mechanical probability is the same as the one that would be obtained by expansion of the state $|e\rangle$ over the basis set of the eigenstates $|\psi_n\rangle$. In other words, by using a fairly short excitation pulse it is possible to prepare our physical system in the excited state $|e\rangle$. The state $|e\rangle$ can then exhibit a fast decay depending on the e–m intramolecular coupling. The RMT described in Section 9.2 shows that such a decay can be damped oscillatory.

The true molecular eigenstate of Eq. 9.4.1 can be prepared by using a fairly long excitation pulse. The relaxation process should depend then on the dissipative properties of any single state, $|e\rangle$ or $|m\rangle$. As a consequence, if the states $|e\rangle$ and $|m\rangle$ are not influenced by strong relaxation coupling, a slow decay should be observed. Rhodes (1980) argued that fluorescence decay can exhibit both an oscillatory behavior (after a short duration pulse) and an exponential one(after a long pulse). The RMT allowed a quantitative treatment of these effects (Section 9.2).

In order to emphasize the generality of these effects, consider the simple molecular system, described by the Hamiltonian:

$$\begin{aligned}\hat{\mathcal{H}} = {} & |g\rangle\epsilon_g\langle g| + 2(|2\rangle\langle g| + |g\rangle\langle 2|)HF(t)\cos\omega t \\ & + |2\rangle\epsilon_2\langle 2| + |1\rangle\epsilon_1\langle 1| + (|1\rangle\langle 2| + |2\rangle\langle 1|)\hat{V} + \hat{\mathcal{H}}_B\end{aligned} \tag{9.4.2}$$

This system has been proposed by Abbott and Oxtoby (1980) to study the problem of vibrational relaxation in liquids. The operator $\hat{V}$ acts on the thermal bath of the system of interest. From a formal point of view the physical system of Eq. 9.4.2 belongs to the same family as those studied in the previous section. In this case the thermal bath is of "external" nature, that is, completely different from the "intramolecular" one used to support the foregoing qualitative remarks on the effects of pulse time duration on the relaxation process.

Abbott and Oxtoby assumed $\hat{V}$ to be a stochastic variable of Gaussian or Poissonian nature and then carried out a computer simulation of this relaxation process, which is semiclassical in nature. In fact, the system of interest is quantum mechanical, whereas the coupling is assumed to be a classical stochastic variable.

The theory developed in the previous section is especially suitable for dealing with the "computer experiment" of Abbott and Oxtoby. Applying this theory we obtain the following Liouville equation:

$$\frac{\partial\sigma}{\partial t} = -i[\hat{\mathcal{H}}_S, \sigma] - i[\hat{\mathcal{H}}_{\text{ext}}(t), \sigma] - i[\hat{\mathcal{H}}_1, \sigma] - \hat{\Gamma}\sigma \tag{9.4.3}$$

where

$$\hat{\mathcal{H}}_S = |g\rangle\epsilon_g\langle g| + |2\rangle\epsilon_2\langle 2| + |1\rangle\epsilon_1\langle 1| \tag{9.4.4}$$

$$\hat{\mathcal{H}}_{\text{ext}}(t) = 2(|2\rangle\langle g| + |g\rangle\langle 2|)HF(t)\cos\omega t \tag{9.4.5}$$

$$\hat{\mathcal{H}}_1 = (|1\rangle\langle 2| + |2\rangle\langle 1|)\hat{v} \tag{9.4.6}$$

The simplest model of stochastic fluctuation is the two-state one described

in the previous section. Using this model we have

$$\hat{\Gamma}|p_0\rangle = 0 \tag{9.4.7}$$

$$\hat{\Gamma}|p_1\rangle = -b|p_1\rangle \tag{9.4.8}$$

$$\langle p_1|\hat{v}|p_0\rangle = \langle p_0|\hat{v}|p_1\rangle = V \tag{9.4.9}$$

If we are interested in evaluating the absorption spectrum of this physical system we can simply use linear response theory (Zubarev, 1974) whereby the spectrum is given by

$$I(\omega) = \text{const} \times \int_0^\infty \langle \hat{\mu}\hat{\mu}(t)\rangle e^{-i\omega t} \tag{9.4.10}$$

where

$$\hat{\mu} = |2\rangle\langle g| + |g\rangle\langle 2| \tag{9.4.11}$$

According to the stochastic approach (Appendix H)

$$\begin{aligned}\langle \hat{\mu}\hat{\mu}(t)\rangle &= \langle \tilde{p}_0|\,\mathrm{Tr}_{\{S\}}\,(|2\rangle\langle g| + |g\rangle\langle 2|)\exp[i(\hat{\mathscr{H}}_S + i\hat{\Gamma})t] \\ &\quad \times (|2\rangle\langle g| + |g\rangle\langle 2|)|g\rangle\langle g||p_0\rangle \\ &= \langle g|\sigma_0(t)|2\rangle \qquad (\sigma_0(0) = |g\rangle\langle 2|)\end{aligned} \tag{9.4.12}$$

From Eq. 9.4.3 we have

$$\frac{\partial}{\partial t}\langle g|\sigma_0(t)|2\rangle = -i(\epsilon_g - \epsilon_2)\langle g|\sigma_0(t)|2\rangle + iV\langle g|\sigma_1(t)|1\rangle \tag{9.4.13}$$

$$\frac{\partial}{\partial t}\langle g|\sigma_1(t)|1\rangle = -i(\epsilon_g - \epsilon_1)\langle g|\sigma_1(t)|1\rangle + iV\langle g|\sigma_0(t)|2\rangle - b\langle g|\sigma_1(t)|1\rangle \tag{9.4.14}$$

In conclusion, the evaluation of the time evolution of $\hat{\mu}$ requires the diagonalization of the matrix:

$$\mathbf{A} = \begin{pmatrix} i\omega_0 & iV \\ iV & -b \end{pmatrix} \tag{9.4.15}$$

where $\omega_0 = \epsilon_2 - \epsilon_1$.

The "intramolecular" model described in Section 9.2 when replaced by a "reduced" scheme only involving a "virtual" state $|M\rangle$ with a damping b results in a free time evolution of the dipole $\hat{\mu}$ connecting $|g\rangle$ with the excited state $|e\rangle$, which will be determined by the effective Hamiltonian (Section 9.2):

$$\hat{\mathscr{H}}_{\text{eff}} = |e\rangle\langle e|\epsilon_e + |M\rangle\langle\epsilon_M - i\gamma_M\rangle\langle M| + |g\rangle\epsilon_g\langle g| \tag{9.4.16}$$

By using the result obtained in Section 9.2, it is possible to show that the dynamics of $\langle g|\rho|e\rangle$ are the same as those of $\langle g|\sigma_0(t)|2\rangle$ provided that $\gamma_M = b$ and $\epsilon_e - \epsilon_M = \omega_0$. As a consequence the two systems have the same

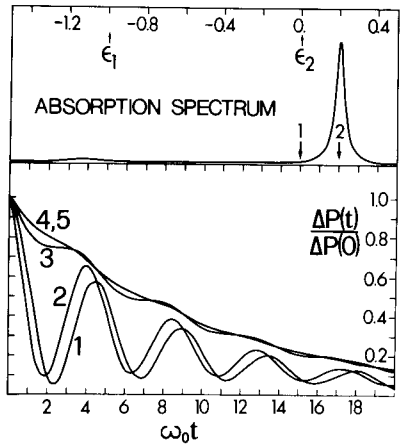

Figure 9.4.1 Decay of the state 2 for excitation pulses of different time duration. $T = 0.01(1)$, $T = 1(2)$, $T = 10(3)$, $T = 100(9)$, $T = 1000(5)$, $V = 0.5$, $\omega_0 = \epsilon_2 - \epsilon_1 = 1$, and $b = 0.2$. The quantity $\Delta P(t)/\Delta P(0)$ is defined as $[P(t) - P(\infty)]/[P(0) - P(\infty)]$, where $P(t)$ is the population of the state $|2\rangle$. $P(\infty)$ is its equilibrium value. $P(0)$ is the value of the population at the time when the excitation pulse is turned off. The excitation frequency is tuned in to the absorption frequencies denoted by arrows 1 (cases 1, 2) and 2 (cases 3–5). The intensity of the electromagnetic coupling is $H = 0.001$.

absorption spectrum. This is illustrated in Fig. 9.4.1 for $V = 0.5$ and $b = 0.2$.

With a square excitation pulse of time duration T, that is, when

$$F(t) = 1 \qquad (0 < t < T) \tag{9.4.17}$$

$$F(t) = 0 \qquad (t \geqslant T) \tag{9.4.18}$$

it is possible to evaluate the time evolution of the physical system starting from the initial condition expressed by the following equation:

$$\sigma(0) = (|g\rangle\langle g|)|p_0\rangle \tag{9.4.19}$$

This means that before excitation the system is found in the ground state in the presence of a thermal bath in its equilibrium distribution. If we are interested in the time evolution of the population of the excited state $|2\rangle$ we can determine the time evolution of $\langle 2|\sigma_0|2\rangle$ from Eq. 9.4.3. It is possible to show that it involves the time evolution of the elements $\langle g|\sigma_0|g\rangle$, $\langle g|\sigma_0|2\rangle$, $\langle 2|\sigma_0|g\rangle$, $\langle g|\sigma_1|1\rangle$, $\langle 1|\sigma_1|g\rangle$, $\langle 2|\sigma_1|1\rangle$, $\langle 1|\sigma_1|2\rangle$, and $\langle 1|\sigma_0|1\rangle$. By making the rotating wave approximation, which is an obvious extension of that illustrated in Appendix A, the corresponding calculation can be performed by diagonalizing the following matrix:

$\mathbf{A} =$

	$\langle g\|\sigma_0\|g\rangle$	$\langle g\|\sigma_0\|2\rangle$	$\langle 2\|\sigma_0\|g\rangle$	$\langle g\|\sigma_1\|1\rangle$	$\langle 1\|\sigma_1\|g\rangle$	$\langle 2\|\sigma_0\|2\rangle$	$\langle 2\|\sigma_1\|1\rangle$	$\langle 1\|\sigma_1\|2\rangle$	$\langle 1\|\sigma_0\|1\rangle$
$\langle g\|\sigma_0\|g\rangle$	0	iH	$-iH$	0	0	0	0	0	0
$\langle g\|\sigma_0\|2\rangle$	iH	$i\Delta_1$	0	iV	0	$-iH$	0	0	0
$\langle 2\|\sigma_0\|g\rangle$	$-iH$	0	$-i\Delta_1$	0	$-iV$	iH	0	0	0
$\langle g\|\sigma_1\|1\rangle$	0	iV	0	$i\Delta_2 - b$	0	0	$-iH$	0	0
$\langle 1\|\sigma_1\|g\rangle$	0	0	$-iV$	0	$-i\Delta_2 - b$	0	0	iH	0
$\langle 2\|\sigma_0\|2\rangle$	0	$-iH$	iH	0	0	0	iV	$-iV$	0
$\langle 2\|\sigma_1\|1\rangle$	0	0	0	$-iH$	0	iV	$i\omega_0 - b$	0	$-iV$
$\langle 1\|\sigma_1\|2\rangle$	0	0	0	0	iH	$-iV$	0	$i\omega_0 - b$	iV
$\langle 1\|\sigma_0\|1\rangle$	0	0	0	0	0	0	$-iV$	iV	0

(9.4.20)

where

$$\Delta_1 = \omega_{2g} - \omega, \qquad \Delta_2 = \omega_{1g} - \omega \tag{9.4.21}$$

When the pulsed external irradiation is turned off ($H = 0$), Eq. 9.4.2 is divided into two noninteracting submatrices. The submatrix involving the matrix elements $\langle 2|\sigma_0|2\rangle$, $\langle 2|\sigma_0|1\rangle$, $\langle 1|\sigma_0|2\rangle$, $\langle 1|\sigma_0|1\rangle$ could be used in order to evaluate the free relaxation if the initial condition were known. The initial condition is correctly defined when the matrix elements $\langle 1|\sigma_1|2\rangle$ and $\langle 2|\sigma_1|1\rangle$ are known in addition to $\langle 2|\sigma_0|2\rangle$, $\langle 1|\sigma_0|1\rangle$. It is not correct to assume that when relaxation begins all matrix elements vanish except $\langle 2|\sigma_0|2\rangle$. In fact, during the excitation process even these elements can be finite. From an intuitive point of view this corresponds to an excitation of the "thermal bath" itself as a result of the irradiation process. Before irradiation our physical system can be assumed to be in the ground state in the presence of a thermal bath in its equilibrium distribution; that is, we can assume that all matrix elements vanish except $\langle g|\sigma_0|g\rangle$. As a result of excitation all the matrix elements of the four-dimensional submatrix are excited.

Excitation by the radiation pulse slightly affects the close similarity between the "external" and "intramolecular" model of vibrational relaxation. In the latter case the dissipation interaction should be provided by the effective Hamiltonian of Eq. 9.4.16. The description of excitation–relaxation process would find in the Schrödinger equation the most convenient theoretical approach. However, in order to study the relation between the two models it is convenient to use the Liouville equation (Appendix G):

$$\frac{\partial \rho}{\partial t} = [\hat{\mathcal{H}}_{\text{eff}} + \hat{\mathcal{H}}_{\text{ext}}(t)]\rho - \rho[\hat{\mathcal{H}}_{\text{eff}} + \hat{\mathcal{H}}_{\text{ext}}(t)]^{\dagger} \tag{9.4.22}$$

where $\hat{\mathcal{H}}_{\text{ext}}$ is the same as that of Eq. 9.4.5. In this case the study of the time evolution of $\langle 2|\rho|2\rangle$ would involve that of $\langle g|\rho|g\rangle$, $\langle g|\rho|2\rangle$, $\langle 2|\rho|g\rangle$, $\langle g|\rho|M\rangle$, $\langle M|\rho|g\rangle$, $\langle 2|\rho|1\rangle$, $\langle 1|\rho|2\rangle$, and $\langle 1|\rho|1\rangle$. We would obtain a matrix very similar to that of Eq. 9.4.20 but with the following differences. The σ_0 matrix elements should be replaced by the corresponding $\langle \alpha|\rho|\alpha'\rangle$. The elements $\langle g|\sigma_1|1\rangle$, $\langle 1|\sigma_1|g\rangle$, $\langle 2|\sigma_1|1\rangle$, $\langle 1|\sigma_1|2\rangle$ should be replaced by $\langle g|\rho|M\rangle$, $\langle M|\rho|g\rangle$, $\langle 2|\rho|M\rangle$, and $\langle M|\rho|2\rangle$, respectively, and the matrix element $A_{9,9} = 0$ by $A_{9,9} = -2b$, that is, when thermodynamic equilibrium is attained the intramolecular model results in a total depopulation of the states $|2\rangle$ and $|M\rangle$. In the "external" case, on the contrary, when $H = 0$ at equilibrium we have $\langle 2|\sigma_0|2\rangle = \langle 1|\sigma_0|1\rangle = \frac{1}{2}$ and $\langle 1|\sigma_1|2\rangle = \langle 2|\sigma_1|1\rangle = 0$. However, as shown by Fig. 9.4.2, in both cases the effect of increasing the pulse time duration is that of washing out the oscillations.

Abbott and Oxtoby carried out their computer "experiment" by using initial conditions corresponding to the excitation of the sharp component of the absorption spectrum (see Fig. 9.4.1). From an experimental point of view we can do that only by using a highly monochromatic excitation

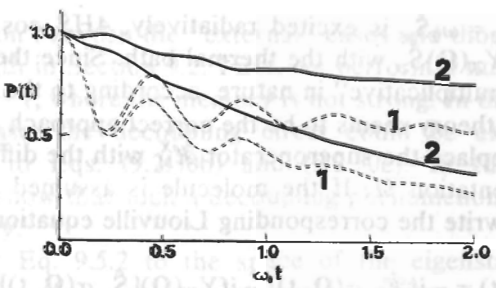

Figure 9.4.2 Time evolution of the population of the states $|2\rangle$, "external" case, and $|e\rangle$, "intramolecular case", $P(t)$, soon after the square excitation pulses of different time duration. The full lines denote the "external" case. The dashed lines denote the "intramolecular" case. The lines denoted by 1 describes the population decay after square pulses of time duration $T = 0.01$. The lines denoted by 2 describe the population decay after square pulses of time duration $T = 10$. The electromagnetic coupling H is $H = 0.0001$ for all curves except the full line 1, the coupling of which is $H = 0.001$.

pulse, the time duration of which must be very large. Figure 9.4.1 shows the results obtained using the theoretical approach described above. The agreement with the results of the computer experiments is good [see the corresponding "experimental" result (Abbott and Oxtoby, 1980)].

9.5 EFFECTS OF STRONG IRRADIATION

The main aim of this section is to show that the decoupling effects discussed in Section 9.2 for the intramolecular case are present also in the case of "external" thermal baths.

In order to show this, consider the case of an electric dipole interacting with a fluctuating magnetic field. This fluctuation is a result of the stochastic motion of the molecule containing the electronic spin under study. We do not give any derivation of the corresponding Hamiltonian. A detailed justification may be found in the literature (Freed et al., 1971). We can limit ourselves to asserting that in the simple case of an axially symmetrical g tensor the Hamiltonian may be written as follows:

$$\hat{\mathcal{H}} = \omega_0 \hat{S}_z + fY_{20}(\Omega)\hat{S}_z + 4H\hat{S}_x \cos \omega t + \hat{\mathcal{H}}_M \tag{9.5.1}$$

where Ω denotes the orientation of the molecule under study, and $\hat{S}_z$ and $\hat{S}_x$ are the z and x components of the spin angular momentum ($S = \frac{1}{2}$). $\mathcal{H}_M$ is the thermal bath of our system of interest. It consists of both the molecule containing the electronic spin and any other molecule of the liquid sample. The tagged molecule, of course, behaves stochastically owing to its interaction with the other molecules in the sample. The system described by the Hamiltonian of Eq. 9.5.1 is similar to that described by Eq. 9.4.2 of the previous section. In fact, the unperturbed part of the

Hamiltonian, $\hat{\mathcal{H}}_0 = \omega_0 \hat{S}_z$, is excited radiatively, $4H\hat{S}_z \cos \omega t$, and interacts dissipatively, $if Y_{20}(\mathbf{\Omega})\hat{S}_z$, with the thermal bath. Since the structure of this interaction is "multiplicative" in nature, according to the definition by Fox (1978), the SLE theory seems to be the correct approach also for this case.

We have to replace the superoperator $\mathcal{H}_M^X$ with the diffusion operator of the angular orientation $\mathbf{\Omega}$. If the molecule is assumed to be a spherical rotator we can write the corresponding Liouville equation as follows:

$$\frac{\partial}{\partial t}\sigma(\mathbf{\Omega}, t) = -i[\hat{\mathcal{H}}_0, \sigma(\mathbf{\Omega}, t)] - if Y_{20}(\mathbf{\Omega})[\hat{S}_z, \sigma(\mathbf{\Omega}, t)] + \hat{\Gamma}_{\Omega}\sigma(\mathbf{\Omega}, t) \tag{9.5.2}$$

where (diffusional limit)

$$\hat{\Gamma}_{\Omega} = R\nabla_{\Omega}^2 \tag{9.5.3}$$

Following a standard approach (Freed, 1964) we can evaluate the correlation function of the fluctuating function $F(t)$ defined as follows:

$$F(t) = \frac{f}{2} Y_{20}[\mathbf{\Omega}(t)] \tag{9.5.4}$$

We obtain

$$\Phi(t) = \langle F(t)F(t+\tau)\rangle = \frac{f^2}{4}\langle Y_{20}(t)Y_{20}(t+\tau)\rangle$$

$$= \left(\frac{\mathfrak{F}}{20}\right)\exp(-6Rt) \tag{9.5.5}$$

where

$$\mathfrak{F}^2 = \left(\frac{5}{4\pi}\right)f^2 \tag{9.5.6}$$

In order to make a comparison with the typical correlation function of the "intramolecular reduced model" used in Section 9.2, Eq. 9.2.16, we can write Eq. 9.5.5 as follows:

$$\Phi(t) = \frac{g^2\gamma^2}{4}\exp(-\gamma t) \tag{9.5.7}$$

provided that

$$\gamma = 6R \tag{9.5.8}$$

and

$$g = (180)^{-1/2}\frac{\mathfrak{F}}{R} \tag{9.5.9}$$

The correlation function of Eq. 9.5.7 has the same form as those involved in Section 9.2. The definition of the "memory" parameter allows us to make a comparison between the "external" cases and those with the same "memory" strength in Section 9.2. First, we perform a numerical "experiment" close to $g \sim 1$, where the memory is not strong. In the corresponding intramolecular case, the decoupling effect could be explained by the remarks leading to Eqs. (9.2.30b) and (9.2.30c). In further numerical experiments, we show that such a decoupling phenomenon is present even for strong memory.

We must refer Eq. 9.5.2 to the space of the eigenstates of ∇_{Ω}^2: the spherical harmonics. As a consequence, we can write

$$\sigma(\mathbf{\Omega}, t) = \sum_{lm}\sigma_{lm}(t)Y_{lm}(\mathbf{\Omega}) \tag{9.5.10}$$

We must also make the standard transformation to the rotating frame of reference. We thus obtain

$$\frac{\partial}{\partial t}\tilde{\sigma}_{lm} = -i\Delta\omega[\hat{S}_z, \tilde{\sigma}_{lm}] - 2iH[\hat{S}_x, \tilde{\sigma}_{lm}] - Rl(l+1)\tilde{\sigma}_{lm}$$

$$- if\sum_{l'm'} C(lm, l'm')[\hat{S}_z, \tilde{\sigma}_{l'm'}] \tag{9.5.11}$$

where

$$C(lm, l'm') = \int d\mathbf{\Omega}\, Y_{lm}(\mathbf{\Omega})^* Y_{20}(\mathbf{\Omega})Y_{l'm'}(\mathbf{\Omega}) \tag{9.5.12}$$

and

$$\Delta\omega = \omega_0 - \omega \tag{9.5.13}$$

We solve the system of differential equations of Eq. 9.5.12 by a matrix diagonalization procedure, in order to try to simulate a relaxation in the presence of external excitation. We assume that the initial magnetization vector is parallel to the y-axis. In the model of Eq. 9.5.1 any relaxation mechanism of longitudinal type is neglected, so that we can assume this physical condition to be achieved by applying a 90° pulse to a magnetization vector. The appearance of this along the z-axis is describable with a longitudinal relaxation process with a very large time constant.

The property studied here is the counterpart of that already discussed in Section 9.2 (the factor $\frac{1}{2}$ affecting the damping in the presence of external excitation). When $T_1 \gg T_2$ in the frame rotating at the resonance frequency, the phenomenological equations of Bloch (Abragam, 1961) can be written as

$$\frac{d}{dt}M_x = -\frac{M_x}{T_2} \tag{9.5.14}$$

$$\frac{d}{dt}M_y = -\frac{M_y}{T_2} - 2HM_z \tag{9.5.15}$$

$$\frac{d}{dt}M_z = 2HM_y \tag{9.5.16}$$

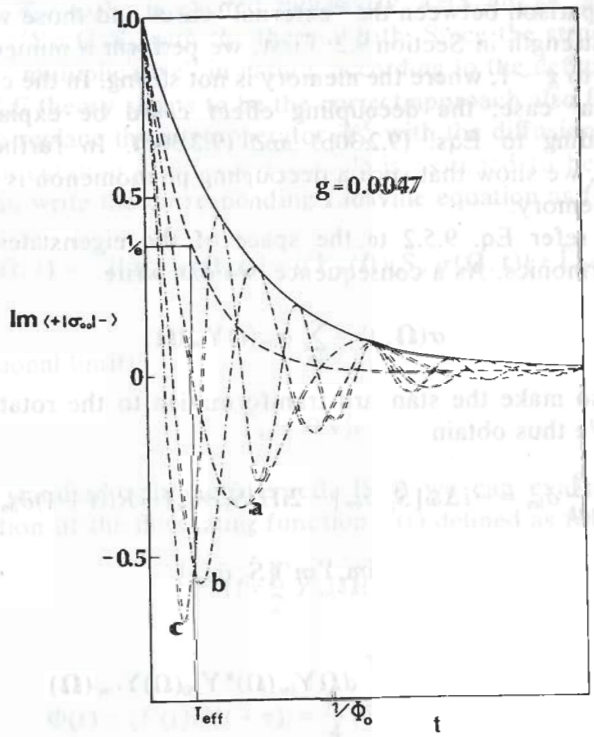

Figure 9.5.1 The imaginary part of $\langle +|\sigma_{\infty}|-\rangle$ as a function of time. The results reported in this figure, as well as those in Figs. 9.5.2–9.5.6, are to be related to initial conditions such that all the $\langle \alpha|\sigma_{Im}(0)|\alpha'\rangle$ vanish but $\langle \pm|\sigma_{\infty}(0)|\mp\rangle = \pm i$. The solid line is a rigorously exponential curve whose damping parameter is $1/(2T_{eff})$. In its turn, T_{eff} is the time at which the free relaxation function (--------) is endowed with the value $1/e$. The electromagnetic strengths, in Φ_0 units, are (*a*) 2.513, (*b*) 5.026, and (*c*) 7.539.

By substituting Eq. 9.5.16 in the derivative of Eq. 9.5.15 we have

$$\frac{d^2}{dt^2}M_y + \frac{1}{T_2}\frac{d}{dt}M_y + 4H^2 M_y = 0 \tag{9.5.17}$$

Since the roots of the corresponding auxiliary polynomial are

$$r = \frac{1}{2}\left[\frac{1}{T_2} \pm \left(\frac{1}{T_2} - 16H^2\right)^{1/2}\right] \tag{9.5.18}$$

it is evident that the condition for oscillation at exact resonance is that $16H > 1/T_2$. Furthermore, Eq. 9.5.17 shows that as oscillation appears, its damping is $1/2T_2$, whereas the free decay damping is $1/T_2$. The appearance of the factor $\frac{1}{2}$ as a simple result in the presence of a large enough irradiation field has already been discussed in the intramolecular case of Section 9.2. When the Markovian approximation is made to the free decay

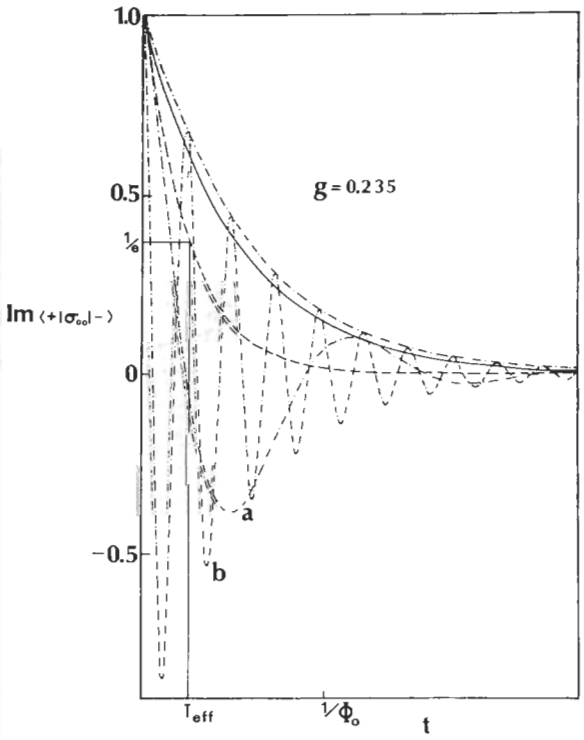

Figure 9.5.2 The imaginary part of $\langle +|\sigma_{\infty}|-\rangle$ as a function of time. The solid line has been derived from the free relaxation curve in the same way as the corresponding one in Fig. 9.5.1. The electromagnetic strengths, in Φ_0 units, are (*a*) 2.513 and (*b*) 12.565.

of the system under study we obtain the following unperturbed damping*:

$$\Phi_0 = \int_0^{\infty} \Phi(t')\,dt' = \frac{g^2\gamma}{4} \tag{9.5.19}$$

which is the counterpart of that of Eq. 9.2.30d. When $g \ll 1$ the phenomenological equations of Bloch (Eqs. 9.5.14–9.5.16) enable one to simulate exactly the relaxation process provided that

$$T_2 = \frac{1}{4\Phi_0} \tag{9.5.20}$$

The condition for oscillation at exact resonance is then that $H > \Phi_0$. Figure 9.5.1 shows that indeed for $g \ll 1$ no significant decoupling effect is exhibited.

From Figs. 9.5.2–9.5.4 it is clear that in the cases where the memory parameter g is not negligibly small, the damping of the oscillations is

*In the next chapter the formal expression of the Markovian approximation is given a complete justification.

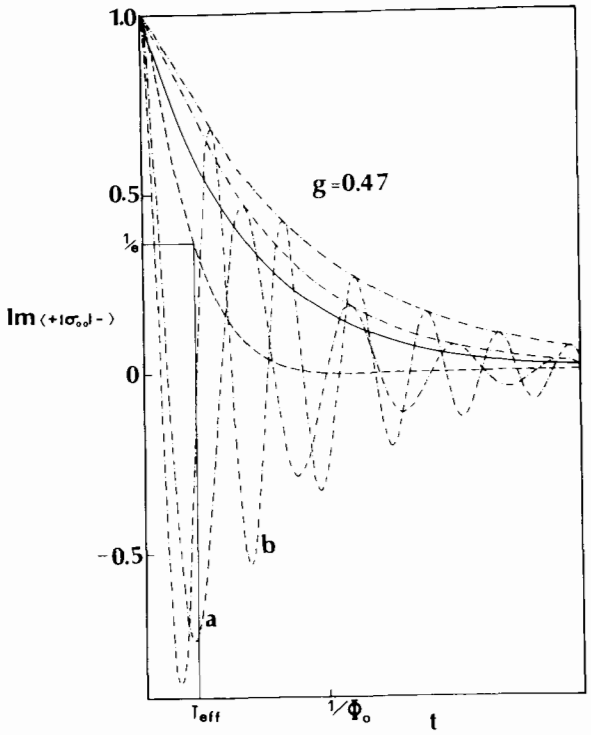

Figure 9.5.3 The imaginary part of $\langle +|\sigma_{00}|-\rangle$ as a function of time. The solid line has been derived from the free relaxation curve in the same way as the corresponding one in Fig. 9.5.1. The electromagnetic strengths, in Φ_0 units, are (*a*) 5.026 and (*b*) 7.539.

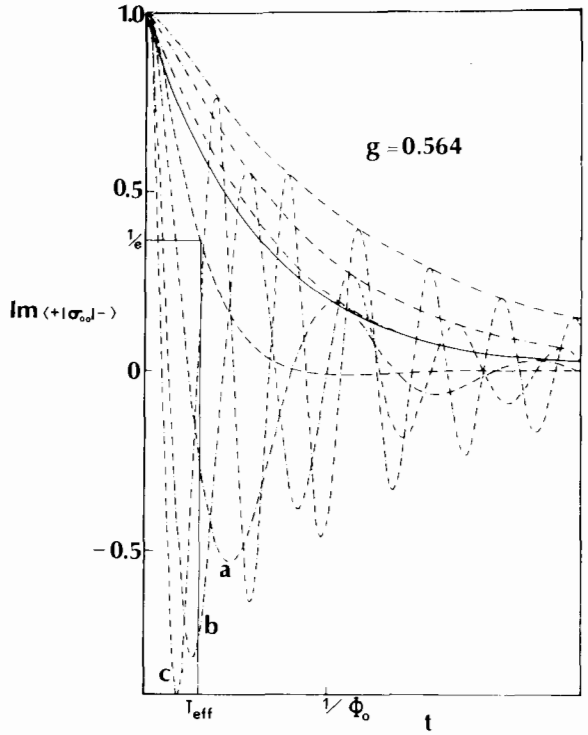

Figure 9.5.4 The imaginary part of $\langle +|\sigma_{00}|-\rangle$ as a function of time. The solid line has been derived from the free relaxation curve in the same way as the corresponding one in Fig. 9.5.2. The electromagnetic strength, in Φ_0 units, are (*a*) 2.513, (*b*) 5.026, and (*c*) 7.539.

significantly reduced by the irradiation fields fulfilling the condition that $H > \Phi_0$. A quantitative evaluation of such effects may be obtained in the following way. First, for each nonvanishing H a suitable decay function is built up from the envelope of the corresponding damped oscillation. Then, the time at which this has the value $1/e$ is assumed to be proportional to $1/\Phi$, where Φ is the damping value to be related to H. For nonnegligible values of g the relaxation process exhibits a significant deviation from rigorous exponential behavior, and therefore such a criterion becomes unrealistic as the parameter g increases.

A complex perturbative evaluation of such decoupling effects have been developed (Grigolini, 1976). In Fig. 9.5.5 we compare the results of the present approach with the approximate ones. As the "memory strength" increases even the approximate theory by Grigolini (1976) becomes progressively less accurate. However, Fig. 9.5.5 shows fairly good agreement between the two approaches. It supports the presence of decoupling effects for "external" thermal baths.

Figure 9.5.6 shows that these are well marked even when $g \gg 1$.

The real experimental detection of such effects could be used for investigating molecular relaxation in liquids.

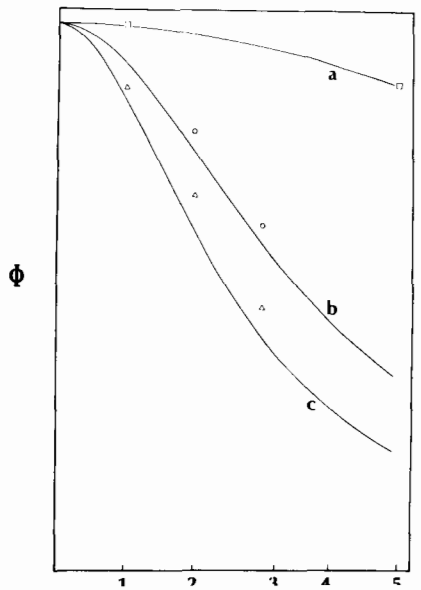

Figure 9.5.5 A plot of Φ versus H. For each g the abscissa unity is provided by the corresponding value $\Phi_0 = g^2\gamma/4$. The solid lines have been obtained using the same perturbation method as the one applied to the secular interaction. The cases *a*, *b*, and *c* are related, respectively, to the following values of g: 0.235, 0.47, and 0.564. The points denoted by □, ○, and △ have been obtained by applying the criterion described in the text to the damped oscillations of Figs. 9.5.2, 9.5.3, and 9.5.4, respectively.

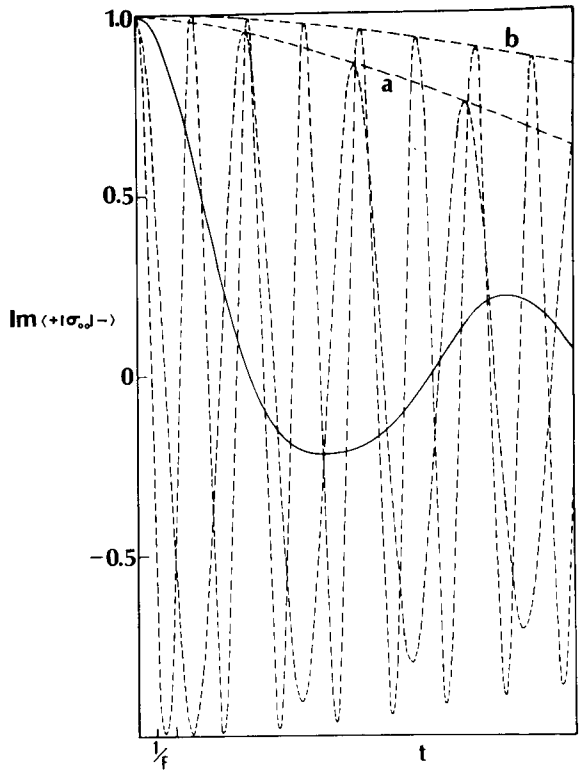

Figure 9.5.6 The imaginary part of $\langle +|\sigma_{00}|-\rangle$ as a function of time. The solid line denotes the free induction decay. The electromagnetic strengths in F units are (*a*) 1 and (*b*) 2. F is defined by $F = f^2/5$ and $f = 1000$.

APPENDIX A

In Chapter 9 we used the rotating wave approximation. We describe here the nature of this approximation and its advantages. We have to deal with an equation of the following form:

$$\frac{\partial}{\partial t}|\psi(t)\rangle = \hat{\mathcal{H}}|\psi(t)\rangle = -i\hat{\mathcal{H}}_S|\psi(t)\rangle - i\hat{\mathcal{H}}_{\text{int}}|\psi(t)\rangle - (i\hat{\mathcal{H}}_M + \hat{\Gamma})|\psi(t)\rangle \tag{9.A.1}$$

where $\hat{\mathcal{H}}_S$, $\hat{\mathcal{H}}_{\text{int}}$, $\hat{\mathcal{H}}_M$, and $\hat{\mathcal{H}}_{\text{ext}}$ are Hermitian matrices, whereas $\hat{\Gamma}$ is usually a real symmetric matrix. $\hat{\mathcal{H}}_{\text{int}}$ expresses the intramolecular interaction with the "thermal bath," the Hamiltonian of which is $\hat{\mathcal{H}}_M - i\hat{\Gamma}$. The interaction with the external excitation is

$$\hat{\mathcal{H}}_{\text{ext}}(t) = 2H\cos\omega t[|e\rangle\langle g| + |g\rangle\langle e|] \tag{9.A.2}$$

We can define a new Hamiltonian of interest, $\hat{\mathcal{H}}'_S$, in such a way that the energy difference between two states coupled by $\hat{\mathcal{H}}_{\text{ext}}$ is exactly equal to ω. As a consequence, the Hamiltonian $\hat{\mathcal{H}}$ can be partitioned as follows:

$$\hat{\mathcal{H}} = \hat{\mathcal{H}}'_0 + \hat{\mathcal{H}}'_1 \tag{9.A.3}$$

where

$$\hat{\mathcal{H}}'_1 = (\hat{\mathcal{H}}_S - \hat{\mathcal{H}}'_S) + \hat{\mathcal{H}}_{\text{int}} + \hat{\mathcal{H}}_{\text{ext}}(t) - i\hat{\Gamma} \tag{9.A.4}$$

and

$$\hat{\mathcal{H}}'_0 = \hat{\mathcal{H}}'_S + \hat{\mathcal{H}}_M \tag{9.A.5}$$

We can now make the following transformation:

$$|\tilde{\psi}(t)\rangle = \exp(i\hat{\mathcal{H}}'_0 t)|\psi(t)\rangle \tag{9.A.6}$$

By differentiating Eq. (9.A.6) we obtain

$$\frac{\partial}{\partial t}|\tilde{\psi}(t)\rangle = i\hat{\mathcal{H}}'_0|\tilde{\psi}\rangle + \exp(i\hat{\mathcal{H}}'_0 t)\frac{\partial}{\partial t}|\tilde{\psi}(t)\rangle \tag{9.A.7}$$

If Eq. 9.A.1 is replaced in Eq. 9.A.7, we have

$$\frac{\partial}{\partial t}|\tilde{\psi}(t)\rangle = i\hat{\mathcal{H}}'_0|\tilde{\psi}(t)\rangle - \exp(i\hat{\mathcal{H}}'_0 t)(\hat{\mathcal{H}}'_0 + \hat{\mathcal{H}}'_1)|\tilde{\psi}(t)\rangle \tag{9.A.8}$$

In the new reference framework the equation of motion becomes

$$\frac{\partial}{\partial t}|\tilde{\psi}(t)\rangle = \tilde{\hat{\mathcal{H}}}_1(t)|\tilde{\psi}(t)\rangle \tag{9.A.9}$$

where

$$\tilde{\hat{\mathcal{H}}}_1(t) = \exp(i\hat{\mathcal{H}}'_0 t)\hat{\mathcal{H}}_1\exp(-i\hat{\mathcal{H}}'_0 t) \tag{9.A.10}$$

In the new system of reference the time scale is determined by the greatest contribution to $\mathcal{H}_1$. We should also take into account the fact that the order of magnitude of $\mathcal{H}_0 - \mathcal{H}'_0$ is the same as that of Γ, for when $|\mathcal{H}_0 - \mathcal{H}'_0| \gg \Gamma$ the effect of the external excitation is negligible.

By expressing Eq. 9.A.2 in the form

$$\hat{\mathcal{H}}_{\text{ext}}(t) = H(e^{i\omega t} + e^{-i\omega t})[|e\rangle\langle g| + |g\rangle\langle e|] \tag{9.A.11}$$

and by using Eq. 9.A.11 in 9.A.10 we find that $\tilde{\hat{\mathcal{H}}}_1(t)$ may be expressed as follows:

$$\tilde{\hat{\mathcal{H}}}_1(t) = \overline{\tilde{\hat{\mathcal{H}}}_1(t)} + \hat{G}e^{2i\omega t} + \hat{G}^+e^{-2i\omega t}, \quad \hat{G} = |e\rangle\langle g| \tag{9.A.12}$$

If we assume that

$$|\hat{\mathcal{H}}_{\text{ext}}| \ll \omega \tag{9.A.13}$$

$$|\Gamma| \ll \omega \tag{9.A.14}$$

We can neglect the rapidly oscillating contributions to Eq. 9.A.12 (rotating

wave approximation). The advantage of using the interaction picture has been that of focusing our attention only on the interaction contribution to the time evolution of the wave function (Eq. 9.A.9). The rotating wave approximation, then, enables us to replace a time-dependent Hamiltonian with a time-independent one.

APPENDIX B

Let us write a matrix $\mathbf{A}$ in the following form:

$$\mathbf{A} = \mathbf{A}_0 + \mathbf{A}_1 \tag{9.B.1}$$

where $\mathbf{A}_0$ is the matrix consisting of the diagonal part of $\mathbf{A}$. Let us assume that the $\mathbf{A}_1$ is very much smaller than $\mathbf{A}_0$. Then the eigenvalue equation

$$\mathbf{A}|\pi\rangle = E_\pi|\pi\rangle \tag{9.B.2}$$

can be expanded in power series of the perturbation, $\mathbf{A}_1$, as follows:

$$\mathbf{A}_0|\pi_0\rangle = E_\pi^{(0)}|\pi_0\rangle \tag{9.B.3}$$

$$\mathbf{A}_1|\pi_0\rangle + \mathbf{A}_0|\pi_1\rangle = E_\pi^{(1)}|\pi_0\rangle + E_\pi^0|\pi_1\rangle \tag{9.B.3a}$$

$$\mathbf{A}_1|\pi_1\rangle + \mathbf{A}_0|\pi_2\rangle = E_\pi^{(2)}|\pi_0\rangle + E_\pi^{(1)}|\pi_1\rangle + E_\pi^0|\pi_2\rangle \tag{9.B.3b}$$

Let us consider the state $|\pi(\alpha)\rangle$ close to the unperturbed state $|\alpha\rangle$. By multiplying Eq. 9.B.3a on its left side by $\langle\alpha|$ we obtain

$$\langle\alpha|\mathbf{A}_1|\alpha\rangle + E_\alpha^{(0)}\langle\alpha|\pi_1(\alpha)\rangle = E_{\pi(\alpha)}^{(1)} + E_\alpha^{(0)}\langle\alpha|\pi_1(\alpha)\rangle \tag{9.B.4}$$

From the definition of $\mathbf{A}_1$ we have $E_{\pi(\alpha)}^1 = 0$.

If we multiply Eq. 9.B.3a by $\langle\alpha'|$, we can write

$$\langle\alpha'|\pi_1(\alpha)\rangle = \frac{1}{E_\alpha^0 - E_{\alpha'}^0}\langle\alpha'|\mathbf{A}_1|\alpha\rangle (E_{\alpha'}^0 \neq E_\alpha^0) \tag{9.B.5}$$

By multiplying Eq. 9.B.3b on the left by $\langle\alpha|$, we have

$$\langle\alpha|\mathbf{A}|\pi_1(\alpha)\rangle + E_\alpha^0\langle\alpha|\pi_2(\alpha)\rangle = E_{\pi(\alpha)}^{(2)} + E_{\pi(\alpha)}^{(1)}\langle\alpha|\pi_1(\alpha)\rangle + E_\alpha^0\langle\alpha|\pi_2(\alpha)\rangle \tag{9.B.6}$$

from which we obtain

$$E_{\pi(\alpha)}^{(2)} = \langle\alpha|\mathbf{A}|\pi_1(\alpha)\rangle = \sum_{\alpha'}\langle\alpha|\mathbf{A}|\alpha'\rangle\langle\alpha'|\pi_1(\alpha)\rangle \tag{9.B.7}$$

By using Eq. 9.B.5 we arrive at

$$E_{\pi(\alpha)}^{(2)} = \frac{\sum_{\alpha'}\langle\alpha|\mathbf{A}|\alpha'\rangle\langle\alpha'|\mathbf{A}|\alpha\rangle}{E_\alpha^0 - E_{\alpha'}^0}$$

which is the formula used to obtain the perturbation energies of Section 9.2.

APPENDIX C

Throughout Chapters 9 and 10, we often deal with non-Hermitian matrices. The eigenvalues of a non-Hermitian matrix can no longer be proved real. As a consequence, after solving the eigenvalue equation

$$\mathbf{A}|\pi\rangle = E_\pi|\pi\rangle \tag{9.C.1}$$

it is convenient to define the left eigenstates of $\mathbf{A}$ as follows:

$$\langle\tilde{\pi}|\mathbf{A} = \langle\tilde{\pi}|E_\pi \tag{9.C.2}$$

The left state $\langle\tilde{\pi}|$ is not the usual dual conjugate to the state $|\pi\rangle$. In fact, from Eq. (9.C.1) we have

$$\langle\pi|\mathbf{A}^+ = \langle\pi|E_\pi^* \tag{9.C.3}$$

The matrix $\mathbf{A}$ will be diagonalized by the similarity transformation

$$\mathbf{SAS}^{-1} = \mathbf{\Lambda} \tag{9.C.4}$$

where, of course,

$$\mathbf{S}^{-1} \neq \mathbf{S}^+ \tag{9.C.5}$$

As a consequence we can write the right and left eigenstates as follows:

$$|\pi\rangle = \sum_\alpha S_{\alpha\pi}^{-1}|\alpha\rangle \tag{9.C.6}$$

$$\langle\tilde{\pi}| = \sum_\alpha S_{\pi\alpha}\langle\alpha| \tag{9.C.7}$$

respectively. Equation 9.C.7 implies

$$\sum_\pi |\pi\rangle\langle\tilde{\pi}| = \mathbf{I} \tag{9.C.8}$$

where $\mathbf{I}$ is the identity operator. Equations 9.C.6 and 9.C.7 also imply

$$\langle\tilde{\pi}\,|\,\pi'\rangle = \delta_{\pi\pi'} \tag{9.C.9}$$

which explains why this basis set of vectors is denoted as biorthogonal.

We provide now an example of a biorthogonal basis set. Let us consider the following symmetrical complex matrix:

$$\mathbf{A} = \begin{pmatrix} x_1 & y \\ y & x_2 \end{pmatrix} \tag{9.C.10}$$

The two right eigenvectors are

$$|\pi_1\rangle = c|\alpha_1\rangle + s|\alpha_2\rangle \tag{9.C.11}$$

and

$$|\pi_2\rangle = -s|\alpha_1\rangle + c|\alpha_2\rangle \tag{9.C.11a}$$

where

$$c = \frac{1}{\sqrt{2}}\left(1 + \frac{1}{(1+t^2)^{1/2}}\right)^{1/2} \tag{9.C.12}$$

$$s = \frac{1}{\sqrt{2}}\left(1 - \frac{1}{(1+t^2)^{1/2}}\right)^{1/2} \tag{9.C.12a}$$

$$t = \frac{2y}{x_1 - x_2} \tag{9.C.13}$$

The corresponding left vectors are

$$\langle \tilde{\pi}_1| = \langle \alpha_1| c + \langle \alpha_2| s \tag{9.C.14}$$

$$\langle \tilde{\pi}_2| = -\langle \alpha_1| s + \langle \alpha_2| c \tag{9.C.15}$$

The eigenenergies are given by

$$E_1 = \tfrac{1}{2}[(x_1 + x_2) + (x_1 - x_2)(1+t^2)^{1/2}] \tag{9.C.16}$$

$$E_2 = \tfrac{1}{2}[(x_1 + x_2) + (x_1 - x_2)(1+t^2)^{1/2}] \tag{9.C.16a}$$

The eigenstates and the eigenvalues of the two-dimensional matrix of Section 9.2 have been evaluated by using Eqs. 9.C.11–9.C.16a.

APPENDIX D

It can be shown that Eq. 9.3.14a requires that the time evolution of the "operator" $\hat{y}$ be defined by

$$\frac{d}{dt}\hat{y} = \hat{\Gamma}^{+}\hat{y} \tag{9.D.1}$$

Let us take into account the simple case of the two-time correlation function $\langle y(t_1)y(t_2)\rangle$. According to the stochastic approach of Section 9.3, we have

$$\langle y(t_1)y(t_2)\rangle = \int dy_1\, dy_2\, y_1 P(y_2 t_2 \mid y_1 t_1) y_2 w_0(y_2) \tag{9.D.2}$$

By using Eq. 9.3.22 we have

$$\langle y(t_1)y(t_2)\rangle = \int y[e^{-\Gamma_y(t_1-t_2)} y w_0(y)]\, dy = \int w_0(y) y (e^{-\Gamma_{y^+}(t_1-t_2)} y)\, dy \tag{9.D.3}$$

This means that y can be regarded as a time-dependent operator $y(t)$ provided that Eq. (9.D.1) is applied. However, if we introduce the left eigenstate

$$\langle \tilde{p}_0 \mid y\rangle = 1 \tag{9.D.4}$$

and the right one [$w_0(y)$ real distribution]

$$\langle y \mid p_0\rangle = w_0(y) \tag{9.D.5}$$

we can write Eq. 9.D.3 as follows:

$$\langle y(t_1)y(t_2)\rangle = \langle p_0|\hat{y}e^{-\Gamma^{+}(t_1-t_2)}\hat{y}|\tilde{p}_0\rangle = \langle \tilde{p}_0|\hat{y}e^{-\Gamma(t_1-t_2)}\hat{y}|p_0\rangle \tag{9.D.6}$$

APPENDIX E

In this appendix we describe the standard derivation of the SLE theory by Kubo (1969b).

We start from the standard Liouville equation:

$$\frac{\partial}{\partial t}\rho = -i[\hat{\mathscr{H}}, \rho] \tag{9.E.1}$$

where the Hamiltonian operator $\mathscr{H}$ involves the whole universe. We make a semiclassical approximation, according to which we keep looking at the part of interest of our physical system, $\mathscr{H}_S$, as being quantum mechanical. The part of interest is assumed to undergo a fluctuating interaction, $V(x)$, depending on the stochastic variable $x(t)$. The stochastic process $x(t)$, furthermore, is assumed to obey the following diffusion equation:

$$\frac{\partial}{\partial t}P(\lambda, t) = \hat{\Gamma}_{\lambda}P(\lambda, t) \tag{9.E.2}$$

where λ is a collection of stochastic variables including x and $P(\lambda, t)$ is the probability of finding λ in a fixed state at time t. We can include in the collection of stochastic variables the statistical density matrix ρ itself.

We can obtain the equation of motion of the composite probability $P(\lambda, \rho, t)$ as follows:

$$\frac{\partial}{\partial t}P(\lambda, \rho, t) = \left\{-\frac{\delta}{\delta\rho}\frac{1}{i}[\hat{\mathscr{H}}(\lambda), \rho] - \Gamma_{\lambda}\right\}P(\lambda, \rho, t) \tag{9.E.3}$$

We can now define a new statistical density matrix σ as follows:

$$\sigma = \int \rho P(\lambda, \rho, t)\, d\rho \tag{9.E.4}$$

By differentiating Eq. 9.E.4 we obtain

$$\frac{\partial\sigma}{\partial t} = \int \rho \frac{\partial}{\partial t}P(\lambda, \rho, t)\, d\rho \tag{9.E.5}$$

If we substitute Eq. 9.E.3 in Eq. 9.E.5 we obtain

$$\frac{\partial\sigma}{\partial t} = -\int \rho \frac{\delta}{\delta\rho}\frac{1}{i}[\mathscr{H}, \rho]P(\lambda, \rho, t) - \int \rho\Gamma_{\lambda}P(\lambda, \rho, t)\, d\rho \tag{9.E.6}$$

The first term on the right side of Eq. 9.E.6 can be integrated by parts. If the integrated part is assumed to vanish at infinity we obtain

$$\frac{\partial \sigma}{\partial t} = -i[\hat{\mathcal{H}}(\lambda), \sigma] - \hat{\Gamma}_\lambda \sigma \tag{9.E.7}$$

In fact $\hat{\Gamma}_\lambda$ acts only on the variable λ. In the text we denote $\hat{\mathcal{H}}(\lambda)$ as $\hat{\mathcal{H}}(\hat{\lambda})$ in order to emphasize that after relating $\hat{\Gamma}_\lambda$ to its eigenstates, it is convenient to regard λ as being an operator in this space.

Equation 9.E.7 is the main result of Kubo theory in the semiclassical case. It is worth noting that this result is based on Eq. 9.E.3, which may be given a hydrodynamic interpretation. In fact, if we are dealing with a classical fluid in the presence of a continuous sink the standard equation of continuity for the time evolution of fluid density $\rho(r, t)$ has to be supplemented by

$$\frac{\partial \rho}{\partial t} = -\operatorname{div} v\rho - \Gamma\rho \tag{9.E.8}$$

where the second term on the right side of Eq. 9.E.8 is a correction to the standard equation expressing the flow of fluid resulting from the presence of the sink. Of course the contribution $-\delta/\delta\rho(1/i)[\hat{\mathcal{H}}(\lambda), \rho]P(\lambda, \rho, t)$ in Eq. 9.E.3 corresponds to $-\operatorname{div} v\rho$, which is the nondissipative contribution to the time evolution of $\rho(r, t)$. A generalized equation of continuity of the same kind as Eq. 9.E.8 plays an important role in the next chapter (Section 10.7).

APPENDIX F

The SLE can be expressed by the following equation:

$$\frac{\partial}{\partial t}\sigma = -i[\hat{\mathcal{H}}_S, \sigma] - i[\hat{\mathcal{H}}_{ext}(t), \sigma] - i[\hat{\mathcal{H}}_1, \sigma] - \hat{\Gamma}_y \sigma \tag{9.F.1}$$

where $\hat{\Gamma}_y$ is the diffusion operator of the stochastic process affecting the system of interest. We can make the general assumption that

$$\hat{\mathcal{H}}_S = \sum_\alpha |\alpha\rangle \epsilon_\alpha \langle\alpha| \tag{9.F.2}$$

$$\hat{\mathcal{H}}_1 = \sum_{\alpha\alpha'} |\alpha\rangle\langle\alpha'| T_{\alpha\alpha'}(y) \tag{9.F.3}$$

$$\hat{\mathcal{H}}_{ext}(t) = 2\boldsymbol{\mu} \cdot \mathbf{H} \cos \omega t \tag{9.F.4}$$

where $\boldsymbol{\mu}$ is the dipole operator of the quantum system under study. The operator $\hat{\Gamma}_y$ can be expressed by its eigenvalues E_n and eigenvectors $|p_n\rangle$. Over this basis set the density matrix σ can be expressed as follows:

$$\sigma = \sum_n \sigma_n |p_n\rangle \tag{9.F.5}$$

The statistical matrix σ_n is independent of the stochastic variable. The contribution σ_0 can be regarded as the part of interest of our physical system. The contributions $\sigma_n (n \neq 0)$ can be regarded as the counterpart of the "virtual" state of Section 9.2.

By multiplying Eq. 9.F.1 on the left by $\langle \tilde{p}_n|$ (for the definition of left state see Appendix C) we obtain

$$\frac{\partial \sigma_n}{\partial t} = -i[\hat{\mathcal{H}}_S, \sigma_n] - i[\hat{\mathcal{H}}_{ext}(t), \sigma_n] - \sum_{\alpha\alpha'} \langle \tilde{p}_n | T_{\alpha\alpha'}(y) | p_{n'} \rangle [|\alpha\rangle\langle\alpha'|, \sigma_{n'}] - E_n \sigma_n \tag{9.F.6}$$

We can see that through the third term on the right side of Eq. 9.F.6 the statistical density σ_0 is coupled with the "unstable" contributions $\sigma_n (n \neq 0)$.

APPENDIX G

We recall the definition of quantum mechanical statistical density matrix. If we have a statistical ensemble of N identical systems the average value of an observable $\hat{A}$ is

$$\langle \hat{A} \rangle = \frac{\sum_i^N p_i \langle \psi(i) | \hat{A} | \psi(i) \rangle}{N} \tag{9.G.1}$$

where i denotes a generic system, and $|\psi(i)\rangle$ is the quantum mechanical state of such a system. The previous average value can be put in the following form:

$$\langle \hat{A} \rangle = \operatorname{Tr} \rho \hat{A} \tag{9.G.2}$$

provided that the statistical density matrix ρ be defined as follows:

$$\langle \alpha | \rho | \alpha' \rangle = \frac{\sum_{i=1}^N p_i \langle \psi(i) | \alpha' \rangle \langle \alpha | \psi(i) \rangle}{N} \tag{9.G.3}$$

where $\{|\alpha\rangle\}$ is a basis set of vectors for the system under study.

Let us assume that the time evolution of the wave function is given by

$$i \frac{\partial}{\partial t} |\psi(t)\rangle = \hat{\mathcal{H}} |\psi(t)\rangle \tag{9.G.4}$$

where $\hat{\mathcal{H}}$ is not necessarily a Hermitian operator. It is quite important to avoid such a mathematical constraint for in Section 9.2 we introduce an effective Hamiltonian operator of non-Hermitian kind. As a consequence the equation conjugate to Eq. 9.G.4 is

$$\frac{\partial}{\partial t} \langle \psi(t)| = \langle \psi(t) | \hat{\mathcal{H}}^+ \tag{9.G.5}$$

Then by differentiating Eq. 9.G.3 and replacing in the resulting expression both Eqs. 9.G.4 and 9.G.5 we obtain

$$\frac{\partial \rho}{\partial t} = \hat{\mathscr{H}}^{\times}\rho = \hat{\mathscr{H}}\rho - \rho\hat{\mathscr{H}}^{+} \tag{9.G.6}$$

This is a generalization of the standard quantum mechanical Liouville equation (Messiah, 1964).

APPENDIX H

As shown in Section 9.3, the SLE is based on the evolution of the time evolution of the stochastic variable y by the equation

$$\frac{d\hat{y}}{dt} = \hat{\Gamma}_{y}^{+}\hat{y} \tag{9.H.1}$$

This is a first example of a dynamic equation for a variable where the dynamic operator is not anti-Hermitian as, for example, $\hat{\mathscr{L}} = i\hat{L}$, when $\hat{L}$ is the total Liouvillian. By using the SLE it is then possible to show that any observable of interest obeys the same kind of equation. If we use, for instance, Eq. 9.4.3 for evaluating the time evolution of $\hat{m} = \hat{\mu}|p_0\rangle$, where $\hat{\mu}$ is given by Eq. 9.4.11, we obtain

$$\frac{\partial \hat{m}}{\partial t} = i[\hat{\mathscr{H}}_S, \hat{m}] + i[\hat{\mathscr{H}}_{\text{ext}}, \hat{m}] + i[\hat{\mathscr{H}}, \hat{m}] - \hat{\Gamma}^{+}\hat{m} \tag{9.H.2}$$

Equation 9.H.2 is a result of the following requirement:

$$\text{Tr}_{\{S\}}\, \sigma_0(t)\hat{\mu}(0) = \text{Tr}_{\{S\}}\, \sigma_0(0)\langle\tilde{p}_0|e^{\hat{\Lambda}t}\hat{\mu}(0)|p_0\rangle \tag{9.H.3}$$

where $\hat{\Lambda}$ is the superoperator to be determined. If we use the invariance of the trace for commutation, from Eqs. 9.H.3 and 9.4.3 we obtain Eq. 9.H.2. When $\Gamma^{+} = \Gamma$, Eq. 9.H.2 is of the same kind as Eq. 9.4.3.

The evolution of the correlation function $\langle\hat{\mu}\hat{\mu}(t)\rangle$ has to be made at the thermodynamic equilibrium. As a consequence

$$\langle\hat{\mu}\hat{\mu}(t)\rangle = \text{Tr}_{\{S\}}\langle\tilde{p}_0|\hat{\mu}(e^{\hat{\Lambda}t}\hat{\mu}|g\rangle\langle g|)|p_0\rangle \tag{9.H.4}$$

From Eq. 9.H.4 we obtain Eq. 9.4.12.

REFERENCES

Abbott, R. J. and Oxtoby, D. W., *J. Chem. Phys.* **72**, 3972 (1980).

Abragam, A. *The Principles of Nuclear Magnetism*, Oxford at Clarendon Press, Oxford (1961).

Argyres, P. N. and Kelley, P. L., *Phys. Rev.* **134**, A98 (1964).

Bixon, M. and Jortner, J., *J. Chem. Phys.* **48**, 715 (1968).

Evans, M. W., Ferrario, M., and Grigolini, P., *Chem. Phys. Lett.* **71**, 139 (1980).

Fox, R. F., *Phys. Rep.* **48**, 179 (1978).

Freed, J. H., *J. Chem. Phys.* **41**, 7 (1964).

Freed, J. H., in *Electron Spin Relaxation in Liquids*, L. T. Muus and P. W. Atkins, Eds., Plenum Press, New York, p. 165 (1972).

Freed, J. H., Bruno, G. V., and Polnaszek, C., *J. Chem. Phys.* **55**, 5270 (1971).

Freed, K. F., *Topics Curr. Chem.* **31**, 105 (1972).

Freed, K. F., *Chem. Phys. Lett.* **42**. 600 (1976).

Gelbart, W. M., Heller, D. F., and Elert, M. L., *Chem. Phys.* **7**, 116 (1975).

Goldberger, M. L. and Watson, K. M., *Collision Theory*, Wiley, New York (1964).

Grigolini, P., *Mol. Phys.* **31**, 1717 (1976).

Grigolini, P., *Chem. Phys. Lett.* **47**, 483 (1977).

Grigolini, P., *Chem. Phys.* **38**, 389 (1979).

Grigolini, P. and Lami, A., *Chem. Phys.* **30**, 61 (1978).

de Groot, S. R. and Mazur, P., *Non-Equilibrium Thermodynamics*, North-Holland, Amsterdam, p. 50 (1962).

Jortner, J. and Mukamel, S., *Proceeding of the First International Congress on Quantum Chemistry, Menton, France*, R. Daudel and B. Pullman, Eds., D. Reidel, Amsterdam, p. 145 (1974).

Kubo, R., *Rep. Prog. Phys.* **29**, 255 (1966).

Kubo, R., in *Stochastic Processes in Chemical Physics*, K. E. Shuler, Ed., Wiley-Interscience, New York (1969a).

Kubo, R., *J. Phys. Soc. (Jap.) Suppl.* **26**, 1 (1969b).

Kushick, J. N. and Rice, S. A., *Chem. Phys. Lett.* **52**, 208 (1977).

Laubereau, A. and Kaiser, W., *Rev. Mod. Phys.* **50**, 607 (1978).

Messiah, A., *Mécanique Quantique*, Dunod, Paris (1964).

Mori, H., *Prog. Theor. Phys.* **33**, 423 (1965a).

Mori, H., *Prog. Theor. Phys.* **34**, 399. (1965b).

Morokuma, K. and Freed, K. F., *J. Chem. Phys.* **61**, 4392 (1974).

Muus, L. T., in *Electron Spin Relaxation in Liquids*, L. T. Muus and P. W. Atkins, Eds., Plenum Press, New York, p. 1 (1972).

Nordholm, S. and Zwanzig, R., *J. Stat. Phys.* **13**, 347 (1975).

Pietenpol, J. L., *Phys. Rev.* **162**, 1301 (1967).

Platz, O., in *Electron Spin Relaxation in Liquids*, L. T. Muus and P. W. Atkins, Eds., Plenum Press, New York, p. 89 (1972).

Rhodes, W., *Chem. Phys.* **4**, 259 (1974).

Rhodes, W., Chapter 5, in *Radiationless Transitions*, S. H. Lin, Ed., Academic Press, New York, (1980).

Robinson, G. W., in *Excited States*, Vol. 1, E. C. Lim, Ed., p. 1 (1974).

Schieve, W. C., *Lect. Notes Phys.* **28**, 1 (1974).

Weisskopf, P. and Wigner, E. P., *Z. Phys.* **63**, 54 (1930).

Zubarev, D. N., *Nonequilibrium Statistical Thermodynamics*, Consultants Bureau, New York, London (1974).

Zwanzig, R., *J. Chem. Phys.* **33**, 1338 (1960).

Zwanzig, R., in *Lectures in Theoretical Physics*, Vol. III, W. E. Brittin, B. W. Downs, and J. Downs Eds., Interscience, New York, pp. 106–141 (1961).

10

Equations of Motion: Mori Theory and Simple Models of Relaxation Processes

LIST OF SYMBOLS

$\mathbf{A}$	A general column vector of variables
Δ^2_{k+1}	The intensity of the coupling between the kth state of the Mori chain and the $(k+1)$th one
$\mathbf{F}(t)$	Multidimensional fluctuating force (Mori theory)
$\tilde{\mathbf{F}}(t)$	Multidimensional stochastic force within the context of the stochastic approach
$\|f_0\rangle$	Monodimensional variable of interest within the context of the Mori theory in a quantumlike form
$\|f_k\rangle$	The kth state of the Mori basis set constructed by projection repeated k times
$\langle\tilde{f}_k\|$	Left state f the generalized Mori theory
$\mathbf{f}_k$	The multidimensional generalization of f_k; $\mathbf{f}_0$ is identified with $\mathbf{A}$ in Eq. 10.4.3
$\hat{\mathscr{L}}_0$	The dynamical operator. When dealing with the problem of intramolecular decay $\hat{\mathscr{L}}_0 = -i\hat{\mathscr{H}}$. When dealing with classical molecular dynamics $\hat{\mathscr{L}}_0 = i\hat{L}$
λ_k	A purely imaginary scalar within the context of the standard Mori theory (Section 2). A complex number also containing a real part within the context of the generalized Mori theory (Section 3)
$\boldsymbol{\mu}$	Molecular dipole moment
$\hat{P}_k$	The kth projection operator of the Mori theory
$\mathbf{Q}$	The matrix of the diffusion coefficients of the components of the stochastic force $\tilde{\mathbf{F}}$. This symbol also denotes the multidimensional observable of Section 10
$\Phi_k(t)$	kth scalar correlation function (corresponding to the variable f_k). $\tilde{\Phi}_k(t)$ is the correlation function corresponding to the left variable $\tilde{f}_k$
$\hat{\Phi}_k(z)$	Scalar correlation function (kth order) in z space, $z = i\omega$
$\boldsymbol{\Phi}_k(t)$	Multidimensional extension of $\Phi_k(t)$, $\tilde{\boldsymbol{\Phi}}_k(t)$ is the corresponding left correlation function
$\mathbf{R}$	Part of the physical world that does not interact directly with $\mathbf{S}$
$\mathbf{S}$	Part of the physical world involving $\mathbf{A}$
u	Monodimensional (scalar) equivalent of $\mathbf{A}$ in Kubo's stochastic oscillator
ω	Equivalent of $\boldsymbol{\Omega}$ in Kubo's stochastic oscillator

ω Molecular angular velocity
Ω Variable linking **M** with **R**. The same symbol also denotes Mori's resonance operator (eq. 10.6.16)

10.1 INTRODUCTION

In Chapter 9 we described the advantages of the "reduced" model theory (RMT), the main idea of which consists in building up "reduced" thermal baths "equivalent" to the real ones. It is possible to reduce the degrees of freedom of the system under study from an overwhelming number. This would be of special relevance in the field of molecular dynamics, where the number of particles to be taken into account should be Avogadro's number. Approaches of the same kind have been developed by Adelman and co-workers (M. Berkowitz et al., 1980; Adelman, 1979) and by Ciccotti and Ryckaert (1980). In accordance with the theory developed by Ferrario and Grigolini (1979a, b), in Section 10.2 we show that Mori theory (1965b) implies rigorously our RMT.

In the field of generalized Brownian motion, however, a simple model such as the two-friction itinerant oscillator studied in earlier chapters requires the use of non-Hermitian Liouvillians. This is described in Section 10.3. A further extension of Mori theory is made in Section 10.4, where the non-Hermitian multidimensional case is dealt with. The latter is useful for large molecules, where interactions of rotation with translations such as those studied in Chapter 5 can take place. The coefficients of the continued fraction expansion are now nondiagonal matrices.

The approach developed in Sections 10.3–10.5 is useful for evaluating the Laplace transform of the correlation function

$$\mathbf{C}_{\mu}(t) \equiv \langle \mu \cdot \mu(t) \rangle \tag{10.1.1}$$

for a variable μ satisfying an equation of motion such as

$$\frac{d}{dt}\mu = \omega(t) \times \mu(t) \tag{10.1.2}$$

where $\omega(t)$ is defined rigorously by the Langevin equation. This is a typical problem in the field of magnetic resonances (Muus and Atkins, 1972) and of dielectric relaxation (Böttcher and Bordewijk, 1978). Section 10.4 provides a general solution. However, for simplicity in Section 10.5 we focus our attention on the simple case where μ is a monodimensional variable. This does not result in loss of generality.

In Section 9.1 we mentioned that the Gaussian and the Markovian approximations are interdependent. In the classical regime no rigorous evidence is available, though Kubo (1966) has argued that when the mass of the Brownian particle, M, is very much greater than the mass m of the particles of the corresponding thermal bath, then both the Markovian and

the Gaussian approximations are acceptable. As is well known (Fox, 1978), these imply a canonical equilibrium distribution for the velocities of Brownian particles, a Maxwellian statistics. Mori et al., (1974) have shown that as the ratio $\delta = m/M$ tends to 1, nonlinear corrections contribute to the corresponding Langevin equation. Since nonlinearity can result in non-Gaussianicity, this might have provided rigorous evidence for the statement of Kubo, if Mori et al. had not based their theory on the mathematical constraint that the equilibrium distribution is Gaussian.† We do not yet have available a theoretical approach which indicates the extent of the deviation from the Gaussian behavior as a function of the interaction between Brownian particle and thermal bath. Nor do we have a rigorous demonstration that Gaussianicity is a natural consequence of the physical condition expressed by $\delta \ll 1$. Only in the quantum mechanical case is it possible to show that the canonical distribution is a consequence of the Markovian approximation (Appendix G).

However, the intuitive discussion by Kubo and recent computational results (Evans et al., 1980b) support the point of view that when the Markovian assumption is not justifiable, neither is the Gaussian. One of the major aims of Sections 10.6–10.8 is to develop a theoretical approach for dealing with non-Markovian, non-Gaussian relaxation processes.

In this chapter we also describe an approach to the study of excitation–relaxation processes more general than that of the preceding chapter. This allows us to study the problem of relaxation in the presence of external excitations (Section 10.9) in a quite general fashion and to evaluate the emission spectra without Markovian or linear response approximations (Section 10.10).

Chapter 10 is theoretically suitable for a wide range of applications in the field of molecular physics, and especially in that of fast relaxation processes such as those usually met in molecular dynamics. However, the powerful approach here described meets with a serious limitation when used in the intriguing problem of long time tails (Section 10.11).

10.2 QUANTUMLIKE APPROACH TO MORI THEORY

In Chapter 1 we derived the generalized Langevin equation of Mori. This was rederived in a slightly different context in Section 9.1.

In this section we construct it again in a form which includes the main results of the preceding chapter. We study a general equation of motion of the following form:

$$\frac{d}{dt}|f_0(t)\rangle = \hat{\mathcal{L}}_0|f_0(t)\rangle \tag{10.2.1}$$

†Their approach, however, results in a dynamical non-Gaussian behavior (P. Marin, and P. Grigolini, 1982).

Equation 10.2.1 could be, for example, the equation of motion of the state $|e\rangle$ of the model of intramolecular relaxation described in the preceding chapter. In this case we would have

$$|f_0(0)\rangle = |e\rangle \tag{10.2.2}$$

$$\hat{\mathcal{L}}_0 = -i\hat{\mathcal{H}} \tag{10.2.3}$$

where $\hat{\mathcal{H}}$ is a suitable intramolecular Hamiltonian operator, such as that of Eq. 9.2.1.

We stress that Eq. 10.2.1 could also be interpreted as the equation of motion of a monodimensional variable. It is, in fact, possible to define the scalar product, $\langle\alpha \mid \beta\rangle$, of the arbitrary operators α and β as follows (Berne and Harp, 1970):

$$(\beta, \alpha^+) = \langle\alpha \mid \beta\rangle = \int d\Gamma \alpha^+(\Gamma)\beta(\Gamma) f_{eq}(\Gamma) \tag{10.2.4}$$

$$(\beta, \alpha^+) = \langle\alpha \mid \beta\rangle = \mathrm{Tr}\ \alpha^+\beta \tag{10.2.5}$$

according to whether we are dealing with classical (Eq. 10.2.4) or quantum mechanics (Eq. 10.2.5). As far as the quantum mechanical case is concerned, Appendix G affords a further example of scalar product. The definition of a scalar product depends, in fact, on a physical problem under discussion.

Classically,

$$\hat{\mathcal{L}}_0|\alpha\rangle = \{\alpha(\Gamma), \mathcal{H}\} \tag{10.2.6}$$

where $\{\cdots\}$ denotes the Poisson bracket, while in the quantum mechanical case we have

$$\hat{\mathcal{L}}_0|\alpha\rangle = -i[\alpha, \hat{\mathcal{H}}] \tag{10.2.7}$$

where $[\cdots]$ denotes the commutator.

For intramolecular relaxation, $|f_0\rangle$ could be defined as follows

$$|f_0\rangle = |e\rangle \tag{10.2.7a}$$

When dealing with the main topic of this book, classical molecular dynamics, the "state" $|f_0\rangle$ denotes a classical variable, for example, the velocity of a Brownian particle. The reason for using a quantumlike formalism is to gain physical insight into Mori theory by using the formal similarity between the equation of motion of a classical variable and that of the quantum mechanical state $|e\rangle$ studied in the preceding chapter. The time evolution of the "state" $|e\rangle$ is given by

$$|f_0(t)\rangle = e^{-i\hat{\mathcal{H}}t}|e\rangle \tag{10.2.8}$$

In the case of radiationless decay (Chapter 9) Eq. 10.2.8 is equivalent to assuming that the molecular system is found at initial time $t = 0$ in the excited state $|e\rangle$. As shown in Chapter 9, this is not a realistic assumption

when dealing with excitation–relaxation processes. Equation 10.2.8 also implies that the manifold $\{|m\rangle\}$ of Fig. 9.2.1 is not populated at $t = 0$. In other words, it is assumed that the thermal bath is found in that condition in which the system finds itself when the absolute temperature T is zero. These intramolecular models expose the main limitations of the standard Mori approach. These are removed using the techniques illustrated in this part of the book.

To describe radiationless decay in molecules a non-Hermitian Hamiltonian or, in other words, a non-anti-Hermitian dynamic operator $\hat{\mathcal{L}}_0$ can be very useful. The ϵ-continuum (Chapter 9) of the model of Fig. 9.2.1 can be eliminated provided that a non-Hermitian Hamiltonian is introduced. However, firstly we consider the Hermitian type.

We define the projection operator $\hat{P}_0$ introduced by Mori as

$$\hat{P}_0 = \frac{|f_0\rangle\langle f_0|}{\langle f_0 \mid f_0\rangle} \tag{10.2.9}$$

Following Mori we can separate $|f_0(t)\rangle$ into its projected and vertical components (Chapter 1) with respect to the $|f_0\rangle$ axis:

$$\begin{aligned} |f_0(t)\rangle &= \hat{P}_0|f_0(t)\rangle + (\hat{1} - \hat{P}_0)|f_0(t)\rangle \\ &= \Phi_0(t)|f_0\rangle + |f_0'(t)\rangle \end{aligned} \tag{10.2.10}$$

where

$$\Phi_0(t) = \frac{\langle f_0|f_0(t)\rangle}{\langle f_0 \mid f_0\rangle} \tag{10.2.11}$$

and

$$|f_0'(t)\rangle = (\hat{1} - \hat{P}_0)|f_0(t)\rangle \tag{10.2.11a}$$

Differentiating with respect to time and using Eq. 10.2.1,

$$\frac{d}{dt}|f_0'(t)\rangle = (\hat{1} - \hat{P}_0)\hat{\mathcal{L}}_0|f_0(t)\rangle \tag{10.2.12}$$

We apply Eq. 10.2.10, so that Eq. 10.2.12 becomes

$$\frac{d}{dt}|f_0'(t)\rangle = \Phi_0(t)(\hat{1} - \hat{P}_0)\hat{\mathcal{L}}_0|f_0\rangle + (\hat{1} - \hat{P}_0)\hat{\mathcal{L}}_0|f_0'(t)\rangle \tag{10.2.13}$$

It is convenient to define

$$\hat{\mathcal{L}}_1 = (\hat{1} - \hat{P}_0)\hat{\mathcal{L}}_0 \tag{10.2.14}$$

$$|f_1\rangle = \hat{\mathcal{L}}_1|f_0\rangle \tag{10.2.15}$$

$$|f_1(t)\rangle = e^{\hat{\mathcal{L}}_1 t}\hat{\mathcal{L}}_1|f_0\rangle = \hat{\mathcal{L}}_1 e^{\hat{\mathcal{L}}_1 t}|f_0\rangle \tag{10.2.16}$$

so that Eq. 10.2.13 can be written as follows:

$$\frac{d}{dt}|f_0'(t)\rangle = \hat{\mathcal{L}}_1|f_0'(t)\rangle + \Phi_0(t)|f_1\rangle \tag{10.2.17}$$

By using Eq. 10.2.16 the solution to Eq. 10.2.17 emerges as

$$|f_0'(t)\rangle = \int_0^t ds\ \Phi_0(s)|f_1(t-s)\rangle \tag{10.2.18}$$

Using Eq. 10.2.18 in Eq. 10.2.10 we have

$$|f_0(t)\rangle = \Phi_0(t)|f_0\rangle + \int_0^t ds\ \Phi_0(s)|f_1(t-s)\rangle \tag{10.2.19}$$

Equation 10.2.19 can easily be generalized provided that we define

$$|f_k\rangle = \hat{\mathscr{L}}_k|f_{k-1}\rangle \tag{10.2.20}$$

$$|f_k(t)\rangle = \exp(\hat{\mathscr{L}}_k t)\hat{\mathscr{L}}_k|f_{k-1}\rangle \tag{10.2.21}$$

$$\hat{\mathscr{L}}_k = (\hat{1} - \hat{P}_{k-1})\hat{\mathscr{L}}_{k-1} \tag{10.2.22}$$

Then we obtain

$$|f_k(t)\rangle = \Phi_k(t)|f_k\rangle + \int_0^t ds\ \Phi_k(s)|f_{k+1}(t-s)\rangle \tag{10.2.23}$$

where

$$\Phi_k(t) = \frac{\langle f_k|f_k(t)\rangle}{\langle f_k \mid f_k\rangle} \tag{10.2.24}$$

Now note that

$$\langle f_k \mid f_{k'}\rangle = 0 \qquad \text{for } k \neq k' \tag{10.2.25}$$

In fact, $|f_1\rangle$ is orthogonal to $|f_0\rangle$ by definition in that from Eqs. 10.2.14 and 10.2.15 we have

$$|f_1\rangle = (\hat{1} - \hat{P}_0)\hat{\mathscr{L}}_0|f_0\rangle \tag{10.2.26}$$

The orthogonality between $|f_1\rangle$ and $|f_0\rangle$ implies that $\hat{P}_1$ and $\hat{P}_0$ are commuting operators. Then the state $|f_2\rangle$, which is orthogonal to $|f_1\rangle$ by construction, in that from Eqs. 10.2.20 and 10.2.22 we have

$$|f_2\rangle = (\hat{1} - \hat{P}_1)\hat{\mathscr{L}}_1|f_1\rangle \tag{10.2.27}$$

is orthogonal also to the state $|f_0\rangle$, for

$$|f_2\rangle = (\hat{1} - \hat{P}_1)(\hat{1} - \hat{P}_0)\hat{\mathscr{L}}_0|f_1\rangle = (\hat{1} - \hat{P}_0)(1 - \hat{P}_1)\hat{\mathscr{L}}_0|f_1\rangle \tag{10.2.28}$$

We thus see that $\hat{P}_0$, $\hat{P}_1$, and $\hat{P}_2$ are operators that commute. It is then possible to show that $|f_3\rangle$ is orthogonal to $|f_0\rangle$ and $|f_1\rangle$, as well as to $|f_2\rangle$, and so on.

It is then evident that Eq. 10.2.25 is equivalent to

$$\hat{P}_k\hat{P}_{k'} = \hat{P}_{k'}\hat{P}_k \qquad \text{for any } k \tag{10.2.29}$$

From Eq. 10.2.21 we have

$$\frac{d}{dt}|f_k(t)\rangle = \hat{\mathscr{L}}_k|f_k(t)\rangle \tag{10.2.30}$$

By applying the property

$$\hat{1} = (\hat{1} - \hat{P}_k) + \hat{P}_k \tag{10.2.31}$$

to Eq. 10.2.30 we have

$$\begin{aligned}\frac{d}{dt}|f_k(t)\rangle &= \hat{\mathscr{L}}_k \exp(\hat{\mathscr{L}}_k t)|f_k\rangle = \exp(\hat{\mathscr{L}}_k t)\hat{\mathscr{L}}_k|f_k\rangle \\ &= \exp(\hat{\mathscr{L}}_k t)\hat{P}_k\hat{\mathscr{L}}_k|f_k\rangle + \exp(\hat{\mathscr{L}}_k t)(\hat{1} - \hat{P}_k)\hat{\mathscr{L}}_k|f_k\rangle \\ &= \lambda_k|f_k(t)\rangle + \exp(\hat{\mathscr{L}}_k t)|f_{k+1}\rangle\end{aligned} \tag{10.2.32}$$

where

$$\lambda_k = \frac{\langle f_k|\hat{\mathscr{L}}_k|f_k\rangle}{\langle f_k \mid f_k\rangle} \tag{10.2.33}$$

Note that the parameters λ_k are purely imaginary numbers due to the anti-Hermitian nature of $\hat{\mathscr{L}}_k$. By substituting again Eq. 10.2.31 in the preceding equation, we have

$$\frac{d}{dt}|f_k(t)\rangle = \lambda_k|f_k(t)\rangle + \frac{|f_k\rangle\langle f_k|\exp(\hat{\mathscr{L}}_k t)|f_{k+1}\rangle}{\langle f_k \mid f_k\rangle} + (\hat{1} - \hat{P}_k)\exp(\hat{\mathscr{L}}_k t)|f_{k+1}\rangle \tag{10.2.34}$$

The operator $\hat{\mathscr{L}}$ is anti-Hermitian and any projection operator $\hat{P}_k$ is Hermitian over the space under study. In consequence, Eq. 10.2.34 can be written as follows:

$$\frac{d}{dt}|f_k(t)\rangle = \lambda_k|f_k(t)\rangle + |f_k\rangle\langle f_k(-t) \mid f_{k+1}\rangle\langle f_k \mid f_k\rangle^{-1} + (\hat{1} - \hat{P}_k)\exp(\hat{\mathscr{L}}_k t)|f_{k+1}\rangle \tag{10.2.35}$$

The anti-Hermiticity of $\hat{\mathscr{L}}_0$ also implies

$$\Phi_k(-t) = \Phi_k(t)^* \tag{10.2.36}$$

From Eq. 10.2.23 then we obtain

$$\begin{aligned}|f_k(-t)\rangle &= \Phi_k(-t)|f_k\rangle + \int_0^{-t} ds\ \Phi_k(s)|f_{k+1}(-t-s)\rangle \\ &= \Phi_k^*(t)|f_k\rangle - \int_0^t ds\ \Phi_k(-s)|f_{k+1}(s-t)\rangle \\ &= \Phi_k^*(t)|f_k\rangle - \int_0^t ds\ \Phi_k^*(s)|f_{k+1}(s-t)\rangle\end{aligned} \tag{10.2.37}$$

The dual vector conjugate to $|f_k(-t)\rangle$ is

$$\langle f_k(-t)| = \langle f_k|\Phi_k(t) - \int_0^t ds\ \Phi_k(s)\langle f_{k+1}(s-t)| \tag{10.2.38}$$

From Eqs. 10.2.38 and 10.2.35, we obtain

$$\frac{d}{dt}|f_k(t)\rangle = \lambda_k|f_k(t)\rangle - |f_k\rangle\int_0^t ds\ \Phi_k(s)\langle f_{k+1}(s-t)|f_{k+1}\rangle\langle f_k \mid f_k\rangle^{-1} + (\hat{1}-\hat{P}_k)\exp(\hat{\mathscr{L}}_k t)|f_{k+1}\rangle \tag{10.2.39}$$

Using the definition of Eq. 10.2.24 and the property of Eq. 10.2.36 this can be written as

$$\frac{d}{dt}|f_k(t)\rangle = \lambda_k|f_k(t)\rangle - |f_k\rangle\int_0^t ds\ \Phi_k(s)\Delta_{k+1}^2\Phi_{k+1}(t-s) + (\hat{1}-\hat{P}_k)e^{\hat{\mathscr{L}}_k t}|f_{k+1}\rangle \tag{10.2.40}$$

where

$$\Delta_{k+1}^2 = \frac{\langle f_{k+1} \mid f_{k+1}\rangle}{\langle f_k \mid f_k\rangle} \tag{10.2.41}$$

By multiplying Eq. 10.2.40 on the left by $\langle f_k \mid f_k\rangle^{-1}\langle f_k|$, we obtain

$$\frac{d}{dt}\Phi_k(t) = \lambda_k\Phi_k(t) - \int_0^t ds\ \Phi_k(S)\Delta_{k+1}^2\Phi_{k+1}(t-s) \tag{10.2.42}$$

which on Laplace transformation becomes

$$\hat{\Phi}_k(z) = (z - \lambda_k + \Delta_{k+1}^2\hat{\Phi}_{k+1}(z))^{-1} \tag{10.2.43}$$

As a consequence the "memory kernel" of the generalized Langevin equation is expressed as follows (cf. Chapter 1):

$$\Delta_1^2\hat{\Phi}_1(z) = \cfrac{\Delta_1^2}{z-\lambda_1+\cfrac{\Delta_2^2}{z-\lambda_2+\cfrac{\Delta_3^2}{z-\lambda_3+\ddots\cfrac{\Delta_n^2}{z-\lambda_n+\Delta_{n+1}^2\hat{\Phi}_{n+1}(z)}}}} \tag{10.2.44}$$

From a practical point of view we have to find sound criteria for truncating this continued fraction expansion as in Chapter 4. If the excited state $|e\rangle$ is coupled with the dissipation continuum via a Lorentzian interaction, then this is equivalent to truncating to first order. The "memory kernels" introduced in Section 9.2.1, Φ_{intra} and Φ_1 are, in fact, related by

$$\Phi_{\text{intra}}(t) = -\langle e|\hat{\mathscr{H}}(1-\hat{P}_0)\hat{\mathscr{H}}|e\rangle\Phi_1(t) \tag{10.2.45}$$

As described in Section 9.2, the right side of Eq. 10.2.45 decays exponentially with damping γ. As a consequence, the Lorentzian model of Section 9.2 results in ($\lambda_1 = i\epsilon_e$)

$$\hat{\Phi}_1(z) = (z - \lambda_1 + \gamma)^{-1} \tag{10.2.46}$$

We can now find a generalized equation for the "variable" $|f_k(t)\rangle$. By

Laplace transforming Eq. 10.2.23 we get

$$|\hat{f}_k(z)\rangle = |f_k\rangle\hat{\Phi}_k(z) + |\hat{f}_{k+1}(z)\rangle\hat{\Phi}_k(z) \tag{10.2.47}$$

Using Eqs. 10.2.43 and 10.2.47, we obtain

$$|\hat{f}_k(z)\rangle = (|f_k\rangle + |\hat{f}_{k+1}(z)\rangle)(z - \lambda_k + \Delta_{k+1}^2\hat{\Phi}_{k+1}(z))^{-1} \tag{10.2.48}$$

which is just the Laplace transform of

$$\frac{d}{dt}|f_k(t)\rangle = \lambda_k|f_k(t)\rangle - \int_0^t ds\ |f_k(s)\rangle\varphi_k(t-s) + |f_{k+1}(t)\rangle \tag{10.2.49}$$

where

$$\varphi_k(t) = \frac{\langle f_{k+1} \mid f_{k+1}(t)\rangle}{\langle f_k \mid f_k\rangle} \tag{10.2.50}$$

By expanding the dynamic operator $\hat{\mathscr{L}}_0$ over the basis set $\{|f_k\rangle\}$ it is possible to show that the $|f_k\rangle$'s form an infinite chain of states replacing the dissipative manifold directly coupled with $|e\rangle$ (Appendix 10.B).

To prove this we use symmetrical matrices such as those of Section 9.2. This is less elegant than the method of Appendix B.

Consider the dynamic operator $\hat{\mathscr{L}}_0'$ defined as follows:

$$\begin{aligned}\hat{\mathscr{L}}_0' = &-i\{|e\rangle\Omega_0\langle e| + (|e\rangle\langle M_1| + |M_1\rangle\langle e|)v_1 + |M_1\rangle\Omega_1\langle M_1| \\ &+ (|M_1\rangle\langle M_2| + |M_2\rangle\langle M_1|)v_2 + \cdots \\ &+ |M_n\rangle\Omega_n\langle M_n| + (|M_n\rangle\langle M_{n+1}| + |M_{n+1}\rangle\langle M_n|)v_n + \cdots\end{aligned} \tag{10.2.51}$$

where the states $|M_1\rangle$ are assumed orthonormal. The use of this operator results in a Mori chain of states defined by the following relations:

$$\begin{aligned}|f_0'\rangle &= |e\rangle \\ |f_1'\rangle &= -iv_1|M_1\rangle \\ |f_2'\rangle &= -v_1v_2|M_2\rangle \\ &\vdots \\ |f_n'\rangle &= (-i)^n v_n v_{n-1}\cdots v_1|M_n\rangle \\ &\vdots\end{aligned} \tag{10.2.52}$$

These equations, in turn, provide the following coupling parameters:

$$\Delta_k'^2 = v_k^2 \tag{10.2.53}$$

The counterpart of Eq. 10.2.33 provides

$$\begin{aligned}\lambda_k' &= \langle f_k'|\hat{\mathscr{L}}_k'|f_k'\rangle/\langle f_k'|f_k'\rangle \\ &= \langle f_{k-1}'|\hat{\mathscr{L}}_0(\hat{1}-\hat{P}_0')\cdots(\hat{1}-\hat{P}_{k+1}') \\ &\quad\times(\hat{1}-\hat{P}_{k-1}')\cdots(\hat{1}-\hat{P}_0')\hat{\mathscr{L}}_0'|f_k'\rangle/\langle f_k'|f_k'\rangle\end{aligned} \tag{10.2.54}$$

By using the fact that the projection operators

$$\hat{P}'_k = \frac{|f'_k\rangle\langle f'_k|}{\langle f'_k | f'_k\rangle} \tag{10.2.55}$$

share the same properties as the corresponding projection operators $\hat{P}_k$ (idempotence and the property of Eq. 10.2.55), Eq. 10.2.54 can be written as follows:

$$\begin{aligned}\lambda'_k &= \langle f'_{k-1}|\hat{\mathscr{L}}'_0(\hat{1}-\hat{P}'_0)\cdots(\hat{1}-\hat{P}'_{k-1})\mathscr{L}'_0|f'_k\rangle/\langle f'_k|f'_k\rangle \\ &= \langle f'_k|\hat{\mathscr{L}}_0|f'_k\rangle/\langle f'_k|f'_k\rangle = -i\Omega_k\end{aligned}$$

In consequence $\mathscr{L}'_0$ is identical with $\mathscr{L}_0$ if

$$-i\Omega_k = \lambda_k \qquad \text{for any } k \tag{10.2.56}$$

and

$$v_k = \Delta_k \qquad \text{for any } k \tag{10.2.57}$$

We have replaced the thermal bath with a chain of "states." The "excited state" $|f_0\rangle$ is depopulated over the Mori chain. When the "irrelevant" part of our physical system is endowed with a sufficiently large number of freedom degrees, the part of interest can exhibit an irreversible behavior provided that the dissipation condition be satisfied (Prigogine, 1966; Grigolini, 1975). Then the Mori chain is infinitely long.

A particular state of the chain evolves temporally in two different ways. One is governed by Eq. 10.2.21, the other by

$$|f_k(t)\rangle = e^{\hat{\mathscr{L}}_0 t}|f_k\rangle \tag{10.2.58}$$

The difference is detailed by Mori and co-workers (Karasudani et al., 1979; Nagano et al., 1980). We deal with the latter kind of time evolution. The standard initial condition of Mori theory can be expressed as follows:

$$|\psi(0)\rangle = |f_0\rangle \tag{10.2.59}$$

where the "wave function" $|\psi\rangle$ expresses the condition of the whole physical system. Any lifting of this restriction will have an effect on the nature of the fluctuating force of the generalized Langevin equation. We can now clarify the general discussion of Section 9.1. Consider the generalized Langevin equation, obtained from Eq. 10.2.49 in the case $k = 0$:

$$\frac{d}{dt}|f_0(t)\rangle = \lambda_0|f_0(t)\rangle - \int_0^t ds|f_0(s)\rangle\Delta_1^2\Phi_1(t-s) + \exp[(1-P)\hat{\mathscr{L}}_0 t](1-P)\hat{\mathscr{L}}_0|f_0\rangle \tag{10.2.60}$$

The fluctuating force, third term on the right side of Eq. 10.2.60, contains on the left the projection operator to the space orthogonal to the "state" $|f_0\rangle$. This implies that the average value of the stochastic force evaluated according to the general indication of Section 9.1, by

$$\langle f_1(t)\rangle = \langle\psi(0)|f_1(t)\rangle \tag{10.2.61}$$

vanishes provided that Eq. 10.2.59 can be satisfied. If $|f_1(t)\rangle$ is governed by Eq. 10.2.58 we obtain

$$\langle\psi(t)|f_1\rangle = \langle\psi(0)|f_1(t)\rangle \neq 0 \tag{10.2.62}$$

This reasoning results in a Langevin type of equation more general in applicability than the one by Mori (1965a, b). This is pursued further in Section 10.6. Mori (1965b) truncates his continued fraction expansion at nth order by assuming that $\Delta_{n+1}^2\hat{\Phi}_{n+1}(z)$ can be replaced by a constant value. This simplifying assumption is equivalent to introducing a bona fide thermal bath, the behavior of which is that of an ideal "thermal source" (at temperature $T = 0$ in the case of the model of radiationless decay described in the preceding chapter).

The states $|f_{n+1}\rangle, |f_{n+2}\rangle, \ldots$ are seen by the state $|f_n\rangle$ as an irreversible sink. Replacing an infinite chain with a sink means that the state interacting with the sink decays exponentially. This technique has been useful, for example, in the description of gas-solid scattering processes (Adelman, 1979). Suppose, therefore, that the state $|f_{n+1}\rangle$ decays with a damping Γ_{n+1}. In accordance with Section 9.2, if $1/\Gamma_{n+1}$ is very much shorter than $1/\Delta_n$ the state $|f_n\rangle$ can also be regarded as interacting with a dissipative sink with a damping rate provided by $\Gamma_n = \Delta_n^2/\Gamma_{n+1}$. This result is valid when $|f_n\rangle$ and $|f_{n+1}\rangle$ can be thought of as being nearly degenerate, so that $|\lambda_{n-1} - \lambda_n| \ll \Gamma_{n+1}$. This can also be understood by looking at the continued fraction of Eq. 10.2.44. Assume that the states $|f_n\rangle$ have the same energy. We can then choose this to be zero. If the contribution $\Delta_n^2/[z + \Delta_{n+1}^2\hat{\Phi}_{n+1}(z)]$ is replaced by $\Delta_n^2/(z + \Gamma_{n+1})$, the latter, in turn, can be replaced by $\Gamma_n = \Delta_n^2/\Gamma_{n+1}$, when $\Gamma_{n+1} \gg z$. The order of magnitude of $|z|$ cannot be larger than that of Δ_n, which is the frequency of exchange of population between $|f_n\rangle$ and $|f_{n+1}\rangle$ (recall that $\Delta_n \ll \Gamma_n$).

The thermal bath of the state $|f_{n-1}\rangle$ is an ideal thermal bath for the whole chain of states $|f_0\rangle, |f_1\rangle, \ldots, ||f_{n-1}\rangle$. In fact, when the excitation reaches the state $|f_n\rangle$ it soon disappears, for $\Gamma_n \gg \Delta_n$. The fluctuations affecting the state $|f_{n-1}\rangle$ are always to be regarded as being vacuum fluctuations.

It is our opinion that no thermal bath of a non-Markovian relaxation process can be regarded as ideal. In fact, excitation can reach the thermal bath and return to $|f_0\rangle$ before an irreversible process has fully taken place. As pointed out in Section 9.1, this results in some ambiguity in the application of Mori theory, which is sometimes (erroneously) supposed to be valid only for ideal thermal baths close to thermodynamical equilibrium. During the relaxation process this condition is destroyed but the generalized Langevin equation by Mori is still valid.

The system consisting of the states $|f_0\rangle, |f_1\rangle, \ldots, |f_{n-1}\rangle$ is taken as that of interest, its relaxation dynamics is described by a standard Langevin

equation, and its thermal bath is an "ideal" thermal bath affecting the system of interest through the vacuum fluctuations.

If, on the other hand, we take the state $|f_0\rangle$ as being the only part of interest our Langevin equation can be used to describe thermal bath excitation phenomena. We can study physical phenomena where at $t = 0$ the thermal bath is already excited; that is, we can study the whole excitation-relaxation process:

We summarize as follows:

1. A rigorous justification is possible for the "reduced" model introduced in Section 9.2. A more general model can be built up and the "virtual" states and their couplings can be expressed in terms of states and couplings of the "complex" model. For example, in the case of the model of Fig. 9.2.1 we have

$$|f_1\rangle = -\sum_m i|m\rangle\langle m|\hat{V}|e\rangle \tag{10.2.63}$$

which is the doorway state of the Ziv and Rhodes theory (1976). The "energy" of this state is

$$\lambda_1 = \frac{\langle f_1|\hat{\mathscr{L}}_0|f_1\rangle}{\langle f_1|f_1\rangle} = -i\sum_m \frac{\langle e|\hat{V}|m\rangle\epsilon_m\langle m|\hat{V}|e\rangle}{\langle e|\hat{V}^2|e\rangle} \tag{10.2.64}$$

The coupling between $|e\rangle$ and the first "virtual" state $|e\rangle$ is given by

$$\Delta_1^2 = \langle e|\hat{V}^2|e\rangle \tag{10.2.65}$$

For higher-order cases, the analytical expressions become more and more complicated. For example, the expression for the state $|f_2\rangle$ is (we neglected both the interaction between $\{|n\rangle\}$ and $\{|m\rangle\}$ and that between $|e\rangle$ and $\{|n\rangle\}$)

$$|f_2\rangle = -\sum_m \epsilon_m|m\rangle\langle m|\hat{V}|e\rangle + \sum_{mm'} \frac{|m'\rangle\langle m'|\hat{V}|e\rangle\langle e|\hat{V}|m\rangle\epsilon_m\langle m|\hat{V}|e\rangle}{\langle e|\hat{V}^2|e\rangle} \tag{10.2.66}$$

For practical applications, therefore, it is quite important to find a sound criterion for truncating the expansion at a fairly low order (cf. Chapter 4).

2. The approximation suggested by Mori is equivalent to breaking the time reversal properties of the nth-order correlation function:

$$\Phi_n(t) = \langle f_n|f_n(t)\rangle/\langle f_n|f_n\rangle = \langle f_n|\exp(\mathscr{L}_n t)|f_n\rangle/\langle f_n|f_n\rangle \tag{10.2.67}$$

with

$$\Phi_n^*(t) = \Phi_n(-t) \tag{10.2.68}$$

After truncation Eq. 10.2.68 is no longer valid. The anti-Hermitian operator of Eq. 10.2.50 has been replaced by

$$\begin{aligned}\hat{\mathscr{L}}_{\text{eff}} = &-i[|e\rangle\Omega_0\langle e| + (|e\rangle\langle M_1| + |M_1\rangle\langle e|)v_1 \\ &+ |M_1\rangle\Omega_1\langle M_1| + (|M_1\rangle\langle M_2| + |M_2\rangle\langle M_1|)v_2 \\ &\cdots \\ &+ |M_{n-1}\rangle\Omega_{n-1}\langle M_{n-1}| + (|M_{n-1}\rangle\langle M_n| + |M_n\rangle\langle M_{n-1}|)v_n \\ &+ |M_n\rangle(\Omega_n - i\Gamma_n)\langle M_n|]\end{aligned} \tag{10.2.69}$$

3. The generalized Langevin equation can be put in a form that makes it possible to study the case of a thermal bath far from its equilibrium distribution.

10.3 MORI THEORY WITH NON-HERMITIAN LIOUVILLIAN OPERATORS

One of the most appealing features of Mori theory is that, when applied to molecular dynamics in liquids, the "reduced" model corresponding to the truncation of $\hat{\Phi}_0(z)$ at $n = 3$ is a mechanical model, the itinerant oscillator (Appendix C). This model has been developed independently of Mori theory (see Chapters 1–4).

Its rotational and monodimensional version is given by

$$\dot{\Omega} = -k_1(\mathscr{O} - \psi) \qquad \left(k_1 = \frac{k}{I_1}\right) \tag{10.3.1}$$

$$\ddot{\psi} = k_2(\mathscr{O} - \psi) - \zeta\dot{\psi} + \lambda(t) \qquad \left(k_2 = \frac{k}{I_2}\right) \tag{10.3.2}$$

These equations correspond exactly to the mechanical model in Eqs. 4.1.4 and 4.1.5. The kinetic energy of the inner disk, the part of interest, is transmitted to the external annulus and if the rate of dissipation of the energy of the external annulus is not too large the mechanical excitation can rebound on the inner disk. A damped oscillatory motion is the result. The similarity with the quantum mechanical "reduced" model is striking. This is because both are "reduced" (e.g., Mori–Evans) models corresponding to a low-order truncation of the "memory kernel." Some variations of the standard itinerant oscillator theory have been developed (in response to spectral data) which assume that the inner disk is affected by friction. We have described this two-friction itinerant oscillator in Chapter 4. This cannot be justified by the standard Mori theory described in the preceding section.

In Section 9.2 we have shown that a background quasi-continuum $\{|n\rangle\}$ is present when dealing with radiationless decay inside molecules. Usually a drastic simplification is made when considering the interaction between

such a background continuum and the remaining part of the physical system under study.

If the quasi-continuum of Fig. 9.2.1 is replaced by a true continuum and the latter, in turn, is eliminated following the suggestions of Bixon et al., (1969), in the absence of external excitation we can replace the Hermitian Hamiltonian of Eq. 9.2.1 with the following one:

$$\hat{\mathcal{H}}_{\text{eff}} = |e\rangle\epsilon_e\langle e| + \sum_m |m\rangle\epsilon_m\langle m| + \sum_m (|e\rangle\langle e|\hat{V}|m\rangle\langle m| + |m\rangle\langle m|\hat{V}|e\rangle\langle e|)$$
$$-i\Big[|e\rangle\Gamma_{ee}\langle e| + \sum_m (|e\rangle\langle m| + |m\rangle\langle e|)\Gamma_{em}$$
$$+ \sum_{\substack{mm' \\ m<m'}} (|m\rangle\langle m'| + |m'\rangle\langle m|)\Gamma_{mm'} + \sum_m |m\rangle\langle m|\Gamma_{mm}\Big] \tag{10.3.3}$$

The Hamiltonian of Eq. 10.3.3 is a sound starting point for further development. For example, the interference effects between different states $|m\rangle$ is taken into account as an effect of a second-order interaction of these states with the ϵ-continuum (Bixon et al., 1969). Furthermore, this Hamiltonian is symmetrical and there is no difficulty in diagonalizing it (Chapter 9, Appendix C).

However, this Hamiltonian is not Hermitian. Therefore the standard Mori approach cannot be followed. We show now that there is a close connection between the fact that standard Mori theory cannot be used to justify the two-friction itinerant oscillator and the fact that it cannot deal with non-Hermitian Hamiltonians (or Liouvillians) such as that of Eq. 10.3.3. Consider the equation of motion

$$\frac{d}{dt}|f_0(t)\rangle = \hat{\mathcal{L}}_0|f_0(t)\rangle \tag{10.3.4}$$

when $i\hat{\mathcal{L}}_0$ is not Hermitian. The expansion for $|f_0(t)\rangle$ obtained in the preceding section

$$|f_0(t)\rangle = \Phi_0(t)|f_0\rangle + \int_0^t ds\ \Phi_0(s)|f_1(t-s)\rangle \tag{10.3.5}$$

where

$$\Phi_0(t) = \langle f_0|f_0(t)\rangle \tag{10.3.5a}$$

can be derived without any assumption concerning Hermitianicity. In consequence, Eq. 10.3.5 is generally valid. In order to extend this result to nth-order in the variable chain, we define

$$|f_k\rangle = \hat{\mathcal{L}}_k|f_{k-1}\rangle \tag{10.3.6}$$

$$|f_k(t)\rangle = \exp(\hat{\mathcal{L}}_k t)\hat{\mathcal{L}}_k|f_{k-1}\rangle \tag{10.3.7}$$

$$\hat{\mathcal{L}}_k = (\hat{1} - \hat{P}_{k-1})\mathcal{L}_{k-1} \tag{10.3.8}$$

From Eqs. 10.3.6 and 10.3.8 we obtain

$$|f_k\rangle = (\hat{1} - \hat{P}_{k-1})(\hat{1} - \hat{P}_{k-2}) \cdots (\hat{1} - \hat{P}_1)(\hat{1} - \hat{P}_0)\hat{\mathcal{L}}_0|f_0\rangle \tag{10.3.9}$$

It is convenient to define now a left eigenstate to be associated with $|f_k\rangle$ in the following way:

$$\langle\tilde{f}_k| = \langle\tilde{f}_{k-1}|\hat{\mathcal{L}}_0(\hat{1} - \hat{P}_0)(\hat{1} - \hat{P}_1) \cdots (\hat{1} - \hat{P}_{k-2})(\hat{1} - \hat{P}_{k-1}) \tag{10.3.10}$$

The projection operator $\hat{P}_k$ can then be written as

$$\hat{P}_k = \frac{|f_k\rangle\langle\tilde{f}_k|}{\langle\tilde{f}_k|f_k\rangle} \tag{10.3.11}$$

which, of course, satisfies the idempotency property

$$\hat{P}_k^2 = \hat{P}_k \tag{10.3.12}$$

When $\hat{\mathcal{L}}_{\text{eff}}$ is not Hermitian, however, the Hermitian property of each projection operator is also lost. We must limit ourselves to using Eq. 10.3.12 and

$$\hat{P}_k\hat{P}_{k'} = \hat{P}_{k'}\hat{P}_k \qquad \text{for any } k \tag{10.3.13}$$

The validity of Eq. 10.3.13 depends on the fact that the vectors $\langle\tilde{f}_k|$ (Eq. 10.3.10) are orthogonal to the vectors$|f_k\rangle$ (Eq. 10.3.9), according to the formula

$$\langle\tilde{f}_k|f_{k'}\rangle = 0 \qquad \text{for } k \neq k' \tag{10.3.14}$$

This is the property exhibited by the biorthogonal set of vectors which in Section 2 were used to deal with non-Hermitian matrices (see Chapter 9, Appendix C). Thus the approach which led us to Eq. 10.2.23 can be repeated and results in

$$|f_k(t)\rangle = \Phi_k(t)|f_k\rangle + \int_0^t ds\ \Phi_k(s)|f_{k+1}(t-s)\rangle \tag{10.3.15}$$

where

$$\Phi_k(t) = \frac{\langle\tilde{f}_k|f_k(t)\rangle}{\langle\tilde{f}_k|f_k\rangle} \tag{10.3.16}$$

We can focus our attention now on the following equation of motion:

$$\frac{d}{dt}\langle\tilde{f}_0(t)| = \langle\tilde{f}_0(t)|\hat{\mathcal{L}}_0 \tag{10.3.17}$$

Its solution is given by

$$\langle\tilde{f}_0(t)| = \langle f_0|e^{\hat{\mathcal{L}}_0 t} \tag{10.3.18}$$

The vector $\langle\tilde{f}_0(t)|$ is not the usual left vector associated with $|f_0(t)\rangle$. The latter one is given by

$$\langle f_0(t)| = \langle f_0|\exp(\hat{\mathcal{L}}_0^\dagger t) \tag{10.3.19}$$

In the Hermitian case we would have had

$$\langle \tilde{f}_0(t)| = \langle f_0(-t)| \tag{10.3.20}$$

If we define

$$\langle \tilde{f}_k(t)| = \langle \tilde{f}_{k-1}|\tilde{\hat{\mathcal{L}}}_k e^{\tilde{\hat{\mathcal{L}}}_k t} \tag{10.3.21}$$

where

$$\tilde{\hat{\mathcal{L}}}_k = \tilde{\hat{\mathcal{L}}}_{k-1}(\hat{1} - \hat{P}_{k-1}) \tag{10.3.22}$$

we can obtain the left equation corresponding to Eq. 10.3.15

$$\langle \tilde{f}_k(t)| = \langle \tilde{f}_k|\tilde{\Phi}_k(t) + \int_0^t ds\, \langle \tilde{f}_{k+1}(t-s)|\tilde{\Phi}_k(s) \tag{10.3.23}$$

where

$$\tilde{\Phi}_k(t) = \langle \tilde{f}_k(t)|f_k\rangle / \langle \tilde{f}_k|f_k\rangle \tag{10.3.24}$$

Equations 10.3.12 and 10.3.13 give, after some algebra,

$$\tilde{\Phi}_k(t) = \Phi_k(t) \tag{10.3.25}$$

and

$$\langle \tilde{f}_k(t)|f_{k+1}\rangle = \langle \tilde{f}_k|\exp(\hat{\mathcal{L}}_k t)|f_{k+1}\rangle \tag{10.3.26}$$

From Eq. 10.3.7 we obtain

$$\frac{d}{dt}|f_k(t)\rangle = \hat{\mathcal{L}}_k|f_k(t)\rangle \tag{10.3.27}$$

As in the preceding section, we can use the property $\hat{1} = (\hat{1} - \hat{P}_k) + \hat{P}_k$ and the definition of $|f_{k+1}\rangle$. Equation 10.3.27 then becomes

$$\frac{d}{dt}|f_k(t)\rangle = \lambda_k \exp(\tilde{\mathcal{L}}_k t)|f_k\rangle \tag{10.3.28}$$

where

$$\lambda_k = \frac{\langle \tilde{f}_k|\hat{\mathcal{L}}_k|f_k\rangle}{\langle \tilde{f}_k \mid f_k\rangle} \tag{10.3.29}$$

Equation 10.3.28 can also be written in the following useful form:

$$\frac{d}{dt}|f_k(t)\rangle = \lambda_k|f_k(t)\rangle + \frac{|f_k\rangle\langle \tilde{f}_k|\exp(\hat{\mathcal{L}}_k t)|f_{k+1}\rangle}{\langle \tilde{f}_k \mid f_k\rangle} + (1 - \hat{P}_k)\exp(\hat{\mathcal{L}}_k t)|f_{k+1}\rangle \tag{10.3.30}$$

We can now exploit the advantage provided by using the left vectors of Eq. 10.3.10, that is, Eq. 10.3.26. By using this equation, Eq. 10.3.30 can be written as follows:

$$\frac{d}{dt}|f_k(t)\rangle = \lambda_k|f_k(t)\rangle + \frac{|f_k\rangle\langle \tilde{f}_k(t)|f_{k+1}\rangle}{\langle \tilde{f}_k \mid f_k\rangle} + (\hat{1} - \hat{P}_k)\exp(\hat{\mathcal{L}}_k t)|f_{k+1}\rangle \tag{10.3.31}$$

Substituting Eq. 10.3.23 into Eq. 10.3.31, we obtain

$$\frac{d}{dt}|f_k\rangle = \lambda_k|f_k(t)\rangle - \int_0^t ds|f_k\rangle\Phi_{k+1}(t-s)\Phi_k(s)\Delta_{k+1}^2 + (\hat{1} - \hat{P}_k)\exp(\hat{\mathcal{L}}_k t)|f_{k+1}\rangle \tag{10.3.32}$$

where

$$\Delta_{k+1}^2 = -\frac{\langle \tilde{f}_{k+1} \mid f_{k+1}\rangle}{\langle \tilde{f}_k \mid f_k\rangle} \tag{10.3.33}$$

By repeating the techniques described in the preceding section we arrive at the generalized Langevin equation:

$$\frac{d}{dt}|f_k(t)\rangle = \lambda_k|f_k(t)\rangle - \int_0^t ds|f_k(s)\rangle\varphi_k(t-s) + |f_{k+1}(t)\rangle \tag{10.3.34}$$

where

$$\varphi_k(t) = \frac{\langle \tilde{f}_{k+1} \mid f_{k+1}(t)\rangle}{\langle \tilde{f}_k \mid f_k\rangle} \tag{10.3.35}$$

The corresponding continued fraction is

$$\hat{\Phi}_1(z) = \cfrac{1}{z - \lambda_1 + \cfrac{\Delta_2^2}{z - \lambda_2 + \cfrac{\Delta_3^2}{z - \lambda_3 + \ddots \cfrac{\Delta_n^2}{z - \lambda_n + \Delta_{n+3}^2\hat{\Phi}_{n+1}(z)}}}} \tag{10.3.35a}$$

identical with Eq. 10.2.45. The expansion coefficients Δ_k^2 and the "energies" $-i\lambda_k$, however, here are complex numbers which contain both a real and an imaginary part. In consequence any state of the generalized Mori chain can be directly damped. In contrast, the standard Mori theory of the preceding section results in a damping only of the last variable of the chain as an effect of truncation.

The theory developed in this section generalizes the two-friction itinerant oscillator of Chapter 4. It is a matter of current investigation whether the non-Hermitianicity of the Liouvillian in such a case depends on a background thermal bath. Further study is required into the real nature of this background.

If the theory of this section is applied to the "intramolecular" Hamiltonian of Eq. 9.21, its second-order truncation results (Grigolini and Rosato, 1981) in the following effective Hamiltonian:

$$\hat{\mathcal{H}} = \begin{pmatrix} \epsilon_e - i\Gamma_{ee} & v - i\Gamma_{eM} \\ v - i\Gamma_{eM} & \epsilon_M - i\Gamma_{MM} \end{pmatrix} \tag{10.3.36}$$

which has more general applicability than that of Section 9.2. This

"reduced" Hamiltonian can result in both damped oscillatory relaxation and biexponential decay. The result is obtained by rejecting the assumption that the state $|e\rangle$ does not interact with the n-continuum and that interference effects on the states $|m\rangle$ can be neglected.

10.4 MULTIDIMENSIONAL VARIABLES

It frequently happens that the variable of interest is multidimensional. The theory can be generalized without difficulty to describe a vectorial variable $\mathbf{A}$ satisfying the following equation of motion:

$$\frac{d}{dt}\mathbf{A} = \hat{\mathscr{L}}_0\mathbf{A} \tag{10.4.1}$$

This is needed to describe the interaction of molecular rotation and translation (Chapter 4 or 5) or that of a discrete set of quantum mechanical states (Appendix G). According to Kivelson and Ogan (1974) the first projection operator can be defined as follows:

$$\hat{P}_0\mathbf{B} = (\mathbf{B}, \mathbf{A}^+)(\mathbf{A}, \mathbf{A}^+)^{-1}\mathbf{A} \tag{10.4.2}$$

The chain of variables can now be built up as follows:

$$\mathbf{f}_0 = \mathbf{A} \tag{10.4.3}$$

$$\hat{\mathscr{L}}_k = (\hat{1} - \hat{P}_{k-1})\hat{\mathscr{L}}_{k-1} \tag{10.4.4}$$

$$\mathbf{f}_k(t) = \exp(\hat{\mathscr{L}}_k t)\hat{\mathscr{L}}_k\mathbf{f}_{k-1} \tag{10.4.5}$$

$$\tilde{\mathbf{f}}_k(t) = \exp(\hat{\mathscr{L}}_k^+ t)\hat{\mathscr{L}}_k^+\tilde{\mathbf{f}}_k \tag{10.4.6}$$

$$\tilde{\mathbf{f}}_0 = \mathbf{f}_0 \tag{10.4.7}$$

The "projection" operator $\hat{P}_k$ is defined as follows:

$$\hat{P}_k\mathbf{B} = (\mathbf{B}, \tilde{\mathbf{f}}_k^+)(\mathbf{f}_k, \tilde{\mathbf{f}}_k^+)^{-1}\mathbf{f}_k \tag{10.4.8}$$

and is not Hermitian in general.

The states $\mathbf{f}_k$ and $\tilde{\mathbf{f}}_k$ are biorthogonal, that is,

$$(\mathbf{f}_k, \tilde{\mathbf{f}}_{k'}^+) = 0 \qquad \text{if } k \neq k' \tag{10.4.9}$$

Repeating the approach of Section 10.2 leading to Eq. 10.2.23, we obtain

$$\mathbf{f}_k(t) = \mathbf{\Phi}_k(t)\mathbf{f}_k + \int_0^t ds\, \mathbf{\Phi}_k(s)\mathbf{f}_{k+1}(t-s) \tag{10.4.10}$$

where

$$\mathbf{\Phi}_k(t) = (\mathbf{f}_k(t), \tilde{\mathbf{f}}_k^+)(\mathbf{f}_k, \tilde{\mathbf{f}}_k^+)^{-1} \tag{10.4.11}$$

The result provided by Eq. 10.4.10 must also be valid for $\tilde{\mathbf{f}}_k(t)$ provided that

$\hat{\mathscr{L}}_k$ is replaced by $\hat{\mathscr{L}}_k^+$, and $\hat{P}_k$ by $\hat{P}_k^+$, defined by

$$\hat{P}_k^+\mathbf{C} = (\mathbf{C}, \mathbf{f}_k^+)(\tilde{\mathbf{f}}_k, \mathbf{f}_k^+)^{-1}\tilde{\mathbf{f}}_k \tag{10.4.12}$$

(and, of course, $\mathbf{f}_k$ changed in $\tilde{\mathbf{f}}_k$); then we obtain

$$\tilde{\mathbf{f}}_k(t) = \tilde{\mathbf{\Phi}}_k(t)\tilde{\mathbf{f}}_k + \int_0^t ds\, \tilde{\mathbf{\Phi}}_k(s)\tilde{\mathbf{f}}_{k+1}(t-s) \tag{10.4.13}$$

where

$$\mathbf{\Phi}_k(t) = (\tilde{\mathbf{f}}_k(t), \mathbf{f}_k^+)(\tilde{\mathbf{f}}_k, \mathbf{f}_k^+)^{-1} \tag{10.4.14}$$

The transpose conjugate of the matrix $\tilde{\mathbf{\Phi}}_k(t)$ is

$$[\tilde{\mathbf{\Phi}}(t)]^+ = (\mathbf{f}_k, \tilde{\mathbf{f}}_k^+)^{-1}(\mathbf{f}_k, \tilde{\mathbf{f}}_k^+(t)) \tag{10.4.15}$$

This is the only difficulty present in the multidimensional case. In fact, in general, the matrix $(\mathbf{f}_k, \tilde{\mathbf{f}}_k^+)^{-1}$ does not commute with $(\mathbf{f}_k, \tilde{\mathbf{f}}_k(t)^+)$. In order to establish a relation between $(\tilde{\mathbf{\Phi}}_k(t))^+$ and $\mathbf{\Phi}_k(t)$ like Eq. 10.3.25, we multiply Eq. 10.4.15 on the left by $(\mathbf{f}_k, \tilde{\mathbf{f}}_k^+)$ and on the right by $(\mathbf{f}_k, \tilde{\mathbf{f}}_k^+)^{-1}$ to obtain

$$\mathbf{\Phi}_k(t) = (\mathbf{f}_k, \tilde{\mathbf{f}}_k^+)[\tilde{\mathbf{\Phi}}(t)]^+(\mathbf{f}_k, \tilde{\mathbf{f}}_k^+)^{-1} \tag{10.4.16}$$

We have also used the property

$$(\mathbf{f}_k(t), \mathbf{f}_k^+) = (\mathbf{f}_k, \tilde{\mathbf{f}}_k(t)^+) \tag{10.4.17}$$

which is the multidimensional counterpart of that used in Eq. 10.3.26. Of course, Eq. 10.4.16 can be written in the following way:

$$[\tilde{\mathbf{\Phi}}(t)]^+ = (\mathbf{f}_k, \tilde{\mathbf{f}}_k)^{-1}\mathbf{\Phi}_k(t)(\mathbf{f}_k, \tilde{\mathbf{f}}_k) \tag{10.4.18}$$

which is, in turn, the multidimensional counterpart of Eq. 10.3.25.

As in the preceding section we obtain the following chain of correlation functions (now to be regarded as matrices):

$$\frac{d}{dt}\mathbf{\Phi}_k(t) = \boldsymbol{\lambda}_k(t)\mathbf{\Phi}_k(t) - \int_0^t ds\, \mathbf{\Phi}_{k+1}(t-s)\boldsymbol{\Delta}_{k+1}^2\mathbf{\Phi}_k(s) \tag{10.4.19}$$

where

$$\boldsymbol{\lambda} = (\hat{\mathscr{L}}_k\mathbf{f}_k, \tilde{\mathbf{f}}_k^+)(\mathbf{f}_k, \tilde{\mathbf{f}}_k^+)^{-1} \tag{10.4.20}$$

$$\boldsymbol{\Delta}_k^2 = -(\mathbf{f}_{k+1}, \tilde{\mathbf{f}}_{k+1}^+)(\mathbf{f}_k, \tilde{\mathbf{f}}_k^+)^{-1} \tag{10.4.21}$$

The important feature now is that $\boldsymbol{\Delta}_k^2$ is not diagonal. By Laplace transforming Eq. 10.4.19 we obtain

$$\hat{\mathbf{\Phi}}_k(z) = (\mathbf{1}z - \boldsymbol{\lambda}_k + \mathbf{\Phi}_{k+1}(t-s)\boldsymbol{\Delta}_{k+1}^2)^{-1} \tag{10.4.22}$$

The generalized Langevin equation can now be written as follows:

$$\frac{d}{dt}\mathbf{f}_k = \boldsymbol{\lambda}_k\mathbf{f}_k(t) - \int_0^t ds\, \mathbf{\Phi}_{k+1}(t-s)\boldsymbol{\Delta}_{k+1}^2\mathbf{f}_k(s) + \exp[(\hat{1} - \hat{P}_k)\hat{\mathscr{L}}_k t]\mathbf{f}_{k+1} \tag{10.4.23}$$

With an Hermitian Liouvillian the result of Section 9.1, Eq. 9.1.21 is completely recovered (for $k = 0$).

10.5 THE CONTINUED FRACTION EXPANSION FOR THE STOCHASTIC LIOUVILLE EQUATION

The theory of Sections 10.3 and 10.4 leads us in a natural way to the solution of an equation of motion such as

$$\frac{d}{dt}\boldsymbol{\mu} = \boldsymbol{\omega}(t) \times \boldsymbol{\mu} \tag{10.5.1}$$

where $\boldsymbol{\omega}(t)$ is a stochastic variable the properties of which are determined by a suitable diffusion equation. In Section 9.3 we dealt with the corresponding problem in the semiclassical case. We showed that the main idea of the SLE consists in replacing the Hamiltonian of the thermal bath of the variable of interest ($\boldsymbol{\mu}$ in the present case) with the diffusion operator of the stochastic variable ($\boldsymbol{\omega}$ in the present case). It is important to discuss how the same idea can be applied to the classical case where the variable of interest is **A**.

We start from the Liouville equation

$$\frac{\partial}{\partial t}\psi(t, \Gamma) = -i\hat{L}\psi(t, \Gamma) \tag{10.5.2}$$

where Γ is a multidimensional phase space coordinate. In order to include in our treatment the system described by Eq. 10.5.1, we assume our physical system to consist of three parts. The first, **S**, is the part involved by our variable of interest, **A**; the second one, **M**, concerns a variable $\boldsymbol{\Omega}$ which is assumed to interact with the third part, **R**. The subsystem **S** does not interact with **R** except indirectly through the **M**–**R** interaction.

As a consequence, we write the Liouvillian as follows:

$$\hat{L} = \hat{L}_{\mathbf{S}}(\mathbf{A}) + \hat{L}_{\mathbf{M}}(\boldsymbol{\Omega}) + \hat{L}_{\mathbf{R}} + \hat{L}_{\mathbf{SM}}(\mathbf{A}, \boldsymbol{\Omega}) + \hat{L}_{\mathbf{MR}}(\boldsymbol{\Omega}) \tag{10.5.3}$$

By following the standard Mori theory (Section 9.1), we can build up the generalized Langevin equation for the variable $\boldsymbol{\Omega}$ as follows:

$$\frac{\partial}{\partial t}\boldsymbol{\Omega} = \mathbf{c}_{\boldsymbol{\Omega}}\boldsymbol{\Omega} + \int_0^t ds\, \mathbf{d}_{\boldsymbol{\Omega}}(s)\boldsymbol{\Omega}(t-s) + \mathbf{F}_{\boldsymbol{\Omega}}(t) \tag{10.5.4}$$

where

$$\mathbf{c}_{\boldsymbol{\Omega}} = (\hat{P}_{\boldsymbol{\Omega}} i\hat{L}_{\boldsymbol{\Omega}}\boldsymbol{\Omega}, \boldsymbol{\Omega}^+)(\boldsymbol{\Omega}, \boldsymbol{\Omega}^+)^{-1} \tag{10.5.5}$$

$$\mathbf{d}_{\boldsymbol{\Omega}}(s) = (\hat{P}_{\boldsymbol{\Omega}} i\hat{L}_{\boldsymbol{\Omega}} \exp[is(\hat{1} - \hat{P}_{\boldsymbol{\Omega}})\hat{L}_{\boldsymbol{\Omega}}](\hat{1} - \hat{P}_{\boldsymbol{\Omega}})i\hat{L}_{\boldsymbol{\Omega}}\boldsymbol{\Omega}, \boldsymbol{\Omega}^+)(\boldsymbol{\Omega}, \boldsymbol{\Omega}^+)^{-1} \tag{10.5.6}$$

and

$$\mathbf{F}_{\boldsymbol{\Omega}}(t) = \exp[it(\hat{1} - \hat{P}_{\boldsymbol{\Omega}})t](\hat{1} - \hat{P}_{\boldsymbol{\Omega}})i\hat{L}_{\boldsymbol{\Omega}}\boldsymbol{\Omega} \tag{10.5.7}$$

We now make some important simplifying assumptions. First, we assume that the dynamics of the variable $\boldsymbol{\Omega}$ is driven mainly by the interaction with its thermal bath. This is equivalent to the one by Kubo (1969) that the molecular thermal bath dynamics are independent of the interaction with the variable of interest itself, **A**. Then, according to Kubo's theory, we can make the further assumption that the dynamics of **M** are Markovian. This physical constraint can be eliminated, as shown in the following (Section 10.7).

If we assume that the time evolution of $\boldsymbol{\Omega}$, Eq. 10.1.4, is Markovian then this variable plays the same role as the intramolecular manifold $\{|m\rangle\}$ of Section 9.2. While the manifold $\{|m\rangle\}$ is driven by a damping matrix, the variable $\boldsymbol{\Omega}$ is driven by an effective Liouvillian. In accordance with the basic idea of Section 9.3 we can replace the Hermitian Liouvillian

$$\hat{L}_{\boldsymbol{\Omega}} = \hat{L}_{\mathbf{M}} + \hat{L}_{\mathbf{MR}} + \hat{L}_{\mathbf{R}} \tag{10.5.8}$$

with the diffusion operator $\hat{R}_{\boldsymbol{\Omega}}$. The new total Liouvillian $\hat{L}_{\text{eff}}$ is then defined as follows:

$$i\hat{L}_{\text{eff}} = i\hat{L}_{\mathbf{S}} + \hat{R}_{\boldsymbol{\Omega}} + i\hat{L}_{\mathbf{SM}} \tag{10.5.9}$$

It is worthwhile to remark that this effective Liouvillian concerns a new "phase space" where the variable $\boldsymbol{\Omega}$ is replaced by an operator $\hat{\boldsymbol{\omega}}$ acting on the space spanned by the eigenstates of the operator $\hat{R}_{\boldsymbol{\Omega}}$. The corresponding Liouville equation provides a time evolution for $\hat{\boldsymbol{\omega}}$ which depends also on the interaction with the variable of interest. This remark, as shown in Appendix E, leads us to eliminate a well-known flaw of the SLE theory (Appendix F) which results in an incorrect equilibrium distribution for the variable of interest.

$\hat{L}_{\text{eff}}$ is no longer Hermitian. However, the theory developed in Sections 10.3 and 10.4 allows us to obtain straightforwardly the Laplace transform of the correlation function of the spectrum of the variable of interest. We write explicitly the general result provided by Eq. 10.4.22 in the simple case where **A** and $\boldsymbol{\Omega}$ are monodimensional variables denoted by u and ω, respectively (Kubo's stochastic oscillator)(Kubo, 1969). When dealing with this problem, we can assume

$$\hat{L}_{\mathbf{SM}} = \hat{\omega} \tag{10.5.10}$$

The diffusion operator

$$\hat{R}_{\boldsymbol{\Omega}} = \gamma\frac{\partial}{\partial\omega}\left(\Delta^2\frac{\partial}{\partial\omega} + \omega\right) \tag{10.5.11}$$

can be expressed over the basis set of its eigenstates

$$p_n(\Omega) = [(2\pi)^{1/2}n!]^{-1/2}2^{-n/2}H_n\left(\frac{\omega}{\sqrt{2}\Delta}\right)e^{-\omega^2/2\Delta^2} \tag{10.5.12}$$

(where the symbol H_n denotes the Hermite polynomials), as follows:

$$\hat{R}_\Omega = \begin{pmatrix} 0 & 0 & 0 & \dots & 0 \\ 0 & -\gamma & 0 & \dots & 0 \\ 0 & 0 & -2\gamma & \dots & 0 \\ \vdots & \vdots & \vdots & \ddots & \vdots \\ 0 & 0 & 0 & \dots & -n\gamma \\ \vdots & \vdots & \vdots & & \ddots \end{pmatrix} \tag{10.5.13}$$

By using the formalism of the simple monodimensional case of Section 10.3 we put

$$|f_0\rangle = |u\rangle|p_0(\omega)\rangle \tag{10.5.14}$$

From Eq. 10.2.15 we obtain

$$\begin{aligned} |f_1\rangle &= [1 - (|u\rangle\langle u|)(|p_0(\omega)\rangle\langle p_0(\omega)|)](i\hat{L}_S + i\hat{\omega} + \hat{R}_\Omega)|\mu\rangle|p_0(\omega)\rangle \\ &= i|u\rangle|p_1(\omega)\rangle\langle p_1|\hat{\omega}|p_0\rangle \end{aligned} \tag{10.5.15}$$

The nth-order state is given by Eq. 10.2.20. In the present case this equation reads

$$|f_n\rangle = i^n|u\rangle|p_n(\omega)\rangle\langle p_n|\hat{\omega}|p_{n-1}\rangle \cdots \langle p_1|\hat{\omega}|p_0\rangle \tag{10.5.16}$$

Equation 10.2.33 provides the following "energies":

$$\lambda_k = \langle\tilde{f}_k|\hat{\mathcal{L}}_k|f_k\rangle\langle\tilde{f}_k|f_k\rangle^{-1} = i\omega_0 - k\gamma \tag{10.5.17}$$

where ω_0 is the proper frequency of the free oscillator ($\omega_0 = \langle\mu|L_S|\mu\rangle$).

Furthermore, by using suitable properties of Hermite polynomials (Spain and Smith, 1970), we obtain

$$\Delta_n^2 = -\frac{\langle\tilde{f}_n \mid f_n\rangle}{\langle\tilde{f}_{n-1} \mid f_{n-1}\rangle} = n\Delta^2 \tag{10.5.18}$$

By using now the general result of Eq. 10.3.35 we arrive at the Sack type continued fraction (Chapter 2):

$$I(\omega) = \frac{1}{\pi}\cfrac{1}{i\omega + \cfrac{\Delta^2}{i\omega + \gamma + \cfrac{2\Delta^2}{i\omega + 2\gamma + \ddots}}}, \quad \omega_0 = 0 \tag{10.5.19}$$

In this simple case Eq. 10.5.19 coincides with that of cumulant expansion, which can be proved to be (Kubo, 1969)

$$I(\omega) = 2\,\mathrm{Re}\int_0^{+\infty} \exp\left(\frac{\Delta^2}{\gamma^2}(e^{-\gamma t} - 1 + \gamma t) - i\omega t\right) dt \tag{10.5.20}$$

The use of the multidimensional continued fraction resulting from Eq. 10.4.22 would enable one to work unaffected by the kind of difficulties present in the cumulant approach for multidimensional stochastic variables (Ferrario and Evans, 1981). This is a fundamentally important result because the generalized version of Eq. 10.5.19 allows us in principle to describe, in terms of one parameter only (the matrix or supermatrix, Chapter 5 γ), the spatial as opposed to planar, rotational, or rototranslational diffusion of the asymmetric top. This circumvents the conceptual difficulties of planar itinerant libration, and generalizes the theory described in Chapter 4.

10.6 THE REPLACEMENT OF THE GENERALIZED LANGEVIN EQUATION WITH A MARKOVIAN ONE OF ENLARGED DIMENSIONS

In this and the following sections we demonstrate some further advantageous features of the Mori approach to relaxation phenomena in molecules. These are revealed through the use of the Fokker–Planck equations associated with non-Markovian processes.

For simplicity we focus our attention on the monodimensional variable of interest a driven by a Hermitian Liouvillian for which the generalized Langevin equation (GLE) reads

$$\frac{d}{dt}a = i\omega(t)a(t) - \int_0^t \varphi(t-s)a(s)\,ds + f(t) \tag{10.6.1}$$

where

$$f(t) = \exp(i\hat{Q}_0\hat{L}t)\hat{Q}_0 iLa \tag{10.6.2}$$

$$\varphi(t) = \frac{(f(t), f^+)}{(a, a^+)} \tag{10.6.3}$$

$$i\omega = \frac{(i\hat{L}a, a^+)}{(a, a^+)} \tag{10.6.4}$$

$$\hat{Q}_0 = 1 - \hat{P}_0 \tag{10.6.5}$$

$\hat{P}_0$ is the projection operator of the variable a defined, as usual, by

$$\hat{P}_0 b = (b, a^+)(a, a^+)^{-1}a \tag{10.6.6}$$

In the previous sections of this chapter we derived the GLE as a zero-order case of an infinite set of generalized Langevin equations using a chain of operators which, in the monodimensional and Hermitian case, may be written as follows:

$$f_k = i\hat{L}_k f_{k-1} \tag{10.6.7}$$

where

$$\hat{L}_k = (1 - \hat{P}_k)\hat{L}_{k-1} \tag{10.6.8}$$

$$\hat{P}_k g = \frac{(g, f_k^+)}{(f_k, f_k^+)} f_k \tag{10.6.9}$$

and

$$\hat{L}_0 = \hat{L} \tag{10.6.10}$$

$$\hat{L}_0 = \hat{L} \tag{10.6.11}$$

It is a natural result of our remarks in Sections 10.2–10.4 to try to understand what happens if we define our variable of interest as being the following multidimensional one:

$$\mathbf{A} = \begin{pmatrix} f_0 \\ f_1 \\ \vdots \\ f_{n-1} \\ f_n \end{pmatrix} \tag{10.6.12}$$

The problem has been dealt with in a paper by Mori and co-workers (Karasudani et al., 1979). The main aim of their work has been that of relating the correlation functions $[\exp(it\hat{L}_{j+1})f_{j+1}, f_{j+1}^+]/(f_j, f_j^+)$ to those of the form $[\exp(itL)f_{j+1}, f_{j+1}^+]/(f_j, f_j^+)$, depending on the total Liouvillian of the system. Our main aim is to find a natural approach to building up multidimensional Langevin equations such as those studied in Appendix A.

In the Hermitian case the multidimensional theory of Section 10.4 results in the following GLE:

$$\frac{d}{dt}\mathbf{A} = i\boldsymbol{\Omega}\mathbf{A}(t) - \int_0^t \boldsymbol{\Phi}(t-s)\mathbf{A}(s)\,ds + \mathbf{F}(t) \tag{10.6.13}$$

where

$$\mathbf{F}(t) = \exp(i\hat{Q}\hat{L}t)\hat{Q}iL\mathbf{A} \tag{10.6.14}$$

$$\boldsymbol{\Phi}(t) = (\mathbf{F}(t), \mathbf{F}^+)(\mathbf{A}, \mathbf{A}^+)^{-1} \tag{10.6.15}$$

$$i\boldsymbol{\Omega}(t) = (iL\mathbf{A}, \mathbf{A}^+)(\mathbf{A}, \mathbf{A}^+)^{-1} \tag{10.6.16}$$

In the present multidimensional case, of course, the projection operators are given by

$$\hat{Q} = \hat{1} - \hat{P} \tag{10.6.17}$$

$$\hat{P} = \sum_{i=0}^{n} \hat{P}_i \tag{10.6.18}$$

Since the variables f_k are mutually orthogonal we obtain

$$\hat{Q} = \prod_{i=0}^{n} \hat{Q}_i \tag{10.6.19}$$

Equation 10.6.19 allows us to obtain an important property of the fluctuating force $\mathbf{F}(t)$ (Eq. 10.6.14). In fact, by using Eq. 10.6.19 we can write

$$\begin{aligned} \hat{Q}iLf_k &= (\hat{1} - \hat{P}_n)\cdots(\hat{1} - \hat{P}_{k+1})(\hat{1} - \hat{P}_k)\cdots(\hat{1} - \hat{P}_0)i\hat{L}f_k \\ &= (\hat{1} - \hat{P}_n)\cdots(\hat{1} - \hat{P}_{k+1})i\hat{L}_{k+1}f_k \\ &= (\hat{1} - \hat{P}_n)\cdots(\hat{1} - \hat{P}_{k+1})f_{k+1} = 0, \quad k < n \end{aligned} \tag{10.6.20}$$

As a consequence, the only nonvanishing component of $\mathbf{F}(t)$ is the last one. The fluctuating force $\mathbf{F}(t)$ can then be written as follows:

$$\mathbf{F}(t) = \begin{pmatrix} 0 \\ 0 \\ \vdots \\ \exp(i\hat{Q}\hat{L}t)\hat{Q}i\hat{L}f_n \end{pmatrix} \tag{10.6.21}$$

By using Eqs. 10.6.15 and 10.6.21 we can write the memory kernel $\boldsymbol{\Phi}$ as follows:

$$\boldsymbol{\Phi}(t) = \begin{pmatrix} 0 \ldots 0 \\ \vdots \quad \vdots \\ 0 \ldots \varphi_n(t) \end{pmatrix} \tag{10.6.22}$$

where

$$\varphi_n(t) = \frac{(f_{n+1}(t), f_{n+1}^+)}{(f_n, f_n^+)} \tag{10.6.23}$$

As far as $i\boldsymbol{\Omega}\mathbf{A}(t)$ (Eq. 10.6.13) is concerned, we note that the element (i, j) of this matrix is the matrix element of the "operator" L on the basis set of the "states" f_j. Such a matrix is tridiagonal in structure. In fact, if $j' > j + 1$ we have

$$\begin{aligned} (\hat{L}_0 f_j, f_{j'}^+) &= ((\hat{1} - \hat{P}_{j'-1})\cdots(\hat{1} - \hat{P}_j)(\hat{1} - \hat{P}_{j-1})\cdots(\hat{1} - \hat{P}_0)\hat{L}_0 f_j, f_{j'-1}^+) \\ &= ((\hat{1} - \hat{P}_{j'-1})\cdots(\hat{1} - \hat{P}_{j+1})f_{j+1}, f_{j'-1}^+) = 0 \end{aligned} \tag{10.6.24}$$

By exploiting the Hermitian property of the "operator" $\hat{L}$ it is also possible to show that

$$(\hat{L}f_{j'}, f_j^+) = 0 \qquad \text{if } j' > j + 1 \tag{10.6.25}$$

We can focus our attention on the nonvanishing matrix elements of the "operator" L.

For the diagonal elements, we obtain

$$\frac{(\hat{L}_0 f_i, f_i^+)}{(f_i, f_i^+)} = \frac{((\hat{1} - \hat{P}_{i-1})(\hat{1} - \hat{P}_{i-2})\cdots(\hat{1} - \hat{P}_0)\hat{L}_0 f_i, f_i^+)}{(f_i, f_i^+)} = \lambda_i / i \tag{10.6.26}$$

and

$$(f_{j+1}, f_{j+1}^+) = ((\hat{1} - \hat{P}_j)(\hat{1} - \hat{P}_{j-1}) \cdots (\hat{1} - \hat{P}_0) i\hat{L}_0 f_j, f_{j+1}^+)$$
$$= (\hat{L}_0(\hat{1} - \hat{P}_j)(\hat{1} - \hat{P}_{j-1}) \cdots (\hat{1} - \hat{P}_0)(\hat{1} - \hat{P}_j) \cdots (\hat{1} - \hat{P}_0)\hat{L}_0 f_j, f_j^+)$$
$$= -i(\hat{L}_0 f_{j+1}, f_i^+) = i(\hat{L}_0 f_j, f_{j+1}^+) \tag{10.6.27}$$

Consequently

$$-\frac{i(\hat{L}_0 f_{j+1}, f_j^+)}{(f_j, f_j^+)} = \frac{(f_{j+1}, f_{j+1}^+)}{(f_j, f_j^+)} = \Delta_{j+1}^2 \tag{10.6.28}$$

$$\frac{i(\hat{L}_0 f_j, f_{j+1}^+)}{(f_{j+1}, f_{j+1})} = \hat{1} \tag{10.6.29}$$

To obtain Eqs. 10.6.28 from Eq. 10.6.24 we have used both the Hermitian and idempotent properties of $\hat{P}_k$. The interesting result of this algebra is that the matrix elements of $\hat{L}$ can be expressed in terms of the parameters λ_i and Δ_j^2, introduced in Section 10.2. It is now clear that the $i\lambda_i$'s can be regarded as being the "energies" of the "states" f_i. The parameters Δ_j^2 can then be regarded as the coupling between two adjacent states of the Mori chain. In the present Hermitian case, of course, this coupling is not dissipative in nature. When dealing with the general case of Section 10.3, Eq. 10.3.33, we could also take into account a dissipative coupling between two adjacent states of the chain.

The matrix $i\boldsymbol{\Omega}$ can thus be written as

$$i\boldsymbol{\Omega} = \begin{pmatrix} i\omega_0 & 1 & 0 & 0 & \cdots & \cdots & \cdots & \cdots \\ -\Delta_1^2 & i\omega_1 & 1 & 0 & \cdots & \cdots & \cdots & \cdots \\ 0 & -\Delta_2^2 & i\omega_2 & 1 & \cdots & \cdots & \cdots & \cdots \\ 0 & 0 & -\Delta_3^2 & i\omega_3 & \cdots & \cdots & \cdots & \cdots \\ \cdots & \cdots & \cdots & \cdots & \cdots & \cdots & \cdots & \cdots \\ \cdots & \cdots & \cdots & \cdots & \cdots & \cdots & \cdots & \cdots \\ \cdots & \cdots & \cdots & \cdots & \cdots & \cdots & i\omega_{n-1} & 1 \\ \cdots & \cdots & \cdots & \cdots & \cdots & \cdots & -\Delta_n^2 & i\omega_n \end{pmatrix} \tag{10.6.30}$$

We can now assume that the memory kernel $\boldsymbol{\Phi}$ of Eq. 10.6.15 has a very short lifetime. If the variable $\mathbf{A}$ does not change very much in the interval τ_c, we can write

$$\int_0^t \boldsymbol{\Phi}(t-s)\mathbf{A}(s)\,ds = \int_{t-t_c}^t \boldsymbol{\Phi}(t-s)\mathbf{A}(s)\,ds = \left[\int_{t-t_c}^t \boldsymbol{\Phi}(t-s)\right]\mathbf{A}(t)$$
$$= \left[\int_0^\infty \boldsymbol{\Phi}(\tau)\,d\tau\right]\mathbf{A}(t) \tag{10.6.31}$$

As a consequence, we obtain the following multidimensional Langevin equation

$$\frac{d}{dt}\mathbf{A} = i\boldsymbol{\Omega}\mathbf{A}(t) - \boldsymbol{\Gamma}\mathbf{A}(t) + \mathbf{F}(t) \tag{10.6.32}$$

where

$$\boldsymbol{\Gamma} = \begin{pmatrix} 0 & 0 & \cdots & 0 \\ 0 & 0 & \cdots & 0 \\ \cdots & \cdots & \cdots & \cdots \\ \cdots & \cdots & \cdots & \cdots \\ \cdots & \cdots & \cdots & \cdots \\ 0 & 0 & \cdots & \int_0^\infty \varphi_n(t)\,dt \end{pmatrix} \tag{10.6.33}$$

If the nth-order of the Mori chain is Markovian in nature this corresponds to replacing the Hermitian Liouvillian governing the dynamics of a with the following:

$$i\hat{L}_0' = \hat{\mathscr{L}}_0' = \begin{pmatrix} i\omega_0 & 1 & 0 & 0 & \cdots & \cdots & \cdots \\ -\Delta_1^2 & i\omega_1 & 1 & 0 & \cdots & \cdots & \cdots \\ 0 & -\Delta_2^2 & i\omega_2 & 1 & \cdots & \cdots & \cdots \\ \cdots & \cdots & \cdots & \cdots & \cdots & \cdots & \cdots \\ \cdots & \cdots & \cdots & \cdots & \cdots & i\omega_{n-1} & 1 \\ \cdots & \cdots & \cdots & \cdots & \cdots & -\Delta_n^2 & i\omega_n - \hat{\varphi}_n(0) \end{pmatrix} \tag{10.6.34}$$

However, this replacement results in a theoretical difficulty. The theory developed in Sections 10.3 and 10.4, in principle, makes it possible to deal with non-Hermitian Liouvillian operators such as that of Eq. 10.6.34. However, the fluctuating force of Eq. 10.6.32 cannot be introduced in a proper way. To circumvent the difficulty we replace Eq. 10.6.32 with its instantaneous average. We know that the instantaneous average of the fluctuating force vanishes unless the thermal bath is far from its equilibrium distribution at $t = 0$ and therefore if the number of "virtual" variables is large enough, the thermal bath of the last variable of the chain can attain its equilibrium distribution very quickly (recall the general discussion of Section 9.2). As a consequence, the assumption that the time instantaneous average of the fluctuating force is zero is sound. The reasoning is valid also in Section 10.5 (SLE). The damping contributions affecting any variable of that generalized Mori chain can be related to a corresponding fluctuating force, the time average of which is assumed to be zero. It is now clear that this assumption has the same consequence as the Markovian assumption that sets up the damping in the first place.

However, the fluctuating force may not have a vanishing average if the system under study is non-Markovian. In order to clarify this important point we follow Ferrario and Grigolini (1979b). From Eq. 10.6.32 we see that the equation of motion of the $(n-1)$th-order component of the Mori chain is determined by the interaction with the last component as follows:

$$\dot{f}_{n-1}(t) = i\omega_{n-1} f_{n-1}(t) + f_n(t) \tag{10.6.35}$$

$$\dot{f}_n(t) = -\Delta_n^2 f_{n-1}(t) + (i\omega_n - \gamma_n) f_n(t) + F(t) \tag{10.6.36}$$

where

$$\gamma_n = \int_0^\infty \varphi_n(t)\, dt \tag{10.6.37}$$

We have to Laplace transform this system. The expression for $\hat{f}_n(z)$ is replaced by that for $\hat{f}_{n-1}(z)$. The new expression is then shown to be the Laplace transform of the following equation:

$$\dot{f}_{n-1}(t) = \lambda_n f_{n-1}(t) - \int_0^t ds\, f_{n-1}(s)\varphi_{n-1}(t-s) + f_n(t) \tag{10.6.38}$$

where

$$\hat{\varphi}_{n-1}(z) = \frac{\Delta_n^2}{z - \lambda_n + \gamma_n} \tag{10.6.39}$$

and

$$\hat{f}_n(z) = \frac{\hat{F}(z) + f_n(0)}{z - \lambda_n + \hat{\varphi}_n(z)} \tag{10.6.40}$$

By repeating this approach n times, we obtain

$$\dot{a}(t) = \lambda_0 a(t) - \int_0^t ds\, a(s)\varphi_0(t-s) + f_1(t) \tag{10.6.41}$$

where

$$\hat{f}_1(z) = \frac{1}{z - \lambda_1 + \hat{\varphi}_1(z)} \left\{ \frac{1}{z - \lambda_2 + \hat{\varphi}_2(z)} \times \left[\ldots \left(\frac{1}{z - \lambda_n + \gamma_n} [\hat{F}(z) + f_n(0)] + f_{n-1}(0) \right) + \cdots \right] + f_1(0) \right\} \tag{10.6.42}$$

$$\hat{\varphi}_0(z) = \cfrac{\Delta_1^2}{z - \lambda_1 + \cfrac{\Delta_2^2}{z - \lambda_2 + \cfrac{\Delta_3^2}{z - \lambda_3 + \ddots \cfrac{\Delta_n^2}{z - \lambda_n + \gamma_n}}}} \tag{10.6.43}$$

Comparing now Eqs. 10.6.41 and 10.6.1, then as far as "memory kernels" are concerned, we see that Eq. 10.6.43 is just the continued fraction expression for $\hat{\varphi}(z)$ given by the theory of Section 10.2 when the Mori chain is truncated at nth order. As far as $\hat{f}_1(z)$ is concerned its average value depends even on the values of the virtual variables $f_1(0)$, $f_2(0), \ldots, f_n(0)$. In consequence the instantaneous average value of $f_1(t)$ can also be different from zero, if the average values of the variables f_1, $f_2, \ldots, f_n$ do not vanish at $t = 0$ (this feature has been emphasized throughout Chapters 9, and the foregoing sections of Chapters 10).

Therefore Eq. 10.6.41 is not completely equivalent to Eq. 10.6.1 if the latter is derived from the standard Mori theory based on the assumption that the thermal bath of the variable a at $t = 0$ is close to its thermal equilibrium.

The theory developed in this section also enables one to obtain the expression of the Liouvillian used in Section 10.2 in a more elegant fashion (Appendix B). It is also possible to apply this approach to the case where $i\hat{\mathscr{L}}_0$ is a non-Hermitian dynamic operator such as that of the preceding section. The multidimensional Langevin equation results then in the same a.c.f. as the SLE, whereas the higher-order correlation functions are not affected by the flaw of Kubo's theory (Appendix D). The kind of generalized Langevin equation under discussion is more general than the well-known one by Mori in the sense both that $i\hat{\mathscr{L}}_0$ is not Hermitian and that the fluctuating force $f(t)$ also depends on the excited thermal bath dynamics.

10.7 THE FOKKER-PLANCK EQUATION ASSOCIATED WITH THE CLASSICAL GLE

Equation 10.6.32 is similar to the multidimensional Langevin equation by Fox and Uhlenbeck (Fox and Uhlenbeck, 1970). These authors were able to build up a Fokker–Planck equation associated with this kind of Langevin equation (Appendix A). After assessing that our multidimensional Langevin equation really belongs to the same family as that of Fox and Uhlenbeck, we use their generalized Fokker–Planck equation.

We can check the validity of the approach which led us to replace the GLE with the Langevin equation of Markovian nature given by Eq. 10.6.32. We show that the latter equation satisfies the fluctuation–dissipation theorem of the Fox–Uhlenbeck theory (Eq. 10.A.15).

The matrix $\mathbf{G}$ of Eq. 10.A.4a can be written as follows:

$$-\mathbf{G} = i\boldsymbol{\Omega} - \boldsymbol{\Gamma} = \begin{pmatrix} i\omega_1 & 1 & 0 & 0 & . & . \\ -\Delta_1^2 & i\omega_2 & 1 & 0 & . & . \\ 0 & -\Delta_2^2 & i\omega_3 & 1 & . & . \\ 0 & 0 & -\Delta_3^2 & i\omega_4 & . & . \\ . & . & . & . & . & 1 \\ . & . & . & . & -\Delta_n^2 & i\omega_n - \gamma_n \end{pmatrix} \tag{10.7.1}$$

Fox and Uhlenbeck used vanishing proper frequencies; therefore we assume

$$\omega_i = 0 \qquad \text{for } 1 \leqslant i \leqslant n \tag{10.7.2}$$

In order to express the parameters Δ_i^2 in the Fox formalism (Fox, 1978) we have to choose a suitable kind of scalar product. In a classical case such as

that under discussion, a convenient scalar product is

$$(F, G^+) = \langle FG^* \rangle = \int \cdots \int FG^+ w_0(\Gamma)\, d\Gamma \tag{10.7.3}$$

where Γ is a point of the classical phase space and w_0 is the corresponding equilibrium distribution. We can then write the fluctuation–dissipation relation of the Mori theory in the Fox formalism as follows:

$$\mathbf{\Phi}(t) = \langle \tilde{\mathbf{F}}(t)\tilde{\mathbf{F}}^*(0)\rangle [\mathbf{A}(0)\mathbf{A}^+(0)]^{-1} \tag{10.7.4}$$

Furthermore, the matrix $[\mathbf{A}(0)\mathbf{A}^+(0)]$ can be identified with the matrix $\mathbf{E}^{-1}$ of the Fox–Uhlenbeck theory. Since our matrix $(\mathbf{A}, \mathbf{A}^+)$ is diagonal the matrix $\mathbf{E}$ also is diagonal. Therefore from Eq. 10.A.15 we have

$$2Q_{ij} = G_{ij}E_{jj}^{-1} + E_{ii}^{-1}G_{ij} \tag{10.7.5}$$

The expression of $\mathbf{G}$ given by Eq. 10.7.1 and Eq. 10.7.5 result in

$$E_{i+1,\,i+1}^{-1} = E_{ii}^{-1}\Delta_i^2 \qquad \text{for } i < n \tag{10.7.6}$$

$$Q_{nn} = \gamma_n E_{nn}^{-1} \tag{10.7.6a}$$

By definition (Eq. 10.2.41)

$$\Delta_i^2 = \frac{(f_{i+1}, f_{i+1}^+)}{(f_i, f_i^+)} \tag{10.7.7}$$

and Eq. 10.7.6 is completely satisfied.

Equation 10.7.6a is the fluctuation–dissipation relation in the Markovian limit. When we make the Markovian constraint on the memory kernel of Eq. 10.6.1, the fluctuation–dissipation theorem of Eq. 10.6.3 results in Eq. 10.7.6a. No theoretical impediment is then encountered in using the results described in Appendix A. Since Eq. 10.6.32 belongs to the same category as Eq. 10.A.1 we arrive at the following result: when the memory kernel of the GLE

$$\frac{d}{dt}a = i\omega a(t) - \int_0^t \varphi(t-s)a(s)\, ds + f(t) \tag{10.7.8}$$

is expressed in the continued fraction expansion

$$\hat{\varphi}(z) = \cfrac{\Delta_1^2}{z - i\omega_1 + \cfrac{\Delta_2^2}{z - i\omega_2 + \ddots \cfrac{\Delta_{n-1}^2}{z - i\omega_n + \gamma_n}}} \tag{10.7.9}$$

then the Fokker–Planck equation to be associated with Eq. 10.7.8 is† (summation on repeated indices is understood)

$$\frac{\partial}{\partial t_2}P_2(\mathbf{a}_1t_1; \mathbf{a}_2t_2) = \frac{\partial}{\partial a_{2i}}(G_{ij}a_{2j}P_2(\mathbf{a}_1t_1; \mathbf{a}_2t_2)) + \frac{1}{2}\frac{\partial}{\partial a_{2i}}(2\mathbf{Q})_{ij}\frac{\partial}{\partial a_{2j}}P_2(\mathbf{a}_1t_1; \mathbf{a}_2t_2) \tag{10.7.10}$$

Using Eq. 10.7.1 for $\mathbf{G}$ we can also write Eq. 10.7.10 as follows:

$$\frac{\partial}{\partial t_2}P_2(\mathbf{a}_1t_1; \mathbf{a}_2t_2) = \sum_{j\neq i}\frac{\partial}{\partial a_{2i}}(G_{ij}a_{2j}P_2(\cdots)) + \hat{\Gamma}_nP_2(\cdots) \tag{10.7.11}$$

where

$$\hat{\Gamma}_n = \gamma_n\left(\frac{\partial}{\partial a_{2n}}a_{2n} + E_{nn}^{-1}\frac{\partial^2}{\partial a_{2n}^2}\right) \tag{10.7.12}$$

Equation 10.7.12 is the standard diffusion operator of the variable a_n assumed to be Markovian and Gaussian. Equation 10.7.11 may be given a suggestive physical interpretation. We can regard the "diffusion" of the stochastic variable $\mathbf{a}$ as driven by a nondissipative part, the first term on the right side of Eq. 10.7.11, plus the sink contribution $\Gamma_nP_2(\cdots)$. The dissipation contribution comes from the fact that the last component of the variable $\mathbf{a}$ is stochastic in nature. In other words, the physical meaning of Eq. 10.7.11 is the same as that of the following generalized continuity equation of fluid dynamics (recall Eq. 9.B.8)

$$\frac{\partial}{\partial t}\rho = -\operatorname{div} v\rho + \Gamma\rho \tag{10.7.13}$$

where the mass conservation is corrected by the presence of the sink contribution Γ. This equation has been used in Chapter 9, Appendix D, to build up the SLE in accordance with Kubo's approach.

When (1) the coupling between the variables of interest and the last stochastic one is linear and (2) the stochastic process affecting the latter is of Gaussian–Markovian kind, Eq. 10.7.13 provides the same result as the Fox–Uhlenbeck theory. However, even in the case when condition 1 or 2, or both, are not satisfied this equation enables us to build up a Fokker–Planck equation. In the next section we consider what happens when condition 2 is not satisfied. Here we comment briefly on the case where condition 1 is not satisfied. We follow the synthetic proof given by van Kampen (1976):

Let $\mathbf{u}$ be an n-dimensional vector, and let $\mathbf{F}(\mathbf{u}, t; y)$ a vector function of $\mathbf{u}$, t, and one additional variable y. Consider the equation

$$\dot{\mathbf{u}} = \mathbf{F}(\mathbf{u}, t; y) \tag{10.7.14}$$

†The observable $\mathbf{A}$ when regarded as being a stochastic variable is denoted by the symbol $\mathbf{a}$.

where $y(t)$ is a stochastic process. The restriction to be made now is that η is taken to be a Markovian process such that its probability density $\Pi(y, t)$ obeys a master equation

$$\dot{\Pi}(y, t) = W\Pi(y, t) \tag{10.7.15}$$

In general the coupling between $\mathbf{u}$ and y may be of nonlinear nature. The idea applied by van Kampen is that for equations of this type the $(n+1)$-component variable $(u_1, u_2, \ldots, u_n\ y)$ is again a Markov process. Its probability density $\mathcal{P}(\mathbf{u}, y, t)$ varies in time owing to the flow in $\mathbf{u}$-space and the stochastic fluctuations of $\mathbf{u}$. The corresponding master equation is found by using Eq. 10.7.13. We obtain

$$\frac{\partial \mathcal{P}(\mathbf{u}, y, t)}{\partial t} = \frac{\partial}{\partial \mathbf{u}}[\mathbf{F}(\mathbf{u}, y)\mathcal{P}(\cdots)] + WP \tag{10.7.16}$$

The theory developed in this section allows us to eliminate the restriction that y be a Markovian process. In fact, we can replace y with a multidimensional variable $\mathbf{Y}$† driven by a master equation such as that of Eq. 10.7.10. Then by following again the kind of approach which led us to Eq. 10.7.16 we can obtain without any difficulty the generalized result

$$\frac{\partial}{\partial t}\mathcal{P}(\mathbf{u}, \mathbf{Y}, t) = \frac{\partial}{\partial \mathbf{u}}[\mathbf{F}(\mathbf{u}, y)\mathcal{P}(\cdots)] + \mathbf{W}_{\mathbf{Y}}\mathcal{P}(\cdots) \tag{10.7.17}$$

where $\mathbf{W}_{\mathbf{Y}}$ is just the multidimensional diffusion operator driving the variable $\mathbf{Y}$ (which can be built up along the lines described above).

By applying the idea to the semiclassical counterpart of Eq. 10.7.14 it has been possible to study a stochastic quantum mechanical oscillator more general than that of Kubo (Ferrario and Grigolini, 1979b).

10.8 NON-GAUSSIAN–NON-MARKOVIAN CASE

In the classical case we have not yet available a rigorous demonstration such as the quantum mechanical one of Appendix G, which can justify the attainment of the canonical distribution at thermodynamic equilibrium. However, even in the quantum mechanical case some difficulties arise as the Markovian constraint is released (Grigolini et al. 1981). The difficulty met in extending the result of Appendix A could be a sign of the incompatibility between the Gaussian constraint and the true (non-Markovian nature) of the molecular ensemble.

In the absence of any rigorous theory computational "experiments" may be of some usefulness in providing insights into this intriguing problem. A suitable field of investigation is provided by the computational "experiments" on molecular dynamics. In molecular dynamics simulation non-

†As usual, $\mathbf{Y}$ is a multidimensional variable the first component of which has to be identified with the variable y.

Markovian and non-Gaussian statistics can be detected. In the Gaussian limit the second-order conditional probability is provided by the well-known formula (Chapter 2)

$$P(\mathbf{u}t;\ \mathbf{u}_0\ 0) = \left(\frac{M}{2\pi kT[1-\psi_{\mathbf{u}}^2(t)]}\right)^{3/2} \times \exp\left[-\left(\frac{M[\mathbf{u}-\mathbf{u}_0\psi_{\mathbf{u}}(t)]^2}{2kT[1-\psi_{\mathbf{u}}^2(t)]}\right)\right] \tag{10.8.1}$$

where

$$\psi_{\mathbf{u}}(t) = \frac{\langle \mathbf{u}\cdot\mathbf{u}(t)\rangle}{\langle u^2\rangle} \tag{10.8.2}$$

for a Brownian particle of mass M at temperature T. It can be obtained as a simple result of the definition of the Gaussian statistical process (Stratonovich, 1963). The Markovian constraint is not implicit in Eq. 10.8.1, which is the solution of the non-Markovian Fokker–Planck equation discussed in Chapter 3. It has the same structure as the general equation found by Stratonovich (1963), obtained without using the Markovian or Gaussian assumptions. Stratonovich did not relate his results to the Langevin type of equation. This is, indeed, a limitation of Stratonovich's approach. However, the GLE, as discussed in Section 9.1, may be obtained by working directly on the Liouvillian of the system under study and, as a consequence, provides useful physical information with which to define the parameters appearing in the corresponding Fokker–Planck type of equation.

As shown by Berne and Harp (1970), Eq. 10.8.1 can be used in order to express the correlation functions

$$\epsilon_2(t) = \frac{\langle u^2(0)u^2(t)\rangle}{\langle u^4\rangle} \tag{10.8.3}$$

and

$$\epsilon_4(t) = \frac{\langle u^4(0)u^4(t)\rangle}{\langle u^8\rangle} \tag{10.8.4}$$

as functions of $\psi_u(t)$.

By evaluating integrals such as the following

$$\epsilon_{2G}(t) = \left(\frac{M}{2\pi kT}\right)^{3/2}\int d\mathbf{u}\int d\mathbf{u}_0\,\mathbf{u}\cdot\mathbf{u}\mathbf{u}_0\cdot\mathbf{u}_0 P_2(\mathbf{u}t;\ \mathbf{u}_0 0)\times\exp\left(-\frac{Mu_0^2}{2kT}\right) \tag{10.8.5}$$

it is possible to obtain

$$\epsilon_{2G} = \tfrac{3}{5}[1+\psi_{\mathbf{u}}^2(t)] \tag{10.8.6}$$

$$\epsilon_{4G} = [\tfrac{225}{945} + \tfrac{600}{945}\psi_{\mathbf{u}}^2(t) + \tfrac{120}{945}\psi_{\mathbf{u}}^4(t)] \tag{10.8.7}$$

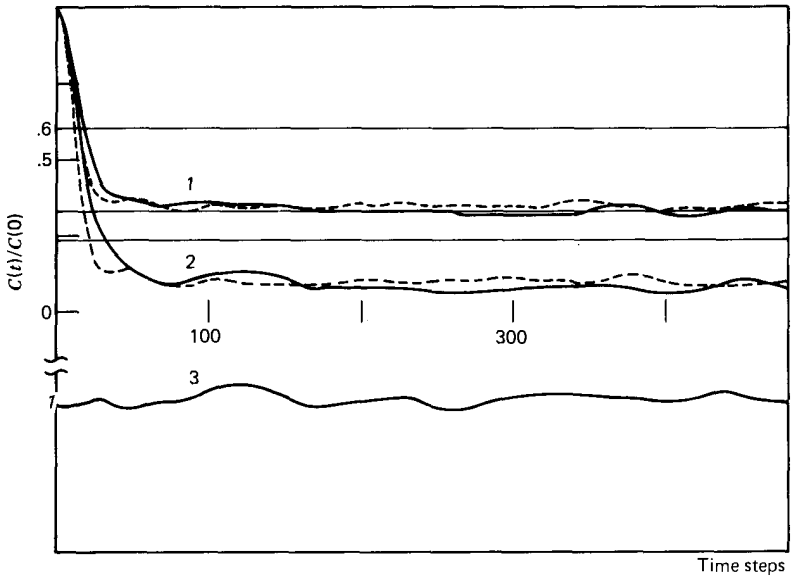

Figure 10.8.1 This is a result of recent computational experiment (Evans et al., 1980). Solid lines: (1) $\langle v^2(t)v^2(0)\rangle/\langle v^2(0)v^2(0)\rangle$; (2) $\langle v^4(t)v^4(0)\rangle/\langle v^4(0)v^4(0)\rangle$ (both in three dimensions); (3) $\langle v_x^2(t)v_y^2(0)\rangle/\langle v_x^2(0)v_y^2(0)\rangle$. Dashed lines: (1) $\langle v_x^2(t)v_x^2(0)\rangle/\langle v_x^4(0)\rangle$; (2) $\langle v_x^4(t)v_x^4(0)\rangle/\langle v_x^8(0)\rangle$.

The subscript G has been used to denote the Gaussian assumption. Equations 60.6 and 10.8.7 imply that for $t\to\infty$, ϵ_{2G} and ϵ_{4G} attain the well fixed Gaussian limits 3/5 and 225/945, respectively.

Computer simulation shows that the actual limit is well below the Gaussian limit (Fig. 10.8.1). When the Brownian particle [the polyatomic molecule of the computational experiment (Evans et al., 1980)] has the same mass as the particle of the thermal bath, then its time evolution is no longer the result of an enormous number of collisions. As a consequence, the central limit theorem (Chapter 1) can be invalidated.

So far, no theory is available in order to interpret this kind of non-Gaussian behavior. In fact, as said before, the theory of Stratonovich (1963) does not contain any indication of practical use. However, Eq. 10.7.11 can usefully be applied in order to reproduce the simulation results. In fact, in principle, the parameters defining the nondissipative interaction may be evaluated by using the Mori theory. The problem of dealing with the non-Gaussian aspects of the phenomenon under discussion is rigorously separated from that of determining the nondissipative interaction in the non-Markovian system. The last variable of the Mori chain satisfies a Markovian kind of equation such as

$$\frac{d}{dt}w = -\beta w + f(t) \tag{10.8.8}$$

The stochastic force is thus a δ-correlated force that will be defined by its moments as follows:

$$\langle f(t_1)\cdots f(t_n)\rangle = n!\epsilon_n\Delta^n\beta\delta(t_1-t_2)\delta(t_2-t_3)\cdots\delta(t_{n-1}-t_n) + (\text{Gaussian contribution}) \tag{10.8.9}$$

where

$$\Delta^2 = \langle w^2\rangle \tag{10.8.10}$$

Stratonovich (1963) showed that the master equation to be associated with Eq. 10.8.8 may be expressed in the following general form:

$$\frac{\partial}{\partial t}P = \sum_{s=1}^{\infty}\frac{1}{s!}\left(-\frac{\partial}{\partial w}\right)^s[k_s(w)P] \tag{10.8.11}$$

where

$$k_s(x) = \lim_{\Delta t\to 0}\frac{m_s(w)}{\Delta t} \tag{10.8.12}$$

and $m_s(w)$ is defined as follows:

$$m_s(w) = \langle[w(t+\Delta t)-w(t)]^s\rangle \tag{10.8.13}$$

By integration of Eq. 10.8.8 we obtain

$$\frac{w(t+\Delta t)-w(t)}{\Delta t} = -\beta w(t) + \frac{1}{\Delta t}\int_t^{t+\Delta t} f(\tau)\,d\tau \tag{10.8.14}$$

Thus, from Eq. 10.8.12,

$$k_1(w) = -\beta w \tag{10.8.15}$$

and, by using Eq. 10.8.9,

$$k_s(w) = s!\epsilon_s\Delta^s\beta \tag{10.8.16}$$

If we assume that the stochastic force is Gaussian, that is, that

$$\langle f(t_1)f(t_2)\cdots f(t_n)\rangle = 0 \qquad \text{if } n \text{ is odd} \tag{10.8.17}$$

and for n even

$$\langle f(t_1)\cdots f(t_n)\rangle = \sum\langle f(t_{i_1})f(t_{i_2})\rangle\langle f(t_{i_3})f(t_{i_4})\rangle\cdots\langle f(t_{i_{n-1}})f(t_{i_n})\rangle \tag{10.8.18}$$

(where the sum is over all the different ways of splitting the n variables into n pairs), this would be equivalent to truncating the expansion of Eq. 8.10.11 at second order. We would then obtain the usual Gaussian Fokker–Planck equation. The multidimensional version, which can be obtained from Eq. 10.7.11, would be identical with the corresponding equation of Fox (1978). As shown in Appendix A, Fox arrived at this result by using a two-time probability like that in Eq. 10.8.1.

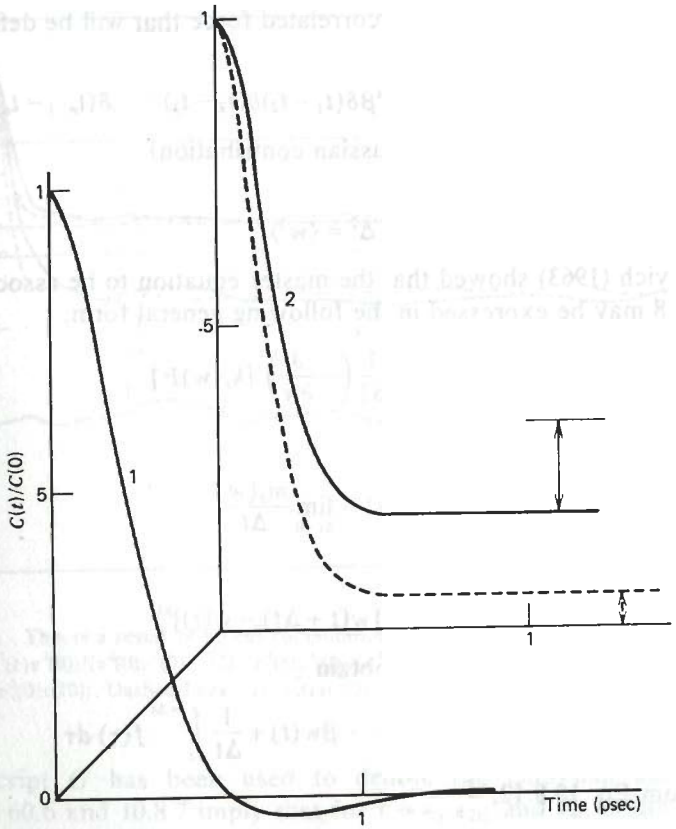

Figure 10.8.2 This is a result of the same computational "experiment" as that of Fig. 10.8.1. (1) Best fit to the simulated velocity a.c.f.; (2) $\langle v_x^2(t)v_x^2(0)\rangle/\langle v_x^4(0)\rangle$ with the non-Gaussian parameter $\epsilon_4 = 1.55$, $\epsilon_3 = 0$, $\epsilon_n = 0$ for $n > 4$; dashed lines $\langle v_x^4(t)v_x^4(0)\rangle/\langle v_x^8(0)\rangle$ with the same non-Gaussian parameters as above. Differences from Gaussian behavior shown by arrows.

If the diffusion operator $\hat{\Gamma}_n$ appearing in Eq. 10.7.11 is built up using the non-Gaussian approach outlined above, we obtain a generalized Fokker–Planck equation which is *neither* Markovian *nor* Gaussian in nature. The simplest equation of this kind is, of course, that which corresponds to a second-order Mori truncation. Its form can easily be obtained by using Eq. 10.7.11 and reads

$$\frac{\partial}{\partial t} P(v, w, t \mid v_0, w_0, 0) = \left[w\left(\frac{\partial}{\partial v} w - \frac{\partial}{\partial w} v\right) + \beta\left(\frac{\partial}{\partial w} w + \Delta^2 \frac{\partial^2}{\partial w^2} + \epsilon_3 \Delta^3 \frac{\partial^3}{\partial w^3} + \epsilon_4 \Delta^4 \frac{\partial^4}{\partial w^4} + \cdots\right)\right] P(\cdots) \tag{10.8.19}$$

where v is the variable of interest and w the "virtual" one. The agreement between theory and "experiment" provided by this equation is encouraging (Fig. 10.8.2).

10.9 RELAXATION PROCESS IN THE PRESENCE OF EXTERNAL EXCITATIONS

In Section 9.1 we mentioned some of the main problems to be solved. That of dealing with non-Markovian–non-Gaussian phenomena has been discussed in the preceding section. In Section 9.2 we showed how a further problem may be solved for "intramolecular" relaxation processes: the evaluation of the transient effects of strong exciting fields when switched on and off. This problem may be given a general solution if the quantumlike formalism of Section 10.2 is used. We show how Eq. 9.1.26 can be solved.

Of course, the quantumlike formalism of Section 10.2 can also be extended for use with multidimensional variables dealt with in Section 10.4 provided that the "scalar product" between two multidimensional variables **B** and **C** is defined as follows:

$$(\mathbf{B}, \mathbf{C}^+) = \langle \mathbf{C} \mid \mathbf{B} \rangle \tag{10.9.1}$$

As a consequence, the equation of motion of the variable $|\mathbf{f}_0\rangle$ in the presence of external interaction $\hat{\mathcal{L}}_1(t)$ is written as follows:

$$\frac{d}{dt}|\mathbf{f}_0(t)\rangle = [\hat{\mathcal{L}}_0 + \hat{\mathcal{L}}_1(t)]|\mathbf{f}_0(t)\rangle \tag{10.9.2}$$

We build up the manifold $\{|\mathbf{f}_i\rangle\}$ of the generalized Mori chain. This means that, in principle, we do not need the assumption that $i\hat{\mathcal{L}}_0$ is Hermitian. Then we define the following wave function:

$$|\psi(t)\rangle = \sum_i c_i(t)|\mathbf{f}_i\rangle \tag{10.9.3}$$

where

$$c_i(t) = \langle \mathbf{f}_i(t)\rangle \tag{10.9.4}$$

By the symbol $\langle \mathbf{f}_i(t)\rangle$ we denote a suitable average value of the variable assumed to be driven by the total dynamic operator as follows:

$$\frac{d}{dt}\mathbf{f}_i(t) = \hat{\mathcal{L}}_0 \mathbf{f}_i(t) \tag{10.9.5}$$

The actual definition of the average $\langle \cdots \rangle$ depends on the kind of problem under study. The "wave function" $|\psi(t)\rangle$ satisfies the following equation of motion:

$$\frac{d}{dt}|\psi(t)\rangle = [\hat{\mathcal{L}}_0 + \hat{\mathcal{L}}_1(t)]|\psi(t)\rangle \tag{10.9.6}$$

We can describe in a concise way the general solution to Eq. 9.1.26. The generalized Mori theory developed in Sections 10.3 and 10.4 emphasizes the importance of the biorthogonal basis set provided by the vectors $|\mathbf{f}_k\rangle$

and $\langle\tilde{\mathbf{f}}_k|$. It seems convenient therefore to relate Eq. 10.9.6 to this basis set. We then obtain

$$\frac{d}{dt}|\psi(t)\rangle = \sum_{\substack{i=1\\j=1}}^{N} |\mathbf{f}_i\rangle\langle\tilde{\mathbf{f}}_i \mid \mathbf{f}_i\rangle^{-1}\langle\tilde{\mathbf{f}}_i|[\hat{\mathscr{L}}_0 + \mathscr{L}_1(t)]|\mathbf{f}_j\rangle \times \langle\tilde{\mathbf{f}}_j \mid \mathbf{f}_j\rangle^{-1}\langle\tilde{\mathbf{f}}_j|\psi(t)\rangle \tag{10.9.7}$$

where N (including the case $N = \infty$) is the number of states required to make the corresponding space complete. In the "intramolecular" case discussed in Section 9.2 N can be finite. Since the basis set of the vectors $|\mathbf{f}_i\rangle$ has been assumed to be complete, Eq. 10.9.7 is totally equivalent to Eq. 10.9.6 and thereby to Eq. 9.1.26. The great advantage of using Eq. 10.9.7 instead of Eq. 10.9.6 is that, as shown in the previous sections, the chain of the states $|\mathbf{f}_k\rangle$ can be truncated and the remaining part of the chain can be simulated by a suitable additional damping on the last variable of the chain (another damping contribution can already be present in the non-Hermitian case). If the chain is long enough the damping is completely unaffected by the external interaction. Of course, in the case where $i\hat{\mathscr{L}}_0$ is non-Hermitian, the relaxation properties involved by this mathematical property have to be assumed as being independent on the external excitation.

In conclusion $\hat{\mathscr{L}}_0$ can be replaced by $\hat{\mathscr{L}}_0'$ of Eq. 10.6.34, even in the presence of external excitation provided that the dynamics of the part of the chain which has been disregarded are fairly rapid with respect to the times of the dynamics induced by the external interaction.

In the "intramolecular" case the thermal baths are described as belonging to the same mathematical space as the part of interest. The scalar products, furthermore, are the usual quantum mechanical scalar products. In the case where one is dealing with external thermal baths one can use a scalar product such as $(g, f^+) = \mathrm{Tr}(f^+ g\rho_b)$, where ρ_b is the equilibrium density matrix, or such as that of Appendix G. Any kind of scalar product, including the previous ones, used to deal with external thermal baths, unfortunately, is incompatible with the assumption of neglecting any direct excitation of the "reduced" thermal bath. As a consequence, in general $\hat{\mathscr{L}}_1(t)$ acts also on the "reduced" thermal bath. However, a difficult feature such as this can be dealt with provided that Eq. 10.9.7 is replaced by

$$\frac{d}{dt}|\psi(t)\rangle = \sum_{\substack{i=1\\j=1}}^{n} |\mathbf{f}_i\rangle\langle\tilde{\mathbf{f}}_i \mid \mathbf{f}_i\rangle^{-1}\langle\tilde{\mathbf{f}}_i|[\hat{\mathscr{L}}_0' + \hat{\mathscr{L}}_1(t)]|\mathbf{f}_j\rangle \times \langle\tilde{\mathbf{f}}_j \mid \mathbf{f}_j\rangle^{-1}\langle\tilde{\mathbf{f}}_j \mid \psi(t)\rangle \tag{10.9.8}$$

where, as shown in Section 10.6, $\hat{\mathscr{L}}_0'$ is obtained from $\hat{\mathscr{L}}_0$ by substituting for $\langle\tilde{\mathbf{f}}_n|\mathscr{L}_0|\mathbf{f}_n\rangle$ the matrix $\boldsymbol{\lambda}_n - \Delta_{n+1}^2\hat{\boldsymbol{\Phi}}_{n+1}(0)$. We hope, of course, $n \ll N$.

The great advantage of replacing Eq. 9.1.26 with Eq. 10.9.8 is then that the relaxation properties are completely independent of the excitation process. Of course, as mentioned in Section 10.6 the replacement of $\hat{\mathscr{L}}_0$ with $\hat{\mathscr{L}}_0'$ prevents us from dealing with stochastic forces, the instantaneous average of which has to be assumed zero. However, if the number of "virtual" states $|\mathbf{f}_i\rangle$ included in the Mori chain is large enough, the corresponding "virtual" bath can be assumed to be always close to equilibrium during all the excitation process.

To preserve the structure of the Langevin equation, one could follow the approach of Section 10.6 using the variable of interest $\mathbf{A} = (\mathbf{f}_0, \mathbf{f}_1, \ldots, \mathbf{f}_n)$. Then the same approach as that of Section 10.6 should be followed with the additional difficulty of dealing with the time-ordered exponential. However, the stochastic force and the memory kernel would have the same matricial structure as that of Eqs. 10.6.21 and 10.6.22. The presence of external excitation on both stochastic force and memory kernel can be neglected because its dynamic effects are not significant when the unperturbed dynamics are extremely fast (the correlation time τ_c vanishes). If $\mathbf{f}_0$ were monodimensional, we would obtain the following Langevin equation:

$$\frac{d}{dt}\mathbf{A} = (i\boldsymbol{\Omega} - \boldsymbol{\Gamma})\mathbf{A} + \mathbf{F}(t) - i\boldsymbol{\Omega}_1(t) \tag{10.9.9}$$

where $\boldsymbol{\Omega}$, $\boldsymbol{\Gamma}$, and $\mathbf{F}$ are provided by Eqs. 10.6.30, 10.6.33, and 10.6.21, respectively. As far as $\boldsymbol{\Omega}_1(t)$ is concerned, it is defined by

$$[\boldsymbol{\Omega}_1(t)]_{ij} = (\hat{\mathscr{L}}_1(t)\mathbf{f}_i, \mathbf{f}_j^+)(\mathbf{f}_i, \mathbf{f}_j^+)^{-1} \tag{10.9.10}$$

Ferrario and Grigolini (1981) have discussed the corresponding multidimensional case.

10.10 EMISSION SPECTRA IN THE PRESENCE OF EXCITATION RADIATION FIELDS

As a last advantageous feature of the approach described in this chapter, we stress its usefulness for dealing with the problem of emission.

To do it, we shall use a general result of quantum optics (Agarwal, 1974). According to Agarwal, the number of photons emitted in the mode $\mathbf{k}s$ is given by

$$N_{\mathbf{k}s}(t) = \sum_{ij} g_{i\mathbf{k}s}g_{j\mathbf{k}s}^* \int_0^t dt_1 \int_0^{t_1} dt_2 \exp[-i\omega_{\mathbf{k}s}(t_1 - t_2)] \times \langle s_i^+(t_1)s_j^-(t_2)\rangle + \text{H.C.} \tag{10.10.1}$$

The rate of change of photons in the mode $\mathbf{k}s$ is then given by

$$\sigma_{\mathbf{k}s}(t) = \sum_{ij} g_{i\mathbf{k}s}g_{j\mathbf{k}s}^* \int_0^t d\tau \exp[-i\omega_{\mathbf{k}s}(t-\tau)]\langle s_i^+(t)s_j^-(\tau)\rangle \tag{10.10.2}$$

Following exactly the notation of Agarwal, s_j^+ and s_j^- denote the operators $(|e\rangle\langle f|)_i$ and $(|f\rangle\langle e|)_j$, descriptions of the molecular states connected by the

radiative decay process. The state $|f\rangle$ has an energy lower than that of the state $|e\rangle$, but in the intramolecular case, for example, it can be different from the state $|g\rangle$ of Section 9.2. With the symbols g_{iks} we denote the coupling coefficients of the corresponding light-matter interaction.

We note that the "macroscopic" signal depends on a macroscopic correlation function involving all the molecules of our sample. For simplicity we neglect any cross correlation between molecules. This means that we are able to replace Eqs. 10.10.1 and 10.10.2, respectively, with the following ones (N is the number of molecules in the sample):

$$N_{ks}(t) = Ng_{ks}g_{ks}^{*}\int_0^t dt_1 \int_0^{t_1} dt_2 \exp[-i\omega_{ks}(t_1 - t_2)]\langle s^{+}(t_1)s^{-}(t_2)\rangle + \text{H.C.} \tag{10.10.3}$$

and

$$\sigma_{ks}(t) = Ng_{ks}g_{ks}^{*}\int_0^t d\tau \exp[-i\omega_{ks}(t-\tau)]\langle s^{+}(t)s^{-}(\tau)\rangle + \text{H.C.} \tag{10.10.4}$$

Of course, to replace Eqs. 10.10.1 and 10.10.2 with Eqs. 10.10.3 and 10.10.4, the assumption is required that any molecule experiences the same environmental influence as any other molecule in the sample; that is, the sample dishomogeneities are completely neglected.

When one is dealing, for example, with condensed phase systems such as those used to study dielectric relaxation (Evans et al., 1980a; Böttcher and Bordewijk, 1978), which frequently exhibit non-Markovian features, the most difficult question to be answered is that Eqs. 10.10.3 and 10.10.4 involve the Markovian constraint. In fact, Agarwal (1974) shows that both the N-spectrum and the σ-spectrum can easily be evaluated by using Eqs. 10.10.3 and 10.10.4 provided that the regression theorem (Lax, 1967, 1968; Haken and Weidlich, 1967) is applied. This theorem, in turn, is based on the Markovian assumption and states that if one-time values are expressed as

$$\langle Q_i(t_1)\rangle = \sum_{\alpha} f_{i\alpha}(t_1 - t_2)\langle Q_\alpha(t_2)\rangle \qquad (t_1 > t_2) \tag{10.10.5}$$

where f_{i_α} are numerical functions and the $Q_\alpha(t_2)$'s form a complete set of operators, then the two-time correlation function, for example, can be written as follows:

$$\langle Q_j(t_1')Q_i(t_1)\rangle = \sum_{\alpha} f_{i\alpha}(t_1 - t_1')\langle Q_j(t_1')Q_\alpha(t_1')\rangle \tag{10.10.6}$$

Equation 10.10.6 is quite useful to evaluate the emission spectra of Eqs. 10.10.3 and 10.10.4. However, Eq. 10.10.5 is derived from a Markovian–Langevin equation where the motion of an observable $\mathbf{Q} = (Q_1, Q_2, \ldots, Q_n)$ can be written in the following form (see Section 10.6):

$$\frac{d}{dt}\mathbf{Q}(t) = -\boldsymbol{\Gamma}\mathbf{Q}(t) + \mathbf{F}(t)\mathbf{Q}(t) + \mathbf{f}(t) \tag{10.10.7}$$

The friction $\boldsymbol{\Gamma}$ and the fluctuating force $\mathbf{f}(t)$ are connected by the Markovian version of the second fluctuation–dissipation theorem. In the preceding sections we have argued that the relaxation contribution's complete independence of the excitation process stems from the Markovian nature of the system under investigation. However, we have also stressed that whether or not a system can be described as being Markovian also depends on the intensity of external excitation. Even when the relaxation time (microscopic time scale) is very much larger than the correlation time (microscopic time scale), the system cannot be regarded as being Markovian if the frequency of the induced dynamics is comparable with the inverse of correlation time. In other words, the Markovian assumption can be invalidated by either of the following physical conditions:

1. The time scale separation cannot be made (fast relaxation phenomena).
2. The excitation pulse is strong (laser spectroscopy by intense excitation pulses).

It is amusing to remark that experimental research in the sorry case where both these constraints apply is currently being initiated (Millar et al., 1979).

If Eq. 10.10.7 were valid we could obtain for the average value $\langle\mathbf{Q}\rangle$ the following equation of motion:

$$\frac{d}{dt}\langle\mathbf{Q}\rangle = -\mathbf{A}\langle\mathbf{Q}\rangle \tag{10.10.8}$$

where $\mathbf{A}$ is a suitable time-independent matrix resulting from the rotating wave approximation. We have to suppose, of couse, that the exciting pulse is monochromatic. A further, more significant assumption required to justify Eq. 10.10.8 is the following:

$$\langle\mathbf{f}(t)\rangle = \mathbf{0} \tag{10.10.9}$$

From the preceding sections it is clear that Eq. 10.10.9 is consistent with the Markovian nature of Eq. 10.10.7. In fact, any subsequent excitation of the thermal bath would relax so rapidly that only negligible effects on the part of interest would result.

It is now quite straightforward to show that Eq. 10.10.6 can be derived from Eq. 10.10.8. Since we assumed that the matrix $\mathbf{A}$ is time independent, we can write

$$\langle\mathbf{Q}(t_1)\rangle = \exp[-\mathbf{A}(t_1 - t_2)]\langle\mathbf{Q}(t_2)\rangle \tag{10.10.10}$$

which is an equation of the same form as Eq. 10.10.5. In fact, it can be written as follows:

$$\langle Q_i(t_1)\rangle = \langle i|\mathbf{Q}(t_1)\rangle = \sum_{j\alpha}\langle i \mid \alpha\rangle\langle\tilde{\alpha} \mid j\rangle\langle j \mid \mathbf{Q}(t_2)\rangle \exp[-\alpha(t_1 - t_2)]$$

$$= \exp\sum_{j\alpha}\langle i \mid \alpha\rangle\langle\tilde{\alpha} \mid j\rangle\langle Q_j(t_2)\rangle \exp[-\alpha(t_1 - t_2)] \tag{10.10.11}$$

where $|\alpha\rangle$ and $\langle\tilde{\alpha}|$ are right and left eigenstates, respectively, of the matrix **A**, and α is the corresponding eigenvalue.

An equation such as Eq. 10.10.11 can always be obtained, when the generalized Langevin equation is replaced by a chain of Markovian variables suitably truncated.

The emission spectra in the work by Grigolini (1978, 1979) have been evaluated by applying the regression theorem to the equivalent Markovian systems which replace the original ones of non-Markovian nature. In this way a generalization can be attained of the theory of Kubo and co-workers (Takagahara et al., 1977) and Hochstrasser and co-workers (Friedman and Hochstrasser, 1974; Hochstrasser and Novak 1977, 1978).

10.11 CONCLUDING REMARKS

In Chapter 10 we have emphasized the possibility of using a generalized version of Mori's theory to model dissipative systems simply. This method makes it possible to deal with excited thermal baths without the restriction of Markov's assumption. In these systems any initial excitation of the bath can significantly affect the subsequent relaxation of the part of interest (recall the effects of the duration of excitation pulse on relaxation described in Chapter 9). This method enables us to overcome the theoretical constraint of linear response (recall the decoupling effects studied in Chapter 9). The experimental challenge (literally unavoidable) is to detect both kinds of effects. As widely emphasized in the other chapters of this book, molecular dynamics is a field of investigation where the non-Markovian character of physical reality plays an important role. Fast developments in picosecond laser technology will soon make possible experimental detection of rapid rotational relaxation in liquids via, for example, fluorescence depolarization methods. Experimental detection of fast relaxation processes will then have to face the important problem of the interplay between excitation and relaxation process. This ineluctable interaction, resulting from the non-Markovian nature of the physical reality, is reminiscent of the role of the observer in the quantum mechanical theory of measurement (Ballentine, 1970). However, the true reason for the physical effects discussed in this part of the book is not quantum mechanical in nature. The use of quantum mechanical formalism, rather, depends on the fact that the excitation process of electronic states, for example, is currently described within the context of quantum mechanical theories. By stressing the features shared by the relaxation of quantum mechanical systems and classical systems, the use of quantum mechanics sheds light on the real meaning of Mori's approach, for example, the close relationship between the Mori chain of variables and the chain of quantum mechanical states of Ziv and Rhodes's (1976) theory. This explains the presence of a quantum mechanical formulation within a book mainly concerning a classical picture of molecular dynamics.

The generalization of the Mori theory to include non-Hermitian operators is a further interesting feature of the theoretical approach developed in this chapter in the sense that it can provide a more rapidly convergent continued fraction expansion. In order to provide further support for this statement consider again the "intramolecular" model of Eq. 9.2.1. Assume, as usual, that the state $|e\rangle$ is coupled to the first quasi-continuum by a Lorentzian type interaction, the bandwidth of which is γ_1. Its interaction with the second is neglected. Let us assume that any state $|m\rangle$ can be coupled to the second quasi-continuum manifold with a Lorentzian whose bandwidth is γ_2. Any interference effect among the states $|m\rangle$ coming from the latter interaction is neglected. This approximation is rigorously satisfied if any state $|m\rangle$ is coupled to its own continuum. In such a case, as many continua would be present as there are states. We can apply the RMT (Section 9.2) to any state $|m\rangle$. This means that any state $|m\rangle$ is regarded as being a state of interest, the decay of which results from the interaction with a Mori chain. We find then that the Hamiltonian of the model of Eq. 9.2.1 has to be replaced by the following ($\hat{\mathcal{H}}_{\text{ext}} = 0$)

$$\begin{aligned}\hat{\mathcal{H}}_{\text{eff}} = {} & |e\rangle\epsilon_e\langle e| + \sum_m (|e\rangle\langle m| + |m\rangle\langle e|)v_m \\ & + \sum_m |m\rangle\epsilon_m\langle m| + \sum_m (|m\rangle\langle M(m)| + |M(m)\rangle\langle m|)V_{2m} \\ & + \sum_m |M(m)\rangle\langle M(m)|(\epsilon_m - i\gamma_2)\end{aligned} \tag{10.11.1}$$

which is no longer Hermitian. For simplicity we assume that the maximum coupling for any state $|m\rangle$ is at $\epsilon = \epsilon_m$.

To evaluate the correlation function expressing the influence of the thermal bath on $|e\rangle$ we follow the approach of Section 9.2 and find that

$$\Phi_{\text{intra}}(t) = \sum_m |v_m|^2\langle m|e^{-i\hat{\mathcal{H}}'t}|m\rangle \tag{10.11.2}$$

where

$$\hat{\mathcal{H}}' = \begin{pmatrix} \epsilon_m & V_{2m} \\ V_{2m} & \epsilon_m - i\gamma_2 \end{pmatrix} \tag{10.11.3}$$

Assuming that any coupling V_{2m} is endowed with the same value v_2, since the diagonalization of the previous matrix is independent of ϵ_m, we may write

$$\Phi_{\text{intra}}(t) = \sum_m |v_m|^2 \exp(-i\epsilon_m t)\langle M|\exp(i\hat{\mathcal{H}}''t)|M\rangle \tag{10.11.4}$$

where

$$\hat{\mathcal{H}}'' = (|M\rangle\langle N| + |N\rangle\langle M|)v_2 - i\gamma_2|N\rangle\langle N| \tag{10.11.5}$$

However, we know (see Section 9.2) that for a dissipative quasi-continuum

with Lorentzian coupling we have

$$\sum_m |v_m|^2 \exp(-i\epsilon_m t) = v_1^2 \exp(-\gamma_1 t) \exp(-i\epsilon_M t) \tag{10.11.7}$$

As a consequence, we can also write Eq. 10.11.4 as follows:

$$\Phi_{\text{intra}}(t) = \langle M| \exp(-i\hat{\mathcal{H}}''' t)|M\rangle v_1^2 \tag{10.11.4a}$$

where

$$\hat{\mathcal{H}}''' = (|M\rangle\langle N| + |N\rangle\langle M|)v_2 + (\epsilon_M - i\gamma_1)|M\rangle\langle M| + (\epsilon_M - i[\gamma_1 + \gamma_2])|N\rangle\langle N| \tag{10.11.8}$$

It is evident that the same result would be obtained if Eq. 10.11.1 were to be replaced by

$$\mathcal{H}'_{\text{eff}} = |e\rangle\langle e|\epsilon_e + (|e\rangle\langle M| + |M\rangle\langle e|)v_1 + |M\rangle(\epsilon_M - i\gamma_1)\langle M| + (|M\rangle\langle N| + |N\rangle\langle M|)v_2 + |N\rangle(\epsilon_M - i[\gamma_1 + \gamma_2])\langle N| \tag{10.11.9}$$

The original theory by Mori cannot produce a chain of states such as that of Eq. 10.11.9, because only the last state would be directly damped. If $\gamma_1 \neq 0$, in order to obtain for $|e\rangle$ the same decay as that provided by Eq. 10.11.9, one should use an infinite chain of standard type.

Lastly, a few lines must be devoted to discussing whether or not the simple models obtained by using the generalized Mori theory have a real existence. By using Section 9.3 the generalized continued fraction when applied to a variable such as a dipole μ satisfying the kinematic relation

$$\frac{d}{dt}\boldsymbol{\mu} = \boldsymbol{\omega}(t) \times \boldsymbol{\mu} \tag{10.11.10}$$

may be interpreted in terms of a chain of coupled dipoles. Within the context of generalized Brownian motion the third-order truncation of the Mori chain is equivalent to the itinerant oscillator (Appendix C), or more usefully (Chapter 4), Mori–Evans theory. If we remove the Markovian constraint this can be written as follows:

$$\dot{v} = \ddot{x} = -\left(\frac{k}{m}\right)(x - y) \tag{10.11.11}$$

$$\dot{w} = \ddot{y} = \left(\frac{k}{M}\right)(x - y) - \int_0^t \xi_M(t - \tau)w(\tau) + f_w(t) \tag{10.11.11a}$$

It is useful to picture the Brownian particle of mass m as being inside a diffusing cage, the mass of which is M. In order to evaluate the "memory kernel" ξ_M, then, one could use a hydrodynamic approach applied directly to the Brownian particle (Metiu et al., 1977). The velocity a.c.f. may be evaluated by the following equation:

$$\langle \mathbf{v} \cdot \mathbf{v}(t)\rangle = \frac{2}{\pi}\int_0^\infty d\omega \frac{\cos \omega t}{-i\omega + \hat{\xi}_H(\omega)} \tag{10.11.12}$$

where (Metiu et al., 1977)

$$\hat{\xi}_H(\omega) = \frac{4\pi a}{3m} f(a, \eta_s^0, \eta_l^0, \tau_s, \tau_l, \rho_0, \beta\omega) \tag{10.11.13}$$

f is a function of a, the radius of the particle η_s^0, and η_l^0, the shear and longitudinal viscosity, respectively, τ_s and τ_l, the shear and longitudinal relaxation times, ρ_0, the particle density, a parameter β, and ω. Equation 10.11.12 provides for $t \to \infty$ the correct time behavior $t^{-3/2}$ (Chapter 7). If an external spherical cage with radius R were endowed with a real existence we could write

$$\hat{\xi}_M(\omega) = \frac{4\pi}{3}\frac{R}{M} f(R, \eta_s^0, \eta_l^0, \tau_s, \tau_l, \rho_0, \beta, \omega) \tag{10.11.14}$$

The Laplace transform of the velocity a.c.f. would then be provided by

$$\mathcal{L}\langle \mathbf{v} \cdot \mathbf{v}(t)\rangle = \frac{2}{\pi}\int_0^\infty d\omega \cfrac{\cos \omega t}{-i\omega + \cfrac{\Delta_1^2}{-i\omega + \cfrac{\Delta_2^2}{-i\omega + \hat{\xi}_M(\omega)}}} \tag{10.11.15}$$

The diffusion parameter is correctly provided by assuming that for $\omega \to \infty$ Eq. 10.11.15 is identical with Eq. 10.11.12. This implies

$$\hat{\xi}_M(\omega) = \frac{m}{M}\hat{\xi}_H(\omega) \tag{10.1.16}$$

which is satisfied only when (Evans et al., 1980b)

$$a = R \tag{10.11.7}$$

It is evident that the real existence of the external cage is inconsistent with this result. The simple example under discussion also emphasizes a limit of the theory developed in Chapters 9 and 10. Any Markovian truncation of our continued fraction cannot produce the hydrodynamic tail. The basic idea of the theory may be preserved provided that the linear expansion of the present approach is replaced by a new kind of expansion involving nonlinear coupling. Work towards such an expansion is in progress.

APPENDIX A

We consider the multidimensional Langevin equation obtained in Section 10.6 (Eq. 10.6.32). When the stochastic force is Gaussian, Fox (1978) has shown that no real difficulty is encountered in building up Fokker–Planck equations to be associated with the Langevin equation under study. The Fokker–Planck equation avoids the difficulty of integrating a stochastic differential equation.

Fox (1978) studied the general case of a Langevin equation written as

follows:

$$\frac{d\mathbf{a}}{dt} = -\mathbf{A}\mathbf{a}(t) - \mathbf{S}\mathbf{a}(t) + \tilde{\mathbf{F}}(t) \tag{10.A.1}$$

He used the usual Gaussian statistics. The stochastic force $\tilde{\mathbf{F}}(t)$ [the tilde denotes the stochastic nature of $\tilde{\mathbf{F}}(t)$] is determined by the first and second moment:

$$\langle \tilde{\mathbf{F}}(t) \rangle = 0 \tag{10.A.2}$$

$$\langle \tilde{F}_i(t)\tilde{F}_j(s) \rangle = 2Q_{ij}\delta(t-s) \tag{10.A.3}$$

If the assumption is made that Eq. 10.A.1 may be integrated as an ordinary differential equation, we obtain the following expression for $\mathbf{a}(t)$:

$$\mathbf{a}(t) = \exp[-t\mathbf{G}]\mathbf{a}(0) + \int_0^t \exp[-(t-s)\mathbf{G}]\tilde{\mathbf{F}}(s)\, ds \tag{10.A.4}$$

where

$$\mathbf{G} = \mathbf{A} + \mathbf{S} \tag{10.A.4a}$$

Fox uses two different kinds of averages. The first, denoted by $\langle \cdots \rangle$, is the average with respect to the stochastic force $\tilde{\mathbf{F}}$. The second, denoted by $\{\cdots\}$ is the average with respect to the initial conditions of the physical system under study. For instance, from Eq. 10.A.4,

$$\langle \mathbf{a}(t) \rangle = \exp[-t\mathbf{G}]\mathbf{a}(0) \tag{10.A.5}$$

$$\{\langle \mathbf{a}(t) \rangle\} = 0 \tag{10.A.5a}$$

We can also define the component (i, j) of a suitable correlation function matrix as follows (repeated indices mean summation):

$$\begin{aligned}\chi_{ij}(t_2 - t_1) &= \{\langle a_i(t_2)a_j(t_1)\rangle\} \\ &= [\exp(-t_2\mathbf{G})]_{il}[\exp(-t_1\mathbf{G})]_{jk}\{a_l(0)a_k(0)\} \\ &\quad + \int_0^{t_2} ds \int_0^{t_1} ds' \{\exp[-(t_2-s)\mathbf{G}]\}_{il}\{\exp[-(t_1-s')\mathbf{G}]\}_{jk} \\ &\quad \times \langle \tilde{F}_l(s)\tilde{F}_k(s') \rangle\end{aligned} \tag{10.A.6}$$

Equation 10.A.6 can be obtained from Eq. 10.A.4 using Eq. 10.A.5a.

Fox (1978) considers in detail the matrix $\mathbf{E}$ defined as follows:

$$E_{ij}^{-1} = \{a_i(0)a_j(0)\} \tag{10.A.7}$$

This defines the equilibrium distribution of a Gaussian process by

$$w_1(a_1, \ldots, a_N) = \left(\frac{\|\mathbf{E}\|}{(2\pi)^N}\right)^{1/2} \exp\left(-\tfrac{1}{2}\, a_i E_{ij} a_j\right) \tag{10.A.8}$$

where $w_1(\mathbf{a}, t)\, dt$ is defined as the probability at time t that the value $\mathbf{a}(t)$ is between $\mathbf{a}$ and $\mathbf{a} + d\mathbf{a}$.

If we denote by $\mathbf{G}^+$ the transpose matrix associated with $\mathbf{G}$, from Eq. (10.A.6) we obtain

$$\begin{aligned}\chi_{ij}(t_2 - t_1) = [\exp(-t_2\mathbf{G})\mathbf{E}^{-1}\exp(-t_1\mathbf{G}^+)]_{ij} + 2(\exp[-(t_2-t_1)\mathbf{G}])_{il} \\ \left\{\int_0^{t_1} ds\, \exp[-(t_1-s)\mathbf{G}]\mathbf{Q}\exp[-(t_1-s)\mathbf{G}^+]\right\}_{lj}\end{aligned} \tag{10.A.9}$$

Defining the following superoperator

$$\mathbf{G}^\times\mathbf{M} = \mathbf{G}\mathbf{M} + \mathbf{M}\mathbf{G}^+ \tag{10.A.10}$$

enables us to write Eq. 10.A.9 as

$$\begin{aligned}\chi_{ij}(t_2 - t_1) &= \exp[-(t_2-t_1)\mathbf{G}]_{il}[\exp(-t_1\mathbf{G}^\times)\mathbf{E}^{-1}]_{lj} \\ &\quad + 2\{\exp[-(t_2-t_1)\mathbf{G}]\}_{it}\int_0^{t_1} ds\{\exp[-(t_1-s)\mathbf{G}^\times]\mathbf{Q}\}_{lj}\end{aligned} \tag{10.A.11}$$

Owing to the stationarity of the process, we have

$$\chi_{ij}(0) = \{\langle a_i(t_1)a_j(t_1)\rangle\} = \{\langle a_i(0)a_j(0)\rangle\} = E_{ij}^{-1} \tag{10.A.12}$$

By applying to Eq. 10.A.12 the superoperator $\mathbf{G}^\times$ we obtain

$$\mathbf{G}^\times\boldsymbol{\chi}(0) = \mathbf{G}\mathbf{E}^{-1} + \mathbf{E}^{-1}\mathbf{G}^+ \tag{10.A.13}$$

If $\boldsymbol{\chi}(0)$ in Eq. 10.A.13 is replaced by the corresponding expression provided by Eq. 10.A.11 we obtain

$$\begin{aligned}\mathbf{G}\mathbf{E}^{-1} + \mathbf{E}^{-1}\mathbf{G}^+ &= \exp(-t\mathbf{G}^\times)\mathbf{G}^\times\mathbf{E}^{-1} + 2\int_0^t d\tau\, \exp(-\tau\mathbf{G}^\times)\mathbf{G}^\times\mathbf{Q} \\ &= \exp(-t\mathbf{G}^\times)\mathbf{G}^\times\mathbf{E}^{-1} - 2\int_0^t d\tau\left[\frac{d}{d\tau}\exp(-\tau\mathbf{G}^\times)\right]\mathbf{Q} \\ &= 2\mathbf{Q} + \exp[-t\mathbf{G}^\times](\mathbf{G}^\times\mathbf{E}^{-1} - 2\mathbf{Q})\end{aligned} \tag{10.A.14}$$

Equation 10.A.14 can be valid only when the following condition is satisfied:

$$\mathbf{G}\mathbf{E}^{-1} + \mathbf{E}^{-1}\mathbf{G}^+ = 2\mathbf{Q} \tag{10.A.15}$$

Equation 10.A.15 is an expression of the second fluctuation–dissipation theorem. This theorem does not depend on the Gaussian assumption. In fact, no force moment higher than the second-order one is required. In Section 10.9 we show that the theory of Section 10.2 can be used to replace the generalized Langevin equation with a Markovian one concerning itself with a variable of higher dimension. Such an equation has been shown to satisfy Eq. 10.A.15. This is a useful check of the validity of our approach.

The Gaussian assumption, however, enabled Fox to obtain the following Fokker–Planck equation to be associated with the Langevin equation of Eq. 10.A.1:

$$\begin{aligned}\frac{\partial}{\partial t_2}P_2(\mathbf{a}_1t_1;\, \mathbf{a}_2t_2) &= \frac{\partial}{\partial a_{2j}}[G_{ij}a_{2j}P_2(\mathbf{a}_1t_1;\, \mathbf{a}_2t_2)] \\ &\quad + \frac{1}{2}\frac{\partial}{\partial a_{2j}}(\mathbf{G}\mathbf{E}^{-1} + \mathbf{E}^{-1}\mathbf{G})_{ij}\frac{\partial}{\partial a_{2j}}P_2(\mathbf{a}_1t_1;\, \mathbf{a}_2t_2)\end{aligned} \tag{10.A.16}$$

where, of course, P_2 is the conditional distribution function (Chapter 1).

APPENDIX B

If we use the quantumlike formalism of Section 10.2 we write the dynamic operator $\hat{\mathscr{L}}_0$ as follows:

$$\hat{\mathscr{L}}_0 = \sum_{kk'} |m_k\rangle\langle m_k|\hat{\mathscr{L}}_0|m_{k'}\rangle\langle m_{k'}| \tag{10.B.1}$$

If the orthonormalized set of vectors $|m_k\rangle$ is defined as

$$|m_k\rangle = \langle f_k \mid f_k\rangle^{-1/2}\langle f_k| \tag{10.B.2}$$

from the remarks in Sections 10.2 and 10.6 (Eqs. 10.6.28 and 10.6.29) we obtain

$$\begin{aligned}\hat{\mathscr{L}}_0 &= \sum_k \langle f_k \mid f_k\rangle^{-1}\lambda_k|m_k\rangle\langle m_k| + \sum_k \langle f_k \mid f_k\rangle^{-1/2}\langle f_{k+1} \mid f_{k+1}\rangle^{-1/2} \\ &\quad \times \{-|m_k\rangle\langle m_{k+1}|\Delta_{k+1}^2\langle f_k \mid f_k\rangle + |m_{k+1}\rangle\langle m_k|\langle f_{k+1} \mid f_{k+1}\rangle\} \\ &= \sum_k \langle f_k \mid f_k\rangle^{-1}\lambda_k|m_k\rangle\langle m_k| \\ &\quad + \sum_k \{-|m_k\rangle\langle m_{k+1}|\Delta_{k+1} + |m_{k+1}\rangle\langle m_k|\Delta_{k+1}\}\end{aligned} \tag{10.B.3}$$

The parameters Δ_{k+1} are real numbers so that we obtain an antisymmetric (Hermitian) matrix instead of the symmetrical real one of Section 9.2.

APPENDIX C

Consider the multidimensional Langevin equation provided by Eq. 10.6.32:

$$\frac{d}{dt}\mathbf{A} = (i\boldsymbol{\Omega} - \boldsymbol{\Gamma})\mathbf{A}(t) + \mathbf{F}(t) \tag{10.C.1}$$

In the three-dimensional case we have

$$i\boldsymbol{\Omega} - \boldsymbol{\Gamma} = \begin{pmatrix} 0 & 1 & 0 \\ -\Delta_1^2 & 0 & 1 \\ 0 & -\Delta_2^2 & -\gamma \end{pmatrix} \tag{10.C.2}$$

$$\mathbf{F}(t) = \begin{pmatrix} 0 \\ 0 \\ f(t) \end{pmatrix} \tag{10.C.3}$$

We want to show that this is equivalent to the monodimensional itinerant oscillator described by

$$\ddot{x} = -\omega_1^2(x - y) \tag{10.C.3}$$

$$\ddot{y} = \omega_2^2(x - y) - \gamma\dot{y} + f_y(t) \tag{10.C.3a}$$

where $f_y(t)$ is the fluctuating force.

Let us define

$$\mathbf{A} = \begin{pmatrix} \dot{x} \\ \alpha \\ \beta \end{pmatrix} \tag{10.C.4}$$

By applying Eq. 10.C.1 we obtain

$$\dot{x} = \alpha \tag{10.C.5}$$

$$\dot{\alpha} = -\Delta_1^2 x + \beta \tag{10.C.5a}$$

$$\dot{\beta} = -\Delta_2^2\alpha - \gamma\beta + f(t) \tag{10.C.5b}$$

If we use

$$\alpha = -\omega_1^2(x - y) \tag{10.C.6}$$

$$\beta = \omega_1^2\dot{y} \tag{10.C.7}$$

$$f = \omega_1^2 f_y \tag{10.C.8}$$

in Eqs. 10.C.5a and 10.C.5a, we obtain

$$\dot{\alpha} = -\omega_1^2(\dot{x} - \dot{y}) = -\Delta_1^2\dot{x} + \omega_1^2\dot{y} \tag{10.C.9}$$

$$\omega_1^2\ddot{y} = \Delta_2^2\omega_1^2(x - y) - \gamma\omega_1^2\dot{y} + f_y(t)\omega_1^2 \tag{10.C.9a}$$

If we put $\omega_1^2 = \Delta_1^2$ Eq. 10.C.9 is an identity. If we put $\Delta_2^2 = \omega_2^2$ Eq. 10.C.9a becomes identical with Eq. 10.C.3a.

APPENDIX D

Assume that the physical system under study is divided into two subsystems, **S** and **M**, interacting with each other. Let **S** be the subsystem of interest and a the corresponding dynamic variable. We mean that the variable $a \equiv a(0)$ depends only on the **S** phase space. The equation of motion of $a(t)$ can be written as follows:

$$\frac{da}{dt} = i(\hat{L}_{\mathbf{S}} + \hat{L}_1 + \hat{L}_{\mathbf{M}})a(t) \tag{10.D.1}$$

where $\hat{L}_1$ is the Liouville operator concerning the interaction between **S** and **M**. Such a kind of partition of the Liouville operator $\hat{L}$ can also be founded on the standard Mori approach outlined in Section 10.6. We can call $\hat{L}_{\mathbf{S}}$ the part of $\hat{L}$ spanned by the "state" f_0 and $\hat{L}_{\mathbf{M}}$ that spanned by all other "states" of the Mori chain. The interaction $\hat{L}_1$ is then proportional to the parameter Δ_1. An approach based on assumptions concerning the modulation of this interaction from the remaining part of the Mori chain results in a new picture of the thermal bath. In this appendix we want to provide a theoretical approach to this new picture.

In the interaction representation Eq. 10.D.1 can be written as follows:

$$\frac{du}{dt} = i\hat{\eta}(t)u(t) \tag{10.D.2}$$

where

$$\hat{\eta}(t) \equiv e^{-i(\hat{L}_S+\hat{L}_M)t}\hat{L}_1 e^{i(\hat{L}_S+\hat{L}_M)t} \tag{10.D.3}$$

and

$$u(t) \equiv e^{-i(\hat{L}_S+\hat{L}_M)t}a(t) \tag{10.D.4}$$

To some extent, $\eta(t)$ (Eq. 10.D.3) is reminiscent of $f(t)$ (Eq. 10.6.1). Both $f(t)$ and $\eta(t)$ exhibit a deterministic dependence on the "irrelevant" part of the physical system under study. When the "irrelevant" part involves a huge number of freedom degrees, it is convenient to replace the deterministic approach by a stochastic one (see Section 10.7). If this suggestion is followed, $\eta(t)$ has to be replaced by the stochastic variable $\omega(t)$ and Eq. 10.D.2 is of the same kind as Eq. 10.5.1 (for simplicity we are considering the case where $\boldsymbol{\mu}$ and $\boldsymbol{\omega}$ are replaced by the monodimensional variables u and ω, respectively). The stochastic variable $\omega(t)$, in turn, obeys an equation of the same form as Eq. 10.6.1:

$$\frac{d\omega}{dt} = i\Xi\omega(t) - \int_0^t \varphi_\omega(t-\tau)\omega(\tau)\,d\tau + f_\omega(t) \tag{10.D.5}$$

We assume that $\hat{\varphi}_\omega(z)$ is given by a truncated continued fraction. Then, according to the theory of Sections 9.3 and 10.7, we can replace Eq. 10.D.5 by

$$\frac{d\hat{\omega}}{dt} = \hat{\Gamma}_\Omega\hat{\omega} \tag{10.D.6}$$

where $\hat{\Gamma}_\Omega$ is the multidimensional Fokker–Planck operator to be associated with the generalized Langevin equation itself. We have to keep in mind that when the thermal bath driving the motion of $\omega(t)$ is assumed to be in its equilibrium state, Eq. 10.D.6 is equivalent to

$$\frac{d}{dt}\hat{\omega} = \hat{\Gamma}^\times_\Omega\hat{\omega} \equiv \hat{\Gamma}_\Omega\hat{\omega} - \hat{\omega}\hat{\Gamma}_\Omega \tag{10.D.6a}$$

As a consequence, if $\eta(t)$ is replaced by $\omega(t)$, Eq. 10.D.1 becomes

$$\frac{d}{dt}a = \hat{\mathcal{L}}_0 a \equiv [i(\hat{L}_S + \hat{\omega}) + \hat{\Gamma}_\Omega]a(t) \tag{10.D.7}$$

In fact, when written in the interaction picture, Eq. 10.D.7 reads

$$\frac{du}{dt} = i\hat{\omega}(t)u(t) \tag{10.D.2a}$$

which is the stochastic counterpart of Eq. 10.D.2 [$\hat{\omega}(t) \equiv \exp(\hat{\Gamma}^\times_\Omega t)\hat{\omega}(0)$].

Though the total "Liouville operator" $i(\hat{L}_S + \hat{\omega}) + \hat{\Gamma}_\Omega$ is not Hermitian, it is still possible to build up an expansion basis set of the same kind as that of Section 10.6 (see also Section 10.3). The theory developed in Section 10.3 can be regarded as a generalization of that of Schneider (1976), who in turn extended the Mori theory. In fact, Schneider only dealt with pseudosymmetric systems, whereas the theory of Section 10.6 can be applied to operators of any mathematical type. Then, following the same approach as the corresponding one in Section 10.6, we can replace Eq. 10.D.7 with

$$\frac{d}{dt}\mathbf{u} = \boldsymbol{\Gamma}\mathbf{u}(t) + \mathbf{F}(t) \tag{10.D.8}$$

where

$$\boldsymbol{\Gamma} = \begin{pmatrix} \lambda_0 & \Delta_1 & 0 & \dots \\ -\Delta_1 & \lambda_1 & \Delta_2 & \dots \\ 0 & -\Delta_2 & \lambda_2 & \dots \\ \dots & \dots & \dots & \dots \end{pmatrix} \tag{10.D.9}$$

The parameters λ_i and Δ_i can be obtained by the prescriptions of Section 10.3. The dimension n of the variable $\mathbf{u}$ is determined by the required degree of accuracy in evaluating, for instance, the correlation function $(u_0(t), u_0)$. However, the matrix $\boldsymbol{\Gamma}$ can be truncated without any need of replacing the remaining part of the chain with an additional damping. In fact, a damping contribution is already present in the parameters λ_i, which are complex numbers also containing a real part.

This subtle characteristic of our approach requires some comments. Once the structure of the matrix $\boldsymbol{\Gamma}$ has been determined, the stochastic force $\mathbf{F}(t)$ has to be related to the dissipation part of the matrix $\boldsymbol{\Gamma}$ itself by a fluctuation–dissipation relation, which affords a correct square average value for the variable of interest. Let us consider the case where the parameters λ_i's are endowed with only the real part (consider, for example, the stochastic oscillator of Section 10.5 when its frequency ω_0 is assumed to be zero). The fluctuation–dissipation relation of the Fox–Uhlenbeck theory can then be written as follows (see also Section 10.7):†

$$(\mathbf{F}(t), \mathbf{F}^*) = 2\boldsymbol{\Lambda}\delta(t) \tag{10.D.10}$$

where $\boldsymbol{\Lambda}$ is a diagonal matrix, the nonvanishing elements of which are given by

$$\gamma_i \equiv (\boldsymbol{\Gamma})_{ii} = -\lambda_i \tag{10.D.11}$$

In the non-Gaussian case, the higher order moments of $\mathbf{F}(t)$ cannot be expressed in terms of $\boldsymbol{\Lambda}$. However, the equilibrium square average value of the variable of interest is independent of their actual value (Grigolini et al., 1980). On the contrary, the correlation functions $(u_0^{2n}(t), u_0^{2n^*})$ are

†We are using normalized variables.

significantly affected by any non-Gaussian contribution to the stochastic force. The present approach could provide a faithful description of such a non-Gaussian behavior as a result of further investigation of the physical properties of the system under study, whereas the "non-Gaussian" behavior of Kubo's stochastic oscillator (see Appendix F) is an artifact of the SLE theory.

Failing information on higher moments of $\mathbf{F}(t)$, we assume that this stochastic force is Gaussian. Then, by using the same approach as that which led us to Eq. 10.7.10, we obtain

$$\frac{\partial}{\partial t_2} P_2(\mathbf{u}^{(1)}, t_1; \mathbf{u}^{(2)}, t_2) = \hat{\Gamma}_{\mathbf{u}} P_2(\mathbf{u}^{(1)}, t_1; \mathbf{u}^{(2)}, t_2) \tag{10.D.12}$$

where $\hat{\Gamma}_{\mathbf{u}}$ is defined by

$$\begin{aligned} \hat{\Gamma}_{\mathbf{u}} \equiv & -\sum_{r=0}^{n-1} \Delta_{r+1} \left(\frac{\partial}{\partial u_r^{(2)}} u_{r+1}^{(2)} - \frac{\partial}{\partial u_{r+1}^{(2)}} u_r^{(2)} \right) \\ & + \sum_{r=0}^{n} \gamma_r \left(\frac{\partial}{\partial u_r^{(2)}} u_r^{(2)} + q_r^2 \frac{\partial^2}{\partial (u_r^{(2)})^2} \right) \end{aligned} \tag{10.D.13}$$

In the case where the "memory kernel" of Eq. 10.D.5 is endowed with a finite lifetime, the theory developed in this appendix leads to a generalization of the SLE theory along the same lines as those of Ferrario and Grigolini (1979). Let us recall, furthermore, that Eq. 10.D.12 has been built up by making the usual Gaussian assumption on the stochastic variable $\omega(t)$. We can then emphasize a further advantageous feature of our approach: the diffusion operator $\hat{\Gamma}_{\mathbf{u}}$ when constructed according to the theory by Evans et al. (1980b) can be unaffected by this limitation.

It is important to stress that Eq. 10.D.8 leads to a generalized Langevin equation with a "memory kernel," the Laplace transform of which exhibits the generalized structure found in Section 10.3. By using the Laplace transform approach of Section 10.6, we find that u_0 satisfies the following generalized Langevin equation:

$$\frac{d}{dt} u_0(t) = \lambda_0 u_0(t) - \int_0^t ds\, \varphi(t-s) u_0(s) + f(t) \tag{10.D.14}$$

where

$$\hat{\varphi}(z) = \cfrac{\Delta_1^2}{z - \lambda_1 + \cfrac{\Delta_2^2}{z - \lambda_2 + \ddots}} \tag{10.D.15}$$

However, Eq. 10.D.14 is not completely equivalent to the generalized Langevin equation derived by using the technique of Mori type of Section 10.3, Eq. 10.3.34 with $k = 0$. In fact, by repeating the method of Section 10.6, we find that the Laplace transform of $f(t)$ is expressed in terms of the

Laplace transforms of the components of $\mathbf{F}(t)$ as follows:

$$\begin{aligned} \hat{f}(z) = \hat{F}_0(z) + & \cfrac{\Delta_1}{z - \lambda_1 + \cfrac{\Delta_2^2}{z - \lambda_2 + \cfrac{\Delta_3^2}{z - \lambda_3 + \ddots}}} \\ & \times \left(u_1(0) + \hat{F}_1(z) + \cfrac{\Delta_2}{z - \lambda_2 + \cfrac{\Delta_3^2}{z - \lambda_3 + \cfrac{\Delta_4^2}{z - \lambda_4 + \ddots}}} \right. \\ & \times \left. \left(u_2(0) + \hat{F}_2(z) + \cfrac{\Delta_3}{z - \lambda_3 + \cfrac{\Delta_4^2}{z - \lambda_4 + \cfrac{\Delta_5^2}{z - \lambda_5 + \ddots}}} \times \left(\cdots \qquad \cdots \right) \right) \right) \end{aligned} \tag{10.D.16}$$

It means that the fluctuating force $f(t)$ also depends on the variables u_i's $(i \geq 1)$, which at $t = 0$ can be found far from their thermodynamical equilibrium, whereas the generalized Langevin equation of the Mori theory, Eq. 10.2.49, for $k = 0$, and its generalized version of Section 10.3 as well, is derived in the presence of a thermal bath assumed to be in its equilibrium state. This is the reason why the present approach can be used to evaluate the spectroscopic effects of thermal bath excitations (Ferrario and Grigolini, 1981).

In Appendix E we show that this approach provides a correct behavior for the higher-order correlation functions $(u^{2n}(t), u^{2n}(t)^{\dagger})$ while resulting in the same $(u(t), u^{\dagger})$ as the SLE theory.

APPENDIX E

The generalized Mori theory of Section 10.3 shares the main features of the standard Mori approach described in Section 10.2. This theory consists in building up a suitable basis set for expanding a non-Hermitian dynamical operator $i\hat{\mathcal{L}}_0$ such as that of Eq. 10.5.9.

In this reference framework, when the "quantum mechanical" method of Appendix B is repeated, $\hat{\mathcal{L}}_0$ can be written as follows:

$$\hat{\mathcal{L}}_0 = \sum_{r=0}^{\infty} |\tilde{m}_r\rangle \lambda_r \langle m_r| - \sum_{r=0}^{\infty} \Delta_{r+1} \{ |\tilde{m}_r\rangle\langle m_{r+1}| - |\tilde{m}_{r+1}\rangle\langle m_r| \} \tag{10.E.1}$$

Consider the simple case of the monodimensional variables ω and u of Appendix D. Furthermore, the variable $\omega(t)$ is assumed to be both Gaus-

sian and Markovian. As a consequence Γ_Ω(Eq. 10.D.6) becomes

$$\hat{\Gamma}_\omega \equiv \gamma\left\{\frac{\partial}{\partial\omega}\,\omega + \Delta^2\frac{\partial^2}{\partial\omega^2}\right\} \tag{10.E.2}$$

By using Eqs. 10.5.17 and 10.5.18, we have

$$\hat{\mathscr{L}}_0 = -\sum_{r=0}^{\infty}|\tilde{m}_r\rangle(r-1)\gamma\langle m_r| - \Delta\sum_{r=0}^{\infty}(r+1)^{1/2}\{|\tilde{m}_r\rangle\langle m_{r+1}| - |\tilde{m}_{r+1}\rangle\langle m_r|\} \tag{10.E.3}$$

We can use $\hat{\mathscr{L}}_0$ (Eq. 10.E.3) for evaluating the time evolution of $\omega(t)$. The main difference between the SLE theory and this approach is that this time evolution is now determined also by the interaction between ω and the part of interest itself. In the case under study the stochastic variable ω must be regarded as being an operator on the space spanned by the states $|m_r\rangle$'s to be denoted by $\hat{\omega}$. Its nonvanishing matrix elements are then given by (see also Section 10.6)

$$-\langle\tilde{m}_r|\hat{\omega}|m_{r+1}\rangle = \langle\tilde{m}_{r+1}|\hat{\omega}|m_r\rangle = (r+1)^{1/2}\Delta \tag{10.E.4}$$

It is straightforward to check that if we replace $\hat{\mathscr{L}}_0$ by

$$\hat{\mathscr{L}}_0' \equiv -\sum_{r=0}^{\infty}|m_r\rangle(r-1)\gamma\langle\tilde{m}_r| \tag{10.E.3a}$$

the corresponding time evolution of ω as given by

$$\frac{d\hat{\omega}}{dt} = \hat{\mathscr{L}}_0'\hat{\omega} \tag{10.E.5}$$

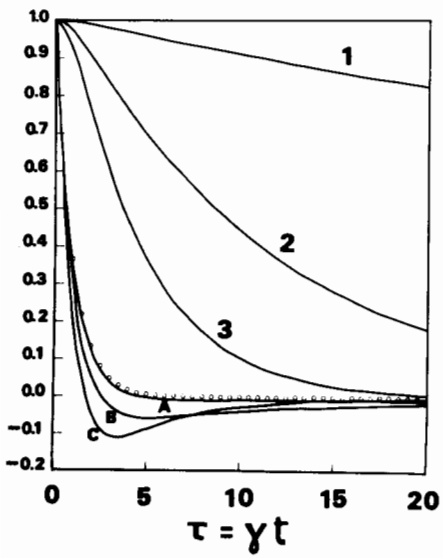

Figure 10.E.1 Time evolution of the correlation function $C_{u_0}(\tau) = (u_0(\tau), u_0^+)$ (1–3) and $C_\omega(\tau) = \langle\omega\omega(t)\rangle$ (A–C). The parameter τ is related to the time t by $\tau = \gamma t$. Values of the parameter Δ: 0.1γ (1, A), 0.3γ (2, B), 0.5γ (3, C). The curves 1–3 coincide with the corresponding ones obtained by using the SLE theory. The circles denote the free decay of the correlation function $C_\omega(\tau)$.

completely satisfies the Gaussian requirements (see Eqs. 9.1.24 and 9.1.25) provided that the moments of $\omega(t)$ are defined by

$$\langle\omega(t_1)\omega(t_2)\cdots\rangle \equiv \langle\tilde{m}_0|\hat{\omega}(t_1)\hat{\omega}(t_2)\cdots|m_0\rangle$$

However, when the total Liouville operator of Eq. (10.E.1) is used, the time evolution of ω is shown to exhibit significant deviations from the free decay behavior. Figure 10.E.1 shows the behavior of the correlation function $C_\omega(t) \equiv \langle\omega\omega(t)\rangle$ for increasing values of Δ. The agreement with the SLE theory is fairly good for small values of the "memory strength" parameter $g \equiv 2\Delta/\gamma$. On the contrary, when $g \sim 1$, the correlation function $C_\omega(t)$ can also have negative values and slowly attains a steady vanishing value for $t \to \infty$. Of course, the correlation function $C_{u_0}(t) \equiv (u_0(t),\ u(0))$ coincides with that given by the SLE theory.

As far as the equilibrium distribution of u_0 is concerned we can have recourse to Eq. 10.D.13. By using again the diffusion operator of Eq. 10.E.2 and the explicit expressions for the parameters Δ_i and λ_i given in Section 10.5, we obtain

$$\frac{\partial}{\partial t_2}P_2(\mathbf{u}^{(1)}, t_1; \mathbf{u}^{(2)}, t_2) = -\sum_{r=0}^{\infty}(r+1)^{1/2}\Delta\left(\frac{\partial}{\partial u_r^{(2)}}u_{r+1}^{(2)} - \frac{\partial}{\partial u_{r+1}^{(2)}}u_r^{(2)}\right)P_2(\cdots) + \sum_{r=1}^{\infty}r\gamma\left\{\frac{\partial}{\partial u_r^{(2)}}u_r^{(2)} + q^2\frac{\partial^2}{\partial(u_r^{(2)})^2}\right\}P_2(\cdots) \tag{10.E.6}$$

It is straightforward to check that the corresponding equilibrium distribution, $w_0(\mathbf{u})$, is

$$w_0(\mathbf{u}) = \prod_{r=0}^{\infty}\left\{\frac{qe^{-(u_r^2/q^2)}}{(2\pi)^{1/2}}\right\} \tag{10.E.7}$$

which results in a Gaussian distribution for the variable of interest u_0 when the other variables are wiped out. As a consequence, the higher-order correlation functions

$$C_{u_0}^{(n)}(t) \equiv (u_0^{2n}(t),\ u_0^{2n^*}) \tag{10.E.8}$$

are shown to attain the correct steady value $C_{u_0}^{(n)}(\infty) = (2n-1)!!$, as required by the Gaussian assumption on the stochastic force $\mathbf{F}(t)$ done in the preceding section. To obtain the simple equilibrium distribution of Eq. 10.E.7 we had to assume all the parameters q_r of Eq. 10.D.13 to have the common value q.

APPENDIX F

Let us consider the stochastic process defined by

$$\frac{du}{dt} = i\omega(t)u(t) \tag{10.F.1}$$

where $\omega(t)$ is a stochastic variable of Gaussian kind defined by its moments as follows:

$$\langle \omega(t_1) \rangle = 0 \tag{10.F.2}$$

$$\langle \omega(t_1)\omega(t_2) \rangle = \Delta^2 e^{-\gamma(t_1 - t_2)} \qquad (t_1 \geq t_2) \tag{10.F.2a}$$

$$\langle \omega(t_1)\omega(t_2)\omega(t_3) \rangle = 0 \qquad (t_1 \geq t_2 \geq t_3) \tag{10.F.2b}$$

$$\langle \omega(t_1)\omega(t_2)\omega(t_3)\omega(t_4) \rangle = \Delta^4 \{ e^{-\gamma(t_1 - t_2)} e^{-\gamma(t_3 - t_4)} + e^{-\gamma(t_1 - t_3)} e^{-\gamma(t_2 - t_4)} + e^{-\gamma(t_1 - t_4)} e^{-\gamma(t_2 - t_3)} \} \qquad (t_1 \geq t_2 \geq t_3 \geq t_4) \tag{10.F.2c}$$

and so on.

The basic idea of Kubo's theory (1963) is as follows. Equation 10.F.1 is integrated to

$$u(t) = \exp\left[i \int_0^t \omega(t_1)\, dt_1 \right] u(0) \tag{10.F.3}$$

When the initial condition $u(0)$ is not a random one, the correlation function $\langle u(t)u(0) \rangle$ is proportional to the stochastic average of the exponential of Eq. 10.F.3. If the latter one, in turn, is developed in cumulants, we obtain

$$\frac{\langle u(t)u(0) \rangle}{\langle u(0)u(0) \rangle} = \exp\left\{ \sum_{m=1}^{\infty} \frac{(i)^m}{m!} \int_0^t \cdots \int_0^t \ll \omega(t_1) \cdots \omega(t_n) \gg \right) \tag{10.F.4}$$

When Eqs. 10.F.2 are satisfied the only surviving cumulant is the following:

$$\ll \omega(t_1)\omega(t_2) \gg = \Delta^2 e^{-\gamma(t_1 - t_2)} \tag{10.F.5}$$

Then, from Eq. (10.F.4) we obtain

$$\frac{\langle u(t)u(0) \rangle}{\langle u(0)u(0) \rangle} = \exp\left(-\frac{\Delta^2}{\gamma} (e^{-\gamma t} - 1 + \gamma t) \right) \tag{10.F.6}$$

Since the equation of motion for $u^n (n > 0)$,

$$\frac{d}{dt} u^n = ni\omega(t) u^n(t) \tag{10.F.7}$$

can be derived from Eq. 10.F.1 by replacing $\omega(t)$ with $n\omega(t)$, the kind of approach which led us to Eq. 10.F.6 when applied to Eq. 10.F.7 results in

$$\frac{\langle u^n(t)u^n(0) \rangle}{\langle u^n(0)u^n(0) \rangle} = \exp\left(-\frac{n^2 \Delta^2}{\gamma} (e^{-\gamma t} - 1 + \gamma t) \right) \tag{10.F.8}$$

The physical consequences of Eq. 10.F.7 are quite disappointing. When $t \to \infty$, $\langle u^n(t)u^n(0) \rangle$ vanish also for even values of n.

APPENDIX G

Here we apply the generalized Mori theory of Section 10.4 to a quantum mechanical system. We consider a discrete set of states interacting with a thermal bath assumed to be in a Boltzmannian equilibrium at the temperature T. If the coupling between the part of interest and its thermal bath is weak enough to allow a Markovian mechanism of relaxation, then we show that the discrete set of state attains a canonical equilibrium distribution. This justifies our use of this result in the classical limit. In the case of a classical particle of mass m interacting with a thermal bath of light particles of mass m, the weak coupling condition can be obtained by assuming that $\delta = (m/M)^{1/2} \ll 1$. The dynamics of the thermal bath are very much faster than those of the Brownian particle. The memory kernel of the GLE therefore has a short lifetime. The analogy with the demonstration of this appendix could be preserved if the fluctuating force resulting from the interaction between Brownian particle and thermal bath could be shown to be Gaussian. According to the standard stochastic theory (Fox, 1978), the Gaussian assumption leads to a Maxwellian distribution for velocity which is the classical counterpart of the canonical equilibrium distribution.

Consider a system defined by the following Hamiltonian:

$$\hat{\mathcal{H}} = \hat{\mathcal{H}}_0^{(S)} + \hat{\mathcal{H}}_0^{(L)} + \hat{\mathcal{H}}_{SL} \tag{10.G.1}$$

where $\hat{\mathcal{H}}_0^{(S)}$ is the unperturbed Hamiltonian defined by

$$\hat{\mathcal{H}}_0^{(S)} = \sum_{\alpha=1}^{n} |\alpha\rangle \epsilon_\alpha \langle \alpha| \tag{10.G.2}$$

$\hat{\mathcal{H}}_0^{(L)}$ is the "thermal bath" Hamiltonian and $\hat{\mathcal{H}}_{SL}$ is the interaction between the system of interest and the thermal bath. We can define as variable of interest

$$\mathbf{A} = \begin{pmatrix} A_1 \\ \vdots \\ A_N \end{pmatrix} \tag{10.G.3}$$

$$A_r = |\alpha_j\rangle\langle\alpha_i| \tag{10.G.4}$$

$$r = n(i-1) + j \tag{10.G.4a}$$

$$N = n^2 \tag{10.G.4b}$$

We assume that the equilibrium distribution of the thermal bath is provided by

$$\rho_0^{(L)} = \frac{\exp(-\beta \hat{\mathcal{H}}_0^{(L)})}{\mathrm{Tr}(e^{-\beta \hat{\mathcal{H}}_0^{(L)}})} \tag{10.G.5}$$

We show in the following that the assumption of Eq. 10.G.5 together with the Markovian constraint result in the Boltzmann canonical distribution for

the part of interest of our physical system. The quantum mechanical counterpart of a Brownian particle with $\delta \sim 1$ is a physical system which does not necessarily attain a canonical distribution.

According to the theory developed in Chapter 10 we first define the scalar product concerning the space of variables such as $\mathbf{A}$ (Eq. 10.G.3). We define the scalar product between the variables B_r and C_r as follows:

$$(B_r, C_r^+) = \mathrm{Tr}\, B_r C_r^+ \rho_0^{(L)} \tag{10.G.6}$$

Consequently

$$(A_r, A_r^+) = \delta_{rr'} \tag{10.G.7}$$

If we define

$$(\mathbf{B}, \mathbf{C}^+) = \begin{pmatrix} (B_1, C_1^+) & (B_1, C_2^+) & \dots & (B_1, C_n^+) \\ (B_2, C_1^+) & (B_2, C_2^+) & \dots & (B_2, C_n^+) \\ \vdots & \vdots & \vdots & \vdots \\ (B_n, C_1^+) & (B_n, C_2^+) & \dots & (B_n, C_n^+) \end{pmatrix}, \tag{10.G.8}$$

we obtain

$$(\mathbf{A}, \mathbf{A}^+) = 1 \tag{10.G.9}$$

the identity operator.

By following the approach described in Chapter 10 (non-Hermitian case) we obtain the following generalized Langevin equation (GLE):

$$\frac{\partial}{\partial t}\mathbf{A}(t) = \mathbf{c}\mathbf{A}(t) + \int_0^t ds\ \mathbf{d}(s)\ \mathbf{A}(t-s) + \mathbf{F}(t) \tag{10.G.10}$$

where

$$\mathbf{c} = (\hat{P}i\hat{L}\mathbf{A}, \mathbf{A}^+) \tag{10.G.11}$$

$$\mathbf{d}(s) = (\hat{P}i\hat{L}\exp[is(\hat{1}-\hat{P})\hat{L}](1-\hat{P})i\hat{L}\mathbf{A}, \mathbf{A}^+) \tag{10.G.11a}$$

$$\mathbf{F}(t) = \exp[it(\hat{1}-\hat{P})\hat{L}](\hat{1}-\hat{P})i\hat{L}\mathbf{A} \tag{10.G.11b}$$

$$\hat{P}\mathbf{B} = (\mathbf{B}, \mathbf{A}^+)\mathbf{A} \tag{10.G.11c}$$

and $\hat{L}$ is the commutator superoperator associated with the Hamiltonian of Eq. 10.G.1.

The reason for following the generalized Mori theory of Section 10.4 depends on the fact that $\hat{L}$ is not Hermitian with respect to the scalar product of Eqs. 10.G.6, 10.G.8.

The projection operator of Eq. 10.G.11c can also be written in the following way:

$$\hat{P}\mathbf{B} = \langle \mathbf{B} \rangle = \underset{\{L\}}{\mathrm{Tr}}\,[\rho_0^{(L)}\mathbf{B}] \tag{10.G.12}$$

The problem is to reduce Eq. 10.G.10 to a Markovian form, assuming

that $\hat{\mathcal{H}}_{SL}$ is fairly small so that the memory kernel $\mathbf{d}(t)$ has a very short lifetime. This allows us to obtain a rigorous expression for the damping operator, as below. The demonstration is similar to that of Deutch (1972).

Following Deutch, we use the following operator identity (see also Chapter 1):

$$\exp[i(\hat{A}+\hat{B})t] = \exp(i\hat{A}t) + \int_0^t d\tau \exp[i(\hat{A}+\hat{B})(t-\tau)]i\hat{B}\exp(i\hat{A}\tau) \tag{10.G.13}$$

We denote with $\hat{L}_0$ the superoperator associated with $\hat{\mathcal{H}}_0^{(S)} + \hat{\mathcal{H}}_0^{(L)}$. Let the symbol $\hat{L}_1$ denote the superoperator associated with $\hat{\mathcal{H}}_{SL}$. Let $A + B = L_0$ and $A = (1-\hat{P})L_1$. It follows that

$$-B = (\hat{1}-\hat{P})L - L_0 = (\hat{1}-\hat{P})\hat{L}_1 - L_0^{(S)}\hat{P} \tag{10.G.14}$$

where $\hat{L}_0^{(S)}$ is the superoperator associated with $\hat{\mathcal{H}}_0^{(S)}$. By applying Eq. 10.G.13 we have then

$$\exp[i(\hat{1}-\hat{P})\hat{L}\tau] = \exp[i\hat{L}_0\tau] + \int_0^\tau d\tau' \exp[i\hat{\mathcal{L}}_0(\tau-\tau')] \times [i(\hat{1}-\hat{P}_0)\hat{L}_1 - \hat{L}_0\hat{P}]\exp[i(\hat{1}-\hat{P})\hat{L}\tau'] \tag{10.G.15}$$

Using this equation, we can write Eq. 10.G.11b as follows:

$$\mathbf{F}(t) = \mathbf{F}_0(t) + \int_0^t d\tau' \exp[i\hat{L}_0(\tau-\tau')][i(1-P)\hat{L}_1]\mathbf{F}(\tau') \tag{10.G.16}$$

Here the random force (to lowest order) is defined as follows:

$$\mathbf{F}_0(t) = \exp(iL_0t)(\hat{1}-\hat{P})iL\mathbf{A} \tag{10.G.17}$$

In order to obtain Eq. 10.G.16 we have applied the property

$$\hat{P}\mathbf{F}(t) = 0 \tag{10.G.18}$$

which can be derived by the analytical expression of Eq. 10.G.11b itself.

Equation 10.G.16 is quite a significant one; it corresponds to saying that replacing $(\hat{1}-\hat{P})\hat{L}$ with $\hat{L}_0$ in the exponential of Eq. 10.G.11a is equivalent to neglecting higher-order contributions in $\hat{\mathcal{H}}_{SL}$. Consequently, when the interaction is small we can replace $\mathbf{F}(t)$ with $\mathbf{F}_0(t)$.

Equation 10.G.18 does not imply that the instantaneous value of the fluctuating force is zero, because this has to be evaluated by taking into account the real initial state of the thermal bath, which could be far from equilibrium (following, for example a laser pulse). In this respect (Section 9.1) our approach is different from that by Mori and Kubo (Mori, 1965a; Kubo, 1966) and more like that of Nordholm and Zwanzig (1975). Nordholm and Zwanzig showed that Eq. 10.G.10 is valid even when the instantaneous average value of the stochastic force is not zero. We are, however, using an approach which is the reverse of that of Nordholm and Zwanzig. We first build up the GLE; then we use it in order to obtain some

information on the reduced density matrix:

$$\sigma = \underset{\{L\}}{\mathrm{Tr}}\,\rho \tag{10.G.19}$$

In accordance with Deutch (1972), we have

$$A_{\alpha\alpha'}(t) = e^{i\hat{\mathscr{H}}t}|\alpha'\rangle\langle\alpha|e^{-i\hat{\mathscr{H}}t} \tag{10.G.19a}$$

$$\langle\alpha|\sigma(t)|\alpha'\rangle = \mathrm{Tr}\{\rho(0)A_{\alpha\alpha'}(t)\} \tag{10.G.19b}$$

We can regard $\langle\alpha|\sigma(t)|\alpha'\rangle$ as being the instantaneous average value of $A_{\alpha\alpha'}$. It then follows that if $\rho(0)$ is expressed as $\rho(0) = \sigma(0)\rho_0^{(L)}$ the instantaneous value of the fluctuating force can be different from zero. The effect of a fluctuating force with nonvanishing instantaneous value has been dealt with by using the approach of Chapter 10 (Ferrario and Grigolini, 1981).

Equation 10.G.16 shows that when the interaction $\hat{\mathscr{H}}_{SL}$ is fairly small we can replace $\mathbf{F}(t)$ with $\mathbf{F}_0(t)$ (Eq. 10.G.17). We can thus define the "memory kernel" $\mathbf{d}(s)$ by the following inner product:

$$\mathbf{d}(s) = -(\mathbf{F}_0(t+s), \mathbf{F}_0^+(s)) \tag{10.G.20}$$

We know that weak coupling results in a long relaxation time. In other words $\mathbf{d}(s)$ is a short lifetime function. However, $\mathbf{c}$, which can be written as:

$$\mathbf{c} = (\hat{P}i\hat{L}\mathbf{A}, \mathbf{A}^+) = i(\hat{L}_0\mathbf{A}, \mathbf{A}^+) = \begin{pmatrix} i\omega_{11} & & & \\ & i\omega_{21} & & \\ & & i\omega_{31} & \\ & & & \ddots \end{pmatrix}, \tag{10.G.21}$$

could contain very high frequencies. Since we do not want to put any constraint on the frequencies $\omega_{\alpha\alpha'}$'s, we make the following transformation into the interaction picture:

$$\tilde{A}_{\alpha\alpha'}(t) = \exp(-i\omega_{\alpha\alpha'}t)A_{\alpha\alpha'}(t) \tag{10.G.22}$$

which allows us to write Eq. 10.G.10 as follows:

$$\frac{\partial}{\partial t}\tilde{A}_{\alpha\alpha'}(t) = -\sum_{\beta\beta'}\exp(-i\omega_{\alpha'\alpha}t)\int_0^t ds(\hat{L}_1\exp(i\hat{L}_0 s)\hat{L}_1 A_{\alpha\alpha'}, A^+_{\beta\beta'}) \times \exp[i\omega_{\beta\beta'}(t-s)]\tilde{A}_{\beta\beta'}(t-s) + \tilde{F}_{\alpha\alpha'}(t) \tag{10.G.23}$$

To obtain this equation we have also used the approximate expression for the "memory kernel" given by Eq. 10.G.20. By making the approximation that the interaction picture "memory kernel"

$$\tilde{\mathbf{d}}(s) = (\hat{L}_1\exp[i\hat{L}_0 s]\hat{L}_1\mathbf{A}, \mathbf{A}^+)\exp(-i\boldsymbol{\Omega}s) \tag{10.G.24}$$

(where $\boldsymbol{\Omega}$ is a diagonal matrix containing the eigenvalues of the superoperator L_0) has a short lifetime, we obtain

$$\frac{\partial}{\partial t}\tilde{A}_{\alpha\alpha'} = -\sum_{\beta\beta'}\exp[i(\omega_{\alpha\alpha'} - \omega_{\beta\beta'})t]R^{\alpha\alpha'}_{\beta\beta'}\tilde{A}_{\beta\beta'} + \tilde{F}_{\alpha\alpha'}(t) \tag{10.G.25}$$

with

$$R^{\alpha\alpha'}_{\beta\beta'} = \int_0^\infty ds(\hat{L}_1\exp(i\hat{L}_0 s)\hat{L}_1 A_{\alpha\alpha'}, A^+_{\beta\beta'})\exp(-i\omega_{\beta'\beta}s) \tag{10.G.26}$$

In order to obtain an explicit expression for the $R^{\alpha\alpha'}_{\beta\beta'}$'s, we make now the fairly unrestrictive assumption that $\hat{\mathscr{H}}_{LS}$ may be written as follows:

$$\hat{\mathscr{H}}_{LS} = \sum_{\alpha\alpha'}|\alpha\rangle\langle\alpha'|\hat{F}_{\alpha\alpha'} \tag{10.G.27}$$

where $\hat{F}_{\alpha\alpha'}$ is an operator acting on the "thermal bath." Then we obtain

$$R^{\alpha\alpha'}_{\beta\beta'} = \delta_{\alpha\beta}\sum_\gamma g^{(-1)}_{\beta'\gamma\gamma\alpha'}(\omega_{\gamma\beta'}) + \delta_{\alpha'\beta'}\sum_\gamma g^{(1)}_{\alpha\gamma\gamma\beta}(\omega_{\beta\gamma}) - g^{(1)}_{\beta'\alpha'\alpha\beta}(\omega_{\beta\alpha}) - g^{(-1)}_{\beta'\alpha'\alpha\beta}(\omega_{\alpha'\beta'}) \tag{10.G.28}$$

where

$$g^{(\mu)}_{\alpha\alpha'\beta\beta'}(\omega_{\gamma\gamma'}) = \int_0^\infty G^{(\mu)}_{\alpha\alpha'\beta\beta'}(t)\exp(i\omega_{\gamma\gamma'}t)\,dt \tag{10.G.29}$$

$$G^{(\mu)}_{\alpha\alpha'\beta\beta'}(t) = \sum_{dd'}\int_{-\infty}^{+\infty} df\,df'\eta_d(f)\eta_{d'}(f')\langle f|\hat{F}_{\alpha\alpha'}|f'\rangle\langle f'|\hat{F}_{\beta\beta'}|f\rangle P(f)e^{i\mu(f-f')t} \quad (\mu = \pm 1), \tag{10.G.30}$$

and

$$P(f) = \langle f|\rho_0^{(L)}|f\rangle \tag{10.G.31}$$

Following Hubbard (1961), we have assumed that the summation over the eigenstates $|f\rangle$ of the thermal bath ($\hat{\mathscr{H}}_0^{(L)}|f_d\rangle = f|f_d\rangle$, d a parameter used to distinguish degenerate states) may be replaced by an integral according to the following formula:

$$\sum_{fd} \to \sum_d \int_{-\infty}^{+\infty} df\,\eta_d(f)$$

To evaluate $G^{(\mu)}_{\alpha\alpha'\beta\beta'}(\omega_{\gamma\gamma'})$, following Hubbard we can write

$$G^{(\mu)}_{\alpha\alpha'\beta\beta'}(t) = \int_{-\infty}^{+\infty}\mathscr{L}^{(\mu)}_{\alpha\alpha'\beta\beta'}(\omega)\exp(-i\omega t)\,d\omega \tag{10.G.30a}$$

where

$$\mathscr{L}^{(\mu)}_{\alpha\alpha'\beta\beta'}(\omega) = \sum_{dd'}\int_{-\infty}^{+\infty} df\eta_d(f)\eta'_d(f+\omega)\langle f|\hat{F}_{\alpha\alpha'}|f+\mu\omega\rangle\langle f+\mu\omega|\hat{F}_{\beta\beta'}|f\rangle P(f) \tag{10.G.30b}$$

Then, from Eq. 10.G.29 we obtain

$$\begin{aligned} g^{(\mu)}_{\alpha\alpha'\beta\beta'}(\omega_{\gamma\gamma'}) &= \int_0^\infty dt\int_{-\infty}^{+\infty}\mathscr{L}^{(\mu)}_{\alpha\alpha'\beta\beta'}(\omega)\exp(-i\omega t)\exp(i\omega_{\gamma\gamma'}t)\,d\omega \\ &= \int_{-\infty}^{+\infty} d\omega\,\mathscr{L}^{(\mu)}_{\alpha\alpha'\beta\beta'}(\omega)\int_0^\infty \exp[i(\omega_{\gamma\gamma'}-\omega)t]\,dt \\ &= \lim_{\gamma\to 0_+}\int_{-\infty}^{+\infty} d\omega\,\mathscr{L}^{(\mu)}_{\alpha\alpha'\beta\beta'}(\omega)\int_0^\infty \exp(-\gamma t)\exp[-i(\omega-\omega_{\gamma\gamma'})t] \\ &= i\lim_{\gamma\to 0_+}\int_{-\infty}^{+\infty} d\omega\,\mathscr{L}^{(\mu)}_{\alpha\alpha'\beta\beta'}(\omega)[i\gamma-(\omega-\omega_{\gamma\gamma'})]^{-1} \end{aligned} \tag{10.G.32}$$

This result implies, of course, that $\mathscr{L}(z)$ is an analytical function. By taking into account the important property

$$p(f+\omega) = e^{-\beta\omega} p(f) \tag{10.G.33}$$

we obtain

$$g^{(-1)}(\omega) = g^{(1)}(-\omega) = e^{-\beta\omega} g^{(1)}(\omega) \tag{10.G.34}$$

Equation 10.G.34 is the detailed balance equation and allows our system to evolve to its canonical distribution. Assume

$$\rho(0) = \rho_0^{(L)} \sigma(0) \tag{10.G.35}$$

Then, from Eq. 10.G.19b,

$$\langle \alpha | \sigma(t) | \alpha' \rangle = \underset{\{S\}}{\mathrm{Tr}} \, \sigma(0) \langle A_{\alpha\alpha'}(t) \rangle \tag{10.G.36}$$

By applying Eq. 10.G.36 to Eq. 10.G.25 and transforming back to the laboratory frame of reference we obtain (the contributions $\omega_{\alpha\alpha'} - \omega_{\beta\beta'} \neq 0$ are disregarded)

$$\frac{\partial}{\partial t} \langle \alpha | \sigma(t) | \alpha' \rangle = -i\omega_{\alpha\alpha'} \langle \alpha | \sigma(t) | \alpha' \rangle - \sum_{\beta\beta'} R^{\alpha\alpha'}_{\beta\beta'} \langle \alpha | \sigma(t) | \alpha' \rangle \tag{10.G.37}$$

By taking into account Eq. 10.G.34 the coefficients $R^{\alpha\alpha'}_{\beta\beta'}$ of Eq. 10.G.38 can be written as follows:

$$R^{\alpha\alpha'}_{\beta\beta'} = -g^{(-1)}_{\beta'\alpha'\alpha\beta}(\omega_{\alpha'\beta'}) - g^{(-1)}_{\beta'\alpha'\alpha\beta}(\omega_{\alpha\beta}) + \delta_{\alpha\beta} \sum_{\gamma} g^{(-1)}_{\beta'\gamma\gamma\alpha'}(\omega_{\beta'\gamma}) \exp(\beta\omega_{\beta'\gamma}) + \delta_{\alpha'\beta'} \sum_{\gamma} g^{(-1)}_{\alpha\gamma\gamma\beta}(\omega_{\beta\gamma}) \exp(\beta\omega_{\beta\gamma}) \tag{10.G.38}$$

Equation 10.G.37 is exactly the Redfield equation (Redfield, 1965). From Eq. 10.G.38 we easily obtain

$$\sum_{\beta} R_{\alpha\alpha'\beta\beta} \exp(-\beta\epsilon_\beta) = 0 \tag{10.G.39}$$

which means that the canonical distribution is a solution to the Redfield equation.

REFERENCES

Adelman, S. A., *J. Chem. Phys.* **71**, 4471 (1979)

Agarwal, G. S., *Springer Tracts Mod. Phys.* **70**, 111 (1974).

Ballentine, L. E., *Rev. Mod. Phys.* **42**, 358 (1970).

Berkowitz, M., Brooks, C. L., III, and Adelman, S. A., *J. Chem. Phys.* **72**, 3889 (1980).

Berne, B. J. and Harp, G. D., *Adv. Chem. Phys.*, **17**, 63 (1970).

Bixon, M., Jortner, J., and Dothan, Y., *Mol. Phys.* **17**, 109 (1969).

Böttcher, C. J. F. and Bordewijk, P., *Theory of Electric Polarization*, Vol. II, Elsevier, New York (1978).

Ciccotti, G. and Ryckaert, J. P., *Mol. Phys.* **40**, 141 (1980).

Deutch, J. M., in *Electron Spin Polarization in Liquids*, L. T. Muus and P. W. Atkins, Eds., Plenum Press, New York, p. 127 (1972).

Evans, M. W., Davies, R., and Evans, G., *Adv. Chem. Phys.* **44**, 255 (1980a).

Evans, M. W., Ferrario, M., and Grigolini, P., *Chem. Phys. Lett.* **71**, 139 (1980b).

Evans, M. W., Grigolini, P., and Resca, L., *Chem. Phys. Lett.* **69**, 97 (1980c).

Ferrario, M. and Evans, M. W., *Adv. Mol. Relax. Int. Proc.*, in press (1981).

Ferrario, M., and Grigolini, P. *J. Math. Phys.* **20**, 2567 (1979a).

Ferrario, M. and Grigolini, P., *Chem. Phys. Lett.* **62**, 100 (1979b).

Ferrario, M. and Grigolini, P., *J. Chem. Phys.* **74**, 235 (1981).

Fox, R. F. *Phys. Rep.* **48**, 179 (1978).

Fox, R. F. and Uhlenbeck, G. E., *Phys. Fluids* **13**, 1893, 2881 (1970).

Friedman, J. M and Hochstrasser, R. M., *Chem. Phys.* **6**, 155 (1974).

Grigolini, P., *Mol. Phys.* **30**, 1229 (1975).

Grigolini, P., *Chem. Phys. Lett.* **58**, 191 (1978).

Grigolini, P. *Chem. Phys.* **38**, 389 (1979).

Grigolini, P., unpublished (1980).

Grigolini, P. Ferrario, M., and Evans, M. W., *Z. Phys.*, (1981).

Grigolini, P. and Rosato, V., in press on *Adv. Molec. Relax. and Inter. Processes* (1981).

Haken, H. and Weidlich, W. *Z. Phys.* **205**, 96 (1967).

Hochstrasser, R. M. and Novak, F. A. *Chem. Phys. Lett.* **48**, 1 (1977).

Hochstrasser, R. M. and Novak, F. A. *Chem. Phys. Lett.* **53**, 3 (1978).

Hubbard, P. S., *Rev. Mod. Phys.* **33**, 249 (1961).

Karasudani, T., Nagano, K., Okamoto, H., Mori, H., *Prog. Theor. Phys.* **61**, 850 (1979).

Kivelson, D. and Ogan, K. *Adv. Mag. Res.* **7**, 72 (1974).

Kubo, R., *J. Math. Phys.* **4**, 174 (1963).

Kubo, R. *Rep. Prog. Phys.* **29**, 255 (1966).

Kubo, R. in *Stochastic Processes in Chemical Physics*, K. E. Shuler, Ed., Wiley-Interscience, New York (1969).

Lax, M., *Phys. Rev.* **157**, 213 (1967).

Lax, M., *Phys. Rev.* **172**, 350 (1968).

Marin, P., Grigolini, P., in press in *J. Molec. Struct.* (1982).

Metiu, H., Oxtoby, D. W., Freed, K. F. *Phys. Rev.* **A15**, 361 (1977).

Millar, D. P., Shah, R. H., and Zewail, A. H., *Chem. Phys. Lett.* **66**, 435 (1969).

Mori, H. *Prog. Theor. Phys.* **33**, 423 (1965a).

Mori, H. *Prog. Theor. Phys.* **34**, 399 (1965b).

Mori, H., Fujisaka, H., and Shigematsu, H. *Prog. Theor. Phys.* **51**, 109 (1974).

Muus, L. T. and Atkins, P. W., Eds., "*Electron Spin Relaxation in Solids*, Plenum Press, New York (1972).

Nagano, K., Karasudani, T. Okamoto, H., and Mori, H., *Prog. Theor. Phys.* **63**, 1904 (1980).

Nordholm, S. and Zwanzig, R., *J. Stat. Phys.* **13**, 347 (1975).

Prigogine, I., *Nonequilibrium Statistical Mechanics*, Wiley, New York, Chapter 14 (1966).

Redfield, A. G., *Adv. Magn. Reson.* **1**, 1 (1965).

Schneider, W. R., *Z. Phys.* **B24**, 135 (1976).

Spain, B. and Smith, M. G., *Functions of Mathematical Physics*, Van Nostrand–Reinhold, London (1970).

Stratonovich, R. L., *Topics in the Theory of Random Noise*, Vol. I, Gordon and Breach, London (1963).

Takagahara, T., Hanamura, E., and Kubo, R. *J. Phys. Soc. Jap.* **43**, 802, 811; **47**, 1522 (1977).

Van Kampen, N. G., *Phys. Rep.* **24C**, 171 (1976).

11
The Dynamics of Collision-Induced Absorption

LIST OF SYMBOLS

$\mathfrak{A}$	Power absorption coefficient
$\underline{\alpha}$	Polarizability tensor
B	Rotational quantum coefficient
$C(t)$	Correlation function
$\mathfrak{D}$	Wigner matrix (elements)
δ	Polarizability anisotropy
F_m, F_n	Fractions of molecules in states m and n
$g(JK)$	Degeneracy
I	Moment of inertia of the linear molecule
I_A	Moment of inertia about the **A** axis
I_B	Moment of inertia about the **B** axis
I_c	Moment of inertia about the **C** axis
I_x	Moment of inertia about the **x** axis
I_y	Moment of inertia about the **y** axis
I_z	Moment of inertia about the **z** axis
I	Spin quantum number
J	Rotational quantum number
$K(t)$	Memory function
$\boldsymbol{\mu}$	Dipole moment
μ	Dipole component
$\bar{\nu}_{mn}$	Wavenumber at which transition from n to m is observable
$\bar{\nu}_{max}$	Far infrared peak frequency
N	Number of molecules per unit volume
ϕ	Potential energy
$\phi_0(t), \phi_1(t)$	Memory functions of induced absorption (section 11.2.5)
Φ	Hexadecapole moment (scalar average)
v	Charge
Q or Θ	Quadrupole moment (scalar average)
Z	Partition function

The far infrared broad band absorption of a dipolar fluid is affected to some extent by collision-induced dipolar absorption. The same is true of Raman and infrared bands and those observed in depolarized Rayleigh

scattering. The far infrared part of the 0–THz spectral range may be used with advantage to study the mechanism of molecular encounters in great detail. The questions to which we must address ourselves in this chapter are to what extent are the band shapes and correlation function $C_u(t)$ affected by this phenomenon, and how may the presence of collision-induced absorption be recognized in the presence of a permanent dipolar contribution. Fortunately the answer is relatively straightforward since any pronounced collision-induced absorption cross section per molecule is proportional to a power of the molecular number density N, while the permanent dipolar absorption is proportional to N, through for example, the Gordon sum rule.

11.1 INTEGRATED INTENSITIES OF PERMANENT DIPOLAR ABSORPTION

The intensity associated with a transition from a g_m-fold degenerate level m to a g_n-fold degenerate level n is given by

$$\bar{A}(m \to n) = \frac{8\pi^3}{3hc} N\bar{\nu}_{mn} \left(\frac{F_m}{g_m} - \frac{F_n}{g_n}\right) \sum_{jk} |\langle nk|\boldsymbol{\mu}|mj\rangle|^2$$

where N is the total number of molecules per unit volume, $\bar{\nu}_{mn}$ is the wave number at which the transition is observed, and F_m, F_n are the fractions of molecules in states m and n, respectively. $\langle nk|\boldsymbol{\mu}|mj\rangle$ is the matrix element of the dipole moment $\boldsymbol{\mu}$ for the states ψ_{mj} and ψ_{nk}, where j and k number the degenerate wave functions belonging to the energy levels E_m and E_n, respectively; the summation is over all degenerate sublevels in the upper and lower states. We make no assumption about line shape since we neglect line width in this representation. The fraction of molecules in state i is given by the Maxwell–Boltzmann expression:

$$F_i = \frac{g_i \exp(-E_i/kT)}{Z}$$

where Z is the partition function:

$$Z = \sum_i g_i \exp\left(-\frac{E_i}{kT}\right)$$

From this it can be shown that

$$\frac{F_m}{g_m} - \frac{F_n}{g_n} = \frac{1}{Z} \exp\left(-\frac{E_m}{kT}\right)\left[1 - \exp\left(-\frac{hc\bar{\nu}_{mn}}{kT}\right)\right]$$

where $E_n - E_m = hc\bar{\nu}_{mn}$. The term in square brackets accounts for stimulated emission, which is important in the far infrared, where $hc\bar{\nu}_{mn} \sim kT$. The rotational energy levels in (cm^{-1}) for rigid, linear molecules, for

example, are given by

$$E(J) = BJ(J+1)$$

where J is the rotational quantum number, and $E = h/(8\pi^2 Ic)$ is the rotational constant in reciprocal centimeters. I is the moment of inertia about the axis through the center of mass perpendicular to the molecular axis. The wave numbers corresponding to rotational transitions are

$$\bar{\nu}(J) = 2B(J+1)$$

for the transition $J \to J+1$.

Each rotational level J has $(2J+1)$ degenerate sublevels labeled by M. The sum involving the matrix elements (for $\Delta J = 1$) is now

$$\sum_{m'm''} |\langle J+1, M'|\boldsymbol{\mu}|J, M''\rangle|^2 = \mu^2(J+1)$$

the rotational partition function being

$$Z_r = \sum_J (2J+1) \exp\left(-\frac{BJ(J+1)}{kT}\right) \doteq \frac{kT}{hcB}$$

The integrated intensity of the complete pure rotational band is then

$$\bar{A} = \int \mathfrak{A}(\bar{\nu})\, d\bar{\nu} = \sum_J \bar{A}(J \to J+1) \tag{11.1.1}$$

with maximum absorption situated at

$$\bar{\nu}_{\max} = \frac{(3kT/I)^{1/2}}{(2\pi c)} \tag{11.1.2}$$

Using the analytical substitution,

$$J+1 = \frac{\bar{\nu}}{2B} \quad \text{and} \quad J(J+1) = \bar{\nu}\,\frac{\bar{\nu} - 2B}{4B^2}$$

and assuming that $2B \ll \bar{\nu}$, $hc\bar{\nu} \ll kT$, we obtain the classical contour:

$$A(\bar{\nu}) \propto \bar{\nu}^3 \exp\left(-\frac{\bar{\nu}^2 hc}{4BkT}\right) \tag{11.1.3}$$

11.1.1 Integrated Intensity for Symmetrical Tops

Define I_A as the unique moment of inertia of the symmetrical top and $I_B = I_C$. The Schrödinger equation then yields the rotational energies of the allowed states (neglecting centrifugal effects):

$$E(J, K) = BJ(J+1) + (A - B)K^2$$

where $A = h/(8\pi^2 I_A c)\ \text{cm}^{-1}$; $B = h/(8\pi^2 I_B c)\ \text{cm}^{-1}$. $J = 0, 1, \ldots$ is the rotational quantum number and $K = 0, \pm 1, \ldots, \pm J$. For each J value there are

$(2J+1)$ sublevels K. Since $E(J,K)$ involves K^2, however, there are only $(J+1)$ closely spaced energy levels for each J. The selection rules for absorption are $\Delta J = 1$, $\Delta K = 0$, giving for each $J \to J+1$ transition

$$\bar{\nu}(J) = 2B(J+1)$$

independent of K, when centrifugal distortions are not considered. The sum over matrix elements for $(J,K) \to (J+1,K)$ is

$$\sum_{M'M''} |\langle J+1, K, M'|\boldsymbol{\mu}|J, K, M''\rangle|^2 = g(J,K)\frac{[(J+1)^2-K^2]\mu^2}{(J+1)(2J+1)}$$

with a rotational partition function:

$$Z_r = \sum_{J=0}^{\infty}\sum_{K=-J}^{J} g(J,K)\exp\left(-\frac{E(J,K)}{kT}\right)$$

For C_{3v} symmetry the degeneracy $g(J,K)$ of the level (J,K) depends on the nuclear spin quantum number (I) of the three identical nuclei, so that:

$$g(J,K) = (2J+1)S(I,K)$$

where $S(I,K) = \frac{1}{3}(2I+1)(4I^2+4I+3)$ for $K=0$

$= \frac{1}{3}(2I+1)(4I^2+4I+3)$ for $K \neq 0$, K = multiple of 3

$= \frac{1}{3}(2I+1)(4I^2+4I)$ for $K \neq 0$, $K \neq$ multiple of 3

The integrated intensity may now be obtained for the $J \to J+1$ transition by summing over the K sublevels:

$$\bar{A}(J \to J+1) = A(I,J)\sum_{K=-J}^{J} S(I,K)\frac{[(J+1)^2-K^2]}{(J+1)}\exp\left(-\frac{E(J,K)}{kT}\right)$$

where

$$A(I,J) = \frac{8\pi^3 N}{3hcZ_r}\mu^2\bar{\nu}(J)\left[1-\exp\left(-\frac{hc\bar{\nu}(J)}{kT}\right)\right]$$

The rotational partition function is easily evaluated on a computer, or alternatively, if hcA, $hcB \ll kT$, then

$$Z_r = \frac{1}{3}(2I+1)(4I^2+4I+1)\left[\frac{\pi}{AB^2}\left(\frac{kT}{hc}\right)^3\right]^{1/2}$$

11.1.2 Comparison with the Sum Rule

A useful sum rule for the integrated intensity of the far infrared absorption in dipolar gases, liquids, and solids is the one derived classically by Brot (Chapter 1) and quantum mechanically by Gordon (1964), who extended the Thomas–Reiche–Kuhn sum rule, which applies to the total optical absorption by a system of *nonpolarizable* particles with spherically symmetrical charge distributions, to molecules with arbitrary mass and charge

distributions. Gordon assumes that the molecules are rigid, and that the wavelengths involved are long compared with molecular dimensions (the so-called dipole approximation). For uncharged molecules with random orientations, as in the gas or liquid:

$$A_1 = \frac{1}{N}\int_0^{\infty}\mathfrak{A}(\bar{\nu})\,d\bar{\nu} = \frac{\pi}{3c^2}\left[\frac{\mu_y^2+\mu_z^2}{I_x}+\frac{\mu_x^2+\mu_z^2}{I_y}+\frac{\mu_x^2+\mu_y^2}{I_z}\right]$$

where I_x, I_y, and I_z are the principal moments of inertia of the molecule and μ_x, μ_y, and μ_z are the components of the dipole along these axes. For a symmetrical top or linear molecule the dipole moment is along one of the principal axes, say, the z-axis. Then, since $I_x = I_y = I$,

$$A_1 = \frac{2\pi\mu^2}{3c^2 I} \qquad (11.1.2.1)$$

where we put $\mu_z^2 = \mu^2$.

This equation should account for the whole of the 0–THz band shape, but induced absorptions are not taken into account and in intensely dipolar fluids the internal field (Chapter 3) must be accounted for. A rule of thumb correction is to employ the Kirkwood factor g in the denominator of Equation 11.1.2.1 but the full dynamic theory should be used whenever possible.

Before proceeding to the detailed quantum mechanical theory of induced absorptions we illustrate the use of the equations in this section to estimate the extent of induced absorption in a linear molecule such as N_2O with a low dipole moment. This is the achievement of Baise (1972), who has clearly demonstrated the importance of the latter effect in comparison with permanent dipolar absorption. The far infrared spectra of the compressed gas are illustrated in Fig. 11.1.2.1. The long high frequency tail is soon developed into a pronounced shoulder. The theoretical $\bar{\nu}_{max}$ from Equation 11.1.2 and the spectra agree very well, additional absorption being indicated by an increase in half-width.

In Fig. 11.1.2.2 are illustrated the contour for liquid N_2O which is *quadrupole*-induced. This peaks at 46 cm^{-1} theoretically. There is also a *dipole*-induced dipole absorption, whose contour is the same as the pure rotational, and may only be distinguished theoretically by assuming a form for the *intermolecular potential energy* using both van der Waals forces (represented by a Lennard–Jones potential) and electrostatic terms as expanded in a convenient mathematical series. This series contains the dipole, quadrupole, octopole, hexadecapole, etc., that is, is a *multipole expansion* of the potential energy. The efficacy of this type of expansion in comparison with charge-charge interactions has been discussed by Brot and co-workers (1978) in a molecular dynamics simulation, which is discussed in Section 11.2.

If we therefore make the assumption that there are three main contributions to the observed integrated intensity $\bar{A}$—pure dipolar, dipole-induced, and quadrupole-induced—then the integrated intensity for the

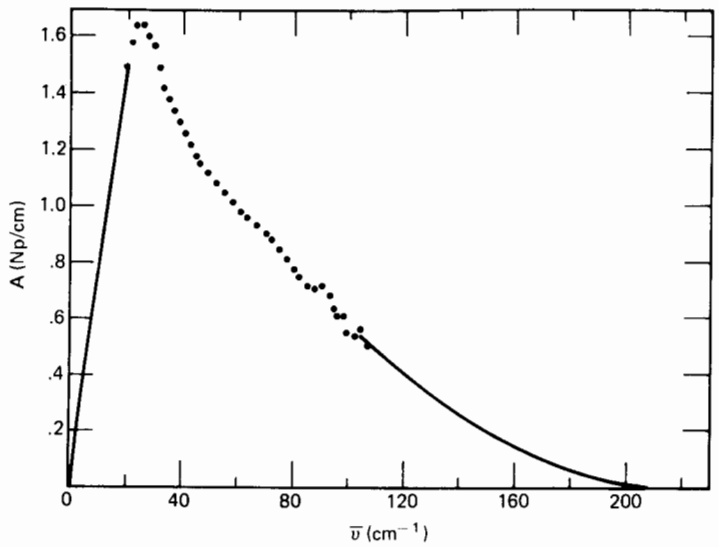

Figure 11.1.2.1 Absorption of N_2O gas just above the critical point at 74.5 bar and 312°K. Note the distortion due to induced dipoles. [Reproduced by permission from A. I. Baise, *J. Chem. Soc. Faraday Trans. II* **69**, 1907 (1972).]

pure rotational transition is proportional to N, so that its contribution to the observed total intensity is A_1N. The constant A_1 can now be evaluated using the sum rule or by summing the quantum mechanical $J \rightarrow J+1$ transitions over all J. For N_2O these methods yield to two significant figures the same result: $A_1 = 0.97 \times 10^{-20}$ cm for each temperature used. We see later that in two-body collisions the contributions from induced absorption

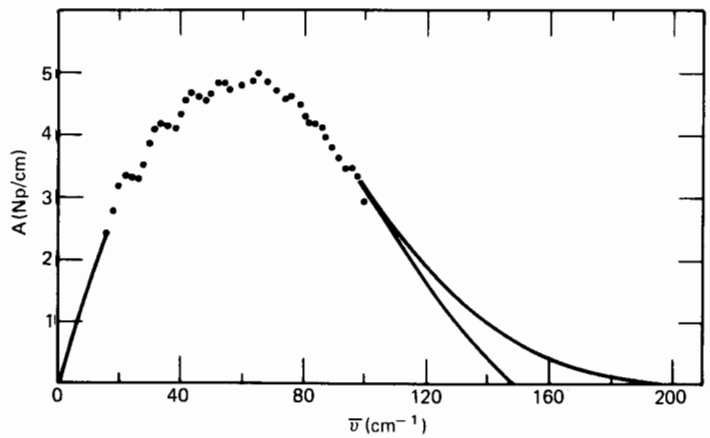

Figure 11.1.2.2 Absorption coefficient of liquid N_2O at 304°K. [Reproduced by permission from A. I. Baise, *J. Chem. Soc. Faraday Trans. II* **69**, 1907 (1972).]

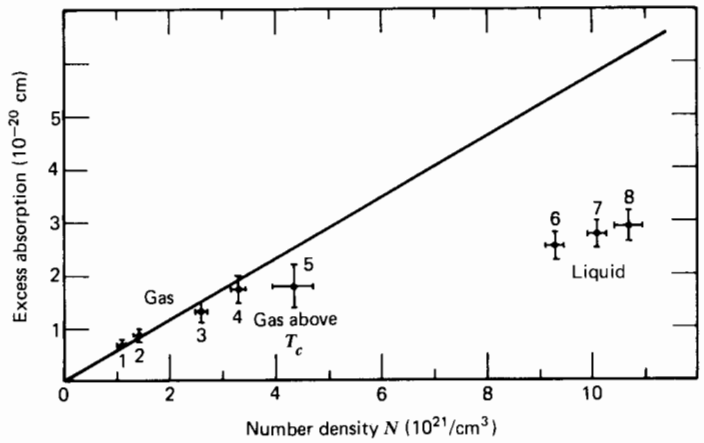

Figure 11.1.2.3 The excess absorption of N_2O as a function of density, showing points for the gas before the critical point (1–4); the gas above the critical point (5); and the liquid (6–8). [Reproduced by permission from A. I. Baise, *J. Chem. Soc. Faraday Trans. II* **69**, 1907 (1972).]

are proportional to N^2 so that

$$\bar{A}^{\mu} + \bar{A}^{Q} = A_2N^2 = \sum_J \bar{A}^{\mu}(J \rightarrow J+1) + \sum_J \bar{A}^{Q}(J \rightarrow J+2)$$

so that the total intensity is

$$\bar{A} = A_1N + A_2N^2 \qquad (11.1.2.2)$$

The "excess" absorption $(A - A_1)$ when plotted against N gives the straight line of Fig. 11.1.2.3. *At high densities the induced absorption becomes larger than the pure dipolar absorption,* $(N^2A_2 > NA_1)$.

Above the critical point in N_2O the induced absorption is very pronounced, and although the density is close to that of the liquid, the spectrum resembles the gas phase contour with $\bar{\nu}_{max}$ still at 25 cm^{-1}. (Notice the great difference in the case of liquid CH_2Cl_2, where the $\bar{\nu}_{max}$ has shifted a great deal away from the gas phase maximum.)

In the liquid itself $\bar{\nu}_{max}$ *has shifted by about* 30 cm^{-1} *to higher frequencies and the contours are now much broader.* It is important now that the "excess" absorption per molecule seems in the liquid to be much smaller. This is a sensitive indication of the fact that in the liquid the two-body collision theory producing A_2N^2 is no longer valid. The far infrared may therefore be used as a guide to the nature of interactions in the *non*dipolar as well as the dipolar condition (Fig. 11.1.2.4).

Since N_2O is isoelectronic with CO_2 it is interesting to compare the far infrared spectra of these compounds under roughly the same conditions, since in CO_2 this is completely collision-induced (Section 11.2). In CO_2 there is a shift of 25 cm^{-1} in $\bar{\nu}_{max}$ in going from the gas to the liquid and the

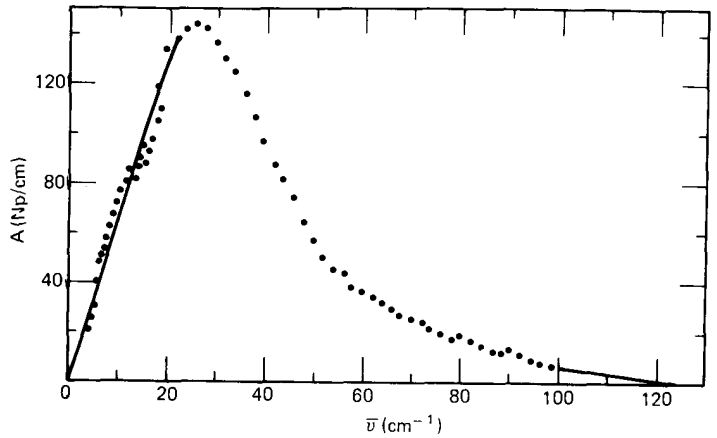

Figure 11.1.2.4 Absorption of liquid CHF_3 at 296°K. [Reproduced by permission from A. I. Baise, *J. Chem. Soc. Faraday Trans. II* **69**, 1907 (1972).]

integrated intensity divided by the square of the amagat density *is a factor of 25 less* in the liquid than in the gas.

11.1.3 Use and "Misuse" of Induced Absorption

The "misuse" of induced absorption may obviously be delineated when a model of purely dipolar dynamics is evaluated against such heavily affected spectra as that of N_2O in all states except the dilute gas and crystalline solid (where the collision-induced absorption cancels by symmetry). This in turn raises the question of when is it reasonably certain that the 0–THz spectrum (or Raman/Rayleigh spectrum) is free from such effects. The answer in strict terms is never, but the induced contribution may be minimized by judicious choice of experimental conditions and of sample. In this section we illustrate these criteria by reference to heavily absorbing specimens such as CHF_3 and CH_2Cl_2.

Fluoroform (CHF_3), studied by Baise (1972) and Gerschel (Fig. 1.2.1) along the gas-liquid coexistence curve, has a large dipole moment, thus minimizing the effect of induced absorption. The general shape of the curves is similar at all states and pressures, peaking at 26 cm^{-1}. However, at sufficiently high molecular number densities, the peak shifts considerably, as Gerschel's data demonstrates. There is no feature to mark the critical point along the gas-liquid coexistence curve. The data of relevance to this chapter are shown in Table 11.1.3.1 where the excess absorption is listed against the total integrated intensity. The competing mechanisms responsible for the high frequency wing may be assigned to the development of libration (in the liquid)-induced absorption from the quadrupole or higher moments, overlap forces, dipole-induced absorption, and even

Table 11.1.3.1 Excess Absorption in Fluoroform due to Induction

Pressure (bars)	n	Polo–Wilson factor	$10^{-21}N$ (cm^{-3})	$10^{20}A$ (cm)	$10^{20}(A - A_1)$ (cm)
10.3	1.01	1.0	0.28	79	1
20.7	1.01	1.0	0.61	88	10
37.9	1.03	0.99	1.5	92	14
Liquid	1.15	0.94	6.4	88	10

multipole-induced effects. However, the overwhelming proportion is due to the motion of the permanent dipole alone. The highest liquid density used by Baise was 0.74 g/cm^3 (the critical density is 0.52 g/cm^3) so that the shift in $\bar{\nu}_{max}$ is not developed to any significant degree.

In this case, then, it is reasonable to assume that the band shapes and correlation functions in the 0–THz region are dominated by the motion of the permanent dipole.

One of the ways of maximizing the contribution of the permanent dipole to the 0–THz band shape is to choose an intensely dipolar molecule for the purposes of extracting an accurate $C_u(t)$. The dipole-induced dipole contribution to the excess absorption is usually much smaller than the quadrupole-induced dipole contribution so that increasing the magnitude of the dipole moment does not introduce extra-induced terms this way. A solution of CH_2Cl_2 in CCl_4, for example (see Chapter 6) is spectrally dominated by the motions of the permanent CH_2Cl_2 dipole moment. The maximum absorption intensity of pure CH_2Cl_2 liquid is about 160 Np/cm, while that of the CCl_4 solvent (*octopole* induced) is about 1.5 Np/cm at ambient temperature. In pure CH_2Cl_2 there are dipole- and quadrupole-induced terms which are of course absent in CCl_4, but the plot of integrated absorption intensity against number density (N) of CH_2Cl_2 in CCl_4 is linear. The absorption cross section seems to depend (within the experimental uncertainty) only on the concentration of the *permanent* CH_2Cl_2 dipoles. The immediate environment of CH_2Cl_2 molecules in CH_2Cl_2 and CCl_4 solution is very different as far as the mechanism of interaction dipole induction is concerned, so that if this were a significant factor in the overall band shape some concentration dependence on powers of N would be expected (compare Chapter 4). Similarly, one of the ways of minimizing the induction effect in depolarized Rayleigh scattering is to choose a highly anisotropic molecule in a solvent such as CCl_4 with scalar polarizability.

One of the most interesting studies of the behavior of far infrared induced absorption upon dilution is that of Davies et al. (1973), who have also investigated the effect of replacing the multipole expansion of the potential by charge-charge interactions. If the absorption of a mixture of two nondipolar liquids is proportional to the concentration of each component

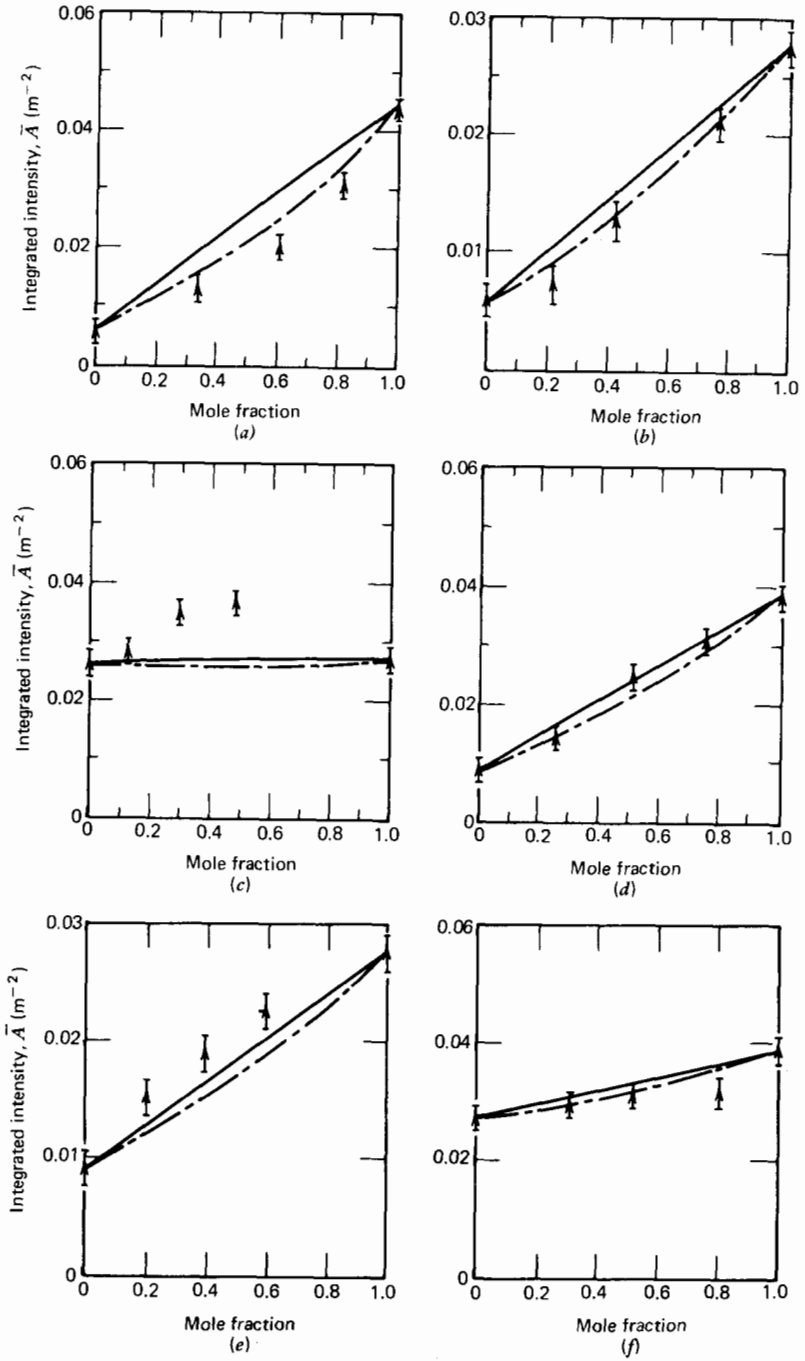

Figure 11.1.3.1 Excess absorption for mixtures of nondipolar liquids. (*a*) *trans*-1,2-Dichloromethylene in cyclohexane; (*b*) *p*-difluorobenzene in cyclohexane; (*c*) *p*-difluorobenzene in CS_2; (*d*) benzene in CCl_4; (*e*) *p*-difluorobenzene in CCl_4; (*f*) *p*-difluorobenzene in benzene. ▲ Experimental points; –·–·–·–, as calculated. [Reproduced by permission from G. J. Davies and J. Chamberlain, *J. Chem. Soc. Faraday Trans. II* **69**, 1739 (1973).]

as is the case for nondipolar liquids, then the absorption coefficient at a spot frequency would be given by

$$\mathfrak{A}(\bar{\nu}) = N_A^2\mathfrak{A}_{AA} + N_B^2\mathfrak{A}_{BB} + 2N_AN_B\mathfrak{A}_{AB} \qquad (11.1.3.1)$$

where N_A and N_B are the mole fractions of the components A and B, and $\mathfrak{A}_A$ and $\mathfrak{A}_B$ are absorption coefficients of the pure liquids. However, if the absorption has its origins in a bimolecular collisional process, then

$$\mathfrak{A}(\bar{\nu}) = N_A^2\mathfrak{A}_{AA} + N_B^2\mathfrak{A}_{BB} + 2N_AN_B\mathfrak{A}_{AB} \qquad (11.1.3.2)$$

provided that only two molecules are involved in the interaction process. In the liquid, this is of course a severe assumption; in general, multibody processes would produce deviations from the simple relation 11.1.3.2. Davies et al. further assume that $\mathfrak{A}_{AB} = (\mathfrak{A}_{AA}\mathfrak{A}_{BB})^{1/2}$. It is important when considering the induced absorption in mixtures of liquids to take into account the volume change on mixing, because the variation with mole fraction of density is not linear. The simple Eq. 11.1.3.2 works well for liquid pairs such as *trans*-1,2 dichloroethylene-cyclohexane, *p*-difluorobenzene-cyclohexane, and *p*-difluorobenzene-benzene, but in some cases (Fig. 11.1.3.1) the variation is in *excess* of a direct proportionality with concentration, the most striking example being *p*-difluorobenzene-carbon disulfide. This is cited as evidence for special kinds of interaction induction of dipole. However, it must be kept in mind that the pair interaction model, although it is the basis of the molecular dynamics simulation method, is unsound when it comes to induction in liquids. This has been shown by Baise in N_2O, where the excess absorption is no longer, in the liquid, proportional to N^2, *but almost to* N (Fig. 11.1.2.3 for N_2O).

This is a point of importance when dealing with liquids such as chlorobenzene and bromobenzene, where the induced absorption seems to be contributing strongly (because the Gordon sum rule value is exceeded by some 50%). However, (Chapter 4), when these are diluted in a solvent such as CCl_4 the absorption cross section remains *linear* in N, the concentration of the dipolar molecule. These apparently contradictory findings may be resolved only by assuming that the dependence on N of the *induced* absorption in the liquid mixture is *also*, within experimental uncertainty, *linear*, or very nearly so. The reason for this is that there is a cancellation of the induction effects of surrounding molecules on a given reference. This means that eventually (in the crystalline solid) there will be *no* dependence on N of the excess absorption (complete cancellation will have been achieved).

11.2 MECHANISMS OF INDUCED ABSORPTION

Nondipolar liquids and compressed gases absorb in the 0–THz frequency region due to a fluctuating (time-dependent) dipole induced by the other

molecules in the ensemble. The basis of the subject have been dealt with lucidly by Möller and Rothschild (1971) and by McQuarrie (1975). Although only broad bands are observable, whose breadth corresponds roughly to the lifetime of the induced dipole, a quantum theory using a multipole expansion of the electrostatic field may be used as an approximate representation (as in Section 11.1). The degree to which the theory and experiment match up is indicative of the type of intermolecular potential active in inducing the temporary absorbing dipole.

Early evidence of an absorption at high microwave frequencies in highly purified nondipolar liquids was presented by Whiffen (1950). The first indication that the absorptions are rototranslational rather than purely translational in origin came via the work of Savoie and Fournier (1970) on CH_4 and CD_4 in the liquid and plastic crystaline states down to 12°K. The liquid exhibits a broad maximum at about 200 cm^{-1} for CH_4 and 150 cm^{-1} for CD_4, which has an $I^{1/2}$ (rotational) rather than $m^{1/2}$ (translational) dependence. Davies et al. (1973) made an attempt to interpret these bands in terms of the torsional oscillation of a molecule within the cage formed by its neighbors. Evidence of a substantial intermolecular mean square torque in the liquid was put forward by Birnbaum et al. (1971) and by Baise (Section 11.1), and verified by Evans (1973) in the intensely quadrupolar species cyanogen.

The nondipolar molecules absorb in the 0–THz region because the overall symmetry of the electron cloud is distorted, producing upon collision a small dipole moment that changes in magnitude and direction rapidly with time. Thus compressed gaseous mixtures of rare gas atoms absorb, whereas the components when separated and moderately pressurized do not. A pair of colliding helium atoms, for example, do not possess a resultant electronic cloud of dipolar asymmetry, whereas a helium-neon pair modulates the electromagnetic field over a broad band of far infrared frequencies commensurate with the most probable frequencies at which interatomic collisions occur. Atomic-induced absorption is purely translational in origin, a mechanism that persists in molecular liquids such as hydrogen and nitrogen as the absorption $\Delta J = 0$, where J is the rotational quantum number. A dipole moment set up between a pair of colliding molecules in addition absorbs by rotational means since even without relative translation of molecular centers, the effect on each other of their rotating electric fields does not cancel. A practical means of dealing with these intermolecular absorption mechanisms is to treat them separately. The rotational absorption is dealt with by expanding the field in terms of *multipole tensors*, which all vanish only in the case of spherical symmetry such as that of atoms.

Pseudospherical molecules such as SF_6 have only the higher multipoles (those above and including the hexadecapole for O_h symmetry), and therefore display a weak, rotational induced absorption band at moderately high number densities. The first nonvanishing multipole in a homogeneous

diatomic such as N_2 is the quadrupole which produces a dipole on molecule A, modulated by the rotational motion of the inducing molecule B. The symmetry of the quadrupole moment is such that it rotates twice as fast as the molecule itself and thus produces quantum absorptions with the selection rule $\Delta J = 2$, in contrast to the $\Delta J = 1$ rule for the rotation of a permanent dipole. Similarly, the first nonzero multipole moment for T_d symmetry, the octopole, produces $\Delta J = 3$, and the hexadecapole $\Delta J = 4$.

11.2.1 The Multipole Moment Tensors

The multipole expression is a means whereby the electrostatic, or time-varying electric field of a collection of charges (representing the molecule) is expanded in successive moments. The standard text is that of Buckingham (1959), and a recent review by Kielich (1973) treats the subject in great detail. In this section we recount briefly the basic concepts and use a computer simulation to compare the multipole-multipole and individual charge-charge representations of electrostatic interaction.

Several different definitions of the multipole tensors are used in the literature, but the basic concept may be illuminated by considering the potential ϕ of just two point charges (e_1 and e_2) at a point P represented by polar coordinates (R, θ). The charges are located (Buckingham, 1959) at Z_1 and Z_2 from an origin 0. Therefore (in c.g.s. units);

$$\phi = \frac{e_1}{r_1} + \frac{e_2}{r_2} = e_1[R^2 - 2RZ_1\cos\theta + Z_1^2]^{-1/2} + e_2[R^2 - 2RZ_2\cos\theta + Z_2^2]^{-1/2} \qquad (11.2.1.1)$$

If R is greater than Z_1 and Z_2 then the expression for r_1^{-1} and r_2^{-1} can be expanded using the binomial theorem:

$$\phi = \frac{e_1 + e_2}{R} + (e_1Z_1 + e_2Z_2)\frac{\cos\theta}{R^2} + (e_1Z_1^2 + e_2Z_2^2)\frac{(3\cos^2\theta - 1)}{2R^3} + \frac{(e_1Z_1^3 + e_2Z_2^3)(5\cos^3\theta - 3\cos\theta)}{(2R^4)} + \cdots$$

$(e_1 + e_2)$	is the zeroth moment (the charge).
$(e_1Z_1 + e_2Z_2)$	is the first moment (the dipole).
$(e_1Z_1^2 + e_2Z_2^2)$	is the quadrupole moment.
$(e_1Z_1^3 + e_2Z_2^3)$	is the octopole moment.
$(e_1Z_1^4 + e_2Z_2^4)$	is the hexadecapole moment.

ϕ is the sum of the potentials of a point charge whose magnitude is $(e_1 + e_2)$, and a point dipole, quadrupole, octopole, and so in, situated at the origin O. Note that the higher moments are increasingly short ranged, and become effective only at increasingly smaller values of R. *If Z_1 and Z_2 are*

not themselves very small (i.e., if the molecule is large) the multipole expansion is increasingly ineffective and should be replaced by direct charge-charge interaction.

By symmetry considerations alone we can proceed to classify molecules in terms of the multipole moments. In the same way this dipole moment of an uncharged body can be thought of as a separation of charges; the quadrupole moment may be treated as a separation of dipoles, which in a linear molecule such as CO_2 are equal and opposite. (The dipole is a separation of equal and opposite charge.) A nondipolar linear molecule has no dipole, but the quadrupole is finite. The octopole is a separation of quadrupoles, and vanishes, but the hexadecapole exists. In a dipolar molecule all the moments above the dipole exist. For molecules of tetrahedral symmetry only moments above the octopole survive, and for O_h symmetry only those above the hexadecapole.

The tensorial nature of these moments is brought out by a consideration of a distribution of charges e_i at points (x_1, y_1, z_1) or $\mathbf{r}_1$ from an origin 0 to e_i. The *distribution* is now placed in an external field produced by distant charges. The potential of the external field at $\mathbf{r}_i$ is denoted by ϕ_i, so that the energy of interaction is

$$\begin{aligned} u &= \sum_i e_i\phi_i \\ &= \sum_i e_i \left\{\phi_0 + \left[\left(\frac{\partial\phi}{\partial x}\right)_0 x_i + \left(\frac{\partial\phi}{\partial y}\right)_0 y_i + \left(\frac{\partial\phi}{\partial z}\right)_0 z_i\right]\right. \\ &\quad + \frac{1}{2}\left[\left(\frac{\partial^2\phi}{\partial x^2}\right)_0 x_i^2 + \left(\frac{\partial^2\phi}{\partial y^2}\right)_0 y_i^2 + \left(\frac{\partial^2\phi}{\partial z^2}\right) z_i^2\right. \\ &\quad \left.\left. + 2\left(\frac{\partial^2\phi}{\partial x\,\partial y}\right)_0 x_i y_i + 2\left(\frac{\partial^2\phi}{\partial y\,\partial z}\right)_0 y_i z_i + 2\left(\frac{\partial^2\phi}{\partial z\,\partial x}\right)_0 z_i x_i\right] + \cdots\right\} \end{aligned}$$

where the subscript 0 denotes the value at the origin 0. In tensor notation this is

$$\begin{aligned} u = \sum_i e_i \left[\phi_0 + \left(\frac{\partial\phi}{\partial r_\alpha}\right) r_{i_\alpha} + \frac{1}{2}\left(\frac{\partial^2\phi}{\partial r_\alpha\,\partial r_\beta}\right)_0 r_{i_\alpha} r_{i_\beta}\right. \\ \left. + \frac{1}{6}\left(\frac{\partial^3\phi}{\partial r_\alpha\,\partial r_\beta\,\partial r_\gamma}\right) r_{i_\alpha} r_{i_\beta} r_{i_\gamma} + \cdots\right] \end{aligned}$$

(i.e., r_{i_α} denotes x_i, y_i, or z_i and repeated suffixes imply a summation over all components: $r_{i_\alpha} r_{i_\beta} = r_i^2 = x_i^2 + y_i^2 + z_i^2$). Introducing, following Buckingham, the parameters

$$q = \sum_i e_i; \qquad \mu_\alpha = \sum_i e_i r_{i_\alpha}; \qquad Q_{\alpha\beta} = \sum_i e_i r_{i_\alpha} r_{i_\beta}; \qquad \text{etc.}$$

$$R_{\alpha\beta\gamma} = \sum_i e_i r_{i_\alpha} r_{i_\beta} r_{i_\gamma}$$

and using Laplace's equation, the usual definitions of the higher multipole moments of the charge distribution may be written as

$$\Theta_{\alpha\beta} = \tfrac{1}{2}(3Q_{\alpha\beta} - Q_{\gamma\gamma}\delta_{\alpha\beta}) = \frac{1}{2}\sum_i e_i(3r_{i_\alpha} r_{i_\beta} - r_i^2\delta_{\alpha\beta})$$

$$\Omega_{\alpha\beta\gamma} = \tfrac{1}{2}(5R_{\alpha\beta\gamma} - R_{\alpha\delta\delta}\delta_{\beta\gamma} - R_{\beta\delta\delta}\delta_{\gamma\alpha} - R_{\gamma\delta\delta}\delta_{\alpha\beta})$$

where $\delta_{\alpha\beta}$ is the substitution tensor ($\delta_{\alpha\beta} = 1$ if $\alpha = \beta$, $\delta_{\alpha\beta} = 0$ if $\alpha \neq \beta$, and $\delta_{\alpha\alpha} = \delta_{xx} + \delta_{yy} + \delta_{zz} = 3$). $\Theta_{\alpha\beta}$ is the quadrupole moment tensor and $\Omega_{\alpha\beta\gamma}$ is the octopole moment tensor. The number of components that are independent depend on the molecular symmetry, and are tabulated by Kielich. For molecules of low symmetry, there are three dipole components, nine quadrupole, components, 27 octopole components, and 81 hexadecapole components (i.e., of the vector, second-, third-, and fourth-rank tensors, respectively).

A further complication is that the multipole moments are not independent of the origin chosen for their calculation. Care must be exercised therefore in treating the values of the multipole moments found in the literature. For an axially symmetrical charge distribution, however, each multipole moment is determined by a single scalar quantity and the principal moments of $\Theta_{\alpha\beta}$; for example, $\Theta_{zz} = \Theta$, $\Theta_{xx} = \Theta_{yy} = -\frac{1}{2}\Theta$. In this case the electric field at the point $p(R, \theta)$ can be obtained in terms of its radial component F_r and those at right angles (F_s and F_t):

$$F_r = -\frac{\partial\phi}{\partial R} = \frac{q}{R^2} + \frac{2\mu\cos\theta}{R^3} + \frac{3\Theta(3\cos^2\theta - 1)}{2R^4} + \frac{2\Omega(5\cos^3\theta - 3\cos\theta)}{R^5} + \cdots$$

$$F_s = -\frac{1}{R}\frac{\partial\phi}{\partial\theta} = \sin\theta\left[\frac{\mu}{R^3} + \frac{3\Theta\cos\theta}{R^4} + \frac{3\Omega(5\cos^2\theta - 1)}{2R^5} + \cdots\right]$$

$$F_t = -\frac{1}{R\sin\theta}\frac{\partial\phi}{\partial\zeta} = 0$$

Davies et al. (1973) have used these equations to discuss an alternative representation of the multipole expansion for large, geometrically anisotropic molecules. It is adequate, perhaps, to use the concept of point multipoles in a theory of two-body collisions (although this is by no means well established) where the separation of molecules is large *on average.* However, in the liquid the situation is obviously beyond the capacity of a two-body theory since the N^2 rule is not even approximately valid. (Fig. 11.1.2.3). The molecules are packed close to the theoretically maximum allowed density and it is no longer possible to distinguish separate collisions per se. The basis of the multipole expansion method is therefore at risk (Eq. 11.2.1.1) and it is desirable to consider charges localized on each of the individual atoms in the interacting molecules.

The method of comparison adopted by Davies et al. is to decompose each axially symmetrical charge distribution into multipoles and equivalent point charges. The alternative charge and multipole fields are then cal-

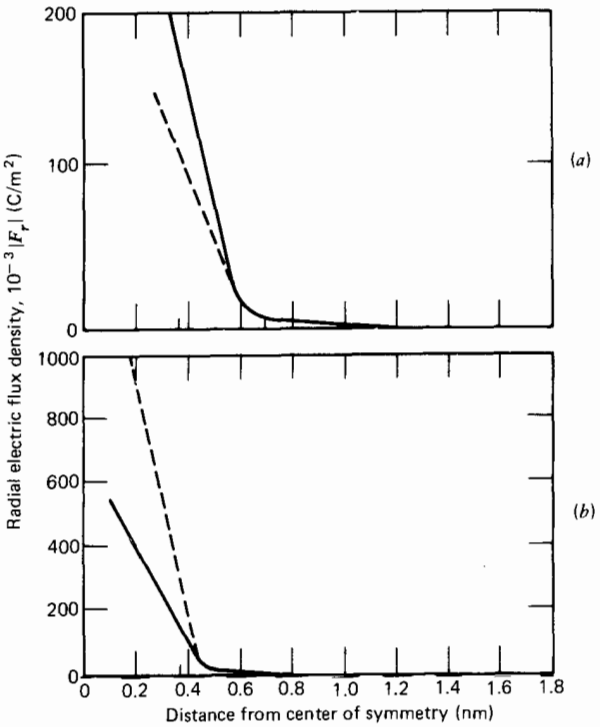

Figure 11.2.1.1 Variation of the radial electric flux density of carbon disulfide (*a*) along its linear axis and (*b*) perpendicular to its linear axis for alternative models of the quadrupole representation. Solid lines, point charges; dashed lines, point quadrupole. [Reproduced by permission from G. J. Davies et al., *J. Chem. Soc. Faraday Trans. II* **69**, 1223 (1973).]

culated at discrete distances from the center of symmetry of the molecule, as illustrated in Fig. 11.2.1.1. There is an increasing discrepancy as the van der Waals profile of the molecule is approached. For molecules such as CS_2, benzene, and CCl_4 the point multipole representation differs appreciably from the point charge model. If the point charge potential is accepted as accurate then the point multipole model is quantitatively in error. However, it is by no means certain that *either* representation is acceptable in the liquid state. Apparently, the local charge model is far preferable to the point dipole model in calculating dipole-dipole interactions of adjacent molecules. The question has lately been taken up by Occelli et al. (1978) using a molecular dynamics simulation.

11.2.2 Simulation of the Coulombic versus Multipolar Intermolecular Potentials

The aim of this simulation (Occelli et al., 1978) was not to discuss the degree of validity of the charge-charge representation but to investigate the

effects of the discrete distribution of charge on the behavior of an assembly of molecules. A direct comparison between this and the multipole expansion was made in two dimensions, in order to minimize the effect of periodic boundary conditions. There are substantial differences at low temperature between the two models, but these disappear when the temperature is increased. *There are important differences between the combined steric plus electrostatic and the steric potential alone.*

The potentials used in the summation were as follows:

1. The coulombic model: a set of n^2 charge-charge terms (there being n discrete charges in each molecule).
2. The multipolar model, involving dipole-dipole, dipole-quadrupole, quadrupole-quadrupole terms, etc.
3. Purely van der Waals type (atom-atom Lennard–Jones potential). This is included to investigate directly the claim that electrical forces have little influence on the local structure of dense liquids (Chandler, 1974).

A two-dimensional system was used in the simulation in order to avoid the difficulty that if the range of the positional-orientational correlations of the molecules reach half the edge of the "box" then the evolution of the system is severely biased by the inevitable periodic boundary conditions. The simulation was run with 225 molecules in a square, at a density equal to $0.39\sigma^{-2}$ where σ is the Lennard–Jones parameter, which is 68% of "close packing" defined with respect to the van der Waals contour of each molecular potential. At any higher densities the strong steric effects would overcome the electrical forces to a greater degree.

The most significant thermodynamic differences between the coulombic and multipolar model manifests itself at low temperatures, but the two forms produce qualitatively the same local order. At high temperatures there is little difference. However, there are always significant differences between the electrostatic potentials and the purely Lennard–Jones system. The effect of the electrical properties is to make the molecule choose the favorable end without *greatly* altering the relative alignment of the unchanged local structure. Most importantly, the structural difference between high and low temperature is *pronounced* for the electrostatic potentials but *very small* for the purely Lennard–Jones type. For *dipolar* fluids, therefore, in the intermediate density region, steric forces alone cannot explain the observed thermodynamics.

Figure 11.2.2.1 illustrates two samples of configuration taken directly from the simulation at a time interval of one to three reduced units. The letters identify molecules that have moved a long way in this time. The *multipolar* potential (or Lennard–Jones base) was used to calculate these trajectories. In the upper left part of the figure can be seen examples of a local structure of the fluid where relative molecular configurations are well

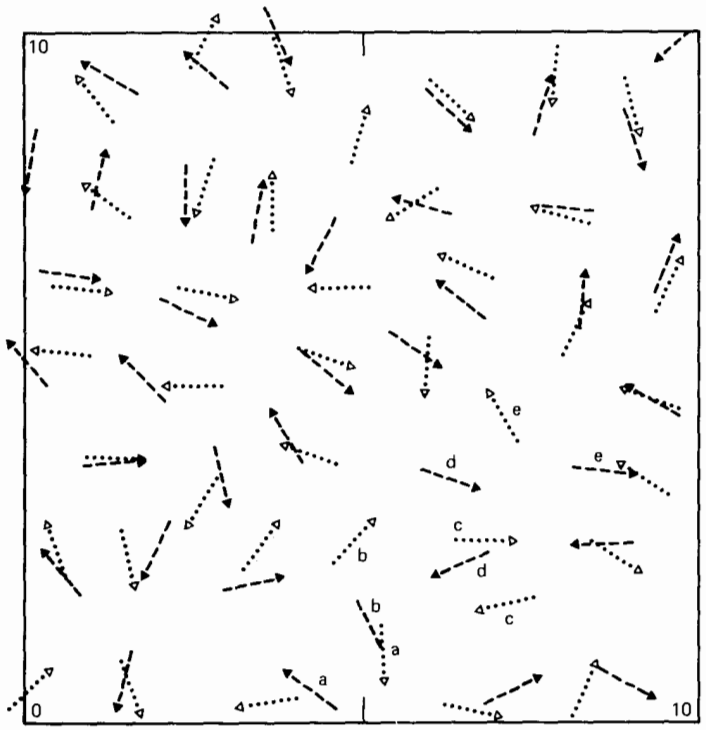

Figure 11.2.2.1 Two samples of configuration of the molecules at $T = 3.2$ for the multipolar model. The two sets of molecules that are distinguishable by solid and open arrowheads, respectively, are "snapshots" taken at a time interval of 1.3 reduced units. The letters help to identify those of the molecules that have moved far away during this time interval. [Reproduced by permission from T. Occelli, B. Quentrec, and C. Brot, *Mol. Phys.* **36**, 257 (1978).]

defined by the multipolar interaction terms. (The time of 1.3 is the order of the *complete* decay of the velocity and angular velocity a.c.f.'s.) In the areas where the local structure is important the displacement of the molecules is small; the molecules are librating and oscillating as in the solid. On the other hand, between the structured areas there is a fracture area where the molecules are drifting quickly. The structure is locally antiferroelectric, but *there are no long range dipolar correlations.* It is obvious by looking at Fig. 11.2.2.1 that the symmetry of the "packing" is such that multipole-induced dipole induction is very much a multimolecular rather than a bimolecular process.

The dynamic properties of the system are embodied in velocity, angular momentum, and $C_u(t)$ a.c.f.'s (Figs. 11.2.2.2–11.2.2.4). The velocity correlation times are 0.17, 0.12, and 0.11 for uncharged, coulombic, and multipole models, respectively, at $T = 9.4$ (reduced units). At $T = 3.2$ these figures are 0.16, 0.14, and 0.12, indicating a slight increase in the hindrance

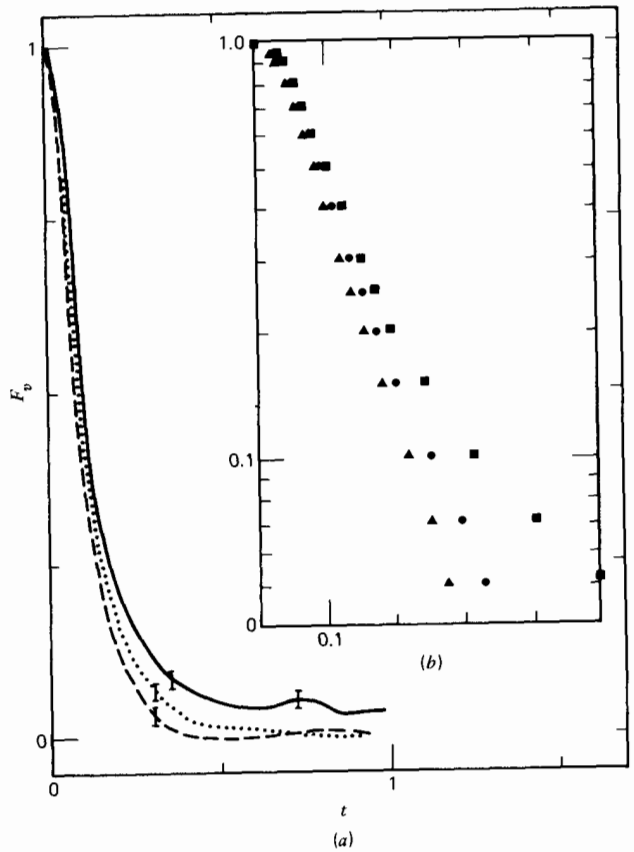

Figure 11.2.2.2 Simulated velocity a.c.f. ($T = 3.2$). (*a*) Linear scale. Solid line, Lennard–Jones potential; dotted line, charge–charge interactions; dashed line, Lennard–Jones + multipole–multipole terms. (*b*) ■ Nonelectric model; ● coulombic model; ▲ multipolar model. [Reproduced by permission from T. Occelli, B. Quentrec, and C. Brot. *Mol. Phys.* **36**, 257 (1978).]

to translation at the lower temperature. An estimate can be made of what these would be if the molecules were approximated by hard spherocylindrical cross sections undergoing uncorrelated collisions. These are 0.42 at $T = 9.4$ and 0.72 at $T = 3.2$. The much larger figures indicate that *attractive Lennard–Jones and electrostatic interactions are vitally important in the dynamics of the condensed phase of matter.* These are, of course, the factors responsible for the characteristic $\bar{\nu}_{max}$ shift of the far infrared and for the broad multipole-induced absorption bands. Brot and co-workers have used the far infrared and molecular dynamics simulations in tandem and this methodology has proved incisive.

The velocity a.c.f.'s for the two electrical models are again very similar, but differ from the purely van der Waals potential in having pronounced

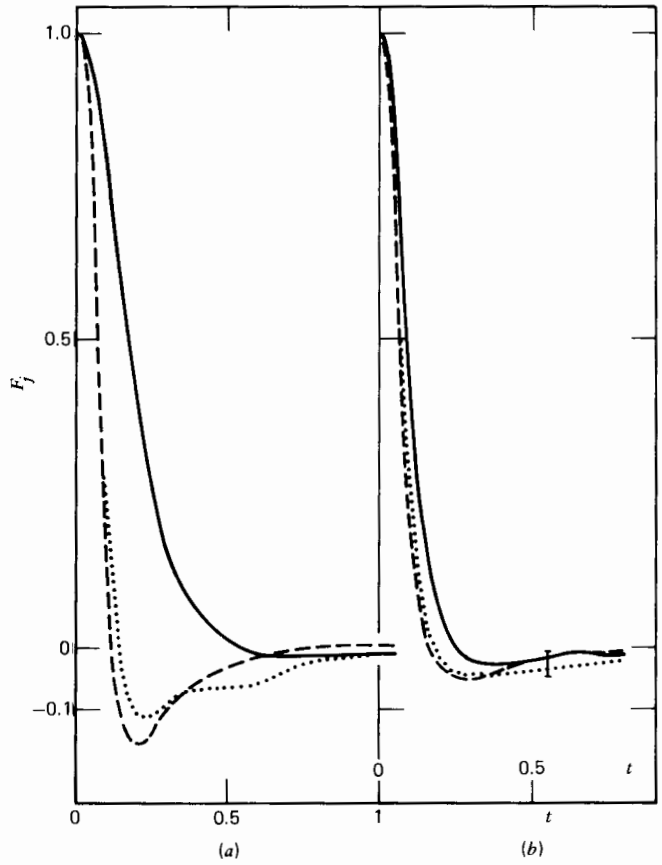

Figure 11.2.2.3 Angular momentum a.c.f., symbols 3 as for Figure 11.2.2.2. (*a*) $T = 3.2$; (*b*) $T = 9.4$. [Reproduced by permission from T. Occelli, B. Quentrec, and C. Brot, *Mol. Phys.* **36**, 257 (1978).]

negative parts, indicating viscoelastic interaction of the molecule with its neighborhood. The fluid is more structured when electrostatic intentions are simulated (i.e., classical Kirkwood theory). A difference between the coulombic and multipolar models appears in the angular momentum decay, but they are almost *indistinguishable* in the orientational a.c.f., $C_u(t)$ (Fig. 11.2.2.4). It would be worth repeating this simulation for induced absorption using multipoles higher than the dipole and octopole used by Occelli et al. (1978). It seems that the discrepancy between point-multipole and charge representations of the potential is not as serious as the simple calculation of Davies et al. (1978) indicates.

11.2.3 Frost's Theory of Multipole-Induced Absorption (1973)

The absorption is attributed to the mutually induced dipole moment $\boldsymbol{\mu}(R)$, dependent on orientations of the molecules and expressed by expanding

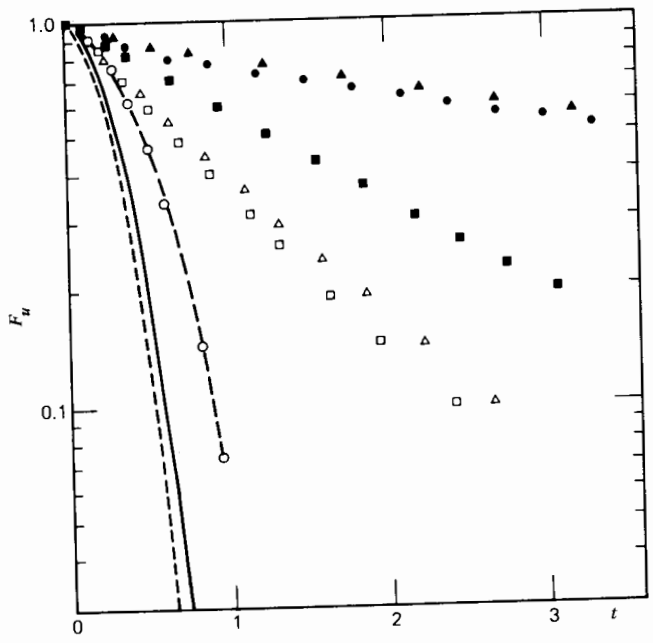

Figure 11.2.2.4 Orientational a.c.f. ----, free rotation for $T = 9.4$; ———, free rotation for $T = 7$; --○--○--, free rotation for $T = 3.2$. □ Lennard–Jones potential for $T = 7$; △ multipole and charge model at $T = 9.4$; ■ nonelectric model, $T = 3.2$; ● coulombic model, $T = 3.2$; ▲ multipolar model, $T = 3.2$. [Reproduced by permission from T. Occelli, B. Quentrec, and C. Brot, *Mol. Phys.* **36**, 257 (1978).]

$\boldsymbol{\mu}(R)$ in terms of Wigner matrices, $\mathcal{D}^{\lambda_1}_{\mu_1\nu_1}(\phi_1, \theta_1, \chi_1)\mathcal{D}^{\lambda_2}_{\mu_2\nu_2}(\phi_2, \theta_2, \chi_2)$, where $\mathcal{D}^{\lambda}_{\mu\nu}$ may be described as the matrix element of an irreducible representation of the rotation group. This permits evaluation of matrix elements of $\boldsymbol{\mu}(R)$ between eigenstates of a molecular pair. The expansion coefficients are then evaluated in terms of the polarizabilities and multipole moments (of any order) of the molecules. Summations are made over "uninteresting" magnetic quantum numbers and expressions are produced for the intensity of pressure-induced absorption in terms of Clebsch–Gordan coefficients (Chapter 2 appendix). The center of mass motion of each molecule is treated classically, with each molecule at rest, so translational absorption is ignored. The pressure-induced intensity of an absorption band is calculated in terms of quantities:

$$\sum_{m_i m_f} |\langle im_i|\boldsymbol{\mu}(R)|fm_f\rangle|^2$$

where $|im_i\rangle$, $|fm_f\rangle$ denote rotation/vibration energy eigenstates for the pair, with m_i and m_f as degenerate magnetic quantum numbers. The dipole moment $\boldsymbol{\mu}(R)$ is the sum of two parts:

$$\boldsymbol{\mu}(R) \equiv \boldsymbol{\mu}(1; R) + \boldsymbol{\mu}(2; R)$$

where $\boldsymbol{\mu}(1; R)$ is the moment induced in molecule 1 by the electric field of molecule 2 and vice versa. The electric field at 1 due to 2 depends on the orientation $(\theta_2, \phi_2, \chi_2)$ and the vibration coordinate S_2 of 2, while the polarizability of 1 depends on its orientation $(\theta_1, \phi_1, \chi_1)$ and vibration coordinates of both molecules. The same applies to $\boldsymbol{\mu}(2; R)$ so

$$\boldsymbol{\mu}(R) \equiv \boldsymbol{\mu}(R; \theta_1, \phi_1, \chi_1, S_1; \theta_2, \phi_2, \chi_2, S_2)$$

Although the molecules are interacting, it is assumed that an eigenstate of the pair is simply a product of eigenstates of the isolated molecules. This result is exact only if the intermolecular potential is independent of the Euler angles, (θ, ϕ, χ) and therefore the theory is restricted to the range where R is determined primarily by the central part $U(R)$ of the interaction potential. Frost now takes the intensity (I) of the absorption band as defined by Colpa and Ketelaar (1958) for two types of molecule, species A of number density n_A and species B:

$$I = I_{AA} + I_{BB} + I_{AB}$$

where

$$I_{AB} = \frac{8\pi^3 \bar{\nu}}{3hc} \frac{(2 - \delta_{AB})}{2} n_A n_B \sum_{\substack{i,f \\ E_f - E_i = h\nu}} \left(\frac{F_i^{AB}}{d_i^{AB}} - \frac{F_f^{AB}}{d_f^{AB}} \right) \times \int 4\pi R^2 \exp\left(- \frac{u_{AB}(R)}{kT} \right) \sum_{m_i, m_f} |\langle im_i | \boldsymbol{\mu}^{AB}(R) | fm_f \rangle|^2 \, dR \quad (11.2.3.1)$$

The summations over the quantum numbers i, f are restricted to those transitions $i \rightarrow f$ for which the absorbed frequency $h^{-1}(E_f - E_i)$ lies in the absorption band of approximate frequency ν. The quantities d_i and d_f are the degeneracies of the quantum numbers i, f; for example, $d_i = (2J_1 + 1)(2J_2 + 1)$. The quantities F_i and F_f are fractional populations of pair states with quantum numbers i, f, respectively; for example,

$$F_i = \frac{d_i \exp(-E_i/kT)}{\sum_j d_j \exp(-E_j/kT)}$$

It is emphasized that $\boldsymbol{\mu}(R)$ is the induced dipole moment of the pair molecules and does not include the permanent dipole moment $(\mathbf{p}^{(1)} + \mathbf{p}^{(2)})$ of the pair. The latter is independent of R and leads to a divergence of Eq. 11.2.3.1 which deals with the transitions of isolated molecules. Evaluation of the dipole moment matrix elements yields, for purely rotational transitions (unbroadened quantum lines),

$$\sum_{m_i m_f} |\langle im_i | \boldsymbol{\mu}(R) | fm_f \rangle|^2 = \sum_{\lambda_1 \lambda_2} \sum_{\mu_1 \mu_2} \sum_m |F_m(R, \lambda_1, \mu_1, K_1' - K_1; \lambda_2, \mu_2, K_2' - K_2)| \times \frac{(2J_1 + 1)\mathscr{C}(J_1, \lambda_1, J_1'; K_1, K_1' - K_1, K_1')^2}{(2\lambda_1 + 1)\mathscr{C}(J_2, \lambda_2, J_2'; K_2, K_2' - K_2, K_2')^2} \left(\frac{2J_2 + 1}{2\lambda_2 + 1} \right) \quad (11.2.3.2)$$

in terms of Clebsch–Gordan coefficients $\mathscr{C}$. Here the dipole moment $\boldsymbol{\mu}(R)$ is regarded through Cartesian components $\mu_j(R)$ $(j = 1, 2, 3)$ relative to the space-fixed frame. These are Hermitian operators. Each of μ_1 in Eq. 11.2.3.2 then ranges from $-\lambda_1$ to λ_1. J and K are defined by the rotational part of the molecular eigenstate of a rigid symmetrical top:

$$|JKM\rangle = \psi_{JKM}(\theta, \phi, \chi) = \left(\frac{2J + 1}{8\pi^2} \right)^{1/2} \mathscr{D}^J_{-M, -K}(\theta, \phi, \chi)$$

where the $\mathscr{D}$ values are the irreducible representations of the rotation group as defined by Rose (Chapter 2 appendix). The expansion coefficient F_m depends on molecular parameters such as the polarizability and is in practice negligible for all but a few values of λ_1 and λ_2. To evaluate F_m we want the Cartesian components in the space-fixed frame of the induced dipole moment $\boldsymbol{\mu}(R)$ in the form:

$$\mu_j(R) = \sum_k \alpha_{jk}^{(1)}(S_1, \theta_1, \phi_1, \chi_1) E_k^{(2)}(R; S_2, \theta_2, \phi_2, \chi_2) + \sum_k \alpha_{jk}^{(2)}(S_2, \theta_2, \phi_2, \chi_2) E_k^{(1)}(R; S_1, \theta_1, \phi_1, \chi_1) \quad (11.2.3.3)$$

where for example, the $\alpha_{jk}^{(1)}$ are the components of the polarizability tensor $\alpha^{(1)}$ of molecule 1, while the $E_k^{(2)}$ are the components of the electric field at molecule 1 due to molecule 2. The polarizability tensor is then cast into a spherical form relative to the space-fixed frame.

Let $\bar{x}_1, \bar{x}_2, \bar{x}_3$ denote the body-fixed principal axes of inertia of a symmetrical top molecule, chosen so that the x_3-axis is the symmetry axis. Then there are also the principal axes of polarizability of the molecule; that is, if it is subjected to an external electric field with Cartesian coordinates $\bar{E}_j$ relative to the $\bar{x}$ frame, the components of the induced moments are

$$\bar{\mu}_j = \sum_k \bar{\alpha}_{jk}(S) \bar{E}_k; \qquad \bar{\alpha} = \begin{pmatrix} \alpha_\perp & 0 & 0 \\ 0 & \alpha_\perp & 0 \\ 0 & 0 & \alpha_\parallel \end{pmatrix} \quad (11.2.3.4)$$

The spherical component version of Eq. 11.2.3.4 is then

$$\bar{\mu}_m = \sum_m \bar{A}_{m'm}(S) \bar{E}_m, \qquad A = \begin{pmatrix} \alpha_\perp & 0 & 0 \\ 0 & \alpha_\parallel & 0 \\ 0 & 0 & \alpha_\perp \end{pmatrix}$$

The next step is to rotate the space-fixed x frame into the $\bar{x}$ frame along with the components of the field and polarizability. As far as polarizability is concerned, symmetrical tops behave as linear molecules do, since for both sorts Eq. 11.2.3.4 has two equal components.

The electric field is now expanded in terms of multipole elements; the electrostatic potential caused by a molecule at a point R with polar

coordinates (R, Θ, Φ) in the x frame is then given by

$$V(R) = \sum_{\lambda=0}^{\infty} \sum_{\mu=-\lambda}^{\lambda} \left(\frac{4\pi}{2\lambda+1}\right)^{1/2} \frac{Q_\mu^\lambda Y_{\lambda\mu}^*(\Theta, \Phi)}{R^{\lambda+1}}$$

Here the μth component of the λth multipole moment of the molecule in the x frame is

$$Q_\mu^\lambda = \left(\frac{4\pi}{2\lambda+1}\right)^{1/2} \int\int\int \xi^\lambda Y_{\lambda\mu}(\alpha, \beta)\rho(S, \xi, \alpha, \beta)\xi^2 \, d\xi \sin\alpha \, d\alpha \, d\beta$$

where ρ is the change density of the molecule at a point with polar coordinates ξ, α, β in the x frame. We have then for the required fields

$$E_m(R^\pm) = \sum_\lambda E_m^\lambda(R^\pm)$$

with

$$E_m^\lambda(R^\pm) = (-1)^{m+1}(\pm 1)^{\lambda+1} \frac{[(\lambda+1)(2\lambda+3)]^{1/2}}{R^{\lambda+2}}$$

$$\times \mathscr{C}(\lambda+1, 1, \lambda; 0, -m, -m) \sum_\nu \mathscr{D}^\lambda_{-m,\nu}(\theta, \phi, \chi)\bar{Q}_\nu^{\lambda *}$$

Here R^+ denotes the case $\Theta = 0$ and R^- denotes $\Theta = \pi$.

The multipole moment components of $\bar{Q}_\mu^\lambda$ of a symmetrical top are severely limited by the fact that the x_3-axis is an n-fold axis of rotational symmetry, with $n \geq 3$. Therefore the following hold:

1. For $\lambda = 1$, only $\bar{Q}_0^1$ is nonzero. Since $Q_\mu^{\lambda *} = (-1)^\mu Q^\lambda$, this quantity is real and is the usual dipole moment of the molecule.
2. For $\lambda = 2$, only $\bar{Q}_0^2$ is nonzero. This real quantity is the usual quadrupole moment defined by $Q_0^2 = q = q_{33}$ where

$$q_{ij} = \frac{1}{2}\int\int\int \rho(S, \bar{\xi}_1, \bar{\xi}_2, \bar{\xi}_3)[3\bar{\xi}_i\bar{\xi}_j - \bar{\xi}^2\delta_{ij}] \, d\bar{\xi}_1 \, d\bar{\xi}_2 \, d\bar{\xi}_3$$

   is the Cartesian quadrupole moment tensor in the principal frame.
3. For $\lambda = 3$, only $\bar{Q}_0^3$ and $\bar{Q}_{\pm 3}^3$ are now zero if $n = 3$, while only $\bar{Q}_0^3$ is nonzero for $n > 3$.
4. For $\lambda > 3$ (hexadecapole moment and higher), the number of nonzero components $\bar{Q}_\mu^\lambda$ depends in an obvious way on n. For a linear molecule $n = \infty$ and each multipole moment has only one nonzero component $\bar{Q}_0^\lambda$.

The expansion coefficient F_m may now be evaluated in terms of polarizability and multipole moments. The dipole moment induced in molecule 1 is then

$$\mu_m(1; R) = \alpha_0^{(1)} \sum (-1)^{\lambda_2+1}[(\lambda_2+1)(2\lambda_2+3)]^{1/2} R^{-(\lambda_2+2)}$$

$$\times \sum_{\mu_2\nu_2} (-1)^{1-\mu_2}\delta_{-\mu_2, m}\bar{Q}_{\nu_2}^{(2)\lambda_2 *}\mathscr{C}(\lambda_2+1, 1, \lambda_2; 0, \mu_2, \mu_2)\mathscr{D}^0_{0,0}(1)D^{\lambda_2}_{\mu_2,\nu_2}(2)$$

$$+ (-1)^m\left(\tfrac{2}{3}\right)^{1/2}\delta^{(1)} \sum_{\lambda_2} (-1)^{\lambda_2+1}[(\lambda_2+1)(2\lambda_2+3)]^{1/2} R^{-(\lambda_2+2)}$$

$$\times \sum_{\mu_1} \sum_{\mu_2\nu_2} (-1)^{1-\mu_2}\bar{Q}_{\nu_2}^{(2)\lambda_2 *}\mathscr{C}(1, 1, 2; -m, -\mu_2, \mu_1)$$

$$\times \mathscr{C}(\lambda_2+1, 1, \lambda_2; 0, \mu_2, \mu_2)\mathscr{D}^2_{\mu,0}(1)\mathscr{D}^{\lambda_2}_{\mu_2,\nu_2}(2) \qquad (11.2.3.5)$$

A similar expression for $\mu_m(2; R)$ is obtained from Eq. 11.2.3.5 by first omitting the factor $(-1)^{\lambda_2+1}$ and then interchanging all superscripts and subscripts 1 and 2. The sum of these yields an expansion of $\boldsymbol{\mu}_m(R)$ in terms of the orientation functions $\mathscr{D}^{\lambda_1}_{\mu_1\nu_1}(1)\mathscr{D}^{\lambda_2}_{\nu_2\mu_2}(2)$. The expansion coefficients contain the polarizabilities α_0, polarizability anisotropies δ, and the multipole moments $\bar{Q}_\mu^\lambda$ of the molecules, quantities that are functions of the vibration coordinates S. It follows that an F_m factor is nonzero only if one of λ_1 or λ_2 is 0 or 2. The value of F_m $(\lambda_1 = 0, \lambda_2 = 0)$ is zero, since we presume each molecule has no net charge, that is, $Q_0^0 = 0$. An $F_m(\lambda_1 = 0$ or $2; \lambda_2 \neq 2)$ is obtained entirely from the expansion of $\mu_m(1; R)$; that is, such an F_m depends only on the dipole moment induced in molecule 1 by molecule 2. An F_m $(\lambda_1 = 2, \lambda_2 = 2)$ is obtained entirely from the expansion of $\mu_m(2; R)$. The coefficient F_m $(\lambda = 2, \lambda_2 = 2)$ is the only one which must be calculated from the sum. The quantities

$$\sum_{m\mu_1\mu_2} |F_m(R, \lambda_1, \mu_1, \nu_1, \lambda_2, \mu_2, \nu_2)|^2$$

may now be evaluated since they reduce the sums of Clebsch–Gordan coefficients.

Selection rules in Eq. 11.2.3.5 come from two sources:

1. General limitations on Clebsch–Gordan coefficients.
2. The nature of symmetrical top molecules is such that $\Sigma|F_m^2|$ is nonzero only for restricted values of ν_1 and ν_2.

A term in Eq. 11.2.3.5 is zero unless

$$\Delta J_1 = J_1' - J = 0, \pm 1, \ldots, \pm\lambda_1$$
$$\Delta K_1 = K_1' - K = 0, \pm n, \ldots, \pm m_1 n_1 \qquad (m_1 n_1 \leq \lambda_1)$$
$$\Delta J_2 = J_2' - J_2 = 0, \pm 1, \ldots, \pm\lambda_2$$
$$\Delta K_2 = K_2' - K_2 = 0, \pm n_2, \ldots, \pm m_2 n_2 \qquad (m_2 n_2 \leq \lambda_2)$$

Here m_1 or m_2 is a positive integer or zero, and n_1 or n_2 denotes the

rotational symmetry class of molecule 1 or molecule 2, respectively. Since one of λ_1 or λ_2 in Eq. 11.2.3.5 must be 0 or 2 the allowed transitions are any ΔJ_1, ΔJ_2, provided one of $|\Delta J_1|, |\Delta J_2| \leq 2$; $\Delta K_1 = \pm m_1 n_1$, $\Delta K_2 = \pm m_2 n_2$ provided one of $m_1, m_2 = 0$; $m_1 = 0$ if $|\Delta J_2| > 2$; $m_2 = 0$ if $|\Delta J_1| > 2$. An allowed transition contributes only through terms with λ_1, λ_2 such that $\lambda_1 \geq \max[|\Delta J_1|, |\Delta K_2|]$, $\lambda_2 \geq \max[|\Delta J_2|, |\Delta K_2|]$. For example, if the dipole and quadrupole moments are the only important ones, the summation is over $\lambda_1 \leq 2$; $\lambda_2 \leq 2$, and the selection rules reduce to $\Delta J_1 = 0, \pm 1, \pm 2$; $\Delta K_1 = 0$, $\Delta J_2 = 0, \pm 1, \pm 2$, $\Delta K_2 = 0$.

If the octopole moments are also important and if both molecules have threefold symmetry, the summation in Eq. 11.2.3.5 is over $\lambda_1 \leq 3$, $\lambda_2 \leq 3$, and the selection rules are

$\pm\Delta J_1 = 0, 1, 2$	0, 1, 2	3	0, 1, 2
$\pm\Delta J_2 = 0, 1, 2$	0, 1, 2	0, 1, 2	3
$\pm\Delta K_1 = 0$	3	0, 3	0
$\pm\Delta K_2 = 0, 3$	0	0	0, 3

where any combination may be chosen within a given block. For a given allowed transition in a pair of true symmetrical tops there will in general be contributions to Eq. 11.2.3.5 from all (λ_1, λ_2) terms with λ_1 and λ_2 bounded below and above by the selection rules, by whatever are taken as the important multipole moments and by the demand that one of λ_1 or λ_2 is 0 or 2. For example, if the transition is $\Delta J_1 = 1$, $\Delta J_2 = 1$, $\Delta K_1 = \Delta K_2 = 0$, then in general all the terms with $(\lambda_1, \lambda_2) = (1, 2), (2, 1), (2, 2), (2, 3), (3, 2), \ldots$ contribute to Eq. 11.2.3.5. Finally only those terms contribute in Eq. 11.2.3.5 for which $(\lambda_1 + \Delta J_1)$ is even.

For a pair of linear molecules the selection rules become any ΔJ_1, ΔJ_2 provided one of ΔJ_1 or ΔJ_2 is 0 or ± 2. An allowed transition contributes only through (λ_1, λ_2) terms for which

$$\lambda_1 \geq |\Delta J_1|, \lambda_1 + \Delta J_1 \quad \text{is even}$$
$$\lambda_2 \geq |\Delta J_2|, \lambda_2 + \Delta J_2 \quad \text{is even}$$

The weakness of the Frost theory is that the anisotropy of the molecules is neglected in using the product of eigenstates of the isolated molecules. The intermolecular potential is therefore purely radial and does not contain angle-dependent electrostatic terms. This is despite the fact that the phenomenon of which the theory is a description depends entirely on such angle-dependent terms except for overlap and translational contributions discussed later. Some mechanism of line broadening should also be included because individual $\Delta J = 2$ bands (quadrupole-induced), for example, are barely resolved even in hydrogen (Fig. 11.2.3.1).

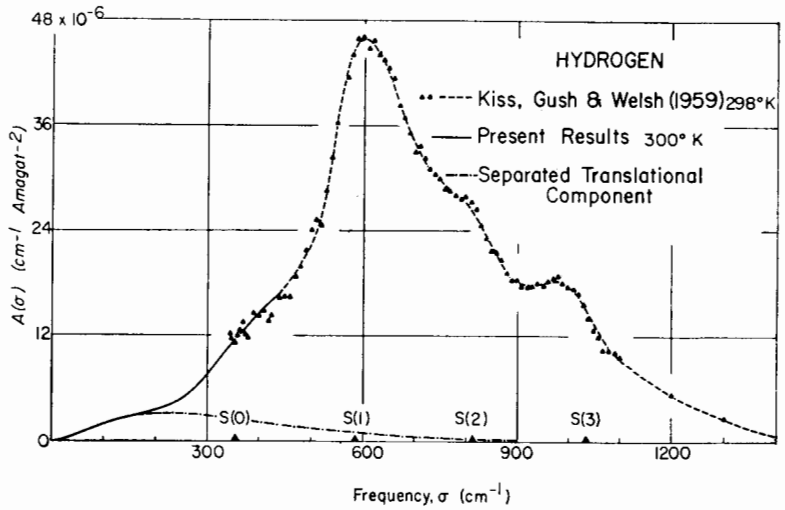

Figure 11.2.3.1 The $J \rightarrow J+2$ quadrupole-induced absorption bands in compressed H_2. [Reproduced by permission from O. R. Bosomworth and H. P. Gush, *Can. J. Phys.*, **43**, 751 (1965).]

11.2.4 Induced Absorption in Linear Molecules

A particularly interesting example is compressed oxygen gas, where we may use the general Frost theory to describe the broad, far infrared band shape in terms of quadrupole and hexadecapole mechanisms of dipole induction. This band, first observed by Bosomworth and Gush (1964) in the region 20–400 cm^{-1}, cannot be explained satisfactorily on the basis of quadrupole-induced dipole absorption alone. Values of $|\mathbf{Q}|$ and $|\mathbf{\Phi}|$, the quadrupole and hexadecapole moments, are obtained from the best fit to the experimental intensity and band shape. A justification for the use of the very short range (R^{-12}) hexadecapole field is based on the evaluation of the approximate range of the induced dipole moment. Equation 11.2.3.1 is conveniently presented in terms of the dipole, quadrupole, octopole, and hexadecapole terms. The anisotropy terms (δ) are small.

Dipole-Induced Dipole Absorption

$$A^{\mu}_{J\rightarrow J+1} = \frac{4\pi^3\mu^2N^2}{3hcZ}\int_0^{\infty} 4\pi R^{-4}\exp\left(-\frac{U_{AA}(R)}{kT}\right)dR \times\left[1-\exp\left(-\frac{hc\bar{\nu}_1(J)}{kT}\right)\right]\exp\left(-\frac{E_J hc}{kT}\right)\bar{\nu}_1(J) \times\left(4\alpha_0^2(J+1)+\frac{8}{3}\delta^2\frac{(J+1)^2(J+2)}{(2J+3)}\right) \qquad (11.2.4.1)$$

where $\bar{\nu}_1(J) = 2B(J+1)$ and $E_J = BJ(J+1)$.

Quadrupole-Induced Dipole Intensity

$$A^{Q}_{J\to J+2} = \frac{4\pi^3 Q^2 N^2}{3hcZ}\int_0^\infty 4\pi R^{-6}\exp\left(-\frac{U_{AA}(R)}{kT}\right)dR \times\left[1-\exp\left(-\frac{hc\bar{\nu}_2(J)}{kT}\right)\right]\exp\left(-\frac{E_J hc}{kT}\right)\bar{\nu}_2(J) \times\left[9\alpha_0^2\frac{(J+1)(J+2)}{(2J+3)}+\frac{18}{5}\delta^2\left(\frac{(J+1)(J+2)}{(2J+3)}\right)^2\right] \tag{11.2.4.2}$$

where $\bar{\nu}_2(J) = 2B(2J+3)$.

Octopole-Induced Dipole Intensity

$$A^{\Omega}_{J\to J+3} = \frac{4\pi^3\Omega^2 N^2}{3hcZ}\int_0^\infty 4\pi R^{-8}\exp\left(-\frac{U_{AA}(R)}{kT}\right)dR \times\left[1-\exp\left(-\frac{hc\bar{\nu}_3(J)}{kT}\right)\right]\exp\left[-\frac{E_J hc}{kT}\right]\bar{\nu}_3(J) \times\left[40\alpha_0^2\frac{(J+1)(J+2)(J+3)}{(2J+5)(2J+3)} +\frac{80}{3}\delta^2\left(\frac{(J+1)(J+2)}{(2J+3)}\right)^2\frac{(J+3)}{(2J+5)}\right] \tag{11.2.4.3}$$

where $\bar{\nu}_3(J) = 6B(J+2)$.

Hexadecapole-Induced Dipole Intensity

$$A^{\Phi}_{J\to J+4} = \frac{4\pi^3\Phi^2 N^2}{3hcZ}\int_0^\infty 4\pi R^{-10}\exp\left(-\frac{U_{AA}(R)}{kT}\right)dR \times\left[1-\exp\left(-\frac{hc\bar{\nu}_4(J)}{kT}\right)\right]\exp\left(-\frac{E_J hc}{kT}\right)\bar{\nu}_4(J) \times\left[\frac{175(J+1)(J+2)(J+3)(J+4)\alpha_0^2}{2(2J+3)(2J+5)(2J+7)} +\frac{875}{12}\delta^2\left(\frac{(J+1)(J+2)}{(2J+3)}\right)^2\frac{(J+3)(J+4)}{(2J+5)(2J+7)}\right] \tag{11.2.4.4}$$

where $\bar{\nu}_4 = 4B(2J+5)$.

By comparison with oxygen, the induced 0–THz absorption in N_2 is much narrower and is fairly well simulated by the frequencies and relative intensities of the unbroadened $\Delta J = 2$ rotational transitions calculated with an equation similar to Eq. 11.2.4.2. With Eqs. 11.2.4.2 and 11.2.4.4 it is possible to simulate the oxygen band with two contributions to the bimolecular collision-induced dipole moment assumed to be the result of quadrupole and hexadecapole fields of the second oxygen molecule, and vice versa. Oxygen has no dipole or octopole moment by symmetry. The hexadecapole field, being R^{-12} dependent, is important only at very short separations R, but justification for its use comes from a simple analysis of

Bosomworth and Gush (1965), involving a rough measurement of the range (p) of the induced dipole moment, which may be obtained from the width of the spectrum. Classically this is proportional to the Fourier transform of the correlation function of the dipole moment, the width function of the induced dipole, which is roughly equal to the duration of the collision. Thus

$$\tau = (2\pi\bar{\nu}_{1/2}c)^{-1}$$

where $\bar{\nu}_{1/2}$ is the width of the spectrum at half peak height. For oxygen at 300°K, $\bar{\nu}_{1/2} = 160\,\text{cm}^{-1}$; thus $t = 0.1$ psec. Then p can be estimated by multiplying the duration of collision (τ) by the average rate of change of the intermolecular distance ($\dot{R}_{Av}$). Now $\frac{1}{2}m\dot{R}^2_{Av} = \frac{1}{2}kT$, where m is the reduced mass of the colliding molecules. Thus $p = R_{Av}\tau = 0.055$ nm at 300°K. The Lennard–Jones diameter (σ) of an O_2–O_2 pair is 0.792 nm; thus the induced dipole moment is practically zero until the colliding oxygen molecules enter the repulsion part of the intermolecular potential, and rise rapidly as the van der Waals contours interpenetrate. In other words the high frequency wing arises from the absorption of the dipole moment induced in the temporary O_2–O_2 pairs.

Values of $|\mathbf{Q}|$ and $|\Phi|$ can be estimated (Fig. 11.2.4.1) by resolving the O_2 profile into a quadrupole-induced and hexadecapole-induced dipole absorption band. These are based on line spectra calculated from the even J values in Eqs. 11.2.4.2 and 11.2.4.4 since oxygen has no odd J due to molecular spin statistics. Of course, the considerable broadening of each line expected in practice might lead to a different overall profile than that suggested by the line spectrum even if this ever exists in practice for molecules other than hydrogen. Nevertheless, a "forced" agreement can be

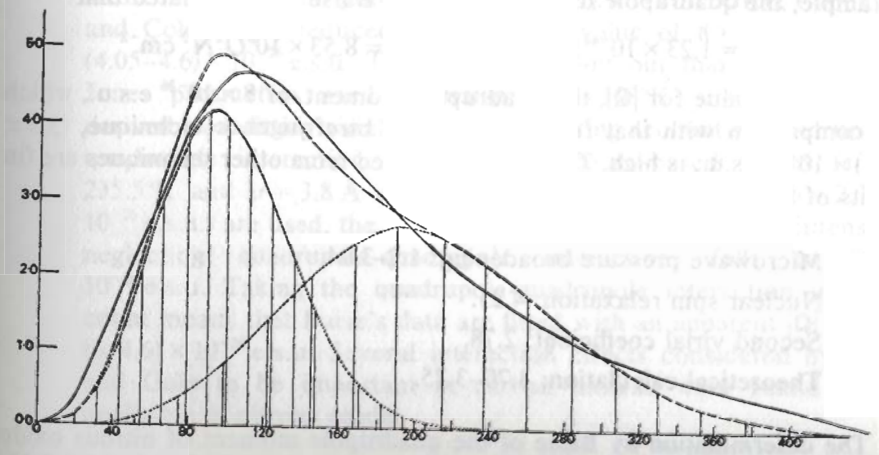

Figure 11.2.4.1 Fitting the far infrared oxygen band with quadrupole- and hexadecapole-induced components. Ordinate, $\alpha(\bar{\nu})/N^2$ (Np cm^{-1} amagat^{-2}); abscissa, $\bar{\nu}$(cm^{-1}). [Reproduced by permission from M. W. Evans, *Mol. Phys.* **25**, 1345 (1975).]

obtained with the values

$$|\mathbf{Q}| = 1.0 \times 10^{-40}\ \text{C m}^2; \qquad |\Phi| = 3.7 \times 10^{-60}\ \text{C m}^4$$

The value of $|\mathbf{Q}|$ compares favorably with that of $|\mathbf{Q}| = -1.34 \times 10^{-40}\ \text{C m}^2$ found by induced birefringence, and $|\Phi|$ is the "expected" order of magnitude.

The hexadecapole moment is one facet of transient O_4 formation which may be interpreted perhaps in other ways that are theoretically less convenient. A "complete" treatment would have to include such complicated factors as

1. The overlap dipole contribution.
2. Translational and rotational contributions of the interference between the quadrupolar and overlap induction and of the hexadecapole and overlap induction.
3. The pure translational ($\Delta J_1 = \Delta J_2 = 0$) contribution observable clearly in the hydrogen-induced absorption.
4. Broadening by stochastic means of the individual quantum lines of the induced absorption spectrum.
5. Others.

11.2.4.1 Induced Absorption in Nitrous Oxide

In this case there is theoretically a contribution due to all the multipoles from the dipole term onward. This is generally the case, of course, in molecules of arbitrary symmetry and it is of interest to check the extent of the dipole-induced contribution to the spectrum in comparison with, for example, the quadrupole induced. For N_2O Baise has calculated that

$$\bar{A}^{\mu} = 1.23 \times 10^{-44} N^2\ \text{cm}^{-2}; \qquad \bar{A}^{Q} = 8.53 \times 10^{8} Q^2 N^2\ \text{cm}^{-2}$$

obtaining a value for $|\mathbf{Q}|$, the quadrupole moment, of 8×10^{-26} e.s.u., which in comparison with that from the induced birefringence technique, $(3.5 \pm 0.3) \times 10^{-26}$ e.s.u., is high. The values obtained from other techniques are (in units of 10^{-26} e.s.u.) as follows:

1. Microwave pressure broadening: 1.2–3.04.
2. Nuclear spin relaxation: 4.25.
3. Second virial coefficient: 2.78.
4. Theoretical calculation: 3.70–3.75.

The determination by Baise of the quadrupole moment of nitrous oxide (N_2O) was the first measurement of its kind, that is, in the presence of a permanent dipole contribution to the overall far infrared broad band. The high value of $(8 \pm 0.7) \times 10^{-26}$ e.s.u. is attributable to the fact that the intermolecular potential of nitrous oxide is not radial (i.e., there are

dipole-dipole, dipole-quadrupole, quadrupole-quadrupole, etc. terms) and to the following complications:

1. Triple and multiple "collisions" which affect the N^2 dependence of the Frost-type theory at liquidlike densities (Fig. 11.1.2.3).
2. Translational absorption, in which $\Delta J_1 = \Delta J_2 = 0$. In this case the absorption of a photon leads to a change in the relative kinetic energy of the two molecules with no change in rotational energy. The induced dipole moment in mixtures of rare gases, for example, arises solely from these overlap *forces*, modulated only by the translational motions of the two colliding molecules. Therefore even in the complete absence of electrostatic factors the far infrared power absorption spectrum of mixtures of rare gas atoms are not elastic, because in this case, the width of the collision-induced band would be infinitely broad. The band is a very direct measure of translational dynamics at close range. In nitrous oxide, the translational absorption is expected below $10\ \text{cm}^{-1}$, and is in this case rototranslational in origin, in contrast to the rare gas mixtures. In fact, as pointed out by Baise, the whole of the induced band is rototranslational rather than purely rotational in origin. Ho et al. (1975) have calculated that as much as 30% of the induced absorption in carbon dioxide, which we consider below, is due to translation/rotation modifications.
3. Absorption associated with the anisotropy of the polarizability, that is, the double transitions $\Delta J_1 = \Delta J_2 = 2$ of the Frost equation.
4. The most important cause is neglect of quadrupole-quadrupole terms in the intermolecular potential. By applying this correction, Copeland and Cole (1975) reduced the *apparent* value of 8×10^{-26} e.s.u. to $(4.05–4.6) \times 10^{-26}$ e.s.u. These authors point out that the Lennard–Jones parameters used by Baise ($\epsilon/k = 193°\text{K}$, $\sigma = 4.54$ Å) were derived from fitting virial data *without* taking account of quadrupole-quadrupole interaction. When the viscosity-based values ($\epsilon/k = 235.5°\text{K}$ and $\sigma = 3.8$ Å consistent with virial data for $|\mathbf{Q}| = 2.78 \times 10^{-26}$ e.s.u.) are used, the derived value of $|\mathbf{Q}|$ from infrared intensity, neglecting quadrupole-quadrupole interaction, falls to 5.2×10^{-26} e.s.u. Taking the quadrupole-quadrupole interaction into account means that Baise's data are fitted with an apparent $|\mathbf{Q}|$ of (4.1 to 4.6) $\times 10^{-26}$ e.s.u. Several interaction effects considered by Bose and Cole to be important in carbon dioxide were found to be negligible in nitrous oxide.

11.2.4.2 Induced Absorption in Gaseous and Liquid CO_2

This molecule is linear, possessing a quadrupole and hexadecapole moment, but no dipole or octopole. It has been intensely studied by microwave pressure broadening and by Ho et al. (1971) in the far infrared

over a wide range of temperature and pressure. The contribution of the quadrupole-quadrupole energy in the interaction potential is particularly important for carbon dioxide, because of its large quadrupole moment. The translational spectrum is considerably stronger than the rotational in the microwave and very far infrared regions (below $10\,cm^{-1}$).

The pair interaction energy contains the quadrupole-quadrupole term

$$U_{\theta\theta} = \left(\frac{3Q^2}{4R_{ij}^5}\right)(1 - 5\cos^2\theta_i - 5\cos^2\theta_j + 17\cos^2\theta_i\cos^2\theta_j + 16\sin\theta_i\cos\theta_i\sin\theta_j\cos\theta_j\cos\phi + 2\sin^2\theta_i\sin^2\theta_j\cos^2\phi)$$

where θ_i and θ_j are the angles between the axes of the axially symmetrical molecules i and j and the R line joining the centers of mass, and ϕ is the angle of tilt. This term is so large for carbon dioxide that $U_{\theta\theta} = kT$ at ambient T. The induced dipole-induced dipole and overlap energy terms are smaller, but still significant. The total integrated intensity in carbon dioxide therefore consists of several terms:

1. A contribution of the pure translational band, including the effect of translational modulation on the rotational motion of the molecules. This is proportional to Q^2.
2. The induced rotational band, consisting of the following:
   - **a.** $\Delta J_1 = 2$, $\Delta J_2 = 0$ transitions.
   - **b.** $\Delta J_1 = 2$, $\Delta J_2 = 0$ transitions due to the polarizability anisotropy.
   - **c.** Double transitions $\Delta J_1 = \pm 2$, $\Delta J_2 = \pm 2$.
   - **d.** *Terms proportional to Q* arising from translational and rotational contributions of the interference between the quadrupolar and overlap induction.
   - **e.** Hexadecapole-induced dipole terms and interference effects.

The spectrum of carbon dioxide in the compressed gas state at 233 and 296°K is shown in Fig. 11.2.4.2.1 together with the profile of the stick spectrum $\Delta J_1 = 2$, $\Delta J_2 = 0$. In the region below $10\,cm^{-1}$ the absorption is mainly purely translational and at each temperature the peak intensity occurs at a frequency roughly 10% higher than predicted by mechanism 2a. On the high frequency side there is considerable disagreement which cannot be accounted for by the double transitions ($\Delta J_1 = \pm 2$, $\Delta J_2 = \pm 2$), since these amount to only about 50% of the total intensity. The situation is different in nitrogen, where there is good agreement between the observed far infrared band and the same type of bar spectrum (Section 11.4). This result rules out asymmetry in the rotational lines as the reason for the enhanced high frequency absorption in carbon dioxide, since the line shape is independent of the quadrupole moment in the usual induction process. In addition overlap induction cannot be the cause since this should be more important in nitrogen, with a smaller quadrupole. This suggests that the shoulder

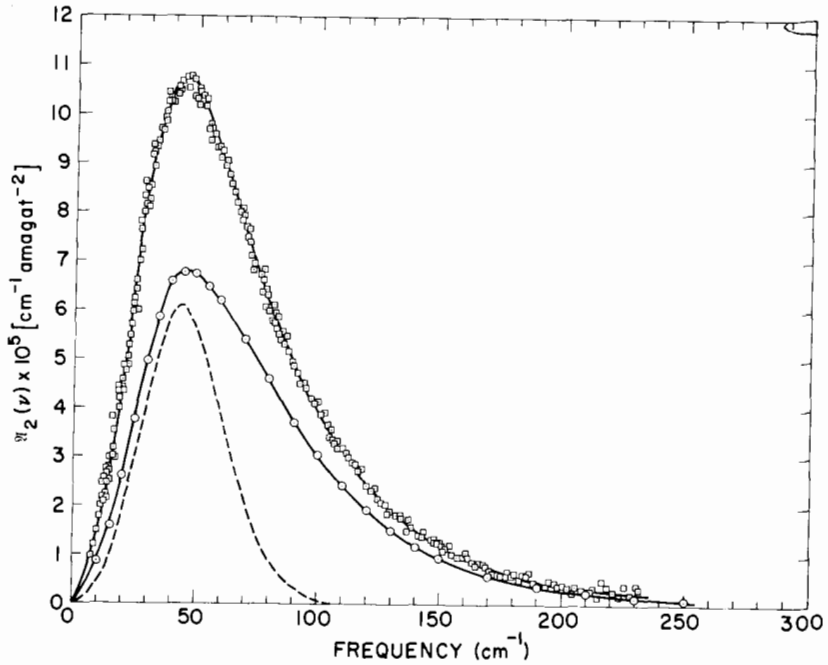

Figure 11.2.4.2.1 Far infrared spectrum of gaseous CO_2 at 233°K (upper curve) and 296°K (lower curve). The dashed curve is the profile of the bar spectrum in which the length of each bar is proportional to the integrated intensity of the rotational absorption lines resulting from $\Delta J_1 = 2$, $\Delta J_2 = 0$ transitions. [Reproduced by permission from W. Ho, G. Birnbaum, and A. Rosenberg, *J. Chem. Phys.* **55**, 1028 (1971).]

either is a hexadecapole-induced dipole effect or is due to the fact that the quadrupole-quadrupole energy is greater than kT, the thermal energy, and therefore having an effect on any rotational type of spectrum.

Ho et al. interestingly emphasize the low frequency part of the band by plotting it in the power representation $\Re(\bar{\nu})/\bar{\nu}^2$, which is the data output in a depolarized Rayleigh scattering experiment on a compressed gas such as methane, where a *polarizability anisotropy* is *induced* by the interaction of molecules. We return to this in Section 11.3. The $\Re(\bar{\nu})/\bar{\nu}^2$ plot shows an inflection at roughly $10\,cm^{-1}$ (Fig. 11.2.4.2.2) due to the separation of the rotational from the *translational* band shape.

An unsatisfactory aspect of the interpretation by these authors is that the hexadecapole-induced contribution to the carbon dioxide spectrum is treated arbitrarily by simply guessing a value for Φ, the hexadecapole moment. In fact, as in oxygen (Fig. 11.2.4.1), the high frequency shoulder in the gas phase spectra may be accounted for quite simply (but empirically) by using $J \to J + 4$ transitions and $J \to J + 2$ transitions. The guess of $\Phi = 4 \times 10^{-42}$ e.s.u. for carbon dioxide is probably small, since Birnbaum et al. themselves estimate 4.2×10^{-42} e.s.u. for oxygen, a molecule with a con-

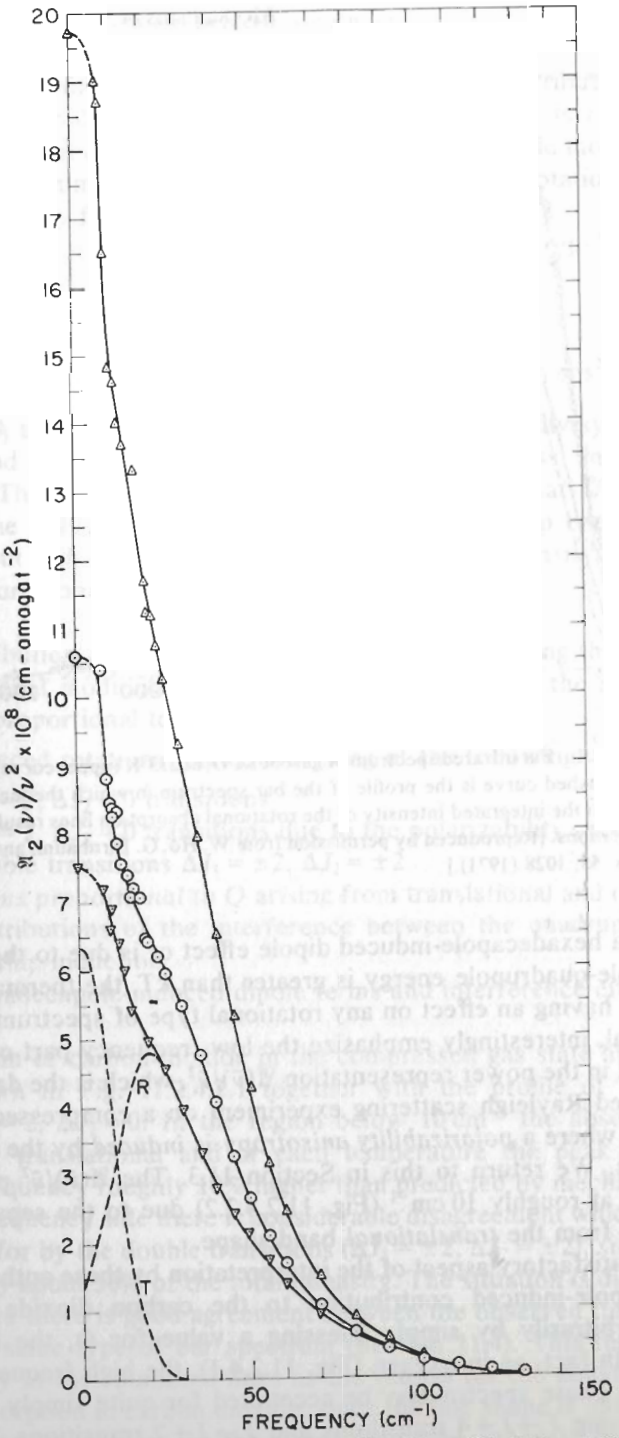

Figure 11.2.4.2.2 $\mathfrak{A}_2(\bar{\nu})/\bar{\nu}^2$ as a function of frequency for CO_2 at 233, 296, and 303°K. Top to bottom, decreasing temperature. The "zero" frequency (microwave) points are shown in order to get a fix on the translational band around zero frequency. The dashed curves are theoretical translation and rotation bands. [Reproduced by permission from W. Ho, G. Birnbaum, and A.

siderably smaller quadrupole moment. It is significant that a recent self-consistent field molecular orbital calculation of the carbon disulfide hexadecapole moment (Buckingham et al., work in progress) indicates a value far higher than that used in the carbon dioxide calculation.

However, it must be kept in mind that the fundamental weakness in all theories such as these is that a product of eigenvectors is used to generate the induced band shape. As pointed out by Frost, this is valid only when the Lennard–Jones radial averaging is used in the calculation. There is an obvious need to extend the theory to take into account angle-dependent terms in a self-consistent manner.

The density dependence of the induced absorption in carbon dioxide was carefully evaluated by Birnbaum and co-workers. The most significant result is that the integrated absorption cross section per molecule in the liquid state is about five times less than that in the gas (the measured integrated intensity per density squared is about 25 times less). This is consistent with the results of Baise for nitrous oxide and Evans for the intensely quadrupolar cyanogen. From this pressure study, Birnbaum and co-workers have drawn the important (but tentative) conclusion that the high frequency tail of the gas *and liquid* absorption is due to short range binary interactions, and that the longer range quadrupolar interactions effectively cancel in the liquid state. The first conclusion follows from analyzing the gas absorption with

$$\mathfrak{A}(\bar{\nu}, N) = \mathfrak{A}_2(\bar{\nu})N^2 + \mathfrak{A}_3(\bar{\nu})N^3$$

The coefficients, $\mathfrak{A}_2$ and $\mathfrak{A}_3$ refer to binary and *ternary* interactions, respectively. Both $\mathfrak{A}_2(\bar{\nu})$ and $\mathfrak{A}_3(\bar{\nu})$ have the *same* frequency distribution (same band shape), the selection rules being $\Delta J_1 = 2$, $\Delta J_2 = 0$ and $\Delta J_1 = 2$, $\Delta J_2 = \Delta J_3 = 0$, respectively. Now $\mathfrak{A}_3(\bar{\nu})$ is actually found to follow the predicted contour quite well, while $\mathfrak{A}_2(\bar{\nu})$ has a high frequency tail. This is taken to mean that binary interactions are responsible for the high frequency tail. However, binary quadrupolar interactions are not expected to contribute in this region, so that short range overlap and hexadecapole forces are possible causes. In view of the very large CS_2 hexadecapole, this is a strong probability.

The suggestion that there is a cancellation of the long range interactions in the liquid follows from the observations that the integrated intensity divided by N^2 is much less in liquid than gaseous carbon dioxide. This is *not* found in SF_6, where the hexadecapole is the first multipole moment. In SF_6 liquid, because of the short range nature of the forces, the molecules must approach closely in order for a dipole to be formed; that is, the interactions are essentially binary. These results are confirmed by Baise's studies on nitrous oxide, but there is a reduction in the absorption per molecular pair, although only by a factor of ~2, and the higher frequency absorption is emphasized in the liquid due to the librational motion of the nitrous oxide permanent dipole. There is also a shift of 25 cm^{-1} to higher

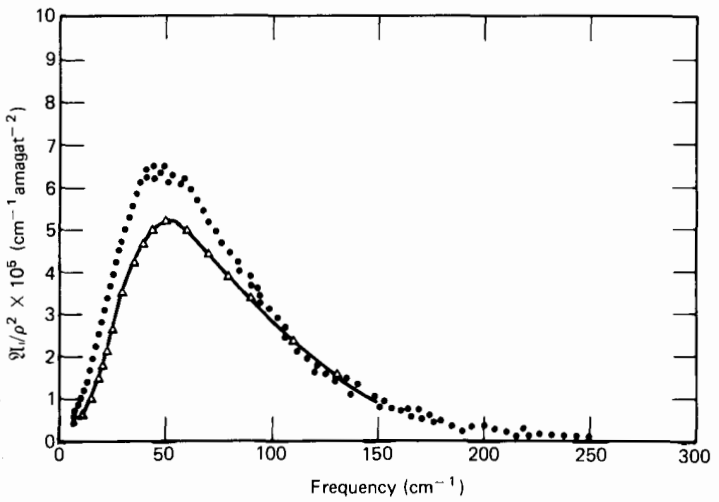

Figure 11.2.4.2.3 Far infrared collision-induced spectrum of CO_2 at room temperature. Upper curve 15 amagat, lower curve 85 amagat units of density. Note the persistence of the long tail. [Reproduced by permission from G. Birnbaum, W. Ho, and A. Rosenberg, *J. Chem. Phys.* **55**, 1039 (1971).]

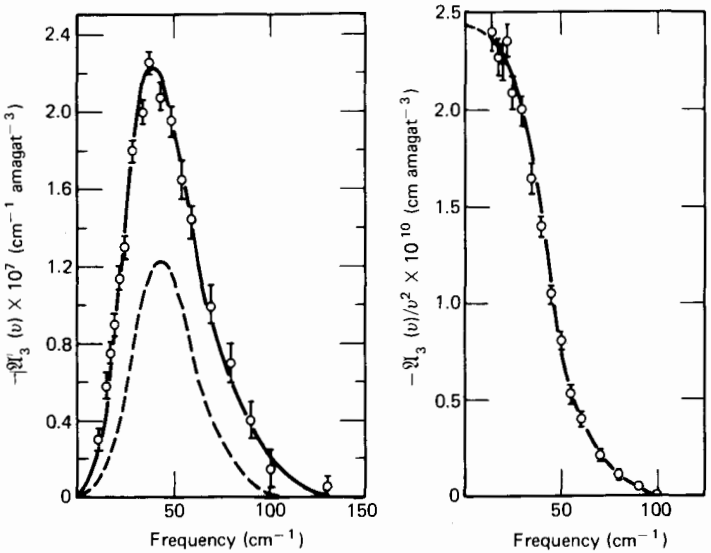

Figure 11.2.4.2.4 Cubic term $\mathfrak{A}_3(\bar{\nu})$ and $\mathfrak{A}_3(\bar{\nu})/\bar{\nu}^2$ as a function of frequency. The dashed curve is the bandshape defined by the relative integrated intensity of the rotational lines due to the radiative transitions $\Delta J_1 = \pm 2$, $\Delta J_2 = 0$, $\Delta J_3 = 0$. [Reproduced by permission from G. Birnbaum, W. Ho, and A. Rosenberg, *J. Chem. Phys.* **55**, 1039 (1971).]

frequency in liquid carbon dioxide compared with the gas, and also a much larger shift in cyanogen, described later. One cannot consider the liquid spectrum just as that of a very dense gas. The beginning of the cancellation effect in the dense gas is illustrated in Fig. 11.2.4.2.3, where the tail is still clearly N^2-dependent while the quadrupole-induced peak begins to fall away.

Figure 11.2.4.2.4 illustrates the three-body function $\mathfrak{A}_3(\bar{\nu})$ for carbon dioxide and a plot of $\mathfrak{A}_3(\bar{\nu})/\bar{\nu}^2$, the depolarized scattering function. On a log scale the latter is exponential at high values of $\bar{\nu}$, in agreement with experimental results for compressed inert gases (Section 11.3). The $\mathfrak{A}_3(\bar{\nu})$ and bar spectrum agree fairly well, but $\mathfrak{A}_2(\bar{\nu})$ does not. A tentative explanation was given in terms of the observation that the relaxation time for three-body interactions, τ_3, is nearly four times greater than for two-body interactions at room temperature. Since these are essentially a measure of the duration of the collision, the more distant and hence weaker interactions are more important in τ_3 then in τ_2. The excess intensity for $\mathfrak{A}_2(\bar{\nu})$ is associated with the very strong Q–Q interaction in close collisions. If then, as suggested by the fact that $\tau_3 \gg \tau_2$, $\mathfrak{A}_3(\bar{\nu})$ reflects the more distant and weaker interactions, then $\mathfrak{A}_3(\bar{\nu})$ should follow the bar spectrum for triple collisions.

11.2.4.3 Quadrupole-Induced Absorptions in Cyanogen: Classical Broadening

The cyanogen molecule N≡C—C≡N has a very large quadrupole moment and the Q–Q interaction is much greater than the thermal energy at ambient temperature. Consequently the $\Delta J = 2$ stick spectrum does not match the observed $\bar{\nu}_{max}$ in the compressed gas (or liquid) (Figs. 11.2.4.3.1 and 11.2.4.3.2) in the region where the N^2 dependence is valid. A molecular orbital calculation (Evans, 1973) of the quadrupole moment suggests that $|\mathbf{Q}| = -9.0 \times 10^{-26}$ e.s.u. By treating the whole of the far infrared band as being quadrupole-induced (dubious but simplifying assumption) the apparent quadrupole moment from the far infrared band of the compressed gas is (13.0 to 15.5) $\times 10^{-26}$ e.s.u. and of the liquid is 6.9×10^{-26} e.s.u. There is a shift of 15 cm^{-1} in $\bar{\nu}_{max}$ between the gas and the liquid, which may be compared with 25 cm^{-1} in carbon dioxide, 30 cm^{-1} in nitrous oxide, and 60 cm^{-1} in propyne, a weakly dipolar, linear species. There is similarly a shift in OCS, librational modes contributing at the higher frequency end of the spectrum.

In order to develop a theory of broadening of the stick spectrum in cyanogen and the other cases already mentioned, we must manipulate Eqs. 11.2.4.1–11.2.4.4 into a continuous form, conveniently with time as a variable. The usual expression for a rotational absorption band shape, in terms of transitions between quantum states, is

$$I(\omega) = \frac{3\hbar c\sigma(\omega)}{\left\{4\pi^2\omega\left[1-\exp\left(-\frac{\hbar\omega}{kT}\right)\right]\right\}}$$

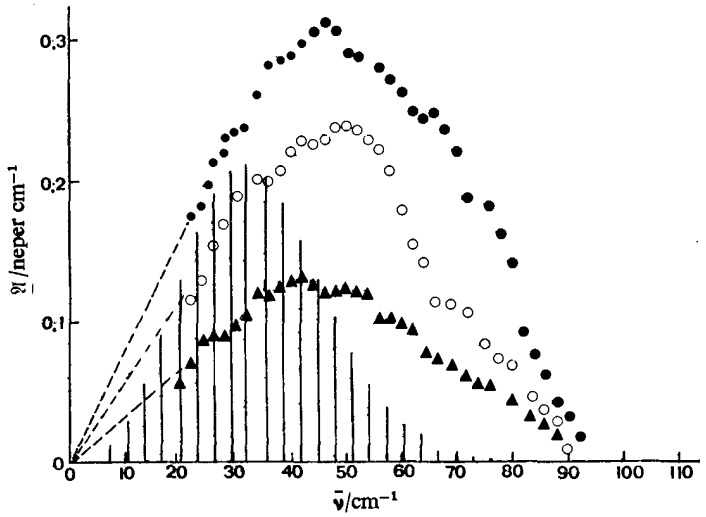

Figure 11.2.4.3.1 Far infrared pleasure-induced spectrum of cyanogen at ● 33.5 ± 0.3 bar, 383°K; ○ 28.4 ± 0.2 bar, 381°K; ▲ 24.0 ± 0.2 bar, 348°K. The bar spectrum represents relative integrated intensities for some of the $J \rightarrow J+2$ lines (quadrupole-induced). [Reproduced by permission from M. W. Evans, *J. Chem. Soc. Faraday Trans. II* **69**, 763 (1973).]

where $\sigma(\omega)$ is the absorption cross section per molecule. The Fourier transform

$$F(t) = \int_{-\infty}^{\infty} \omega^2 I(\omega) \exp(i\omega t)\, d\omega$$

may be used to weight the intensity toward the higher frequencies ($10 \leqslant \bar{\nu} \leqslant 450\ \text{cm}^{-1}$) where accurate data are available. Here $\sigma(\omega) = \mathfrak{A}(\omega)/N$,

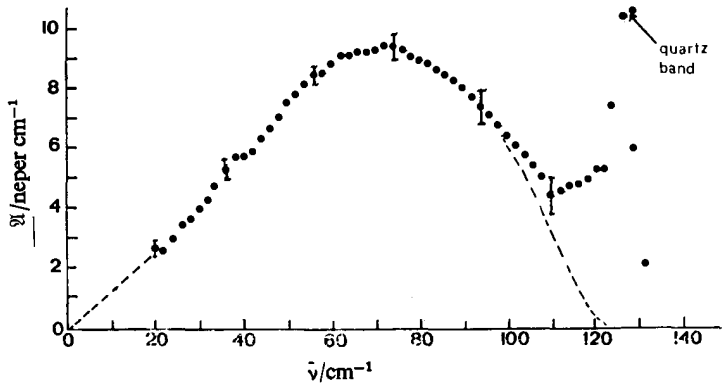

Figure 11.2.4.3.2 Spectrum of liquid cyanogen at 301°K. [Reproduced by permission from M. W. Evans, *J. Chem. Soc. Faraday Trans. II* **69**, 1011 (1973).]

where $\mathfrak{A}$ is the power absorption coefficient and N the number density in molecules per cubic centimeter. The theoretical functions of time are obtained by substituting into Eq. 11.2.4.2 using the continuous expression for the contours passing through the points of $I(\bar{\nu})$ obtained by eliminating J. For a linear molecule in the absence of broadening one has then the theoretical contour:

$$I_{\text{th}}(\bar{\nu}) \propto \left(\frac{\bar{\nu}}{2B} - \frac{2B}{\bar{\nu}}\right) Q^2 \exp\left[-\frac{hcB}{4kT}\left(\frac{\bar{\nu}}{2B} - 3\right)\left(\frac{\bar{\nu}}{2B} - 1\right)\right] A_8$$
$$\times \left[12\alpha_0^2 + \frac{24}{5}\left(\frac{\bar{\nu}}{2B} - \frac{2B}{\bar{\nu}}\right)\delta^2\right] + \frac{(\bar{\nu}+4B)(\bar{\nu}+12B)}{\bar{\nu}(\bar{\nu}+8B)}\Phi^2$$
$$\times \exp\left[-\frac{hcB}{4kT}\left(\frac{\bar{\nu}}{4B} - 5\right)\left(\frac{\bar{\nu}}{4B} - 3\right)\right] A_{12}\left[\frac{175}{96}\alpha_0^2\left(\frac{(\bar{\nu}-12B)(\bar{\nu}-4B)}{B(\bar{\nu}-8B)}\right.\right.$$
$$\left.\left. + \frac{875}{36}\delta^2\left(\frac{\bar{\nu}}{2B} - \frac{2B}{\bar{\nu}}\right)^2\right]\right]$$

where

$$A_n = \frac{\pi^3 N^2}{hcZ}\int_0^{\infty} 4\pi^2 R^{-n} \exp\left(-\frac{U_{AA}(R)}{kT}\right) R^2\, dR$$

In the time domain, therefore,

$$C_{\text{th}}(t) = \int_0^{\infty} I_{\text{th}}(\bar{\nu})\bar{\nu}^2 \exp(2\pi i\bar{\nu}ct)\, d\bar{\nu} \Big/ \int_0^{\infty} I_{\text{th}}(\bar{\nu})\bar{\nu}^2\, d\bar{\nu}$$

is the associated correlation function of the induced dipole dynamics. The direct Fourier transform of the experimental data can be made in the same way, giving

$$C_{\text{exp}}(t) = \int_{-\infty}^{\infty} \frac{\bar{\nu}\alpha(\bar{\nu})\exp(2\pi i\bar{\nu}ct)\, d\bar{\nu}}{1 - \exp(-hc\bar{\nu}/kT)} \Big/ C_{\text{exp}}(0)$$

The functions $C_{\text{th}}(t)$ and $C_{\text{exp}}(t)$ are compared for various values of $|\mathbf{Q}|$ and $|\Phi|$ in Figs. 11.2.4.3.3–11.2.4.3.5 in the compressed gaseous states of oxygen, carbon dioxide, and cyanogen. Fourier transforms are carried out directly using different algorithm designs. The time functions are sensitive to small changes in $|\mathbf{Q}|$ and $|\Phi|$ used. This is illustrated in Fig. 11.2.4.3.3 for oxygen, where the preceding section's frequency domain curve fittings, using values of $|\mathbf{Q}| = 0.30 \times 10^{-26}$ e.s.u., yields a $C_{\text{th}}(t)$ function which is quite severely underdamped compared with $C_{\text{exp}}(t)$. However, with slight changes, $|\mathbf{Q}| = 0.36 \times 10^{-26}$ e.s.u. and $|\Phi| = 0.4 \times 10^{-42}$ e.s.u., a much better fit is obtained, $C_{\text{th}}(t)$ now showing very short time "oscillations," although they are slightly displaced along the time axis from those of $C_{\text{exp}}(t)$. Analysis in the time domain, then, is quite pronouncedly more sensitive than that in the frequency domain.

However, for cyanogen, no satisfactory fit can be obtained. The subtraction of a continuous time domain function $C_{\text{th}}(t)$ by transforming the

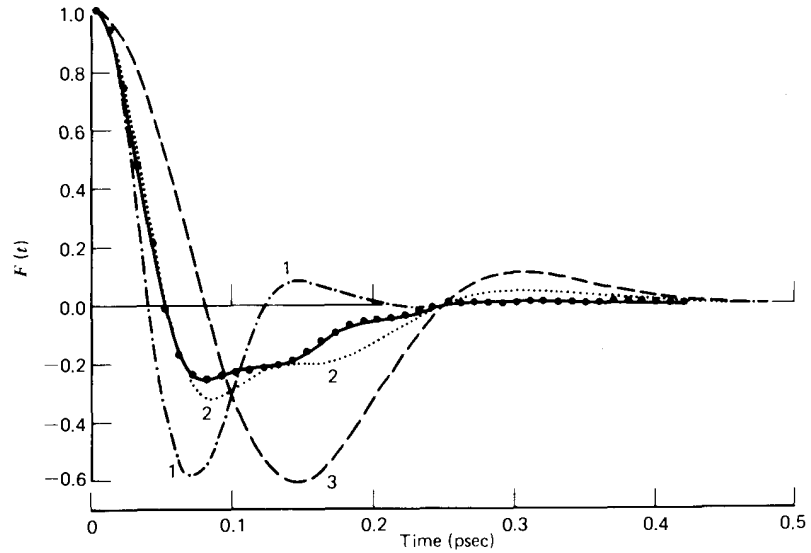

Figure 11.2.4.3.3 Fourier transforms for O_2 gas at 300°K, 35–75 amagat. ●—●—●—● $C_{exp}(t)$ as derived from two different algorithms. (1) $C_{th}(t)$ calculated with $\|\mathbf{Q}\| = 0.30 \times 10^{-26}$ e.s.u., $|\Phi| = 1.1 \times 10^{-42}$ e.s.u. (2) $C_{th}(t)$ with $|\mathbf{Q}| = 0.36 \times 10^{-26}$ e.s.u. $|\Phi| = 0.4 \times 10^{-42}$ e.s.u. (3) $C_{th}(t)$ with $|\mathbf{Q}| = 0.38 \times 10^{-26}$ e.s.u., $|\Phi| = 0$. [Reproduced by permission from M. W. Evans, *J. Chem. Soc. Faraday Trans. II*, **71**, 1257 (1975).]

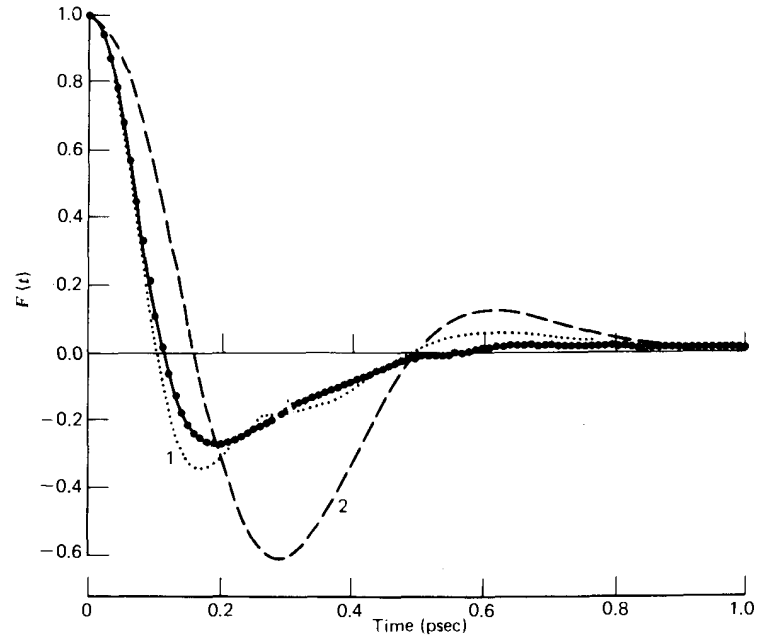

Figure 11.2.4.3.4 Fourier transforms for CO_2 gas at 273°K, 85 amagat. ●—●—● $C_{exp}(t)$ as derived from two separate algorithms. (1) $C_{th}(t)$ with $\|\mathbf{Q}\| = 5.0 \times 10^{-26}$ e.s.u., $|\Phi| = 6.1 \times 10^{-42}$ e.s.u. (2) $C_{th}(t)$ with $|\mathbf{Q}| = 5.2 \times 10^{-26}$ e.s.u., $|\Phi| = 0$. [Reproduced by permission from M. W. Evans, *J. Chem. Soc. Faraday Trans. II*, **71**, 1257 (1975).]

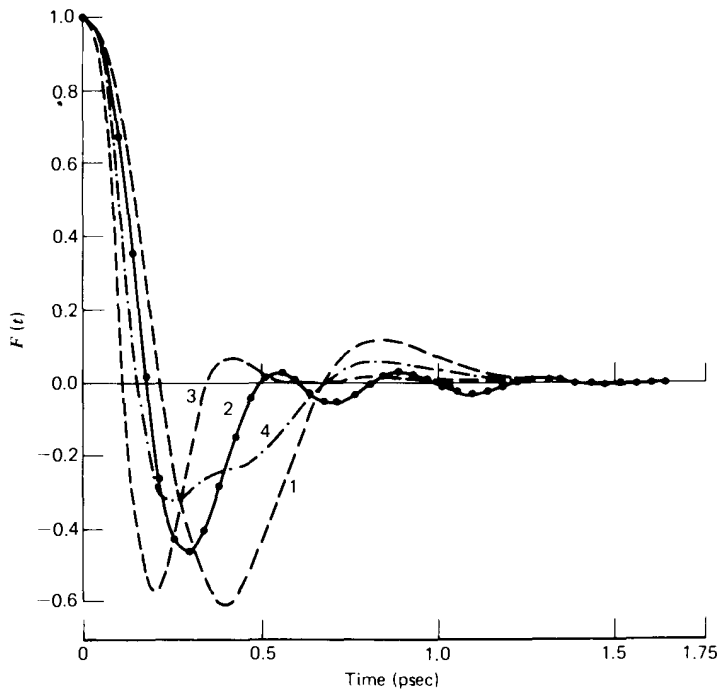

Figure 11.2.4.3.5 Fourier transforms for $(CN)_2$ gas at 383°K, 33.5 bar. ●—●—● $C_{exp}(t)$ from two separate algorithms. (1) $C_{th}(t)$ with $|\mathbf{Q}| = 15.5 \times 10^{-26}$ e.s.u., $|\Phi| = 0$. (2) $C_{th}(t)$ with $|\mathbf{Q}| = 12.0 \times 10^{-26}$ e.s.u., $|\Phi| = 44 \times 10^{-42}$ e.s.u. (3) $C_{th}(t)$ with $|\mathbf{Q}| = 9 \times 10^{-26}$ e.s.u., $|\Phi| = 56 \times 10^{-42}$ e.s.u. (4) $C_{th}(t)$ with $|\mathbf{Q}| = 14.5 \times 10^{-26}$ e.s.u., $|\Phi| = 24 \times 10^{-42}$ e.s.u. [Reproduced by permission from M. W. Evans, *J. Chem. Soc. Faraday Trans. II* **71**, 1257 (1975).]

sum of the profiles of the functions may be affected by neglect of the classical broadening of each line observed in practice; that is, the experimental absorption is a broad band and not an assembly of lines. A broadening mechanism based on the Gordon J-diffusion is considered presently, but a few remarks on the cyanogen spectrum are needed first.

The only satisfactory feature of Fig. 11.2.4.3.5 is that the $|\mathbf{Q}|$ and $|\Phi|$ used confirm an intuitive expectation of certainly a large molecular quadrupole moment, and possibly a large hexadecapole moment as well. The $C_{th}(t)$ curves are not underdamped compared with the $C_{exp}(t)$ curves, suggesting that triple collisions are not important at 33.5 bar. Attempts to modify the Frost theory with angle-dependent intermolecular potentials such as $U_{AA}(R) + U_{QQ}$ have no effect on the normalized line shape because U_{QQ} is independent of the rotational state of a molecule provided the rotational wave functions are assumed to be unperturbed, while the absolute values of $|\mathbf{Q}|$ and $|\Phi|$ are very sensitive to the Lennard–Jones parameters ϵ/k and σ; the relative values of A_2 are not greatly changed. Therefore ϵ/k and σ have little effect on the normalized line shape represented by $C_{\ldots}(t)$

Quantum mechanically, therefore, a theory of pressure-induced absorption is needed which either disposes of point multipole expansions of the electrodynamic field, or retains this approximation and then proceeds, albeit discordantly, to take into account the effect of molecular anisotropy on the eigenstate of a pair of molecules.

To broaden the set of $\Delta J = 2$ absorptions is compressed cyanogen, oxygen, or carbon dioxide we assume that the broadened contour $C_b(t)$ has the general property of being an even function of time, and is also a solution of the integro-differential equation:

$$\dot{C}_b(t) = -\int_0^t K_b(t-\tau)C_b(\tau)\,d\tau \qquad (11.2.4.3.1)$$

where the memory kernel may be expanded in a set of coupled integro-differential equations analogous to the Mori expansion:

$$\frac{\partial}{\partial t}K_{n-1}^{(b)}(t) = -\int_0^t K_n^{(b)}(\tau)K_{n-1}^{(b)}(t-\tau)\,d\tau$$

To effect broadening we now forge a link analogous to that leading to J-diffusion in the case of permanent dipolar absorption:

$$K_0^{(b)}(t) = K_\delta(t)\exp\left(-\frac{|t|}{\tau}\right) \qquad (11.2.4.3.2)$$

where $K_\delta(t)$ is associated through an equation identical with Eq. 11.2.4.3.1 with $C_\delta(t)$, the correlation function of the set of unbroadened $J \to J+2$ transitions. For bimolecular, quadrupole-induced dipolar absorption in linear, nondipolar molecules, neglecting the hexadecapole term, we have

$$C_\delta(t) = \frac{\int_0^\infty f_0(\Omega)\cos\Omega t\,d\Omega}{\int_0^\infty f_0(\Omega)\,d\Omega}$$

for each $J \to J+2$ transition, where

$$f_0(\Omega) = \left(\frac{\Omega}{4\pi Bc} - \frac{4\pi Bc}{\Omega}\right)\exp\left[-\frac{hcB}{4kT}\left(\frac{\Omega}{4\pi Bc}-3\right)\left(\frac{\Omega}{4\pi Bc}-1\right)\right]$$

For nondipolar symmetrical tops, up to the quadrupole term a similar more complicated expression may be derived. $C_b(t)$ and $C_\delta(t)$ may be linked now by equations identical with Eqs. 11.2.4.3.2. The broadened set of $J \to J+2$ lines is extracted from

$$C_b(\omega) = \mathrm{Re}[C_b(i\omega)] = \mathrm{Re}\left[\frac{C_\delta(i\omega+\tau^{-1})}{1-\tau^{-1}C_\delta(i\omega+\tau^{-1})}\right] \qquad (11.2.4.3.3)$$

where

$$C_\delta(i\omega+\tau^{-1}) = \Gamma + i\Lambda$$

with

$$\Gamma(\omega) = \int_0^\infty f_0(\Omega)\left(\frac{\tau^{-1}(\Omega^2+\omega^2+\tau^{-2})}{(\Omega^2-\omega^2+\tau^{-2})^2+4\omega^2\tau^{-2}}\right)d\Omega \Big/ \int_0^\infty f_0(\Omega)\,d\Omega$$

$$\Lambda(\omega) = \int_0^\infty f_0(\Omega)\left[\frac{\omega(\Omega^2-\omega^2-\tau^{-2})}{(\Omega^2-\omega^2+\tau^{-2})^2+4\omega^2\tau^{-2}}\right]d\Omega \Big/ \int_0^\infty f_0(\Omega)\,d\Omega$$

The absorption coefficient is then given by

$$\mathfrak{A}(\omega) = \frac{(\epsilon_s-\epsilon_\infty)\omega^2 C_b(\omega)}{n(\omega)c}$$

where $n(\omega)$ is the frequency-dependent refractive index and c is the velocity of light. For quadrupole-induced dipole absorption in pair collisions,

$$\epsilon_s - \epsilon_\infty = \frac{16\pi^2}{kT}N^2\bar{\alpha}_P Q\int_0^\infty R^{-6}\exp\left(-\frac{U_{AA}(R)}{kT}\right)dR$$

Figure 11.2.4.3.6 shows how Eq. 11.2.4.3.3 produces an absorption which simulates the broadening and eventually fuses the $J \to J+2$ lines in cyanogen ($B = 0.1570\ \mathrm{cm}^{-1}$). A broad continuum is reached at $\tau = 10$ psec, which according to kinetic theory, means a free path of about 38 Å. Therefore a continuum is reached well before triple collisions become statistically significant. Equation 11.2.4.3.3 is matched with nitrogen data in Figs. 11.2.4.3.7 and 11.2.4.3.8 (gas and liquid). An effective quadrupole

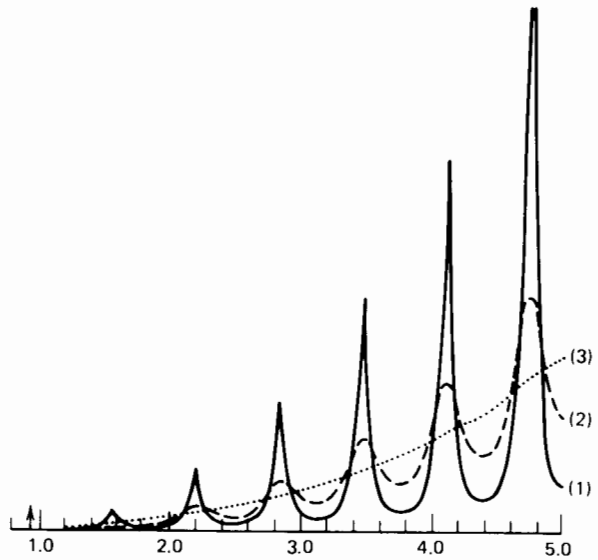

Figure 11.2.4.3.6 The first few $J \to J+2$ transitions for $(CN)_2$ broadened by a J-diffusion mechanism, with times between collisions of (1) $\tau = 100$ psec, (2) $\tau = 35$ psec, (3) $\tau = 10$ psec. [Reproduced by permission from M. W. Evans, *Spectrochim. Acta* **32A**, 1253 (1976).]

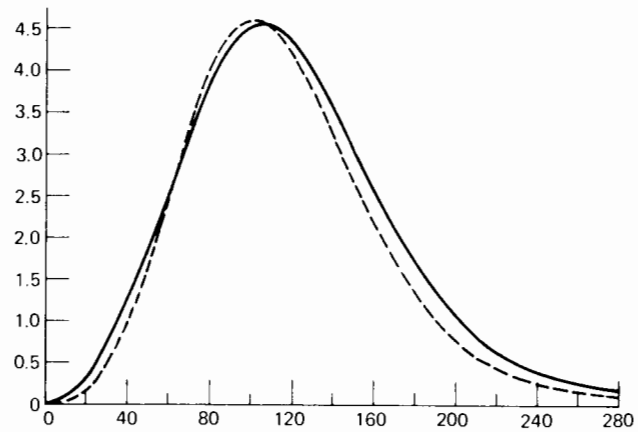

Figure 11.2.4.3.7 Solid line, Experimental absorption of compressed N_2 at 300°K compared with (dashed line) the J-diffusion broadening with $\tau = 0.4$ psec. $|\mathbf{Q}| = 5 \times 10^{-40}$ C m^2. Ordinate, intensity (10^6 cm^{-1} amagat^{-2}); abscissa, $\bar{\nu}$ (cm^{-1}). [Reproduced by permission from M. W. Evans, *Spectrochim. Acta* **32A**, 1253 (1976).]

moment of $|\mathbf{Q}| = 5 \times 10^{-40}$ C m^2 was extracted from this curve-fitting procedure for the total dispersion ($\epsilon_s - \epsilon_\infty$). Despite the neglect of many factors such as translational and electronic overlap absorption, this estimate of $|\mathbf{Q}|$ compares well with Kielich's tabulated values of $(4.5\text{–}6.9) \times 10^{-40}$ C m^2. Equation 11.2.4.3.3 is less accurate for liquid nitrogen at 76.4°K (Fig. 11.2.4.3.8). The calculated curve is for $\tau = 0.1$ psec and normalized to the $\bar{\nu}_{max}$ of the observed band. The $|\mathbf{Q}|$ estimated from this is 3×10^{-40} C m^2, significantly less than that deduced from the gas, owing to the cancellation effect.

Equation 11.2.4.3.3 does not work (Fig. 11.2.4.3.9) for cyanogen liquid at

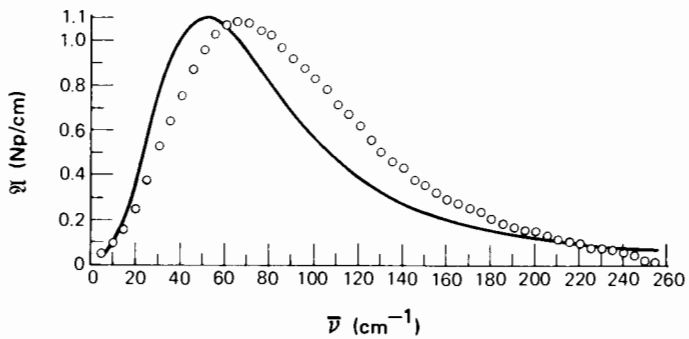

Figure 11.2.4.3.8 ○ Absorption for N_2(l) at 76.4°K. ——, J-diffusion broadening with $|\mathbf{Q}| = 3 \times 10^{-40}$ C m^2. [Reproduced by permission from M. W. Evans, *Spectrochim. Acta* **32A**, 1253 (1976).]

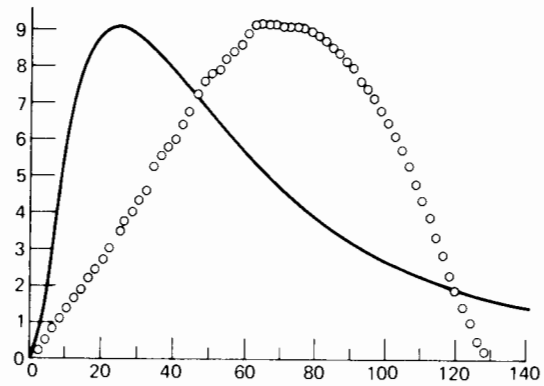

Figure 11.2.4.3.9 ○ Absorption of $(CN)_2$(l) at 301°K. Solid line, $J \rightarrow J + 2$ lines, broadened by a J-diffusion mechanism, Ordinates; $\mathfrak{A}(\bar{\nu})$ (Np/cm); abscissa; $\bar{\nu}$(cm^{-1}). [Reproduced by permission from M. W. Evans, *Spectrochim. Acta* **32A**, 1253 (1976).]

301°K where, analogously to the case of permanent dipole absorption, there is a large discrepancy between the observed and calculated $\bar{\nu}_{max}$. This shift can be interpreted (as in the earlier chapters on the permanent dipole) in terms of the increased amount of shorter range interactions in the liquid phase, where the torques in the rodlike molecule cyanogen will be greater than those of nitrogen. This is saying merely that collision-interrupted free rotation is not the case in the liquid phase of dipolar or nondipolar liquids. The "J-diffusion" type of mechanism does not shift $\bar{\nu}_{max}$.

11.2.5 Absorptions of Nondipolar Liquids—a Continued Fraction Empiricism

An absorption band in the infrared, whatever its molecular dynamical origin, is a probability distribution of frequencies $C(\omega)$, and is related to a correlation function $C(t)$ by Fourier's integral theorem in the form

$$C(t) = \int_0^\infty \cos \omega t \, dC(\omega) \qquad (11.2.5.1)$$

The quantum theory of induced absorptions in an N-body interaction is hugely complicated, but in the classical limit Eq. 11.2.5.1 holds quite generally if we define the correlation function $C(t)$ as follows:

$$C(t) = \sum_{ij} \langle \boldsymbol{\mu}_j(t) \cdot \boldsymbol{\mu}_i(0) \rangle$$

where $\boldsymbol{\mu}_i$ is the reduced dipole on molecule i at time t. $C(t)$ is an orientation/interaction correlation function dependent simultaneously at time t on the orientation of a molecule with respect to all the others. The correlation function can now be expanded in a continued fraction formally

Table 11.2.5.1 Parameters of Eq. 11.2.5.2 for Various Liquids

Liquid	Temp. (°K)	$10^{40} I_B$ (g cm^2)	$\gamma(I_B/2kT)^{1/2}$	$K_0(I_B/2kT)$	$K_1(I_B/2kT)$	$\epsilon_s - \epsilon_\infty$
Nitrogen	76.4	12.2	10.6	5.9	37.8	0.005
Carbon dioxide[a]	273	71.2	11.5	8.6	51.9	0.007
CCl_4	296	484	14.2	10.9	80.6	0.019
CH_4 (rotor phase I)	76	5.34	10.6	14.7	47.9	0.009
Cyanogen[a]	301	155	10.9	14.9	66.5	0.050
Methane	98	5.34	14.5	16.8	75.7	0.007
Benzene	296	198	12.8	20.8	110.6	0.023
CS_2	296	259	20.3	26.2	170.2	0.026
Cyclohexane	296	178	21.1	28.4	194.3	0.040
trans-Decalin	296	1020	22.7	70.7	335.3	0.003
1,4-Dioxane[b]	296	160	7.8	10.4	46.5	0.060

[a] Liquids of low density under several atmospheres of the vapor.
[b] Anomalous behavior.

identical with that of Mori (see earlier chapters), truncated with

$$\tilde{\phi}_1(s) = \frac{\tilde{\phi}_1(0)}{s + \gamma} \tag{11.2.5.2}$$

Using an equation such as this then allows us to fit directly the frequency domain data, iterating on $\phi_0(0)$, $\phi_1(0)$, and γ (Table 11.2.5.1).

The three-variable fit is very close in the far infrared (Figs. 11.2.5.1 and 11.2.5.2) and there is a tendency for $\phi_0(0)$ and $\phi_1(0)$ to increase as the geometric anisotropy of each molecule increases. The absolute magnitude of the absorption can be related via the effective $\epsilon_s - \epsilon_\infty$ to an "effective" dipole moment, or higher multipole, given some simplifying assumption about the microscopic dynamic and electrical origin of these very broad bands. The physical meaning of $\phi_0(0)$, $\phi_1(0)$, and γ is obscured by the complexity of the induction process, but it is clear that all three are interaction dependent. The curves for $C(t)$ can then be calculated and are illustrated in Fig. 11.2.5.3, together with a "cell" model due to Litovitz and the model of multipole-induced absorption in a two-molecule collision. The latter is of course inaccurate in the liquid phase.

In deriving Eq. 11.2.5.2 it is assumed that the molecular ensemble obeys classical equations of motion ($\hbar \to 0$). This is consistent with our basic assumption that Mori formalism is applicable to the classical correlation function defined in Eq. 11.2.5.1. Classically (Chapter 3), the latter can be derived for a canonical ensemble using the Liouville equation, and quantum mechanically the Poisson brackets are replaced by the commutator $\hbar^{-1}[\ ]$. The relation between the classical and quantum mechanical correlation functions is discussed in Chapters 1, 9, and 10. Mori has shown that the equation of motion of an arbitrary dynamical variable of an arbitrary system can be transformed rigorously to a linear generalized Langevin

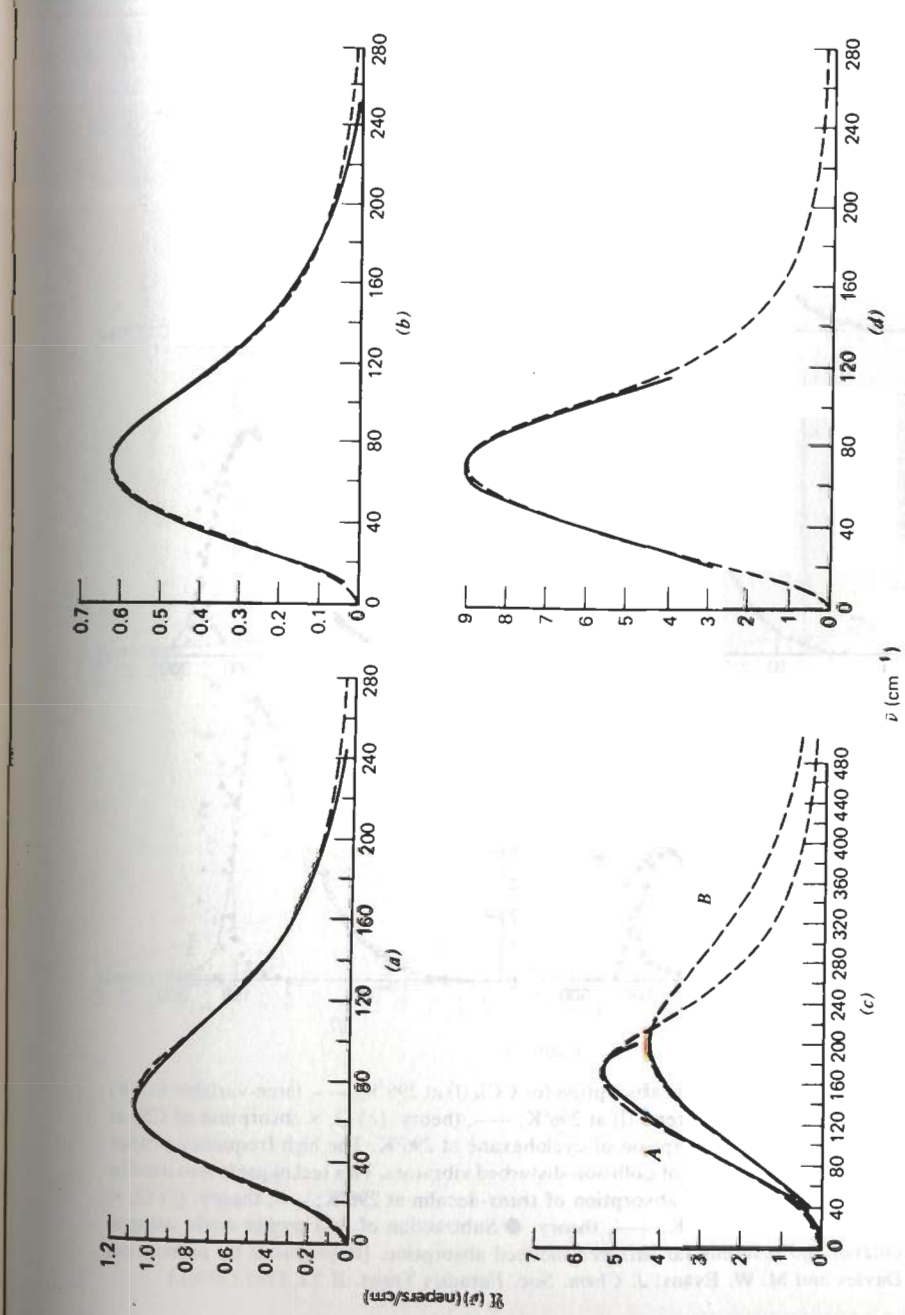

Figure 11.2.5.1 (*a*) Experimental absorption for $N_2(0)$ at 76.4°K, ——, Mori three-variable fit. (*b*) Liquid CO_2 at 273°K. (*c*) A, CH_4 (rotator phase) at 76°K; B, CH_4(liquid) at 98°K. (*d*) Liquid $(CN)_2$ at 301°K. [Reproduced by permission from G. Davies and M. Evans, *J. Chem. Soc. Faraday Trans. II* **72**, 1194 (1976).]

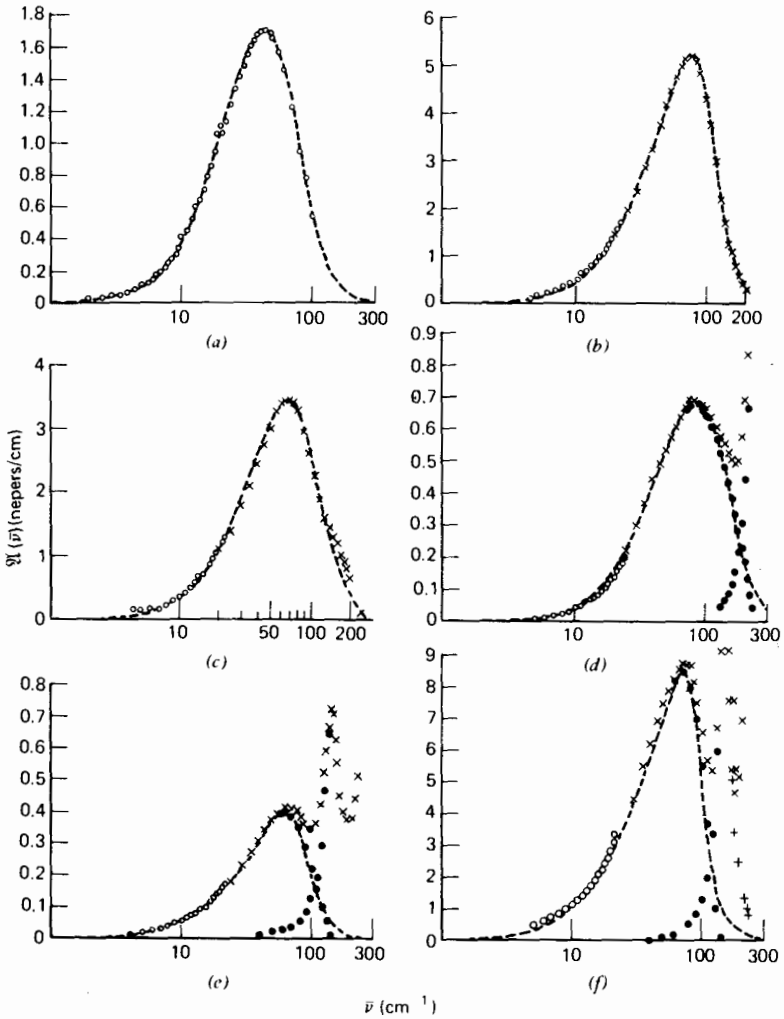

Figure 11.2.5.2 ○ (*a*) Experimental absorption for CCl_4 (l) at 296°K; ---, three-variable fit. (*b*) ○, × absorption observed for benzene (l) at 296°K; ---, theory. (*c*) ○, × absorption of CS_2 at 296°K; ---, theory. (*d*) ○, × absorption of cyclohexane at 296°K. The high frequency proper mode is extrapolated using a model of collision-disturbed vibrators. This technique is also used in (*e*) and (*f*). ---, Theory. (*e*) ○, × absorption of *trans*-decalin at 296°K; ---, theory. (*f*) ○, × absorption of 1, 4-dioxane at 296°K; ---, theory. ● Subtraction of first proper mode using a simple Lorentzian and resulting far infrared induced absorption. [Reproduced by permission from G. J. Davies and M. W. Evans, *J. Chem. Soc. Faraday Trans. II* **72**, 1195 (1976).]

equation form; and Kubo shows that a subsystem of an ensemble when perturbed relaxes to thermal equilibrium via the same generalized Langevin equation. Neither the arbitrary subsystem nor the variable need be quantized. That an ensemble of molecules as small as nitrogen or methane can be treated with classical equations of motion is the basis of the technique of computer molecular dynamics

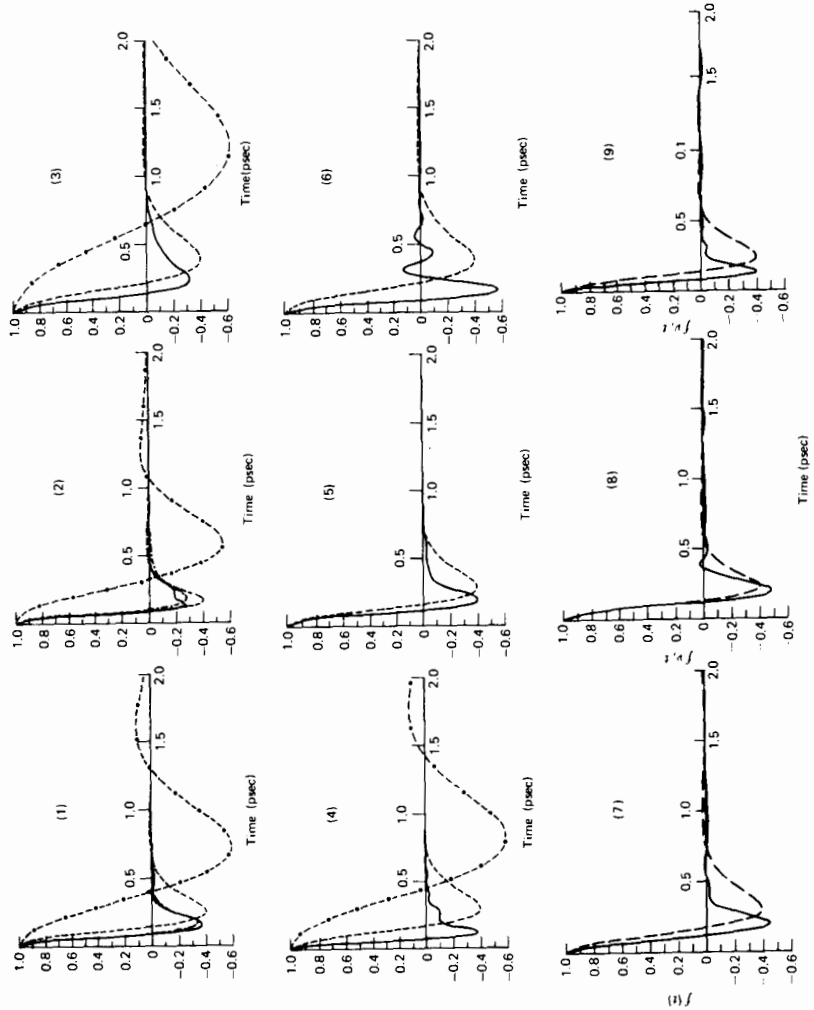

Figure 11.2.5.3 Fourier transforms of the power absorption coefficient $\mathfrak{A}(\bar{\nu})$ for some nondipolar liquids. (1) Benzene; (2) carbon disulfide; (3) carbon tetrachloride; (4) cyclohexane; (5) *p*-difluorobenzene; (6) bicyclohexyl; (7) *trans*-decalin; (8) 1, 4-dioxane; (9) *trans*-1, 2-dichloroethylene. [Reproduced by permission from G. Davies and M. Evans, *J. Chem. Soc. Faraday Trans. II* **72**, 1195 (1976).]

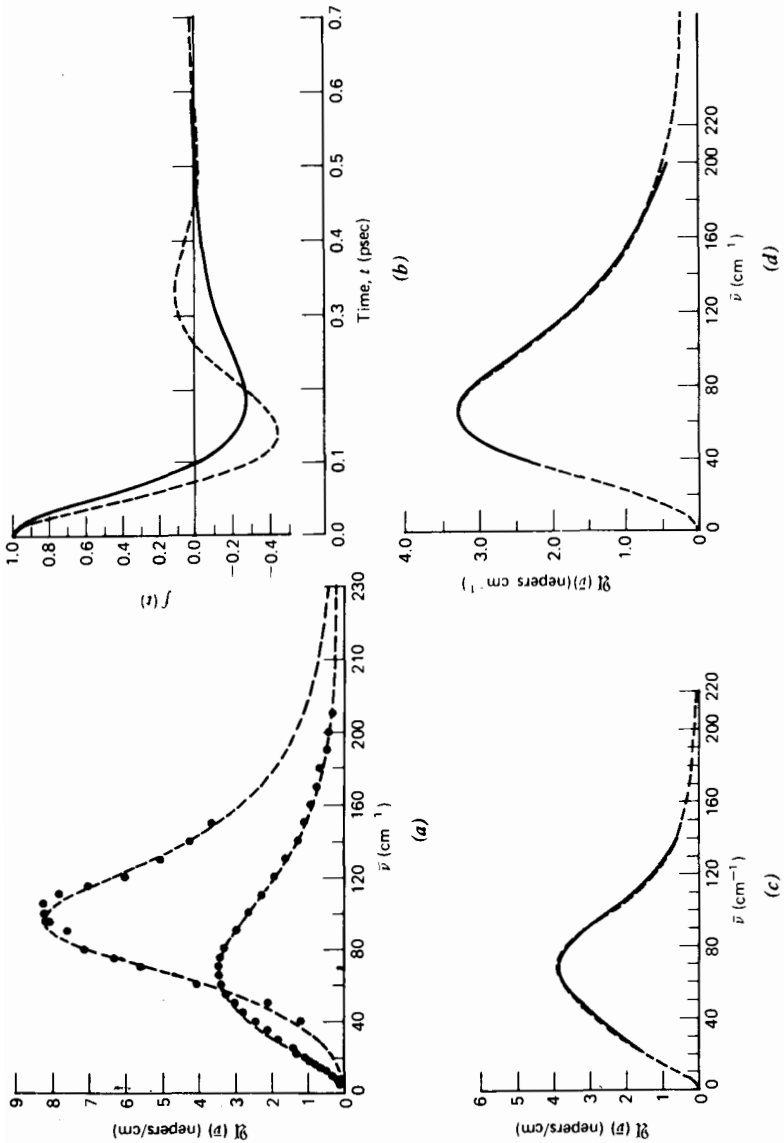

Figure 11.2.6.1 (*a*) ● Some experimental observations of the CS_2(l) absorption at 11.6 kbar, 293°K; ----, Mori three-variable theory, best fit. ○ Absorption of CS_2(l) at 296°K, 1 bar; ---, three-variable theory. (*b*) Fourier transforms of (*a*): ——, CS_2(l) at 296°K, 1 bar; ---, CS_2(l) at 293°K, 11.3 kbar. (*c*) ——, Experimental absorption of CS_2(l) at 232°K; ---, three-variable theory. (*d*) 315°K. [Reproduced by permission from M. W. Evans et al., *J. Chem. Soc. Faraday Trans. II* **72**, 1206 (1976).]

11.2.6 Effect of Pressure on Liquid Phase Induced Absorption

In this section we are concerned with the approach to the solid state in nondipolar fluids by application of external hydrostatic pressure and by freezing. Carbon disulfide can be solidified at room temperature by the application of 12–13 kbar of external pressure. The only far infrared study available of the dependence of the induced absorption on pressure is still that of Bradley et al. (1964) using pressures of up to 11.6 kbar. They found that the absorption peak shifts by about 35 cm^{-1} to higher frequency through the pressure-induced phase change at 293°K. This is equivalent to a large increase in both $\phi_0(0)$ and $\phi_1(0)$, that is, an increase in the mean square torque (in the slope of the intermolecular potential dependence on orientation). Such pressure data are technically very difficult to come by, we have taken the other approach (temperature) in liquid CCl_4, 298–343°K. The change in $\phi_0(0)$ and $\phi_1(0)$ with temperature is less pronounced, but real. The results are summarized in Table 11.2.6.1 and Figs. 11.2.6.1 and 11.2.6.2. They were obtained by fitting Eq. 11.2.5.2 to the experimental data

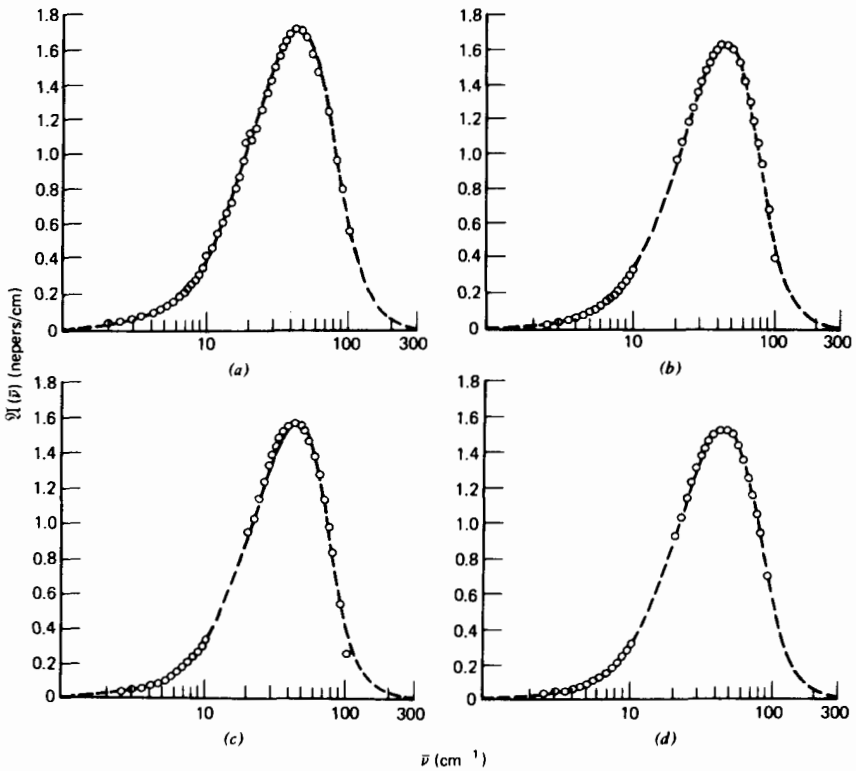

Figure 11.2.6.2 Far infrared absorptions of CCl_4 (l). ○ Experimental; ----, Mori three-variable theory. (*a*) 296°K; (*b*) 313°K; (*c*) 328°K; (*d*) 343°K. [Reproduced by permission from M. W. Evans et al., *J. Chem. Soc. Faraday Trans. II* **72**, 1206 (1976).]

on the three-variable basis. At 11.6 kbar in liquid carbon disulfide it is clear from the 0–THz band that there is a greater probability that the motion of the induced dipole moment is associated with the central frequency (ω_0) of $\sim 100\,\text{cm}^{-1}$ (0.33 psec). This process is reflected in the behavior of the correlation function associated with these bands (Fig. 11.2.6.2). The less-damped behavior at 11.6 kbar is an indication that the orientational correlation is greater. The angular forces resulting from mechanical anisotropy seem to be enhanced at the greater pressure, an effect that can be seen reflected in the very large increase in the torque-dependent parameters $\phi_0(0)$ and $\phi_1(0)$. The equivalent correlation function of depolarized Rayleigh scattering has recently been observed with applied pressure of up to 1 kbar. The effect of temperature is not as pronounced on $\phi_0(0)$ and $\phi_1(0)$ as that of pressure, but for CS_2(l) both increase with T. This dependence of mean square torque on temperature is predictable both by harmonic well dynamics and hard core collisions, but is a more subtle one than either of these theories can deal with. Therefore no discernible "loosening up" of internal structure can be observed in liquid carbon disulfide over the temperature range 232–315°K, the intermolecular torques and forces being determined by the thermal energy available to each molecule in kT.

The situation is different in the spherical top CCl_4 (Fig. 11.2.6.2) over the range 296–343°K, the latter being a few degrees below the boiling point at 1 bar. Both $\phi_0(0)$ and $\phi_1(0)$ *decrease* as T increases, although the values at 343 K are slightly anomalous (Table 11.2.6.1). Therefore there must be a considerable increase in free volume, and thereby translational freedom, as the boiling point is approached in order to overcome the purely thermal increase ($\propto kT$) in the mean square torque. An important indication is that the mean square torque is always much smaller for CCl_4 than CS_2, implying that molecular geometry plays an important part in rotational freedom of motion. This is particularly so in the plastic crystalline phase of CBr_4 dealt with below.

Table 11.2.6.1 Parameters[a] of Eq. 11.2.5.2 for CS_2 (l) and CCl_4 (l)

Liquid	T (K)	P (bar)	$10^{40}I$ (g cm^2)	$xK_0(0)$	$xK_1(0)$	$x^{1/2}\gamma$	$\epsilon_s - \epsilon_\infty$
CS_2	296	1	258.6	26.2	170.2	20.3	0.026
	293	11 600	258.6	79.9	247.6	32.7	0.018
	232	1	258.6	21.9	114.3	12.0	0.034
	315	1	258.6	29.9	212.0	27.0	0.020
CCl_4	296	1	242	10.9	80.6	14.2	0.019
	313	1	242	10.2	65.1	12.2	0.017
	328	1	242	9.1	51.2	10.1	0.016
	343	1	242	10.3	77.7	14.6	0.016

[a] $x = I/2kT$.

It is relevant to note that the NMR spin-rotation relaxation time T_1 of liquids is observed to decrease as temperature is raised, following an Arrhenius law. T_1 is inversely proportional to τ_J, the angular momentum correlation time, which thus increases with temperature. τ_J is a measure of the mean time during which a molecule seems to retain its angular momentum, and in spherical top molecules in the liquid state it is known that spin-rotation interaction is the dominant relaxational mechanism, τ_J becoming long even at temperatures well below the critical point. In contrast, for asymmetric tops and sticklike molecules, spin-rotation interaction becomes appreciable only at high temperatures, the ratio between dielectric and NMR relaxation times being close to the Hubbard ratio of 3 (rotational diffusion). In sticklike molecules, the motions about different symmetry axes is often observed to be highly anisotropic; for example, in liquid propyne near the critical point, the rotation about the C_{3v} axis is eight times faster than that about the perpendicular, the contribution of spin-rotation relaxation being about equal to that of the spin-spin magnetic dipolar correlation time, and not dominant, as in spherical tops.

The apparent dispersion ($\epsilon_s - \epsilon_\infty$) is lower at 11.6 kbar than at 1 bar in CS_2(l) and also decreases with temperature for both liquids. There remains a considerable amount of theoretical work to do, probably with the aid of computer simulations before the observables can be interpreted in terms of molecular constants.

11.2.7 Induced Absorption in Plastic Crystals

The 0–THz-induced far infrared absorptions in plastic crystalline and liquid CBr_4 can be used in order to study the changes in rotational dynamics brought about by the increased translational constraint and packing symmetry of the solid. It turns out that the barrier to rotational motion is slightly increased on going from the solid to the liquid a few degrees above the melting point. The integrated intensity per molecule is slightly greater in the liquid, which suggests that the spatial disposition of the electrostatic part of the intermolecular potentials is important in determining the magnitude of the molecular mean induced dipole moment. The dipole cross-correlation function corresponding to these bands is compared with that of octopole-induced dipole absorption arising from collision of spherical tops, and with the a.c.f. for a Maxwellian ensemble of freely rotating molecules of this symmetry. The mean square torque is greater initially in the condensed phase, and rotational motion is thereafter correlated.

In the plastic crystalline phase of CBr_4, in comparison with the room temperature monoclinic form, each molecule is left with a characteristically generous amount of rotational freedom, but translational freedom is limited, though not entirely absent. In contrast both types of dynamics are available and strongly coupled in the liquid. The broad bands centered near $32\,\text{cm}^{-1}$ (Fig. 11.2.7.1) in both liquid and rotator phase are interpreted as

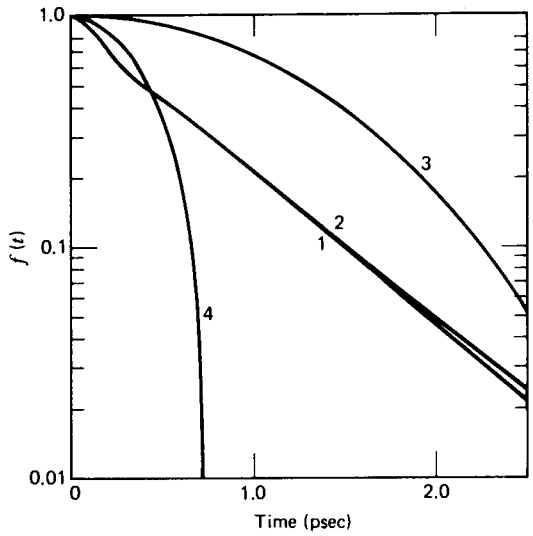

Figure 11.2.7.1 Correlation functions for CBr_4 from induced far infrared bands. (1) $C(t)$ (liquid); (2) plastic crystal; (3) $C_{FR}(t)$; (4) $C_\Omega(t)$. [Reproduced by permission, G. J. Davies et al., *J. Chem. Soc. Faraday Trans. II* **72**, 2147 (1976).]

intermolecular in origin since they do not correspond to any known difference modes or overtones or fundamentals, and occur at frequencies where such bands are prevalent for nondipolar molecules. In the $Th^6(Pa^3)$ monoclinic phase at 298°K this band is replaced by a doublet, both components of which are considerably broader than the fundamentals at 125 and 270 cm^{-1}. In the plastic crystalline phase at 376°K the fundamental at 124 cm^{-1} is broadened compared with the monoclinic phase, and considerably so in the liquid.

If a CBr_4 molecule whose center of mass is at the point $R(r, \theta, \phi, \chi)$ is assumed to develop a temporary dipole moment under the influence of the electrostatic fields of its neighbors then the vector sum of these fields at **R** at any instant is determined by the relative positions of all other molecules in the ensemble at that time, and consequently is a measure of the disorder or ordering in the lattice of molecules near enough for their fields to be influential. In order then to estimate absolutely the degree of rotational freedom retained in these condensed phases it is profitable to compare the correlation function derived experimentally (Fig. 11.2.7.1) with those estimated using models of rotational motion in the gas phase. The a.c.f. for the free rotation of an assembly of spherical tops is given by the classical expression:

$$C_{FR}(t) = \frac{2}{3}\left(1 - t^2\frac{kT}{I}\right)\exp\left(-t^2\frac{kT}{2I}\right) + \frac{1}{3}$$

(Chapter 2). This is illustrated in Fig. 11.2.7.1 for CBr_4 at 376°K and decays much more slowly than the functions $C(t)$ of the condensed phase. Thus

the effect of intermolecular force is clearly seen in the time domain. The bimolecular octopole-induced band produces in the classical limit a correlation function $C_\Omega(t)$ as follows, and is compared with $C_{FR}(t)$ and $C(t)$ in Fig. 11.2.7.1.

The total integrated intensity of an octopole-induced dipole absorption band in spherical tops is given by Ozier and Fox (1970) as

$$A = \sum_{J \neq J'} A(J, J') \tag{11.2.7.1}$$

where

$$A(J, J') = \frac{(8\pi)^4 N^2 \Omega^2 \alpha_0^2}{280hcZ}\int_0^\infty R^{-8}\exp\left(-\frac{U(R)}{kT}\right)dR \times \bar{\nu}(J, J')(2J+1)(2J'+1)\{\exp[-aJ(J+1)] - \exp[-aJ'(J'+1)]\}$$

with $a = Bhc/kT$; $\bar{\nu}(J, J') = B[J'(J'+1) - J(J+1)]$ and where $\Delta J = J' - J = 0, 1, 2, 3, \ldots$ are allowed. Here N is the molecular number density, α_0 the polarizability, B the rotational constant (cm^{-1}), and Z the rotational partition function:

$$Z = \sum_J (2J+1)^2 \exp[-aJ(J+1)]$$

Thus the overall band is the sum of the individual transition intensities $A(J, J+1)$, $A(J, J+2)$, $A(J, J+3)$. The correlation function is thus given by

$$C_\Omega(t) = \sum_{i=1}^{3}\int_0^\infty \frac{A(J, J+1)\cos(2\pi\bar{\nu}ct)\,d\bar{\nu}}{{}^{(i)}\bar{\nu}[1 - \exp(-h{}^{(i)}\bar{\nu}c/kT)]}$$

with

$${}^{(1)}\bar{\nu} = 2B(J+1); \qquad {}^{(2)}\bar{\nu} = 2B(2J+3); \qquad {}^{(3)}\bar{\nu} = 6B(J+2)$$

It may be shown that

$$A(J, J+1) \propto {}^{(1)}\bar{\nu}(2J+1)(2J+3)\exp[-aJ(J+1)][1 - \exp(-hc{}^{(1)}\bar{\nu}/kT)]$$

$$A(J, J+2) \propto {}^{(2)}\bar{\nu}(2J+1)(2J+5)\exp[-aJ(J+1)][1 - \exp(-hc{}^{(2)}\bar{\nu}/kT)]$$

$$A(J, J+3) \propto {}^{(3)}\bar{\nu}(2J+1)(2J+7)\exp[-aJ(J+1)][1 - \exp(-hc{}^{(3)}\bar{\nu}/kT)]$$

the proportionality constant being in each case the J-independent part of Eq. 11.2.7.1. We have, finally, in the classical sense:

$$C_\Omega(t) \propto \int_0^\infty \left\{\left(\frac{\bar{\nu}}{B} - 1\right)\left(\frac{\bar{\nu}}{B} + 1\right)\exp\left[-a\left(\frac{\bar{\nu}}{2B} - 1\right)\frac{\bar{\nu}}{2B}\right] + \left(\frac{\bar{\nu}}{2B} - 2\right)\left(\frac{\bar{\nu}}{2B} + 2\right)\exp\left[-a\left(\frac{\bar{\nu}}{4B} - \frac{3}{2}\right)\left(\frac{\bar{\nu}}{4B} - \frac{1}{2}\right)\right] + \left(\frac{\bar{\nu}}{3B} - 3\right)\left(\frac{\bar{\nu}}{3B} + 3\right)\exp\left[-a\left(\frac{\bar{\nu}}{6B} - 2\right)\left(\frac{\bar{\nu}}{6B} - 1\right)\right]\right\} \times \cos(2\pi\bar{\nu}ct)\,d\bar{\nu}$$

Table 11.2.7.1 Langevin Parameters for CBr_4 ($I = 1.33 \times 10^{-37}$ g cm^2)

	$\left(\frac{2kT}{I}\right) K_0(0)$	$\left(\frac{2kT}{I}\right) K_1(0)$	$\left(\frac{2kT}{I}\right)^{1/2} \gamma$	t (°K)
Liquid	21 ± 0.4	247 ± 5	21 ± 0.4	376 ± 1
Rotator	20 ± 0.4	227 ± 5	20 ± 0.4	358 ± 1

This function looks very little like the correlation function of the condensed phase bands, which fall off initially faster and thereafter exponentially and more slowly. This octopolar function becomes negative after 0.7 psec, exhibits a minimum at 1.2 psec, and is damped to zero after 5.0 psec. The fact that $C_\Omega(t)/C_\Omega(0)$ falls off faster than $C_{FR}(t)$ means that a_2 is affected in some way by molecular interaction in the classical expansion:

$$C(t) = 1 - \frac{a_2 t^2}{2!} + \cdots$$

From Table 11.2.7.1 it is clear that CBr_4 molecules in both the liquid and plastic crystalline phase experience a torque almost immediately after the arbitrary $t = 0$. This is greater in magnitude than that in a bimolecular encounter of octopole fields, since $C(t)$ falls off faster initially than $C_\Omega(t)/C_\Omega(0)$. Rotation motions are then correlated in the condensed phases, and after $\sim$0.7 psec both $C(t)$ become exponential and decay relatively slowly compared with $C_\Omega(t)/C_\Omega(0)$. O'Dell and Berne (1975) have discovered that rotational motion is freer in the solid just below the melting point in rough hard sphere ensembles. This seems to be the case here since $C(t)$ for the liquid falls off a little faster initially. The greater initial torque in the condensed phases can be explained superficially in terms of the greater packing density since the intermolecular potential would be much greater on average with van der Waals radii overlapping (repulsive domain) for a greater percentage of the time. However, this is as always too simple a view, since the packing density in the plastic solid is greater, and the mean torque is smaller. This can only mean that symmetry of packing and the resultant restriction on molecular diffusion are factors that are important in determining the ease of rotational movement in the plastic phase.

11.3 INDUCED ABSORPTION AND LIGHT SCATTERING

If incoming light, polarized in the z-axis, is incident upon liquid or gas samples in the x direction and scattered light is observed in the y direction polarized in the x-axis, then what is observed is the radiation spectrum $I_{VW}(\omega)$ from a dipole induced in the x direction by an electric field along the z-axis. Such a dipole is proportional to the xz element of the electric

polarizability of the scattering volume. The depolarized Rayleigh spectral intensity $I_{VH}(\omega)$ is the Fourier transform of a correlation function which can be written as

$$C(t) = C_{perm}(t) + C_{ind}(t) + C_{ip}(t) \tag{11.3.1}$$

with

$$C_{perm}(t) = \mathrm{Tr}\langle\beta_1(0)\beta_2(t)\rangle + \sum_{i \neq 1} \mathrm{Tr}\langle\beta_1(0)\beta_1(t)\rangle$$

where β_i is the anisotropy of the electric polarizability tensor for the ith molecule and the trace is over the x, y, and z components of β. In Eq. 11.3.1 $C_{ind}(t)$ is a contribution arising from intermolecular collisions which exists in molecules such as CH_4 or CCl_4 which are optically isotropic. $C_{ip}(t)$ accounts for cross correlation between permanent and induced anisotropies.

In the specific case of self-correlation in linear molecules, $C_{perm}(t)$ is given by

$$C_{perm}(t) = \langle P_2[\cos\theta(t)]\rangle = \tfrac{1}{2}\langle 3[\mathbf{u}(0)\cdot\mathbf{u}(t)]^2 - 1\rangle$$
$$= 1 - 3\frac{kTt^2}{I} + \left[4\left(\frac{kT}{I}\right)^2 + \frac{\langle N^2\rangle}{8I^2}\right] t^4 - \cdots$$

where $\mathbf{u}$ is a unit vector along atomic centers, I is the moment of inertia, $T$the temperature, and $\langle N^2\rangle$ the mean square torque on a molecule. We are interested in the induced term $C_{ind}(t)$.

11.3.1 Molecular Dynamics Simulation

A simulation of the depolarized band shape of atomic fluids has been carried out by Alder and Wainwright (1970) using Lennard–Jones, hard sphere, and square well potentials to simulate the induced dipole-induced dipole a.c.f. $C_{ind}(t)$. The total intensity of the light scattering depends on the mean square of the irreducible second-rank part of the total polarizability tensor, and this includes contributions from the change of the polarizability of each atom due to changes in its environment (polarizability distortion). The simulation of the band shape requires knowledge of the autocorrelation of the polarizability at various times. However, too little is known about the detailed dependence of the polarizability distortion terms on the atomic density to evaluate anything except the induced dipole-induced dipole a.c.f. in a practical way. Two further assumptions are made:

1. The electronic motion and the resulting polarizability anisotropy must follow the fluctuations of the atomic density instantaneously. This is met very well because the electronic motion is very fast

compared with the atomic motion. The latter, simulated on the computer, determine the temporal behavior of the polarizability.

2. The distortion must be pairwise additive, and the polarizability anisotropy must vary with the interatomic distance in the same way as does the induced dipole-induced dipole term, that is, as $1/r^3$. The behavior of the complete polarizability anisotropy for many particles may be much more complicated.

Statistical averaging in the simulation was performed with a special distribution function involving up to four particles, with a number of different potentials. The induced-dipole a.c.f.'s were averages of six different components of the autocorrelation tensor. The variation of the hard sphere band shape with density is shown in Fig. 11.3.1.1, a long tail developing at the higher values in the same way as in the far infrared. It is interesting to compare the band shape (Fig. 11.3.1.1) with $\mathfrak{A}(\bar{\nu})/\bar{\nu}^2$ from the far infrared results (Fig. 11.2.4.2.2) for carbon dioxide.

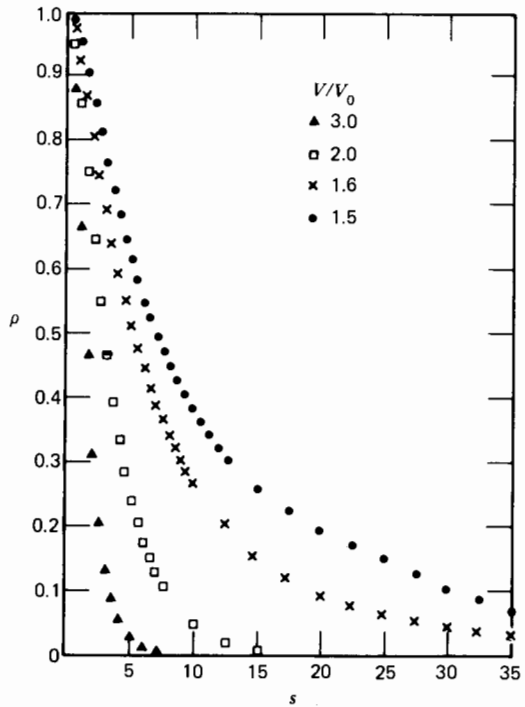

Figure 11.3.1.1 The average of the six components of the induced dipole-induced dipole tensor a.c.f. versus time, measured in units of the mean collision time, calculated for a system of hard spheres at various densities, expressed as the volume relative to the close packed volume v/v_0. [Reproduced by permission from B. J. Alder, H. Strauss, and G. Weiss, *J. Chem. Phys.* **59**, 1002 (1973).]

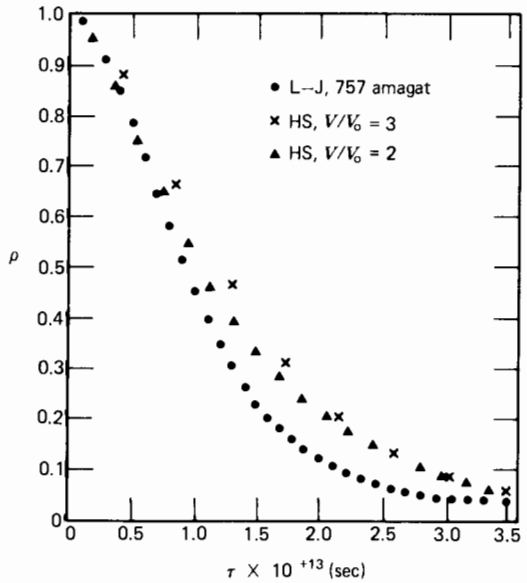

Figure 11.3.1.2 The computer simulation of the central Lorentzian in the band shape of argon at 960°K, 757 amagat. The experimental curves are scaled. [Reproduced by permission from B. J. Alder, H. Strauss, and G. Weiss, *J. Chem. Phys.* **59**, 1002 (1973).]

The dependence of the a.c.f. on the kind of intermolecular potential used is illustrated in Fig. 11.3.1.2. It is interesting to note that the significant range of intermolecular distances involved in the density anisotropy is of the order of the distance for which the attractive part of the potential changes rapidly. If this is the case, relatively small changes in the details of the potential might have a large effect on the correlation function, and the nature of this effect would be hard to predict but manifested in the induced band shapes of far infrared and Rayleigh scattering spectroscopy. The band shapes (the Fourier transform of the correlation functions), however, agree closely with each other and with experimental results but this is with the reservation that the latter were rather insensitive to detail. The latest results (Section 11.3.2) are more sensitive and discriminatory.

The comparison with data for compressed neon shows once again that the intermolecular potential is not purely repulsive, but intermediate between a hard sphere and Lennard–Jones system. The simulation method does not reproduce very well the high and low frequency scattering data in CCl_4 (liquid), so that more complex intermolecular factors are at work in more complex molecules.

The induced correlation function may therefore by written as

$$C_{\text{ind}}(t) = \sum_{k \neq l} \sum_{i \neq j} \langle \beta[r_{ij}(0)]\beta[r_{kl}(t)]P_2[\mathbf{u}_{ij}(0) \cdot \mathbf{u}_{kl}(t)] \rangle$$

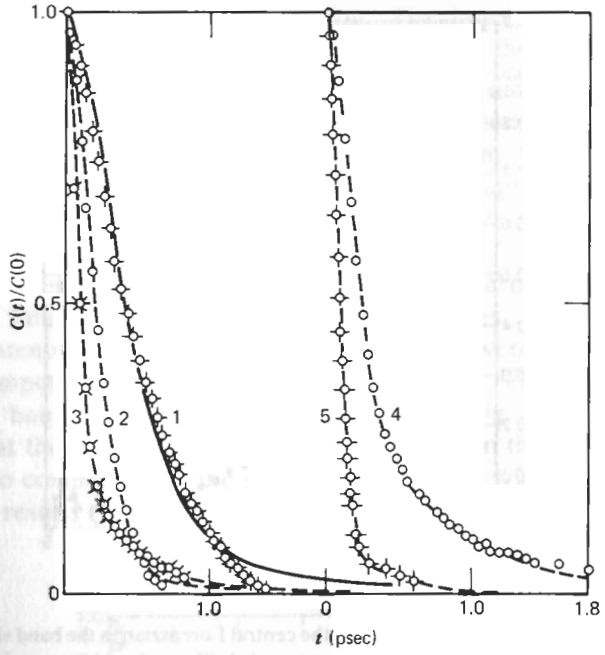

(a)

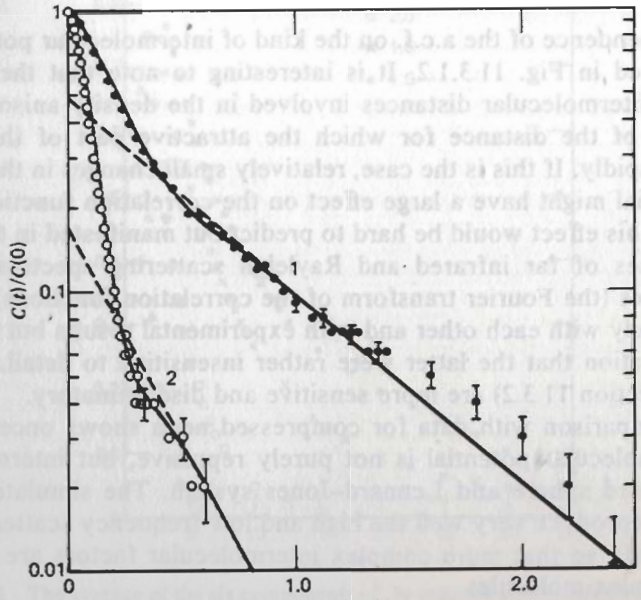

(b)

Figure 11.3.2.1 (*a*) and (*b*)

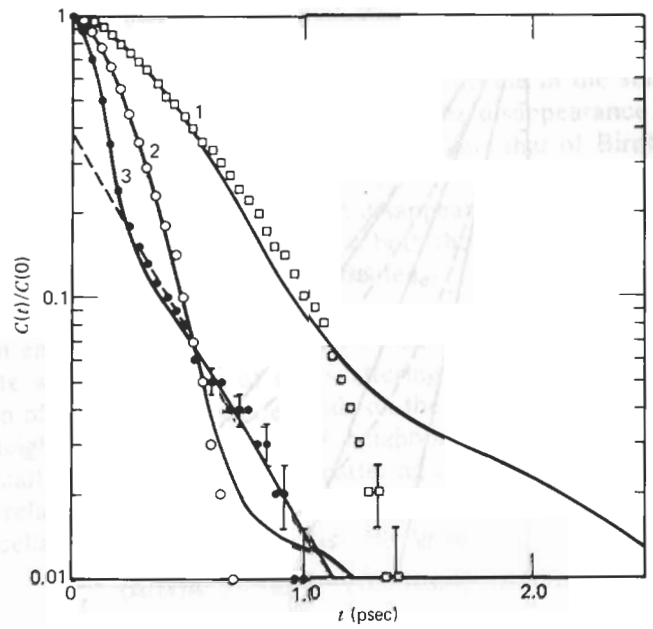

(c)

Figure 11.3.2.1 (*a*) -◇- Correlation function for argon simulated by Alder et al. Solid line, three-variable empirical least mean squares fits. (1) 300°K, 67 amagat; (2) 300°K, 473 amagat; (3) 300°K, 905 amagat; (4) 960°K, 757 amagat; (5) 90°K, 795 amagat. (*b*) As for (*a*), on a logarithmic scale designed to emphasize the long time exponential tailing of the theoretical correlation functions. (1) 90°K, 795 amagat; (2) 960°K, 757 amagat. (*c*) (1) 67 amagat, 300°K; (2) 473 amagat, 300°K; (3) 905 amagat, 300°K. [Reproduced by permission from M. W. Evans, *J. Chem. Soc. Faraday Trans. II* **71**, 485 (1977).]

where $\beta(r) = 6\alpha_0^2/r^3$, where α_0 is the atomic polarizability and r the interatomic distance. Here $\mathbf{u}_{ij}$ is the unit vector along the line joining the pair ij.

11.3.2 Continued Fraction Representation

The continued fraction theorem may be used to describe the total correlation function $C(t)$ of Section 11.2.1 and the depolarized line shape via the relation

$$I_{VH}(\omega) \propto \int_{-\infty}^{\infty} \exp(i\omega t) C(t)\, dt$$

$$\propto \frac{\phi_0(0)\phi_1(0)\gamma}{\gamma^2[\phi_0(0) - \omega^2]^2 + \omega^2[\omega^2 - (\phi_0(0) + \phi_1(0)]^2} \qquad (11.3.2.1)$$

This form reproduces all but one of Alder et al.'s computed correlation function for induced absorption in fluid argon and also the results of Dill et al. (1975) for the *permanent* polarizability a.c.f. $C_{perm}(t)$ in liquid acetone pressurized up to several thousand bar.

The least mean squares best fits to the experimental correlation functions of Eq. 11.3.2.1 are shown in Figs. 11.3.2.1 and 11.3.2.2. Equation 11.3.2.1

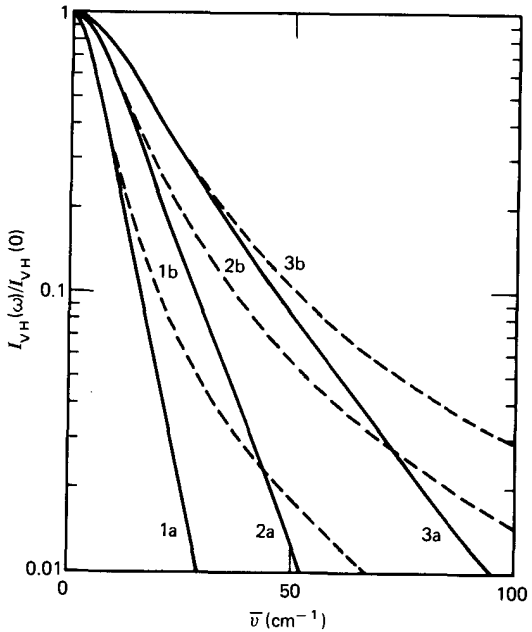

Figure 11.3.2.2 (*a*) Normalized line shape calculated from the least mean squares best fit of Fig. 11.3.2.1. 1a, 67 amagat; 2a, 473 amagat; 3a, 905 amagat; 300°K. 1b–3b, the Lorentzians to which these reduce at low frequency. [Reproduced by permission from M. W. Evans, *J. Chem. Soc. Faraday Trans. II* **71**, 485 (1977).]

for interaction-induced scattering is a Lorentzian at short times and exponential at long, reproducing well the band shape of scattered depolarized light from compressed argon at five thermodynamic states, where a roughly Lorentzian component in the band shape accounts for about half of the total depolarized intensity. The $C_{ind}(t)$'s estimated by best fit to the computer data all have natural exponential tails which are significantly positive at fairly long times. This could be indicative of the hydrodynamic power tails discussed in Chapter 5 but Alder et al. found no conclusive evidence for them in the molecular dynamics experiment.

11.3.2.1 Madden's Theory of Collision-Induced Scattering (1978)

The rapid improvement in theoretical and experimental techniques in this field has resulted in novel spectral features:

1. The integrated scattered intensity per molecule in the liquid state falls, as in the far infrared. The exponential regions of the induced line shape fall away more slowly with frequency (i.e., a high frequency tail develops, again as in the far infrared).
2. An additional Lorentzian feature appears at low frequency. There are high and low frequency deviations from the exponential.

3. The high frequency slope and its frequency dependence show a remarkably universal scaling behavior from one fluid to another.
4. The integrated scattered intensity per molecule in the solid phase is lower than that in the liquid, owing to the disappearance of the low frequency contribution. This result parallels that of Birnbaum et al. for carbon dioxide (Section 11.2.4.2) where the lower frequency part of the induced *absorption* band disappears with increasing density. The higher frequency behavior in both the scattering and absorption experiments is consistently unaffected.

Madden emphasizes the inadequacy of the pair interaction model in the liquid state where the width of the scattering spectrum, as in the induced absorption of the far infrared, depends on the temporary anisotropy of the nearest neighbor cage (the shell of neighbors is *on average* spherically symmetrical). The lifetime of the "scattering configuration" is the time this takes to relax to equilibrium. Madden calculates directly this departure from cancellation using Mori theory in the form

$$\langle \mathbf{A}(\omega)\mathbf{A}^T\rangle = [i\omega\mathbf{1} - i\hat{\Omega} + \mathbf{K}(\omega)]^{-1}\langle \mathbf{A}\mathbf{A}^T\rangle$$

which leads to an expression for the band shape in terms of the Fourier components of the *bilinear* number density, $B(\mathbf{K}-\mathbf{K}')$. The correlation function of $B(\mathbf{K}-\mathbf{K}')$ at different $\mathbf{K}'$ reflects atomic motions over a range of distances which feature their diffusional, librational, and free translational limits. The free parameters of the theory are eliminated using neutron scattering data. Here $\mathbf{K}$ denotes the scattering vector.

The induced spectrum is written as the Fourier transform of correlation functions involving components of the spatial Fourier transform of the anisotropic polarizability *density* of the medium (i.e., the temporary polarization density induced by molecular interaction). The use of the *density* (hydrodynamic in nature) means that a summation over many particles is involved from the start. The equivalent for far infrared induced absorption would be the summed induced-dipole density. The following assumptions and methods are then used for the sake of tractability:

1. The m-particle distribution function is written as a product of two-particle distribution functions.
2. The anisotropy function $\beta(r)$ of the interatomic separation is calculated using a correct $r \to 0$ form, ensuring convergent integrals.
3. Two-, three-, and four-body terms contribute to the intensity as 1, −1.3, and 0.8, respectively. This means that the three-body contribution is *negative*, as in the work on carbon dioxide (Section 11.2.4.2). However, the intensity arises from a near cancellation of one-, two-, and three-body terms, so that it is fruitless to attempt a discussion in terms of each individual n-body contribution.

4. The spectrum is finally related to the *bilinear* number density correlation function:

$$\lim_{K\to 0}\langle n_{\mathbf{K}-\mathbf{K}'}n_{\mathbf{K}'})(\omega)(n_{-\mathbf{K}+\mathbf{K}'}n_{-\mathbf{K}'})\rangle$$

where $n_{\mathbf{K}}$ is the Fourier transform of the number density.

Madden then uses the neutron scattering results from liquid argon at the same density and frequency range for *incoherent* scattering:

$$\mathbf{A}=\begin{bmatrix} n_{\mathbf{K}}^{(i)} \\ i\mathbf{K}\cdot\mathbf{p}_{\mathbf{K}}^{(i)} \\ i\mathbf{K}\cdot\boldsymbol{\sigma}_{\mathbf{K}}\cdot i\mathbf{K}+\dfrac{K^2}{m\beta}n_{\mathbf{K}}^{(i)} \end{bmatrix} \tag{11.3.2.1.1}$$

as a set of slow variables (in Kivelson terminology) coupled to $n_{\mathbf{K}}^{(i)}$. Note that this is a very similar approach to that used in the empirical Eq. 11.3.2.1. In Eq. 11.3.2.1.1 $\mathbf{p}_{\mathbf{K}}^{(i)}$ is the Fourier transform of the momentum *density* of i and $\boldsymbol{\sigma}_{\mathbf{K}}^{(i)}$ of the force acting on i:

$$i\mathbf{K}\cdot\boldsymbol{\sigma}_{K}^{(i)}=\frac{\partial}{\partial t}\mathbf{p}_{\mathbf{K}}^{(i)}$$

The decay rates of $n_{\mathbf{K}}^{(i)}$ and $i\mathbf{K}\cdot\boldsymbol{\sigma}_{\mathbf{K}}\cdot i\mathbf{K}$ are intuitively comparable because of the following:

1. The important contributions to the decay of $n_{\mathbf{K}}^{(i)}$ arise from atomic motions over distances comparable to the near neighbor separation.
2. Such motions also determine the rate of change of the interatomic forces.

Naturally, in Eq. 11.3.2.1.1 rates of changes of intermolecular force are assumed very fast, and correlation functions of all higher derivatives of $\sigma_{\mathbf{K}}$ decay very rapidly compared with those involving the set **A** only. The incoherent scattering cross section is of the three-variable form:

$$S_I(\mathbf{K},\omega)=\langle n_{\mathbf{K}}^{(i)}(\omega)n_{-\mathbf{K}}^{(i)}\rangle$$
$$\propto \mathrm{Re}\left(\frac{i\omega-\delta_2}{i\omega-\delta_4/(i\omega-t_I^{-1})}\right)$$

which is identical with Eq. 11.3.2.1, and is, of course, Lorentzian at low frequencies.

The coherent neutron scattering spectrum may be described similarly and the Mori data are thereafter used by Madden as an "input" to the calculation of the more complicated bilinear density function of the *induced* light scattering spectrum.

The problem is therefore reduced to choosing a set of slow variables

which couple to the bilinear primary variable $n_{\mathbf{K}-\mathbf{K}}n_{\mathbf{K}'}$. The neutron scattering formalism is suggestive of

$$\mathbf{A}^T(\mathbf{K}')=(nn,\ pn,\ pp,\ n\sigma',\ p\sigma',\ \sigma\sigma')$$

where

$$nn=n_{\mathbf{K}-\mathbf{K}'}n_{\mathbf{K}'}$$

$$pn=\frac{\partial}{\partial t}(nn)$$

$$pp=-\frac{1}{m^2}(\mathbf{K}-\mathbf{K}')\cdot\mathbf{p}_{\mathbf{K}-\mathbf{K}'}\mathbf{p}_{\mathbf{K}'}\cdot\mathbf{K}'$$

$$n\sigma'=n\sigma-\langle n\sigma(nn)^*\rangle\langle nn(nn)^*\rangle^{-1}nn$$

(see Chapter 3), and

$$n\sigma=\frac{\partial}{\partial t}(pn)-2pp$$

$$p\sigma'=p\sigma-\langle p\sigma(pn)^*\rangle\langle pn(pn)^*\rangle^{-1}pn$$

$$p\sigma=\frac{\partial}{\partial t}(pp)$$

$$\sigma\sigma'=-\frac{1}{n^2}(\mathbf{K}-\mathbf{K}')\cdot\boldsymbol{\sigma}_{\mathbf{K}-\mathbf{K}'}\cdot(\mathbf{K}-\mathbf{K}')\mathbf{K}'\cdot\boldsymbol{\sigma}'_{\mathbf{K}}\cdot\mathbf{K}'$$

Here $\boldsymbol{\sigma}'_{\mathbf{K}}$ is related to the stress tensor.

This is a complicated set to work out in general but in the $\mathbf{K}\to\mathbf{0}$ limit of depolarized, quasi-elastic, light scattering ($\mathbf{K}''\neq\mathbf{K}'$ terms being neglected), only components parallel to $\mathbf{K}'$ remain coupled. The result is that

$$\lim_{K\to 0}\langle(n_{\mathbf{K}-\mathbf{K}'}n_{\mathbf{K}'})(\omega)(n_{-\mathbf{K}+\mathbf{K}'}n_{-\mathbf{K}'})^*\rangle$$
$$=\pi^{-1}\,\mathrm{Re}\left[S(\mathbf{K}')^2\Big/\left(\frac{i\omega+2\omega_c^2}{(i\omega+T)}+\frac{2\omega_c^2(1-HT)^2}{i\omega+2H(\omega_e^2-\omega_c^2)[1-HT\omega_c^2(\omega_e^2-\omega_c^2)^{-1}]}\right)\right]$$

with

$$H=\left(i\omega+\tau^{-1}+\frac{2(\omega_e^2-\omega_c^2)}{i\omega+2\tau^{-1}}\right)^{-1}$$

$$T=\frac{\omega_e^2-\omega_c^2}{i\omega+\tau^{-1}+\omega_c^2H} \tag{11.3.2.1.2}$$

which is similarly structured to Eq. 11.3.2.1. The frequencies ω_e and ω_c are defined in terms of elements of $\langle\mathbf{AA}^*\rangle$, and τ^{-1} by the $K_{44}(0)$ component of the memory matrix.

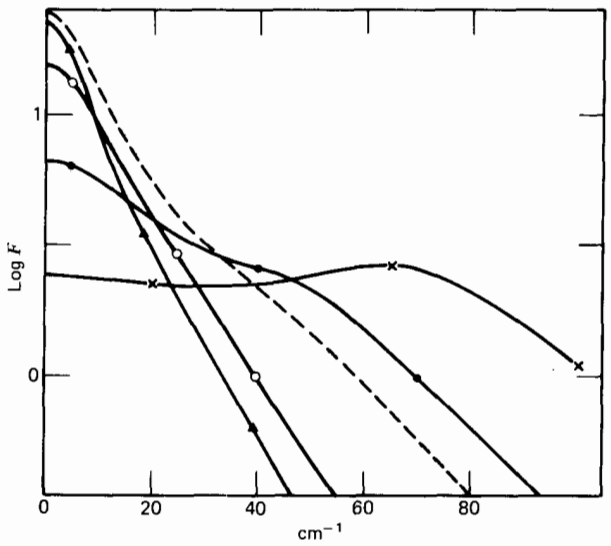

Figure 11.3.2.3 Log $F(\mathbf{K}', \omega)$ versus ω at a series of $|\mathbf{K}'|$: ○ 1.8 Å^{-1}, ▲ 2.0 Å^{-1}; ● 3.4 Å^{-1}; × 4.3 Å^{-1}. The dashed line is the log of the experimental spectrum. Note that the empirical formalism of Figure 11.3.2.2 cannot apparently reproduce the hump at about 50 cm^{-1}. [Reproduced by permission from P. Madden, *Mol. Phys.* **36**, 365 (1978).]

The low frequency Lorentzian of induced light scattering from this theory has a width which is related to twice the width of the coherent neutron scattering peak and reflects motions that are diffusional (in much the same way that the Debye peak does in *permanent*-dipolar absorption in 0–THz spectroscopy). If **A** is restricted to *nn*, then what results is the spectrum of *two independent pairs* of particles moving apart by diffusion. The fuller theory corrects for the assumed independence of the forces acting on each particle in the diffusion model.

The frequency-dependent part of the spectrum $[F(\mathbf{K}', \omega)]$ shows some interesting structural details that harmonize well with the experimental features. This is shown for various $\mathbf{K}'$ in Fig. 11.3.2.3 along with the experimental features in the region of the second observable shoulder [compare this with Fig. 11.2.4.2.2 for CO_2 (l)]. The observable change of slope coincides with the position of an observable peak in solid argon, which has been associated with the Debye limiting frequency of the solid. We have $\mathbf{K}' = \mathbf{K}_\sigma$ as the first peak of the structure factor, and $\mathbf{K}' \doteqdot 2\mathbf{K}_\sigma$ as the second peak. The shape of $F(2\mathbf{K}_\sigma, \omega)$ is determined by motions of atoms around spatially fixed sites as distinct from the shape of $F(\mathbf{K}_\sigma, \omega)$, which arises predominantly from diffusional motions (interchange of atoms among sites). If two atoms are, at time zero, at their most probable relative separation, then $\exp(i\mathbf{K} \cdot \mathbf{r}_{12}) = 1$. In order that $\exp(i\mathbf{K} \cdot \mathbf{r}_{12})$ change to zero $\mathbf{r}_{12}$ must change by $\sigma/2$ for $\mathbf{K} = \mathbf{K}_\sigma$ and by $\sigma/4$ for $\mathbf{K} = 2\mathbf{K}_\sigma$. The latter type

of motion may be accommodated without lattice reorganization whereas the former cannot, and entails cooperation diffusion, absent in the solid induced scattering spectrum.

At high frequencies, Madden uses a model of the dynamics based on the fact that at very short times

$$\mathbf{r}_i(t) = \mathbf{r}_i(0) + \mathbf{v}_i(0)t$$

where $\mathbf{v}_i$ is the velocity of particle i, and consequently the number density correlation function is

$$\langle n_{\mathbf{K}}(t) n_{-\mathbf{K}} \rangle = \sum_{i,j} \langle \exp i\mathbf{K} \cdot [\mathbf{r}_{ij}(0) + \mathbf{v}_i(0)t] \rangle$$

$$= \sum_{i,j} \langle \exp i(\mathbf{K} \cdot \mathbf{r}_{ij}) \rangle \langle \exp(i\mathbf{K} \cdot \mathbf{v}_i t) \rangle$$

because velocity and positional averages are independent. The distribution of velocities is Gaussian with a standard deviation of $(2/m\beta)^{1/2}$, so that

$$\langle n_{\mathbf{K}}(t) n_{-\mathbf{K}} \rangle = NS(K) \exp\left(-\frac{K^2 t^2}{2m\beta}\right) \qquad (11.3.2.1.3)$$

Liquid structure is retained, through the factor $S(K)$, but the effect of intermolecular interactions on the frequency dependence is ignored, as in ideal gas. The correlation function which describes the interaction-induced light scattering is now

$$\lim_{\mathbf{K} \to 0} \sum_{ij}{}' \sum_{mn}{}' \langle \exp[i(\mathbf{K} - \mathbf{K}') \cdot \mathbf{r}_{ij}] \exp[-i\mathbf{K}' \cdot \mathbf{r}_{mn}] \rangle$$
$$\times \exp[i(\mathbf{K} - \mathbf{K}') \cdot \mathbf{v}_i(0)t] \rangle \langle \exp(-i\mathbf{K}' \cdot \mathbf{v}_m(0)t \rangle$$
$$= N^2 S(K')^2 \exp\left(-\frac{K^2 t^2}{m\beta}\right)$$

which involves two-, three-, and four-body terms. A hard sphere calculation is used for the frequency independent term $S(\mathbf{K})$.

At frequencies higher than that of the maximum atomic oscillation this gas-like theory represents the motion as free translation. The range $|\mathbf{K}'| > 3$ Å^{-1} accounts for almost the full contribution for $|\mathbf{K}'| > 60$ cm^{-1}.

The above approach is that of reducing the equation of motion for the multiparticle correlation function to a form in which only one- and two-particle properties appear. The resulting problem was solved by use of the superposition approximation for the configuration distribution function (i.e., by factorizing the *equilibrium* correlation functions). Alternatively, one may use the following factorization:

$$\langle (n_{\mathbf{K}-\mathbf{K}'} n_{\mathbf{K}'})(t) n_{-\mathbf{K}+\mathbf{K}'} n_{-\mathbf{K}'} \rangle$$
$$= N^4 \langle \exp\{i(\mathbf{K} - \mathbf{K}') \cdot [\mathbf{r}_1(t) - \mathbf{r}_2(0)]\} \exp\{-i\mathbf{K}' \cdot [\mathbf{r}_3(t) - \mathbf{r}_4(0)]\} \rangle$$
$$= N^4 \langle \exp\{i(\mathbf{K} - \mathbf{K}') \cdot [\mathbf{r}_1(t) - \mathbf{r}_2(0)]\} \rangle \langle \exp\{-i\mathbf{K}' \cdot (\mathbf{r}_3(t) - \mathbf{r}_4(0)]\} \rangle$$

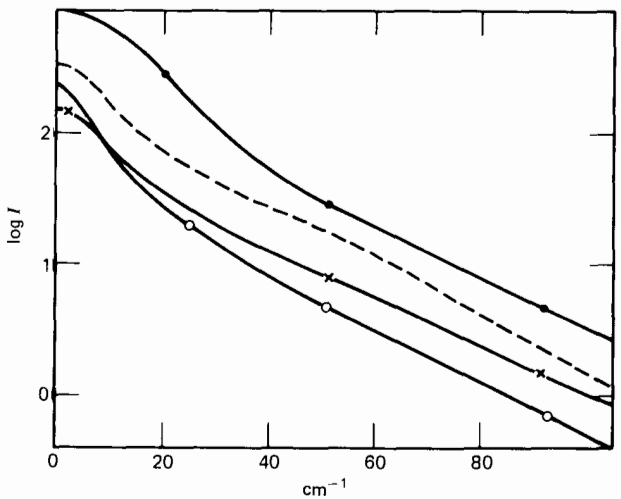

Figure 11.3.2.4 Comparison of theories of induced light scattering. ● Structured gas; × Madden–Mori; ○ Stephen. Dashed line, experimental. The first and last are offset. [Reproduced by permission from P. Madden, *Mol. Phys.* **36**, 365 (1978).]

that is, directly that of the time-dependent correlation function. In this way the correlation function is reduced to that of two independent pairs of particles. The resulting spectrum may be directly related to the coherent neutron-scattering spectrum through the work of Stephen. This approach is apparently inaccurate in compressed argon, but is identical with the Madden theory in the absence of intermolecular interactions.

Figure 11.3.2.4 compares the Madden–Mori theory (Eq. 11.3.2.1.2), the Stephen theory, and the "structured gas" model of Eq. 11.3.2.1.3 with the experimental data. The Stephen type of factorization does not accurately reproduce the low frequency Lorentzian and fails qualitatively to reproduce the change of slope at $\sim 60\,cm^{-1}$ associated with the "solidlike" motions of the atoms. The "structured gas" calculation fails to describe either the low frequency Lorentzian or the change of slope, which are both cooperative in origin.

11.3.3 High-Accuracy Study of Scattering from Atoms

An et al. (1979) have recently reported some accurate scattering data on compressed gaseous krypton at four thermodynamic states. At liquidlike densities there exists a Lorentzian at below $20\,cm^{-1}$ from the exciting line and a weak shoulder at around $50\,cm^{-1}$. The existence of the low frequency Lorentzian is of course corroborated by the molecular dynamics simulations of Alder et al. (Section 11.3.2) and is describable either by Evans's empirical Eq. 11.3.1.1 or Madden's self-consistent Eq. 11.3.2.1.1.

The shallow peak at around $50\,cm^{-1}$ is a deviation from the apparent exponential appearance of the induced scattering, which has its analogue in the by now familiar far infrared shift to higher frequencies as liquid densities are approach. An et al. (1979) makes the interesting observation that the simulation of Chapter 7 on glassy argon produces a pronounced peak at $50\,cm^{-1}$ or so. The far infrared power representation of compressed nitrogen (Fig. 11.4.1.1) or compressed carbon dioxide (Fig. 11.2.4.2.2) brings out the same kind of overall feature. The weak $50\,cm^{-1}$ scattering shoulder in krypton disappears as the density is lowered below the critical, as in spherically polarizable molecules such as CCl_4, where the shoulder is the direct counterpart of the far infrared absorption, described empirically in Figs. 11.2.5.1 and 11.2.5.2, by Evans's three-variable Mori formalism. It is reported once more that the intensity of the total depolarized spectrum decreases with density in the range studied. This again echoes the earlier far infrared results.

Madden's theory makes it possible to assign these features to the dynamic evolution of fluctuations with different wave vectors. The Lorentzian comes from fluctuations with $|\mathbf{K}'_\sigma| \sim 2$ and, as we have seen, reflects the collective motion of a central particle with its first shell of neighbors. An aspect of the motion is probed which reflects the relaxation of an asymmetric molecular arrangement around a given particle to the "symmetrical" equilibrium state. According to An et al. the breadth of the central Lorentzian establishes the time scale of this phenomenon involving both the rearrangement of atoms within the first coordination shell as well as the atoms out of this shell. Madden uses the latter as the Mori primary variable, but according to An et al. no such distinction can be made because of the relatively long times associated with the Lorentzian half-width of $5–10\,cm^{-1}$.

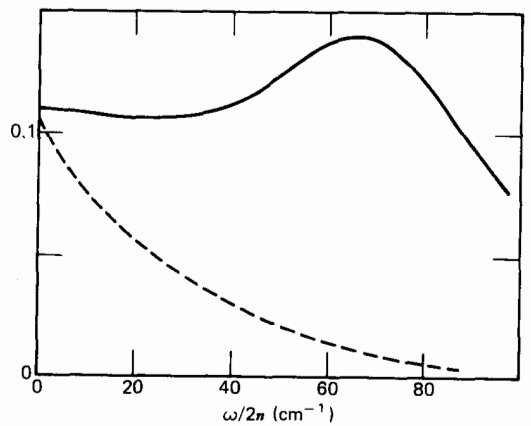

Figure 11.3.3.1 Reduced scattering function $F(K', \omega)$ (arbitrary units) and dynamic structure factor for liquid argon for $|\mathbf{K}'| = 4.4\,Å^{-1}$. [Reproduced by permission from An et al., *J. Chem. Phys.* **70**, 4626 (1979).]

In discussing the 50 cm^{-1} shoulder An et al. point out the absence of the equivalent signature in the dynamic structure factor of a neutron scattering experiment (Fig. 11.3.3.1). Its appearance in the depolarized Rayleigh spectrum $[F(\mathbf{K}', \omega)]$ is traceable to the fact that the induction process imposes a moving frame of reference on the observation of atomic motions so that only *relative motion* of an atomic pair is measured. Spectral features associated with the motions of isolated atoms (neutron scattering) are suppressed, thereby emphasizing the oscillating character of the *relative* velocities. Note that in the liquid it is not meaningful to speak of motion relative to a fixed lattice site, because this has no meaning in the laboratory frame. Similarly *relative angular* velocities are highlighted in far infrared induced spectra.

By consideration of the Lorentzian half-width these authors seem to have found evidence for a limitation of the Madden theory to densities below the critical.

11.4 COMPUTER SIMULATION OF INDUCED ABSORPTION

The ensemble averages of squares of dipole-dipole interatomic quantities have been calculated by Alder et al. (1973) using molecular dynamics simulations of spheres with a constant polarizability. The dielectric dispersion and loss has been evaluated by these authors using the dipole-dipole tensor a.c.f.:

$$R^{ab}(\tau) = \frac{\sigma^6}{N^2}\left\langle \sum_j \left[\sum_{i\neq j} T_{ij}^{ab}(0)\right]\left[\sum_{k\neq j} T_{kj}^{ab}(\tau)\right]\right\rangle$$

where σ is the Lennard–Jones diameter, N is the number of particles in the system, and T_{ij}^{ab} is a component of the dipole-dipole tensor between atoms i and j with $a, b = X, Y, Z$. For example,

$$T_{ij}^{xy} = \frac{1}{r_{ij}^3}\left(\delta_{XY} - \frac{3X_{ij}Y_{ij}}{r_{ij}^2}\right)$$

where atoms are separated by $\mathbf{r}_{ij}$ and δ_{XY} is the Kronecker δ. The R^{ab} quantities may be broken into two- and three-body terms:

$$R^{ab} = S_2^{ab} + S_3^{ab}$$

where S_2 includes only terms with $i = k$ and S_3 with $i \neq k$. At low densities only the S_2 terms remain, but as the results of Section 11.2 and those of Madden (Section 11.3) show at higher densities there is cancellation between the S_2 and S_3 terms. The tensor $\mathbf{R}$ does not contain four-body terms as does the light scattering form of Section 11.3.1. The components are related by

$$R^{zz} = R^{xx} = R^{yy}; \qquad R^{xy} = R^{yz} = R^{zx} = \tfrac{3}{4}R^{zz}$$

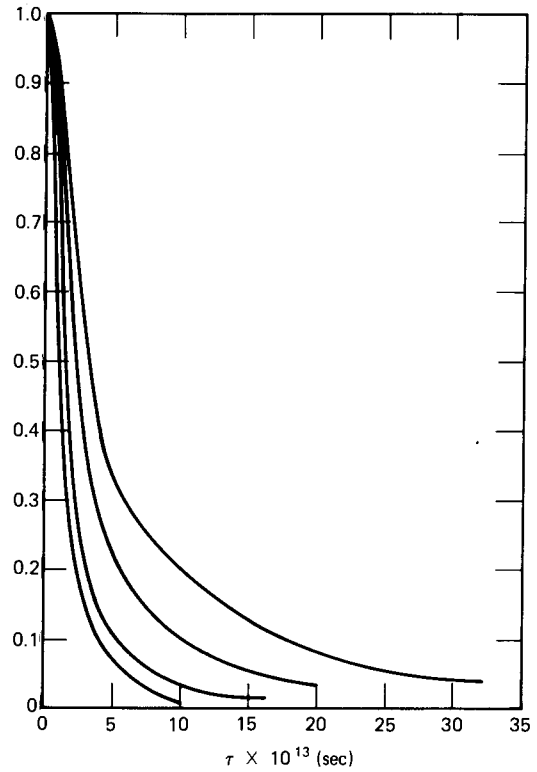

Figure 11.4.1 The calculated dielectric R and light scattering S a.c.f.'s for argon. (1) R, 90°K, 795 amagat; (2) S, 90°K, 795 amagat; (3) R, 300°K, 905 amagat: (4) S, 300°K, 908 amagat. [Reproduced by permission from B. J. Alder et al., *J. Chem. Phys.* **62**, 2328 (1975).]

The tensors $\mathbf{R}$ and $\mathbf{S}_2$ were simulated separately by averaging the six components of each. *The shape of* $\mathbf{R}(\tau)$ *is very similar* (*Fig.* 11.4.1) *to that of the light scattering autocorrelation of Section* 11.3.1, except that it decays more slowly for two states of argon.

The static dielectric constant may be evaluated from these tensors using, for example, a series expansion of the Clausius–Mossotti equation:

$$\frac{\epsilon_s - 1}{\epsilon_s + 2} = \frac{4\pi}{3}\rho\alpha[1 + \Delta + 0(\alpha^3)] \tag{11.4.1}$$

with

$$\Delta = \frac{\alpha^2}{3}\sum_{\substack{i\neq j\\ k\neq j}}\left\langle \sum_{a,b}\langle T_{ij}^{ab}T_{jk}^{ab}\rangle - \sum_{a,b}\langle T_{ij}^{ab}\rangle\langle T_{jk}^{ab}\rangle\right]$$

In the molecular dynamics simulation of Alder and co-workers the dielectric constant is calculated from an isotropic sample using, as usual, periodic boundary conditions so that the mean values $\langle T^{ab}\rangle = 0$. The last term of Eq.

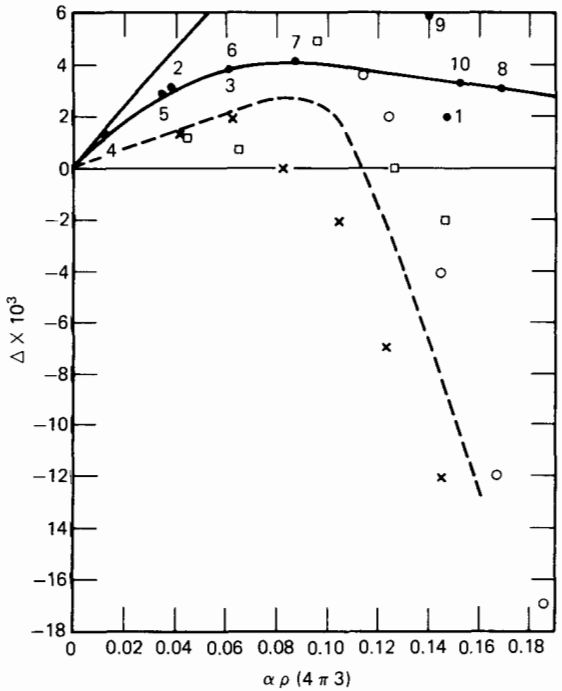

Figure 11.4.2 Computer-simulated (solid line) and experimental (dashed line) values of Δ (see text) for a polarizable sphere (argon). The experimental values are given for argon at 298°K (×), 273°K (○), and 190°K (●). The refractive index values are shown (□) for the gas at 173°K and for the liquid at the gas/liquid coexistence temperature. [Reproduced by permission from B. J. Alder et al., *J. Chem. Phys.* **62**, 2328 (1975).]

11.4.1 therefore vanishes and

$$\Delta = \frac{5}{2}\frac{\alpha^2}{\sigma^6} R^{zz}(0)$$

The calculated and experimentally measured values of Δ are plotted in Fig. 11.4.2. Deviations from the ideal Clausius–Mossotti relation are small, so that experimental errors seem large. However, the calculated Δ term does not account for the observations. Δ is intrinsically positive and the observed deviations are negative at the higher densities, and the cause of the ϵ_s variation lies in the variation of α itself with density.

The dielectric dispersion in a system of polarizable atoms must be due, to mechanisms that have something to do with density fluctuations as discussed by Madden in his theory of light scattering. The simulations show an interesting persistence of the electronic absorptions of the rare gases into the far infrared.

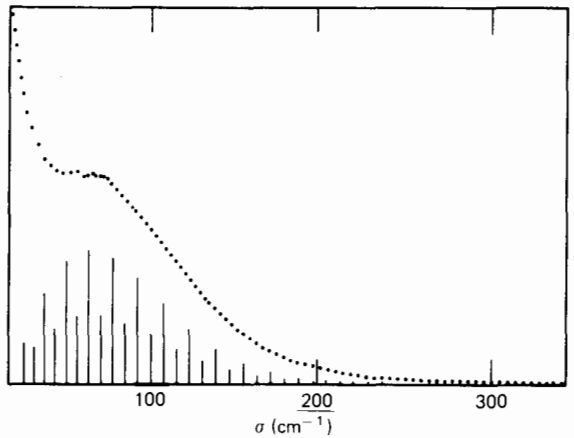

Figure 11.4.1.1 The line shape of N_2 at 300°K, "light scattering representation" of the far infrared power absorption $\alpha(\bar{\nu})$. The vertical lines are the unbroadened quadrupole induced intensities. Note that the similarity to the induced light scattering features. [Reproduced by permission from Buontempo, Cunsolo, Jacucci, and Weis, *J. Chem. Phys.* **63**, 2570 (1975).]

11.4.1 Molecular Dynamics Simulation of the Far Infrared Band of Liquid Nitrogen

This was carried out by Buontempo et al. (1973) using atom-atom potential interaction on 500 N_2 molecules arranged cubically with periodic boundary conditions. The "light scattering" intensity function $[\mathfrak{N}(\bar{\nu})/\bar{\nu}^2]$ is illustrated for gaseous nitrogen in Fig. 11.4.1.1, the translational component ($\Delta J = 0$) being well resolved. In the liquid (Fig. 11.4.1.2) there is the shift to high frequencies we have already noted and a decrease in the integrated absorption intensity per molecule. Two-body interaction theory again breaks down, the calculated bimolecular induced absorption being much too intense. The cancellation effect is even stronger in the solid phase. The cross section per molecule is smaller by a factor of two in the liquid than in the gas. The interference of the induced dipole moments plays a major role in the cancellation effect.

The object of the molecular dynamics simulation in this liquid nitrogen was to attempt to reproduce the broader liquid spectrum using only quadrupole mechanisms of dipole induction, using zero polarizability anisotropy so that double transitions ($\Delta J_1 = 2$, $\Delta J_2 = 2$) are not present. A five-step predictor-corrector integration routine was used the run lasting for 24,000 time steps of $\Delta t = 5 \times 10^{-15}$ sec each. The thermodynamics state was close to the triple point. The density and temperature in reduced units were $\rho\sigma_a^3 = 0.696$, $Tk/\epsilon_a = 1.60$, respectively.

The time a.c.f. $C(t)$ of the total dipole moment was calculated as follows. The induced dipole $\boldsymbol{\mu}_i$ on the ith molecule results from the resultant

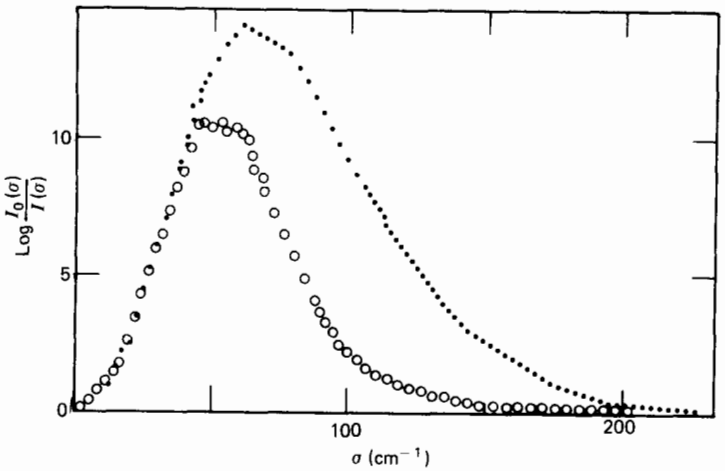

Figure 11.4.1.2 The experimental far infrared optical density of liquid N_2 at 66°K (●). The estimated gas profile (○) peaks at the lower frequency. [Reproduced by permission from Buontempo, Cunsolo, Jacucci, and Weis, *J. Chem. Phys.* **63**, 2575 (1975).]

electric field $\mathbf{E}_i$ due to the surrounding quadrupole moments:

$$\mu_i^\gamma = \sum_\delta \alpha_i^{\gamma\delta} E_i^\delta$$

Nonadditive effects are neglected and the molecular polarizability tensor taken to be *spherically symmetrical*, that is, $\mu_i^\gamma = \alpha E_i^\gamma$ and the total induced dipole moment is $\mu^\gamma(t) = \Sigma_i \alpha E_i^\gamma(t)$. The contribution of the quadrupole

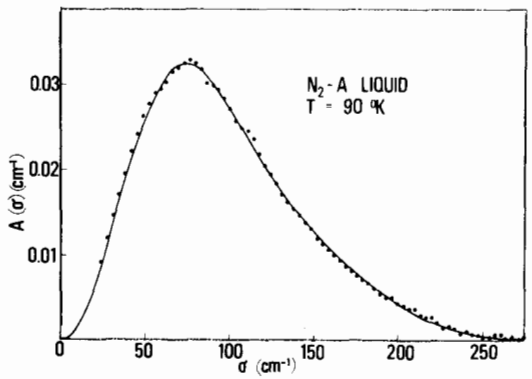

Figure 11.4.1.3 Comparison between the experimental absorption coefficient and that simulated (———). The intensities are normalized for direct band *shape* comparison. The simulated intensity is too low. The shift to higher frequencies is simulated satisfactorily. [Reproduced by permission from Buontempo, Cunsolo, Jacucci, and Weis, *J. Chem. Phys.* **63**, 2570 (1975).]

moment of the jth molecule to the electric field on the ith molecule is written as

$$E_{ij}^\alpha = -\tfrac{1}{2} \sum_{\beta\gamma} u_i^{\alpha\beta\gamma} Q_j^{\beta\gamma}$$

where $Q_j^{\beta\gamma} = Q u_j^\beta u_j^\gamma$ and

$$u_{ij}^{\alpha\beta\gamma} = -\frac{3}{r^7}\left[5r^\alpha r^\beta r^\gamma - r^2(r^\alpha \delta_{\beta\gamma} + r^\beta \delta_{\alpha\gamma} + r^\gamma \delta_{\alpha\beta})\right]$$

where $r = r_{ij}$ and u_j is a unit vector parallel to the axis of molecule j. Q is the molecular quadrupole moment. The absorption coefficient obtained from the molecular dynamics calculation of $C(t)$ is shown in Fig. 11.4.1.3 and compared with the experimental data. The two curves are normalized at the frequency of the maximum of the molecular dynamics results.

The absorption profile is very well described by the *quadrupolar* induction mechanism. It is particularly important to note that the high frequency wing is accurately reproduced so that apparently there is no need to take into account such factors as hexadecapole-induced absorption. The shift in the peak frequency is produced solely by the angular constraints on the molecules in the liquid state, and by accurately accounting for the quadrupole-quadrupole part of the interaction energy. Note that a hard sphere or hard dumbbell potential would be useless in this respect, and in this regime electrostatic factors predominate. It would naturally be interesting to repeat this simulation for CO_2, N_2O, and $(CN)_2$, again using quadrupole-quadrupole interactions.

11.5 FEATURES OF INDUCED ABSORPTION IN WEAKLY DIPOLAR SYMMETRICAL TOPS

In C_{3v} symmetry symmetrical tops such as $CClF_3$ and $CBrF_3$, which are weakly dipolar, the induced absorption appears as a high frequency tail on the $\Delta J = 1$ contour of the permanent dipolar motions. The Frost theory may be used to evaluate the multipoles which appear to contribute to this process. In this final section we illustrate briefly how the spectral profile of $CClF_3$ and $CBrF_3$ change on self-pressurization and liquefaction (Figs. 11.5.1–11.5.3). The position of the permanent dipolar $\bar{\nu}_{max}$ does not change significantly so that even in the liquid state there is considerable freedom of rotation. This is the best possible situation for such gas phase models as J-diffusion and at intermediate densities the theory seems to be fairly adequate (Fig. 11.5.4). However, the very long liquid tail and the similar features in the compressed gas at liquidlike densities are collision induced in origin, and establish the role of inelastic, electrical interactions as opposed to the elastic collisions of the extended diffusion models. Faced with data such as these, the diffusion modes seem to be tremendously

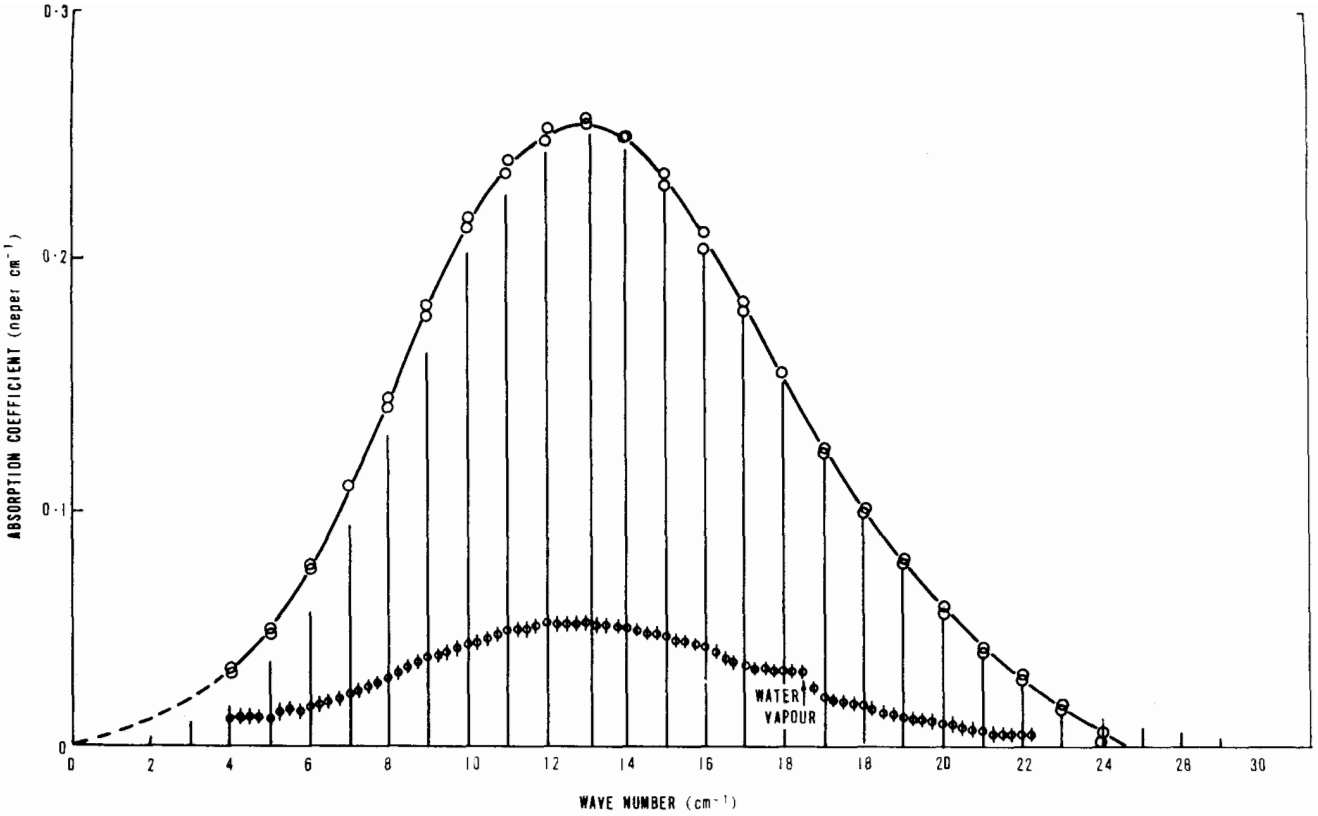

Figure 11.5.1 Power absorption coefficient of $CClF_3$ at low pressures. 1 atm, 288°K (ϕ) and 4.4 atm, 288°K (○). The vertical lines give the frequencies and relative integrated intensities of the pure rotational $J \rightarrow J + 1$ transitions up to $J = 150$. [Reproduced by permission from G. J. Davies and M. W. Evans, *J. Chem. Soc. Faraday Trans. II* **71**, 1275 (1975).]

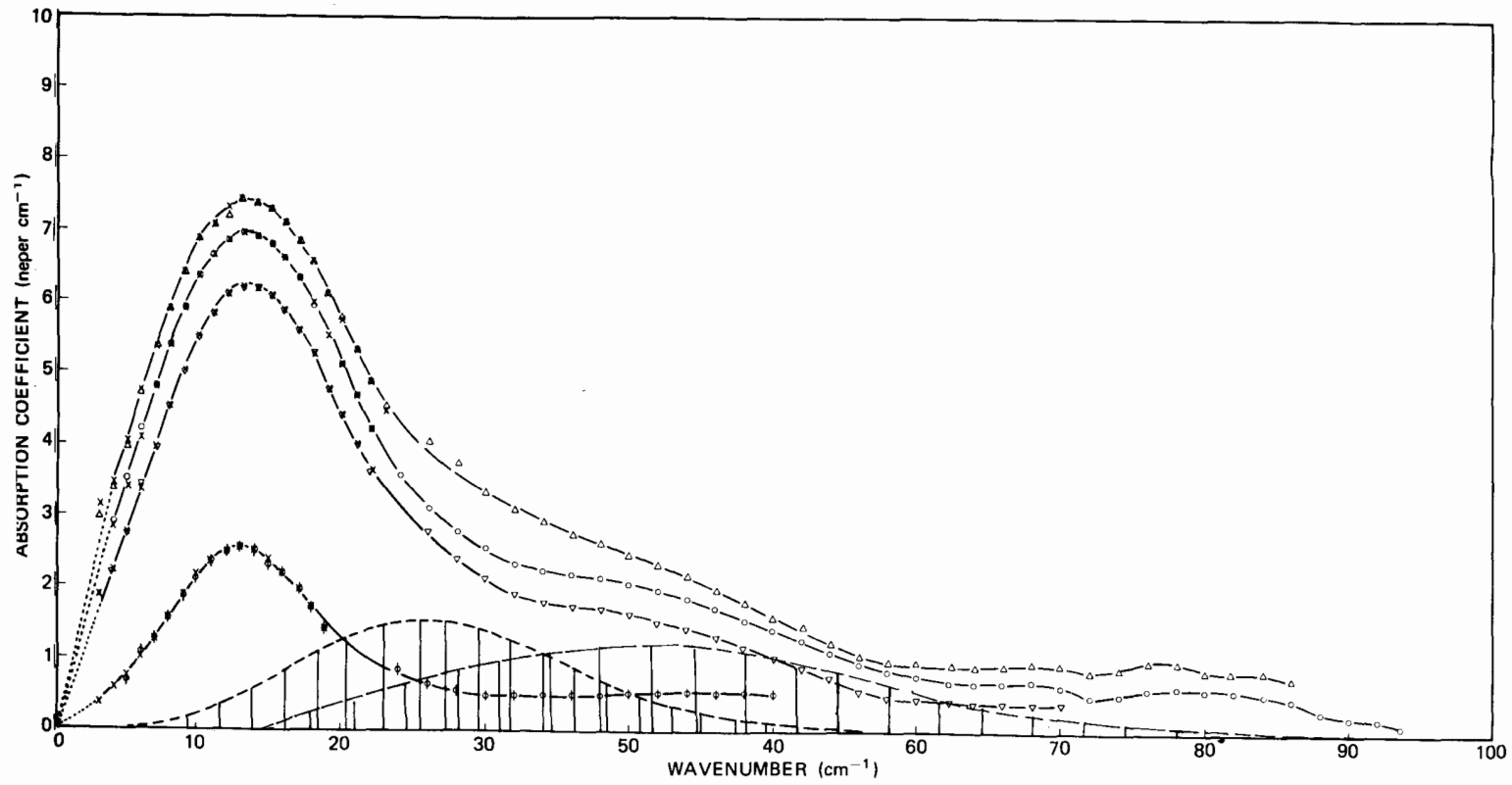

Figure 11.5.2 Power absorption coefficient of $CClF_3$ at high pressures. Top to bottom: Curve 4, 40.4 bar and 323°K; curve 3, 67.7 bar and 323°K; curve 2, 104.3 bar and 323°K; curve 1, 147.7 bar and 323°K. The vertical solid lines are the $J \rightarrow J + 2$ (quadrupole-induced) and $J \rightarrow J + 3$ (octopole-induced) transitions. [Reproduced by permission from G. Davies and M. Evans, *J. Chem. Soc. Faraday Trans. II* **71**, 1275 (1975).]

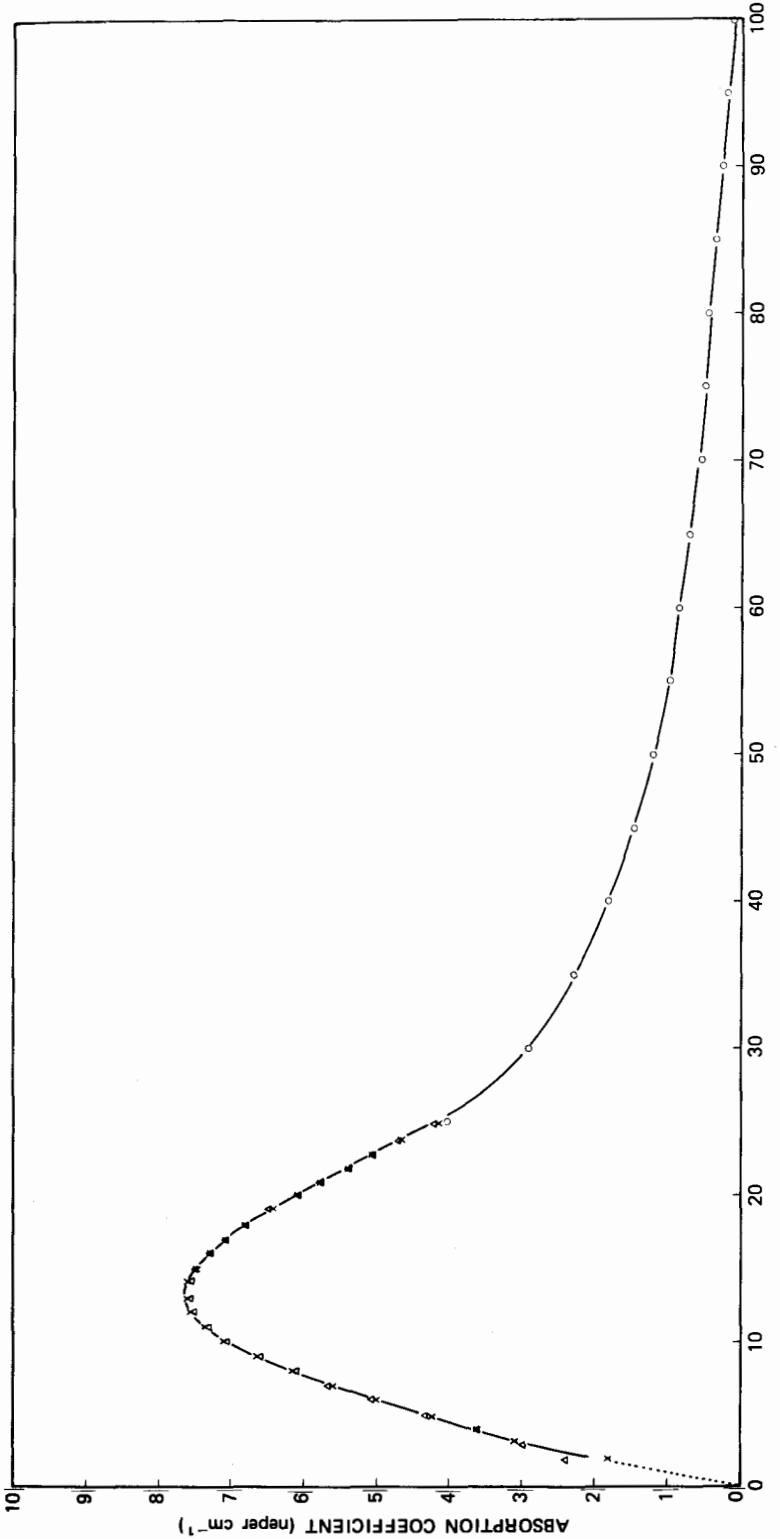

Figure 11.5.3 Power absorption coefficient (runs △, ×, and ○) of liquid $CClF_3$ at 288°K. Note the development of the long tail. Obviously the liquid density is gas-like (cf. Fig. 11.5.2) but J-diffusion (Fig. 11.5.4) is not appropriate. [Reproduced by permission from G. Davies and M. Evans, *J. Chem. Soc. Faraday Trans. II* **71**, 1275 (1975).]

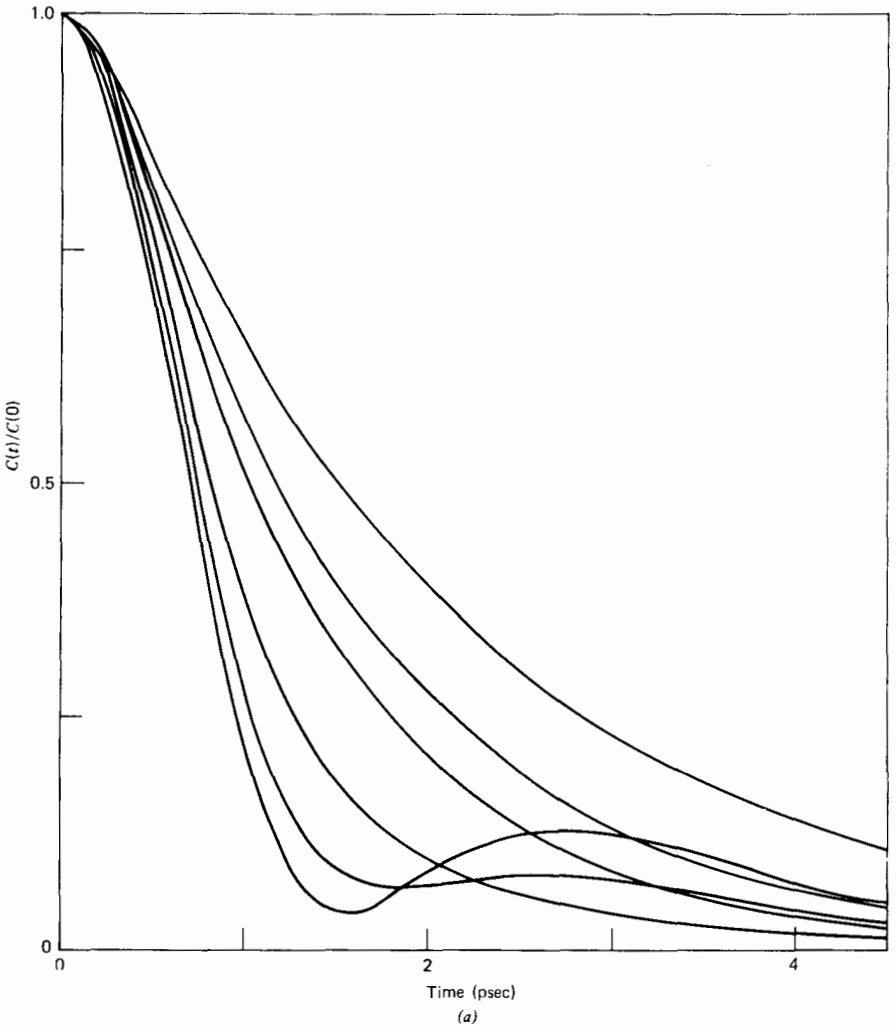

Figure 11.5.4 (*a*) J-diffusion $C_u(t)$ for $CClF_3$ at 288°K. Top to bottom: $\tau_J = 0.2$, 0.3, 0.4, 0.9, 3.0 psec, $\tau_J \to \infty$. (*b*) Experimental Fourier transforms equivalent to $C_u(t)$ Top to bottom: liquid; gas at 67.7 bar, 320°K; gas at 40.4 bar, 320°K. [Reproduced by permission from G. Davies and M. Evans, *J. Chem. Soc. Faraday Trans. II* **71**, 1275 (1975).]

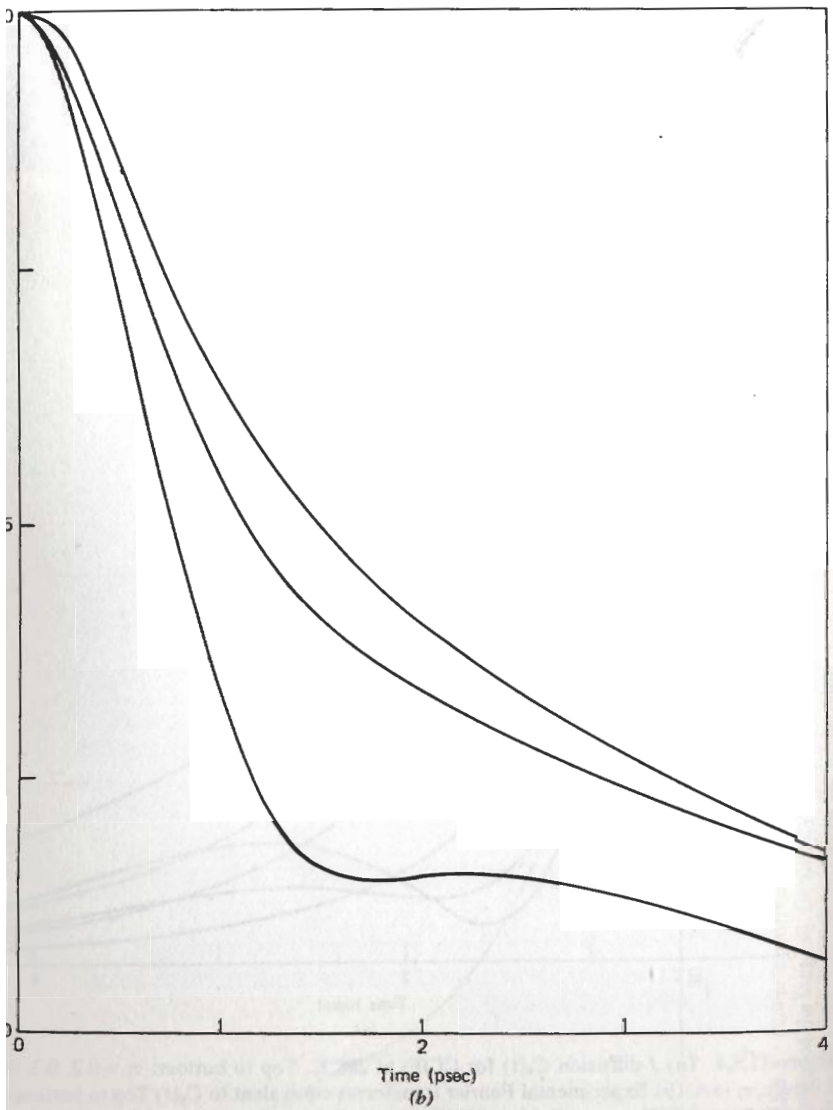

Figure 11.5.4 (*Continued*)

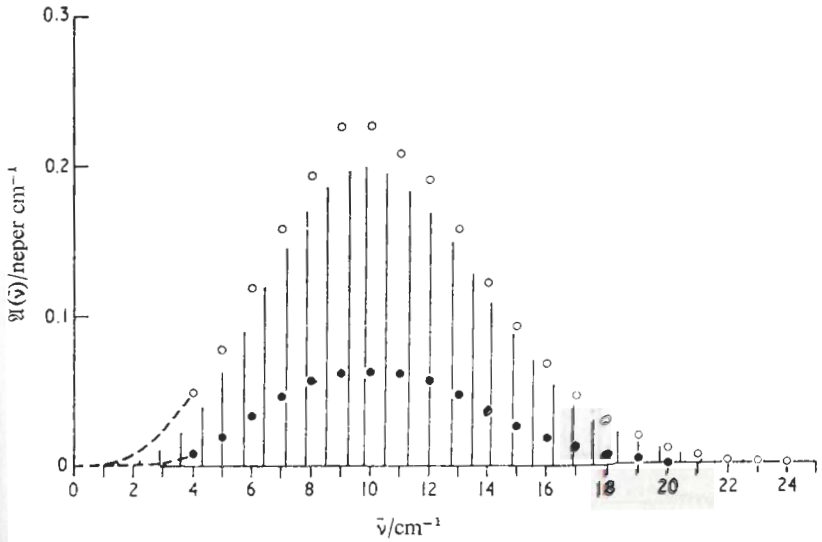

Figure 11.5.5 (*a*) Theoretical and measured absorption of $CBrF_3$ at 1.2 bar (●) and 3.3 bar (○), 295°K. [Reproduced by permission from Davies and Evans, *J. Chem. Soc. Faraday Trans. II* **72**, 43 (1976).]

oversimplified. Again there is an indication that the apparent two-body $|\mathbf{Q}|$ is halved on going from $N = 1.5 \times 10^{21}$ cm^{-3} (the gas) to $N = 4.46 \times 10^{-21}$ cm (the liquid) (from 11×10^{-40} C m^2 to 6×10^{-40} C m^2). The calculated octopole is about 3.3×10^{-50} C m^3. The binary *J*-diffusion mechanism is therefore likely to be unrepresentative of molecular dynamics conditions even in a $CClF_3$ liquid of very low density, such as that of Fig. 11.5.2.

The situation is echoed in $CBrF_3$ fluid where deviation from "free rotor behavior" is clearly seen in the Fourier transforms of Figs. 11.5.5 and 11.5.6. Again the $\bar{\nu}_{max}$ position does not shift significantly but the induced high frequency tail becomes increasingly prominent in the gas (Fig. 11.5.7) and in the liquid (Fig. 11.5.8). Again the *J*-diffusion model fails qualitatively to describe the liquid dynamics accurately. A great deal more—and more accurate—work of this nature is needed before the wide range of kinetic and electrical interactions contributing to these spectra will begin to be delineated and understood. Spectral features in this section are in themselves rather beyond the theoretical reach of present theory (analytical or computer simulation) and reflect the penetrating nature of far infrared spectroscopy when dealing with subtleties of condensed phase molecular dynamics and interactions.

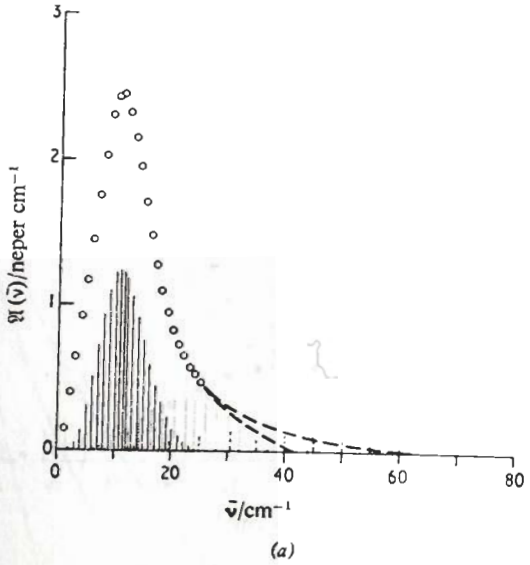

(a)

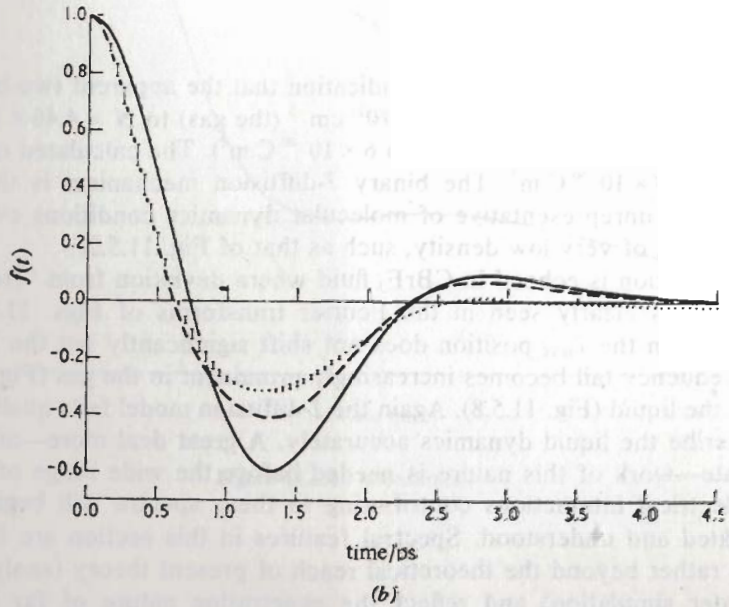

(b)

Figure 11.5.6 (*a*) Measured absorption at 28.4 bar, 357°K (○). Dashed lines, alternative extrapolations of high frequency tail. Vertical solid lines, $J \rightarrow J+1$ lines; vertical dotted lines, $J \rightarrow J+2$; vertical dashed line, $J \rightarrow J+3$. (*b*) Corresponding Fourier transform. Solid line, free rotor curve; dashed line, curve with $|\mathbf{Q}| = 4.0 \times 10^{-26}$ e.s.u., $|\Omega| = 10 \times 10^{-34}$ e.s.u. Φ error bar illustration. [Reproduced by permission from G. Davies and M. Evans, *J. Chem. Soc. Faraday Trans. II* 72, 43 (1976).]

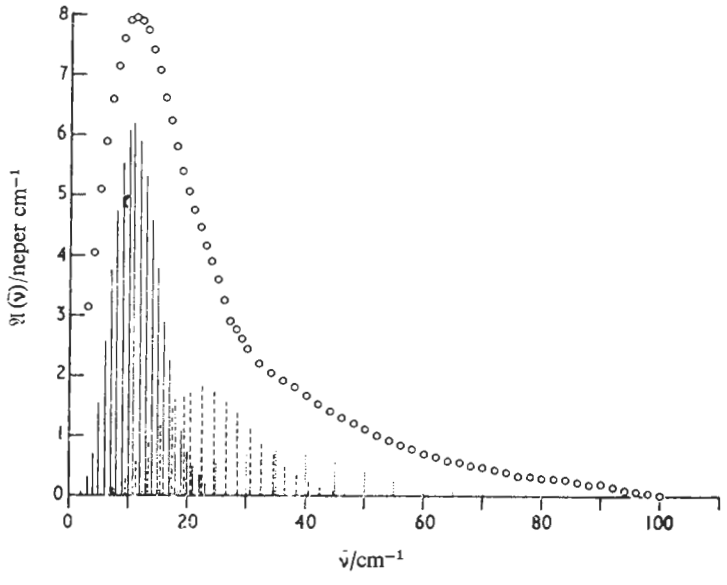

(a)

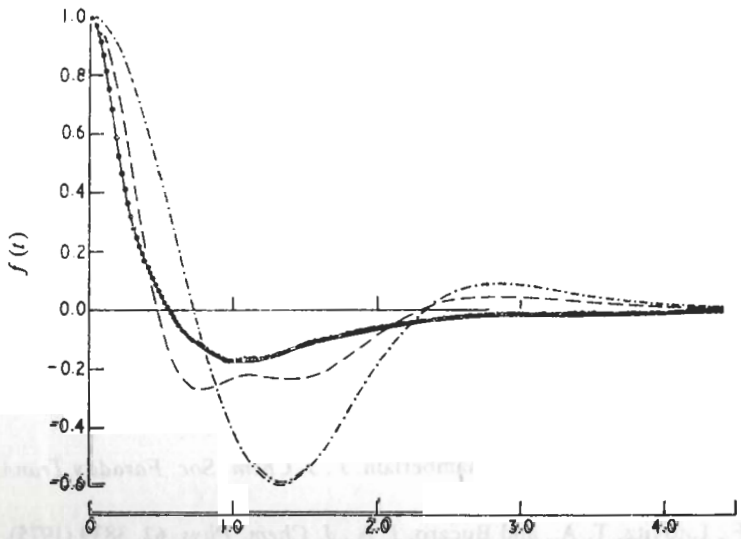

(b)

Figure 11.5.7 (*a*) Data as for Fig. 11.5.6, 46.2 bar, 357°K. (*b*) Fourier transform (as in Fig. 11.5.6
[Reproduced by permission from G. Davies and M. Evans, *J. Chem. Soc. Faraday Trans. II*, 72, 4
(1976).]

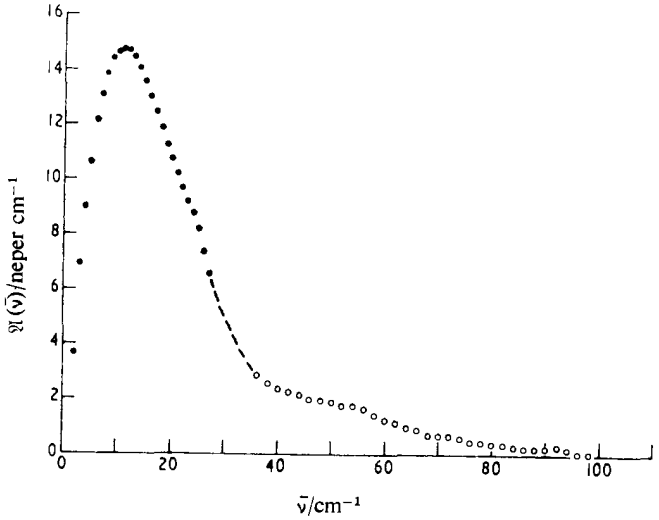

Figure 11.5.8 The far infrared absorption of $CBrF_3$ (liquid) at 295°K. [Reproduced by permission from G. Davies and M. Evans, *J. Chem. Faraday Trans. II* **72**, 43 (1976).]

REFERENCES

Alder, B. J., Strauss, H., and Weiss, G., *J. Chem. Phys.* **59**, 1002 (1973).

Alder, B. J. and Wainright, T. E., *Phys. Rev.* **A1**, 18 (1970).

An, I., Montrose, P., and Litovitz, T. A., *J. Chem. Phys.*, **70**, 4626 (1979).

Baise, A. I., *J. Chem. Soc. Faraday Trans. II* **69**, 1907 (1972).

Birnbaum, G., Ho, W., and Rosenberg, A., *J. Chem. Phys.* **55**, 1028 (1971).

Bosomworth, O. R. and Gush, H. P., *Can. J. Phys.* **43**, 751 (1965).

Brot, C., *Dielectric and Related Molecular Processes*, Chem. Soc. Spec. Per. Rep. 2, Chemical Society, London, p. 1 (1975).

Brot, C. and Lassier, B., *Chem. Phys. Lett.* **1**, 581 (1968).

Buckingham, A. D., *Quart. Rev. Chem. Soc.* (1959).

Chandler, D., *J. Chem. Phys.* **60**, 3508 (1974).

Colpa, J. H. and Ketelaor, J. A. A., *Mol. Phys.* **1** 873 (1958).

Copeland, T., and Cole, R. H., *Chem. Phys. Lett.* (1975).

Davies, G. J., Davies, M., and Chamberlain, J., *J. Chem. Soc. Faraday Trans. II* **69**, 1223 (1973).

Dill, J. F., Litovitz, T. A., and Bucaro, J. A., *J. Chem. Phys.* **62**, 3839 (1975).

Evans, M. W., *J. Chem. Soc. Faraday Trans. II* **69**, 1011 (1973).

Gordon, R. G., *J. Chem. Phys.* **41**, 1819 (1964).

Ho, W., Birnbaum, G., and Rosenberg, A., *J. Chem. Phys.* **55**, 1039 (1971).

Kielich, S., *Dielectric and Related Molecular Processes*, Vol. 1, p. 192, Chem. Soc. London (1973).

McQuarrie, D. A., *Statistical Mechanics*, Harper and Row, New York (1975).

Madden, P., *Mol. Phys.* **36**, 365 (1978).

Möller, K. D. and Rothschild, W., *Far Infra-red Spectroscopy*, Wiley-Interscience, New York (1971).

Ozier, T. and Fox, K., *J. Chem. Phys.* **53**, 3768 (1970).

Occelli, T., Quentrec, B., and Brot, C., *Mol. Phys.* **36**, 257 (1978).

O'Dell, J. O., and Berne, B. J., *J. Chem. Phys.* **63**, 2376 (1975).

Rose, M. E., *Elementary Theory of Angular Momentum*, Wiley, New York (1957).

Savoie, R., and Fournier, R. P., *Chem. Phys. Lett.* **7**, 1 (1970).

Whiffen, D. H., *Trans. Faraday Soc.* **46**, 124 (1950).

12
Intercomparison of Experimental Techniques

12.1 INTRODUCTION

The investigation of molecular dynamics in the liquid state of matter has reached the stage where coordination is essential (Chapter 6) before further advances can be made. There are three major areas of investigation, roughly classified as follows:

1. Spectroscopy of band shapes, which when Fourier transformed produce correlation functions. These can be either cross-correlation functions or a.c.f.'s, depending on circumstance and technique.
2. Analytical theory, which depends on the methods of statistical mechanics, designed to reduce the number of dynamic variables involved from Avogadro's order of magnitude to not more than two or three thermodynamic averages.
3. Simulation of the individual trajectories of about 10^2–10^3 model potentials using Newton's equations. This requires a great deal of computer time but within the framework of assumptions used essentially provides a complete bank of data that can be used to build up correlation functions and consequently spectral band shapes.

The third area has been expanded steadily since its inception in the early 1950s; with the increase in computer power it is now possible to simulate the motion and interaction of increasingly more complicated and presumably more "realistic" model potentials. For the first time it is becoming possible to simulate dipolar molecules such as the substituted methanes.

It therefore seems that the time is ripe to select molecules for a combined investigation using all three modes of investigation simultaneously, under identical conditions of pressure and temperature over the whole of the range of existence of the liquid phase.

With this purpose in mind several laboratories have agreed to coordinate their research into three molecules, CH_3F, CH_3I and CH_2Cl_2 with the following major objectives:

1. To study, by various spectroscopic techniques, dipolar fluids, at thermodynamic conditions agreed upon by each laboratory. The end result is a collection of band shapes that can be analyzed for the information they contain about molecular motion and interaction.
2. To simulate the band shapes by the technique of molecular dynamics under the same thermodynamic conditions. To use a number of different model potentials to test the sensitivity of the simulated spectral features to changes in interaction potential by direct comparison.
3. To develop an analytical model in an attempt to describe the range of data from (1) and (2).
4. To carry out second virial coefficient and related measurements to aid in the choice of potential for simulating band shape.
5. To discuss the results of the project in a number of conferences.

The purpose of this chapter is primarily to provide a review of the reasons why such a project is necessary, and to provide a source of reference concerning the preset conditions under which the investigations are planned.

12.1.1 Survey of the Problem of Consistency

Hildebrand (1978) has recently produced a number of criteria that should be borne in mind when dealing with a problem as complex as ours, namely that of explaining the liquid state of matter in molecular terms.

1. Firstly, consider carefully the basic concepts. For liquid systems it is apparent that a number of these concepts are inconsistent with each other and with the pertinent facts. Following Marcus (1975), they include "holes, cells, clusters, cages, lattices, scaled particles, fluidised vacancies, hypernetted chains and molecules with solid-like degrees of freedom". This range of concepts reflects on the comparative failure of analytical modeling of the liquid state even at the stage where molecular dynamics are not considered. Computer simulations are not based on so many conflicting preconceptions.
2. A model should be regarded as suspect if it yields inferences in serious conflict with any of the pertinent properties of a system regardless of how closely it can be made to agree with some, especially if there are adjustable parameters. A model that is consistent with all properties, even if only approximately, can probably be made more precise, but if it is in irreconcilable conflict with any

part of the evidence, it is destined to be discarded, and predictions and extrapolations based upon it should be regarded as unreliable.

3. The entropy of vaporization of all simple liquids to the same concentration of vapor is the same. It is larger for associated liquids; hence simple liquids are in a state of maximum disorder and have no structure.
4. Simple liquids flow freely when expanded by only a few percent over their intrinsic volume. There is no room for "holes" or "lattices" or jumps greater than a small fraction of the molecular diameter. Self-diffusion occurs because thermal motion presents any molecule from remaining in the same spot.
5. The molar volume V_t is defined as that volume at which soft molecules begin to be sufficiently separated between collisions to acquire fractions of their momentum in free space. At volumes smaller than V_t they are in fields of force not appropriately described by pair potentials. The role of temperature is only to determine volume. Values of V_t depend on the capacity of a molecular species to absorb collision momentum by bending, vibrating, or rotating. Pair interaction is an assumption that is involved even in computer simulation. There is only one type of algorithm that does not use this, and that at the same time takes into account the effect of polarizability on molecular interactions (and vice versa), and that is the Birkbeck group's (Finney, 1978). Significant evidence of non-pair additivity has been produced during test runs with this algorithm.

Bearing in mind these criteria, it is clear that there has been a tendency for the analytical theoreticians to model the molecular dynamics with simplistic and subjective ideas. Over-parameterized molecular models tend to simplify the problem further so that ultimately it seems we have a number of solutions to our problem.

It is obvious that only the combined use of the three methods of assessment we have available to us (spectroscopy, simulation, and theory) can lead to an objective evaluation of the state of the art as it stands concerning liquid state dynamics. The project will be built, therefore, around a triad methodology (spectroscopy, simulation and theory). There will be available a variety of molecular dynamics algorithms, each of which is to be tested as thoroughly as possible with the thermodynamic and spectral data. By using the simulation method (which is still in its infancy for dipolar molecular liquids, we can use a much more realistic form of the intermolecular potential than is currently implied in a model of the liquid state such as the itinerant oscillator. Using a combination of algorithms it is possible to increase the complexity of the potential under consideration from an atom–atom Lennard–Jones basis, for example, by gradually adding polarizability, multipole-multipole interactions, intermolecular vibrational

effects, and non-pair additivity. The problem of the reaction field itself is beginning to be tackled using molecular dynamics, especially in the context of water. The algorithms written for this purpose can be adopted for use with CH_2Cl_2, for example, because the symmetry is the same. The newly developed nonequilibrium methods of molecular dynamics can be used to great advantage to build up multiparticle (cross) correlation functions observable with certain techniques. The equivalent a.c.f.'s are observable with other types of spectroscopy and the analytical macro-micro theorems linking the two types can be directly tested.

The spectroscopic techniques referred to below (see literature search) have been used in the past to study molecular dynamics from different angles. They have not been used previously in combination, and there have only been few attempts to compare the results of more than one technique. Notable in this respect is the work of Brier and Perry on CH_2Cl_2 (1978).

There are fundamental problems in trying to extend some concepts of the theory of, for example, the Brownian motion to the case of the asymmetric rather than spherical top molecules (Chapter 2). Not least is deciding the correct frame in which to diagonalize the friction tensor when this is different from the frame defining the principal axes of inertia. How is it possible to evaluate separately the components of the grand friction matrix of rotation/translation (Chapter 5) when using the Einstein relation between friction and diffusion and Langevin's idea of the molecular dynamics? There are well-known inconsistencies in the latter equation (Chapter 1) which balance force or torque with a strong combination of stochastic and hydrodynamic terms. The velocity or angular velocity of the Langevin equation has no time derivative, which directly contravenes the fact that probability hypotheses are imposed (i.e., relations are assumed between the stochastic force and the velocity). These inconsistencies, instead of leading to the rejection of the Langevin equation, have led to discoveries such as the Ito–Stratonovitch calculi, and more lately to the use of Wiener processes in the analysis (Chapters 1 and 5).

However, it is clear that after the full realization (about 1968) of the meaning of the Debye plateau in the far infrared that the technique of 0–THz frequency spectroscopy alone poses an unsolved problem at a fundamental level (Chapter 4 and 6). The 1970s have seen attempts to use the projection operator techniques (e.g., Chapters 9 and 10) of Kubo, Zwanzig, Mori, and many others to reproduce (usually with adjustable parameters) the spectroscopic broad band data up to *and including* tera Hertz frequencies. The Mori continued fraction has proved useful here but only in an empirical fashion because of the use of a truncation procedure. It is still not known whether the fraction "converges" or, if taken to infinity, is physically meaningful. On the one hand, it is possible to give such truncations physical meaning by unraveling the implied equations of motion, but Scaife (1980) has criticized many of the basic assumptions made in this field. The evolution of the friction into a memory function is

therefore providing us with both solutions and problems. There has been almost no attempt to see if the memory function makes simultaneous sense of results from different spectroscopic fields. There is a basic reason for this in that the relation between the angular velocity a.c.f. $[C_\omega(t)]$ and the orientational a.c.f. $[C_u(t)]$ in all but the simplest and most uninformative models based on Brownian motion theory is exceedingly intricate. The only reasonable stopgap at present is to consider the orientational dynamics of the symmetrical top with an embedded dipole (orientation) vector **u** constrained geometrically. This leads to the use of models as already discussed which are semiempirical but capable of describing semiquantitatively the far infrared as well as the low frequency part of the 0–THz electromagnetic absorption and dispersion profiles. For spherically isotropic libration of the asymmetric top dipole there is a relation between $C_\omega(t)$ and $C_u(t)$ and also higher Legendre polynomials of the orientational a.c.f. This means that the results from different spectroscopies can be interrelated on the same basis. When all constraints are removed there is no closed relation between $C_\omega(t)$ and $C_u(t)$ even in the case of diffusion of the hypothetical dipole embedded in the spherical top. This is of course the model originally considered by Debye, but *without* the inertial and memory effects. We have already illustrated the behavior of the Debye model in the far infrared when three-dimensional diffusion is considered analytically. The only case where it is possible to relate $C_\omega(t)$ and $C_u(t)$ in a simple way is that which produces the unrealistic result of the Debye plateau. There are of course several methods of relating $C_\omega(t)$ to $C_u(t)$ based on "collisional" models such as the well-known m- and J-diffusion (Chapter 2), and lately methods of using projection operators have been developed to deal with two or three molecule interactions in the presence of N others (Chapter 5).

The above analytical considerations of course leave aside completely the everpresent problem of the internal field (Chapter 3), or multipole-multipole interaction, beginning with dipole–dipole interaction. However, there is a danger that these elaborate theories will lose touch with experimental findings without the intervention of molecular dynamics simulation as a source of reference for thermodynamic averages not easily accessible experimentally.

Hydrodynamic equations of energy, momentum, and particle density conservation have always been of use in dealing with light scattering (Chapter 7). The linearized Navier–Stokes equations have recently been modified with significant results such as the theoretical prediction and subsequent simulation of long time tails in various molecular a.c.f.'s, and the successful description of the Rytov dip. The modification has been used in the mixing of hydrodynamic modes within the overall framework developed by Mori and others (see appendixes to Chapters 7 and 8). In this area of research there are different ideas of mode–mode coupling which lead to the same spectral result (i.e., analytical frequency dependence of the intensity of polarized or depolarized scattered light), so that there is

scope for resolving the issue (*a*) by computer simulation, or (*b*) by exploring the implications of the mode–mode theory in parallel spectroscopies such as 0–THz, neutron scattering, and the techniques of NMR relaxation. It seems that there has been little consideration given to the high frequency wings of light scattered from a molecular liquid where the available theories can, in fact, be evaluated more thoroughly. There has been a tendency in the treatment of these spectra to mix "molecular" and "hydrodynamic" ideas, so that the final result might work in some respects, but nobody at the end of the day quite knows why.

The study of molecular dynamics by infrared and Raman band shape analysis is of course well established, and particularly for methylene chloride there have been a great number of studies (about 70 papers, roughly the same number as with NMR spectroscopy). In theory the band shape analysis provides information on the a.c.f. of the transition dipole involved which involves a consideration of rotation/vibration mixing. *It is clear that it is not possible in general to factorize the relevant a.c.f. into a vibrational a.c.f. multiplied by a rotational a.c.f.* (Chapter 6). This has been made clear for CH_2Cl_2 liquid in papers by van Woerkom et al. (1974). Unfortunately the factorization is made a priori in many papers, whose results therefore are not meaningful. The same is true to an extent with Raman scattering. The problem of vibration/rotation coupling is difficult to tackle analytically, especially when memory effects are to be taken into account, so that this is a field which is acutely in need of some aid from computer simulations, providing as they do multiparticle and single-particle correlation functions under well-defined conditions of intermolecular potential.

There are a large number of papers available for all three molecules considered here (CH_3F, CH_2Cl_2, and CH_3I) which consider the dynamics from the point of view of NMR relaxation of different atoms in the molecule. For CH_2Cl_2 it is possible to look at the movement of the carbon, hydrogen, and chlorine atoms separately and evaluate the anisotropy of the reorientational motion. Despite some quite surprising inconsistencies between NMR data from different laboratories Brier and Perry have attempted to use the NMR infrared and Raman data as an aid for evaluating their neutron scattering experiment on liquid CH_2Cl_2. This comparison involved many scaling assumptions because the literature results are normally at different temperatures. Brier and Perry did not attempt an analysis past the stage of the m- and J-diffusion models, which are unrealistic in the far infrared (Chapters 1, 2, and 4). They bring to light the confusion that results from the application by different groups of different models to the NMR spin-spin and spin-rotation relaxation data. By considering in isolation various NMR correlation times it is not possible even to distinguish between alternative models easily. Brier and Perry run into the fundamental difficulty already mentioned that there is no way of extending the concept of a spherical top diffusing against a hydrodynamic friction to the case of the asymmetric top (methylene chloride) or even the symmetrical

tops (Methyl fluoride and methyl iodide) without introducing too many phenomenological parameters as in Chapters 2 and 5. Accordingly, one of the first aims of the molecular dynamics simulations would be to produce NMR correlation times and to compare these with a freshly measured set at precisely the same thermodynamic states. It would be immediately of interest to compare these with the infrared, Raman, and Rayleigh correlation data remeasured under the same conditions. At present Brier and Perry emphasize that the infrared and NMR data provide an almost diametrically *conflicting* picture of the anisotropy of the molecular motion in methylene chloride (Chapter 6). Which is the more nearly correct should be answerable with the molecular dynamics simulation. Concepts such as mean time between collisions or mean size of angular jumps are almost meaningless, and in this are echoed (*a*) Hildebrand's remarks and (*b*) the likelihood of conflict instead of harmony when these ideas are used with more than one technique. An example with CH_2Cl_2 is the opposing conclusions based on consideration of these quantities reached by Dardy et al. (1972) (Rayleigh scattering) and Larkin (1973) (0–THz spectroscopy) despite the fact that both techniques measure in principle closely complementary multiparticle correlation functions. All this points us away from analytical modeling toward its much more comprehensive (and comprehensible) counterpart, computer simulation.

Where does this leave neutron scattering from liquids? The interpretative problems with this technique are acute, if not overwhelming. For example, translation/rotation/vibration is widely accepted as being uncoupled in the sense that the relevant correlation functions are factorized—a dubious procedure that often results in the incorrect use of *different* models for each type of motion. To base the interpretation of neutron scattering data on the results of other techniques can be acceptable only when there is a strong coordination *and* simulation backup. The project therefore provides a unique opportunity to assess critically the idea of using neutron scattering as a probe into the dynamical behavior of molecules in the liquid and condensed phases of matter.

It is important to take into account (Chapters 9 and 10) the rapidly developing nonlinear electrooptic techniques such as the Kerr effect (Chapters 7 and 8) as well as the more established, such as hyper- and ultrasonic dispersion and Brillouin scattering. Sound dispersion has been used extensively on liquid methylene chloride, but the interpretation of the results is not often incisive on the molecular scale. However, when used in combination with Brillouin scattering and molecular dynamics simulation of the correlation function of the relevant off-diagonal elements of the microscopic stress tensor, it can provide a valuable viewpoint to complement the other spectroscopies. It is in principle possible to simulate the correlation function at high frequencies with the new computer technique of "nonequilibrium molecular dynamics."

Among the new electrooptic techniques now available is the dynamic

Kerr effect, either with picosecond pulse lasers (Chapter 9) or at lower frequencies. The interpretation of the data from the Kerr effect is not of course free from complications, not least because it is not strictly valid to use a theory of linear response with transient responses dependent on pulsed electric fields. However, Grigolini et al. (Chapters 9 and 10) have considered the problem in detail when intense laser pulses are used to produce either fluorescence or birefringence transients. There should be little technical difficulty in simulating a picosecond pulse on the computer and directly testing linear response theory at a fundamental level. In fact, computer simulation runs are quenched into a glassy state at present over picosecond periods (Chapter 7).

The impulse methods developed by Malecki (1962, 1976) have introduced the possibility of overcoming the heating effects caused by conductivity. There are now available at low frequencies nonlinear dielectric transients on aqueous systems. It is becoming possible to extend the study to the far infrared range using carcinotron radiation (or alternatively, submillimeter laser radiation), ultra-short high voltage pulses, and fast response pyroelectric detectors. It is possible to detect a minute of arc change in the plane of polarization of the carcinotron beam which has passed simultaneously through the liquid and field pulse. This is the far infrared Kerr phenomenon recently described qualitatively by Evans et al. (1980) in aniline using conventional interferometry. It is also possible to pursue the far infrared Faraday effect in the same way with powerful magnet pulses. In dealing with electromagnetic absorptions, dispersion, and scattering, consideration should always be given to collision-induced absorption. One of the reasons for choosing methylene chloride and methyl fluoride for a coordinated project is that the far infrared, infrared, etc. absorption intensities of these two molecules are large enough to counteract the induced absorption which always affects the band shape (Chapter 6). Whenever there is absorption (or scattering) of electromagnetic radiation by permanent dipoles there is induced absorption or scattering due to temporary dipoles.

In conclusion, we may discern a trend away from analytical modeling of the spectroscopic band shapes of molecular liquids toward the increased use of molecular dynamics simulation. It is therefore necessary for the theoretical work to develop in new, well-defined directions. If the recent criticisms of Scaife are corroborated then the existing methods used by the theoreticians (e.g., the various generalized Langevin equations) would be undermined.

12.2 PRESET CONDITIONS AND LIQUIDS FOR THE COORDINATION PROJECT

At the very basis of the aim of coordination is the selection of thermodynamic conditions that should be adhered to closely for easy inter-

comparison of a wide range of data. The range of conditions of course depends on the choice of molecules. Methylene chloride has the following advantages which typify the selection procedure:

12.2.1 Methylene Chloride (CH_2Cl_2)

1. This is a dipolar asymmetric top (C_{2v}) which is a liquid at room temperature. It has been widely used in industry as a solvent and degreasing agent and consequently many of its basic physical properties have been measured, and are listed below.
2. It has a wide liquid range of almost 140° from the melting point to the boiling point at 1 bar. Its critical temperature and pressure have been measured.
3. The variation of solidification temperature with applied pressures in the kilobar range has been reported up to 30 kbar. The dependence of static permittivity on kilobar pressure over a different (more restricted) range is also known. This facilitates measurements at constant volume over a temperature range. The relevant physical data are listed in Section 12.3.
4. With reference to the comprehensive (but not exhaustive) bibliography of Section 12.4, it becomes clear that methylene chloride has been investigated with a variety of spectroscopies, especially with infrared and NMR. The results of all this effort have been discussed briefly in Section 12.1.
5. There are infrared active vibrations with transition moment vectors parallel to any one of the axes of inertia so that the rotational motion of each axis may be studied by choosing an appropriate vibrational band. In CH_2Cl_2, isotopic broadening factors are negligible compared with other sources of uncertainty. The infrared band intensities are presumably enough to ensure that the collision-induced absorption is small in comparison. There is no way of corroborating this statement quantitatively at present.
6. The liquid absorbs strongly in the 0–THz region (static to far infrared) so that the multimolecule orientational correlation function can be measured (Chapter 4) with minimal interference from collision-induced absorption. The same goes for scattering techniques such as depolarized Rayleigh and Raman. The 0–THz spectra of methylene chloride in a range of environments have been investigated (e.g., Chapter 7). The behavior in viscous and vitreous solvents such as decalin is especially significant.
7. It has a predominantly incoherent scattering cross section with cold neutrons owing to the presence of the equivalent hydrogen atoms. There are no low frequency vibrational inelastic features in a low energy neutron scattering experiment. This implies that the far infrared Poley absorption is also free from distortion at the high frequency side.
8. The C_{2v} symmetry of the molecule is that of water, so that the available water algorithms of the molecular dynamics simulators can be adapted straightforwardly for methylene chloride, which is believed to be weakly hydrogen bonded in the neat liquid state.
9. Inertial or molecular shape considerations would predict symmetrical top behavior. However, the complex nature of the intermolecular interaction with the dipole moment along the b-axis might invalidate such simple arguments. There is a need to attack completely the problem of asymmetric top reorientation in an attempt to resolve some of these problems.
10. For NMR spectroscopy the presence of C, H, D, and Cl nuclei is an advantage in determining the anisotropy of reorientation.
11. The large amount of work on acoustic relaxation (Section 12.4) means that it will be relatively straightforward to coordinate this technique with Brillouin and neutron scattering to investigate center of mass motions and their relation to reorientation.
12. A number of different simulation algorithms has been developed to the stage where the coordinated treatment of a molecule such as methylene chloride is now possible from different computational viewpoints. The project will provide the necessary range of data needed to test out these algorithms at a fundamental level.

The choice of methylene chloride is therefore well supported by a variety of (albeit uncoordinated) results already in the literature. To pull all these threads together the following section deals with the preset conditions for methylene chloride.

12.2.1.1 Suggested Conditions for Spectroscopic Technique and Simulation

The reader is referred to Section 12.4.1 for a comprehensive bibliography. Among these conditions are listed studies up to kilobar pressures, which are technically difficult:

1. Liquid from the melting point to the boiling point at 1 atm, that is, −96 to 40°C at 10° increments, thus at −96°C (as close to the melting point as possible), −85°C, . . . , 35°C and one point as close to the boiling point as possible.
2. Liquid under hydraulic pressure. In this study we have 1 atm = 1.01325 bar = 1.03323 kg/cm^2.

a. The following conditions should be followed accurately, that is,

Pressure (kg/cm²)	Melting Temp. (°C)
Atmospheric	−96.7
5,000	−46.0
10,000	0.0
15,000	42.0
20,000	82.0
25,000	120.0
30,000	157.0

All measurements should be carried out just above the melting temperature at each pressure, therefore, at −90, −40, 5, 50, 85, 125, and 160°C.

It would be useful to carry out measurements at constant volume by increasing the temperature of the pressure cell, if this is technically feasible. The complete set of pressure measurements would be as follows:

Starting Pressure (kg/cm²)	Temperatures (°C)			
5,000	−40	−20	0	20
10,000	5	25	45	65
15,000	50	70	90	110
20,000	85	105	125	145
25,000	125	145	165	185
30,000	160	180	200	220

There are points to make clear about this table.

i. As the temperature is raised the initial pressure increases at constant volume.
ii. At the extreme of pressure and temperature the liquid might decompose.
iii. Laboratories might find that it is not technically feasible to push the pressure too far.
iv. The measurements should be continued to the boiling point at each pressure if possible.

b. At room temperature (30°C) the external pressure should be varied in increments of 500 kg/cm² until the liquid solidifies. A measurement of the liquid should be taken just before solidification and of the solid at 30°C. This should be repeated at 50°C.

3. Measurements in the liquid along the gas/liquid coexistence line from the boiling point (40°C) to the critical point (245°C, 60.9 atm) at increments of 25°C. Specifically, the liquid under its own vapor pressure at b.p. (40°C), 50, 75, 100, 125, . . . , 225°C, and at the critical point itself. Measurements at further 25°C increments into the supercritical region are desirable if technically possible.

4. In solution in carbon tetrachloride and in decalin at room temperature (25°C) in pressure. Concentrations (in mole % CH_2Cl_2): 100, 90, 80, 70, . . . , 10, 0.
5. In ultraviscous and vitreous environments.
   a. In 10% decalin at 106, 110, 113, 115, 118, 138, and 140°K (α, β, γ loss peaks known at these temperatures).
   b. 10% v/v CH_2Cl_2 in mixed glass-forming solvents.
      i. 1:7 cholesteryl oleyl carbonate (OCC)-decalin: 106, 110, 112, 116, 144, 146, and 150°K.
      ii. 1:9 toluene–decalin at 115, 118, 120, 123, 137, 141, and 144°K.
      iii. 3:7 toluene–decalin 125.5, 128, 130, 133, 136°K.
      iv. 10% v/v CH_2Cl_2 in 10% pyridine–toluene at 110°K.

These last conditions may seem without obvious reasons, but they repeat those of Reid's work (Chapter 7) dealing with measurements across the (α, β, γ) features of the 0–THz loss spectrum for methylene chloride solute over about 12 decades of frequency. In each case of condition 5 the CH_2Cl_2 dynamics are drastically different from those at room temperature and its (α, β) behavior is unique with high activation energies in both cases.

6. The glassy state is one instance where the translation of the CH_2Cl_2 solute molecules takes place on a scale which is much slower than their torsional oscillation (which appears as the far infrared γ process in vitreous decalin solvent, e.g.). The problem of rotation/translation coupling should therefore be eliminated when considering the ν process from the point of view of molecular dynamics simulation and inelastic neutron scattering. Another way of eliminating translation is to use the rotator phase of CCl_4 as a solvent for methylene chloride and to compare the rotator phase and liquid spectra.

12.2.2 Methyl Fluoride (CH_3F)

The details of the methyl fluoride potential function are exceptionally well known, partly because of the availability of second and third pressure virial coefficient data. It is a gas at room temperature and for this reason much less is available in the literature on the liquid phase. The work of Gerschel et al. (1976) along the gas/liquid coexistence line is taken as the basis for further spectroscopic study. The measurements provide an ideal basis for extension to other techniques and for simulation with molecular dynamics.

In this study it was found that there is apparently a weak density dependence of the mean square torques, since molecular multipole interactions are long range and not sensitive to the mean intermolecular

Table 12.2.1 Mean Square Torques from Gerschel et al. (1976): Methyl Fluoride along the Orthobar

$T_R = \frac{T - T_c}{T_c - T_t}$	0.01	0.1	0.2	0.3	0.4	0.5	0.6	0.7	0.8	0.9
$\langle N_1^2 \rangle (10^4\,\mathrm{cm}^{-2})$	97	94	91	88	86	84.5	83	82	81	80
$\langle N_1^2 \rangle^{1/2}/kT$	10.75	9.2	8.1	7.2	6.5	5.9	5.4	4.9	4.6	4.3

separation. The local anisotropy of the structure appears to be a consequence of specific molecular properties other than shape factors; therefore multipolar interaction should be used in the molecular dynamics simulation. These are adapted from the paper in Table 12.2.1. Here T_t denotes the triple point temperature and T_c the critical temperature.

In this paper the methyl fluoride was studied at 15°K intervals from T_t to T_c. The liquid was maintained in equilibrium with its own vapor along the orthobaric or coexistence curve. This is a set of conditions that is easily reproducible by other experimentalists, by simply heating the liquid (in equilibrium with the vapor) in a closed cell.

In this table we have ϵ_s = static permittivity; $\bar{\nu}_{\max}$ = far infrared peak absorption frequency; n_{IR} = refractive index at the end of the far infrared dispersion; $\epsilon_{\infty D}$ = intersection point on the ϵ' axis of the Debye semicircle; τ_D and τ_μ are versions of the Debye relaxation time with and without internal field corrections. In addition a set of measurements of methyl fluoride in carbon tetrachloride is essential to remove dipole–dipole interaction as in Chapter 4. The concentrations should be ideally the same as those for CH_2Cl_2, that is, 100, 90, 80, 70, . . . , 10, 0 mole %. Carbon tetrachloride is chosen as

Table 12.2.2 0–THz Data for CH_3F along the Orthobar

T_R	$\bar{\nu}_{\max}$ (cm^{-1})	ϵ_s	n_{IR}^2	$\epsilon_{\infty D}$	τ_D (psec)	τ_μ (psec)
0.01	92	49	1.79	3.7	6.6	4.57
0.10	84	40	1.775	3.5	4.4	3.06
0.20	79	32.8	1.76	3.25	3.1	2.17
0.30	75	26.9	1.73	2.95	2.2	1.55
0.40	71	22.5	1.695	2.7	1.55	1.10
0.50	66.5	18.6	1.65	2.4	1.1	0.78
0.60	62.5	15.6	1.60	2.1	0.8	0.57
0.70	58.5	12.9	1.55	1.9	0.6	0.43
0.80	54.0	10.4	1.475	1.7	0.5	0.36
0.90	50.0	8.2	1.405	1.5	0.45	0.33
0.93		7.2	1.35	1.45	0.42	0.31

Table 12.2.3 Pressure/Temperature Data for CH_3F (l)

Temp. (°K)	Vapor Pressure ($\mathrm{kN/m^2}$) (°K)	T_R
132.9	0.675 (135)	0.01
149.6	3.638 (150)	0.1
168.2	20.508 (170)	0.2
186.8	57.02 (185)	0.3
205.4	172.17 (205)	0.4
224.0	419.62 (225)	0.5
242.0	737.82 (240)	0.6
261.2	1410.7 (260)	0.7
279.8	2460.4 (280)	0.8
298.4	3999.4 (300)	0.9

being suitable for light scattering and for NMR and neutron scattering (no interference with the solute properties because there are no hydrogens).

It is emphasized that as far as possible these conditions should be matched exactly by all experimentalists and also by simulators, if dilution studies by simulation are not too costly.

For convenience the vapor pressure data for methyl fluoride are reproduced in Table 12.2.3. Note $T_c = 317.6$°K, $T_t = 131.0$°K; $T_c - T_t = 186$°K.

There are no kilobar pressure data available to our knowledge to date for methyl fluoride liquid, but the same pressures (or their nearest equivalents) should be used for methyl fluoride as for methylene chloride. Specifically, this means the following:

1. Just above the melting temperature at each kilobar pressure.
2. At room temperature, vary the external pressure in increments of 500 $\mathrm{kg/cm^2}$ until the liquid solidifies. Take a measurement of the liquid just before solidification and of the solid.

These essentially constant volume measurements should of course be supplemented by those on the liquid from the normal freezing point (at 1.0 bar) of 131.2°K to the boiling point at 1.0 bar, 194.65°K. *Note that methyl fluoride has a much smaller liquid range than methylene chloride (about half in °K).* Specifically these measurements on the liquid should be carried out (at 1.0 bar):

1. As close to the freezing point as possible.
2. At 140°K, and in 10°K increments to 190°K.
3. As close to the boiling point as possible.

Finally, it has already been mentioned that dilution studies for methyl fluoride in carbon tetrachloride would be essential for the problem of electrodynamics typified in dipole–dipole interaction. This might well persist in dilute solution but presumably would not be so powerful a force in setting up the collective oscillations mentioned by Gerschel and co-workers (1976).

In carbon tetrachloride rotator phase solvent the translational movement of the methyl fluoride solute molecules would be slowed substantially compared with that in liquid carbon tetrachloride solvent. Methyl fluoride itself does not form a rotator phase. It would be advantageous therefore to measure and simulate methyl fluoride in dilute solution in rotator phase carbon tetrachloride if technically feasible. It might be difficult to dissolve enough methyl fluoride in carbon tetrachloride for this purpose. In this case benzene might prove a substitute. Benzene forms a reorientational solid phase as opposed to a true rotator phase. Conditions for this experiment may be specified as "very dilute solution of methyl fluoride carbon tetrachloride just below normal freezing point of the solution."

12.2.3 Methyl Iodide

Again for this species there seem to be no available literature data yet on the liquid subjected to kilobars of pressure. In consequence the set of conditions drawn up below are based on a linear extrapolation method:

1. Liquid from melting point (207°K) to the boiling point (315°K) at 1 atm pressure ($\equiv$1.013 bar $\equiv$ 101.3 kN/m^2) at 10°K increments, that is, as close to the melting point as possible, at 210°K, etc., up to 310°K, and as close to the boiling point as possible.
2. Liquid under hydraulic pressure.
   a. Study of the liquid just above the melting point for pressures up to 30 kbar, and hence at increments of 20°K for each pressure.

Pressure (kg/cm^2)	Melting Point[a] (°C) (°K)
1 atm	−66 (207)
1,000	−52 (221)
5,000	3 (276)
10,000	72 (345)
15,000	142 (415)
20,000	211 (484)

[a]Obtained from values at 1 atm and 1000 kg/cm^2 using a linear relationship.

   b. Temperature/pressure studies at constant volume.

Pressure (Initial) (kg/cm^2)	Temp. (°C)				
1 atm	−65	−15	35	85	135
5,000	5	25	45	65	
10,000	75	95	115	135	
15,000	145	165	185	205	
20,000	215	235	255	275	

3. Measurements of the liquid along the gas/liquid coexistence line from the boiling point (315°K) to the critical point (528°K, 66.3 atm.) This involves study of the liquid under its own vapor pressure at the following temperatures at 25°C increments:

Temp. (°K) (°C)	Vapor pressure (kN/m^2)
315 (42)	99.379
340 (67)	216.73
365 (92)	419.52
390 (117)	740.10
415 (142)	1213.90
440 (167)	1879.4
465 (192)	2779.5
490 (217)	3701.3
515 (242)	5489.4

   and at further 25°C increments into the supercritical region, if feasible.
4. In solution in carbon tetrachloride and in decalin at room temperature (250°C) and pressure; concentrations (in mole % methyl iodide) 100, . . . , 90, 80, 70, . . . , 10, 5, 2, 1% (low concentrations in an attempt to extrapolate to "single-particle" dynamics, as in Chapter 4).
5. In ultraviscous and vitreous environments. In 10% decalin, from liquid nitrogen temperature to room temperature. As in methylene chloride careful measurements should be made around the glass transition temperature.

12.3 PHYSICAL PROPERTIES

12.3.1 Methylene Chloride

The following is a selection of useful physical properties for methylene chloride, structural, thermodynamic and electrostatic:

1. *Structure and moments of inertia* have been determined by Myers and Gwinn (Section 12.4.1, references in CH_2Cl_2) using microwave spectroscopy.

Average of All Isotopes

$C—Cl = 1.7724 \pm 0.0005$ Å
$C—H = 1.068 \pm 0.005$ Å
$L_{ClCCl} = 111°47' \pm 1'$

Isotope	$10^{40}I_A$ (g cm^2)	$10^{40}I_B$ (g cm^2)	$10^{40}I_C$ (g cm^2)	μ (D)
$CH_2Cl_2^{35}$	26.2142	252.64	273.69	1.61(8)
$CH_2Cl^{35}Cl^{37}$	26.3157	259.60	280.73	1.62(3)
$CH_2Cl_2^{37}$	26.419	266.88	288.11	
$CDHCl_2^{35}$	30.844	253.80	277.16	1.61(6)
$CDHCl^{35}Cl^{37}$	30.966	260.74	284.23	1.62(5)
$CD_2Cl_2^{35}$	35.432	255.43	280.23	1.64(4)
$CD_2Cl^{35}Cl^{37}$	35.575	262.37	287.31	1.64(0)

2. *Static dielectric permittivity and density as a function of pressure* have been measured recently in two papers by Schormak et al. and Hartmann et al.

At 30°C			At 50°C		
P (atm)	ϵ_s	Density (g/cm^3)	P (atm)	ϵ_s	Density (g/cm^3)
1	8.649	1.3078	40	7.757	1.2587
178	8.860	1.3325	205	7.939	1.2716
697	9.298	1.3886	502	8.239	1.3087
959	9.524	1.4103	747	8.451	1.3279
1342	9.770	1.4387	1057	8.673	1.3506
2048	10.171	1.4893	1446	8.923	1.3852
3074	10.708	1.5505	1963	9.198	1.4219
4063	11.159	1.5963	2685	9.550	1.4658
4883	11.545	1.6276	3491	9.878	1.5064
			4280	10.167	1.5401
			5121	10.439	1.5725

It is emphasized that the permittivity and density should be remeasured at the set conditions; any extrapolation is merely a guide.

*12.3.1.1 Thermodynamic Conditions**

(Critical temperature = 245°C; critical pressure = 60.9 atm)

A paper by McGovern gives the vapor pressure versus temperature curve from −15 to 220°C, the density of the liquid versus temperature, the

*Nonstandard units of the original paper.

density of the saturated vapor versus temperature, and a table of physical properties. Some selected values for CH_2Cl_2 are as follows:

Molecular weight = 84.94
Freezing point = −96.7°C
Boiling point = 39.8°C
Latent heat of vaporization (at b.p.) = 78.7 cal/g
Specific heat of the liquid at 20°C = 0.28 cal/g/°C
Specific heat of the vapor (at 40°C at 1 atm) = 0.155 cal/g/°C
Thermal conductivity of the liquid at 20°C = 0.092 C.H.U./hr/ft^2/(°C/ft)
Thermal conductivity of the vapor (b.p.) = 0.00438 C.H.U./hr/ft^2/(°C/ft)
Density of the liquid (d_4^{20}) = 1.326 g/cm^3
Viscosity of the liquid at 20°C = 0.425 cP
Refractive index, n, of the liquid = 1.4244 at 20°C
Dielectric static permittivity of the liquid = 9.1 (20°C)
Dielectric static permittivity of the vapor = 1.0109 (40°C)
Heat of formation of the liquid = 28.6 kcal/mole
Heat of formation of the vapor = 2.17 kcal/mole

Also in this paper are charts of solubility in water, latent heat, specific heat (liquid and vapor), viscosity (liquid and vapor), thermal conductivity (liquid and vapor), and diffusivity in air at 1 atm, all against temperature.

12.3.1.2 Dielectric Properties and Polarizability

The polarizability and the anisotropy of the polarizability are known from a paper by Iszak and le Fevre (Section 12.4.1) on the molar Kerr constant in solution: $P_2(CCl_4) = 69.24$ cm^3; P_2(benzene) = 69.05 cm^3. This paper lists a range of experimentally determined liquid state dipole moments, the majority in benzene solution (1.44–1.62 D). In CCl_4 they are 1.49–1.59 D. The paper provides a detailed description of attempts to reproduce the measured Kerr constant theoretically with bond polarizabilities, induction, etc.

In gaseous methylene chloride at 83.5°C/750 mm, $b_1 = 5.96$ Å^3; $b_2 = 8.47$ Å^3; $b_3 = 5.02$ Å^3 are given by Stuart (1967), which compare with the values of Iszak and le Fevre: $b_1 = 6.25$ Å^3; $b_2 = 7.82$ Å^3; $b_3 = 5.21$ Å^3 (at infinite dilution).

12.3.1.3 Collected Values of the Dipole Moment

In the dilute gas, according to isotope, from 1.61(6) to 1.64(4) D. In benzene, from 1.44 to 1.62 D. In CCl_4, from 1.49 to 1.59 D. There is one value of 1.91 D by Myers and Sun.

The quadrupole and higher moments of methylene chloride are apparently unknown experimentally.

12.3.1.4 Hyperpolarizabilities

Miller et al. provide the second- and third-order nonlinear optical polarizabilities.

12.3.1.5 Charge Distributions

A study by Del Ré (Section 12.4.1.13, Ref. 1), using a simple molecular orbital LCAO method, provides a calculated dipole moment of 1.7 D.

Atoms			(1)	(2)	(3)
H_2	C	Cl_2	$+0.105e$	$+0.024e$	$-0.117e$
(1)	(2)	(3)			

where e is the charge on the electron. These can be used to calculate rough values of the higher multipoles about a given reference origin.

12.3.1.6 Second Virial Coefficients

One of the most valuable methods of studying intermolecular forces consists of the direct measurement of the deviations of real gases from the equation of state of the perfect gas. The state of a real gas is described by means of the well-known equation:

$$PV_m = A + \frac{B}{V_m} + \frac{C}{V_m^2} + \cdots$$

due to Kammerlingh–Onnes. A, B, and C are the first, second, and third virial coefficients, and are temperature dependent.

For methylene chloride:

T (°C)	$-B_p$ (cm³/mole)
50	676.5
75	544.8
100	467.2
125	389.2
150	348.9

The virial coefficient method is applicable to arbitrary quantities Q describing the property of a real gas:

$$Q = A_Q + \frac{B_Q}{V_m} + \frac{C_Q}{V_m^2} + \cdots$$

where A_Q, B_Q, C_Q are the first, second,... virial coefficients of the measurable quantity Q. For example, Q can be molecular electric polarization. Buckingham (1959) proposes its use for molecular refraction and Kerr constants, and Kielich (1972) for the Cotton–Mouton effect, light scattering, and field gradient-induced optical birefringence. So far no experimental values are available for methylene chloride.

12.3.2 Basic Physical Properties of Methyl Fluoride

Molecular weight = 34.034
Boiling point at 1 bar = 194.65°K
Freezing point at 1 bar = 131.2°K
Triple point = 131°K
Critical temperature = 317.6°K
Gas density at 273°K (1 bar) = 1.5451 g/l
Density of liquid at 213°K = 0.8328 g/ml
Critical pressure = 58 bar (852.6 psia)
Critical density = 0.275 g/cm³
Latent heat of vaporization at b.p. = 118.46 cal/g
Specific heat at 298°K (1 bar) = 0.3221 cal/g/°C
Entropy, gas, at 298°K (1 bar) = 53.25 cal/mole °C
Heat of formation at 298°K = -59 ± 2 kcal/mole
Dipole moment = 1.8555 ± 0.0015 D
C—F bond dist. = 1.3852 Å; C—H = 1.106 Å
$\angle_{HCH} = 109°50' \pm 3'$
Polarizability = 2.97×10^{-24} cm³/mole
Moment of inertia $I_x = I_y = 33 \times 10^{-40}$ g/cm²
$I_z = 5.5 \times 10^{-40}$ g/cm²
Liquid Densities (g/cm³), 133°K, $\rho = 0.955$; 153°K, $\rho = 0.93$; 173°K, $\rho = 0.91$; 193°K, $\rho = 0.88$; 233°K, $\rho = 0.79$; 270°K, $\rho = 0.675$; 293°K, $\rho = 0.59$

12.3.3 Physical Properties of Methyl Iodide

Molecular weight = 142
Melting point = 66.45°C
Boiling point = 42.5°C (760 mm)
Static permittivity, $\epsilon_s = 7.1 \pm 0.1$ at 20°C
Density, $\rho = 2.3346$ g/cm³; $\rho_4^{20} = 2.2819$ g/cm³; $\rho_4^{30} = 2.25102$
Density in the solid at −195°C, $\rho = 2.994$ g/cm³; at −79°C, $\rho = 2.840$ g/cm³
Refractive index, $n_D^{20} = 1.53173$; n_{He}^{15} (yellow) = 1.534

12.3.3.1 Structural Factors

r(C—H) = 1.0958 Å
r(C—I) = 2.1387 Å
$\angle_{HCH} = 111°50'$
$\angle_{HCI} = 106°58'$

12.3.3.2 Second Virial Coefficients

$-B_p$ (cm³/mole)	T (°K)
600	323
490	353
420	383

12.3.3.3 Viscosity

$\eta = 0.594$ cP
$\eta_{15} = 0.518$ cP
$\eta_{30} = 0.460$ cP

12.3.3.4 Critical Constants

$T_c = 255°C$
$P_c = 66.3$ atm
$\rho_c = 0.83$ g/cm^3

12.4 BIBLIOGRAPHY

This is a compilation of papers on the topics of interest to the proposed scheme. It is not exhaustive but fairly comprehensive up to the end of 1979.

12.4.1 Methylene Chloride

12.4.1.1 Infrared Spectroscopy

1. "Vibrational Intensities in Halogenated Methanes. III Interpretation of solution Data," Mallard, W. C. and Straley, J. W., *J. Chem. Phys.* **27**, 877–879 (1957).
2. "Intensity of the Valence Vibration Bands of the Methylene Groups in CH_2Cl_2. Abnormal Influence of the Concentration," Josien, M. L., Fuson, N., and Lafaix, A., *Compt. Rend.* **249**, 256–258 (1959).
3. "Effect of Pressure on the Valence Vibration of C—H of Dissolved Gases up to 50,000 Atmospheres," Slykhouse, T. E. and Drickamer, H. G., *Coll. Int. Centre, Natl. Rech. Sci. (Paris)* **77**, 129–135 (1959).
4. "Intensities of C—H Vibration Bands in Haloform and Methylene Halides," Robinson, C. C., Tare, S. A., and Thompson, H. W., *Proc. R. Soc.* **269A**, 492–499 (1962).
5. "Infra-red Solvent Shifts and Molecular Interactions. II Carbon–Halogen Dipoles," Hallam, H. E. and Ray, T. C., *Trans. Faraday Soc.* **58**, 1299–1308 (1962).
6. "Infrared Spectroscopic Study of Valence Vibrations Carbon–Halogen for Various Halides of Methyl and Methylene," Jacob, J. and Symvoulidou, H., *Compt. Rend.* **257**(3), 639 (1963).
7. "Methylene Chloride Spectrum. C—H Stretching Vibration Bands of Methylene Chloride," Kagarise, R. E., *Spectrochim. Acta* **19**(8), 1371–1374 (1963).
8. "The C—H Stretching Spectra and Intensities of Dihalogenomethane and Intermolecular Interaction," Kanbayeshi, U., *Bull. Chem. Soc. Jap.* **36**(9), 1173–1177 (1963).
9. "Vapour-Liquid Frequency Shifts in Some Substituted Methanes," Kagarise, R. E., *Spectrochim. Acta* **19**(12), 1979–1987 (1963).

10. "The C—H Stretching Spectra and Intensities of Methylene Halides," *Proc. Int. Symp. Mol. Struct. Spectrosc., Tokyo, C209*, 4 pp. (1962).
11. "Far Infrared Spectra of Twelve Organic Liquids," Wyss, H. R., Werder, R. D., and Guenthard, Hs. H., *Spectrochim. Acta*, **20**(4), 573–579 (1964).
12. "Infra-red Dispersion Studies," Prichard, W. H. and Orville–Thomas, W. J., *Proc. Colloq. Spectros. Int., 10th, Univ. Maryland*, 563–568 (1968).
13. "Recalculation of the Bond Moments and the Bond Derivatives of the Dichloromethane Molecule," Kambayashi, U. and Nukada, K., *Bull. Chem. Soc. Jap.* **38**(3), 497–498 (1965).
14. "Infra-red Intensities in CH_2F_2, CH_2Cl_2 and CF_2Cl_2," Morcillo, J., Zamorano, L. J., and Heredia, J. M. V., *Spectrochim. Acta* **22**, 1969–1980 (1966).
15. "Band Intensities and Widths of Some RCX_2-type Compounds in Different Solvents," Dervil, E., *C.R. Acad. Sci., Paris, Ser. C.* **264**, 168–170 (1967).
16. "Effect of Weak Intermolecular Interaction on the Intensity of Valence Vibration Bands of the Methylene Group in Dichloromethanes," Rasulov, A. Ya. and Chulanovskii, V. M., *Opt. Spektrosk.* **22**(5), 763–767 (1967).
17. "Relation between Absolute Intensities in the Vapour and Condensed Phases of the Valence Vibrations. CH_2 in Methylene Chloride and Methylene Iodide," Levi, G. and Chalaye, M., *C.R. Acad. Sci., Paris, Ser. A, B*, **265B**, 1093 (1967).
18. "Calculation of Oscillator Coupling in the Liquid State. Infra-red Absorption Bandwidths as Evidence of the Phenomenon," Vincent-Geisse, J., *Spectrochim. Acta* **24A**, 1–8 (1968).
19. "Infra-red Spectra of CH_2Cl_2, CH_2Br_2 and CH_2I_2 in the Solid State," Kartha, V. B., *J. Mol. Spectrosc.* **24**, 368–377 (1967).
20. "Relation Between Overtones of the Symmetrical and Asymmetrical Frequency in Groups of the XH_2 Type," Shman'ko, I. I. and Finkel'shtein, A. I., *Opt. Spektrosk.* **23**(3), 506–508 (1967).
21. "Rotation-like Motion of Molecules in Liquids: Far Infra-red Absorption of Polar Molecules in an Invert Solvent," Datta, P. and Barrow, G. M., *J. Chem. Phys.* **48**(10), 4662–4666 (1968).
22. "Effect of the Electron Cloud Distribution on the Infra-red Absorption Intensities of the C—H Bond of Halomethane Derivatives of the Type CHX_3, CH_2X_2, CH_3X," Chalaye, M. and Levi, G., *C.R. Acad. Sci., Paris, Ser. A, B*, **267B**(1), 45–47 (1968).
23. "The Effect of Molecular Interaction in the Intensity of Vibrational Absorption Bands of Dihalomethanes. I. Stretching Vibrations of the Methylene Chloride Methylene Group," Rasulov, A. Ya., *Ref. Zh. Khim*, Abstr. No. 22B300 (1967).
24. "Infra-red Study of Matrix-isolated Chlorinated Tetrahedral Molecules," King, S. T., *J. Chem. Phys.* **49**(3), 1321–1330 (1968).
25. "Quantitative Study of the Effect of Temperature on the Intensity of Infra-red Absorption Bands in Liquids," Zabiyakin, Yu. E. and Bakhshiev, N. G., *Opt. Spektrosk.* **25**(1), 58–61 (1968).
26. "Molecular Constants of Some Tetrahedral XY_4-type Molecules and their

Substituted Derivatives by Green's Function Analysis," Ramaswamy, K. and Ranganathan, V., *Indian J. Pure Appl. Phys.* **6**(12), 651–655 (1968).

27. "CCl and CBr Valence Vibrations of Organic Compounds in the Gaseous State and in Solution in Various Solvents," Derril, E. and Vincent-Geisse, J., *J. Phys. Chim. Physiochim. Biol.* **65**, 1417–1424 (1968).

28. "Calculation of Electrooptical Parameters and Absolute Intensities in the Infra-red Spectra of Halo-substituted Methanes," Mokhnatkin, V. M. and Sverdlov, L. M., *Zh. Prikl. Spektrosk.* **10**(2), 276–282 (1969).

29. "Solute-solvent Interactions. III Solvent Shifts of Carbon–Chlorine Infra-red Stretching Frequencies of some Chlorinated Hydrocarbons," Oi, N. and Coetzee, J. F., *J. Am. Chem. Soc.* **91**, 2473–2477 (1969).

30. "Vibrational Spectra of Single Crystals and Polycrystalline Films of CH_2Cl_2 and CH_2Br_2," Brown, C. W., Allkins, J. R., and Lippincott, E. R., *J. Chem. Phys.* **51**(4), 1376–1384 (1969).

31. "Infra-red Intensities of Some Fundamentals of Methylene Chloride in the Condensed Phase," Jayadevoppa, E. S. and Haibatti, S. K., *Z. Phys. Chem. (Leipzig)*, **242**(1–2), 67–73 (1969).

32. "Infra-red Spectrum of Crystalline CH_2Cl_2 and CD_2Cl_2. Polarization Measurements and Crystal Structure," Marzucchi, M. P. and Manzelli, P., *J. Chem. Phys.* **52**(5), 2630–2639 (1970).

33. "Effect of a Weak Intermolecular Interaction on the Intensity of Valence Bands of the CH_2 Group in Dihalomethanes," Rasulov, A. Ya. and Chulanovskii, V. M., *Ref. Zh. Khim.*, Abstr. No. 24B489 (1969).

34. "Rotational Diffusion Tensor of Liquid Methylene Chloride from Its Infrared Spectrum," Rothschild, W. G., *J. Chem. Phys.* **53**(3), 990–997 (1970).

35. "Calculation of Infra-red Band Intensities of Various Chlorinated Methanes," Tanabe, K. and Saeki, S., *Spectrochim. Acta* **26**, 1469–1479 (1970).

36. "Infra-red Spectrum of Crystalline Dichloromethane and Dichloromethane-d_2. Phase Transition and Doublet Structure of Mixed Crystals," Manzelli, P., Marcucchi, M. P., and Califano, S., *J. Chem. Phys.* **54**(3), 1409–1410 (1971).

37. "Comparative Study of the Profile of Infra-red Absorption Bands of Liquid Compounds in the Pure State and in Dilute Solution. Analysis of the Interpretation as a Function of the Local Field Effect and Coupling of Oscillators in Pure Liquids," Lafaix, M. and Vincent-Geisse, J., *Spectrochim. Acta* **29**(1), 177–191 (1973).

38. "Determination of the Anharmonicity of the $\partial(CH_2)$ Scissoring Vibration. Fermi Resonance between the $\nu_8(CH_2)$ Symmetrical Vibration and $2\nu(CH_2)$ Harmonic Levels," Saur, O., Travert, J., Lavalley, J. C., and Sheppard, N., *Spectrochim. Acta* **29**(2)A, 243–252 (1973).

39. "Isotopic Dilution Effect on the Infra-red Absorption Bandshape of Dichloromethane," van Woerkom, P. C. M., De Bleyser, J., and Leyte, J. C., *Chem. Phys. Lett.* **20**(6), 592–593 (1973).

40. "Effect of Fluctuations in Solution Concentrations on Line Widths in Vibrational Molecular Spectra," Bondarer, A. F. and Mardaeva, A. I., *Opt. Spektrosk.* **35**(2), 286–288 (1973).

41. "Simple Models of the Far Infra-red Absorption of Polar Molecules in Liquid and Rotator Phases," Larkin, I. W., *J. Chem. Soc. Faraday Trans. II* **69**, 1278–1290 (1973).

42. "Intermolecular Vibrational Relaxation in Liquids," van Woerkom, P. C. M., De Bleyser, J., De Zwart, M., and Leyte, J. C., *Chem. Phys.* **4**(2), 236–248 (1974).

43. "Evaluation of Atom Polarization from Infra-red Intensity Measurements," Rao, D. S. R. and Thyagarajan, G., *Indian J. Pure Appl. Phys.*, **12**(3), 242–243 (1974).

44. "Infra-red Dispersion Studies. 12. Infra-red Dispersion of Dichloro-, Dibromo-, and Diiodomethane and their Deuterated Analogs," Rendell, C. H., Ford, T. A., Redshaw, M., and Orville-Thomas, W. J., *J. Mol. Struct.* **24**(1), 187–204 (1975).

45. "Solvent Effect on the ν_8 Bandshape of Dichloromethane," Tanabe, K., *Spectrochim. Acta* **30A**, 1891–1900 (1974).

46. "Infra-red Investigation of Electronic Interactions in Di- and Tri-substituted Methanes," Zatsepina, N. N., Kolodina, N. S., and Tupitsyn, I. F., *Reakts. Sposobn. Org. Soedin* **11**(2), 399–415 (1974).

47. "Vibrational Relaxation in Liquids. Some Applications of the Isotopic Dilution Method," van Woerkom, P. C. M., deBleyser, J., De Zwart, M., Burgers, P. M. J., and Leyte, J. C., *Ber. Bunsenges. Phys. Chem.* **78**(12), 1303–1318 (1979).

48. "Infra-red Intensity Measurements by ATR (Attenuated Total Reflection). I. Survey of Results for some Pure Liquids," Chambers, J. G., Barnes, A. J., and Orville-Thomas, W. J., *Chem. Phys.* **9**(1–2), 165–173 (1975).

49. "General Local Mode Theory for High Energy Polyatomic Overtone Spectra and Application to Dichloromethane," Hayward, R. J. and Henry, B. R., *J. Mol. Spectrosc.* **57**(2), 221–235 (1975).

50. "Temperature and Concentration-dependence of ν_8 Bandwidth of Dichloromethane," Tanabe, K., *Spectrochim. Acta* **31A**, 1611–1616 (1975).

51. "Infra-red Absorption Bandwidth and Molecular Rotational Motion of Dichloromethane," Tanabe, K., *Spectrochim. Acta* **32A**, 1129–1133 (1976).

52. "Study of Orientational and Vibrational Relaxation of Molecules in Pure Liquids and Solutions," Pogorelov, V. E., Boldeskul, A. E., and Salivon, G. I., *Fiz. Zhidk. Sostoyaniya* **4**, 115–120 (1976).

53. "Far Infra-red Study of Cation Motions in Dry and Solvated Mono and Divalent Carion Containing Zeolites X and Y," Butler, W. M., Angell, C. L., McAlister, W., and Risen, W. M., *J. Phys. Chem.* **81**, 2061–2068 (1977).

54. "Mass Effects on the Applicability of a Local Mode Description—an Analysis of the High Energy Overtone Spectra of Difluoro-, Dichloro-, Dibromo- and Diiodomethane," Henry, B. R. and Hung, I-Fu, *Chem. Phys.* **29**(3), 465–475 (1978).

55. "Dipole Moment Derivatives, Polar Tensors and Effective Atomic Changes for the Dihalogenomethanes, CH_2X_2 (X = Fluorine, Chlorine, Bromine)," Ford, T. A., Aroca, M. R., and Robinson, E. A., *Spectrochim. Acta* **34A**, 77–82 (1978).

12.4.1.2 Raman and Hyper-Raman Spectroscopy

1. "Raman Spectral Data Assignments, Potential Energy Constants, and Calculated Thermodynamic Properties for CH_2Cl_2, $CHDCl_2$, and CD_2Cl_2," Palma, F. E. and Sathianandan, K., *Dev. Appl. Spectrosc.* **2**, 58–64 (1963).
2. "Comparison of the Fine Structure of Raman Spectra of Polyhalogenated Methane Derivatives," Delwaulle, M.-L. and Cerf, C., *J. Chim. Phys.* **60**, 1195–1198 (1963).
3. "Intensities of the Raman Lines of Some Chloromethanes," Miroue, P., Patella, P., and Rastelli, A., *Atti Acad., Nazl. Lincei, Rend. Classic Sci. Fis., Mort. Not.* **34**(4), 422–429 (1963).
4. "Raman Spectra of Polycrystalline Methylene Halides," Ito, M., *J. Chem. Phys.* **42**, 391–394 (1965).
5. "Raman and Infrared Studies of the Solvent Dependence of the Intensities of the CH_2 Fundamental Stretching Modes of the Methylene Halides," Evans, J. C. and Lo, G. Y.-S., *Spectrochim. Acta* **21**, 33–44 (1965).
6. "The Measurement of the Raman Spectra of Organic Compounds in Solution," Jones, R. N., Di Giorgio, J. B., Elliott, J. J., and Nonnenmacker, G. A. A., *J. Org. Chem.* **30**, 1822–1832 (1965).
7. "Absolute Raman Intensities of Symmetrical Stretching Modes in Some Molecules and Ions from the *S* Function Model of Chemical Bonding," Lippincott, E. R. and Nagarajan, G., *Bull. Soc. Chim. Belg.* **74**, 551–554 (1965).
8. "Resonance Raman Spectra of the Halomethanes Excited by Ultraviolet Nitrogen Pulsed Laser," Kaya, K., Mikami, N., Udagawa, Y., and Ito, M., *Chem. Phys. Lett.* **13**(3), 221–224 (1972).
9. "Comparison of Raman Spectra of Methane Derivatives in Liquid and Gaseous State," Vorob'eva, G. A. and Timonin, S. P., *Zh. Prikl. Spektrosk.* **18**(5), 860–864 (1973).
10. "Effect of the Internal Field on Raman Scattering Cross Sections," Nestor, J. R. and Lippincott, E. R., *J. Raman Spectrosc.* **1**(3), 305–318 (1973).
11. "Degrees of Polarization of the Raman Bands of Totally Symmetric Fundamental Vibrations in Liquid Halogen substituted Methanes," Fukushi, K., Ikawa, S., and Kimura, M., *Proc. Int. Conf. Raman Spectr. 5th.*, 470–471 (1976).
12. "Reorientational Molecular Motion in Liquids. Comparison of Raman and Rayleigh Scattering," Amorim da Costa, A. M., Norman, M. A., and Clarke, J. H. R., *Mol. Phys.* **29**, 191–204 (1975).
13. "Evaluation of Force Constants from Raman Intensity Analysis of Molecules I. Methylene Chloride," Padma, V. A., Kumar, S. P., and Rao, N. R., *Indian J. Pure Appl. Phys.* **13**(1), 31–34 (1975).
14. "Calculation of Raman Intensities by a Modified CNDO/2/INDO Method," Bleckmann, P. and Wiegeler, W., *J. Mol. Struct.* **42**, 227–234 (1977).
15. "Vibrational Population Lifetimes of Polyatomic Molecules in Liquids," Laubereau, A., Fischer, S. F., Spanner, K., and Kaiser, W., *Chem. Phys.* **31**, 335–344 (1978).

16. "The Hyper Rayleigh and Hyper Raman Spectra of some Group IV and Group V Halides," Dines, T. J., French, M. J., Hall, R. J. B., and Long, D. A., *Proc. Int. Conf. Raman Spectrosc. 5th.*, 707–716 (1976).
17. "Measurements of Nonlinear Optical Polarisabilities for Some Halogenated Methanes: the Role of Bond–Bond Interactions," Miller, C. K. and Ward, J. F., *Phys. Rev. A*, **16**(3), 1179–1185 (1977).

12.4.1.3 NMR Spectroscopy

1. "Anomalous Solvent Shifts in High Resolution NMR Spectra," Evans, D. F., *Proc. Chem. Soc.* **1958**, 115–116.
2. "Applicability of the Macroscopic Magnetic Susceptibility Model to Solvent Effects in Proton NMR," Glick, P. E., Kates, D. F., and Ehrenson, S. J., *J. Chem. Phys.*, **31**, 567–568 (1959).
3. "Solvent Shifts of ^{19}F NMR Spectra," Evans, D. F., *J. Chem. Soc.* **1960**, 877–880.
4. "Proton Nuclear Spin Resonance Spectroscopy. XIA ^{13}C Isotope Effect," Tiers, G. vD., *J. Phys. Chem.* **64**, 373–374 (1960).
5. "Temperature Dependence of the Chlorine Pure Quadrupole Resonance Frequency in Molecular Crystals," Gutowsky, H. S. and McCall, D. W., *J. Chem. Phys.* **32**, 548–552 (1960).
6. "Nuclear Pure Quadrupole Relaxation and its Temperature Dependence in Solids," Woessner, D. E. and Gutowsky, H. S., *J. Chem. Phys.* **39**, 440–456 (1963).
7. "Nuclear Quadrupole Resonance of Organic Compounds," Lucken, E. A. C., *Tetrahedron* **19**, 123–141 (1963).
8. "Electrically Induced Perturbations of Halogen Nuclear Quadrupole Interactions in Polycrystalline Compounds. I. Phenomenological Theory and Experimental Results," Dixon, R. W. and Bloembergen, N., *J. Chem. Phys.* **41**(6), 1720–1738 (1964).
9. "Phase-Transition Characteristics Determined by M.M.R. in Dihalomethanes," Babushkina, T. A. and Semin, G. K., *Zh. Strukt. Khim.* **7**, 114–116 (1966).
10. "Substitutents Effects. V. Correlation of ^{13}C Chemical Shifts by Pairwise Interactions," Malinowski, E. R., Vladimiroff, Th., and Tavares, R. F., *J. Phys. Chem.* **70**(6), 2046–2048 (1966).
11. "Geminal Isotope Effects on the Proton m.r. of some First-Row Molecules," Bernheim, R. A. and Batiz-Hernandez, H., *J. Chem. Phys.* **45**, 2261–2269 (1966).
12. "A N.M.R. Study of Polar Gases, Either Pure or Perturbed by Gaseous Impurities," Widenblocher, G., *Ann. Phys.* **1**, 327–352 (1966).
13. "Solvent effects on ^{13}C—H Coupling Parameters and Chemical Shifts of some Halomethanes," Watts, V. S. and Goldstein, J. H., *J. Phys. Chem.* **70**, 3887–3892 (1966).
14. "N.M.R. Solvent Effects and Molecular Interactions," Kintz., I. D. and Johnston, M. D., *J. Am. Chem. Soc.* **89**, 6008–6017 (1967).

15. "Semiempirical Method for the Calculation of Some Parameters for High Resolution N.M.R. Spectra," Maslov, P. G., *J. Phys. Chem.* **72**(5), 1414–1424 (1968).

16. "Relaxation in N.M.R. for Multi-spin Systems," Blicharski, J. S., *Inst. Nucl. Phys., Cracow, Rep. No. 508*, 6–17 (1967).

17. "Anomalous Features of N.M.R. Spectra of Methyl and Methylene Halides Oriented in a Nematic Solvent. Unusual Ordering due to Specific Solute-Solvent Interaction," Morishimia, I., Mizuno, A., and Yonezawa, T., *J. Am. Chem. Soc.* **93**, 1520–1522 (1971).

18. "Field-dependent Contributions to ^{13}C Nuclear Relaxation," Lyerla, J. R., Grant, D. M., and Bertrand, R. D., *J. Phys. Chem.* **75**, 3967–3971 (1971).

19. "Proton NMR Spectra of Dichloromethane and 1,4-Di-bromo-2-butyne Molecules Dissolved in the Nematic liquid Crystal Phase," Borodin, P. M. and Ignat'ev, Yu. A., *Vestn. Leningrad Univ. Fiz. Khim.* **46**(1), 157–158 (1972).

20. "Deuterium Isotope Effects on ^{13}C N.M.R. Spectra," Colli, H. W., Gold, V., and Pearson, J. E., *J. Chem. Soc. Chem. Commun.* **1973**(12), 408–409.

21. "Measurement of Nuclear Magnetic Spin-Lattice Relaxation Times by the Use of Repetitive Sweep Techniques," Heatley, F., *J. Chem. Soc. Faraday Trans. II* **69**, 831–841 (1973).

22. "NMR Measurement of the Hydrogen Bonding Ability of the CH Groups of Some Halogenated Hydrocarbons. Limitations of the NMR Method for XH_2 and XH_2 Groups," Pang, T. S. and Ng, S., *Spectrochim. Acta* **29**, 207–212 (1973).

23. "NMR Spin-Lattice Relaxation in the Lyotropic Polypeptide Liquid Crystal," Hines, W. A. and Samulski, E. T., *Macromolecules* **6**, 793–795 (1973).

24. "Concerning the Theory of Chemical Shifts in ^{19}F NMR in Polar Solvents," Mukhomorov, V. K., *Teor. Eksp. Khim.* **12**(1), 64–70 (1976).

25. "Proton Spin Relaxation in the HaloMethanes," Brown, P. M., Krishna, N. R., and Gordon, S. L., *J. Magn. Reson.* **20**, 540–543 (1975).

26. "Medium Effects in Chlorine Magnetic Resonance," Forsem, S., Gustavsson, H., Lindman B., and Persson, N. E., *J. Magn. Reson.* **23**(3), 515–518 (1976).

27. "Nuclear Spin Relaxation in Liquid Methylene Chloride," Sandhu, H. S., *J. Magn. Reson.* **29**, 563–572 (1978).

For a critical review of the NMR work see Brier and Perry (1978).

12.4.1.4 Dielectric Relaxation and Far Infrared

1. "Dielectric Dispersion in Gases at 9400 Megacycles," Boggs, J. E., Whiteford, J. E., and Thompson, C. M., *J. Phys. Chem.* **63**, 713–715 (1959).

2. "Mobility of Small Molecules in Viscous Media. I. Rotational Motion of Methylene Chloride Molecules in Polystyrene by Far Infra-red Spectroscopy," Rothschild, W. G., *Macromolecules* **1**(2), 43–47 (1968).

3. "Relaxation of Physical Properties and Reactivity of Substituted Methanes with their Structure. III," Papulov, Yu. G., *Zh. Obshch. Khim.* **37**, 2591–2598 (1967).

4. "Effect of Pressure on the Static Dielectric Constants of Liquids at 30.0°C and 50.0°C," Hartmann, H. and Schmidt, A. P., *Ber. Bunsenges. Phys. Chem.* **72**, 875–877 (1968).

5. "Effect of Pressure on the Density and Dielectric Constant of Polar Solvents," Schornack, L. G. and Eckert, C. A., *J. Phys. Chem.* **74**(15), 3014–3022 (1970).

6. "Molecular Motion in Liquids: Prevalence of large-size Rotational and Translational Diffusion Steps," Rothschild, W. H., *J. Chem. Phys.* **53**(8), 3265–3271 (1970).

7. "Self Diffusion Coefficients and Rotational Correlation Times in Polar Liquids, IV. Dichloromethane and Pyridine," O'Reilly, D. E., Peterson, E. M., and Yasaitis, E. L., *J. Chem. Phys.* **57**, 890–894 (1972).

8. "Molecular Dynamics in Dichloromethane/Decalin Glass," Reid, C. J., Evans, G. J., Evans, M. W., and Coffey, W. T., *Chem. Phys. Lett.* **56**, 529–532 (1978).

9. "Far Infra-red Absorption Intensities and the Dipole Moments of Some Molecules in Solutions," Sato, K., Ohkubo, Y., Moritsu, T., Ikawa, S., and Kimura, M., *Bull. Chem. Soc. Jap.* **51**(9), 2493–2495 (1978).

10. "Experimental Measure of the Planar Itinerant Oscillator," Coffey, W. T., Evans, G. J., Evans, M., and Wegdam, G. H., *J. Chem. Soc. Faraday Trans II* **74**, 310–323 (1978).

11. "Far Infra-red Absorption of Dichloromethane in Isotropic and Cholesteric Solvents," Evans, G. J., Reid, C. J., and Evans, M. W., *J. Chem. Soc. Faraday Trans. II* **74**, 343–352 (1978).

12. "Far Infra-red and Related Studies of Molecular Motion in Condensed Phases," Reid, C. J., Ph.D. Thesis, University of Wales (1979).

12.4.1.5 Light Scattering

1. "Intensity and Width of the Components of the Fine-Structure Line of Scattered Light in Liquids and the Damping of Hypersound," Mash, D. I., Starunov, V. S., Tiganov, E. V., and Fabelinskii, I. L., *Zh. Eksp. Teor. Fiz.* **49**(6), 1764–1773 (1965).

2. "Brillouin Scattering in Liquids at 4880 Å," Shapiro, S. L., McClintock, M., Jennings, D. A., and Barzer, R. L., *J. Quantum Electron.* **2**(5), 89–93 (1966).

3. "Thermodynamics of Binary Liquid Mixtures by Rayleigh Light Scattering," Schmidt, R. L. and Clever, H. L., *J. Phys. Chem.* **72**, 1529–1536 (1968).

4. "Angular Time Correlation Functions from Spectra for Some Molecular Liquids," Van Konynenburg, P., and Steele, W. A., *J. Chem. Phys.* **56**, 4775–4787 (1972).

5. "Reorientational Molecular Motion in Liquids. Comparison of Raman and Rayleigh Scattering," Amorim da Costa, A. M., Norman, M. A., and Clarke, J. H. R., *Mol. Phys.* **29**, 191–204 (1975).

12.4.1.6 Acoustic Relaxation/Brillouin Dispersion

1. "Ultrasonic Relaxation in Liquid Methylene Chloride," Andreae, J. H., Joyce, P. L., and Oliver, R. J., *Proc. Phys. Soc. (London)* **75**, 82–86 (1960).

2. "Sound Velocity and Molecular Structure. I. Some General Points of View on the Molecular-Kinetic Calculation of the Sound Velocity in Liquids. II Temperature Dependence of the Sound Velocity. III Sound Velocity and the

Potential of the Intermolecular Forces," Altenburg, K., *Z. Phys. Chem.* **216**, 126–138, 138–145, 146–162 (1961).

3. "Ultrasonic Relaxation in Polyatomic Gases and Vapours," Jatkar, S. K. K. and Deshpande, D. D., *Br. J. Appl. Phys.*, **12**, 243–247 (1961).
4. "Vibrational Relaxation in Liquid Dichloromethane," Hunter, J. L. and Dardy, H. D., *J. Chem. Phys.* **42**, 2961–2966 (1965).
5. "Vibrational Relaxation and Hypersonic Velocity in Liquids," Piercy, J. E. and Hanes, G. R., *J. Chem. Phys.* **43**, 3400–3402 (1965).
6. "Intensity and Width of the Components of the Fine-Structure Line of Scattered Light in Liquids and the Damping of Hypersound," Mash, D. I., Starunov, V. S., Tiganov, E. V., and Fabelinskii, I. L., *Zh. Eksp. Teor. Fiz.* **49**(6) 1764–1773 (1965).
7. "Supersonic Vibrations in Liquids," Pesin, M. S., *Tr. Fiz. Inst. Akad. Nauk. SSSR* **30**, 158–220 (1964).
8. "A Method of Investigating the Acoustical Properties of Liquids at 300–1000 Mc," Berdyev, A. A. and Lezhnev, N. B., *Akust. Zh.* **12**, 247–250 (1966).
9. "Relaxation Phenomena in the Generation of Supersonic Molecular Beams," Campargue, R., *Chem. Soc. Spec. Publ. No. 20*, 287–296 (1966).
10. "Absorption of Ultrasound in a Benzene–Methylene Chloride Mixture," Bergyev, A. A. and Khemraev, B., *Isv. Akad. Nauk. Turkm. SSR. Ser. Fiz. Tekh. Khim. Geol. Nauk* **1966**, 116–118; *ibid.*, **1967**(1), 102–104.
11. "Spectrum of Thermal and Forced Molecular Scattering of Light in Liquids," Starunov, V. S., *Tr. Fiz. Inst. Akad. Nauk SSSR* **39**, 151–218 (1967).
12. "Temperature Coefficient of Hypersonic Sound and Relaxation Parameters for Some Liquids," Eastman, D. P., Hollinger, A., Kenemuth, J. R., and Rank, D. H., *J. Chem. Phys.* **50**, 1567–1581 (1969).
13. "Absorption of Ultrasound in Liquids in the 20–3000 MHz Frequency Range," Bergdyev, A. A., Lapkin, V. V., and Lezhnev, N. B., 1969, *Izv. Akad. Nauk. Turkm. SSR, Ser. Fiz.-Tekh. Khim. Geol. Nauk*, **1969**(3), 108–110.
14. "Hypersonic Absorption Measurements in a Series of Liquids at 1–2 GHz Frequencies," Parpiev, K., Khabilbullaev, P. K., and Khaliulin, M. G., *Akust. Zh.* **15**(3), 466–468 (1969).
16. "Vibrational Relaxation in Liquids," Plass K. G., *Ber. Bunsenges. Phys. Chem.* **74**, 343–347 (1970).
16. "Ultrasonic Relaxation in Liquid Thiophene, Methylene Chloride, and Methylene Bromide," Khabibullaev, P. K., Khaliulin, M. G., and Parpiev, K., *Vestn. Mosk. Univ. Khim.* **12**, 111–113 (1971).
17. "Acoustical Relaxation in Fluids," Bergyev, A. A., Lapkin, V. V., and Lezhnev, N., 1971, *Izv. Akad. Nauk. Turkm. SSR, Ser. Fiz.-Tekh., Khim. Geol. Nauk.* **1971**(4), 28.
18. "Dependence of Ultrasound Velocity on the Concentration and Temperature in the Methylene Chloride-Ethyl alcohol Water Mixture," Voleisis, A., Domarkas, V., and Jaronis, E., *Nauch. Tr. Vyssh. Ucheb. Zaved, Litov. SSR, Ul'trazvuk* **1969**(1), 169–173.
19. "Mechanism of Vibrational Relaxation in Liquids," Davidovich, L. A., Ivanov, A. A., Makhkamov, S., Pulatova, L., Khabibullaev, P. K., Khalivlin, M. G., and Sharinov, Sh., *Akust. Sh.* **19**, 26–31 (1974).
20. "Study of the Vibrational Relaxation in Polyatomic Liquids By Brillouin Scattering Spectral Analysis," Caloin, M. and Candam, S., *J. Phys. (Paris)* **33**, 7–14 (1972).

12.4.1.7 Kerr Effect, Anisotropy of Polarizability, Polarization

1. "Kerr Effect in the Liquid State," Okabayashi, H., *Bull. Chem. Soc. Jap.* **34**, 1010–1015 (1961).
2. "Molecular Polarizability. The apparent Anisotropies of Carbon–Halogen Bonds in Methylene Dihalides," Izsak, D. and Le Fevre, R. J. W., *J. Chem. Soc. Phys. Org.* **1966**(1), 102–106.
3. "Dependence of the Molecular Electrical Field Gradient q_{zz} on the Average Molecular Polarisability $\bar{\alpha}$," Machmer, P., *Z. Naturforsch. b* **23**(3), 295–298 (1968).
4. "Atom Dipole Interaction Model for Molecular Polarizabilities. Application to Polyatomic Molecules and Determination of Atom Polarizabilities," Applequist, J., Carl, J. T., and Fung, K. -K., *J. Am. Chem. Soc.* **94**(9), 2952–2960 (1972).
5. "Evaluation of Atom Polarization from Infrared Intensity Measurements," Rao, D. S. R. and Thyagarajan, G., *J. Pure Appl. Phys.* **12**(3), 242–243 (1974).
6. "Polarizability of Interacting Chemical Bonds," Vullfson, S. G., Khamatullina, I. M., and Vereshchagin, A. N., *Izv. Akad Nauk SSSR, Ser. Khim.* **1977**(6), 1325–1332.
7. "Measurement of Nonlinear Optical Polarizabilities for Some Halogenated Methanes: the Role of Bond–Bond Interactions," Miller, C. K. and Ward, J. F., *Phys. Rev.* **16**(3), 1179–1185 (1977).

12.4.1.8 Second Virial Coefficients

1. "The Second Virial Coefficient of Organic Vapours. I. Experimental Results," Perez Masiá, A. and Diaz Peña, M., *An. Real. Soc. esp. fis. Quím. (Madrid)* **54B**, 661–668 (1958).
2. "Real Gas Behaviour in Systems with Ethyl Chloride," Raetzsch, M., *Z. Phys. Chem. (Leipzig)* **238**, 321–328 (1968).
3. "Second Virial Coefficients of Polar Haloalkanes," Tsonopoulos, C., *A.I.Ch.E. J.* **21**(4), 827–829 (1975).
4. "Second Virial Coefficient of Organic Vapours. I. Apparatus," Vilcu, R. and Birhala, Al., *Rev. Roum. Chim.* **20**(7), 889–899 (1975).

12.4.1.9 Critical Properties

1. "A Thermodynamic Method of Reproducing Ultra-high Pressures," Zhokhovskii, M. K., *Tr. Vses. Nauchn.-Issled. Inst. Fiz.-Tekh. Radiotekh. Izmen.* **1960**(46), 68–80.
2. "Correlation of Molecular Volume and Critical Pressure with the Number of Atoms in a Molecule," Benko, J., *Acta Chim Acad. Sci. Hung.* **34**, 217–228 (1962).

3. "Vapour Pressures and Critical Points of Liquids. V. Halogenated Methanes," Engineering Sciences Data Unit, Eng. Sci. Data Item 75010 (1975).

4. "Correlation Between Energies of Vapourization, Molecular Parameters and Critical Temperatures and Pressures," Hajjar, R. F., *Rev. Roum. Chim.* **21**(2), 217–222 (1976).

12.4.1.10 Compressibility and Isochore

1. "Compressibilities and Isochores of $(C_3F_7COOCH_2)_4C$, cyclo-$Si_4O_4(CH_3)_8$, *n*-C_5H_{12}, *n*-C_8H_{18}, 2,2,4-$C_5H_9(CH_3)_3$, cyclo-C_5H_{10}, cyclo-C_6H_{12}, cyclo-$C_6H_{11}CH_3$, $C_6H_5CH_3$, *p*-C_6H_4-$(CH_3)_2$, *s*-$C_6H_3(CH_3)_3$, CH_2Cl_2," Shinoda, K. and Hildebrand, J. H., *J. Phys. Chem.* **65**, 183 (1961).

2. "New Method for Measuring Liquid Compressibilities," Schamp, H. W., Hastings, J. R., and Weissman, S., *Phys. Fluid* **8**(1), 8–11 (1965).

3. "Low-pressure Studies of the Isothermal Compressibilities and Specific Volumes of Organic Liquids," Burkat, R. K. and Richard, A. J., *J. Chem. Thermodyn.* **7**(3), 271–277 (1975).

12.4.1.11 Viscosity

1. "Spin-Lattice Relaxation Times of Protons in Some Organic Compounds," Pendred, T. L., Pritchard, A. M., and Richards, R. E., *J. Chem. Soc. A, Inorg. Phys. Theor.* **1966**(8), 1009–1012 (1966).

2. "Liquid Viscosity of Halocarbons," Phillips, T. W. and Murphy, K. P., *J. Chem. Eng. Data* **15**(2), 304–307 (1970).

3. "Gas Phase Viscosity of Some Halohydrocarbons," Ruiz Panego, A. and Guil Pinto, J. C., *An. Fis.* **65**, 343–349 (1969).

4. "Planar Correlations between Lennard–Jones m-6 Potential Parameters and Molecular Structure," Bishop, P. J. and Liley, P. E., *Proc. Symp. Thermophys. Prop. 6th*, 111–116 (1973).

5. "Attempt to Interpret the Variations in Excess Viscosity in Non-ideal Homogenous Binary Liquid System," Singh, R. P. and Singh, S. S., *J. Indian Chem. Soc.* **51**(a), 790 (1974).

6. "Rotational Microviscosity Factor from Intramolecular Dipole–Dipole Contribution and Deuteron Relaxation Time," Sandhu, H. S., *J. Am. Chem. Soc.* **97**, 6284–6285 (1975).

12.4.1.12 Thermal Conductivity of CH_2Cl_2

1. "Thermal Conductivity of Air and Some Organic Vapours. I.. Variation with Temperature, II Variation with Pressure-Accommodation Coefficients," Perez Masia, A. and Roig, A., *An. real Soc. Esp. Fis. quim.* **54B**, 639–650, 651–660 (1958).

2. "Thermal Conductivity: Reduced State Correlation for Ethylene and its Application to Gaseous Aliphatic Hydrocarbons and their Derivatives at Moderate Pressures," Owens, E. J. and Thodos, G., *A.I.Ch.E. J.* **6**, 676–681 (1960).

3. "Estimated Viscosities and Thermal Conductivities of Gases at High Temperatures," Svehla, R. A., *NASA Tech. Rep. R132*, 140 pp. (1962).

4. "Estimation of Thermal Conductivities of Organic Liquids over Useful Temperature Ranges," Robbins, L. A. and Kingrea, C. L., *Proc. Am. Petrol. Inst., Sect. III*, **42**, 52–61 (1962).

5. "Measurements of the Thermal Conductivity of Liquid Refrigerants at Low Temperatures," Djalalian, W. H., *Bull. Inst. Int. Froid, Ann.* **1964**(2), 153–165.

6. "Heat Transfer in Polar Organic Vapours," Manna, A., Das Gupta, A., and Srivastava, B. N., *Proc. Phys. Soc., London, Gen.* **21**(2), 272–276 (1968).

7. "Measurement of the Thermal Conductivity of Refrigerants and Salt Solutions," Grassmann, P., Tauscher, W., and Chiquillo, A., *Proc. Symp. Thermophys. Prop., 4th*, 282–285 (1968).

8. "Thermal Conductivity of Liquid Refrigerants Measured by an Unsteady-state Hot Wire Method. II," Tauscher, W., *Kaeltech.-Klim.* **20**(9), 287–290 (1968).

9. "Measurement of the Thermal Conductivity of Liquid Refrigerants by an Unsteady-state Hot-wire Method," Tauscher, W. A., *Am. Soc. Heat., Refrig., Air-Cond. Eng. J.* **11**(1), 97–104 (1969).

10. "Coefficient of Thermal Conductivity of Some Freons of the Methane Series," Sadykov, A. Kh., Gabdrakohmanov, R. G., Brykov, V. P., and Mukhamedzyonov, G. Kh., *Tr. Kaz. Khim.-Tekhnol. Inst. No. 47*, 35–39 (1971).

11. "Thermal Conductivity of Binary Liquid Mixtures," Jamieson, D. T. and Irving, J. B., *Adv. Therm. Conduct. Pap. Int. Conf. Therm, Conduct., 12th*, 185–193 (1974).

12. "Thermal Conductivity of Chlorosubstituted Methane and Silane," Prostov, V. N. and Popova, O. G., *Zh. Fiz. Khim.* **49**, 631–633 (1975).

12.4.1.13 Intermolecular Potential Estimates for CH_2Cl_2

1. "A simple M.O.–L.C.A.O. Method for Calculating the Charge Distribution in Saturated Organic Molecules," Del Ré, R., *J. Chem. Soc.* 4031–4040 (1958).

2. "Gas-Kinetic Collision Diameters of the Halomethanes," Miller, G. A. and Bernstein, R. B., *J. Phys. Chem.* **63**, 710–713 (1959).

3. "Intermolecular Forces and Chain Flexibilities in Polymers. I. Internal Pressures and Cohesive Energy Densities of Simple Liquids," Allen, G., Gee, G., and Wilson, G. J., *Polymer* **1**, 456–466 (1960).

4. "Raman Spectral Data, Assignments, Potential Energy Constants, and Calculated Thermodynamic Properties for CH_2Cl_2, $CHDCl_2$, and CD_2Cl_2," Palma, F. E., and Sathianandan, *Dev. Appl. Spectrosc.* **2**, 58–64 (1962).

5. "Force Constants of Small Molecules," Shimanouchi, T., *Pure Appl. Chem.* **7**, 131–145 (1963).

6. "Bond and Interaction Contributions for Calculating the Heat of Formation, Diamagnetic Susceptibility, Molar Refraction and Volume, and Thermodynamic Properties of Some Substituted Methanes," Bernstein, P. B., *J. Phys. Chem.* **69**(5), 1550–1564 (1965).

7. "Relation of Physical Properties and Reactivity of Substituted Methanes with their Structure, III," Papulov, Yu. G., *Zh. Obshch. Khim.* **37**(12), 2591–2598 (1967).

8. "Calculation of Unique force Constants for the Dihalomethanes," Dennen, R. S., *J. Mol. Spectrosc.* **29**, 163–173 (1969).

9. "Geometry of Molecules and Energies of Atomization. III. Halo Derivatives of Methane," Dashevskii, V. G., *Zh. Struck. Khim.* **11**(5), 912–918 (1970).

10. "Comparison of Quantum Chemically Calculated Atomic Net Charges with Data from X-Ray Photoelectron Spectroscopy," Gruendler, W. and Schaedler, H. D., *Z. Chem.* **13**(4), 156–157 (1973).

11. "Theoretical Prediction of the Thermodynamic Properties of Refrigerant Fluid Mixtures," Bougand, J. and Jadot, R., *Bull. Inst. Int. Froid, Ann.* **1973**(4), 57–64.

12. "Bond Strengths and Other Constants for the Substituted Methanes. IV. Calculated Values of the Energies at 0°K, Equilibrionic Energies, Constants in the Exponential Part of the Morse Function for the Potential Energy, and Asymmetries of the Morse Curves," Dhar, A. I. and Cleveland, F. F., *Spectrosc. Mol.* **24**(276), 20–22 (1975).

13. "Crystal Chemical Analysis of Structures Formed by C_2-symmetry Molecules. II. Calculations of Intermolecular Interaction Potentials," Beliskii, V. K. and Dzyabchenko, A. V., *Zh. Strukt. Khim.* **16**(3), 441–445 (1975).

14. "Conformational Analysis CXIX. Charge Distribution in the Molecular Mechanics Method," Allinger, N. L. and Wensthoff, M. T., *Tetrahedron* **33**, 3–10 (1977).

15. "Intermolecular Potential of Real Gases. II. Comparison with Experience," Novak, J., *Zh. Fiz. Khim.* **51**(6), 1339–1343 (1977).

16. "A Critical Evaluation of Lennard-Jones and Stockmayer Parameters and of Some Correlation Methods," Maurits, F. M. and Rummens, F. H. A., *Can. J. Chem.* **55**(16), 3007–3020 (1977).

17. "Molecular Structure Factors of Carbon Tetrachloride, Chloroform and Dichloromethane," Orton, B. P., and W. B. Streett, *Mol. Phys.* **34**(2), 583–587 (1977).

18. "A New type of Parametrization Among the Approximate SCF-LCAO-MO Methods," Moldoveanu, S., *Rev. Roum. Chim.* **23**(3), 453–465 (1978).

19. "Dipolar Correlation and Entropy Variation," Greffe, J.-L. and Grosse, C., *J. Chim. Phys. Phys.-Chim. Biol.* **75**(2), 127–131 (1978).

12.4.1.14 Neutron Scattering and Intertechnical Review

1. "Neutron Inelastic Scattering Measurements and Liquid Dynamics of Dichloromethane," Brier, P. N. and Perry, A., *Adv. Mol. Rel. Inter. Proc.* **13**(1), 1–46 (1978).

12.4.1.15 Dynamics of CH_2Cl_2 in the Viscous and Vitreous States

1. "A Free Volume Interpretation of the Influence of the Glass Transition on Diffusion in Amorphous Polymers," Vrentas, J. S. and Duda, J. L., *J. Appl. Polym. Sci.* **22**(8), 2325–2339 (1978).

2. "Molecular Dynamics in Dichloromethane/Decalin Glass," Reid, C. J., Evans, G. J., and Coffey, W. T., *Chem. Phys. Lett.* **56**(3), 529–532 (1978).

3. "Glass Transition Temperature for Simple Molecular Liquids and their Binary Solutions," Angell, C. A., Sare, J. M., and Sare, E. J., *J. Phys. Chem.* **82**(24), 2622–2629 (1978).

12.4.1.16 Surface Tension

1. "Relation Between Viscosity and Surface Tension of Liquids," Moritz, P., *Period. Polytech.* **3**, 167–176 (1959).

12.4.2 Methyl Fluoride (Liquid and Gas)

12.4.2.1 Neutron Scattering

1. "Thermal Neutron Scattering from Gaseous and Liquid Fluoromethane and Iodomethane," Malm, W. C., *Diss. Abstr. Int. B* **33**(9), 4437 (1972).

2. "Cold Neutron Scattering from Gaseous Methyl Halides," Malm, W. C., Danner, H. R., and Lurie, N. A., *J. Chem. Phys.* **61**(9), 3863–3864 (1974).

12.4.2.2 Virial Coefficients

1. "Dielectric and Pressure Virial Coefficients of Imperfect Gases. VII. Trifluoromethane–Argon and Fluoromethane Argon Mixtures," Copeland, T. G. and Cole, R. H., *J. Chem. Phys.* **64**, 1747–1751 (1976).

2. "Dielectric and Pressure Virial Coefficients of Imperfect Gases. VI. Analysis of Results for Trifluoromethane and Fluoromethane," Copeland, T. G. and Cole, R. H., *J. Chem. Phys.* **64**(4), 1741–1746 (1976).

3. "Second Virial Coefficients of Polar Haloalkanes," Tsonopoulos, C., *A.I.Ch.E. J.* **21**, 827–829 (1975).

4. "Pre-averaged Potential Model and Equilibrium Properties of Polar Gases," Singh, S. and Singh, Y., *J. Phys. B* **5**(11), 2039–2050 (1972).

5. "Study of the 2nd Dielectric Virial Coefficients of Polar Gases. I. Fluoromethane, Chloromethane and Bromomethane," Wohlfarth, C. and Raetzsch, M. T., *Z. Phys. Chem. (Leipzig)* **258**(6), 1117–1128 (1977).

6. "On the Second Dielectric Virial Coefficient of Nonspherical Polar Fluids," Singh, S., *Physica A* **89A**, 219–222 (1977).

7. "Second Virial Coefficients of Polar Gases for a Four-Parameter Model," Lin, H.-H. and Stiel, L. I., *Can. J. Chem. Eng.* **55**(5), 597–601 (1977).

8. "Calculation of the Second Virial Coefficient for Dipolar and Quadrupolar Polyatomic Gases," Burns, H. A., *Rep. IS-T-703, ex. ERDA Energy Res. Abstr. 1976 1(10)*, Abstr. No. 21526 (1976).

12.4.2.3 Far Infrared and Dielectric Spectroscopy

1. "Angular Correlations from the Relative Permittivity of Some Halogenated Methanes at Orthobaric Densities," Gerschel, A., *Mol. Phys.* **31**, 209–220 (1976).

2. "Hierarchy of Memory Functions for Dipolar Absorption in Fluoromethane, Chloromethane and Fluoroform," Bossis, G. and Quentrec, B., *Mol. Phys.* **32**, 591–596 (1976).

3. "Liquid Absorption—Dispersion of Highly Polar Symmetric Top Molecules," Gerschel, A., Dimicoli, I., Joffre, J., and Riou, A., *Mol. Phys.* **32**, 679–697 (1976).
4. "Absorption of Liquids in the Far Infra-red and Extraction of Statistical Function of Motion," Gerschel, A., *J. Chim. Phys. Phys.-Chim. Biol.* **75**, 97–109 (1978).
5. "The Dielectric Constant of a Polar Fluid of Heteronuclear Molecules," Martina, E. and Stell, G., *J. Chem. Phys.* **69**, 931–932 (1978).
6. "An Evaluation of Two Theoretical Models for the Reorientation of Polar Symmetric Top Molecules," Evans, G. J. and Evans, M. W., *J. Chim. Phys.* **75**, 522 (1978).
7. "Static Dielectric Constants of the Liquified Fluoromethanes," Tremaine, P. and Robinson, M. G., *Can. J. Chem.* **51**, 1497–1503 (1973).
8. "Dielectric Relaxation in Symmetric Top Molecules at Radio Frequencies," Clark, R. and Bloom, M., *Can. J. Phys.* **51**, 149–152 (1973).

12.4.2.4 NMR Relaxation

1. "Anisotropy in Molecular Reorientational Motions in Simple Liquids," Griffiths, J. E., *Mol. Motions Liq., Proc. Ann. Meet. Soc. Chim. Phys., 25th, 1972*, 327–335 (1974).
2. "Nuclear Spin Relaxation Study of the Spin-Rotation Interaction in Symmetric Top Molecules," Armstrong, R. L. and Courtney, J. A., *Can. J. Phys.* **50**(12), 1262–1272 (1972).
3. "Nuclear Relaxation in Gaseous Methyl Fluoride and Fluoroform," Pausak, S. and Waugh, J. S., *J. Chem. Phys.* **61**, 2165–2166 (1974).
4. "^{13}C N.M.R. Spectroscopy. VIII. Aliphatic Hydrocarbon Derivatives," Miyajima, G. and Nishimoto, K., *Org. Magn. Reson.* **6**(6), 313–321 (1974).
5. "Role of Nuclear Spin Symmetry of Symmetric Top Molecules in Gas Phase N.M. Relaxation," Sanctuary, B. C., *Can. J. Phys.* **52**(5), 387–395 (1974).
6. "Critical Anomaly in the Proton Chemical Shift of Methyl Fluoride," Trappeniers, N. J. and Van Emden, F. W., *Chem. Phys. Lett.* **54**, 203–206 (1978).

12.4.2.5 Polarizability and Hyperpolarizability

1. "Kerr Constants, Depolarization Ratios, and Hyper-polarisabilities of Substituted Methanes," Burnham, A. K., Buxton, L. W., and Flygare, W. H., *J. Chem. Phys.* **67**, 49 (1977).
2. "Rayleigh Scattering Depolarisation Ratio and the Molecular Polarizability Anisotropy for Gases," Bogard, M. P., Buckingham, A. D., Pierens, R. K., and White, A. H., *J. Chem. Soc. Faraday Trans. I* **74**, 3008–3015 (1978). Also for methylene chloride.
3. "Atom–dipole Interaction Model for Molecular Polarizability. Application to Polyatomic Molecules and Determination of Atom Polarizabilities," Applequist, J., Carl, J. R., and Fund, K.-K., *J. Am. Chem. Soc.* **94**, 2952–2960 (1972).
4. "Molecular Second- and Third-order Polarizabilities from Measurements of Second-harmonic Generation in Gases," Ward, J. F. and Bigio, I. J., *Phys. Rev. A* **11**(1), 60–66 (1975).

5. "Tensor Autocorrelation Functions of the Polarisability of Some Polyatomic Molecules in the Gaseous State," Cattani, M., Ngyen, V. T., and Rossi, I., *Can. J. Phys.* **52**, 2321–2328 (1974).

12.4.2.6 Infrared Spectroscopy, Microwave Spectroscopy

1. "Pressure Induced Spectra of Axially Symmetric and Slightly Asymmetric Quadrupolar Molecules," Zwicker, J. O. and Cole, R. H., *J. Chem. Phys.* **60**, 4780–4789 (1974).
2. "Dipole Moment Derivatives and Infra-red Intensities. II. Polar Tensors in Methyl Halide Molecules," Newton, J. H. and Person, W. B., *J. Chem. Phys.* **64**, 3036–3049 (1976).
3. "Infra-red Absorption Spectra of Solid Fluoromethane," Blanchard, J., Brunel, L. C., and Peyron, M., *Chem. Phys. Lett.* **14**(4), 481–484 (1972).
4. "Infrared Absorption Intensities of Methane and Fluoromethanes," Saeki, S., Mizuno, M., and Kondo, S., *Spectrochim. Acta* **32A**, 403–413 (1976).
5. "Molecular Zeeman Effect in Methyl Fluoride," Norris, C. L., Pearson, E. F., and Flygare, W. H., *J. Chem. Phys.* **60**, 1758–1760 (1974).
6. "Molecular Constants of Some Axially Symmetric XYZ_3 Molecules," Thirungnanasambandam, P. and Karunanidhi, N., *Indian J. Phys.* **50**, 527–543 (1976).
7. "Determination of A_0 for Methyl Fluoride from Ground-State Combination Differences," Graner, G., *Mol. Phys.* **31**(6), 1833–1843 (1976).

12.4.2.7 Field Effects on Transport Properties

1. "The Viscomagnetic Effect in Polar Gases," van Ditzhuysen, P. G., Thijsse, B. J., van der Meij, L. K., Hermans, L. J. F., and F. Knaap, H. F. P., *Physica* **88A**, 53–87 (1977).
2. "Non-resonant Absorption/Senftleben–Beenakker Effect," Moraal, *Z. Naturforsch.*, **29**(2), 299–304 (1974).

12.4.3 Methyl Iodide

12.4.3.1 Infrared, Raman, and Light Scattering

1. "Vibrational Intensities. XV. Error Treatment and its Application to the Methyl Halides," Russell, J. W., Needham, C. D., and Overend, J., *J. Chem. Phys.* **45**(9), 3383–3398 (1966).
2. "Intensity Calculation for the Infrared Spectra of Methyl and Methylene Groups of Aliphatic Hydrocarbons," Higuchi, S., Tanaka, S., Kamada, H., *Nippon Kagaku Zasshi* **88**, 930–937 (1967).
3. "Infrared Dispersion in Methyl Iodide," Pratt, H. A. and King, W. T., *J. Chem. Phys.*, **47**, 3361–3365 (1967).
4. "Vibrational Anharmonicity in the Methyl Halides," Reichmann, S. and Overend, J., *J. Chem. Phys.* **48**, 3095–3102 (1968).
5. "Rotationlike Motion of Molecules in Liquids; Far Infrared Absorption of Polar Molecules in an Inert Solvent," Datta, P. and Barrow, G. M., *J. Chem. Phys.* **48**, 4662–4666 (1968).

6. "Linewidths of the Rotational Spectra of Symmetric-Top Molecules," Roberts, J. A., Tung, T. K., and Lin, C. C., *J. Chem. Phys.* **48**(9), 4046–4099 (1968).
7. "Solvent Effect on Half-width of Infrared Absorption Band," Tanaka, S. and Kamada, H., *Nippon Kagaku Zasshi* **89**(9), 849–852 (1968).
8. "Solvent Effect on the Infra-red Absorption Intensities of Methyl Iodide and Methyl Iodide-d_3," Higuchi, S., Tanaka, S., and Kamada, H., *Spectrochim. Acta* **24A**, 1929–1938 (1968).
9. "Raman Band Widths of the Carbon–Iodine Band Stretching Vibrations of Methyl Iodide in the Liquid Phase," Doege, G., *Z. Naturforsch., A*, **23**(9), 1405–1407 (1968).
10. "Calculation of Electrooptical Parameters and Absolute Intensities in the Infra-red Spectra of Halo-substituted Methane," Mokhnatkin, V. M. and Sverdlev, L. M., *Zh. Prikl. Spektrosk.*, **10**(2), 276–282 (1969).
11. "Molecular Constants of Some Tetrahedral XY_4-type Molecules and their Substituted Derivatives by Green's-function Analysis," Ramaswamy, K. and Ranganathan, V., *Indian J. Pure Appl. Phys.* **6**(12), 651–655 (1968).
12. "Dipole Correlation Functions from Infrared Transmission and Reflection Measurements: a Comparison on Methyl Iodide," Rothschild, W. G., *J. Chem. Phys.* **51**(11), 5187–5189 (1969).
13. "^{13}C Frequency Shifts and the General Harmonic Force Fields of Methyl Chloride, Bromide and Iodide," Duncan, J. L., Allan, A., and McKean, D. C., *Mol. Phys.*, **18**(3), 289–303 (1970).
14. "Raman Spectra of the Crystalline Methyl Halides," Brown, C. W. and Lippincott, E. R., *J. Chem. Phys.* **52**(2), 786–790 (1970).
15. "Direct Measurement of the Rotational Constant Ao of Methyl Iodide," Matsuura, H., Nakagawa, T., and Overend, J., *J. Chem. Phys.* **53**(6), 2540–2541 (1970).
16. "Molecular Motion in Liquids: Prevalence of Large-size Rotational and Translational Diffusion Steps," Rothschild, W. G., *J. Chem. Phys.* **53**(8), 3265–3271 (1970).
17. "Group Theory of Molecular Angular Autocorrelation Functions," Keller, B. and Kneubuehl, F., *Chem. Phys. Lett.* **9**(2), 178–180 (1971).
18. "Comparative Study of Liquid-Phase Orientation Motion from Raman Scattering and Dipolar Absorption Spectra," Constant, M. and Fauquembergue, R., *C. R. Acad. Sci. Ser. B*, **272**, 1293–1296 (1971).
19. "Indexes of Refraction, Susceptibilities and Correlation Functions," Fulton, R. L., *J. Chem. Phys.*, **55**, 1386–1394 (1971).
20. "Far-infrared Absorption of Some Organic Liquids," Walker, S. and Jain, S. R., *J. Chem. Phys.* **75**, 2942–2947 (1971).
21. "Equilibrium Geometries of the Methyl Halides," Duncan, J. L., *J. Mol. Struct.* **6**(6), 447–456 (1970).
22. "Empirical Force Field for Ethylene III. Application to some Methyl Halides, Methyl Cyanide, and Propane," Ramaswamy, K. and Devarajan, V., *Indian J. Pure Appl. Phys.* **9**(9), 700–702 (1971).

23. "Raman Study of Rotational Diffusion in Methyl Iodide," Griffiths, J. E., *Chem. Phys. Lett.* **21**(2), 354–356 (1973).
24. "Raman Scattering. Vibrational and Reorientational Motions in Liquid Methyl Iodide," Constant, M. and Fauquembergue, R., *Adv. Raman Spectrosc.* **1**, 413 (1972).
25. "Dideuteriomethyl Spectra and Fermi Resonance Effects in the Methyl and Trideuteriomethyl Stretching Regions. Symmetrical Methyl Groups," McKean, D. C., *Spectrochim. Acta* **29A**, 1559–1574 (1973).
26. "Determination of the Ao Rotational Constant for C_{3v} Molecules. ν_4 Raman Band of Methyl Iodide," Freedman, P. A. and Jones, W. J., *J. Chem. Soc. Faraday Trans.* II **71**, 650–653 (1975).
27. "Rotational Contributions to the Dipole-Moment Derivatives," van Straten, A. J. and Smit, W. M. A., *J. Mol. Spectrosc.*, **56**, 484–493 (1975).
28. "Infrared and Raman Studies of Rotational Correlation Functions in Liquids," Jones, D. R., Andersen, H. C., and Pecora, R., *Chem. Phys.* **9**(3), 339–358 (1975).
29. "CH-valance Vibrations in $X(CH_3)_4$(X = carbon, silicon, germanium, tin and lead) Compounds. Co-ordination and Fermi Resonance at ν_{13} and ν_{14}", Buerger, H. and Biedermann, S., *Spectrochim. Acta* **28**, 2283–2286 (1972).
30. "Raman Scattering. I Vibrational Correlation in Methyl Iodide," Constant, M. and Fauquembergue, R., *J. Chem. Phys.* **58**(9), 4030–4031 (1973).
31. "Exciton Splitting and Fermi Resonance in Solid Solutions," Lisitsa, M. P., Ralko, N. E., and Yarenko, A. M., *Phys. Lett.* **48A**, 241–243 (1974).
32. "Depolarized Rayleigh Light Scattering and Reorientation of Molecular Liquids under High Pressure," Claesson, S. and Jones, D. R., *Chem. Scr.* **9**(3), 103–109 (1976).
33. "Single Particle Reorientation and Pair Correlations of Methyl Iodide Solutions Studied by Depolarised Rayleigh and Raman Scattering," Cheung, C. K., Jones, D. R., and Wang, C. H., *J. Chem. Phys.* **64**, 3567–3572 (1976).
34. "Vibrational Energy Transfer in Methyl Iodide," Langsam, Y., Lee, S. M., and Ronn, A. M., *Chem. Phys.* **14**(3), 375–383 (1976).
35. "Raman Spectroscopic Studies on Temperature Dependence of Reorientational Motions of Methyl Iodide and Deuterated Methyl Iodide Molecules," Arndt, R., Moormann, R., and Schaeffer, A., *Mol. Motions Liq., Proc. Ann. Meet. Soc. Chim. Phys., 24th, 1972*, 217–224 (1974).
36. "Raman Spectroscopic Observation of Collective Excitation of Molecular Vibrations in Liquid Methyl Iodide," *ibid.*, 225–231.
37. "Potential Energy Distributions and Normal Co-ordinates of Methyl, Methyl-d_3 and Partially Deuterated Methyl Chloride, Bromide and Iodide," Whitmer, J. C. and Lewis, B. D., *J. Mol. Struct.* **24**(2), 317–324 (1975).
38. "Molecular Reorientation in Liquids by Rayleigh Scattering. Pressure Dependence of Rotational Correlation Functions," Dill, J. F., Litovitz, T. A., and Bucaro, J. A., *J. Chem. Phys.* **62**, 3839–3850 (1975).
39. "Examination of Two Theories for Absorption of Microwave and Far Infrared Radiation by Polar Liquids," Benson, M., Martin, G. D., Walker, J., Warren, J., and Wilson, R., *Can. J. Chem.* **50**, 2610–2616 (1972).

40. "Angular Time-Correlation Functions from Spectra for Some Molecular Liquids," van Konynenberg, P. and Steele, W. A., *J. Chem. Phys.* **56**, 4776–4787 (1972).

41. "Equilibrium Structure of Methyl Iodide," Matsuura, H. and Overend, J., *J. Chem. Phys.* **56**, 5725–5727 (1972).

42. "The ν_4 Band of Methyl Iodide," Connes, P., Pinard, J., Guelachivili, G., Maillard, J. P., Amiot, Cl., Grenier-Besson, M. L., Camy-Peyret, C., and Fland, J. M., *J. Phys. (Paris)* **33**, 77–84 (1972).

43. "Temperature Dependences of Half-band Widths of Infrared Absorption Bands," Higuchi, S., Tanaka, S., and Kamada, H., *Spectrochim. Acta* **28**, 1721–1730 (1972).

44. "Analysis of Orientational Broadening of Raman Line Shapes," Bartoli, F. J. and Litovitz, T. A., *J. Chem. Phys.* **56**, 404–412 (1972).

45. "Raman Scattering. Orientational Motions in Liquids," Bartoli, F. J. and Litovitz, T. A., *J. Chem. Phys.* **56**, 413–425 (1972).

46. "Reorientational Correlation Functions obtained from Raman Line Shapes," Johnson, E. F. and Drago, R. S., *J. Am. Chem. Soc.* **95**(5), 1391–1398 (1973).

47. "Raman Line Shapes in Liquid Methyl Iodide and Methyl-d_3 Iodide," Goldberg, H. and Pershan, P. S., *Adv. Raman Spectrosc.* **1**, 437–443 (1972).

48. "Raman Scattering. II. Orientational Motions in Methyl Iodide," Constant, M. and Fauquembergue, R., *J. Chem. Phys.* **58**(9), 4031–4033 (1973).

49. "Dielectric Relaxation of Rigid Solute Molecules in Benzene–Paraffin Solutions," Balogun, G. A., and Cumper, C. W. N., *J. Chem. Soc. Faraday Trans. II* **69**, 1172–1182 (1973).

50. "Temperature Dependent Raman Study of Molecular Motions and Interactions of Methyl Iodide in the Liquid Phase," Wright, R. B., Schwartz, M., and Wang, C. H., *J. Chem. Phys.* **58**, 5125–5134 (1973).

51. "Raman Line Shapes in Liquid Methyl Iodide and Methyl-d_3 Iodide," Goldberg, H. S. and Pershan, P. S., *J. Chem. Phys.* **58**(9), 3816–3827 (1973).

52. "Reorientation Broadening of the ν_4 Raman Band of Methyl Iodide in Liquid Phase," Doege, G. and Schaeffer, A., *Ber. Bunsenges. Phys. Chem.* **77**(9), 682–684 (1973).

53. "Density and Temperature Effects on the Molecular Reorientation and Vibrational Relaxation in Liquid Methyl Iodide," Campbell, J. H., Fisher, J. F., and Jonas, J., *J. Chem. Phys.* **61**(1), 346–360 (1974).

54. "Dephasing Processes of Molecular Vibrations in Liquids," Fischer, S. F. and Laubereau, A., *Chem. Phys. Lett.* **35**(1), 6–12 (1975).

55. "Solvent Effects in the Absolute Intensities of Infrared Absorption Bands and the Dipole–Dipole Interaction," Kakimoto, M. and Fukiyama, T., *Bull. Chem. Soc. Jap.* **48**(8), 2258–2263 (1975).

56. "Use of the Memory Function in the Interpretation of the Dipole Absorption Spectra of Symmetric Top Molecules in the Liquid Phase," Desplanques, P., Constant, E., and Fauquembergue, R., *Mol. Motions Liq. Proc. Ann. Meet. Soc. Chim. Phys. 24th, 1972*, 133–149 (1974).

57. "Dipole Moment Derivatives and Infra-red Intensities. II. Polar Tensors in Methyl Halide Molecules," Newton, J. H. and Person, W. B., *J. Chem. Phys.* **64**(7), 3036–3049 (1976).

58. "Infrared Band Shape of the Carbon–Iodine Stretching Vibration of Methyl Iodide in Solutions," Fujiwara, K., Fukushi, K., Ikawa, S., and Kimura, M., *Bull. Chem. Soc., Jap.* **48**(12), 3464–3469 (1975).

59. "Molecular Vibrational Excitations in Liquids. General Consideration of the Effect on Raman Band Profiles and Experimental Studies with Methyl Iodide," Doege, G., *Z. Naturforsch., Teil A*, **28**(6), 919–932 (1973).

60. "Raman Spectra and Crystal Structures of Methyl Halides," Takeuchi, H., Brikes, J. L., Harada, I., and Shimanouchi, T., *J. Raman Spectrosc.* **4**(3), 235–243 (1976).

61. "Vibrational Relaxation and Line-widths in Liquids: A Comparison of Theory and Experiment," Lynden-Bell, R. M. and Tabisz, G. C., *Chem. Phys. Lett.* **46**, 175–177 (1977).

62. "Vibrational Relaxation in Liquid Methyl Iodide. I. Comparison of the Three A_1 Vibrations," Doege, G., Arndt, R., and Khuen, A., *Chem. Phys.* **21**(1), 53–59 (1977).

63. "The Infrared Band Shapes of Methyl Iodide in Solution," Ikawa, S., Fukushi, K., Fujiwara, K., and Kimura, M., *Bull. Chem. Soc. Jap.* **50**(1), 60–64 (1977).

64. "An Atom–Dipole Interaction Model Study of the Molecular Second Hyperpolarisability of Selected Haloalkanes," Sundberg, K. P., *J. Chem. Phys.* **66**, 1475–1476 (1977).

65. "The Concentration Dependence of the Raman Intensity in Binary Mixtures and the Determination of Polarisability and Hyperpolarisability Derivative Tensors," Koike, J., Suzuki, T., and Fujiyama, T., *Bull. Chem. Soc. Jap.* **49**(10), 2724–2730 (1976).

66. "Infrared Band Intensities and Polar Tensors: Properties of Effective Charge ξ_α and its Relation to the Sign of Dipole Moment Derivatives," Prasad, P. L. and Singh, S., *J. Chem. Phys.* **66**(4), 1621–1630 (1977).

67. "Raman Spectral Studies on Vibrational Relaxation Functions using Overtone Bands," Arndt, R. and Yarwood, J., *Chem. Phys. Lett.* **45**(1), 155–157 (1977).

68. "Vibrational Energy Redistribution of Polyatomic Molecules in Liquids after Ultrashort Infrared Excitation," Spanner, K., Laubereau, A., and Kaiser, W., *Chem. Phys. Lett.* **44**, 88–92 (1976).

69. "Hyperpolarisabilities of Organic Molecules," Levine, B. F., *Dig. Tech. Pap.—Int. Quantum Electron Conf. 8th*, 21 (1974).

70. "The Influence of Reorientational Motions on Vibration Relaxation Functions in Liquids", Doege, G., *Proc. Int. Conf. Raman Spectrosc. 5th*, 372–373 (1976).

72. "Microwave Radii in Non-Resonant Spectra," Buffa, G. and Tarrini, O., *Phys. Rev.* **16A**, 1612–1616 (1977).

72. "Comment on 'A Comparison of the Rough Sphere Rotational Diffusion Model with Experimental Results for Liquid Methyl Iodide'," McClung, R. E. D., *J. Chem. Phys.* **67**(11), 5410–5411 (1977).

73. "Comparison of Depolarised Rayleigh–Wing Scattering and Far Infra-red Absorption in Molecular Liquids," Lund, P. A., Faurskov–Nielson, O., and Praestgaard, E., *Chem. Phys.* **28**, 167–173 (1978).

74. "Far Infrared Absorption Intensities and the Dipole Moments of Some Molecules in Solutions," Sato, K., Ohkubo, Y., Moritsu, T., Ikawa, S., and Kimura, M., *Bull. Chem. Soc. Jap.* **51**(9), 2493–2495 (1978).

75. "Method for the Adjustment of a Vibrational Potential Function to the Frequencies of Two Isotopic Derivatives," Nieto, J. L. and Herranz, J., *An. Quim.* **74**, 363–370 (1978).

76. "Vibrational Relaxation and Reorientation Correlation of the First Overtone of the Symmetric Carbon–Hydrogen Bending Vibration of Methyl Iodide in some Liquids," Doege, G. and Khuen, A., *J. Mol. Struct.* **45**, 101–106 (1978).

12.4.3.2 NMR Relaxation, etc.

1. "Empirical Correlation between NQR Frequencies and Infrared Absorption Data," Gerdil, R., *Nature* **212**, 922–923 (1966).

2. "Solvent Effects on ^{13}C—H Coupling Parameters and Chemical Shifts of Some Halomethanes," Watts, V. S. and Goldstein, J. H., *J. Phys. Chem.* **70**, 3887–3892 (1966).

3. "Effects of Excitation Energies on Nuclear Spin Coupling Constants," Saika, A., *J. Chem. Phys.* **45**(7), 2715–2716 (1966).

4. "Effects of Molecular Motions on the NQR Frequencies and Linewidths in Some Solid Alkyl Halides," Tadashi, T., *J. Chem. Phys.* **47**, 2353–2361 (1967).

5. "NMR Solvent Effects and Molecular Interactions," Kuntz, I. D. and Johnston, M. D., *J. Am. Chem. Soc.* **89**, 6008–6017 (1967).

6. "Chemical Shift Anisotropy in Liquid-Crystal Solvents. II. Theoretical Calculations for the Methyl Halides," Caesar, G. P. and Dailey, B. P., *J. Chem. Phys.* **50**(10), 4200–4204 (1969).

7. "Enhancement and Reversal of ^{13}C Resonances in Nuclear-Electron Double Resonance," Cannon, T. C., Richards, R. E., and Taylor, D., *J. Chem. Soc.* **1970**(8), 1180–1184.

8. "Dipolar Contributions to ^{13}C Relaxation Times," Grant, D. M., Lyerla, J. R., and Harris, R. K., *J. Phys. Chem.* **75**(4), 585–588 (1971).

9. "NMR Relaxation Time Studies in Liquid Methyl Iodide," Gillen, K. T., Schwartz, M., and Noggle, J. H., *Mol. Phys.* **20**(5), 899–912 (1971).

10. "Pressure Dependence of the Proton Relaxation Rate in Liquid Methyl Iodide and Acetonitrile at Several Temperatures," Franck, E. U., Hertz, H. G., and Raedles, C., *Z. Phys. Chem. (Frankfurt)* **73**(1–3), 18–28 (1970).

11. "^{13}C Spin–Rotational Relaxation in Methyl Iodide and Methyl Cyanide," Lyerla, J. R., Grant, D. M., and Wang, C. H., *J. Chem. Phys.* **55**(9), 4676–4677 (1971).

12. "NMR Proton Shifts of Polar Solutes," Weiner, P. H. and Malinowski, E. R., *J. Phys. Chem.* **75**, 3971–3975 (1971).

13. "Temperature-dependent ^{13}C Relaxation Studies of Small Molecules," Farmer, T. C., Druck, S. J., Shoup, R. R., and Becker, E. D., *J. Am. Chem. Soc.* **94**(3), 699–703 (1972).

14. "Spin–Echo Experiments on ^{13}C, D, ^{1}H, ^{19}F, in Some Small Molecules in the Liquid Phase," Haeberlen, U., Spiess, H. W., and Schweitzer, D., *J. Magn. Reson.* **6**(1), 39–54 (1972).

15. "Coefficient of Self-Diffusion in Liquids using Pulsed NMR Techniques," Sandhu, H. S., *J. Magn. Reson.* **17**(1), 34–40 (1975).

16. "Spin-lattice Relaxation Times of ^{13}C Satellites in Proton NMR Spectra and their use in Determining Molecular Rotational Diffusion Constants," Heatley, F., *J. Chem. Soc. Faraday Trans. II* **70**(1), 148–167 (1974).

17. "Proton Spin Relaxation in the Halomethanes," Brown, P. M., Krishna, N. R., and Gordon, S. L., *J. Magn. Reson.* **20**(3), 540–543 (1975).

18. "Intermolecular Field Interaction and Chemical Shift of Protons," Lutski, A. E. and Gordienko, V. G., *Zh. Fiz. Khim.* **51**(11), 2717–2721 (1977).

12.4.3.3 Neutron Scattering

1. "Molecular Dynamics Study by the Neutron Inelastic Scattering Method. II. Methyl Iodide," Janik, J. A., Janik, J. M., Bajorek, A., Parlinski, K., and Sudnik–Hoynkiewicz, M., *Physica* **35**(4), 451–456 (1967).

2. "Microdynamic Behaviour of Hydrogenous Liquids by Cross Section Measurements with Cold Neutrons," Fischer, C. O., *Phys. Lett.* **30**(7), 393–394 (1969).

3. *Thermal Neutron Scattering from Gaseous and Liquid Fluoromethane and Iodomethane*, Malm, W. C., 173 pp. (1972).

4. "Motions of Protons in CH–, CH_2–, CH_3–, and C_2H_5–Halides by Cold Neutron Transmission Experiments," Fischer, C. O., *Ber. Bunsenges. Phys. Chem.* **75**(3/4), 361–365 (1971).

12.4.3.4 Electrical Interactions

1. "Atom Dipole Interaction Model for Molecular Polarizability. Application to Polyatomic Molecules and Determination of Atom Polarizabilities," Applequist, J., Carl, J. R., and Fund, K. K., *J. Am. Chem. Soc.* **94**(9), 2952–2960 (1972).

2. "Molecular Multipole Moments Derived from Collisional Quenching of Atomic Hydrogen (2s)," Dose, V. and Semini, C., *Helv. Phys. Acta* **47**(6), 623–629 (1974).

3. "Molecular Orientational Relaxation Times in Liquids," Mouron, G. and Malley, M. M., *Opt. Commun.* **13**(4), 412–417 (1974).

4. "Orienting Polar Molecules in Molecular Beams. Symmetric Tops," Brooks, P. R., Jones, E. M., and Smith, K., *J. Chem. Phys.* **51**(7), 3073–3081 (1969).

5. "Absolute Signs of Hyperpolarizabilities in the Liquid State," Levine, B. F. and Bethea, C. G., *J. Chem. Phys.* **60**(10), 3856–3858 (1974).

6. "Second and Third Order Hyperpolarisabilities of Organic Molecules," Levine, B. F. and Bethea, C. G., *J. Chem. Phys.* **63**(6), 2666–2682 (1975).

7. "Molecular First Hyperpolarizabilities of Cyanomethane and Iodomethane," Battaglia, M. R. and Ritchie, G. L. D., *Mol. Phys.*, **31**(4), 1283–1286 (1976).

8. "Semiclassical theory of Collision-Induced Vibrational-Rotational Transitions. Application to Methyl Halides," Miklava, A. and Fischer, S. F., *J. Chem. Phys.* **69**(1), 281–287 (1978).

12.4.3.5 Ultrasonic Absorption

1. "Vibrational Relaxation in Liquids," Plass, K. G., *Ber. Bunsenges. Phys. Chem.* **74**(4), 343–347 (1970).

12.4.3.6 Crystal Properties

1. "Crystal Vibrations and Intermolecular Interactions of CH_3X and CD_3X (X = Cl, Br and I), "Takeuchi, H., Bribes, J.-L., Harada, I., and Shimanouchi, T., *Bull. Chem. Soc. Jap.* **49**(12), 3483–3492 (1976).
2. "Harmonic Frequencies of Vibration in Molecular Crystals. Anharmonic Vibrations and Inter-molecular Harmonic Potential. Methyl Iodide," Aubard, J. and Dumas, G. G., *C. R. Acad. Sci., Ser. B.*, **275**(12), 419–422 (1972).
3. "Crystal Structures of Methyl Bromide and Methyl Iodide," Kawaguchi, T., Hijikigawa, M., Hayafuji, Y., Ikeda, M., Fukushima, R., and Tomiie, Y., *Bull. Chem. Soc. Jap.* **46**(1), 53–56 (1973).

12.4.3.7 Review Article

1. "The Rotation of Molecules in Dense Phases," Steele, W. A., *Adv. Chem. Phys.* **34**, 1–104 (1976).

12.5 RESULTS OF LITERATURE SEARCH*

12.5.1 Methylene Chloride

A literature search of the relevant material on CH_2Cl_2(Freon 30) has revealed the following conclusions:

1. A great deal of infrared, acoustic, and NMR work has been carried out, as well as a smaller amount of Raman work.
2. The thermodynamics is fairly well covered, but there is a lack of virial coefficient data. There are no second dielectric virial coefficients in the literature.
3. There is a fairly large amount of intermolecular potential work, but it is difficult to say whether this will be sufficient to build a reliable potential for the simulations until these specialists begin their investigation during the course of the project.
4. There is a sparse amount of modern spectral work such as light scattering but the 0–THz region has been used in some papers as an entity for analysis (Chapter 4).

*References cited in this section are listed in the bibliography of Section 12.4 under the corresponding headings.

5. There is one available Kerr effect study. The polarizability of the molecule is known, but the anisotropy of polarizability less accurately so. However, some estimates are available for the effective charges on each atom which could be used to calculate a quadrupole.

A completely blank field spectroscopically seems to be that of the methylene chloride liquid under kilobars of applied pressure, first studied thermodynamically by Bridgman between 4 kbar (−46°C m.p.) and 30 kbar (157°C m.p.). These factors have influenced the choice of conditions. The kilobar pressures in pure methylene chloride liquid can be simulated, although to simulate methylene chloride in an ultraviscous or vitreous environment such as decalin or toluene-pyridine is probably outside present-day capability, especially because the molecular dynamic evolution is spread over at least 12 decades of frequency via the α, β, and γ dielectric loss peaks. Nevertheless this does not preclude spectroscopic study by near infrared, Raman, etc., and especially acoustic, NMR, and viscoelastic methods.

12.5.1.1 Infrared Spectroscopy

Key papers in this field have been published by van Woerkom et al., which emphasize the role of vibration/rotation mixing when discussing the correlation function associated with infrared band shapes. The influence of intermolecular vibrational relaxation due to intermolecular interactions depends on the reorientational behavior of the molecules. An a priori separation of the dipole moment into independent rotational and vibrational parts is not possible. The implications for various procedures used to correct Raman and infrared band shapes for vibrational relaxation are discussed in this paper and isotope dilution experiments carried out. Two more papers have appeared by these authors, using isotope dilution methods. The temperature-dependent isotopic dilution effect was explained by intermolecular transition dipole-transition dipole interactions modulated by molecular reorientation. From these papers it is clear that it is not valid to assess the orientational a.c.f. by simply factorizing it from the vibrational a.c.f.

There is one very recent paper from Karlsruhe (Buback et al., 1979) which deals with the effect of kilobar pressure on liquid methylene chloride, and this work could certainly be pursued with incisive results during the course of the project. It would be best to take the methylene chloride spectra over the complete infrared range, because extra information is often available from overtones and combination modes.

12.5.1.2 Raman Spectroscopy

Boldeskal et al. have measured the Al type Raman bands of the liquid in both V and H plane polarization during excitation by a He/Ne laser.

Contours of the anisotropic and isotropic Raman band components were obtained. The correlation functions of vibrational and orientational relaxation for the Al vibrational bands were calculated but there is no indication as to whether the vibration/rotation coupling is factorized or not.

Baranov et al. have recorded infrared and Raman spectra over a large interval of temperature in the solid, liquid, and gaseous states. The predominant role of dipole–dipole interaction in the condensed phase was confirmed by the magnitude of the frequency shifts in the gas to liquid phase transition. At temperatures much greater than the melting point the log of the antisymmetric line broadening due to Brownian motion was linearly related to $1/T$. The infrared or Raman work pursued during the course of the project will be of interest to establish the role of vibration/rotation coupling over the complete liquid range.

The effect of the internal field on Raman scattering cross sections has been studied by Nestor et al. The effect of the internal field (the increasing amplitude of incident Raman scattered radiation brought about by the dielectric nature of the liquid) on Raman scattering cross section was studied in this paper using liquid and gas phase Raman spectra. The cross section for each Raman band is greater for molecules in the liquid state due to the internal field effect. The Placzek polarizability theory may be applied to molecules in the liquid phase only when the internal field effect is included and when strong intermolecular association such as hydrogen bonding is absent.

12.5.1.3 Rayleigh and Brillouin Scattering, Ultrasound Relaxation

Van Konynenberg and Steele (Section 12.4.1.5, Ref. 4) have produced a study of CH_2Cl_2 by depolarized light scattering at one temperature. Collision-induced contributions are important at short times. The long time behavior of the correlation functions was compared with several models. Infrared vibration/rotation data were used to supplement the Rayleigh wing data, the former being corrected for refractive index variability, isotope splitting, and hot bands. Stokes and anti-Stokes intensities were measured to about 100 cm^{-1} shift.

Brillouin scattering measurements of vibrational relaxation have been made by Caloin et al. as a function of temperature and scattering angle (90° and backscattering). Experimental spectra were compared with the calculated ones by assuming a single or double relaxation of the vibrational specific heat. The observed vibrational relaxation was interpreted by assuming that energy transfer was produced in bimolecular collisions. This is not an interpretation that is based on molecular theory, but this is now possible by simulation of such correlation functions as the off-diagonal elements of the molecular stress tensor. The paper by Caloin covers a range of temperature, and it would be interesting to repeat the Brillouin scattering measurements at the same conditions as the hyper and ultrasonic experiments planned for the project as a whole. There are some 50 papers

available on acoustic studies in liquid methylene chloride. A laser-stimulated Brillouin scattering experiment at 4416 and 4765 Å was carried out by Gustafsson et al. The Brillouin scattering at 90° was obtained with an Ar ion laser and He/Cd laser and a pressure-scanned Fabry-Perot spectrometer. The hypersonic velocities of the thermal wave at 4.8–7.2 GHz were determined from the frequency shift between the Stokes and anti-Stokes lines. No hypersound dispersion was observed. The recent papers on sound dispersion in liquid methylene chloride can be briefly summarized as follows.

Ultra and hyperacoustic properties of methylene chloride in the region 0.2–3 GHz were carried out by Markhkamov et al. Scattering of the absorption coefficient occurs if sound is observed in methylene chloride in this region. Acoustic dispersion produces vibrational relaxation. Takagi et al. have recently observed considerable velocity dispersion in the range 60–700 MHz at 293°K. Relaxation strengths are described by using vibrational relaxation. Hypersonic velocity in methylene chloride was measured by Brillouin scattering. There was no dispersion between the frequency region 700 MHz and 1 GHz. The volume viscosity is much greater than three times the shear viscosity.

12.5.1.4 NMR Relaxation

There has been a great deal of work on NMR relaxations of various kinds in liquid methylene chloride, some of which covers a broad temperature range, but as Brier and Perry point out, the results between different groups are not directly comparable in the majority of instances. In this section one or two representative papers of the 1970s are briefly described in an attempt to define a little more clearly the course of future work in this field.

O'Reilly et al. cover the liquid from the freezing point to the normal boiling point (i.e., at 1 bar). Intramolecular ^{35}Cl, D, and ^{13}C relaxation rates were measured in methylene chloride from 178 to 310°K. Papers such as this are covered in the review by Brier and Perry. An important point of experimental information is provided by Homer et al. in that degassing of O_2 from CH_2Cl_2 with $Co(bipy)_3(ClO_4)_2$ (bipy = 2,2 bipyridyl) results in spin-lattice relaxation times of up to 7 sec longer than previously observed. Recently Sandhu has measured the spin-lattice relaxation time T_1 of protons and deuterons in oxygen-free samples of CH_2Cl_2–CD_2Cl_2 and CD_2Cl_2, respectively, over the temperature range from the melting point to the boiling point at 1 bar. The spin-rotation interaction makes no contribution and the rotational and translational contributions are 70 and 30% of the total relaxation rate. It is clear that in NMR the broadest range of temperature and pressure is relevant in the attempt to extract incisive molecular dynamic information. The simulation backup in the project will no doubt help to clarify the modeling problems that the NMR spectroscopists encounter in their work. These are typified in Sandhu's paper,

because apparently he finds no easy route to interpretation of the overall data. NMR studies up to 1 kbar of pressure will no doubt help to define these problems even more closely. The rotational correlation times in Sandhu's paper disagree with the values predicted by more than one model.

12.5.1.5 Far Infrared/Microwave (or 0–THz) Spectroscopy

During the 1970s papers have been produced that describe attempts to extend low frequency dielectric work to far infrared frequencies, and to interpret the complete band shape as an entity (by the Aberystwyth group). Using this method provides any modeling technique with a difficult challenge, as we have already seen. The analytical difficulties are more fully exposed when the spectroscopic work is extended to supercooled and vitreous solution of CH_2Cl_2 in, for example, decalin. Dielectric losses of a glassy solution of CH_2Cl_2 in decalin have been determined at kilohertz and terahertz frequencies at 107–148°K as discussed in Chapter 7. It is argued that in addition to the well-documented primary and secondary (α and β) losses in glasses and polymers, there exists in general a tertiary (γ) process at far infrared frequencies. This process is part of the dynamic evolution in a wide range of disordered solids. This initial research was subsequently followed by investigations aiming to characterize the (α, β, γ) loss triad over the 12 decades of frequency experimentally available. These show that the molecular dynamic evolution in methylene chloride under certain conditions is much more complicated than hitherto envisaged, because significant dynamic features are discernible on picosecond time scales (the far infrared) which evolve gradually into those occurring on immensely longer time scales (seconds and longer) in a "continuing metamorphosis." The whole process must in principle be describable by the orientational correlation function of the resultant dipole in the sample. This would require a conventional (but not semistochastic) molecular dynamics simulation (on present-day computers) lasting approximately 10^9 years! It is possible, however, to simulate the γ part of the overall loss, which appears in the far infrared and is measurable as a power absorption coefficient, $\mathfrak{A}(\omega)$. This in itself would be a major achievement of the molecular dynamics simulators.

12.5.1.6 Incoherent, Inelastic Neutron Scattering

As Brier and Perry point out in their review, there has been no attempt to derive or deduce detailed models for the translational or rotational dynamics of the asymmetric molecular dynamics associated with this molecule. The neutron scattering data obtained in their paper were on the INS time-of-flight instrument at the high flux beam reactor of ILL, Grenoble. Restrictions on the maximum rotor speeds meant that the full design resolution capability of this spectrometer was not available. As a compromise between energy resolution and momentum transfer requirements, the experiments were performed with an incident neutron energy of $E_0 = 1.236$ meV and an energy resolution of 4%. Scattering angles were 14–90°. There is scope for adding to all these variables in a new series of experiments. The experimental results were presented as efficiency-corrected neutron counts per second (scattered neutron flux) for the given sample dimensions and orientation, normalized to unit incident flux. Multiple scattering seems to be a practical difficulty with neutron scattering from liquids.

To describe the conclusions of the work we can do no better than quote Brier and Perry:

> The second half of the paper demonstrates the considerable difficulties of liquid dynamics investigation. Firstly, there is the problem of assembling reliable dynamical data for a given molecular liquid. Secondly there is the problem as to whether the available data are sufficiently varied and accurate to make a critical test of any model of the liquid dynamics. Thirdly there is the general problem of the lack of theoretical models particularly for the case of non-isotropic angular motion.
>
> In the case of CH_2Cl_2, the first problem of assembling and assessing available dynamical data has been fully discussed [in Chapter 6]. We conclude that, for different reasons, neither the infra-red nor the neutron scattering measurements provide reliable first order ($l = 1$) data for this molecule. The available n.m.r. ($l = 2$) data have required particularly careful consideration and some adjustments and corrections of the published data have been proposed. ... Our overall conclusion was that despite the numerous studies on CH_2Cl_2 no clear picture of the reorientational dynamics has yet emerged, even of a semi-quantitative nature. By no means can this be totally ascribed to the low symmetry of the CH_2Cl_2 molecule. Admittedly, with a true symmetric top molecule there is the considerable advantage of knowing 'a priori' that the reorientational motion about two of the principal axes is equivalent. Nevertheless, investigations of these systems are not without similar serious difficulties. The recent evaluation by Steele of the data for CH_3I, a liquid which has been extensively studied by many techniques, contains several cautionary statements concerning the presence of some serious unresolved problems in the interpretation of the correlation time data and that 'the correlation time data should be regarded as subject to revision when better methods of estimating non-rotational spectral intensities have been developed for non-spherical molecules.' Already since that review, it has been shown that correlated motions most probably do contribute to the depolarised Rayleigh scattering measurements, contrary to the earlier evidence.

It seems that the availability of molecular dynamics algorithms will ease the problem of interpretation encountered previously in neutron scattering *providing* realistic potentials are used in the simulations.

12.5.1.7 Vibrational Population Lifetimes of Polyatomic Molecules in Liquids

There is one paper, by Laubereau et al., on C–H stretching modes first excited by picosecond infrared pulses (Chapter 9). The generated excess population is monitored by anti-Stokes scattering of subsequent ultrashort

probe pulses. The observed time constants vary between 1 and 2 psec, depending on the individual molecule and surroundings. Theoretical calculations show rotational coupling, Fermi resonance, Coriolis coupling, and resonance energy transfer can strongly affect the vibrational population lifetime. Experimental data were reported on five molecules. The experimental results on methylene chloride are such that the anti-Stokes scattering signal decays rapidly at first, before turning to a much lower decay rate of approximately 40 ± 10 psec. The data points suggest the same result for different experimental conditions. With infrared radiation of 2985 and 3050 cm^{-1} both the ν_1 and ν_6CH stretching modes were excited using pulses of bandwidth $\Delta\nu = 30\ cm^{-1}$. The initial rapid decay of the measuring signal is explained with fast transfer between the neighboring C–H stretching modes, and the longer relaxation times as transition to overtones and combination modes of the molecule.

12.5.1.8 Pulsed High Field Dielectrics and Electrooptics

These techniques are still in the development stage but are potentially very revealing. We include among them the first attempts to define the extent of the Faraday and Kerr effects in the far infrared using carcinotron radiation and impulse methods. The results would be interpreted with a theory of nonlinear response for the rise and decay transients. It is expected that in analogy with such work on liquid crystals (or mesophases) the application of electric and magnetic fields to liquids monitored in the far infrared will result in information on collective effects rather than on individual molecular motion.

12.5.2 Methyl Fluoride

12.5.2.1 Infrared Spectroscopy and Raman Spectroscopy

A great number of papers have lately appeared which deal with laser induced processes such as infrared/microwave double resonance in gaseous methyl fluoride. Naturally these papers virtually all concentrate on the molecule in the gas phase and there are few available of relevant interest in the liquid state of methyl fluoride. There is, however, one by Brunel et al. that deals with the infrared and Raman spectra of solid methyl fluoride. The crystal structure is centrosymmetric, with four molecules in the unit cell. Infrared polar tensors and effective charges were evaluated by Prasad et al. The rotation/vibration constants of methyl fluoride have been evaluated by Arnondo et al. from the ν_3 band. Rotational constants are given by Harmony et al.

12.5.2.2 Far Infrared and Dielectric Spectroscopy

The work of Gerschel et al. (1976) on the liquid in this frequency region forms the basis of the conditions for methyl fluoride and is described briefly in this section and Chapter 6. The relative permittivity and far infrared absorption were used to evaluate angular correlations in methyl fluoride, avoiding the approximations inherent in dielectric theory. Static permittivities were evaluated in terms of the Kirkwood factor g. The data were compared with a derivation using Onsager's formula and Wertheim's mean spherical model solution. These results are supplemented to some extent by Tremaine et al., who measured the static permittivity ϵ_s in the liquid from the melting point to the boiling point. The deviation of the dielectric constants of the polar fluoromethanes from the values predicted from the Onsager equation cannot be fully due to nonspherical shape.

Gerschel et al. have produced a series of papers on the 0–THz spectroscopy of liquid methyl fluoride from the triple point to the critical point upon which the project conditions are based. Microwave relaxation times and far infrared spectra of methyl fluoride were determined over the complete liquid range beneath the critical point. On gradual approach of the dense gase-like situation from the expanded liquid the far infrared and microwave characteristic times converge. The occurrence of specific alignment effects caused local enhancement of dipole moments, as indicated by the refractive index of methyl fluoride along the bands, giving increased integrated intensities.

Bossis and Quentrec have used a hierarchy of memory functions (as in Chapter 3) to test the above results. Agreement is good along the coexistence line to the triple point. At low temperatures there is evidence of coupling of local orientational order to hydrodynamic modes. The conditions in one of the papers form the basis of the methyl fluoride projected conditions. Evans et al. used the Langevin equation for the symmetrical top to describe the far infrared/dielectric data of Gerschel et al. An inertia-corrected Langevin equation used with no further refinement fails qualitatively to explain the short time details of the reorientational process.

12.5.2.3 NMR Relaxation Spectroscopy

Again there has been a great deal of coverage of the gaseous state by NMR spectroscopy. Armstrong has measured the spin-lattice relaxation times at room temperature from 0.03 to 10 amagat. Values were derived of the effective spin-rotation constant and cross section for molecular reorientation. Pausak et al. have determined the density dependence of the spin-rotation relaxation time of $^1H_1$ and Miyagima et al. have measured the ^{13}C NMR spectrum. Some NMR work has also been carried out in liquid crystal solvents which partially order the molecule. Burnell et al. find that CH_3F is rapidly exchanging between at least two sites which have slightly different geometries and orientational parameters of different sign.

It is clear that not much is available on NMR relaxation in liquid, as opposed to gaseous, methyl fluoride, and experiments at the conditions defined by Gerschel would be interesting and revealing.

12.5.2.4 Brillouin and Ultrasonic Relaxation

There is little information available about these in methyl fluoride and work completed during the course of the project would be original.

12.5.2.5 Thermal Neutron Scattering

There is a thesis available on microfilm by W. C. Malm (Section 12.4.2.1, Ref. 1). The work is summarized in another paper (see Section 12.4). In the latter a small amount of data is presented for the methyl halides, including CH_3F and CH_3I. Time-of-flight spectra were measured at 22°C (CH_3F) and 50°C (CH_3I), and compared with the Gaussian formalism of Agarwal and Yip. This means of course that only the gas phase spectrum is given for CH_3F and for CH_3I. High purity samples were used and contained in a thin-walled (0.075 cm) cylindrical aluminum holder 6 in. in diameter. The scattering experiments were carried out using a cold neutron time-of-flight spectrometer in which the full cold spectrum transmitted by a refrigerated beryllium filter is incident on the sample and the analysis of the scattered beam is accomplished using a pulse modulator. All the data were taken at a scattering angle of 27° using a chopper speed of 5000 rpm. Under these conditions the time resolution of the instrument varies from 1% at 4 Å to 2.5% at 1 Å. This corresponds to an energy resolution of 2% at 5 meV to 5% at 85 meV. However, these values must be modified due to the energy spread in the incident beam. In practice this was taken into account by folding all calculated cross sections with the measured incident spectrum before comparing with experiment. The spectra were corrected for background, detector efficiency, air and aluminum absorption in the scattered beam, and modulator transmission. The authors state that the inclusion of multiple scattering corrections, which tend to increase inelastic scattering while decreasing elastic contributions, would further improve the agreement. Practically the only conclusion from this work is that the Agarwal/Yip formalism describes reasonably well the observed differential scattering cross section from CH_3F gas (or CH_3I vapor at 50°C). A non-Gaussian correction gives only slight improvement.

12.5.2.6 Kerr Effect, Polarizability Anisotropy, and Birefringence

There have been very recent measurements of the Rayleigh scattering depolarization ratios and molecular polarizability anisotropy for the gas at 488, 514.5, and 632.8 nm by Buckingham et al. The hyperpolarizability term in methyl fluoride is significantly large. An atom-dipole interaction study of the molecular second hyperpolarizability has been carried out by Sundberg. The theoretical and experimental second hyperpolarizabilities agree to within 15%. Beenakker et al. have considered gradients in the stream velocity of a gas consisting of optically anisotropic molecules which give rise to an alignment of rotational angular momenta, observable as a birefringence. Comparison was made with data from light scattering and the Senftlebeen–Beenakker effect. It is clear that measurements on the dynamic Kerr effect will be revealing at all frequencies, especially when carried out with carcinotron apparatus in the far infrared. If methyl fluoride were to be dissolved in a viscous or glassy environment it is probable that the relaxational features observable in electric permittivity experiments on the α and β processes could also be observable by birefringence. The far infrared Faraday effect at the preset conditions would also prove revealing as regards collective behavior, especially if the order of magnitude of the increment in the power absorption coefficient is larger than expected on the basis of classical theory. There have been no measurements to date of nonlinear (high field) dielectric increments or transients.

12.5.2.7 Thermodynamics

The choice of methyl fluoride as a species for coordinated study is significantly supported by the amount of information available about the intermolecular potential function. The dielectric and pressure second virial coefficients were reported by Copeland and Cole from 273 to 417°K. These data were reproduced to 5% or better with a model pair potential that incorporated the following:

1. A Lennard–Jones (12,6) central-force potential from viscosity data of Casparian and Cole.
2. Electrostatic interactions described in terms of the permanent dipole moment (μ), quadrupole moment (Q), and average polarizability (α) and effects due to the anisotropy of repulsive forces in terms of the Buckingham–Pople shape factor (D). Optimum values (for CH_3F) $\epsilon/k = 199$°K; $\sigma = 3.80$ Å; $\mu = 1.85$ D; $\alpha = 2.97 \times 10^{-24}$ cm^3; $Q = 2.3 \times 10^{-26}$ e.s.u.; $D = 0.25$. These parameters are useful for any future attempt to produce a satisfactory potential for simulation purposes.

Singh and Singh have studied second and third virial coefficients using a preaveraged pair potential model which includes a dipole repulsion term. The dipole dispersion and repulsion three-body nonadditive interactions were taken into account in evaluating the third virial coefficient. A large number of sets of force parameters were found and all reproduce the second virial data with equal consistency and accuracy. Using these parameters the third virial coefficient was calculated. The values of the third are different for different sets of parameters. A comparison of the experimental and calculated values of the third virial therefore leads to a unique set of force parameters for an assumed potential model. For methyl fluoride a set of force parameters was found which gives good agreement between theory and experiment. Transport properties such as viscosity and thermal conductivity are also well known for methyl fluoride. For example, Casparian and Cole have described a method in which capillary flow is

measured by the decay of the capacitance difference of gases in two reservoirs connected to the ends of the capillary. The viscosity is determined from the time constant in the temperature range 20–150°C. The parameters for the Lennard–Jones (12,6) intermolecular potential were derived by using the theory of Monchik and Mason. These parameters give a much better description of the central force than those from pressure virial coefficients.

There is therefore plenty of evidence for constructing reliable intermolecular potential in simulations of methyl fluoride. Work is already in progress in this field by Finney et al., using the unique multibody algorithm developed initially for water. Nonadditive effects are clearly important in the results already obtained by this group, and dynamic work is planned jointly with the Aberystwyth group. There is scope also for attempting to simulate subtle effects of external fields on transport properties. In conclusion:

1. There is surprisingly little dynamic work available for liquid methyl fluoride as opposed to the gas. The only work of the any note in the dielectrics/far infrared field, for example, is that of Gerschel and co-workers on which the project conditions are based.
2. There are no literature data of any kind on kilobar pressure work on methyl fluoride. It would therefore be interesting for one or two laboratories to measure the solidification temperatures of liquid methyl fluoride at a set of kilobar pressures, which for convenience should be those for methylene chloride: 5, 10, 15, 20, 25, and 30 kbar. The methyl fluoride liquid can of course be simulated under kilobar conditions and the solidification points predicted in advance. It would be interesting to see how well these agree with the measured solidification points when these are eventually available.

12.5.3 Methyl Iodide

Overall there has been a great deal of spectroscopic (Chapter 6) and other work on this liquid (and gas), and following is a list of key papers.

12.5.3.1 Infrared and Raman Spectroscopy/Rayleigh Scattering

There have been several papers on Raman measurements combined with those on Rayleigh scattering. There is a review by Griffiths which gives a complete list of all the data available on going to press. This deals with Raman, infrared, and nmr dynamics studies. Both temperature and pressure ranges have been covered in the Raman and Rayleigh methods (e.g., Campbell et al.) The consistency problem has already been discussed by Steele.

Dill et al. have provided Rayleigh scattering data from 1 to 2500 bar. The reduced $\langle \tau_2 \rangle^*$ changes from 1.9 to 3.8 on raising the pressure from 1 bar to 2.5 kbar. This type of work is exemplified by Cheung et al., who also use the technique in combination with Raman scattering to evaluate what is taken conventionally as the relation between single particle and multiparticle correlation functions. The Rayleigh time in these papers is measured as a function of concentration in isopentane-CCl_4.

Patterson and Griffiths have used this method with temperature variation. This paper is useful for its wide range of data over a wide range of temperature. Correlation factors are evaluated. A series of very recent papers by Yarwood and Döge et al. has appeared or is in press. One particularly interesting paper has appeared which shows how extra information can be obtained from Raman overtones.

Collision-induced absorption or scattering is not usually given enough attention if any at all. With methyl iodide this is potentially much more important than with methyl fluoride or methylene chloride, and this is clearly seen in the far infrared. The above interpretations rarely take enough account of this phenomenon, which gives the project an opportunity to redress matters by using the molecular dynamics algorithms in combination with polarizability effects and without them. The analytical task of separating the effects of permanent dipolar absorption from those of the impermanent (induced) dipole is beyond the capability of present-day methods without heavily relying on phenomenological variables.

12.5.3.2 Far Infrared/Microwave Spectroscopy

The proper interpretation of these data requires a sufficient awareness of the extent of induced dipolar effects, which is unknown at present. It can nevertheless be estimated by correlation with other data and by an experiment along the coexistence line at the present conditions, following the precedent of Blaise (1972) with nitrous oxide. The induced absorption can in principle be used to give very subtle hints as to how the molecular interaction evolves with time (e.g., Chapter 11). Only molecular dynamics algorithms which take account of molecular polarizability can in principle be used to simulate collision-induced spectra. Any interpretation of infrared, Raman, Rayleigh, or 0–THz spectra which discards this phenomenon should in turn be discarded.

12.5.3.3 NMR Spectroscopy

Grant et al. have evaluated ^{13}C relaxation times and spin-lattice relaxation times (T_1). Nuclear Overhauser effect data were obtained. The molecular nuclear Overhauser factor T_1 for ^{13}C was calculated. For complete analysis the T_1 and η values of more than one magnetic nucleus in the molecule are required.

Sandhu has measured the coefficient of self-diffusion in oxygen-free samples of liquid methyl iodide using a pulsed NMR technique. The results show that D is temperature dependent and logarithmic in $1/T$ for each liquid. The experimental value agree with the Stokes–Einstein relation,

modified to include the microviscosity factor for translational motion introduced by Gierer and Wirtz. The significant structure theory of liquids developed by Eyring and Ree also gives reasonable agreement.

Heatley has developed a method for ^{13}C relaxation for both methyl iodide and methylene chloride. The relaxations were exponential with an effective time which depended on the ^{13}C relaxation probabilities as well as on the proton relaxation mechanism. Inter and intramolecular and spin-rotation contributions to the proton relaxation were determined. Molecular rotational diffusion constants were also calculated.

12.5.3.4 Neutron Scattering

This is covered in the thesis by Malm described for methyl fluoride.

Fischer has measured the neutron scattering cross section (in barn/proton) for methyl iodide. This increases with increase in neutron wavelength in the range 4–17 Å. The cross section for methyl iodide at 17 Å is 254 barn/proton and the slope (in barn/Å) of σ versus neutron wavelength is 13.9. The latter is related to rotational barriers and decreases smoothly with increase of the NMR rotational relaxation times. The neutron method shows some advantages for the separation of internal molecular rotations from reorientations of the whole molecule.

A molecular dynamics study by the neutron inelastic scattering method has been made by Janik et al. The lattice molecular dynamics of solid and liquid methyl iodide were studied by the inelastic neutron scattering method. The spectrum obtained for solid methyl iodide was caused by lattice vibrations (wave number region below $\sim 120\,cm^{-1}$) and by intramolecular vibrations of the methyl iodide molecules (above $\sim 500\,cm^{-1}$). Peaks obtained in the intermediate region were higher harmonics of the torsional vibrations. The spectrum obtained for liquid methyl iodide was regarded as proof of the freedom of translational motions in the liquid phase.

12.6 INTERCOMPARISON OF EXPERIMENTAL DATA

The methods used to compare the insights of certain spectroscopies in order to obtain a coherent aspect of the liquid state involve the intercomparison of correlation functions. There are several articles in the literature which deal with this, notably the Berne and Harp review of 1970. It has become clear, however, that in their enthusiasm to make one analytical model do for several spectroscopies, some authors in this field have overlooked the several assumptions involved in reducing what is actually observed (say, by dielectric and far infrared spectroscopy) to accessible *auto*correlation functions. In this section we review these assumptions for each of half a dozen of the project spectroscopies and indicate how the growing power and speed of computer simulation can be used to build a more realistic criterion of intercomparison of observable correlation functions.

12.6.1 Dielectric and Far Infrared (or 0–THz) Spectroscopy

The analytical theory of dielectric polarization and relaxation runs into the difficulties caused by the shape of the cavity taken for consideration. These are discussed in Chapter 3, where, we recall, the relation of the macroscopic dipole moment a.c.f. $\langle \mathbf{M}(t) \cdot \mathbf{M}(0) \rangle$ to the dipole a.c.f. $\langle \boldsymbol{\mu}(t) \cdot \boldsymbol{\mu}(0) \rangle$ involves consideration of the displacement and orientational polarization, together with that of dipole–dipole interaction. Most analytical theories are constructed for $\langle \boldsymbol{\mu}(t) \cdot \boldsymbol{\mu}(0) \rangle$, but the fact remains that only $\langle \mathbf{M}(t) \cdot \mathbf{M}(0) \rangle$ is the usual observable. The relation between polarizability $\alpha(\omega)$ and the complex permittivity $\epsilon(\omega)$ is not independent of several assumptions usually involving cavities.

An important aim of the project would be to use molecular dynamics algorithms to *assume* well-defined mechanisms of molecular interaction and to calculate the four correlation functions:

$$C_{\mathbf{M}}(t) = \langle \mathbf{M}(t) \cdot \mathbf{M}(0) \rangle; \qquad C_{\boldsymbol{\mu}}(t) = \langle \boldsymbol{\mu}(t) \cdot \boldsymbol{\mu}(0) \rangle;$$

$$C_{\dot{\mathbf{M}}}(t) = \langle \dot{\mathbf{M}}(t) \cdot \dot{\mathbf{M}}(0) \rangle; \qquad C_{\dot{\boldsymbol{\mu}}}(t) = \langle \dot{\boldsymbol{\mu}}(t) \cdot \dot{\boldsymbol{\mu}}(0) \rangle$$

the latter two being related to Fourier transforms of the far infrared spectrum. The macro-micro correlation theorems in the literature can therefore be tested directly. For example, Madden and Kivelson (1975, Chapter 3) state that if $\langle \boldsymbol{\mu}(t) \cdot \boldsymbol{\mu}(0) \rangle$ is a sum of complex exponentials, then so is $\langle \mathbf{M}(t) \cdot \mathbf{M}(0) \rangle$. Brot et al. (Chapter 3 appendix) have recently tested directly the Fatuzzo–Mason theory using molecular dynamics. The aim of the project is to produce experimental far infrared/dielectric data over a wide range of liquid density and temperature which will be the common denominator, or reference set, for specific kinds of simulation, each simulation dealing with specific aspects of the complete dielectric problem.

For example, Bellemans et al. (Chapter 3) have used the molecular dynamics method to isolate the effect of dipole–dipole interaction on the dielectric response function by simulating weakly interacting dipoles on a rigid lattice. The approach to equilibrium of an assembly of dipoles on a lattice is a direct case of application for the fluctuation–dissipation theorem. The first point that emerges is that a weak interaction involving two dipoles only cannot drive the system to equilibrium. This may be shown analytically using the Prigogine formalism. The time equilibrium state is attained by means of processes involving at least three interacting dipoles. This illustrates the difficulty of using analytical theories with only pairs of interacting dipoles. The molecular dynamics simulations in two dimensions of Kohler and Bellemans (Chapter 3) corroborate this point. The same type of molecular dynamics simulation may be used to obtain the

following information concerning the dielectric response function:

1. The form of the dielectric response function is strongly related to the nature of the orientational interactions between the molecules.
2. If this interaction is purely dipolar in nature the response function is not very different from its limiting form at zero coupling (free rotation) even if the dipolar interaction is quite strong.
3. The long range part of the dipolar interactions seems to play a very limited role in the response function.

These conclusions were reached in the simulation (Chapter 3) by Bellemans et al. of the total moment $\mathbf{M}(t)$ of dipoles located in a plane on the sites of a rigid square lattice involving 101, 193, and 421 entities, respectively. In this simulation the usual central forces (van der Waals) do not appear in the Hamiltonian since the molecules are translationally fixed. In the simulation the correlation function $C_M(t)$ was calculated using time averages and not phase space averages, that is, by assuming that the system is ergodic. The error caused by this is of the order N^{-1} where N is the number of molecules (i.e., the difference between the microcanonical and canonical ensembles). Starting from randomly oriented dipoles with random angular momenta, correlations grow within the system so that its potential energy becomes slightly negative with respect to the start level. The simulated dipole–dipole interactions are not capable of producing an exponentially decaying response function; instead they have a tendency to make it oscillate.

The far infrared region is rich in information concerning interactions. The most extreme case is that of water (Chapter 3) and in liquids where electrostatic forces are relatively important, such as methyl fluoride and methylene chloride, there is a large shift away on dilution from the neat liquid value of the far infrared power absorption coefficient. The anisotropy of the total intermolecular potential strongly depends on the contributions of multipole–multipole interactions. Another sign of electrostatic influence is a weak density dependence of the torques, coming from the fact that the dipole interactions are long range, and not sensitive in consequence to the mean intermolecular separation. Experimental measurements of the molecular mean square torque provide, therefore, a direct and unambiguous measure of the strength of angle-dependent intermolecular forces, and nowhere is this more evident than in the far infrared, which provides a sensitive means of evaluating the type of intermolecular interaction taken as suitable for a molecular dynamics simulation. To obtain unambiguous information on the mean square torque the relationship between $C_M(t)$ and the a.c.f. and between $C_M(t)$ and the observables in 0–THz spectroscopy $\mathfrak{A}(\omega)$, the power absorption coefficient, and $\epsilon''(\omega)$, the loss, must be defined unambiguously.

Gerschel et al. have put the problem of the internal field, or cavity theory complications, into the far infrared context. In Chapter 3 we illustrated one of these corrections for the intensely dipolar liquid fluoroform. The corresponding correlation functions are also shown there. Despite the fact that there is a considerable amplitude of dispersion and absorption in these compounds there is little appreciable difference between the cavity corrections used by Gerschel et al. What follows is therefore designed to produce correlation functions microscopically by computer simulation using various forms of intermolecular interaction. The problem of relating these to the polarization and then to the observables enters at a later stage.

1. A simulation for the four correlation functions mentioned above should be carried out using only dipole interactions in three dimensions, extending the work of Kohler and Bellemans to the methyl fluoride, methyl iodide, and methylene chloride dipoles. This would isolate the dipole–dipole contribution to the far infrared spectrum, and the dependence of the far infrared spectrum on the dipole–dipole strength. In this and following simulations the simplest kind of procedure should be used to relate the calculable response function to the power absorption coefficient. We suggest the Lorenz–Lorentz procedure or more, accurately, that developed by Gerschel et al. specifically for the far infrared.
2. The second simulation is intended to look at the far infrared/dielectric region with purely atom–atom interactions, pairwise additive. It is particularly important to see whether this kind of 5×5 (or 3×3) atom–atom interaction can reproduce the major features of 0–THz spectra along, for example, the gas–liquid coexistence curves, where the far infrared peak shifts considerably in frequency.
3. Several algorithms are available that can be adapted easily for methylene chloride simulations using charge–charge interactions along the lines of Rahman and Stillinger (Chapter 3) for water. These are apparently fairly successful for simulating the spectral data for water, but probably their limitations have not yet been exposed by a joint spectroscopic effort. The Rahman–Stillinger algorithm would probably fail to describe the far infrared spectrum of water even in the most qualitative manner because of the two-body interaction assumption built into the algorithms.
4. The restriction of pairwise additivity can be lifted (Finney et al., 1978) by using polarizibility considerations that might also allow the simulation of collision-induced absorption to be carried out on a nonpairwise basis, which is clearly the case experimentally; the cross sections of infrared and far infrared induced absorptions cease to vary as the square of the molecular number density as the liquid densities are approached. Strong evidence for multibody effects have

been found in liquid methyl fluoride using this simulation algorithm.

5. It is clear that the simulation of collision-induced absorption cannot proceed without the inclusion of molecular polarizability.
6. A "hybrid potential" consisting of atom–atom interactions + multipole–multipole forces could be used to evaluate the extra effect of electrostatic forces on the 0–THz spectrum.
7. In some cases the effect of removal of boundary conditions could be evaluated (Chapter 3 appendix).
8. Semistochastic methods and nonequilibrium molecular dynamics (1980, CECAM workshop, Orsay, Paris) should be used whenever possible to save computer time when evaluating $\langle \mathbf{M}(t) \cdot \mathbf{M}(0) \rangle$ with complicated intermolecular potentials.

The microscopic response functions or correlation functions from all these techniques should be compared in both time and frequency domains before introducing macroscopic cavity theories of any kind to relate the orientational correlation functions to loss and power absorption coefficient. Brot has discussed the relation in detail (1975).

Finally in this section, it is important that the simulators produce the angular velocity a.c.f. to provide analytical theoreticians with a reference set of results for testing ways of relating this a.c.f. to the orientational a.c.f. for the symmetrical and asymmetric tops in three-dimensional space. This particular analytical problem is one of the most difficult ones confronting theoreticians involved in the Langevin and Fokker–Planck approach to molecular motion in the condensed phases of matter.

12.6.2 Infrared Band Shapes

Sections 12.4 and 12.5 list the papers of interest in this field for methylene chloride, methyl fluoride, and methyl iodide. Clearly the main problem that emerges is that of rotovibrational relaxation as emphasized in Chapter 6.

Lynden-Bell has given a convenient general formalism for expressing the line shape from any experiment as a function of angular frequency ω. This is the real part of

$$I(\omega) = \{S|[-i(L-\omega)-K]^{-1}|S\}$$

where S is the operator corresponding to the observation of the vibrational system and L and K are superoperators describing the propagation and relaxation of the system. S depends on experiment; in infrared absorption the observed quantity is the total electric moment of the sample induced by the electromagnetic field; for Raman scattering it is the total induced electric moment, which, at each point, is proportional to the isotropic or anisotropic parts of the molecular polarizability (VH scattering measures the anisotropic part; VV–$\frac{3}{4}$VH the isotropic part). In each experiment, S is

a sum over all the molecules in the system:

$$S = \sum_{n,b} \exp(i\mathbf{k} \cdot \mathbf{r}_n) \mathscr{D}^{(\lambda)}_{aa}(\Omega_n) S^{(\lambda)}_b(n)$$

where molecule n is at $\mathbf{r}_n$ with axes related by Euler angles Ω_n to the laboratory frame. $S^{(\lambda)}_b$ is the value of the (λ, b) spherical component of the transition moment (or polarizability) referred to molecular axes. These types of equations also describe the loose coupling of spin systems to a thermal bath and are derived using time-dependent perturbation theory.

The vibrational dephasing relaxation time T_2 is expressed by Lynden-Bell as

$$T_2^{-1} = \sum_{l,i} \int_0^\infty \langle A^*_{lj}(0) A_{ij}(t) \rangle_j \, dt$$

which is averaged over all molecules j, and which depends on both three particle ($l \neq i$) and two-particle ($l = i$) correlations.

A is a matrix designed by Lynden-Bell to take into account contributions to vibrational relaxations from such intermolecular sources as dipole–dipole interaction and isotropic dispersion.

An important result is that *even excluding reorientational effects*, the vibrational widths of the isotropic and anisotropic scattering may differ.

In arriving at the results, Lynden-Bell produces an interesting remark on the interaction of vibrations with intermolecular forces. The principal contributions to intermolecular forces are (*a*) very short range repulsive overlap; (*b*) van der Waals or dispersive forces; (*c*) multipole forces (which we have previously termed electrostatic) exemplified by dipole–dipole interaction. All these can be expressed in the following form for the energy of interaction between two molecules (1 and 2);

$$U_{12} = \sum_\gamma F_\gamma R_\gamma(r_{12}) \left[\sum_{m_1 m_2} \begin{pmatrix} L & l_1 & l_2 \\ M & m_1 & m_2 \end{pmatrix} \mathscr{D}^{(l_1)}_{\nu_1 m_1}(\Omega_1) \mathscr{D}^{(l_2)}_{\nu_2 m_2}(\Omega_2) \mathscr{D}^{L}_{0M}(\Omega, r) \right]$$

where the Wigner rotation matrix elements (Chapter 2 appendix) relate the angles of molecules 1, 2 and the intermolecular vector $\mathbf{r}$ to the laboratory frame, respectively, R is a function of the intermolecular separation r only, and F_γ is a property of the pair of molecules, independent of their separation and transforming like spherical tensors. γ enumerates the interaction. For dipole–dipole interaction F is the product of the molecular dipole moments and R is proportional to r^{-3}. Coupling of the vibrational system to the bath of translational degrees of freedom occurs because these F's vary with nuclear displacements. Changing the density of the liquid by kilobars of pressure effects the time correlation functions of the relative molecular position, but not the F operators. Within the assumptions of slow molecular reorientation and independent translational

diffusion and correlation times for the intermolecular potentials are inversely proportional to the translational diffusion constant D. If three-body correlations are neglected the line width is inversely proportional to the number density of oscillators. Therefore, whichever terms in the intermolecular potential cause the coupling of the vibrational system to the bath, the vibrational line width and dephasing time should decrease slowly with temperature at constant density and increase rapidly with density. The temperature and pressure effects should be the same for all normal modes of the same molecule.

In real liquids three-body correlations may be important. The simulation by Finney et al. (1978) has already shown that non-pair additivity is important in methyl fluoride. According to Lynden-Bell such contributions give a term in the line width proportional to density squared. If the molecules are not taken merely as hard spheres, the effective distance of closest approach decreases with temperature.

There are symmetry restrictions on the terms in the intermolecular potential which can provide relaxation pathways. There are cross terms in the symmetrical Raman scattering between self and exchange contribution which may be either positive or negative. The relative importance of the various contributions and the total line width depend on the particular normal mode being excited. Considering the methyl halides, the C—X (X = F or I) stretch affects both the polarizability and the dipole moment to a considerable extent so that intermolecular contributions from both dispersion and dipolar interactions should appear, giving a comparatively large vibrational line width compared with the symmetrical C—H stretch. Since the partial charges on the atoms must decrease to zero as the bonds dissociate and the dipole–dipole cross term is negative. Therefore, if dipolar relaxation dominates and self and exchange terms are comparable, the symmetrical Raman spectrum of the methyl halide stretches may be narrower than the corresponding depolarized Raman line spectrum, even in *the absence of vibration/rotation coupling.* If dispersion relaxation dominates, the reverse is likely to be true.

Lynden-Bell also predicts the change in line width on isotropic substitution, provided that the normal mode analysis is unaltered by the mass charge. Assuming negligible changes in the molecular dynamics and intermolecular potentials, isotropic dilution should change the line width by a factor proportional *to the square of the ratio of the reduced masses.*

Energy exchange occurs to a significant extent only between molecules whose normal modes have frequencies which differ by less than $(2\pi\tau)^{-1}$, where τ is the correlation time for the fluctuations causing relaxation. In consequence, dilution with an isotopically substituted molecule reduces the exchange terms without significantly altering the self terms (defined by Lynden-Bell's analysis) or the correlation times. All spectra except the symmetrical scattering should narrow and have longer relaxation times; the symmetrical scattering may broaden or narrow according to the sign of the cross term and should reach the same width as the anisotropic spectra on dilution. In each case the width should vary linearly with the mole fraction of the substance.

Dilution with other molecules alters the dynamics and may introduce new relaxation pathways. A solvent (such as carbon tetrachloride) with no dipole moment and low polarizability and viscosity leads to longer dephasing time, whereas a polar solvent with high viscosity increases the line widths.

In vibrational spectroscopy of liquids overtone and combination bands are seen. Lynden-Bell points out that the symmetry restrictions on the various mechanisms are the same for the overtone as for the fundamental. Combination modes have a line width which is the sum of the self line widths of both fundamentals.

Lastly, vibrational states are not exactly harmonic, and there is a small contribution to bandwidth from this source.

The paper by Lynden-Bell presents a theory of vibrational bandwidths in liquids for both the infrared and Raman. The width is caused by interaction of molecular vibrations with translations and rotations by rapidly varying terms in the intermolecular potential dependent on both internal and external coordinates. The vibrational dephasing is assumed to be slow compared with the time scale of decay of intermolecular correlation. Bratos et al. have considered the opposite extreme.

It would be a task for the analytical theoreticians attached to the project to use the methods of Lynden-Bell to develop predictions as described above for pressure, temperature, isotope dilution, etc. behavior via the *same* types of intermolecular potential being used by the molecular dynamics simulators. In this way it might become possible to use the information coming from the molecular dynamics runs to predict what should be happening experimentally in the infrared and Raman spectra.

12.6.3 Vibration/Rotation Coupling

As we saw in Chapter 6 vibrational dephasing has often been assumed to be decoupled from rotational relaxation, allowing the experimentalists a basis for deconvoluting the depolarized Raman spectrum with the infrared or polarized Raman spectrum to obtain a "pure" reorientational line shape. Secular terms in the fluctuating vibrational Hamiltonian are normally responsible for dephasing. These come from the second derivative of the intermolecular potential with normal coordinate (and also from the first derivative if the vibrations are anharmonic). These may be divided into self and exchange (or resonant energy transfer) terms, the latter being important in neat liquids. Efficient dephasing comes from those parts of $\partial^2 U_{12}/\partial q^2$ that have a large amplitude and vary slowly (but still rapidly compared with the dephasing time). Coupling of vibrational and reorientational dephasing occurs when these parts depend on the orientation of

the observed molecules. Orientation-dependent intermolecular interactions are affected by relative molecular translation and by reorientation. The translational motion can be related to neutron scattering data, the reorientational motion to 0–THz, NMR, Kerr effect, etc.

However, the traditional approach of the 1970s as outlined above by Lynden-Bell should not be adopted. It would be preferable to use the technique of molecular dynamics as the common theoretical denominator, and to attempt to avoid any ad hoc assumptions about rotation/vibration interaction. To use correlation functions from one technique in the analysis of data from another merely compounds approximation, leading to discord when taking into account the totality of work on a specific molecular liquid. It is much more satisfactory to take a particular model of the liquid, develop it on the computer, and then produce band shapes across the spectrum of spectroscopies available.

Van Woerkom et al. (1974) have pointed out, for example, that intermolecular vibrational relaxation is important (e.g., because of transition dipole-transition dipole interaction). Vibrational relaxation is not in general temperature independent and may be strongly affected by the reorientational motions of the molecules. This means that the methods developed to obtain the rotational and vibrational contributions to infrared band shapes separately *are not valid.*

One method is typified by Rakov (1962) and has been extended by Bartoli and Litovitz (1972). Here temperature independence of the vibrational relaxation is assumed. From the infrared band shape at low temperature, the intrinsic vibrational line width is then used to determine the reorientational line width at higher temperatures by subtracting from the whole band width the intrinsic width at a given temperature. This method is applicable only if the band shape is Lorentzian (or nearly so) over a large temperature range. Another incorrect procedure in the literature assumes the independence of rotational and vibrational relaxation. Using this method the vibrational line shape is obtained from Raman scattering data. Therefore the applicability of the method is confined to infrared active vibrations that are also Raman active. Fourier transformation of Raman bands yields information about the correlation functions for the elements of the polarizability tensor. The correlation function of the isotropic part of the polarizability tensor obtained in this way is assumed to be the vibrational correlation function for both the infrared correlation function (overall) and that of the anisotropic part of the polarizability tensor. The vibrational correlation function is then used to extract from the infrared correlation function the "reorientational" correlation function. This method is valid only if the assumption of additivity of the rotational and vibrational relaxation is independent of rotational relaxation. Van Woerkom et al. have shown that this is *not* the case, and in consequence Lynden-Bell has developed the ideas used above.

Methylene chloride and CH_2Cl_2/CD_2Cl_2 mixtures have been investigated

most important change in the interaction of the CH_2Cl_2 molecules with their environment is due to a shift in the frequency spectrum of the surrounding oscillators. In this way, the probability for resonant vibration energy transfer is diminished. The microdynamical behavior may be expected to be unchanged. A possible intermolecular coupling mechanism between the CH_2Cl_2 oscillators is the transition dipole-transition dipole interaction. The importance of the magnitude of the transition dipole is illustrated by the fact that the weak absorptions of CH_3I at 525 cm^{-1} and CD_3I at 495 cm^{-1} are *not affected* by isotopic dilution.

12.6.4 Neutron Scattering

In view of the assumptions that must be made in obtaining orientational a.c.f. from infrared and Raman spectroscopy, it seems clear that the use of these functions in the analysis of neutron scattering data again will serve only to compound uncertainty. Sears's method (1967) of expanding the van Hove function in terms of orientation functions was specifically designed to allow easy comparison with infrared and Raman functions, but the theoretical formalism is available only for the spherical top and only for incoherent scattering. Accordingly, it is better to redefine the criterion for intertechnical comparison when dealing with neutron inelastic scattering. In the present context this means specifically that molecular dynamics simulation should be the common denominator.

12.6.4.1 Coherent and Incoherent Cross Sections

In view of the uncertainties surrounding Sears's method of relating these functions to orientational correlation functions it is preferable to simulate these probabilities directly by constructing histograms in the molecular dynamics method and building up the experimentally observed scattering law directly.

Brier and Perry (1978) have discussed the theoretical problems of treating the neutron scattering from a rotationally diffusing asymmetric top. Careful quantitative studies of molecular liquids by neutron scattering are extremely limited in both kind and number. In particular, no liquid of nonspherical molecules had been investigated prior to that of methylene chloride by these authors. For the case of spin incoherent scattering ^1H nuclei, the double differential scattering cross section per nucleus is given in terms of the incoherent scattering law function $S(\mathbf{K}, \omega)$ by

$$\frac{d^2\sigma}{d\Omega\, d\tau} = \frac{k^4}{k_0}\left(\frac{\hbar}{m}\right)^2 a^2 S(\mathbf{K}, \omega)$$

where, as above, with a slight change of notation,

$$S(\mathbf{K}, \omega) = \frac{1}{2\pi}\int_{-\infty}^{\infty} I(\mathbf{K}, t)\exp(-i\omega t)\, dt$$

$$I(\mathbf{K}, t) = \langle \exp[-i\mathbf{K}\cdot\mathbf{r}(0)]\exp[i\mathbf{K}\cdot\mathbf{r}(t)]\rangle$$

This is for incoherent scattering and a is the bound incoherent scattering length of ^{1}H. $\hbar\omega$ is the energy gained by the neutron in the scattering event, and $\hbar\mathbf{K} = \hbar(\mathbf{k} - \mathbf{k}_0)$ is the momentum transfer. τ denotes the time-of-flight energy scale. $\mathbf{r}(t)$ is the time-dependent vector position of the scattering nucleus.

The first incorrect assumption made in the attempt to develop a theory for the intermediate scattering function $I(\mathbf{K}, t)$ is that of, (Chapter 6), factorizing into a translational part, $I_t(\mathbf{K}, t)$ and a rotational part, $I_r(\mathbf{K}, t)$. Berne and Montgomery have investigated this problem for rough hard spheres. In Chapter 5 we illustrated the effects of translation/rotation coupling in the simplest of molecules. Vibrations contribute a further Debye–Waller factor to the final expressions, but apparently with a value close to unity for the range of momentum transfers covered in a slow neutron scattering experiment.

The Sears expansion of $I_r(\mathbf{K}, t)$, that is,

$$I_r(\mathbf{K}, t) = \sum_{l=0}^{\infty} (2l+1) j_l^2(Kb) F_l(t)$$

is therefore not useful in practice because of rotation/translation coupling. Here j_l is a spherical Bessel function of order 1 and the rotational relaxation functions are defined in terms of the usual Wigner matrix expansion.

The only valid method of treating experimental incoherent neutron scattering data is therefore via molecular dynamics simulation, where the huge complexity involved can be handled by the machine in a more realistic way than is possible analytically. If Mori theory is used, for example, the memory function is a rotation/translation supermatrix (Chapter 5) whose elements are themselves matrices, each with nine phenomenological elements. The situation is obviously overparameterized. Models such as the M- and J-diffusion of Gordon (and variants) cannot be developed exactly for the asymmetric top because the free rotor a.c.f. for the asymmetric top is not known analytically in a closed form (Chapter 2). It would be more fruitful in the long run for theoreticians to devote their attentions to the technical problems of the molecular dynamics method (e.g., removal of pairwise interactions and boundary conditions, development using Mori theory of the semistochastic molecular dynamics approach). We remark finally that the idea of using infrared and Raman data to interpret neutron scattering data is a nonstarter. One need go no further in the argument than to point out that Sears's rotational theory was developed a dozen years ago for a *spherical top*, methane, and has not been extended to a dipolar molecule with any real success. This argument of course implies that incoherent (or coherent) neutron inelastic scattering data from a liquid are uninterpretable without molecular dynamics simulation, where we can reduce the band shapes to molecular dynamical properties, embodied essentially in an analytical form for the mode of

molecular interaction. In other words, there is no purpose in trying to use only phenomenological theory, such as that of Brownian motion, with the computer power now available.

12.6.4.2 Comparison of Far Infrared and Rayleigh Wing Scattering in CH_3I (References to lit. search)

This has been carried out for several liquids including methyl iodide in an interesting paper by Lund et al. The study of the depolarized Rayleigh-wing scattering has been intensified in recent years, but as Lund et al. point out, without any attempt to compare with the corresponding far infrared band shapes. An exception is the theory of Litovitz et al. These workers claim that collision-induced far infrared absorption and depolarized Rayleigh-wing scattering of dipolar anisotropic liquids are due to the same local fluctuations in the orientations of the individual molecules.

The authors use the relation

$$\mathfrak{A}(\omega) \propto \omega \tanh\left(\frac{\hbar\omega}{2kT}\right) \int_{-\infty}^{\infty} e^{-i\omega t} \langle \boldsymbol{\mu}(t) \cdot \boldsymbol{\mu}(0) \rangle \, dt$$

$$\equiv \omega \tanh\left(\frac{\hbar\omega}{2kT}\right) C_{ir} \qquad (12.6.4.3.1)$$

The intensity of scattered light of frequency ω_f is

$$I_{if}(\mathbf{q}, \omega_f, R) = \left(\frac{I_0 k_f^4}{16\pi^2 R^2 \epsilon_0^2}\right) \frac{1}{2\pi} \int_{-\infty}^{\infty} e^{-i\omega t} \langle \delta\epsilon_{if}(\mathbf{q}, 0) \delta\epsilon_{if}(\mathbf{q}, t) \rangle \qquad (12.6.4.3.2)$$

in standard notation. In this expression $\omega = \omega_i - \omega_f$. Owing to the high exciting frequency used compared to the low frequency shift studied, k_f may be regarded as a constant. For molecular liquids one usually assumes that $\delta\epsilon_{if}$ may be expressed in terms of molecular polarizabilities.

$$I(\omega_f) \propto \int_{-\infty}^{\infty} e^{-i\omega t} \langle \alpha(0) \alpha(t) \rangle \, dt \equiv S(\omega) \qquad (12.6.4.3.3)$$

$$S(\omega) = \frac{1}{2} [S^{>}(\omega) + S^{<}(\omega)] \qquad (12.6.4.3.4)$$

$S^{>}(\omega)$ and $S^{<}(\omega)$ are used for the Stokes and anti-Stokes side. The principle of detailed balance states

$$\frac{S^{<}(\omega)}{S^{>}(\omega)} = \exp\left(\frac{-\hbar\omega}{kT}\right) \qquad (12.6.4.3.5)$$

$$S(\omega) = \frac{1}{2} S^{>}(\omega) \left[1 + \exp\left(\frac{-\hbar\omega}{kT}\right)\right]$$

Lund et al. do not compare the dipolar and polarizability correlation functions directly, as is often done; instead they construct a quantity $R(\omega)$

proportional to the energy absorbed in a scattering experiment:

$$R(\omega) = \omega[S^{>}(\omega) - S^{<}(\omega)]$$
$$= S^{>}(\omega)\omega\left[1 - \exp\left(\frac{-\hbar\omega}{kT}\right)\right]$$
$$= 2S(\omega)\omega \tanh\left(\frac{\hbar\omega}{2kT}\right) \qquad (12.6.4.3.6)$$

$R(\omega)$ is now compared with the infrared power absorption $\mathfrak{A}(\omega)$ to see if they show the maximum for the same value of the frequency. This is the case if the dipolar and the polarizability correlation functions have the same time dependence for the times studied in this paper which are smaller than the rotational diffusion times, that is, $<10^{-12}$ sec. This procedure is chosen because the far infrared absorption maxima are very pronounced so that a comparison should be very easy.

Eq. 12.6.4.3.6 has sometimes been used in its lower frequency or high temperature form:

$$R(\omega) \propto S(\omega)\omega^2$$

For symmetrical tops with a permanent dipole moment [$CHCl_3$, CH_3I, $CHBr_3$, CH_3CCl_3, $(CH_3)_3CCl$, $(CH_3)_3Br$] the maxima for $R(\omega)$ and $\mathfrak{A}(\omega)$ coincide in frequency. The discrepancy is largest for CH_3CCl_3 and $(CH_3)_3CCl$; this may be due to the considerable contribution of the convolution of the apparatus slit function and the "true" Rayleigh line due to molecular diffusion to low frequency shifts ($<20 \sim 25\,cm^{-1}$), but the discrepancy could also be caused by a strong variation of the refractive index for these compounds.

Lund et al. also investigated the Rayleigh and far infrared spectra of the nondipolar species C_6H_6, C_6D_6, and CCl_4, which are without a permanent dipole moment and show maxima in the $R(\omega)$ curves coinciding with the corresponding ω_{max} in the absorption spectra. The shift in the far infrared absorption maximum going from C_6H_6 to C_6D_6 is reproduced in the $R(\omega)$ curves.

The maximum in the $R(\omega)$ curves for the asymmetric tops C_6H_5Cl and C_6H_5Br is very close in frequency to the maximum in benzene, whereas the absorption maximum is at a lower frequency. An examination of the $R(\omega)$ curves for C_6H_5Cl and C_6H_5Br show that these curves have an augmented intensity compared with the corresponding benzene curve on the low frequency side of the maximum, especially pronounced for C_6H_5Br. Lund et al. suggest that the $R(\omega)$ curves for C_6H_5Cl and C_6H_5Br are composed of two curves: one with a frequency maximum at $\sim 75\,cm^{-1}$ (benzene) and another showing a maximum at the frequency of the absorption maximum in the far infrared, the latter curve being less intense than the former.

Finally, these authors mention that the $R(\omega)$ curve for CCl_4 is very similar to the far infrared spectrum with bands of very weak intensity at

~ 95 and $\sim 140\,cm^{-1}$. These far infrared bands have been assigned as difference bands: $146\,cm^{-1}$, $\bar{\nu}_1(a_1) - \bar{\nu}_4(f_2)$, and $96\,cm^{-1}$, $\bar{\nu}_2(e) - \bar{\nu}_4(f_2)$. The difference bands are also Raman active.

The similarity between the far infrared absorption and the "Raman absorption" $R(\omega)$ for symmetrical top molecules with a permanent dipole moment makes it plausible that the same component of the short time motion is responsible. Lund et al. go on to propose a molecular mechanism involving molecular rotation around an axis perpendicular to the top axis. This leads to a change both in the component of the permanent dipole moment in the direction of the field and in the static polarizability in the laboratory frame, whereas a rotation around the top axis cannot give rise to far infrared absorption in a slowly varying field.

The hypothesis that librations around axes perpendicular to the top axis are responsible for both the depolarized Rayleigh-wing scattering and the far infrared absorption bands for symmetrical top molecules with a permanent dipole moment could be tested if symmetrical tops with the dipole moment perpendicular to the top axis existed, because librations around the top axis would give rise to a far infrared absorption, while they would be Raman inactive and $\mathfrak{A}(\omega)$ and $R(\omega)$ would not look alike. The asymmetric top molecules chlorobenzene and bromobenzene almost fulfill the condition.

The difference between α_{xx} and α_{yy} is too small to show a significant contribution from a libration around the z-axis to the Raman spectrum, which will be due to libration around the axis in the molecular plane; it is to be expected that the similar values of I_x for C_6H_5X and C_6H_6 will result in similar values of ω_{max} for $R(\omega)$ for libration around the x-axis, and this is the case. The libration around the y-axis gives a contribution which in itself should result in a maximum around

$$\bar{\nu} = \frac{\omega}{2\pi c} = 75(89/320)^{1/2} = 40\,cm^{-1} \text{ for } C_6H_5Cl$$
$$\bar{\nu} = \frac{\omega}{2\pi c} = 75(89/513)^{1/2} = 31\,cm^{-1} \text{ for } C_6H_5Br$$

In the measured $R(\omega)$ they are seen as an augmented intensity [compared to $R(\omega)$ for benzene], and they give rise to a slight decrease in the position of the maximum ω_{max}. The libration around the x-axis only gives rise to far infrared absorption through induced dipoles. The main contribution caused by the permanent dipole is due to libration around the y-axis and the libration around the z-axis, and $\mathfrak{A}(\omega)$ looks quite different from $R(\omega)$. The observed far infrared maxima, $\bar{\nu}_{max} = 44$ and $38\,cm^{-1}$ for C_6H_5Cl and C_6H_5Br, respectively, agree well with the moments of inertia for the y and z librations; the values of the moments are so close that we cannot separate the two modes.

The comparison between the x and y librations leads us to expect a slightly lower $\bar{\nu}_{max}$ than the one measured if the intermolecular force field

were isotropic, so that $\bar{\nu}_{max}$ depends only on the moment of inertia. It is, according to Lund et al., obvious that the resistance to a movement around the y- and z-axes that involves a displacement of the halogen atom is stronger than a motion around the x-axis and that it will lead to an augmented frequency of the free librator.

The far infrared and Rayleigh spectra of the spherical molecule carbon tetrachloride arise from induced dipole moments and distortions of the ellipsoid of polarizability, respectively. The similarity of $R(\omega)$ and $\mathfrak{A}(\omega)$ again makes it plausible that the same librational motion is responsible.

This brings to an end our manuscript on molecular dynamics. We have tried to describe the state of the art as it stands and suggested a course for the most profitable future study. To this end we have proposed a scheme of research for inter-technical experimental cooperation to be pursued in close collaboration with molecular dynamics simulators and theoreticians. We end the book on this note in the hope that it may help bring the project to fruition and remind the reader that we have always insisted that molecular dynamics are those of a crowd.....

REFERENCES

Bartoli, F. J. and Litovitz, T. A., *J. Chem. Phys.* **56**, 414 (1972).

Berne, B. J. and Harp, G. D., *Adv. Chem. Phys.* **17**, 163 (1970).

Brier, P. N. and Perry, A., *Adv. Mol. Rel. Int. Proc.* **13**, 1 (1978).

Brot, C., *Dielectric and Related Molecular Processes*, Vol. 2, Chemical Society, London, p. 1 (1975).

Buckingham, A. D., *Chem. Soc. Quart. Rev.* p. 63, (1959).

Dardy, H., Volterra, V., and Litovitz, T. A., *Chem. Soc. Symp. No. 6*, p. 71 (1972).

Dill, J. F., Litovitz, T. A., and Bucaro, J. A., *J. Chem. Phys.* **52**, 3839 (1975).

Evans, M. W. and Evans, G. J., *J. Chem. Soc. Faraday Trans II* **76**, 667 (1980).

Finney, J. L., in *Water: A Comprehensive Treatise*, Vol. 6, F. Franks, Ed., Plenum, New York (1978).

Gerschel, A., Dimicoli, I., Joffre, J., and Riou, A., *Mol. Phys.* **32**, 679 (1976).

Hildebrand, J. H., *Faraday Disc. No. 66*, p. 151 (1978).

Kielich, S., *Dielectric and Related Molecular Processes*, Vol. 1, Chemical Society, London, p. 253 (1972).

Larkin, I. W., *J. Chem. Soc. Faraday Trans II* **69**, 1278 (1973).

Lynden-Bell, R., *Mol. Phys.* **33**, 907 (1977).

Malecki, J., *Acta Phys. Pol.* **21**, 13 (1962); *J. Chem. Soc. Faraday Trans. II* **72**, 104 (1976).

Marcus, Y., *Introduction to Liquid State Chemistry*, Wiley, New York (1975).

Rakov, A. V., *Opt. Spectrosc.* **13**, 203 (1962).

Scaife, B. K. P., Dielectrics Society Meeting, Aussois (1980).

Sears, V. F., *Can. J. Phys.* **45**, 237 (1967).

Stuart, H.-A., *Molekulstruktur*, Springer, Berlin (1967).

Baise, A., Ph.D. Thesis, University of Wales (1972).

van Woerkom, P. C. M., de Bleyser, J., de Zwart, M., Burgers, P. M. J., and Leyte, J. C., *Ber. Bunsenges. Phys. Chem.* **78**, 1303 (1974).

Wolynes, P. and Deutch, J. M., *J. Chem. Phys.* **66**, 178 (1977).

Index